DEFENSE TECHNICAL INFORMATION CENTER

Information for the Defense Community

DTIC® has determined on 06/11/2010 that this Technical Document has the Distribution Statement checked below. The current distribution for this document can be found in the DTIC® Technical Report Database.

☒ **DISTRIBUTION STATEMENT A.** Approved for public release; distribution is unlimited.

☐ **© COPYRIGHTED**; U.S. Government or Federal Rights License. All other rights and uses except those permitted by copyright law are reserved by the copyright owner.

☐ **DISTRIBUTION STATEMENT B.** Distribution authorized to U.S. Government agencies only (fill in reason) (date of determination). Other requests for this document shall be referred to (insert controlling DoD office)

☐ **DISTRIBUTION STATEMENT C.** Distribution authorized to U.S. Government Agencies and their contractors (fill in reason) (date of determination). Other requests for this document shall be referred to (insert controlling DoD office)

☐ **DISTRIBUTION STATEMENT D.** Distribution authorized to the Department of Defense and U.S. DoD contractors only (fill in reason) (date of determination). Other requests shall be referred to (insert controlling DoD office).

☐ **DISTRIBUTION STATEMENT E.** Distribution authorized to DoD Components only (fill in reason) (date of determination). Other requests shall be referred to (insert controlling DoD office).

☐ **DISTRIBUTION STATEMENT F.** Further dissemination only as directed by (inserting controlling DoD office) (date of determination) or higher DoD authority.

Distribution Statement F is also used when a document does not contain a distribution statement and no distribution statement can be determined.

☐ **DISTRIBUTION STATEMENT X.** Distribution authorized to U.S. Government Agencies and private individuals or enterprises eligible to obtain export-controlled technical data in accordance with DoDD 5230.25; (date of determination). DoD Controlling Office is (insert controlling DoD office).

SCIENTIFIC COUNCIL
OF THE RUSSIAN ACADEMY OF SCIENCES
ON THE PROBLEMS OF MOTION CONTROL
AND NAVIGATION

THE STATE RESEARCH CENTER
OF THE RUSSIAN FEDERATION
CENTRAL SCIENTIFIC AND RESEARCH
INSTITUTE ELEKTROPRIBOR

9th SAINT PETERSBURG INTERNATIONAL CONFERENCE ON INTEGRATED NAVIGATION SYSTEMS

27 - 29 MAY, 2002

RUSSIA

CO-SPONSORED BY:

- THE INTERNATIONAL PUBLIC ASSOCIATION ACADEMY ON NAVIGATION AND MOTION CONTROL (ANMC)
- THE AMERICAN INSTITUTE OF AERONAUTICS AND ASTRONAUTICS (AIAA)
- THE INSTITUTE OF ELECTRICAL AND ELECTRONICS ENGINEERS (IEEE), USA
- L'ASSOCIATION AÉRONAUTIQUE ET ASTRONAUTIQUE DE FRANCE (AAAF)
- L'INSTITUT FRANÇAIS DE NAVIGATION (IFN)

SCIENTIFIC COUNCIL
OF THE RUSSIAN ACADEMY
ON THE PROBLEMS OF MOTION CONTROL
AND NAVIGATION

THE STATE RESEARCH CENTER
OF THE RUSSIAN FEDERATION
CENTRAL SCIENTIFIC AND RESEARCH
INSTITUTE "ELEKTROPRIBOR"

9th SAINT PETERSBURG INTERNATIONAL CONFERENCE ON INTEGRATED NAVIGATION SYSTEMS

27 - 29 MAY, 2002

RUSSIA, ST. PETERSBURG

CO-SPONSORED BY:

- THE INTERNATIONAL PUBLIC ASSOCIATION ACADEMY OF NAVIGATION AND MOTION CONTROL (ANMC)
- THE AMERICAN INSTITUTE OF AERONAUTICS AND ASTRONAUTICS (AIAA)
- THE INSTITUTE OF ELECTRICAL AND ELECTRONICS ENGINEERS (IEEE), USA
- L'ASSOCIATION AÉRONAUTIQUE ET ASTRONAUTIQUE DE FRANCE (AAAF)
- L'INSTITUT FRANÇAIS DE NAVIGATION (IFN)

In the present publication the materials of the 9th Saint Petersburg International Conference on Integrated Navigation Systems (May 27–29, 2002) are presented.

*This publication includes the full texts of plenary papers and abstracts of poster presentations (marked with * in the Contents).*

Editor-in-Chief

Vladimir G. Peshekhonov

ISBN 5-900780-37-6

CONTENTS

SESSION I: SATELLITE SYSTEMS

SESSION II: INTEGRATED SYSTEMS

SESSION III: INERTIAL SYSTEMS AND SENSORS

HIGH ELLIPTICAL ORBIT-BASED INFORMATIONAL AND NAVIGATIONAL FUNCTIONAL AUGMENTATION OF GLOBAL NAVIGATION SATELLITE SYSTEMS

Yu.P.Semenov*, V.P.Legostaev, B.Ye.Chertok***, V.P.Gavrilov****, G.A.Berzin*****.**
S.P.Korolev Rocket and Space Corporation Energia,
4a, Lenina st., 141070, Korolev, Moscow Region, Russia
Phone 7095 5138242; Fax: 7095 5138620; e-mail: post2@rsce.ru.

V.A.Udaloy****, S.G.Revnivykh*******, V.N.Pochukaev********
Mission Control Center
4, Pionerskaya st., 141070, Korolev, Moscow region, Russia
Phone 7095 5135806; Fax: 7095 5868380; e-mail: CNSS@mce.rsa.ru.

Abstract

Keywords: satellite, navigation, user, augmentation, corrections.

This paper presents a concept for a Russian space-based wide-area functional augmentation of global navigation satellite systems (GNSS). This augmentation was given the name of Informational and Navigational Functional Augmentation (INFA). In contrast to WAAS and EGNOS systems using for relay satellites SC in GEO, the space segment of INFA consists of SC based on Yamal bus flying in High Elliptical Orbits (HEO) of Tundra type. The paper provides a rationale for the desirability of creating INFA for Russia, with its large area and northerly location.

Introduction

There are plans for the near future (2008-2011) to introduce in Russia a Positioning and Time Support (PTS) system based on the use of global navigation satellite system GLONASS (as well as GNSS GPS, GALILEO), to provide control to all kinds of mobile objects.

The key elements of the PTS system are: navigation satellites (NS), user equipment (UE), functional augmentations to GNSS (FA), monitoring and control centers, communications lines.

The task of integrated optimization of the following problems must be addressed: providing the maximum achievable positioning accuracy to the PTS system users, continuity and reliability of positioning, including users located in difficult environments (cities, mountains, etc.), providing communications to traffic control, servicing and other kinds of centers; minimization of total costs.

In the interests of accomplishing this task, this paper proposes a concept for Russian wide-area functional augmentation, Informational and Navigational Functional Augmentation (INFA), the space segment of which consists of satellites in HEO.

It shows the architecture of INFA and functions of its elements, possible options for satellite constellations of SC in HEO, orbital parameters for these SC.

It demonstrates the advantages of SC in HEO as compared to relay satellites in GEO.

It provides performance data for HEO satellite that is being designed at RSC Energia to be used as a space component of INFA

INFA effectiveness analysis has been completed.

1. INFA architecture and functions of its elements

Major INFA elements are: Navigation Data Processing and Generation Center or Navigation Center (NC); a network of Monitoring and Correction Stations (MCS) equipped with multi-channel GLONASS/GPS/GALILEO receiving hardware; HEO satellite constellation; Satellite Communications Ground Stations (SC GS); Central

---

* Full member of RAS, chief designer.
** Corresponding member of RAS, first deputy chief designer.
*** Full member of RAS, honorary member of the Academy of Navigation and Motion Control, chief scientific adviser.
**** Senior scientist
***** Leading engineer.
****** Ph.D, first deputy leader.
******* Head of department.
******** Doctor of sciences, leading scientist.

Station, which is a system that includes JEO SC mission control center, Monitoring and Control System Ground Station, transmitting station based on GLONASS SC transmitter, etc.

MSC continuously receive radio signals from navigation satellites. All the received data are transmitted to NC via SC in HEO (other communications channels may also be involved). NC generates: data on the integrity of NS that are being controlled; current corrections to the ephemeris and time data stored on-board navigation satellites; ephemeris and time data for SC in HEO.

The generated data array is distributed throughout the entire coverage area of HEO SC via transmitting station and HEO SC which serves as a relay for these data.

Transmitting station also generates a navigation signal similar to GLONASS SC signal which is also distributed via HEO SC over its entire coverage area. This signal is also received by an MCS located near transmitting station. The processing of this signal together with the signal generated by the transmitting station allows to factor in the time it takes for the radio signal to travel between the transmitting station and HEO SC with high degree of accuracy. Thus, the HEO SC becomes a conventional navigation satellite. It goes without saying that an accurate geodetic fixation of the transmitting station and the MCS will be required.

The number of MCSs is an issue which needs to be determined. There are plans to use both specialized MCSs, and Monitoring and Correction Stations for local augmentations.

Top-level INFA architecture is shown in Fig.1.

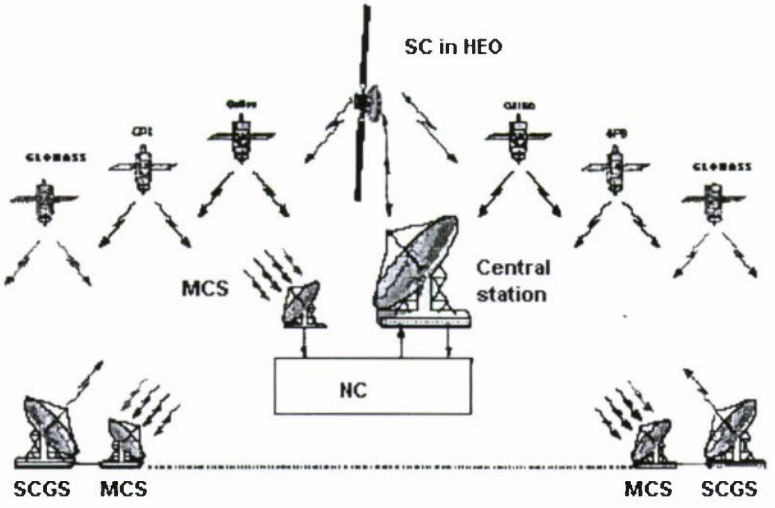

Fig.1. Top-level architecture of the Information and Navigation Functional Augmentation

NC has the following additional functions: continuous monitoring and periodic certification of navigation fields over Russia and adjoining territories; it is possible to integrate INFA with other wide-area augmentations.

Additional functions of SC in HEO are: transmission of digital data on the location and status of objects that are the users of the navigational data to monitoring and control centers; transmission of command data in the opposite direction.

2. Parameters of the satellite constellation in high elliptical orbits

The orbital constellation of relay satellites is to be built on the basis of Yamal SC flying in HEO with the following parameters:

period	T ~ 24 h,
apogee altitude	$H_{\text{♋}}$ ~ 47-50 thou. km,
perigee altitude	$H_{\square}$ ~ 25-22 thou. km,
inclination	i ~ 63°,
argument of perigee	• ~ 270°.

The advantages of these orbits are: high perigee altitude, which allows the SC to fly above radiation belts; large coverage area with the minimal number of satellites in the constellation; less propellant required to put the SC in such an orbit as compared with putting SC in GEO.

There are several options for HEO constellation: a constellation which consists of 3, 4 SC flying over the same ground track; a constellation consisting of 4 SC flying over two different ground tracks.

Fig. 2-4 shows these constellation options, their respective orbital parameters, ($H_{\text{♋}}$ - apogee altitude, $H_{\square}$ - perigee altitude), SC ground tracks, active SC change latitudes ($\varphi_{\text{♋}}$), one-moment critical coverage areas. It is assumed that, taking into account external obstacles (urban environments, mountains), navigation and

communications services must be provided to the user at mask angle γ of up to 25°. It can be seen that such constellations provide a 100% coverage of the Russian territory at γ=25°.

Fig.5 shows similar coverage areas for two SC in GEO. They demonstrate that it would be disadvantageous to use such SC for a Russian wide-area functional augmentation.

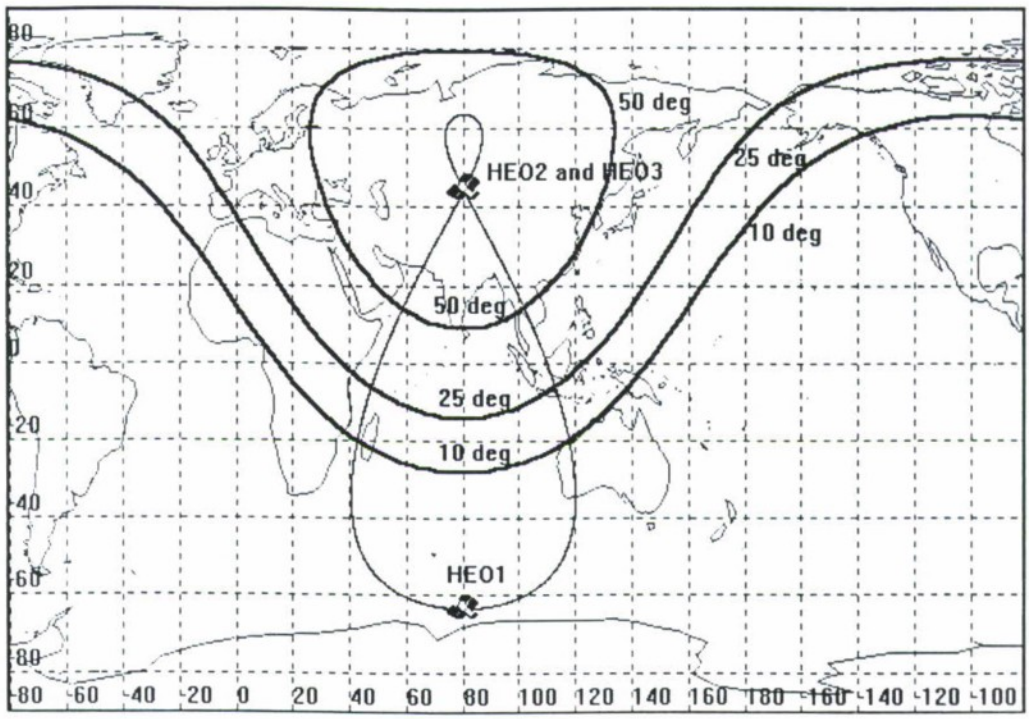

Fig.2 Satellite Constellation in HEO consisting of three SC flying over the same ground track (H_α=47 thou. km, H_π=25 thou. km, φ_α=45°)

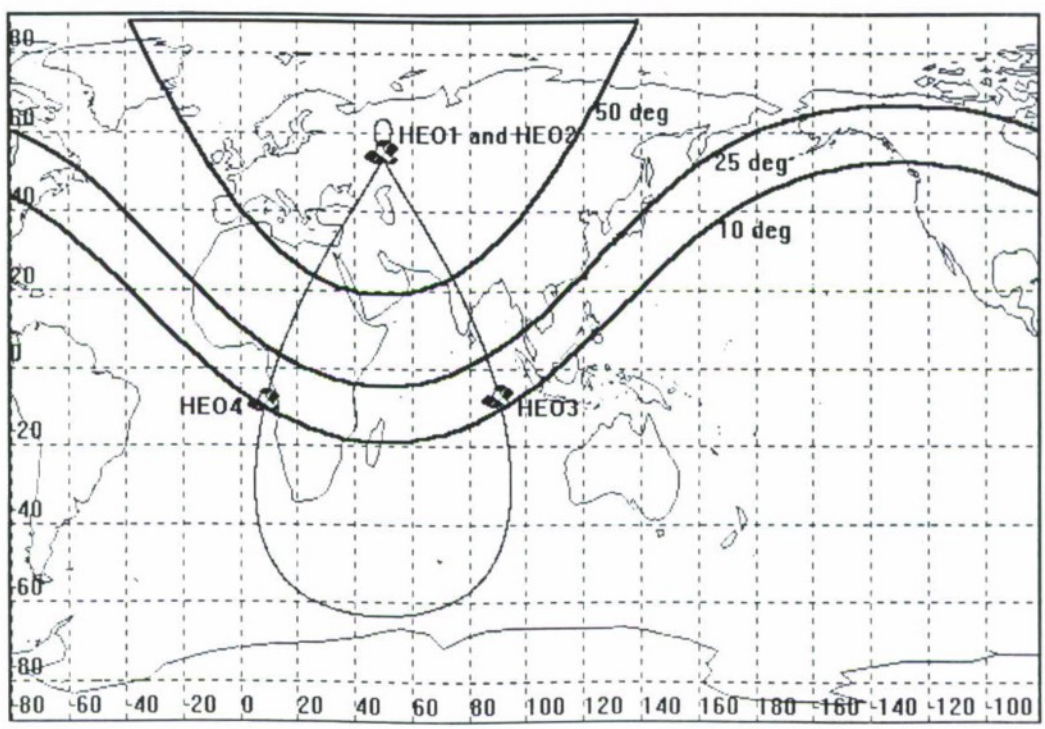

Fig.3 Satellite Constellation in HEO consisting of four SC flying over the same ground track (H_α=50 thou. km, H_π=22 thou. km, φ_α=54°)

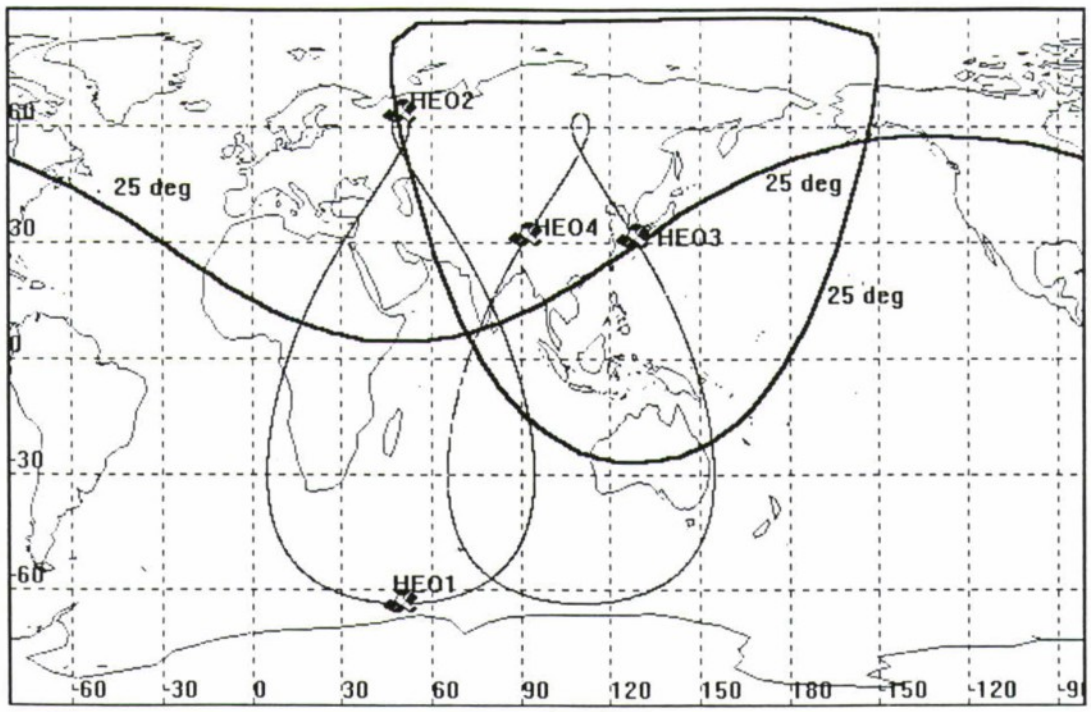

Fig.4 Satellite Constellation in HEO consisting of four SC flying over two different ground tracks (H_a=50 thou. km, $H_п$=22 thou. km, φ_a=31°)

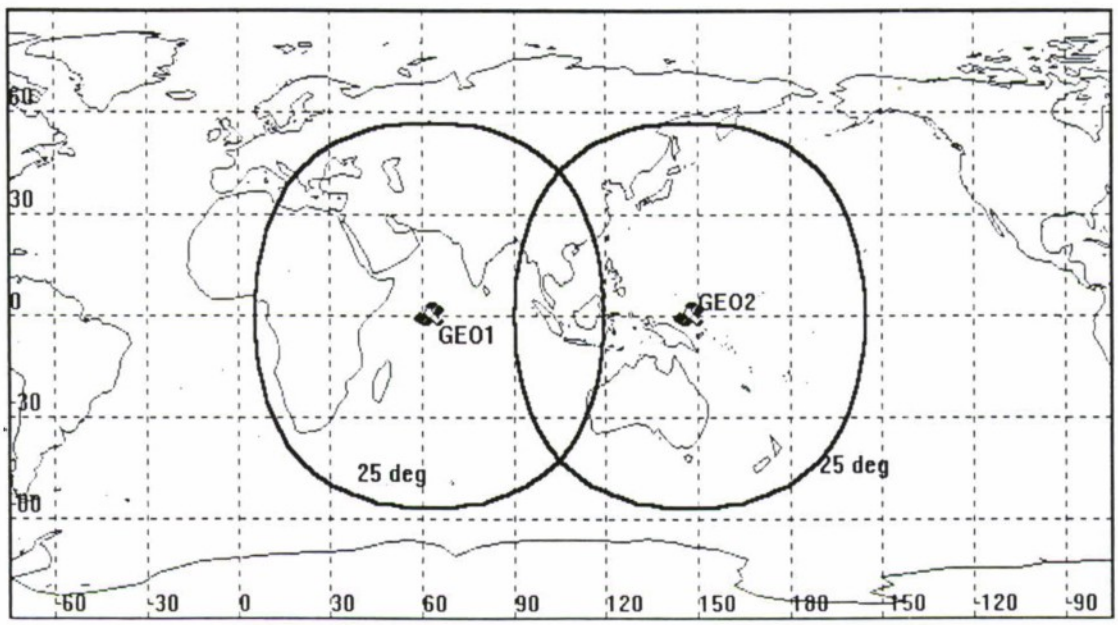

Fig.5 Coverage areas of two SC in GEO (γ=25°).

3. Properties of the SC based on Yamal bus and used as a space component of the INFA

Fig.6 provides key performance data on a high-apogee SC (Tundra-type orbit) based on Yamal bus, which is being designed in RSC Energia as a radio broadcast and communications satellite, and which can be used as a space component of INFA.

Fig.7 shows the architecture of the on-board radio system of that SC.

The functions of this SC on-board radio system are: radio broadcasts in L-band, mobile communications in Ku-band on the CIS territory, mobile communications in Ku-band in the area of northern air-routes, implementation of INFA functions.

Energy and mass resources of the on-board radio system spent on the implementation of the INFA functions does not exceed 10-15% of the total on-board radio system resources.

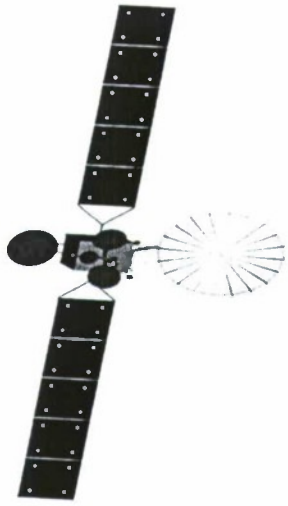

- Mass 1600 kg
- Mass of the Applications Payload 450 kg
- Power required for the Applications Payload 5,5 kW
- Transponder bands C, Ku, L
- Stabilization in three axes
- Life in orbit 12 years and more
- Can be put into a high elliptical orbit using Soyuz LV with Fregat upper stage

Fig.6 SC based on Yamal bus in HEO

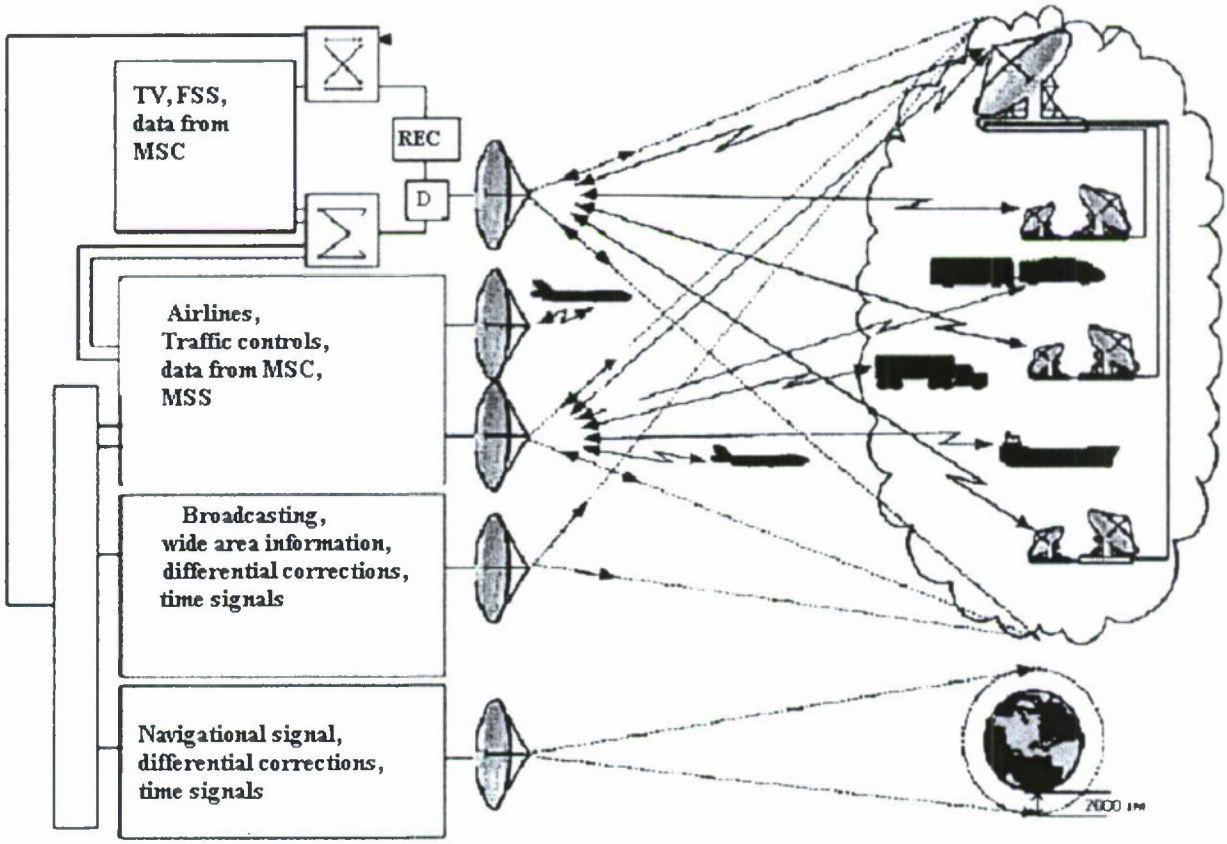

Fig.7 Block-diagram of the SC on-board RF system

4. INFA efficiency evaluation

One of the most important functions of INFA is to accumulate at NC all the navigation data from MCS, and, based on its processing, to provide real-time monitoring of GNSS GLONASS, GPS, GALILEO navigation field parameters. It is expected that providing the data from such monitoring to all interested parties, will allow to reduce work load at monitoring centers at the level of specific regions and industries.

Introduction of INFA will also allow integration with other wide-area augmentations (WAAS, EGNOS).

The next important function of INFA is to provide communications services between PTS system users and centers for controlling mobile objects via HEO SC. This task is important for Russia because of its large territory and underdeveloped infrastructure of ground communications lines.

And finally, INFA functions include improving navigation accuracy for PTS system users.

Let us review this problem in more detail.

We shall proceed from the following assumptions.

No later than 2008, NSs of the GLONASS, GPS, GALILEO systems will be transmitting navigation signals on two (three) frequencies available to all the users. The user will have multi-channel (12 channels and more) equipment capable of receiving signals from GLONASS, GPS, GALILEO, as well as signals relayed via HEO SC. It is assumed that the design performance data of the upgraded GLONASS and GPS systems, as well as of the new GALILEO GNSS will be achieved.

Expected navigation accuracy of the upgraded GLONASS GNSS (GLONASS K), GPS (GPS III) and GALILEO system, as well as GLONASS K GNSS plus INFA are given in Table 1.

For the purposes of comparison, the Table also lists accuracy data for the previous phases of GLONASS and GPS GNSS (one- and two-frequency signal options).

Table 1 lists major sources of errors in pseudo range measurements, total pseudo range errors, horizontal and vertical errors in one-moment positioning (1σ) in meters. Positioning errors were determined as a result of using the method of geometric dilution of precision at mask angles $\gamma=5\div10°$.

Table 1

Pseudo range error sources	GLONASS		GPS			GLONASS K, GPS III, GALILEO	GLONASS K +INFA
	GLONASS	GLONASS - M	GPS	GPS II RM	GPS II F		
Positioning and Timing Support of NS	9.2	2.6÷3.4	2.3	2.3	1.25	0.65÷0.8	0.2÷0.4
Ionosphere	I0	-	7	-	-	-	-
Troposphere	0.2÷2.5	0.2÷2.5	0.2÷2.5	0.2÷2.5	0.2÷2.5	0.2÷2.5	0.1÷0.5
Hardware errors and multi-paths	5.2	4	1.6	2.1	2.1	0.57÷2.3	0.1÷2.0
Total pseudo range error	I4.7	4.8÷5.8	7.5	3÷3.9	2.5÷3.5	0.9÷3.5	0.25÷2.1
Horizontal positioning error	22.0	7.2÷8.7	11.2	4.5÷5.8	3.7÷5.2	I.4÷5.2	0.4÷3.2
Vertical positioning error	29.5	9.6÷11.6	15.0	6÷7.8	5.0÷7.0	1.8÷7.0	0.5÷4.2

The above data demonstrate that one can expect a significant effect from introduction of INFA.

In order to achieve this, in our opinion, one must purposefully carry out a large amount of work on procedures and experiments.

One must solve the problems of improving models of NS motion and operating conditions of mobile objects using navigation information, models of slowly and quickly changing errors in navigation parameter

measurements, eontents of the information transmitted from MCS to NC and from NC to the users, optimization of algorithms for the measured data preproeessing, evaluation algorithms in NC and user hardware.

One neeessary eondition is coordination of ealculation methods between NC and user equipment, whieh must support INFA operation in a way similar to a local FA in case where a navigation data user is located near one of MCSs.

It is assumed that the user equipment will simultaneously proeess radio signals from all visible NSs or from a maximum number of them (taking into aceount constraints on the number of user equipment ehannels). From this standpoint, the optimal option is to use the total navigation field ereated by GNSS GLONASS, GPS, GALILEO.

The wide spread of navigation aeeuraey estimates in the last two eolumns of Table 1 is eaused, firstly, by different levels of external interferenee (troposphere, multipath), secondly, by our eurrent lack of knowledge.

Also done was a preliminary effieieney analysis of ineluding HEO SC into the Russian GNSS as additional navigation satellites. Compared were a eomplete (24 SC) and an ineomplete GLONASS systems, and extended systems (eomplete or ineomplete GLONASS systems plus one or two aetive HEO SC).

The analyses were performed in aeeordance with the following proeedure.

First, aecessibility areas were ealeulated at N = 4, 6 for all the navigation system options under review in the ease of mask angles $\gamma = 5^\circ - 20^\circ$.

Where N is the number of satellites simultaneously observed by the user.

Then, for various locations on the Russian territory, the horizontal (HDOP) and vertical (VDOP) geometric dilutions of precision were calculated as funetions of time. Geometric dilutions of precision were taken as criteria for the navigation data user positioning accuracy.

The following preliminary results were obtained:

1. Adding one or two HEO navigation satellites to the complete GLONASS constellation on the average improves the positioning aeeuracy on the Russina territory by 10÷20% and 15÷30% for $\gamma = 5^\circ$ and $\gamma = 20^\circ$, respeetively.

2. A system of 18 GLONASS SC and two aetive HEO SC is roughly equivalent to a complete GLONASS system of 24 SC. In ease one GLONASS SC fails, additional HEO navigation satellites will allow to preserve high charaeteristies of the Russian navigation field over Russia.

As a result, the effeet of introducing INFA and HEO SC based on Yamal bus ean be summarized as follows:

- a eentralized monitoring of all navigation fields over Russia is provided, thus allowing to reduce the amount of work in departmental and regional monitoring and eontrol centers;
- a capability for integration with wide-area FA of other eountries is provided:
- mobile objects navigation accuracy is significantly increased, which, in our opinion, will allow to forgo the deployment of regional FAs and to reduee the number of loeal FAs in Russia;
- HEO SC as a navigation satellite will improve the aceuraey and reliability of the Russian GNSS;
- SC based on Yamal bus will provide additional eommunications and traffic control serviees;
- costs of the additional HEO SC payload that supports INFA operation are eomparatively low

Conclusion

It is expected that the implementation of the INFA eoneept will clear the way for creation of a common navigation field over Russia, which will support mobile objeet positioning accuracy of 1 to several meters. this objeetive ean be achieved by both the use of the common navigation field created by GLONAS, GPS, GALILEO systems, and by means of only the Russian GNSS

Implementation of INFA will solve the problems of centralized monitoring of navigation fields over Russia and of integration with wide-area funetional augmentations of other countries.

Radio broadeast and eommunications satellite based on Yamal bus that is currently under development at RSC Energia fits nicely into the INFA concept.

References

1. **Dmitriev P.P., Shebshaevich V.S.** Network satellite navigational systems. - M.:Radio and communication, 1982.
2. **Harisov V.N., Petrov A.I., Boldin V.A.** Global satellite navigational system GLONASS. - M.: IPRGR, 1999.
3. **Turner D., Shaw M., Sandhoo K.** Modernization of the GLOBAL positioning system // UN/USA Workshop on Use and Aplication of GNSS, 2002.
4. **Salabert F.** Status and development of EGNOS // UN Workshop, Santiago de Chile, 2002.

GNSS FUNCTION IN NAVIGATION AND CONTROL SYSTEMS:TRENDS OF IMOPROVEMENT AND DEVELOPMENT

I.K. Konarzhevsky, S.B. Pisarev, B.V. Shebshaevich

The russian institute of radionavigation and time, St. Petersburg, Russia

The outstanding performances of the Global Navigation Satellite Systems /GNSS/ demonstrated and approved by GPS and GLONASS during about 20 years clearly defined GNSS function as an integral part of the most navigation and control systems all over the world.

Accuracy on the global basis was the initial object of interest nevertheless availability and integrity of GNSS function became the main objects of critical studies, development and improvement soon.

GNSS function availability, as probability of PVT (Position, Velocity, Time) determination everywhere and every time it is necessary, depends on the current status of space and ground control segments and user equipment segment as well. The GPS Block II R satellites now, GLONASS-M for the nearest future, GALILEO for the future can provide more than 99,99 % availability. Actually GNSS function availability is strongly influenced by user equipment capabilities and quality in changing environment and operational conditions such as:

- signal shadowing /low power signal/;

Signal reception in standard conditions implies free path signal propagation from satellite transmitter to users receiver. Actually, various shadowing for example foliage or constructions and buildings in urban conditions reduce signal power level and make difficult signal reception and processing. In addition only some signals may be shadowed while others are of standard power level. That means that dynamic signal power range may exceed the standard automatic gain control range of the users equipment or cross correlation products may mask the auto correlation products and bring to fault signal acquisition.

- multipath signal propagation /multipath effect/;

Signal reflections from various natural objects and construction elements result in the situation when the signal at antenna comprises the superposition of direct path signal and multiple reflected signals (multipath effect). The discriminator of code locked loop becomes then distorted and introduces significant errors into pseudorange measurements and correspondingly to position and time determination.

- intentional and non intentional electromagnetic interference/EMI/

and signal jamming;

Intentional and non intentional EMI is a real problem especially now when satellite and mobile telecommunication standards are competing with GNSS for frequency band and special aids for radio counteraction against GNSS signals have already demonstrated jamming efficiency in various local conflicts. The GNSS improvement in particular implies the transmitted signal power increase but still the user equipment is the final border of protection against EMI.

- high dynamics;

Correctly designed GNSS signal phase locked loops and code locked loops can bear highest dynamics coming out of reasonable applications, with corresponding losses in noise protection indicators due to locked

loops bandwidth expansion. Nevertheless, spatial rotations raise one more problem, namely, the interruptions in signal continuous reception in the rotation phase when the satellite is out of radio vision from users antenna.

- short term missions bringing strict limitation to the time to first PVT fix.

Standard first PVT fix procedures are finite in time. Nevertheless some applications are even shorter in time. Special first PVT fix procedures with reduced time are necessary to use GNSS function in short time missions.

The presence of these factors or their combination can ruin the GNSS function availability never the less the GNSS signals are available. The counter – measures comprise, a set of hardware and soft ware advanced techniques discussed in the present report.

In particular:

- low power signal processing techniques;
- multipath effect reduction techniques;
- signal spatial and frequency selection techniques;
- redundant and external measurements (long range navigation based on LORAN-C/CHAYKA low frequency radionavigation systems, inertial navigation) processing techniques;
- signal processing technique under high dynamics conditions including spatial rotation;
- fast signal acquisition and reacquisition techniques.

Integrity as the ability of a system to provide timely warnings to the user when the system should not be used is the main system performance characterizing output data reliability.

GNSS integrity monitoring carried out by ground control segment does not meet the strictest requirements. The additional failure detection and exclusion capabilities rely on corresponding user equipment internal and external data processing techniques.

The internal data processing techniques well known as Receiver Autonomous Integrity Monitoring (RAIM) is based on redundant GNSS measurements processing. Depending on the number of redundant measurements RAIM enables to detect and exclude the faulty measurements that are inconsistent to the measurement majority. The consistency checks based on the history of measurements and on the instantaneous processing of the redundant number of satellite signals are discussed in the present report.

External data processing techniques is based on an independent GNSS monitor network and space-based and ground-based transmitters for integrity information broadcasting such as:

- Wide Area Augmentation System (WAAS)
- European Geostationary Navigation Overlay System (EGNOS)
- LORAN-C/CHAYKA network
- Marine Radiobeacon network

These augmentations to the GNSS function are also discussed in the present report.

Internal and external data processing techniques in combination with inertial navigation leads to a correct integrity problem solution in applications with the strictest requirements for integrity level.

A FLEXIBLE GPS TRACKING SYSTEM FOR SUB-ORBITAL AND SPACE VEHICLES

M. Markgraf, O. Montenbruck, S. Leung

DLR, German Space Operations Center, 82230 Wessling, Germany
markus.markgraf@dlr.de, phone: +49 (8153) 28 3513, fax +49 (8153) 28 1450

Abstract

Key words: GPS, navigation, satellite, sounding rocket

This paper describes the development of a GPS based navigation system for the use on highly dynamical platforms, comprising sounding rockets, re-entry vehicles and low earth orbit satellites. The tracking system comprises the GPS receiver itself as well as a mission specific antenna system. So far, the system has successfully been tested during several sounding rocket campaigns and on a small radio amateur satellite. In the near future the first flight onboard a re-entry capsule will be performed. For all three mission types a brief introduction to the employed system is provided. Besides this, a performance valuation based on actual flight results is presented where available.

Introduction

GPS based tracking systems for all kind of vehicles have become increasingly important over the recent years. Even though a major effort has been put into the development of GPS systems for mass market applications, there is still a strong demand for receiver for high dynamic platforms. While a large number of GPS systems for ground based and civilian aeronautic applications can nowadays be purchased at low prices all over the world, commercial-off-the-shelf systems for highly dynamical environment are still rare and costly. Nearly all of these systems are produced in the US and access to those systems is limited due to rigorous export limitations resulting at least in unacceptably long delivery times.

Motivated by these restrictions and the need for GPS based tracking systems within DLR internal projects, the development of an independent GPS system for high dynamics applications has been initiated. A first goal of the project was to build up a receiver system for the use on sounding rockets [1]. The Mobile Rocket Base (MORABA) of DLR's German Space Operation Centre plans, prepares and carries out sounding rocket missions and balloon campaigns in the whole world. Traditionally tracking services for those vehicles are provided utilizing bulky and costly C-band radar equipment. As an alternative, a GPS based tracking system can help to minimize expenses and the maintenance requirements. In 2001, such a system has successfully been flown onboard three sounding rockets (TestMaxus-4, Maxus-4 and Texus-39) launched from Kiruna, Sweden. The results obtained from these flights are presented and discussed to demonstrate the actual receiver performance.

Aside from the use on sounding rockets, a nearly identical system will be flown on an experimental re-entry vehicle IRDT-2 in 2002. The mission serves for the conceptual validation of a download system that has been developed by German and Russian space industry as an alternative for returning small payloads from the International Space Station. The Orion GPS navigation system has been supplemented by a dedicated data handling unit for this mission. Due to differing mission requirements in comparison with the sounding rocket campaigns, a software adaptation to the new constraints became necessary. Aside from a short mission and system description, the results of various signal simulator tests, performed to assess the receivers tracking performance during all mission phases, will be presented.

Aside from ballistic flight trajectories the GPS tracking system can likewise support the navigation of satellites in low Earth orbit. As part of a demonstration project a taylored Orion system has been made available to the US Naval Academy (USNA) for the flight onboard the Pcsat radio amateur satellite. Several additional working payload has been activated and started providing highly accurate navigation data. The paper provides a short system overview as well as an analysis of the so far received tracking data. steps had to be carried out to adapt the hardware to the satellite's environment. PCsat has successfully been launched on 30 September 2001 from Kodiak Island, Alaska. One month after the launch the GPS receiver.

1. Receiver System

Despite obvious differences in the characteristics of the various space applications demanding a GPS tracking system, all missions described in the following share the common problem of host vehicle dynamics and environmental conditions. This suggests the development of a single GPS platform supporting a wide range of different mission types. Traditional GPS systems are mainly designed for usage near the Earth's surface and onboard of relatively slow host vehicles. Furthermore, in accordance to the regulations of the US department of

defcnee (DoD), all GPS receiver built for export purposes must have height and velocity limits implemented, disabling the computation of a navigation solution above these limits. Henee, almost all available commercial systems are unsuitable for use onboard sub-orbital and spaee vehieles. Moreover, signal simulator tests with various GPS reeeiver showed big problems in aequiring new satellites at high velocity, even if continuous traeking at high velocities is possible.

The Mitel Orion receiver has been selected as base for the development of a GPS based tracking system for space applieations, sinee on the onc hand the availability of detailed design information allowed a fast manufaeturing of the required hardware platform in the DLR workshop. On the other hand, a development kit [2] could earlier be obtained from Mitel. The kit included the souree code for a simple ground based application, resulting in an essential simplification of the development of a firmware version ensuring accurate and reliable traeking under a highly dynamical environment. Thc GPS Orion receiver (Fig. 1) makes use of the GP2000 [3] ehipset, which comprises a GP2015 RF down-eonverter, a DW9255 SAW filter, a GP2021 eorrelator and a 32-bit ARM-60B mieroprocessor. Using a single aetive antenna and RF front-end, the reeeiver supports C/A code traeking of up to 12 channels on thc L1 frequency. The main receiver board is supplemented by an interface board, which comprises a power regulator, a backup battery for real-time clock operation and memory retention as well as a TTL-to-RS232 serial interface converter.

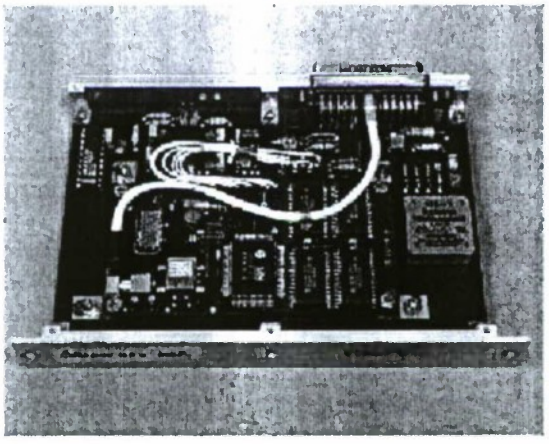

Fig. 1. Orion GPS unit for the Maxus-4 mission

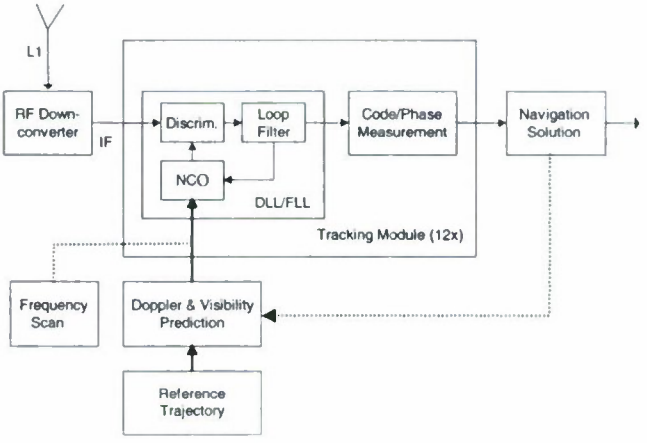

Fig. 2. Doppler and visibility prediction for code and frequency tracking on highly dynamical host vehicles. An open-loop prediction based on the nominal flight path (bold line) replaces the cold start frequency search and the feed back of the receiver's navigation solution (dashed line)

Numerous modifieations have been applied to the standard receiver software in order to adapt the system to the requirements of a use in a spaee mission. Above all, a pronouneed improvement of the aequisition eapability under high dynamics could be aehieved by implementing a novel position-velocity-aiding algorithm, making use of a piece-wise polynomial approximation of the nominal flight path in Cartesian WGS84 eoordinates [4]. To minimize the computational workload of the ARM processor, second-order polynomials in position have been seleeted, which provide a first-order approximation of the sounding rocket velocity.

Up to 15 polynomials ean be eonfigured and stored via a suitably modified eommand interface, whieh is sufficient to provide a position accuracy of about 2 km and a velocity accuracy of roughly 100 m/s. Based on the polynomial approximation of the nominal trajectory, the reference position and velocity of a sounding rocket or a re-entry vehiele in the WGS84 reference frame are eomputed onee per seeond. The result is then used to obtain the line-of-sight velocity and Doppler frequeney shift for eaeh visible satellite, whieh in turn serve as initial values for the steering of the delay and frequency locked loops (Fig. 2). The position-velocity aiding thus assists the reeeiver in a fast aequisition or re-aequisition of the GPS signals and ensures near-continuous tracking throughout the all flight phases.

For satellite applieations, the above deseribed pieee-wise approximation is replaeed by an SGP4 analytieal orbit model for the prediction of the reeeiver's eoarse position and veloeity required for the prediction of visible satellites and the steering of the Doppler seareh [5]. The model is fed by standard two line elements that are for most satellites routinely generated by NORAD and distributed for public use. At the orbiting altitude of LEO satellite, updates of the twoline elements need to be commanded at intervals of about one to two weeks, which provides an only minor effort for the ground operations.

Further modifieations eomprise correetions to software limits for altitude and velocity, an extension of the Doppler computation to properly aeeount for the reeeiver veloeity and a replaeement for the kinematie position

and velocity determination. By default the least-squares estimation of the host vehicles state vector is carried out in spherical coordinates to support the implementation of an altitude hold-mode in case of lacking GPS satellite visibility. Since the frame rotation of the co-moving North-East-Up system is not properly accounted for in the original firmware, the velocity estimation exhibits a severe degradation in case of fast moving host vehicles. This is particularly notable for near-polar trajectories and high ground velocities. As a remedy, a traditional, Cartesian formulation has been implemented, which does not support fixed-altitude operation but provides accurate navigation solutions (WGS84 position and velocity) even for ballistic trajectories and orbiting spacecraft.

Besides, several hardware modifications have been performed, mainly concerning the interface module, to adapt the system to the particular requirements of each envisaged mission. A short description of these mission specific modifications can be found in the following chapters. Likewise, specific antenna concept has been developed for each application. Since the antenna has to be considered as the "eye" of the GPS sensor, the importance of the antenna subsystem as an integral part of each GPS unit and therewith the influence on the performance of the entire system may not be neglected. In particular notable effort has been put into the design of a sophisticated antenna concept for sounding rocket missions. A brief introduction to the various, mission specific antenna systems is provided within each corresponding chapters.

2. Sounding Rockets

The first assessment of the modified GPS Orion system in a real mission has been performed during three sounding rocket flights, conducted in 2001. All missions have been carried out from the European rocket range Esrange near Kiruna, Sweden. The qualification flights were performed on an Improved Orion rocket (Test Maxus-4 campaign [6]), a Castor-4B rocket (Maxus-4), and a dual stage Goldfinch/Raven rocket (Texus-39)). The results obtained throughout the three flights convincingly demonstrated the great benefit of the soft- and hardware modifications applied to the Orion receiver regarding the tracking and acquisition capability under high dynamic. In all missions the receiver kept lock throughout the entire flight except during outages caused by an intentional switching of GPS antennas. Re-acquisition times after interrupts amounted to at most five seconds. The number of tracked GPS satellites was sufficient for a stable and continuous determination of a 3-D navigation solution. As a representative example for all test flights, the Test Maxus-4 mission will be presented in more detail with a discussion of the achieved results.

2.1 Test Maxus-4 Campaign

The first flight valuation of the GPS Orion receiver was performed on 19 February 2001 during the test flight of an Improved Orion rocket in Kiruna. The primary mission goal consisted in the validation of existing range safety facilities (radar and one-way slant-range system) prior to the Maxus-4 campaign.

The Test Maxus-4 rocket was powered by a single stage Improved Orion motor (*note*: by accident the rocket motor and the GPS receiver shared the same name). During the 24s boost phase, the rocket built up a spin rate of 3.8 Hz along the longitudinal axis. Accordingly, the rocket maintained a constant and stable attitude with a near zenith-facing tip. During the first 6s boost phase a maximum acceleration of 18g was reached, followed by a sustenance phase of 1g and 5g. After burnout a maximum rate of climb of 1100 m/s and a speed over ground of 280 m/s were measured. The rocket reached the apogee 2 minutes and 17 seconds after lift-off at an altitude of 81 km. Briefly thereafter the spin was removed by a yo-yo system and the top cone as well as the motor have been separated (Fig. 3). The service and recovery module started a tumbling motion from about h=40 km downwards. Between 25 and 15 km altitude the module decelerated to sub-sonic speed before parachute deployment at h=5 km. The payload and nose cone landed at a distance of 60 km from the range and were finally recovered by helicopter.

The Orion receiver was placed inside a DLR/MORABA provided service module, which housed a data handling unit and telemetry system. To support the different mission phases and to assess the suitability of different antenna concepts, the rocket was equipped with the multi-antenna system illustrated in Fig. 4 [7]. A helical antenna mounted in the tip of the rocket cone provides a near hemispherical coverage during the ascent trajectory. After separation of the cone, an R/F switch connects the GPS receiver to a pair of antennas mounted opposite to each other at the walls of the service module and combined via a power divider. This results in a near omni-directional coverage and can thus be applied even in case of a tumbling motion of the module. Compared to wrap-around antennas that are otherwise used for GPS tracking of launchers, a blade antenna system can be manufactured at less than 10% of the overall system cost and does not require special milling of the sounding rocket structure for mounting. Finally, a separate antenna was mounted on the arm of the launch pad and connected to the receiver through a supplementary R/F switch prior to lift-off. Thus the receiver could be properly initialized and acquire all visible GPS satellites prior to launch.

In addition to the ORION receiver, an Ashtech G12 HDMA receiver and a BAE (Canadian Marconi) Allstar receiver, both connected to a wrap-around antenna, have been flown on the same rocket as part of an

independent experiment provided by the Goddard Space Flight Center. This allowed an in-depth verification and trade-off of different receiver and antenna concepts.

Analysis of the Orion GPS data recorded during the Test Maxus-4 campaign shows that the receiver and the

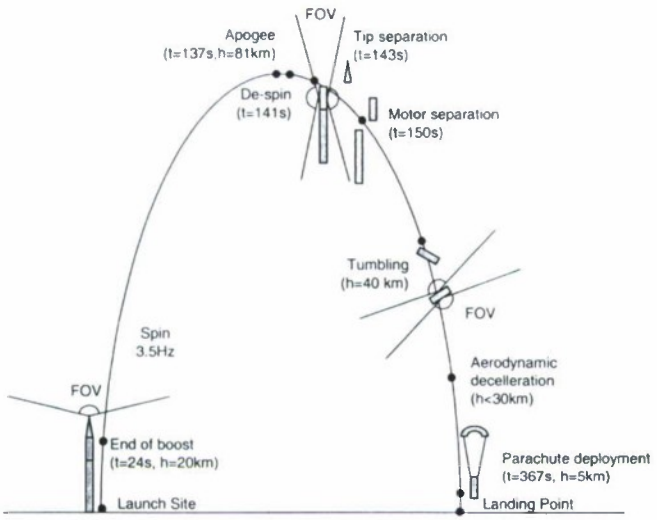

Fig. 3. Test Maxus-4 mission profile

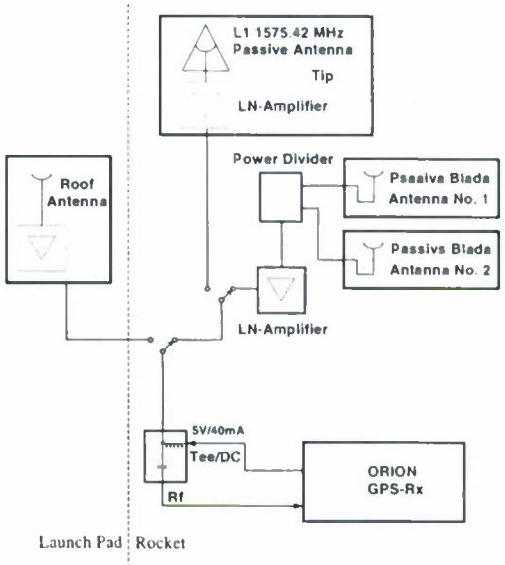

Fig. 4. Schematic view of the GPS antenna system

antenna system worked well during the entire flight. The receiver has continuously been in 3D-navigation mode from payload activation on the launch pad (20 minutes before lift off) to the time when DLR telemetry lost contact near landing. Typically, the receiver had 10 to 11 GPS satellites in lock. Only during the first few seconds of the boost phase and during the reentry into the atmosphere a loss of some satellites can be observed (Fig. 5). Continuous tracking was even available near apogee, where short outages had to be expected due to the antenna switching at this time. Likewise, the tracking behavior during atmospheric reentry was expected to be critical due to the uncontrolled tumbling motion of the payload and the pronounced sensitivity gaps in the antenna diagram described above. While the performed ground tests indicated a moderate robustness in case of single axis rotation, the actual body motion and system performance during reentry could neither be simulated nor tested on ground prior to the mission.

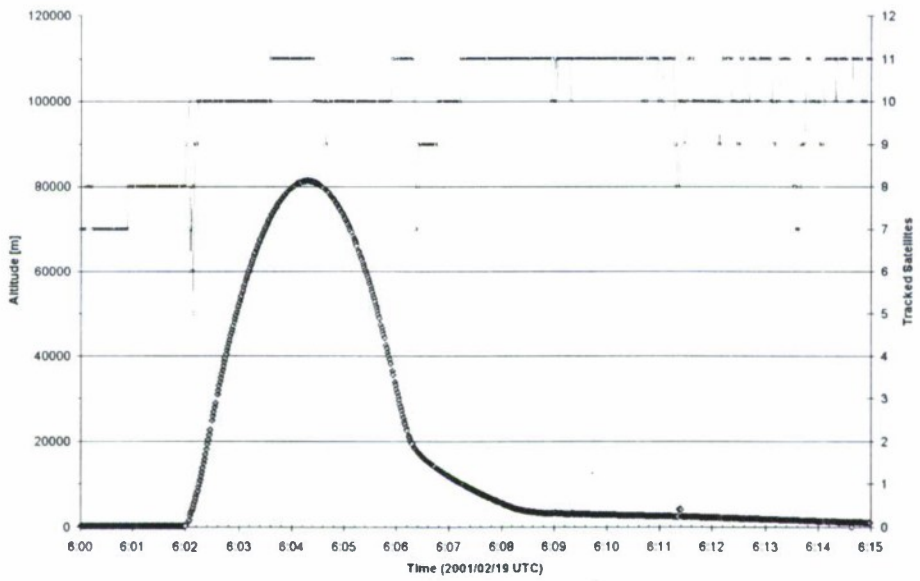

Fig. 5. History of the number of tracked satellites (solid line) and rocket altitude during the mission (diamonds)

Since GPS is usually more accurate than ground based radar tracking, its absolute accuracy is difficult to prove if only one GPS receiver is flying on a sounding rocket. As mentioned above, in the case of the Test Maxus-4 flight three different and independent GPS receivers were providing data. This gave the unique chance to make a detailed analysis of the accuracy of the obtained GPS solutions. Likewise it was a good opportunity to find out the pro and cons of each individual sounding rocket tracking systems. The Ashtech G12 HDMA flown by NASA in combination with a commercial wrap-around antenna can be considered as a reference in performance and accuracy for the other systems, since from a technical point of view it is the most advanced and best evaluated GPS receiver for the use on highly accelerated vehicles.

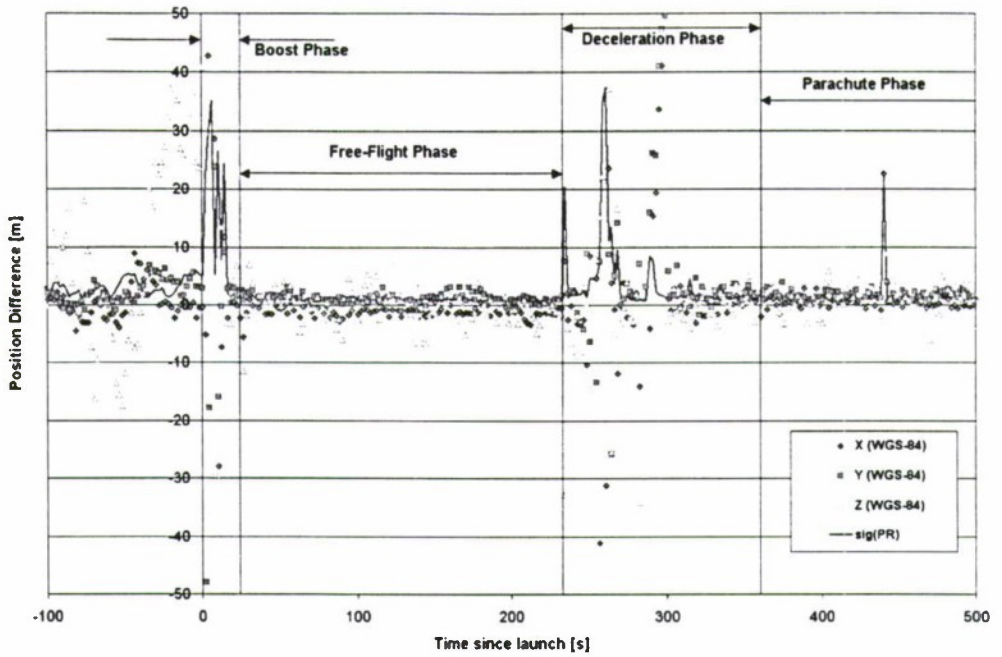

Fig. 6. Difference between the Ashtech G12 and the Orion position solution.

The differences between the Ashtech G12 on-board computed single point solution and the unfiltered Orion single point solution recorded during the TestMaxus-4 flight is illustrated in Fig. 6. In addition the r.m.s. values for the total position difference are given in Table 1, for the different flight phases.

Table 1 R.M.S. values for the difference between Ashtech G12 and Orion position solution

#	Time / UTC From	To	R.M.S [m]	Remarks
1	6:00:00	6:01:59	0.9	Before lift-off
2	6:02:00	6:02:24	90.0	Boost phase
3	6:02:27	6:05:52	1.5	Free-flight phase
4	6:05:55	6:06:44	29.0	Re-entry (h=39..14km)
5	6:07:00	6:09:19	3.4	Descent (h=12..2km)

During the periods of good tracking the GPS solutions obtained from the two receivers match each other to better than 6.5 meters, which is well in accord with the expected overall accuracy of a GPS tracking system. The large perturbations after lift-off and during the re-entry phase can be attributed to frequency variations of the reference oscillator as well as a temporary loss of satellites during the descent. Furthermore, deficiency the receiver tracking loops has been identified, which contributes to the degradation of the obtained navigation solution. A further verification flight with a modified receiver software and a better suited quartz oscillator is planned for September, 2002.

3. Re-entry Experiment

Under contract of ESA and the European Community the German Astrium GmbH is presently preparing the second test flight (Inflatable Rentry and Descent Technology IRDT-2) for the demonstration of a novel reentry technology making use of an inflatable aerobraking shield [8]. The project conducted jointly with the Babakin Space Center, Moscow, aims at the development of a download system for the International Space Station, which is able to return small payloads to the ground independent of the US Space Shuttle. IRDT makes use of technologies originally developed within the Russian Mars program and differs from common recovery systems for reentry capsules or sounding rockets. Instead of a parachute an inflatable heat shield is employed to decelerate the capsule and land it safely on ground.

The launch has originally been scheduled for 2001 but had to be postponed to the year 2002 due to a failure in the electronic of the sensor module found during the final check-out at the launch site in Severomorsk. Presently, the IRDT-2 capsule is planned to be launched in the last week of May 2002 by a Volna rocket from a Kalmar type submarine in the Baltic sea north of Murmansk and injected into a ballistic trajectory passing across the arctic sea and northern Siberia (Fig. 7). Following deployment of the first shield, the capsule reaches the rentry point at a 100 km altitude and a velocity of roughly 7 km/s. Here, a second shield is deployed which introduces a steep descent of the capsule. The actual landing takes place on the Kamshatka peninsula within 25 min after separation.

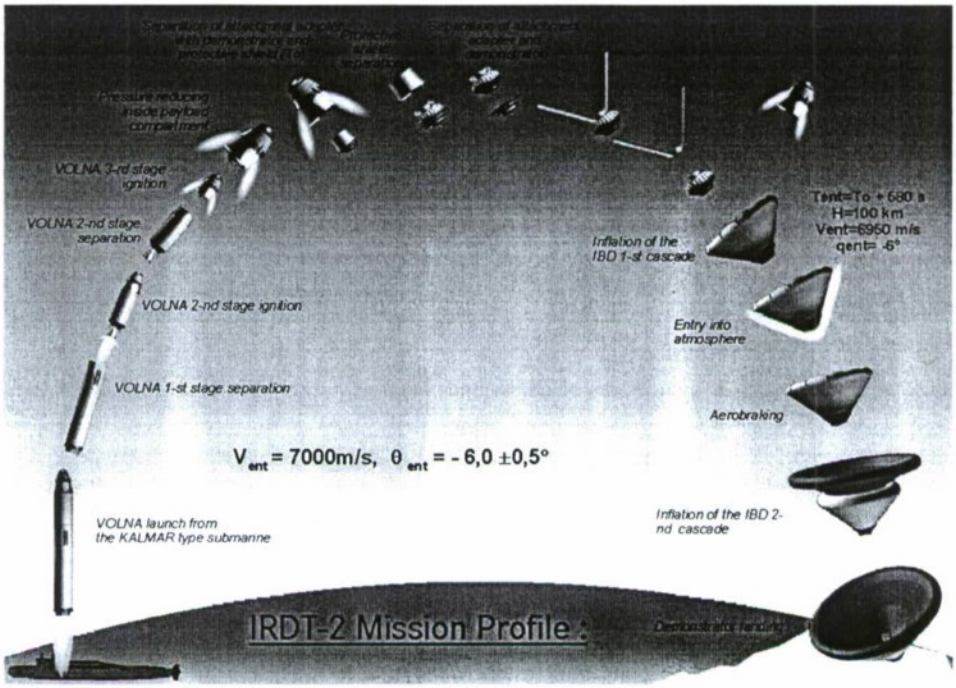

Fig. 7. IRDT-2 mission profile

As part of the IRDT-2 payload, a DLR/GSOC provided Orion GPS receiver system will be flown and the resulting navigation data will complement other sensors and experiments in the post mission analysis [9]. Within the IRDT flight unit, the main receiver board is supplemented by a tailor-made interface unit, which comprises basic support functions (power regulator, backup battery and serial interface converters) as well as a dedicated data handling system (Fig. 8). It provides a separate micro-controller and an EPROM memory, which are used to store GPS navigation data during the flight of the IRDT-2 capsule for read-out after landing. The available storage volume of 900 kByte is sufficient to hold 2 Hz samples of position and velocity as well as raw data (pseudoranges, pseudorange rates) and status information at a reduced data rate. Thus a dynamical post mission adjustment of the reentry trajectory is even possible in case of limited tracking conditions with less than 4 satellites in lock. The receiver and interface board measure 95 x 50 mm each and are stacked on top of each other inside the housing shown in Fig. 9. The power consumption of the complete GPS unit amounts to roughly 3W. Even though the mission scenario resembles a sounding rocket flight at first sight, it involves a much higher maximum speed and critical differences in the receiver initialization. In a sounding rocket campaign the receiver is switched on several minutes prior to lift-off, which allows a proper initialization of the system at the launch pad. In contrast to this, the activation of the GPS system onboard the re-entry capsule takes place shortly after

separation when the vehicle has reached its maximum speed. Furthermore, the exact launch time and thus the receiver boot time is not known in advance. Due to these facts, a slightly different initialization procedure had to be implemented in the receiver software. Prior to the final integration the receiver will be briefly activated and connected to an outside antenna.

This allows the receiver to synchronize itself to the current time and to receive a recent almanac of the GPS constellation. Following the subsequent power-down the correlator's internal real-time clock is kept alive by a backup battery. Likewise, relevant auxiliary data like the almanac and the IRDT reference trajectory are stored in a non-volatile part of the memory. Using the above information, the absolute time is available to the receiver at start-up with an accuracy of a few seconds, which in turn allows the prediction of the GPS satellite constellation. Likewise the time since boot (i.e. the time since separation) is available within the receiver, which is required to read-out the nominal trajectory. In this way the receiver is both able to predict its approximate position and velocity as well as the position and velocity of the GPS satellites. Using these data the channel allocation and the Doppler offset for the signal acquisition are determined. This allows a full warm start of the receiver irrespective of the actual launch date and time of the mission. Based on corresponding signal simulator tests, it is expected that position, and velocity measurements are available within a minute after activation, provided that the tumbling of the capsule after separation does not impose major restrictions to the GPS satellite visibility.

Using a GPS signal simulator, different hardware-in-the-loop simulations were carried out to validate the receiver design and operations concept. The simulation scenario was configured to start at separation of the

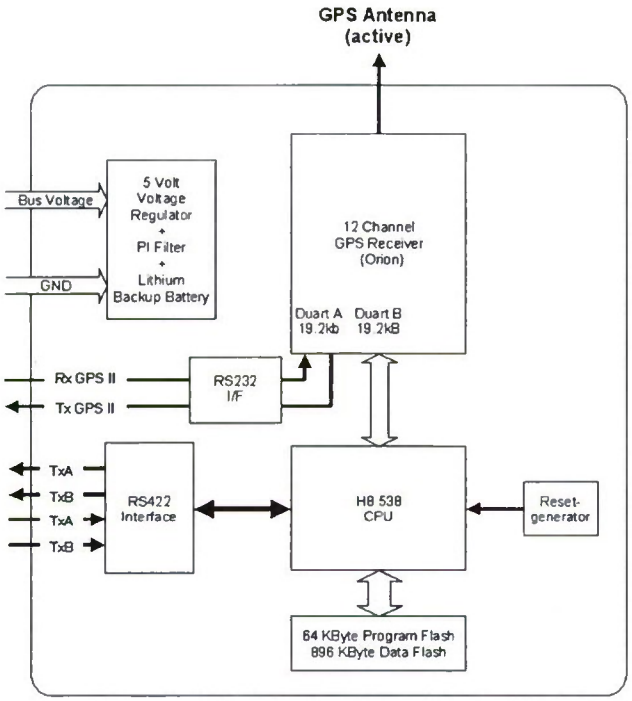

Fig. 8. Schematic view of the IRDT GPS system.

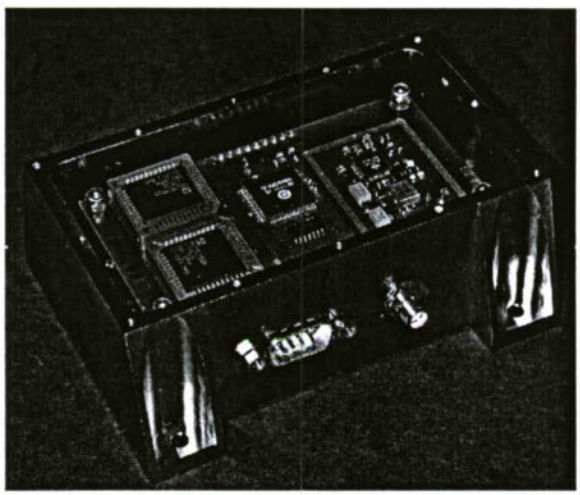

Fig. 9. IRDT-2 GPS flight unit.

IRDT capsule from the upper stage and continue up to the time of landing. In accord with the operations concept described above, the IRDT GPS receiver had to be switched on simultaneously with the start of the simulator and it had to be ensured that the time propagated by the battery buffered real-time clock matched the simulated separation epoch.

An initial test that matched these requirements to within about a second provided an overall conceptual verification of the receiver design and showed that the receiver is nominally able to perform a warm start under the given conditions. Within 15 s, the receiver achieved frame lock for eight satellites but was still unable to produce a navigation solution due to the lack of suitable broadcast ephemeris parameters. At 37 s after the boot, 3D navigation was obtained with 7 satellites in use. Since then the receiver provided uninterrupted tracking troughout the free-flight phase and atmospheric reentry down to the landing point.

Additionally, an off-nominal test has been performed, simulating a complete loss of real-time clock and non-volatile memory as a consequence of a battery failure. In addition an offset of roughly 11 s was introduced between the simulator start and the receiver boot. As a result the receiver started with a default date (2000/07/30) and an 80 km position offset, but was nevertheless able to acquire a first satellite after 23 s and adjust its clock to the scenario time. Using the hardcoded almanac and reference trajectory, the receiver started searching for other visible GPS satellites in highest elevation mode and achieved 3D navigation within about 2 minutes.

4. Satellite Application

While space borne GPS receivers can in general be considered as a well established tracking tool for low Earth orbit (LEO) satellites, their use on miero- or nano-satellites poses multiple problems from a systems engineering point of view. Representative examples include the mass budget, the lack of a suitable attitude stabilization, antenna allocation problems, restricted command and telemetry links as well as limited onboard power resources. The recent flight of a DLR built GPS system onboard the PCsat Prototype Communications satellite (Fig. 10) provides an illustrative example of GPS operations on a 25 kg class of micro-satellites.

Fig. 10. The Prototype Communication Satellite (PCSat) built by the US Naval Academy

The Prototype Communication satellite PCsat has been designed and built by midshipmen of the US Naval Academy (USNA), Annapolis. It serves as a space borne extension of the terrestrial Amateur Radio Automatic Position Reporting System (APRS), which allows the distribution of position/status reports and short messages using handheld or mobile radios. PCsat is a cubic satellite of 10" (25 cm)size. Solar cells on five faces of the spacecraft provide a typical power of 7 W in full Sun, which is buffered in a set of 12 NiCd cells to allow operations during eclipses (with minimum GPS receiver activities). The minimum power consumption amounts to 3 W when sending only safe mode beacon messages, thus leaving a best case value of 4 W for thermal control, digipeating, and experiment operations. PCsat has been launched on an Athena 1 rocket on 30 September 2001 from Kodiak Island, Alaska. It orbits the Earth at an altitude of 800 km and an inclination of 67° with respect to the equator. US and European radio amateurs can access the satellite for up to six passes of 10-15 min each per day.

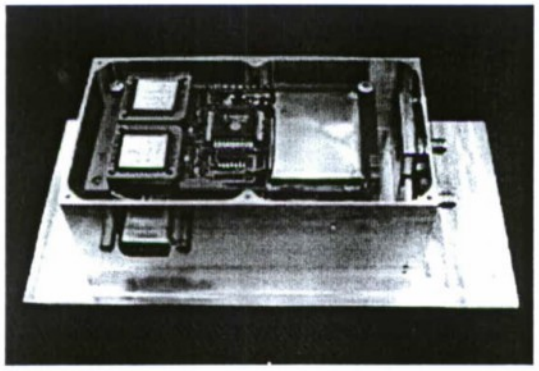

Fig. 11 PCsat GPS Orion flight unit

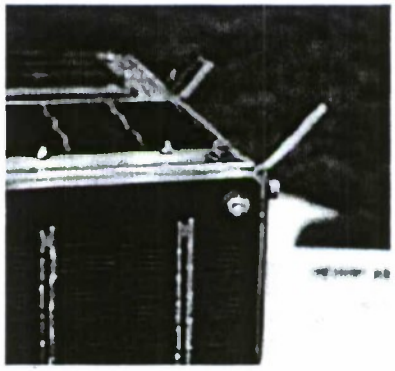

Fig. 12 Monopole antenna ($\lambda/4$) for GPS reception

While the main purpose of PCsat consists in the relaying of APRS communication messages, it also carries an experimental Orion GPS receiver provided by DLR/GSOC (Fig. 11). Prior to the integration into the satellite, the position-velocity-aiding concept for LEO satellites has extensively been tested in a signal simulator environment. These tests have demonstrated that the receiver is able to perform hot starts with a typical time to first fix of better than 20s under adequate GPS visibility conditions. During the actual mission, where the output

sampling interval was reduced to 30-60 s, the receiver was found to be back on track within 60 s after various power cyclings due to temporary battery shortages. In case of extended off times that exceeded the validity of broadcast ephemeris parameters stored in non-volatile memory, representative times-to-first fix of 3 minutes were observed during the actual mission.

Compared to terrestrial or big LEO applications, the signal acquisition onboard PCsat is seriously hampered by the use of a low gain antenna and the uncontrolled attitude of the spacecraft. Due to lacking surface area for the accommodation of a standard antenna patch, a quarter-wavelength monopole mounted in the corner of the cubic spacecraft structure is used instead (Fig. 12). It provides a roughly toroidal antenna diagram with a sensitivity dip in the boresight direction, but allows tracking down to negative elevations with respect to the antenna equator. Other than a patch or helical antenna, the monopole is linearly polarized and does not provide a proper impedance matching. As a result of the sub-optimal antenna system, signal-to-noise ratios are, on average, 4-5 dB less than observed otherwise with the same receiver.

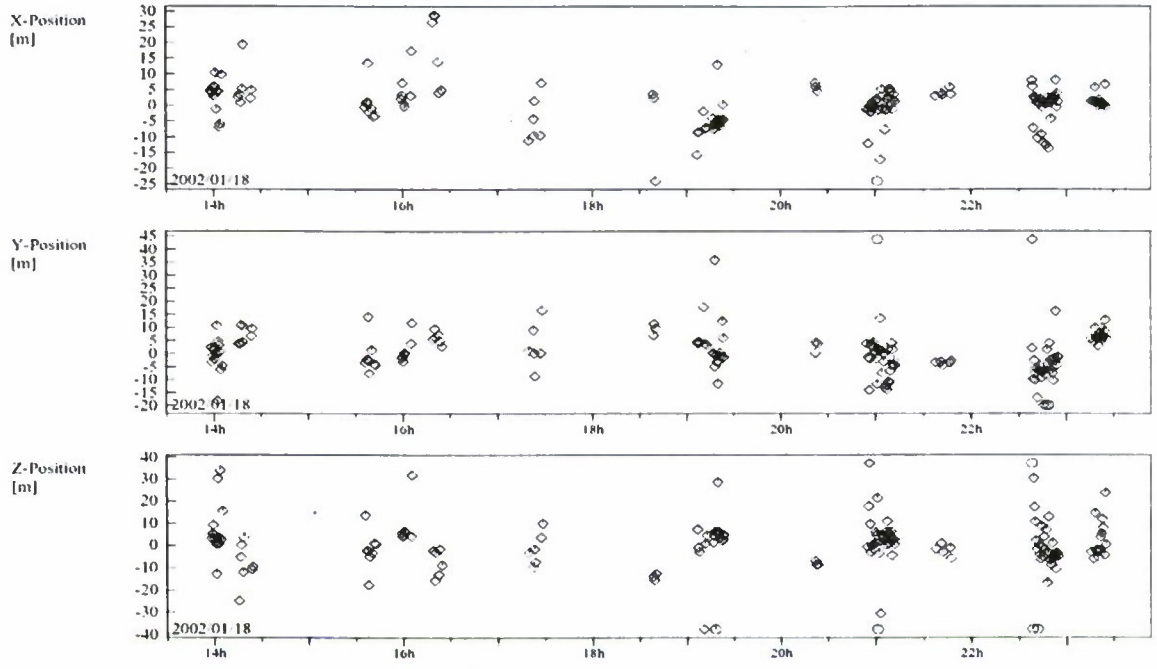

Fig. 13 Position residual plot (from single point code range solutions) for a 12 hour data arc recorded in mid-January, 2002

A near continuous activation of the GPS receiver became possible in mid-January, when PCsat was in a full-Sun orbit for about on week. NMEA type GPGGA position message as well as state vectors, raw measurements (pseudorange and Doppler), and channel status data were collected by a worldwide net of radio amateurs. Batch filtering of the GPS position data in a dynamical orbit determination system indicates an 3-D r.m.s. accuracy of 15 m (Fig. 13). This is slightly worse than observed in other missions but can be understood by the large fraction of low (including negative) elevation pseudoranges that are affected by media effects (ionospheric path delay) and tracking errors near signal acquisition.

5. Summary and Outlook

Starting from a prototype design of a terrestrial receiver, a GPS tracking system for high dynamics applications has been developed. A preliminary qualification of the Orion GPS receiver has been performed in various test flights onboard sounding rockets and a small low Earth satellite. A first flight on a re-entry capsule is planned in the summer of 2002. Compared to commercial receivers, the in-house developments offers a notably improved flexibility and a reduced time to mission. Aside from sounding rocket missions benefiting from a robust tracking under high dynamics, the receiver is also well suited for small satellite missions in view of its small size and power requirements. New applications under study include the onboard computation of the expected impact point of a sounding rocket to improve range-safety operations at the launch site [10] and the precision relative navigation of spacecraft in close proximity [11].

Acknowledgment

The authors are grateful to all individuals and institutions that have supported the development and qualification of the Orion receiver. We'd like to thank Kayser-Threde GmbH for providing access to a GPS signal simulator and enabling the flight tests onboard the Texus and Maxus missions. The IRDT-2 flight experiment would not have been possible without the active support of ASTRIUM and Vectronic Aerospace GmbH. Finally, our special thanks are due to Bob Bruninga and the United States Naval Academy for their contribution to the successful performance of the PCsat GPS experiment.

References

1. **Markgraf M., Montenbruck O., Hassenpflug F., Turner P., Bull B.,**; *A Low Cost GPS System for Real-time Tracking of Sounding Rockets*; 15th Symposium on European Rocket and Balloon Programmes and Related Research, Biarritz, 28 May - 1 June 2001.
2. **Mitel Semiconductor**; *GPS Architect 12 Channel GPS Development System*; DS4605 Issue 2.5; March 1997.
3. **Mitel Semiconductor;** *GP2000 GPS Receiver Hardware Design*; AN4855 Issue 1.4, Feb. 1999.
4. **Montenbruck O., Enderle W., Schesny M., Gabosch V., Ricken S., Turner P.**; *Position-Velocity Aiding of a Mitel ORION Receiver for Sounding-Rocket Tracking*; C5-5; ION GPS 2000 Conference, Salt Lake City, 19-22 Sept. 2000.
5. **Leung S., Montenbruck O., Bruninger B.**; *Hot Start of GPS Receivers for LEO Microsatellites;* 1st ESA Workshop on Satellite Navigation User Equipment Technologies NAVITEC'2001, ESTEC Noordwijk, 10-12 Dec. 2001.
6. **Bull. B., Diehl J., Montenbruck O., Markgraf M.**; *Flight Performance Valuation of three GPS receivers for Sounding Rocket Tracking;* ION National Technical Meeting, San Diego California, 28-30 Jan. 2002.
7. **Markgraf M., Montenbruck O., Hassenpflug F.**; *A Flexible GPS Antenna Concept for Sounding Rockets*; DLR-GSOC TN 01-04; Deutsches Zentrum für Luft- und Raumfahrt, Oberpfaffenhofen, 2001.
8. **Wilde D., Walther S., Steckling M., Pitchadze K., Serdjuk V.**; Inflatable Reentry and Descent Technology (IRDT); 15th International Symposium on Spaceflight Dynamics, Biarritz , 26-30 June 2000.
9. **Montenbruck O., Gill E., Markgraf M., Schule R., Wilde D.**; *GPS Tracking of the IRDT-2 Re-entry Capsule;* 16th International Symposium on Space Flight Dynamics, Pasadena, 3-7 Dec. 2001.
10. **Montenbruck O., Markgraf M., Jung W., Bull B., Engler W.**; *GPS Based Prediction of the Instantaneous Impact Point for Sounding Rockets*; in press: Aerospace Science and Technology, 2002.
11. **Montenbruck O., Ebinuma T., Lightsey E.G., Leung S.**; *A Real-Time Kinematic GPS Sensor for Spacecraft Relative Navigation*; submitted to: Aerospace Science and Technology, 2002.

THE ACCURACY OF DGPS SYSTEM IN THE AREA OF ZALEW SZCZECIŃSKI*

Dołgopolow*, Z. Kozłowski, M. Kaczmarek***, T. Turczyn****,**
Maritime Office, Plac Batorego 4, 70-207 Szczecin, Poland
A. Wolski***
(2) Maritime University of Szczecin, Wały Chrobrego 1-2, 70-500 Szczecin, Poland

Abstract

Key words: navigation, accuracy

The safety of navigation, hydrographic survey and water engineering work requires constant accurate positioning of the craft. The area of Zalew Szczeciński is covered by the radionavigational system located at the Dziwnów station.

In spring 2001 the transmitting aerial of the station was modernized to improve transmission conditions. In summer 2001 the levels of signal strength (SS) and the signal to noise ratio (S/N) were examined in order to evaluate the effectiveness of the modernization.

The research was carried out in summer 2001 with the use of two Leica receivers:

- GPS MX 9400N receiver,
- MX 52R corrections receiver.

The reception aerials of the two receivers were installed at the elevation of 4 metres above the water level. The CDU 5.10 program was used for recording data, whilst the information was entered through a port enabling raw data logging. The research method was the same as applied during routine sounding, i.e. the vessel proceeded along north-south and east-west profiles at 2.5 km intervals (Fig. 1).

:

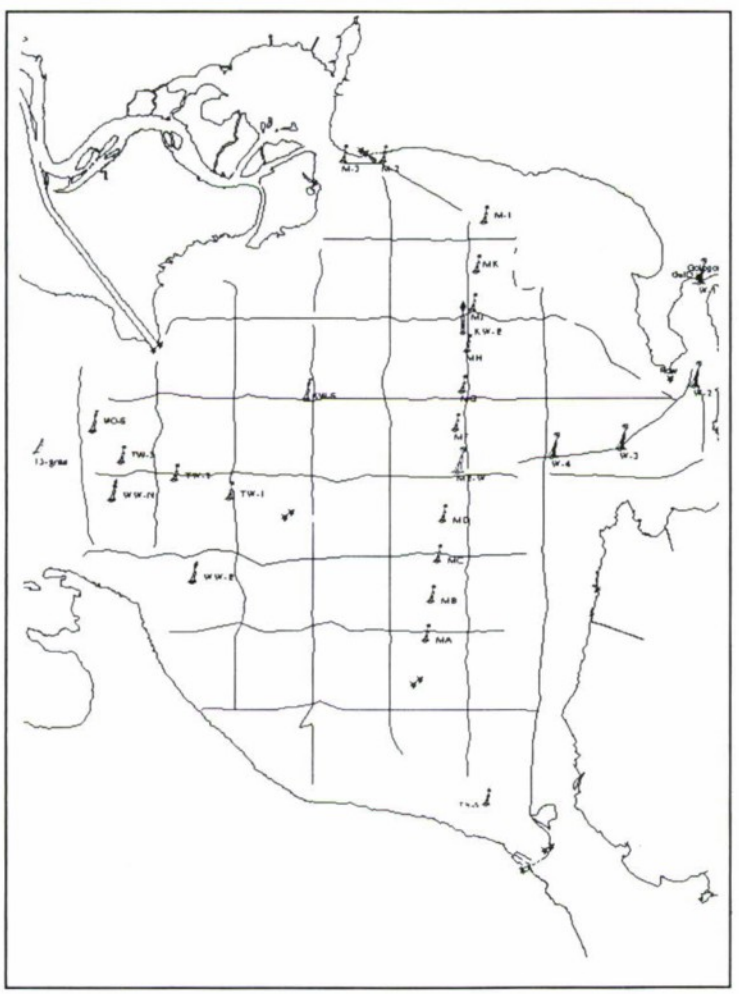

Fig. 1. Tracks of the survey ship during measurement

* Researchers of Maritime Office.
** Researchers of Maritime Office.
*** Researchers of Maritime Office.
**** Researchers of Maritime Office.
***** Ass.Prof. (docent).

Fig. 2. Zalew Szczeciński. Signal strength (SS) [dB/μV] Fig. 3. Zalew Szczeciński. Signal to noise ratio (S/N) [dB]

The measurement results were recorded every minute by using the data line no 799, recording φ, λ, SS and S/N. The research vessel moved at the average speed of 7 knots, that is the distance between readout was 215 m.

Gathered data were processed, then maps with measurement profiles in the 1:5000 scale were done, including the values of SS (Fig. 2) and S/N (Fig. 3). Both maps were plotted for the co-ordinate system WGS 84 UTM – zone 33 with basic navigational marks.

According to the manufacturer, the receivers used in the research work in the DGPS mode if the signal strength is not less than:

$$SS = 9\ dB/\mu V,$$
$$S/N = 6\ dB$$

The reference receiver of the Dziwnów station located 40 metres away from the transmitting aerial shows maximum values that are, respectively, SS = 99 dB/μV and S/N = 25dB.

The minimum values observed in the area of Zalew Szczeciński were as follows: SS = 44 dB/μV and S/N = 13 dB. The respective maximum values equalled 52 dB/μV and 13 dB. The values of SS and S/N were not found to drop below the minimum admissible values. Records of minimum and maximum SS and S/N values in the Zalew Szczeciński area can be summarised as follows:

- the minimum values, found in the western part of Zalew Szczeciński. The level of these values, however, is good and equal to at least: SS – 44 dB/μV and S/N = 13 dB;
- in the area of greatest traffic intensity, where measurements are performed most frequently, i.e. within the Świnoujscie-Szczecin fairway, the level of signals reached, respectively: SS – 46 to 48 dB/μV and S/N = 13 dB;
- the maximum values of SS and S/N occurred in the northeast part of the examined area;
- no sudden disappearance or oscillation of the signal have been found in the whole examined area of Zalew Szczeciński.

The research results lead to a conclusion that over the entire Zalew Szczeciński area the level of corrections signals transmitted by the Dziwnów station is at least good. A range of hills between the location of the aerial and Zalew Szczeciński only slightly affects the levels of SS and S/N.

The results of research have justified the changes in aerial parameters and aerial field. It has been found that the power and stability of GPS corrections signal have been improved.

References

1. **Dolgopolow A., Wolski A.,** 1997, "Radionavigational DGPS System for the Safety Navigation in West Pomerania", Reports on Geodesy, IG&GA WUT, No. 3(26), Warsaw.
2. **Dolgopolow A., Wolski A.,** 1998, "Application of DGPS System for Surveys of Hydrotechnical Objects", Reports on Geodesy, IG&GA WUT, No. 9(39), Warsaw.
3. **Dolgopolow A., Wolski A.,** 1999, "Accuracy of radionavigational DGPS system in Zalew Szczeciński", Reports on Geodesy, IG&GA WUT, No. 4(45), Warsaw.
4. **Dolgopolow A., Kozlowski Z., Kaczmarek M., Turczyn T., Wolski A.,** 2001, "An examination of the DGPS system capabilities in Zalew Szczeciński", Reports on Geodesy, IG&GA WUT, No. 2(57), Warsaw.

SOLUTION OF PHASE AMBIGUITY IN ONE-BASE INTERFEROMETER*

Yu. L. Fateev*

Krasnoyarsk State Technical University
26, Kirenskogo St., 660074, Krasnoyarsk, Russia. E-mail: chmyh@ns.kgtu.runnet.ru

Abstract

In the report the algoritlun of a solution of phase ambiguity for an one-base interferometer which is included in a structure angular of the satellite navigational equipment ГЛОНАСС/GPS is analysed. The solution is selected on a criterion of a maximum probability. The cumulative distribution function of errors, probability of skip of a right solution and gross errors, and also choice of an optimum threshold level for a various structure of constellations of navigational space vehicles and various level of noise of measurements is analysed. The potential possibilities of algorithm of a solution of phase ambiguity, in particular, maximum admissible measurement error of phase shifts are determined, and also maximum length of basis of an interferometer at specific noise of measurements, at which the work of algorithm is possible.

Now large interest is represented by equipment of customers of navigational satellite systems ГЛОНАСС and GPS, which measure space orientation of plants. To a measurement of space orientation in quality by an antenna of a system are applied one and two-base interferometers. The equation of an one-base interferometer, with the help of which is determined it orientation has an aspect

$$k_{xi}X + k_{yi}Y + k_{zi}Z = \frac{\lambda_i}{B}\frac{\Phi_i}{2\pi},$$

where *kx, y, zi* – direction cosines of a vector – direction on a navigational satellite (NS), *X, Y, Z* – direction cosines of a vector – basis, $i = 1,2, \ldots N$ – serial number observed NS, λ_i – wavelength of signals NS, *B* – length of basis, Φ_i – measured phase shift between antennas.

At angular measurements the serious problem is made by a solution of ambiguity of a measurement of a phase shift, as length of basis In much exceeds a wavelength l signals NS. One from modes of a solution of phase ambiguity is the method of a maximum probability, in which the redundancy of constellation NS is used.

At angular measurements the serious problem is made by with a solution of ambiguity of a measurement of a phase shift, as length of basis In much exceeds a wavelength l signals NS. One from methods of a solution of phase ambiguity is the method of a maximum probability, in which the redundancy of constellation NS is used.

The purpose of researches is the definitions of potential possibilities of algorithm of a solution of phase ambiguity at one-time measurements, in particular, maximum admissible measurement error of phase shifts, and also maximum length of basis of an interferometer at specific noise of measurements, at which the work of algorithm is possible.

The researches were carried out by a method of the analysis of function of a probability. It is possible to set an angular position of a vector – basis by two parameters, therefore function of a probability will be two-dimensional. At a solution of phase ambiguity the special interest represents probability of gross errors, i.e. cases, at which the phase ambiguity is determined with errors. The gross errors arise then, when the function of a probability has accessory maximums, which magnitude is commensurable with magnitude of a basic maximum appropriate to a valid solution. Such situation is characterised by Fig.1, where the function of a probability for one NS is reduced. From Figure follows, that the solution of phase ambiguity at a measurement on one basis on everyone NS is impossible, as the function of a probability accepts extreme, besides greatest possible values, in the whole areas.

At magnification of number observable NS the log of function of a probability represents a weighed sum of quadrates of discrepancies on all NS. The discrepancies on everyone NS represent wavy function, which extremes in space *K, q* draw closed curves. The summarised discrepancy represents a sum of wavy functions and grows out interference's of these functions. On Fig. 2 the function of a probability is reduced at four observable NS. Here basic and accessory maximums precisely differ.

*PhD, Research assistant.

Fig. 1. The graph of function of a probability at a measurement of signals one NS

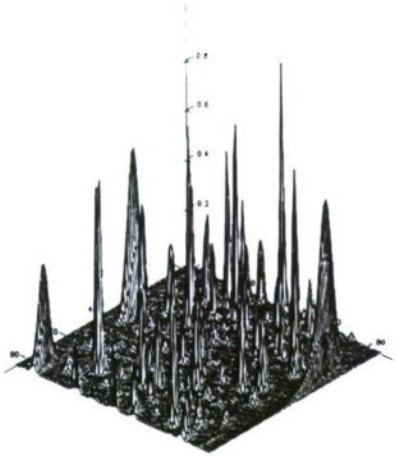

Fig. 2. The graph of function of a probability at a measurement of signals four NS

The function of a probability is rather complicated for the analysis, therefore there is a necessity of introduction of one parameter, on which it is possible to estimate probability of skip of a right solution and probability of gross errors, i.e. acceptance of a false solution. For such parameter can be a summarised discrepancy equal to a sum of quadrates of discrepancies on all NS, or radical square of this magnitude.

Discrepancies have two component: one from them is stipulated by discrepancies in accessory maximums at the expense of acceptance of a false solution, and another – at the expense of a variance of the measured phase shifts. At the analysis noise component measurements of phase shifts on reliability of a method of a solution of phase ambiguity we shall consider discrepancies originating in accessory maximums at a lack of noise of a measurement as expectation of discrepancies, and discrepancies – distributed on the normal law.

If the expectations of magnitudes x_i are equal to zero, and their variances are equal, the magnitude $\chi^2 = x_1^2 + x_2^2 + \ldots + x_n^2$ is distributed under the law χ^2 with n by degree of freedoms. It has a place in a principal maximum of function of a probability at uniformly precise measurements of phase shifts. In accessory maximums of expectations are not equal to zero, and in a classical aspect the law of distribution χ^2 cannot be applied. Unfortunately, at presence of expectations the cumulative distribution function of a summarised discrepancy does not express in elementary and special functions, expression in the integrated form for a probability density and integrated cumulative distribution function however was obtained which can be used for calculations.

On an integrated cumulative distribution function it is possible to define threshold values, at which the right solution hits in the list of possible solutions with specific probability, by accepting $m = 0$.

Component discrepancies at the expense of an incorrect solution of phase ambiguity is determined magnitude, it can be calculated is a priori for each combination of phase ambiguities. Obviously, the concrete values by this component depend on geometry of satellites and position of a vector – basis. However evaluation of discrepancies for each concrete case meets significant difficulties, first of all because of large number of combinations of phase ambiguity. Researches with the purpose therefore were carried out to reveal common regularities, in particular, distribution of values of discrepancies because of errors of a solution of phase ambiguities in maximums of function of a probability. In a course of a research the discrepancies were analysed at various constellations NS, from 4 up to 13 satellites in constellation, various positions and lengths of a vector – basis and the following conclusions are made:

1). The distribution of discrepancies does not depend on length of a vector – basis. At a modification of length of basis from 0.5 up to 100 m at constant constellation NS the cumulative distribution function practically does not vary.

2). A cumulative distribution function at identical number NS and geometric factor less than 3 depend on geometry of constellation NS and from a position of a vector – basis very little.

3). The square root from a sum of quadrates of discrepancies (summarised discrepancy) is enough precisely described by normal distribution, and the average quadratic deviation does not depend about number NS in constellation. The elimination makes case at a measurement on 4 NS.

4). The expectation of a summarised discrepancy at number NS more than 5 linearly depend on number NS in constellation. At 4-th NS she a little less and at 3-rd NS is equal to zero, as at an evaluation of discrepancies the algorithm with three unknown parameters was used.

It is necessary to mark, that the cumulative distribution function in this case is used not as the probability law, and for an evaluation of number of solutions having a summarised discrepancy in a specific range.

The probability of acceptance of a false solution in many respects is characterised minimum discrepancy in accessory maximums. Using an integrated cumulative distribution function of a summarised discrepancy, it is

possible to calculate probability of acceptance of a false solution at a specific threshold and limiting average quadratic error of a noise of a measurement of phase shifts. By results of researches it is possible to make the following conclusions:

1). Limiting average quadratic error of a noise of a measurement of phase shifts for one – times of methods it is necessary to consider magnitude 50 ... 60°, that there correspond 25 ... 30 mm.

2). The limiting noise error of a measurement of a phase shift depends on number observable NS. For example, by work on navigational constellation consisting from 4-th NS, the work one-time of algorithms is impossible. At 5-6 observable NS the unambiguous solution is possible only at small noise of a measurement of phase shifts (1-2° or 0.5-1мм). Optimum number NS in navigational constellation – 8 and more observable NS.

3). The probability of gross errors depends on length of basis. This association is explained by square-law increase of number of possible positions of a vector – basis at increase of its length. At length of basis 1 m the work of algorithm is possible already at 5 observable NS at a noise error of a measurement of a phase shift 5°, while at length of basis 10 m at the same exactitude of a measurement of phase shifts the observation 7-8 NS is necessary.

It is important to mark, that one-time the algorithm on one basis in practice is applied to compiling an initial gang of solutions, therefore major performance is the probability of skip of a valid solution, which is determined by a threshold value of function of a probability. The presence of false solutions in an initial gang does not mean a gross error, if the valid solution also is present at an initial gang.

A TECHNIQUE OF THE ANOMALY MEASUREMENTS REJECTION FOR SPACE VEHICLE TRAJECTORY DETERMINATION BASED ON GPS/GLONASS DATA*

V.E. Hertzman*
(Science Engineering Center of St.Petersburg's State Electro Technical University, Russia, e-mail: nic@eltech.ru),
V.V. Chistyakov**
(SoftNav Ltd St.Petersburg, Russia, e-mail: vchistyakov@mail.ru)

Abstract

Key words: GPS, GLONASS, RAIM, rejection, failure detection

The following aspects of the anomaly measurements rejection for the GPS/GLONASS user equipment based on a board of the space boosters, are considered: the pre-computations of the signal reception conditions, the methods of the failure detection and exclusion in real-time and post-mission processing. The pre-computations have the goal to determine the trajectory sectors (flight time intervals) with critical conditions of the signal reception. The methods of the measurements rejection in real-time processing are based on the analysis of the signal-to-noise density of the measurement errors and comparison of the least-squares residual's sum with the permissible bounds. Chi-square distribution of the probability is used for determination of the permissible bounds. The methods of the measurements rejection in post-mission processing are based on the analysis of the residuals, determined by polynomial smoothing in the sliding time intervals. The results of the anomaly measurements processing are illustrated on the data obtained from GPS/GLONASS receiver "Terminator".

1. The GPS/GLONASS user equipment, placed on a board of the vehicles, is used to determine the trajectory parameters of the space booster and orbital elements of the spacecraft. During the launch and insertion into final orbit, measurement data (UTC time, satellite identification number, channel number, signal-to-noise ratio, pseudorange, integrated Doppler shifts or carrier phase) are transmitted from the on-board user equipment to the control center for real time and/or post-mission processing. The rejection technique includes three stages of the computations:

- A pre-computation on the stage of measurement séance planning,
- Data processing in real time,
- Post-mission data processing.

During space-booster launch and spacecraft orbit insertion the specific conditions of signal reception can be occurred, which cause the signal tracking failure and/or appearance of anomaly measurement errors. Therefore the corresponding time intervals should be determined on the stage of the séance planning.

In real time processing the anomaly measurements are detected and isolated on ensemble of the all-simultaneous sighting GPS/GLONASS navigation satellite vehicles (NSV).

In post-mission processing the anomaly measurements are detected and isolated on ensemble of data are transmitted from everyone during the measurement's seance.

2. On the planning stage a priory conditions of the signal reception along NSV-to-user tracing path are calculated on the basis of the following data:

- Predetermined space-booster movement (translation and rotation) in celestial reference axis;
- Antenna pattern in body-fixed axis;
- GPS/GLONASS system almanac.

The critical measurement time intervals and NSV identification numbers are used in the post-flight analysis. The following conditions of signal reception are presented for these time intervals and satellites:

- NSV-user sight line sets out boundary of the antenna pattern;
- Derivative of the acccleration, paralleled to sight line, exceeds the critical level;
- Component of the user's angular velocity, perpendicular to sightline, exceeds the critical level.

3. In the real-time processing the following criterions are used for detection of the anomaly measurements.

1) Comparison of the signal-to-noise density in receiver channels with permissible level.

$$SN_k \le SN_{lim}, k = 1 : N.$$

2) Comparison of the least - squares residuals sum with the confidence bound on prescribed probability significance.

---

*Ph.D., Leading Research Scietist.
** Engineer.

$\left(\frac{R_W}{s}\right)^2 \le \chi^2(p, N-4)$ - the measurements are normal.

$\left(\frac{R_W}{s}\right)^2 > \chi^2(p, N-4)$ - the measurements are anomalous.

$W = Y - G \cdot \hat{X}$ - the $N \times 1$ range residual vector, Y - the measurement's vector, $\hat{X}$ - the least - squares estimate (single - point solution),

$R_W = sqrt(W^T \cdot W)$ - the norm of the residual vector,

s - a priory root mean square of the measurement's erros,

$\chi^2(p, N-4)$ - the p – fractiles of χ^2 - distribution with $(N\text{-}4)$ degrees of freedom,

p - prescribed probability significance,

N - the numbers of NSV in the work constellation.

The results of the residual's norm calculation, obtained for real measurements, are presented on Fig. 1. The curve 1 characterizes the quantities of the residual's norm before the rejection, the curve 2 – after the rejection (probability significance is equal 5%), in the sector 3 the anomaly measurements are absent.

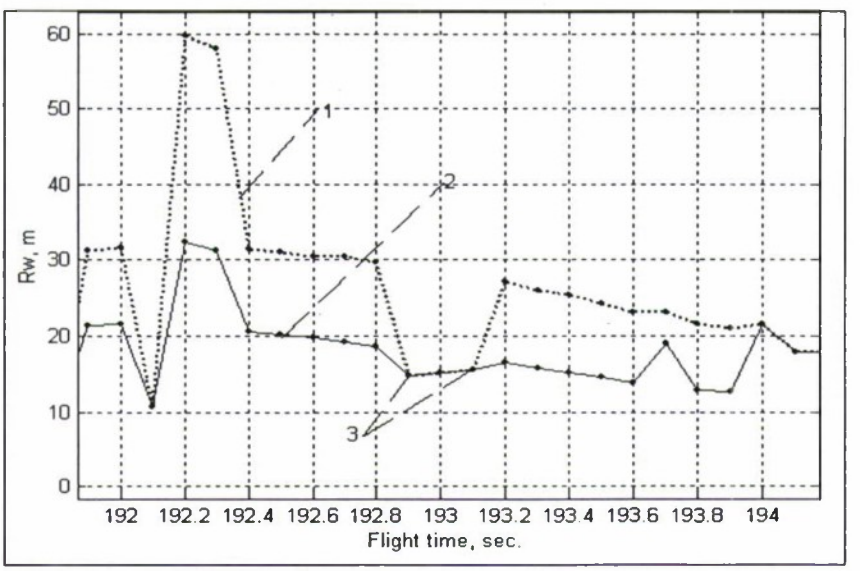

Fig.1. Residuals norma

The following criterions are used for detection and exclusion of the anomaly measurements.

- Criterion *Kr1*, based on *QR*-factorization of the connection matrix, described linearized measurement equation, and on transformation of the *N*-dimensional least-squares residuals vector *W* with correlated components to *(N-4)*-dimensional parity vector *V* with independent random components ("Parity" method [1]);
- Criterion *Kr2* used one by one satellite exclusion from the work constellation with subsequent calculation of the least-squares residuals sum, corresponding *(N-1)* remained NSV.

$G = Q \cdot R$ - qr - factorization of the matrix G,

$V = P \cdot W, P = Q^T(5:N, 1:N), V_i = \frac{P(1:N, i)}{norm(P(1:N, i))}, W_i = W(1:(i-1):(i+1):N,), i = 1:N,$

$Krl(i) = \max_i \langle V^T \cdot V_i \rangle, Kr2(i) = \max_i \langle W_i^T \cdot W_i \rangle$ - criterions of the exclusion of failure NSV (SVID = i)

The results of the NSV-residuals calculation for one of the satellites *(SVID=22)*, obtained before and after the rejection anomaly measurements (satellite *SVID=1)*, are presented on Fig. 2. The curve's marks correspond to Fig. 1.

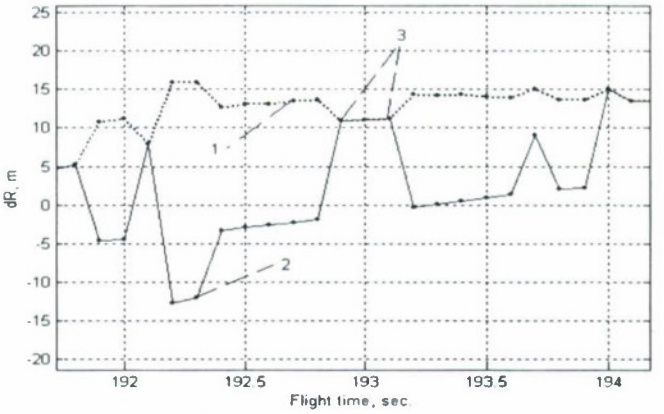

Fig.2. SV-residuals. SV = 22

4. In post-mission processing the range residuals for each NSV $dR(t_i)$, determined by polynomial smoothing in the sliding time intervals $[t_i-T/2, t_i+T/2]$, were represented as random time series on the entire measurement's seance. For this random process the estimates of the mean $m(dR)$ and the root mean square $std(dR)$ are calculated and anomaly level excesses are found (Gaussian distribution of measurement's errors is assumed) [2].

$$dR(t_i) = Y(t_i) - \int_{t_i-T/2}^{t_i+T/2} F(\tau)\cdot Y(t_i+\tau)d\tau,$$

$$D = \max_i \left| \frac{dR(t_i) - m(dR)}{std(dR)} \right| \le PH(p),$$

$PH(p)$ - the p – fractiles of Pearson and Hartley Biometrika Tables.

Then out-of-tolerance time intervals are compared with the time intervals of critical signal reception, determined on the planning stage. In the result NSV data, corresponding this conditions, are rejected out the navigation solution.

The quantities dR of the NSV-residuals and the estimates of the root mean square std, obtained by polynomial smoothing for two NSV $(SVID=1;22)$, are presented on Fig. 3. The measurements for $SVID=1$ were passed in the optimal conditions of signal reception, the measurements for $SVID=22$ – in the critical conditions.

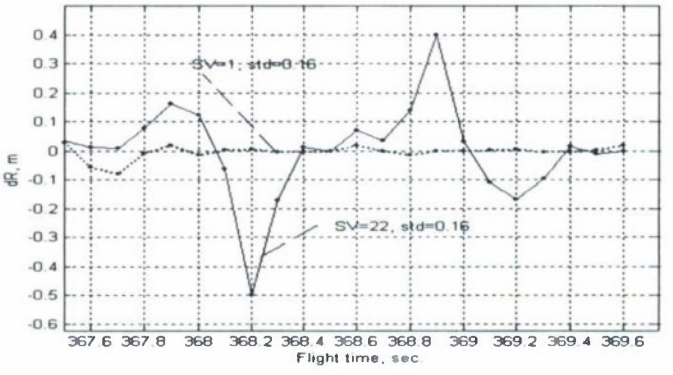

Fig.3. Smooth residual

5. The suggested technique of the anomaly measurements detection and isolation is implemented in the real time processing and post-processing software for space vehicle trajectory determination based on GPS/GLONASS measurements [3]. This software is utilized on the computing centers of the Russian experience cosmodroms during the launch of missiles and spacecraft with the user equipment "Terminator" on a board.

References

1. **R. Grover Brown.** Receiver Autonomous Integrity Monitoring, Chapter 5, "Global Positioning System: Theory and Applications", Volume II, Edited by Bradford W. Parkinson, James J. Spilker Jr.
2. **H.A. David.** . Order Statistics. 1970.
3. **V.E. Hertzman, A.V. Ekalo.** "Software for space vehicle trajectory determination based on GPS/GLONASS measurements// Proceedings of the 7-th Saint Petersburg International Conference on Integrated Navigation Systems. 29-31 May, 2000/Russia, St.Petersburg:CSRI Elektropribor, 2000.

ONBOARD BALLISTIC-NAVIGATIONAL SUPPORT OF SPACECRAFT "SOLAR SAIL"*

V.D. Dishel, A.K. Bikov, D.K. Churikiov

N.A.Pylugin Automatics &Instruments Scientific Production Center (AISPC), Moscow, Russia
Tel: 334-33-85. E-mail: nicolas@email.ru Fax 330-53-29

The description of onboard ballistic - navigational support of a spacecraft " Solar sail " is given. Spaceeraft "Solar Sail" is created for improvement of technology of control of a solar sail with the purpose of cheek of an opportunity of formation of desirable trajeetories of flight at thc expense of purposeful use of force of a solar wind. The system of navigation is construction on the basis of subsystems with use of measurements:

- ground one point of system;
- onboard 12-channel receiver GPS of signals.

The system of navigation is intendcd for definition of parameters of movement with accuracy allowing to reveal and to estimate influence of effect solar sail on movement of object in view of eharaeter light exposure of this or that site of a coil and orientation on it of blades solar sail. In the greatest measure these tasks are answered by opportunities, which has GPS- receiver.

With the purpose of operative reception of estimations of parameters of trajectory the target data of the receiver are proeessed directly in the onboard eomputer. The part of crude measurements of the receiver together with the processed onboard information in structure of telemetry acts in Mission Control Center.

After disclosing solar sail of the spacecraft twists concerning an axis of symmetry. As a result of it the axis Spaceeraft "Solar Sail" continuously is guided on Sun. During each eoil the antenna field of view of the receiver continuously varies from as much as maximum disclosings up to eomplete a hidden by the Earth, and it is possible also by separate elements of Spacecraft "Solar Sail". These eircumstances are taken into account in algorithms of planning of sessions of navigating definitions and formation of the telemetering information.

Each second from GPS of thc receiver in the onboard computer the crude measurements act. These measurements are processed in rate of flight. In result the set of qualitative residuals of measurements pseudorange and pseudospeeds on 32 second site of flight is formed.

During the subsequent interval on generated on the previous session average residual the estimation of parameters of trajectory is made. The methodieal basc of algorithms of an estimation is served by the speeial form of the Kalman filter , in which basis the idea of deeomposition covariances of a matrix of error of an estimation on multipliers as diagonal and two triangular matrixes lays. Due to this the preservation covariances by a matrix of property of positive definiteness is guaranteed. It provides high quality of a filtration in conditions of limitcd length of a digit grid of onboard computer. The elimination of probable instability of proeess of a filtration because of incomplete conformity to the aeeepted mathematical model of movement to a physical pieture is achieved by a choiee of the appropriate strueture of the filter and adjustment of a number of its parameters.

Estimated is extended a veetor, the first 6 which components eonsist of errors of eoordinates ($\Delta L,\Delta H,\Delta Z$) and speeds (($\Delta VL,\Delta Vh,\Delta Vz$) object in orbital frame. Two others - regular errors of range and radial speed caused divergenees of phases both frequencies of generators of the GPS-receiver and GPS satellites.

In the same orbital frame the fundamental matrix of estimated dynamic system is construction. It has allowed its account to carry out on analytical dependences, that has simplified and has sped up process of propagation of eovariances matrix (more precisely than its matrixes - multipliers) from one moment of binding average of measurements to another.

The integration of the equations of movement is carried out by a method Runge-Kutta of the fourth order with a step 32 s. On a step of integration a trajeetory approximate sedate near to faetors being funetions from meanings of the right parts of the equations of movemcnt. Due to this technique the high spced of algorithms of aeeount of a vector of a condition in internal points of a step is provided.

Onboard computer is constructed on the basis of 386 proccssors. The onboard software of the considered tasks is developed in language C ++ in view of features of representation machine given as numbers with the fixed point.

ESTIMATING IONOSPHERIC GLONASS AND GPS SIGNAL DELAY BY SINGLE FREQUENCY MEASUREMENTS

A.V. Grebennikov*, M.Yu. Kazantsev, Yu.L. Fateev*****
Scientific & Research Institute of Radio Engineering, Krasnoyarsk State Technical University
26, Kirenskogo St., 660074, Krasnoyarsk, Russia. E-mail: chmyh@ns.kgtu.runnet.ru

Abstract

Key words: ionosphere, satellite navigation, single frequency receiver

Method of ionospheric delay determination by GLONASS/GPS one-frequency receiver is presented. It is based on using a difference of increments of code and phase pseudoranges. Results of experimental researches are presented.

Introduction

The user equipment (receivers) of global satellite navigational systems is applied for creation of modern integrated systems of navigation and orientation. It is stipulated first of all by their such performance as a possibility of determination with a high exactitude of coordinates, velocity and orientation of object located in any point of globe. Main defects of receivers are: a susceptibility to influence of an environment and parasites; possible unauthenticity of satellite signals; miss of satellite signals, in particular, for origin of shadowings.

Noticeable influence to an exactitude of navigational determinations on signals of GLONASS and GPS render the conditions of passing of a signal from satellite up to receiver. As show researches [1,2], the large contribution to an error of GLONASS and GPS measurements is introduced by an ionosphere. In the report, the method of ionospheric delay determination for single-frequency receiver is represented.

1. Influence of ionosphere to an error of a measurements

The determination of coordinates and velocity using by GLONASS and GPS signals is carried out in an outcome of processing measurements, such as

- code pseudorange – pseudorange up to satellite, measured on a ranging code;
- phase pseudorange – pseudorange up to satellite, measured on a phase of a carrier frequency of a signal;
- range rate – radial velocity rather satellite.

To the greatest degree ionosphere renders influence to an error of a measurement of code and phase pseudoranges, that expresses through accordingly group and phase delay of signals. The systematic errors of a measurement of code and phase pseudoranges up to satellite caused by influence of an ionosphere, will be equal, but to have a different sign.

Ionospheric delay depends on sunspot activities (approximately 11-year cycle), seasonal and diurnal variations of total electronic concentration in an ionosphere, the line of sight which includes elevation of the satellite, and the position of the observation site. Measured pseudorange may be wrong from about 0.15 m to 50 m [3].

2. Methods eliminating of ionospheric influence on single-frequency GLONASS and GPS receivers

Each GLONASS and GPS satellite transmits navigational signals in two frequency L1 and L2. Two-frequency receiver, working on two frequency signals, is capable to exclude influence of an ionospheric refraction of radiowaves to an error of measurements. The access to GLONASS and GPS navigational signal on frequency L2 is limited [4,5].

In the navigational message of GPS the parameters of a global model of an ionosphere – Klobuchar model are transmitted, thus a single-frequency user can realize an ionospheric correction. Agrees [5], the application of a Klobuchar model will provide at least a 50% reduction in the Standard Position Service user's RMS error due to ionospheric propagation effects. GLONASS gives no possibility of a correction of influence of an ionosphere for a single-frequency user.

---

* Ph.D., Deputy Chief.
** Research Scientist.
*** Ph.D., Research Scientist.

The error of majority of empirical models of ionospheric parameters (International Reference Ionosphere, Chiu, Bent) is high (20-40 %), empirical models are capable to work, only in mid-latitude areas and quiet geomagnetic conditions.

Most perspective is the method of elimination of influence of an ionosphere on satellite signals in single-frequency receiver, based on the account of contrast of signs of phase and group delay. The proposed approach allows to determine delay of a signal in an ionosphere with the help of single-frequency receiver. It based on a difference between code and phase pseudoranges[6,7]. A residual of code and phase pseudoranges is equal to the double ionospheric delay of a signal, and can be used for determination of it

$$I_i(k) = \frac{r_i(k) - \varphi_i(k) + N_i(k)\lambda_i}{2},$$

where $I_i(k)$ – ionospheric delay of a satellite signal at epoch k ($k = 1,2,\ldots$); $r_i(k)$ – code pseudorange measured on a ranging code; $\varphi_i(k)$ – phase pseudorange measured on a phase of a carrier frequency of a signal; $N_i(k)$ – initial carrier phase cycle ambiguity; λ_i – wavelength of a satellite signal; i – serial number of satellite, $i = \overline{1, n(k)}$; $n(k)$ – number observed satellites.

The given approach has received the development in the beginning of the 90-th years in works listed in [7]. To the present time in the foreign publications there are mentions of realization of the considered approach in practice [8], the researches of the given approach were conducted and in our country [9].

Main obstacle in a path of realization of the considered approach of indemnification of ionospheric errors is the problem of the determination of initial ambiguity of phase measurements $N_i(k)$ in absence of additional measuring frequencies [6,7]. One from methods of a solution of the given problem is the inclusion of initial ambiguity of phase measurements $N_i(k)$ in a vector of estimated parameters of a Kalman filter, as it was made in work [7]. Such method of an evaluation $N_i(k)$ has some disadvantages, which explicitly are circumscribed in [7].

3. Ionosphere Model

The purpose of construction or choice of a model of an ionosphere is, the possibility of determination, with its help, delay of a signal in an ionosphere, having at the command of an only measurement NP on single frequency. Height of working orbits of GLONASS and GPS satellite is above than upper bound of an ionosphere. As a rule, the main mass of the users is under a low bound of an ionosphere, behind an elimination receivers, established on low-orbit space vehicle. The vertical profile of electronic concentration has essential significance only for objects were in an ionospheric stratum. Therefore for the account of ionospheric errors essential is all ionosphere. For air and ground objects the ionospheric single-error correction practically completely is determined by significance by total electron content in a vertical direction. Therefore for a basis we shall take, so-called, single-layer model of an ionosphere, where it is supposed, that all electrons are concentrated in a lamina located at some height h Above a surface of the Earth [7, 10, 11].

Ionospheric shell height h usually understand as height, where 50 % of total electron content in a vertical direction [11] is reached. There is a daily variation of ionospheric shell height. In night time height h is higher, than in day time. Ionospheric shell height can will be changed in limits from 250 up to 500 km.

The magnitude of an error caused by influence of an ionosphere will depend on an expansion of a path S of satellite signal in an ionosphere. For satellite with low elevation angles the expansion of a path of signal will be more, than for satellite with high elevation angles. Therefore ionospheric error will be inversely proportional to satellite elevation angle. Distinguish vertical delay (satellite elevation angle $\gamma = 90^\circ$) and slant delay (satellite elevation angle $\gamma < 90^\circ$). Their relation is determined by following expression [7, 10]

$$I_i(k) = Ob(\gamma_i(k)) I_v(k), \tag{3.1}$$

Where $I_i(k)$ – (slant) ionospheric delay of signal in an ionosphere; $Ob(\gamma_i(k))$ – mapping function; $I_v(k)$ – vertical delay of a signal in an ionosphere; $\gamma_i(k)$ – satellite elevation angle. The mapping function is intended for recalculation of vertical delay in slant and is determined as the relation of slant and vertical delay of a signal in an ionosphere [10]

$$Ob(\gamma_i(k)) = \frac{I_i(k)}{I_v(k)} = \frac{1}{\sqrt{1 - \left(\frac{R_\oplus}{R_\oplus + h} cos\gamma_i(k)\right)^2}}, \tag{3.2}$$

where $R_\oplus$ – radius of the Earth; h – ionospheric shell height.

Depending on an elevation angle and ionospheric shell height, the significance of function $Ob(\gamma)$ will vary an approximately range from 3.5 up to 1 (fig. 1).

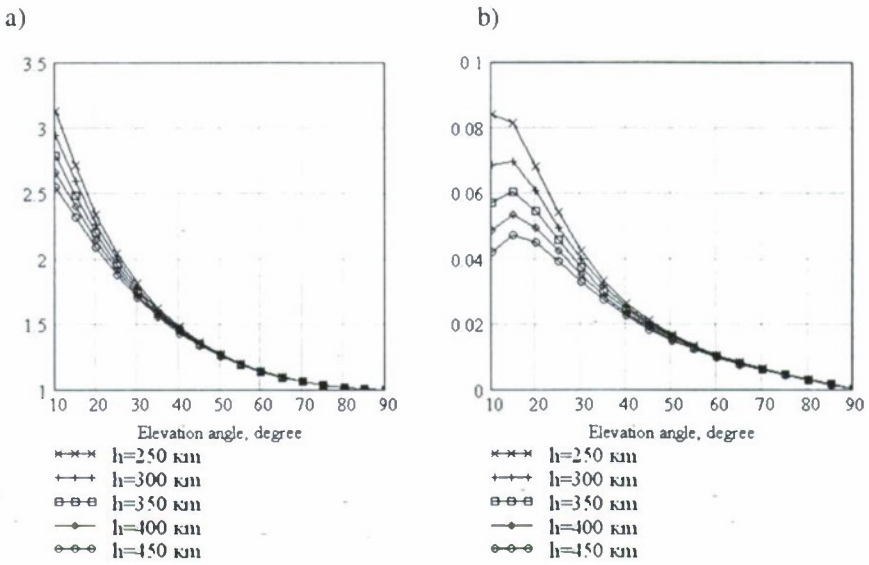

Fig. 1. Properties of mapping function: a) significance of mapping function $Ob(\gamma)$ depending on an elevation angle and γ ionospheric shell height h ; 6) an increment of mapping function of magnification of an elevation angle on 1 degree.

4. Algorithm description

Let's note input equations for determination of delay of a signal in an ionosphere. Code pseudorange is determined by expression [3]

$$r_i(k) = \rho_i(k) + I_i(k) + T_i(k) + \Delta\tau(k)\cdot c + \delta_i(k) + \xi_i(k),$$

(4.1)

where $\rho_i(k)$ – distance up to satellite; $T_i(k)$ – delay of a satellite signal in troposphere; $\Delta\tau(k)$- receiver clock error; c – speed of light; $\delta_i(k)$ – part of a systematic error, which includes satellite orbit error, satellite clock error, etc.; $\xi_i(k)$ – random error. The phase pseudorange is determined by expression [3]

$$\varphi_i(k) = \rho_i(k) - N_i(k)\lambda_i - I_i(k) + T_i(k) + \Delta\tau(k)\cdot c + \delta_i(k) + \zeta_i(k), \quad (4.2)$$

where $\zeta_i(k)$ – random error.

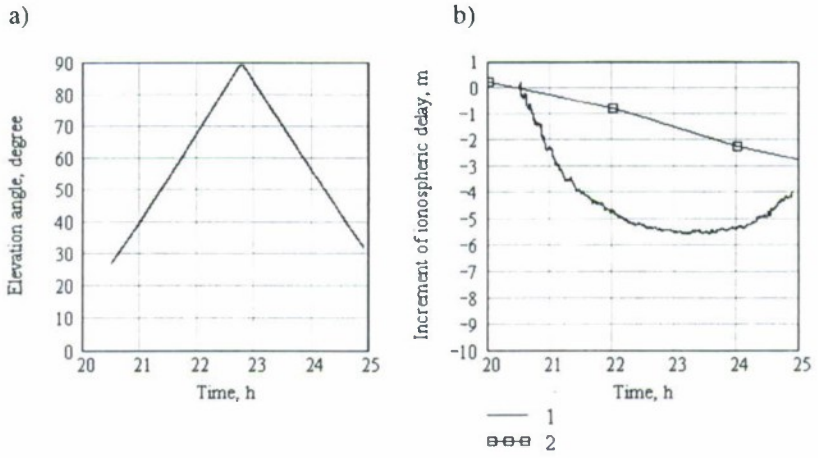

Fig. 2. The figures a) variation of satellite elevation angle and b) increment of ionospheric delay (1 – increment of vertical delay, 2 – increment of slant delay)

Proceeding from the equations (4.1) and (4.2), residual of increments of code and phase pseudoranges during $\Delta t = k - l$ (Δt – an interval of measurements) is equal to the double increment of delay of a signal an ionosphere for the same slice of time

$$(r_i(k) - r_i(k-l)) - (\varphi_i(k) - \varphi_i(k-l)) = 2 \cdot (I_i(k) - I_i(k-l)).$$

First step of researches was experimental check of equality on magnitude and contrast on a sign of phase and group delay of satellite signals in an ionosphere. The experimental researches were conducted and the increments of delay of a signal in an ionosphere are obtained. In a fig. 2. the outcomes of measurements of a GPS satellite signal are represented. The experiment has confirmed, that the diminution or magnification of delay of a signal in an ionosphere for rather small spaces of time (1-2 hours) happens, mainly, at the expense of a modification of an satellite elevation angle, much smaller influence renders a daily variation of an ionosphere. The experimental researches have shown, that with the help of single-frequency receiver it is possible to observe a variation of delay of a signal in an ionosphere.

Following pitch of researches was development of algorithm of determination of ionospheric delay. The algorithm is divided into two stages. At first with the help of Kalman filter the vertical delay of a signal is evaluated, and then it is recalculated for each satellite, with allowance for of its elevation angle. With allowance for (3.1) we shall note the equations (4.1), (4.2) as follows

$$r_i(k) = \rho_i(k) + Ob(\gamma_i(k)) I_v(k) + T_i(k) + \Delta\tau(k) \cdot c + \delta_i(k) + \xi_i(k), \tag{4.3}$$

$$\varphi_i(k) = \rho_i(k) - N_i(k)\lambda_i - Ob(\gamma_i(k)) I_v(k) + T_i(k) + \Delta\tau(k) \cdot c + \delta_i(k) + \zeta_i(k). \tag{4.4}$$

Let's make a difference set of equations, deducting from each equation of a system (4.3) and (4.4) at epoch k for i-th satellite the appropriate equation at epoch $k-1$. Let's define increments of pseudo-distances (4.3) and (4.4)

$$\Delta r_j(k) = \rho_j(k) - \rho_j(k-1) + (Ob(\gamma_j(k)) - Ob(\gamma_j(k-1))) I_v(k) + \xi_i(k) - \xi_i(k-1),$$

$$\Delta\varphi_j(k) = \rho_j(k) - \rho_j(k-1) - (Ob(\gamma_j(k)) - Ob(\gamma_j(k-1))) I_v(k) + \zeta_i(k) - \zeta_i(k-1),$$

where $\Delta r_j(k) = r_j(k) - r_j(k-1)$ – increment of code pseudorange; $\Delta\varphi_j(k) = \varphi_j(k) - \varphi_j(k-1)$ – increment of phase pseudorange; j – serial number of satellite, which was observed at epochs k and $k-1$, $j = \overline{1, \tilde{n}(k)}$; $\tilde{n}(k)$ – satellite number, which were observed at epochs k and $k-1$. Then we shall define a residual of increments of code and phase pseudoranges

$$2 \cdot (Ob(\gamma_j(k)) - Ob(\gamma_j(k-1))) \cdot I_v(k) = \Delta r_j(k) - \Delta\varphi_j(k) + \varepsilon_j(k), \tag{4.5}$$

where $\varepsilon_j(k)$ – random error. In the total we have received a set of equations (4.5), where is absent of initial phase ambiguity $N_i(k)$. With the help of equations (4.5) the vertical delay of a signal in an ionosphere is determined. The evaluation of vertical delay is made with the help of Kalman filter. Then the obtained vertical delay will be transformed to slant delay of a signal for i-th satellite in the correspondence with expression (3.1).

Obtained algorithm have a number of distinctive features. As measurements not differences of pseudoranges, but difference of increments of pseudoranges act. In an outcome the necessity in disclosure of initial phase ambiguities disappears, the number of unknown variables decreases which are necessary for evaluating, on a comparison with a method circumscribed in work [7], that considerably simplifies algorithm.

From a set of equations it is possible to find significance of vertical delay for j-th satellite

$$I_v(k) = \frac{\Delta r_j(k) - \Delta\varphi_j(k)}{2 \cdot (Ob(\gamma_j(k)) - Ob(\gamma_j(k-1)))}. \tag{4.6}$$

From expression (4.6) and properties of mapping function (Fig.1) follows, that the evaluation of magnitude of vertical delay will depend on selected ionospheric shell height h. Ionospheric shell height can be given a priory. The choice of optimum height of an ionosphere for mapping function was considered in work [10]. Leaning on the indicated outcomes of researches indicated in [10], was selected significance of ionospheric shell height $h = 432.5$ km.

5. Outcomes of experimental researches

By closing stage were the experimental researches of the developed method, with the help of MRK receiver, developed in Scientific & Research Institute of Radio Engineering placed in Krasnoyarsk State Technical University (KSTU). GLONASS/GPS MRK receiver works on single-frequency L1. MRK receiver has important for realization of the developed method in practice of performances

- Measurement of a phase of a carrier frequency of a signal;
- Low frequency of failures of tracing behind a phase of a carrier frequency of a signal;
- Low level of a random component error of a of code pseudorange measurement (RMS 0.2 – 0.3 m).

During of experiment, measurements, made with the help MPK receiver was recorded. Then, using by noted information, the ionospheric delay of satellite signals was determined. During a 2001 some measuring companies (see table) in various geomagnetic conditions (perturbed and quiet ionosphere) were conducted. In the table for performance of geomagnetic activity the Ap-index is indicated.

For check of an exactitude of the developed method the information about ionosphere state of centre of data storage Crustal Dynamics Data Information System (CDDIS) was used [12]. CDDIS gives for a free access the data files of global distribution of total electron content (TEC) in a format IONEX [13]. These data are obtained from Analytical Centres of International GPS Service (IGS). The correspondence of a information about state of ionosphere for Krasnoyarsk is determined by that in KSTU is located two-frequency TurboRugue receiver, included in structure of IGS, it has allowed to accept data IGS as true measurements.

Date	Duration, h	Global magnetic activity: Ap-index, nT	RMS error of single frequency method σ_1, m	RMS error of Klobuchar model σ_2, m	$\frac{\sigma_2}{\sigma_1}$
25 April	26	6	0.49608723	1.84167667	3.71240494
26 April		6			
28 April	29	40	0.81335721	2.02093429	2.3388889
29 April		13			
16 May	46	7	0.3878384	1.23400857	3.18175996
17 May		6			
18 May		8			
8 October	24	16	1.08973087	2.24708779	2.06205756
9 October		18			
Average			**0.69675343**	**1.76357926**	**2.7712769**

On the figures 3-4 the evaluation of vertical ionospheric delay obtained with the help of developed method, Klobuchar model, and as evaluations of vertical delay on an information of IGS Analytical Centres is indicated: CODE (Center for Orbit Determination in Europe), Bern, Switzerland; JPL (Jet Propulsion Laboratory), Pasadena, USA. On the figures on an axes of abscissas the number of hours, past from a beginning of the first day of experiment is resulted. The beginning of day is determined on local winter time ZT =UTC + 6 h + 1 h, or otherwise, ZT = GLONASS system time + 4 h).

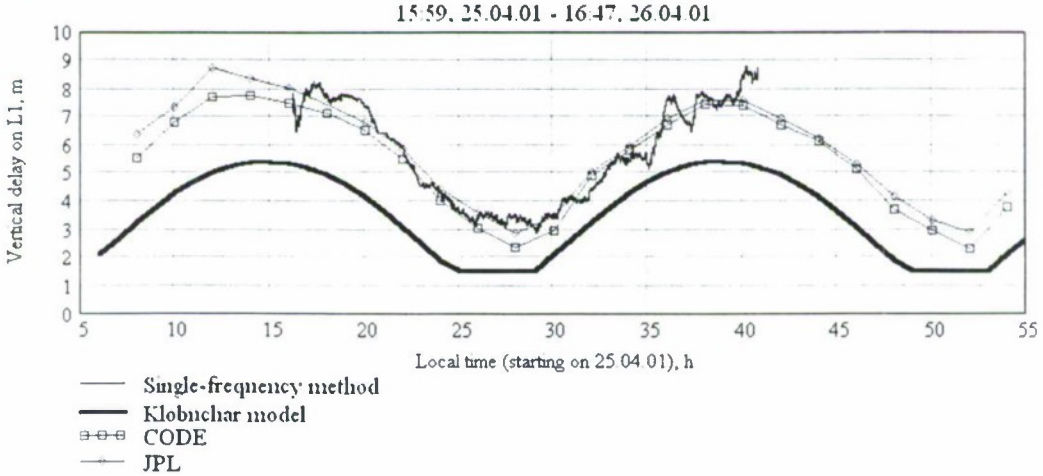

Fig. 3. Outcomes of experiment conducted at April 25-26, 2001

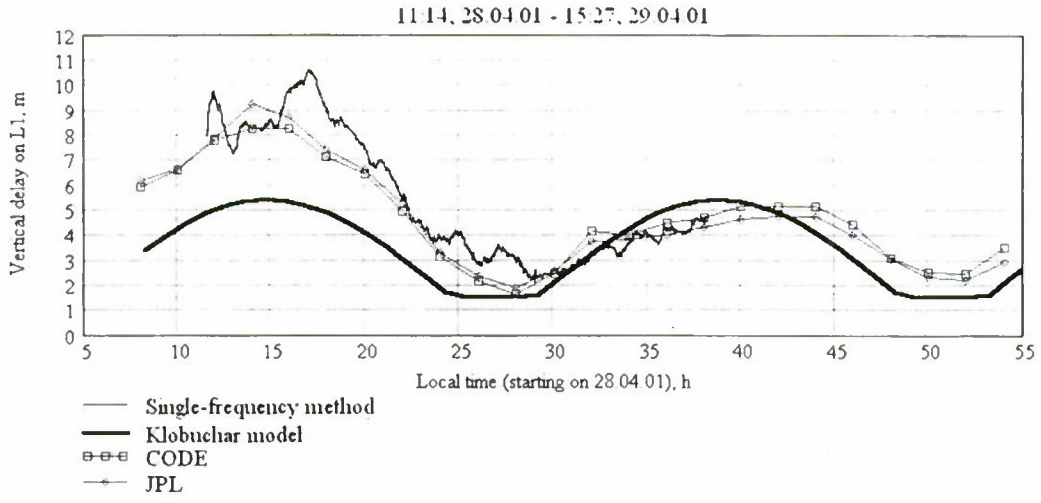

Fig. 4. Outcomes of experiment conducted at April 28-29, 2001

6. Influence of an ionosphere to an error of solution of a navigational problem

Let's try to clarify a character of influence of ionospheric delay on the measured coordinates of object. The research of ionospheric delay by an one-frequency method has shown a rather good exactitude of a measurement of vertical delay. At the same time to attempt of elimination of an ionospheric error the rather specific influence on evaluated coordinate and time was clarified it.

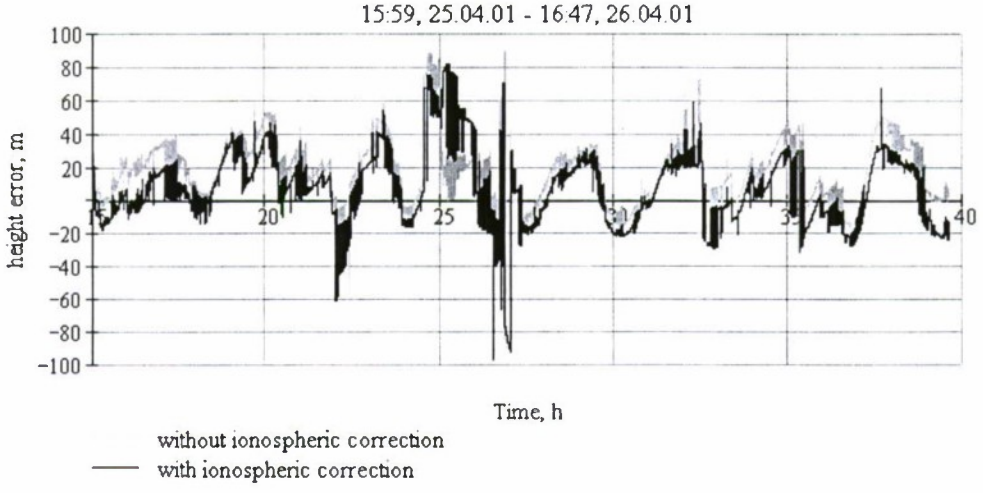

Fig. 5. Height error (without filtration)

The researches have shown, that the error of obtained coordinates caused by ionospheric delay, depends on a configuration of satellite constellation very little. First of all the ionospheric error effects on altitude component error of coordinates of object and time (fig. 5). Research of a character of influence of ionospheric delay for the measured coordinates and time we shall conduct, proceeding from the following suppositions:

- The navigational equations, being nonlinear, at the same time in each point of space have a very small curvature, that allows to linearize them in a point of a disposition of object. With an adequate accuracy it is possible to consider, that the errors of a measurement of pseudoranges are connected to an error of calculation of coordinates of object and time by linear transformation, i.e. the total error of a measurement of coordinates and time is equal to the sum of errors caused separate component ionospheric error of a pseudorange measurement.
- Proceeding from linear transformation of an error of a measurement of pseudorange to an error of coordinates and time, it is possible to consider an ionospheric error separately from a remaining component error.

By aeeepting a hypothesis that the ionospheric error influenees in main height and time, is separable an ionospheric error on two component. First component ealls only deviation of height and time. Second component – residual ionospheric error, in the sum with first component they give a full ionospheric error.

First eomponent of an ionospheric error ean be found as follows. Let's assume, that in a point with known eoordinates the pseudorange up to satellite are measured. The similar measurements are made in other point loeated above first on the magnitude H. The linearization of the navigational equations eorresponds to the supposition, that the satellite signals eome from an indefinitely deleted point, having a flat wavefront set. A residual of satellite signals between two points is equal

$$\Delta R = -H \cdot \sin\gamma \tag{6.1}$$

Residual equal to an error of a measurement of pseudoranges, whieh displaees the measured coordinates up on magnitude H. For a displaeement of a time seale t_{iono} it is enough to all pseudoranges to add the same magnitude $c \cdot t_{iono}$, where c – speed of light.

The resulting error of a measurement of pseudo-distanee displacing eoordinates up on magnitude H And time on magnitude t_{iono} Is equal

$$I_{HT} = c \cdot t_{iono} - H \cdot sin\gamma\,. \tag{6.2}$$

The residual ionospheric error is equal

$$I_{res} = I - I_{HT} = \frac{I_v}{\sqrt{1-\left(\frac{R_\oplus}{R_\oplus + h}\cos\gamma\right)^2}} - c \cdot t_{iono} + H \cdot \sin\gamma\,. \tag{6.3}$$

It is necessary to select parameters H and t_{iono} so that to minimize a residual error. The minimization ean be made on a criterion of minimum root-mean-square magnitude of a residual ionospheric error

$$\int_0^{\pi/2} (I_{res})^2 d\gamma = min\,. \tag{6.4}$$

For minimization of function (6.4) we shall take derivatives with parameters t_{iono} and H and we shall equate them to zero

$$\frac{\partial}{\partial t_{iono}} \int_0^{\pi/2} (I_{res})^2 d\gamma = \int_0^{\pi/2} -2c \left(\frac{I_v}{\sqrt{1-\left(\frac{R_\oplus}{R_\oplus + h}\cos\gamma\right)^2}} - c \cdot t_{iono} + H \cdot \sin\gamma \right) d\gamma = 0\,, \tag{6.5}$$

$$\frac{\partial}{\partial H} \int_0^{\pi/2} (I_{res})^2 d\gamma = \int_0^{\pi/2} \left(\frac{I_v}{\sqrt{1-\left(\frac{R_\oplus}{R_\oplus + h}\cos\gamma\right)^2}} - c \cdot t_{iono} + H \cdot \sin\gamma \right) \cdot \sin\gamma \cdot d\gamma = 0\,. \tag{6.6}$$

In an outeome have reeeived two equations eoneerning two unknown parameters t_{iono} and H. The integration of the equation (6.5) gives

$$\int_0^{\pi/2} \left(\frac{I_v}{\sqrt{1-\left(\frac{R_\oplus}{R_\oplus + h}\cos\gamma\right)^2}} - c \cdot t_{iono} + H \cdot \sin\gamma \right) d\gamma = I_v \int_0^{\pi/2} \frac{d\gamma}{\sqrt{1-\alpha^2 \cos^2\gamma}} - c \cdot t_{iono} \cdot \pi/2 + H\,, \tag{6.7}$$

where $\alpha = \left(\frac{R_\oplus}{R_\oplus + h} \right)$. The integral $\int_0^{\pi/2} \frac{d\gamma}{1 - \alpha^2 \cos^2 \gamma}$ is reduced to a kind

$$\int_0^{\pi/2} \frac{d\gamma}{1 - \alpha^2 \cos^2 \gamma} = F\left(\pi/2,\ 1 - \frac{\alpha^2}{1 - \alpha^2} \right),$$

where $F(\cdot)$ – full elliptic integral of the 1-st kind. The integration of the equation (6.6) gives

$$\int_0^{\pi/2} \left(\frac{I_v}{\sqrt{1 - \left(\frac{R_\oplus}{R_\oplus + h} \cos\gamma \right)^2}} - c \cdot t_{iono} + H \cdot \sin\gamma \right) \cdot \sin\gamma \cdot d\gamma = I_v \beta \cdot \arcsin \frac{1}{\beta} - c \cdot t_{iono} + H \cdot \pi/4 ,$$

where $\beta = \frac{R_\oplus + h}{R_\oplus}$. In the total we have a set of equations

$$\begin{cases} -c \cdot t_{iono} \cdot \pi/2 + H = -I_v \cdot F(\alpha) \\ -c \cdot t_{iono} + H \cdot \pi/4 = -I_v \cdot \beta \cdot \arcsin \frac{1}{\beta} \end{cases} \tag{6.8}$$

Solution of a system (6.8)

$$c \cdot t_{iono} = I_v \frac{\beta \cdot \arcsin(1/\beta) - F(\alpha) \cdot \pi/4}{1 - \pi^2/8},$$

$$H = I_v \frac{[\beta \cdot \arcsin(1/\beta) + F(\alpha)(1 - \pi/4)] \cdot \pi/2}{1 - \pi^2/8}.$$

The factors α And β of accepted model of an ionosphere ($R_\oplus = 6371$ km, $h = 432.5$ km) will be equal $\alpha = 1.067$, $\beta = 1/\alpha = 0.936$. In this case $c \cdot t_{iono} = 2.797 \cdot I_v$, $H = 1.913 \cdot I_v$ And then the formula (6.2) will look like

$$I_{HT} = (2.797 - 1.913 \cdot \sin\gamma) \cdot I_v . \tag{6.9}$$

In a fig. 6 the schedules of full ionospheric delay and its part responsible for high-altitude and temporary component errors are represented. In a fig. 7 the residual ionospheric error is represented.

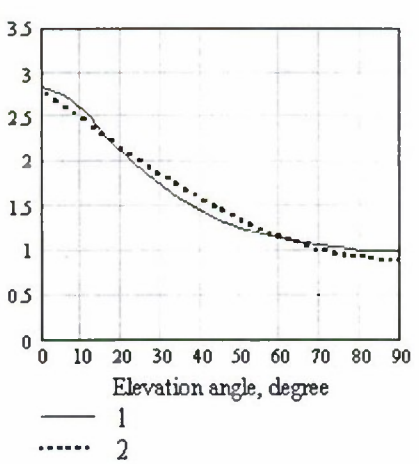

Fig. 6. 1 – full ionospheric error
2 – first component of ionospheric error

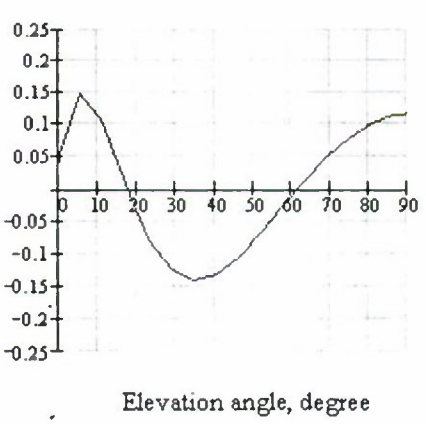

Fig. 7. Residual ionospheric error

From the figures it is visible, that is valid, the ionospheric error in main is determined by first component. The residual error makes only 15-20 % from vertical delay. First component of ionospheric delay calls merging coordinates on height and displacement of a time scale, and these effects do not depend on structure and configuration of satellite constellation, and bodily and completely are determined by magnitude of vertical delay. The residual error is recalculated in an error of coordinates and time scale through a matrix of linear transformation, the magnitude of an error of coordinates depends on a concrete kind of this matrix, i.e. from a configuration of constellation, and the magnitude is determined by magnitude of the appropriate geometric factor.

Let's evaluate magnitude of a residual error of coordinates. Normal conditions the magnitude of the geometric factor makes magnitude from 1.5 up to 3, therefore residual error of coordinates will make 30-60 % from vertical delay. For example, for want of to vertical delay $I_v = 5$ m the magnitude of a residual error will make 1.5-3 m. At the same time, the magnitude of a vertical displacement will be equal 10.8 m.

Conclusions

1. The determination of ionospheric delay of satellite signal based on single-frequency GLONASS and GPS measurements is possible.
2. The developed method has allowed in some times to increase an exactitude of definition(determination) of vertical delay on a comparison with a Klobuchar model.
3. The developed method is stable works in various condition of an ionosphere (quiet and perturbed ionosphere).
4. The ionospheric delay of satellite signal influences on error of determination of height and receiver time error.

References

1. **Conley R., Lavrakas J. W.** The world after Selective Availability // Proceedings of ION GPS-99. The Satellite Division of the Institute of Navigation 12th International Technical Meeting. – Nashville, Tennessee, September 14-17, 1999. – P. 1353-1361.
2. **Camargo P.O., Monico, J.F.G., Ferreira L.D.D.** Application of ionospheric corrections in the equatorial region for L1 GPS users // Earth Planets Space. – 2000. – V.52. – P. 1083-1089.
3. **Hofmann-Wellenhof B., Lichtenegger H., Collins J.** Global Positioning System. Theory and Practice. Springer-Verlag Wien New York, 1994. – 356 p.
4. **Global Navigational Satellite System GLONASS.** The interface control document (edition fourth). – M.: KNITS VKS, 1998. – 54 p. (In Russian)
5. **ICD-GPS-200**, Revision C, U.S. Government, October 10, 1993.
6. **Network satellite radio navigational systems.** / Editing by V. S. Shebshaevich. – M.: "Radio i svyaz", 1993. – 408 p. (In Russian)
7. **Nisner P., Trethewey M.** GPS Ionospheric Determinations Using L1 Only // Proceedings of the 5th International conference on "Differential Satellite Navigation Systems", Additional Volume, St. Petersburg, Russia, May, 1996.
8. **Brunet M., Lamy A., Suard N.** EURIDIS System Test Measurement Station // Proceedings of ION GPS-99. The Satellite Division of the Institute of Navigation 12th International Technical Meeting. – Nashville, Tennessee, September 14-17, 1999. – P. 2325-2333.
9. **Dubinko Yu.S.** Some directions of development of user equipment in firm "KB NAVIS" // Proceedings of the III International conferences "Planning of global navigation" (October 9 -11 2000, Moscow, Russia).– M.: NTTS «Internavigatsiya», 2000. (In Russian)
10. **Schaer S.** Mapping and Predicting the Earth's Ionosphere Using the Global Positioning System // Ph. D. dissertation, Astronomical Institute of the University of Bern, Switzerland, 1999. – 208 p.
11. **Komjathu A., Langley R.B.** The Effect of Shell Height on High Precision Ionospheric Modelling Using GPS // Proceedings of the IGS Workshop in Silver Spring, Maryland, USA, 19-21 March, 1996. – P. 193-203.
12. **Noll C.E.** CDDIS 2000 Global Data Center Report // IGS 2000 Technical Report. – 2001.
13. **Schaer S., Gurtner W., Feltens J.** IONEX: The IONosphere Map EXchange Format Version 1, February 25, 1998 // Proceedings of the IGS Analysis Center Workshop ESA/ESOC, Darmstadt, Germany, February 9-11, 1998. – P. 233-247.

GALILEO – ONLY AN OTHER GPS OR MORE? PERFORMANCE ANALYSE WITH THE TOOL NAV–SIM

J. Furthner*
German Aerospace Centre (DLR e.V.) – Institute of Communications and Navigation,
Münchner Straße 20, D-82234 Weßling, Germany. E-mail: Johann.Furthner@dlr.de

Abstract

Key words: simulation system, navigation, GPS, GALILEO, GNSS

Since the European Commission (EC) decided to built up an own civil global navigation satellite system called GALILEO, many people are asking why the EC want to built up an additional system. They say that they can use without any costs the U.S. navigation system GPS and, therefore, there is no need for the European GALILEO for the applications. But this is not really true. For some special applications GPS is not utilisable because it is no guarantee for the availability of the system.

In this paper I want to present a few technical reasons, why GALILEO is necessary in addition to GPS. For analysing the effects in navigation and positioning of a global navigation satellite system GNSS like GALILEO and GPS or GLONASS the DLR developed an end-to-end software simulation system called NAV–SIM. The software package offers the possibility to simulate simultaneously different satellite systems.

In many cases we will be asked, what we understand under 'end–to–end' simulation tool. The answer is very easy: we can simulate the signal propagation from the satellite down to the receiver in two interconnected simulation levels. The two levels are the signal simulation level and the application simulation level. Both levels are necessary to determine the positioning performance of a GNSS under consideration of nearly realistic conditions. A detailed description of this tool is given in the paper.

We are able to analyse with this tool, which global navigation satellite system of both GALILEO or GPS is the better system for special applications or if it is needful to use both systems simultaneously.

1. Introduction

Existing navigation systems like GPS and GLONASS are well–known and have shown that the reachable accuracy and availability in the navigation solution depends on the complexity of natural influences and used technical equipments. For some applications like flight navigation (CAT1 .. CAT3) all the available satellite navigation system don't fulfil the requirements in case of accuracy and availability. These are the gist's why the European Commission decided to develop an own civil satellite navigation system called GALILEO. The verification of the preliminary system specifications of GALILEO is necessary in its early development phase if the assumed requirements can be fulfilled under the aspect of technical possibilities and of costs for development and operation.

The allocated frequency bands for GALILEO are in the L–band which is used by a lot of other signals (c.g. GPS, GLONASS, MLS). The bandwidth for the GALILEO signals are not so wide as in the case of GPS or GLONASS and, therefore, different modulation schemas are discussed based on the definition, that a Code Division Multiple Access (CDMA) is used by GALILEO. In addition, different services shall be available for the new navigation system: Open Service, Safety–of–Life Service, Commercial Service and Public Regulated Service. For all theses services the signal has to be optimised related to service requirements like accuracy, availability and reliability.

The paper will give you at first an overview of the architecture of the NAV–SIM tool. show some results concerning errors introduced by multipath or atmospheric effects and display the

2. Architecture of NAV–SIM

The German Aerospace Centre has developed a simulation tool for GNSS, because it was seen the need of a suitable software tool for design, investigation and verification since a the last few years beginning at the first ideas about an own European navigation system. The problem of simulating navigation systems is the GNSS complexity considering on one hand the component and parameter variety in the space and user segment and on the other hand the spatial and temporal variation of natural impacts during signal transmission and reception. The projection of all processes into a simulation system contains a time–scale conflict resulting from the large physi-

* Scientific Staff Member.

cal transmission bandwidth (thcrefore high sampling frequencies of several 10 MHz) and from the comparatively slowly changing scenario determined by satellite tracks, user movement, ionospheric and tropospheric influenccs, clock drifts and other effects. This conflict normally results in excessively long simulation times and in the demand of large data storage capacities. To avoid this detected problem and to achieve a suitable handling of the GNSS software simulation system, the project NAV–SIM uses a multi–layer architecture.

The multi–layer architecture has two levels: the first level is the signal simulation level (SSL), and the second application simulation level (ASL). The SSL is responsible for the estimation and modelling of the signal specific range performance. It allows to investigate the signal structures (e.g. spreading codes, pulse shaping, chip rates) and the corresponding design of signal generation and receiver components (e.g. high power amplifier HPA, delay or phase lock loops DLL/PLL). Based on these simulations, where essential transmission impacts are considered (e.g. multipath), the system performance will be derived using a very short signal section (e.g. 30 seconds) for a sufficient number of carrier–to–noise ratios C/No. Due the highly detailed simulation at sampling frequencies of several 10 MHz and the high computational complexity each of these short time simulations takes about one day on high performance workstation. With the results of these simulation – a set of statistical parameters – a model of physical signal processing is generated.

The ASL simulates the very slowly changing system aspects compared to the signal simulation: The satellite tracks, ser movement, atmospheric influences, system and satellite time behaviour and the solution of the navigation equation. This level is used, on the one hand, for generating the signal states characterized by C/No, ranges, phases and the corresponding rates for the SSL and, on the other hand, for composing the delay measurements of the natural and physical part and of the technical simulations to get the positioning solution. Because of the flexible and block-based design an adaptation of changes can be quickly implemented. It is also possible to change the implemented algorithms with new and test the influences of these new algorithms on the positioning solution.

Fig.1 shows the block structure of the two layer navigation simulation system NAV–SIM. Both simulation layers can be used independently of each other. Therefore, it is possible to decide which level have to be used for analysing a special problem.

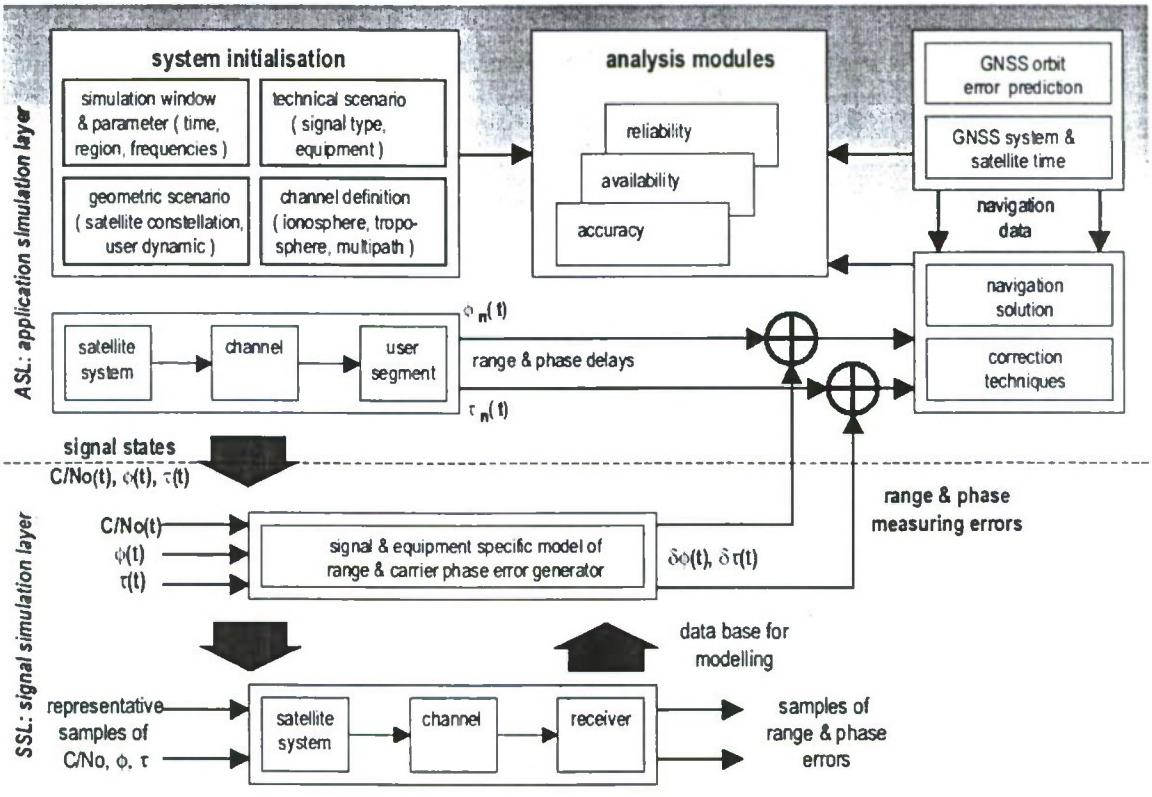

Fig.1 NAV–SIM architecture with the two layers for signal (SSL) and application simulation (ASL)

Each module is initialised by its own dialog window. The first window defines a set of global parameters like time and region of simulation and makes the selection of optional modules. To guarantee the correct parameters and its consistency of each module a parameter controlling is implemented. The simulation system can be used in four different basic modes depending on the composed system and selected modules:

- analysing the behaviour and influence of single components
- analysing the signal states like C/No, temporal and regional influence after estimation of attenuation, noise, code and phase delays and the corresponding rates
- estimation the navigation accuracy without signal and receiver influences for statistical analyse of accuracy and availability, and
- analysing the navigation solution including the signal level.

With these basic modes and the possibility of using each simulation level as a stand–alone tool the following results are generated by the NAV–SIM tool.

3. Effects on ranging performance by using different signal types

To get an improved bandwidth efficiency a suitable pulse shaping has to be used for the navigation signals of GALILEO. The Cramer Rao bound have to be determined to estimate the best ranging accuracy of a defined modulation format [1]. The performance of the ranging signal in the case of a rectangular (RECT) and root raised cosine (RRC) signal is shown in Fig.2. The RRC is the most promising option for the modulation pulse for the new navigation system, because of the allocated frequency bands and their bandwidths. The performance analysis of both options was calculated by simulations using an additive white Gaussian noise (AWGN) channel and an incoherent DLL. It can be seen, that the RRC option achieves the same performance with a lower C/No ratio than the RECT option. The observed gain is in the order of 1 – 2 dB–Hz [2].

To get a more realistic estimation of the achieved performance requires to look on the one hand on the influence of satellite components and on the other hand on the signal behaviour in the case of multipath afflicted environment. The first part is a point of interest for system engineers of satellite design and not discussed in this paper. To evaluate the influence of multipath on the signal performance five different sample channels are used in the simulation and their influence on the signal is shown in Fig.3 for selected C/No values. The most important outcome is the fact, that faster channel variations corresponds with smaller errors and vice visa. That the phase isn't influenced in any case was shown by additional simulations [2]. These simulations show also that a better ranging performance is achieved by using a RRC pulse shape instead of RECT pulse shape.

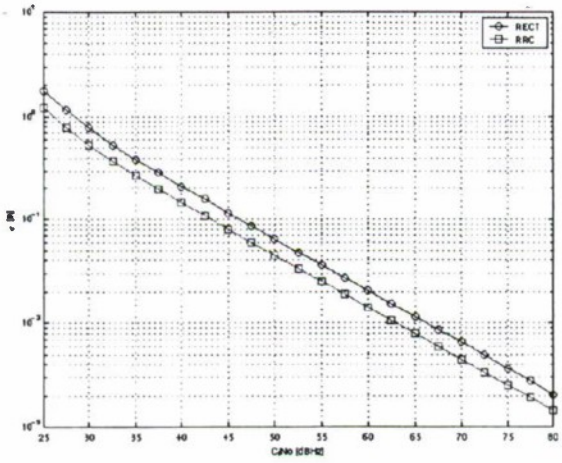

Fig. 2. Ranging Performance of Rectangle (RECT) and Root Raised Cosine (RRC) Pulse Shape

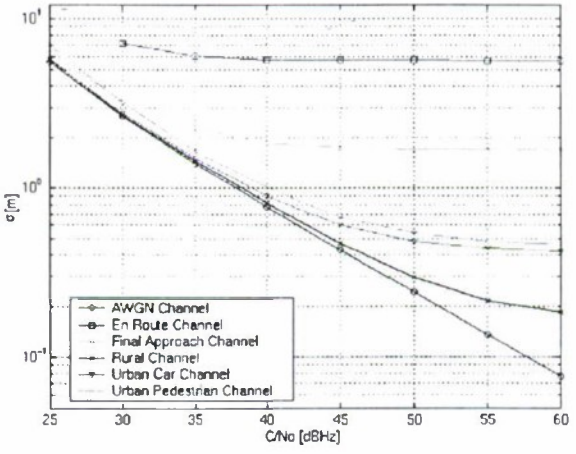

Fig. 3. Ranging Errors in Presence of different Kinds of Multipath Environments

4. Carrier–to–noise Ratio in Dependence on Ionosphere

To compare simulation results between the European navigation system GALILEO with the U.S. system GPS we have to use a defined satellite constellation for GALILEO. The satellite constellation which is finally used is still open. It looks like that a similar constellation is used to GPS, a so–called MEO–only Walker constellation with 27 satellites. The satellites will be symmetrically distributed over three planes with an anomaly shift between 0 and 20 degrees (27/3/1) plus 3 in–orbit spares on an additional Walker constellation(3/3/F) with an inter–plane phasing F of 0,1 or 2). For all simulation where a satellite constellation is necessary following scenario is used:

- Walker constellation 27/3/1
- anomaly shift 0 degrees

- In-orbit spares 3/3/0
- 23600 km altitude of circular orbits

In the case for GPS simulations the actual constellation of 27 operable satellites is used.

One important task is the estimation of the signal states at the receiver input described by the carrier to noise ratio C/No to analyse which signals should be used for positioning. The use depends on the occurred disturbances during transmission and on the tracking performance of the receiver equipment. Fig.4 shows the carrier to noise distribution of GPS L5 frequency at the Greenwich meridian over 12 hours. The simulation was done for stand ionosphere without scintillations. The influence by the ionosphere onto the carrier to noise ratio in middle Europe for the allocated GALILEO frequency bands E1 and E3 is displayed in Fig.5. For this simulation a transmitting power of 18,4 dBW was used. C/No without ionospheric scintillations are distributed between 47 and 54 dB-Hz for the frequency E1 (red graph) and between 49 and 57 dB-Hz for the frequency E3 (blue graph).

The magenta and green graph shows the influence of ionospheric scintillations. The spreading can be temporary in the order of several 10 dB-Hz, therefore, this effect must be considered for improved accuracy, availability and reliability estimations. The probability for C/No ratios lower than 20 dB-Hz is only 0.02 percent for both frequencies. Assuming that such value of carrier to noise ratio causes a loss of locks the occurrence of scintillations should not to be sneezed.

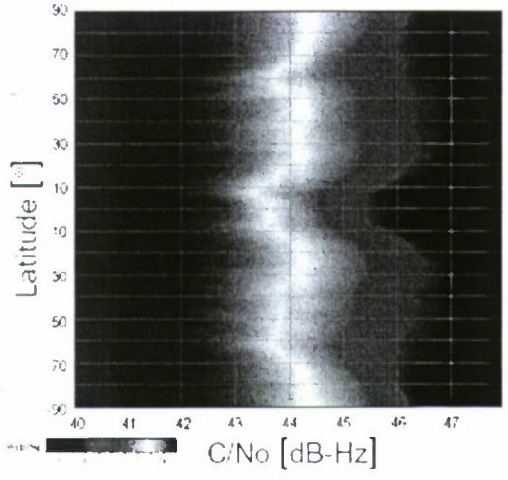

Fig. 4. Carrier-to-Noise Ration of GPS L5 at the Greenwich Meridian over 12 hours

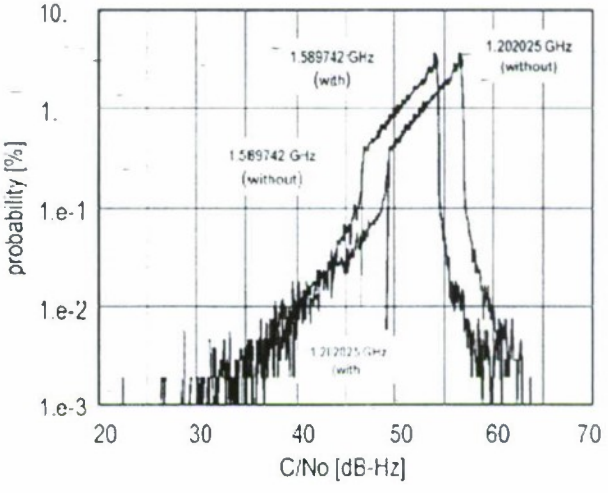

Fig. 5. Carrier-to-Noise Ratio of GALILEO E1 and E5 with and without ionospheric scintillations over 24 hours

5. Satellite Availability

One of the most interest point is the satellite availability of GALILEO compared to GPS. In Fig.6 four different situation are displayed. Fig.6a) shows the satellites in view at the 60th longitude over 1 day for the normal GPS satellite constellation and an elevation angle of 10°. The number of visible satellites is varied between four , which is the minimal number to get a position solution, and a maximum number of 12 satellites for short time. Looking on the subfigure b) the same situation is calculated for the GALILEO constellation and it is easy to see that in the worst case a minimal number of 6 satellites are visible for the complete simulation time.

For some applications a greater number of visible satellites are useful. Therefore, a combination of both satellite system is discussed. This means that both systems have to be compatible in a special way, but they must not be identical. In this case the number of available satellites grows up to minimal number of 10. If the user want to navigate in urban environments he has two problems: first problem is the multipath influence on to the signal, which can be solved with new signal forms, and the second problem is the number of satellites in view under high elevation angles (e.g. 35°). Using both systems the second point is solved displayed in Fig.6d). Comparing GPS only with GPS & GALILEO under an elevation angle of 35° it can be seen that both have nearly the same distribution (see Fig.7 and Fig.8, St. Petersburg, 23rd of May 2002). In 97% of the simulation time six and more satellites are available for the positioning solution under high elevation angles. This one of the best reasons to built-up an own European satellite navigation system.

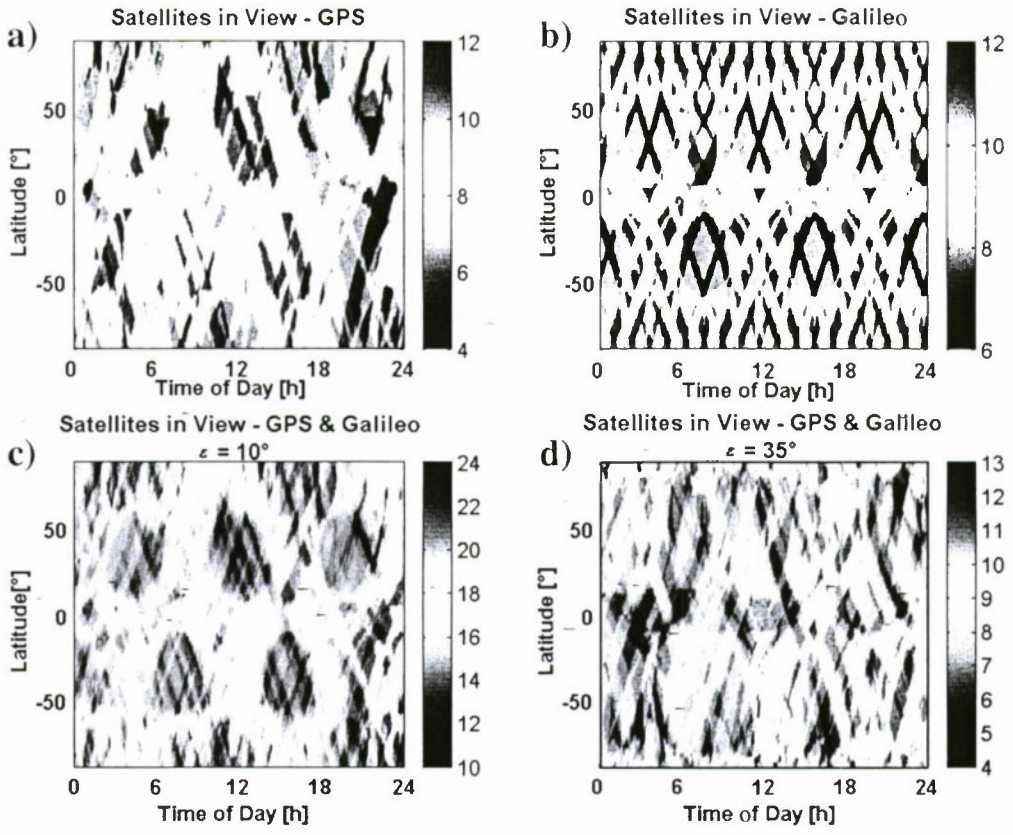

Fig.6. Satellite Availability of GPS (a), GALILEO (B), GPS & GALILEO with an Elevation Angle of 10° (c) and 35° (d) over 24 hours at Longitude 60°

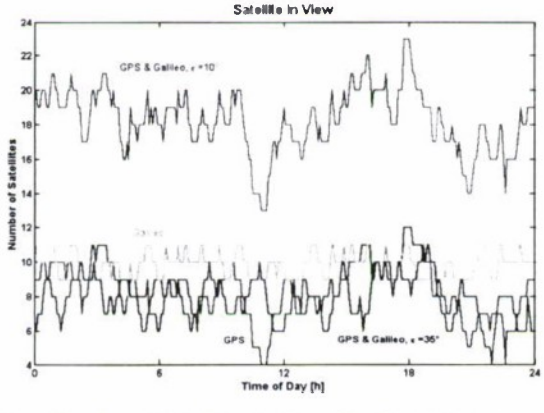

Fig. 7 Number of Satellites in View for St. Petersburg (23rd of May 2002)

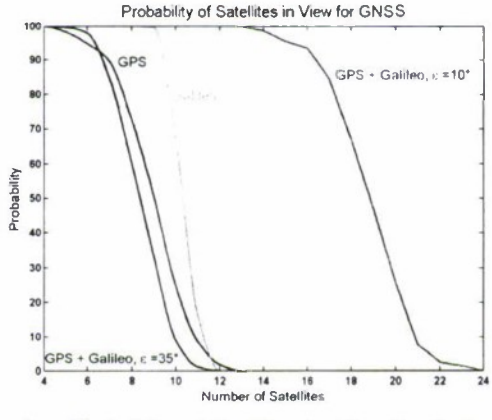

Fig. 8 Probability of Satellites in View for St. Petersburg (23rd of May 2002)

6. GALILEO Clock and System Time

For all satellite navigation systems like GPS, GLONASS and GALILEO it is necessary to have a precise synchronisation of all satellite clocks to a common time scale, called system time. The deviations of the satellite clocks from this system time directly impact the accuracy of the navigation solution. Therefore, it is planned to use passive H-maser onboard the satellite as the main clock in GALILEO. The passive H-maser has a greater stability as the caesium and rubidium clocks used by all other existing systems. In the case of a failure a switch between this H-maser and a hot redundant working rubidium clock will be realised. The system time will be provided by two Precision Timing Facility (PTF). One of the discussed assumptions contain that each PTF contain

an ensemble of 12 high precise caesium clocks steering an active H-maser. These clock ensembles ensure the necessary stability of the system time.

The model of the time error of a physical clock can be divided into a deterministic and a stochastic component, where the deterministic part can simply be modelled with a second order polynomial. The simulation of the stochastic error behaviour of the clock based on the well known power law model for the output of an oscillator. This model says that the stochastic error signal of an oscillator $y_s(t)$ can be represented most suitably by means of the following spectral density

$$S_y(f) = \begin{cases} \sum_{\alpha=-2}^{+2} h_\alpha \cdot f^\alpha & for \quad f \le f_h \\ 0 & for \quad f > f_h \end{cases} \tag{1}$$

where f_h is the cut-off frequency and h_α is a coefficient.

The model covers all known stochastic noise types of an oscillator, which are called 'random walk frequency modulated noise ($\alpha = -2$)', 'flicker frequency modulated noise ($\alpha = -1$)', 'white frequency modulated noise ($\alpha = 0$)', 'flicker phase modulated noise ($\alpha = 1$)' and 'white phase modulated noise ($\alpha = 2$)'. The system time of a satellite navigation system is normally not the time of a single clock but a so called ensemble time, which is calculated from the measurements of many high stable atomic clocks.

The system time is normally calculated by using a weighted least square formulation. The NAV–SIM tool allows the simulation of the error effects caused by real physical clocks as well as the resulting system time error. In Fig. 8 the results of the simulation of the GALILEO clocks is depicted, which are passive H-masers and rubidium clocks onboard the satellites and caesium clocks as the clocks for the system time generation on ground over a long (about 34 days) time period. It is easy to see that the rubidium clock has the worst long time behaviour and the caesium standard has the best long time stability. Therefore the Caesium clocks are the best choice for generating a precise system time with a high long time stability. Fig.10 shows the simulation results of the system time stability for the supposed use of 24 Caesium clocks and the stability of the emitted system time from the satellites. The short time stability of the emitted system time is not so good than the ground generated system time but better than a single Caesium clock.

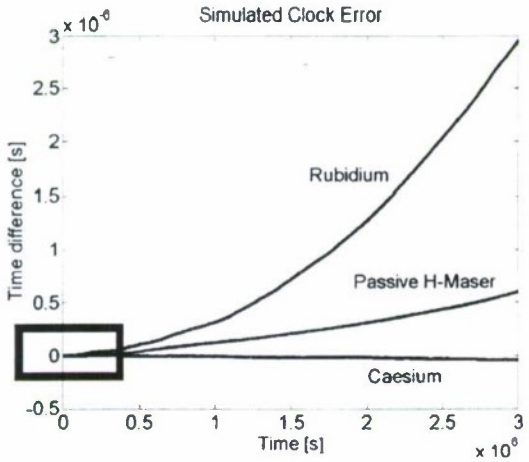

Fig. 9. Clock Error over a Long Time Period

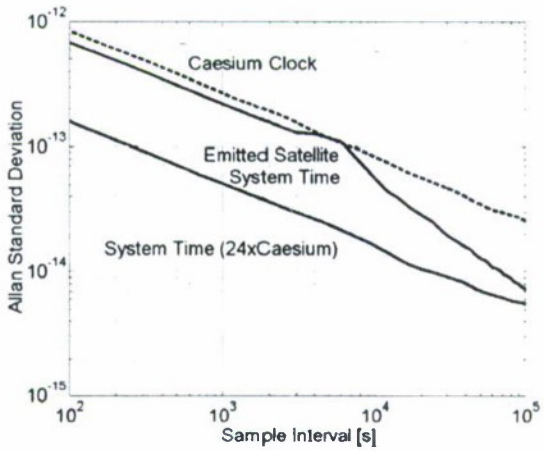

Fig. 10. Allan Deviation of the System Time

7. Conclusion

This paper presents at first an overview of the software tool NAV–SIM which was developed by the German Aerospace Centre. It has highlighted some of the features of NAV–SIM which are suited to demonstrate the possibilities of this simulation tool.

The currently available simulator can be used for the following types of analyses independent of the satellite navigation system:

- estimation of signal states at the receiver input described by range and phase delays, the corresponding rates and the carrier to noise ratio inside a temporal and spatial window
- composition of GNSS observations (ranges & phases) and corresponding estimation of the accuracy and availability of positioning

- extended composition of GNSS observations (range & phases) including an error generator model (receiver type dependent accuracy of range and phase measurements) and corresponding estimation of the accuracy and availability of positioning
- estimation of GNSS reliability by evaluation of several simulation runs with different spatial and temporal windows for typical static and dynamic applications

It was shown that many aspects of satellite navigation system can be simulated with high accuracy comparing to realistic effects (e.g. satellite clocks, system time, signal pulse shape). Using a special simulation scenario the paper shows the necessity to built–up the European navigation system GALILEO, too.

Acknowledgement

The author would like to acknowledge the German Government (BMBF) represented by PT-BEO as the sponsor of the project (contract number 03 NC 9706). He would also thank Thoralf Noack, Stefan Schlüter and Alexander Steingaß for the execution of simulations and motivated discussion. At last all members of the project team should be mentioned: Michael Angermann, Evelin Engler, Achim Hornbostel, Rainer Krämer, Hans-Peter Müller, Helmut Nickl and Jesus Selva.

References

1. **B.W. Parkinson and J.J. Spilker**: "GPS: Theory and Applications Volume I", Progress in Astronautics and Aeronautics, Vol. 163, 1996
2. **J. Clynch, C. Henry :** "Ionospheric Effects on GPS and DGPS in Polar Regions ", Proceedings of the ION GPS-94, Salt Lake City, September 1994, pages1579-1587
3. **A. Steingass:** "Pulse Shape for Navigation Systems in a Multipath Environment", Proceedings of the 2001 National Technical Meeting, ION, Long Beach 2001, pages 614-617.
4. **E. Engler, A. Steingass, S. Schlüter:** "End to End Simulator for the Evaluation of GALILEO", GALILEO's World, Summer 2001.
5. **R.Lucas, J. Hahn, S. Dinwiddy, J. Benedicto, M. Lugert, G. Gatti**: "Galileo Space and Ground Segment Definition: System and Performance", Pre-Print of a publication for ION-GPS 2000, Salt Lake City, Utah, 19-22 September 2000
6. **S. Schlüter, T. Noack:** "Simulation of Scintillation Effects in NavSim", ect 2000, Mai 2000
7. **E. Engler:** "Capability of the SW simulation system developed by the DLR in the project NavSim", etc2000, Mai 2000
8. **R. Krämer:** "High Precise Clock Simulation Included in the Modular Software Simulator for Navigation Systems NavSim", etc 2000, Mai 2000
9. **R. Schweikert, T. Wörz, R. De Gaudenzi, A. Steingass, A. damman:** "On Signal Structures for GNSS2", International Journal of Satellite Communications, Vol. 18, 2000, pages 271-291
10. **Steingass, J. Furthner, E. Engler et al:** "Modular end-to-end software simulator for navigation systems", GNSS 1999, Genua, 8.10.1999
11. **S. Schlüter, E. Engler:** "Simulation of Ionospheric Corrections Regarding of Solar Activity on GNSS", ETT /SATNAV 99, Potsdam, 10.11.1999
12. **E. Engler, A. Jungstand, H.-D. Bettac:** "Ionospheric Influence in Satellite Signals in the GHz Range", Proceedings of the European Telemetry Conference, Germany, May 04 to 07, 1998, pages 437-444.
13. **J. Nichols, A. Hansen, T. Walter and P. Enge:** "Observations of Equatorial Scintillation Using GPS Receiver", Proceedings of the ION GPS-99, Nashville, September 1999, pages1451-1460.
14. **Steingass, A. Dammann, M. Angermann, R. Schweikert, T. Wörz:** " The Impact of High Powwer Amplifier and their associated Lowpass Filters on Pseudorange accuracy and the Spectrum of the Signal", Proceedings of the Global Navigation Satellite Systems Conference, Genua 1999, Italy.

ASSESSMENT OF USING C-BAND FOR NAVIGATION SIGNALS

J. Hammesfahr, A. Dreher, A. Hornbostel, Z. Fu

Deutsches Zentrum für Luft- und Raumfahrt (DLR)
Institute of Communications and Navigation
Postfach 1116, D-82230 Wessling, Germany; E-mail: jens.hammesfahr@dlr.de

Abstract

Key words: Satellite navigation, C-band, Galileo, digital-beamforming antenna

Current satellite navigation systems are based on signals-in-space in the range of some 1.2 to 1.6 GHz. A lot of experience exists about the quality of signals and their decoding in receivers within this band. Due to a recent frequency allocation, C-band additionally offers a new quality to satellite navigation which has to be carefully investigated before it can be used in any operational service. The aim of this paper is to shortly summarize status and expected performances when using C-band frequencies for navigation by Galileo satellites. The paper assumes that the reader is well aware about the performance of L-band navigation. That's why mainly the differing aspects of C-band with respect to L-band use are highlighted.

The paper describes the main technical aspects which affect the navigational accuracy of Galileo signals when making use of C-band. Political or legal matters have not been addressed. The paper considers the signal chain which generally is split into 3 sections, namely signal generation and transmission, signal propagation, and signal reception and decoding. Emphasis is put on the atmospheric signal delay (being smaller in C-band) and on the signal attenuation (being higher).

Additionally, a short overview is given on in-band interferences which are a very important issue because C-band provides low interference levels, thus making it attractive for safety critical applications (at least on a regional basis).

This is followed by some assessments on the user terminal, including the antenna. It's because of the low signal levels that the receiver antenna design plays a very important role and is discussed in detail. Advanced beamforming and receiver technologies can solve this problem and at the same time enhance the performance of the whole system decisively.

Finally, a condensed summary of all the findings with an interpretation of their effect on the total system performance is given.

1. Introduction

Current navigation systems are based on signals-in-space in the range of some 1.2 to 1.6 GHz. Also the present design of the European Galileo system is looking to use this band. However, several navigation frequency bands were allocated at WRC2000 by ITU. One of it is a 20MHz band from 5010 to 5030 MHz. This "C-band" shall be used for downlink (space to earth) directions. The band is ARNS (aeronautical radio navigation) protected. Another frequency band had been allocated to Galileo. That's the band from 5000 to 5010 MHz. This is to be used for RNSS (radio navigation satellite service) earth-to-space links and will not be assessed for navigational use in this paper.

C-band offers a new quality to satellite navigation which has to be carefully investigated before it can be used in any operational service. The aim of this paper therefore is to shortly summarize status and recent investigations on the special qualities when using C-band frequencies for navigation by Galileo satellites. The paper highlights the differing aspects of C-band with respect to L-band use.

Stress is laid on those aspects where differences exist between the use of L-band signals — as being used with GPS — and the use of C-band frequencies. The following table presents an overview of the main different properties related to the signal:

Table 1 — Main signal properties being different between L-band and C-band

parameter	L_1-band	C-band	consequences for C-band
carrier frequency	1575 MHz	5020 MHz	♦ higher free space transmission losses ♦ higher attenuation (rain, foilage) ♦ higher atmospheric noise ♦ less propagation delays (ionosphere)
max. carrier Doppler shift (static user)	5 kHz	17 kHz	♦ PLL search time longer if not optimized ♦ PLL loop bandwidth affected by user acceleration and jerk
downconversion mixing frequency for baseband frequency of 40 MHz	1535 MHz	4980 MHz	higher complexity if double conversion to IF needed

A signal design for C-band services within Galileo has not been performed yet. On the other hand, the frequency band to be used will have a width of 20 MHz. Accordingly it is assumed that the signal spectrum will be limited by the 20 MHz requirement without considerable power in spectral lines outside this band. Therefore the design of navigation signals within C-band is expected to be made very similar to L-band frequencies.

Resulting from these considerations it is very likely that navigation signals generated on board the Galileo satellites in C-band will have more or less an identical signal spectrum with regard to L-band, the only difference being the carrier frequency.

Also signal transmission in C-band is mostly a state-of-the-art technique because of the widespread use in communication systems, but with some higher frequencies in navigation. The following sections therefore address primarily aspects of signal propagation and receive antenna. This includes considerations about the link budget for C-band navigation signals.

2. Signal Propagation

In this section, signal propagation in the atmosphere is addressed, subdivided into ionospheric and tropospheric effects. Special emphasis is put on the signal delay (being smaller in C-band) and on the signal attenuation (being higher).

Tropospheric delay

Since the atmosphere is not a homogeneous medium it generally will be divided into different layers. The atmospheric delay in the lower layer (neutral atmosphere) is commonly called tropospheric delay, although it includes contributions both by the troposphere and stratosphere. The refractive index ($n > 1$) of the earth's neutral atmosphere reduces the propagation speed of radio frequency signals. The gradient of the refractive index with height causes additionally a curvature of the propagation path. Both effects lead in the sum to a delay of satellite navigation signals in comparison to free space propagation. Delays in C-band and L-Band are identical and the same correction models can be applied. Typical models of the tropospheric delay calculate the delay in vertical direction (zenith delay) and derive the delay at other elevation angles by multiplication with so-called mapping functions.

The tropospheric delay can be expressed as an excess path in addition to the geometric path length by integration of the tropospheric refractivity $N=10^6 \cdot (n-1)$ along the curved path through the neutral atmosphere, where n is the real part of the refractive index:

$$\Delta L = 10^{-6} \int_L N(s) ds. \qquad (1)$$

Tropospheric attenuation

The path attenuation due to atmospheric gases is generally low both for L-band and C-band (less than 0.1 dB at zenith). At L-band frequencies which are used by the current satellite navigation systems GPS and GLONASS attenuation and noise due to rain are negligible. However, in C-band the rain attenuation and noise increase and can reduce the signal-to-noise ratio during intense rainfall by some dB.

The specific attenuation γ_R in dB/km depending on the rain rate R in mm/h can be calculated by:

$$\gamma_R = aR^b [\mathrm{dB}]. \qquad (2)$$

The coefficients a and b are listed for linear and vertical polarization and different frequencies in [1] . Finally, the following values are obtained for L-Band and C-band by linear interpolation of the values and conversion to circular polarization, with equations also given in [1].

Table 2. — Coefficients for specific rain attenuation

Coefficient	L1 (1.2 GHz)	L2 (1.6 GHz)	C (5.02 GHz)
a	0.000059	0.000102	0.001146
b	0.9063	0.9252	1.1954

For L-Band, rain attenuation is negligible. For C-band, the specific rain attenuation is 0.28 dB/km for R=100 mm/h and 0.65 dB/km for 200 mm/h.

The following figure shows the zenith attenuation due to rain and atmospheric gases for different rain rates for a rain height (vertical extension of the rain layer) of 3 km.

For elevation angles ε decreasing from zenith, the path attenuation rises by a factor of $1/\sin\varepsilon$.

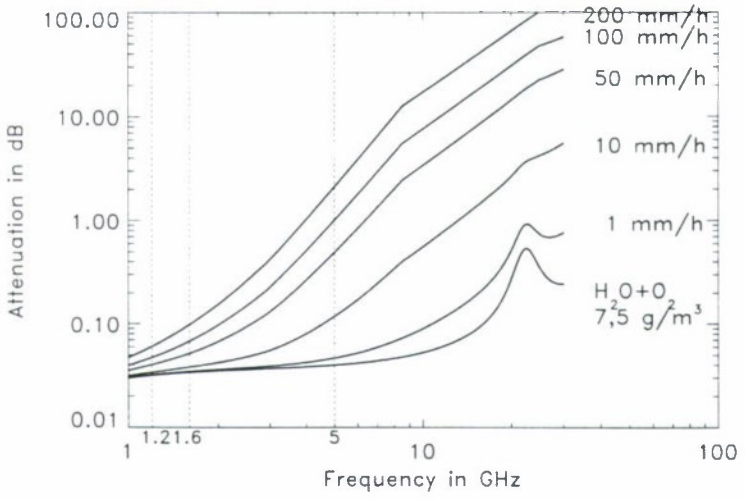

Fig.1. Zenith attenuation versus frequency for different rain rates (rain height 3 km)

Tropospheric noise

By the realistic assumption that tropospheric attenuation is only due to absorption there is a direct relation between thermal noise temperature and attenuation (Kirchhoff's law).

The noise temperature in path direction depends on the effective medium temperature of the troposphere (ca. 270 K) and the path attenuation. Thus the antenna noise temperature depends on the beam characteristic. However, the antenna picks up noise from all directions. For clear sky, the zenith attenuation in C-band is about 0.05 dB. 3 dB is an upper value for zenith rain attenuation.

For high elevation angles the noise figure for a hemispherical antenna is higher than the path noise, but for low elevation angles it is vice versa.

Tropospheric scintillations are fast noise-like fluctuations of signal amplitude and signal phase due to short scale variations of the refractive index, which are caused by turbulences in the atmosphere, rain and clouds. For elevation angles above 15 degrees, the fade depth for L-band caused by amplitude oscillations is less than 0.7 dB. For C-band, the fade depths are about 2 times higher than in L-Band.

Ionospheric delay and attenuation

In the ionosphere, the refractive index is dispersive and the delay decreases with the square of the frequency. Therefore the delay in C-Band is reduced by a factor of 10 in comparison to L_1 and by a factor of 17 compared to L_2. Because all correction models are based on the determination of the total electron content in the ionosphere (TEC), the residual error depends linearly on the uncertainity of the TEC estimation. Due to the frequency dependency, the resulting range error in C-band is also by the factor 10 to 17 smaller than in L-Band for the same TEC uncertainty. Therefore in C-band simple correction models are sufficient. For most of the applications two frequency measurements for determination of the TEC are not required. It is known that ionospheric scintillations (amplitude and phase) can lead to a signal loss in L-Band. However, when the signal still is locked, the range variations due to phase scintillations should also be reduced compared to L-Band.

In contrary to the troposphere and stratosphere, the ionosphere is a dispersive medium, where group and phase delay of radio waves have different signs and depend on frequency.

The delay of signals at frequencies above 100 MHz due to ionospheric refraction can be calculated by neglecting high order effects by [2]:

$$d_{ion} \approx \pm \frac{40.3}{f^2} TEC \,, \qquad (3)$$

where d_{ion} is the range error due to ionospheric delays in meters, having positive sign for code measurements and negative sign for carrier phase measurements. f is the carrier frequency (Hz) and TEC the number of free electrons within a column of 1 m² cross section along the propagation path.

Other effects like rotation of the polarization plane or the geometric Doppler shift will not be considered here.

The magnitude of the effects depends on the carrier frequency and on the concentration and distribution of the electron densities within the ionosphere. Similar to the temperature distribution within the troposphere, the electron density distribution is a very complex parameter.

Table 4 shows the ionospheric range error for typical maximum and minimum TEC values in zenith direction (VTEC) for different frequencies. In L-Band, the zenith error can reach 18 m, in C-band the error is reduced by a factor of 11 having a maximum value of 1.6 m. For lower elevations the error can increase by a factor of 3 to 3.5 due to the longer path lengths.

Table 3. Ionospheric range error in zenith direction for low and high limits of vertical TEC values

Frequency	TEC=10^{16}el/m²	TEC=10^{18}el/m²
100 MHz	40 m	4030 m
400 MHz	2.5 m	250 m
1.5 GHz	0.18 m	18 m
5 GHz	0.016 m	1.6 m
10 GHz	0.004 m	0.4 m

Additionally, short scale and short term variations of the electron density occur in the ionosphere, e. g. due to particle showers in the polar regions or instabilities in the equatorial region. Those ionospheric scintillations can lead to short time signal fades of up to 20 dB and finally to the loss of a signal in L-band. This amplitude effect is expected to decrease with frequency ,thus being smaller in C-band (roughly by a factor of 0.2).

Atmospheric influence

To summarize the frequency dependency of both tropospheric and ionospheric effects, Fig. 2 represents an overlay of tropospheric attenuation and of ionospheric delay which are the driving factors for signal propagation. It demonstrates that C-band represents a good compromise with respect to rain attenuation and ionospheric delay. The probabilities shown for the rain rate are indicated for ITU-R rain zone K (e.g. Munich).

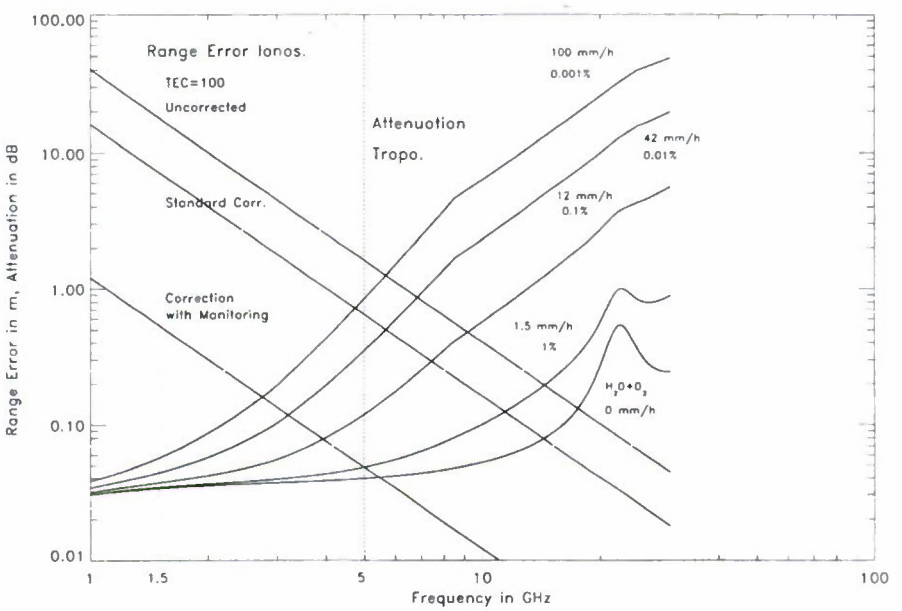

Fig.2. Frequency dependency of atmospheric errors in zenith direction

Free space loss

The investigations on atmosphere have demonstrated that signal delays in C-band are lower than in L-band and also reduce the uncertainty by improper modelling or measuring (2 frequencies). On the other hand, signal attenuation plays a dominant role in C-band. Two terms of attenuation are important. The first one has been described already and is caused mainly by the content of rain in the atmosphere. The second type of "attenuation" is the loss γ_{fs} between two isotropic radiators in free space. It depends on the range r and on the wavelength λ:

$$\gamma_{fs} = \left(\frac{4\pi r}{\lambda}\right)^2. \qquad (4)$$

That is why for C-band (shorter wavelength) this loss is considerably higher than for L-band. However, it must be taken into account that the RX signal level is independent of the wavelength, if transmitting-antenna gain and receiving aperture are kept constant.

3. Link Budget

Having investigated the most important attenuation effects, now a representative link budget for 5° elevation is presented. It is based on Galileo orbits and the assumption that signal properties on board the satellites are the same for L-band and for C-band. Results are given for two different rain zones (assuming a system availability of 99.99% and 99.999% respectively) and two different types of receive antennae for C-band.

Table 4. Link budgets for equal L_1 and C band transmit powers

	Rain zone L , 5°, 99.99%			Rain zone Q, 5°, 99.999%		
	L_1	C	C high gain	L_1	C	C high gain
Satellite power [dBW]	14.7	14.7	14.7	14.7	14.7	14.7
Satellite antenna gain [dB]	15	15	15	15	15	15
Output filter insertion loss [dB]	-1.5	-1.5	-1.5	-1.5	-1.5	-1.5
EIRP [dBW]	**28.2**	**28.2**	**28.2**	**28.2**	**28.2**	**28.2**
Free space loss [dB]	-184.4	-195.5	-195.5	-184.4	-195.5	-195.5
Troposheric attenuation [dB]	-0.4	-1.6	-1.6	-0.4	-3.8	-3.8
RX signal level [dBW]	**-156.6**	**-168.9**	**-168.9**	**-156.6**	**-171.1**	**-171.1**
RX antenna gain [dB]	3	3	18	3	3	22
Noise power density [dBW/Hz]	-210	-208.9	-206.8	-210	-205.8	-205.4
C/N_0 (antenna output) [dB/Hz]	**56.4**	**43**	**55.9**	**56.4**	**37.7**	**56.3**

The table reveals the wider range of received signal levels in C-band with respect to L-band. This is caused by the variations in troposphere depending on the severeness of precipitation. The attenuation varies largely from dry air to wet air. Such a variation comes in addition to the variation of free space attenuation due to the change in distance to the satellite. Larger signal level variations require a more sophisticated gain control within the receiver equipment.

For Europe (rain zone L) there is a 13 dB degradation in C-band when similar receive antennae are to be used. This could be compensated by an 18 dB antenna gain leading to a comparable C/N_0 . For worst precipitation conditions (rain zone Q with a 0.001% probability) at a very low elevation angle of 5°, the receive antenna gain theoretically has to be 22 dB to get equal carrier-to-noise performance between L-band and C-band. This requirement will be further discussed in section 6.

This comparison shows the most critical issue when using C-band frequencies for navigation, i.e. signal level. Some countermeasures have to be taken to compensate for this considerable deterioration of the received power level. But before discussing this, an additional noise effect of the receiver hardware has to be studied.

4. Receiver Noise

In order for the GNSS receiver to successfully derive pseudoranges to the selected space vehicles (SV), the code and the carrier signals of the desired SV must be restituted simultaneously. Consequently the GNSS signal acquisition and tracking process is a two-dimensional (SV code and carrier) signal correlation process. The GNSS receiver must keep the phase and frequency of its own replica of the code and carrier signals at maximum correlation with the desired SV code and carrier phase, including Doppler shifts.

Operation in C-band affects the signal processing by the shorter wave length and by higher dielectric losses. The wavelength has to be considered for the antenna design (discussed in later paragraph). The effect of additional material losses is assumed to be less than 0.5 dB and will be neglected here.

In GNSS receivers, the PLL to track the carrier frequency is the most critical signal restitution part. Thus the performance of the PLL can be used to express the performance of the whole receiver. A scheme for a typical carrier tracking loop is shown in the subsequent figure.

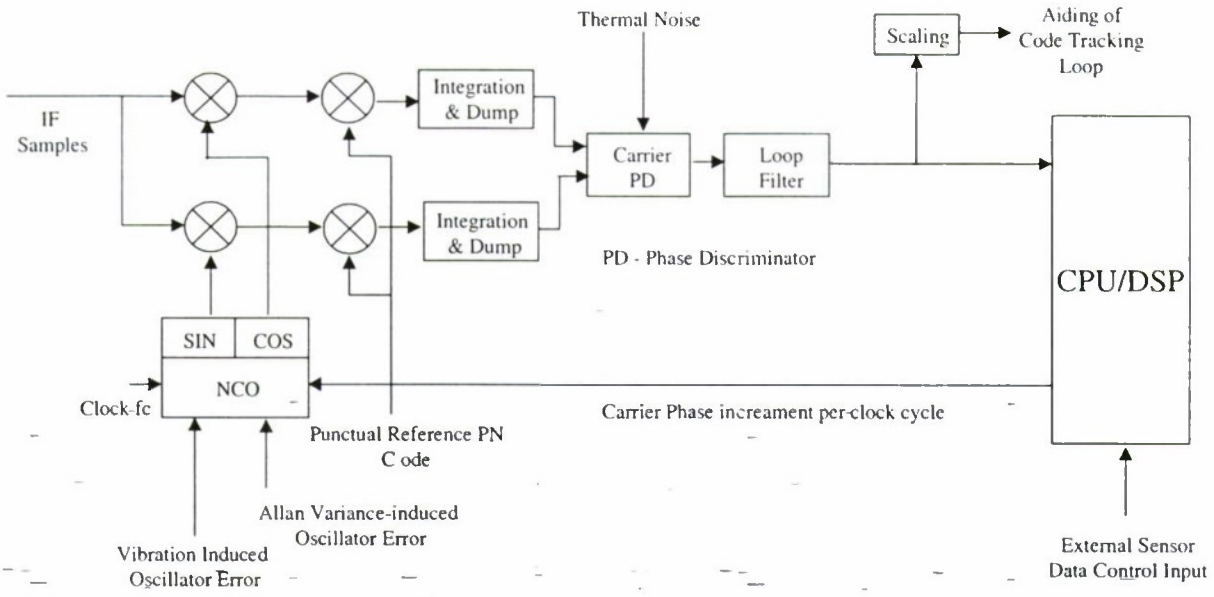

Fig. 3. Structural block diagram of a carrier tracking loop

Without explaining this structure, attention should be concentrated on the numerical controlled oscillater (NCO) in the lower left corner, producing I and Q reference frequencies. This oscillator is steered by a processor, but also is influenced by external physical factors illustrated in the scheme by two arrows from beneath. That is because a crystal oscillator is affected by temperature changes (mostly long term variations) but also by very short variations (vibrations, gravity when changing attitude). Those short-term variations induce an additional noise on the carrier frequency within the receiver.

Generally the carrier tracking error varies with the square of the carrier frequency. This is caused by the low frequency phase noise of the local oscillator. If the total measurement errors induced by the PLL/FLL exceed the tracking thresholds (i.e. the effective C/N_0 below which the carrier tracking loop no longer can be hold locked) the receiver cannot detect the signal. Because of the high non-lincarity of the tracking loops, it is very difficult to analyze the true tracking performance of the receiver. However, rules-of-thumb can be used based on equations that can approximately predict the dominant measurement errors [3].

As an example, for a PLL the 1-sigma rule-of-thumb lock condition can be expressed by the following formula:

$$\sigma_{TPLL} = \sqrt{\sigma_{PLL}^2 + \sigma_A^2 + \sigma_V^2} + \frac{\theta_{Dy}}{3} \leq 15^\circ \qquad (5)$$

with
- σ_{TPLL} PLL total measurement error
- σ_A jitter induced by the Allan variance of the crystal oscillator
- σ_V jitter induced by vibrations of the oscillator
- θ_{Dy} dynamic stress error of the PLL

Several simulations have been run to test the expected performance of a C-band receiver carrier tracking loop in comparison to a similar L-band receiver. The results are depicted in figure 4.

It can be seen that because of the vibration and stress error and the Allan variance jitter, the C-band PLL at $B_L=18$ Hz cannot operate in lock state. In order for the PLL to operate in lock, the bandwidth has to be changed from 18Hz to 25Hz. Then the minimum C/N_0 required to achieve a tracking threshold of better than 15 degrees changes from about 27dB-Hz in L-band to about 32 dB-Hz in C-band. Therefore a comparable tracking performance to L-band can be reached in C-band by a 5dB-Hz larger C/N_0 only.

In order to compensate at least partially for this 5 dB loss, an FLL-aided PLL can be used for C-band. That's because a FLL greatly outperforms a PLL in dynamic stress situations but the measurement accuracy is lower than that of a PLL. Therefore an optimal combination of PLL and FLL has to be developped. The disadvantage of C-band for such a technique is anticipated to be 2.5 dB (in table 5 named "equivalent dynamic PLL loss").

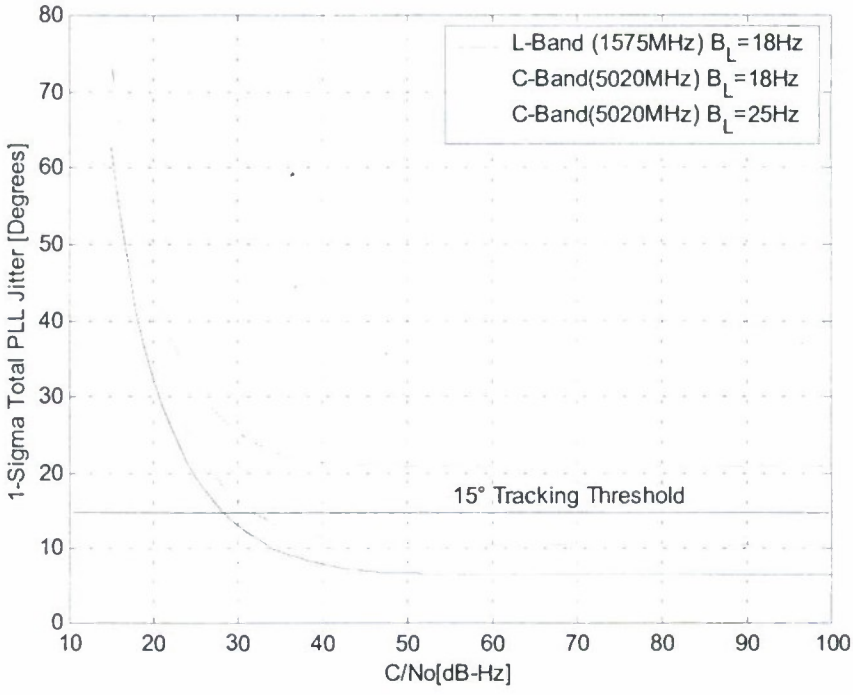

Fig. 4. Total PLL tracking jitter for a third order carrier loop

5. Interference

The band 5000 –5100 MHz is primarily allocated to acronautical radionavigation. Currently it is being used for operation of Microwave Landing Systems (MLS).

The band 5010-5030 MHz was allocated for satellite navigation on a primary basis. To date, there are no other satellite navigation services besides Galileo planned for this band. There are some (less then 5) aircraft-carrier based systems known in the UK which operate in the band 5000 - 5030 MHz but are only used on sea. In the operational radius of these systems, disturbances to satellite navigation receivers may be expected [4]. These are the only in-band interferers known for C-band.

More critical is the MLS Band, where sometimes out-of-band interference from MLS above 5030 MHz could occur. Until December 2015 the frequency range 5091-5150 MHz is also used by feeder links for fixed satellite services. Galileo C-band receivers in aircrafts must be protected by suitable filtering, to make sure that they do not receive power above 5030 MHz on one hand and do not cause harmful interference to the MLS equipment on the other hand.

A new source of interference could appear with the introduction of ultra-wideband systems (UWB) . These are systems which transmit very short pulses in a bandwidth of up to 25% around the center frequency and therefore could cover several allocated neighbouring bands. The peak power can be 1 kW. Potential applications are in radar detection, remote sensing and communications as well as for the mass market and industry. First tests in the USA have shown that a single UWB can cause harmful interference to GPS-receivers [5]. In the near future, UWB systems will be used only with low power as unlicensed services. This type of interference is a similar threat to C-band as well as to L-band. However, signal power decreases much faster in C-band with growing distance from the interfering source.

Thus, presently the danger of harmful interference to satellite navigation receivers is considerably smaller in C-band than it is in L-band. In-band interferers are not known with the exception of some aircraft-carrier based systems in the UK. Due to the higher free space transmission loss the range of interference sources is smaller in C-band than in L-band.

6. Requirement for user antenna gain

Having investigated all factors for the carrier-to-noise ratio, now we are able to look at a representative link budget comparison between L and C. This calculation uses the same signal propagation assumptions as in table 4 but a different transmit power of 125W for C-band. This power level is technically feasible but requires additional ressources (power, weight). Results are given in Table 5.

Table 5. Representative link budgets for equal C/N_0 (rain zone L — Europe, 5° masking angle)

	L_1	C
Satellite power [W]	30	**125**
Satellite power [dBW]	14.7	20.9
Satellite antenna gain [dB_i]	15	15
Output filter insertion loss [dB]	-1.5	-1.5
EIRP [dBW]	28.2	34.4
Freespace attenuation [dB]	-184.4	-195.5
Troposheric attenuation [dB]	-0.4	-1.6
RX signal level [dBW]	-156.6	-162.7
RX antenna gain [dB]	3	**15**
Noise power density [dBW/Hz]	-210	-206.8
Equivalent dynamic PLL loss [dB]	0	-2.5
PLL effective C/N_0 [dB/Hz]	**56.4**	**56.6**

This budget demonstrates that navigation by using C-band signals is possible if a directive antenna of some 15dB gain is used at user sites. On the other hand, without such a type of antenna, tracking of the signals in most cases is not possible. At rare occasions of higher rain rates, tracking performance is degraded further. However, this can be compensated by excluding low elevation angles (results above are for a mask angle of 5 degrees). Moreover, there is less interference noise in C-band. However, presently this cannot be quantified.

7. User Antenna

The explanations on signal propagation above indicate that in C-band a compensation is needed to cope with the signal attenuation by free-space loss and troposphere. One countermeasure is to use directional user antennae with medium gain instead of low-gain hemispherical characteristics. Interferences caused by multipath propagation and jammers can be reduced by enhancing the signal-to-noise ratio in the direction of the satellite and lower the gain or generate nulls towards the interferer. This results in a higher accuracy of the navigation system. For the navigation process, at least four satellites are necessary. Including more satellites will enhance the exactness and reliability of positioning. Thus, the antenna must generate at least four beams with autonomous beamforming and steering to guarantee the required links for any satellite constellation and any alignment of the user terminal. For all-in-view receivers, generally a higher number of beams is required. Moreover, suitable algorithms are necessary to track the satellites and detect code multipath propagation and interferers.

An advanced technique to realise a smart multibeam antenna with the required flexibility is the concept of digital beamforming (DBF) [6]. To demonstrate the principle, a scheme is shown in Figure 5 for a system of four antenna elements. Each antenna element is equipped with a complete receiver path including low-noise amplifier, mixer and analog-to-digital converter, whereby the beamforming procedure is completely shifted to the processor. In contrast to conventional phased arrays which require complicated and costly multibeam architectures and networks, no electronically tuned components are necessary at RF-level. The accuracy can be enhanced significantly using calibration and error-correction procedures to compensate for drift effects and keep the quality of data independent of external physical influences.

Within the framework of a recent user antenna development, a demonstrator with a 5×5 C-band array was developped and tested [7]. The size of this 5×5 array is about 23 cm × 23 cm which is significantly smaller than a comparable antenna in L-band (80 cm × 80 cm). A precise beam-steering capability for scan angles of ±180° in azimuth and 0...60° in elevation direction was demonstrated. Figure 6 shows the pattern for one beam. A gain of 12dB could be achieved (figure 8). However, the gain decreases for low elevations at higher scan angles. This effect may be compensated by a larger antenna using more than 25 elements. An example for side-lobe control is depicted in Figure 7. An overall side-lobe level of -25 dB can be achieved for all scan angles.

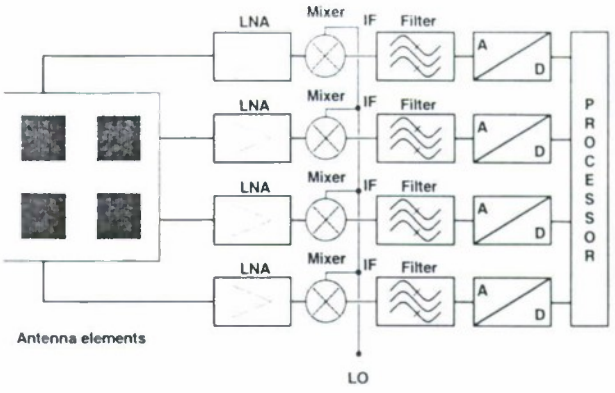

Fig. 5. Principle of a digital beamforming antenna with 4 elements

The generation of multiple deep pattern-nulls was also demonstrated (Figure 8). A cut in the plane $\phi = 0°$ (A-B) shows the very accurate location of the null with a signal rejection better than 45 dB. This was only achieved by using calibration and error-correction procedures taking into account mutual couplings of the antenna elements.

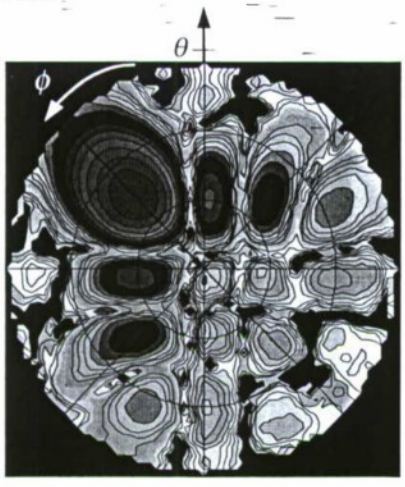

Fig.6. Radiation characteristic with beam pointing in two dimensions
$\phi = 45°$, $\theta = 45°$

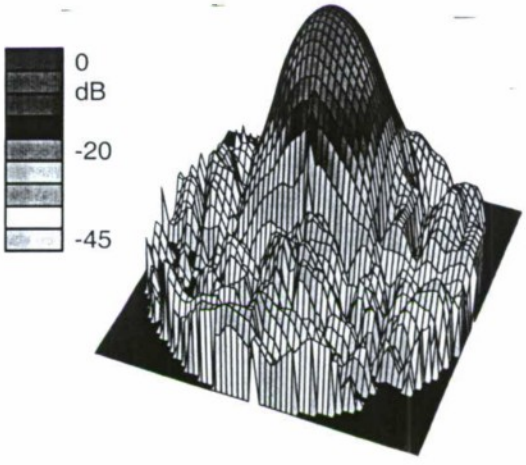

Fig.7. Scan with $\Phi=0°$, $\theta = 20°$ using side-lobe level control (<-25 dB)

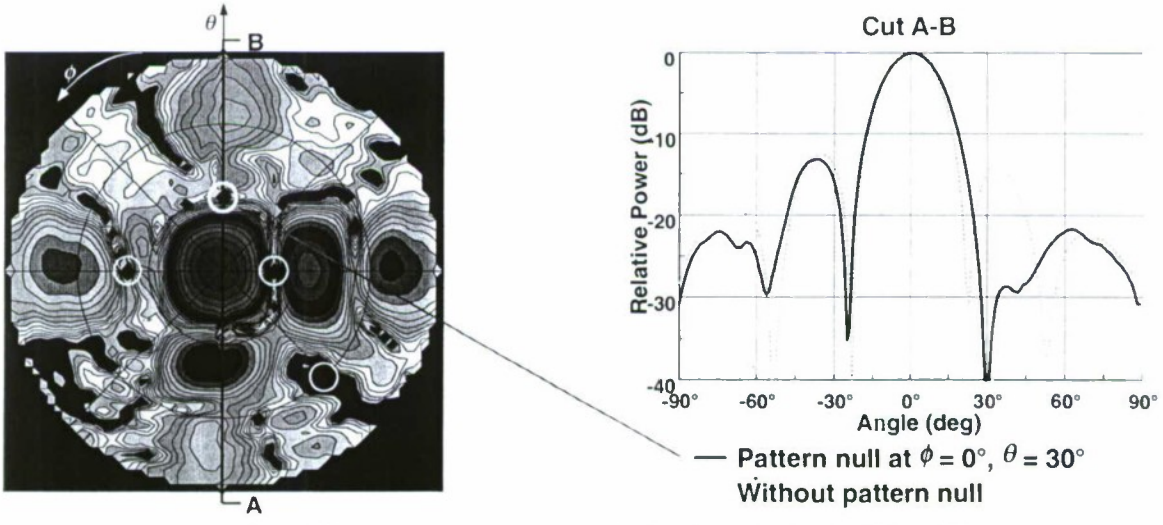

Fig. 8. Multiple pattern-null generation at ($\phi = 0°, \theta = 30°$), ($\phi = 90°, \theta = 39°$), ($\phi = -135°$, $\theta = 60°$), ($\phi = -90°, \theta = 21°$). The cut for $\phi = 0°$ shows the radiation characteristic with (—) and without ( ) pattern-null at ($\phi = 0°$, $\theta = 30°$)

8. Conclusions

Although the investigations presented here do not cover all aspects of C-band for navigation, it is obvious that there is a degradation of the received signal-to-noise power ratio with respect to L-band. On the other hand, C-band provides a nearly interference-free environment with low signal delays in ionosphere.

The signal propagation loss can only be compensated by increasing the power of the radiated signal on board the satellite and by using a directive antenna on board the user platform (directive antennae on board the satellite for regional services have not been considered in this paper). The effective link budget of paragraph 6 has shown that a transmit power of 125 W may be effective and a receive antenna gain of 15 dB is needed.

By using modern antennae techniques such a gain seems to be achievable although the present technological development is not yet in a state that the antenna gain requirements will be met by a compact antenna (5×5 elements), particularly in critical situations (low elevation angles, high user dynamics).

Additionally the receiver for C-band will also be more complex. It is due to these complexities on receiver and antenna unit (and on the satellite) that navigation in C-band is expected to be be reserved only to specific services, in particular safety-critical applications because digital beamforming antennae additionally improve the ability of the receiver to suppress multipath and jamming interference.

C-band is less susceptible to ionospheric disturbances but more sensitive to atmospheric effects (in particular precipitation). This leads to a less uniform performance level on a world-wide basis.

The MLS-band above 5.03 GHz may be phased out in the future. If this will happen, an extension of the 20 MHz navigation band to higher frequencies will offer more bandwidth which can be used for additional services. Therefore C-band offers the potential for future expansions.

Without going into technical details, the results of the investigations can be summarized in a simple table showing the most important advantages and drawbacks for navigation by C-band signals:

pros	cons	remarks
	additional ressources on board the satellites required	• high power amplifier • increased power consumption
	more complex user equipment	• beam forming antenna needed • low noise local oscillator needed • Doppler tracking more complicate
increased interference and multipath resistance		• low-interference band • use of compact directive user antenna • higher power forced for an intentional external jamming signal
low propagation delay		reduced ionospheric influence
potential for future expansion		if frequency band extended to frequencies above 5.03 GHz

9. References

1. **ITU-R** : Specific Attenuation Modell für Rain For Use in Prediction Methods//ITU-R Recommendation PN 838, 1994
2. **Hargreaves, J.K.** The solar-terrestrial environment". Cambridge University Press, 1992
3. **Ward, P.W.**Performance Comparison between FLL, PLL and a novel FLL-assisted PLL carrier tracking loop//Conference proceedings of ION GPS-98, Nashville, USA, 1998
4. **CEPT Brief** // World Radiocommunication Conference 2000. May / June 2000, Istanbul, Turkey.
5. **Pelmoine, C.** Some Elements Regarding Rule Making for UWB Technology". Eurocontrol DIS/COM, 07/09/00.
6. **Litva, J.;. Lo, T. K** : Digital Beamforming in Wireless Communications// Norwood Artech House, 1996.
7. **Dreher, A.; Hekmat, T.; Niklasch, N. E.; Lieke, M.; Klefenz, F.; Schroth, A.** Planar C-band antenna with digital beamforming//IEEE Antennas Propagation Society. International. Symposium, Salt Lake City, USA, July 2000, pp. 906-909

AIRBORNE MONITORING SYSTEM OF INTEGRITY OF NAVIGATIONAL DATA BASED ON STATISTICAL PROCESSING

N.A. Golovanov*, Yu.V. Gavrilenko, V.V. Groshev***, N.A. Zaitseva****, I.V. Kalinina*****, E.V. Kochneva******, V.G. Potekhin*******, T. P. Tkacheva********
Moscow institute electromechanics and automatics
5, Aviatzionny Pereulok, Moscow, 125319, Russia. E-mail: aomiea@aviapribor.ru

Abstract

Key words: control, navigation, accuracy, integrity

The problem of usage of the information from satellite navigators is connected to mining of the applicable monitoring facilities, which one will allow to supply an indispensable level of navigational data integrity. The primary estimation of quality of the satellite information grounded on the autonomous control of integrity of the receiver, appears poor and for these purposes it is necessary to elaborate the onboard monitoring system, which one would use the data from everything, included in a structure of a navigational complex of sensors. In the article it is offered as such system to use a system built on principles of a statistical check and permitting to define veracity of the information or to give warning message. The function ability of a tendered method confirms by outcomes of mathematical modelling.

Introduction

The introducing of satellite navigation systems introduces the new contents to navigational maintenance of flights. The split-hair accuracy of definition of navigational parameters allows to fly in conditions of high intensity of an air traffic, and the full deployment of systems GPS and GLONASS allows to fly, in any geographic region, making modifications in concept "no oriented" terrain. Having the rather small cost, on the one hand, and split-hair accuracy of definition of navigational parameters on the other hand, SNS are entered in a structure existing and again of developed an integrated flight navigation system (IFNS).

1. Structure of a navigational complex

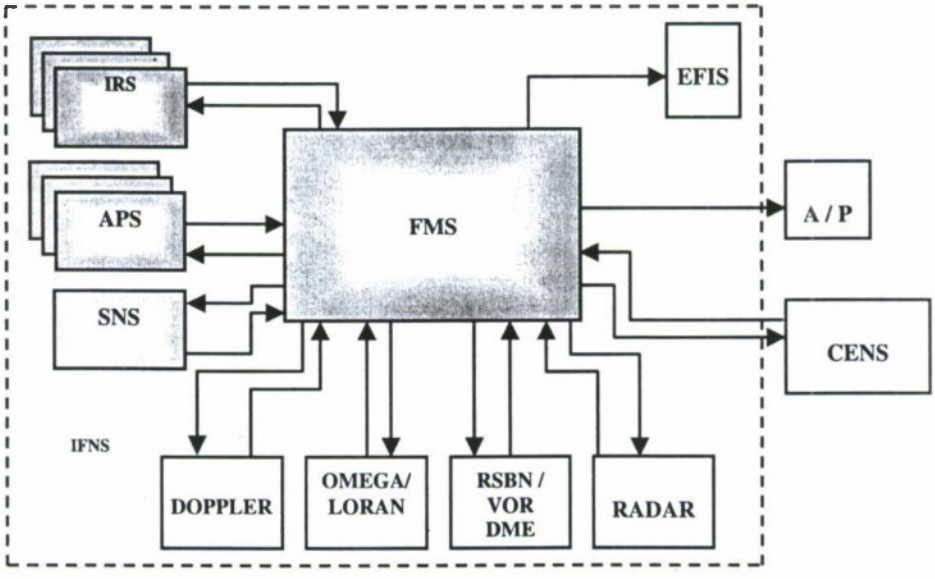

Fig. 1 Pattern of a navigational complex

The structure IFNS is determined by assigning of an aircraft and circle of problems, which one it should decide. In the general case, the structure of a navigational complex actuates following (fig. 1):

---

* Depute General Director, candidate of science, Superior Research Fellow.
** Engineer.
*** Leading engineer, candidate of science.
**** Chief of department, candidate of science, Superior Research Fellow.
***** Engineer.
****** Leading engineer.
******* Leading engineer, candidate of science.
******** Superior Research Fellow, candidate of science.

- Means ensuring autonomous dead-reckoning;
- Compass systems;
- System of air signals measuring true air speed, altitude of flight and parameters of atmosphere;
  - Doppler sensors of ground speed and angle of drift;
  - Radio systems;
  - Satellite navigation system;
  - Navigational computing system.

Such structure of IFNS provides fulfilment of flights, using principles of an area navigation, in any physics-geographic conditions.

The off-the-shelf onboard flight manager systems (FMS) concern to the most composite equipment IFNS, which one represent an overall system, a leading particular by which one is the calculator. Operating the large database, FMS provides problem solving of navigating with a given level of accuracy for an established airspace, using for this purpose the data of navigation aids which are included in a structure IFNS.

The algorithmic maintenance FMS, decisive problems of navigating, controls input data, rejecting a unreliable information, and at the expense of usage of information redundancy achievable by usage of the information from all navigational sensors IFNS, the high reliability of an output information is reached at minimum interference of flight crew.

2. Principles of construction of a integrated data processing

The integrated data processing, as a means of increase of accuracy of definition of navigational parameters, is esteemed as a problem of applying of an optimum Kalman filter (KF) or suboptimal filter for an estimation of inaccuracies of all-inertial calculation.

At formation algorithm pattern of an integrated data processing the following factors were taken into account:

1. Split-hair accuracy of definition of navigational data by aircraft receivers of satellite signals, which one on one - two order of above conventional radio systems.
2. Distinctive features of the satellite information: influencing of poor geometry on accuracy of definition of output parameters SNS, capability of interruption of the information, bound with poor quantity of satellites in a field of view, uncertainty of knowledge of the statistical characteristics of inaccuracies SNS in a current instant, gang of constellations and gentle noiseproof features.
3. Necessity of maintenance of a given level of accuracy and integrity at each phase of flight in an airspace with the established type RNP and signal conditioning of warning about impossibility of fulfilment of scheduled operation.

The parameter of accuracy of holding of the navigational characteristics represents the determining factor of the new concept of the demanded navigational characteristics (Required Navigation Performance - RNP), which one modern FMS should provide, but at usage SNS in a structure IFNS with the relevant parameter to become not only accuracy of holding of lateral and longitudinal separation, but also information integrity. It requires mining such methods of verification of navigational data, which one would allow to use this system at all phases of flight and in any locales, even with the very stringent type RNP.

Numerically integrity expresses by a degree of confidence to a regularity of the information giving IFNS and time of warning to crew when the information should not be used for fulfilment of planned operation.

In a fig. 2 the skeleton diagram of algorithm of an integrated data processing is adduced. Presence in a structure of such functional modules, as module input and outgoing control, module of crude estimates and module of a reconfiguration allows to provide continuous monitoring behind a condition input, intermediate and output information.

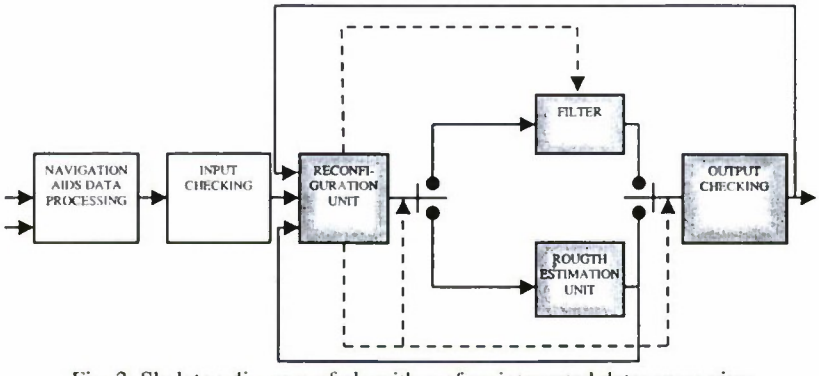

Fig. 2. Skeleton diagram of algorithm of an integrated data processing

3. Principles of a building of a system of the control

In the general theory of monitoring systems select a functional check executed during operation of a system, which one actuates the monitoring system grounded on coprocessing of the information, entering from several sensors.

The problem of the control actuates four ports of reference are problems of failure detection, localization of failure, estimation of its level and reconfiguration. As a result of a reconfiguration the information aggravating common quality of system operation, is eliminated from further processing.

Pursuant to definition of integrity, apparently, that problems of the control, bound with definition of hardware failures in IFNS, are supplemented by necessity to analyze aloft quality intermediate and output information with the purpose of definition of impairment of its quality and exception of the unsuitable data of processing and process of calculus of output navigational data.

The necessity of maintenance of the requirements RNP1 or even more stringent requirements on accuracy of holding of navigational parameters, and also feature of operation SNS and nature of behavior of inaccuracies SNS, results in a problem of mining of such principles and methods of verification, which one would allow to execute of monitoring behind a condition of output parameters IPD in each current instant, providing a given level of integrity. The solution of this problem is grounded on principles of a statistical check used as for the intermediate information - algorithm of crude estimates, and for an output information. Intermediate and outgoing control are founded on usage the identical approaches and methods of a statistical sorting of abnormal measurements.

The **monitoring system** apart from all functions tolerance and parameter monitoring executes functions of maintenance of an output information integrity.

The **rough estimation unit** is intended for smoothing of the information and exception of abnormal signals received from SNS.

The special place takes a module of a reconfiguration, which one depending on a condition of an input information, phase of flight, of outcomes of an outgoing control and solved problem should reshape pattern IPD.

The incoming control is grounded on feature analysis of a condition of systems participating in an integrated data processing, on the analysis of outcomes of the test control and parameter checking (in a case triple or dual inertial system).

The outgoing control is a closing stage on a state estimation of output navigational data IPD. Presence of uncertainty in knowledge of the statistical characteristics of inaccuracies SNS, dynamic effect of aircraft motion, the geometrical factor of arrangement of constellations can render negative influencing on an estimation of navigational parameters, that requires the continuous control.

For an estimation of quality of the information the following problems (fig. 3) are decided:

- The t-second sliding interval is selected, the selection which one is conditioned:
  - by sufficiency of quantity of measurements for realization of a statistical analysis (definition of expectation and dispersion);
  - by a simplicity of definition of a detection time of an abnormal signal;
  - by a small data volume, that allows to realize algorithm of a statistical check in the onboard calculator.
- Outgoing from a normality of a distribution law of inaccuracies of the data SNS [3] and probability of a false alarm equal $Q=Q_{set}$ the confidence interval is under construction.
- The abnormal measurement is determined, which one is identified at fulfilment of a following inequality:

$$X_i \geq \sigma_{set} \sqrt{\theta_{set}} .$$

- The ranging of abnormal signals with usage of statistics $\theta(k)$, given accuracy of definition of parameter and frequency of occurrence of an abnormal signal is carried out on the basis of a dispersion two adjacent t of intervals k, $k+1$ statistics $\theta(k)$ is evaluated; the excess of statistics $\theta(k)$ of boundary value $\theta_{boundary}$ determines an abnormal signal and time of its occurrence.
  - $\theta(k) \geq \theta_{boundary}$ the abnormal signal such as "rejection" is identified;
  - at $\theta(k) \leq \theta_{boundary}$ and $X_i \geq \sigma_{set} \sqrt{\theta_{boundary}}$ signal such as "spike" is identified;
  - if there are some series abnormal signals, these measurements are assorted as "serial".

- The boundary value $\theta_{boundary}$ demonstrates, that the large value $\theta(k)$ is not random, and the normality is upset. The value $\theta(k)$ obeys to a distribution law χ^2 and is selected is tabular [4] on the basis of degree of freedoms of compared sampling.

  Permissible θ_{per} is selected outgoing from maintenance of the given requirements on accuracy with given probability. It also tabular value [5].

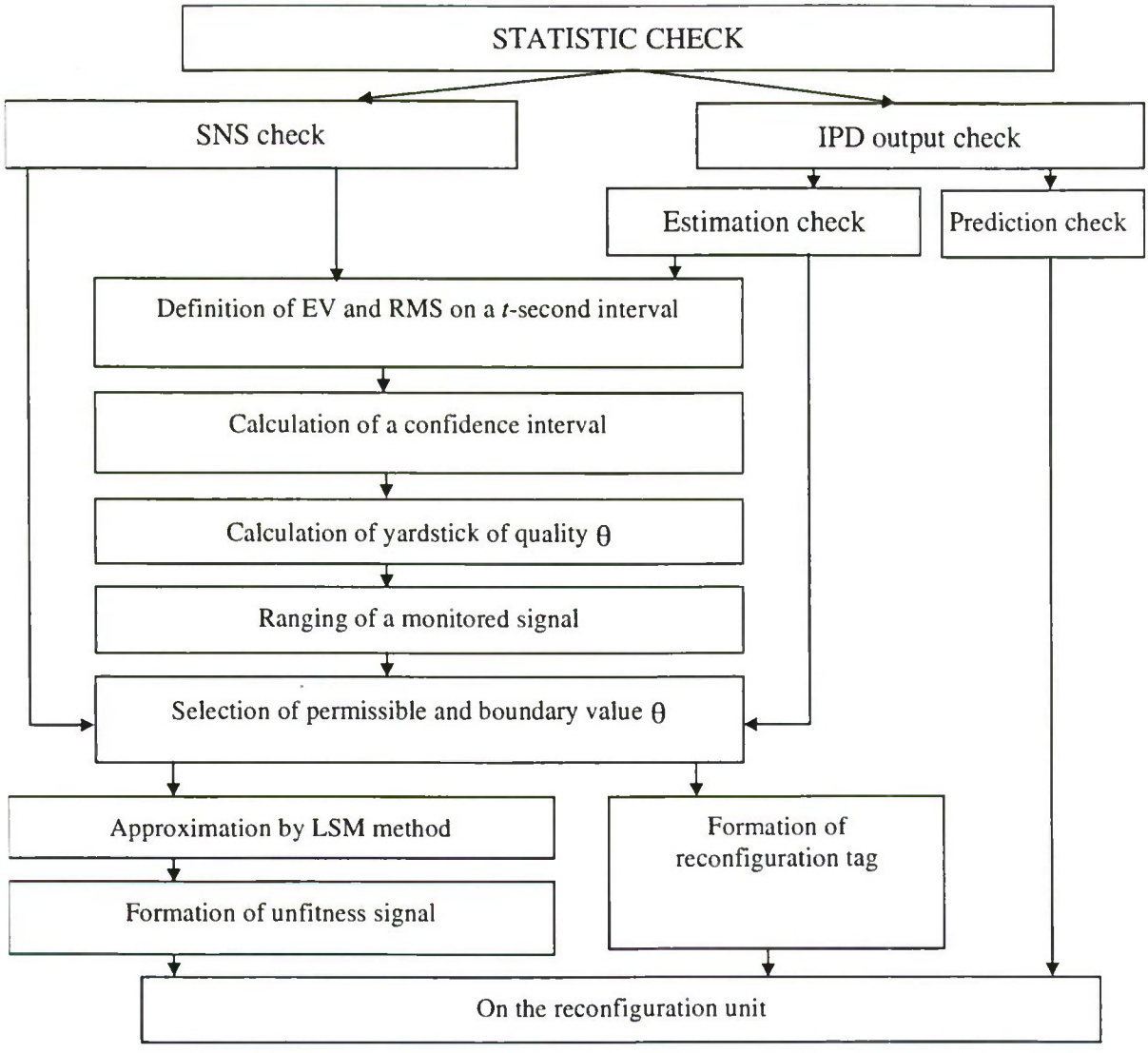

Fig. 3. The scheme of construction of a statistical check

- At usage as an output information of the data SNS the approximating of an instrument parameters $X(t)$ by a method LSR on a t-second interval will be used. The approximating curve $X(t)$ is expectation of parameter computed from a condition of maximum likelihood.
- On the basis of the analysis of statistics $\theta(k)$ on an output IPD the tag of a reconfiguration of output navigational data or signal of unfitness is reshaped, if the reconfiguration does not allow to ensure demanded accuracy and integrity for fulfilment of scheduled operation.
- Outgoing from boundaries of integrity demanded for a definite phase of flight, aircraft running speed and given time of an illegal crossing of the frontier the alarm signal is reshaped.

The offered technique was tested by an analytical method and method of mathematical modelling under the data obtained at test of systems "SNS-2" and "SNS-3" (a fig. 4 -5).

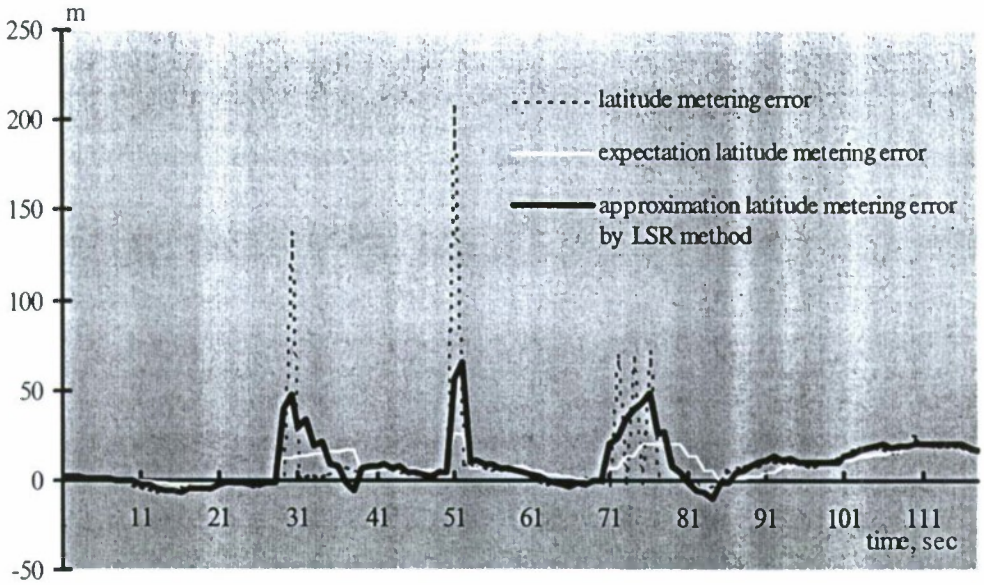

Fig. 4. Signals, its expectation and approximation
(1 spike+1 rejection + serial of bad signals)

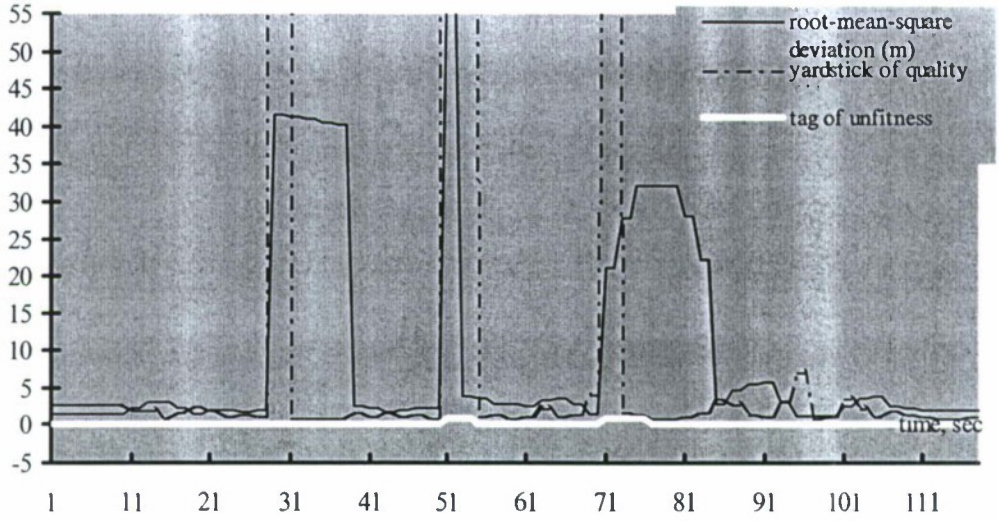

Fig. 5. root-mean-square deviation of a signal, yardstick of quality and tag of unfitness
(1 spike + 1 rejecting + serial of bad signals)

4. Principles of construction of an outgoing control

Module complcting pattern of a integrated data processing, is the module of an outgoing control. The given module executes continuous diagnosing of output navigational data, controlling them accuracy characteristic, and decides two problems:

- using methods of a statistical check, finds out an abnormal signal, arresting time of its occurrence, carries out matching with θ_{per} and reshapes tag for a reconfiguration unit;
- by activity of the filter in a mode "predic" is conducted continuous monitoring of an output information and the time is determined, at which one the inaccuracies of definition of navigational parameters can leave for established boundaries of accuracy.

In a fig. 6 the flowchart of an output statistical check is adduced, the pattern repeats which one in many respects algorithm of crude estimates, but the qualitative values of yardsticks have other filling.

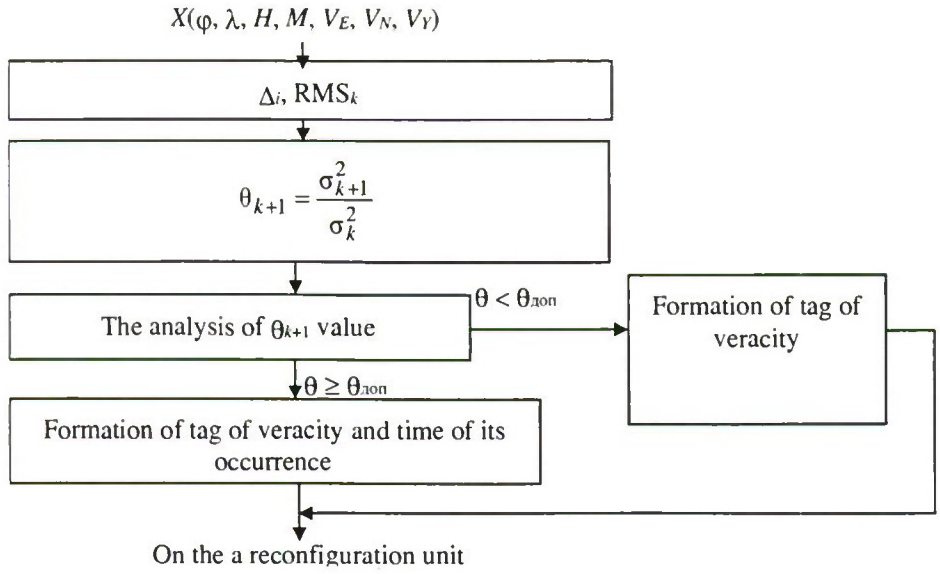

Fig. 6. The flowchart of algorithm of an outgoing control

For the solution of a problem of an output statistical check the t-second sliding interval will be used.

The algorithm of an outgoing control decides following problems:

- definition of expectation (M) and root-mean-square deviation (σ), received representative on a k-ohm an interval:

$$M_k = \frac{\sum_{1}^{n} X_i}{n};\ \sigma_k = \sqrt{\frac{\sum_{i=1}^{n} \Delta_i^2}{n}},$$

Where n - number of measurements, k - number of an interval;

- definition of a parameter $\theta_{k+1} = \frac{\sigma_{k+1}^2}{\sigma_k^2}$ [4], which one allows to check up a hypothesis about presence of abnormal measurement. The value θ_{k+1} is random, obeying to a distribution law $\chi 2$;
- matching of value of an index θ_{k+1} with the applicable acceptable value, which one is selected from a condition of maintenance of permissible probability of an output for established boundary of an accuracy index. At excess of selected value θ_{per} the tag for a module of a reconfiguration is reshaped.

5. Output "prediction" check

By activity of the filter in a mode "predict" for definition of preventing of an aircraft output for established boundaries of given accuracy is executed by output "prediction" check. The designed algorithm decides following problems:

- determines aircraft position determination navigational component errors depending on an parameter of accuracy, phase of flight or from accuracy of an aircraft position determination for the solution of special problems, flying speed;
- determines magnitude of error of position during a given time period Тзад, which one is determined by a run time of planned operation both magnitude of error of a coordinates setting and speed at the moment of the filter drift in "predict";
- on the basis of the comparative analysis of given and computational inaccuracies the tag K_{pred} for a module of a reconfiguration is reshaped in case of excess T_{giv}.

Navigational component inaccuracies Δ_{nav} is determined:

$$\Delta_{nav} = \Delta - \Delta_{FTE},$$

Where - Δ - given accuracy of a coordinates setting of aircraft position;

Δ_{FTE} - inaccuracy of a piloting technique.

The magnitude of error of a coordinates setting and speed at the moment of the filter drift in "predict" is determined in a module of an output statistical check on the basis of the statistical characteristics: expectations m_φ and σ_φ, received on a t-second interval.

Computational prediction the value of navigational component inaccuracy on a time period T_{giv} is determined:

$$\Delta_{pred_Z} = \left(m_{v_Z} + 2\sigma_{v_Z}\right)T_{\text{giv}},$$
$$\Delta_{pred_S} = \left(m_{v_S} + 2\sigma_{v_S}\right)T_{giv},$$

where m_{v_Z}, m_{v_S} - expectations of inaccuracies of component ground speed in lateral and longitudinal directions;

σ_{v_Z}, σ_{v_S} - root-mean-square deviation of component inaccuracy of ground speed.

At omission even of one of inequalities:

$$\Delta_{nav} \le \Delta_{pred_Z}, \qquad \Delta_{nav} \le \Delta_{pred_S},$$

the tag for a module of a reconfiguration is reshaped.

The outcomes input, intermediate and outgoing control can be such, that at the selected configuration IPD the scheduled operation can be executed only at some limitations (for example, there can be time constraints of fulfilment of operation) or can not be executed.

6. Reconfiguration unit

The reconfiguration unit, collecting the information from all modules IPD, should select such operational mode and use that information, which one would provide the solution of a scheduled problem, i. e. would provide property of an adaptivity of algorithms IPD to varied conditions of operation. The module of a reconfiguration should allow:

- Structure of input navigational vector;
- Conditions of operation (fig. 7): a phase of flight, condition of intelligence systems and sensors, requirement on accuracy, which one are determined by the type RNP or the special requirements are set, which one are indispensable for fulfilment of scheduled operation;
- Outcomes of an outgoing statistical and prediction check, which one provides integrity of output navigational data.

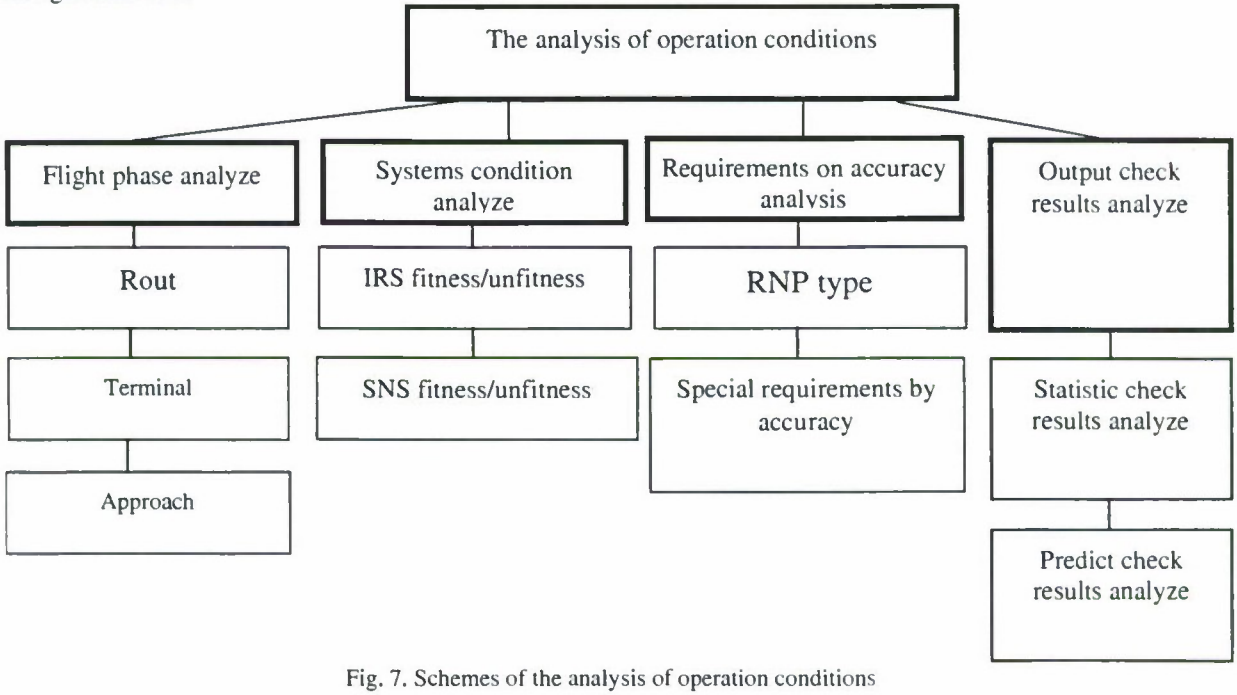

Fig. 7. Schemes of the analysis of operation conditions

Depending on what equipment installs aircraft on board, the module of a reconfiguration selects indispensable pattern IPD.

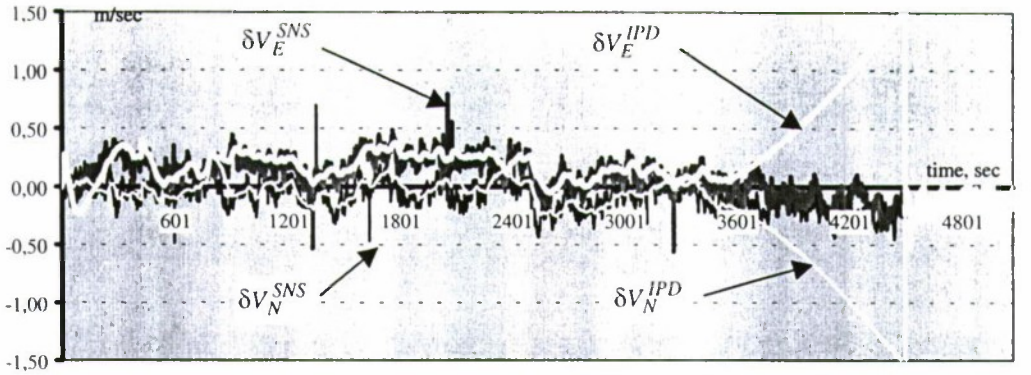

a) inaccuracies by nothern and eastern speed component

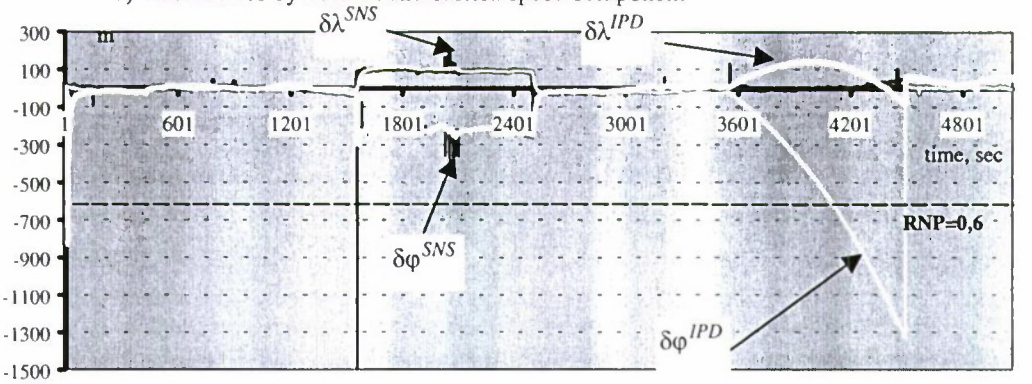

b) inaccuracies by coordinates

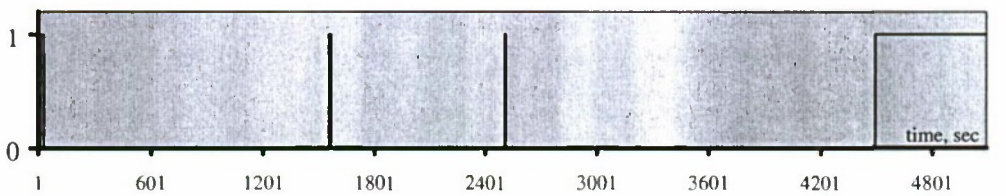

c) tag of unauthenticity of coordinates estimation

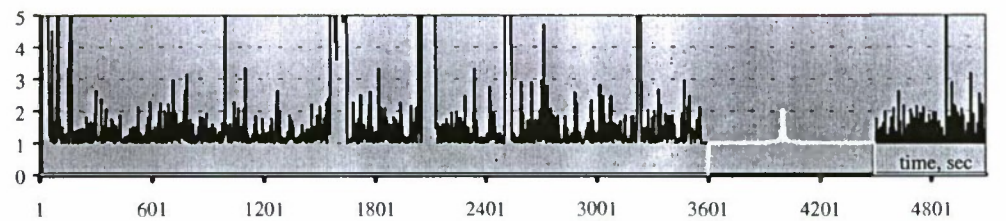

d) yardstick of quality Θκ. *Kpred*

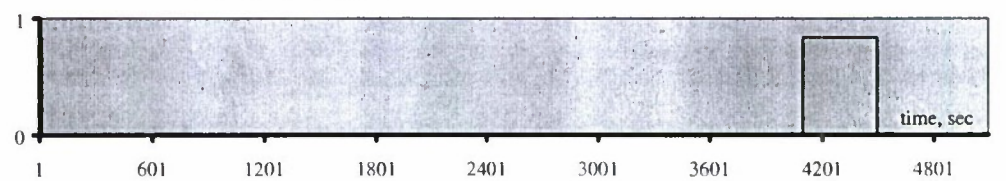

e) alarm signal

Fig. 8. Case history activity check and reconfiguration units

The conditions of operation are determined:

- By phase of flight, which one is characterized by a given level of accuracy and integrity of definition of navigational parameters;
- By fulfilment of aircraft manoeuvring, which one can result in occurrence of transients of a filtration and instability of estimations;
- By condition of systems and sensors participating in an integrated data processing, the data which one communicate with a system of incoming control by results of a built-in check, tolerance check and parameter check. The module of a reconfiguration reshapes pattern IPD and selects a filtration mode from a case:
  - Faultiness or inauthenticity of output parameters of one of sensors,
  - Failure or unfitness detected by results of incoming control of the receiver SNS at realization of the autonomous integrity control,

By the type of a solved special problem, which one can be characterized by a heightened tolerance requirement of navigational data, and also requirements to maintenance of a self-sufficiency of fulfilment of aircraft flight. In this case reconfiguration unit also should select the applicable mode of a filtration and structure of input navigational data.

The outcomes of an output statistical and prediction check provide integrity of navigational data. In case of impossibility of fulfilment of scheduled operation, the warning message in a module of a reconfiguration, which one is given on the basis of bulk analysis of a condition of systems, of a phase of flight makes a decision on a reconfiguration of algorithms IPD or the warning message, with the indicating of time is given, when the given requirements will exceed an established level.

7. Outcomes of mathematical modelling

The method of mathematical modelling affirmed functionability of designed algorithm of a reconfiguration IPD of a federated system receiving the information from an inertial system and SNS. In a fig. 8 the chart of behavior of error of coordinate (latitude) is adduced at flight in a zone of an aerodrome at normally operating sensors (accuracy of a coordinates setting according to the requirements should to make 660 м) and at the introducing of contingencies by activity IPD. As contingencies were esteemed:

- Impairment of instrument error of an inertial system (on a time period t=550-1000 sec);
- Dilution of precision of definition of navigational parameters SNS (on a time period t=1550-2500 sec);
- Absence of the data SNS (at t=3550-4500 sec).
- Failure of an inertial system.

As it is visible from the reduced chart, the algorithm of a reconfiguration reacts to a contingency, controlling activity IPD and providing fulfilment of scheduled operation.

Conclusions

The designed monitoring system, apart from conventional tolerance and parameter check, provides detection and sorting of abnormal signals, bound with features of measurements SNS and quality of operation of algorithms of a filtration

The introduced system of an in-flight monitoring of integrity of navigational data grounded on principles of statistical processing and optimum filtration, provides demanded quality of the navigational data at all phases of flight, including not precision landing approach, at the expense of actuation in a structure of a reconfiguration unit. In case of impossibility of fulfilment of scheduled operation gives to crew a clearance signal..

References

1. **Manual** under the requirement navigation performance, Doc 9613-AN/937, ICAO, 1999.
2. **Gavrilenko I.V., Zaitseva N.A., Kochneva E.V., Tkacheva T.P. Applying** of a statistical processing techniques of the information of navigation systems for maintenance of integrity of the integrated navigator, Aerospace instrument making of Russia, Avionics, St.-Petersburg, 2001.
3. **Gavrilenko I.V., Zaitseva N.A., Kochneva E.V., Tkacheva T.P.** Outcomes of statistical processing of the navigational data of an onboard satellite system of a mixed type obtained by results of flight tests. The accumulator cell of the reports III of conference of the young scientists "Navigating and mission control", St. Peterburg, State Research Center of Russia-Central Scientific & Research Institute "Electropribor", 2001.
4. **Dlin A.M.** Mathematical statistics in science. M.: Sovetsckaya Nauka, 1958.
5. **Bolshov L.N., Smirnov N.V.** The tables of mathematical statistics. M.: Science, 1965.

INSTANTANEOUS AMBIGUITY RESOLUTION FOR GPS/GALILEO RTK POSITIONING

Bernd Eissfeller[1]
Institute of Geodesy and Navigation, University FAF Munich
85577 Neubiberg, Germany. E-mail: Bernd.Eissfeller@unibw-muenchen.de
Christian Tiberius[2]
Section of Mathematical Geodesy and Positioning, Delft University of Technology
Thomas Pany[3], **Robert Biberger**[4], **Torben Schueler**[5]
Institute of Geodesy and Navigation, University FAF Munich
Günter Heinrichs[6]
MAN Technologie AG, Dept. Satellite Navigation, Augsburg

Abstract

Key words: Ambiguities, GPS, Galileo, RTK receiver

We review the planned modernization of the Global Positioning System (GPS) and the development of the European Galileo system, thereby concentrating on the high-precision carrier phase and code signals eventually available to the GNSS user community for fast and precise Real-Time Kinematic (RTK) positioning.

High-precision GNSS positioning results are obtained with carrier phase measurements, once the integer cycle ambiguities have been successfully resolved using also code measurements. A geometry free and a geometry based approach for ambiguity resolution are discussed. The first approach is conceptual simple but we will show that high ambiguity success rates for a combined hybrid GPS/Galileo system can only be obtained with the second one. The reason is that all ranges are linked to the same three baseline coordinate unknowns, instead of dealing with a double difference range unknown per satellite-pair.

RTK positioning requires forming of double differences of carrier phase and code observations between two satellites, a reference station and the roving receiver. Three scenarios (short, medium and long baseline) are discussed. The categorization refers to the baseline length (<3 km, 20 km and 400 km) but more important than baseline length are atmospheric conditions which are characterized by double differenced tropospheric and ionospheric delays.

Ambiguity success rates for each scenario and for each satellite configuration are calculated as a function of time for a whole day. Each attempt to resolve ambiguities relies on data from only one epoch, i.e. we consider instantaneous ambiguity resolution. The method to calculate (instantaneous) success rates is a based on an approximation called bootstrapping, a sequential process in which ambiguities are fixed (hard-constrained) to integers one-by-one, each time accounting for the statistical correlation with the remaining ambiguities.

As a result we find a decrease of the ambiguity fail rate (i.e. one minus success rate) for a 4 frequency hybrid GPS/Galileo system compared to the dual frequency GPS system. The improvement is largest for the short baseline scenario where the fail rate decreases from 0.24 % to less than 0.000001 %. For medium baseline lengths it decreases from 63% to 6% and no improvement can be seen for long baselines. The improvement is attributed mainly to the increased number of satellites and to the improved geometry. The main performance limiting factors are the uncertainty in the ionospheric delay and to less extend the code measurement error.

The ultra high instantaneous ambiguity success rate for short baselines opens new fields of applications for RTK positioning like avionics. In that fields the high RTK positing accuracy might yield new applications of satellite based navigation.

1. Introduction

Undoubtedly, the GPS modernization program (GPS II R-M, GPS IIF/III) as well as the setup of the anticipated European counterpart Galileo will prove to be highly beneficial for Real-Time Kinematic (RTK) positioning. GPS Block IIR-M and IIF will both transmit the unencrypted L2 civil signal on the second carrier frequency making the tracking of this signal much more easier and reliable. GPS IIF/III and Galileo will also provide a third frequency that can substantially aid in the process of carrier phase ambiguity resolution, often called TCAR (triple carrier phase ambiguity resolution) or MCAR (multiple carrier phase ambiguity resolution).

This paper focuses on the high-end receiver and RTK application market. After outlining the anticipated frequency scenario for a combined GPS/Galileo receiver, a brief review of current RTK systems is provided. Technological improvements for RTK positioning are expected to be made with software correlation receivers, tightly coupled inertial navigation systems and modern wireless communication technologies within the next receiver generations. Galileo specific improvements regard a more reliable ambiguity resolution method. The ambiguity success-rate (resp. fail-rate) is calculated with a geometry-based

---

1 Univ.- Prof. Dr.- Ing., Vice-Director of the Institute of Geodesy and Navigation
2 Dr.Ir., Research Associate
3 Mag., Research Associate
4 Dipl.-Ing., Research Associate
5 Dr.-Ing., Head of the GNSS/INS Laboratory
6 Dr.-Ing., Research and Development Manager

model for a GPS only receiver and a hybrid GPS/Galileo receiver based on the LAMBDA method [Teunissen, 1993]. Since only instantaneous ambiguity resolution is considered, which is based on a single epoch of data, no distinction between a moving and a stationary receiver is necessary. The ambiguity success-rate increases significantly for short and medium baselines by using a hybrid GPS/Galileo receiver. It depends for a given satellite constellation mainly on the uncertainty of the differential ionospheric delay. Therefore accurate ionospheric modeling by a network of reference receivers is necessary. In principle also very accurate code measurements (<10 cm) yield very high success-rates. The implications of both points on the receiver design are discussed at the end of the paper.

2. New RTK Boundary Conditions due to GPS IIF /Galileo

(A) The GPS Case

Current Situation – GPS C/A Code

The current constellation of GPS Block II and IIA satellites provides C/A code on L1 only, whereas the encrypted P-code is modulated on both carriers, L1 and L2. The actual transmission power lies approximately 5.5 dBW above the specified one.

GPS Modernization – L2 Civil Signal

GPS Block IIR, the so-called replenishment satellites, are launched since 1997 to replace the older Block II (and IIA) vehicles. The major difference between Block IIA and IIR satellites lies in the altered antenna phase center and the longer design life time. A modernized version (Block IIR-M) is planned for 2003 with the C/A code and an the L2 civil signal (CS) being implemented on L1 resp. L2. Furthermore, the military M-code is expected to be modulated on both carriers.

Albeit GPS Block IIR-M will not offer a third frequency, tracking the L2 carrier will become significantly easier and the signal-to-noise ratio on the second frequency will improve. This fact is also important for kinematic applications since ionospheric disturbances may cause loss-of-lock esp. on L2 much easier for current GPS than for GPS IIR-M due to the accessible civil code on L2.

GPS Modernization – New GPS Signal on L5

Generally speaking, apart from the availability of an additional third frequency itself that may enable fast ambiguity resolution (see below), the civil code on L5 can be considered to be similar to the existing P(Y) code, i. e. the power spectrum is analogous and the multipath envelopes are identical to those for the P-code ranges. The L5 signal allows coherent tracking of phase and code and avoids the squaring loss. The integration time does not depend on the data bit rate since code and data bits are separated from each other making L5 a much more robust signal than L1 and L2.

Table 1. GPS modernization schedule. Adopted from [Shaw et al., 2000].

Activity	Implementation Date
SA set to zero GPS IIR Enhancements - L2CS on L2 - M-code on L1 & L2	May 2000 2003 – 2006
GPS IIF Enhancements - L2CS on L2 - M-Code on L1 & L2 - L5	2005 – 2010
GPS III Enhancements - L2CS on L2 - M-code on L1 & L2 with greater power - L5 - Future Capabilities	2010 - ... (to be determined)
Operational Control Segment (OCS) Enhancements	2000 – 2008

Figure 1. Available frequency bands for GPS (in green) and Galileo (in yellow).

(B) The Galileo Case

The investigations for this work are based on a frequency scenario compatible with one outlined by the European Commission (EC) Galileo Signal Task Force and published in [Hein et al., 2001]. The frequency plan is shown in Fig. 1.

Frequency Choice

Many of the Galileo signal properties and the choice of the carrier frequencies have been discussed or are still being discussed in the Galileo definition phase. Each possible frequency band has specific advantages and disadvantages, e.g. the E6 offers a very wide frequency band, but an E6-signal may suffer from radar interference and the risk of signal degradation has not yet been assessed in detail. A split spectrum signal with the main lobes in E1 and E2 has only a small cross-correlation (spill over) with the GPS L1 signal but the ionospheric influence on such types of signals has not been quantified yet. The advantage of E5 is that this signal would be located in the Aeronautical Radio Navigation Service (ARNS) band, shown gray in Fig. 1 and therefore it is suitable for aviation.

Codes

Low-noise code ranges with small multipath sensitivity would be desirable to aid in the ambiguity resolution process. Generally speaking, the codes for Galileo can be made as good as the GPS L5 code (see Table 2). However, depending on the implementation of the service concept (data bit rate), the quality and the statistical properties of the codes may have to be compromised resulting in an inferior performance. The implementation of services through encryption of data is not that critical, but may also have a slight impact on the required data rate. However, the implementation of security features through encryption of the codes is to be considered as a quite critical affair.

The scenario outlined by the EC Galileo Signal Task Force [Hein et al., 2001] forms the background for this investigation. The signal design in the upper L band shows a binary offset carrier BOC(14,2) signal having its main lobes in the E1 and E2 frequency bands with a spill-over into GPS L1 and two overlay signals of type BOC(2,2). The three split spectrum signals are combined by majority voting. The carrier is centered at the very same frequency (1575.42 MHz) as GPS L1. Coherent (split spectrum) processing of both side bands in the RTK receiver is necessary to obtain the carrier phase at the center frequency.

At the lower end of the L-band spectrum the E5-band (denoted as E5b in [Hein et al., 2001]) is chosen, at a center frequency of 1202.025 MHz, separate from the GPS L5-band. Both bands are 24 MHz wide and are allocated for ARNS. Employing L5 and E5 in this study, anticipates on an (eventually) not too bad interference by Distance Measuring Equipment (DME) in use for aviation. A signal in the E6-band, not allocated for ARNS, is not considered because of possible radar inferences from existing pulsed radar systems.

The Galileo L1 and E5 band are part of the Galileo Open Service Signals and comprise un-encrypted ranging codes and navigation data.

(C) The GLONASS Case

Since the future of GLONASS is not very certain and a modernization of the system is even more questionable GLONASS is not considered in this study.

(D) Hybridization

Digital technology together with sub-micron silicon technology has made receivers cheap and has lead to small linear dimensions and low power consumption. In building hybrid GPS/Galileo RTK receivers, which will be the case for high-end applications, it is very important to minimize the effort on the front-end. This is a primary issue for interoperability between different satellite navigation systems. The lesson learned from GLONASS was, that its FDMA concept lead to a disadvantage of GLONASS receivers in comparison to GPS. Having to process the signals on many different carriers leads to high front-end complexity (advanced synthesizer, multiple front-ends, multiple antennas). Higher burden in signal processing in hybrid

receiver architectures is only a secondary problem, because it is solved with low-cost digital circuitry and software. Based on the used reference scenario, a hybrid RTK GPS/Galileo receiver will have in minimum three front-ends (L1, L5, E5). An additional front-end could is required, if also L2 or E6 are used. It is to be noted that with different carrier frequencies also different equipment or hardware delays are involved. These delays are frequency dependent. Each additional frequency induces an additional unknown, which can of course be solved for, if many satellites are in view. However, RAIM (Receiver Autonomous Integrity Monitoring) needs redundancy and RAIM availability will be affected by spending observations to continuously calibrate the front-ends.

Table 2. GPS and Galileo frequency overview. Code noise is calculated from a Minimum Variance Unbiased Estimator for coherent code delay estimation. Adopted from [Winkel et al., 2000]. The C/A code is assumed to modulated on L2 instead of the civil signal (L2CS).

Acronym	L1 *GPS*	L2 *GPS*	L5 *GPS*	L1 *Gal.*	E5 *Gal.*
Frequency [MHz]	1575	1228	1176	1575	1202
Wavelength [cm]	19.0	24.4	25.5	19.0	24.9
Bandwidth [MHz]	24-30	24-30	24	33	24
Code Type	C/A	C/A	Direct Seq.	BOC	Direct Seq.
Power Level [dbW]	-157	-157	-154	-158	-152
Chip rate [Mcps]	1.023	1.023	10.23	10.23	10.23
Code noise [m]	0.38	0.38	0.12	0.12	0.10

To summarize we list all used frequencies for this study in Table 2. A hybrid GPS/Galileo RTK receiver uses L1/L5/L1/E5 (for one investigation additionally GPS L2 is taken into account) and a GPS-only receiver is assumed to work with L1/L2. Table 2 also shows that the code noise varies significantly for different signal types. For this reason and because the signal structure is not definitely fixed yet, we assume in the following sections a code measurement accuracy of 30 cm common to all signals unless indicated differently.

3. RTK System Overview

Most of the currently available RTK receiver systems use double differenced GPS and/or GLONASS carrier phase measurements to determine the position of the roving receiver. The typical nominal accuracy for dual frequency systems is 1 cm ± 2 ppm (horizontal) and 2 cm ± 2 ppm (vertical). The accuracy refers to kinematic positioning, but not all manufacturers indicate if the receivers operate in fast RTK or synchronized RTK mode. The latency for position outputs varies from <20 ms to 100 ms for different receiver systems. If the receiver works in the synchronized RTK mode the latency depends of course on the latency of the radio data link.

The position accuracy drastically decreases if the double differenced ambiguities are not resolved or are resolved incorrectly. In the latter case errors in the order of 1 m can easily occur. Therefore reliable ambiguity fixing is probably the most important design aspect for an RTK system. All other error sources like unmodeled atmospheric effects, (carrier) multipath, orbital errors or receiver measurement noise are of the order of several millimeters up to some centimeters.

Possible Receiver Improvements

Hybrid RTK receiver systems for GPS and Galileo will be available at the earliest 2005. The receivers will not only differ from currently available RTK systems due to Galileo, they will also show significant improvements due to the rapid digital hardware and communications development.

A simplified sketch of a future RTK system is shown in Fig. 2. An important difference regards the antenna, which has to be designed for all processed frequency bands (3 for the case considered here). Especially for high-precision applications all the antenna phase centers and their variations have to be calibrated or at least determined with sub-millimeter accuracy.

The demands on the low noise amplifiers and on the RF down-conversion remains basically unchanged.

We expect that in the next years economic inertial navigation sensors (INS) will come on the market. If they are integrated into the RTK system, they will allow to reduce the bandwidth of the PLL and DLL tracking loop, reducing the thermal noise error influence and allowing faster reacquisitions [Kreye et al., 2000]. Of course the INS will also be used to bridge satellite outages.

A change in the receiver design may occur in the signal correlation and processing part. Especially for the initial phase of Galileo an improved flexibility will allow to test various signal options and processing algorithms to optimize the RTK system performance. This could be achieved by so-called software correlator receivers (SWC). They will probably gain a privileged position in comparison with hardware correlator receivers due to the least expensive hardware development. Of course the demands on the digital signal processor are extremely high for an RTK system. To process a single C/A code channel with a 1 chip correlator spacing a processing capacity of 4 MIPS is necessary [Botchkovski et al., 1999]. Increasing the bandwidth from 2 to 20 MHz, to cope with wide-band signals, increases the capacity by a factor of 10. To reduce the quantization noise level the sampling of the signal should be performed with at least 2 bits instead of 1, which also puts a factor of 3 on the processing demands. Finally, a multitude of 48 (12 channels for L1, L5, L1, E5) channels has to be processed simultaneously and continuously to obtain carrier phase measurements. Combining all factors leads to an overall DSP throughput of 5760 MIPS. These demands are on the edge of currently available DSP processors. For example the high performance DSP TMS320C6416 from Texas Instruments provides 4800 MIPS [Texas Instruments, 2001]. Recalling Moore's law (the microchip capacity doubles every 18-24 months) it should however become clear that SWC receivers will be possible at the launch time of the Galileo system.

Important improvements are also expected for the navigation processor. Not only the implementation of algorithms for reliable ambiguity fixing will yield a significant performance improvement, but also the usage of new telecommunication possibilities. Since accurate ionospheric information is indispensable for RTK performance over medium to long baselines (see below), ionospheric modeling shall be done by a network of reference receivers, instead of only by double differencing at the roving receiver. Many different techniques exist for this purpose. In all cases the different reference receivers have to communicate. Since RTK positioning requires only moderate data rates the usage of enhanced GSM data channels like GPRS, HSCSD or UMTS would be ideally suited. The major advantage of these technologies is that the setup is done easily and quickly and independent of fixed telecommunication lines. Ideally the network RTK software shall be part of each individual RTK receiver. The consequent use of new communication possibilities would also allow to establish a real time connection with a Geographical Information System (GIS) and many other applications.

4. Reliable Instantaneous Ambiguity Resolution

Satellite Constellation

The constellation used in this study is based on a YUMA-almanac for January 2001 [USCG, 2001]. The GPS constellation consisted of 28 satellites. Four satellites have been removed (those in the fifth slot), to arrive at a more or less nominal GPS constellation, with four satellites in each of the six orbit planes.

The 30-MEO Galileo constellation in [Salgado et al., 2001] is designed to offer a good performance even in case of a satellite failure. The constellation consists of 27 satellites (as 27/3/1) plus three active spares. The designation is according to the Walker type of orbit constellation, which implies circular orbits with equally spaced satellites and orbit planes. A designation as T/P/F means T satellites, P uniformly spaced planes (with each T/P satellites) and a relative phasing between satellites in adjacent planes of 360°F/T, see e.g. chapter 5 in [Parkinson and Spilker, 1996].

The key parameters of the Galileo constellation are listed in Table 3. The three orbit planes are equally spaced. Any pro- or retrograde motion of the orbit plane is assumed to be absent, as only a short period of time is considered here. The positions of the satellites within the orbit are specified by the mean anomaly; they are separated by 360°/9 = 40°.

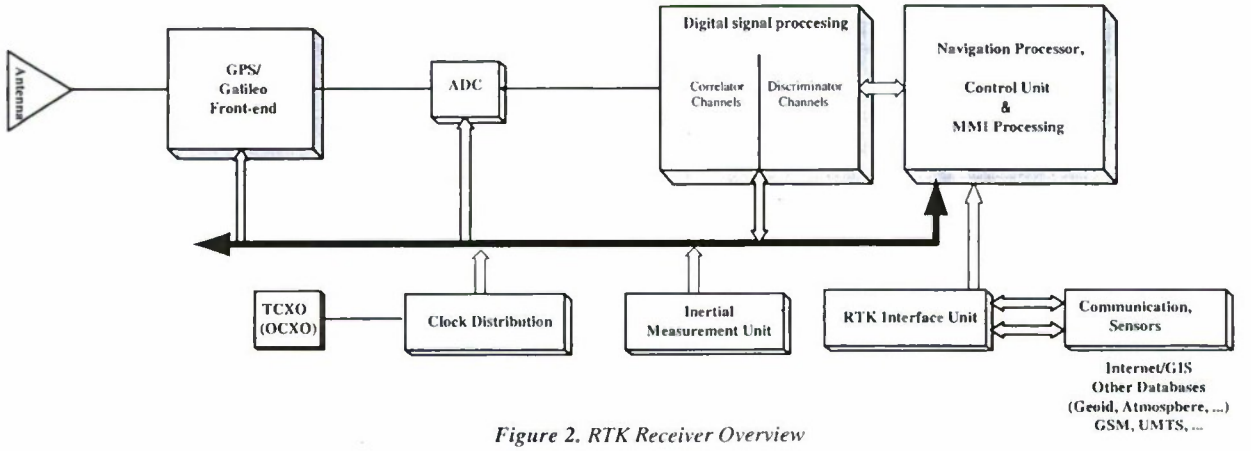

Figure 2. RTK Receiver Overview

Table 3. Almanac parameters for Galileo satellites, as Keplerian elements.

Semi-major axis	a	29994 km
Inclination	i	56°
Eccentricity	e	0.0
Right ascension	Ω_o	-120°,0°,120°
Rate of right ascension	$\dot{\Omega}$	0.0°/day
Argument of perigee	ω	0.0°
Mean anomaly (1^{st} orbit plane)	M_o	-160°,-120°, ..., 120°,160°

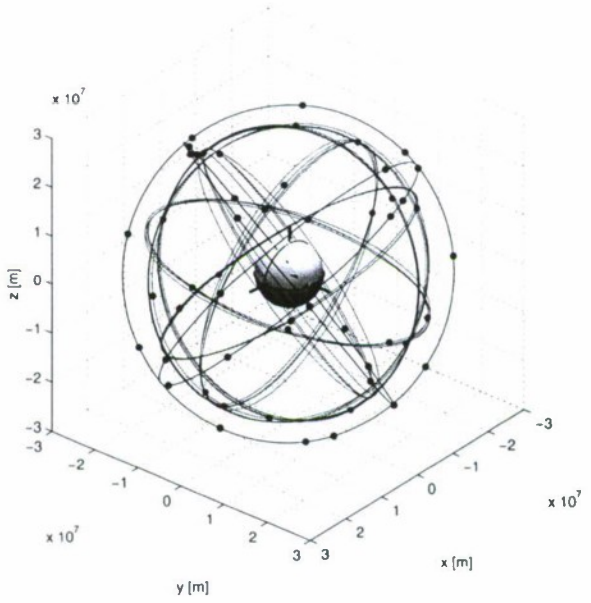

Figure 3. Hybrid GNSS satellite constellation with 24 GPS satellites (in red) and 30 Galileo satellites (in blue). Situation at 00:00h on 19-JAN-2001 (GPS time). The orbit of each satellite has been projected one full revolution ahead.

The Galileo constellation has been added-in, at time of GPS almanac applicability, without any phase offset. Comparing the first Galileo satellite with the first GPS satellite (PRN09 in slot 1 of orbital plane A) yields a difference of -46.6° in angle of Right Ascension (at weekly epoch), and of –50.0° in position in orbit, as angle with respect to the ascending node. Positioning the Galileo constellation as to have the three orbit planes coinciding with three out of six GPS planes (each time skipping one), or as to have the Galileo orbit planes halfway between two adjacent GPS planes, of course did change the results obtained at a particular epoch, but the general behavior of the parameters considered in the sequel remained the same.

The final hybrid GPS-Galileo constellation is viewed in Fig. 3, looking to the Earth from above the Middle-East. The coordinate system is the non-rotating (hence pseudo-inertial) WGS84, coinciding with the ECEF WGS84 at GPS week turnover. In the following we anticipate on full compatibility of the reference systems of GPS and Galileo.

Ambiguity Resolution

A critical step in precise Real-Time Kinematic (RTK) positioning is resolving the ambiguities. The potential of millimeter-centimeter accurate position coordinates, within a short observation time span, is available only after correct determination of the integer ambiguities. In this study the LAMBDA method is used to resolve the carrier phase ambiguities, see [Teunissen,

1993] and [de Jonge and Tiberius, 1996]. By this method, ambiguities of both satellite systems, GPS and Galileo, on one, two, three (or even more) carrier frequencies, can be treated *all* in one integral integer adjustment. In this study we consider dual frequency hybrid GPS and Galileo, with code and carrier phase measurements on L1, for both systems, and on L5 for GPS and E5 for Galileo. Measures on ambiguity resolution performance presented hereafter refer to simultaneously resolving all ambiguities, in one go, as to achieve highest possible accuracy for the position coordinates; the rates given are 'all-included'.

The integer least-squares principle embodied in the LAMBDA method has been proven to be optimal [Teunissen, 1999]. The integer least squares estimator is best in the sense of maximizing the probability of correct integer estimation, i.e. in maximizing the ambiguity success-rate. This measure expresses, given a certain scenario, how successful one can expect to be in resolving the integer carrier phase ambiguities correctly.

Exact evaluation of the success-rate is complicated when integer least-squares estimation is employed and therefore an easy to compute approximation is used in the sequel. This approximation is based on bootstrapping, a sequential process in which ambiguities are fixed (hard-constrained) to integers one-by-one, each time accounting for the statistical correlation with the remaining ambiguities. Provided that bootstrapping is applied to ambiguities that have been transformed using the ambiguity decorrelation of the LAMBDA method, it provides a good approximation. Bootstrapping is however sub-optimal compared with integer least-squares estimation and the actual success-rate for integer least-squares with the LAMBDA method is always better or at least equal to the success-rate for bootstrapping as computed in this study. The bootstrap success-rate consequently provides a guaranteed and safe lowerbound to the actual success-rate. An introduction to the LAMBDA method and the success-rate can be found in [Joosten and Tiberius, 2000].

The success-rate, as a statistical probability, can range from 0 to 1. In order to discriminate between different high levels of success-rates, the *fail-rate* is presented in the sequel. The fail-rate is simply one-minus-the-success-rate. The fail-rate should have a small value, preferably be zero.

Modeling and Processing

In the light of GPS modernization and Galileo, techniques for triple frequency ambiguity resolution have been proposed, see e.g. [Hatch et al., 2000] and [Vollath et al., 1998]. Carrier phase ambiguities are resolved using a parametrization of the measurements in ranges, the so-called geometry-free model. Geometry-free ambiguity resolution, with respect to the GPS three frequency scenario, in the context of optimal integer least-squares ambiguity estimation with the LAMBDA method, has been analysed in [Joosten et al., 1999].

The mathematical model used in the present study employs instead a parametrization of the satellite-receiver ranges in terms of baseline coordinates, i.e. the so-called geometry-based model. The LAMBDA method for ambiguity resolution is applicable to both modeling approaches, directly, without any algorithmic change.

The geometry-based model - the geodesist's and navigator's workhorse in practice - is believed to yield in general a more powerful approach to ambiguity resolution than the geometry-free model, as all ranges are linked to the same three baseline coordinate unknowns, instead of dealing with a double difference range unknown per satellite-pair. Moreover, the purpose of *positioning* is to get position coordinates eventually. On a short baseline, formulated in terms of double difference observations, the unknown parameters are the baseline coordinates and associated with the carrier phases, the integer ambiguities. On long(er) baselines differential atmospheric delays have to be taken into account. A tropospheric zenith delay will be included, together with double difference combinations of ionospheric slant delays.

To meet the condition of fast positioning in the context of Real-Time Kinematic (RTK) applications, in a strict sense, only a single epoch of data will be considered each time. Therefore no distinction needs to be made for a moving or stationary receiver. The ambiguities will be resolved instantaneously and the precise fixed solution for the baseline coordinates is directly available. Several examples, also kinematic ones, of processing dual frequency GPS phase and pseudorange code data on an epoch-by-epoch basis can be found in e.g. [de Jonge et al., 2000].

The separation in single epochs has in practice the advantage of robustness. As the data processing is started completely anew every next epoch, as opposed to a so-called accumulated solution, the effect of an anomaly or error is always restricted to (at maximum) the epoch on which it occurs. A serious drawback of this strategy is that valuable information on the nature of the problem is lost each time from one epoch to the next. The ambiguities are constants, when no cycle slips occur, and the baseline coordinates are as well, when the receiver is stationary, or only slowly varying in the case of low motion. Epochwise obtained position or trajectory coordinates could be subject to further processing as averaging or smoothing.

Concerning the measurements' noise characteristics, the initial stochastic model for the analyses includes a standard deviation for code measurements of 30 cm and of 3 mm for phase measurements. These values pertain to undifferenced measurements and for code and phase it is assumed that measurements are all equally precise. Correlation between channels (of one receiver) and between measurement types (code and phase) is assumed to be absent. As only one epoch of data is considered per solution, time correlation is not an issue.

The combined GPS and Galileo constellation, discussed earlier, is, over a full day of 24 hours, considered ('sampled') at a 3 minutes interval. After each interval of 3 minutes only one epoch of data is taken and consequently processed and analysed. Results, as the ambiguity fail-rate, are often presented later on as 95% (sample) percentiles. The value given can be interpreted as an upperbound for 95% of the time, and the value is exceeded in only 5% of the 1440 single epoch solutions considered.

By default the city of Munich in Germany is chosen as a sample location, at 48° 08' N and 11° 34' E. It is thought to represent the middle-European area. The satellite elevation cut-off angle was set to 10 degrees.

More Frequencies – More Ambiguities

Current dual frequency GPS positioning (on L1 and L2) serves as a benchmark. Employing in future also signals from Galileo satellites, yields more observational data for the determination of the same three baseline coordinates. With precise carrier phase positioning however, before reaching the fixed baseline solution, there are also more unknown ambiguities to solve for. For dual frequency GPS, and dual frequency hybrid GPS and Galileo, Table 4 summarizes the number of (integer double difference) ambiguities, when m_1 GPS, and m_2 Galileo satellites are available.

Table 4. Number of ambiguities with m_1 GPS and m_2 Galileo satellites and ambiguity fail-rate (95% percentile over the full day), on a short baseline, at location Munich, for dual frequency GPS at present (top) and future dual frequency hybrid GPS and Galileo (bottom).

System	# of amb	Fail-rate
GPS L1+L2	$2(m_1-1)$	2.4×10^{-3}
GPS+Galileo L1/L1+L5/E5	$2(m_1-1)+2(m_2-1)$	$<10^{-8}$

For various locations across Europe (from latitude 38° N in the South of Italy to 63° N halfway up Scandinavia) the ambiguity fail-rate, on a short baseline, lies in the order of 10^{-4} to 10^{-3} with dual frequency GPS at present (95% percentile over the 24 hours period). With dual frequency hybrid GPS and Galileo the fail-rate is always smaller than 10^{-8}, i.e. none of the individual solutions at the locations considered had a fail-rate ever exceeding this value.

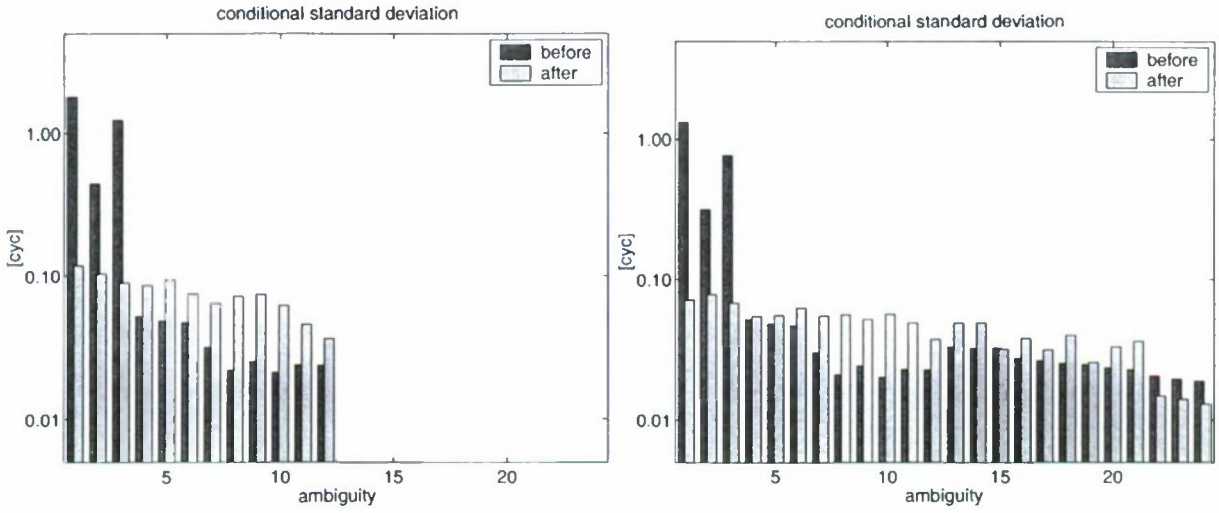

Figure 4. Spectrum of standard deviations of conditional ambiguity float estimators, in cycles. Dual frequency GPS on top, with 7 satellites, and dual frequency hybrid GPS and Galileo at bottom, with a total of 14 satellites. The orange bars refer to the original double difference ambiguities (in the order GPS L1 and L5, followed by Galileo L1 and E5), the green bars to the LAMBDA transformed ones.

Figure 4 presents the spectrum of standard deviations of the conditional ambiguity estimators both for original double difference ambiguities (in orange), as well as for decorrelated ambiguities (in green). These standard deviations are the key and only parameters determining the approximate ambiguity success-rate, by means of bootstrapping. Figure 4 pertains to a short baseline at epoch 00:00h, at which both 7 GPS satellites and 7 Galileo satellites are available. The standard deviation is given,

along the vertical axis, in cycles, in a logarithmic scale. The ambiguities, 12 on top and 24 at bottom, are ordered along the horizontal axis.

The graphs give the value of the standard deviation when the concerning ambiguity is to be fixed to an integer in the sequential bootstrap process. A standard deviation of for instance 0.1 cycle, much smaller than 1 cycle, gives good hope for successful resolution; with a value of 1 cycle, or larger, this is quite unfeasible.

Both graphs show, in orange, the very typical behavior with three larger standard deviations and 9 (on top) or 21 (at bottom) smaller ones, cf. [Teunissen et al., 1994]. The larger ones are at the 1 cycle level, prescribed by the precision of the code measurements. These three larger ones are caused by the fact that simultaneously the three baseline coordinates are unknown. Once the baseline coordinates are known, on a short baseline, all remaining ambiguities can be easily determined as then only the noise of the carrier phase measurements plays a role, which is at the 10^{-2} cycle level.

The decorrelating transformation of the LAMBDA method clearly flattens the spectrum of standard deviations of the sequential conditional ambiguity estimators and correlation between them has been reduced considerably. The resulting standard deviations, in green, are all about 0.1 cycle, indicating to more or less extent a substantial chance to successful ambiguity resolution. The standard deviations (in green) for dual frequency GPS, on top, start slightly above the 0.1 cycle level; those for dual frequency hybrid GPS and Galileo, at bottom, with more satellites and improved geometry, are smaller.

Short Baseline

Table 4 of the previous section pertains to the short baseline. The values for current dual frequency GPS, at least when 'success' and 'fail' are properly indicated during field operation and data processing, are generally acceptable for surveying types of applications, but definitely not for precise navigation of aircrafts and vehicles. The values for hybrid GPS and Galileo are promising, also for the latter applications.

Figure 5 shows the ambiguity fail-rate over the full day on the short baseline for a station in the South of Italy at 38° 07' N and 13° 22' E with present dual frequency GPS. The vertical scale is logarithmic and ranges from 10^{-8} to 1. The 95% percentile over the full day is 2.4×10^{-3}. At least 5 GPS satellites are visible all day round.

Medium and Long Baseline

On a short baseline differential ionospheric and tropospheric delays are simply absent (or perfectly known). On longer baselines differential atmospheric delays have to be taken into account however. In starting from a short baseline and extending its length, the differential atmospheric delays do not get completely unknown at once. Unknown parameters are introduced to account for the delays, but at the same time, the uncertainty about the parameters' values is bounded. The amount of uncertainty thereby depends on the actual length of the baseline. The approach followed is the same as described in [Odijk, 2000] for differential ionospheric delays.

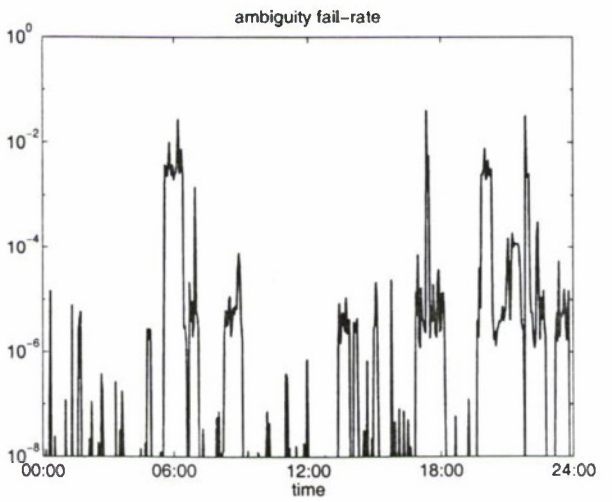

Figure 5. Ambiguity fail-rate at Palermo for current dual frequency GPS.

In the sequel we consider a medium and a long baseline. On the medium baseline we allow for an uncertainty (standard deviation) of 1.4 cm in the tropospheric zenith delay, differential between the two stations, and of 4 cm in each of the double difference slant delays (which we have one per satellite-pair). Such uncertainties are typically left on a 50 km baseline after applying correction data from a permanent active reference network. User station and reference network are thereby assumed not to differ significantly in height. With a long baseline a length of several hundreds of kilometers is meant. The aforementioned uncertainties are increased to 14 cm for troposphere and to 80 cm for ionosphere. Satellite positions are assumed to be known at a sufficient accurate level.

Table 5. *Instantaneous ambiguity fail-rate on a short, medium and long baseline for dual frequency GPS (L1+L2) at left, and dual frequency hybrid GPS and Galileo (L1/L1+L5/E5) at right. Given are 95% percentiles over the 24 hours period for location Munich.*

Baseline	GPS	GPS+Galileo
Short	2.4×10^{-3}	$<10^{-8}$
Medium	6.3×10^{-1}	6.3×10^{-2}
Long	1.0	1.0

Table 5 gives the ambiguity fail-rates for the three types of baseline lengths. On the medium length baseline one order of magnitude is gained by switching from GPS only to hybrid GPS and Galileo. On long baselines there is no chance at all to correctly resolve the ambiguities on the basis of just one epoch of data, not with dual frequency GPS, nor with dual frequency hybrid GPS and Galileo. The success-rates are respectively 3.4×10^{-5} and 1.3×10^{-3}.

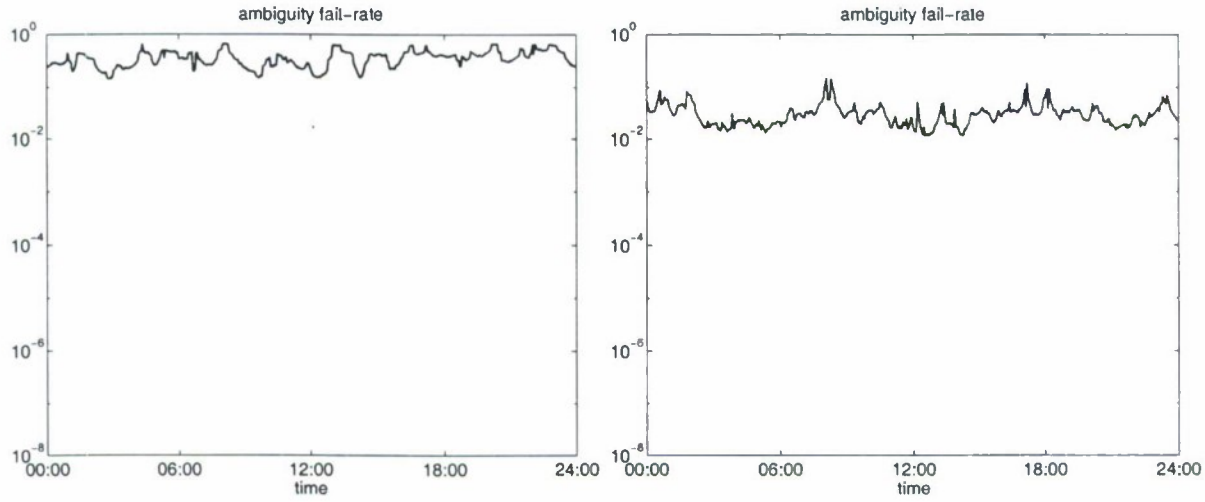

Figure 6. *Instantaneous ambiguity fail-rate for dual frequency GPS on top and dual frequency hybrid GPS and Galileo at bottom, on a medium baseline, at location Munich.*

Figure 6 presents the ambiguity fail-rate as a function of time. The 24 hours period is 'sampled' at a 3 minutes interval. As can be seen, the fail-rate behaves at a more or less constant level on this medium baseline. With dual frequency GPS the fail-rate amounts to several tens of percents (on top) and with dual frequency hybrid GPS and Galileo a few percent (at bottom).

The ambiguity fail-rate is likely to increase with increasing baseline length and this behaviour is shown explicitly in Fig 7. The tropospheric delay uncertainty was maintained at 1.4 cm (differential) and the ionospheric delay uncertainty, expressed by standard deviation σ_I was varied. For illustrative purposes the horizontal axis of Fig. 7 is expressed (logarithmic) in terms of baseline length l in [km], according to $\sigma_I=0.001\times l$ with standard deviation σ_I in [m] (at the undifferenced level), which corresponds to a 1 ppm effect. The horizontal axis ranges from 1 km to 100 km, the vertical axis from 10^{-8} to 1 (also logarithmic). Figure 7 pertains again to epoch 00:00h, with both 7 GPS and 7 Galileo satellites.

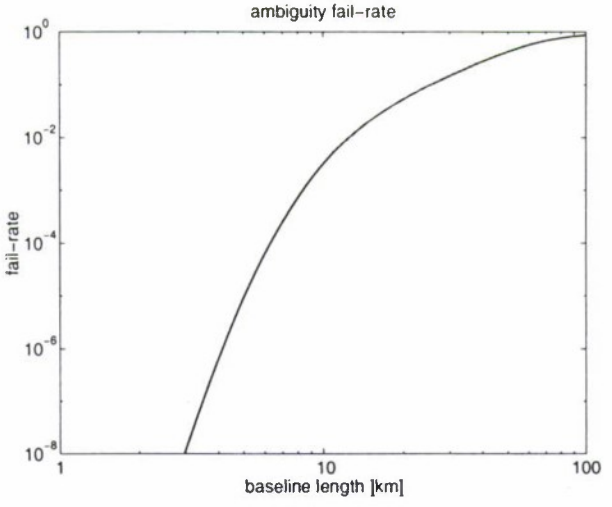

Figure 7. Instantaneous ambiguity fail-rate for dual frequency hybrid GPS and Galileo versus baseline length at location Munich. The (undifferenced) ionospheric slant delay uncertainty expressed in standard deviation σ_l [m] has been converted according to $\sigma_l = 0.001 \times l$, with baseline length l in [km].

It should be kept in mind that the fail-rates presented pertain to integer bootstrap estimation, which has been proven to be sub-optimal compared with integer least-squares estimation. The bootstrap rate tends to yield a sharp bound on the integer least-squares rate when it is based on decorrelated ambiguities, as always has been done here.

Figure 8 presents the spectrum of standard deviations of the conditional ambiguity estimators both for original double difference ambiguities (in orange) as well as for decorrelated ambiguities (in green), similar to Fig. 4, but now for a long baseline, where the tropospheric zenith delay has been left out for clarity. The graph shows, concerning the GPS ambiguities, six large standard deviations, followed by three moderate ones. There are seven satellites, hence six (unknown) double difference ionospheric slant delays, together with three baseline coordinates. With the Galileo ambiguities (ambiguity numbers 13 through 24) there are again six large standard deviations, referring to the six ionospheric delays to the Galileo satellites. The GPS and Galileo measurements share the baseline coordinates.

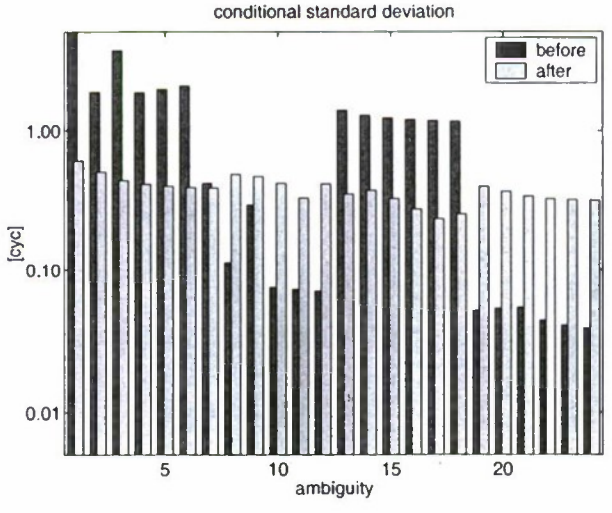

Figure 8. Spectrum of standard deviations of conditional ambiguity float estimators, in cycles, for dual frequency hybrid GPS and Galileo (L1/L1+L5/E5), on a long baseline with uncertainties of 0.80 m (standard deviation) in the double differenced ionospheric (slant) delays.

The spectrum helps to explain why ambiguity resolution can not be expected to be successful on the long baseline considered. The spectrum is well flattened, as shown in green, by the decorrelating transformation, but the standard deviations of the transformed ambiguities are at the half cycle level and that is simply too much for having any serious chance on successful resolution. Introducing only a tropospheric zenith delay (not shown here), yields still a low fail-rate, comparable to that of the short baseline.

Improved Medium Baseline

Two attempts are made to increase the ambiguity success-rate on the medium length baseline. In the first one the precision of the code measurements on L5 and E5 is increased; the standard deviation is assumed to be 10 cm instead of the default 30 cm (undifferenced), see also Table 2. The second one implies the inclusion of code and phase measurements on the GPS L2-frequency. These two cases are compared with standard dual frequency hybrid GPS and Galileo in Table 6.

The fail-rate decreases, but only a very little. It basically stays at the 5% level. The few centimeters uncertainty in the tropospheric and ionospheric delays on a single epoch medium length baseline can apparently not be compensated by either more precise code measurements or code and phase measurements on an additional frequency. Single epoch solution were considered and it should be kept in mind that with only a single epoch of data, the code measurements solely determine the float solution.

Table 6. Instantaneous ambiguity fail-rate on a medium baseline. Given are 95% percentiles over the 24 hours period for location Munich.

Case	fail-rate
Hybrid GPS+GALILEO	6.3×10^{-2}
Precise code L5/E5	5.6×10^{-2}
GPS L2 code+phase	6.1×10^{-2}

Figure 9 finally details on the relation between the precision of the code measurements and the ambiguity fail-rate for a single epoch solution on a medium baseline. The standard deviation of the L1 code measurements was kept at 30 cm (undifferenced) and the standard deviation of the GPS L5 and Galileo E5 code measurements was varied from 5 mm at left to 50 cm at right, on the horizontal axis (logarithmic). The fail-rate is given along the vertical axis from 10^{-8} to 1, also logarithmic. This figure shows that a significant reduction in the ambiguity fail-rate can be achieved only at centimeter code measurement precision.

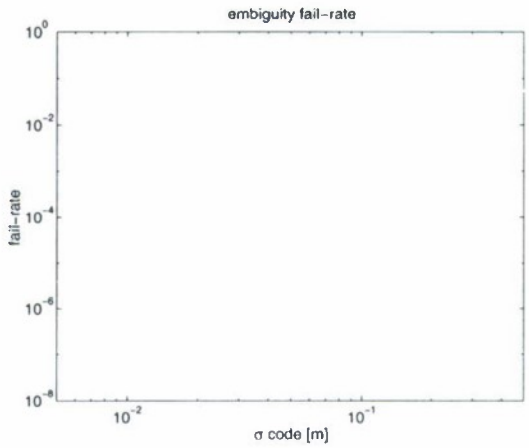

Figure 9. Ambiguity fail-rate as function of the code measurement standard deviation in [m], on a medium baseline with dual frequency hybrid GPS and Galileo.

5. Implications On Receiver Design

From the last section it can be concluded that ultra reliable instantaneous ambiguity resolution is possible with hybrid GPS and Galileo if one of the following conditions is met.

- Centimeter accuracy for the code measurements is achieved.
- The differential ionospheric slant delays are known at a few millimeter level (expressed as a standard deviation at the undifferenced level) and the differential tropospheric delays can be adequately modeled by one zenith delay parameter and a mapping function.

Accurate Code Measurements

Referring to Table 2 we conclude that code observations with 1-2 cm accuracy are virtually not achievable with civilian signals. Only the GPS military M code has the potential if it is emitted in the high power spot beam mode. However other error sources like multipath or inter channel biases, will become more significant as the code accuracy increases and will probably put a limit on that approach.

Another possibility to reduce the code measurement error due to noise is carrier smoothing. In Fig. 10 we show the RMS code error as a function of the integration time. This method potentially decreases the code error by a factor of 5. However code and phase measurements become correlated and the resulting influence on ambiguity resolution have to be investigated. Low frequency multipath is generally not reduced by carrier smoothing.

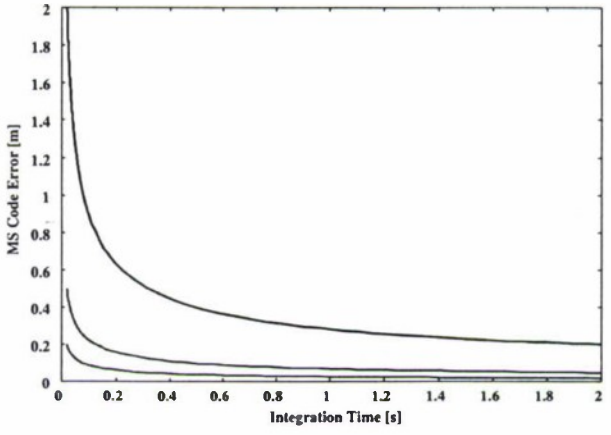

Figure 10. Initial code errors after carrier phase smoothing in the GNSS receiver (assuming a loop update rate of 20 ms)

Code measurement errors of 1-2 cm seem to be theoretically achievable if multipath and other errors are completely controlled. This would allow to instantaneously solve the ambiguities even over medium baselines. It should be noted that carrier phase measurements can be performed with 0.5-1.5 mm accuracy and thus would improve the already high code measurement accuracy by a factor of 10.

High Demands on Atmospheric Modeling: Active GNSS Reference Station Network

Ionospheric modeling for an RTK reference network is best performed by bilinear interpolation between 3 or more reference stations [Wanninger, 1999]. In that way all effects having a wavelength longer than the extension of the reference network are removed. Over Europe especially medium-scale travelling ionospheric disturbances and phase scintillations can have a wavelength shorter than 50-100 km. Latter number is the typical extension for a reference network. Wanninger [1999] reports that under undisturbed ionospheric conditions virtually all ionospheric delay can be determined by bilinear interpolation for a network with a size smaller than 100 km. Under solar maximum conditions the residual ionospheric delay on undifferenced observations is about 8 mm for a network extension of 50 km, and about 33 mm for an extension of 100 km.

It should be noted that the one-dimensional power spectrum of ionospheric refractivity fluctuations shows an approximate power law behaviour of λ^2 (λ lambda being the horizontal wavelength) for a range of 70 m to 7 km [Yeh and Chao-Han, 1982] implying that ionospheric modeling can be performed arbitrarily precisely, depending only on the distance of the reference receivers.

From that we conclude that within a small scale RTK network ultra high instantaneous ambiguity resolution reliability can be achieved. Setting up such a network is easy if the receivers have the capability to communicate with each other automatically via for example GSM data channels.

Tropospheric demands are not that stringent because only one parameter, namely the (differential) zenith delay, is estimated per baseline. Treuhaft et al. [1992] showed that the most variable component of the delay, the wet zenith delay, is correlated within 1 cm for distances below 30 km. Tropospheric modeling could be further improved, by a network of RTK receivers and by including data from a numerical weather prediction model. Latter one also gives vertical tropospheric refractivity profiles. In that case one RTK reference receiver must have a real time access to the predicted weather model fields, via for example the internet.

Conclusions

Future RTK receiver systems will be developed incorporating remarkable technological improvements. Software correlation receivers will offer a great flexibility and allow for optimization of the RTK system performance. A combined use of the new signals in space of the modernized GPS and the upcoming Galileo system will drastically reduce the instantaneous ambiguity fail-rate from 10^{-3} to 10^{-8} on short baselines.

An hybrid RTK receiver will be most effective, if full use of the ultra high ambiguity success-rate is exploited. The increased success-rate is caused by the increased number of satellites and the improved satellite geometry. Of less importance seem to be a possible use of a third frequency (i.e. L2 for GPS) or an increased code measurement accuracy, as long as it is above approx. 5 cm. The difference between a GPS only and a hybrid GPS/Galileo system is largest for short baselines and vanishes as the ionospheric uncertainty (i.e. the baseline length) increases. Therefore also for a future RTK system atmospheric, especially ionospheric, modeling is of utmost importance. Here we expect that new wireless communication technologies will facilitate the convenient setup of a complete RTK reference network.

Acknowledgement

The investigations and developments of a future GNSS RTK receiver are supported within the scope of the research project FKZ: 50NA0003 in contract with DLR.

References

Botchkovski A. et al. (1999): Softflex, An Advanced Approach to Design of GNSS Receiver with Software Correlator, Proc. ION GPS 1999, Nashville, September 14-17, pp. 353-362.

Hatch, R., J. Jung, P. Enge and B. Pervan (2000): Civilian GPS: the Benefit of Three Frequencies, GPS Solutions, Vol. 3, No. 4, pp. 1-9.

Hein G. et al., (2001): The Galileo Frequency Structure and Signal Design, Proc. ION GPS 2001, Salt Lake City, September 11-14.

Jonge, P. de and C. Tiberius (1996): The LAMBDA Method for Integer Ambiguity Estimation: Implementation Aspects, Technical Report Delft Geodetic Computing Center, LGR-series, No. 12, August, 49 pp.

Jonge, P. de, Y. Bock and M. Bevis (2000): Epoch-by-Epoch™ Positioning and Navigation, Proc. ION GPS 2000, Salt Lake City, September 19-23, pp. 337-342.

Joosten, P., P. Teunissen and N. Jonkman (1999): GNSS Three Carrier Phase Ambiguity Resolution using the LAMBDA-method, Proc. GNSS'99, Genova, October 5-8, pp. 367-372.

Joosten, P. and C. Tiberius (2000): Fixing the Ambiguities: Are You Sure They're Right? GPS World, Vol. 11, No. 5, pp. 46-51.

Kreye, C., B. Eissfeller and J. Winkel (2000): Improvements of GNSS Receiver Performance Using Deeply Coupled INS Measurements, Proc. ION GPS 2000, Salt Lake City, September 19-23, pp. 844-854.

Odijk, D. (2000): Weighting Ionospheric Corrections to improve Fast GPS Positioning over Medium Distances. Proc. ION GPS 2000, Salt Lake City, September 19-23, pp. 1113-1123.

Parkinson, B. and J. Spilker (1996): Global Positioning System: Theory and Applications. Progress in Astronautics and Aeronautics, Vol. 163 and 164, AIAA Washington.

Salgado G., S. Abbondanza, R. Blondel and S. Lannelongue (2001): Constellation Availability Concepts for Galileo, Proc. ION NTM 2001, Long Beach, January 22-24, pp. 778-786.

Shaw, M., K. Sandhoo, and D. Turner (2000): Modernization of the Global Positioning System, GPS World, September 2000, pp. 36-44.

Teunissen, P. (1993): Least-Squares Estimation of the Integer GPS Ambiguities, Invited Lecture, Section IV 'Theory and Methodology', IAG, Beijing, China, August.

Teunissen, P., P. de Jonge and C. Tiberius (1994): On the Spectrum of the GPS DD Ambiguities, Proc. ION GPS 1994, Salt Lake City, September 20-23, pp. 115-124.

Teunissen, P. (1999): An Optimality Property of the Integer Least-Squares Estimator, J. Geod., Vol. 73, pp. 587-593.

Texas Instruments (2001): TMS320C6416, Fixed-Point Digital Signal Processor, http://dspvillage.ti.com/.

Treuhaft, R. and G. Lanyi (1987): The Effect of the Dynamic Wet Troposphere on Radio Interferometric Measurements, Radio Sci., Vol. 22, No. 2, pp. 251-265.

Wanninger, L. (1999): The Performance of Virtual Reference Stations in Active Geodetic GPS-networks under Solar Maximum Conditions, Proc. ION GPS 1999, Nashville, September 14-17, pp. 1419-1427.

Winkel, J., B. Eissfeller, G. Hein and P. Hartl (2000): Requirements on the Galileo Signal Structure, GNSS2000, Edinburgh, May 1-4.

United States Coast Guard (2001): YUMA-Almanac, http://www.navcen.uscg.mil/gps/default.htm#Almanacs

Vollath, U., S. Birnbach, H. Landau, J.M. Fraile-Ordonez and M. Martin-Neira (1998): Analysis of Three-Carrier Ambiguity Resolution (TCAR) Technique for Precise Relative Positioning in GNSS-2, Proc. ION GPS 1998, Nashville, September 15-18, pp. 417-426.

Yeh, C.Y. and L. Chao-Han (1982): Radio Wave Scintillations in the Ionosphere, Proc. IEEE Vol. 70, No. 4, pp. 324-360.

PRECISE RELATIVE NAVIGATION OF SPACE VEHICLES WITH GPS

M. Mittnacht*, M. Hartrampf **
Astrium GmbH, Munich, Germany
M. Vasilev *, N. Mikhailov******
Soft Nav Ltd., St. Petersburg, Russia

The GPS technique is considered now as a preferred tool to implement the real time autonomous systems for sub-centimeter relative navigation of Earth-orbiting satellites and piloted orbital vehicles. The reason is that the usage of approximately inexpensive GPS receiver allows cutting down expenses on sufficiently complex and expensive classical navigation system without any losses of accuracy. This paper describes the adaptation of a low cost space borne GPS receiver MosaicGNSS developed by Astrium GmbH for relative navigation of the space vehicles including such types of satellites as LEO and GEO. It is necessary to mention that the main peculiarity of the MosaicGNSS receiver is the implementation of all function of signal correlator in software. As sequence, there are several limiting features of the Mosaic GNSS receiver as applied to the task of the spacecraft relative navigation:

- Relatively low accuracy of pseudorange measurements (RMS is about 3-4 meters)
- Limited number of tracked GPS satellites. Number of tracked satellites is limited by the throughput of the receiver processor and strongly depends on the strength of the GPS satellites signals.
- Large time to first valid measurements from the moment when GPS satellite becomes visible.

It is shown in the paper that these shortcomings are not critical ones and may be overcome by using algorithms described below.

There are two technical approaches to attain sub-centimeter relative navigation accuracy: methods based on accounting of the satellite dynamics and "dynamics free" solutions. The first group of methods is applicable for all types of non-maneuvering satellites. The second one works only if at least five GPS satellites are visible simultaneously. "Dynamics free" approach may be used only for LEO satellites and has the following features:

- Absolute position of the reference LEO satellite is determined from the pseudorange processing
- Combine processing of double differenced phase and pseudorange measurements is performed to estimate relative satellite-satellite position and to resolve phase ambiguity

The main features of the "dynamics dependent" (GEO is the typical case) approach are the following ones:

- Orbital parameters of the reference satellite are determined from the pseudorange processing
- Combine processing of single differenced phase and pseudorange measurements is performed to estimate the difference between the orbital parameters (elements) of reference and driven satellites. The phase ambiguities are estimated as well.

Modeling of the different scenarios of LEO and GEO relative navigation was performed using multi-channel GPS simulator and MosaicGNSS receivers as onboard navigation tools. It is shown that the LEO relative position may be determined with the accuracy of about 1 centimeter (RMS) in all analyzed cases: zero, 1, 10 and 100 kilometer baselines.

It is demonstrated also that the mean time to first fix (TTFF) is about two minutes. Note, that TTFF fix was calculated as time from the moment when the measurements from at least 5 satellites become available to time when phase ambiguities are fixed. It is shown also that TTFF might be reduced significantly in case of usage of more powerful GPS receiver, which can produce more accurate pseudorange measurements.

Test scenarios for GEO relative navigation are under processing now.

---

*Engineer.
**Engineer.
***Engineer.
****General Manager.

INTEGRATION OF MULTI-STATION LONG-RANGE DGNSS DATA

T. Willems*
Department of Applied Mathematics and Computer Science, Ghent University, Belgium,
E-Mail: Tom.Willems@rug.ac.be
A. De Wulf**,
Department of Geography, Section Land Surveying, Ghent University, Belgium,
E-Mail: Alain.DeWulf@rug.ac.be
M. Brondeel***
Department of Geography, Section Land Surveying, Ghent University, Belgium,
E-Mail: Marijke.Brondeel@rug.ac.be

Abstract

Key words: RAAS, error propagation, simulation

The accuracy of differential GNSS positioning is, as we all know, inversely proportional to baseline length. This is commonly labeled decorrelation, which we can define as the decreasing relevance of reference station data to the user when baseline length is increased. It can be decomposed into spatial decorrelation, which includes atmospheric decorrelation, and temporal decorrelation, which is a real-time issue.

In order to overcome spatial decorrelation one clearly needs to employ, either implicitly (e.g. in case of SBAS systems) or explicitly, data from different reference sites. For terrestrial applications, however, SBAS systems often cannot meet strict availability requirements because of signal masking. On the other hand, terrestrial networks providing differential data are often confined to a rather slow data rate, which implies that they cannot conveniently accommodate WADGNSS data. Even if they could, costly additional infrastructure would be required.

It is particularly interesting against this background to investigate user equipment algorithms for merging different sources of differential data. This technique, in which networked differential corrections are computed by the user equipment, effectively implements regional area augmentation (RAAS). It has been discussed previously with regard to the Loran-C/Chayka Eurofix service, since Eurofix could potentially make two or more long-range differential data streams available over large areas. It could also be of interest in the context of maritime DGNSS radio beacons.

To gain a better understanding of decorrelation, it is interesting to look at scatter plots associated with long-range differential code fixes. These plots demonstrate a shift on the mean position along the baseline in the direction away from the reference station. This systematic baseline stretching in differential code positioning is a result of spatial decorrelation.

As with any parameter estimation process, the study of the propagation of random and systematic errors on the observation data into the results, is relevant to GNSS observation data processing. By using different simulation techniques, Santerre et al. have obtained important results in this field for GPS ambiguities-fixed and ambiguities-free carrier phase solutions. In the context of long-range differential code positioning, we focus on the propagation of residual ionospheric errors into the horizontal coordinates.

The ionospheric delay on a satellite that is simultaneously visible at the reference station and the rover will be different at both sites. This so-called ionospheric decorrelation increases with baseline length and results in residual errors on the corrected pseudoranges. These errors, which depend on the relative satellite-receiver position and time, propagate into the estimated parameters i.e. receiver coordinates and clock error. We illustrate this by an examplatory plot of horizontal error induced by the ionosphere as a function of time for stand-alone operation and for differential code over a distance of 150 km and 400 km.

We developed a simulation technique using MatLab software in which the only errors imposed on the measurements are ionospheric delays. The Klobuchar model was used with post-processed coefficients provided by CODE (Center for Orbit Determination in Europe, University of Berne, Switzerland) for estimating the ionospheric delays. Simulated corrected pseudorange data that is only affected by ionospheric decorrelation was generated and then processed in a standard least squares estimation of the receiver position and clock error. The plot of horizontal error referenced above was generated using the simulation procedure. It was also used to construct simulated scatter plots, in which the directional spatial decorrelation effect was clearly recovered.

Wide area augmentation systems are able to estimate various error components individually because of the very long baselines present in their vast tracking network. On a regional scale, however, we limit ourselves to modelling the total error. Additionally we assume that the error is basically a linear function of the location over the regional area. The reference stations provide the total error as observed on-site in the form of pseudorange

* M.Sc., Assistant** Ph.D., Professor,*** Ph.D., Assistant,

corrections.

Suppose that three non-collinear reference sites, located at (x_i, y_i) $(i = 1,2,3)$, provide a pseudorange correction PRC_i $(i = 1,2,3)$ for a certain satellite to a user located at (x_r, y_r). The three points (x_i, y_i, PRC_i) $(i = 1,2,3)$ define a plane in three-dimensional space. A point (x_r, y_r, PRC_r) also lies in this plane and PRC_r can subsequently be used as a pseudorange correction for the satellite at the user's location. We present the mathematical formulation and solution of this problem, including least-squares techniques in case data from more than three reference stations is available.

This augmentation approach was introduced into the simulation software described previously. Several tests were carried out using different numbers of reference nodes, different baseline lengths within the network, different geometries of the reference nodes, etc. Only minor residual errors due to decorrelation were observed when using three reference stations distributed evenly around the rover at a distance of approximately 1000 km. In this case the networked corrections appear to be quite effective, despite the great distance of the reference nodes to the rover. The residual decorrelation effects are more explicit when a less optimal arrangement of the different nodes is used. However, the results were still found to be better than when operating stand-alone, while using only one of the reference stations produced results even worse than in stand-alone mode.

Substantial spatial decorrelation effects occur when operating differentially with a single reference station over a long range. When different sources of differential data are available, however, we conclude that user equipment based augmentation appears to be a useful technique for mitigating these effects, even over fairly large areas. A uniform arrangement of the reference nodes over the intended coverage area is advisable.

The most attractive feature of user equipment based augmentation undoubtedly is that an expensive communications network, which permanently links all reference sites and a control station, is unnecessary. Each reference site transmits directly to the user, where all processing takes place. In case one of the reference nodes goes down, the other nodes serve as a backup. Temporal decorrelation due to data latency is minimised since each site only needs to transmit its own data. The computational load on the user equipment for carrying out the data fusion is low.

1. Spatial and Temporal Decorrelation

Introduction

It is surely sufficiently well known that the accuracy of differential GNSS positioning is inversely proportional to baseline length. This is commonly labeled decorrelation, which we can define as the decreasing relevance of reference station data to the user when baseline length is increased. It can be decomposed into spatial decorrelation, which includes atmospheric decorrelation, and temporal decorrelation, which is a real-time issue.

Particularly interesting in the context of decorrelation are scatter plots associated with long-range differential code fixes. Figure 1 shows one such scatter plot for a baseline length of 350 km, baseline orientation of 30 degrees (as seen from the roving station), session length of 24 hours (Jan. 4, 2001), interval of 30 seconds and a cut-off angle of 10 degrees. The processed data originates from the EUREF (European Reference Frame) permanent observation stations BORK (Borkum, Germany) and BRUS (Brussels, Belgium) for the reference station and rover respectively. Both the mean and exact position are indicated on the scatter plot, as well as baseline orientation. Note that when studying scatter plots, one has to keep in mind that they obscure any time-dependent effect that may be present on the underlying data.

Figure 1 indicates a shift on the mean position along the baseline in the direction away from the reference station. This systematic baseline stretching in differential code positioning is a result of spatial decorrelation [1,4].

Propagation of residual ionospheric error

As with any parameter estimation process, the study of the propagation of random and systematic errors on the observation data into the results, is relevant to GNSS observation data processing. By using different simulation techniques, Santerre et al. [2] have obtained important results in this field for GPS ambiguities-fixed and ambiguities-free carrier phase solutions. In the context of long-range differential code positioning, we will now focus on the propagation of residual ionospheric errors into the horizontal coordinates. The fact that a receiver clock error parameter is included in the least squares adjustment complicates a purely geometric interpretation.

The ionospheric delay on a satellite that is simultaneously visible at the reference station and the rover (under a large enough elevation angle) will be different at both sites. This so-called ionospheric decorrelation increases with baseline length and results in residual errors on the corrected pseudoranges. These errors, which depend on

the relative satellite-receiver position and time, propagate into the estimated parameters i.e. receiver coordinates and clock error.

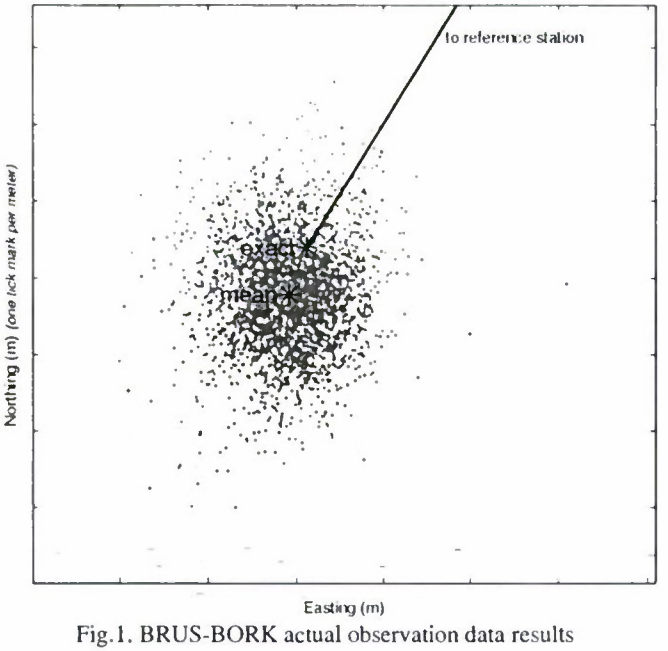

Fig.1. BRUS-BORK actual observation data results

In order to illustrate ionospheric decorrelation, Figure 2 shows a plot of horizontal error induced by the ionosphere at BRUS as a function of time (on Jan. 27, 2001) for stand-alone operation and for differential code over a distance of 150 km and 400 km, baseline orientation of 90 degrees, cut-off angle of 10 degrees. Note that the ionosphere is at its maximum activity level around 14h local time. For a baseline length of 150 km, most of the ionospheric error is compensated for, with only slightly more residual error when the ionosphere is at its most active state. A less pronounced improvement is seen over the 400 km baseline because of increased ionospheric decorrelation.

Simulation technique and results

Figure 2 is the result of a simulation, using MatLab software, in which the only errors imposed on the measurements are ionospheric delays. The Klobuchar model was used with post-processed alpha and beta coefficients provided by CODE (Center for Orbit Determination in Europe, University of Berne, Switzerland) for estimating the ionospheric delays. Using this model with post-processed coefficients is computationally light while performance is sufficient for our purposes. For each simultaneously visible satellite (i.e. each satellite visible under at least the minimum elevation angle at both sites simultaneously), at each epoch, the ionospheric delay was estimated for both the reference station and the rover.

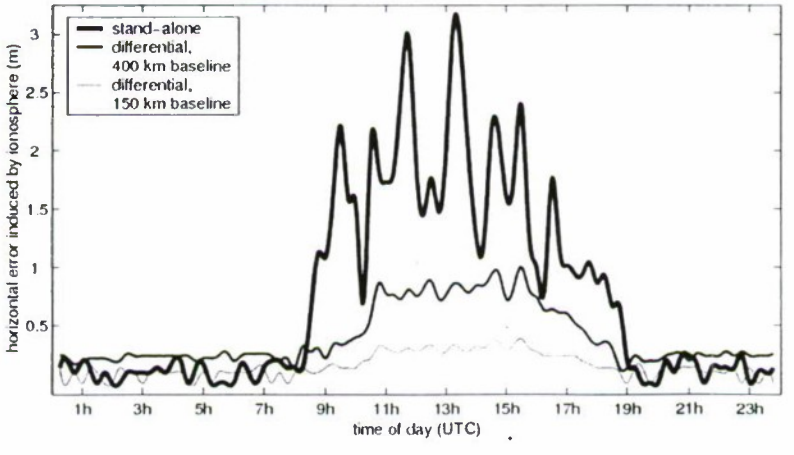

Fig.2. Ionospheric decorrelation

Simulated corrected pseudorange data that is only affected by ionospheric decorrelation, is generated by adding an estimate of the residual range error caused by ionospheric decorrelation to the exact geometric distance between rover and satellite. An estimate of the residual range error can be found by subtracting the

estimated ionospheric delay at the reference station from the estimated ionospheric delay at the rover.

The simulated observation data for each epoch is processed in a standard least squares estimation of the receiver position and clock error. In order not to bias the results, the iterative estimation process starts at the exact receiver position and at zero clock error. The primary output of the simulation thus is one position fix per epoch (except for epochs with insufficient common satellites) and its associated horizontal error. The only inputs basically are: exact rover and reference station coordinates, satellite ephemerides, alpha and beta ionospheric coefficients, cut-off angle, interval, start and stop time.

While the simulation procedure facilitates analysis in the sense of Figure 2, it can also be used to construct simulated scatter plots. In Figure 3, a simulated scatter plot is shown for the rover set at BRUS, reference station at BORK, cut-off angle of 10 degrees, session length of 24 hours (Jan. 4, 2001), interval of 15 minutes. This setup corresponds to the scatter plot, generated from actual observations at the BRUS and BORK permanent stations, presented in Figure 1.

In comparing Figure 3 to Figure 1, it seems that we have recovered the directional effect that was mentioned previously. Figure 4 shows some other simulated scatter plots at BRUS for a baseline orientation of 45, 135, 225 and 315 degrees (Figure 4(a), 4(b), 4(c) and 4(d) respectively), baseline length of 300 km, cut-off angle of 10 degrees, session length of 24 hours (Jan. 4, 2001), interval of 15 minutes. The systematic baseline stretching is demonstrated in each subplot.

2. User Equipment Based Regional Area Augmentation

Introduction

In order to overcome spatial decorrelation one clearly needs to employ, either implicitly (e.g. in case of SBAS systems such as EGNOS) or explicitly, data from different reference sites. For terrestrial applications, however, SBAS systems often cannot meet strict availability requirements because of signal masking. On the other hand, terrestrial networks providing differential data are often confined to a rather slow data rate, which implies that they cannot conveniently accommodate WADGNSS data. Even if they could, costly additional infrastructure would be required.

It is particularly interesting against this background to investigate user equipment algorithms for merging different sources of differential data. This technique, in which networked differential corrections are computed by the user equipment, effectively implements regional area augmentation (RAAS). It has been discussed previously with regard to the Loran-C/Chayka Eurofix service [3], since Eurofix could potentially make two or more long-range differential data streams available over large areas. It could also be of interest in the context of maritime DGNSS radio beacons.

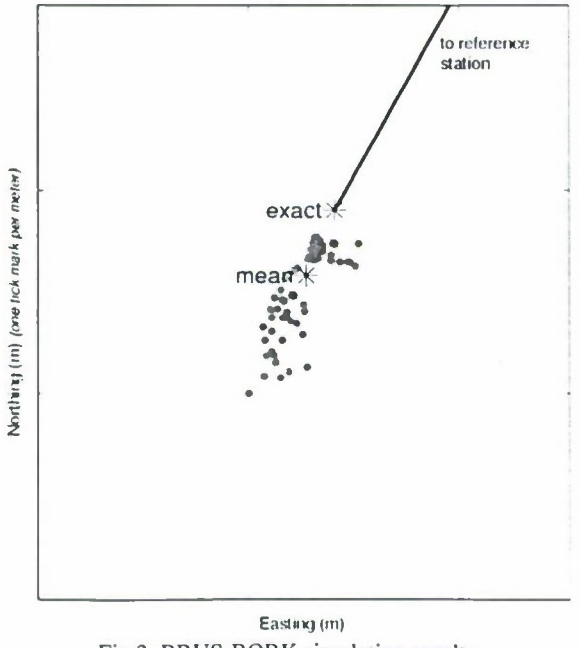

Fig.3. BRUS-BORK simulation results

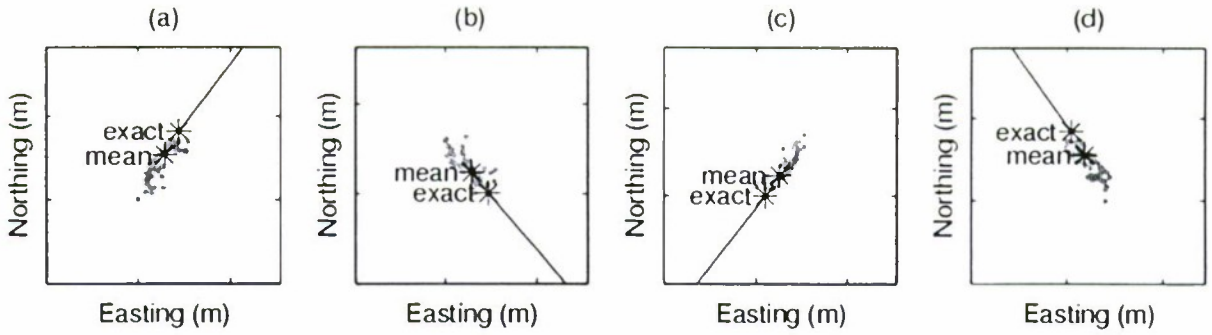

Fig.4. Further simulation results

Networked pseudorange corrections

Wide area augmentation systems are able to estimate various error components individually because of the very long baselines present in their vast tracking network. On a regional scale, however, we limit ourselves to modelling the total error. Additionally we assume that the error is basically a linear function of the location over the regional area. For each satellite, the reference stations provide the total error as observed on-site in the form of pseudorange corrections.

Suppose that three non-collinear reference sites, located at (x_i, y_i) $(i = 1,2,3)$, provide a pseudorange correction PRC_i $(i = 1,2,3)$ for a certain satellite to a user located at (x_r, y_r). The three points (x_i, y_i, PRC_i) $(i = 1,2,3)$ define a plane in three-dimensional space. A point (x_r, y_r, PRC_r) also lies in this plane and PRC_r can then be used as a pseudorange correction for the satellite at the user's location. If data from more than three reference stations is available, least-squares techniques can be used.

Suppose that data for a satellite j is available from n reference stations $(n \geq 3)$, located at (x_i, y_i) $(i = 1,2,\ldots,n)$, at the rover's location (x_r, y_r). Denote the pseudorange corrections received for this satellite as PRC_i^j $(i = 1,2,\ldots,n)$. Recall that a plane can be defined as $z(x,y) = \alpha_0 + \alpha_x x + \alpha_y y$. The pseudorange correction PRC_r^j for satellite j at the rover can then be calculated as:

$$PRC_r^j = \alpha_0^j + \alpha_x^j x_r + \alpha_y^j y_r \text{, with } \begin{bmatrix} \alpha_0^j \\ \alpha_x^j \\ \alpha_y^j \end{bmatrix} = (A^T A)^{-1} A^T \begin{bmatrix} PRC_1^j \\ PRC_2^j \\ \cdots \\ PRC_n^j \end{bmatrix}, A = \begin{bmatrix} 1 & x_1 & y_1 \\ 1 & x_2 & y_2 \\ & \cdots & \\ 1 & x_n & y_n \end{bmatrix}. \quad (1)$$

In case data from only two reference stations is available, assuming that the error varies linearly along the line connecting both reference stations, we project the rover's position onto this line. We then find that:

$$PRC_r^j = PRC_1^j + \frac{\begin{bmatrix} x_r - x_1 & y_r - y_1 \end{bmatrix} \begin{bmatrix} x_2 - x_1 \\ y_2 - y_1 \end{bmatrix}}{\begin{bmatrix} x_2 - x_1 & y_2 - y_1 \end{bmatrix} \begin{bmatrix} x_2 - x_1 \\ y_2 - y_1 \end{bmatrix}} (PRC_2^j - PRC_1^j). \quad (2)$$

Simulation technique and results

This augmentation approach was introduced into the simulation software described previously. The reference values for the ionospheric delays at the rover and each reference station are first calculated (see above). The delays at each of the reference stations are then combined into a networked estimate of the delay at the rover. Next, the networked estimate is subtracted from the delay calculated for the rover in the first step, in order to obtain an estimate of the residual range error at the rover. This estimate is then added to the exact geometric distance between rover and satellite in order to obtain a simulated corrected pseudorange. The simulated measurements resulting from this procedure, which is repeated for each satellite and each epoch, are processed as described above.

Several tests were carried out using different numbers of reference nodes, different baseline lengths within the network, different geometries of the reference nodes, etc. Only satellites under common view at all reference

stations and the rover were used. When using this common view approach, the cut-off angle should be chosen low enough to ensure availability over the intended area (but not a lot lower). Each of the results shown below were obtained using a session length of 24 hours, a cut-off angle of 10 degrees, an interval of 15 minutes and under mild ionospheric activity conditions.

Figure 5 shows the result of a test using three reference stations distributed evenly around the rover at a distance of approximately 1000 km. Despite the great distance of the reference nodes to the rover, the networked corrections appear to be quite effective thanks to the favourable arrangement of the different nodes. Only minor residual errors due to decorrelation are observed.

In Figure 6, the arrangement of the different nodes is much less optimal and the residual decorrelation effects are consequently more explicit. The results are still better than when operating stand-alone, while using only one of the reference stations was found to produce results even worse than in stand-alone mode.

The arrangement of reference stations in Figure 7 reflects a possible Eurofix setup within the NELS (Northwest European Loran-C System) [3]. The performance at the rover's location is somewhat in-between what we have seen previously, which is not surprising considering its location with respect to the reference stations.

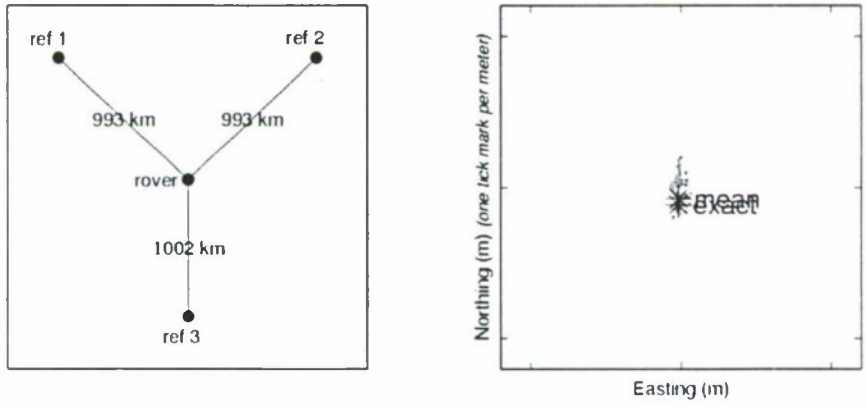

Fig.5

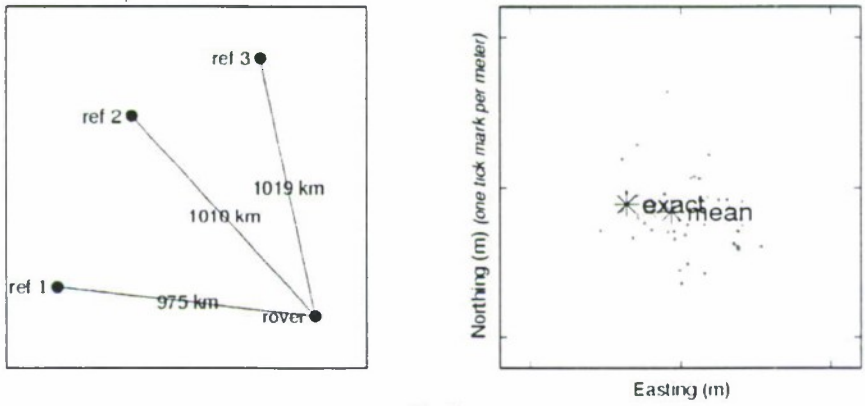

Fig.6

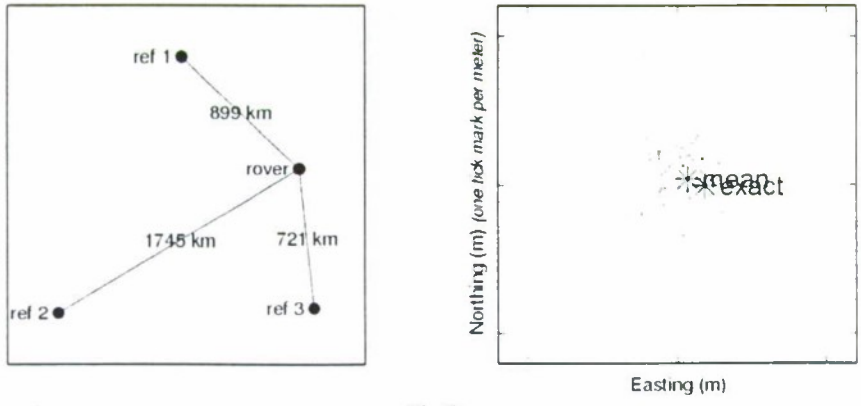

Fig.7

3. Conclusions

Substantial spatial decorrelation effects occur when operating differentially with a single reference station over a long range. When different sources of differential data are available, however, user equipment based augmentation appears to be a useful technique for mitigating these effects, even over fairly large areas. A uniform arrangement of the reference nodes over the intended coverage area is advisable.

The most attractive feature of user equipment based augmentation undoubtedly is that an expensive communications network, which permanently links all reference sites and a control station, is unnecessary. Each reference site transmits directly to the user, where all processing takes place. In case one of the reference nodes goes down, the other nodes serve as a backup. Temporal decorrelation due to data latency is minimised since each site only needs to transmit its own data. The computational load on the user equipment for carrying out the data fusion is not high since the pseudo-inverse of A in (1) only needs to be computed once for each encountered combination of reference nodes.

This augmentation technique could be used in combination with maritime DGNSS radio beacons. Given that the validity of correction data is (in the absence of selective availability measures) in the order of several minutes, one beacon receiver would suffice for this purpose. We could tune to the different available beacons one by one, retuning each time a complete set of corrections has been received. It is possible to do this automatically since the tuning of most beacon receivers can be controlled by software. An implementation is currently under development at Ghent University.

User equipment based regional area augmentation has been discussed previously in the context of the Loran-C/Chayka Eurofix service [3]. Indeed, it seems that Eurofix is particularly suitable since its full-scale implementation would make two or more long-range differential data streams available over large areas and its arrangement of sites would be quite favourable. User equipment based regional area augmentation could revalidate DGNSS as a useful mode for Loran-C/Chayka.

Acknowledgments

This work has been carried out with the highly appreciated support of the Department of Geography and the Department of Applied Mathematics and Computer Science at Ghent University, Belgium. The first author would like to express his appreciation to W. Blanchard, A. Muls and A. De Clercq for their support.

References

1. **Blanchard, W.** (2000), "The Characteristics of Long Range DGPS", Proceedings of GNSS 2000, Fourth European Symposium on Global Navigation Satellite Systems, Edinburgh, Scotland.
2. **Santerre, R., Beutler, G. & Geiger, A.** (1990), "GPS Error Analysis and Modelling", Proceedings of the Second International Symposium on Precise Positioning with the Global Positioning System, Ottawa, Canada.
3. **Van Essen, R.F., Offermans, G.W.A, Helwig, A.W.S. & van Willigen, D.** (1997), "Regional Area Augmentation Concept for Eurofix - Reducing Spatial Decorrelation Effects through Multi-station DGNSS", Proceedings of the 26th Annual Technical Symposium of the International Loran Association, Ottawa, Canada.
4. **Willems, T., Blanchard, W. & De Wulf, A.** (2001), "DGNSS Directional Spatial Decorrelation at European Latitudes", Proceedings of GNSS 2001, Fifth European Symposium on Global Navigation Satellite Systems, Sevilla, Spain.

BLUNDER DETECTION AND ESTIMATION WITH FUZZY LOGIC: APPLICATIONS TO GPS CODE- AND CARRIER-PHASE MEASUREMENTS

N. Crocetto*, S. Ponte**
Second University of Naples – Via Roma, 29 – 81031 Aversa (CE), Italy

Abstract

Key words: GPS measurements, fuzzy logic, outlier detection

This paper presents a new strategy of localisation and estimation of gross errors (blunders) in code-phase (pseudorange) and carrier-phase GPS (Global Positioning System) measurements. Our FLOOD (Fuzzy LOgic-based Outlier Detection) procedure localises in a single iteration several (in particular cases, all of the) observations affected by blunders, in contrast to typical least-squares compensation procedures which require iterations and have significant computational cost. The devised three-step approach consists of a conventional blunder detection statistical test (first stage), a fuzzy-logic based blunder localization procedure (second stage), and a blunder estimation module (third stage). The FLOOD approach saves computational time and allows one to use the whole observation vector, without discarding the measurements affected by blunders. The procedure is applied to a typical set of Coarse/Acquisition (C/A) code measurements. Three and five blunders were injected into the measurement vector, respectively, and in both cases the FLOOD core localised the outliers by assigning to the residuals membership values to the fuzzy set "observations affected by blunders" and defuzzifying on a threshold-based value (α-cut criterion). Similar results are found on carrier-phase measurements.

1. Introduction and rationale

Detection and estimation of the magnitude of gross errors (outliers, or blunders) is a crucial issue in navigation and geodetic measurements (for example, platform trajectory or orbit determination from GPS position fixes, least-squares (LS) solutions for user state vector estimates with redundant pseudorange measurements, orbit reconstruction from tracking radar estimates, triangulation and/or trilateration networks). Outliers in the GPS observables (pseudorange or carrier phase) can be attributable to hardware receiver errors, such as correlator noise and measurement noise, as well as to multipath, i.e. secondary-path signals reflected from the ground or from structures in the vicinity of the GPS antenna. Unpredicted or partially compensated anomalies (such as GPS satellite ephemeredes and clocks, ionospheric and tropospheric propagation delay) produce position and phase errors. Moreover, secondary-path signals reflected by the structure of the platform can significantly distort the signal's waveform amplitude and phase, inducing blunder in the observables.

Throughout this work, the assumed functional model of the GPS observations is Gauss-Markov [1]:

$$\mathbf{H}\Delta\mathbf{u}=E[\Delta\mathbf{l}]=\Delta\mathbf{l}+\mathbf{v}, \tag{1.1}$$

where $E[\cdot]$ is the expectation operator, $\mathbf{v}$ is the zero-average vector of the true measurement errors, rank($\mathbf{H}$)=4, i.e. the columns of $\mathbf{H}$, the geometry or design matrix, are independent, and $\mathbf{H}^T\mathbf{H}$ is non-singular ($\mathbf{T}$ stands for transposition). The ordinary LS solution for the n linearized pseudorange equations, n being the number of visible GPS satellites or the number of acquisition epochs multiplied by the number of visible satellites is [2, 3]:

$$\Delta\mathbf{u}=(\mathbf{H}^T\mathbf{P}\mathbf{H})^{-1}\mathbf{H}^T\mathbf{P}\Delta\mathbf{l}, \tag{1.2}$$

where $\Delta\mathbf{u}$ is the vector offset of the four-element user's position and clock bias vector $\mathbf{u}=[x\ y\ z\ b]^T$ from the values at the linearization point, $\Delta\mathbf{l}=[\Delta l_1\ \ldots\ \Delta l_n]^T$ is the $n\times1$ vector difference between the pseudorange values associated with the user's position and those associated with the linearization point, and $\mathbf{H}$ is the $n\times4$ design (or geometry) matrix, whose rows contain the direction cosines of the line of sight from the user's linearization position to the satellite. $\mathbf{P}$ is the weight matrix of the observations.

The purpose of this work is to present a new methodology of blunder detection and estimation in a vector of LS-adjusted observations, regardless of the choice of the adjustment model (Gauss-Markov, Gauss-Helmert, condition only, with constraints on the parameters, etc.), exploring logical relationships between abnormal misclosures and blunders, and their mathematical formalisation by means of descriptions using the everyday spoken language.

The mathematical tools and concepts used belong to fuzzy set theory and the extensions of Boolean logic to multi-valued logic (fuzzy logic). The interested reader may refer to [4, 5, 6, 7] for a basic introduction on fuzzy sets and fuzzy logic.

The main advantages of the fuzzy logic-based approach to our detection and estimation problem are:

* Associate Professor, Dept. Civil Engineering. E-mail: nicola.crocetto@unina2.it
** Ph. D., Assistant Professor. Dept. Aerospace and Mechanical Engineering. E-mail: salvatore.ponte@unina2.it

1. A correct (unbiased) estimate of the outlier (or the outliers) allows removal of the gross error from the affected measurement, and the observation is not discarded, thus leaving the redundancy unaltered;
2. The LS-adjustment with the corrected measurements is improved;
3. Use of fuzzy set theory and fuzzy logic is shown to be effective in correct localisation and estimation of one and more than one single gross error in the observations as well.
4. Blunder detection and estimation is not performed iteratively, but in a single step, with significant CPU time saving;
5. Typical statistical tests on the normalized LS-residuals for blunder detection are avoided, thus implementing cost-effective procedures.

The Fuzzy-LOgic-based Outlier Detection (FLOOD) algorithm presented here is a post-adjustment procedure by means of which in a single step (i.e. after only one LS-adjustment) one or more than one blunder are localized in the uncorrelated pseudorange measurements needed for the GPS single-point-positioning problem. Furthermore, we show a final statistical procedure in which these blunders are estimated and the estimates are submitted to two-tailed tests of significance, in order to confirm the FLOOD-derived localization.

The paper is structured as follows. After some background on fuzzy set concepts, necessary to define the sets of interest and their characterisation in the fuzzy sense, and on the adopted statistics in the presence of gross errors, the conceptual stages of the methodology are presented, putting in evidence the innovative aspects and the advantages with respect to classical techniques. Successively, the technique is applied to real datasets gathered from GPS campaigns, and its effectiveness and power in detecting and estimating gross errors is shown. Concluding remarks and direction for further work close the article.

The basic concept of fuzzy set is briefly recalled here. Given a non-empty set U, called "universe of discourse", a fuzzy set is a pair $\{\tilde{S}, \mu_{\tilde{S}}(x)\}$, with $x \in U$. The mapping $\mu_{\tilde{S}} : \tilde{S} \rightarrow [0,1]$ is called "membership function", and expresses the degree of truthfulness of the statement "the element x belongs to $\tilde{S}$". Thus if $\mu_{\tilde{S}}(x)=0$, x is "absolutely not belonging to $\tilde{S}$", and if $\mu_{\tilde{S}}(x)=1$, x is "completely belonging to $\tilde{S}$". Every intermediate situation, i.e. $0<\mu_{\tilde{S}}(x)<1$ is "fuzzy". In this framework, classical (non-fuzzy, or *crisp*) sets have membership functions of the kind $\mu_S(x) \in \{0, 1\}$, whereas $\mu_{\tilde{S}}(x) \in [0, 1]$.

Much work has been done in the past to devise statistical techniques for blunder detection, localisation and estimation in LS-adjusted data [1, 8]. Basically, given a set of observations, hypothesis testing algorithms such as the Fisher Global Model Test [8, 9] allow one to accept or reject to some degree of confidence the null hypothesis H_0 about the absence of gross errors in the observation vector **l**. The *a-priori* variance factor σ_0^2 is assumed known, as well as the n×n variance-covariance matrix Σ of the observations, assumed Gaussian and uncorrelated, so that $\mathbf{P}=\sigma_0^2\Sigma^{-1}$ is diagonal. The adopted functional model has r=n−4 degrees of freedom (r is also called redundancy, being the difference between the number of measurement equations and the number of unknowns). In order to test the null hypothesis H_0, i.e. the assumption of "absence of blunders in the vector **l**", the Fisher test uses the statistic:

$$\frac{s_o^2}{\sigma_o^2} = \frac{\hat{\mathbf{v}}^T \mathbf{P} \hat{\mathbf{v}}}{r\,\sigma_o^2}, \tag{1.3}$$

where s_o^2 is the *a*-posteriori variance factor, and $\hat{\mathbf{v}}$ is the n×1 vector of the LS residuals. In the absence of blunders, the estimate of s_o^2, i.e. $\hat{\mathbf{v}}^T \mathbf{P} \hat{\mathbf{v}}/r$, is a Best Invariant Quadratic Estimator (BIQUE) [8], and the statistic (1.3), assuming no gross errors and Gaussian observations, is a central chi-square with r degrees of freedom:

$$\frac{s_o^2}{\sigma_o^2} \sim \frac{\chi_r^2}{r} \tag{1.4}$$

The one-tailed hypothesis test with significance level α accepts H_0 if:

$$\frac{s_o^2}{\sigma_o^2} = \frac{\hat{\mathbf{v}}^T \mathbf{P} \hat{\mathbf{v}}}{r\,\sigma_o^2} \leq \frac{\chi_{r,1-\alpha}^2}{r}, \tag{1.5}$$

whereas the presence of outliers in the observations is inferred in case of failure of the test, that is, when the statistic becomes unacceptable, or abnormal:

$$\frac{s_o^2}{\sigma_o^2} = \frac{\hat{\mathbf{v}}^T \mathbf{P} \hat{\mathbf{v}}}{r\,\sigma_o^2} > \frac{\chi_{r,1-\alpha}^2}{r} \tag{1.6}$$

In case of rejection of H_0, the successive step, i.e. localisation of all the possible blunders in **l**, is typically accomplished by using methodologies whose effectiveness depends on the correctness of the chosen functional and stochastic models, and on some hypotheses on the statistical behaviour of data (Gauss distribution, uncorrelated observations, presence of one single outlier in **l**). In particular, if Σ is known, iterative post-LS adjustment procedures such as Baarda's data snooping [9] are used to localize outliers, whereas if in Σ only an unknown variance factor is assumed, Pope's method [10] localises correctly the single blunder. Under the above mentioned hypotheses, simple relations are available in the GPS literature [11] for estimating the magnitude of the outlier.

Baarda's approach assumes diagonal Σ and $\mathbf{P}$ matrices [9, 10], i.e. uncorrelated observations, and applies two-tailed hypothesis testing to the standardised LS residuals $\hat{w}_i = \hat{v}_i / \sigma_{\hat{v}_i}$ (i=1,...,n), where $\sigma_{\hat{v}_i}$ is the standard deviation associated with each $\hat{v}_i$. A blunder is localised in the observation with the maximum absolute value of $\hat{w}_i$. The anomalous observation is discarded, the LS-adjustment is repeated, obtaining a new global solution, and the Fisher test is applied. If H_0 is rejected again (there is at least another outlier in the observations), then Baarda's data snooping is repeated, the $\hat{w}_i$ are tested until all the blunders are localised and all the anomalous observations are discarded.

In the presence of only one blunder ∇_i affecting the i-th observation l_i (which has variance σ_i^2), an estimate of its magnitude is obtained from the i-th LS-residual [10]:

$$\hat{\nabla}_i^* = -\frac{\hat{v}_i}{r_i}, \tag{1.7}$$

where r_i is the local redundancy, i.e. the (i,i)-element of the n×n redundancy matrix $\mathbf{R}$, given by:

$$r_i = \frac{\sigma_{\hat{v}_i}^2}{\sigma_i^2} \tag{1.8}$$

since $\mathbf{P}$ is diagonal. It can be shown that $\mathbf{R} = \mathbf{Q}_{\hat{v}}\mathbf{P}$, where $\mathbf{Q}_{\hat{v}}$ is the (singular) cofactor matrix of the LS residuals [8]:

$$\mathbf{Q}_{\hat{v}} = \sigma_0^2\left(\mathbf{P}^{-1} - \mathbf{H}\left(\mathbf{H}^T\mathbf{P}\mathbf{H}\right)^{-1}\mathbf{H}^T\right). \tag{1.9}$$

The standard deviation of the estimate (1.7) is obviously, using (1.8):

$$\sigma_{\hat{\nabla}_i^*} = \frac{\sigma_{\hat{v}_i}}{r_i} = \frac{\sigma_i}{\sqrt{r_i}} \tag{1.10}$$

The case of correlated observations, but still assuming a single blunder, is thoroughly investigated in [8] and [12], where it is shown that the iterative use of Baarda's data snooping is still effective but at the cost of heavy computational effort, since the whole n×n cofactor matrix $\mathbf{Q}_{\hat{v}}$ is needed to calculate the variance of the i-th element of $\mathbf{w}_p = \mathbf{P}\hat{\mathbf{v}}$, the n×1 vector of the weighted LS residuals. Moreover, errors that could impair convergence of the solution are unlikely to be found with this procedure.

When more than one blunder affects **l**, the algorithm is performed iteratively, but in many cases its weaknesses can seriously impair the whole procedure of blunder detection and estimation. First, in the presence of set of measurements of large dimensions and with complicated models, the computational effort can be very cumbersome, for example when dealing with carrier phase cycle counts or phase measurements from three or four antennas in a GPS receiver for attitude determination. Second, the effect of blunders on the magnitude of residuals and on misclosure errors is not taken correctly into account [9] and could lead to erroneous estimates of the outliers, if not their erroneous localisation. This could lead to unwanted propagation of a measurement error on several estimates of **u**. Third, some pre-adjustment analysis, performed through statistical control of conditional misclosures (i.e. errors of closure of the condition equations) and their logical relationships, is required for effective results, but great effort to formulate all the functionally independent condition equations is usually required. This problem is frequently dealt with in post-processing analysis of GPS positioning solutions with some constraints.

Localization of the blunders could generally be performed by a pre-adjustment analysis considering the functional model of the so-called "Conditions-only" [1], by checking conditional misclosures (i.e. closure errors of the condition equations). The analysis is performed through statistical control of the misclosures and investigation about the presence of some, say *k*, of the *n* measurements in condition equations which exhibit abnormal misclosures and, at the same time, about the absence of the same *k* observations in condition equations

with non-abnormal misclosures. Therefore, blunder detection can be expressed in linguistical terms with the following IF-THEN rule with the standard logic connective AND:

> **IF** there are k (of n) measurements in some condition equations which exhibit abnormal misclosures **AND** the same k measurements are absent in condition equations with non-abnormal misclosures **THEN** the k observations are likely to be affected by outliers (1.11)

2. Outlier detection in LS-adjusted observation vectors: description of the methodology

A conceptual flow diagram of the proposed mixed fuzzy/statistic methodology for outlier detection and estimation is illustrated in Fig. 1, starting from the measurement vector **l** and the weight matrix of the observations **P**.

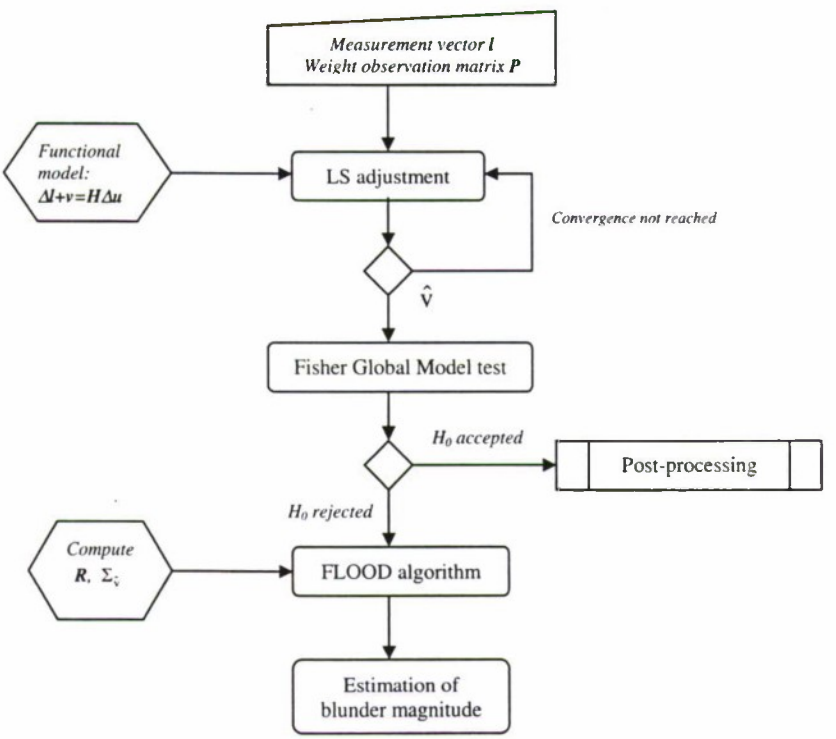

Fig. 1. Conceptual flowchart of the proposed methodology for blunder detection and estimation.

The procedure can be partitioned in three main blocks:

Block 1. A standard LS adjustment is performed on all the available observations until convergence is reached, a global solution for the user state vector is obtained and the LS-residual vector $\hat{\mathbf{v}}$ is computed. The Fisher test for the absence of gross errors is performed on the residuals. If H_0 is accepted, the user vector estimate is validated and passed to a post-processing block (e.g. orbit reconstruction, filtering, data smoothing, etc.). If the test fails, the n×n covariance matrix of the LS residuals $\boldsymbol{\Sigma}_{\hat{v}}$ and the redundancy matrix **R** are computed and passed to the FLOOD module.

Block 2. The FLOOD core, entirely based on fuzzy logic, implements fuzzification, which converts the input data to degrees of membership to some (fuzzy) sets, evaluates a logic rule on the basis of the fuzzified input, and finally performs defuzzification, which converts the resulting output fuzzy set into a single numerical value, used to infer the presence of blunders in the analyzed measurement vector and localize it in **l**. As it will be shown in Sec. 3, the FLOOD module locates the observations affected by gross errors even if they are more than one. A simplified block diagram of the fuzzy module is shown in Fig. 2.

Block 3. After identification of the GPS measurement (or measurements) affected by a gross error, a statistical module performs estimates of the magnitude of the blunders. Furthermore, in order to confirm the FLOOD-derived outlier localization, the estimates are submitted to two-tailed significance tests.

In the following subsections, a description of each of the modules will be given in detail.

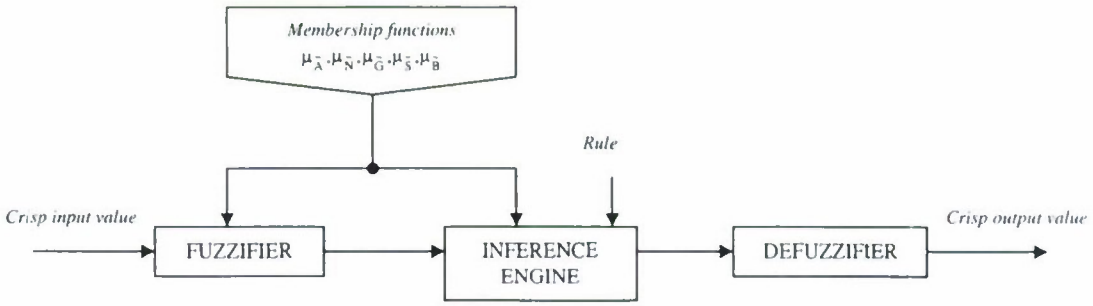

Fig. 2. Simplified block diagram of the fuzzy system (FLOOD core).

2.1. The FLOOD algorithm

Implementations of the FLOOD procedure for detection of outliers in the vector **l** starts from the definition of the crisp inputs to the fuzzy system of Fig. 2. To this end, we consider the following relation between $\hat{\mathbf{v}}$, **R**, the n×1 vector **v**=–**l** of the true errors and the vector of the uncorrelated observations **l** [13]:

$$\hat{\mathbf{v}} = \mathbf{R}\,\mathbf{v} = -\mathbf{R}\,\mathbf{l} \tag{2.1}$$

Successively we define the n×1 vector of the standardized LS-residuals $\mathbf{v} = \left\{\hat{v}_i / \sigma_{\hat{v}_i}\right\}$ (i=1, ..., n), and the n×n matrix $\tilde{\mathbf{R}} = \left\{\tilde{r}_{i,j} = r_{i,j} / \sigma_{\hat{v}_i}\right\}$, which we call "relative redundancy matrix". From (2.1):

$$\mathbf{v} = \tilde{\mathbf{R}}\,\mathbf{e} = -\tilde{\mathbf{R}}\,\mathbf{l} \tag{2.2}$$

Eq. (2.2) can be considered a set of condition equations (functionally dependent because of the singularity of **R** and of $\tilde{\mathbf{R}}$) among the observation errors, and the standardized LS-residuals v_i can assume the significance of misclosures. The basic idea of the FLOOD algorithm is to translate in fuzzy linguistic terms the pre-adjustment procedure identified by the rule (1.11), and to define in the fuzzy sense the sets of interest in the blunder detection procedure.

The fundamental hypothesis is that the observations (pseudoranges or carrier phases) are uncorrelated, and the rule implemented by the FLOOD strategy is the following:

> *if the contribution of a measurement l_i (by means of the corresponding error) to the abnormal standardized LS-residuals v_i, (i=1,... n) is great* **and** *the contribution of l_i to the non abnormal standardized LS-residuals is small,* **then** *the i-th observation is affected by a blunder.*

(2.3)

In other words, the FLOOD fuzzy inference engine interprets the values of the input vector **l** and, based on the rule above, assigns degrees of membership of the elements of **l** to the output set $\tilde{H}$ (see later). The fuzzy sets to be defined in the FLOOD algorithm and the symbols used in assigning the membership functions are summarized in Tab. 1.

Table 1: Definition of fuzzy sets in the FLOOD procedure

Linguistic meaning of the fuzzy set	*Symbol used*
Abnormal standardized LS-residuals	$\tilde{A}$
Non-abnormal standardized LS-residuals	$\tilde{N}$
Measurements with great contribution to the abnormal standardized LS-residuals	$\tilde{G}$
Measurements with small contribution to the non-abnormal standardized LS-residuals	$\tilde{S}$
Measurements affected by blunders	$\tilde{B}$

Obviously, the linguistic terms "abnormal", "non-abnormal", "great", "small", have to be defined in the fuzzy sense, that is, as fuzzy variables with their membership functions (belonging to a "term set") defined over

a "base variable" [4]. In our case, the base variables are "Standardized LS residuals" for the term set {Abnormal, Non-abnormal} and "Contribution to the standardized LS residuals" for the term set {Great, Small}.

The measurements l_i, the standardized LS-residuals $\hat{v}_i/\sigma_{\hat{v}_i}$ and the relative redundancy matrix $\tilde{\mathbf{R}}$ constitute the crisp input to the FLOOD block (Fig. 2), i.e. the input numerical values which will belong to the fuzzy sets of Tab. 1 with some degree of membership. The fuzzifier assigns membership functions to the fuzzy sets $\tilde{A}$, $\tilde{N}$, $\tilde{G}$, $\tilde{S}$: the elements of $\tilde{A}$ and $\tilde{N}$ are the $\hat{v}_i/\sigma_{\hat{v}_i}$, whereas the elements of the input fuzzy sets $\tilde{G}$ and $\tilde{S}$ are the observations l_i, i=1, ..., n. The membership function of the standardized LS residuals to the fuzzy set $\tilde{A}$ of the abnormal standardized LS-residuals is defined as follows:

$$\mu_{\tilde{A}}\left(\frac{\hat{v}_i}{\sigma_{\hat{v}_i}}\right)=\frac{\left|\frac{\hat{v}_i}{\sigma_{\hat{v}_i}}\right|}{\max\limits_{k=1,\ldots,n}\left\{\left|\frac{\hat{v}_k}{\sigma_{\hat{v}_k}}\right|\right\}} \qquad (i=1, \ldots, n) \qquad (2.4)$$

with the denominator acting as a normalizing factor. Eq (2.4) reproduces Baarda's approach to the analysis of the residuals, assigning maximum membership to the greatest value of $\hat{v}_i/\sigma_{\hat{v}_i}$, and considering a linear function.

The fuzzy set $\{\tilde{N}, \mu_{\tilde{N}}(\cdot)\}$, the complement of $\tilde{A}$, has a membership function given by:

$$\mu_{\tilde{N}}\left(\frac{\hat{v}_i}{\sigma_{\hat{v}_i}}\right)=1-\mu_{\tilde{A}}\left(\frac{\hat{v}_i}{\sigma_{\hat{v}_i}}\right) \qquad (i=1, \ldots, n) \qquad (2.5)$$

and, as obvious, small values of the standardized LS-residuals have high degree of membership to $\tilde{N}$. The crisp input values l_i belong to the fuzzy set $\tilde{G}$ (measurements with great contribution to the abnormal standardized LS-residuals) with a membership function which takes account of $\mu_{\tilde{A}}$, introducing a weighting factor extracted from the elements of $\tilde{R}$ and normalized to 1, and finally applying the square root as a linguistic modifier, or hedge [7] which models the term "Great":

$$\mu_{\tilde{G}}(l_i)=\sqrt{\mu_{\tilde{A}}\left(\frac{\hat{v}_j}{\sigma_{\hat{v}_j}}\right)\cdot\frac{|\tilde{r}_{ji}|}{\sqrt{\sum_{k=1}^{n}\tilde{r}_{ki}^2}}} \qquad (i=1, ..., n), \qquad (2.6)$$

where the index j is given by:

$$|\tilde{r}_{ji}|=\max_{k=1,\ldots,n}\{|\tilde{r}_{ki}|\}=\max_{k=1,\ldots,n}\left\{\left|\frac{r_{ki}}{\sigma_{\hat{v}_k}}\right|\right\} . \qquad (2.7)$$

The meaning of the value $\tilde{r}_{ji}$ is as follows: it represents the maximum influence that the observation l_i has on all the standardized LS residuals. This influence is normalized to 1 by considering the whole i-th column of $\tilde{\mathbf{R}}$. It has to be stressed that (2.6) approaches 1 only if both the factors are close to 1: that is, when l_i gives a strong contribution to the residual $\hat{v}_j/\sigma_{\hat{v}_j}$ *and* the membership of the residual to $\tilde{A}$ is high, l_i belongs to $\tilde{G}$ with high degree of membership.

The measurements with small contribution to the non abnormal standardized LS-residuals belong to $\tilde{S}$ with membership function given as follows, using (2.5):

$$\mu_{\tilde{S}}(l_i)=\mu_{\tilde{N}}\left(\frac{\hat{v}_{j^*}}{\sigma_{\hat{v}_{j^*}}}\right)\cdot\left[1-\frac{|\tilde{r}_{j^*i}|}{\sqrt{\sum_{k=1}^{n}\tilde{r}_{ki}^2}}\right]=\left[1-\mu_{\tilde{A}}\left(\frac{\hat{v}_{j^*}}{\sigma_{\hat{v}_{j^*}}}\right)\right]\cdot\left[1-\frac{|\tilde{r}_{j^*i}|}{\sqrt{\sum_{k=1}^{n}\tilde{r}_{ki}^2}}\right] \qquad (i=1, ..., n), \qquad (2.8)$$

where the index j^* is given by:

$$\left|\tilde{r}_{j^*i}\right| = \min_{k=1,\ldots,n}\left\{\left|\tilde{r}_{ki}\right|\right\} = \min_{k=1,\ldots,n}\left\{\left|\frac{r_{ki}}{\sigma_{\hat{v}_k}}\right|\right\} . \qquad (2.9)$$

Dually with respeet to $\tilde{G}$, the value $\tilde{r}_{j^*i}$ represents the minimum influenee of l_i on the standardized LS-residuals vector. When l_i gives small contribution to the residual $\hat{v}_{j^*}/\sigma_{\hat{v}_{j^*}}$, the difference in (2.8) approaches 1, and if the j*-th residual belongs strongly to the set of the non-abnormal residuals, the whole membership of l_i to $\tilde{S}$ becomes high.

As far as the fuzzy inference engine is coneerned, the input members of the rule are numerical values of the membership functions associated with $\tilde{G}$ and $\tilde{S}$, and the output defines the fuzzy set $\tilde{H} = \tilde{G}$ **and** $\tilde{S}$ of the observations affected by blunders. The AND operator used is the fuzzy intersection (often referred to as *T-norm* [5]), and the membership function assoeiated with $\tilde{B}$ is deduced assuming as T-norm the min-operator:

$$\mu_{\tilde{B}}(l_i) = \min\left\{\mu_{\tilde{G}}(l_i), \mu_{\tilde{S}}(l_i)\right\} \qquad (i=1, \ldots, n). \qquad (2.10)$$

The defuzzifier maps the fuzzy set $\tilde{B}$ to the crisp (non-ambiguous) set B of the observations affected by blunders. The set B is assumed equal to the ordinary *α-level*, or *α-cut* subset of $\tilde{B}$ [13]:

$$B = B_\alpha = \left\{ l_k \in \mathbf{l} \;\middle|\; \mu_{\tilde{B}}(l_k) \geq \alpha_c \right\} . \qquad (2.11)$$

As stated by (2.11), the observations affeeted (with eertainty) by blunders are eonsidered those that belong to $\tilde{B}$ at least to a degree α_c. The numerical value of α_c, determined experimentally with different datasets, has been set to 0.60.

2.2. Estimation of the blunder magnitude

Denoting with *b* the number of blunders that have been deteeted and loeated by the FLOOD eore, and with **g** the b×1 vector of the (unknown) numerical values of the blunders, we extract from the redundancy matrix **R** the diagonal and off-diagonal elements that correspond to the respeetive positions of the *b* located blunders, thus obtaining a b×b matrix **C**. We also extract from the vector of the LS residuals $\hat{\mathbf{v}}$ the elements that correspond to the respective positions of the *b* blunders, thus obtaining a b×1 veetor $\hat{\mathbf{v}}^*$. Henee, we have the system:

$$\mathbf{C}\mathbf{g} = \hat{\mathbf{v}}^* \qquad (2.12)$$

from whieh the b×1 vector of the unbiased (if **C** is invertible) estimates of the magnitude of the blunders is:

$$\hat{\mathbf{g}} = \mathbf{C}^+ \hat{\mathbf{v}}^* , \qquad (2.13)$$

where $\mathbf{C}^+$ is the pseudo-inverse matrix of **C**. Sueeessively, eaeh eomponent of $\hat{\mathbf{g}}$ is submitted to a two-tailed test of significanee with 1%-significance level. The b×b cofaetor matrix of $\hat{\mathbf{v}}^*$, $\mathbf{Q}_{\hat{v}^*}$, is then derived from $\mathbf{Q}_{\hat{v}}$, and finally the b×b variance-covariance matrix of the estimated blunder vector $\hat{\mathbf{g}}$ is evaluated as:

$$\mathbf{\Sigma}_{\hat{g}} = \sigma_o^2 \mathbf{C}^+ \mathbf{Q}_{\hat{v}^*} (\mathbf{C}^+)^T . \qquad (2.14)$$

The null hypothesis is:

$$H_o : E\left[\hat{g}_i\right] = 0 \quad (i=1, \ldots, b). \qquad (2.15)$$

Assuming Gaussian uncorrelated observations and a known *a-priori* variance factor σ_o^2, each estimated blunder $\hat{g}_i$ is Gaussian as well. If the value $\hat{g}_i/\sigma_{\hat{g}_i}$ of the i-th standardized estimated blunder is greater than the eritieal value $u_{1-\alpha/2} = 2.57$ (with α=1%) of the standardized Gaussian density [15]:

$$\hat{g}_i/\sigma_{\hat{g}_i} \geq u_{1-\alpha/2} = 2.57 \qquad (2.16)$$

then $\hat{g}_i$ is judged signifieant and (with 1%-signifieanee level) the eorrespondent observation is affected by a gross error. If (2.16) is not satisfied, the observation is considered normal, i.e. not affeeted by a blunder.

3. Numerical results

The FLOOD detection and estimation procedure has been tested on several datasets. The first example (determination of the GPS antenna phase center by means of more than four measurements) used an antenna fixed on a point in Poggiorenatico (Ferrara, Italy) of the new Italian geodetic network "IGM95". The GPS orbital data were deduced from a precise ephemerides file in the SP3 format [16]. Pseudorange (code-phase) measurements were obtained from the C/A (Coarse/Acquisition) code and were input as a RINEX (Receiver-INdependent EXchange) format file. The data of one session obtained via dual-frequency receivers were elaborated, with eight satellites in view. We employed four epochs with fifteen-minute sampling interval, and eight pseudorange measurements for each epoch, dealing therefore with n=32 uncorrelated observations, 4 unknowns (the elements of **u**), and a total redundancy *r* equal to 28.

In the stochastic model we assumed two unknown variance factors: the variance of each observation has been modeled as the sum of a constant and a term inversely proportional to the square of the SNR (Signal-to-Noise Ratio), evaluated from the values written in the RINEX files as flags from 0 to 9. The BIQUE estimates of the two variance factors were performed following a rigorous procedure [10] and a simplified method developed by one of the authors [12]. Both techniques gave identical results.

In order to test the whole approach to blunder detection, the gathered dataset has been intentionally corrupted with three blunders and successively, in a second experiment, with five. In the first case the injected blunders were equal to 2 km in the 4th pseudorange observation, -2 km in the 13th, and 3 km in the 25th. After performing the ordinary LS adjustment, the Fisher test on the statistic (1.3) failed as expected:

$$\frac{s_o^2}{\sigma_o^2} = \frac{\hat{\mathbf{v}}^T \mathbf{P} \hat{\mathbf{v}}}{r\sigma_o^2} = 391.2 > \frac{\chi^2_{r,1-\alpha}}{r} = \frac{48.3}{28} = 1.725 \qquad (3.1)$$

at 1%-significance, thus confirming the presence of blunders in **l**. The FLOOD core of our methodology allowed us to locate the three blunders exactly in the 4th, 13th and 25th observations. Table 2 shows the pseudorange measurements whose membership function in the fuzzy set $\tilde{B}$ (observations affected by blunders) is greater than the critical value α_c=0.60, reporting the observation number, the LS residual, the standardized LS residual and the numerical value of the membership functions $\mu_{\tilde{A}}, \mu_{\tilde{N}}, \mu_{\tilde{G}}, \mu_{\tilde{S}}, \mu_{\tilde{B}}$.

Table 2: Three blunders injected in the observation vector l.
The table reports the GPS measurements with $\mu_{\tilde{B}} \geq 0.60$

Observation number (i)	*LS residual* $\hat{v}_i$ [m]	*Standardized LS residual* $\frac{\hat{v}_i}{\sigma_{\hat{v}_i}}$	*Membership function values*				
			$\mu_{\tilde{A}}$	$\mu_{\tilde{N}}$	$\mu_{\tilde{G}}$	$\mu_{\tilde{S}}$	$\mu_{\tilde{B}}$
4	1727.0	50.76	0.693	0.307	0.810	0.956	0.810
13	-1887.1	-54.37	0.742	0.258	0.836	0.832	0.832
25	2655.8	73.26	1.000	0.000	0.972	0.933	0.933

After blunder localization, we estimated their magnitude (block 3 of the procedure). The unbiased estimates (2.13) are reported in Tab. 3, second column. The fifth column reports the numerical results of the two-tailed test evaluated in correspondence of each standardized blunder. As it can be seen, each $\hat{g}_i/\sigma_{\hat{g}_i}$ satisfies the condition (2.16).

Table 3: Estimates of the three injected blunders and of the standardized blunders

Observation number (i)	*Blunder estimate[m]*	*Injected value in l, [m]*	*Estimation error*	*Standardized blunder* $\hat{g}_i/\sigma_{\hat{g}_i}$
4	2025.9	2000	1.3%	53.57
13	-1980.7	-2000	0.97%	-50.77
25	3004.0	3000	0.13%	74.12

In the second experiment, two additional blunders were injected in the observations, namely -0.5 km in the 10th pseudorange and 0.5 km in the 29th. Again, application of the Fisher test confirms the presence of blunders:

$$\frac{s_o^2}{\sigma_o^2} = \frac{\hat{\mathbf{v}}^T \mathbf{P} \hat{\mathbf{v}}}{r\sigma_o^2} = 410.2 > \frac{\chi^2_{r,1-\alpha}}{r} = \frac{48.3}{28} = 1.725 \qquad (3.2)$$

Table 4 reports the main numerical results related to this case. It has to be stressed that by retaining the experimental value of 0.60 of the α-cut threshold, the procedure is able to detect only three of the five blunders, locating them in the 4-th, 13-th and 25-th pseudoranges. Lowering α_c to 0.40 allows us to locate correctly all the five gross errors.

Table 4: Five blunders injected. Observations with membership function $\mu_{\tilde{B}} \geq 0.40$ (α_c=0.40)

Observation number (i)	*LS residual* $\hat{v}_i$ *[m]*	*Standardized LS residual* $\frac{\hat{v}_i}{\sigma_{\hat{v}_i}}$	*Membership function values*				
			$\mu_{\tilde{A}}$	$\mu_{\tilde{N}}$	$\mu_{\tilde{G}}$	$\mu_{\tilde{S}}$	$\mu_{\tilde{B}}$
4	1768.2	51.97	0.701	0.299	0.815	0.959	0.815
13	-1886.6	-54.35	0.733	0.267	0.831	0.849	0.831
25	2686.6	74.11	1.000	0.000	0.972	0.769	0.769
10	-597.7	-18.14	0.245	0.755	0.479	0.991	0.479
29	631.8	16.26	0.219	0.781	0.456	0.898	0.456

The unbiased estimates of the magnitude of the first three located blunders are reported in the second column of Table 5. As before, the two-tailed test on the first three standardized blunders confirms at 1%-significance level the previously identified locations.

Table 5: Estimates of the first three blunders and standardized blunders (second case, five outliers, α-cut threshold=0.60)

Observation number (i)	*Blunder [m]*	*Injected value [m]*	*Estimation error*	*Standardized blunder* $\hat{g}_i/\sigma_{\hat{g}_i}$
4	2073.4	2000	3.7%	54.83
13	-1977.9	-2000	-1.1%	-50.70
25	3041.0	3000	1.4%	75.03

Eliminating from the observation vector the three anomalous pseudoranges (Nos. 4, 13 and 25), the available observations reduce to n=29, with total redundancy r equal to 25. After a new LS adjustment, the Fisher test confirms the presence of other blunders, providing for α=1%:

$$\frac{s_o^2}{\sigma_o^2} = \frac{\hat{\mathbf{v}}^T \mathbf{P} \hat{\mathbf{v}}}{r \sigma_o^2} = 12.1 > \frac{\chi^2_{r,1-\alpha}}{r} = \frac{44.3}{25} = 1.77 \qquad (3.3)$$

Successive application of the FLOOD algorithm on this new measurement vector allows us to locate the remaining two blunders exactly in the 10th and 29-th measurement, considering only the pseudorange measurements whose membership function values $\mu_{\tilde{B}}$ are greater than 0.60 (α_c=0.60). Table 6 summarizes the statistical analysis and the membership values.

Table 6: Two blunders left in the observation vector

Observation number (i)	*LS residual* $\hat{v}_i$ *[m]*	*Standardized LS residual* $\frac{\hat{v}_i}{\sigma_{\hat{v}_i}}$	*Membership function values*				
			$\mu_{\tilde{A}}$	$\mu_{\tilde{N}}$	$\mu_{\tilde{G}}$	$\mu_{\tilde{S}}$	$\mu_{\tilde{B}}$
10	-415.6	-12.76	1.000	0.000	0.961	0.899	0.899
29	443.8	11.49	0.900	0.100	0.920	0.974	0.920

The unbiased estimates of the magnitude of the last two located blunders are reported in the second column of Table 7. The two-tailed test on the remaining two standardized blunders (fifth column of Table 7) confirms their locations.

Table 7: Estimates of the two remaining blunders

Observation number	*Blunder [m]*	*Injected value [m]*	*Estimation error*	*Standardized blunder* $\hat{g}_i/\sigma_{\hat{g}_i}$
10	-458.6	-500	-8.3%	-12.01
29	462.8	500	7.4	10.65

. As a remark, the estimation errors become greater: this is due to the small numerical entity of the injected blunders (500 m absolute value, with typieal pseudorange values of the order of $2.5 \cdot 10^7$ m). After disearding the observations Nos. 10 and 29, the Fisher test does not indicate anymore the presenee of blunders in the measurement vector.

Finally, the whole proeedure has been applied to carrier phase measurements (eyele counts) gathered from a eommereial GPS board (Garmin® GPS25LP), connected to a PC by means of a RS-232-like interface, and aequiring pseudoranges and number of carrier cycles at 1-seeond epoehs. Statie measurements were aequired over different 10-minute aequisition eampaigns. By injeeting sensibly wrong eounts in some of the cyele measurements with the same strategy adopted for the pseudorange observations, we found similar results, not reported here for the sake of brevity. The choice of 0.60 for the α_c threshold for the definition of B has been found to be effeetive, even if in the ease of "small" blunders.

4. Conelusions

The mixed fuzzy/statistical methodology described in this work performs eorrectly blunder detection (with statistical tests), localization (with a fuzzy-logic based approaeh) and estimation (Eq. (2.13)). Application of our approaeh to real datasets (GPS pseudorange and carrier phase measurements) enabled us to localize blunders even in the presenee of more than one gross error in the observations, allowing us to skip classieal iterative methodologies for blunder detection. Furthermore, the methodology implements a statistical module capable of providing unbiased estimates of the magnitude of the previously located blunders. The eomputational saving with respect to iterative techniques such as Baarda's data snooping is significant. In the first case of our example (See. 3, with only three blunders), Baarda's teehnique would have required three iterations and the estimate of the blunders would not have been correct, whereas our methodology required only one step and gave correct estimates of the blunders. In the seeond ease (with five blunders), five iterations would have been required, whereas the FLOOD core of our methodology required only two steps and again eorreet estimates of the blunders were obtained. It is worth noting that (see Tab. 4) if in the ease of five blunders we had assumed the eritieal value α_c of the membership function in the fuzzy set $\tilde{B}$ equal to 0.45, only one step would have been suffieient to locate all the five blunders. Further research is needed to modify the defuzzification algorithm in order to improve the FLOOD core: there is a degree of arbitrariness in the funetional ehoice of α_c, which eould impair the methodology (or at least require more than a single inspection of I) for particular datasets. The authors are eurrently developing alternative strategies for the definition of the output set of the observations affeeted by blunders, and effective defuzzification techniques.

Aeknowledgement

This work has been carried out under a research project sponsored by the Italian Ministry of the Univcrsity and Scientific Research.

Referenees

1. **Mikhail E. M.** *Observations and Least Squares*. Thomas Y. Crowell Company, Inc., University Press of America, Lanham/New York/London, 1976.
2. **Kaplan E. D. (Ed.)** *Understanding GPS – Principles and Applications*, Artech House, Boston/London, 1996.
3. **Ponte S., De Paris G.** SMART orbit determination by means of GPS techniques: accuracy and simulation results, *49th International Astronautical Federation Congress*, Sep. 28- Oct. 2, Melbourne, Australia, Paper IAF-98-A.2.02, 1998.
4. **Zimmermann H.J.** *Fuzzy Sets Theory and Its Applications*. Kluwer Academie Publishers, 1994.
5. **Zadeh L. A.** Fuzzy logic. IEEE Computer, Vol. 21, No. 4, pp. 83-93, 1988.
6. **Kaufmann A.** *Introduction to the theory of fuzzy sets*. Academic Press, New York, 1975.
7. **Yager R.R., Ovchinnikov R., Tong M., Nguyen H.T.** *Fuzzy sets and applications – selected papers by L. A. Zadeh*. John Wilcy and Sons, Ncw York, 1987.
8. **Koch K.R.** *Parameter Estimation and Hypothesis Testing in Linear Models*. Springer–Verlag Berlin Heidelberg, 1999.
9. **Kraus K.** *Photogrammetry. Volume 2: Advanced Methods and Applications*. 4th Ed., Dümmler Verlag, Bonn, Germany, 1997.
10. **Caspary W.F.** *Concepts of network and deformation analysis*. School of Surveying. The University of New South Wales, Kcnsington, N.S.W., Australia, 1987.
11. **Leick A.** *GPS Satellite Surveying*. John Wiley & Sons, Inc., New York, 1995.
12. **Crocetto N.** Correct estimation and localization of single blunders in LS adjusiment of correlated observations. Submitted to Journal of Geodesy, 2002.
13. **Crocetto N., Gatti M., Russo P.** Simplified formulae for the BIQUE estimation of varianee components in disjunctive observation groups. Journal of Geodesy, No. 74, pp.447-457, 2000.
14. **Sun W.** A new method for localisation of gross error. Survey Review, Vol. 32, No. 252, pp. 344-358, 1994.
15. **Papoulis A.** *Probability, Random Variables, and Stochastic Processes, 3rd Edition*. McGraw-Hill International Editions, 1991.
16. **Remondi B.W.** The NGS GPS Orbital Formats. Available on the Internet at http://www.navcen.uscg.gov, 1991.

EXPERIENCE OF INVESTIGATIONS PERFORMED WITH THE HELP OF NAVIGATION SYSTEM ABOARD THE RESEARCH PRIRODA MODULE ON THE MIR SPACE STATION

M.Yu.Beliaev, D.N.Rulev, T.V.Matveeva
(Korolev Rocket Space Corporation Energia, Russia)

V.V.Sazonov
(Keldysh Institute of Applied Mathematics, Russia)

S.Foeckersperger
(Kayser Threde, Germany)

H.Frank, W.Paeffgen
(DLR/GSOC, Germany)

Abstract

Results of processing GPS measurements obtained on Space Station Mir are presented and processing technique is described. Processing is performed in two steps. First, the interval being processed is divided into short (a few minutes in length) subintervals and measurements on every subinterval are approximated by normal points. In generating the normal points the station motion is considered as Keplerian. Then, using the obtained normal points, the functional of least square method is constructed. Minimization of the functional on solutions of rather detailed equations of the station motion gives an approximation of its actual motion. This approximation is used to provide the navigational reference for results of researches performed on the station and can be used in coping with the flight control problems.

Introduction

The GPS-receiver is installed on Space Station Mir to provide a high-precision navigational reference for the MOMS-2P scientific equipment accommodated on the Priroda module. The receiver operates only with the C/A code and, together with the module angular rate gyro unit, makes a set of MOMSNAV equipment. The equipment is accommodated inside and outside of the Mir pressurized volume and includes such elements as GPS-receiver (antenna modules, avionics), gyro unit (2 sets of gyro modules), power supply unit, service and science data distribution and management unit connected with the station telemetry and telecommand systems.

The GPS-receiver has two antenna modules, each containing two antennas. The antennas are accommodated outside the Prioda module. The antennas are positioned and oriented so that to minimize their shadowing by solar arrays and other structural elements of Space Station Mir. To meet thermal requirements the antennas are protected with radio-transparent heat-shielding fabric.

As far as the GPS-receiver is included into the MOMSNAV equipment set, it is controlled via a link provided to control this equipment. Two operational modes are envisaged for the MOMSNAV equipment. The first mode "GPS + gyro module" is used in measuring sessions of the Earth remote sensing equipment MOMS-2P for purpose of referencing the scientific information. The second mode "GPS only " is intended for determining the station phase vector. The both modes can be used for the MOMSNAV data downlink via the station data systems.

Commands to control the GPS-receiver are generated at the ground stations and uplinked to the Priroda on-board computer. The commands will be implemented either at the present time, or immediately. In the first case the commands are served out from the onboard computer in accordance with the specified time references, in the second case these commands enter the receiver immediately.

1. GPS measurements results

The Mir phase vector measurements results obtained via GPS make a sequences of values of coordinates z_1, z_2, z_3 and the station velocities $z_4 = dz_1/dt$, $z_5 = dz_2/dt$, $z_6 = dz_3/dt$ within the Greenwich coordinate system on a uniform grid with a time step of 4 s. In some rarely encountered grid points no measurements are available. Lengths of measurement intervals are within a range from several dozens of minutes to several hours. The GPS-receiver accommodated on the station ensures the definition of coordinates z_1, z_2, z_3 with nominal errors being 100 m and velocities z_4, z_5, z_6 with nominal errors of 0.5 m/s. However in some subintervals several minutes long the errors can be sufficiently higher.

Despite a rather high accuracy the "shoddy" data of GPS measurements do not allow to solve those problems of processing the results of scientific experiments which require to use a smooth approximation of the station orbital motion, for example, such approximation that can be given by solutions of motion equations resulted from processing the traditional trajectory measurements. However, the GPS data can be used instead of trajectory measurements while looking for the appropriate approximating solutions. Such a method of determining the station motion parameters appears to be no less accurate and offers more convenience against traditional. Principal mathematical models and algorithms making a basis of PC software designed for calculating the station motion parameters from the GPS measurements within short (up to several days) time intervals are described hereafter. As far as the accuracy of the velocity constituents of GPS data are not high, the only coordinate measurements are used in the capacity of initial measurement information.

2. Data processing technique

The station motion mathematical model is based on differential motion equations of the station mass center written in the Greenwich coordinate system. The model takes into account the Earth's gravitation field and atmospheric drag. The field is considered up to harmonics of the order of (8,8) inclusively in the expansion of the Earth's gravitational potential into a series by spherical functions. Atmosphere is assumed to be motionless relative to the Earth's surface, the atmospheric density is calculated from the GOST 22721-77 model. Variables in the motion equations are $z_1,\dots,z_6$. Introduce vector $z=(z_1,\dots,z_6)^T$. By the numerical integration of these equations z can be found as a function of time t. Designate the solution of motion equation having an initial condition $z(t_0)=\alpha$ as $z=\varphi(t,\alpha)$.

There is a too large amount of GPS data and their accuracy is rather uncertain to use them directly in generating the solution of differential equations approximating these measurements. It would be much more convenient (especially when carrying out calculations on PC) to compress data being available and, in parallel, access its quality rejecting inaccurate measurements. The measurement data is compressed by generating normal points.

Assume the station coordinates to be measured in moments of time t_k $(k=1,2,\dots,N)$. Designate the result of measuring coordinate z_i at moment t_k as $z_i^{(k)}$ $(i=1,2,3)$. Divide the measurement interval containing points t_k on intervals I_μ $(\mu=1,2,\dots,M)$. Interval I_μ contains n_μ points t_k numbered by $k=N_{\mu-1}+1,\dots,N_\mu$, where $N_0=0$, $N_\mu=N_{\mu-1}+n_\mu$, $N_M=N$. Suppose that errors in all measurements are independent and distributed normally with a mean value equal to zero. Errors in measurements of each coordinate z_i in interval I_μ have similar but unknown standard deviations σ_μ. With the given assumptions the definition of initial conditions of the station motion $z(t_0)=\alpha$ and the unknown standard deviations σ_μ is reduced within a framework of maximum likelihood method to the minimization of functional

$$\Phi=\sum_{\mu=1}^{M}\left(\frac{\Psi_\mu}{2\sigma_\mu^2}+3n_\mu\ln\sigma_\mu\right),\qquad \Psi_\mu=\sum_{k=N_{\mu-1}+1}^{N_\mu}\sum_{i=1}^{3}[z_i^{(k)}-\varphi_i(t_k,\alpha)]^2.$$

Minimize Φ in several steps. At the first step, taking α as constant, find estimates of standard deviations and $\Phi_1=\min\Phi$ for σ_μ. This step is easy to accomplish analytically. We have

$$\sigma_\mu^2=\frac{\Psi_\mu}{3n_\mu},\qquad \Phi_1=\frac{3}{2}\sum_{\mu=1}^{M}n_\mu\ln\Psi_\mu.$$

Here, in the expression for Φ_1 the unessential additive constant is omitted. At the second step $\alpha^*=\arg\min\Phi_1$ will be found. Within a framework of maximum likelihood method vector α^* is the estimate the unknown vector α.

Practically, the direct performance of the second step is associated with certain problems the greatest of which is a large amount of measurement points (coarse errors encountered in measurements are not yet under consideration). When each of the points has to be processed while $\varphi(t,\alpha)$ is being calculated, either rather complex software has to be used, or much time has to be expended to calculate functional Φ_1. Simple and effective techniques for calculating Φ_1 are desirable. These are possible to obtain by using normal points. In the given case the normal points serve to approximate functions $\Psi_\mu=\Psi_\mu(\alpha)$ and are arranged in the following way.

Suppose $z=\chi(t,\beta)$ – Keplerian approximation of the station motion in interval I_μ, $\beta=(a,e,L_0,\Omega,i,\omega)^T$

– a set of Keplerian elements of orbit: a – semimajor axis, e – eccentricity, L_0 – mean longitude for a certain epoch, Ω – longitude of ascending node, i – inclination, ω – argument of perigee latitude. An epoch selection for task L_0 is unessential. The first point with measurements, $t_{N_{\mu-1}+1}$, in interval I_μ is taken for convenience. Lengths of intervals I_μ are supposed to be such that in each of them, provided the relation between α and β is proper, relationship $\varphi(t,\alpha) \equiv \chi(t,\beta)$ can be considered fulfilled. Let's name values α and β meeting such a relation as equivalent. Actually, lengths of intervals I_μ must be selected so that the equivalence is expressed as the Kepler problem formulae. For example, to express dependence $\varphi(\tau_\mu,\alpha) = \chi(\tau_\mu,\beta)$, where τ_μ – is a middle point of interval I_μ.

Designate $z_i^{(k)} - \varphi_i(t_k,\alpha) = A_{ik}(\beta) + B_{ik}(\alpha,\beta)$, where $A_{ik}(\beta) = z_i^{(k)} - \chi_i(t_k,\beta)$, $B_{ik}(\alpha,\beta) = \chi_i(t_k,\beta) - \varphi_i(t_k,\alpha)$, and present the expression for Ψ_μ in the form

$$\Psi_\mu(\alpha) = \Psi_\mu^a(\beta) + \Psi_\mu^b(\alpha,\beta) + \Psi_\mu^c(\alpha,\beta),$$

$$\Psi_\mu^a(\beta) = \sum_{i,k} A_{ik}^2(\beta), \quad \Psi_\mu^b(\alpha,\beta) = \sum_{i,k} B_{ik}^2(\alpha,\beta), \quad \Psi_\mu^c(\alpha,\beta) = 2\sum_{i,k} A_{ik}(\beta)B_{ik}(\alpha,\beta).$$

Here, summing up with respect to i is performed from 1 to 3, with respect to k – from $N_{\mu-1}+1$ to N_μ.

Take $\beta_\mu = \arg\min \Psi_\mu^a$ and suppose that such β_μ is unique. From the definition of β_μ the following relation is derived

$$\frac{\partial \Psi_\mu^a(\beta_\mu)}{\partial \beta} = -2\sum_{i,k} A_{ik}(\beta_\mu)\frac{\partial \chi_i(t_k,\beta_\mu)}{\partial \beta} = 0. \qquad (1)$$

As far as the above equivalence of functions $\varphi(t,\alpha)$ and $\chi(t,\beta)$ is concerned, with α values close to β_μ, we obtain

$$\varphi(t,\alpha) - \chi(t,\beta_\mu) \approx \frac{\partial \chi(t,\beta_\mu)}{\partial \beta}\Delta\beta,$$

where $\Delta\beta$ – a certain function of α. The last relationship enables to find approximated formulae for If we substitute them in the expression for $\Psi_\mu^c(\alpha,\beta)$ and consider equality (1), then $\Psi_\mu^c(\alpha,\beta_\mu) \approx 0$ can be obtained. From this the approximated formula is derived

$$\Psi_\mu(\alpha) \approx \Psi_\mu^a(\beta_\mu) + \Psi_\mu^b(\alpha,\beta_\mu). \qquad (2)$$

Estimates s_μ^2 of dispersions σ_μ^2 of errors in coordinates measurements can be calculated via formulae

$$s_\mu^2 = \frac{\Psi_\mu^a(\beta_\mu)}{3n_\mu} \qquad (\mu = 1,2,\ldots,M). \qquad (3)$$

Now find the approximated expression for $\Psi_\mu^b(\alpha,\beta_\mu)$. There are two ways for this.

The first way. Suppose, that interval I_μ is sufficiently short, then difference $\varphi(t,\alpha) - \chi(t,\beta_\mu)$ hardly varies within it and it can be assumed that

$$\Psi_\mu^b(\alpha,\beta_\mu) \approx n_\mu \sum_{i=1}^{3} [\varphi_i(\tau_\mu,\alpha) - \chi_i(\tau_i,\beta_\mu)]^2,$$

where τ_μ – is a middle point of this interval as before. The middle point selection is particularly attractive in the event when moments with measurements form a uniform grid on the time axis. A set of values s_μ^2, n_μ and $\chi_i(\tau_\mu,\beta_\mu)$ $(i = 1,2,3)$ will be taken as a normal point in the described way of approximating the function $\Psi_\mu^b(\alpha,\beta_\mu)$. Such an approach to constructing normal points is widely used.

The second way is described in [3,4]. In the first way a more simple approximation is used. In the second way the approximation is more complex and more accurate. In the case of large values of M the both ways, when used to process measurements, will lead to similar results.

Consider now the further conversions of functional Φ_1, having the solved relations (2) at $(\mu = 1,2,\ldots,M)$. In other words, assume the following expression to be valid

$$\Phi_1 \approx \frac{3}{2}\sum_{\mu=1}^{M} n_\mu \ln[\Psi_\mu^a(\beta_\mu) + \Psi_\mu^b(\alpha,\beta_\mu)].$$

Suppose, that in the considered range of α the following relations are valid

$$\Psi_\mu^b(\alpha,\beta_\mu) << \Psi_\mu^a(\beta_\mu) \qquad (\mu = 1,2,\ldots,M). \tag{4}$$

Hence, using formula $\ln(1+x) \approx x$, valid at $|x| << 1$, it can be written

$$\Phi_1 \approx \frac{3}{2}\sum_{\mu=1}^{M} n_\mu \ln\Psi_\mu^a(\beta_\mu)\left[1 + \frac{\Psi_\mu^b(\alpha,\beta_\mu)}{\Psi_\mu^a(\beta_\mu)}\right] \approx \frac{3}{2}\sum_{\mu=1}^{M} n_\mu \ln\Psi_\mu^a(\beta_\mu) + \frac{3}{2}\sum_{\mu=1}^{M}\frac{n_\mu\Psi_\mu^b(\alpha,\beta_\mu)}{\Psi_\mu^a(\beta_\mu)}.$$

The first sum in the right part of the last equality does not depend on α, and it can be omitted. The second sum is converted considering relations (3). As a result, the problem of minimization of the functional

$$\Phi_2 = \frac{1}{2}\sum_{\mu=1}^{M}\frac{\Psi_\mu^b(\alpha,\beta_\mu)}{s_\mu^2}. \tag{5}$$

is obtained. Functional (5) is a functional of least square method. Now, the problem is to minimize it. Functional (5) is also reasonable to be considered when conditions (4) are violated because, owing to inequalities of $\Psi_\mu^b > 0$ and $\ln(1+x) \le x \quad (x > -1)$ the following bounds are valid

$$0 \le \Phi_1 - \frac{3}{2}\sum_{\mu=1}^{M} n_\mu \ln\Psi_\mu^a(\beta_\mu) \le \Phi_2.$$

From these bounds it follows that value α, minimizing (5) must be close to the estimation found through minimizing Φ_1.

Let $\alpha^* = \arg\min\Phi_2$. Then, with the assumptions regarding measurement errors α^* is a random vector having approximately normal distribution with a mean value equal to a true value of α, and covariance matrix $K_\alpha = \left[\partial^2\Phi_2(\alpha^*)/\partial\alpha^2\right]^{-1}$. However, when the covariance matrix is calculated in the aforesaid way, the α^* assessment accuracy will be strongly exaggerated. The more accurate estimation of K_α can be obtained following the least square scheme. Consider vector $\chi_i(\tau_\mu,\beta_\mu)$ as result of measuring vector $\varphi_i(\tau_\mu,\alpha)$ $(i = 1,2,3)$; errors made during such measurements taken at different moments of time are independent and have normal distributions with the mean values equal to zero and the covariance matrices proportional to s_μ^2, the coefficient of proportionality being similar for all μ. In this case

$$K_\alpha \approx \frac{2\Phi_2(\alpha^*)}{3M-6}\left[\frac{\partial^2\Phi_2(\alpha^*)}{\partial\alpha^2}\right]^{-1}. \tag{6}$$

The given technique for processing measurement results is referred to the ideal model of errors contained in the measurements. As it was already mentioned above, the measurement data contain a certain number of coarse errors. To exclude such errors from processing the following technique has been applied in calculating β_μ $(\mu = 1,2,\ldots,M)$. First, by the Gauss-Newton method a value of $\beta'_\mu = \arg\min\Psi_\mu^a$, was found and median m'_μ of residual module $\left|z_i^{(k)} - \chi_i(t_k,\beta'_\mu)\right| \quad (i = 1,2,3;\ k = N_{\mu-1}+1,\ldots,N_\mu)$ was calculated. Value of $s'_\mu = 1.48m'_\mu$ was assumed as an estimate of a standard deviation was assumed as an estimate of a standard deviation σ_μ. Then, the Gauss-Newton procedure was iterated, each iteration excluding from the sum defining

Ψ_μ^a, the terms related to those values of k for which at least one of inequalities $z_i^{(k)} - \chi_i(t_k, \beta'_\mu) < 2.5 s'_\mu$ $(i = 1,2,3)$ is violated. As a result of this process the value of β_μ was determined as well as median m_μ of module of those residues which were included in the Ψ_μ^a sum in the last iteration. In sum (5) defining functional Φ_2 only those normal points were included for which the estimation of standard deviation $s''_\mu = 1.48 m_\mu$ was not beyond a specified threshold. In the calculations described hereafter this threshold was 40 m.

3. Results of measurement data processing

To commence, let's give an example of standard point characteristics. For one thing, rather large lengths of intervals I_μ, are desired to enable a large number of measurements. For another thing, increasing these lengths will lower the accuracy of the station motion approximation by solution of the Kepler problem. In the calculations described thereafter lengths of intervals I_μ (except for I_M) were assumed to be 5 min and the maximum possible value of n_μ up to 75. For typical one of those intervals: $n_\mu = 72$, $s'_\mu = 23$ m, $s''_\mu = 13$ m, $s_\mu = 12$ m with only 57 moments of time with measurements at the final step of constructing a normal point. Values $n_\mu = 57$ and $s_\mu = 12$ m were used in (5).

Eigenvalues of matrix $\frac{1}{2}\partial^2 \Psi_\mu^a(\beta_\mu)/\partial\beta^2$ appeared to be: 0.000010, 0.78, 7.6, 240, 2200, 11000 (to explain the order of values with no dimensional representation it should be noted that in calculations 1000 km and 1000 s were used as the length and time measuring units and angles were measured in radians), a normalized eigenvector corresponding to minimal eigenvalue of matrix is equal to $(0.01, 0.00, 0.00, 0.00, 0.00, 1.00)^T$. Standard deviations of vector β_μ, components defined within standard assumptions of least square method are: $\sigma_a = 43$ m, $\sigma_e = 4.2 \cdot 10^{-6}$, $\sigma_{I_0} = 4.0° \cdot 10^{-4}$, $\sigma_\Omega = 2.1° \cdot 10^{-4}$, $\sigma_i = 8.1° \cdot 10^{-5}$, $\sigma_\omega = 0.21°$. Thus, in generating normal points the argument of perigee latitude is determined least accurately.

Consider the other characteristics of the normal point concerned. Standard deviations of the $\chi(\tau_\mu, \beta_\mu)$: 1.9 m, 1.9 m, 1,9 m, 24 mm/s, 24 mm/s, 24 mm/s.

Now, come to the description of results obtained from processing the long intervals with GPS measurements. Consider three intervals which characteristics are given in Table 1. The Table gives numbers of intervals for reference, dates covering initial points of intervals, moments of time τ_1 and τ_M in seconds from the day outset at the Greenwich mean time, duration of intervals $\tau_M - \tau_1$ in hours and number M of normal points included in processing. Besides the intervals indicated in Table 1, interval $1 \vee 2$, obtained by combining intervals 1 and 2 will be also considered. Its length is 30.77 h.

Table 1. Processed intervals

Int.	Date	τ_1, c	τ_M, c	$\tau_M - \tau_1$, ч	M
1	27.01.97	21763.5	27262.5	1.53	13
2	28.01.97	39463.0	46145.0	1.86	16
3	02.02.97	12440.5	22824.0	2.88	24

For all aforesaid intervals the functional (5) was minimized by the Gauss-Newton method [Ref. 1]. In all cases an initial point of interval was selected as t_0. A condition number of matrix of corresponding normal equations (the quotient of maximal and minimal eigenvalues of this matrix) in a minimum of Φ_2 does not exceed several thousands for intervals 1, 2 and 3, for interval $1 \vee 2$ this number is equal to $1.2 \cdot 10^5$. The covariance matrix of estimation α^* of initial conditions vector was calculated from expression (6).

Values describing the accuracy of processing all listed intervals are given in Tables 2, 3 and 4. Table 2 shows standard deviations $\sigma_{\alpha i}$ $(i = 1,2,\ldots,6)$ of α^* components. Tables 3 and 4 give the corresponding mean and mean square values of components of vectors $\varphi_i(\tau_\mu, \alpha) - \chi_i(\tau_\mu, \beta_\mu)$. The values are designated δ_i and S_i $(i = 1,2,\ldots,6)$ respectively.

Table 2. Standard deviations of α^* components

Int.	$\sigma_{\alpha 1}$, m	$\sigma_{\alpha 2}$, m	$\sigma_{\alpha 3}$, m	$\sigma_{\alpha 4}$, mm/s	$\sigma_{\alpha 5}$, mm/s	$\sigma_{\alpha 5}$, mm/s
1	8.8	15.1	18.3	15.8	15.9	8.5
2	12.4	9.8	7.5	8.2	12.9	13.0
3	9.9	12.0	15.6	14.6	16.0	10.5
1 ∨ 2	5.1	5.2	6.7	6.8	5.6	4.9

Table 3. Mean values of components of residual differences $\varphi(\tau_\mu,\alpha)-\chi(\tau_\mu,\beta_\mu)$

Int.	δ_1, m	δ_2, m	δ_3, m	δ_4, mm/s	δ_5, mm/s	δ_6, mm/s
1	10	-2	13	-115	-80	-43
2	-9	-1	3	57	186	89
3	-3	-3	3	-194	4	-15
1 ∨ 2	0	21	11	-21	65	20

Table 4. Mean square values of components of residual differences $\varphi(\tau_\mu,\alpha)-\chi(\tau_\mu,\beta_\mu)$

Int.	S_1, m	S_2, m	S_3, m	S_4, mm/s	S_5, mm/s	S_6, mm/s
1	33	27	34	378	276	356
2	29	40	32	397	415	411
3	67	50	55	403	290	328
1 ∨ 2	41	42	36	389	362	384

As it is suggested by the Tables, the normal points can be fitted with the solution of the station motion equations, the errors being of several dozens of meters for each coordinate and of several hundreds of mm/s for each velocity component. Usually, maximum errors are not exceeding 100 m and 1m/s, respectively. These accuracy characteristics are the same that referred in [Ref. 2].

References

1. **Akim E.L., Eneev T.M.** Determining spacecraft motion parameters from trajectory measurements. Cosmic Research, 1963, vol. 1, No. 5, p. 5-50.
2. **Gill E.** Analysis of the first MOMS-2P GPS navigation data of the Mir space station. DLR GSOC TN 96-06, November 15, 1996.
3. **Belyaev M.Yu., Rulev D.N., Chernopyatov A.N., Sazonov V.V., Foeckersperger S., Paeffgen W.** Use of GPS for determining motion parameters of space station Mir. Proc. of the 12th International Simposium on Space Flight Dynamics, ESOC, Darmstadt, Germany, 2-6 June 1997, p. 109-114.
4. **Belyaev M.Yu., Rulev D.N., Chernopyatov A.N., Sazonov V.V., Foeckersperger S., Paeffgen W.** Determining motion of space station Mir with the help of GPS navigation data. Cosmic Research, 1999, vol. 37, No. 3, p. 276-282.

DIGITAL MAGNETIC COMPASS AND GYROSCOPE INTEGRATION FOR PEDESTRIAN NAVIGATION

Q. Ladetto[*], B. Merminod[**]
Faculté ENAC - Institut du Développement Territorial, Geodetic Laboratory (TOPO)
CH-1015 Lausanne, Switzerland.
WWW: http://topo.epfl.ch
E-mail: quentin.ladetto@epfl.ch

Abstract

Keywords: Pedestrian Navigation, Dead Reckoning, Magnetic Compass, Gyroscope

When satellite signals are available, the localisation of a pedestrian is fairly straightforward. However, in cities or indoors, dead reckoning systems are necessary. Our current research focuses on the development of algorithms for pedestrian navigation in both post-processing and real-time modes. Experience shows that the main source of error in position comes from the errors in the determination of the azimuth of walk. By coupling a magnetic compass with a low-cost gyroscope in a decentralized Kalman filter configuration, the advantage of one device can compensate the drawback of the other.
If we compare the rate of change of both signals while measuring the strength of the magnetic field, it is possible to detect and compensate magnetic disturbances. When these disturbances do not take place, the continuous measurement of the azimuth allows to estimate and compensate the bias and scale factor of the gyroscope. The reliability of indoor and outdoor navigation gets significantly improved due to the redundancy of the information. Numerous tests conducted with different subjects and in various environments validate this approach.

Introduction

The nice aspect about human displacements is its unpredictable freedom of motion. The worst hypothesis in modelling human trajectories is precisely this liberty of movements. Such aspect will play a major role in the filtering of the azimuth. Sudden rotations measured by a magnetic compass can be caused either by the movement itself or by a magnetic disturbance. Intuitively, if there is a disturbance, the total value of the earth magnetic field changes too. Some examples show that this condition might be sufficient but not necessary to reliably determine a disturbance. In order to improve the reliability of the azimuth determination, a gyroscope will be used. The motivation doesn't come to navigate with a gyroscope heading only, as presented in Gabaglio (2002), but to bridge the gaps when the compass gets disturbed. Vice versa, the magnetic azimuth will contribute to determine the absolute direction of the gyroscope as well as a continuous calibration of its errors (bias and scale factor) even when no satellite signals are available. The suggested methodology takes into account the possibility of a non-aligned system. It is therefore possible to use a gyroscope having multiple tasks. Using the factual approach with the combination of such sensors has the advantage of keeping cost relatively low compared to the classical mechanization that requires a full high grade IMU (Figure 1).

This paper will present a calibration procedure

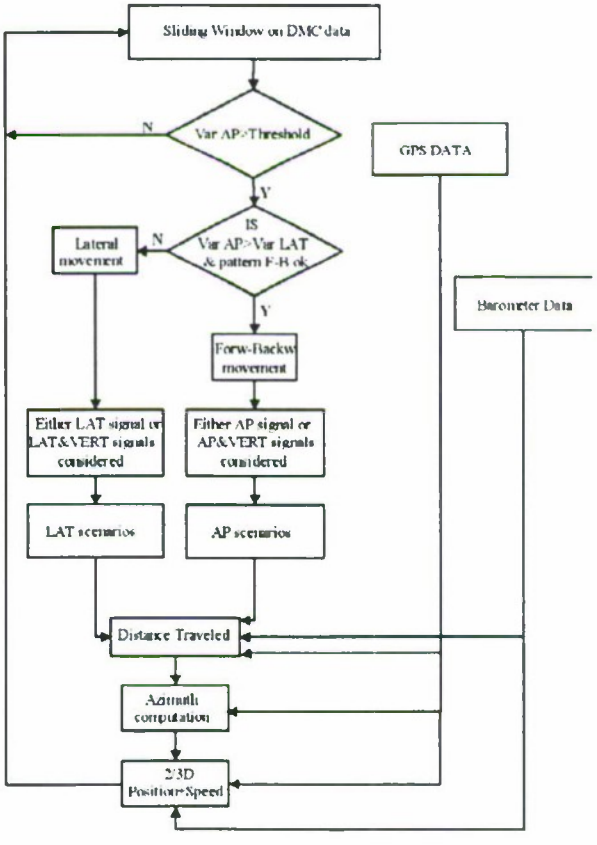

Figure 1: Flow chart of the factual approach considering each step occurrence instead of a double integration of the acceleration

[*] PhD Student, Research Scientist
[**] Professor, Head of Laboratory

necessary to compensate magnetic apparent disturbances induced by human motions. Trajectories comparisons in a non-disturbed area between the factual and total mechanization approach are described. The identification of magnetic disturbances as well as the continuous calibration of the gyroscope errors for indoor and outdoor navigation are detailed. Finally, a reliability concept complementing the indicator of precision is presented.

1. Compass Navigation: errors, disturbances and solutions

The magnetic azimuth is the horizontal component of the Earth field. Its determination requires implicitly the knowledge of the horizontal or vertical plane. This is commonly done by sensing the gravity vector at rest. To compute then the azimuth of walk, one has to constantly compute the attitude of the sensor in order to correct the measured magnetic values. Using the 3D rotation matrix with the Yaw(ψ)-Pitch(φ)-Roll(θ) sequence, the horizontal components H_y and H_x are

$$H_x = b_x \cos\varphi - b_y \cos\varphi \sin\Theta + b_z \sin\varphi \cos\Theta \quad (1.1)$$

$$H_y = b_y \cos\Theta - b_z \sin\Theta \quad (1.2)$$

where b_i are the components measured by the sensor. The azimuth derived from these values will contain and propagate the errors present in the attitude angles themselves. According to the first order Taylor development of the azimuth computation, this uncertainty becomes

$$\alpha + \Delta\alpha = \arctan(\frac{-H_y}{H_x}) + \frac{\partial(-\arctan(\frac{H_y}{H_x}))}{\partial H_y}\Delta H_y + \frac{\partial(-\arctan(\frac{H_y}{H_x}))}{\partial H_x}\Delta H_x \quad (1.3)$$

Simplifying (1.3) and taking into account that

$$H_e = H_h \begin{bmatrix} \cos\alpha \\ -\sin\alpha \\ \tan\delta \end{bmatrix} \text{ where } \delta \text{ is the inclination of the magnetic vector} \quad (1.4)$$

we get that the error produced can be written as

$$\Delta\alpha = -\Delta\theta \cdot \tan\delta \cdot \cos\alpha - \Delta\varphi \cdot \tan\delta \cdot \sin\alpha \quad (1.5)$$

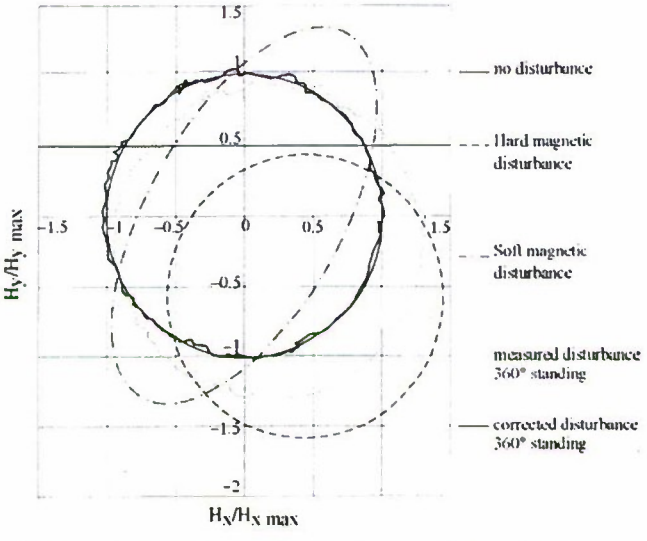

Figure 2: Description of the different effect of magnetic disturbances. The result of the simplified procedure adapted for pedestrian navigation corrects the disturbances caused by clothes and accessories.

This relation shows that the error in determining the attitude angles affects directly the azimuth and its effect strongly depends on the azimuth itself. The same errors will have different effects according to the latitude of displacement. This can be understood considering that the higher the latitude, the weaker the measured horizontal field. Therefore, the secondary component induced by the attitude errors will have a more important influence. For mid-latitude, the average value of 2 for $tan\delta$ can be considered. A complete theoretical description can be found in Denne (1979).

Independently to these errors, disturbances, divided into *soft* and *hard* categories will affect the Earth magnetic field in the tree dimension of the space. A rigorous approach would require the determination of 12 parameters at known elevations, which, considering the previous remark, would also be affected by some errors. A simplified approach (Caruso 1997) consisting of determining only the corrections in the horizontal plane is more convenient considering also that the pedestrian navigation system is worn by a person at the belt level. The four parameters are two scale

factors (X_{sf} Y_{sf}) and two translations (X_0, Y_0). Applying the corrections to the projected magnetic values, the components of equation (1.3) become

$$H_x = X_{sc} \cdot H_{xmes} + X_0 \text{ and } H_y = Y_{sc} \cdot H_{ymes} + Y_0 \quad (1.6)$$

The result of the calibration procedure to determine the disturbances caused by the clothes and accessories of a person is illustrate in Figure 2.
If this static procedure already takes into account an important part of the azimuth error, a second dynamic calibration will be necessary to compensate the individual errors occasioned by walking. Low-pass filtering the additional accelerations allows to get rid of the typical oscillations in walking. If the computed pitch and roll values reflect the movements done by the hips, virtual values have to be defined to compensate the displacement effects on the horizontal plane. These additional constant corrections don't have a physical meaning but reflect the individual characteristics of a walk and the symmetry between left and right strides. Figure 3 shows the effects of the different calibration phases and their additional effects for a 400 m track on an Olympic stadium. The lower parts show the pitch and roll computed step by step from the filtered accelerations. The optimal constant values are 1.48° for the pitch and 3.92 for the roll angles. Without any calibration process, these values are impossible to retrieve from the data.

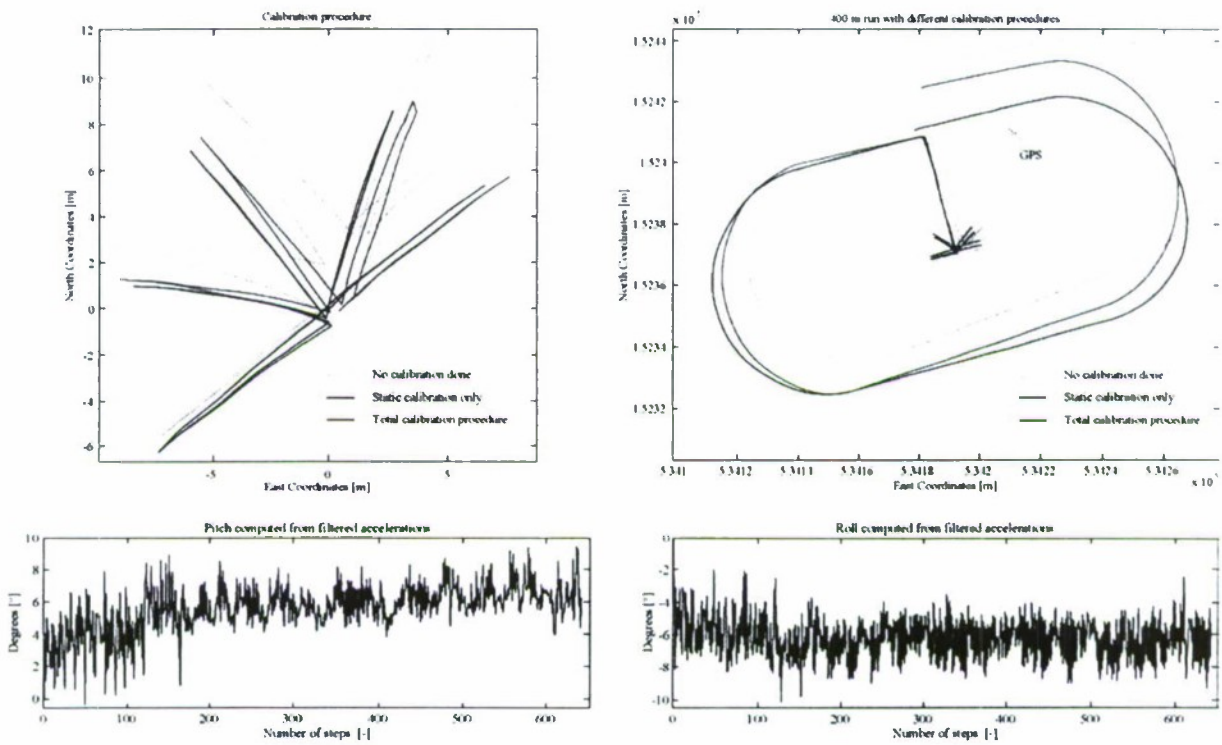

Figure 3: Effects of the different and complementary calibration phases (up). The pitch and roll angle values computed directly from the filtered acceleration doesn't provide the optimal attitude virtual values to correct the horizontal projection plane (down).

2. Factual vs. total mechanization approach

In order to test this approach versus a golden standard, trajectories were covered using two different devices (Figure 4). The measurement procedure as well as the data integration is completely different. The reference path is computed with the POS/LS™ system of Applanix by double integration of the acceleration 3D vector coupled to a triad of gyroscope. The measurement frequency was set to 200 Hz. In order to keep an optimal precision and avoid any divergence, Zero Velocity Updates (ZUPT) were performed every 1 or two minutes during less than 10 seconds. After an alignment procedure between 5 and 10 minutes, the strict respect of such procedure allows maintaining accuracy at a decimetre, even centimetre, level over several kilometres. As this system only measures effective displacements, it is independent of the type of ground and environment.
The different tests, realised in standard conditions, show the limits in precision as well as in reliability between *navigation* and *surveying*, Figure 5. If the maximal difference remained always below the 10 m, it cannot be

reliably improved with the factual approach and therefore its performance does not meet surveying requirements. On counterpart, the necessary repeated stops for the ZUPTs, are very constraining in navigation, showing simultaneously the functional limits of such approach. Future research will focus on the integration and complementarities of both approaches.

Figure 4: Pedestrian Navigation System (left) developed together with Leica Vectronix. With a size of 73.7 mm x 48.3 mm x 18 mm and a weight inferior to 50 grams, it fulfills all ergonomic requirements for such application. Right, the POS/LS™ (Position and Orientation System for Land Survey) system of Applanix for high precision surveying.

3. Handling magnetic disturbances

Once walking, magnetic disturbances have an important influence on the quality of the azimuth signal. These are sometimes identifiable thanks to the magnetic field itself, however, the simultaneous use of a gyroscope allows providing a heading, even in sensible areas.

3.1 Optimising the magnetic information

The Earth magnetic field can be considered as a constant within the area normally covered by a pedestrian. All sudden variation of this field will be logically and indicator of a disturbance. Unfortunately, when someone is moving, the magnetic ambient is always changing and small random variation are caused by the environment. If low-pass filter and the factual approach take care of the majority of these fluctuations, the determination of a threshold is indispensable. Ideally this should be determined in a magnetic neutral area. This stage being unfortunately too constraining, the value of 3μT has been empirically defined as threshold on the root mean square of the magnetic field during three steps. Passed this value, the last good azimuth is held constant until the field variation becomes stable again. The error introduced with such simplification is directly correlated to the sinuosity of the path during the disturbed period. As the effect of a disturbance decreases with the square (even cube) of the distance from the source, the majority of effects are visible only over tens of meters. Considering the way people walk, and the strong influence of the cadastre (straight line between blocs), this approach provides a much better result than considering indistinctively disturbed and undisturbed azimuths.

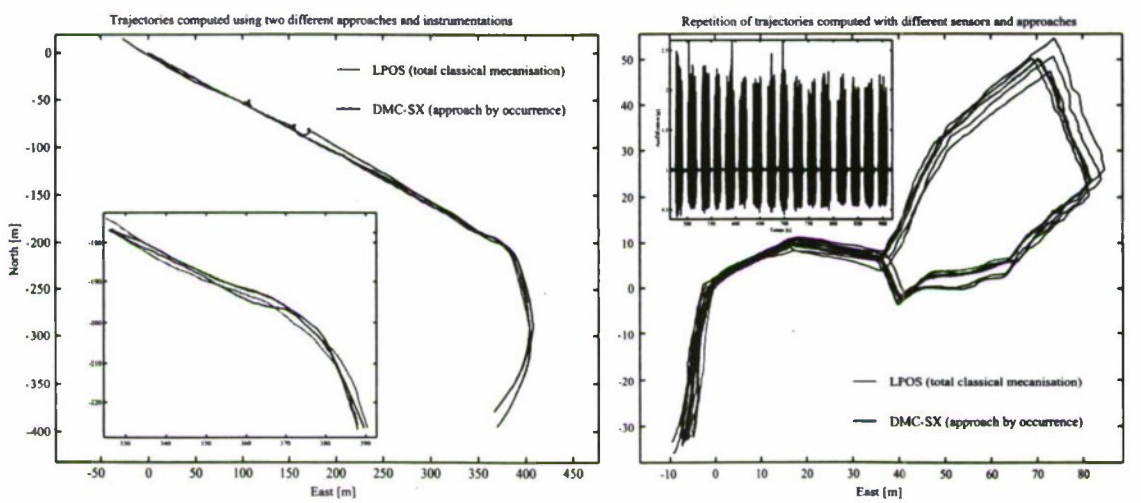

Figure 5: Comparison of the trajectories obtained with the two approaches. On the left, a rectilinear return walk of 1'331.5 m. The end-loop position error computed by the factual approach is 21.4 m (1.6 %) and -6.4 m on the travelled distance. On the right, the repetitions of the same trajectory (304.8 m) show the perfect reproducibility of the classical approach. On 4 trials with the factual approach, the dispersion on the travelled distance is 7.8 m (from 299.4 m to 307.2 m), that is an error of 2 cm/step. The inserted box presents the vertical accelerations bringing to the fore the frequent ZUPTS (10 sec. Each 30 sec).

3.2 Using gyroscope

Although gyroscopic azimuth is broadly used in dead reckoning navigation, the intention here is to use it only as a back up system in definite situations when the compass is confused or during quick turns. The exclusive use of the gyroscope during these period, even if they are reasonably short (one to two minutes maximum) requires its permanent and complete calibration. Bias and scale factor are therefore continuously up-dated by the compass data or/and with GPS data when the signal is available. The use of non-aligned sensors force the gyroscope angles to virtually harmonized itself with the compass. The misalignment towards the direction of walk can in a second time only be defined if given absolute directions are known or if satellites signals are present.

Numerous tests (Moix 2002) using a low cost vertical gyroscope have shown a scale factor error of 1%. For 90° turn, keeping the scale factor to unity would cause an error of 0.9°. That is the same order of precision in the azimuth as we get from the compass. The parameter of a scale factor will therefore be neglected under the hypothesis that the gyroscope is set perpendicularly to the plane of movement. The bias determination is, however, of major importance and requires an initialisation phase before each run. This will be done standing or along a line, important being that the gyroscope doesn't sense any angular velocity (Earth rate neglected). The simplified model is the following

$$\tilde{\omega}_i = \omega_i - b_i + \varepsilon_i \tag{3.2}$$

where $\tilde{\omega}_i$ is the true value, ω_i the measured value and ε_i a white noise affecting the measurements.

If we consider the azimuth we can write:

$$\varphi_{begin}^{gyro} - \varphi_{end}^{gyro} = \sum_{i=1}^{n} (-b_i) \cdot \Delta t \tag{3.4}$$

where n is the number of time interval considered and Δt is the time interval itself (here 1/30). If we make the hypothesis that during this initial phase the bias is constant, its value can be approximated by

$$\bar{b} = \frac{1}{n} \cdot \sum_{i=1}^{n} b_i = \frac{\varphi_{begin}^{gyro} - \varphi_{end}^{gyro}}{\Delta T} \tag{3.5}$$

where $T = n \cdot t$. This value $\bar{b}$ is then continuously updated when no magnetic disturbance is detected. As the value of the bias varies in time, an estimation of the error of both azimuths in required.

3.3. Unweighted bias update and error propagation

Starting from the assumption that the azimuth of the compass is considered as true, the bias will be computed projecting the gyroscope heading on the compass azimuth. At the update, this is expressed by:

$$\varphi_{j+1}^{gyro} = \varphi_{j}^{compass} + \sum_{i=j}^{j+1} (\omega_i - b_j) \cdot t = \varphi_{j}^{gyro} + \sum_{i=j}^{j+1} (\omega_i - b_j) \cdot t \tag{3.6}$$

where j represents the epoch of bias update. Such modelisation requires a constant bias between updates. This is unfortunately not the case but considering the time frame between updates, such assumption can be made. The azimuth of the compass can also be written

$$\varphi_{j+1}^{compass} = \varphi_{j}^{compass} + \sum_{i=j}^{j+1} (\omega_i - b_i) \cdot t \tag{3.7}$$

where $b_i = b_j + \Delta b_i$ and Δb_i being the bias increment by unit of time i. Subtracting (3.7) from (3.6), the average bias correction is

$$\overline{\Delta b}_{j+1} = \frac{1}{n} \sum_{i=j}^{j+1} \Delta b_i = \frac{\varphi_{j+1}^{gyro} - \varphi_{j+1}^{compass}}{T} \; [°/s] \tag{3.8}$$

with $\Delta T = n \cdot \Delta t = t_{j+1} - t_j$. By correcting simultaneously the bias $b_{j+1} = b_j + \overline{\Delta b}_{j+1}$, the azimuth of the gyroscope becomes

$$\varphi_{j+1}^{gyro^*} = \varphi_j^{gyro^*} + \sum_{i=j}^{j+1} (\omega_i - b_{j+1}) \cdot \Delta t = \varphi_{j+1}^{gyro} - \overline{\Delta b}_{j+1} \cdot \Delta T \tag{3.9}$$

An error on the bias will therefore logically influence the error on the gyroscopic azimuth. The evolution of this value is computed applying the error propagation to (3.8)

$$\sigma_b^2 = \sigma_{\Delta b}^2 = \frac{\sigma_{\varphi^{COMPASS}}^2 + \sigma_{\varphi^{Gyro}}^2}{\Delta T^2} \tag{3.10}$$

As $\sigma_{\varphi^{Gyro}}^2$ is dependent of the precision of the bias, both errors are not independent. In order to remedy to this problem, the equation (3.8) allows to write

$$\overline{\Delta b}_{j+1} = \frac{1}{n} \sum_{i=j}^{j+1} \Delta b_i = \frac{\varphi_j^{compass} - \varphi_{j+1}^{compass}}{\Delta T} + \overline{\omega}_i - b_j \quad \text{i.e.} \quad b_{j+1} = \frac{\varphi_j^{compass} - \varphi_{j+1}^{compass}}{\Delta T} + \overline{\omega}_i \tag{3.11}$$

The error on the bias is therefore

$$\sigma_b = \sqrt{\frac{2 \cdot \sigma_{\varphi^{COMPASS}}^2}{\Delta T^2} + \frac{1}{n} \cdot \sigma_\omega^2} \tag{3.12}$$

that leads to the error on the gyroscopic azimuth itself

$$\sigma_{\varphi_{j+m}^{GYRO}} = \sqrt{\sigma_{\varphi^{COMPASS}}^2 + m \cdot \Delta t^2 \cdot \sigma_\omega^2 + m^2 \cdot \Delta t^2 \cdot \sigma_b^2} \tag{3.13}$$

m is the number of sampled values elapsed since the last update. At this stage, the assumption of the constancy of the bias can influence the results. The bigger the *m* value becomes, the greater the influence of the bias drift on the azimuth. The maximal time interval is directly related to the quality of gyroscope used. In the given conditions, tests show that pure gyroscope dead reckoning is achievable up to a time interval of 120 seconds.
As the magnetic azimuth presents an error, it should not be considered as true in the updating process. A weighting of its value can therefore be obtained with the use of either an exponential or a Kalman filter.

3.4. Weighted bias update and error propagation

Using an exponential filter has the advantage of taking into account an evolution of the bias without forgetting its past values. This can be seen as a security in environments where undetected magnetic disturbances could influence its value. The updated bias can then be expressed by (3.14) where the parameter α regulates the influence of the new measurement on the bias value.

$$b_{j+1}^* = (1 - \alpha) b_{j+1} + \alpha b_j^* \tag{3.14}$$

The expression (3.9) becomes then

$$\varphi_{j+1}^{gyro^*} = \varphi_j^{gyro^*} + \sum_{i=j}^{j+1} (\omega_i - b_{j+1}^*) \cdot \Delta t \tag{3.15}$$

The gyroscopic azimuth is corrected by the value

$$\Delta \varphi_{j+1}^{gyro^*} = \varphi_{j+1}^{gyro^*} - \varphi_{j+1}^{gyro} = (\alpha - 1) \cdot \Delta T \cdot \overline{\Delta b}_{j+1} \tag{3.16}$$

Applying the error propagation law to (3.14)

$$b_j^* = \alpha^j b_0 + \sum_{i=1}^{j+1} \alpha^{(j-i)} \cdot (1-\alpha) b_i \tag{3.17}$$

With the hypothesis of a constant time interval between the updates as well as a white noise on the averaged measured angular velocities, the error on the bias is

$$\sigma_{b_j^*} = \sqrt{\frac{2\cdot(1-\alpha)^2}{\Delta T^2} \cdot \left(\sum_{i=0}^{j+1} (-\alpha)^i \right) \sigma^2_{\varphi^{compass}} + \alpha^{2j} \cdot \sigma^2_{b_0}} \tag{3.18}$$

Considering (3.16) the error of the azimuth given by the gyroscope becomes

$$\sigma_{\varphi_{j+m}^{gyro^*}} = \sqrt{\sigma^2_{b_0} \left(\Delta T^2 \left(\sum_{i=1}^{j} (\alpha^i) \right)^2 + m^2 \Delta t^2 \alpha^j \right) + \sigma^2_{\varphi^{compass}} \left(2 \sum_{i=1}^{2j} (-\alpha)^i + 1 + \frac{2m^2 \Delta t^2 (1-\alpha)^2}{\Delta T^2} \sum_{i=0}^{j+1} (-\alpha)^i \right)} \tag{3.19}$$

3.5. Update of the bias using a Kalman filter

A commonly used approach to integrate different sources of information is a Kalman filter, as described in Gelb (1971). The parameters considered are the gyroscope bias and the azimuth. The bias is modelled as a first order Markov process (Ladetto et al 2001) that leads for the equations of movement to

$$\begin{pmatrix} d\dot{\varphi}_k \\ d\dot{b}_k \end{pmatrix} = \begin{pmatrix} 0 & -1 \\ 0 & -\alpha \end{pmatrix} \cdot \begin{pmatrix} d\varphi_k \\ db_k \end{pmatrix} + \begin{pmatrix} 1 \\ a \end{pmatrix} w \tag{3.20}$$

The increment k represents here a step occurrence and not a time interval. The values of 0.05 for a and $\sqrt{0.05}$ [$^\circ/\sqrt{s}$] for the spectral density of the driving noise have been empirically determined for the employed gyro.

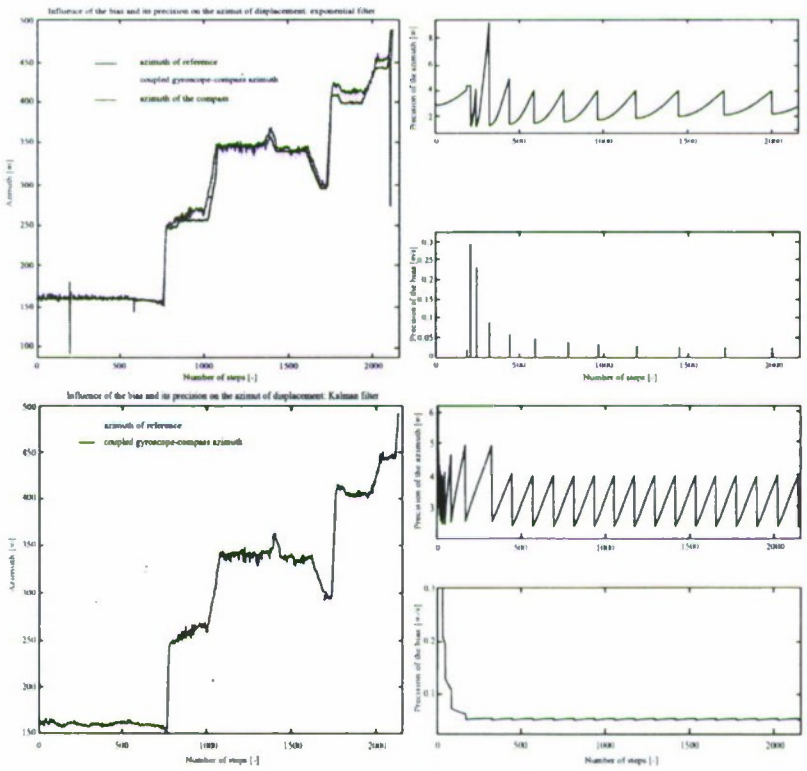

Figure 6: Update of the bias of the gyroscope using the two different approaches and their consequence on the precision of the gyroscope azimuth. In the Kalman filter, the frequent updates of the beginning are cause by the hypothesis of an unknown bias (precision of 100°). The threshold for the updates is set to 4°.

The Figure 4 presents the two different method of integration with their precision. The initial value of 3° takes into account that residual magnetic disturbances might have not been identified during the bias determination. This value is empirical and reflects the precision one can expect in such application. The differences between the two approaches are very small and, in the majority of the tests done, inferior to the precision of the compass. The main distinction is in the precision of the given gyroscopic azimuth. In the exponential filtering, the precision becomes weaker from one update to the other, cumulating the errors of the previous bias that are maintained present thanks to the factor α. The opposite is observed with the Kalman filter where the gain matrix tends to become smaller and smaller and therefore to trust the model. The error of prediction must be artificially augmented in order to avoid any convergence of the

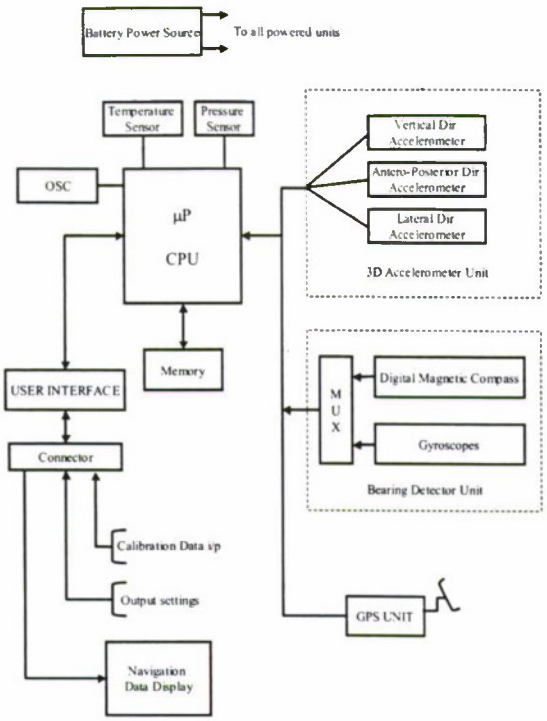

Figure 7: Schematic representation of the Pedestrian Navigation System. The different sensors work in parallel at a frequency that can be individually chosen in function of the specificity of the application.

gain to zero, which consequence would result in ignoring new measurement. Even if the exponential approach doesn't converge, this fits the reality better than the Kalman filter. As the magnetic field can present undetectable disturbances, it is desirable that the imprecision of the gyroscope azimuth also augments with time, when the bias updates are done using the compass data only. The presence of satellite signals will improve the precision of the updates, as it is the case with the Kalman filter.

4. Reliability concept in pedestrian navigation

The concept of reliability used mainly to predict industrial process failures has been introduced in geomatics by Baarda (1968) and can be adapted to the particularity of pedestrian navigation. The integration of different measurements sources coming from several independent sensors allows, because of the redundancy of the information, the detection of a bad calibration as well as mistakes and systematic errors in the models. The developed Pedestrian Navigation System (PNS) offers the following redundancies: 3 azimuths (compass - gyroscope - GPS), 2 altitudes (barometer - GPS), 2 travelled distances (dead reckoning - GPS). The Figure 7 presents the structure of the PNS.

The indicators should take into account the degradation of precision (spatial or temporal) dependent of the chosen technologies. Accuracy and reliability are theoretically well distinct notions, and the evolution of the first one should normally not affect the second. If this is true for well-defined models, generally fixed and constant in time, such affirmation in the context of walk, is less categorical. Situations might occur such that the precision of the compass is so bad in magnetically disturbed areas, that its reliability can be call in question. A similar conclusion can be deduced for a gyroscope azimuth after a long time without bias control. Two indicators will be set to reflect the situation in which the azimuths and positions are computed.

1. The first indicator expresses the part of redundancy of the information. This represents the degree of certitude of one observation against the presence of an error. This notion is called the **internal reliability** of the system. For the azimuth, compass, gyroscope (and GPS), provide orientations that control one-another. The considered values are shown in Table 1. The given percentages take into account the different filtering effectuated. For example, even if the gyroscopic azimuth cannot be processed because of a too long time without bias update, the information of the angular velocity helps to validate or invalidate the magnetic azimuth. A similar argument can be applied to the other measurements.

Value	Situation of computation of the azimuth
0 %	Magnetic disturbances / Long period without any gyroscope bias update
25 %	Magnetic disturbances / Recent bias update of the gyroscope
50 %	Area magnetically stable / Long period without any gyroscope bias update
75 %	Area magnetically stable / Recent bias update of the gyroscope
+25 %	Add to each case if a GPS azimuth was computed

Table 1: Empirical weighting of the different scenarios allowing the computation of the azimuth of walk

2. The second indicator is closer to its geodetic use. It presents the effect on the coordinates of the biggest non-detected error on the different observations. The term of **external reliability** is commonly used. In the given application, only the indicator relative to the azimuth of walk presents a real meaning. As magnetic disturbances are detected using an empirical defined threshold, every disturbance inferior to this value will induce an error.

The latter will propagate on the East-North components according to the azimuth of walk as presented in Figure 8. An impreeision on the bias will also eause eumulated errors that are diffieult to identify on a short time period.

It is important to mention that in pure dead reekoning mode, one single non-deteeted disturbed area eould have important consequences on the following positions. Without any absolute update, the error will tend to remain eonstant on the trajeetory. The measured path after the disturbanees is parallel to the true one at a distanee that is proportional to the number of steps done during the disturbed period. The use of satellite signals allows bounding the influenee of sueh error. The time interval between two GPS positions will therefore influenee the external reliability of the system.

Indicator of reliability	Value	Situation of computation of the position
	0 %	No satellite available
Altimetry: 50 %	50 %	Altitude measured by barometer, ealibrated on a known point
	50 %	Calibrated step model
Planimetry: 50 %	50 %	Compass valid but no reeent update of the gyroseope bias

Table 2: Typical solution provided by the Pedestrian Navigation System in Dead Reckoning mode. The notion of time will be present for the altimetry. If no update can take place within a given time frame, the possible atmospheric variation will not permit to give a reliable absolute altitude. The value will therefore fall to 0.

The use of thesc two indicators is mainly already present inside the algorithms of navigation with thc use of numerous plausibility tests. An indieator is however eomputed with the eumuli of the pereentages aeeording to a conditional logic. Its value doesn't have any precise mathematical meaning but allows intuitively to assess the quality of the computed coordinates. As it is eommon in geodesy, planimetry and altimetry are separated. Table 2 shows a typical solution provided by the PNS during a dead reckoning period.

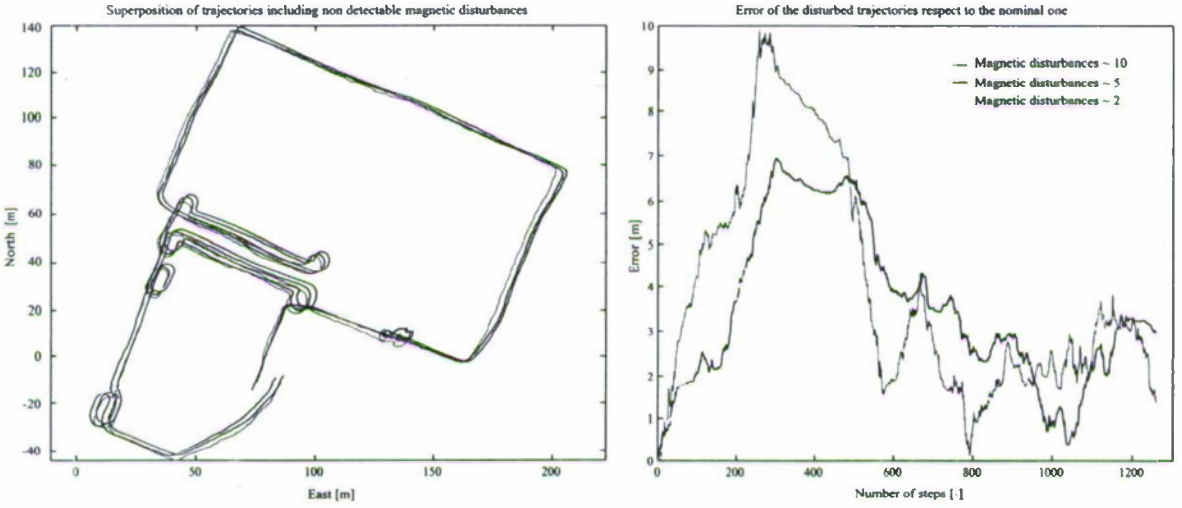

Figure 8: Representation of the notion of internal reliability. As the thresholds are empirically fixed for the determination of a magnetic disturbanee, the non-detected disturbances will induee errors in positions. Disturbanees from 2° to 10° have been introduced in thc measurements. Superior disturbances are detected. It is of interest to mention that in general, the considered error in position is inferior to the preeision of the GPS solution of navigation.

Conclusion

This paper showed the achievable accuracy and reliability of the factual, stride-dependant, approach that replaces the temporal, double integration, evolution. The development of a Pedestrian Navigation System based mainly on a digital magnetic compass was tested against the 3D inertial navigation. In non-magnetically disturbed areas, the results are elose to each other and errors in position are below the 10 meters. In order to improve the reliability of the system, the addition of a gyroscope helps bridging the gaps when the compass is strongly disturbed. No operational ZUPTs constrain is required by the approach. The analytic error propagation of the gyroscope bias and its consequence on the azimuth determination were described. Finally, two indicators on reliability are presented, providing information on the quality of the position that is given.

The numerous tests effectuated proved the validity of the concept for a navigation system that aims to offer reliable several-meter accuracy position in all kinds of environments.

Acknowledgments

Special thanks to Mr Jack Runyon from Locametric LLC, Virginia, for the testing and data collection as well as to Dr. Silvio Gnepf and Mr. Josephus van Seeters of Leica Vectronix for their advices.

This research is performed under a collaboration scheme financed jointly by the Swiss Government and Leica Geosystems AG.

References

Baarda, W (1968) *A testing procedure for use in geodetic networks.* Publication on geodesy, Netherlands geodetic commission, Delft.

Caruso, M. J. (1997) *Applications of magnetoresistive sensors in navigation systems*, Sensor and Actuators, SAE SP-1220:15-21

Denne, W (1979) *Magnetic Compass Deviation and Correction*. Brown, Son & Fergusson Ltd, Scotland

Gabaglio, V (2002) *GPS/INS System Integration for Low-Dynamic Application.* PhD thesis, Swiss Federal Institute of Technology, Lausanne (EPFL)

Gelb, A (1971) *Applied Optimal Estimation.* MIT Press, Cambridge, Massachusetts.

Ladetto, Q (2002) *Capteurs et algorithmes pour la localisation autonome en mode pédestre.* PhD thesis, Swiss Federal Institute of Technology, Lausanne (EPFL), in press.

Ladetto, Q, **Gabaglio**, V, **Merminod**, B (2001) Combining Gyroscopes, Magnetic Compass and GPS for Pedestrian Navigation, Proc. Int. Symposium on Kinematic Systems in Geodesy, Geomatics and Navigation (KIS 2001), pp 205-213.

Moix, S. (2002) *Améliorer la navigation pédestre en integrant un gyroscope et une boussole*, Msc thesis, Swiss Federal Institute of Technology, Lausanne (EPFL)

THE MARINE SIMULATION SYSTEM PANORAMA TS

A.A. Koshevoy*, A.V.Maranov, A.S. Grib, V.V.Ivanov, I.E.Nagirnaya**
Central Scientific & Research Institute Navigation and Control,
5, Dimitrova St., 03006, Kiev, Ukraine. E-mail:office@kvantn.com.ua

Abstract

Key words: simulator, radar/ARPA/ECDIS/navigation simulation, algorithms, accuracy

During 30 years the "KVANT-NAVIGATION" company works in sphere of navigation. In times of USSR existence we worked out one of the most well-known navigation system "Briz E", which then was manufactured in Bulgaria and was installed on hundreds of ships. Also we worked out a lot of navigation systems of military use.

To the present day our company has expended the assortment of production offered on the market of Russia and Ukraine. Among our production there are as systems of radar navigation, so systems of satellite electronic cartography, hydrographer automated working places, dispatching systems of transport control, systems of exact agriculture and one of the youngest and most prospective directions - working out of simulation system (further called "traines"..

The experience received in elaboration of working stations and the practical knowledge from testing in real conditions let us as complexly as possible to estimate problems confronting other researchers. Working out trainers we don't use modules of other researchers. Mathematic models of ships are calculated by our engineers, which guarantee high stability and exactness of real condition imitation.

The marine simulation system "Panorama TS" offered on the market in three versions (single-user, multi-user and net version; each of them may be with hardware (pro) or only software (box)) are live example of aforesaid. In the present time we carry on negotiations with BSS Company about creation of joint trainer navigation radar and the system of automatic radar lay plus GMBSS.

Net version of trainer is one of the most adequate from the standpoint of real situation imitation, and one of the most useful from the teacher point of view.

Using this version every working place of student (WPS) is linked on net by means of protocol TSP/IP with other WPSs and a working place of instructor (WPI). With such a topology an imitated ship driven by student is allotted to every WPS and on WPI an instructor has a possibility to interfere actively in the process of studying inputting additional parameters (to change a stream, to give SOS and so on). The system of electronic cartography working with electronic navigation maps in format S-57 is also installed in the trainers.

Due to the flexibility of the engine net exchange, trainers of different purpose can be created on its basis. Now the working out of trainers for railroad and air transport is carrying on.

The principle of net engine work is in the following: "Master engine" is created on WPI and with connecting to a server every WPS clones "Master engine" on its terminal. Then every event from every WPS appears in the server and is analyzed by it. If any event causes changes in "Master engine", a signal of synchronization comes and all WPS correct its clones according to changes in "Master engine".

This technology allows us to reduce to minimum the quantity of transmitted information in the net. 300 bit/sec speed is sufficient for the work. As the system is not demanding to net recourses and not limited in the quantity of working places and exchange is carried out by means of TCP/IP protocol, so this system can be used for trainer work through the Internet. There is a possibility to carry out distant studying and certification directly on a ship with the help of accurate registration system. The work of one instructor in many trainer centers situated in different places of the world at once is also possible!

Introduction

The research institute "KVANT-NAVIGATION" is known as the developer of program for a military-industrial complex and transport industry, which include ARPA, the systems of electronic cartography, dispatching systems of transport control, and as trainers. The trainers "Panorama TS" pools in itself group of training simulators for preparing navigators in such complete sets as single-user, multi-user and net version.

The net version of the trainer is most professional from all kind of trainers. It can include as image of running cabin with a complete set of equipment working in an imitative mode (the interaction of several running cabins is possible), up to trainer PJIC ARPA which cooperate on the network of any topology down to internet.

---

* D.Nat.Sci., Professor, Director.
** D.Sc., Leading Research Scientist.

The trainer can be delivered as software version installed on any computer which satisfy the requirements and as hardware version. The trainer allows executing the following tasks: RADAR, ARPA, ECDIS using; route planning; definition of position and navigational tasks solution, etc. There is a possibility to carry out distant observation, introducing amendments and sending off of the helps through the internet by the instructor.

The multi-user version can include in all components of the net version and differs by absence of network interaction between every working place of student. There is using the simulators on the basis of an artificial intelligence as nearby ships. There is a possibility to carry out distant observation, introducing amendments by the instructor too.

The single-user version is local variant of the trainer "Panorama TS". It can be used (individually) on the personal computer for self-preparation or the running cabin can be completed by without handle of the instructor. This version is such as net version, but despite of this it is available for training centers of any scale.

CHARACTERISTICS radar/ARPA trainer.

1. Problems decided radar/ARPA trainer.

Radar/ARPA trainer provides the decision of the following problems(tasks):

- Display of the combined radar-tracking, navigating and stylized cartographical information to the screen of television type;
- Manual or automatic input on support up to 120 objects;
- Automatic support and definition of parameters on 120 objects;
- Autodetection of radar-tracking objects in a zone of autocapture;
- Input both semi-automatic support and definition of parameters on 10 objects;
- Definition of dangerous objects by the given criteria and distribution of the danger warning;
- Detection of maneuvering objects;
- Imitation of maneuver and distribution of recommendations for a safe divergence;
- The control of courts on anchor parking;
- Calculation of routing coordinates;
- The control of courts on a waterway;
- Calculation of parameters for an output(exit) of a vessel in the given point;
- The control for buoy (driff buoy);
- Input of additional graphic objects for the task of security zones and zones of autocapture;
- Registration and reproduction of the secondary radar-tracking information.

2. Structure radar/ARPA trainer.

Into structure radar/ARPA trainer enter:

- The central processor (CENTRAL PROCESSING UNIT);
- The controller of initial and secondary processing;
- The device of interface with radar;
- Analog-digital converter (A/D);
- The device of coding of video signal (DC);
- The shaper of signals;
- The monitor;
- The keyboard;
- Unit of imposing;
- The converter.

The converter of the signals which have been built - in the system block of the computer, carries out digital processing radar-tracking signals in real time. Multilevel coding of amplitude of video signal and preliminary digital processing for display to the indicator of the videomonitor are carried out with the device of quantization. Processing of signals radar with the purpose of an estimation of parameters of a trajectory of accompanied objects is made by the microcontroller connected to the device of transformation of a consecutive code of video signal in parallel through trunk RS - 104.

The device consists of the amplifier of video signal, the shaper of a signal "Beginning readout of range ", the counter of a course corner of the aerial, the counter of the address of the RAM of video signal, the counter of the address of the RAM of code APU, quantizer, circuits of management of record of video signal, the circuit of management of reading of codes APY, the register of video signal, the register of code APU, the multiplexer.

The device works as follows. Signals "ISR" or "Null range distance" act on an input(entrance) of the device, allowing(resolving) record of video signal and reading of codes of pulse APU.

Video signal from an input(entrance) of the device acts in the amplifier of video signal or, across the amplifier, on an input(entrance) quantizer. binary -quantizer video signal with quantizer (comparator) acts in the register of video signal and the circuit of management of record corresponds in the RAM of video signal to the address, generated by the counter of the address of the RAM. The code which has been read out from a cell of RAM ARU with the address, the generated counter of the address of the RAM of code APU, enters the name in the register of code APU.

The register of code APU is connected to the shaper of pulses APU which makes distribution of pulses of amplification(strengthening) sling supports.

Record of codes APU and reading binary -quantizer video signal is carried out by the controller of the device on trunk RS-104 or PC on trunk ISA on a signal of interruption which sanction of distribution is made by the program.

The device carries out the following functions:

1. Digitization and storing binary -quantizer video signal in a range of support, with the subsequent (at input) mathematical slinging his(its) areas the program of the microcontroller
2. Formation of amplitude and range of pulses APU in стробе supports.
3. Program management of time of an exchange with the buffer RAM of the device.
4. Connection of the device to two processor modules on standard trunks ISA, PC-104 serially, that allows to process and display video signal by one or two processors.

The device is executed on a payment of expansion in standard PC with application of element base for the expanded temperature range.

3 Block diagram radar/ARPA trainer.

Radar/ARPA consists of the central processor, the controller of initial and secondary processing radar a signal, the device of digital coding of radar signal (DC) of the device of interface with radar (MOUSTACHE), the converter of an analog signal in digital code (A/D), the shaper of signals: "0" KUa, KUa, Vc, code F of recurrence, interruption, and as signals of management.

Into structure radar/ARPA trainer enter as the monitor, the keyboard, unit of imposing and the converter for transformation of interface RS-232 in RS-422.

On input(entrance) ARPA act from radar video signal, a pulse of start radar, a pulse "0" a course corner of the aerial, a pulse code of a corner of turn of aerial (KUa) and as a pulse code of speed of the vessel from a log and a digital code of a rate of the vessel, acting from a navigating complex or a gyrocompass on consecutive interface RS-422 under report NMEA 0183. From output(exit) ARPA in a navigating complex and to other consumers parameters of the accompanied purposes are given out.

Electric parameters, frequency characteristics of entrance signals are coordinated with concrete radar with the help of the appropriate adjustment of the device of interface with radar and parameters of the software.

In case of need interfaces to additional devices on other channels (analog or other) the opportunity of installation of additional devices of interface, controllers in слоты expansions of trunks ISA, PCI the central processor is stipulated. Thus development of the program of the driver of the appropriate device and binding of software ARPA to the concrete project is required.

As the central processor in ARPA the processor of industrial execution(performance) such as ROCKY with clock frequency up to 800 МГц is used. The processor has trunks ISA, PCI, standard liaison channels with the keyboard and mouse interface RS-232C, the parallel interface. At use in onboard conditions of the program may be loaded in solid-state memory FLASH - the store.

The Processor has the built - in graphic controller which provides interface to monitors to the sanction 1280x1024 pixil.

Structurally the processor is intended for installation in a passive unifying payment.

The Controller ON / IN is realized on the built in industrial processor such as 486-DX2 or 586. The processor has FLASH-the store, trunk PS-104 (16-ти digit), standard interface RS-232C and the parallel interface.

The Device of coding (DC) has two buffer two-port RAMS through which the exchange with the controller is made.

From the device of interface with radar on input(entrance) DC signals act: video signal, Impulse "0" D, Imp. KUa, Imp, "0" KUa.

Video signal acts on an input(entrance) of the converter of an analog pressure(voltage) in binary coded signal (CVC) which further acts on an input(entrance) of shifting register: which makes record of a binary code in sling, formed by the circuit of management, and then through the buffer register enters the name in DOZE BC.

The eode of management BC generated by the eontroller in sling acts through DOZE APU on an input(entrance) of the converter of a code in a pressure(voltage) from which output(exit) a pulse of automatic adjustment of amplification(strengthening) in sling moves or on an input(entrance) of reception device radar, or if in radar such input(cntrance) is not stipulated, is used for regulation of a threshold of quantization DC.
Counter KUa serves for coding a corner of turn of aerial radar which after input in the controller is shared with a code of a rate of the vessel for calculation of parameters slings and parameters of accompanied objects.

For maintenanee of the eontrol of system and a mode "Trainer" in DC there is a shaper of the eontrol purpose.

The device of interfaee with radar serves for reception and the coordination of signals with radar and their translations in DC and the Shaper of signals.

As the converter analog a signal in digital code (A/D) it is used high-specd A/D PCI-9810. Frequency of coding BC acts on input(entrance) A/D from the external generator. The video signal aeting with matching unit of the/adder, will be transformed in A/D to 1024 coded readout whieh through trunk PCI on the channel of direct access act in the central processing UNIT for processing, transformations and the subsequent display to screen ARPA.

The shaper of signals serves for binding video signal with radar to code KUa, and as formations of frequency of recurrence of a pulse of start radar, formations of a signal "0" to range (the detained pulse of start radar) and buffering of pulses of a code of speed of the vessel.

The shaper of signals is interfaeed(integrated) to the central processing UNIT on trunk ISA.

The eode of frequency of recurrence of a pulse of start radar serves for the coordination of scales established in radar with ARPA.

The central processing UNIT is interfaced(integrated) to the controller ON / IN with the help of channel RS-232C and the parallel channel.

The controller receives from the eentral processing UNIT of coordinate of the purposes taken on support by the operator manually and modes of operation of system.

In the central processing UNIT codes of parameters of the accompanied purposes and a code of a rate arc transferred.

The monitor serves for display radar of signals, graphic symbols of the purposes, the stylized cartographical information, dialogue messages and thc alphanumeric information of the purposes.

The keyboard provides dialogue of the operator from CENTRAL PROCESSING UNITS on the standard interface.

The unit of imposing provides management of a marker at manual eapture on support, identification of parameters and at the decision of other dialogue problems(tasks).

The converter is necessary for transformation of the standard interfaee of controller RS-232C to interface RS-422A.

The process engineering which was used at creation of the trainer

The process engineering which was used at creation of the trainer allows collecting from separate units the necessary complete set of the trainer, and each unit ean be delivered both with a hardware complex, and without it. The training system is developed for the operating system such as the Windows NT but it working optimally under handle of the Windows 2000 and other operating systems except the Windows 3.X.

The proeess engineering of network exehange developed by us in 2001 is a basis of trainer. It permits to link any quantity of objects in the uniform network. In this scheme the exchange through the network is minimum and for transmission of large stream of information enough channel for 2400 kb/see. It makes possible integrations of the trainer and internet, which gives a number of features which were not applied by any of the produeers of the trainers.

As is known most challenge at creation of anyone trainer is the creation of an imitated situation which is maximum approximate to real. It is very diffieult to ereate an artificial intelligenee which will operate by adjacent ships so that it looks as if real crew operating by. For reaching maximum effect the network versions of the trainer are ereated, where the vessel is fixed to everyone trained. But for a eonstruction of training center with several workplaces many finaneial expenditures are neeessary, but unfortunately majority of time an equipment will be simply to stand that not favorable from an eeonomie point of view. At use ours trainer is not present neeessity in one training eenter to create at onee some workplaees; it is enough to construct one and to eonneet it to the internet. Thus, it is neeessary only to synehronize time of studies in other training center arranged by ours trainer, that it is possible to make on ours site in internet, and to carry out share studying in geographically separate points, in various training centers but on one water area working through, for example, the rule of safe discrepancy. For today two training centers are equipped by our trainers in Ukraine. One of them is the Kiev State Academy Driving by Water Carrier, and in nearest future some more systems will be installed.

The complete set of simulator

The complete set of each simulator includes the editor of situations which allows to create any variety of situations in the given water area. After the situation was created it will be send to a database, which sent on a workplace of a student. During occupations on a simulator the instructor on the workplace visually chooses a situation on subjects of occupation or a level of the student, and confirms his choice then code number of a situation and a name of situations base is transferred to a workplace of the student. The situation is loading on the workplace of the instructor and if the situation assumes presence of other workplaces as simulators in not an artificial intelligence the attribute of readiness is transferred to a server (the workplace of the instructor), but only if the student has passed procedure of registration. If the situation is designed for use as simulators an artificial intelligence that the situation at once begins after procedure of registration. In the net version of the situation on the workplace of the instructor the status of all workplaces trained is displayed *Is joined, ready, Is not ready*. If the workplace of the student is presence in a physical network then the status *Is joined* will be on the workplace of the instructor and until the student will not pass procedure of registration it will be with a status *Not ready*. The instructor makes a decision on start of improvement of a situation. After command on start was sending by the instructor it bypasses all workplaces with an attribute *Is ready* and improvement of a situation begins. There is a hot connection of additional workplaces is probably during improvement of a situation (before students observe not connected workplaces as for example court worth on road). In the editor of situations it is set default characteristics of the simulator such as: type of a ship, the geographic location on an electronic navigation map, initial a rate speed. In one minute after start of a situation student may change parameters of movement of his ship simulator. The instructor during improvement of a situation may observe of all event in the given group trained, and may observe actions of the separately taken student and also he can give the help through the special interface of an exchange of text messages.

Some features, which are developer by us for the working navigations systems, were applied in the trainer. One of them is the PLAYING of MANEUVER, which differs from similar systems of other manufactures. There is possible to see not only final point in which our ship will get at speed or course changes, but also dynamics of our ship and other ships movement in our system. Depending on quantity of degrees on which turn for one iteration (usually it is 5 degrees) is made, the time and extrapolation of our vessel are calculated depending on internal characteristics of the vessel. Extrapolation of the vessel is made with taking into account the curvature of an arch dependent on the given laying of a rudder and extrapolation of the objects are made on vectors of true movement.

References

1. **Зурабов Ю.Г.** и др. Судовые средства автоматизации предупреждения столкновений судов. М. :Транспорт,1985.
2. **Удалов В.И.** и др. Управление крупнотоннажными судами М. «Транспорт,1986.
3. **Graham Danton.** The theory and practice of seamanship. London. 1996, -522p.
4. **Nathaniel Bowditch.** The Ameriean practieal navigator (An epitome of navigation). 1995. –481p.

APPLICATION OF A STABILIZED VEHICLE MODEL BASED NAVIGATION FILTER ON THE AUTONOMOUS UNDERWATER VEHICLE "DEEPC"

Armin U. Schmiegel*
STN ATLAS Elektronik GmbH, Sebaldsbrücker Heerstr. 235,
D-28305 Bremen, Germany, E-mail: schmiegel.a@stn-atlas.de

Abstract

Key words: model based navigation, inertial navigation, sensor fusion, Kalman filter

Accurate long-term navigation is one of the most crucial aspects of autonomous underwater vehicles (AUVs), especially if the AUV is being used in unexplored and hence unknown regions. To achieve the necessary data accuracy, the navigation system must have a performance comparable to that found in conventional submarines. Using an AUV for seabed mapping, the customer requirements for position data accuracy correspond to less than 100 m during the entire mission.

To meet these requirements for the German autonomous underwater vehicle "DeepC", STN ATLAS decided to use a model based Kalman filter. A filter design has been developed which permits accurate navigation even if the dynamics of the vehicle model does not coincide with the real dynamics on larger scales. This filter improves the overall navigation performance and is also robust against sensor failures. This presentation describes this stabilized model based Kalman filter, which is part of the navigation system.

Introduction

Most navigation systems used for autonomous underwater vehicles (AUVs) consist of an inertial measurement unit, a Doppler velocity log (DVL) and a CTD sensor (conductivity, temperature, depth). A Kalman filter estimates position, velocity, orientation and turn rates of the vehicle by fusing the sensor data [1-3] and performing dead reckoning navigation.

Besides the depth information, which is measured by the CTD sensor, no further position measurements are available. Therefore, underwater navigation has to deal with a growing position error, which can only be corrected at the surface, where GPS position fixes can be made. For some missions, additional position fixes are possible by the use of long base line (LBL) or ultra short base line (USBL) methods, where acoustic beacons at known positions transmit signals [3]. Other authors support the system with known landmarks or use measured features [4-6]. Unfortunately, LBL and USBL cannot always be applied at great depths and the latter methods can only be employed if the vehicle is diving in known regions.

In addition, the navigation system has to be highly reliable. In the case of a sensor failure, the position error should not diverge. Furthermore, it should be highly adaptable for different sensor ensembles.

To meet both requirements, STN ATLAS decided to equip the German "DeepC", an AUV developed by a consortium of eight companies and universities in which STN ATLAS is participating, with a model based navigation filter.

The integration of a vehicle model into the predictor of a Kalman filter has several advantages: for instance, such a filter is quite fault-tolerant, since all navigation sensors are used within the corrector. Therefore, malfunctioning sensors can easily be disregarded. Such a filter is also less sensitive to sensor drift and it uses all the available knowledge of the problem.

Unfortunately, this Kalman filter is sensitive to mismodeling, i.e. if the vehicle model does not match the real dynamics, the performance is suboptimal or even disastrous [7]. Hence, an accurate vehicle model is needed or the filter design has to take account of possible mismodeling effects. We followed the latter strategy and developed a vehicle model based Kalman filter which is more stable against mismodeling effects. This filter consists of two Kalman filters. The first estimates position, orientation, velocity and turn rate of the vehicle, using the vehicle model for prediction and a subset of the available sensor data for correction. The second one estimates the errors of these quantities: its predictor uses an error model derived from the vehicle model of the state filter. The corrector uses the remaining sensor data. The estimates of this filter are used to modify the estimates of the previous filter.

This filter is an additional component of the navigation system of the autonomous underwater vehicle "DeepC". "DeepC" will have a maximum mission time of 60 h at 4 kts and the capability of diving down to 4000 m. In addition, a postprocessing unit uses the historic sensor data to improve the data accuracy.

This presentation focuses on the stabilized vehicle model based Kalman filter. The presentation starts with a brief description of the vehicle and the architecture of the navigation system. In chapter 2, the stabilized model based Kalman filter is described. In chapter 3, the performance of this filter is indicated.

---

*PhD Scientist.

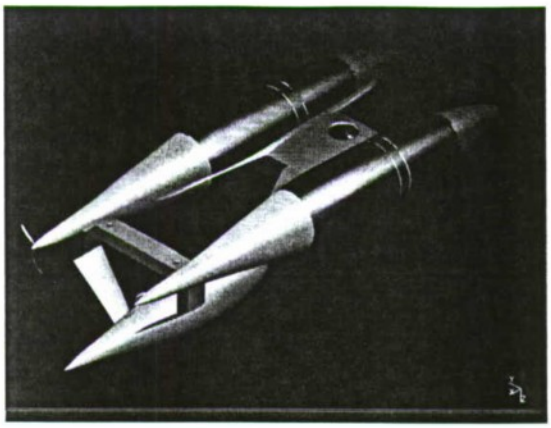

- Length: 5.8 m
- Width: 2.25 m
- Height: 1.6 m
- Speed: max.6 kts
- Maximum depth: 4000 m
- Operation time: 60 h (4 kts)

Fig. 1. Sketch of DeepC. The AUV consists of three bodies. The upper bodies contain the propulsion, energy and control systems. The one below contains the payload

1. The German AUV "DeepC"

The German AUV "DeepC" is being developed by a consortium of eight companies and universities, in which STN ATLAS is participating. The project is funded by the German Federal Ministry of Research and Education. Fig. 1 shows a sketch of this vehicle. It consists of three bodies. The upper two bodies contain the propulsion, energy, navigation and guidance systems. The third body situated below the other two contains the payload, for example a side-scan sonar, and can be easily exchanged.

Table 1 lists the components of the navigation sensor ensemble used in "DeepC". The vehicle is equipped with a GPS, a Doppler velocity log, a CTD sensor and an inclinometer. GPS, DVL and CTD are coupled to the inertial navigation system. The latter consists of high precision laser gyros and acceleration sensors. It combines the DVL, CTD and, if available, GPS data to calculate the position using closed integration of the dead reckoning problem.

The accuracy of this system is comparable to that of other AUV applications which use a similar sensor ensemble [1]. Unfortunately, there are still some problems. To reach a depth of about 4000 m, the vehicle has to dive for about an hour. During this transit phase, the DVL has no bottom track capability. No sensor measures the current velocity. Hence, a change in the current leads to a position error.

Table 1: List of the components of the sensor ensemble used for navigation in "DeepC"

Type of instrument	Measurand
Doppler velocity log	Bottom velocity (bottom track) Water reference velocity Temperature Tilt Heading Distance to ground (bottom track only)
CTD sensor	Conductivity Temperature Pressure
Inclinometer	Roll Pitch Heading
Inertial navigation system	Position Velocity with respect to earth Acceleration Roll / pitch / heading Turn rates
GPS	Position Velocity with respect to earth

Furthermore, in the case of a malfunction of the DVL or CTD, the error of the inertial navigation system grows very fast, presumably too fast. Therefore, STN ATLAS decided to add an extra navigation system, working complementarily to the inertial navigation system. The difference between these two systems is shown in

Fig. 2. The inertial navigation system uses the inertial sensors to calculate the predicted position, while it uses the DVL, CTD and GPS data to correct this prediction. The disadvantage of this well known technique [2] is its "asymmetric" design. Some navigational sensor data are distributed into the predictor, while other data is distributed into the corrector. In the case of a sensor malfunction, either the predictor or the corrector cannot work properly. Furthermore, no knowledge about the vehicle and its movement enters the navigational system. This knowledge helps the filter to ignore "unphysical" movements and improves long-term stability of the system. Therefore, a more "symmetrical" architecture based on a vehicle model is added (

Fig. 2). In this case, the vehicle model is used to predict the position of the vehicle, and all sensor data is used for correction.

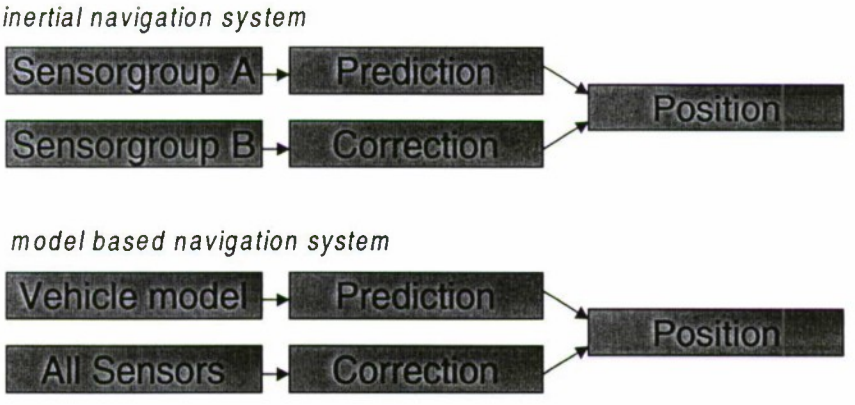

Fig. 2: Sketch of the two navigational systems used in "DeepC". The inertial navigation system uses one sensor group, i.e. the inertial sensors, to predict the position, and another sensor group, i.e. CTD, DVL and GPS, for correction of this estimation. The model based navigation system uses a vehicle model for prediction and all available sensor data for correction of this estimation

2. Model based navigation system

Complementary to the inertial navigation system, "DeepC" is equipped with a model based navigation filter. This filter consists of a vehicle model derived from first principles. Instead of a classic model based approach, we developed a modified design, which stabilizes the filter against mismodeling effects.

In this chapter, the model design and the filter design are illustrated.

2.1 Vehicle model

The original concept of Extended Kalman filtering is to predict the state of the system by means of some model and to correct this prediction via measurements [7]. This concept cannot always be followed since sometimes a good prediction of the vehicle motion is difficult to achieve.

One approach is to make a low-dynamics assumption. In this case the equation of motion consists of the integration of Newton's second law and it is assumed that neither the velocity nor the turn rate changes with time. The next step is the use of heuristic models. In this case, aspects of the whole dynamics are modeled [8]. For example, the low-dynamics assumption is modified with a heuristic model of the influence of different flap angles on the turn rate.

The consistent improvement of this idea is to come back to the original idea of Kalman filtering and use a model derived from first principles. The system state of a vehicle is described by a 12-dimensional vector (η, ν), as follows:

$$\eta = (l, \mu, h, \phi, \theta, \psi), \tag{2.1}$$

$$\nu = (u, v, w, p, q, r), \tag{2.2}$$

l, μ, h are the position in latitude, longitude and height. The orientation is determined by the Euler angles ϕ, ϑ, ψ. Changes of these quantities are described by ν within the body frame of the vehicle. The resulting equation of motion of this vehicle is as follows [9]:

$$M\dot{\nu} + C(\nu)\nu + D(\nu)\nu + g(\eta) = \tau, \tag{2.3}$$

where

M = inertia matrix (including added mass),

$C(\nu)$ = matrix of Coriolis and centripetal terms (including added mass),

$D(\nu)$ = damping matrix,

$g(\eta)$ = vector of gravitational forces and moments,

τ = vector of control inputs.

The 6x6-matrices M, C, D combine two physical aspects. They consist of terms derived from the mechanics of rigid bodies and terms approximating the hydrodynamic interactions between the body and the fluid. The former can be measured very accurately and can be derived from first principles. The latter is only an approximation of the complex hydrodynamic interactions. These values depend on both the state of the vehicle and the state of the fluid. These values are approximated by some heuristic models supported by both experimental and numerical measurements. We assume that we will have an average accuracy between 1% and 20% for the most common system and environmental states.

2.2 The stabilized model based Kalman filter (SMK)

Since the interaction between the fluid and the vehicle is very complex, it cannot be expected that such a vehicle model will coincide with the real dynamics under all environmental conditions and in all maneuvers. Hence, standard model based Kalman filters are expected to give rather poor performances.

Because the number of different system and environmental states is rather high, filter bank techniques [10-11], where for each state a different Kalman filter is working, cannot be applied. Similar difficulties arise if one uses H_∞-filters[12] or adds unknown parameters into the Kalman filter [7], since the number of parameters is also very high.

Another strategy would be the use of varying filter coefficients, i.e. under conditions in which the model and reality coincide the model is given a higher statistical weighting. Unfortunately, this does not improve the navigational accuracy [13]. Therefore, we developed a stabilized model based Kalman filter, which is fairly robust against mismodeling effects.

Fig. 3 illustrates the stabilized model based Kalman filter (SMK) design. The SMK filter consists of two Kalman filters: one Extended Kalman filter which estimates the system state $\hat{x}$, and one Kalman filter which estimates the error of the former $\delta\hat{x}$. Since the dynamics model, which describes the motion of the vehicle, needs information about the thruster, flaps, etc., these control parameters also enter the two filters.

The measurements of the sensor ensemble are split between these two filters into z_1 and z_2 to avoid statistically dependent measurements. z_2 is used to measure the difference of the estimate $\hat{x}'$ and the real state. This difference corrects the prediction of the error δx.

The basic concept of the SMK filter is to investigate the dynamics within the state space and the dynamics in the tangent space in the vicinity of a specific state.

Consider the following system:

$$\dot{x} = f(x,t), \tag{2.4}$$

f models the dynamics of the state vector $x(t)=(\eta,\nu)$ and corresponds to the vehicle model. The dynamics within the tangent space is:

$$\delta\dot{x} = F\delta x, \tag{2.5}$$

where δx is an element of the tangent space at x and $F = \left.\frac{\partial f(x)}{\partial x}\right|_{x,t}$ corresponds to the linearization of f at x.

The dynamics of δx is

$$\delta x(t) = \sum_i \langle \delta x(t=0) | \Lambda_i \rangle e^{\lambda_i t}, \tag{2.6}$$

where λ are the eigenvalues and Λ the eigenvectors of F. $\langle \delta x(t=0) | \Lambda_i \rangle$ are the projections of the initial condition on each eigenvector. The dynamics of δx is dominated by the dynamics in the subspace of the eigenvectors with the highest eigenvalues. These eigenspaces do not change very much for small variations of f if these changes do not imply a drastic change of the topology of the phase space. Hence, if the phase space of the model f has a structure similar to that of the phase space of the real dynamics, i.e. only slight variations of some parameters exist, the dynamics within the tangent space will be fairly similar.

The equations for the Extended Kalman filter, estimating the system state, are as follows [7]:

$$\dot{x} = f(x,t) + w, \quad w \sim N(0,Q),$$
$$z = h(x,t) + u, \quad u \sim N(0,R). \tag{2.7}$$

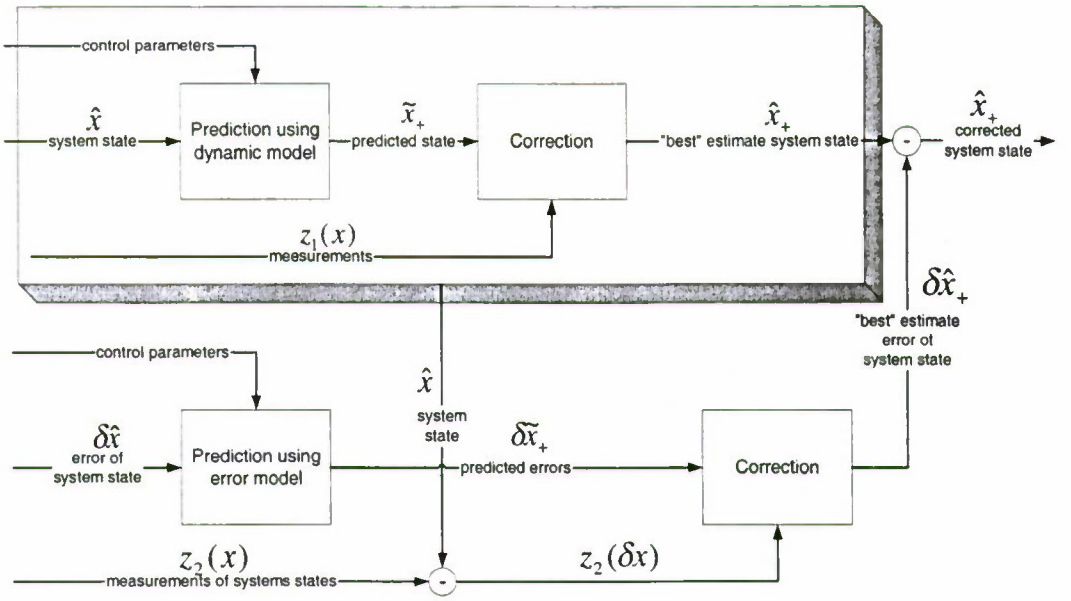

Fig. 3: Illustration of the SMK filter design. This filter consists of two Kalman filters: the boxed filter estimates the state, and the second filter estimates the error of the boxed filter. The available measurements are split between these two filters to guarantee statistically independent measurements

f models the dynamics of the state vector $x(t)$. h is the model of measurements z. w and u are the zero-mean Gaussian white system and measurement noise. The Extended Kalman filter calculates the best estimation of the state $\hat{x}$ and its covariance P:.

$$\dot{\hat{x}} = f(\hat{x}) + PH^T R^{-1}(z - h(\hat{x})),$$
$$\dot{P} = FP + PF^T + Q - PH^T R^{-1} HP, \tag{2.8}$$

with the local linearizations $F = \left.\frac{\partial f(x)}{\partial x}\right|_{x=\hat{x},t}$ and $H = \left.\frac{\partial h(x)}{\partial x}\right|_{x=\hat{x},t}$.

The model of the error state filter is as follows:

$$\delta\dot{x} = F\delta x + w_\delta, \quad w_\delta \sim N(0,Q_\delta),$$
$$z_\delta = h(\delta x) + u_\delta, \quad u_\delta \sim N(0,R_\delta). \tag{2.9}$$

The filter equations for this second filter are:

$$\dot{\delta\hat{x}} = F\delta\hat{x} + P_\delta H_\delta{}^T R_\delta{}^{-1}(z_2 - \hat{x} - H_\delta\delta\hat{x})),$$
$$\dot{P}_\delta = FP_\delta + P_\delta F^T + Q_\delta - P_\delta H_\delta{}^T R_\delta{}^{-1} H_\delta P_\delta. \tag{2.10}$$

The error state filter benefits from two effects. Firstly it benefits from the low changes of the dynamics within the tangent space, and secondly the term $(z_2 - \hat{x} - H_\delta\delta\hat{x}))$ stabilizes the filter additionally, since the measurement of the system error is a combination of mismodeling and noise measurements.

The coupling between these two filters can be highly closed. In this case one can formulate the whole problem within one pair of filter equations. However, we prefer a loose coupling. While the external output of the filter is always $\hat{x} + \delta\hat{x}$, the internal updates are only performed at intervals.

Fig. 4 illustrates these updates. In this figure the hydrodynamic coefficients had an average accuracy of about 50%. The dotted line shows the error of the state filter. The other line shows the output of the SMK filter. Between the updates the error of the state filter grows rapidly, while the error of $\hat{x} + \delta\hat{x}$ grows less fast. Note

that if the error of the state filter grows too fast, the assumption made in eq. 2.9, i.e. that $\delta\hat{x}$ is only a small deviation of the real state, no longer holds, and the error state filter might destabilize the state filter.

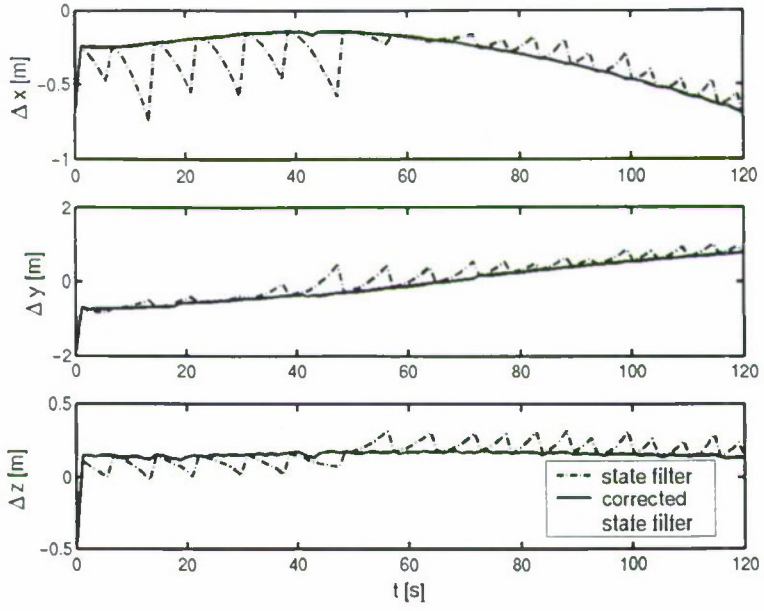

Fig. 4. Influence of the error state filter in the case of mismodeling. The dotted line corresponds to the position error of the state filter. The other line includes the corrections made by the error state filter

3. Application

In this chapter, the overall performance of the SMK will be discussed. The vehicle is equipped with the sensor ensemble described in Table 1. The vehicle dives performing a spiral turn until it reaches a depth of about 400 m. Then at t=0.4 h it starts to perform a line survey until t=3.6 h, where it spirals up to reach the surface. Hence, the first part and the last part of the mission consist of a system state presumably difficult to model, and a middle part which is quite simple to model. So far, no controlling algorithms have entered the vehicle simulation. Therefore, no corrections are made if the current forces the vehicle to leave its original track. In this simulation, the current has a random spatial and temporal modulation. Its average velocity is about 2.5 m/s.

We investigate ideal conditions. In this case, all sensor inputs except the GPS after the start of the diving phase are available; in particular, the DVL works both in water track and in bottom track, and the velocity with respect to water and earth can be measured. We assume a relative accuracy of the hydrodynamic coefficients of about 20%. During the line survey, at t=0.58 h all sensors failed for 10 seconds.

3.1. SMK filter with a vehicle model

In this section, we investigate the behavior of the SMK filter if a vehicle model is installed in the predictor. Fig. 5 shows the position error of the SMK with a vehicle model. The dotted lines are the covariance of the error. During the diving phase, the position error oscillates. This oscillation has its origin in the mismodeling of the hydrodynamic coefficients. Since these coefficients change the distribution of masses, the turn rate differs from the real one. During the line survey, only a few hydrodynamic coefficients have an influence on the vehicle behavior. Hence, the error increases quite slowly between t=0.4 h and t=3.6 h, where the vehicle starts with another spiral to reach the surface. During this line survey, the error growth is less than 0.5 m/h.

The covariance of the position error shown in Fig. 5 differs from the real value of the position error. This difference originates from the mismodeling effects. Since the measurements have no influence on the covariance of the error filter and the state filter, the only compensation being performed originates from the robustness of eigenvectors and eigenvalues within the tangent space. This implies that during the spiral dive of the vehicle the evolution of the covariance did not follow up the evolution of the true covariance, but during the line survey, where vehicle model dynamics and real dynamics coincide quite well, the covariance of the filter follows up the true values.

During the phase when all sensors fail, the covariance and also the error make a single jump. Without the support of some sensors, the mismodeling cannot be compensated, and therefore the error grows rapidly. If the

hydrodynamic coefficients correspond to the real values, this effect is less significant. In Fig. 6 the performance of the SMK filter is shown, with the hydrodynamic coefficients being equal to the real values. In this case, the covariance follows the observed errors rather more and the jump is less significant. However, since the current has not been modeled accurately, the performance is not perfect. There is still a position error of about 0.25 m/h.

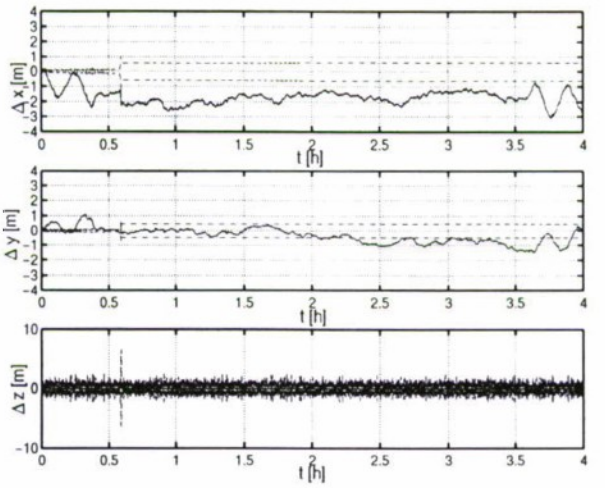

Fig. 5. Performance of the SMK with vehicle model. The average accuracy of the hydrodynamic coefficients is about 20%. The sensor ensemble is working under ideal conditions, i.e. the DVL is working in water track and bottom track mode. At t=0.58 h, all sensors fail for 10 seconds

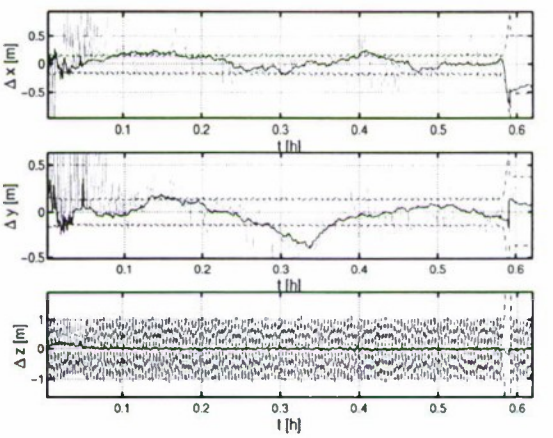

Fig. 6. Performance of the SMK filter with a "perfect" vehicle model. In this case the hydrodynamic coefficients correspond to the real values. The gray lines are the errors of the state filter without compensation. At t=0.58 h, all sensors fail for ten seconds

3.2. SMK filter with a low-dynamics assumption

A simple approach to improve the overall performance of the SMK filter during complex maneuvers is the complementary use of a vehicle model and a low-dynamics assumption. In the latter case it is assumed that v does not change with time. With this assumption, the filter performance does not depend on the maneuver of the vehicle. This can be seen in Fig. 7. The error growth corresponds to a random walk, i.e. the covariance increases with the square root of time. During the diving phase, the error does not oscillate, but increases to 2 m. During the sensor malfunction at t=0.58 h, the error increases more than in the model-supported case, even if the hydrodynamic coefficients are not determined accurately.

During the whole mission the error growth follows the expected behavior of a random walk with a higher diffusion rate than in the model-supported case. Hence, the performance of the SMK filter without a vehicle model is less accurate for a long-term survey than the SMK filter with a vehicle model.

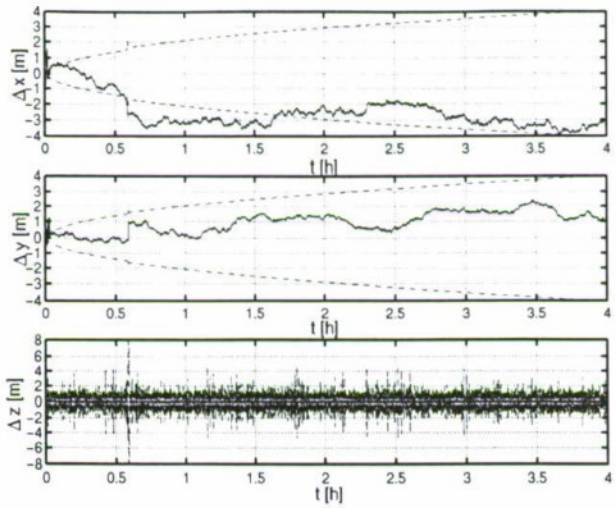

Fig. 7. Performance of the SMK filter replacing the vehicle model with a low-dynamics assumption. During the spiral dives at t<0.4 h and t>3.6 h, the error increase is less fast than in the model-supported case shown in Fig. 5

Conclusions

The design of the stabilized model based Kalman filter (SMK) has been presented. The SMK filter consists of two Extended Kalman filters, one estimating the system state and the other estimating the error of the former filter. This filter design is quite stable against mismodeling effects. The basic idea is that the dynamics within the tangent space is less sensitive against mismodeling effects than the dynamics within the phase space. Furthermore, the sensor ensemble used for the error state filter measures the deviation of the state filter, ignoring its origin.

There are still some open questions not investigated so far. For instance, the coupling between the state filter and the error state filter can be realized in different ways. It can be either closed or loose. In the former case one can represent the two filters as one. In the latter case, two additional degrees of freedom exist - the update rate and the correction method, because the correction of the state and of its covariance is not obvious.

While the stabilization of the positioning data works quite well, the behavior of the covariance is still not well stabilized, since both the covariance of the state filter and the covariance of the error state filter have the same propagator and they are not compensated by means of measurements.

This SMK filter is used to improve the navigation of the autonomous underwater vehicle "DeepC". First simulations show that, under ideal conditions, the performance of the SMK filter using a vehicle model is better than that of common inertial navigation methods. The error growth during long-term surveying is smaller than the error growth of a navigation filter without a vehicle model, and its "symmetrical" design allows quite a fault-tolerant navigation system for long-term underwater survey missions.

References

1. **M. S. Grewal, L. R. Weill, A. P. Andrews.** Global positioning systems, inertial navigation and integration. Wiley, New York, 2001.
2. **C. I. Thornton, J. L. Weston,** Strapdown inertial navigation technology. Peter Peregrinus, Stevenage, United Kingdom, 1997.
3. **M. B. Larsen,** High Performance Doppler-Inertial Navigation – Experimental Results. http://www.maridan.dk/publica/highperfdoppler.pdf
4. **H.J. S. Feder,** Simultaneous stochastic mapping and localization, PhD thesis, MIT Dept. Of Mechanical Engineering, June 1999
5. **J. J. Leonard, H. J. S. Feder,** Decoupled Stochastic Mapping, Marine Robotics Laboratory Technical Memorandum 99-1, December 1999
6. **J. J. Leonard, R. N. Carpenter, H. J. S. Feder,** Stochastic mapping using forward looking sonar data for autonomous underwater vehicles. Proceedings of International conference on field and service robotics, pages 69-74, Pittsburg, PA, August 1999
7. **A. Gelb,** Ed., Applied optimal estimation. MIT Press, Cambridge, 1974.
8. **A. Svensson, J. Holst,** Integration of navigation data, Int. Journal of Navigation, Vol. 48, No. 1, 114 – 135, 1995
9. **T. I. Fossen,** Guidance and control of ocean vehicles. Wiley, New York, 1994.
10. **C. B. Chang,** State estimator for discrete systems with switching parameters. IEEE Transactions of electronic systems, Vol. 14, No. 4, 1978.
11. **P. D. Hanlon, P. S. Maybeck.** Multiple-model adaptive estimation using residual correlation Kalman filter banks. IEEE Transactions of aerospace and electronic systems, Vol. 36, No. 2, 2000.
12. **I. R. Peterson, A. V. Savkin,** Robust Kalman Filtering for Signals and Systems with Large Uncertainties, Birkhäuser Boston, 1999
13. **A. U. Schmiegel,** A stabilized model-based Kalman filter for underwater navigation, Proceedings of the BAE SYSTEMS signal & data processing conference, 2002.

RKF BASED INTEGRATED RADIO/INS ALTIMETER *

Ch.M. Hajiyev*
Istanbul Technical University, Faculty of Aeronautics and Astronautics, Maslak,
80626 Istanbul, Turkey. E-mail: cingiz@itu.edu.tr

Abstract.

Key words: integrated navigation, robust Kalman filter, altimeter, accuracy

In this study, the integrated navigation system, consisting of radio and INS altimeters, is presented. INS and the radio altimeter have different benefits and drawbacks. The reason for integrating these two navigators is mainly to combine the best features, and eliminate the shortcomings. At the next step of the study, in case of abnormal measurements, the performance of the integrated system is examined. The optimal Kalman filter reacts with abnormal estimates to this situation as expected. To recover such a possible malfunctioning, the Robust Kalman Filter algorithm is suggested.

The core task of this study is to combine two different navigation sources with the use of Kalman filter. In fact, the main task for any kind of navigation study is to fight with the disadvantages of a navigation equipment, thus to increase correctness and reliability. By integrating Radio and INS altimeters, the objective is to benefit from the advantages of both of the systems, while eliminating the shortcomings. The presented integrated Radio-INS altimeter contains the following components:INS altimeter; Radio altimeter; Data (central) processing unit; Display (avionics users).The main source of altitude data is INS, and the radio altimeter acts as a correcting element supporting the Kalman filter for estimations. By the use of the data processing unit, radio altimeter output is transformed to the main coordinate system of the aircraft navigation and control.When this condition is set, the real altitude value at the Kalman filter input will be compensated, and the input signal will be designated as the difference between the altitude measurements of the two sources.

$$r(t) = H_I(t) - H_R(t) = (H_g(t) + \Delta H_I(t)) - (H_g(t) + \Delta H_R(t)) = \Delta H_I(t) - \Delta H_R(t). \quad (1)$$

In the expression (1), $H_I(t)$ and $H_R(t)$ are the altitude measurements of INS and radio altimeter, $\Delta H_I(t)$ and $\Delta H_R(t)$ are the measurement errors of the two sources respectively, $H_g(t)$ is the real altitude value.

In this integrated system, INS is the main error source and a severe error of measurement, increasing by time.

The mathematical models of the INS and the radio altimeter given in this study are first or second order stochastic Markov processes [1]. The model parameters are estimated by the use of the Kalman filter. The filter will give the optimum (estimated) value of the INS error $\Delta\hat{H}_I(t)$, in the condition where the standard error is minimized.

Finally, the estimated value of error $\Delta\hat{H}_I(t)$ is subtracted from the altitude measurement of the INS

$$\hat{H}_{Int} = H_I(t) - \Delta\hat{H}_I(t). \quad (2)$$

The calculated altitude value is the output of the integrated system, and it would be used for navigation and control purposes [2,3].

One of the most important improvements of the integrated radio altimeter is that, a dynamic error of measured altitude is not generated. As this is an open loop system for the measured altitude, the filter will not limit the operation rate of the navigators. For this reason, the radio-INS altimeter will have outstanding dynamic character like a stand-alone INS.Another important feature is that, an in-flight failure at the Kalman filter will not result in a whole system breakdown. In such a case, when the Kalman block at the integrated system fails, the INS measurements could be used without corrections for a certain period of operation.

---

* D.Sc., Professor.

The elements of the state veetor $X(k)$, are the measurement error eomponents, where the open form of the veetor is depicted in the following expression.

$$X^T(k) = [\Delta H_I(k) \quad \Delta W_z(k) \quad \Delta a_z(k) \quad \Delta g(k) \quad \Delta H_R(k)]. \tag{3}$$

These terms in (3) are the main four error parameters of the INS altimeter, whieh are the error of finding the altitude $\Delta H_I(k)$, vertical speed $\Delta W_z(k)$, aeceleration $\Delta a_z(k)$, and gravitational aceeleration $\Delta g(k)$; and the altitude finding error of the radio altimeter $\Delta H_R(k)$.

In ease of a failure at the measurement ehannel of a system, a robust Kalman filter is developed to eonsider, and take action against these measurement errors. Tthe following suboptimal filter algorithm is proposed [4].:

$$\hat{X}(k/k) = \hat{X}(k/k-1) + p(1/k)K(k)\Delta(k). \tag{4}$$

Here, $K(k)$ - gain matrix of the Kalman filter ,$\Delta(k)$- innovation sequence, $p(1/k)$ - *a posteriori* probability of the normal operation of the measurement ehannel at the k time step. When $p(1/k)=1$, this filter will bc exactly same with the optimal Kalman filter, but when $p(1/k)=0$, it disregards the new measurements, aeting as an extrapolator.At the abnormal measurement eonditions, when there beeomes a failure at the measurement ehannel, $p(1/k)$ will be equal to 0. This time, the Kalman filter will disregard the new measurements and consider extrapolation values for the output vector.

The results were quite satisfactory in the simulation of the integrated system equipped with the optimal Kalman filter (OKF) without abnormal measurements. In all altimeter parameters, Kalman estimations were able to eateh the model values, and this tendeney was kept until the last iteration. As the estimations are correet, the integrated system error is kept around zero through the simulation. That is one of the goals of this study, as the system error has been stabilized, thus the drifting character of the INS error has been eliminated. Abnormal measurements are implemented into 100th, 200th, 300th, and 400th iterations.The optimal Kalman filter reaets with *abnormal* estimates to this situation as it is expected.

The results of the *Robust Algorithm* simulation were almost perfect, as the system was sueeessful to get rid of the measurement failures, and it produeed aeeeptable estimations. In this case estimations did not divert from the model value, as observed in Figure 1. In this figure, the solid and dotted lines stand for INS and integrated system errors respeetively. Figure 2 is the combined graph of altitude error, model (solid line) and estimated (dotted line), in *Robust Algorithm* simulation. The success of this robust algorithm could again be concluded on this graph.

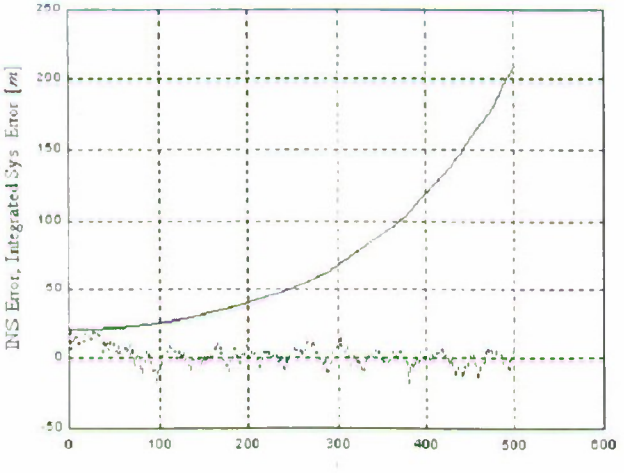

Fig. 1. INS error versus integrated system error
(Robust Algorithm was used)

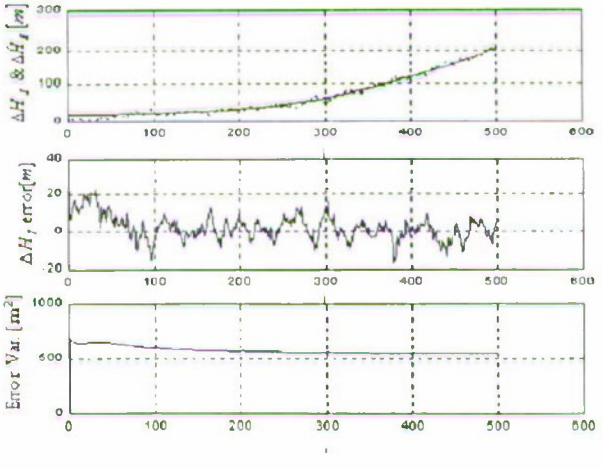

Fig. 2. Altitude error (INS)
(Robust Algorithm was used)

TV the compensation of biases of low cost angular rate and acceleration sensors is one of the most important problems, because biases of these sensors (FOG, micro-mechanical gyros and accelerometers, etc.) are essentially large. These biases not only deteriorate the accuracy of navigation, but also adversely influence the steady state accuracy of flight control system [5]. That is why development of simple and reliable fusion algorithms is one of the objectives of this paper. In accordance with modern theoretical stream flow [6] the main method for increasing Kalman filter convergence and accuracy is the factorization of covariance matrices, which we would call as finding generalized Cholesky factors. In this paper QR – factorization was used for determination of these factors [1]. In comparison with traditional algorithms [7] this one is using factorization of the matrices of smaller sizes. It is necessary to note also, that this factorization is very simple and reliable for practical implementation in inexpensive airborne computers.

In this connection the possibility of compensation of systematic sensors' errors using extended Kalman filter is discussed. This filter is similar to [8], in which 6 variables of systematic errors of rate gyros and accelerometers are included besides obligatory errors of attitude, position and velocity. Note that results of GPS+INS fusion filter simulation for systems allowing neglecting of systematic sensors' errors are presented in [1].

3. Simulation results

Results of simulation of INS/GPS integrated system are presented below for estimation of ability to compensate systematic errors using EKF. Likewise the example in [1] it is supposed, that the vehicle is moving along the circle in horizontal plane with period T=300 sec and velocity 60 m/sec. Its attitude during the process of motion is determined by the following time variations of Euler angles ψ, ϑ, φ (precession, nutation, pure rotation): $\psi = \frac{2\pi}{T}$; $\varphi = 0{,}3\sin(10\psi)$; $\vartheta = \frac{\pi}{2}$. Variances of rate gyros' and accelerometers' errors (for each axis) are equal 60 angular sec/sec and 0.01 m/sec^2 respectively. Systematic errors were generated by random number generator and were accepted as follows (with respect to x, y, z-axes): for accelerometers -0.025, -0.014, -0.02 m/sec^2 and for rate gyros
94, -56, 22 angular sec/sec. Sampling frequency is equal 20 Hz (for INS) and 0.5 Hz (for GPS). It was supposed that at the initial moment the errors of position and velocity determination are absent, attitude determination errors (values of small turns about axes x, y, z) being accepted as 2000, -2000, 2000 angular sec. Also it was supposed that GPS system provides the following r.m.s. magnitudes of velocity and position determination: 0.1 m/sec, 50 m. Simulation results are represented at Fig. a-d.

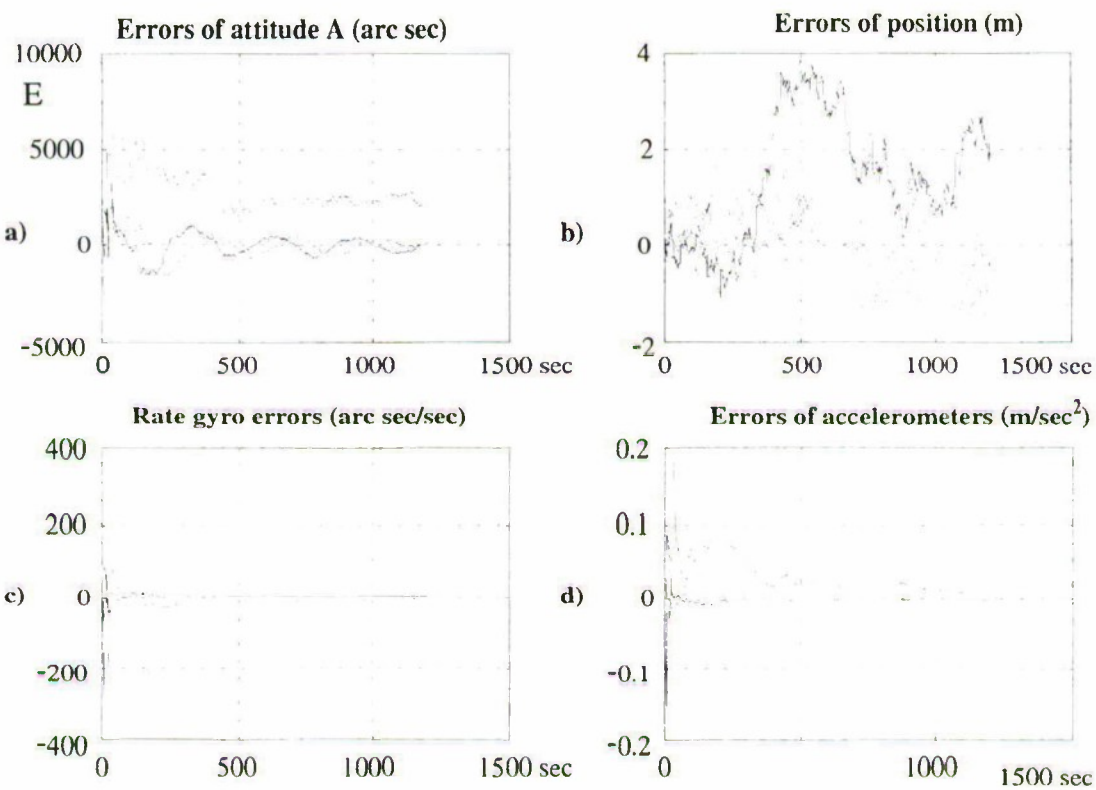

It is necessary to underline the efficiency of proposed algorithms, because it can compensate the accelerometers' errors (see Fig.1d), which (as it is stated in [8]), are practically unobservable.

Conclusions

1. Usage of elementary un-normalized quaternion (1.1) permits to acquire acceptable accuracy of navigation and simultaneously simplify rotational mechanization algorithm.
2. Usage QR-factorization of covariance matrices permits to produce simple and effective Kalman filtering procedure.
3. Simulation of the Kalman filtering fusion algorithm proves its efficiency, because it can compensate sensors' including biases of accelerometers.

References.

1. **V.B.Larin** Attitude-determination problems for a rigid body // Int. App. Mechanics.– **37**, № 7.–2001,pp 870-898.
2. **В.Н.Бранец, И.П.Шмыглевский.** Применение кватернионов в задаче ориентации твёрдого тела. –М.: Наука, 1973.-320с.
3. **Van Bronkhorst A.** Strapdown System Algorithms.// AGARD Lecture Series 95, NATO. –1978.-pp.3-1- 3-22.
4. **R.E.Phillips, G.T.Schmidt**. GPS/INS Integration. // AGARD Lectures Series 207, NATO, 1996, pp. 9-1,9-18.
5. **A.A.Tunik, H.Ryu, I.K.Ahn, C.H.Lim.** Robust Control Design Procedure for Unmanned Aerial Vehicles. Proceedings of Korea Society of Aerospace Science Annual Meeting 2000, KARI, Taejon, Korea, pp.293-299.
6. **M.S.Grewal, A.P.Andrews**. Kalman Filtering. – Prentice Hall, 1993, -381 p.
7. **M.Verhaegent, P.Van Dooren.** Numerical Aspects of Different Kalman Filter Implementation. IEEE Transactions of Automatic Control, Vol. AC-31, No.10, 1986, pp.907-917.
8. **He X., Chen Y., Iz H.B.** A Reduced-order model for integrated GPS/INS // IEEE AES Systems Magazine. – 1998. – N 3. – pp.40 – 45.

APPLICATION OF SISON-GPS FOR THE POSITIONING OF LINE OF UNDERGROUND PIPELINE*

P.K. Plotnikov*, A.I. Sinev**, V.B. Nikishin***, A.P. Ramzaev***

Saratov State Technical University, 77, Polytechnichcskaya Str., Saratov, 410054, Russia.
E-mail: pribor@star.sstu.runnet.ru, pribor@net.sstu.runnet.ru

Abstract

The method and results of experimental research of integrational navigation inertial-satellite system based on low-precision inertial sensors and GPS are described. This system as a component of the interpipeline inspection pig (IIP) was applied for underground main pipeline (MP) tracing with simultaneous defect searching and location.

Key-words: orientation, navigation, main pipeline

Introduction

Now strapdown inertial systems of orientation and navigation (SISON) are widely applied in IIP for the positioning of MP lines. In this work, the algorithms of functioning are developed and results of experimental research of SISON's operation for determining of space models of underground lines on the base of three fiber-optical gyros (FOG) type ВГ-910, three sensors of linear accelerations (SLA) type ДЛУММ-3, completing with GPS and odometer, mechanically uniting with case of moving object. During the experimental research it is found that developed algorithms of SISON's functioning allow its to estimate and successfully correct the systematic components of speed of drifts of gyroscopes this fact ensures precisions of solution of orientation and navigation's task and in total the space model of passing line even under using of gyroscopes and accelerometers with errors 50°/h and $3 \cdot 10^{-3}$g.

Non stability of speed drifts gyroscopes owing to change of temperature and other facts limit the time of work of analogical system in autonomous regime and thus leads to the necessity of organization of correction from the sources of noninertial information.

The signals of GPS are inaccessible for IIP that's why the correction is introduced for the reaper points MP in which there is the exit on the Earth's surface.

System operation

After placing of interpipe inspectional pig in camera of start up is endured in immovable state during T_b for guarantee of initial exposition of system with data processing and than pass it by inspectional plot noting under direction of board processor on flash-memory the current value of system's time and specific forces, angular velocity, passing distance, temperature inside of block of inertial sensor and also of signals of other sensors supporting MP's fault detection. After extraction of pig from receiving camera the information is rewritten in stationary computer where the processing of written signals of IIP sensors with the finding of reper points MP coordinates determined by GPS signal. For this moment the information about azimuth Ψ_m^* angle and coordinates camera of start up (m=0), and than reper points (m=1,2,... running number of reper points) is introduced in stationary computer.

At the initial stage of SISON $\left(t \in [t_0, t_0 + T_B]\right)$ exposition in camera of start up by signals FOG, the values of ω_{xi} are determined the values of zero's shift

$$\omega_{x_1}^0 = \frac{1}{T_B} \int_{t_0}^{t_B+T_B} \bar{\omega}_{xi} d\tau, \ (i = \overline{1,3}), \tag{1}$$

and then their compensation in FOG's signals with finding of angular velocity of Earth's rotation is produced. Then the values of projection of accelerations of force of gravity are calculated, and the angles of IIP [1, 2] orientation are defined by correcting Eiler equations.

During the pass of pig by reper point the capture of values of parameters of orientation and drift SISON velocities is produced. By running values of parameter's orientation $\bar{\psi}, \bar{\theta}, \bar{\gamma}$ the matrix of directional is formed

---

* Dr.Prof. chief of Chair of Instrument Making (SSTU).

** The director ITZ "Orggazdefectoskopya", Saratov.

*** Dr.-Ing. Docent Chair of Instrument Making (SSTU).

cosine $\hat{A}$ whose elements are used for update odometer's signal about increment of count of way passed for time in horizontal system of coordinates $O\zeta_1\zeta_2\zeta_3$:

$$\begin{bmatrix} \Delta\hat{\zeta}_{1k} \\ \Delta\hat{\zeta}_{1k} \\ \Delta\hat{\zeta}_{1k} \end{bmatrix} = \hat{A}^T \begin{bmatrix} x^+_{1,k} - x^+_{1,k-1} \\ 0 \\ 0 \end{bmatrix} \quad (k = 1,2,...), \tag{2}$$

where k is the number of time calculations from the moment of pig pass by next reper point. Then the calculation of values of Cartesian coordinates of pig carried out:

$$\hat{\zeta}_i = \hat{\zeta}_i^{m-1} + \sum_{k=1}^{n} \Delta\zeta_{ik}, \qquad (i = \overline{1,3}). \tag{3}$$

In moment t=tm of pass of pig by next reper point carried out the capture of values of Cartesian coordinates of pig and also of running values is done, and the values of Cartesian coordinates are read from memory of computer and of azimuth of pipeline ψ^*_m for this reper point.

On the base of receiving parameters for given reper point the calculation of difference of geodetics coordinates is carried out and determined with GPS add.

$$\Delta\zeta_i^m = \hat{\zeta}_i^m - \zeta_i^m, \qquad (i = \overline{1,3}). \tag{4}$$

Then azimuth angles are calculated by increment of coordinates between two last reper point. After that non-compensational systematic component of azimuthal drift of block FOG and systematical error of determination of pitch's angle stipulated by zero signal and by inaccuracy of exposition of length accelerometer are definited. As a result are introduced the corrections in estimation of azimuth drift of block FOG and removal of zero length SLA:

$$\omega^o_\psi[m] = \omega^o_\psi[m-1] - \Delta\omega^o_\psi, \quad W^o_{x1}[m] = W^o_{x1}[m-1] - g\,\Delta\theta. \tag{5}$$

Precision estimations of Cartesian coordinates $\hat{\zeta}_1, \hat{\zeta}_2, \hat{\zeta}_3$ of parameters orientation are derived as exit of system information.

Results

Experimental type of navigation-topographie IIP on base IPP «ДСУ-1200» in May of 2000 year was passed by main pipeline (50 km) twice: at first-with mean velocity more than 3 m/s, at second time with mean velocity more than 4 m/s. In accessible places of this part of gas-main coordinates of 9 reper points were definited with add of transducer GPS "Magniscan".

The result of positioning are presented in fig.1,where reper points are marked by cireles.

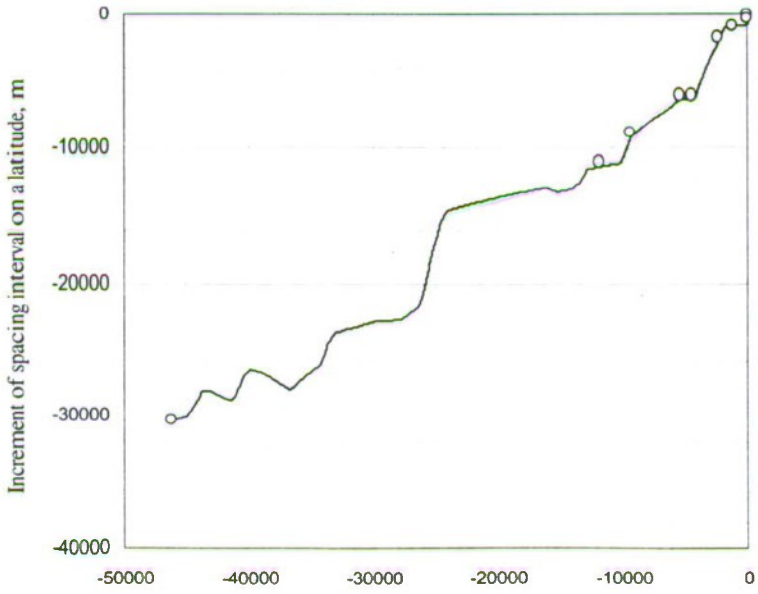

Fig.1. Phase of trajectory of main pipeline

During natural testing trials, the sensor signals in board computer were fixed with frequency 100 Hz by 12 digital ADC. In composition of odometer's channel is realized the buffer apparatus-counter of pulse of odometer with update 1 cm. So, on each tact of interrogation of odometer's canal was written the passed IPP distance from start up camera in memory of board computer. The notice of indicated signals was realized during all time of IIP moving.

Results of processing of system SISON odometer –GPS information shows that:

1) the algorithms of functioning under interrogation's frequency of sensor 100 Hz are stable, fast-operating activity, providing the acceptable precision of positioning;

2) application of non differential GPS and odometer allowed to minimize the error of positioning by comparison with application of autonomous SISON approximately two orders (variable components of angular velocities of drifts FOG 15-45^0/h, shifts of accelerometers $3 \cdot 10^{-3}$ g) in form value for 20-30% exceeding the GPS error.

References

1. **Plotnikov P.K., Andrianov V.A., Nikishin V.B., Ponomarev V.G., Ramsaev A.P.** Constructing the Algorithms of Funktioning and the Research Results of Integrated Strapdown INS of the Automobile. 4-rd Saint Petersburg International Conference on Integrated Navigation Systems., S.P., 1997, CSRI "Elektropribor", p.p. 81-87.
2. **Plotnikov P.K., Nikishin V.B., Sinev A.I., Rassudov V.M.** Determining of Spatial Models of Automobile Traces and Pipelines from the Board of Ground and Intropipeline Vehicle. Thrid Turkish-German Joint Geodetic Days. June1-4, 1999, Istanbul, 1999. p.p.561-570.

ITERATIVE MMSE METHOD FOR ISAR IMAGE RECONSTRUCTION*

Andon D. Lazarov*
Military Academy, Shoumen, No 1 K.Shkorpil Str., e-mail: lazarov@pv-ma.bg

Abstract

Key words: Inverse synthetic aperture, ISAR, LFM signal, MMSE method

This work presents an approximate iterative approach for image reconstruction from inverse synthetic aperture radar (ISAR) data. Mathematical models of the quadrature components of the ISAR signal, reflected by an object with a complex geometry, are devised. Approximation matrix functions are used to describe linear frequency modulated deterministic signals reflected by point scatterers located at nodes of the uniform grid (model) during inverse aperture synthesis. Minimum mean square error (MMSE) equations is derived. To prove the validity and correctness of the developed iterative MMSE method, numerical experiments were performed. The computational results demonstrate high-resolution images, unambiguous and convergent estimates of the point scatterers' intensities of a target from simulated ISAR data.

1. Introduction and Background

The inverse aperture synthesis is a process of registering the complex amplitude of a complex trajectory signal from a moving target. The target image described as a spatial distribution of the object reflectivity function can be retrieved from the complex trajectory signal by applying correlation and spectral techniques, high resolution joint time-frequency transforms, such as the short-time Fourier transform and bilinear transform, such as the Wigner-Ville distribution [1,2]. The traditional tools for target imaging from ISAR data are correlation and fast Fourier transform (FFT) procedures [3]. As it is known to yield high resolution the correlation and FFT procedures require large ISAR length.

In this paper new ISAR image reconstruction technique, called the iterative minimum mean square error (MMSE) method is presented. This method can cope with a small inverse synthetic aperture data set and yield a high-resolution image. This paper deals with the approximate iterative MMSE image restoration method from ISAR data, received by the rectilinear motion of the target, illuminated by linear frequency modulated transmitted (LFM) signal. The iterative procedure requires approximation functions. Thus, the main objectives of the present work are to reveal the composition of these functions in linear approximation and to develop ISAR image reconstruction method for iterative quasi-linear estimation of invariant vector geometrical parameters of the complex amplitude of the trajectory LFM ISAR signal.

2. ISAR Geometry

The object presented as an assembly of point scatterers is detected in a 2-D object's space in a form of a grid of reference points, which is described in the 2-D Cartesian coordinate system $O'XY$. The object's space is moving rectilinearly with a constant vector velocity V in the 2-D Cartesian coordinate system Oxy. Point $O'(0)$ is the location of the coordinate system $O'XY$ at the moment $p = N/2$, which corresponds to the middle of the ISAR length; point $O'(p)$ is the location of the coordinate system $O'XY$ at the pth moment.

The range vector $\mathrm{R}_{ij}(p) = \left[x_{ij}(p), y_{ij}(p)\right]^T$ from ISAR placed in the origin of the coordinate system Oxy to the ijth reference point of the object at the pth moment is defined by the vector equation [4]

$$\mathrm{R}_{ij}(p) = \mathrm{R}_{00}(0) + \mathrm{V}\left(\frac{N}{2} - p\right)T_p + \mathrm{AR}_{ij}, \qquad (1)$$

where $\mathrm{R}_{ij} = \left[X_{ij}, Y_{ij}\right]^T$ is the geometric distance vector of the ijth reference point in coordinate system $O'XY$; $\mathrm{V} = \left[V_x, V_y\right]^T$ is the vector velocity of the object; $\mathrm{R}_{00}(0) = \left[x_{00}(0), y_{00}(0)\right]^T$ is the range vector to the object's geometric center, point $O'(0)$, in the coordinate system Oxy at the moment $p = N/2$; $\mathrm{A} = \begin{bmatrix} \cos\varphi & \sin\varphi \\ -\sin\varphi & \cos\varphi \end{bmatrix}$ is the transformation matrix; φ is the angle between the coordinate axes Ox and $O'X$; $X_{ij} = i(\Delta X)$ and $Y_{ij} = j(\Delta Y)$ are the discrete coordinates of ijth reference point; ΔX and ΔY are the dimensions of the 2-D grid cell on the coordinate axes $O'X$ and $O'Y$ respectively, $i = \overline{1,I}$ is the number of the reference point on the axis

* Prof. Dr. Sc.

$O'X$; $j=\overline{1,J}$ is the number of the reference point on the axis $O'Y$, I is the full number of the reference points placed on the axis $O'X$ in the object space, J is the full number of the reference points placed on the axis $O'Y$ in the object space.

3. Modeling deterministic Components of ISAR signal

The ISAR signal return is an additive sum of a deterministic component $\dot{S}(p,k)$ and zero mean complex Gaussian noise $\dot{n}(p,k)$, i.e. $\dot{\xi}(p,k)=\dot{S}(p,k)+\dot{n}(p,k)$. The deterministic complex component of the LFM ISAR signal can be written as

$$\dot{S}(p,k)=\sum_i\sum_j a_{ij}\,\mathrm{rect}\left[\frac{(t-t_{ij}(p))}{T}\right]\exp\left\{-j\left[\omega\left(t-t_{ij}(p)\right)+b(t-t_{ij}(p))^2\right]\right\}, \tag{2}$$

where $\mathrm{rect}\dfrac{t-t_{ij}}{T}\begin{cases}1, 0<\dfrac{t-t_{ij}(p)}{T}\le 1\\ 0, 0>\dfrac{t-t_{ij}(p)}{T}>1\end{cases}$; a_{ij} is the reflection coefficient (intensity) of the point scatterer of the object space. In common case the parameter a_{ij} is random value with mathematical expectation of the intensity of the target point scatterers $\bar{a}_{ij}>d$, and for all the rest point scatterers from the object space $\bar{a}_{ij}\le d$, d is the threshold of signal detection (noise level); ω is the signal angular frequency, C is the light speed, $b=\pi\Delta F/T$ is the LFM rate, T is the time duration of a LFM pulse, ΔF is the bandwidth of the transmitted pulse; $t=t_{ij\min}(p)+(k-1)\Delta T$, $k=\overline{1,K+L}$ is the sample number of a LFM pulse, $K=T/\Delta T$ is the number of samples of the LFM pulse, L is the normalized time dimension of the object. The expressions (1) and (2) can be used for modeling the ISAR signal return in case the object is moving on rectilinear trajectory in 2-D coordinate system.

4. MMSE Iterative ISAR Image reconstruction Procedure

The vector estimates of the invariant geometric parameters, $\dot{\bar{\lambda}}_r=\left[\dot{a}_{11},\ldots\dot{a}_{ij}\ldots\dot{a}_{IJ}\right]^T$ with dimension $[I\times J;1]$ can be extracted from ISAR data by implementing the iterative MMSE procedure [5]

$$\dot{\bar{\lambda}}_r=\dot{\bar{\lambda}}_{r-1}+\Delta_\lambda, \tag{3}$$

where Δ_λ is the vector of mean square errors of the estimated parameters and has dimension $[I\times J;1]$; r is the iteration number. The vector Δ_λ is given by

$$\Delta_\lambda=\left[\mathrm{B}^T\mathrm{PB}\right]^{-1}\mathrm{B}^T\mathrm{P}\Delta_\xi. \tag{4}$$

Matrix P is diagonal with dimensions $[2(N\times K);2(N\times K)]$, its terms being the squared reciprocals of the standard deviations of the measured return values, $\xi_c(p,k)$ and $\xi_s(p,k)$. The vector Δ_ξ is the difference between the measured quadrature components of the return signal (10) and the corresponding approximation functions, has dimensions $[2(N\times K),1]$, and is given by

$$\Delta_\xi=\left[\xi_c(p,k)-\mathrm{S}_c\left(p,k;\dot{\bar{\lambda}}\right);\xi_s(p,k)-\mathrm{S}_s\left(p,k;\dot{\bar{\lambda}}\right)\right]^T, \tag{5}$$

where $\mathrm{S}_c\left(p,k;\dot{\bar{\lambda}}\right)$ and $\mathrm{S}_s\left(p,k;\dot{\bar{\lambda}}\right)$ are the approximation quadrature vector functions, defined by the expression (3), replacing a_{ij} with its estimate $\dot{a}_{ij}$, and model the ISAR signal, reflected by two-dimensional regular grid of point scatterers. The grid moves with the same dynamic parameters as the observed object.

The matrix $\mathrm{B}=\left[\mathrm{b}_c,\mathrm{b}_s\right]^T$ has dimensions $[2(N\times K);I\times J]$. Each element of the quadrature submatrices b_c and b_s consist of the coefficients of the linear terms of the Taylor's expansion of the quadrature approximation functions in the domain of the invariant parameters can be calculated as follows

$$b^{c}_{(p-1)K+k,(i-1)J+j} = \partial S_c\left(p,k;\dot{\bar{\lambda}}\right)/\partial \dot{a}_{ij} = \cos\left[\omega\left(t-t_{ij}\right)+b(t-t_{ij})^2\right]; \quad (6)$$

$$b^{s}_{(p-1)K+k,(i-1)J+j} = \partial S_s\left(p,k;\dot{\bar{\lambda}}\right)/\partial \dot{a}_{ij} = \sin\left[\omega\left(t-t_{ij}\right)+b(t-t_{ij})^2\right].$$

5. Numerical experiment

To substantiate the properties of the developed 2-D model of LFM ISAR trajectory signal and to verify the correctness of developed MMSE image reconstruction procedure a numerical experiment was carried out. It is assumed that the target is moving rectilinearly in a 2-D observation Cartesian coordinate system Oxy and is detected in 2-D coordinate system $O'XY$. The trajectory parameters are $V = 600$ m/s, $\alpha = \pi$, $\varphi = 0, x_{00}(0) = 0$ m, $y_{00}(0) = 1000$ m. The ISAR parameters are: $T_p = 10^{-4}$ s, $T = 10^{-6}$ s, $f = 10^{10}$ Hz, $\lambda = 3.10^{-2}$ m, $\Delta T = \frac{T}{K}$ s, $\Delta F = 10^8$ Hz, $b = 6.28.10^{14}$, $N = 128$, $K = 128$. Geometrical parameters of the ISAR signal are $\Delta X = \Delta Y = 1$ m, $I = 15$ and $J = 18$, intensities of the point scatterers placed on the target are $a_{ij} = 0.01$, intensities of the point scatterers placed out of the target are $a_{ij} = 0.001$. The initial values of the intensities of point scatterer of the geometrical model in the form of regular grid before starting MMSE image reconstruction procedure are $\dot{a}_{ij} = 0.001$. The complex values of the additive noise $\dot{n}(p,k)$ are modeled by standard procedure by signal to noise ratio equal to 10 dB.

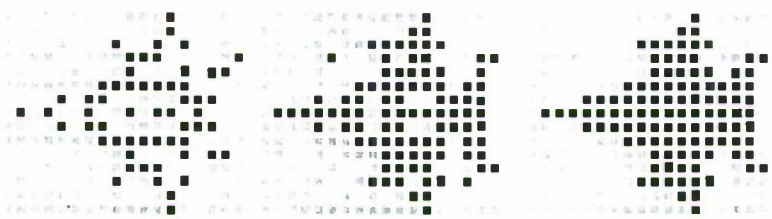

(a) (b) (c)

Fig. 1. Three images of the aircraft obtained after $r = 3$ (a), $r = 7$ (b), and $r = 9$ (c) iteration of the MMSE procedure

6. Conclusion

In the proposed work 2-D ISAR geometry and an ISAR signal model with linear frequency modulation are presented. An image reconstruction procedure grounded on the minimum mean square error estimation of invariant geometrical parameters of the ISAR complex amplitude is implemented. A complex approximation function describing LFM ISAR signal reflected from the regular grid of isotropic point scatterers is constructed. Numerical experiment carried out over simulated ISAR data proves the correctness of the theoretical analysis, mathematical models and consistency of the iterative procedure. The computational results demonstrate high-speed convergence of the algorithm, and no great number of iterations (5-10) is needed to obtain satisfactory images of the aircraft.

References

1. **Chen, V. C., Quian, SH.** Joint time frequency transforms for radar range-Doppler imaging, IEEE Transactions on Aerospace and Electronic Systems, vol. 34, pp. 486-499, April 1998.
2. **Quian, S., Chen, D.** Decomposition of the Wigner-Ville distribution and time-frequency distribution series, IEEE Transactions on Signal Processing, **42**, 10, pp. 2836-2842, Oct. 1994.
3. MARR, R. A., LAMMERS, U.H.W. Coherent 3-D imaging of model targets, IEEE National Radar Conference, Syracuse, New York, May 13-15 1997, pp 289-294.
4. **A.D.Lazarov.** Spatial Correlation Algorithm for ISAR Image Reconstruction. 2000 IEEE International Radar Conference, Alexandria, Virginia, USA, May 7-12, 2000.
5. **A.D.Lazarov.** Iterative Minimum Mean Square error Method and Recurrent Kalman Procedure for ISAR Image Reconstruction. IEEE AES, Transactions, Vol. 37, No 4, Oct. 2001.

APPLICATIONS AND NAVIGATION SYSTEMS FOR PEDESTRIANS IN URBAN AREAS*

D. Klinec
University of Stuttgart, Institute for Photogrammetry,
Geschwister-Scholl-Str. 24, 70174 Stuttgart, Germany. E-mail:darko.klinec@ifp.uni-stuttgart.de

Abstract

Key words: location-based applications, navigation, sensors

Applications providing support for mobile users (pedestrians) are becoming more and more important in a lot of different situations. People using little digital helpers are able to access information wherever they are, e.g. navigation information or information about the next store, etc.

The poster will show two location-based applications and functionality aspects for user support, especially for use in urban areas. As the position is an important requirement for location based applications, also some techniques will be pointed out. Different to systems for car navigation, pedestrians also want to access on information about surrounding objects, e.g. buildings, while walking. Therefore applications and sensors for positioning have to support the pedestrian in a different way.

1 Introduction

Mobile information services can be subdivided into two categories, depending on the way information access is controlled: Usual information services that access on information without regarding the users current location and so-called location-based services (LBS), which use the location information as one of the most important parameters. NEXUS, which is a project currently being carried out at the University of Stuttgart, aims at the development of a generic platform that supports users regarding their current position. For LBS solutions not only data are relevant, also the provision of location information is an important prerequisite. Beside GPS and GSM, also hybrid methods exist which offer the possibility to use images for the positioning process. Since not only the position of the user is of interest but also that of real world objects, the solution of using images can provide also the location information of them.

2 Applications for Mobile User Support

Based on the prototype of the NEXUS platform two applications have been developed, which demonstrate some functionalities. The CityNav application includes some features in order to offer an easier map handling and an automated access on object information [Klinger 2000]. It includes a user interface and the telepointing functionality, which offers the possibility to access information about objects by pointing at them. Since the mobile device is equipped with a differential GPS receiver and a digital compass the position and direction a user is looking in can be superimposed with map information. The line of sight can be drawn into the map. Due to inaccuracies of the digital compass and the GPS receiver a triangle has to be constructed that represents the tolerance, in which the line of sight can actually be. By intersecting the triangle with the geometry of other object classes represented within the map, an identification of the objects a user is looking at can be realised.

The second application uses virtual objects, so-called Virtual Information Towers (VITs), as metaphors to structure information spatially [Leonhardi 00]. The VITs are an electronic equivalent to real-world advertising columns. VITs have a certain geographical position and a given range of visibility attached to it. They host information and services that are relevant at the given location [Volz 00]. A mobile user has access to the information on all the VITs that are "visible" from his current position. Moving through an area, the application selects and displays those VITs. The current position of the user is detected by a differential GPS receiver and indicated within the map. The application allows to browse through the hierarchical content of the available VITs. Via the VITs not only information stored within the NEXUS databases can be accessed, but also external resources like web pages or digital libraries are accessible so that, for instance, information stored in the WWW can be assigned to a geographical position or area, respectively.

3 Positioning Methods for LBS

Within the field of information services two main classes exist, as illustrated in the introduction. In case of location-based services the position information is one of the most important parameters. When LBS are described everybody has in mind small digital helpers that run different applications. As digital helpers are small, also positioning tools should be wearable, too. Of course it is not essential in case of a prototype, but the technology must offer the possibility to be minimised in future. In case of proprietary solutions often GPS technology or positioning techniques using the GSM infrastructure are recommended. In GSM Networks different approaches exist to compute position information depending on wave propagation between GSM device and re-

ceiver antennas. But not only the availability of position information is essential in case of LBS, in the same way also its accuracy is of interest. Some applications are only possible if position accuracy is high, e.g. if the mobile user want to access on object based information that depends on his current position. The major functionality of positioning sensors can be divided into two categories: self-positioning and remote positioning. In self-positioning, the objects themselves determine where they are. Positioning receivers are able to make the appropriate signal measurements from geographically distributed transmitters and use these measurements to determine their own position. As an example, GPS is a self-positioning system. In remote positioning systems, receivers at one or more locations measure a signal originating from, or reflecting off, the object to be positioned. The use of GSM for determining the position can be classified as remote positioning.

In case of NEXUS, not only approved technology for positioning is of interest, but also new approaches are considered. One approach is the use of images and landmarks to provide positions of the mobile user or that of objects. It is of interest because this is also the way how people do their positioning. With the help of a small camera, a part of the environment the user is located at is captured. The idea is, that any captured image only can be provided from one special position or orientation, respectively. Using image analysis techniques, a geometric model (3D-model) of the environment and spatial resection, the coordinates of the camera could be processed. Since users will move both outdoor and indoor, the advantage of this method is the usability for positioning in both areas.

3.1 Hybrid Positioning Systems

As described before different methods for positioning exist. Hybrid location systems combine technology in a way that allows the strengths of one to compensate for the weakness of the other to provide a more reliable and robust location solution. In the chapter before the use of digital camera systems was mentioned as a method for position estimation. Within the field of close range photogrammetry this technique is well known, whereas the idea is relatively new to use it as a hybrid system within the LBS sector. To delimit to close range photogrammetry the approach in context to LBS is called mobile photogrammetry. It combines conventional systems for navigation and a digital camera to improve positioning. In addition to technical equipment the use of mobile photogrammtry also requires a model of the environment, to be able to compute position information. As a model, e.g. a highly detailed 3D city model or a more abstract one can be used, depending on the required accuracy of location information. In case of NEXUS, a 3D representation of the city of Stuttgart is available, containing highly detailed geometrical information about the buildings. The prototype sensory for mobile photogrammetry consists of several devices combined into one tool. In addition to images the device also collects the approximate orientation by means of a digital compass and the position using a differential GPS receiver. The hybrid system allows to combine GPS measurements and further information. In case of mobile photogrammetry images, a city model and compass measurements are combined within a spatial resection algorithm [Klinec 01].

4 Conclusion

The NEXUS concept focuses on the development of a global platform in order to support different kinds of location-based applications. It is intended to facilitate the access to required services and information by means of the infrastructure. As a prerequisite for the realization of location-based applications, the position of the users has to be known. For some applications a high accuracy of location information is required. It can be derived by hybrid positioning. So far, some prototypical implementations of NEXUS-based applications are available which are demonstrating basic features. Ongoing work is aimed at integrating further services of the platform like GeoCast or Spatial Events into the existing prototypes.

5 References

[Klinec 01] **D. Klinec and D. Fritsch (2001).** Acquisition of Position Information for Location Aware Applications using Multi Sensors and Mobile Photogrammetry, Proceedings of ION'01, Salt Lake City, USA.

[Klinger 00] **Klinger, R. (2000).** Konzeption und Entwicklung eines NEXUS Demonstrators. Student Thesis Nr. 1971. Faculty of Computer Science, University of Stuttgart.

[Leonhardi 00] **Leonhardi, A. and Bauer, M. (2000).** The VIT-System: Experiences with Developing a Location-Aware System for the Internet, Workshop on Infrastructure for Smart Devices, How to Make Ubiquity an Actuality, at the HUC2k, Bristol, Great Britain.

[Volz 00] **Volz, S., Sester, M., Fritsch, D. and Leonhardi, A. (2000).** Multi-Scale Data Sets in Distributed Environments. International Archives of Photogrammetry and Remote Sensing, Vol..XXXIII, Part B4, Technical IV/1, Amsterdam.

EXACT SYSTEMS POINTING WITH THE HELP OF INTELLIGENT CONTROL*

Vladimir N. Pilishkin ,
Bauman Moscow State Technical University
2-nd Baumanskaya st. 5, Moscow, 107005, Russia ,E-mail: pilishkin@hotmail.com

Ingmar Tollet
Espoo-Vantaa Institute of Technology (EVITech)
Vanha maantie 6, 02600 Espoo, Finland. E-mail: ingmar.tollet@evitech.fi

Abstract

Key words: represented and mapped models, the intelligent environment, system with intelligent properties.

The task of complex systems pointing is considered on the basis of the intelligent control, synthesized in the real time. Task solving is carried out by forming in the intelligent environment of continuously corrected represented model of system and comparison of its behavior dynamics with mapped model. Formalizing the control task the intelligent law synthesis is carried out by a phase-constraints variation method.

Introduction

To the problems of navigational intelligent systems (IS) construction numerous works are devoted [1] . In these works both general questions of IC forming, and the questions directly connected with functioning features of IC are considered. To these questions the direct relation has the problem of complex dynamic objects intelligent control synthesis. In many known works [2] basically ways of IS construction for a certain type of objects are considered. In the given work for systems with intelligent properties (SIP) the approach for the solving of the considered problem is offered. The construction of intelligent control laws is carried out in real time [3].

1. Task statement

Let's mark considered system as D. We suppose, that D has intelligent properties if it has own representation about character of the functioning. The system D structure can be presented as follows:

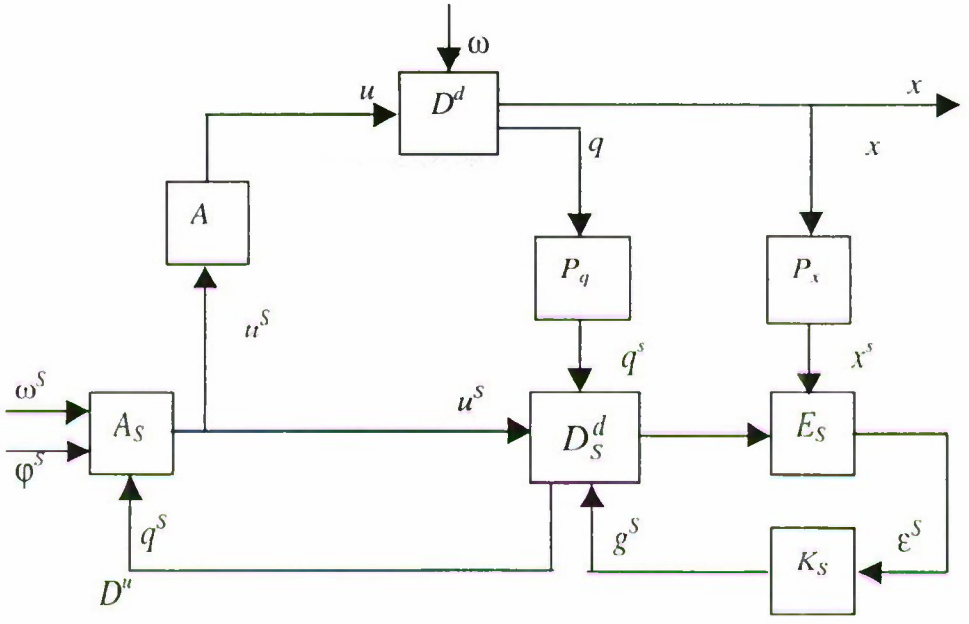

Fig. 1. General structure of SIP

On the fig. 1 the following markings are used: D^d and D^u – dynamic and intelligent part of SIP; x, u, w, – vectors of a condition, control and disturbance in the space state H; q – vector of parameters of model D^d; x^s, u^s, w^s, q^s -images of vectors x, u, w, q, formed in the intelligent environment (IE) S; ϕ^s – signal of the image of the target C_s in the environment S; x_p^s – vector of condition of the image of system's dynamic model; E_s – block of comparison of signals x^s, x_p^s; ε^s – error signal in the environment S, g^s – vector of correction of model's image; D_s^d – image of a dynamic part of SIP in the environment S; K_s – correction operator of model's image; P_q, P_x – operators of images for vectors q and x from H to S; A_s – control vector former in the environment S; A – transformer of a control vector from the environment S to the space H; S – intelligent environment representing certain set of elements s, on the basis of which the analysis of character of target's fulfilling is carried out and the required control law is chosen.

Under the target C we shall understand providing of given system required behavior in space and time. It can be presented as follows:

$$C \Leftrightarrow x(t) \in Q(t) \forall t \geq t_0 \text{ where } Q(t) = \{x \in H : \psi(x,t) \leq 0\} \tag{1}$$

We also suppose that dynamic part D^d is described by the following equation:

$$\dot{x} = f^d(x,u,q,w,t), \quad x(t_0) = x_0, t \geq t_0 \tag{2}$$

On system variables (2) the following limitations are imposed

$$u \in U(t), w \in W(t), q \in \Theta(t), \quad t \geq t_0 \tag{3}$$

where $U(t), W(t), \Theta(t)$, – are some sets. $U(t)$ is given, and about $W(t), \Theta(t)$ the information can be corrected during system functioning. It is required to synthesize such object control algorithm (2), which would provide execution of target C as (1) at presence of limitations (3) and allow to take into account any properties and a kind change of sets $W(t), \Theta(t)$. Control forming should be carried out in real time mode.

The new approach for synthesis of intelligent control directly on the basis of general SIP structure is offered.

2. Model forming in the intelligent environment

We shall suppose that the intelligent part D^u of SIP contains the information about objeet D^d and about environment in the following form:

The equation of objeet in the intelligent environment S

$$\dot{x}_p^s = f_s^d(x_p^s, u^s, q^s, g^s, w^s, t^s), x_p^s(t_0^s) = x_{p0}^s, \quad t^s \geq t_0^s; \tag{4}$$

Target for the objeet in the environment S

$$x_p^s \in Q_s(t^s) = \{x_p^s \in S : \psi_s(x_p^s, t^s) \leq 0\}; t^s \geq t_0^s; \tag{5}$$

Limitation on system variables in the environment S are:

$$u^s \in U_s(t^s), w^s \in W_s(t^s), q^s \in \Theta_s(t^s) \tag{6}$$

As in the environment S, according to SIP definition, the direct forming of system representation about itself is carried out, then at each moment of time $t^s \geq t_0^s$ object model (4) and values of vectors u^s, q^s, g^s, w^s should be completely determined. And as q^s, w^s any realizations can be used, which satisfy to the limitation (6).

We suppose that forming of u^s is carried out according to the equation:

$$\dot{u}^s = v^s(u^s, x_p^s, q^s, g^s, w^s, t^s), u^s(t_0^s) = u_0^s, \quad t^s \geq t_0^s \tag{7}$$

or directly as

$$u^s = \tilde{u}^s(x_p^s, q^s, g^s, w^s, t^s), t^s \geq t_0^s \tag{8}$$

We suppose, that for some fixed model D_s^d the law $\tilde{u}^s(\cdot)$ providing the target (5) is chosen

Let $\tilde{u}(\cdot)$ – is the control law in the state space H

$$\tilde{u}(\cdot) = \alpha(\tilde{u}^s(\cdot)), \tag{9}$$

Efficiency of the chosen control is analyzed from the following relationship

$$x^s \in Q_s(t^s) \tag{10}$$

or

$$\rho_s(\varepsilon^s, t^s) \le 0; t^s \ge t_0^s, \tag{11}$$

where $\varepsilon^s = \mu^s(x^s, x_p^s)$ – a discrepancy signal in IS,

To provide (10), (11) the models D_s^d correcting, which is formed as representation of an environment S about object D^d, is carried out. Therefore further we shall name D_s^d as represented model in the environment S. Correcting is carried out by a signal $g^s = k(\varepsilon^s)$, where $k(\cdot)$ – some unknown dependence. It is necessary to have the full information about vector x^s for check of relationships (10) or (11). To get such information it is offered on the basis of the object model directly mapped onto environment S. Mapped model $D^{d,s}$ we shall define as follows. Let's $x^s = Px$, where P – is non-degenerate operator, then $D^{d,s}$ with the account of (1) will become

$$\dot{x}^s = P \cdot f^d(P^{-1}x^s, \alpha(u^s), q, w, t), x^s(t_0) = x_0^s, \quad t \ge t_0 \tag{12}$$

The given relationships represent the model of SIP in the environment S.

3. Control synthesis in the intelligent environment.

We shall present the relative synthesis scheme in the following form (see fig. 2)

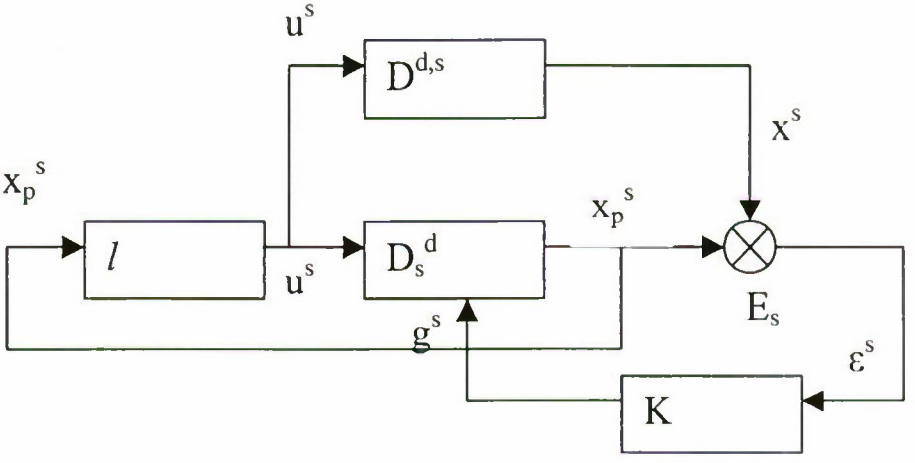

Fig. 2. Synthesis scheme

The dependences $l(\cdot)$, $k(\cdot)$ should be determined so that in view of (3) or (6) the relationships (5), (10) or (11) were provided. The synthesis relationships are

$$\left.\begin{aligned} &\dot{x}_p^s = f_s^d(x_p^s, u^s, q^s, g^s, w^s, t^s), \dot{x}^s = P \cdot f^d(P^{-1}x^s, \alpha(u^s), q, w, t), \\ &u^s = l(x_p^s, t^s), g^s = k(\varepsilon^s), \varepsilon^s = \mu^s(x^s, x_p^s) x^s(t_0) = x_0^s, \quad t \ge t_0; x_p^s(t_0^s) = x_{p0}^s, \quad t^s \ge t_0^s. \end{aligned}\right\} \tag{13}$$

In the (13) there are two time modes: t and t^s. If $t = t^s$, then the control laws synthesis $u^s = l(\cdot)$ and $k(\varepsilon^s)$ corrections of represented model D_s^d are carried out simultaneously. In this case $l(\cdot)$ and $k(\cdot)$ it is necessary to choose so that conditions (5) and (10) were provided. The given task can be solved on the basis of phase constraints variation method [3]. According to this method the following inequalities should be provided:

$$(\nabla_{x_p^s}\psi_s, f_s^d(\cdot)) + \frac{\partial \psi_s}{\partial t} \le 0, \text{ when } x_p^s \in \Gamma Q_s, (\nabla_{x^s}\psi_s, P \cdot f^d(\cdot)) + \frac{\partial \psi_s}{\partial t} \le 0, \text{ when } x^s \in \Gamma Q_s, \quad (14)$$

where ΓQ_s – is a border of set $Q_s(t), t \ge t_0$. It is expedient to use a condition (11) for correction of D_s^d. In this case in (14) instead of the second equation will be the following: $(\nabla_{x^s}\mu^s \cdot \nabla_{\mu^s}\rho_s, P \cdot f^d(\cdot)) + \frac{\partial \rho_s}{\partial t} \le 0$ and $\rho_s(\mu^s(x^s, x_p^s), t) = 0$. Let in (13) time modes t and t^s do not coincide. Then in the environment S it is expedient to use the speeded up time mode $t^s = \eta(t), t \ge t_0$ where $\eta(t) < t$ $(or << t)$. It is obvious that $t_* + T < (<<)\eta^{-1}(t_*^s + T)$, t_*^s – is a moment of time corresponding to the moment $t_* = \eta^{-1}(t_*^s)$, at which vectors $x_p^s(t_*^s)$ and $x^s(t_*)$ it is possible to compare. As $t_1^s = \eta(t_* + T) < (<<)t_* + T$ then on segment of accelerated time $[t_1^*, t_* + T]$ the values of the vector x_p^s, which are received as a result of D_s^d model correction at the moments t_*^s and $t_1^s = \eta(t_* + T)$, it is possible to compare between each other at the same moments of time. Generally it is possible to write down the following: $x_p^s(\cdot) = x_p^s(t^s, g^s)$. As the model D_s^d functions in the speeded up time mode, then for every t^s it is possible to choose such Δt^s, on which by the moment of comparison t^s the model D_s^d was already functioning along the trajectory $x_p^s(t^s, g^s)$. However after x^s and x_p^s signals comparison at the moment t^s the model D_s^d will function during the same period Δt^s, but on another trajectory $x_p^s(t^s, g^s + \Delta g^s)$, where Δg^s – is an increment of correction As $x_p^s(t^s, g^s) = x_p^s(t^s, g^s + \Delta g^s)$, then $\Delta x_p^s(t^s + \Delta t^s, g^s) = \nabla_{g_s} f_s^d(\cdot) \cdot \Delta g^s \cdot \Delta t^s$ or $\nabla_{g_s} f_s^d(\cdot) \cdot \Delta g^s = \Delta x_p^s(t^s + \Delta t^s, g^s) / \Delta t^s$ and characterizes the speed of model D_s^d change, which is carried out as a result of its correction. Then $\Delta g^s = \tilde{K}(x_p^s, x^s, w^s)$ and $g^s = k(\varepsilon^s) + \tilde{K}(x_p^s, x^s, w^s)$.

Conclusion

The considered approach allows to solve various tasks of pointing effectively. Thus it is possible to provide required accuracy of pointing with help of phase limitations. Task solving is carried out due to use of intelligent control. In the intelligent environment the so-called represented system model is constructed, which is continuously corrected in view of the current information about real model. More effective correction is carried out in the speeded up time mode . Intelligent control allows to reach sufficient proximity between real and represented models to provide required pointing accuracy.

References

1. **Albus J. Meystel A.M.** Behaviour Generation in Intelligent Systems. – NISTIR, №6083, NIST, Gaithersburg, MD, 1997.
2. **Cai Z.,** Intelligent Control: Principles, Techniques and Applications. – World Scientific, 1997.
3. **Pilishkin V.N.** Research of Complicated Objects with Intelligent Properties with Virtual Component in the Circuit of Control. – Robotics and Mechatronics Congress, ACRA and ICMT 2001, Singapore, 2001.

ASTROINERTIAL NAVIGATION SYSTEM FOR AIRCRAFT APPLICATIONS*

A.V.Zbrutsky*, O.I.Nesterenko**
National Technical University of Ukraine "Kiev Polytechnic Institute", 37, Peremogy Av., Kiev, 03056, Ukraine
E-mail: nest@cisavd.ntu-kpi.kiev.ua
N.I.Lykholit*, S.K.Fedorenko****, B.P.Goncharov*****
Central Design Office "Arsenal", 8, Moskovskaya Str., Kiev, 01010, Ukraine. E-mail: cdoars@gu.kiev.ua

Abstract

Key words: astronavigation, inertial navigation system, integrated navigation system, Kalman filter

The problems of astronavigation system (ANS) design, which intended for inertial navigation system (INS) error correction, are considered. ANS is integrated with INS by using of optimal Kalman filtering. It is shown that usage of such astroinertial navigation system increases accuracy of aircraft position determination essentially on comparison with separately used ANS and INS. The errors of coordinates determination are not accumulated in time. Furthermore the accuracy of aircraft spatial orientation determination is increased too.

There is a necessity of precise and reliable long-term determination of current airplane coordinates at large distance flights. The main facility for solution of this problem is an inertial navigation system (INS), which is autonomous, reliable and jamming resistance. At the same time the errors of INS position determination increase with time and flight distance. Therefore for the INS error correction the additional navaids, first of all radio navigation systems (Global Positioning Systems, Loran etc) are used. However such radioinertial navigation system looses autonomous and jamming-protected features. In situations, when the advantages of autonomous high-precision navigation systems become principal, the mentioned requirements can be satisfied with the help of astroinertial navigation system.

The problems of astronavigation system (ANS) design, which intended for INS error correction, are considered. ANS star tracker is built on the controlled telescopic unit in azimuth-altitude suspension, which located on the stabilized platform. The platform stabilization is realized by motors which mounted on gimbal suspension axes. INS code information about aircraft roll, pitch and heading is used for the platform stabilization.

A few variants of the ANS platform stabilization making are considered.

The simplest technical solution of this task is control of the stabilization motors by signals of misalignment between angles of roll γ, pitch θ and heading ψ, that measured by INS, and angles γ_3, γ_2, γ_1 of gimbal rotation relative to aircraft fuselage, which are measured by angle-data transmitters mounted on platform gimbal suspension axes:

$$\Delta\gamma_3 = \psi_{\text{инс}} - \gamma_3 ; \qquad \Delta\gamma_2 = \theta_{\text{инс}} - \gamma_2 ; \qquad \Delta\gamma_1 = \gamma_{\text{инс}} - \gamma_1 . \qquad (1)$$

Research results show that for high precision of the platform stabilization at aircraft swinging, the frequency of the INS output information about aircraft attitude must be not less 300 Hz. At the same time developed ANS should be connected to different types of INS that are exploited on aircraft and have rather low-level frequency of navigation data output (50 Hz and less). Such frequency is enough for aircraft control, however it is completely unacceptable for ANS platform stabilization.

In order to decrease requirements to frequency of INS output data, the gyroscopic stabilization of ANS platform can be utilized. Gyro stabilized platform (GSP) keeps its angular position in the inertial space to within a gyroscopes drift. For keeping of platform position in horizon and meridian planes the correction of platform position is realized using external information. As such information the signals of misalignment (1) between angles of aircraft declination relative to geographic frame and angles of the platform declination relative to aircraft are used. Since angular velocities of gyroscope drift are small and geographic frame is slowly rotated in the inertial space, above correction may be done enough weak to decrease effect of INS outputs quantization on level and on time and low frequency of INS output code.

Presented simulation results show that the maximum dynamic error of the ANS GSP stabilization is not exceed 10 arc seconds at aircraft swinging around three axes with amplitude of 2 degrees and frequency 1 Hz; vibration at three axes with amplitude of 2g and frequency 5 Hz. During simulation INS outputs quantization

---

* D.Sc., Professor, Head of Chair.
** Ph.D., Associate Professor.
*** Ph.D., Associate Professor, First Deputy Director - Chief Designer.
**** Deputy Chief of Department.
***** Leading Designer.

frequency was 20 Hz and quantization level was 0.01 degrees. Analog-digital converters (ADC) for gimbal angle-data transmitters had quantization frequency 20 Hz and quantization level 2.5 arc seconds. Static errors of the GSP stabilization are completely defined by ADC and angle-data transmitters errors. During researches it was also shown, that the dynamic error of the GSP stabilization are almost not depend on quantization frequency of INS outputs (for real frequency ranges). This allows using of low frequency code information from INS about angular position of aircraft for ANS work. The simulation has confirmed a capability of lowering of frequency of INS information up to 5 Hz without increasing of the GSP stabilization errors.

With the purpose of increase of aircraft position determination accuracy, the ANS is integrated with INS by using of optimal Kalman filtering. Essentially such astroinertial navigation system represents INS aided by the angular information supplied from astronavigation system.

The INS/ANS integration algorithm is based on INS error equations [1] and ANS errors model [2] which are modified for solution of the task of an optimum estimation of that errors.

INS determines a geographic latitude φ, longitude λ and heading K of aircraft with errors $\Delta\varphi$, $\Delta\lambda$, α:

$$\varphi_{INS} = \varphi + \Delta\varphi\,; \qquad \lambda_{INS} = \lambda + \Delta\lambda\,; \quad K_{INS} = K + \alpha. \tag{2}$$

The state vector of INS errors $X(t)$ consists of 12 components:

$$X(t) = [\Delta\varphi\ \Delta\lambda\ \Delta V_N\ \Delta V_E\ \beta\ \gamma\ \alpha\ m_{aN}\ m_{aE}\ m_{\omega E}\ m_{\omega N}\ m_{\omega V}]^T, \tag{3}$$

where ΔV_N, ΔV_E are errors of determination of north and east components of flight velocity; β, γ are errors of determination of aircraft angular orientation relatively to horizon plane; m_{aN}, m_{aE}, $m_{\omega E}$, $m_{\omega N}$, $m_{\omega V}$ are slowly changed random zero drifts of accelerometers and gyroscopes.

ANS determines the coordinates and heading of aircraft with periodicity of Δt =2 minutes by a serial sighting of two heavenly bodies. Let φ_{ANS}, λ_{ANS}, K_{ANS} are aircraft latitude, longitude and heading that are measured by ANS:

$$\begin{aligned}
\varphi_{ANS} &= \varphi - \beta + \Delta_{\varphi SS} + \Delta^n_{\varphi SS} + \Delta_\varphi + \Delta^n_\varphi\,;\\
\lambda_{ANS} &= \lambda + (\gamma + \Delta_{\lambda SS} + \Delta^n_{\lambda SS})/\cos\varphi + \Delta_\lambda + \Delta^n_\lambda\,;\\
K_{ANS} &= K + \Delta_{KSS} + \Delta^n_{KSS} + \Delta_K + \Delta^n_K\,,
\end{aligned} \tag{4}$$

where $(-\beta + \Delta_{\varphi SS} + \Delta^n_{\varphi SS})$, $(\gamma + \Delta_{\lambda SS} + \Delta^n_{\lambda SS})$ are overall declinations of ANS platform relatively to horizon plane, which include INS errors β, γ, constant components $\Delta_{\varphi SS}$, $\Delta_{\lambda SS}$ and high-frequency (noisy) components $\Delta^n_{\varphi SS}$, $\Delta^n_{\lambda SS}$ of platform servosystem errors; $(\Delta_{KSS} + \Delta^n_{KSS})$ are overall error of azimuth channel servosystem of ANS platform, which includes constant and high-frequency components Δ_{KSS}, Δ^n_{KSS}; Δ_φ, Δ_λ, Δ_K are slowly changed ANS errors of determination of corresponding values concerning to platform; Δ^n_φ, Δ^n_λ, Δ^n_K are noisy components of ANS errors.

The task of INS aiding is decided by an estimation of the INS errors (3) with help of optimal Kalman filter (KF). As measurements for KF there are differences between aircraft coordinates φ_{INS}, λ_{INS} and heading K_{INS}, which are determined by INS (2), and appropriate parameters φ_{ANS}, λ_{ANS}, K_{ANS} (4), which are determined by astro-navigation:

$$\begin{aligned}
y_1 &= \varphi_{INS} - \varphi_{ANS} = \Delta\varphi + \beta - \Delta\varphi_{st} - v_1\,;\\
y_2 &= \lambda_{INS} - \lambda_{ANS} = \Delta\lambda - \gamma/\cos\varphi - \Delta\lambda_{st} - v_2\,;\\
y_3 &= K_{INS} - K_{ANS} = \alpha - \Delta K_{st} - v_3\,,
\end{aligned} \tag{5}$$

where $\Delta\varphi_{st}$, $\Delta\lambda_{st}$, ΔK_{st} are overall static (rather slowly changed) ANS errors; v_1, v_2, v_3 are overall noisy ANS errors.

The analysis of errors observability has shown that not all INS errors, included in the state vector $X(t)$ (3), can be estimated at measurements (5). For example, slowly changed random zero drifts of accelerometers m_{aN},

m_{aE} are not estimated. But the most important errors for solution of the considered task, namely aircraft position determination errors $\Delta\varphi$, $\Delta\lambda$ and heading error α, are estimated.

The real accuracy of the developed astroinertial navigation system (AINS) depends on accuracy of used INS and available capabilities on correction of it errors. In the report the simulation results are presented that confirm the essential decreasing of INS errors even at a loosely coupled ANS and INS at which AINS only estimates the INS errors without their compensation. For example, below figure shows INS error of latitude determination $\Delta\varphi$ in comparison with appropriate AINS error, which defined as inaccuracy of error $\Delta\varphi$ estimation in the integrated INS/ANS system. Note that AINS errors are not accumulated in the time. Furthermore the accuracy of aircraft spatial orientation determination is increased too. At tightly coupled ANS and INS the better accuracy is obtained.

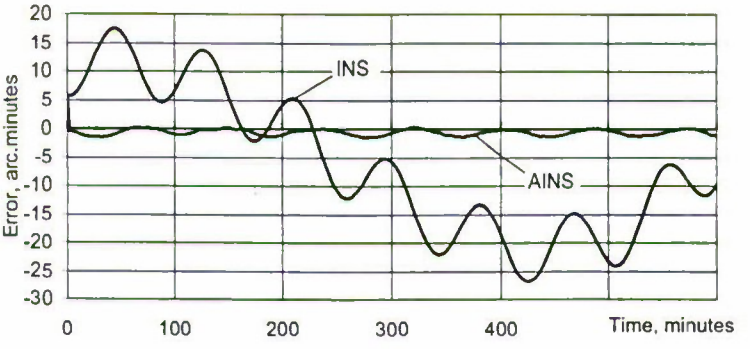

INS and AINS errors of latitude determination

AINS structure is made as the separate ANS module including the star tracker mounted on a stabilized platform and digital computing device that solves the problems of celestial navigation and integration with INS. The capability of ANS connection to various types of airborne INS (both gimbaled and strapdown) is provided. The various levels of ANS and INS integration can be realized, which defined by availability of INS inputs for providing of correction signals on aircraft speed and gyros drift compensation.

References

1. **Бромберг П.В.** Теория инерциальных систем навигации. – М.: Наука, 1979. -296 с.

2. **Каменский А.М.** Теория астрономической коррекции. – М.: Машиностроение, 1974. –220 с.

EFFICIENT ALGORITHM OF GEOMETRIC MODELING FOR THE PROBLEM OF NAVIGATION AND GUIDANCE OF MOVING OBJECTS*

V.B. Kostousov*, I.G. Onuchin
Institute of Mathematics and Mechanics,
Urals Branch of Russian Academy of Sciences
S.Kovalevskaja str., 16, 620219, Yekaterinburg, RUSSIA.
Tel (3432)-49-32-20, E-mail vkost@imm.uran.ru

Abstract

Key words: navigation, guidance, 3D modeling

The main idea of the correlative extremal method of navigation consists in comparison of the reference image to the results of observation, received during the movement. The procedure of polygonal figures intersection is the base of algorithm of generation reference image. Traditionally, high sensitivity to float-point calculation errors is main defect of such procedure. In this case, small inaccuracy in intermediate calculations brings about essential change of result. We present the robust algorithm of polygonal figures intersection.

Introduction

During the latest years the investigation of the problem of precise autonomous navigation and vehicle guidance was developed in the Institute of Mathematics and Mechanics (IMM) of the Ural Branch of RAS. This investigation is based on the comparison of a sensor image to a reference image.

The main idea of the correlative extremal method of navigation consists in comparison of the reference image to the results of observation, received during the movement. This comparison is made in a board computer by special algorithm, which is called the algorithm of binding of measurement to the reference image. Then relative position of the object is determined by results of binding.

The process of comparison of the sensor image to the reference image usually includes the following three stages:

1. Preliminary processing of the sensor image, extracting of the image features or image segmentation;
2. Generation of the reference image or taking out suitable copy of reference image from the data base;
3. Image matching (searching relative position of the sensor image and reference image) or sensor image recognition with the help of reference image.

The subject of this report is connected with the problem of efficient generations of reference image from the three-dimensional database of the scene (stage 2).

This problem is just the problem of computer 3D graphics. Computer graphics algorithms are algorithms, which usually are worked in the picture domain. Usually they are easy realized in hardware because these algorithms are greatly based on raster nature of the images. The modifications of Z-buffer are good examples of such algorithms. Another class of the algorithms consists of the algorithms which are worked in the object domain.

Because of absence of raster restrictions the accuracy of calculations is the main advantage of such algorithms. The main difference of results of algorithms of these two classes consists in the following. The first result is a pixels matrix, which are corresponding to observed spatial scene. In the second case, the result will be a set of polygonal figures, which are corresponding visible parts of objects of spatial scene. We use algorithms of second class in the problem of high-precise navigation and guidance of moving objects.

The polygons intersection procedure is a kernel of algorithm for the reconstruction of observed scene. Usually the high sensitivity to calculation errors is a main defect of such procedure. So, small inaccuracies in intermediate calculations have the essential influence to the result. Many other algorithms of computational geometry possess such a defect. The development of the efficient algorithm of the polygons intersection, which is robust with respect to the rounding errors, is a purpose of current work.

Algorithm

Let the polygon is a set of plane with a boundary which consist of the finite number of edges. The polygon boundary direction is such that at boundary pass-by an interior of polygon stays on the right on the pass-by direction. Let us consider the following known algorithm of building of polygons intersection.

Algorithm POLYGON INTERSECTION

1. Intersection points of the boundaries are to be found;
2. Constructing of the merged graph of borders;

* D.Sc, Leading Research Scientist.

3. All contours of merged graph are traversed. The direction of the path-by is chosen by rule "first on right". Thereby, closed contours of graph, which correspond to results polygons, are to be found.

4. The selected areas are sorted with respect to inclusion order.

The realization of such algorithm brings about the problem of instability, caused by limited accuracy of calculations. Because of the limited representation of the real numbers in the CPU it is impossible to present the range of real numbers in whole, but only some finite subset. We simulate such situation by means of ε-net. Let us consider the next problem.

Problem INTERSECTION OF POLYGONES WITH VERTEXES IN THE NODES OF THE FIXED ε-NET

Let A and B are two polygons. Let the vertexes of A and B are situated in the nodes of ε-net. It is necessary to get a set of result polygons, which correspond to $A \cap B$. The vertexes of the result polygons must be situated in the nodes of ε-net. The difference between this result and ideal result (unlimited precise of calculation) must be no more than ε in Hausdorff metric.

The main difficulties and particularities of problem are defined by the following problem, which we will consider in detail.

Problem INTERSECTION OF SECTIONS WITH VERTEXES IN THE NODES OF THE FIXED ε-NET

Let $\{e_1, e_2, \ldots e_N\}$ be the set of segments on plane. There is the ε-net over the plane. It is necessary to get the set of segments intersected in their own ends only and situated in the nodes of the ε-net. Besides this, each resulting segment must be situated in ε-neighborhood of its own parent segment.

Without loss of generality we suppose that coordinates of nodes of the ε-net are integers ($\varepsilon = 1$).

The problem of calculation accuracy of intersection points is very important in the current problem. Because the coordinates of ends of segments are integer, the coordinates of intersection point are rational. That allows exact calculation of coordinates of intersection point. However a good algorithm must be correct at presence of certain mistake of calculation of intersection point. The notion of δ-*intersection* had been entered to solve this problem.

The using of δ-intersection of segments guarantees that intersection point between two segments will be found, if the errors of calculations of coordinates will be less then δ. Thereby, value δ is an "resolution" of the algorithm and, consequently, δ is a certain threshold of stability to errors. Hereinafter, we shall understand intersection points as δ-intersection points ($\delta < \varepsilon/2$).

The difficulty of the problem arises when the intersection points are moved to nodes of the ε-net. When this occurs, the new false points of intersection can appear. It is not guarantee, that if this **false** points move to the nodes of ε-net again, the **new false** points not appear again. It is not known, that this process will be completed. We suggest algorithm that solves this problem.

Conclusion

Thus in this investigation the algorithm of the polygons intersection, which correctly works on complex dynamic scenes with given level of errors has been offered. Algorithm released on the personal computer and checked for complex scenes contained tens of thousands segments. The analysis of computing difficulty of algorithm has been conducted. The ways of enlarging its efficiency have been determined.

Work was supported in part by Russian Foundation for Basic Research (projects N 00-01-00346, N 01-07-90210).

References

1. **V.B. Kostousov, I.G. Onuchin** «Robust parallel algorithm of intersection of line segments for efficient modeling of 3D-scene » // Algorithms and software for parallel computation, IMM UB RAS, Yekaterinburg, 2002, vol. 5,

THE RESULTS OF THE RESEARCH ON THE MEASURING BLOCK OF THE INTEGRATED SYSTEM FOR MOTOR TRANSPORT*

V.A Tikhonov*, V.E. Plekhanov

The work is executed by the order of joint-stock company "PRIN", Moscow, at participation of the Moscow state aviation institute

Joint-stock company "PRIN", 4, Volokolamskoye shosse, Moscow, 125871, Russia

Tel. (095) 158-69-67, fax. (095) 158-69-65. Moscow state aviation institute, ", 4, Volokolamskoye shosse, Moscow, 125993, Russia.el. (095) 158-43-59, fax: 158-2977.

E-mail: v _ tikhonov pochtamt.ru, ve _ plekhanov pochtamt.ru

Abstract

Key word: an integrated navigation system, magnetometer, microaccelerometer, fibre-optical gyroscope, odometer.

The results of researches of the measuring block of an integrated navigational system for motor transport are represented. The system is intended for a raise of an exactitude of navigation in a complex with the receiver GPS and security of an autonomous condition of navigation in case of short-term (100s) miss of a signal GPS.

Introduction

The basis of a modern navigational system of the automobile is made with the receiver of a satellite navigational system (GLONASS or GPS). Just it is for today the exactest source of an information about a location of the automobile position the acceptable cost. However, an essential shortage of the receiver of a satellite navigational system is it bad noise protection and miss of a signal at a lack of direct visibility of the GPS satellite, that is characteristic of the urban operation conditions of the automobile. Therefore distinguish complex work of a navigation system with use of an information of all sensors, including the receiver of a satellite system, and autonomous work without use of an information from the receiver of a satellite system. The exactitude of work in this condition characterizes quality of a navigational system.

We obtain a statistician on slice of times of miss of a signal GPS of the receiver on two test standard urban routes in Moscow. Slice of observation times 4 and more satellites necessary for deriving of a rigorous navigational solution, make 87 % from common time of the first route and 47.7 % second.

One of the purposes of researches was the definition rational, from a point of view of the cost and exactitude, variants of a construction of an integrated navigational system intended for maintenance on motor transport in urban conditions. For this purpose the experimental model of the measuring block (fig. 1,2), containing a surplus amount of sensors was made. A structure of the researched measuring block: the 3-rd component magnetometer include magnetoresistive sensors of a series HMC100X (Honeywell), two 2-nd component microaccelerometers ADXL210 (Analog Devices), velocity sensor on an information about number of revolutions of a wheel (odometer); two azimuth (rough and exacter) fiber-optical gyroscope VG 910 and VG 951 (Fizoptika); the receiver GPS (Trimble Navigation); the controller with 14 digit analog-digit convertor. The data transfer was carried out on the sequential interface RS-232. Gathering and the data processing was produced by notebook.

The test results

The results of trials of separate sensors and field tests of the measuring block in various conditions of navigation are represented. The handling of results of field tests was carried out both in a condition postprocessing, and in an actual time scale. As the measurement reference of navigation parameters the parameters obtained in the condition DGPS c by the help of phase receivers, and also signals of an exacter fibre-optical gyroscope VG 951 were used.

---

*Associate professor.

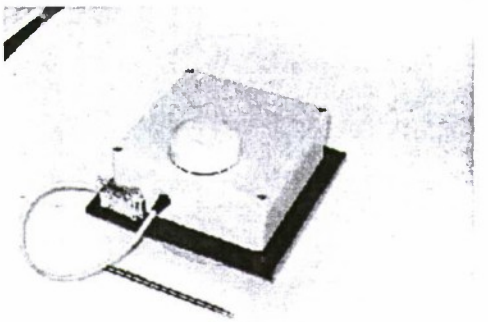

Fig. 1

As a fundamentals the complex including receiver of a satellite system of navigation, odometer and fiber-optical gyroscope is adopted. The remaining sensors are used as auxiliary. The sensor, alternate to a gyroscope, of an information about attitude of plant - compass is investigated. As have shown field tests, the gimballess compass constructed because of of the magnetometer and microaccelerometers in the urban operation conditions is subject to large random disturbances. Basic radiants of perturbations are a vehicle and urban communications (such, for example, as single-wire lines of electrotransmissions for trams and electrotrains).
The error in the definition of magnetic course reaches magnitudes of the order 5°.

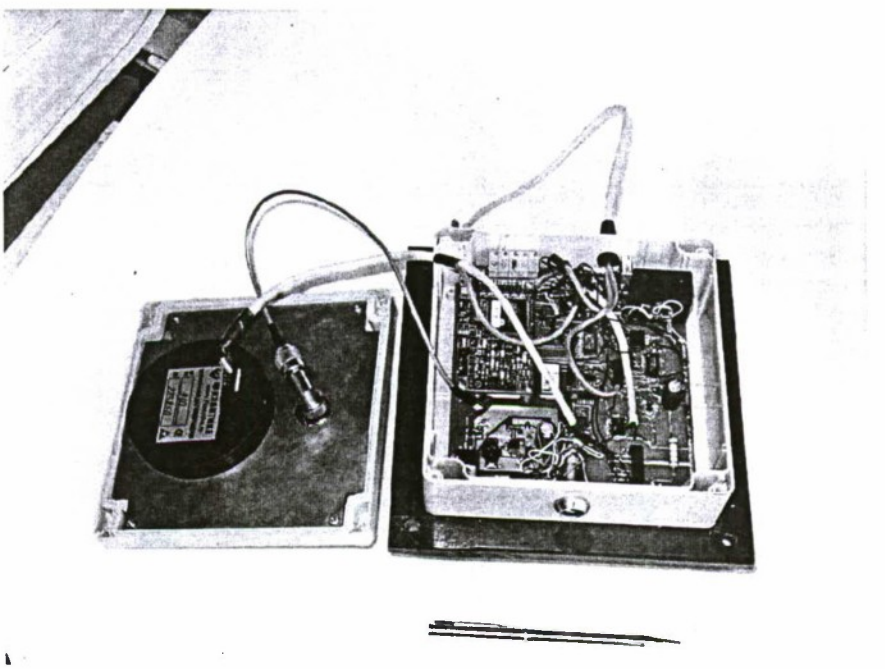

Fig. 2

The algorithm of work of a system includes as a basis algorithm of complex information processing of sensors on the basis of an extended Kalman filter or method of least squares (LSM). To an evaluation are subject both coordinate of a location of plant, and parameters of a gyroscope and sensors. During complex handling the continuous calibration of sensors happens. After loss of a signal GPS of the receiver the filter works in a condition of the prognosis. At handling of experimental datas the common duration of work of a system included an interval of complex work (150s) and interval of the prognosis of navigational parameters in autonomous operational mode of a system (100s).

The basic problem of synthesis of an extended Kalman filter is connected from it by nonlinearity (nonlinearity of a used state model). In particular, the convergence of estimations of this filter depends on an initial approximation of estimations (by results of researches the tolerance on area of convergence - 10-20 %) and degree of adequacy of a filter parameters is defined. The method of least squares has the greater stability. The handling on LSM included two phases: a parameter estimation of a gyroscope on measurements of a travelling angle obtained from the receiver GPS, and improvement of parameters of a model of a gyroscope on measurements of coordinates.

The results of data processing obtained at driving on one from test routes are shown on fig.3.

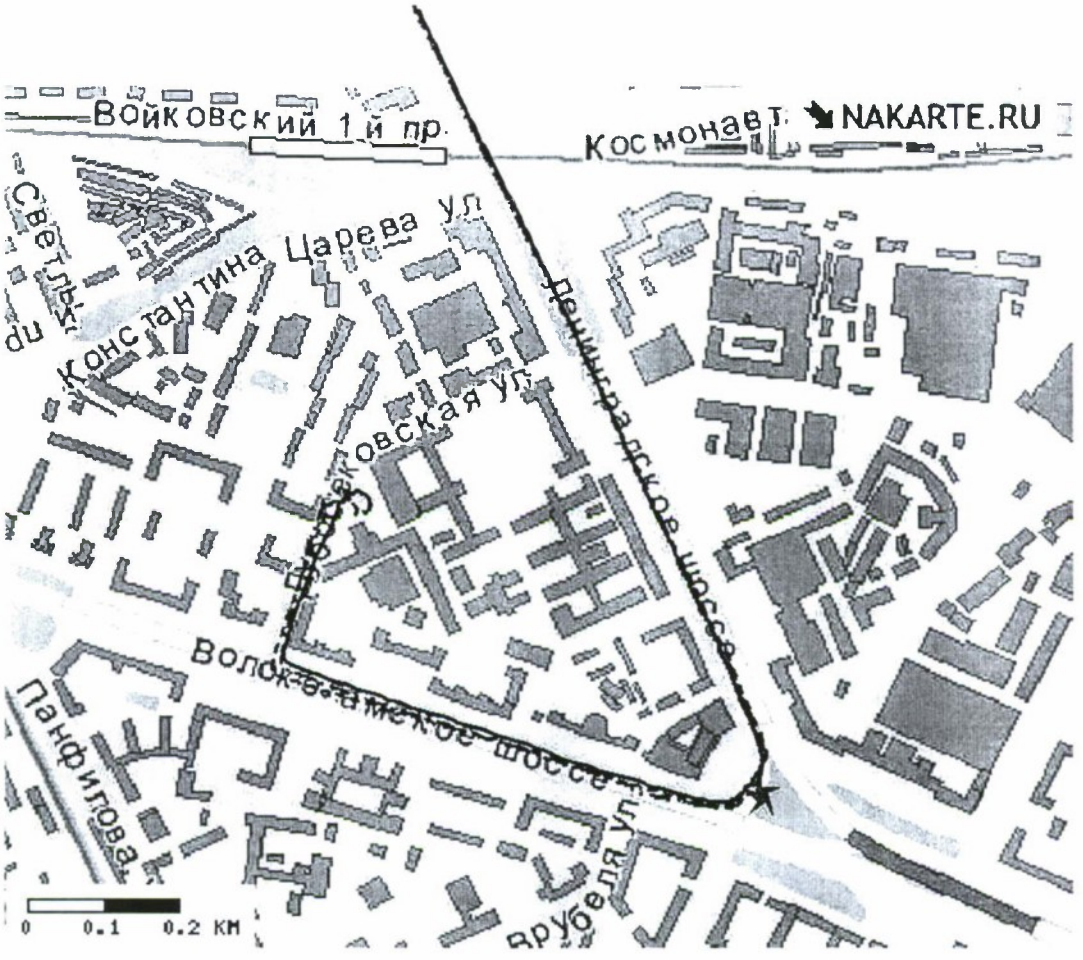

Fig. 3

The "true" trajectory is constructed on datas GPS of the receiver (solid line). On the same Figure the trajectory obtained by complex information processing with use of an extended Kalman filter (dash - dotted line) and a method of least squares (dotted line) is constructed. The asterisk marks a place of passage of a system from complex operational mode in a condition of the prognosis. The values of errors of coordinates the ambassador 100s of the prognosis are those: 23.2 m for estimations of an extended Kalman filter and 14.2 m for a method of least squares. The low bound of an error of an estimation of coordinates stipulated only by error одометра, makes 7-10 m.

The standard deviations of an error of the definition of coordinates obtained in an result of data processing of several test routes, are:

- 5-10 m in a condition of share work of the receiver GPS and number system of a path;
- 10-20 m for 100s - in an autonomous mode of navigation.

Conclusions

Thus, the obtained results of a research of the measuring block of the integrated system allow to hope for satisfactory work of a system in conditions, when deriving coordinates of a object location without interraptions in time is required.

LINEAR JOINT IPDA (LJIPDA) ALOGRITHM*

D. Mušicki*, R. Evans**
Center for Sensor and Signal Proeessing – University of Melbourne,
Parkville, VIC 3010, Australia.

Abstract

Key words: data association, estimation, joint PDA, target tracking

This paper presents a new approach to multi-target tracking. Rather than forming complex hypotheses based on all possible combinations of measurement origins, we attempt to decouple individual tracks based on the probabilities of measurement origins. The Linear Joint IPDA (LJIPDA) algorithm, presented in this paper, recalculates IPDA using the probabilities of measurement origin. This algorithm is recursive and yields formulae for both data association and probability of track existence, which makes it ideal for automatic target tracking applications. Furthermore, the number of operations for this algorithm is linear in the number of tracks and the number of measurements. Simulations are used to verify the performance of the LJIPDA algorithm and compare it with the performance of IPDA, IPDA-DLL, JIPDA and IJPDA algorithms in a dense and non-homogenous clutter environment, and in crossing target situations.

Introduction

Data assoeiation algorithms deal with situations where there are measurements of uneertain origin. In many radar and sonar applications, for example, measurements (detections) originate not only from targets being trackcd, but also from thermal noise as well as from various obstacles such as terrain, clouds etc. Unwanted measurements are often termed clutter. Furthermore, true measurcmcnts from the target are present in each scan only with a certain probability of detection. In a multi-target situation, and assuming infinite sensor resolution, the measurements may have originated from one of various targets.

Automatic track initiation and termination under such conditions requires some knowledge about track existencc. A track exists if it is based on target (whieh follows a speeified dynamie and detection model) measurements, and is not a product of random clutter. If a traek follows a target, wc call it a true track otherwise we eall it a false traek.

One of the most often used algorithms for data association in target traeking is Probabilistie Data Association (PDA) [1,2]. PDA uses all measurements in the validation gate (window) of the track being updated and approximates the probability distribution funetion of the target state after each update with a Gaussian probability distribution. All algorithms mentioned in the text below use the same approaeh and the same approximation.

The PDA algorithm is derived conditioned on track existence, which effectively removes the track existence information. The Integrated PDA (IPDA) [3,4,5,6,7,8] algorithm does not assumc track existenee and provides data association (PDA) formulae together with thc expressions for probability of track existence in a recursive manner. Data Assoeiation eoeffieients (denoted by β in [1]) are identical for PDA and IPDA algorithms. A different approaeh was taken in [11, 12] where it is assumed that a target exists behind eaeh traek, and the probability of pereeivability of the target is reeursively ealculated instead of the probability of the existenee of the target. That algorithm will be denoted as IPDA-DLL, where DLL are the initials of its authors.

IPDA and PDA are derived under the assumption of a single target (single track). Eaeh measuremcnt ean be either elutter or a mcasuremcnt of the target being followed. In real-life situations with multiple targets with crossing trajectories, this is no longer true. It has been shown [13,14] that PDA often gets "confused" under these circumstances and starts following a different target, or it can diverge altogether and stop following any target. To remedy this situation, the Joint PDA (JPDA) [13,14] algorithm has been created.

The JPDA algorithm allows the possibility that a measurement may have originated from one of a number of eandidate tracks or from clutter. In each scan JPDA partitions traeks into elusters, where traeks in eaeh eluster have eommon measurements. It generates all possible joint measurement to track assignments, which are ealled joint events, and ealeulates the a-posteriori probability of eaeh joint event. From these probabilities, the data assoeiation coefficients of each traek are caleulated and then used to update the traek estimates.

---

* Work supported by CSSIP Melbourne and DSTO

* Senior Research Fellow, CSSIP Melbourne, e-mail: d.musicki@ee.mu.oz.au.
** Professor, University of Melbourne, e-mail: r.evans@ee.mu.oz.au.

JPDA suffers from the same problem as PDA, since it assumes that the track(s) exist. Tracks are not differentiated according to probability of track existence, and track maintenance is difficult without probability of track existence information. It is also rather complex because it creates a joint event for each possible combination of measurement origin. Thus the number of joint events can grow very rapidly in a dense clutter situation. Another problem is that the area of each cluster is assumed to encompass the whole surveillance region.

To improve upon JPDA, the Integrated JPDAF (IJPDA) algorithm [15] has been published. It builds upon [12] and also uses the probability of target perceivability to develop recursive expressions for the a-posteriori probability of target perceivability and data association for each track. The use of target perceivability results in the number of joint events being much higher than in the case of JPDA. The IJPDA also assumes the area of each cluster to encompass the whole surveillance region.

The Joint IPDA (JIPDA) algorithm [10] is developed in a similar fashion to the IPDA algorithm. It uses the probability of track existence and results in recursive expressions for the probability of track existence and data association coefficients. The number of joint events is the same as in the case of JPDA. JIPDA uses an efficient approximation to calculate the volume of each cluster (no longer is the entire surveillance region used), and uses a better approximation for the number of false measurements within the cluster. When a cluster consists of a single track, JIPDA becomes identical to IPDA. However, it still has the same complexity as JPDA, which may preclude it from being used on all tracks in a dense clutter situation.

The algorithm presented here, as well as in [9], has a completely different approach. Instead of enumerating all possible hypothesis of measurement origin, it uses the probability of measurement origin as the conduit of inter-track information. LJIPDA processes individual tracks in multi-target situations, while allowing the possibility that measurements may have originated from targets being followed by other tracks. For each track, the probability that the measurement originated from other targets is calculated. The Linear Joint IPDA (LJIPDA) algorithm uses these probabilities to recalculate IPDA data association probabilities using measurement modified IPDA (MMIPDA), also presented here.

The number of calculations for LJIPDA is linear (hence the name) in both the number of tracks and in the number of selected measurements. Thus LJIPDA can be used on all tracks, not just the confirmed ones, even in very dense clutter situations. It performs better than IPDA in target trajectory crossing situations, while not deteriorating the basic false track discrimination properties of IPDA. This paper will present both the false track discrimination properties as well as track crossing performance, and compare these with other single-target and multi-target tracking algorithms. This is done in a dense, non-uniform clutter situation, first described in [8].

The original IPDA algorithm and its derivatives [3,4,5,6,7,8] have two models of track existence propagation. Markov Chain One recognizes two possibilities: the target either does not exist, or it exists and is visible with a probability of detection. Markov Chain Two recognizes the possibility of target existing, but not being visible, in addition to the two possibilities of the Markov Chain One. This paper will present only the Markov Chain One version of LJIPDA.

Section 1 outlines the three-step structure of the LJIPDA algorithm and details the calculation of a-priori probabilities of measurement origin for single-tracks and the calculation of the probabilities of measurement visibility for multiple tracks. Section 2 presents the details of the MMIPDA algorithm. The MMIPDA algorithm delivers the a-posteriori probabilities of each track's existence and data association coefficients. The use of the data association coefficients for track estimation is well covered in [1,2,4,13], as well as other publications, and will not be repeated in this paper. Section 3 presents simulation results illustrating the false track discrimination properties and track crossing performance of LJIPDA compared to IPDA, IPDA-DLL, IJPDA and JIPDA in a dense non-uniform clutter situation.

1. Linear Joint Integrated Probabilistic Data Association (LJIPDA)

LJIPDA is a three step algorithm.

Step one processes individual tracks: First, the candidate measurements are selected using a windowing (gating) procedure, as in [1,4,5]. Then, the algorithm calculates the probability that the track exists and the probability that the measurements have originated from the target being followed by the track (referred to below as "originated by track"), given single-track possibilities:

$$P\left\{\chi_{iMeas}^{iTrack}, \chi^{iTrack} \middle| Z^{k-1}, iTrack\right\} = P_D P_W P_{\chi,k-1} \frac{p_T^{iTrack}\left(z_{iMeas}\right)}{\sum_{meas} p_T^{iTrack}\left(z_{jMeas}\right)}, \tag{1.1}$$

where k denotes current scan, Z^{k-1} denotes set of measurements up to and not including the current scan, P_D is the probability of detection, P_W is the probability of a target measurement falling in the track window, $P_{\chi,k-1}$ is

the a-priori probability of track *iTrack* existence for scan k, and $p_T^{iTrack}(z_{iMeas})$ is the probability density function of measurement *iMeas* for track *iTrack*. Of course, the probability (1.1) is zero if track *iTrack* does not select measurement *iMeas*. The term *meas* denotes the set of all selected measurements.

Probabilities (1.1) are input to Step 2. (At least) two sensor models exist: The Infinite Resolution Sensor, where each measurement can originate from either one track or clutter only, and the Finite Resolution Sensor, where each measurement can originate from one or more tracks, as well as from clutter. Only the Infinite Resolution Sensor is presented here.

Define

$$P_{iMeas}^{iTrack} = P\left\{\chi_{iMeas}^{iTrack}, \chi^{iTrack} \middle| Z^{k-1}, iTrack\right\} \tag{1.2}$$

and let

$$P_{m,iMeas}^{iTrack} = P\left\{\chi_{iMeas}^{iTrack}, \chi^{iTrack} \middle| Z^{k-1}, tracks\right\} \tag{1.3}$$

denote the a-priori probability that measurement *iMeas* originated from the track *iTrack*, given all tracks. Then

$$P_{m,iMeas}^{iTrack} = \frac{\dfrac{P_{iMeas}^{iTrack}}{1-P_{iMeas}^{iTrack}}}{1+\sum\limits_{tracks}\dfrac{P_{iMeas}^{jTrack}}{1-P_{iMeas}^{jTrack}}}. \tag{1.4}$$

The probability that the measurement did not originate from any tracks is

$$P_{m,iMeas}^{0} = \frac{1}{1+\sum\limits_{tracks}\dfrac{P_{iMeas}^{jTrack}}{1-P_{iMeas}^{jTrack}}}. \tag{1.5}$$

The probability that the measurement *iMeas* is visible to track *iTrack*, given all tracks, is

$$P_{V,iMeas}^{iTrack} = P_{m,iMeas}^{iTrack} + P_{m,iMeas}^{0} = \frac{1+\dfrac{P_{iMeas}^{iTrack}}{1-P_{iMeas}^{iTrack}}}{1+\sum\limits_{tracks}\dfrac{P_{iMeas}^{jTrack}}{1-P_{iMeas}^{jTrack}}}. \tag{1.6}$$

2. Measurement Modified Integrated Probabilistic Data Association (MMIPDA)

The notion of probability of the measurement visibility is new for the LJIPDA and MMIPDA algorithms. All data association algorithms mentioned in this paper treat the measurement as a continuous (in coordinates) variable with binary visibility. The LJIPDA and MMIPDA algorithms treat each measurement as a continuous variable with continuous probability of visibility.

MMIPDA processes each track in isolation, using $P_{V,iMeas}^{iTrack}$ calculated in step 2 of LJIPDA. The superscript *iTrack* is omitted in most symbols in this Section for reasons of brevity. Denote by m the number of selected measurements. The expected number of selected clutter measurements is

$$\hat{m} = \sum_{meas} P_{V,jMeas}^{iTrack} - P_D P_W P_{\chi,k-1}\left(1-\prod_{meas}\left(1-P_{V,jMeas}^{iTrack}\right)\right). \tag{2.1}$$

Using V to denote the volume of selection window and

$$\delta = \begin{cases} P_D P_W & m=0 \\ P_D P_W\left(1-\dfrac{V}{\hat{m}}\sum\limits_{meas}\left(\left(P_{V,jMeas}^{iTrack}\right)^2 p_T^{iTrack}\left(z_{jMeas}\right)\right)\right) & m>0 \end{cases} \tag{2.2}$$

the expression for the a-posteriori probability of track existence in scan k becomes

$$P_{\chi,k} = \frac{1-\delta}{1-\delta P_{\chi,k-1}} P_{\chi,k-1}. \tag{2.3}$$

The conditional a-posteriori probability that the measurement *iMeas* on this scan originated from the target being tracked, provided that the track *iTrack* exists, is expressed as

$$\beta_{iMeas} = \frac{P_D P_W \frac{V}{\hat{m}} \left(P_{V,iMeas}^{iTrack}\right)^2 p_T^{iTrack}(z_{iMeas})}{1-\delta} \tag{2.4}$$

and the corresponding probability that no measurement on this scan has originated from the target being tracked is

$$\beta_0 = \frac{1 - P_D P_W}{1-\delta}. \tag{2.5}$$

Expressions (2.4 and 2.5) are used to update track estimations in the classic PDA manner [1,4].

Steps 1, 2 and 3 have number of operations, which are linear to the number of tracks and the number of measurements. Other multi-target tracking algorithms mentioned in this paper (JPDA, JIPDA, IJPDA) have number of operations which grows exponentially with the number of tracks in the cluster. In a dense clutter situation a large number of false tracks is initiated and LJIPDA uses substantially fewer resources than JIPDA, JIPDA or IJPDA. Furthermore, Steps 1 and 3 process each track separately, thus it is very easy to use parallel processing to process a large number of concurrent tracks. Step 2 appears to be a bottleneck as it deals with all tracks simultaneously; however the number of operations per track in Step 2 is small thus this overhead is not significant. If the tracks are separated in clusters, even Step 2 can be done for each cluster simultaneously.

Another benefit of using LJIPDA in a multi-target tracking situation is the ability to process each track individually. Maneuvering algorithms such as IMM, can be implemented on each track directly.

3. Simulation

The simulation experiments presented in this paper compare the LJIPDA algorithm with the IPDA, IPDA-DLL, IJPDA and JIPDA algorithms with respect to track discrimination and target crossing situations, in a heavy and non-homogenous clutter environment. The tracks are initiated automatically, using two-point differencing and initial track probability assignment as described in [7,8].

Two different clutter scenarios were implemented. The first scenario, which we refer to as the "lighter clutter environment" has a small enough clutter density to allow the JIPDA and IJPDA algorithms to be implemented on all tracks, from initiation onwards. This will allow a direct comparison of the LJIPDA, JIPDA and IJPDA algorithms. The second scenario, which we refer to as the "heavier clutter environment" has higher clutter density. In this case, JIPDA and IJPDA are computationally not feasible on all tracks; thus they are implemented on confirmed tracks only. In the case of JIPDA, IPDA is used on non-confirmed tracks and in the case of IJPDA, IPDA-DLL is implemented on non-confirmed tracks.

A two-dimensional surveillance situation was considered. The area under surveillance was 1000 m long and 400 m wide. The clutter measurements satisfied a uniform Poisson distribution with a base density with two higher clutter density patches. The high clutter density patches are rectangular with corner coordinates $(x_{min}, x_{max}, y_{min}, y_{max})$ of (330, 490, 203, 303)m and (718, 840, 100, 200)m. The heavier clutter environment has the base density of 1.0×10^{-4} $/scan/m^2$ and sevenfold clutter density in the 'patches' and the lighter clutter environment has the base density of 0.2×10^{-4} $/scan/m^2$ and fivefold clutter density in the 'patches'.

The experiments consisted of 1000 and 800 runs each for the heavier and lighter clutter situation respectively. Each run consists of 24 scans. In each simulation run target one reappears in scan 1 with an initial state of $x'(1) = [130m \quad 35m/s \quad 200m \quad 0m/s]$, and maintains constant speed thereafter. This trajectory will just edge the high-clutter areas and this will tend to 'diverge' tracks from the true trajectory and into the high intensity clutter, thus turning true tracks into false ones. Target two always follows another straight-line uniform speed trajectory, designed to intersect the first target trajectory in scan 19, with the angle of the two trajectories of 10°. The true track situation is observed on scan 14 and then again on scan 24 to determine the effects of target crossing.

The target motion is modelled in Cartesian coordinates as

$$x(k+1) = Fx(k) + v(k) \tag{3.1}$$

where $x(k)$ is the target state vector at time k and consists of the position and the velocity in each coordinate

$$x' = [x \quad \dot{x} \quad y \quad \dot{y}] \tag{3.2}$$

with the transition matrix F of

$$F = \begin{bmatrix} F_T & 0 \\ 0 & F_T \end{bmatrix}; \qquad F_T = \begin{bmatrix} 1 & T \\ 0 & 1 \end{bmatrix} \tag{3.3}$$

where T is the sampling period of 1s. The plant noise $v(k)$ is the zero-mean white Gaussian noise with covariance

$$E[v(k)v(j)'] = Q\delta(k,j) \tag{3.4}$$

where $\delta(k,j)$ is the Kronecker delta function and

$$Q = q\begin{bmatrix} Q_T & 0 \\ 0 & Q_T \end{bmatrix}; \qquad Q_T = \begin{bmatrix} T^4/4 & T^3/2 \\ T^3/2 & T^2 \end{bmatrix} \tag{3.5}$$

with $q = 0.75$.

The detection probability was 0.9 throughout the experiment and the sensor introduced independent errors in x and y coordinates with the root mean square of 5m. The tracking estimation filter was a simple Kalman filter based on the described trajectory and sensor models. The selection window size for both algorithms was chosen so that the a-priori windowing probability P_W was 0.9999. The algorithms used a Markov Chain One track existence propagation model with parameters

$$\begin{aligned} p_{11} &= 0.98; \quad p_{21} = 0; \\ p_{12} &= 0.02; \quad p_{22} = 1. \end{aligned} \tag{3.6}$$

After initialization, tracks evolve according to the algorithm simulated, as discussed above. The tracks get confirmed if the probability of track existence exceeds the confirmation threshold and are terminated if the probability falls below the termination threshold. Termination thresholds were kept separate for confirmed and unconfirmed tracks. Thresholds were optimized separately for each algorithm. For reasons of simplicity, the thresholds were kept constant during each simulation experiment, although better results would be obtained if they were made dependent on track 'age'. The sum of confirmed false track scans was approximately equal for each simulation experiment, and in the vicinity of 600 over 24000 scans in each of the heavier clutter simulation experiments and about 100 over 19200 scans in each of the lighter clutter experiments.

The track discrimination performance of LJIPDA, JIPDA, IJPDA, IPDA and IPDA-DLL are illustrated in Figures 1 and 2 (heavier clutter) and 3 and 4 (lighter clutter). Each curve shows the number of scans in which a confirmed track using one of the algorithms was following one of the targets. The horizontal axis depicts the time in scans from the start of the simulation run.

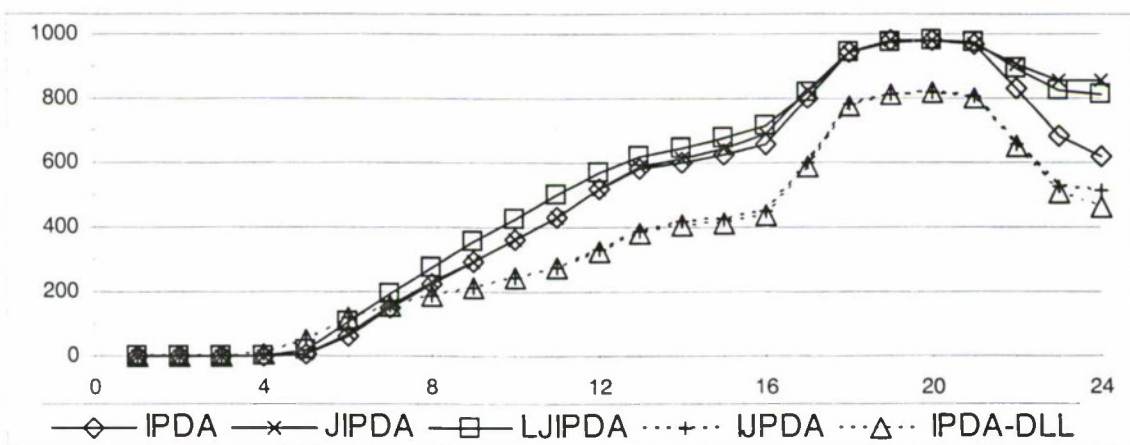

Fig. 1. Target One Discrimination Comparison – The Heavier Clutter Situation (1000 runs)

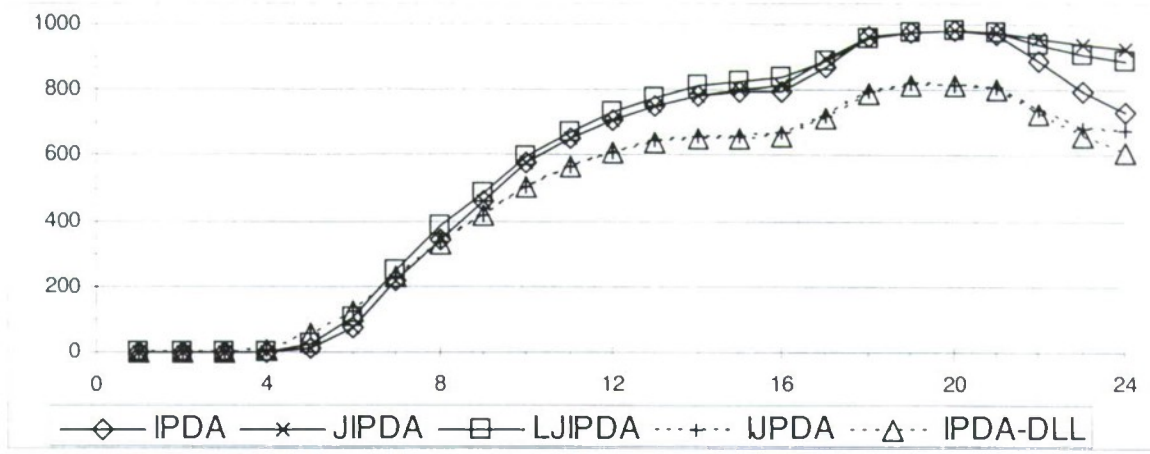

Fig. 2. Target Two Discrimination Comparison – The Heavier Clutter Situation (1000 runs)

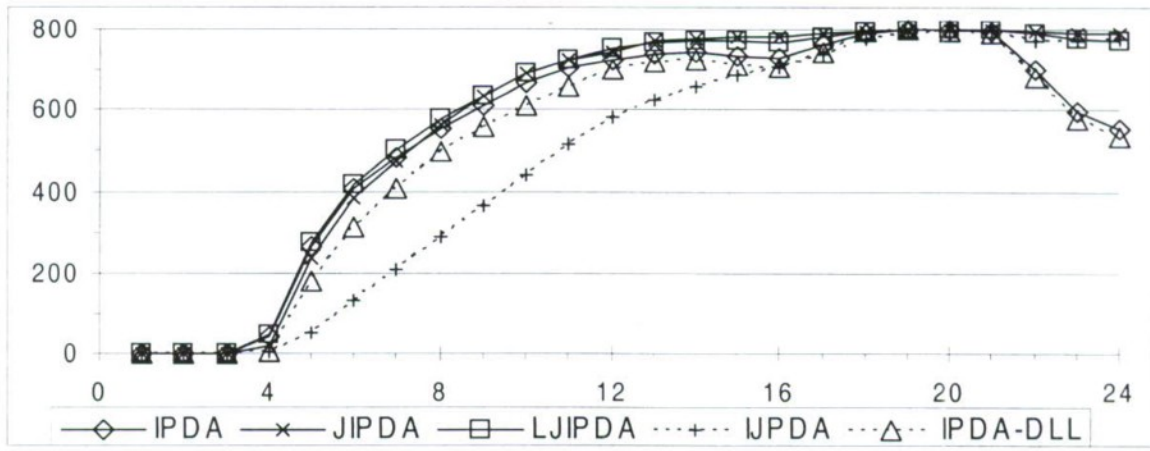

Fig. 3.Target One Discrimination Comparison – The Lighter Clutter Situation (800 runs)

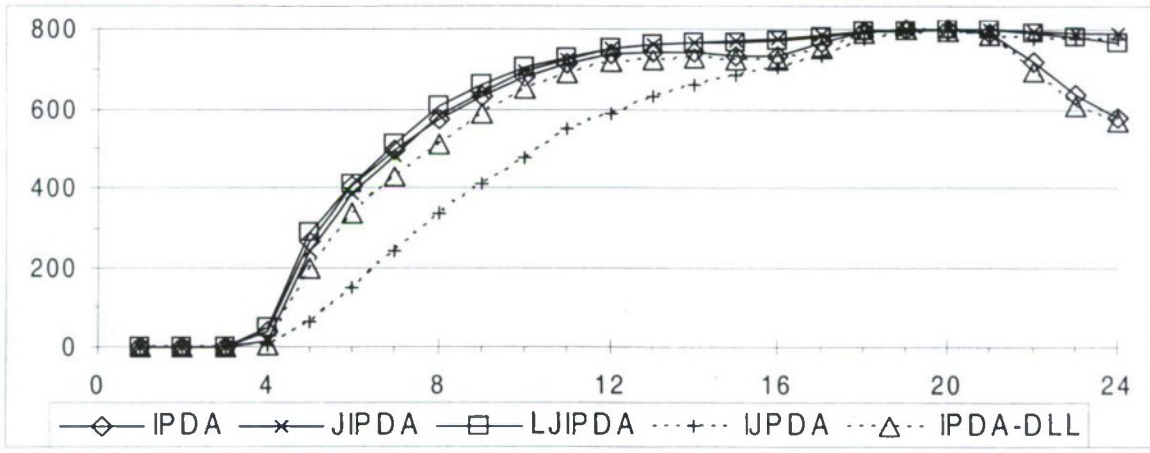

Fig. 4.Target Two Discrimination Comparison – The Lighter Clutter Situation (800 runs)

The target crossing performance of the LJIPDA, JIPDA, IJPDA, IPDA and IPDA-DLL algorithms are shown in Table 1 and 2 for the heavier and lighter clutter situation respectively. Only the cases where two confirmed

tracks were following each of the two targets at scan 14 were considered. Five possible outcomes were recognized on scan 24:

(a) Both tracks continue to follow their original targets,
(b) Only one track continues to follow the original target. The fate of the other target is irrelevant,
(c) Both tracks switch targets,
(d) One track switches a target, the other tracks becomes false or terminated,
(e) Both tracks become false or terminated.

Table 1. 10° trajectory intersection results – the heavier clutter case

	LJIPDA	*JIPDA*	*IJPDA*	*IPDA*	*IPDA-DLL*
Total	*530*	*487*	*280*	*478*	*271*
(a)	*504*	*470*	*271*	*230*	*186*
(b)	*24*	*17*	*6*	*225*	*84*
(c)	*0*	*0*	*2*	*0*	*0*
(d)	*2*	*0*	*1*	*17*	*1*
(e)	*0*	*0*	*0*	*6*	*0*

Table 2. 10° trajectory intersection results – the lighter clutter case

	LJIPDA	*JIPDA*	*IJPDA*	*IPDA*	*IPDA-DLL*
Total	*741*	*747*	*540*	*685*	*655*
(a)	*694*	*738*	*533*	*316*	*301*
(b)	*47*	*9*	*6*	*327*	*322*
(c)	*0*	*0*	*1*	*0*	*0*
(d)	*0*	*0*	*0*	*27*	*21*
(e)	*0*	*0*	*0*	*15*	*11*

The LJIPDA algorithm clearly improves the IPDA algorithm in track-crossing situations and the false track discrimination performance of IPDA. It was observed during the simulations that LJIPDA adds insignificant time to the IPDA simulations, and can be used in much denser clutter situations than either JIPDA or IJPDA. In the lighter clutter density simulations, JIPDA uses significantly (order of magnitude) less CPU time than IJPDA.

It should also be noted that the track crossing statistics from Table 1 and 2 are not completely fair. IJPDA and IPDA-DLL algorithms manage to confirm a significantly smaller number of tracks. These tracks are generated with better measurement data statistics (detection and measurement noise), thus they have better quality tracks as input to the trajectory intersection situations than IPDA, JIPDA and LJIPDA.

Conclusions

1. The LJIPDA algorithm for multi-target tracking has been presented.
2. This algorithm uses a new approach (probability of measurement origin) to model inter-track influence.
3. The number of LJIPDA operations is linear in number of tracks and number of measurements. The number of operations of other multi-target tracking algorithms is exponential.

4. The simulations have shown the advantages of using LJIPDA in multi-target situations, where it has been shown to perform better than IPDA, comparable to JIPDA, and much better than IJPDA and IPDA-DLL.

References

1. **Bar-Shalom Y., Tse E.** Tracking in a cluttered environment with Probabilistic Data Association. *Automatica*, vol. 11, pp 451-460, Sept. 1975.
2. **Bar-Shalom Y.** Tracking Methods in a Multitarget Environmen, *IEEE Trans. Automatic Control*, Vol.23, No.4, 1978.
3. **Mušicki D., Evans R.** Integrated probabilistic data association - finite resolution, *32nd IEEE Conference on Decision and Control*, San Antonio, Texas, Dec.16-18, pp. 912-917, 1993.
4. **Mušicki D., Evans R., Stanković S.**, Integrated probabilistic data association (IPDA), *IEEE Trans. Automatic Control*, AC-39, no. 6, pp 1237-1241, June 1994.
5. **Mušicki D.** Automatic tracking of maneuvering targets in clutter using IPDA, *PhD thesis*, University of Newcastle, New South Wales, Australia, Sept 1994.
6. **Mušicki D., Evans R.** Integrated probabilistic data association - finite resolution, *Automatica*, Vol. 31, pp 559-570, April 1995.
7. **Mušicki D., Evans R.** Data Association using clutter map information, *WOSPA conference*, Brisbane, Australia, December 1997.
8. **Mušicki D., Evans R.**, Clutter Map Information for Data Association and Track Initialization, Submitted for publishing, *IEEE Trans. Aerospace and Electronic Systems*.
9. **Mušicki D., Evans R.** Track Decoupling: Linear Joint IPDA (LJIPDA) and Milti Target Linear JIPDA (MLJIPDA), *IEEE IDC 2002 Conference*, Adelaide, South Australia, Feb. 11-13, 2002.
10. **Mušicki D., Evans R.** Joint Integrated Probabilistic Data Association – JIPDA, *Submitted for FUSION 2002 conference*.
11. **Colegrove S. B., Ayliffe J. K.** An extension of Probabilistic Data Association to Include Track Initiation and Termination, *20th IREE International Convention*, Melbourne, pp 853-856, 1985.
12. **J. Dezert, Li N., Li X. R.** *A New Formulation of IPDAF for Tracking in Clutter, European Control Conference (ECC99)*, Karlsruhe, Germany, Sept. 1999.
13. **Formann T.E., Bar-Shalom Y., Scheffe M.** Sonar Tracking of Multiple Targets Using Joint Probabilistic Data Association, *IEEE Jonrn. Oceanic Engineering*, OE-8, No.3, pp 173-183, July 1983.
14. **Chang K.C., Bar-Shalom Y.** Joint Probabilistic Data Association for Multitarget Tracking with Possibly Unresolved Measurements and Maneuvers, *IEEE Trans. Automatic Control*, AC-29, pp 585-594, July 1984.
15. **Dezert J., Li N., Li X. R.** Theoretical development of an Integrated JPDAF for multitarget tracking in clutter, *Proc. Workshop ISIS-GDR/NUWC*, ENST, Paris, 1998.

AN INTEGRATED ANGULAR MOTION CONTROL SYSTEM FOR A REMOTE SENSING SATELLITE

G.P. Anshakov [**], Yu.G. Antonov [**], A.I. Manturov [***], Yu.M. Ustalov [****]
State Research and Production Space Rocket Center TsSKB-Progress
Samara, Russia
B.Ye. Landau [*****], V.G. Peshekhonov [******]
State Scientific Center of Russian Federation –Central Research Institute Elektropribor
St. Petersburg, Russia

Abstract

The main aspects of the development of an angular motion control system for a remote sensing satellite that provides imaging of observation routes lying arbitrarily to the satellite flight track are considered in the paper. The problems concerned with preparation of satellite angular motion control programs are discussed. The functional diagram of the satellite angular motion control system that is responsible for autonomous preparation of control programs (using satellite navigation) and their implementation by the attitude control system based on highly sensitive inertial sensors is presented.

Key words: angular motion, observation route, inertial system

Present-day low-orbit remote sensing satellites (RSS) are equipped with control systems intended to image strips on the Earth surface - observation routes lying, as a rule, along a flight track. The practical problems the users of sensing data have to solve at present have motivated the necessity to image observation routes of different configurations that lie arbitrarily to the flight track [1]. The requirements have increased: high-quality on-demand information about local areas of the Earth surface should be obtained with observation equipment (OE) with a swath from a few to ten kilometers. The remote sensing satellite RESURS-DK, shown in Fig. 1, was designed to obtain information that meets these requirements [2]. The programs for the satellite angular motion are specified by location of routes relative to flight tracks and conditions for their scanning with the OE swath.

The efficiency of remote sensing depends both on how accurate and efficient the program for the angular motion of the satellite is and on the parameters of the satellite attitude control system that implements this program during the flight. Included in the satellite onboard control complex, the integrated angular motion control system for the remote sensing satellite was specifically developed to provide efficient remote sensing. This system is intended to determine parameters of the satellite center-of-mass motion, prepare an angular motion control program on the sensing interval by specified characteristics of routes and implement this program with a required accuracy.

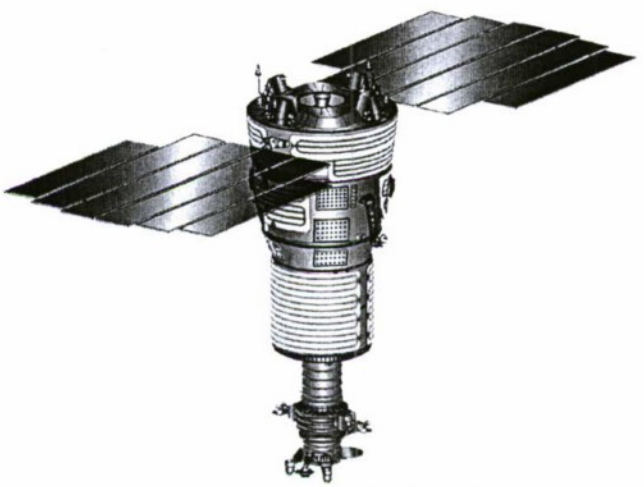

Fig. 1. The satellite RESURS - DK

At the beginning let us consider the problem on autonomous preparation of an angular motion program for imaging of observation routes in the following statement.

The statement of the problem on preparation of an angular motion program. Let the motion of the RSS center of mass be described in a rectangular geocentric inertial coordinate system (ICS) O_3XYZ by the system of differential equations given in /6/, provided the initial conditions of the motion $\bar{r}(t_\circ)=\bar{r}_\circ$, $\bar{V}(t_\circ)=\bar{V}_\circ$ are known at an instant of time t_0, where $\bar{r}$ - the radius-vector, and $\bar{V}$ - the satellite velocity vector.

---

[*] Corresponding Member of Russian Academy of Sciences, First Deputy General Designer of the Center;
[**] Doctor of Technical Sciences, Deputy General Designer of the Center;
[***] Doctor of Technical Sciences, Head of Department;
[****] Deputy Head of Department;
[*****] Doctor of Technical Sciences, Deputy Director of Research Subsidiary;
[******] Academician of the Russian Academy of Sciences, Director of the Institute.

To determine the satellite angular motion programs during sensing, let us enter the program coordinate system (PCS) (Fig. 2). The PCS center is coincident with the satellite center of mass; the axis $OY_П$ is opposite to the line of sighting that originates in the satellite center of mass and is directed to the observed point of the route center line, i.e., it is opposite to the vector of the distance $\overline{D}$ from the satellite center of mass to the observed point on the Earth surface; suppose that the optic axis of the OE is fixed relative to a certain satellite-fixed coordinate system and the vector $\overline{D}$ determines the program position of the OE optic axis; the axis $OX_П$ is parallel with the vector $\overline{W}$ - the vector $\overline{W}_м$ projection of the relative velocity of the intersection point of the line of sighting and the Earth surface at the route level onto the plane perpendicular to the line of sighting; the axis $OZ_П$ complements the system to the right one. The projections of the vector $\overline{W}$ onto the axes $OX_П$ and $OZ_П$ are denoted, respectively, as $W_{x_П}$ and $W_{z_П}$. The program coordinate system is assumed to determine the required angular motion of the satellite-fixed coordinate system on routes and interroute intervals at each instant of time. Also suppose that the plane of the satellite -fixed coordinate system corresponding to the plane $X_ПOZ_П$ is parallel to the focal plane of the OE lens, and the axis of the satellite-fixed coordinate system relative to the plane axis $OX_П$ has the same direction as the image motion compensation rate Vk realized in the observation equipment and defined by the relation:

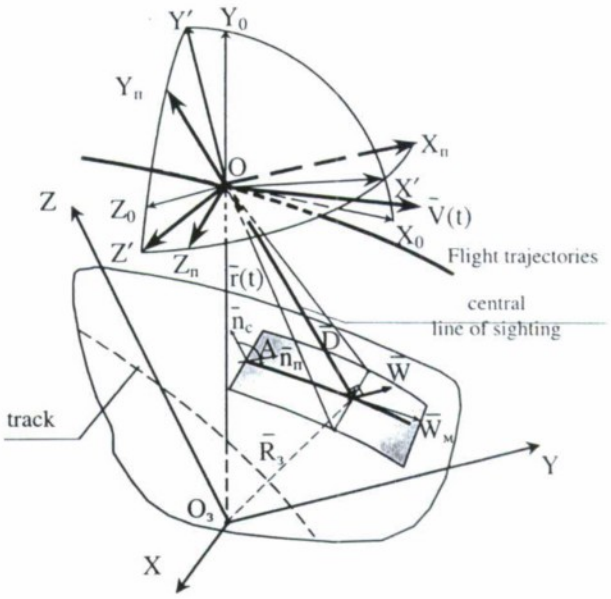

Fig. 2. Coordinate system

$V_k = f\dfrac{W_{x_П}}{D}$, where f is a focal distance of the OE lens.

The axes of the orbital coordinate system ($OX_oY_oZ_o$) given in Figure 2 are directed just as those in /6/.

The satellite angular motion control program will be specified by a matrix of direction cosines Q (t), vectors of absolute angular velocity $\overline{\omega}(t)$ and acceleration $\overline{\varepsilon}(t)$ of the PCS axes in the ICS. The specified orts of the PCS axes, their angular velocities and accelerations relative to the ICS for each instant of time completely determine the satellite angular motion program, i.e. the satellite attitude control program on required flight intervals /4/.

Let there be specified a set of time-ordered routes on a certain time interval of the satellite flight (sensing interval). Each route is specified by a set of characteristics:

$$\left\{\varphi^м, \lambda^м, A, \tau, \vartheta_н, \Delta H, \left(W_{x_П}/D\right)^{зад}\right\}_i, \; i=\overline{1,I} - \text{a route number}, \tag{1}$$

where: $\varphi^м, \lambda^м$ - the latitude and longitude of the initial point of the central route line, A – the azimuth of the central route line, t – the route observation time, ΔH – an average elevation above the global ellipsoid on the route, $\left(W_{x_П}/D\right)^{зад}$ - the parameter determining the required image motion velocity for the central line of the route, $\vartheta_м$ - the specified pitch angle at the beginning of the route observation.

Also specified are the conditions that are to be fulfilled during preparation of the satellite angular motion program on the route intervals for the average route line:

$$W_{x_П}/D = \left(W_{x_П}/D\right)^{зад} = const; \; W_{z_П}/D = 0 \tag{2}$$

There are some constraints on ranges allowable for PCS program angles of rotation with respect to the OCS in pitch g, roll γ and yaw ψ:

$$\vartheta_{min} \le \vartheta \le \vartheta_{max}, \; \gamma_{min} \le \gamma \le \gamma_{max}, \; \psi_{min} \le \psi \le \psi_{max}, \tag{3}$$

as well as on allowable values of the PCS angular velocity module $\left|\overline{\omega}(t)\right|$ and acceleration $\left|\overline{\varepsilon}(t)\right|$ with respect to the ICS:

$$\left|\overline{\omega}(t)\right| \le \omega^{max}, \; \left|\overline{\varepsilon}(t)\right| \le \varepsilon^{max}. \tag{4}$$

The instants of time at which scanning of each route $t^{K}_{M_i}$ is to start were determined for the characteristics of routes (1) on the sensing interval $[t_H, t_K]$, depending on different specified conditions, for example, the instants at which the initial points of routes are coincident with the satellite traverse plane, or with the plane that makes a specified yaw angle with the traverse plane. The instants of time $t^{K}_{M_i}$ at which scanning ends are determined as $t^{K}_{M_i} = t^{H}_{M_i} + \tau_i$.

The problem on preparation of the satellite angular motion control program for a sensing interval is formulated as follows /4/.

For a specified sequence of routes $i = \overline{1,I}$ with the characteristics (1) to define on route and interroute intervals from $[t_H, t_K]$ the satellite angular motion control program as a matrix for the direction cosines Q (t), angular velocity vector $\bar{\omega}(t)$, vector of angular acceleration $\bar{\varepsilon}(t)$ of the program coordinate system in the ICS, provided the conditions (2), conditions of continuity of the function $\varepsilon(t)$ and constraints (3), (4) are fulfilled.

The scheme of solution. The parameters Q (t), $\bar{\omega}(t)$, $\bar{\varepsilon}(t)$ for the satellite angular motion control program (AMCP) on the sensing interval $[t_H, t_K]$ are generated in accordance with the scheme given below for time intervals corresponding to route imaging and interroute intervals.

The satellite angular motion control program is prepared for each route in the following steps:

knowing the radius-vector and velocity vector of the satellite center of mass $\bar{r}_\circ, \bar{V}_\circ$ in the ICS at the moment $t_\circ$, it is possible to predict their values at the instant of time at which the route begins $t^{K}_{M_i}$. The specified route characteristics (1) and motion parameters $\bar{r}\left(t^{H}_{M_i}\right)$, $\bar{V}\left(t^{H}_{M_i}\right)$ allow calculating:

-- the distance to the initial point of the route

$$\bar{D}(t^{H}_{M_i}) = \bar{R}_{З_\circ}(\varphi^{M}, \lambda^{M}, \Delta H) - \bar{r}(t^{H}_{Mi}); \tag{5}$$

-- the unit vector of the route scanning direction

$$\bar{l}_m(t^{H}_{M_i}) = \bar{n}_в \sin A - \bar{n}_c \cos A, \tag{6}$$

where: $\bar{n}_в = \left\{-\sin\lambda^{M}, \cos\lambda^{M}, 0\right\}$ - the unit vector of the route direction to the east;

$\bar{n}_c = \left\{\bar{R}_З \times \bar{n}_в \Big/ \left|\bar{R}_З \times \bar{n}_в\right|\right\}$ - the unit vector of the route direction to the north;

-- the unit vectors of the PCS axes in the ICS:

$$\bar{Y}_П = -\frac{\bar{D}}{|\bar{D}|}, \quad \bar{Z}_П = \frac{\bar{l}_m \times \bar{Y}_П}{\left|\bar{l}_m \times \bar{Y}_П\right|}, \quad \bar{X}_П = \bar{Y}_П \times \bar{Z}_П \tag{7}$$

-- the PCS orientation angles relative to the ICS, namely: roll γ, pitch g and yaw ψ angles

$$\gamma = \arcsin\left(\bar{Y}_П \cdot \bar{n}\right), \vartheta = -\arcsin\left(\frac{\bar{Y}_П \cdot \bar{\tau}}{\cos\gamma}\right); \quad \psi = -\arcsin\left(\frac{\bar{X}_П \cdot \bar{n}}{\cos\gamma}\right); \tag{8}$$

The distance $\bar{D}$ to the specified point of the central line of the route with a time increment of Δt is calculated by the formula

$$\bar{D}_{j+1} = \bar{R}_{З_{j+1}} - \bar{r}(t_{j+1}), \tag{9}$$

where $t_{j+1} = t^{H}_{M_i} + j\Delta t$; $j = \overline{0,J}$, $J = \tau/\Delta t$.

$$\bar{R}_{З\,j+1} = k\left(\bar{R}_{З\,j} + \bar{W}_{m_j}\Delta t\right), \quad \bar{W}_{m_j} = \bar{D}_j\left(W_{x_П}/D\right)^{зад} \cdot \bar{l}_{m_j}$$

k – the reduction factor of the current route point coordinates to the surface of the global ellipsoid with allowance for ΔH;

$\bar{l}_{m_j}$ -- the unit direction vector of scanning of the line of sighting along the route at the moment t_j.

The PCS orientation angles ϑj, γj, ψj in the ICS at the moments t_j are determined by the formulas (7), (8) by substituting $\overline{D}_{j+1}$ in them. Based on the orientation angle values obtained in the ICS for each route interval, the functional dependencies γ(t), ϑ(t), ψ(t) are determined as polynomials of degree *n* with a required accuracy, and then, by selected polynomials, their derivatives - $\dot{\gamma}(t)$, $\dot{\vartheta}(t)$, $\dot{\psi}(t)$, $\ddot{\gamma}(t)$, $\ddot{\vartheta}(t)$, $\ddot{\psi}(t)$. These time functions allow determining the control program parameters with the required increment at the required instant *t* - matrix Q (t) using relations (7), as well as the values $\overline{\omega}(t)$, $\overline{\varepsilon}(t)$ by transferring the parameters $\dot{\gamma}(t)$, $\dot{\vartheta}(t)$, $\dot{\psi}(t)$, $\ddot{\gamma}(t)$, $\ddot{\vartheta}(t)$, $\ddot{\psi}(t)$ from the OCS (orbital coordinate system) into ICS at the moment *t*.

The satellite angular motion program on interroute intervals (intervals of reorientation $\left[t_{\text{п}}^{н}, t_{\text{п}}^{к}\right]_n$, $n = \overline{1,\text{N}}$, where n – the number of interroute intervals) is prepared as follows: the angular motion control program Q (t), $\overline{\omega}(t)$ and $\overline{\varepsilon}(t)$ is determined on the basis of continuity and differentiability of angular velocities and accelerations on these intervals with fulfillment of edge conditions at the beginning and the end of each interroute interval. Edge conditions are the parameters of the angular motion control program at the moment at which the current route $t_{\text{м}_i}^{к}$ ends and at the moment at which the following route $t_{\text{м}_{i+1}}^{к}$ begins in the OCS, specified in the following way:

$$\begin{aligned} t_{\text{п}}^{н} &= t_{\text{м}_i}^{к}, \quad \varphi_{l\,\text{п}}^{н} = \varphi_l\left(t_{\text{м}_i}^{к}\right), \quad \dot{\varphi}_{l\,\text{п}}^{н} = \dot{\varphi}_l\left(t_{\text{м}_i}^{к}\right), \quad \ddot{\varphi}_{l\,\text{п}}^{н} = \ddot{\varphi}_l\left(t_{\text{м}_i}^{к}\right), \\ t_{\text{п}}^{к} &= t_{\text{м}_{i+1}}^{н}, \quad \varphi_{l\,\text{п}}^{к} = \varphi_l\left(t_{\text{м}_{i+1}}^{н}\right), \quad \dot{\varphi}_{l\,\text{п}}^{к} = \dot{\varphi}_l\left(t_{\text{м}_{i+1}}^{н}\right), \quad \ddot{\varphi}_{l\,\text{п}}^{к} = \ddot{\varphi}_l\left(t_{\text{м}_{i+1}}^{н}\right), \end{aligned} \tag{10}$$

where: $l = 1, 2, 3$, $\varphi_1 = \gamma$, $\varphi_2 = \vartheta$, $\varphi_3 = \psi$.

Generally, the angular motion control program on the reorientation interval $T = t_{\text{п}}^{к} - t_{\text{п}}^{н}$ can consist of: an acceleration stage $\Delta t_1 = \Delta\bar{t}$, stage of motion with a constant (in the OCS) angular velocity on the interval $\Delta t_2 = T - 2\Delta\bar{t}$ and deceleration stage $\Delta t_3 = \Delta t_1 = \Delta\bar{t}$. In the case that $\Delta t_2 = 0$ the functions φ_l are determined as polynomials of degree 5:

$$\varphi_l = \sum_{n=0}^{5} A_l^{(n)}\left(t - t_{\text{п}}^{н}\right)^n, \text{ where } t \in \overline{t_{\text{п}}^{н}, t_{\text{п}}^{к}} \tag{11}$$

Polynomial factors are evaluated by the formulas:

$$\begin{aligned} A_l &= \varphi_{\kappa_i}; A_1^{(1)} = \dot{\varphi}_{\kappa_i}; \quad A_1^{(2)} = \frac{1}{2}\ddot{\varphi}_{\kappa i} \\ A_l^{(3)} &= \frac{10}{T^3}\left(\varphi_{l_{\text{п}}}^{к} - \varphi_{l_{\text{п}}}^{н}\right) - \frac{4}{T^2}\left(\dot{\varphi}_{l_{\text{п}}}^{к} + \frac{3}{2}\dot{\varphi}_{l_{\text{п}}}^{н}\right) + \frac{1}{T}\left(\ddot{\varphi}_{l_{\text{п}}}^{к} - 3\ddot{\varphi}_{l_{\text{п}}}^{н}\right) \\ A_l^{(4)} &= \frac{15}{T^4}\left(\varphi_{l_{\text{п}}}^{к} - \varphi_{l_{\text{п}}}^{н}\right) + \frac{7}{T^2}\left(\dot{\varphi}_{l_{\text{п}}}^{к} + \frac{8}{7}\dot{\varphi}_{l_{\text{п}}}^{н}\right) + \frac{1}{T}\left(\frac{3}{2}\ddot{\varphi}_{\kappa_i} - \ddot{\varphi}_{н_i}\right) \\ A_l^{(5)} &= \frac{6}{T^5}\left(\varphi_{l_{\text{п}}}^{к} - \varphi_{l_{\text{п}}}^{н}\right) - \frac{3}{T^4}\left(\dot{\varphi}_{l_{\text{п}}}^{к} + \dot{\varphi}_{l_{\text{п}}}^{н}\right) + \frac{1}{T^3}\left(\ddot{\varphi}_{l_{\text{п}}}^{к} - \ddot{\varphi}_{l_{\text{п}}}^{н}\right) \end{aligned} \tag{12}$$

Given the stage Δt_2, the angular velocity values of the PCS in the OCS φ_l, $l = 1, 2, 3$ for this stage are determined by the formula:

$$\tilde{\dot{\varphi}}_l = \frac{-\varphi_{l_{\text{п}}}^{к} + \varphi_{l_{\text{п}}}^{н} - 2\kappa\dot{\varphi}_l^{cp}\cdot\Delta\bar{t}}{T - 2\Delta\bar{t}}, \tag{13}$$

where: $\dot{\varphi}_l^{cp} = \dfrac{-\varphi_{l_{\text{п}}}^{к} + \varphi_{l_{\text{п}}}^{н}}{T}$, k – a certain scale factor.

Thus, at aeeeleration and deceleration stages the functions φ_l, $l = 1, 2, 3$ are determined as polynomials of degree 5 (11), (12), only in these relations T is substituted for Δt. The boundary conditions at the moment at whieh the acceleration stage ends and at the moment at whieh the deeeleration stage begins are as follows:

$$\begin{aligned} &\varphi_l\left(t_{\text{п}}^{н} + \Delta\bar{t}\right) = \varphi_{l\,\text{п}}^{н} + \kappa\dot{\varphi}_l^{ср} \cdot \Delta\bar{t}, \quad \dot{\varphi}_l\left(t_n^{н} + \Delta\bar{t}\right) = \tilde{\dot{\varphi}}_l, \quad \ddot{\varphi}_l\left(t_n^{н} + \Delta\bar{t}\right) = 0; \\ &\varphi_l\left(t_{\text{п}}^{к} - \Delta\bar{t}\right) = \varphi_{l\,\text{п}}^{к} - \kappa\dot{\varphi}_l^{ср} \cdot \Delta\bar{t}, \quad \dot{\varphi}_l\left(t_n^{к} - \Delta\bar{t}\right) = \tilde{\dot{\varphi}}_l, \quad \ddot{\varphi}_l\left(t_n^{к} - \Delta\bar{t}\right) = 0. \end{aligned} \tag{14}$$

The control program parameters Q (t), $\bar{\omega}(t)$ and $\bar{\varepsilon}(t)$ in the ICS for interroute intervals are evaluated for the required instant of time using relations (11) - (14), just the way they were evaluated on routes.

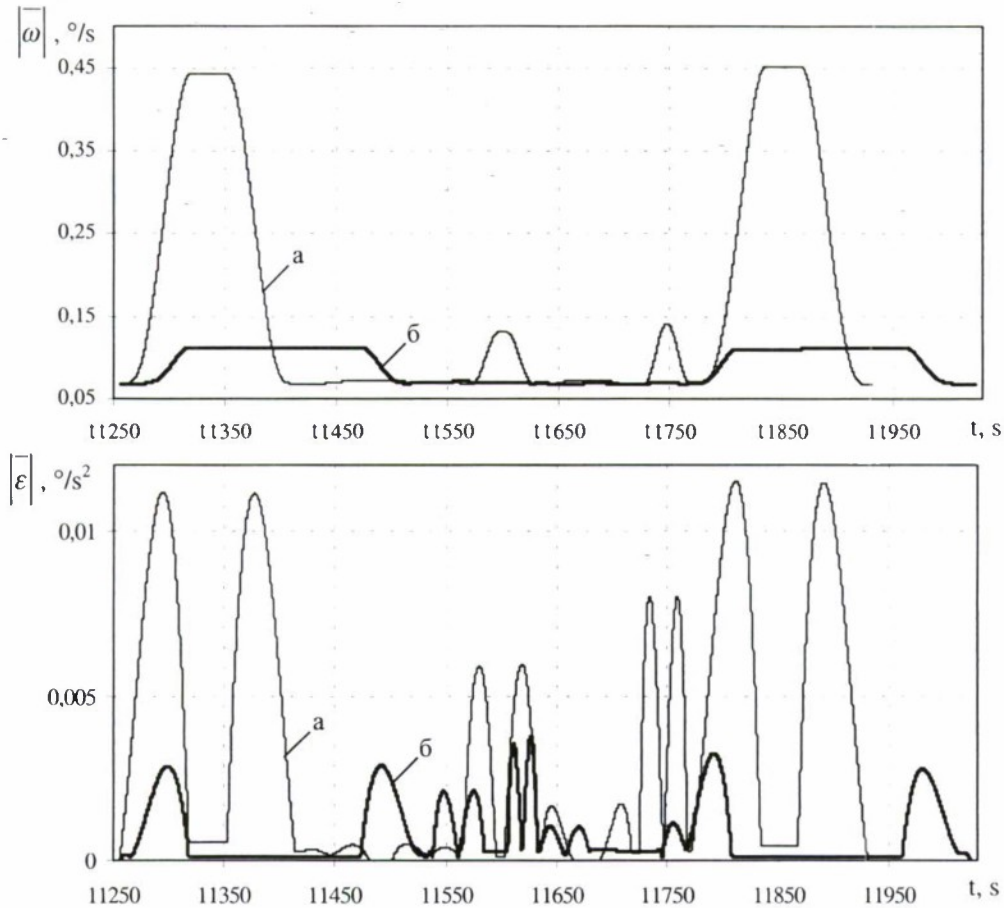

Fig. 3.

Fig. 3 illustrates $|\bar{\omega}(t)|$ and $|\bar{\varepsilon}(t)|$ relations on a sensing interval for two AMCP versions:

а) observation of five routes with roll angles from 38 to 43°;

б) observation of four routes with roll angles from -18 up to -19°.

The functional diagram of the angular motion control system. The development of the angular motion control system that implements the above-mentioned control programs is based on the effeetive realization of the satellite funetional capabilities. RESURS – DK must satisfy the following requirements to:

- aeeuraey of the program trajeetories developed and their aeeurate tracking;
- dynamie eharaeteristies of program trajeetories, namely, ranges of angular velocities and aeeelerations;
- minimization of mass, power consumption, eost of the equipment, etc.

These requirements have motivated the use of the most promising measuring, sensing and actuating elements for the eontrol system.

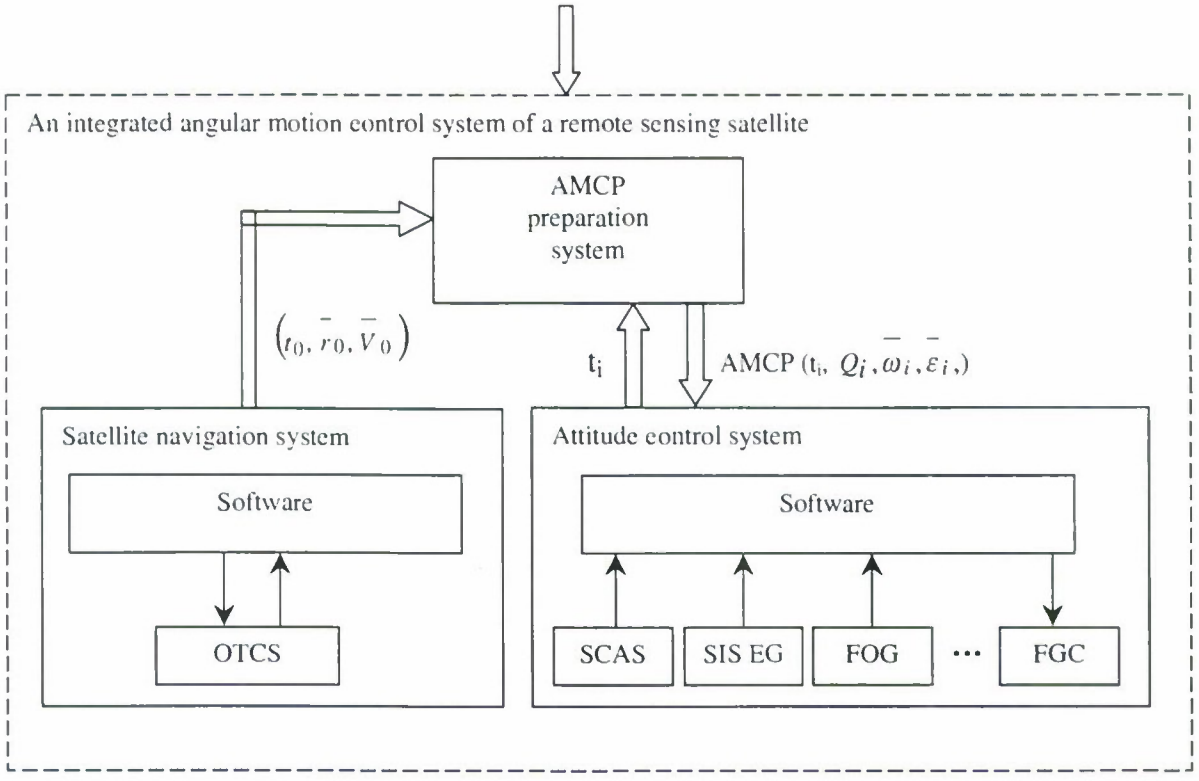

Fig. 4 .The functional diagram of the satellite angular motion control system

As a subsystem, the satellite angular motion control system, presented in Fig. 4 as a functional diagram, consists of three systems: the AMCP preparation system, satellite navigation system and attitude control system.

Making use of the initial data about the satellite operation program on the interval $[t_o, t_n]$ with account of the current state of the satellite onboard system, the AMCP preparation system is intended to organize control of the navigation system with the aim to obtain current parameters of the satellite center-of-mass motion, solve ballistic and navigation problems, organize control of the attitude control system in its implementing the program trajectories developed.

The major principles of preparation of angular motion control programs that ensure efficient sensing can be formulated, in brief, as follows:

- use of the satellite center-of-mass motion parameters determined by the navigation system for the instant of time, closest to the beginning of the calculated interval of the route imaging, to determine the angular motion control programs;
- preparation of satellite angular motion control programs (program motion) that meet the requirements to accuracy in determination of the image motion compensation rate on the central route line and to continuity of control program parameters during the flight both on routes and between imaging routes.

The basic factor on which the accuracy of control programs depends is the accuracy of navigational data used. In this connection the time interval, for which a program trajectory can be prepared, depends on the intervals for which motion parameters are predicted with allowable accuracy. To meet the requirements to the prediction accuracy, the parameters for the satellite center-of-mass motion must be periodically updated. This process, ensuring high accuracy of motion parameters, is implemented within the navigation system and prediction of the center-of-mass motion parameters on the basis of high-accuracy motion models. The satellite center-of-mass motion parameters determined with the Consumer Navigation Equipment (CNE) that makes use of the radio navigation system GLONASS are used as primary navigation information by the navigation system /5/. Statistical processing of the primary navigational data obtained allows increasing the accuracy of motion parameters and use them on forecasting intervals of up to 1-1.5 circuits of the satellite flight. After the data from CNE is periodically processed by the dynamic filtring method, the center-of-mass motion parameters obtained by the navigation system are used in the algorithms for ballistic and navigation problems to determine the satellite angular motion control program on planned imaging intervals. An Onboard Time-Coordinate Synchronizer (OTCS) is used in the system as CNE.

Tracking of the prepared program angular motion trajectory is implemented by the attitude control system. A Strapdown Inertial System based on an Electrostatic Gyroscope (SIS EG) /6/ is used to provide high-accuracy tracking of the satellite angular motion program trajectory in this system as a sensor of angular position of coordinate trihedron related to the satellite with regard to a stored base inertial coordinate.

This system has the highest characteristics in comparison with the other sensing elements used. The results of the SIS EG development in /7/ and /8/ concerning, in particular, the construction, configuration, drift models, algorithms used to solve the problem on determination of satellite angular orientation have shown that it is possible to obtain the drift of the inertial trihedron of no worse than 10^{-4} ... 10^{-5} deg/h, and angular position accuracy - no worse than 30 arc s. High-accuracy performance of the SIS EG was verified experimentally in space conditions. To verify the potential accuracy of a gyroscope operating under zero-gravity conditions, one usually needs to carry out mathematical simulation (for the majority of various gyroscopes). In this case the accuracy of the problem solution depends on the quality of the applied drift model that takes into account the influence of absolute accelerations on the gyroscope drift. Physical simulation of zero-gravity conditions in ground tests require either conditions that provide supersmall accelerations or conditions for tests with controllable change of parameters of the gyroscope drift model

$$\left\{\varphi^{M}, \lambda^{M}, A, \tau, \vartheta_{H}, \Delta H, \left(W_{x_{\Pi}}/D\right)^{\text{разб}}\right\}_{i} \quad \text{for } [t_{O}, t_{K}].$$

Thus, the estimation of the apparent rotor motion under these conditions is compared with the theoretically expected program motion. The coincidence of the gyroscope drift implementations with the program motion lends support to the validity of the drift model used and therefore allows a reliable prediction for the accuracy under zero-gravity conditions.

The SIS EG drift model presented in /7/ includes parameters that depend on the level of the reference voltage in the channels of the rotor electrostatic suspension. So, for the SIS EG there is a possibility to reduce the reference voltage of the suspension under zero-gravity conditions, thus allowing substantial increase of the gyroscope accuracy. The change in the reference voltage allows the gyroscope operation under space conditions to be simulated physically. The analytical relations for the change of drift model coefficients at the reference voltage V_0 reduced by a factor of k are given in the Table. In this Table k_0, k_1, k_2, k_3, k_4 are the conservative components of the drift model caused by the rotor nonsphericity, V – control voltages in the suspension channels. In this case, the drift component that does not depend on acceleration reduces by a factor of k^2; the one proportional to acceleration does not change; the drifts caused by interaction of radially unbalanced rotor with the anisoelastic suspension reduce by a factor of k^2; the drifts proportional to squared acceleration increase by a factor of k_2. The changes in reference voltages do not influence the dissipative components caused by the influence of residual magnetic fields.

Refcrence voltage	Coefficients			Products	
V_0	k_0	μ_{ij}	ν_{ij}	k_1V , k_3V	k_2V^2 , k_4V^2
V_0/k	k_0/k^2	μ_{ij}/k^2	ν_{ij}/k^2	k_1V , k_3V	$k^2(k^2V^2$, $k_4V^2)$

During the tests of the SIS EG designed for a low-orbit satellite attitude control system the parameters of the apparent motion were compared for the polar orientations of the gyro at normal, for the Earth conditions, values V_0 and at the values reduced by a factor of 2.85 (accordingly, at 450V and 140V). In so doing, the maximum deviation of the rotor apparent motion trajectory from the program one over the test period of 110 hours did not exceed 100 arc s, including the errors of gyro rotor readout system. For this level of accuracy no additive components due to dissipative influences of residual magnetic fields were observed, which is indicative of sufficient protection of the gyroscope from these influences.

During these tests the following qualitative changes of apparent motion parameters have been obtained:

- increase of the rotor motion period at the polar orientation up to the value, close to the period of Earth diurnal rotation;
- severe reduction of the rotor motion damping factor.

It was proved that SIS EG accuracy increases essentially under zero-gravity conditions.

To fix the base inertial coordinate trihedron to the inertial coordinate system, in which the satellite angular motion control program is used, the attitude control system employs automatic sensors to determine stellar coordinates – SCAS (Stellar Coordinate Automatic Sensors) /9/. They allow algorithmical determination of both the initial alignment of the base inertial coordinate trihedron relative to the ICS and data information to correct this inertial trihedron as it drifts from the initial position (trihedron drift).

A fiber-optic gyroscope (FOG) is used in the system to provide the initial alignment of the satellite (for example, after it separates from the launch vehicle), track the program trajectory with high accuracy and improve reliability.

Coincidence of the satellite-fixed coordinate system with its program position during the satellite flight, i.e. with the PCS, is provided by force gyroscopic complexes (FGC) used in the attitude control system /3/.

The software for the angular motion control system and technical aids employed have passed experimental testing and confirmed the capability to provide high tactic and technical characteristics of the system.

References

1. **В.Аганов**. Первый снимок метрового разрешения с КА Ikonos//Новости космонавтики, №12, 1999, с. 37.
2. **Д.И.Козлов, Г.П.Аншаков, Г.Е.Фомин и др.** Дистанционное зондирование Земли из космоса – универсальная технология получения информации для решения социально-экономических задач, исследование природных ресурсов и экологии//Сб. научно-технических статей по ракетно-космической тематике. г.Самара, 2001,с.7-13.
3. **Г.П.Аншаков, Ю.Г.Антонов, В.П.Макаров и др**. Этапы и результаты создания систем управления движением космических аппаратов наблюдения//Сб. научно-технических статей по ракетно-космической тематике. г.Самара, 1999, с.88-98.
4. **Г.П.Аншаков, Ю.Г.Антонов, А.И.Мантуров, Ю.М.Усталов.** Формирование программ управления ориентацией космических аппаратов наблюдения//Сб. научно-технических статей по ракетно-космической тематике. г.Самара, 2001, с.16-25.
5. **В.С.Шебшаевич, П.П. Дмитриев и др.** Сетевые спутниковые радионавигационные системы. М. Радио и связь. 1993.
6. **Основы** теории полета космических аппаратов/Под ред. Г.С.Нариманова.– М.:Машиностроение,1972,601 с.
7. **S.S.Gurevich, V.Z.Gusinsky, B.Ye.Landau, V.M.Lesyuchevsky, S.L.Levin, Yu.A.Litmanovich, V.G.Peshekhonov, V.N.Tzvetkov.** An Attitude Reference System with Solid-Rotor ESGs for Orbital Satellites// 8th Saint Petersburg international conference on integrated Navigation Systems:CSRI Elektropribor,2001, p.57-64.
8. **Б.Е.Ландау, В.Д.Аксененко и др**. Электростатический гироскоп со сплошным ротором и бескарданная система ориентации космического аппарата на его основе//Гироскопия и навигация, №1, 2001,с.3-14.
9. **V.N.Branets, N.N.Sevastianov.** Control System of YAMAL 100 Communication Satellite// 7th Saint Petersburg international conference on integrated Navigation Systems:CSRI Elektropribor,2000, p.7-10.

INTEGRATING NAVIGATION AND COMMUNICATION SYSTEMS FOR INNOVATIVE SERVICES

Ernst Kesseler*, **Ronald Grosmann****, **Rudy Ehrmanntraut*****
National Aerospace Laboratory, NLR, P.O. Box 90502, 1006 BM Amsterdam, The Netherlands
e-mail: kesseler@nlr.nl, grosmann@nlr.nl
Eurocontrol Experiment Centre, EEC, P.O. Box 15, F-91222 Brétigny-sur-Orge, France
e-mail: rudiger.ehrmanntraut@eurocontrol.int

Abstract

Key words: Java, Air Traffic Management, Communication, Intelligent Services, TALIS

In air transport safety is rightly is a prime concern, which led to safe proprietary solutions but a conservative approach to innovation. Forecasted traffic growth, economic pressure and passenger preferences require more responsiveness. Both new air traffic management concepts, Eurocontrol's COOPATS and FAA's DAG-TM, are based on extensive information sharing between all parties concerned. The Total Information Sharing for Pilot Situational Awareness Enhanced by Intelligent Systems (TALIS) project has chosen to use COTS based Internet technology to provide the enabling data sharing. This open solution also allows for easy integration with non-traditional actors like airports, passenger services etc. The planned 2½ year realisation time for the TALIS prototype versus the decades typical for the industry and the relatively minor investment, of which already half is allocated to applications, testify to the success of the approach.

Introduction

Air transport is a safety conscious industry. Its good safety records testify to the success in this area. The downside of this success is the industry's conservative approach to innovation. Economic pressure will force it to be become more competitive and hence more responsive to other user needs. This paper describes an approach to use the Internet based service paradigm in which services are provided to customers. These services are based on, or use, other services. In this way communication services and navigation services can be integrated to provide innovative services to satisfy user needs in a timely fashion.

The first section will provide some background or a high level view of the current practise in air transport. The second section argues why innovation is needed. Subsequently section 3 describes the two major user-driven new Air Traffic Management (ATM) concepts, Eurocontrol's Co-operative Air Traffic Services (COOPATS) and FAA's Distributed Air-Ground Traffic Management (DAG-TM). Section 4 elaborates the Total Information Sharing for Pilot Situational Awareness Enhanced by Intelligent Systems (TALIS) services approach, illustrated by an en-route example and an airport one. The TALIS solution is elaborated in section 5, including its underlying Internet technology. Finally section 6 discusses some safety issues before the conclusion summarises this paper.

1. Background

Air transport technology is heavily influenced by safety concerns. Air transport's safety record justifies this approach. As in any industry concerned with safety, proven technology is favoured above innovative solutions. Compared with the general market, the volume, both for aircraft avionics and for ground systems is relative minor. This reinforces in a slow evolution of the technology deployed and a very limited use of commercial off-the-shelf (COTS) products. Nevertheless the evolution tends to be technology driven in stead of user driven due to the complex aeronautical issues involved. Typical implementation times for new technologies are measured in decades, as illustrated by certified GPS approaches in the navigation domain (versus massive GPS use in the general domain, cars and the maritime domain), and the still incumbent Aeronautical Telecommunication Network (ATN) versus massive use of mobile communication in the general domain. The COOPATS document [1] provides a vivid example of these long implementation times by contemplating the use of data link technologies, which it mentions started in the early 1970's.

2. Need for change

Air transport is expected to grow in the long term, despite the temporal downturns like the one after the September 11, 2001 attacks, see [2]. It is a widely held view [1], [3], that this expected traffic volume can only be accommodated by a paradigm shift away from the current concepts and ways of working. Rising delays reinforce the business need for more responsiveness of the air transport system to user needs instead of the

* Drs., Head of Embedded Systems Department of NLR.
** Ing., Senior research scientist of Embedded Systems Department of NLR.
*** Head of CNS Studies Business Area of EEC.

current practise of innovation based on teehnologieal opportunities. Cost concerns imply that an effort should be made to harness the power of COTS to concentrate the resources on air transport specific problems. Some observations on the relevanee of COTS for ATM are provided in [4].

Apart form these high level incentives for ehange, other factors reinforce this need for more responsiveness. Based on the finding that weather related accidents have the highest fatality rate, [5] studied the use of data linked weather update for general aviation pilots Conclusions include that on-board intelligenee is needed to transform weather information to a usable service supporting the pilot. Also the important but not well understood issue of the Human Machine Interface (HMI) makes updates of any initial service and its supporting software likely, reinforeing the need for responsive user-driven services.

3. User driven concepts

Currently a number of air-ground integration operational concepts are being conceived. These range from short term improvements based on ADS-B and Controller/Pilot Data Link Communications (CPDLC), through Airbornc Separation Assurance System (ASAS) to the long term vision of Co-operative ATS (COOPATS) of Eurocontrol for the European Civil Aviation Conference (ECAC) area or Distributed Air-Ground Traffie Management (DAG-TM) of NASA for the USA. These coneepts are based on integrating the air-side and the ground-side comprising amongst others integration of the navigation capabilities with the eommunication systems. These communication systems are an enabling teehnology, just now being deployed in the air transport domain. The need for flexibility and more responsiveness of the air transport information technology systems will be illustrated by the following eursory deseription of COOPATS and DAG-TM.

3.1 COOPATS concept

The COOPATS eonecpt is defined in [1] as "a concept of Air Traffie Management (ATM) that enhances the productivity and safety of Air Traffic Services by optimising the involvement of (air traffie) eontrollers, airerew and airline operators through integrated Data Communieations and improved forms of surveillanee and automation". The high level objective of Co-operative ATS is to support controllers, pilots and all potential ATM users, in all phases of flight, up to enabling autonomous flight operations in Free Flight Airspaee by progressively implementing fully seamless communications, data exchange, situational awareness and automation eapabilities. The Co-operative ATS coneept is based on the human centred automation paradigm, as a consequence of the responsibilities defined by ICAO in [6]. It identifies the following concept goals:

- Fully seamless communieation between air traffic controllers and pilots,
- Fully seamless data exchange capabilities between all involved ground systems and aircraft,
- Optimal provision of flight information data in real time, for use by airerew and any other involved parties, sueh as meteorological ccntres.

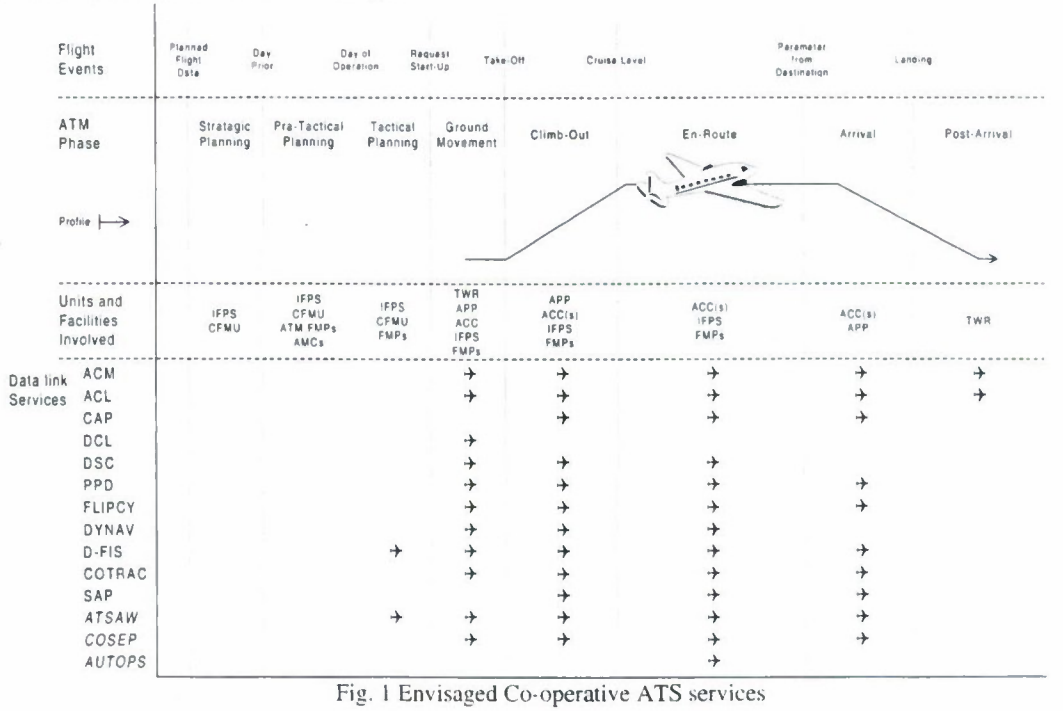

Fig. 1 Envisaged Co-operative ATS services

The key principle is improved situational awareness for both pilot and controller, enabled by data link technologies. ATM will become increasingly dependent upon the efficiency and quality of supporting processes and services such as System-wide Information Management (SWIM), Aeronautical Information Services (AIS) and aviation meteorological services (MET). For planning purposes, Co-operative ATS is divided into two concept levels, level 1 for evolution up till 2008 / 2010 and level 2 for realisation between 2007 and 2015. Figure 1 provides an overview of the data link services per flight phase. The bottom three services, in Italics, relate to level 2 services. Note that the Co-operative ATS concepts naturally uses the word services and the notion that advanced services build upon more primitive services.

Co-operative ATS assumes the ATM system to evolve in a gradual and interactive way towards its final form. Consequently Co-operative ATS implies a mechanism for continuous change of the software and applications which implement these services.

3.2 DAG-TM concept

The Distributed Air-Ground Traffic Management (DAG-TM) concept is defined in [7] as "a concept in which flight deck crews, air traffic service providers and aeronautical operational control personnel use distributed decision making to enable user preferences and increase system capacity, while meeting air traffic management constraints. DAG-TM will be accomplished with a human centred operational paradigm enabled by procedural and technological innovations. These innovations include automation aids, information sharing, communication, navigation and surveillance (CNS) air traffic management technologies". The fundamental objective of DAG-TM is to minimise static restrictions i.e. the users can plan and operate according to their preferences (as the rule) with ATM deviations only when inevitable (by exception). The DAG-TM concept will be implemented using a spiral development approach, as known from the information technology [8]. The DAG-TM concept, as described in [3], is referred to as the gate-to-gate concept. Taking the user needs and individual return-of-investment decisions into account, it assumes a mixed fleet equipage for the additional DAG-TM capabilities. The centrepiece of the DAG-TM concepts is distributed decision making between the three parties involved

- The flight deck, operated by the flight crew,
- The aeronautical operational control centre, operated by the flight planners and flight dispatchers,
- The air traffic service provider, including air traffic controllers and traffic flow managers.

This is depicted in figure 2.

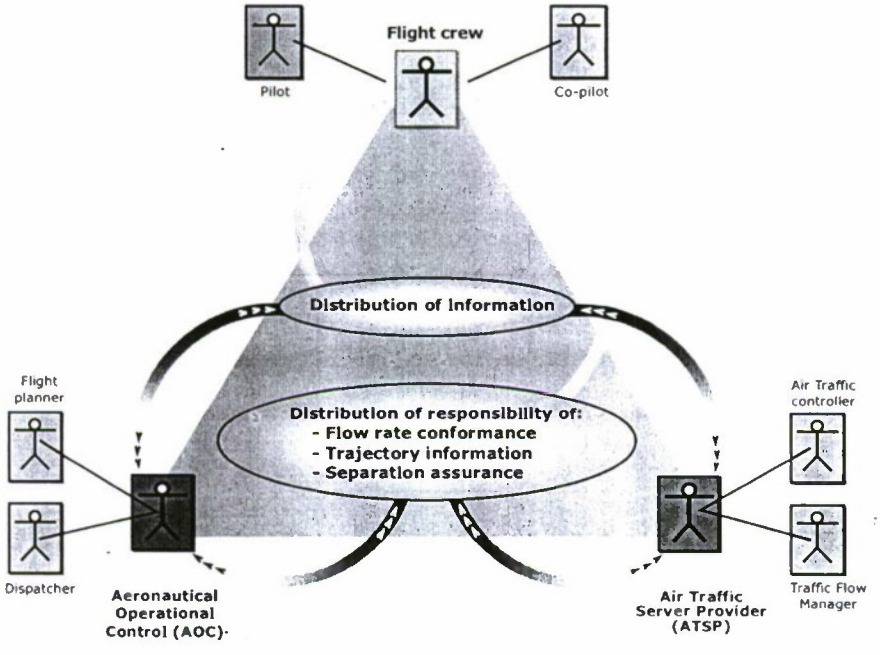

Fig. 2. DAG-TM concept triad

The flight deck plus the aeronautical operational control centre together constitute the DAG-TM users. The DAG-TM concept is based on extensive information sharing and subsequent distributed decision-making responsibility by all three parties. To exchange information the 4–D trajectory is considered fundamental. Table 1 provides the fundamental gate-to-gate concept plus the 14 derived DAG-TM concept elements and their provided services.

Table 1. DAG-TM concept elements and provided services

DAG-TM concept element	provided services
1. Gate-to-gate	Information access / exchange for enhanced decision support
2. Pre-flight planning	NAS constraint considerations for schedule / flight optimisation
3. Surface departure	Intelligent routing for efficient pushback times and taxi
4. Terminal departure	Free manoeuvring for user-preferred departures
5. Terminal departure	Trajectory negotiation user-preferred departures
6. En route (departure, cruise, arrival)	Free manoeuvring for • user-preferred Separation assurance • user-preferred local traffic flow management conformance
7. En route (departure, cruise, arrival)	Trajectory negotiation • user-preferred Separation assurance • user-preferred local traffic flow management conformance
8. En route (departure, cruise, arrival)	Collaboration for mitigating local traffic flow management restrictions due to weather, Special Use Airspace and complexity
9. En route / Terminal arrival	Collaboration for user-preferred arrival metering
10. Terminal arrival	Free manoeuvring for weather avoidance
11. Terminal arrival	Trajectory negotiation for weather avoidance
12. Terminal arrival	Self spacing for merging and in-trail separation
13. Terminal arrival	Trajectory exchange for merging and in-trail separation
14. Terminal arrival	Airborne conflict detection and resolution for closely spaced approaches
15. Surface arrival	Intelligent routing for efficient active-runway crossing and taxi

The DAG-TM concept is based on decision support tools. The determination of the required information exchange is one of the foremost research issues to determine its feasibility. The information sharing and the improved situational awareness aim to increase both safety and capacity. For the arrival phase, the Estimated Time of Arrival (ETA) will be replaced by a Desired Time of Arrival (DTA). This will allow the users to either accept some delays using their preferred route or to avoid congested airspace and arrive earlier (e.g. using another runway with increased taxiing time). This mimics car drivers, which might take the shortest but congested route or take a longer not congested route.

The DAG-TM concept states information sharing and distributed decision making as fundamental enabler. As research continues, current ideas evolve and new ideas are expected to arise necessitating new procedures and algorithms. A software characteristic is that even stable products evolve over time, so the DAG-TM concept comprising evolving ideas and relying heavily on software implicitly needs a mechanism to cost-effectively and swiftly disseminate new software or software updates to the existing fleet i.e. it needs a flexible communication infrastructure.

4. TALIS services approach

The aforementioned need for change results in user driven concepts enabled by a way to share information. Based on this, the Total Information Sharing for Pilot Situational Awareness Enhanced by Intelligent Systems (TALIS) project is being executed. Its objective is to provide an architecture that supports a layered services concept. To achieve this, the architecture builds upon (or uses in Internet parlance) navigation and communication services to provide more advanced services like ADS-B (Automatic Dependant Surveillance) and Traffic Information Services (TIS). By using general hardware and software components i.e. COTS technology and Internet based solutions, the time-to-market of the services can be reduced drastically. Uplinking new data, or even new software, facilitates a swift deployment of new or updated services, also for aircraft with legacy avionics. This is a big advantage when new requirements arise, as is currently the case for security. Figure 3 depicts this layered services concept. Viewing the Flight Management System (FMS) in an analogue way, the FMS provides the capability (service) to navigate from any designated point to any point, based on ground

beacons plus the aircraft's Inertial Navigation System (INS) combined with local processing capabilities or intelligence, the supporting or lower level services.

TALIS aims to be an enabler for the Co-operative ATS and DAG-TM concepts as well as for many other services, including non-ATM services like aeronautical operational control and passenger services. The next two services describe two sample services, both from the ATM domain, the first being realised in the TALIS project and the second being considered for implementation. Both services focus primarily on pilot users.

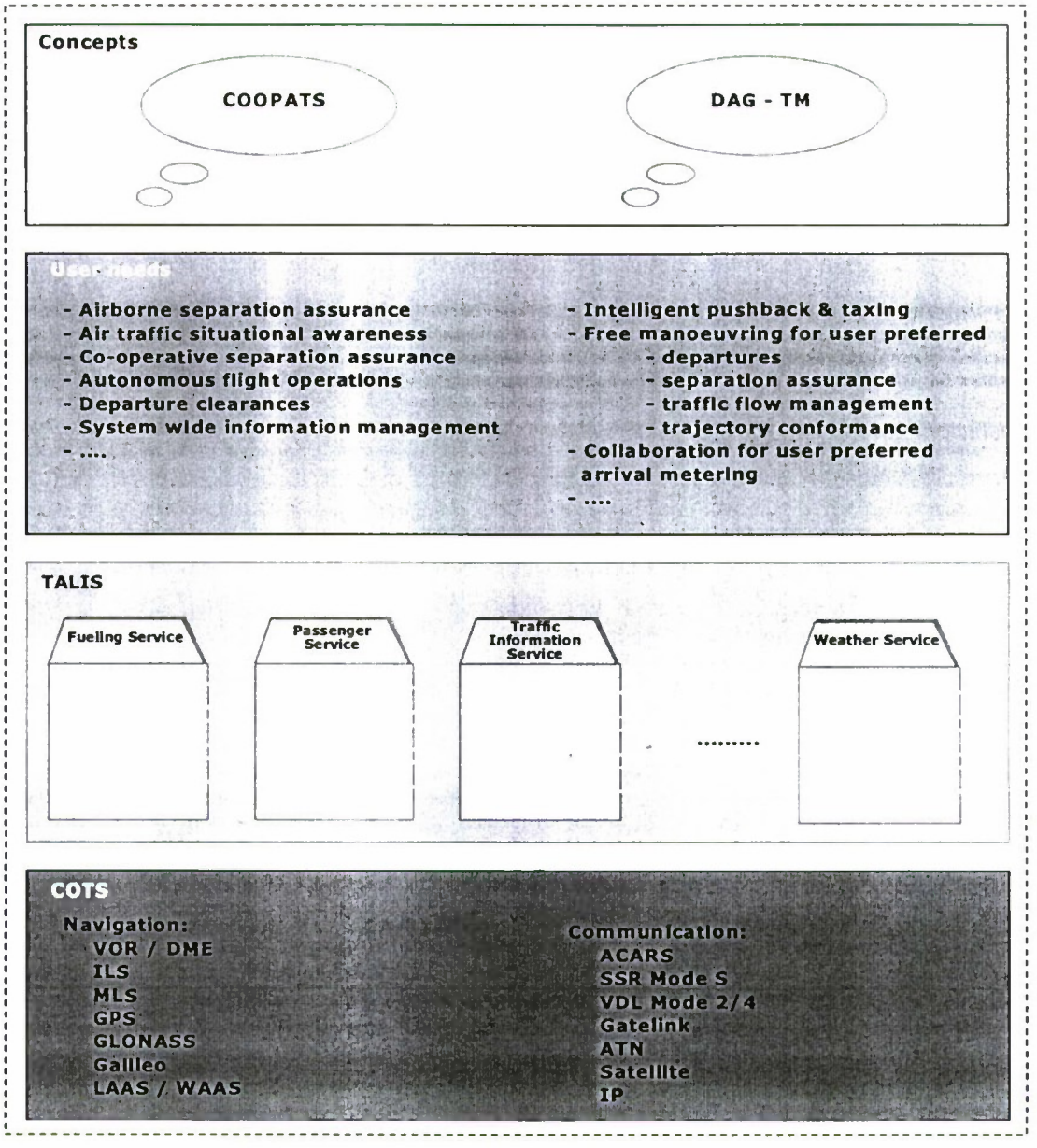

Fig. 3. TALIS layered services concept

4.1 En-route example services

Some en-route services with their TALIS support are illustrated in figure 4 using the Airborne Separation Assurance System (ASAS) concept. Depending on the navigation and communication services available, a different level of ASAS service can be supplied. When no radar is available, ASAS will be Automatic Dependent Surveillance Broadcast (ADS-B) based and provides protection for equipped aircraft only. Where radar and ATN are available, the aircraft in the immediate surrounding of the own ship can be uplinked providing protection to all aircraft. In the approach phase, when radar, ATN and Traffic Information Service-Broadcast (TIS-B) are available, these services will allow station keeping. Figure 4 illustrates these context dependant services. TALIS is currently working on the Traffic Information Service part.

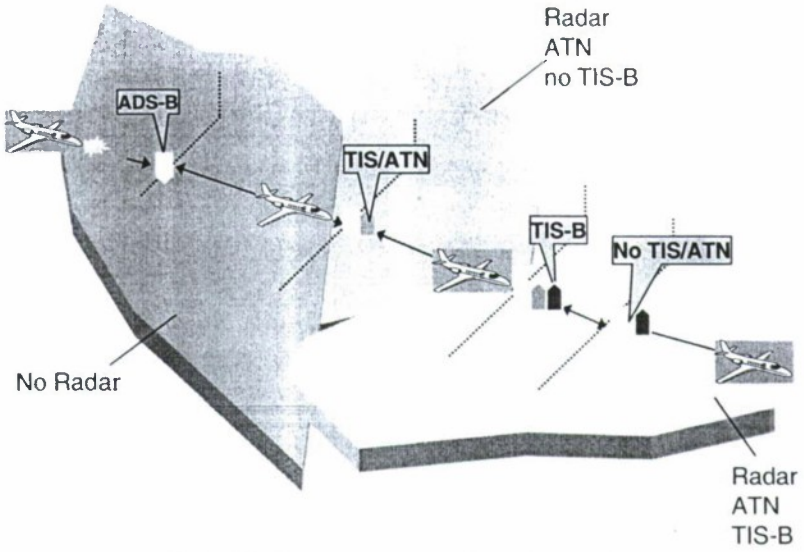

Fig. 4 TALIS en-route context dependant services

4.2 Airport example services

On an airport the pilot has different information needs, depending on the flight phase. Figure 5 provides some sample services. The co-ordinated pushback service will allow the pilot to improve the reliability of on-time pushback taking information of all relevant parties into account. The pilot needs amalgamated information from fuelling services, baggage-handling services, catering services, security services, gate personnel, AOC for information on connecting passengers etc. This co-ordinated pushback service optimises usage of the taxi-way linking the various gates and prevents two aircraft from blocking each other or ending up in the wrong take-off order. Subsequently taxi-services [9] guide the aircraft to the correct runway, optimised for the other airfield traffic. Finally runway incursion services improve the safety during take-off. For arriving aircraft taxi services can guide the aircraft and the ground handling vehicles to the (re)allocated gates. These services illustrate the power of integrating navigation and communication capabilities based on updateable software.

Fig. 5. Example TALIS airport services

5. TALIS solution

Summarising, some important requirements for the TALIS solution will be to

- Support a variety of applications, the mix of which will evolve over time, for a diverse set of users

- Support a mix of hardware and software platforms, both on-board the aircraft and for the various ground systems involved
- Be responsive to evolving user requirements
- Be able to accommodate the safety and security concerns of some of the envisaged applications.

To accomplish this, TALIS has chosen to harness the power of COTS tools by choosing Java[tm] technology. As Java[tm] is being used in a.o. many Internet applications a lot of work is being done on Java[tm] technology, resulting in investments which are much larger then possible for dedicated air transport solutions. The general usage of Java[tm] also implies that TALIS can be used for other applications then air traffic management alone, like aeronautical operational control, passenger information and even for security services. This will improve the return-on-investments, or increase the passenger service and hence the competitiveness of the airline. For a solution which interfaces with so many independent parties as TALIS, it is important that the solution is vendor independent i.e. open. Open solutions provide a level playing field for all competitors, prevent monopolies, foster innovation by competition and tend to generate standard solutions that are easier to integrate in a business organisation. Java[tm] complies with this requirement.

Note that independently of this work, in the automotive transport industry a similar approach of Internet based service provision is being aimed at [10]. Interestingly both security services and a number of charged passenger services are being envisaged, like tourist information, news, weather /news / stock and location based information. A car is even referred to as a Java[tm] browser on wheels. In another independent work stream for military pilots, [11] investigates the concept of on-board intelligence combined with a network connection and supporting ground services. It seems the time is set for this type of network-centric solutions.

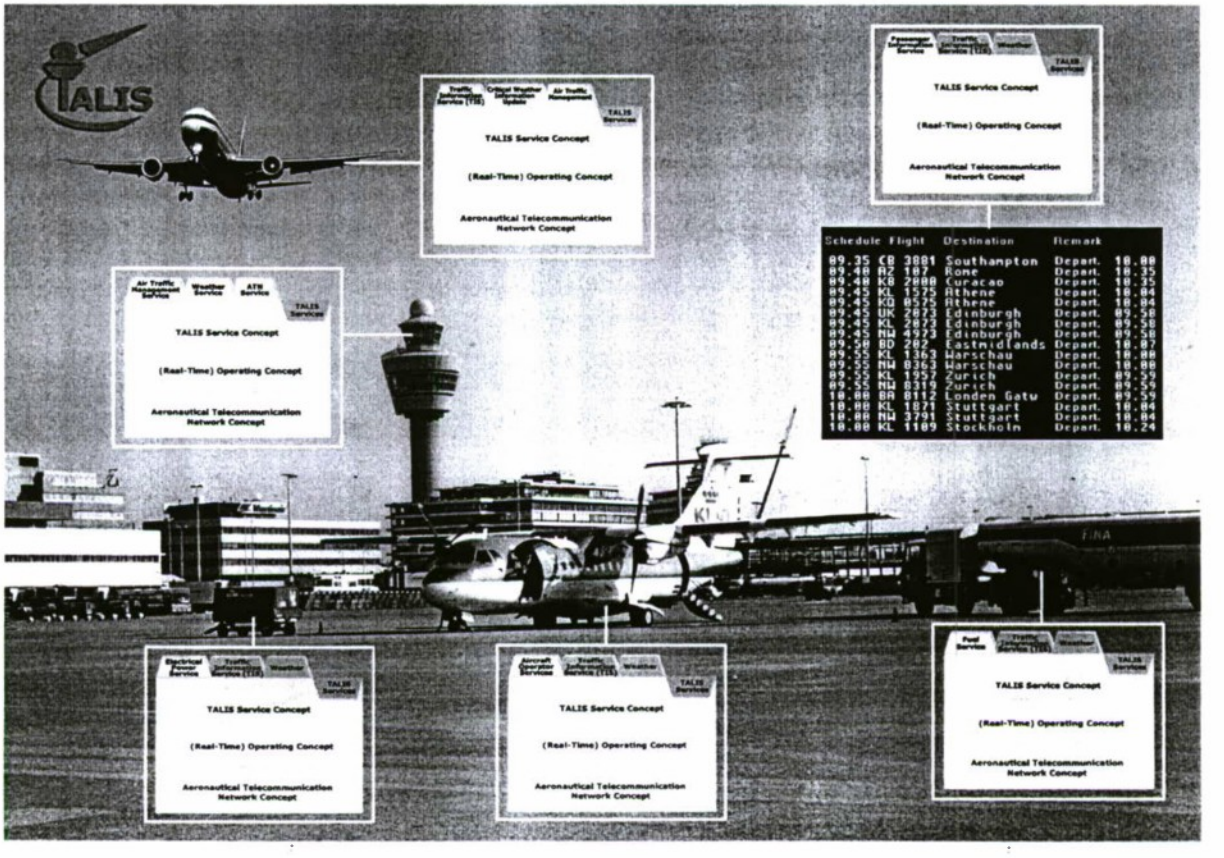

Fig. 6. TALIS concept

Fig. 6 depicts the general philosophy of the TALIS solution. A standard infrastructure will be provided, which will connect all relevant actors, or people performing functions. On top of this infrastructure applications (or services) will be provided, which support the person(s) involved. By using the TALIS infrastructure these applications will be easier to develop than in the current business practise. An advantage of the shared infrastructure is that applications can interact, allowing for more advanced services or even entirely new innovative services to be offered building upon existing services. The TALIS architecture consists of TALIS applications complemented by TALIS services. The application provides the services to the user e.g. a weather update to the pilot. The corresponding TALIS service will be a meteorological service, probably ground based, which can provide the requested weather. As is common in Internet, many applications will also provide services

to other applications. This is depicted in the TALIS application and TALIS services boxes in figure 7. The mapping of the TALIS architecture to the COTS based implementation is shown in figure 7.

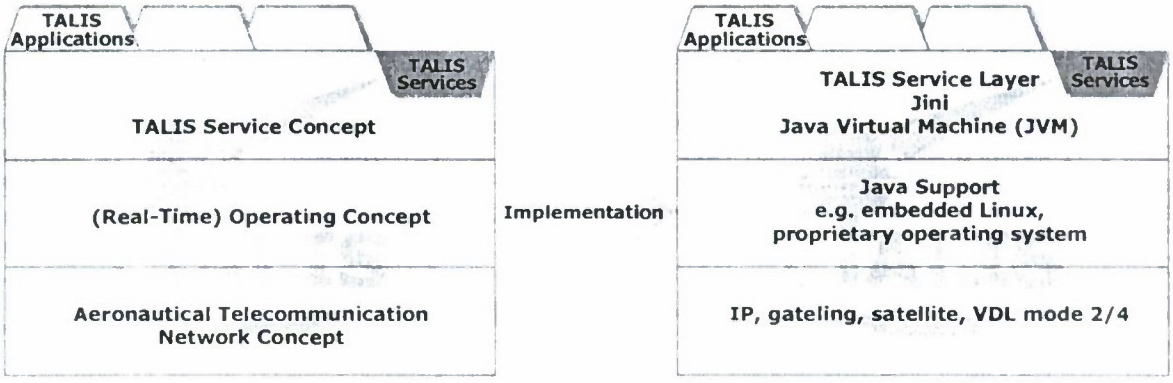

Fig. 7 TALIS architecture and implementation

The TALIS service concept layer hides all network and operating system implementation specific details from the TALIS application developer. By using Java™ TALIS will be able to dynamically detect new services, and servers. Java™ has been designed to run unmodified on any computer platform where a Java™ Virtual Machine (JVM) is available. The Java™ compiler translates the TALIS application in Java™ to intermediate Java™ byte codes. The Java™ Virtual Machine then executes these Java™ byte codes. Depending on the type of application, the amount of functions required from the JVM may vary and consequently several Java™ Virtual Machines are available, from the full J2EE (Java™ 2 platform Enterprise Edition) to the smallest J2ME (Java™ 2 Platform Micro Edition). To illustrate the power of COTS, in March 2002 the standard Java™2platform software was already downloaded over one million times. Also, due to the recent security concerns, work is being done to include some security features into Java™. This is possible for COTS products that are in common use. For air transport specific products the cost of such additions would be prohibitive and the realisation time, even for a limited implementation, would be far longer.

Jini network technology is an open architecture that enables developers to create network-centric services. Jini technology is designed to build adaptive networks that are scalable and can evolve. These are the characteristics needed by TALIS. As can be seen from figure7, TALIS will need to add a specific interface for communication over the Aeronautical Telecommunication Network. Due to the substantial deployment of Java, it is expected that it will be easy to add wireless portable and wearable devices when they will become available in the future, as all of these will be COTS products. This architecture will allow the air transport actors to concentrate on providing added value by exploiting new technologies, as they become available.

The use of the chosen COTS technologies pays off for TALIS. A study of airborne certification issues and project management plus consortium management account for nearly one third of the TALIS effort. Of the remaining effort, half is spend on the two demonstration applications, a meteorological update service and Traffic Information Service. The other half is spend on technical issues related to the TALIS federated architecture, the common infrastructure.

6. Certification issues

Air transport could benefit from a number of services, which can be provided by the TALIS infrastructure. Some of these services are not critical, like passenger information services, but many of these services incur a safety concern in case the TALIS infrastructure would fail. Consequently there is a requirement to certify TALIS services and the supporting TALIS infrastructure. Due to historic reasons, for the airborne part of TALIS DO-178B [12] is available, but for the ground part no standard is mandated yet. In the US DO-278 / ED-109 [13], the ground equivalent of DO-178B, has just been completed. For the ECAC area DO-278 is busy with a European standard. This European standard is based on combining elements of DO-178B, IEC 61508 [14] and addresses both safety concerns as well as quality issues. For the latter the Capability Maturity Model (CMM) [15] is used. All of these standards classify applications depending on the hazardous consequences software failure can incur for system behaviour. This information is obtained from Functional Hazard Analysis (FHA) plus (Preliminary) System Safety Assessment (P)SSA. The number of software classes, the definition of these classes and the required assurance for each class differ for each standard. DO-178B has levels A till E, IEC 61508 has Safety Integrity Levels SIL 1 to SIL 4, DO-278 has assurance levels AL1 to AL6 and European standard will probably have 6 assurance levels.

The TALIS approach will be to study the safety and certification issues starting with applications with low safety classification levels. This practical approach is chosen as no FHA or (P)SSA for any data link application is known, which has been accepted by a certifying authority. When the FHA and (P)SSA classify a new TALIS application to a higher class, the certification activities of the relevant services of the TALIS federated architecture could be extended to higher levels, if feasible. This approach is based on the experience that considerable effort can be saved by applying the costly safety critical development process only to those parts that really need them and by partitioning the application according to its safety critical functions [16]. Like many other languages, certification concerns will lead to the definition of a safe subset of the language complemented by programming standards limiting the use of some other unavoidable constructs. In the Open Group work on Java[tm] and DO-178B is being discussed [17].

It is expected that some TALIS applications will require some form of real time behaviour. Those applications will need a real time operating system kernel to support those services. Again the COTS paradigm can be exploited. The Real Time Java[tm] (RTJ) working group recently completed the definition of a hard real-time version of Java[tm] [18], on which already some comment is available [19]. Due to the communication delays incurred by the ATN, it is expected that for TALIS currently soft real-time will suffice. The real time Java[tm] working group also addresses related DO-178B certification issues.

7. Conclusions

1. Both new ATM concepts, Eurocontrol's COOPATS and FAA's DAG-TM, are based on information sharing. They implicitly assume many applications which will evolve over time. A more responsive ATM necessitates a reduced time-to-market for new applications. The current proprietary solutions can not cope with this.
2. The TALIS approach is based on layered services. This approach is extensively used in other domains and hence validated.
3. TALIS uses proven Commercial of the Shelf (COTS) Java[tm] technology, thereby capitalising on a lot of effort and allowing for easier integration of future updated capabilities.
4. The layered open TALIS architecture
   - allows for easy adaptation of innovative services, innovative technologies and innovative solutions
   - reduces time-to-market in accordance with user / operational needs
   - benefits fully from COTS solution(s) which have proven itself
   - eases integration with other business applications of the actors involved
   - fosters competition
   - promotes innovation
5. TALIS will address some safety / certifiability aspects, starting with expected classification levels for the initial applications.
6. The resulting air transport system will be more responsive to user needs while maintaining its good safety record.

Acronyms and abbreviations

ACARS	Aircraft Communication Addressing and Reporting System
ACC	Area Control Centre
ACLATC	Clearance and Information (Service)
ACM	ATC Communications Management (Service)
ADS-B	Automatic Dependant Surveillance – Broadcast
AIS	Aeronautical Information Services
AL	Assurance level
AMC	Airspace Management Cell
AOC	Aeronautical Operational Control
APP	Approach Control (Service) (Unit)
ATSAW	Air Traffic Situation(al) Awareness
ATSP	Air Traffic Server Provider
ASAS	Airborne Separation Assurance System
ATM	Air Traffic Management
ATN	Aeronautical Telecommunication Network
ATS	Air Traffic Services
AUTOPS	Autonomous Flight Operations
CFMU	Central Flow Management Unit
CMM	Capability Maturity Model
CNS	communication, navigation and surveillance
COOPATS	Co-operative ATS (Air Traffic Services)
COSEP	Co-operative Separation Assurance
COTRAC	Common Trajectory Co-ordination (Service)
COTS	commercial off-the-shelf
CPDLC	Controller/Pilot Data Link Communications
DAG-TM	Distributed Air-Ground Traffic Management
DCL	Departure Clearance (Service)
DSC	Downstream Clearances (Service)
DFIS	Digital Flight Information (Services)

DME	Distance Measuring Equipment
DTA	Desired Time of Arrival
DYNAV	Dynamie Route Availability (Serviee)
ECAC	European Civil Aviation Conference
ETA	Estimated Time of Arrival
FHA	Funetional Hazard Analysis
FLIPCY	Flight Plan Consisteney (Serviee)
FMP	Flight Management Position
FMS	Flight Management System
GPS	Global Positioning System
HMI	Human Machine Interfaee
IFPS	Initial Flight Plan Proeessing System
ILS	Instrument Landing System
INS	Inertial Navigation System
IP	Internet Protoeol
J2EE	Java™ 2 platform Enterprise Edition
J2ME	Java™ 2 Platform Miero Edition
JVM	Java™ Virtual Maehine
LAAS	Loeal Area Augmentation System
MLS	Microwave Landing System
NAS	US National Airspaee System
PPD	Pilot Preferenees Downlink (Serviee)
PSSA	Preliminary System Safety Assessment
RTJ	Real Time Java™
SAP	System Aeeess Parameters (Service)
SIL	Safety Integrity Level
SSA	System Safety Assessment
SSR	Secondary Surveillanee Radar
SWIM	System-wide Information Management
TALIS	Total Information Sharing for Pilot Situational Awareness Enhanced by Intelligent Systems
TIS-B	Traffic Information Serviees-Broadcast
TWR	Tower Control Serviee (Unit)
VDL	VHF Data Link
VOR	VHF Omni-Directional Radio Range
WAAS	Wide Area Augmentation System

References

1. **Eurocontrol,** Towards Co-operative ATS, The COOPATS Concept // Eurocontrol DIS/ATD/AGC/MOD/DEL 01, Version 0.5, 01/11/2000
2. **Eurocontrol,** Performance Review Commission // http://www.eurocontrol.int/prc/reports/prr4/reference.html
3. **S.M. Green, K.D. Bilimoria, M.G. Ballin,** Distributed air/ground traffic management for en route flight operations // Air Traffic Control Quarterly, volume 9, number 4, 2001, P. 259-285
4. **E. Kesseler,** Cheaper / faster / better and safer?, searching the perfect balance // Institute for Information Industries, the 5th CNS/ATM conference, March 2000, Taipei
5. **D. E. Yuchnovicz, et al,** Use of data-linked weather information display and effects on pilot navigation decision making in a piloted simulation study // NASA / CR-2001-211047, august 2001
6. **International** Civil Aviation Organisation, Human Factors Digest No. 10: Human Factors, Management and Organisation.// ICAO circular, n.249, 1994
7. **K.D. Bilimoria,** Distributed air/ground traffic management // Air Traffic Control Quarterly, volume 9, number 4, 2001, P.255-258
8. **B. Boehm,** A spiral model for software development and enhancement // IEEE, Computer, Volume 21, number 5, P. 61-72, 1988
9. **P. van Leeuwen,** Scheduling aircraft using constraint satisfaction // 11th International workshop for functional and logic programming, June 2002, Grado, Italy http://www.dimi.uniud.it/~wflp2002/
10. **S. Ashley,** Driving the info highway // Scientific American, October 2001, P. 44-50
11. **H.H. Hesselink, et al.,** On-board decision support through the integration of advanced information processing and human factors techniques // NLR-TP-2001-611, NATO SCI lecture series on Tactical Decision Aids and Situational awareness, Amsterdam November 2001, Sofia November 2001, Madrid November 2001, Patuxent River (MD) November 2001 and NVvL November 2001
12. **DO-178B / ED12B,** Software Considerations in Airborne Systems and Equipment Certification // RTCA / EUROCAE (December 1992)
13. **DO-278 / ED-109** Guidelines for Communication, Navigation, Surveillance, and Air Traffic Management (CNS/ATM) Systems Software Integrity Assurance // RTCA / EUROCAE 2002
14. **IEC 61508** Functional safety: safety related systems, 7 parts // , (June 1995)
15. **M. C. Paulk, C. V. Weber, S. M. Garcia, M. B. Chrissis, M. W. Bush,** "Key Practices of the Capability Maturity Model, Version 1.1" // Software Engineering Institute, CMU/SEI-93-TR-25, DTIC Number ADA263432, February 1993 or http://www.sei.cmu.edu/cmm/obtain.cmm.html
16. **E. Kesseler,** Applying theory to practice: Airworthy software measured and analysed // 16th IFIP World Computer Congress (WCC2000), Beijing, China August 21-25, 2000
17. **John Joseph Chilenski,** Software development under DO-178B // The open Group, Anaheim, January 28, 2002
18. **Greg Bollella et al,** The real-time specification for Java™ // http://www.rtj.org/rtsj-V1.0.pdf
19. **E. D. Jensen,** Requirements For Real-time Extensions For the Java™ Platform // The open Group, Anaheim, January 28, 2002

CREATION OF HYPERBOLIC SYSTEM FOR SEARCH OF DISTRESS MOVING OBJECTS ON THE SEA, IN AIR, ON LAND USING RADIATION FROM THEIR TRANSMITTERS*

A.A. Koshevoy*, A.V.Maranov, O.T. Chigirin**, Y.T.Chigirin**, A.A. Ostapov*****
Central Scientific & Research Institute Navigation and Control,
5, Dimitrova St., 03006, Kiev, Ukraine. E-mail:kvantn@i-c.com.ua

Abstract

Key words: transmitting object, transmitter, reception station (post), location, timedifference, difference-distance (hyperbolic) method, accuracy, measuring error

Creation of the distress alerting and locating systems (DALS), based on transmitter signals receiving of distress moving objects (vessels, aircraft, automobiles etc.) and also mobile phone. The pulse hyperbolic system using "back" Loran" method can be used as DALS. In the pulse hyperbolic system, based on "back" Loran" method use hyperbolic lines of position are determined by measuring the difference in time of reception of signals from one transmitter on two receive station (post). The receive station can be placed both on the land in that number on the towers of mobile phone net and the vessels. Proposed systems can be used in following radio frequencies bands: 1,8 – 2,0 MHz (as in system "Loran"), 90-110 kHz (as in system "Loran-C"), 800 –1500 MHz (as in mobile phones).Pulse signal format must correspond "come quick" signal (CQ) or CQD.The accurate position pulse hyperbolic system can be used for Cost Guard Service, Vessel Traffic Service, Aircraft Traffic Service, USA E911 Service. The analysis of precision characteristics is executed. As mistakes of measurement are use mean square errors, marked by a symbol.

Introduction

One of the major problems facing to Cost Guard Service, Vessel Traffic Service, Aircraft Traffic Service, services E911 USA and similar in other countries, is duly detection and definition with required accuracy of a position of the suffering objects disaster on the sea, in air and on land.

Effective detection method of such objects is use of radio channels for reception of suffer signals from them. For this the special radio-electronic equipment, which makes radiation of suffer signals after inclusion of onboard transmitters, should be established on board of moving objects. Inclusion of transmitters on radiation is carried out automatically or by the operator, after creation of some situations which unequivocally define transition of object in emergency operation. Without considering in detail algorithm of decision making on inclusion of transmitters, we shall consider only their modes of functioning; such modes may be two: – the first mode – is not made electromagnetic radiation. It considers to a normal mode operation of the object; second – is made electromagnetic radiation. It considers to an emergency mode operation of the object.

To the moving suffering objects are included:

- flying objects (planes, helicopters, balloons, etc.);
- surface objects (the vessels, boats, yachts, etc.);
- ground moving objects (automobiles, trains, etc.);

There are can be used a mobile phones onboard of moving and standing objects except the special radio electronic equipment.

1. The methods of definition of a position of a source of electromagnetic radiation

Detection and definition of a position of the specified objects on radiation of their transmitters can be made by passive methods as network of ground (coastal) or vessel reception stations. In the future the network of strong points of the distant navigation systems "Loran", "Loran-C", and network of mobile phones is advanced.

It is possible to allocate three methods from variety of possible methods of position definition of sources of electromagnetic radiation, which meets acceptable accuracy:

- difference distance (hyperbolic) or a "back"Loran" method;
- difference frecuency method or a Doppler method;
- triangulable (bearing) method.

Application of this or other methods depends on initial requirements and potential opportunities of these methods. Hyperbolic method provides higher accuracy of coordinates definition of sources of electromagnetic

---

* D.Nat.Sci., Professor, Director.
** D.Sc., Leading Research Scientist.
** * Chief Engineer.

radiation and speed. In work [1] comparison on size of a circular probable mistake σ_r of hyperbolic and bearing methods is executed at use of three measuring places of acceptance. It is shown, that hyperbolic systems have advantage over bearing if all points on one line are located symmetrically and the condition $5c\,\sigma_{T_p} < L\sigma_\varphi$ is carry out, where $\sigma_{T_p}, \sigma_\varphi$ - is a mistake of measurement of time difference, an angular direction; L – distance between extreme reception stations; c – speed of light.

The task was to assess the opportunity of definition with high accuracy of source of radiation position ($\sigma_r \approx 50-100m$), which is commensurable with accuracy of the satellite navigation systems (ground position system) GPS (USA), ГЛОНАСС (Russia), at use frequency ranges $f_I = 90-110kHz$, as is in system "Loran-C", $f_{II} = 1{,}8-2MHz$, as is in system "Loran", $f_{III} = 800-1500MHz$, as is in system of mobile telecommunication GSM.

The specified frequency ranges are chosen proceed from that they are widely used now and there is enough plenty of theoretical and experimental works on research of the basic characteristics of a liaison channel (multiplier easing, peak and time fluctuations of a signal in a point of reception, correlation characteristics etc.).. Accuracy of definition of a source radiation position is defined by product measuring M and geometrical G factors: $\sigma_r = MG$ [1]. If G = 100 ÷ 1, that corresponds to the big changes of mutual position of a radiation source and reception stations ($d/R = 0{,}1-10$, where d - base between stations, R – distance), it is necessary to make range measurement of arrival time of a signal with a mistake $\sigma_t = 0{,}1-0{,}2 \bullet 10^{-8} s$ for reception of the given accuracy.

2. A kind of a signal

In practice the devices based on interruption of work of the oscillator are frequently used for transfer of radio impulses. We choose as a signal on an output of the transmitter amplitude manipulated signal as

$$S(t) = \begin{cases} A\cos(\omega t + \varphi_0), & at \;\; 0 \prec t \prec T \\ 0 & at \;\; t \prec 0 \;\; ; \;\; t \succ T, \end{cases}$$

where $\omega = 2\pi f$, f - frequency of fluctuation, φ_0 - a phase of fluctuation. T - duration of a radio impulse which repeats with frequency F.

The signal on an input of reception devices spatially – carried reception stations is defined by expression

$X_j = k_j S(t) + \overline{n}_j(t)$,

where $S(t)$ - a signal on an output of the transmitter;

k_j – the factor which is taking into account easing of a signal on a line;

$\overline{n}_j(t)$ - noise of the reception device.

3. The methods of measurement of time of a signal arrival

For an accession of mistakes of measurement numerical values of the attitude signal / noise on capacity (P_s / P_n) were set in an interval $10^4 \div 10^8$.

There is widely known method of measurement on forward front of a video pulse which is based on crossing by forward front of some threshold level was chosen as one of methods of measurement of arrival time of a signal. At the big parities signal / noise the steepness of forward front of the pulse, which is deformed by noise, remains same as well as undistorted [2].

The mistake of measurement of delay time is defined by expression $\sigma_t = \tau_f / k_f \sqrt{P_s / P_n}$ for constant amplitude of a pulse , if time of increase of a video pulse τ_f is limited by a passband on intermediate frequency .The opportunity of increase of measurements accuracy at change of value P_s / P_n in a range $P_s / P_n = 10^4 - 10^8$ may be provided at passage of a signal through the linear device. It is necessary to note, that there is a regular peak mistake Δt_A, which reaches the size equal to duration of forward front of a pulse appear when the amplitude of a pulse on an output of the video amplifier, which is caused by various factors (change of distance, a signal fluctuations in a point of reception, change of a passband of the receiver) is changed. The

analysis of mistakes of time delay measurement shows that in considered ranges f_I, f_{II}, f_{III} at duration of fronts τ_f required accuracy of measurement of time delay accordingly $10^{-4}s$, $5 \bullet 10^{-5}s$, $10^{-6}s$ is not provided.

The method of measurement based on use of thin structure of a signal as which are understood was considered, agrees Woodword, signals of high and intermediate frequency is used as second method. Measurements of arrival time, a difference of times at use of signals of high and intermediate frequeney are more exaet, but they result in ambiguity of measurements [2]. The results received at measurement repeats through half of length of a high-frequency wave. The kind of a signal $s_B(t)$ on an output of the filter is in detail enough analyzed in [3]. Elimination of ambiguity of measurements may be executed for the following conditions: $P_s / P_n \geq 6 - 10 \bullet 10^3$; $\Delta f / f = 0{,}015 - 0{,}1$; $A_{\max} \geq 3 \div 5\overline{n}(t)$ on an interval $t \leq 0{,}015 \div 0{,}1\tau_f$. The high accuracy of measurements may be provided at processing of high-frequency fluctuations of a radio impulse on an interval T under eondition that $T \geq 10\tau_f$ and results averaging of measurements. Mistakes of time delay in frequeney ranges f_I, f_{II}, f_{III} are accordingly equal at $0{,}15 \bullet 10^{-8}s$, $0{,}15 \bullet 10^{-9}s$, $0{,}15 \bullet 10^{-10}s$, if $P_s / P_n = 10^4$. Assess of a mistake of time delay of a sine wave signal was carried out under the formula $\sigma_t = 1/2\pi f\sqrt{P_s / P_n}$ [2].

The conclusion

1. The opportunity of use of thin strueture of a signal (signals of high and intermediate frequency) for measurement of time of delay of amplitude manipulated signals in ranges 90-110 kHz, 1,8-2 MHz, 800-1500 MHz is shown.

2. The estimation of mistakes of definition of a site of a souree of electromagnetic radiation is exeeuted. The opportunity of development of precision passive hyperbolie systems whieh aeeuraey is eommensurable with accuraey of systems of satellite navigation sueh as GPS (USA), ГЛОНАСС (Russia) is shown.

References

1. **Южаков В.В.** Современные методы определения местоположения источников электромагнитного излучения.//Зарубежная радиоэлектроника. –1987. –N8 – стр. 67-79.

2. **М. Сколник.** Введение в технику радиолокационных систем. Из-во "Мир", М., -1965.- 748 с

3. **Гоноровский И. С.** Радиотехнические цепи и сигналы. Изд-во "Советскос радио", М., -1971.- 678 с.

UNIVERSAL HARDWARE AND SOFTWARE COMPLEX FOR PROCESSING AND DISPLAYING RADAR AND CHART INFORMATION*

A.A Koshevoy*, A.S.Grib, V.M.Konshin, A.V.Maranov, V.Ph.Medvedev ,V.N.Sadiy, I.P.Smaglyuk, G.I.Reshetnikov**

Central Scientific & Research Institute Navigation and Control,
5, Dimitrova St., 03006, Kiev, Ukraine. E-mail:kvantn@i-c.com.ua

Abstract

Key words: radar, ARPA,navigation, simulation, algorithms, accuracy

There is software device complex for processing of navigation and other radars information intended for:

1) *ARPA*
2) *Control of ship movement in ports and limited areas of water*
3) *Watching after situation on anchor moorages, berths, distant areas of water and coastal zones.*

The complex meets the corresponding requirements of IMO resolution with its performed functions, precision characteristics, noise stability and range of technical means. SDC provides decision above-mentioned problems in the range from 0.1 to 180 miles depending on the type of the aerial system and the altitude of phase center of the aerial. The results of practical task decision in the range from 0.1 to 128 miles are evidence of stability of objective disclosure and escorting. To the present day SDC is exploited in complex with radar systems as "NAYADA", "OCEAN" and other more powerful station. Also it can work with radar system as "KRUPH-ATLAS", Litton, Kelvin Hughes, Furuno, Data Bridge – 7 Norcontrol, Digiplot, Iotron, CAS-1, Sperry - USA

. The functional possibilities of SDC allow: to register a video information of circle survey indicator synchronically with talks (with re-recording after 3 days) with following saving, playing and printing;

to receive radar signal from CSI for a distant (up to 12 miles) notebook with the aim of using of the later as ARPA; to adapt automatically to conjugate type of aerial systems; to adapt (if there is necessary cartography information) to different water areas. In complete set SDC contains five processors (of modern type, more than 200 MHz) and fitted in IBM case controller with the signal transformer. The software of SDC has been worked out in operation systems MS-DOS and Windows. 32 Mb RAM for software and hard drives up to 40 Gb are used in each system. In the present time SDC are in industrial exploitation at many objects.

Introduction

The modern means of navigation and management of vessel movement include the difficult program complexes, which allows providing traffic safety at technical operation of vessels. The tendency of the maximal integration of information services of mobile objects and motionless objects of management now is planned. In this case the prosess of making decisions define automatic means of information processing. Processes of an observation now are automated -definition of a vessel position according to systems information: satellite; hyperbolic; combined.

The attendants receives the information about a course of processes as the message of digital information panels: type of working system; quantity of their elements;accuracy characteristics of measurements; time of separate measurements; degree of the data integration.

However, it is necessary to set the current parameters of astable elements for maintenance of sufficient accuracy: condition of an atmosphere and ionosphere; radio engineering handicapes; time of day; the geographical data; local conditions.

It is obvious, that all given parameters should participate during automatic acceptance of decisions which consequence the increase of time of the data integration, connection of filters of handicapes, a choice of an optimum set of means. So in modern mathematical models of making desitions, based on a method of the maximal plausibility, include additional elements as dot statistical processes with discrete intervention of accident. The models based on the given model of making-decision are called to adapt the computing processes for sharply varied situations: refusal of elements of the big systems; sharp shading at moving in narrow waters; atmospherie faetors.

Together with it it is necessary to expect, what even the small degree of a doubtful situation on the aprioristic data in a considered case will result in deterioration of resulting indications.

Alternative to the given direction is the deterministic approach - inclusion in decision-making process of the aprioristie information such as a card of active and industrial handicapes, card of possible natural and artificial

---

* D.Nat.Sci., Professor, Director.
** D.Sc., Leading Research Scientist.

shadings, card of reflecting properties of objects, removal on recommended trajectories and other type of the information which it is possible to receive including regular onboard means.

The considered examples allow to draw a conclusion, that in the real conditions the means of automation of decision-making processes should be orientate to friendly contact with the operators, which are responsible for consequences of acceptance decisions.

According to stated technicho-methodical bases develop a complex of control facilities by movement of a vessels including in ports both the limited water areas and the control of surface conditions. The task of the maximal visualization and automation of labourious processes of signals processing, registration of operator's actions, works with local and system-wide databases were practically put. Dialogue of the operator of the basic monitor is based on these principles. In particular the following elements: high quality of the image on the monitor; independent choice of a display palette of the information which is displayed by the operator; the arrangement of elements of management is direct in places of the screen on which his attention is concentrated; the minimal set of actions for performance of the appropriate functions; protection of operation against incorrect actions; the opportunity of return to background is perceived by consumers of the considered equipment as at a walk in a correct direction of designing.

The analog part includes reception of signals, automatic adjustment of amplification according to the processor, maintenance of sending frequencies of signals and duration of signals, and also transformation of signals to the digital form (it is possible with management dynamically a range) and record of signals in real time in the remembered device of the processor. Also analog means are used for interface of the developed complex to existing send-receive systems (Nayada, Ocean, specialized, of foreign manufacture). The basis in volume of development of the given complex is made with the software (ON) - up to 90 % of development. On an opportunity of these devices ON provides necessary characteristics: reception of signals with required accuracy; scales of display of the information; the sanction; protection against noise

The program complex in a full complete set includes five processors: managements - displays; initial - secondary processing of signals; tablet with display of the long-term information: condition of anchor parking; condition of moorings; courts on the control. the synchronous registrar audio and video of the information; system of independent display of the data.

The given division allows to raise(increase) reliability of system, complexities however take place at simultaneous work of the operator with several monitors. For overcoming last factor the integrated complex with two monitors for monitoring systems of surface conditions in ports (one multipurpose monitor and the monitor of management audiorecoder), and also directly ship means of automatic radar-tracking lining (ARPA) is developed. Further it is supposed to add a program complex means of radionavigation and positioning on СНС, hyperbolic phase systems. The general(common) software in volume more than 1 М байта is made in language C^{++} For 32 digit calculations. The basic operational system of real time DOS, last updatings as Windous does not support a mode of real time about 3 кГц and in a complex with graphic package DirectX, on supervision, works not stably. Taking into account, that standard DOS does not support diagrams and expansions of memory is used compandor the own universal graphic package such as Visual C is developed.

Now the given hardware-software complex in structure of a product of central scientific research institute navigation and control_ is maintained on a number(line) technical objects..

Block diagram ARPA

ARPA consists of the central processor, the controller of initial and secondary processing radar a signal, the device of digital coding of radar-signal (DC) of the device of interface with radar (MOUSTACHE), the converter of an analog signal in digital code (A/D), the shaper of signals: _0_ KUa, KUa, Vc, code F of recurrence, interruption, and as signals of management.

Into structure ARPA enter as the monitor, the keyboard, unit of imposing and the converter for transformation of interface RS-232 in RS-422.

On input(entrance) ARPA act from radar video signal, a pulse of start radar, a pulse _0_ a course corner of the acrial, a pulse code of a corner of turn of acrial (KUa) and as a pulse code of speed of the vessel from a log and a digital code of a rate of the vessel, acting from a navigating complex or a gyrocompass on consecutive interface RS-422 under report NMEA 0183. From output(exit) ARPA in a navigating complex and to other consumers parameters of the accompanied purposes are given out.

Electric parameters, frequency characteristics of entrance signals are coordinated with concrete radar with the help of the appropriate adjustment of the device of interface with radar and parameters of the software.

In case of need interfaces to additional devices on other channels (analog or other) the opportunity of installation of additional devices of interface, controllers in слоты expansions of trunks ISA, PCI the central processor is stipulated. Thus development of the program of the driver of the appropriate device and binding of software ARPA to the concrete project is required.

As the central processor in ARPA the processor of industrial execution(performance) such as ROCKY with clock frequency up to 800 МГц is used. The processor has trunks ISA, PCI, standard liaison channels with the keyboard and mouse interface RS-232C, the parallel interface. At use in onboard conditions of the program may be loaded in solid-state memory FLASH - the store.

The Processor has the built - in graphic controller which provides interface to monitors to the sanction 1280x1024 pixel.

Structurally the processor is intended for installation in a passive unifying payment.

The Controller ON / IN is realized on the built in industrial processor such as 486-DX2 or 586. The processor has FLASH-the store, trunk PS-104 (16-ти digit), standard interface RS-232C and the parallel interface.

The Device of coding (DC) has two buffer two-port RAMS through which the exchange with the controller is made.

From the device of interface with radar on input(entrance) DC signals act: video signal, Impulse."0" D, Imp. KUa, Imp, "0" KUa.

Video signal acts on an input(entrance) of the converter of an analog pressure(voltage) in bineryo coded signal (CVC) which further acts on an input(entrance) of shifting register: which makes record of a binary code in sling, formed by the circuit of management, and then through the buffer register enters the name in DOZE BC.

The code of management BC generated by the controller in sling acts through DOZE APU on an input(entrance) of the converter of a code in a pressure(voltage) from which output(exit) a pulse of automatic adjustment of amplification(strengthening) in sling moves or on an input(entrance) of reception device radar, or if in radar such input(entrance) is not stipulated, is used for regulation of a threshold of quantization DC.

Counter KUa serves for coding a corner of turn of aerial radar which after input in the controller is shared with a code of a rate of the vessel for calculation of parameters slings and parameters of accompanied objects.

For maintenance of the control of system and a mode _Trainer_ in DC there is a shaper of the control purpose.

The device of interface with radar serves for reception and the coordination of signals with radar and their translations in DC and the Shaper of signals.

As the converter аналового a signal in digital code (A/D) it is used high-speed A/D PCI-9810. Frequency of coding BC acts on input(entrance) A/D from the external generator. The video signal acting with matching unit of the/adder, will be transformed in A/D to 1024 coded readout which through trunk PCI on the channel of direct access act in the central processing UNIT for processing, transformations and the subsequent display to screen ARPA.

The shaper of signals serves for binding video signal with radar to code KUa, and as formations of frequency of recurrence of a pulse of start radar, formations of a signal "0" to range (the detained pulse of start radar) and buffering of pulses of a code of speed of the vessel.

The shaper of signals is interfaced(integrated) to the central processing UNIT on trunk ISA.

The code of frequency of recurrence of a pulse of start radar serves for the coordination of scales established in radar with ARPA.

The central processing UNIT is interfaced(integrated) to the controller ON / IN with the help of channel RS-232C and the parallel channel.

The controller receives from the central processing UNIT of coordinate of the purposes taken on support by the operator manually and modes of operation of system.

In the central processing UNIT codes of parameters of the accompanied purposes and a code of a rate are transferred.

The monitor serves for display radar of signals, graphic symbols of the purposes, the stylized cartographical information, dialogue messages and the alphanumeric information of the purposes.

The keyboard provides dialogue of the operator from CENTRAL PROCESSING UNITS on the standard interface.

The unit of imposing provides management of a marker at manual capture on support, identification of parameters and at the decision of other dialogue problems(tasks).

The converter is necessary for transformation of the standard interface of controller RS-232C to interface RS-422A.

References

1. **Зурабов Ю.Г.** и др. Судовые средства автоматизации предупреждения столкновений судов. М. :Транспорт 1985.

2. **Удалов В.И.** и др. Управление крупнотоннажными судами М. :Транспорт, 1986.

3. **Graham Danton.** The theory and practice of seamanship. London, 1996, -522p.

4. **Nathaniel Bowditch.** The American practical navigator (An epitome of navigation). 1995. –481p.

RESTRICTION OF MAXIMUM ERRORS IN GUIDANCE, NAVIGATION AND MOTION CONTROL SYSTEMS*

Alexander Nebylov*

State University of Aerospace Instrumentation,
67, Bolshaya Morskaya, St.Petersburg, 190000, Russia. E-mail: nebylov@aanet.ru

Abstract

Key words: maximal error, linear system, synthesis

Motion control systems and other automatic systems with accuracy indexes which are within the assigned tolerance limits for a broad class of input excitations are considered. A maximum error is adopted as the main index of accuracy. The limitations on several derivatives values determine the class of input excitations. The maximum total error is calculated taking into account the features of reference input and different noises and disturbances applied to the system. At system syntheses the problems of minimization of a maximum total error or limitation of a maximum dynamic error at, for example, minimum possible pass-band of a system can be solved. The importance of maximal error restriction in the absolute majority of guidance, navigation and motion control systems is underlined.

The maximum error e_m is not the statistical characteristic and can be reached at the particular determined input in a definite instant. Therefore its controlling is possible only at the given prior information about properties of inputs and disturbances in categories of the rigid determined limitations. A standard case of such task is the limitation of maximum values of one, two or more derivatives of a signal [1]

$$\left|g^{(i)}(t)\right| \le g_m^i, \; i = \overline{K, N}, \; 0 \le K \le N .$$

At limitation of only one i-th derivative of input (N=K) the maximum dynamic error is easily determined by a method of disturbances accumulation which fundamentals were established at the paper of B.V.Bulgakov [2], and expresses by the formula

$$e_m = g_m^i \int_0^\infty \left|w_{eK}(t)\right| dt ,$$

where $w_{eK}(t)$ is the applicable impulse response of a system.

At growing the number of input restricted derivatives the complexity of solution of the task of maximum error finding sharply increases, that generally causes to use the numerical methods. At the same time it is essential, that in the majority of the practical applications the number of authentically restricted derivatives can be not less than two or three. That makes the most unfavorable input sufficiently smooth, and the estimation of a maximum error many times stronger in compare with the case of one restricted derivative. It causes to develop analytical method of estimation and restriction (at system synthesis) of a maximum error at a heightened volume of the prior information on inputs properties. One of them was presented in [3] and permits to prove that the maximum error appears under the input which n-th derivative shape is shown in Fig.1 for three different relationship between the values of limited derivatives. It was established that the frequency λ meets the formula

$$\lambda \ge \eta_{N-1}^* \sqrt[N-i]{g_m^{(N)}/g_m^{(i)}} , \text{ where } \eta_1^* = 1.57 , \; \eta_2^* = 1.11 , \; \eta_3^* = 1.09, \; \eta_4^* = 1.06 , \ldots$$

Certainly, the exact definition of the original maximum directly from the Laplace transform, without finding the original, is principally impossible. However, the frequency domain method, connected with searching of the most unfavorable input as the sum of several harmonic functions, has been designed by the author. It gives the maximum error estimation in the form

$$e_m \cong c_K g_m^{(K)} + c_{K+1} g_m^{(K+1)} + \ldots + c_N g_m^{(N)}, \qquad (1)$$

where $\{c_i\}_K^N$ are the multipliers of the polynomial

$$C_{N-K}(\omega) = \sum_{i=K}^{N} c_i \omega^{i-K} ,$$

* D.Sc., Professor, Director of International Institute for Advanced Aerospace Technologies of SUAI.

which deliver performing the condition $C_{N-K}(\omega) \geq |H_{eK}(j\omega)|$. Here $H_{eK}(j\omega)=H_e(j\omega)/(j\omega)^K$, and $H_e(s)$ is the corresponding transfer function of the system which connected the transforms of input and dynamic error.

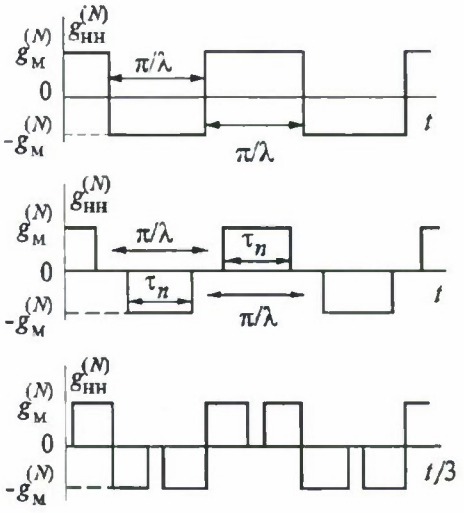

Fig.1

The estimation (1) will be of top strength if the coefficients $\{c_i\}_K^N$ are optimal under the criterion

$$\sum_{i=K}^{N} c_i g_{..}^{(i)} \to \min_{c}.$$

In this case the points of curves $C_{N-K}(\omega)$ and $|H_{eK}(j\omega)|$ tangency correspond to the frequencies of harmonic functions which sum has to be the most unfavorable input of the system. The number of such harmonics V depends on the number of limited derivatives of input and is equal to $v = \frac{N-K}{2} + 1$ at even $(N\text{-}K)$

and $v = \frac{N-K+1}{2}$ at odd $(N\text{-}K)$.

As a rule V is equal to 2 or 3.

This method gives a quite reasonable estimation of maximum error. It has been established that the relative understatement of the estimation of maximum error can not surpass 27% even in a highly oscillating system with very small margin of stability, and in actual cases of a well-damped system makes only a few percent.

Often even a single harmonic with the most unfavorable frequency can provide the error rather close to maximal one. It can be determined by the graphic constructions which were described in [3].

It is essential, that in the majority of the technical applications just maximum error instead of r.-m.-s. error is the most objective characteristic of automatic system accuracy. This is very important for motion control systems, in which at a quite reasonable r.-m.-s. error even a single large surge of an error can result in disastrous consequences. This fact is among the main reasons of the limited efficiency of the optimal filtration theory at real systems constructing. The finding of the refined solution of r.-m.-s. error minimization problem, as a rule, does not give for the designer a final version of a system dynamic properties choice. The successful solution of the majority problems of guidance is also determined not by r.-m.-s. error but maximum error.

At consideration the system synthesis methods with maximum error of control restriction two options have to be considered: (1) of minimization of a maximum total error and (2) limitation of a maximum dynamic error at, for example, minimum possible pass-band of a system. It could be shown that in both cases the construction of allowed "corridor" for the Bode magnitude plot of an open-loop circuit of a system [3] is an effective method of control accuracy investigation.

The examples of comparison of systems synthesized under criteria of r.-m.-s error minimum and a maximum error minimum show the difference of their dynamic properties and variance of extremum points of control accuracy. The requirement of total r.-m.-s. error minimization at the action of an input noise results in narrower bandwidth of a system as contrasted to the requirement of minimization of a maximum total error. In this case maximum error increases approximately on 50 % in compare with its minimum accessible level.

The influence of system parameters instability on the different indexes of control accuracy have to be taken into account. . It was shown that the indexes of accuracy in a system which is optimal under the criterion $D_e \rightarrow \min$ are less critical to instability of system parameters than in the case of criterion $e_m \rightarrow \min$. Besides, the criticality to instability of parameters decreases with decrease of a system order, i.e. its simplification. The simplest system of the first order has rather smooth dependence of maximal error on the open loop gain factor K_1 instability according to the formula

$$e_{m\,\min} = \frac{3^{2/3}}{2^{1/3}} \frac{1+\chi(1+\chi)}{(1+\chi)^{2/3}\chi^{2/3}} \left(g_m^{(1)} S_v\right)^{1/3}.$$

Here index χ characterizes the deepness of K_1 instability with reference to the nominal value K_{1nom}: $K_1 \in [K_{1nom}/\chi, K_{1nom}\chi]$, $\chi \geq 1$, and S_v is the level of spectral density of input noise. Naturally, at $\chi \rightarrow 1$ when the gain factor is absolutely stable,

$$e_{m\,\min} \rightarrow 3^{5/3} \cdot 2^{-1} \left(g_m^{(1)} S_v\right)^{1/3} = 3.12 \left(g_m^{(1)} S_v\right)^{1/3}.$$

Among the problems of motion control, where the restriction of a maximum error is specially relevant, the blind landing of an airplane, the collusion avoidance at vessels moving at clashing heading, homing missile control [4] and similar tasks are of top importance. The problem of accuracy ensuring at automatic control of relative motion of two winged vehicles at their approach with the purpose of docking could be also reviewed as an example (the project of Ekranoplane use at aerospace plane assist at for horizontal start and landing [5]).

The examples of two-channel and multi-channel invariant and non-invariant integrated navigation systems synthesis under the criterion $e_m \rightarrow \min$ could be considered. In these cases the values of derivatives of gyros and accelerometers errors and measured parameters of motion were assumed as limited ones, and for positional sensor (GPS, radar or other) the spectral density of wide-band error were given.

The reasoning of importance of maximum error restriction criterion in a lot of practical tasks of navigation and motion control could be considered as the objective of the paper.

References

1. **Besekerski V.A., Nebylov A.V.** Robust automatic control systems. Nauka, Moscow, 1983 (in Russian).
2. **Bulgakov B.V.** About disturbances accumulation in linear oscillation systems with constant parameters. // USSR Academy of Sciences reports, 1946, V.51, №5, pp.339-342(in Russian).
3. **Nebylov A.V.** Ensuring control accuracy. Nauka, Moscow, 1998 (in Russian with abstract in English).
4. **Besekerski V.A., Eliseev A.A., Nebylov A.V., etc.** Radioautomatics. Visshaya Shkola, Moscow, 1985 (in Russian).
5. **Nebylov A.V., Ohkami Y., Tomita N.** Control Strategies and Means of Spaceplane Landing with Ekranoplane Assist. 14th World Congress of International Federation of Automatic Control. Beijing, 1999, Vol. P, pp. 395-400.

ESTIMATION OF GYROCOMPASSING ACCURACY AND TECHNIQUES OF COURSE AND GYRO DRIFT CORRECTION IN INTEGRATED NAVIGATION SYSTEM*

A.A.Fomitchev*, A.B.Koltchev, K.Yu.Schastlyvets***, V.B.Uspensky****
JSC "Lasex". **V.V.Timofeev*****, RDI AE
9, Institutsky per., Dolgoprudny Moscow Area, Russia. E-mail: laser@pop3.mipt.ru

Abstract

Key words: accurancy gyrocompassing, course and drift correction, algorithms

The estimations of coarse gyrocompassing accuracy at a strapdown inertial navigation system are received with the account of regular and random gyro drift, measured data quantization and gyrocompassing duration. In these conditions the actual course error, the estimation of accuracy for any gyro start and the guaranteed estimation of accuracy are received. The obtained results may be to use for definition the initial covariance matrix of the state vector errors and for the planning technique of coarse gyrocompassing duration. For decrease these errors the technique of current course correction and restoration of the actual regular gyro drift in moving integrated navigation system is offered also. It includes the algorithm of the course computation in moving, the algorithm of the guaranteed course accuracy computation and the algorithm of the gyro drift correction.

Introduction

At alignment realization of a strapdown inertial navigation system (SINS) it fails to share a course mistake and "horizontal" gyro regular drift. Thus by a coarse course estimation the not authentic values gyro drift are calculated. It results that the decision of a navigating task begins with large errors of the initial parameters. The report is devoted to analysis of the coarse gyrocopmassing error for the motionless object with the account regular and random gyro drift, information quantization effect, data accumulation duration, object position (geographical latitude) and actual orientation. The obtained results may be to use for definition the initial covariance matrix of the state vector errors and for the planning technique of coarse gyrocompassing duration. For decrease these errors the technique of current course correction and restoration of the actual values of "horizontal" gyro regular drift in moving integrated navigation system is offered also.

1. The analysis of accuracy gyrocompassing

Influence of each of the tool errors was investigated separately. Thus the total error is the sum of errors which are brought in by each factor. High-frequency perturbations of actual angular movement are interpreted as random gyro drift.

In these conditions three kinds of estimation of the gyrocompassing accuracy are received and listed in ascending order of absolute meanings:

- **actual error**. It is defined by concrete realization of regular drift and actual course object. It corresponds to actual error received for one gyro start;

- **estimation of accuracy for any gyro start**. It corresponds to the "worse" regular drifts, concrete course object and serve for definition of guaranteed gyrocompassing accuracy (i.e. for any gyro start), if something is known about object actual course a priori;

- **guaranteed estimation of accuracy**. It corresponds to the "worse" regular drift gyros and the "worse" probable course object and can be used as the generalized characteristic of the coarse gyrocopmassing accuracy. It can be used also for formation of the requirements to tool errors depending on planned gyrocopmassing duration and required accuracy.

For difference tool errors the following results are received.

1.1. Model of measurements algorithmically "leveling" gyros (X and Z-gyros) with account regular gyro drift is set as:

$$\omega_x = \Omega \cos\varphi \cos\psi^* + \Delta\omega_x, \quad \omega_z = -\Omega \cos\varphi \sin\psi^* + \Delta\omega_z.$$

---

* D.Sc., General Director.
** Chief of Department.
*** Chief of Division.
**** Ph.D., Senior Scientist.
***** Ph.D., Senior Scientist.

Here ω_x, ω_z - displayed by gyros rotation rate, Ω - Earth angular rate, φ - geographical latitude of an alignment position, ψ^* - actual course, $\Delta\omega_i \ (i = x, z)$ - regular gyro drift.

In linear approximation the actual error of computed course looks as

$$\delta\psi = -\frac{1}{\Omega \cos\varphi}(\Delta\omega_x \sin\psi^* + \Delta\omega_z \cos\psi^*).$$

Let values $\Delta\omega_x$ and $\Delta\omega_z$ are realized for one gyro start from a range $[-\Delta\omega_{max}; \Delta\omega_{max}]$ according to the uniform distribution. Then for a computed course we have an estimation of accuracy for any gyro start as

$$\delta\tilde{\psi} = \max_{\Delta\omega_X, \Delta\omega_Z} |\delta\psi| = \frac{\Delta\omega_{max}}{\Omega \cos\varphi}\left(|\sin\psi^*| + |\cos\psi^*|\right).$$

For any course we shall receive guaranteed estimation of accuracy

$$\delta\bar{\tilde{\psi}} = \max_{\psi^*} \delta\tilde{\psi} = \frac{\sqrt{2}\Delta\omega_{max}}{\Omega \cos\varphi}.$$

1.2. For the analysis of random gyro drift error the following model of measurements is accepted in view of averaging by the data on an interval of time T - data accumulation duration:

$$\omega_x(T) = \Omega \cos\varphi \cos\psi^* + \frac{1}{T}\int_0^T \delta\omega_x(t)dt, \quad \omega_z(T) = -\Omega \cos\varphi \sin\psi^* + \frac{1}{T}\int_0^T \delta\omega_z(t)dt.$$

Here $\omega_x(T), \omega_z(T)$ - indications displayed by gyros, $\delta\omega_i(t) \ (i = x, z)$ - random drift set as white noise with zero average and intensity $\sigma^2_{\delta\omega}$. In this case for mean square deviation we have

$$\sigma_{\delta\psi} = \frac{1}{\Omega \cos\varphi}\frac{\sigma_{\delta\omega}}{\sqrt{T}}.$$

The piece $[-\sigma_{\delta\psi}, \sigma_{\delta\psi}]$ can be interpreted as a range of a course error caused random gyro drift.

From last expression, in particular, it is possible to receive an estimation of data accumulation time $T_{\delta\omega}$ for achievement of an admissible error Δ_ψ, caused random drift:

$$T_{\delta\omega} = \frac{\sigma^2_{\delta\omega}}{\Delta^2_\psi}\frac{1}{\Omega^2 \cos^2\varphi}.$$

1.3. For reception of course error caused by information quantization, is used the following model of measurements:

$$\Delta\Theta_x(T) = \Omega \cos\varphi \cos\psi^* \cdot T - \nu_x \, sign(\cos\psi^*), \quad \Delta\Theta_z(T) = -\Omega \cos\varphi \sin\psi^* \cdot T + \nu_z \, sign(\sin\psi^*),$$

here $\nu \in [0; K)$ - random value submitting according to the uniform distribution, K - size of quantum.

In these conditions is received the actual course error, the estimation of accuracy and the guaranteed estimation of accuracy accordingly

$$\delta\psi_\nu(T) = -\frac{\sin\psi^* \cos\psi^*}{\Omega \cos\varphi \cdot T}\left(-\frac{\nu_x}{|\cos\psi^*|} + \frac{\nu_z}{|\sin\psi^*|}\right), \quad \delta\tilde{\psi}_\nu(T) = \frac{|\cos\psi^*| \cdot K}{\Omega \cos\varphi \cdot T}, \quad \delta\bar{\tilde{\psi}}_\nu(T) = \frac{K}{\Omega \cos\varphi \cdot T}.$$

Basing on last estimation, minimal time of data accumulation, at which the course error caused by quantization will not exceed Δ_ψ, we shall define as $T_\nu = \frac{K}{\Delta_\psi \Omega \cos\varphi}$.

2. The technique of course and gyro drift correction

The problem of current course correction and restoration of the actual regular drift of "horizontal" gyros in moving integrated navigation system is considered. The decision of the problem is realized according to the following technique.

Upon alignment termination the algorithm of autonomous navigation realizing computation of object orientation, speed and position concerning some inertial frame (IF) is initialized. This algorithm provides autonomous data organization about object reorientation and change vector of the speed. In the beginning object movement the algorithm of course correction is initialized. With comparison of speed change vector in the IF received from SINS and the same one from GNSS the current course is defined. The end of the algorithm is carried out at achievement of required guaranteed course accuracy. Further, the new accurate object orientation in alignment time is recomputed and the actual values gyro drift are restored.

For protection the course correction algorithm against casual mistakes in GNSS measurements using hybrid information is more preferred.

The more dynamic object movement guarantees the better efficiency of the stated technique because influences of a course error and gyro drift are shared better. The results of modeling demonstrate the acceptable course accuracy is provided after some seconds of moving aircraft on runway.

The following algorithms to realize described technique are developed:

- Algorithm of the course computation in moving.
- Algorithm of the guaranteed course accuracy computation.
- Algorithm of the gyro drift correction.

The modeling of algorithms on simulation model of movement, and also real data confirms efficiency of the offered technique.

MOBILE VEHICLE TRACKING SYSTEM TESTS*

D. A.Antonov*, A. I.Chernomorsky, A. I.Peterburg***, A. Tuvin****, K. K.Veremeenko*****, R. Yu.Zimin******

Moscow Aviation Institute (Technical State University),

4, Volokolamskoyc shosse, 125993, GSP-3, A-80, Moscow, Russia. E-mail: k_veremeenko@pein.msk.su

Abstract

Key words: satellite navigation system, vehicle-tracking system, test.

The outcomes of work on mock-up realization for a system determining mutual disposition and transition of two floating objects are considered in the presentation. Satellite navigation receivers and modern data links are the basis of the considered solution. Block diagram of the system mock-up and results of the test at a freshwater testing area are presented.

The outcomes of work on realization of one practical method of solving a problem of accurate and fast determination of a mutual disposition and transition of two floating objects are considered in the presentation.
The purpose of the work was to create a mockup of the system for detecting and tracking of a mobile object that could be up to tens kilometers away from a mobile dispatch point. The following requirements were made of the developed system:

- the coordinate determination error should be not greater than 20 m;
- the following information should be displayed at the mobile dispatch point: time, coordinates of the mobile dispatch point and a tracking objcct, velocity projections of the dispatch point and an object, distance between the dispatch point and an object, an azimuth from dispatch point to an object, indication of lack of information concerning object and dispatch point positions (signal of the failure of the system);
- the indicated information should be updated and be mapped on a screen of the monitor of the dispatch point with a rate of 1 Hz, and should be recorded and stored in memory of the computer of mobile dispatch point;
- thc systcm must indicate fails in any operational mode by special signals.

The delivered problem of tracking system creating could be solved with the use of satellite navigation and modern communication technologies. To solve the navigation part of the problem it is most expedient to use satellite navigation systems GLONASS/GPS. The positioning accuracy of these systems is about 20 м (2 RMS). Thus, the solution of the problem within the framework of a required accuracy is possible without differcntial mode that considerably simplifies and makes cheaper the system.

The main idea of the offer consists of the use of industrial packet radio modems operating jointly with commercially produced radio stations. Thc system consists of the following constituents:

1. Onboard set installed on a tracked mobile object that consists of:
   - Plaser GPS 450GPS receiver;
   - GPS antenna;
   - Radio modem TRIMTALK Modcm;
   - Radius GM 300 Motorola radio station (with a power of 45 W).
2. Onboard set installed on mobile dispatch point that consists of:
   - UHF antenna;
   - Radio modem with the built-in TRIMTALK 450 receiver;
   - personal computer with two COM ports;
   - Plaser GPS 450 GPS recciver;
   - GPS antenna.

The main function of the Plaser GPS 450 GPS receiver is to determine position, velocities and track angle of the objects. Data exchange between Plaser GPS 450 GPS receiver and other equipment is carried out with the use of the TAIP protocol (Trimble ASCII Interface Protocol).
Data represented in TAIP protocol arrivcs from GPS receivcr located on a tracked mobile objcct through RS-232 port to thc radio modem TRIMTALK Modem that is intended for data link communication shaping. The Modem operates in UHF band (from 450 up to 470 MHz). It executes the following functions:

- partition of digital information generatcd by GPS receiver into packages of certain size;
- further digital-to-analog or analog-digital transformation of a signal.

---

*Student,
** Head of the Department, professor,
*** Chief designer,
**** Associate professor,
***** Associate professor,
****** Student.

After digital-to-analog transformation information packages are broadcast by Radius GM-300Motorola radio station, operating in VHF band (from 146 up to 176 MHz) and in UHF band (from 403 up to 433 MHz, from 438 up to 470 MHz, from 465 up to 495 MHz).

The reception of information broadcast by radio station of the tracked mobile object is carried out with the help of a built-in receiver of the TRIMTALK 450 radio modem operating in the same frequency band as TRIMTALK Modem and performing the following functions:

- reception and transfer of radio signal by means of built-in receiver and low-power (0,5 W) transmitter that allows to realize a double-side digital data link communication between objects within a distance of up to 3 km, i.e. to configurate a set of the onboard equipment of the tracked mobile object through RS-232 port of dispatch PC;
- further digital-to-analog or analog-digital transformation of a signal.

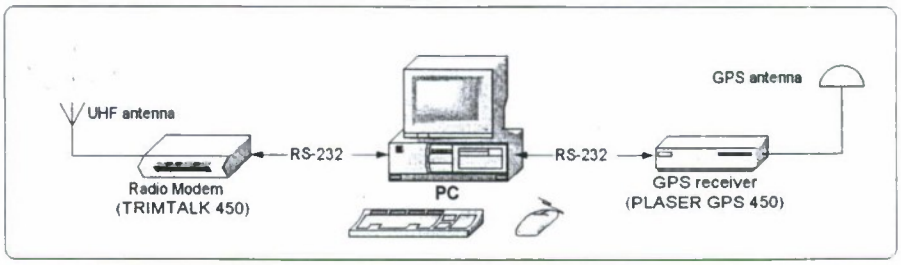

Fig.1. Mobile dispatch point diagram.

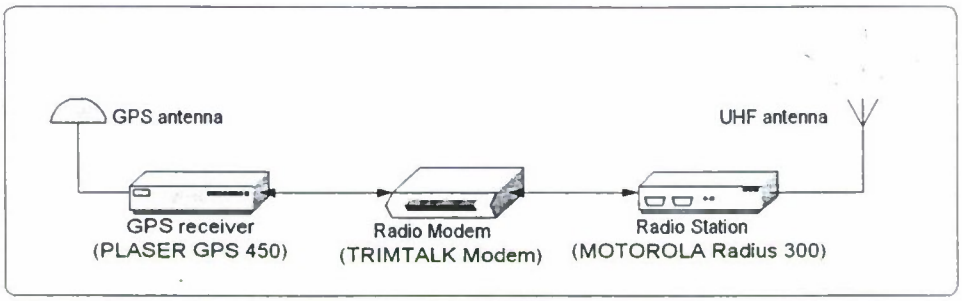

Fig.2. Onboard set installed on a tracking object.

After analog-digital transformation the information package is transferred to PC through RS-232 port. PC is intended for configuration of the system, processing, systematization and indication of the received data using specially developed software that grants sufficient possibilities to the developer for the solution of the given problem.

The software consists of eleven modules. They can be divided into three parts according their functionality:

- main module that performs operations on dispatching of the requests, reception and consequent data processing, displaying of the received and processed information;
- auxiliary module that is necessary for GPS receivers and serial ports set-up and for organization of the convenient interface;
- graphic module that performs graphic representation of the processed information.

The developed software is intended for work in 3 modes:

- indication of GPS receiver outputs of a tracked mobile object;
- indication of GPS receiver outputs of the mobile dispatch point;
- joint indication of both GPS receivers outputs, calculation of mutual orientation parameters and recording of the information in the output data file.

The possibility of change-over of GPS receivers serial ports and of dispatch mobile point computer to any data rate supported by the equipment is stipulated by the developed software. Components of visualization of mutual position of an object and dispatch point and components of a posteriori processing of experiment outcomes that give a qualitative and quantitative evaluation for the accuracy of GPS positioning are integrated into developed software.

The created mockup passed successfully development-testing, tests in dynamic environments at a ground and aquatic testing polygons. It showed high accuracy and stability of work. The serviceability of the system in urban conditions was demonstrated. Tests at an aquatic polygon showed that the system works stable within a distance up to 13 km. It was demonstrated also that there are no noticeable effects of interference between GPS antenna of the satellite navigation receiver and transmitting UHF antenna. Graphical results of the tests are presented in presentation.

ADAPTIVE FLIGHT CONTROL BASED ON PARAMETRIC IDENTIFICATION IN SLIDING MODE*

A. L. Fradkov*, B. R. Andrievsky**

Institute for Problems of Mechanical Engineering of the Russian Academy of Sciences,
61 Bolshoy ave., V.O., Saint Petersburg, 199178, Russia.
Fax: +7(812) 321–4771, Tel: +7(812) 321–4766.
E-mails: {alf,andrh}@ipme.ru

Abstract.

Keywords. Combined adaptive control, Flying vehicle, Attitude reference control, Homing guidance.

Combined adaptive control scheme is presented for attitude control of the flying vehicle with uncertain parameters. The adaptive algorithm includes the variable structure controller with forced sliding motion, parametric identification algorithm and the parallel feedforward compensator. The proposed controller ensures finite time decay of augmented error due to relay term in control law. Exponential convergence of the parameter error under the condition of persistent excitation is provided. The adaptation algorithm provides the prescribed dynamic properties of the attitude control system for various flight conditions. The problems of the attitude reference control and homing guidance control are considered and numerically examined. Simulation results demonstrate high performance and adaptivity properties of the proposed controller.

Introduction

The demands on modern autopilots are becoming more stringent than in the past. The flying vehicle autopilots have to be able to produce a response that is accurate and fast despite severe variations in speed and altitude of the airframe. Hence the challenge for autopilot design is to produce closed loop airframe responses that are much faster than the nature weathercock frequency of the airframe, and to produce accurate and fast response in the face of large parametric uncertainty [1].

The promising way to fulfill these requirements is application of the *adaptive control technique*. Chosen method of adaptation has to meet the conflicting requirements on the tuning rate and performance quality under the conditions of lack of the flying vehicle state measurements. The *variable*-structure control technique, utilizing forced *sliding motions* ensures high adaptability in the some region of flying vehicle parameters [2], but in the general case can not provide the optimal closed-loop system performance. The adaptation methods based on the *parameter identification* make the optimality easier to secure, but have relatively long period of tuning.

The *combined* adaptive controller [3] uses both variable-structure and identification approaches and is able to meet the claims indicated above.

In the paper [3] the general scheme of the combined adaptive controller is presented and proof of overall system efficiency for LTI (Linear Time-Invariant) plant model for the case of fulfillment the *persistent excitation condition* is given. This condition is well known one for convergence of the parameter estimates to their true values [4, 5].

Fulfillment of that requirement is an open question for the considered system, because the flying vehicle controlling input (the rudder deflection) is produced by the autopilot as a function on current attitude. Besides, for practical applicability of the proposed scheme more realistic plant model (in comparison with [3, 6, 9, 10]) has to be taken. First of all, it is necessary to take into account *nonlinearities* of the vehicle model, *atmospheric disturbances* and *sluggishness* of the steering gears.

1. Combined adaptive controller

The combined adaptive controller consists of the following subsystems [3].

The *adaptation algorithm* includes the *variable structure* (VS) controller with forced sliding motion, parametric *identification algorithm*, *tunable pre-filter* and the *parallel feedforward compensator* (or *shunt*) [3, 9, 6, 10]. The adaptation algorithm is aimed to provide prescribed dynamic properties of the internal system when the plant parameters are changed in the wide range. The control aim is to achieve desired closed-loop system performance described by an *implicit reference-model* [7, 8] and imposes fewer restrictions on system performance than for explicit one. To achieve that aim an accurate tracking to transformed reference signal is provided. This signal is generated by adjustable pre-filter. Pre-filter adjustment is provided on the basis of the parameter estimates.

The posed tracking problem is solved by means of organizing the *sliding motion* [2]. By means of the shunt [3] the plant attitude angular velocities are not used in the control law.

The identification algorithm provides real-time parameter estimates. It uses the *augmented error signal*, generated by means of two low-pass filters and can be treated as an *Extended Kalman Estimator.*

The sliding-mode control law is used to ensure an ideal tracking of the *extended plant* (the shunt in parallel with the aircraft) output after the reference signal, produced by means of the tunable pre-filter. The nonlinear flying vehicle model is used for adaptive control system performance analyses. To use the design method of [3], the LTI flying

---

* D.Sc., Head of the Laboratory
**Ph.D., Senior Researcher

vehicle model had been taken. The model parameter values depend on the flight conditions and assumed to be *a priory* unknown.

For the algorithm design it is assumed that the time lag of autopilot servo is absent. In simulation is used the first-order dynamical servo model. The yaw angle only (without the yawing rate) is assumed to be measurable by means of the flying vehicle onboard sensors.

2. Numerical examples

The lateral angle control problem for a small-size hypothetical flying vehicle is considered. The transients of the *yaw* and the *rudder* angles are shown in Fig. 1.

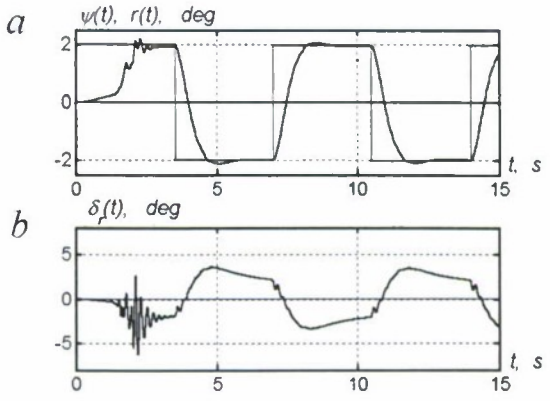

Fig. 1. Transients of the yaw (*a*) and the rudder (*b*) angles

The time histories of the flying vehicle linear model parameters estimations are shown in Fig. 2. It can be seen, that the transient time of estimation processes is approximately 2.5 *s*, and, therefore, the rate of estimation is close to that of flying vehicle attitude motion. The "ideal" parameter values had been found numerically by linearization of the vehicle model near the basic point.

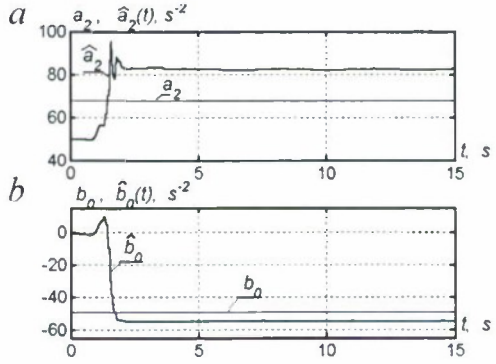

Fig. 2. Time histories of the flying vehicle parameters estimations

Figure 3 shows the fight path in the relative coordinates for homing guidance by means of the direct pointing method to the movable target point, having 20 *m/s* and the initial distance 10 *km*.

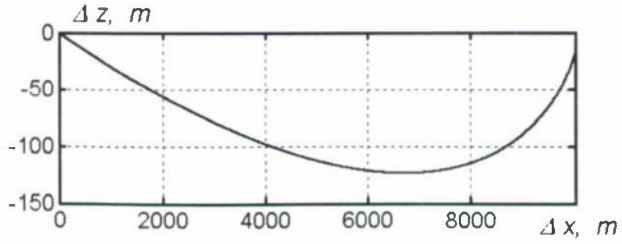

Fig. 3. The homing guidance fight path

3. Conclusions

The combined adaptive control law for flight attitude control system is proposed. The adaptive algorithm for flight control includes the variable-strueture controller with foreed sliding motion, parametrie identifieation algorithm and the parallel feedforward compensator. The adaptation algorithm provides the preseribed dynamic properties of the flight eontrol system for uneertain parameters of the vehicle. Simulation results verify effieieney of the combined adaptive controller in the ease of significant uneertainty of the flying vehiele parameters, its nonlinearity and the servo time lag.

Aeknowlgements

This work was partly supported by Russian Foundation of Basie Researeh (RFBR), grant 02-01-00765 and Seientifie Program of RAS No 17 (projeet 3.1.4).

References

1. **White, B A and Tsourdos, A.** Modern missile flight control design: an overview. 15th IFAC Symposium on Automatic Control in Aerospace, Bologna, Italy, 2–7, Sept. 2001, pp. 431–436.
2. **Utkin, V.I.** Sliding Modes in Control and Optimization. Berlin: Springer-Verlag, 1992.
3. **Andrievsky B.R., Fradkov A.L., Stotsky A.A.** Shunt compensation for indirect sliding mode adaptive control. Proc. of 13th Triennial IFAC World Congress, S.F., USA, 1996, v. **K**, pp. 193–198.
4. **Narendra K.S., Annaswamy A.M.** Persistent excitation in adaptive systems. Int. J. Control, 1987, **45**, 1, pp.127–160.
5. **Fradkov, A.L., I.V. Miroshnik and V.O. Nikiforov.** Nonlinear and Adaptive Control of Complex Systems, Dordrecht: Kluwer, 1999.
6. **Bartolini G., Ferrara A.** A simplified discontinuous control scheme for uncertain linear systems: an Input/Output approach. Proc. of the IEEE Workshop "Variable Structure and Lyapunov Control of Uncertain Dynamical Systems", Shefficld, UK, 1992, pp. 6–11.
7. **Fradkov, A.L.** Synthesis of adaptive system for stabilization of linear dynamic plants. Autom. Rem. Contr., **35**, 12, 1974, pp. 1960–1966.
8. **Andrievsky, B.R. and A.L. Fradkov.** Implicit model reference adaptive controllers based on feedback Kalman-Yakubovich lemma. Proc. 3rd IEEE Conf. on Control Applications, Glasgow, 1994, pp. 1171–1174.
9. **Bartolini G., Ferrara A., Stotsky A.** Stability and exponential stability of an adaptive control scheme for plants of any relative degree. IEEE Trans. Autom. Contr. **40**, No 1, 1995, pp. 100 – 103.
10. **Iwai Z., Mizumoto I.** Realization of simple adaptive control by using parallel feedforward compensator. Int. Journ. Contr., v. **59**, 1994, pp. 1543 – 1565.

PRIVACY CONCERNS WHEN INTRODUCING TELEMATICS IN THE MARKET*

Carlos Rodriguez Casal*
Departamento de Ingenieria Electrica y Electronica, Universidad Publica de Navarra
Pamplona, Navarra, 31.006 Spain
Tel: +34.948.169.094 Fax: +34.948.169.169 E-mail: crosal@unavarra.es

Abstract

Keywords: location data, car industry, user's intimacy

The car industry is introducing location and communication possibilities in order to improve the traveller's safety and security. This new infrastructure is also used to provide support services to the driver and entertainment to the passengers. One of the most controversial characteristics of these systems is the processing of personal data: the car's position is going to be stored and the speed, brake, car performance and the chronology of requested services can also be processed. For a service provider to use location data is it important to keep an eye on the legal restriction imposed to the processing of such data.

Location techniques

The function of the systems typically included in the term "telematics", differs according to manufacturer, but the underlying idea is common to all of them: to compute the vehicle's position, to communicate with an information centre and to facilitate services to the travellers. Many manufacturers (such as Fiat, General Motors or Daimler Chrysler) develop their own systems and services (Connect, OnStar and Tegaron respectively), other manufactures may opt for the installation of other's providers platforms, such as Scoobi.

In order to compute the car's position, different location techniques can be used: The most typical technique is GPS, however improved versions of GPS such as "Assisted-GPS", "Differential-GPS" or "Augmented-GPS" will be used. Alternative constellations may also exit, such as the Russian GLONASS,[1] the pan-European GNSS[2] 1 and 2 (EGNOSS[3] and Galileo respectively) or the Chinese "Beidou Navigation System".

Considering that the most solicited service will probably be "to communicate", it will be convenient to involve a telephone operator, and other possibilities such as "Cell Identification", "E-OTD" (Enhanced – Observed Time Difference) or "OTDOA" (Observed Time Difference Of Arrival) could be used to provide geographic information.

Moreover, some manufacturers are thinking further. For example, Mercedes Benz with Infofueling, will use WLAN (Wireless – Local Area Networks) for their wireless connection, which agrees with the fact that the North American FCC (Federal Communications Commission), back in 1991, allocated the 5,9 GHz band to provide car services following the WLAN standard IEEE 802.11a. Wireless LAN, as well as Bluetooth could also be used to provide location information.

Privacy protection

Drivers and passenger could get traffic, parking and navigation information, weather conditions, medical or breakdown assistance, concierge services such as hotel booking, theatre tickets, yellow pages, music on demand and films or games for passengers. In accordance with the service desired, the user's interface will be different, the basic infrastructure involving a hands-free terminal with voice recognition, a keyboard, a screen and an emergency button. This emergency connection would work at any moment, whether the car is running or not, whether the SIM[4] card has been inserted or not, and it should be automatically activated in case of an accident.

Movements of a vehicle usually coincide with the movement of its driver. If so, the processing of location data has to be considered processing of personal information and the existing legislation has to be examined.

From an international point of view the OECD[5] has already tackled privacy issues and has adopted the OECD Guidelines on the Protection of Privacy and Transborder Flows of Personal Data in 1980. Following these Guidelines, the European Union issued the Directive 95/46[6] on privacy protection. This Directive does not mention the term "location", but protects personal privacy in a general way.

---

* PhD, Master of Laws, Associate Prof., Director.
[1] GLObal NAvigation Satellite System
[2] Global Navigation Satellite System
[3] European Geostationary Navigation Overlay System
[4] Subscriber's Identity Module
[5] Organisation for Economic Co-operation and Development
[6] Directive 95/46/EC on the protection of individuals with regard to the processing of personal data and on the free movement of such data.

In June 2000 a new regulatory framework was proposed. This framework followed the spirit of the Lisbon summit, establishing in six Directives the end of the telecommunications liberalisation process. Within these proposals, the Proposal 385 covers location data and is destined to substitute Directive 97/66[7]. In December 2001, the European Council and the European Parliament approved the new regulatory package, but the controversial Directive on data protection was excluded. Among other problems discussed were the need to erase location data and the treatment that should be given to non solicited commercial mail. The general idea within the new regulatory framework is that location data can only be processed with the user's consent or in order to provide an emergency service.

The situation is analogous in the USA where the Congress passed in 1999 the "Wireless Communications and Public Safety Act", amending the Article 222 of the Telecommunications Act. Through this amendment the privacy rules will not be applied to the processing of location data in emergency situations and in case of automatic crash notifications.

Medical data

When a user dials the emergency number on his phone, he is connected to an operator who analyses the situation and dispatches the appropriate emergency service (police, fire-fighters, etc.). If the emergency warning is generated from a vehicle system, the private call centre has two possibilities: on the one hand to dispatch the company's private emergency services, on the other hand to forward the call to the public emergency services (such as the 911 in the USA, the 112 in the EU or the 000 in Australia). Within the former option new organisations could be involved, such as insurance companies or private medical services.

In the case of a mobile phone, it is typical that the phone is linked to a single user. In the case of a vehicle it is also common that the vehicle is associated to a single driver and certain passengers. In case of an emergency it would be very useful to know the medical records of the driver, and the typical passengers (if any). The data subject may be unwilling to provide such data, but if he is conscious of the possible benefits (for him and his relatives), he probably will be the one asking for such data processing.

Who should be depository of such joint information? It could be the telephone operator in charge of processing the data, since the majority of the current telematics systems base their communications on inserting the SIM card (a duplicate of the card) in the vehicle system. It is also true that there are systems that obtain the position through a GPS and transmit it through a SMS without the operator participation. From this, it could be inferred that the provider of the telematics services could also provide medical information. Looking a step further, there may be situations in which each vehicle has an IP address. In such situations there could be a database where medical data is stored in reference to IP numbers. Finally, the ENUM[8] database could keep personal contact information and a document with the medical record.

Taking for granted the convenience of providing the medical record in case of emergency, the protection of the privacy of the medical record must also be considered. Privacy Protection Directive (95/46) protects the privacy of European citizens. Moreover, and regarding the processing of medical data there is a Recommendation (a non-binding text although of great interest due to the attention paid by the EU Member States), that regulates the collection and automatic processing of medical data and seeks to ensure both the security and the proper conservation of the data[9]. In the USA and regarding medical data processing, it will shortly enforce the largely debated HIPAA ("Health Insurance Portability and Accountability"), passed in 2001, which will protect personal medical information and will impose, at a federal level, restrictive measures to the use and disclosure of medical information in any medium. This Act will be enforced in April 2003.

Other privacy threats

There are different devices that are being used nowadays by the car industry. All of them have some interesting applications, but simultaneously, all of them are keeping private data regarding the driving.

The first one is a data recorder, a videocassette sized black box, used to determine the car's safety features. More advanced devices are being included now that record up to 16 different parameters including vehicle speed, brake status and gas pedal position. Black boxes have become a key element to solve liability lawsuits and vehicle's owners have agreed to turn over the information or have been forced by a court order. Insurance companies are also aware of the significance of these boxes.

---

[7] Directive 97/66/EC concerning the processing of personal data and the protection of privacy in the telecommunications sector.

[8] ENUM has been said to stand for "tElephone NUmber MApping", "Electronic NUMber", "E-NUMber" and "E.164 NUmber Mapping", www.itu.int (January 2002).

[9] Recommendation 97-5 of the Committee of Ministers to Member States on the protection of medical data.

Other ways of surveillance are license plate readers and automated toll-collection tags. License plate readers are used in parking garages to prevent customers from swapping tickets and paying lower fees. Authorities or traffic information centres use plate readers to monitor traffic conditions and it is also possible to use them to keep a log of vehicles that enter security areas or to detect potentially suspicious activity (such as vehicles that pass through too many times). Regarding automated toll-collection tags (like those used in the E-ZPass system) they can be used for payments at drive-through windows as McDonald's, Dunkin' Donuts, gas stations and parking garages. Again, here is a huge repository of information about personal habits and some control could protect consumers.

Acknowledgements

The author gratefully acknowledges the support of the industrial sponsors of the MIT Program on Internet & Telecoms Convergence (ITC), listed at http://itc.mit.edu. This work has also been partially supported by the Spanish Government as CICYT TIC 2000-1025.

normalized on the sum of all members of this matrix. The minimum variance of error of estimation is equal to reverse value of the sum of members of the same matrix.

For the estimation of errors of a filtration, founded on average of data measurements, we shall mark, that the transfer function of the equivalent filter has identical factors, equal $1/N$. Using for this case the concluded above formula for variance of error, we shall receive:

$$Disp_{med} = I^T \cdot C \cdot I \; / \; N^2$$

Let's conduct comparison the efficiency of *PF*-filtration concerning methods, founded on average of signal. For this purpose we investigate the relation of variance $Disp_{med}$ to value $Disp_{opt}$. (factor P). On figure 1 show the family of relations $P = F(N)$ at different times of process of measurements as contrasted to by reference time of a correlation (time constant *Tcor*). As it is visible, each function has a maximum, which is increased in due course correlation of disturbance.

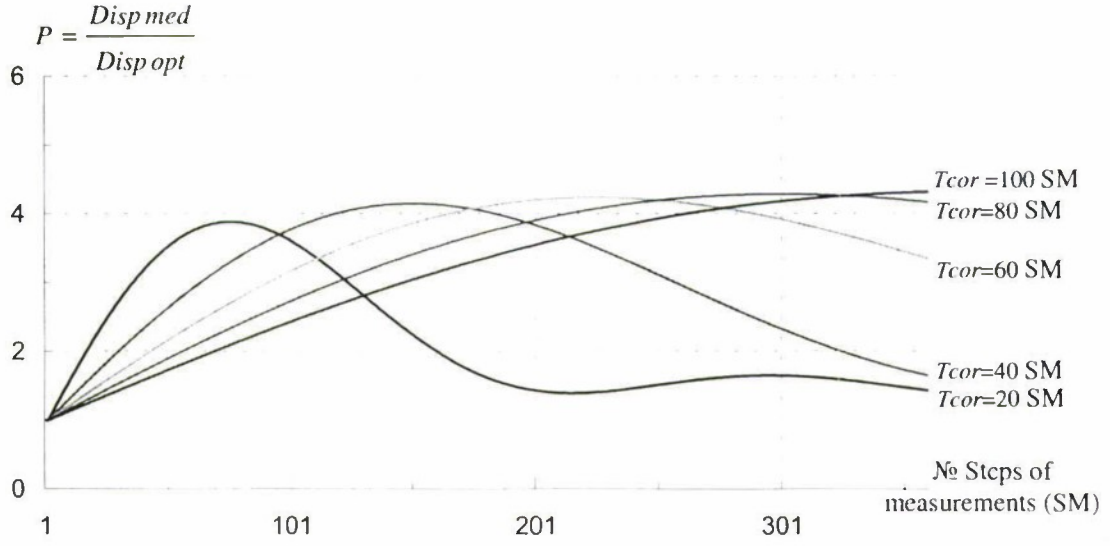

Fig. 1

The citation data are obtained at mathematical modelling. For experimental check the filtration of real output signal of the laser gyroscope in conditions of unstable temperature was conducted. On the figure 2 the relation, obtained at processing, of parameter P from duration of an interval of measurement is adduced. The theoretical function $P(N)$, counted on measured in experiment of an autocorrelation function there is showed.

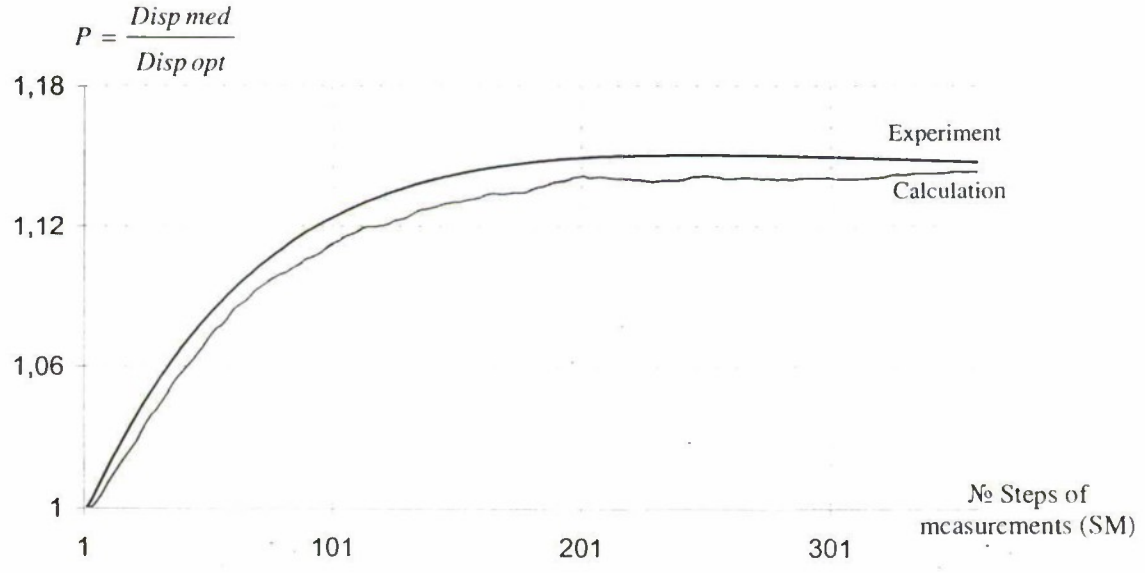

Fig. 2

As it is visible, the data of experiment well enough coincide the theoretically obtained relations, that proves analytical investigations and productivity of the made proposal.

SIMULATION MODEL OF THE AIRCRAFT MOVEMENT*

Yu.Yu.Broslavets*, A.A.Fomitchev, A.B.Koltchev***, V.B.Uspensky****
JSC "Lasex",
9, Institutsky per., Dolgoprudny Moscow Area, Russia. E-mail: laser@pop3.mipt.ru

Abstract

Key words: simulation model, aircraft, back dynamics problem

On the basis of the back dynamics problem decision the simulation model of the aircraft movement is developed. This model is generating etalon values of navigating parameters and indications of inertial sensors. The developed model allows to reproduce all characteristic modes of a trajectory and angular aircraft movement. The angular movement is set by means of angles close to "roll", "attack" and "sliding", most adequately describing plane orientation concerning a trajectory of movement. The simulation model is intended for debugging and research of SINS algorithms in various conditions of movement.

Introduction

Now, due to development of global satellite navigating systems, the precision navigating information became accessible to the consumers in various branches of a national economy. At the same time the perfection of means and systems of inertial navigation still is an urgent scientific and practical problem. One of stages of creation strapdown inertial navigation system (SINS) is the development, debugging and reception of efficiency estimations of SINS algorithms in various conditions. Taking into account the limited opportunity of reception the experimental information about object movement, the decision is based on the model-made data. So simulation model should satisfy to the following requirements:

– to generate the indications of inertial gauges adequate to their real work;
– to generate etalon values of navigating parameters;
– to simulate various kinds of movement, characteristic for the given object;
– to be of detailed elaboration, adjusted on a degree, and mathematical model parameters of sensors, and also parameters of simulated movement of object.

Given report is devoted to development of simulation model of the aircraft movement.

The considered problem can be solved from positions direct or back dynamics problem. Both approaches have both advantages and lacks. Considering high complexity of aircraft dynamic model, no stationary and the uncertainty of its many parameters is offered simulation model of aircraft movement, constructed on the basis of a back problem. Is important, that the navigating algorithm in itself is a direct method of the decision of a problem. Therefore it is represented expedient generation input data for such algorithm to base on other methodical principles.

The contents of the report

For modeling aircraft movement we shall divide it on trajectory and angular movement around of the centre of mass. The trajectory movement we shall describe in three coordinates $\bar{x} = (\varphi, h, \lambda)$ – accordingly terrestiral latitude, altitude, longitude and three geographical components of a vector of speed $\bar{v} = (V_N, V_h, V_E)$ – northern, vertical and east components. Believing initial and final values of a state vector given at the fixed duration of movement T, we shall define their evolution as polynomials of time $t \in [0, T]$:

$$\bar{x}(t) = \bar{b}_0 t^3 + \bar{b}_1 t^2 + \bar{b}_2 t + \bar{b}_3 .$$

In these conditions

$$V_N(t) = \dot{\varphi}(t) \cdot R_2(t), \; V_h(t) = \dot{h}(t), \; V_E(t) = \dot{\lambda}(t) \cdot R_1(t) \cos \varphi(t),$$

where

$$(\dot{\varphi}(t), \dot{h}(t), \dot{\lambda}(t)) = \dot{\bar{x}}(t) = 3\bar{b}_0 t^2 + 2\bar{b}_1 t + \bar{b}_2, \; R_1(t) = (a_0 + h(t)) \cdot \chi^{-1}(t),$$

$$R_2(t) = (a_0 + h(t))(1 - e^2) \cdot \chi^{-3}(t).$$

---

* Ph.D., Research Scientist.
** D.Sc., General Director.
*** Chief of Department.
**** Ph.D., Senior Scientist.

$\chi(t)=\sqrt{1-e^2\ sin^2\ \varphi(t)}$; a_0, e – accordingly major semiaxis and Earth eccentricity.

The factors $\bar{b}_j, j=\overline{0,3}$ are calculated from a condition of the coordination polynomial with initial and final values of coordinates and speeds.

The vector of the apparent acceleration causing movement along a nominated trajectory, is defined as

$$\bar{a}(t)=\dot{\bar{v}}(t)-\bar{g}'(t)-[\bar{v}(t)\times(\bar{\Omega}(t)+\bar{\omega}(t))],$$

here $\dot{\bar{v}}=(\dot{V}_N,\dot{V}_h,\dot{V}_E)$, and $\dot{V}_N(t)=\ddot{\varphi}(t)\cdot R_2(t)+\dot{\varphi}(t)\cdot\dot{R}_2(t)$, $\dot{V}_h(t)=\ddot{h}(t)$,

$$\dot{V}_E(t)=\ddot{\lambda}(t)\cdot R_1(t)\cdot\cos\varphi(t)+\dot{\lambda}(t)\cdot\dot{R}_1(t)\cdot\cos\varphi(t)-\dot{\lambda}(t)\cdot R_1(t)\cdot\sin\varphi(t)\cdot\dot{\varphi}(t);$$

$$(\ddot{\varphi},\ddot{\lambda},\ddot{h})=\ddot{\bar{x}}(t)=6\,\bar{b}_0 t+2\,\bar{b}_1,\ \dot{R}_1(t)=\dot{h}(t)\cdot\chi^{-1}(t)-(a_0+h(t))\cdot\chi^{-2}(t)\cdot\dot{\chi}(t),$$

$$\dot{\chi}(t)=-e^2\ \sin\varphi(t)\cos\varphi(t)\cdot\dot{\varphi}(t)\cdot\chi^{-1}(t),$$

$$\dot{R}_2(t)=(1-e^2)\cdot\dot{h}(t)\cdot\chi^{-3}(t)-3\cdot(a_0+h(t))(1-e^2)\cdot\dot{\chi}(t)\cdot\chi^{-4}(t);$$

$\bar{g}'(t)$ – free-fall acceleration calculated according to the accepted model of an Earth gravitational field; $\bar{\Omega}(t)=(\Omega\cdot\cos\varphi(t),\Omega\cdot\sin\varphi(t),0)$ – Earth rotation rate,

$\bar{\omega}(t)=\{\Omega\cdot\cos\varphi(t)+\frac{V_E(t)}{R_1(t)},\ \Omega\cdot\sin\varphi(t)+\frac{V_E(t)}{R_1(t)}tg\varphi(t),\ -\frac{V_N(t)}{R_2(t)}\}$ – absolute rotation rate of the local level frame. All vectors are set in local geographical frame (LGF).

When define angular evolutions aircraft concerning a trajectory we shall take into account, that most adequate from the point of view of its characteristic movements are the angles of "roll", "attack" and "sliding" belonging to various angles systems. The closest these 3 angles is the angle system specifying transformation trajectory frame to fixed-body frame (FBF) in following sequence of turns, μ (around the first axis), β (around of the second transformed axis) – angle of "sliding" and α (around of the third transformed axis) – angle of "attack". Here we should note that if $\beta=0$ the angle μ coincides with an angle of "roll", and at small β – is close to it.

Let's set dynamics of the entered angles as some analytical functions of time, for example periodic, $\mu(t),\beta(t),\alpha(t)$, having coordinated them with the given initial and final value of angles.

We shall accept a formal designation of unit vectors $\bar{e}_1=(1,0,0)$, $\bar{e}_2=(0,1,0)$, $\bar{e}_3=(0,0,1)$. In these conditions the transformation LGF to trajectory frame is set quaternion

$$M_0(t)=(\cos\frac{\psi(t)}{2}-\sin\frac{\psi(t)}{2}\cdot\bar{e}_2)\circ(\cos\frac{\theta(t)}{2}+\sin\frac{\theta(t)}{2}\cdot\bar{e}_3),$$

here $\psi(t)=\arccos\frac{V_N(t)}{\sqrt{V_N^2(t)+V_E^2(t)}}$ – angles of yaw, $\theta(t)=\arccos\frac{\sqrt{V_N^2(t)+V_E^2(t)}}{\sqrt{V_N^2(t)+V_E^2(t)+V_h^2(t)}}$ – angles of a trajectory inclination, $\circ$ – mark quaternion of product.

To transformation trajectory frame to FBF is corresponds quaternion

$$M(t)=(\cos\frac{\mu(t)}{2}+\sin\frac{\mu(t)}{2}\cdot\bar{e}_1)\circ(\cos\frac{\beta(t)}{2}+\sin\frac{\beta(t)}{2}\cdot\bar{e}_2)\circ(\cos\frac{\alpha(t)}{2}+\sin\frac{\alpha(t)}{2}\cdot\bar{e}_3).$$

In this case vector of apparent acceleration $\bar{a}$ is projected on the connected axes according to expression

$$\bar{a}^*(t)=\tilde{M}(t)\circ\tilde{M}_0(t)\circ\bar{a}(t)\circ M_0(t)\circ M(t).$$

Thus the absolute rotation rate of the aircraft $\bar{\omega}^*(t)$ in FBF for everyone $t\in[0,T]$ is calculated as

$$\bar{\omega}^*(t)=2\cdot[\tilde{M}(t)\circ\tilde{M}_0(t)\circ\tilde{N}(t)\circ(\dot{N}(t)\circ M_0(t)\circ M(t)+N(t)\circ\dot{M}_0(t)\circ M(t)+N(t)\circ M_0(t)\circ\dot{M}(t))],$$

where $N(t)=(\cos\frac{\lambda(t)}{2}+\sin\frac{\lambda(t)}{2}\bar{e}_1)\circ(\cos\frac{\varphi(t)}{2}-\sin\frac{\varphi(t)}{2}\bar{e}_3)$; $\tilde{}$ – mark of interface quaternion. $\dot{N}(t),\dot{M}_0(t),\dot{M}(t)$ – derivative quaternion.

Thus, the speeds of object and its angular navigating parameters for various kinds of movement are given the expressions allowing with a required step on time analytically exact to calculate of a vector absolute rotation rate and a vector of apparent acceleration aircraft in FBF and also exact value of geographical coordinates. Character of movement and its duration are defined by adjustment of model. At modeling the program of flight including parking, rise, upward flight, horizontal flight, landing, it is broken into separate characteristic sites, and then the data "are sewed".

In the report the questions connected to modeling of work of inertial sensors with integrated quantized output are considered also. The input data for them are an absolute rotation rate vector and an apparent acceleration vector. Set parameters serve takeoff frequency, and also characteristic of tool errors (regular and random gyro drift, accelerometers bias, errors of scale factors, and sensitive axes non orthogonal parameters). Thus the reception an apparent turn vector and an apparent speed vector is realized by a method of numerical integration of the high order. The step of integration will be coordinated to entered sensors errors. In order to prevent excessive accumulative error the simulated trajectory is broken on short enough on time sites, which then "are sewed" on regional conditions. At transition from a site on a site of the sensors indication zeroed lost-free movement information.

The conclusion

The using of offered simulation model allows to testing SINS algorithms for various types of movement, to estimate its methodical error (on ideal sensors with arbitrary high takeoff frequency), to estimate the contribution of various tool errors to a general efficiency of algorithms at a concrete kind of movement.

NUMERICAL REALIZATION OF ADAPTIVE ALGORITHM FOR NONLINEAR FILTERING MANEUVERING OBJECT TRAJECTORY PARAMETERS *

O.S. Amosov*
Komsomolsk-on-Amur State Technical University.
27, Lenina St., 681013, Komsomolsk-on-Amur, Russia. E-mail: is@knastu.ru

Abstract

Key words: nonlinear filtering, adaptive algorithm, artificial intelligence, accuracy

The solution of the task of adaptive nonlinear discrete filtering of parameters of a trajectory of the maneuvering object on the Bayesian basis approach is given. The various numerical methods of approximation and the recurrent calculation of a posteriori density of probability are analyzed. The numerical models of nonlinear estimation of coordinates and parameters of the trajectory of the movement of objects which have good maneuverable properties are received. The computer models for supervisions in a spherical coordinate system are realized. The accuracy and speed of adaptive algorithms of nonlinear discrete filtering for the considered task are analyzed. The opportunities of use are discussed at realization of the radiolocation information processing of effective methods of programming, heuristic devices, methods of artificial intelligence and neuroinformatics allowing to reduce the time of the processing and to increase its quality.

Introduction

Fast growth of productivity of computer systems, the application of modern architecture taking advantage of conveyor and parallel processing, neural computers result now in appearing of the improved methods of signal processing. For modern control systems of aerial and sea objects urgent still remains a decision of a task of boosting of accuracy estimating in real time of coordinates and parameters of movement of objects. The special complexity is caused by the decision of a task in conditions of a priori ambiguity, when the model of dynamics of object and stochastic characteristics of live perturbations and noises varies in time. As the theory of linear filtering finds optimum transformation in a class of linear transformations, and the theory of nonlinear filtering - in a class of all transformations, nonlinear filtering gives obviously the best results. The question consists about the value of a divergence. Therefore the extreme achievable accuracy at the decision of concrete tasks in practice only the use of nonlinear filtering can give. And it also represents the main interest for the developers of the practical systems and instruments.

1. The formulation of a task of the adaptive nonlinear estimation

It is necessary to receive the optimum ratings of stochastic vector of the dynamic process by the available vector supervisions at the lack of a priori items of information on a vector of accompanying parameters, and (or) about the characteristics of noise of the channel of measurement, and (or) of forming noise. The noises can depend on the vector of a state and the vector of accompanying parameters. In a vector of accompanying parameters it is taken into account a priori ambiguity in the task of model of estimated process and perturbations [1].

For discrete supervisions the nonlinear models of processes of dynamics and measurements are resulted which are recorded as three difference vector equations.

The description of the mathematical formulas of adaptive filtering is resulted. On the Bayesian basis approach [1, 2] are recorded the recurrent formulas of adaptive estimating for the nonlinear equations of dynamic processes and nonlinear equations of supervision at an incomplete a priori information. The expressions for a posteriori of density of probabilities of extrapolated values of a vector of state and vector of accompanying parameters in the absence of the sample of supervisions and for a posteriori density of probabilities for the following moment of time after the reception of the sample of supervision are received. The knowledge of a posteriori density of probabilities allows to receive a rating by any criterion.

The received results can be used in practical tasks, at which decision of the greatest accuracy of a rating should be achieved under conditions of influence on the object of real perturbations, taking into account nonlinear of the object of testing and nonlinear of the measuring sets. The given results can, for example be used for tracking the maneuvering object in radiolocation and determinations of both coordinates and parameters of

* C. Sc., Docent.

movement of the maneuvering of the flying apparatus. In these cases as a component of a vector one can use the distance to the object, its speed and acceleration, and accompanying parameter can characterize the control influence (manoeuvre) or sharp variations of the turbulence of the atmosphere [1, 3].

2. The numerical realization of adaptive filter

The numerical realization of the algorithms of adaptive nonlinear discrete filtering for tracking the maneuvering purpose on a basis Bayesian approach is offered. As an uncertain perturbation semi-Markov stochastic process is chosen [3], which includes as a special case the pulse stochastic process. It allows to simulate various uncertain influences, which take place in practice.

The task of the optimum estimation of a vector of the system condition at square-law function of losses is reduced to the weighed averaging of ratings, which represent the decision of the task of filtering at the fixed values of the revolting parameter [3]. For the case, when the revolting parameter receives only fixed values, according to a general arrangement of the application of the Bayesian formula the expressions for a posteriori probability of the revolting parameter on current sample of measurements are received. For the reception of the optimum ratings the numerical realization of the nonlinear discrete filter is used.

The various numerical methods of approximation of a posteriori density of probabilities are analyzed: the replacement of the continuous function of the density of probabilities by a set of discrete points, using of the poly-Gaussian distributions, the approximation with the help of Hermit polynomials, spline-functions, and Fourier numbers [2]. For the numerical simulation analysis the first of the above methods is used. For the solution of the multiple integrals in Bayesian algorithms for the recurrent calculation a posteriori density of probability the method of cells, convolution and fast Fourier transform are used.

The computer models of the optimum nonlinear estimation of coordinates and parameters of the trajectory of the movement of airplane are realized at nonlinear measurement. The model of movement is characteristic of the flight of airplane, which have good maneuverable properties and during supervision carry out a number of manoeuvres. For simplification of calculations and opportunity of visual supervision of a time variation of a priori density of probability the separate filtering for coordinates in a rectangular system of coordinates with the beginning in a point of stand Radar is carried out. The measurement is carried out in a spherical system of coordinates of the two-coordinate Radar, metering the distance to the object and azimuth with the preset period of the review. At performance of a trajectory by the polynomial of the first degree as estimated parameters the coordinates and speeds are considered.

Model of indignant polynomial trajectory on each coordinate and nonlinear equation of measurements in a spherical system of coordinates are resulted. The formulas for recurrent of calculation of conventional density of probabilities and ratings of a vector of a state for each discrete value of revolting parameter and weighed values of ratings, and also for calculation of ratings of dispersions are resulted. The various ways of construction of a discrete grid for the following iteration are discussed.

For comparison the computer model is realized on the basis of the adaptive Kalman filter. The models of adaptive and non-adaptive filters are compared by a dynamic mistake estimating in execution time manoeuvre and in its absence. The prize by a dynamic mistake estimating in the nonlinear adaptive filter is reached at significant temporary expenses.

Depending on noise levels of measurements, models of movement, models of measurement, parameters of the manoeuvre the scoring on accuracy in researched models for nonlinear filters makes from several percents up to several tens percents.

3. Elements of artificial intelligence

The opportunities of use are discussed at realization of the radiolocation information processing of effective methods of programming, heuristic devices, methods of artificial intelligence and neuroinformatics allowing to reduce the time of the processing.

For a method of array it is offered at choice of the center of the new array for next iteration as the first approximation usage of estimations of a Kalman filter, and estimations which are worked out by the neural network. The models of different architectures of the neural networks for detection of manoeuvres of the object, the estimation of the perturbing parameter, preliminary extrapolation of coordinates and parameters of a trajectory are researched.

At problem solving of secondary information processing usage of a knowledge base built on the basis of heuristic rules, in the form of rule-oriented models is offered. It is necessary for build-up of fuzzy model operating empirical knowledge on sizing of strobes of support, the criteria of detection and reset of trajectories,

starting conditions, the information identification from primary and secondary radars, the detection of false objects and trajectories.

Conclusions

1. The computer models of adaptive nonlinear discrete filter for the maneuvering object on the Bayesian basis approach are received.

2. The research of the accuracy and speed of adaptive algorithm of the filtering is given. For increase of the speed and efficiency at problem solving of supervision for the maneuvering objects usage neural networks and knowledge bases is offered.

References

1. **Тихонов В.И., Харисов В.Н.** Статистический анализ и синтез радиотехнических устройств и систем.–М.: Радио и связь, 1991.–608 с.
2. **Степанов О.А.** Применение теории нелинейной фильтрации в задачах обработки навигационной информации – СПб: ГНЦ РФ – ЦНИИ «Электроприбор», 1998. – 370 с.
3. **Кузьмин С.З.** Основы проектирования систем цифровой обработки радиолокационной информации.–М.: Радио и связь, 1986.–352 с.

CNS/ATM FOR TACTICAL MILITARY AIRCRAFT

Steven Frain*
Naval Air Systems Command
47204 Buse Road, Building 500, Patuxent River, MD 20670
(301) 757- 0921, *FrainSG@navair.navy.mil*
Garth Van Sickle**
DCS Corporation
46641 Corporate Dr. Lexington Park, MD 20653
(301) 862-2390x286, *gvansick@dcscorp.com*

Abstract.

Key words: CNS/ATM, Navigation, Surveillance, Military, Aircraft, Tactical

Worldwide, civil aviation is transitioning to a new airspace architecture called Communication, Navigation, Surveillance / Air Traffic Management (CNS/ATM). The International Civil Aviation Organization (ICAO) is leading this effort by establishing standards and addressing minimum equipage for aircraft to operate within this new architecture. Military aircraft are classified as State Aircraft and are not subjected to International Registration. Many do not have the space available to utilize civil approved avionics. To enable military aircraft to operate within this new CNS/ATM airspace, they must capture civil functionality within their military avionics equipment. Specifically, military aircraft must transition from ground based navigation aids (VOR/TACAN) to area navigation in performance-based airspace (RNP RNAV). Likewise, they must transition from RADAR surveillance, both primary and secondary, to Automatic Dependent Surveillance Broadcast (ADS-B).

With GPS as the source of accurate positioning, the transition to RNP RNAV is accomplished through cockpit integration, improved processing power, digital databases, modular software and digital cockpit displays. Specific procedures for Departure, Enroute, Terminal and Non Precision Approach must be established and presented to the aircrew without increasing the workload. Data base validity must be established and software qualification must be maintained. Since the specific functionalities of RNP RNAV are still not fully defined by the various certifying authorities, we started by drafting a Functional Requirements Document (FRD) that conforms with presently published RNP performance requirements. If these requirements change, the upgrades will be incorporated in future revisions of the FRD and cockpit software. We are prepared to present the details of the FRD at the conference.

Likewise, with GPS installed, the most accurate locating information for each military aircraft will be the self-generated position displayed in that aircraft. Today, this accurate GPS-based aircraft position is not available to the air traffic controller. With the installation of a standard data link and a common reference, a line-of-site broadcast of the accurate GPS-based aircraft self-reports (ADS-B) is possible. These self-reports of aircraft identity WGS-84 geodetic position (Lat-Long-Alt) and velocity vector and will be transmitted up to twice a second. Aircraft within line of sight can use these transmissions to automatically produce a cockpit display of traffic information (CDTI). If all civil and military air traffic participated in an ADS-B network, improved situational awareness and aviation safety would be possible. The same processing power, modular software, and cockpit displays used for RNP RNAV will be used for ADS-B and CDTI. Today, three different data links are being considered for ADS-B but only the Mode S 1090 MHz Extended Squitter is being installed. Both the RNP RNAV and the ADS-B have considerable military utility and improved situational awareness is anticipated within the battlespace as well as within civil airspace.

Introduction

Military aircrews are beginning to experience the benefits of having quality Global Positioning System (GPS) navigation information available in the cockpit to support their tactical missions. However, another big improvement in situational awareness and tactical effectiveness will be available when military aircraft capture the new capabilities known as Communications, Navigation, Surveillance / Air Traffic Management (CNS/ATM). Since tactical military aircraft do not have the space available to install civil approved avionics, they must develop dual use avionics and capture CNS/ATM functionality with military avionics equipment. Specifically, military aircraft must transition from airways flying using ground based navigation aids to area navigation (RNAV) and Required Navigation Performance (RNP) using GPS with a geodetic database. For access to some airspace, tactical military aircraft must transition from surveillance with Identification Friend or Foe (IFF) (Modes 3/A and C) to Mode S and eventually Automatic Dependent Surveillance Broadcast (ADS-B). Significant improvement in situational awareness and tactical effectiveness will be possible when tactical

* Assistant Program Manager.
** Technical Advisor.

military aircraft can file and fly with GPS and also self-report position and identification via the Mode S ADS-B data link.

Civil Transition to Required Navigation Performance Airspace

The primary function of civil airspace management is to support air traffic in a safe and efficient manner during both visual and non-visual meteorological conditions. Since most aircraft flying in civil airspace do not have the capability to locate and avoid other aircraft during non-visual conditions, the airspace management rules were established to provide this function. For example, aircraft flying east are at a different altitude than aircraft flying west, east is odd and west is even. Likewise, other rules were established to allow aircraft at the same altitude to avoid conflicts during overtaking and crossing situations. The simplest solution to this problem is to put the aircraft on airways, highways in the sky, and keep slow aircraft on different airways and altitudes than faster aircraft. The basic form of overland aircraft navigation since the early 1950s, VHF Omni-directional Range (VOR), supports the airways system. The principle of operation of the VOR is very simple: the VOR facility transmits two signals at the same time. One signal is an omni directional 30 Hz pulse, while the other signal rotates in the horizontal plane about the station at 30 Hz. The airborne equipment receives both signals, looks (electronically) at the difference between the phases of the two signals, and interprets the result as a radial from the station. With 2 VOR stations, an aircraft is capable of determining its location by knowing its magnetic radial from each VOR station. Aircraft navigation to and from VOR stations is fairly simple and the overland airways system today is based on aircraft doing exactly that. With VOR, aircraft can also locate airway intersections, establish holding, and fly non-precision approaches to the destination airfield.

Tactical military aircraft use an equivalent Tactical Air Navigation (TACAN) instead of VOR. TACAN introduced another useful navigation tool called Distance Measuring Equipment (DME). In the operation of DME, paired pulses at a specific spacing are sent out from the aircraft and received at a ground station. The ground station then transmits paired pulses back to the aircraft at the same pulse spacing but on a different frequency. The time required for the round trip signal exchange is translated into slant range distance (nautical miles) between the aircraft and the ground station. Usually TACAN, DME and VOR stations are located together and the airways system based on these navigation stations is usable by aircraft equipped with any or all this equipment. When an aircraft is authorized to fly in the airways system because it has an approved VOR, DME, or TACAN installed, this authorization is called equipment-based certification.

The concept of flying from one TACAN/VOR to another TACAN/VOR does not yield the most direct route costing time and money. The ability to navigate from any given geodetic fix to another geodetic fix is called Area Navigation (RNAV). Modern aircraft with Flight Management Systems (FMS) can use several VORs, VOR/DME, or even DME/DME/DME to locate their present position and calculate the proper course to fly to another geodetic fix selected by the aircrew. RNAV is becoming fairly common. RNAV is also useful when using other positioning sources such as LORAN or GPS. With RNAV, the route of flight can be much shorter than flying the airways route and this direct routing saves both time and money.

To obtain the navigation benefits of CNS/ATM, accurate, repeatable and predictable navigation performance must be demonstrated regardless of the positioning source. The capability to perform to a specified level of navigation performance regardless of the positioning source is called Required Navigation Performance (RNP). With RNP, aircraft will be authorized to fly in instrument conditions not due to specific certified equipage but because the entire navigation system, including the aircraft and the pilot, has demonstrated a specified, repeatable and predictable, level of navigation performance. For example, if the required accuracy for a designated airspace is 4 NM (RNP 4), it is assumed that for 95% of the total flying time an aircraft flying in this airspace will maintain a position within ± 4 NM of its Air Traffic Control (ATC) cleared route. With RNP RNAV, an aircraft will also be required to achieve a specified level of integrity and continuity guaranteeing the aircraft shall not error outside twice the accuracy (for RNP 4, 2 x 4 NM = 8 NM) without an annunciation to the aircrew. For tactical military aircraft, the transformation from TACAN to RNP RNAV as a primary means of navigation will be a significant achievement since tactical aircraft will not use civil approved avionics but capture this new capability in avionics designed for military missions.

A Tactical Aircraft Solution for Required Navigation Performance

For large military cargo and troop transports, the transition to CNS/ATM will leverage commercial system design used by commercial aviation. By using the civil CNS/ATM solutions, the certification of the military transports will be fairly simple since the civil commercial air carriers will have already received civil certification. However, for tactical military aircraft where the addition of civil avionics is not possible, guidance was found in the Chairman of the Joint Chiefs of Staff Master Positioning Navigation and Timing Plan. This guidance states: "The development of minimum performance standards for military users is the responsibility of

the Services. These military standards must conform with civil airspace required navigation performance (RNP) requirements, prevent violation of civil air traffic clearances, and ensure safe separation of military and civil air traffic." From this guidance, a performance based requirements document was developed to capture civil RNP RNAV functionality appropriate for Navy and Marine Corps tactical military aircraft.

Scope and Limitations of RNP RNAV Specification

The first step in the effort to achieve RNP in tactical military aircraft was to decide what level of RNP would be the goal. Presently, there is airspace where RNP 5 (BRNAV) has been implemented and additional airspace where RNP 10 or RNP 4 is required. Future plans also call for RNP 2 and RNP 1 in selected airspace. Since the US DOD policy is to transition to GPS as the primary positioning source, the decision was made to use Precise Positioning Service (PPS) GPS as a primary means of navigation. The PPS GPS based navigation system will provide accurate positioning to RNP 0.3 which is required for approach and departure

Looking at the various documents published by ICAO, RTCA, FAA, and JAA, we discovered various contradictions and ambiguities related to the minimum functional requirements for RNP RNAV. There were contradictions as to required capabilities such as route leg types, containment limits, and required augmentation for GPS. Some of the RTCA publications have been updated several times and are still not implemented by the FAA. Since official guidance for RNP RNAV is still pending and the tactical military aircraft will not be using commercial avionics, guidance was needed to establish the appropriate functionality for RNP RNAV in tactical military aircraft. This new guidance is called RNP RNAV Functional Requirements Document (FRD). Tactical military aircraft with navigation systems that are designed, integrated, and tested to meet the functional performance specified in the RNP RNAV FRD will be capable of meeting minimum RNP RNAV operational approval requirements to file and fly RNP RNAV flight plans from takeoff through a published Non Precision Approach (NPA).

Obviously, a document that establishes the minimum requirements will not contain capabilities that may later be desired or required. We accept this possibility and view the RNP RNAV FRD as a living document with plans to review this document on a regular basis and incorporate new functionalities, if required. We anticipate most future capabilities will be captured with software updates. A precision approach capability is a future requirement and is not contained within this document. Neither is the requirement for vertical guidance. The RNP accuracy requirement pertains to cross track deviation, only. Along track deviation is really a function of ground speed and the RNP RNAV FRD does not address required timing issues or 4-D navigation. If these, or other functionalities that are not covered by this document, become a requirement somewhere in the world, aircraft integrated and tested in accordance with the current RNP RNAV FRD will not be qualified to participate.

Even though the requirements are limited to the minimum functionality required, this limitation does not restrict the aircraft integrator from providing increased functionality above the specification. This document will provide the Naval Air System Command testers the minimum functionality that must be demonstrated during developmental testing of RNP RNAV on board an aircraft. Other capabilities, not covered by this document, will need to be properly defined and tested prior to being utilized.

Navigation Sensors

All civilian applications of GPS use the Standard Positioning Service (SPS) GPS. Both Ground Based Augmentation Systems (GBAS) and Space Based Augmentation Systems (SBAS) are planned to support SPS GPS. One very good reason why the RNP RNAV FRD is required is the requirement to use PPS GPS for primary positioning. There are no ICAO, FAA or JAA documents that address PPS GPS utility. DOD policy dictates that military platforms will use PPS GPS receivers and those receivers shall be operated in the keyed mode. This means that there is no civilian guidance available and it will be DOD responsibility to ensure military aircraft are compatible with civil standards using the military PPS GPS. We do not anticipate a problem demonstrating the required accuracy, availability, continuity, and integrity to meet the civil standards for RNP 0.3. However, it is important that civil air authorities realize that the required functional performance is met even though not by the commercially available means. This realization may require an educational effort to explain how equivalent civil functionality is achieved with military avionics.

PPS GPS is a two-frequency signal that measures and corrects for the error introduced by ionospheric distortion and supplies position information at ten times the rate of the single frequency SPS signal. The greater accuracy of PPS GPS provides the user the needed integrity availability to fly in RNP 0.3 airspace without augmentation. No attempt is made to fly precision approaches, where RNP 0.15 is required, based on this document. SBAS implementations such as the United States Wide Area Augmentation System, the European Geostationary Navigation Overlay Service, and Japan's Multifunctional Transport Satellite Space-based Augmentation System provide enhanced accuracy over the SPS GPS signal but their use is not required. PPS GPS will provide tactical military aircraft the required performance worldwide to support air operations from take-off through enroute recovering to Non-Precision Approach minimums.

Few publications address the contribution of an Inertial Navigation System (INS) to augment the GPS navigation solution. Since most naval aircraft are either equipped or plan to equip with at least one INS, the ability to provide PPS GPS with aircraft based augmentation (ABAS) is planned. The RNP RNAV FRD does not require INS augmentation to meet the RNP 0.3 requirements but if an INS is available, full utilization is anticipated. The possibility of using inertial navigation system "coasting" for periods when the GPS signal is unavailable will augment the navigation system continuity capability of the GPS/INS integration. The full utility of the Embedded GPS INS (EGI) to meet the accuracy, integrity, continuity and availability requirements for RNP RNAV is a topic for further study.

Vertical Guidance

Although the requirements for vertical guidance or VNAV are listed in an appendix to the RNP RNAV FRD, there is no mandate for VNAV in the initial publication of the document. If individual platforms have a need or desire to implement a VNAV capability, the VNAV capability must meet the requirements in the FRD. In some discussions, a glide slope could be considered as part of a non-precision approach but until these issues are more mature, no attempt to provide a glide slope is established as a minimum requirement for RNP RNAV. The precision approach capability for naval aviation is part of the Joint Precision Approach and Landing System (JPALS) program, which will establish the minimum requirements for a precision approach separately.

Path Definition Requirements

The list of required leg types for the RNP RNAV FRD are limited to Track to Fix, Initial Fix, Direct to Fix, and Course to Fix legs. These leg types are as defined in RTCA/DO-236A. Other leg types such as Radius to Fix, Fix to Altitude, and Hold legs were discussed but not considered a minimum requirement. The Radius to a Fix algorithm is considered a function associated with an autopilot vice manually flying the aircraft. The RNP RNAV FRD contains no functionality that will require an autopilot upgrade to military aircraft for two reasons. First, military pilots of tactical aircraft do not let the autopilot fly the aircraft as much as commercial air pilots and it is not our intention to change the normal procedures and training of the military pilots. Second, there is no requirement for an autopilot as a distinct requirement to fly RNP RNAV. Likewise, Fix to Altitude and Holding legs are related to requirements for vertical guidance and since VNAV is not required, these leg types are also not required.

The procedures for the terminal area are described in detail with strict guidance to prevent human error. No manual changes will be allowed to an approach procedure found in the electronic database and the approach must be selectable with a single keystroke. The aircraft shall provide auto sequencing of successive waypoints from procedure initiation until the designated Missed Approach Holding Point. Likewise, "direct to" the Missed Approach Point shall not be permitted due to the obstacle rich environment in close proximity to the airport.

Database Management

Flight with GPS is very dependent on the quality of the digital database being used. Most civil air carriers use a commercial product database that is compatible with the Flight Management System (FMS) installed in the aircraft. For the United States military, the National Imagery and Mapping Agency (NIMA) is responsible for providing electronic Digital Aeronautical Flight Information Files (DAFIF) database. This federal agency performs the database maintenance and controls DAFIF distribution. Database integrity is a critical component in RNP RNAV and the assurance of database integrity is vital to the aircraft. An undetected error in the database can be as fatal as an undetected error in positioning.

To ensure database integrity on board the aircraft, the navigation system is required to perform hardware fault detection initially and periodically as a regular course of operation. The software shall perform error detection and correction of information read from the database to ensure that corrupted data is not used. The aircraft system prohibits the manual modification of stored data. Should the database become corrupted, the pilot shall be alerted. All RNP RNAV is referenced to the World Geodetic Survey – 84 (WGS-84). WGS-84 is the standard geodetic reference used throughout the world by the GPS system and has been accepted by ICAO and the US Department of Transportation for air navigation.

Naval Aviation RNP RNAV Certification Process

The RNP RNAV FRD will establish the requirement and initiate the certification process for naval aviation. When the RNP RNAV FRD is signed, the minimum functionality that each type aircraft must obtain will be established. The contradictions and ambiguities found in the various ICAO, RTCA, JAA, and FAA documents

related to RNP RNAV will be resolved. The systems engineering teams can then start to integrate this defined functionality into the lead aircraft. The various components will include a PPS GPS receiver with integrity, INS aiding (if available), electronic DAFIF database, various cockpit displays, and a cockpit processor to host the RNP RNAV software. During this developmental process, software industry standards will be followed appropriate for the severity of the potential failure condition.

A Test and Evaluation Master Plan will be written to ensure all details of the defined functionality are completely demonstrated. Reliability and maintainability will be evaluated as well as appropriate aircrew training. At the completion of developmental testing, the properly integrated aircraft will be given to the operational testers for a through evaluation in the operational environment. When the fleet representative aircraft is declared operational effective and operational suitable by the operational testers, the paperwork will be routed to the decision authority for the authorization for fleet use. This authorization for fleet use is the naval aviation equivalent of civil certification. It is important to note that all the functionality defined in the RNP RNAV FRD will be obtained or the aircraft will not be authorized for fleet use.

Civil Transition to Aircraft Self Reports

The monitoring of air traffic with RADAR, whenever possible, allows controllers to ensure flight clearances are followed and supports the direct vectoring of traffic as required to promote safety and efficiency. To support this monitoring function, civil air traffic service providers use both Primary Surveillance Radar (PSR), the reflected energy off the aircraft's skin, and Secondary Surveillance Radar (SSR), the triggered response from the aircraft's transponder. Air traffic surveillance requires that the aircraft must first be detected, then identified and then continuously tracked. Due to the safety of flight and time critical nature of air traffic control, little tolerance is allowed for misidentification or inaccurate tracking of aircraft.

Today, civilian air traffic controllers use SSR to both detect and identify air contacts. Primary surveillance radar is used as a detection backup and for weather surveillance. Air Traffic Control Radar Beacon System (ATCRBS) is the civilian version of SSR and it uses Question and Answer (Q&A) procedures with Modes A, and C, to track air traffic. Civil Mode A is the same as military IFF Mode 3 and is usually called Mode 3/A. Mode C, which was first implemented by civil aviation, is the altitude readout (100 ft increments) and is the basis for altitude separation monitoring. Even after Mode S functionality is installed, Mode 3/A capability will still be required. The deficiencies associated with SSR Modes 3/A and C include:

- Signal garble due to overlapping replies from two or more aircraft that are in the main beam with approximately the same slant range (synchronous garble)
- Signal interference caused by replies from a transponder in response to an interrogation from another interrogator (FRUIT)
- No response from a transponder due to over-interrogation and the resultant transponder unavailability (fanning the transponders)
- Ghost targets displayed due to reflections off obstacles (multipath)
- Inefficient use of frequency spectrum with multiple interrogations and multiple replies and total reliance on 2-party Q & A procedures
- Only 4,096 codes available with Mode 3/A

Civil aviation is transitioning to Mode S because Mode S enables improved target degarbling and provides more information from the targets. Mode S is a digital data link with protocol formats, error detection, and correction. Mode S permits selective interrogation since each interrogator and transponder has its own unique Mode S address. The operation of Mode S airborne equipment requires assigning a unique 24-bit aircraft address code to each individual aircraft. Within the high traffic density airspace of Europe, Mode S will be required by 2003 for instrument flight clearance and by 2005 for visual flying. All Mode S transponders also broadcast their unique aircraft address once per second. This "squitter" is the first step in the transition to broadcast architecture for air traffic surveillance with information available to the entire line-of-site network. Specific advantages of Mode S include:

- Improved target degarbling due to unique discrete address, selective interrogation, and error detection/correction
- Improved target azimuth accuracy due to Monopulse interrogator with single replies
- Improved spectrum channel efficiency with lockout, scheduled transponder replies and squitters for network information broadcasts

- Digital data link capability that is used for Enhanced Surveillance, Extended Squitter, and Resolution Advisory (RA), and aircraft-to-aircraft coordination
- Compatible with the Aeronautical Telecommunications Network (ATN)
- 2 to the 24^{th} power or > 16 Million unique 24 Bit aircraft addresses available

The concept of aircraft self-reporting their geodetic location, both in the air and on the ground, via a periodic line of sight broadcast is called ADS-B. The goal is to routinely use ADS-B self reports as a primary source of aircraft surveillance. The accuracy of the GPS position and the positive aircraft identifications can be captured to improve the quality of air traffic surveillance. Three different data links are under consideration for civilian ADS-B utility. They are Mode S Extended Squitter (1090ES), VHF data link Mode 4 (VDL 4), and Universal Access Transceiver (UAT). All three data links capture aircraft self reports, provide the aircraft a Cockpit Display of Traffic Information (CDTI), and have potential to bring value to the air traffic surveillance problem. However, interoperability will always be an issue. The FAA plans to use both 1090ES and UAT within the National Airspace System (NAS) with a multi-link gateway in the terminal area.

All ADS-B reports use the same geodetic reference, World Geodetic Survey of 1984 (WGS-84). WGS-84 is the standard geodetic reference used throughout the world by the GPS system and has been accepted by the US Department of Transportation for use in the NAS. This use of one standard geodetic reference for all ADS-B reports enables uncomplicated aircraft integrations regardless of which data link to improve situational awareness and empower traffic deconfliction from the cockpit. Airborne Collision is used. By using WGS-84, ADS-B will facilitate a cockpit display of traffic information that can be used Avoidance System (ACAS II) is capable of using this ADS-B information to reduce the number interrogations. ADS-B is truly a major step toward Air Traffic Management (ATM) vice Air Traffic Control (ATC) and a big step toward Free Flight.

Civil ADS-B for Tactical Military Aircraft

Since the military aircraft will be installing Mode S transponders for civil interoperability, the first ADS-B opportunity for the military aircraft should be 1090ES ADS-B. Another advantage of using 1090ES self-reports for ADS-B is its interoperability with ACAS II equipped aircraft. All aircraft that install Level II Mode S functionality will be able to provide the 1090 MHz Extended Squitter broadcast required for 1090ES ADS-B. This includes aircraft that install Mode S with their 2 box ACAS II system and also those aircraft that install Mode S but do not install ACAS II box. However only the aircraft that install ACAS II will have the 1090 MHz receiver required to receive the Extended Squitter broadcast of other aircraft in the vicinity. Without the ability to receive on 1090MHz, tactical military aircraft that will not install the ACAS II box will not have a functional 1090ES ADS-B and will not be able to build the CDTI picture.

To address the requirement for Mode S in tactical aircraft, the Naval Air Systems Command is developing a digital common transponder, APX-118, with legacy Mark XII IFF functionality and also Mode S functionality as a baseline capability. The new APX-118 has the form factor of the APX-100, will fit in all tactical aircraft, and also has a growth option for a 1090 MHz receiver; see Fig. '

	1030 MHz Tx	1030 MHz Rx	1090 MHz Tx	1090 MHz Rx
MK XII IFF Transponder		YES	YES	
MK XII IFF Interrogator	YES			YES
Digital				
Mode S Transponder (Box # 1)		YES	YES	
Mode S Interrogator	YES			YES
ACAS II (Box # 2)	YES	Mode S box	Mode S box	YES
1090 MHz ADS-B (One Box)		YES	YES	YES
	1030 MHz Tx	1030 MHz Rx	1090 MHz Tx	1090 MHz Rx

ADS-B Capability; The key requirement for 1090ES ADS-B is to be able to receive on 1090 MHz

When this growth option of the APX-118 is completed, the ability to receive on 1090 MHz will enable tactical military aircraft to participate in civil 1090ES ADS-B. Even though there are two other data links available for ADS-B, (UAT and VDL-4), 1090ES appears to be the cost effective way to go. There are several reasons why ACAS II, with its automatic interrogations of other aircraft, is not appropriate for tactical military fixed wing or rotary winged aircraft. With 1090ES ADS-B, there will be no capability to interrogate other aircraft but even without the ability to interrogate, military aircraft will still be able to use the self-reports of other civil and military aircraft to build a quality picture of participating aircraft in the vicinity. Other services in development such as Traffic Information Service (TIS & TIS-B) will complete the air picture by providing information on local aircraft without ADS-B. This 1090 MHz receive transponder upgrade will promote safety, facilitate civil interoperability, improve situational awareness, and greatly improve both military and civil air traffic surveillance.

ADS-B also has the potential to play a significant role in improving military as well as civil air surveillance. GPS is at least 20 times more accurate than military air search radar in determining the location of any aircraft. However, aircraft have not been able to share their improved location accuracy since they do not have a common data link available for that purpose. The biggest improvement in battle space situational awareness will come when military aircraft start to share their new level of location accuracy with a self-report. A functional requirements document is in work to establish the minimum requirements for Mode S and 1090ES ADS-B.

Conclusion

Commercial aviation will use RNP RNAV in the near future. Likewise, ADS-B self-reports will improve air traffic surveillance and provide sufficient situational awareness in each cockpit to support free flight. If tactical military aircraft are to operate within this new performance based airspace, they will require operational RNP RNAV, Mode S, and 1090ES ADS-B functionality. To achieve these new functionalities, dual use avionics and integrations must be found to capture civil functionality with military equipment. The bottom line is that tactical military aircraft will achieve the required functionality or they will not be authorized for fleet use. This paper describes one way to get RNP RNAV, Mode S, and 1090ES ADS-B capability in tactical military aircraft.

Acknowledgments

We would like to thank Mr. Wilfred Volkstadt, Mr. John Praktish, and Mr. Mike Germain for their comments on this work.

References

1. **CJCSI 6130.01B, 2000 CJCS** Master Positioning, Navigation and Timing Plan, 15 June 2000
2. **Doc 9613-AN/937, ICAO** Manual on Required Navigation Performance, Second Edition, 1999
3. **AWOP-WP/756, ICAO** Manual on Required Navigation Performance (RNP) for Approach, Landing and Departure Operations, **(DRAFT)**
4. **RTCA/DO-236A,** Minimum Aviation System Performance Standards: Required Navigation Performance for Area Navigation, 13 September 2000
5. **RTCA/DO-229C,** Minimum Operational Performance Standards for Global Positioning System/Wide Area Augmentation Systems Airborne Equipment, 28 November 2001
6. **RTCA/DO-178B,** Software Considerations in Airborne Systems and Equipment Certification, 10 December 1992
7. Specimen Aeronautical Information Circular (AIC) titled "Carriage and Operation of SSR Mode S Airborne Equipment in European Airspace," 28 July 2000
8. **ICAO SARPs Annex 10,** Volume IV, Amendment 73, second edition -July 1998
9. **ICAO Doc 9688,** "The Manual on Mode S Specific Services"

Acronyms

- 1090ES---1090 MHz Extended Squitter
- ABAS---Aircraft Based Augmentation System
- ACAS II---Airborne Collision Avoidance System
- ADS-A---Automatic Dependent Surveillance - Addressed
- ADS---Automatic Dependent Surveillance
- ADS-B---Automatic Dependent Surveillance - Broadcast
- APX-118---Common IFF Digital Transponder
- ATC---Air Traffic Control

- ATCRBS---Air Traffic Control Radar Beacon System
- ATM---Air Traffic Management
- ATN--- Aeronautical Telecommunications Network
- CDTI---Cockpit Display of Traffic Information
- CJCS---Chairman, Joint Chiefs of Staff
- CNS/ATM--- Communications, Navigation, Surveillance / Air Traffic Management
- DAFIF--- Digital Aeronautical Flight Information File
- DME---Distance Measuring Equipment
- EGI---Embedded GPS INS
- EUROCAE---European Organization for Civil Aviation Equipment
- FAA----Federal Aviation Administration
- FMS---Flight Management System
- FRD---Functional Requirements Document
- FRUIT---Friendly Replies Uncorrelated In Time
- GBAS---Ground Based Augmentation
- GPS---Global Positioning System
- ICAO---International Civil Aviation Organization
- IFF---Identification Friend or Foe
- INS---Inertial Navigation System
- JAA--- Joint Aviation Authorities
- JPALS--- Joint Precision Approach and Landing System
- MASP---Minimum Aviation System Performance Standards
- MHz---Megahertz
- Mode S---Mode Select
- MOPS---Minimum Operational Performance Standards
- NAD-83---North American Datum of 1983
- NAS---National Air Space System
- NIMA--- National Imagery and Mapping Agency
- NM---Nautical Miles
- NPA---Non-Precision Approach
- PPS---Precise Positioning Service
- PSR---Primary Surveillance Radar
- Q&A---Question and Answer
- RA---Resolution Advisory
- RNAV---Area Navigation
- RNP----Required Navigation Performance
- RTCA---RTCA Inc.
- SARPs---Standards And Recommended Practices
- SBAS--- Space Based Augmentation
- SPS---Standard Positioning Service
- SSR---Secondary Surveillance Radar
- TACAN---Tactical Air Navigation
- TIS-B---Traffic Information Service - Broadcast
- TIS---Traffic Information Service
- UAT--- Universal Access Transceiver
- VDL 4---VHF data link mode 4
- VNAV---Vertical Navigation
- VOR----VHF Omni-directional Range
- WGS-84--- World Geodetic Survey of 1984

INTEGRATED MOBILE GRAVIMETRIC SYSTEM. DEVELOPMENT AND TEST RESULTS

B.A.Blazhnov *, L.P.Nesenjuk **, V.G.Peshekhonov *, A.V. Sokolov ****, L.S.Elinson *******
The State Research Center of Russia - Central Scientific & Research Institute Elektropribor
30, Malaya Posadskaya St., 197046, St.Petersburg, Russia. E-mail: elprib@online.ru
L.K. Zheleznyak******
Institute of Physics of the Earth of the Russian Academy of Sciences
10, Bolshaya Gruzinskaya St., 123995, Moscow, Russia. Fax: (095) 255-60-40

Abstract

Key words: gravity, gravimeter, gyrostabilizer

The paper discusses a mobile gravimeter as the evolution of sea gravimetric systems, which have been created by the CSRI Elektropribor for thirty years. The principle of the gravity sensor design based on the double quartz elastic system with an optoelectronic converter using charge couple devices of linear type as a photodetector is considered. The gyrostabilizer of the gravimeter is built on floated gyros with accelerometer correction. The gyrostabilizer control system uses built-in microcontrollers. The mobile gravimeter is integrated with the satellite navigatiin system. The results of bench tests and preproduction operation of the first specimen of the mobile gravimeter onboard a geophysical vessel carrying out marine seismic work with the aim to search for oil and gas are analyzed.

Introduction

A gravimetric system of the third generation was presented at the First St.Petersburg International Conference in 1994 [1]. The gravimeter integrated with the satellite navigation systems GPS/GLONASS allows gravity survey in the open sea to be carried out with an error of less than 1 mGal.

The research on the development of the fourth-generation mobile gravimeter was conducted in two basic directions with the aim to:

- reduce weight and dimensions and at the same time increase the reliability of the gravity sensor and gyrostabilizer;
- synchronize measurements and refine techniques for coprocessing of gravity and navigation data.

As a result, it was made possible to install all devices and functional modules of the gravity sensor and the gyrostabilizer in a single device.

The conventional quartz gravity sensor has become much smaller, thus enabling it to be fitted in the compact-size gyrostabilizer. At the same time the reliability of the gravity sensor has increased due to the use of an optoelectronic converter with a photodetector based on two charge couple devices of linear type.

The gyrostabilizer design is unified with those of modern marine inertial navigation systems. It contains floated gyros with gas bearings practically of unlimited service life, miniature accelerometers with built-in electronics, digital servo drives and a digital gyro control system.

The gravity information and navigation data from the GPS/GLONASS receiver is received, recorded, processed in real-time and off-line in a personal computer.

1. The gravity sensor

Like the previous analogues, the gravity sensor is based on a Double Quartz Elastic System (DQES) developed by Elektropribor in collaboration with the Institute of Physics of the Earth [2,3]. Physically DQES consists of two torsions made of particularly pure quartz glass contained in a common housing. The torsions are turned in a horizontal plane at an angle of 180° to each other. The housing is filled with silicone liquid to afford damping, temperature compensation and pressure insulation of the torsions. Quartz glass, as a material, has a number of advantages: it is manufacturable; when being deformed, it obeys Hook's law even to destruction; it has a positive thermoelastic factor, which allows temperature compensation to be carried out in simple constructive methods.

A schematic of the gravity sensor is given in Fig 1. The DQES output magnitude is a turning angle φ of the pendulum lever. The angle φ changes under the influence of the gravity increment Δg in accordance with the formula:

---

*Ph.D., Leading Researcher
** D.Sc., Professor, Head of Department
*** D.Sc., Academician of the Russian Academy of Sciences, Director
**** Researcher
***** Ph.D., Head of Laboratory
****** D.Sc., Leading Researcher

$$\Delta\varphi = K \cdot \Delta g ,$$

where K – DQES sensitivity, which, depending on the torsion rigidity, may be in the range from 0.3 "/mGal to 1.5 "/ mGal.

The torsion string is preliminary twisted so that the initial position of the pendulum will be close to horizontal.

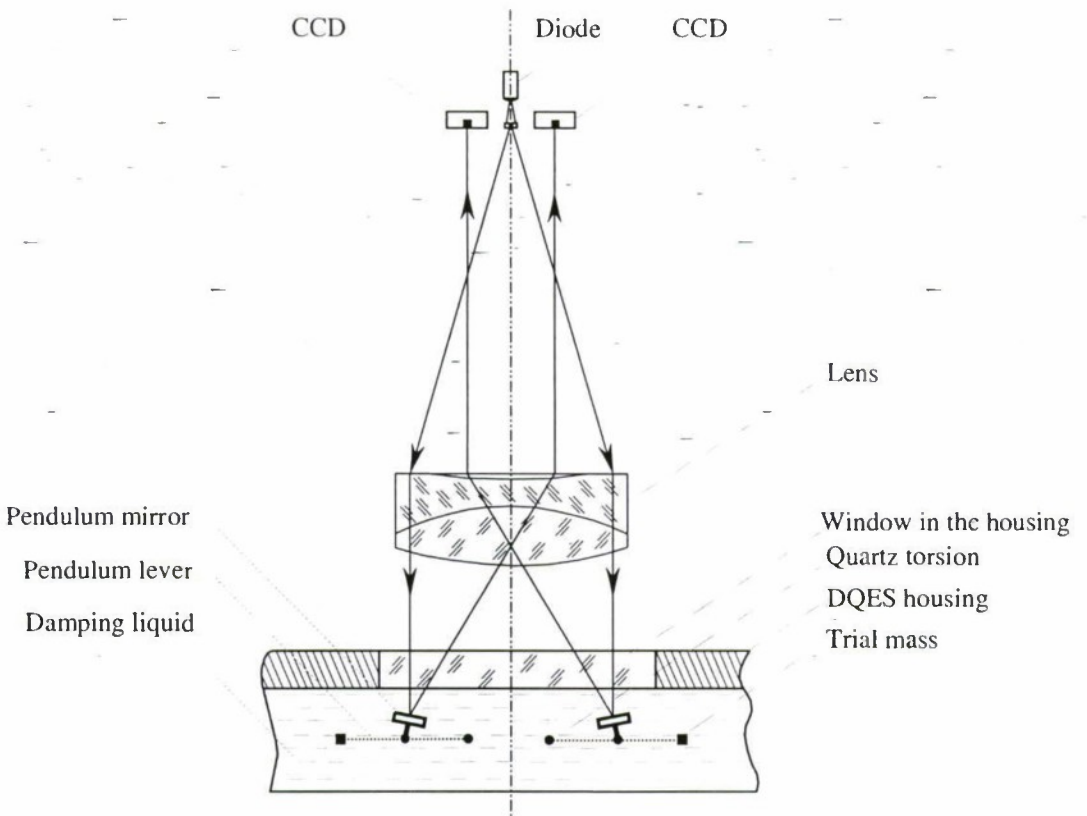

Fig.1. A schematic of the Gravity Sensor Construction

The dynamic range of the measurement is no less than 15 Gal, which makes it possible to carry out gravity survey without readjusting the measurement range all over the World ocean water area even at rather rough sea. The elastic system placed in the damping liquid practically fully eliminates the influence of vibrations and shocks caused by seismic work.

As the DQES is all-welded and has no adjusting elements, it is highly reliable. The advanced manufacturing technology of DQES provides a high degree of identity of the quartz systems both in sensitivity K and damping. Non-identity of two systems does not exceed 0.2 %, resulting practically in full elimination of an error due to the Cross Coupling Effect (CC-effect) caused by interaction between vertical and horizontal accelerations. For the double system it is less than 0.2 mGal at rocking accelerations of up to 1 m / s^2.

Elimination of the CC-effect is an important advantage of the DQES in comparison with other types of gravity sensors.

Concurrent with the improvement of the DQES, a new OptoElectronic Converter (OEC) was developed to measure tilt angles of the pendulum deflection. To increase the system resolution, the OEC photodetector is based on two Charge Couple Devices (CCD) of linear type, thus allowing the lens focal length to be extended from 40 mm to 150 mm.

Physically the CCD cases are placed at some distance from each other, which corresponds to a turn angle of the pendulum mirrors in the direction perpendicular to that of scanning. The CCD photosensitive surfaces are directed along the motion of autocollimation images of the mark.

A Light Emitting Diode is used in the pulse mode to allow for synchronization of the gravity data output with an external source of information including GPS receiver.

The change in the autocollimation mark image position ΔL is proportional to the change in the twisting angle $\Delta\varphi$ of the quartz torsion and, consequently, proportional to the gravity value increment.

The autocollimation mark image positions *L1* and *L2* are measured by a Video-Code Converter (VCC) fabricated as a single printed circuit board with two CCDs. The VCC block diagram is given in Fig 2. The board includes two AD converters (ADC), a shaper of control signals and a unit of calculation based on a logic integrated circuit.

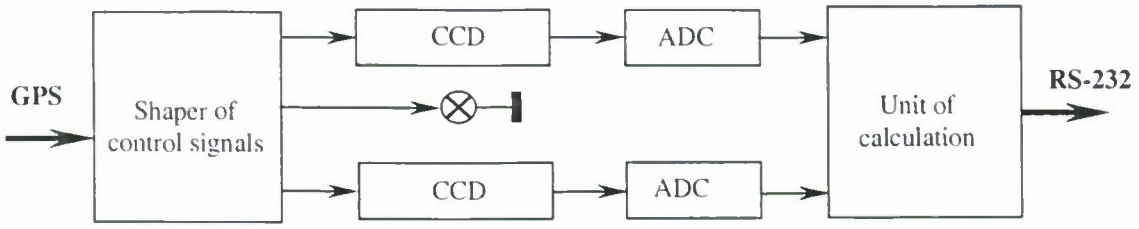

Fig. 2.The Block Diagram of the Video-Code Converter

The CCD is illuminated during 1 ms after the sync pulse arrives. Then the volume charges accumulated in the CCD elements are transferred to the reading registers. After that the volume charges are sequentially transmitted to the ADC input that forms a 12-bit code. The parameters describing the position of the autocollimation mark are transmitted to the computer via the serial interface. The computer calculates *L1* and *L2* values with an error of less than 0.001 pixel.

The development presented here employs two Sony ILX526A CCDs of linear type, each of 3000 pixels. A pixel is 7x200 μm in size, the length of photosensitive surface is 21 mm. The diode has the maximum of spectral brightness on the wavelength λ = 626 μm and operates in the pulse mode with a frequency of up to 50 Hz.

Integration of the gravimeter with the satellite navigation system is its distinctive feature. Data binding to the satellite time is provided with an error of less than 1 ms by synchronization of the gravity sensor operation with a TTL-pulse with a frequency of 48 Hz.

The bench test results of the gravity sensor are presented in Fig. 3. It is obvious that the reading spread of the double system is essentially less than that of each of the elastic systems. This effect was achieved owing to the turning round of the CCD cases at an angle of 180° to each other. As a result, when the board is displaced because of some external influence, the readout of one of the CCDs increases, at the same time of the other decreases.

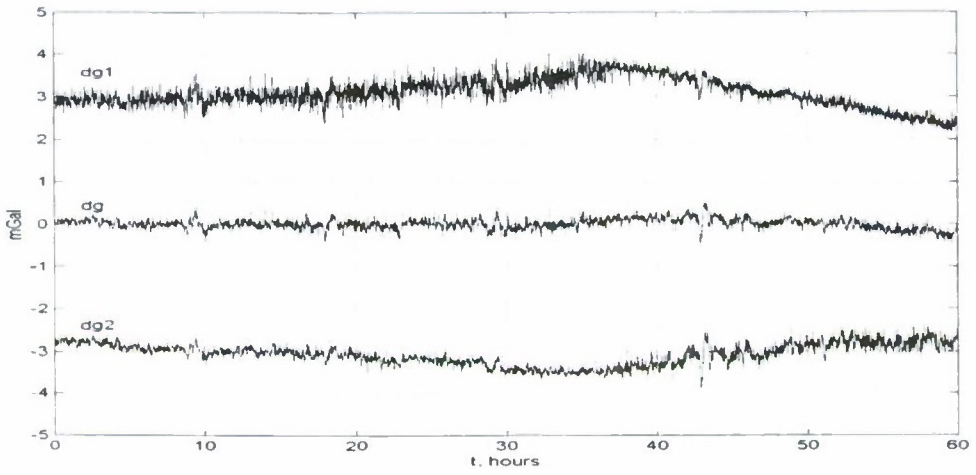

Fig. 3.The Gravity Sensor Output Data

The standard deviation calculated from the double system data is about 0.2 mGal. After this data is processed by the lowpass filter with the bandwidth *Fc* = 0.01 Hz, it decreases down to 0.05 mGal.

Changes in the ambient temperature exert a profound effect on the instrumental error of the gravity sensor. In spite of the fact that the DQES is placed in a thermostat, whose wall temperature is kept within an error of about 0.1°C, sharp fluctuations of the ambient temperature result in discontinuous change of readings of 1-2 mGal. This is caused by the difference between the temperature factors for quartz glass and damping liquid of

about two orders. To provide the required accuracy of the gravity sensor, the ambient temperature should be stabilized to an error of no more than 1°C.

2. The gyrostabilizer

The gyrostabilizer design is unified with those of modern marine inertial navigation systems. The general view of the gyrostabilizer with the gravity sensor is shown in Fig. 4. The overall dimensions of the device are Ø430x450 mm, the weight is about 55 kg.

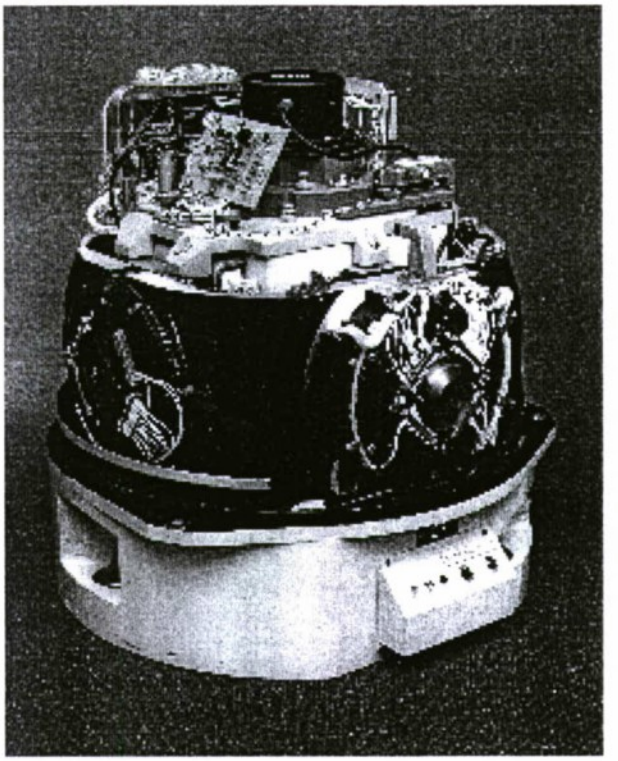

Fig. 4 The general view of the gyrostabilizer with the gravity sensor

The gyrostabilizer contains two floated gyros with gas-dynamic rotor suspension, tiny accelerometers with built-in electronics and gearless servo drives. The gyros have practically unlimited service life. The signals from the gyro pick-offs arrive at the servo drive inputs.

The torque motors on stabilization axes are controlled by two single-channel microcontrollers based on a SIEMENS processor. Unlike the preceding analogs, in which the units of the servo drive were placed in a separate device, in this construction the microcontrollers are fabricated as printed circuit boards built in the gyrostabilizer. This essentially raises the reliability of the servo drive, as there is no transfer of analog signals through current wires, connectors and cables.

Two other single-channel microcontrollers mounted on the inner gimbal of the gyrostabilizer supply power to the gyros, receive and digitize the accelerometer signals used to correct the position of the gyro axis by the gyro torquers control. The selected correction and stabilization parameters provide the required dynamic responses of the gyrostabilizer. The microcontrollers are interconnected via CAN-interface.

The gyrostabilizer software allows entering corrections for the constant component of the gyro drift and initial deviation of the gyro axis from horizon, for the gyro scale factor error and for the zero shift of the accelerometers. All corrections are determined at the manufacturing plant during the gyrostabilizer calibration.

The algorithm of accelerometer corrections corresponds to the Butterworth filter of the 3^{rd} order with response time of about 50 s. The information about the horizontal velocities and the heading, incoming from GPS receiver, is used to provide the gyrostabilizer unperturbance in maneuvering. To reduce the error caused by the vessel maneuver, the heading value is integrated with the turn angle generated by the fiber-optic gyro VG-910 mounted on the stabilized base of the gyrostabilizer.

The results obtained during the tests on the rolling stand show that the gyrostabilizer dynamic error does not exceed 15". Automotive tests were carried out to estimate the error caused by abrupt change of the heading. It

was established that during circulation the deviation of the stabilized platform from horizon does not exceed 3', and transient process lasts no more than 3 minutes after the maneuver finishes.

3. Software

The software for real time provides reception in the computer and recording on a hard disk of the gravity sensor output data, accelerometer signals and navigation information incoming from the GPS receiver. Concurrent with filing, the current information is displayed on the monitor in graphic and digital form (Fig. 5).

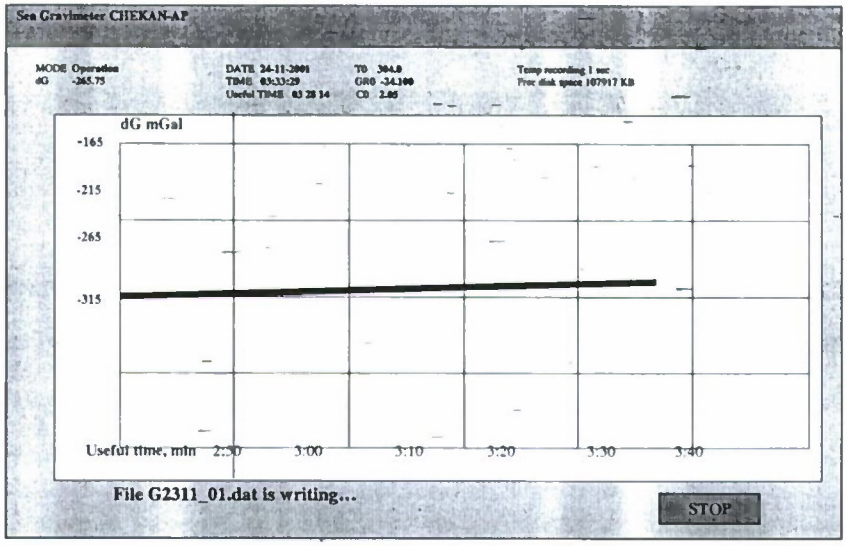

Fig. 5. View of the Monitor

During marine gravity survey the initial processing of the gravity data are also carried out in real-time. It includes scale linearization and smoothing of the gravity sensor output data by using the digital lowpass filter. After the each tack filtering is done in the opposite direction, thus excluding any time delay of gravity relative to navigation data. The operator can change the filter bandwidth in a wide range, depending on the sea state. The frequency of data storage is 1 Hz.

Off-line processing involves calculation and filtering of Eotvos correction and creation of a gravity catalogue including both gravity and navigation data. The software also allows for calculating differences at the tacks cross points. It is by these differences that the survey accuracy is estimated and the gravity sensor null-point drift rate is determined.

During the aerogravity survey only gravity and navigation data is recorded in real time with a frequency of 48 Hz synchronized with the GPS receiver. This high frequency provides elimination of the transfer effect of the high-frequency error component in the low-frequency area during the off-line processing of the gravity and navigation data. The required altitude correction accuracy is achieved by coprocessing of the data obtained from the GPS receivers installed both aboard an aircraft and at the ground station, together providing a phase differential mode of the system operation.

4. The results of the bench tests

The prototype mobile gravimeter was tested on special dynamic benches to study the influence of angular and vertical rolling, vertical motion of the object, as well as mechanical and climatic effects. It was found that in rolling with an amplitude of up to 15 degrees, the standard deviation of the gravimeter error was about 0.15 mGal with the use of the lowpass filter with the bandwidth of 0.02 Hz. This error practically does not exceed the static error. The same estimation was obtained in vertical motion tests with small values of the vertical motion period (up to 20 s) with amplitude of about 2 m. It is interesting to note that in this case the fluctuations in the readings of the double system turned out to be much less than the readings of each of the quartz systems (Fig.6).

However the error increases up to 0.5 mGal at vertical motion with a period of 50-200 s and the same amplitude. These conditions are typical for an air survey. It should be noted that the most essential factor is the error in determining response time τ in the damped gravity sensor, which determines the accuracy of reproduction of input action using the gravity sensor output signal. Originally the value of response time is calculated with an error of about 1 s by using the transient process measured when the gravity sensor is returning

rapidly from the inclined to the vertical position. The vertical motion tests allowed the accuracy in determination of response time to increase up to 0.1 s.

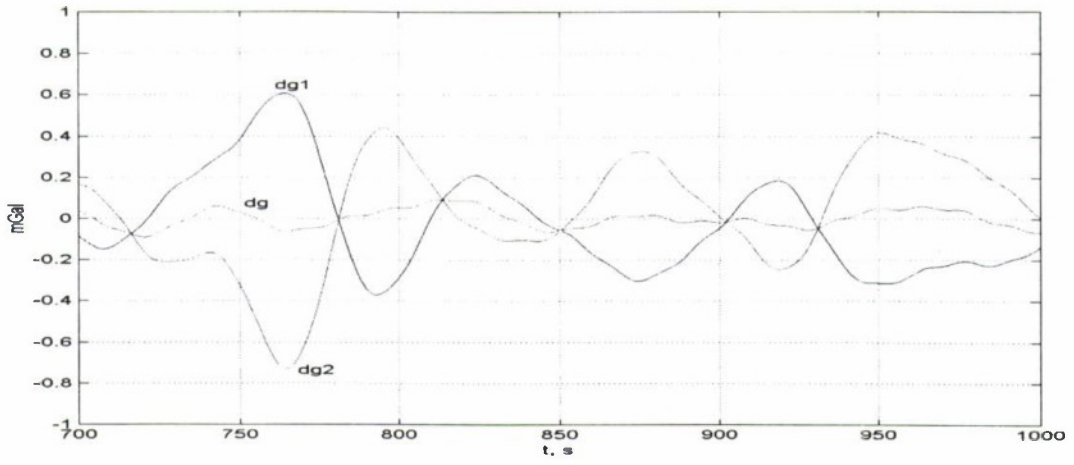

Fig. 6. The results of the vertical motions tests

The vibration tests showed that vibrations do not increase the error in the frequency range between 2 and 35 Hz, but there was constant displacement of up to 0.5 mGal at some frequencies of vibration.

The climatic tests showed that it is sufficient to install a fan in the gyrostabilizer cover to provide the gravimeter operation onboard a vessel where the temperature is kept in the range from 18 to 23 °C. Aboard an aircraft the cover is replaced with a thermostabilization device to keep the temperature inside the gyrostabilizer at a level of 22-24 °C.

5. The operational test results of the mobile gravimeter onboard a hydrographic vessel

The first specimen of the mobile gravimeter was installed onboard the research vessel Northern Access in accordance with the agreement on technical cooperation with the Norwegian geophysical company TGS NOPEC in June, 2001, the purpose being the gravity survey in the course of marine seismic work aimed at oil and gas searching. At the same time the survey was carried out by a LaCosta-Romberg gravimeter. The results of measuring the same tack by two gravimeters are shown in Fig. 7. It is easy to see that the data obtained is very close. The survey standard deviation error calculated by the data of 73 differences at tacks cross points was about 0.36 mGal.

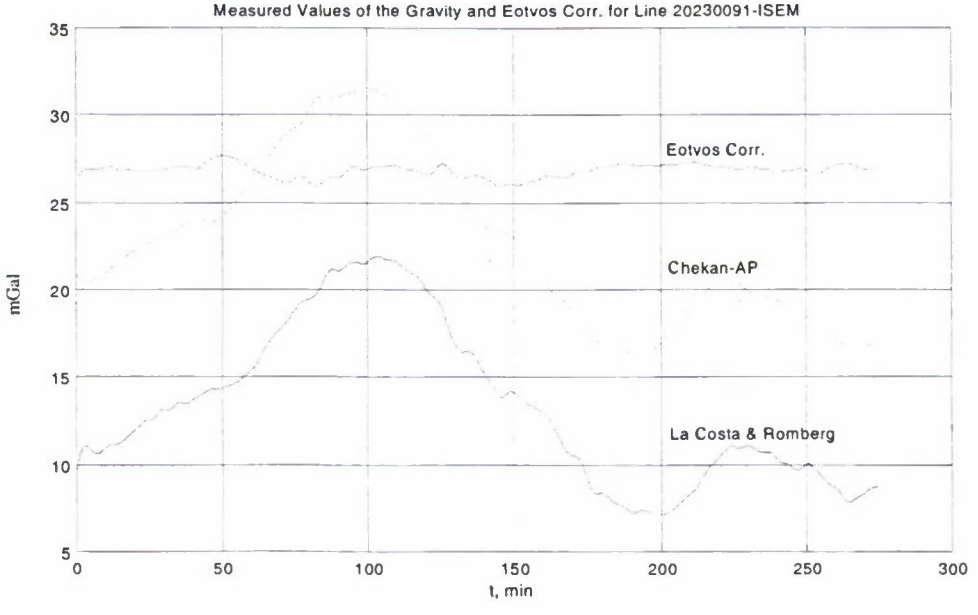

Fig. 7. Gravity Measurement of the Tack

The data given in Fig. 8 shows a high degree of correlation between the gravity data and the seismic profile, proving that the methods of gravity survey hold much promise for oil and gas searching on the shelf.

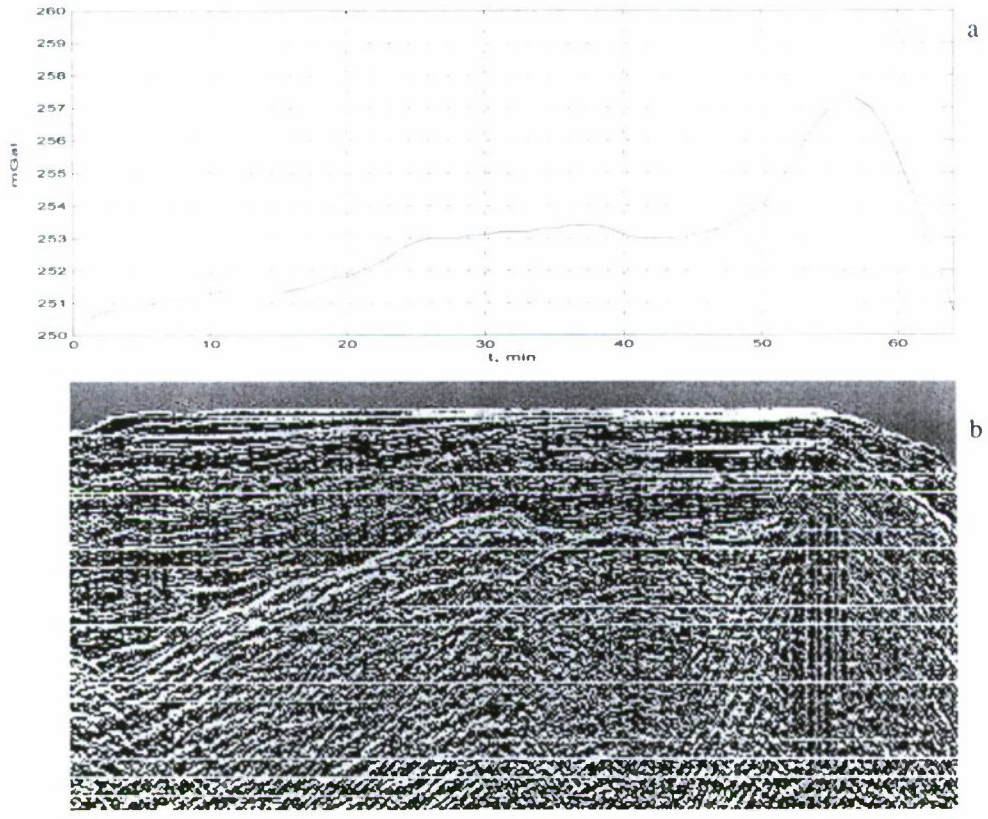

Fig. 8. Gravity Data (a) and Seismic Profile (b) for One Tack

The operational performance and reliability of the gravity equipment are of vital importance along with the measurement accuracy. The prototype mobile gravimeter installed onboard the vessel ZEPHYR-1 has been operation without any failures and interruptions for more than three years [5,6]. The significant advantage of the mobile gravimeter is the possibility to transfer it from one vessel to another without any special requirements to transportation.

6. The outlook for using the mobile gravimeter in regional air survey

The first flight tests of the gravimeter of the previous generation were carried out in 1992-1993 aboard airplanes AN-12 and AN-30 over Ladogskoe Lake. The tests showed the gravimeter serviceability in the flight conditions, but the navigation equipment was not perfect enough to allow a reliable assessment of the gravity survey aecuracy. The results obtained showed that the GPS reeeiver should have been used in the phase mode to measure altitude variations with an error of less than 1cm [1].

In 1999-2000 the further work earried out in cooperation with Braunschweig Technical University (BTU) was aimed at improving the equipment and methods of air gravity survey. The tests were eonducted in Braunschweig (Germany) aboard an airplane Dornier. The airplane navigation equipment ineluded a NovAtel GPS receiver operating in the phase mode and a Honeywell inertial navigation system LaserNav. The estimation of survey accuracy obtained by the experts from BTU was ~1 mGal [7]. The results of the survey data processing carried out by the experts from the CSRI Elektropribor are given in [8].

The flight tests of the mobile gravimeter aboard an airplane IL – 114 are scheduled for June, 2002 together with Geologorazvedka Company. The gravimeter automobile tests have been carried out in preparation for the flight trials. The mobile gravimeter operation was cheeked using the gyrostabilizer correction by GPS data, the measurement error was estimated at the Pulkovo gravity testing area. Besides, the off-line processing of the test

results included estimation of altitude determination error by using integrated data from GPS receivers installed on the automobile and at the ground reference station.

The tests were carried out in two modes: when moving along a short closed trajectory to check dynamic features of the gyrostabilizer corrected by GPS data and in motion with constant values of course and speed to estimate the accuracy of the gravity measurements. The test areas and routes are given in Fig.9.

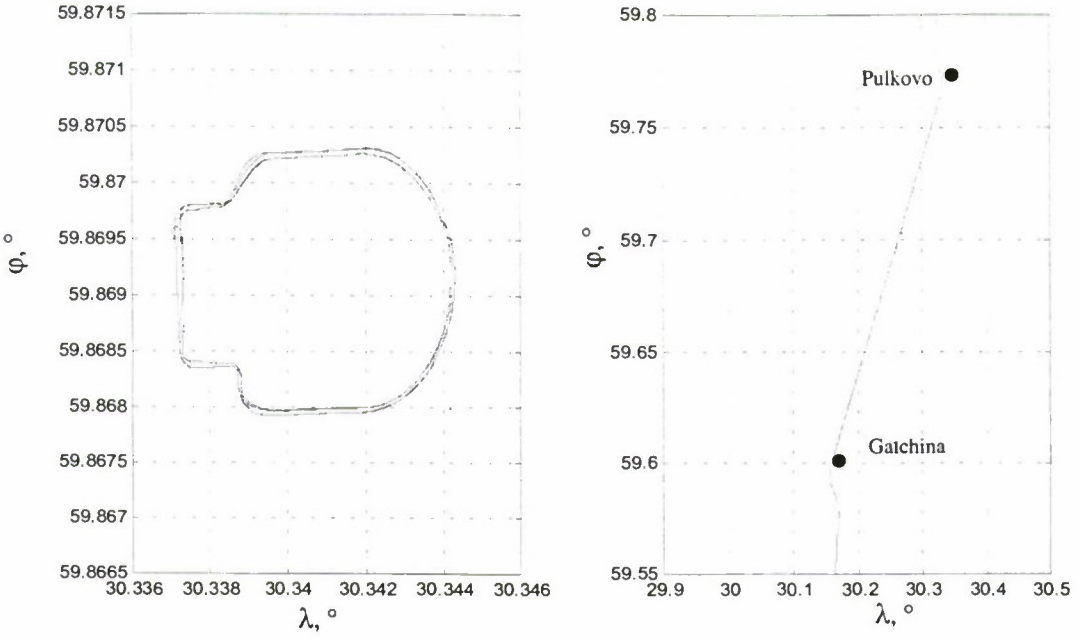

Fig.9. The Areas of the Mobile Gravimeter Automobile Tests:
a) – The Route Along a Closed Trajectory; b) – A Leg of the Route Pulkovo-Gatchina

The gyrostabilizer error was estimated from the differences of the linear speeds generated by the gyrostabilizer and received from satellites. The curves of the gyrostabilizer deviations α, β for the case that the automobile is moving along the closed trajectory at a speed of ~ 5 m/s are given in Fig.10. It also shows curves for the northern *Vns* and eastern *dVes* components of the speed calculated by the GPS data. The gyrostabilization error during motion was no more than 5'. The gyrostabilizer transient process lasted about 5 minutes after the automobile stopped. The deviations α, β did not exceed 30″ along the linear part of the route in the steady state.

The analysis of the obtained data shows that in general the gyrostabilization error during a maneuver is caused by the usage of the GPS heading instead of the true course. It may be expected that the use of additional information from the fiber-optic gyro will cause the gyrostabilization accuracy to increase during the maneuver and the transient process duration to reduce.

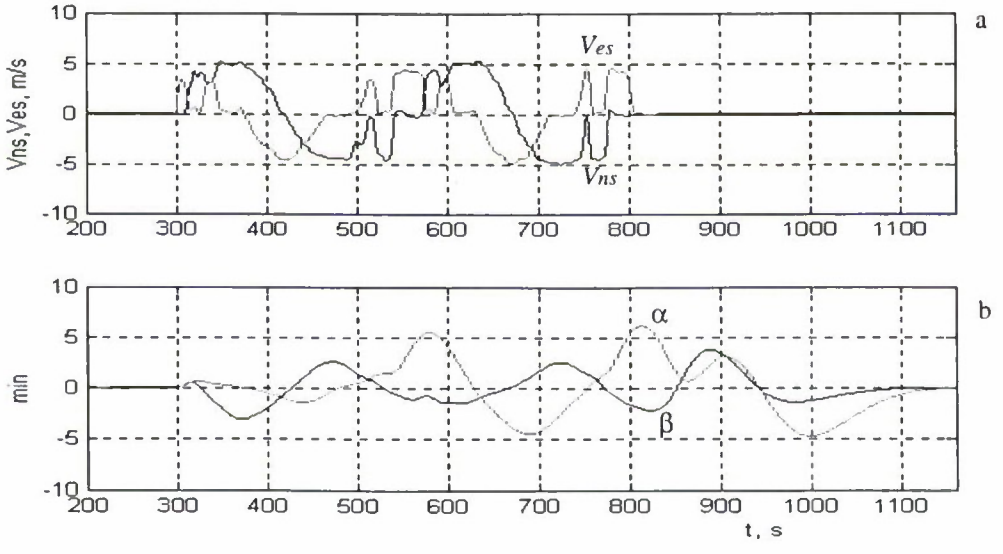

Fig.10. The curves of the horizontal speed components (a) and the gyrostabilizer errors (b)

A fragment of gravity measurements obtained on a leg of the route Pulkovo-Gatchina is given in Fig.11. The diagram of the vertical acceleration *Wz* calculated by double differentiation of the altitude value *H* is shown in the upper part of the figure. The disturbing acceleration values are as high as 10 Gal, which is close to the acceleration level in flights [7].

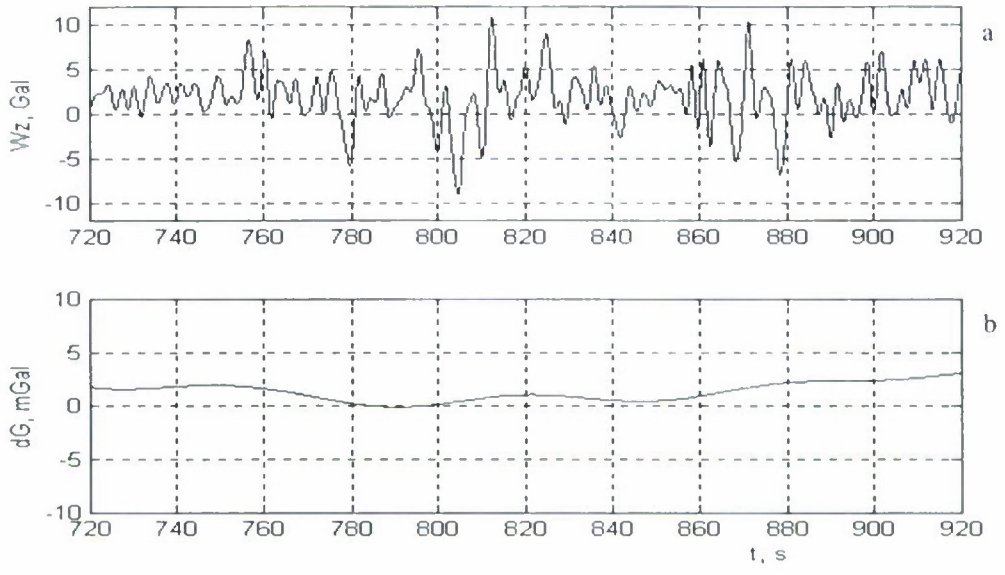

Fig.11. Vertical accelerations (a) and gravity measurements (b)

However the spectrum of the automobile vertical acceleration given in Fig.11 differs in the increased level in the low-frequency area. Due to this circumstance the measurement accuracy of 1 mGal was achieved using the lowpass filter with narrow band - $Fc = 0.007$ Hz.

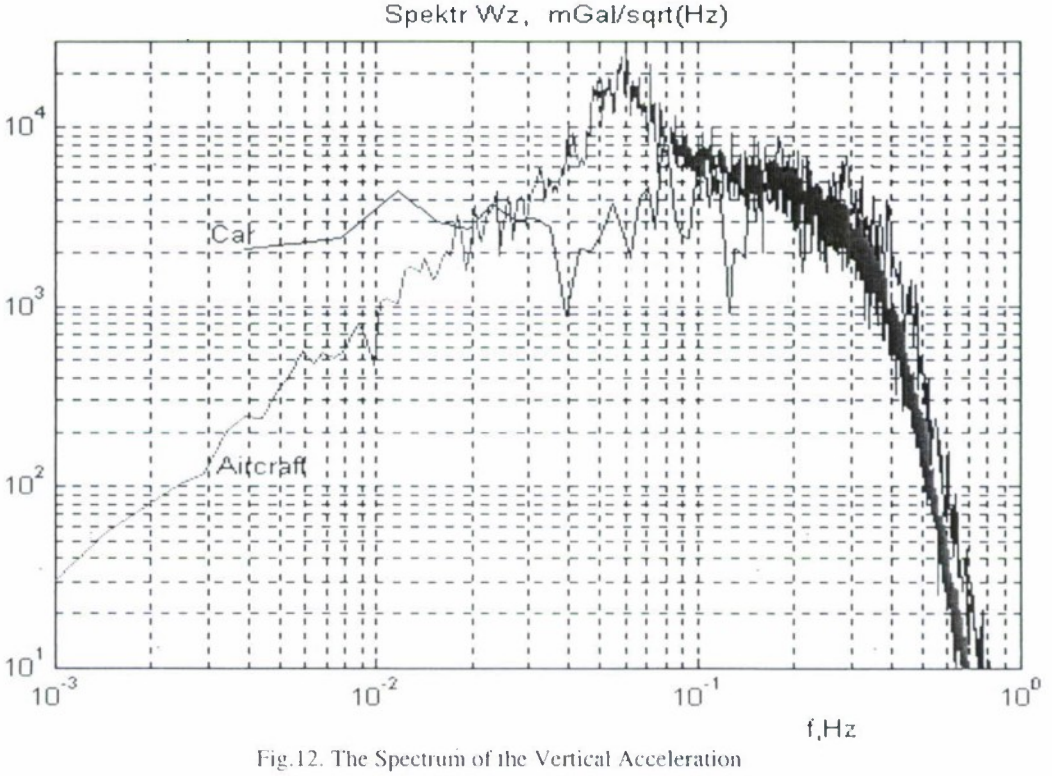

Fig.12. The Spectrum of the Vertical Acceleration

The estimation of the gravimeter error was carried out by comparing the gravimeter readings against the gravity data of at the reference points of the Pulkovo gravity testing area. The root-mean-square error of the gravimeter readings was 0.6 mGal.

Conclusions

The results of bench tests and operational testing of the mobile gravimeter have confirmed its high accuracy and reliable operational performance when it was used in marine seismic work for searching of hydrocarbonic deposits.

The flight tests of the gravimeter of the previous version and bench tests of the mobile gravimeter shows considerable promise for regional air survey.

References

1. **Блажнов Б.А., Несенюк Л.П., Пешехонов В.Г., Элинсон Л.С.** Морские и авиационные гиростабилизированные гравиметры, разрабатываемые в ЦНИИ «Электроприбор» // Материалы I Санкт-Петербургской международной конференции по гироскопической технике. – 1994. – С.114-121.
2. **Nesenjuk L.P., Peshekhonov V.G., Elinson L.S.** Marine Gravity Systems. // First Annual Workshop."Russian Airborn Geophysics and Remote Sensing", 13-17 September 1992, Colorado School of mines, Golden, Colorado, USA. SPIE, V2111, 93.
3. **Несенюк Л.П., Пешехонов В.Г., Элинсон Л.С., Железняк Л.К.** Морские гравиметрические комплексы // Морская и аэрогравиметрия. – 1994 – N 1.
4. **Блажнов Б.А., Несенюк Л.П., Элинсон Л.С.** Особенности выработки параметров вертикального движения объекта по данным сильно демпфированного гравиметра // Гироскопия и навигация. – 1996. – N 4.
5. **Соколов А.В., Усов С.В., Элинсон Л.С.** Опыт проведения гравиметрической съемки в условиях выполнения морских сейсмических работ // Гироскопия и навигация. – 2000. – N 1. – С.39-51.
6. **Ржевский Н.Н., Соколов А.В., Усов С.В., Элинсон Л.С.** Опыт использования гравиметрического комплекса «Чекан-А» при морских сейсмических работах за рубежом // Геофизический вестник – 1999. – N 12. – С.8-11.
7. **Abdelmoula F.** Ein Beitrag zur Bestimmung der Eerdbeschleuigungsanomalien an Bord eines Flugzeuges.
8. **O.A. Stepanov, B.A.Blazhnov, D.A.Koshaev.** The efficiency of using velocity and coordinate satellite measurements in determining gravity aboard an aircraf (In the present issue, p. 255).

GT-1A INERTIAL GRAVIMETER SYSTEM DESIGN CONSIDERATIONS AND RESULTS OF FLIGHT TESTS

V.N. Berzhitzky [*], **V.N. Ilyin** [**], **E.B.Saveliev** [***], **Y.L. Smoller** [****], **S.S. Yurist** [*****]
Scientific and Technological company "Gravimetric Technologies ",
Russia 119361 Moscow Ozernaja 42,
e-mail: gravitech@mtu-net.ru
Yu.V. Bolotin [†], **A.A.Golovan** [††], **N.A.Parusnikov** [†††]
Lomonosov Moscow State University, Russia 119899, Moscow, Vorobjovy Gory
e-mail navlab@moids.math.msu.su
G.V. Popov [‡], **M.V. Chichinadze** [‡‡]
Central Scientific & Research Institute "Delphin", Russia 119361 Moscow Ozernaja 42
e-mail: delfin@sl.ru

Abstract

Keywords: gravimeter, airborne gravimeter, gyro system, data processing

A brief description of the functional scheme, system organization and software operation of the GT-1A inertial gravimeter, developed by JSK STC "Gravimetric Technologies", is given. The software system for processing of airborne gravimetry data, developed by MSU Laboratory of Control and Navigation, is described. The results of laboratory and flight tests are discussed.

Introduction

During 2000 and 2001 the closed stock scientific and technological company "Gravimetric Technologies" (GT) developed, under a government contract with the Ministry of Science, Industry and Technology, a high precision, compact inertial gravimeter system with a broad range of applications (airborne, marine and surface-based). Central Scientific & Research Institute "Delphin" manufactured the prototype version of this system.

The software for off-line data processing was developed by Lomonosov MSU Laboratory of Control and Navigation.

During the period July to September 2001, the GT-1A airborne system was subjected to extended laboratory and flight tests [1].

1. Problem statement

In airborne gravity measurement, an Inertial Gravimetry System (IGS) is used to obtain the anomaly of gravitational force along the flight lines of the aircraft.

The main stages of the airborne gravity evaluation are as follows.

On-board algorithms:

1. Control of platform levelling using information from the accelerometers, with gyroscope moment sensors and possibly data from the on-board GPS receiver.
2. Recording of the information delivered by the IGS and the rover GPS receiver. This information includes: GSU and accelerometer readings; information required to estimate the platform misalignment; Cardano angles; and raw readings from the GPS receiver including phase measurements

Off-line processing:

1. Differential phase solution of GPS navigation problem

---

[*] Senior researcher , candidate of science.
[**] General director, candidate of science
[***] Leading researcher , candidate of science.
[****] Head of group
[****] Leading researcher , candidate of science.
[†] Leading researcher , candidate of science.
[††] Senior researcher , candidate of science.
[†††] Professor, doctor of science.
[‡] General director, candidate of science.
[‡‡] Deputy director, doctor of science.

2. Determination of platform misalignment
3. Calculation of the forces of inertia (Eötvös correction)
4. Determination of the gravity force along the flight line
5. Construction of anomalous gravity maps

The principal equation of airborne gravimetry is the equation of motion of the material point M of unit mass in the gravity field of the Earth under the action of a measured external force projected onto the vertical axis of the local geographic frame

The equation can be written as [6]:

$$\ddot{h} = f_3 + f_E + g_0 + \Delta g \,.$$

Here f_3 is the vertical component of specific force acting on the point M, $g_0 = g_0(\varphi, h)$ is the regular component of the gravitational force. The Gelmert formula is commonly used.

The value f_E, which includes inertial terms, is called in gravimetry the Eötvös correction term

$$f_E = \frac{V_E^2}{R_E} + \frac{V_N^2}{R_N} + 2uV_E cos\varphi \,.$$

Here R_N, R_E are the curvature radii of the ellipsoid in the north and east directions, V_E, V_N are the eastern and northern components of relative linear velocity of the point M.

The value $\Delta g(\varphi, \lambda, h)$ is the anomalous value of the gravitational force, which is to be determined. To solve the principal gravimetric equation is to extract the value of Δg from it.

The main difficulty of the airborne gravimetry problem, as opposed to, for example, marine gravimetry, is the fact that the spectrum of anomalies coincides with the spectrum of perturbing vertical accelerations. Hence, high-precision external measurements of the aircraft altitude are required. The value of h is derived from GPS measurements, which are also used for calculation of the Eötvös correction. Residual errors, after the elimination of $\ddot{h}$ and f_E, are filtered out using optimal methods of filtering and smoothing [5].

2. Description of inertial gravimeter system GT-1A

2.1. Functional scheme and structure

The functional scheme of the GT-1A inertial gravimeter system (IGS) is shown in Fig. 1. The IGS consists of:

- central inertial gravimeter device mounted on a shock absorbing base
- control, display and data acquisition unit (CDU) using an industrial-grade Asmet 08-12-PC 14 computer
- on-board Ashtech Z-12 GPS receiver
- power supply system
- one or more surface-based GPS receivers supporting differential mode operation

The IGS central device contains a gyro-stabilized platform which is non-perturbed by motion and stabilized in an azimuth-free coordinate frame. The following parts are mounted on the platform: a gravimetrical sensing unit (GSU); two horizontal accelerometers (HA), a dynamically tuned gyro (DTG) with vertical orientation of the kinematic moment; a fibre-optic gyro (FOG) with a vertical sensitive axis; and two gravimeter calibration devices (GCD).

The GSU has an axial structure with a proof mass on an elastic suspension, a photoelectric position sensor and magneto-electric sensors of the feedback force and the compensation force. A current, proportional to the vertical apparent acceleration, originates in the coil of the feedback force sensor and runs through a series reference resistor. The output signal (W_z) is the voltage on the reference resistor which passes through an integrating analogue-to-digital converter (ADC) into an Octagon Systems' MicroPC central processing unit (CPU). The stabilized reference current runs though the coil of the compensation force sensor which compensates the fixed value of the gravitational force. The integrating ADC of the GSU consists of serially connected converters: voltage-to-frequency and frequency-to-code. The ADC has two channels: one narrow-band with a range of $\pm 0.25g$ and one wide-band with a range of $\pm 0.5g$ [1], which allows, through selective operation, achieving the accuracy of the narrow-band converter together with the large dynamic range of the wide-band converter.

The GSU in conjunction with the ADC has a bandwidth of approximately 100 Hz and a random noise error

of 0.1 to 0.2 mGals (1 σ) with an averaging time of 60 sees. The scale factor instability of the GSU is 10^{-4}.

The GB-23 dynamically tuned gyro has a random noise error of 0.01° per hour (3 σ) for an averaging time of 10 minutes.

The VG910FOA FOG has a random noise error of 0.5° per hour (1 σ) for an averaging time of 60 sees and a scale factor instability of approximately 10^{-3}.

The AK-10 quartz accelerometers have a random noise error of $2 \cdot 10^{-6}$g (1 σ) over 60 sees, a long-period systematic error with correlation interval of the order of 20 hrs of $5 \cdot 10^{-5}$g (3 σ), and a scale factor instability of $6 \cdot 10^{-4}$.

The gravimeter calibration device is based on AK-10 accelerometers. The DGC performs highly accurate measurement of the gyro-platform tilt about its horizontal axes, which allows calibration of the GSU by inclination without removing it from the instrument. During calibration, the GSU scale factor, the scale factors of the accelerometers and the misalignment of the GSU sensitive axis from the platform vertical are determined.

The gyro-stabilized platform is mounted on a triaxial Cardano gimbal with external azimuthal axis located outside of the device case [3]. This gimbal scheme, compared with a biaxial arrangement, allows the virtual elimination of errors due to instability of the FOG scale factor and the non-orthogonality of the DTG kinematic moment to the platform plane. Compared with a traditional triaxial scheme, it eliminates the so-called "bearing" error, induced by varying orientation of the platform with respect to spurious sources of magnetic and thermal fields caused by the gimbal axes and the device case.

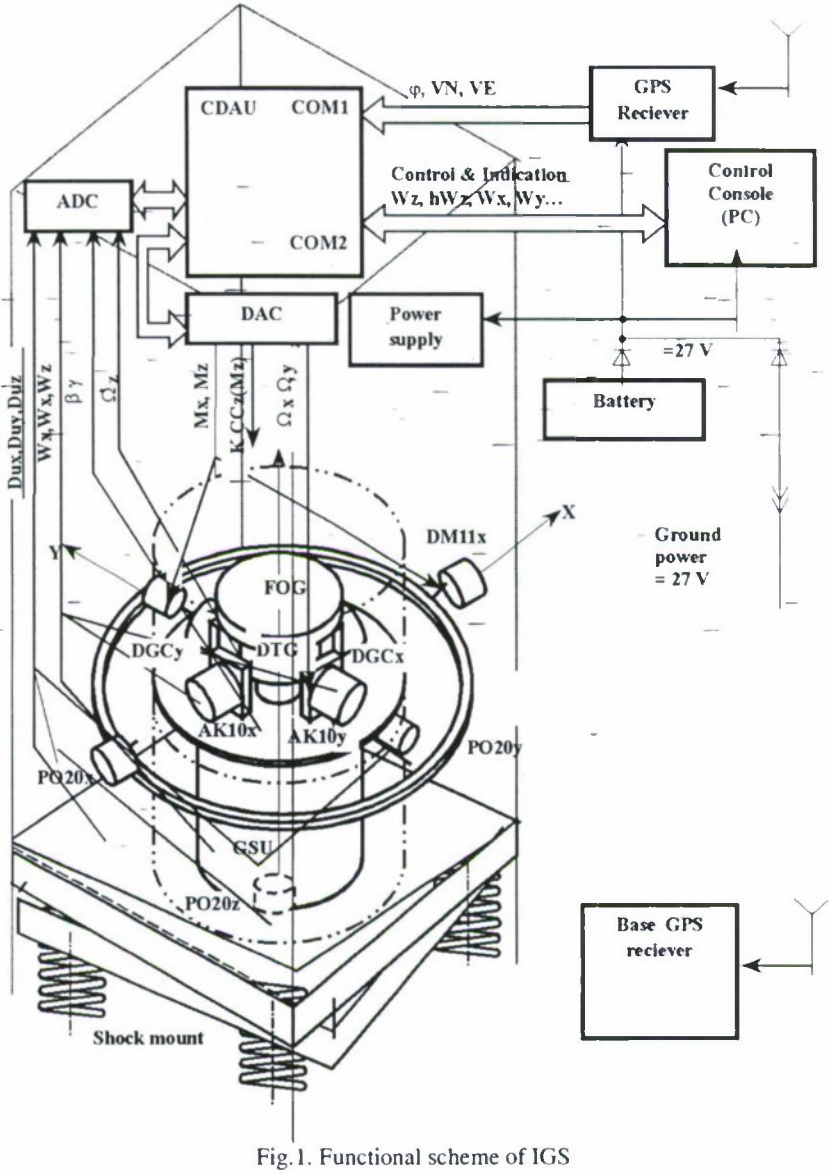

Fig.1. Functional scheme of IGS

The model PO-20 angle sensors and motors for the servo stabilization systems (SS) are mounted on the axes of the Cardano gimbal (in Fig. 1 the azimuthal SS motor is not shown). The angle sensors are used to measure the roll, pitch and course angles of the aircraft.

To ensure constant operating temperature of the sensitive units and the principal components of the gravimeter, three thermal control systems (TCS) are used:

- Double-circuit TCS of the GSU and the reference voltage source
- Single-circuit TCS of the DTG controller DAC
- Single-circuit TCS of the DTG, AC and DGC.

Control of the functional elements of each TCS, consisting of heating coils and fans, is performed by the CPU according to signals received from the thermo-sensors via the ADC. Information exchange with the CDU and the on-board GPS receiver is through the serial COM-ports of the CP.

All processes in the IGS, including start-up, GSU calibration and monitoring of the system state, are fully automated. The CDU displays all necessary information to the operator grouped by function: start-up, warm-up, operating mode, reference measurements, system monitoring, GSU calibration, and maintenance. The monitoring mode indicates monitoring results and the isolation of failures to the operator. The CDU allows the operator to enter control commands plus various constants, and also shows moving plots of many selectable system variables in real time. During gravimetric surveys, files of gravimetric and navigation data are stored on the CDU hard disk. Operation of the IGS during surveys does not require manual intervention.

The small power consumption of the IGS (150 W from 27 Vdc) allows the use of a rechargeable battery as a power source in the aircraft, which assures full independence from the aircraft electrical system.

2.2. On-board software

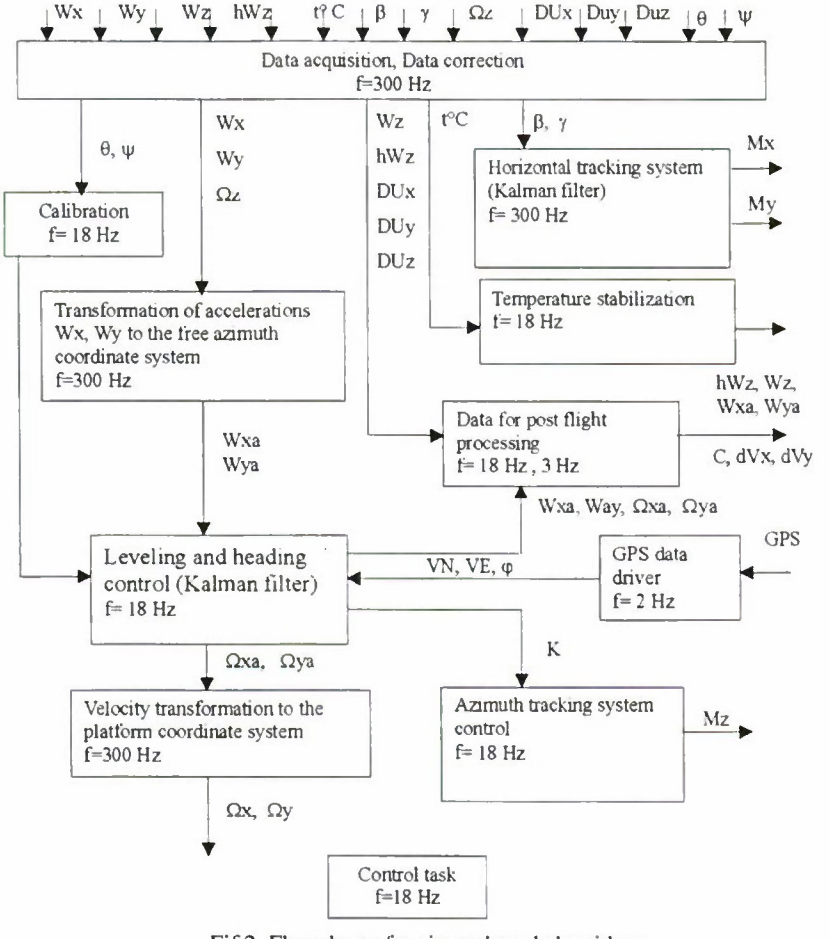

Fif.2. Flowchart of main on-board algorithms

A flowchart of the main on-board IGS algorithms is shown in Fig. 2. Sensor sampling is performed at a rate of 300 Hz. The output of the GSU is corrected with respect to the joint influence of horizontal accelerations and platform tilts (Harrison correction) [7], non-orthogonality of the GSU sensitive axis to the platform plane, and influence of the square acceleration. The platform tilt correction is incorporated into the accelerometer measurements [9].

With the FOG data sampled at 300 Hz, a coordinate frame free in azimuth is constructed and accelerometer data is projected onto this coordinate system. Integration of the dynamic equations of inertial navigation is carried out at a rate of 18 Hz in this azimuth-free coordinate system.

External information on aircraft velocity and latitude, delivered by the on-board GPS receiver, is used for correction. The values of absolute angular rates Ω_{xa}, Ω_{ya}, generated at a rate of 300 Hz, are projected onto the platform coordinate frame and control the sensors of DTG moments. The value of platform course angle thus obtained is passed to the input of the servo system for azimuthal stabilization. The servo system for horizontal stabilization operates at a frequency of 300 Hz, and azimuthal stabilization occurs at a frequency of 18 Hz. The algorithms for both horizontal orientation control and for the stabilizing servo systems are built around stationary Kalman filters.

Calibration of the GSU and accelerometers is fully automated. The calibration process takes 3 hours and can be performed while the aircraft is parked on the ground and oriented in any direction.

The monitoring algorithms perform logical control of all sub-systems of the inertial gravimetric device. The results of monitoring are passed to the CDU for display to the operator.

3. Software for off-line processing

In this section the software for off-line processing of gravimetric information is briefly described. The software takes into account peculiarities of operation and error models of the GT-1A.

The flowchart of information processing is shown in Fig. 3. The three main stages of processing arc: determination of coordinates with GPS data; gyro-platform correction with the GPS data (determination of platform misalignment in particular); and solution of the principal gravimetric equation.

Software for processing GPS phase measurements uses algorithms developed by the Laboratory of Control and Navigation for applications in gravimetry. It differs from most commercial GPS data processing packages in its approach to the problem of cycle slips [6]. The software allows the incorporation of information from an arbitrary number of GPS base stations.

To solve the gyro-platform correction problem with GPS data, the gyro-horizon control signal is used. The problem is solved using sub-optimal Kalman smoothing. The algorithms allow the estimation of platform misalignment with high accuracy.

The design of the shock mount results in tilting of the gravimeter due to the action of horizontal accelerations. This lead to the requirement to model the compliance of the shock mount during the calculation of relative motion of the GPS antenna and GSU using Cardano angle measurements of the IGS. The compliance parameters were determined on a swinging Scorsby table (Fig. 7) using special identification software.

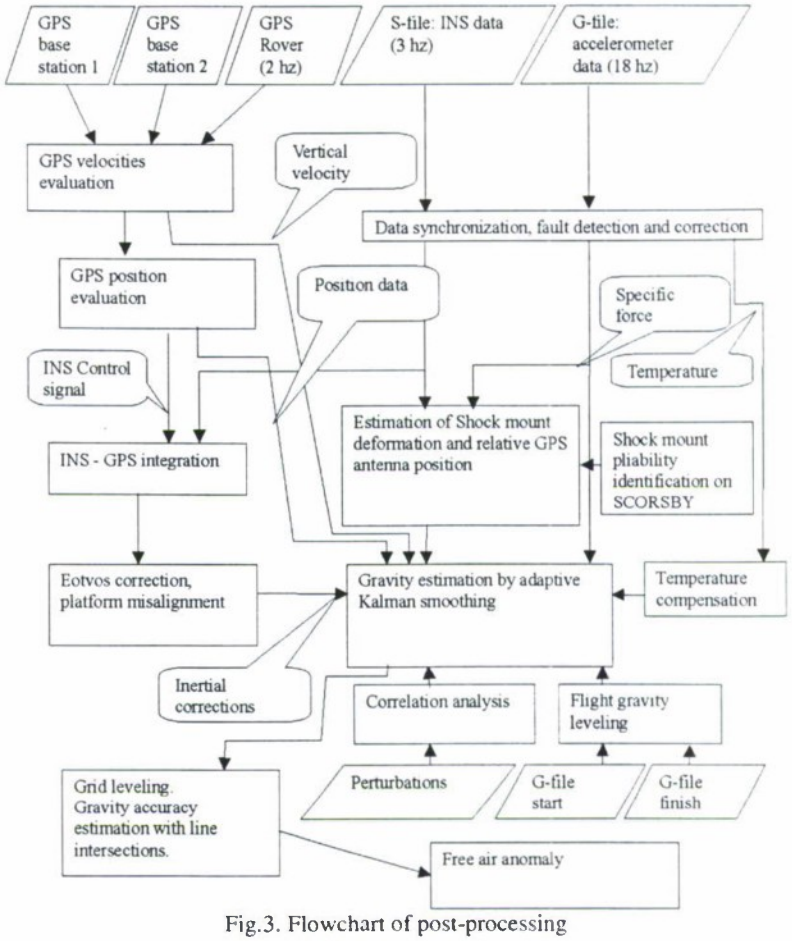

Fig.3. Flowchart of post-processing

Solution of the principal gravimetric equation is performed using non-stationary adaptive Kalman filtering and smoothing [11]. This approach allows more flexibility in reaction to possible data corruption, provides for non-stationary correlations of various kinds and minimizes the influence of boundary effects at the beginning and end of survey lines and during aircraft turns.

4. Results of laboratory tests

The IGS was put through a vast amount of laboratory tests over the past two years: on a stationary bench: on a vibration table; on a rotating Scorsby table; and in motion over the ground. For all the laboratory tests a gravity filter with a bandwidth of 0.017 Hz was used

On the bench the anomaly RMS for the fine channel was 0.2 mGal, while for the coarse channel it was 0.42 mGal. The gravimeter trend was 0.22 mGal per day.

The results of the vibration table tests are presented in Fig. 4.

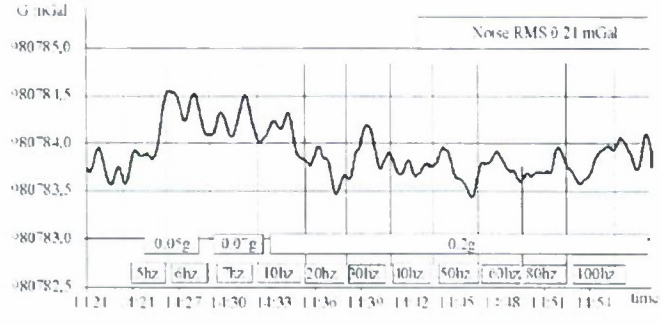

Fig.4. Gravity on vibrating table

These results illustrate the high effieieney of the shoek mount in damping frequeneies above 10 Hz.

Fig. 5 shows the results of system tests with large horizontal aeeelerations.

The results from the Seorsby table are given in Fig. 6 and a photo of the gravimeter mounted on the table is shown in Fig. 7. The IGS was located 1.4 m from the eenter of motion and the parameters of motion were.

a) Yaw: amplitude 6°, period 10 sees
b) Roll: amplitude 6°, period 6 secs
c) Pitch: amplitude 6°, period 8 secs.

The operational integrity of the eomplete IGS system and the validity of data obtained were verified in motion over the ground, where the GPS base and rover reeeivers were used. For this test, the system was installed in a small cart which was pulled over a horizontal asphalted surface outdoors (Fig. 8).

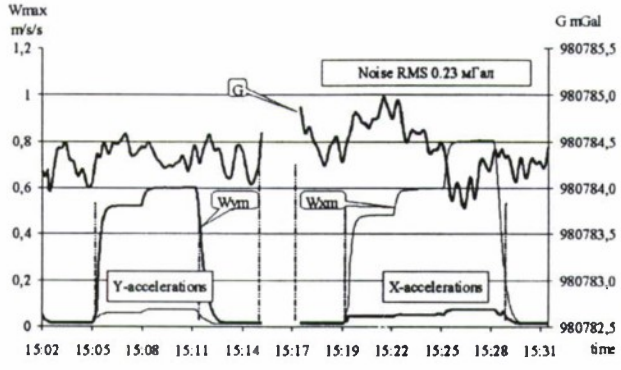

Fig.5. Gravity with horizontal aeeelerations

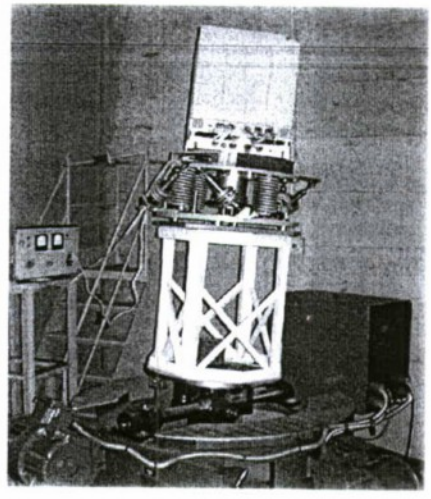

Fig.7

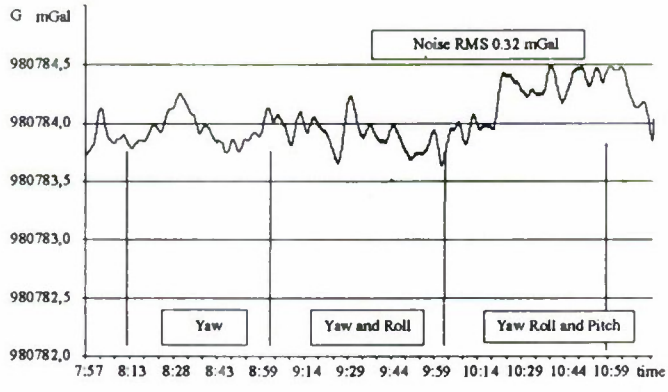

Fig.6. Gravity on SCORSBY table

Fig.8

5. Results of test flights

5.1. *Flight conditions*

In order to test the gravimeter in the air, four flights were made near Vologda on an An-30 aircraft. The aircraft was based at the Cherepovets airfield for the duration of the test flights. Due to internal RAM memory limitations of the GPS base station reeeivers, the length of each record was limited to 2.5 hours per flight. The flight plan is shown in Fig. 9. A short flight was undertaken on 2001.09.04 to test the operational integrity of the entire system and also to test the means of eommunications with the GPS base stations. The three production flights are described below:

1. Wednesday, 5th September, 2001. Flight time: 14:15 to 16:45 GMT. Flight duration: 2 hours 30 minutes. Mean speed on flight lines: 90 m/sec. Mean flight altitude (over WGS84 ellipsoid): 1,000 m. Weather: clear skies.

2. Thursday, 6th September, 2001. Flight time: 02:15 to 05:15. Flight duration: 2 hours 30 minutes. Mean speed on flight lines: 90 m/sec. Mean flight altitude: 1,000 m. Weather: clear skies.
3. Saturday, 8th September, 2001. Flight time: 07:50 to 10:10 GMT. Flight duration: 3 hours 20 minutes. Mean speed on flight lines: 90 m/sec. Mean flight altitude: 1,200 m. Weather: cloudy.

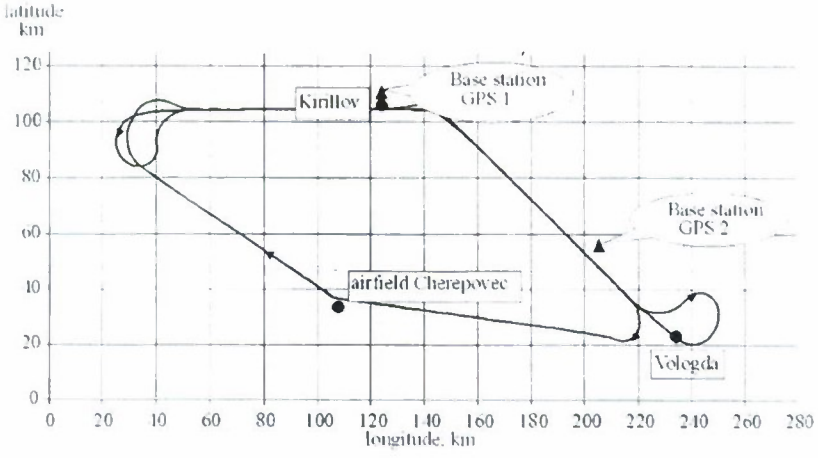

Fig.9. Flight path

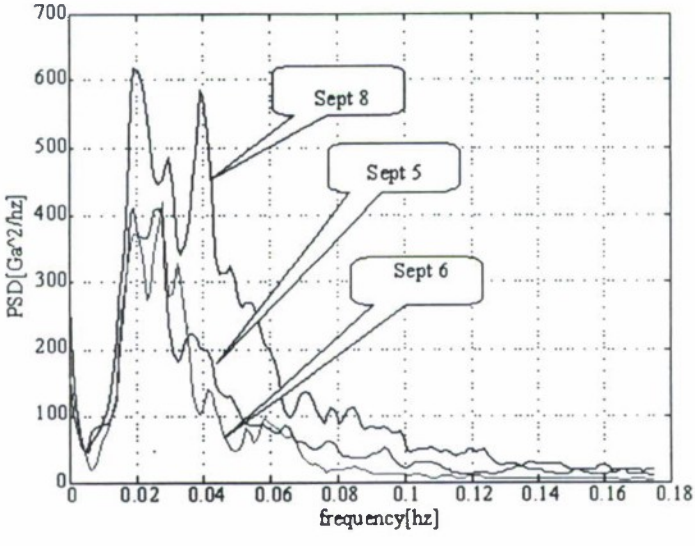

Fig.10. Acceleration PSD

The spectral density of the vertical acceleration on all three production flights is shown in Fig. 10. The vertical acceleration during flights of 2001.09.05 and 2001.09.06 was up to 150 Gals. The vertical acceleration on 2001.09.08 was up to 300 Gals, which required the data from the wide-band channel of the gravimeter. The altitude was maintained to within ±10 m by the aircraft's autopilot linked to a barometric altimeter. During turns, the value of the roll angle was kept to within ±5° due to the ±12° limits for roll angles on the prototype instrument being tested. The commercial GT-1A gravimeters have both roll and pitch limits of ±45°.

The location of the GPS antenna relative to the gravimeter GSU in terms of the aircraft axes was: X = -0.80 m, Y = 1.57 m, and Z = 0.17 m. A photo of the IGS mounted inside the aircraft is shown in Fig. 11.

Ashtech Z-12 GPS receivers were used as the rover and as base station number 2. A Z-Xtreme GPS receiver from Ashtech (Magellan) was used as base station number 1. The measured data was recorded in the built-in RAM memory of the receivers and was transferred after each flight to a PC. The recording rate of all GPS data was 2 Hz.

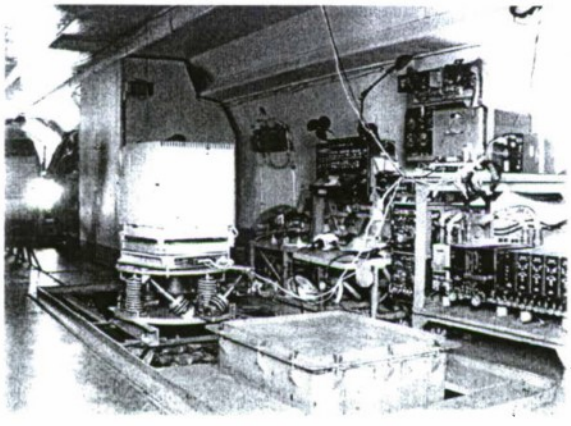

Fig.11

Fig.12

5.2. *Navigation conditions*

Figs. 13 present graphs of navigation data for each of the three production flights. They show: the number of visible satellites (SVs); the geometric factor (PDOP); the error of the differential mode phase solution for base station number 1 in Kirillov (RMS); the length of the baselines for both of the base stations; and estimates of the platform leveling errors (misalignment).

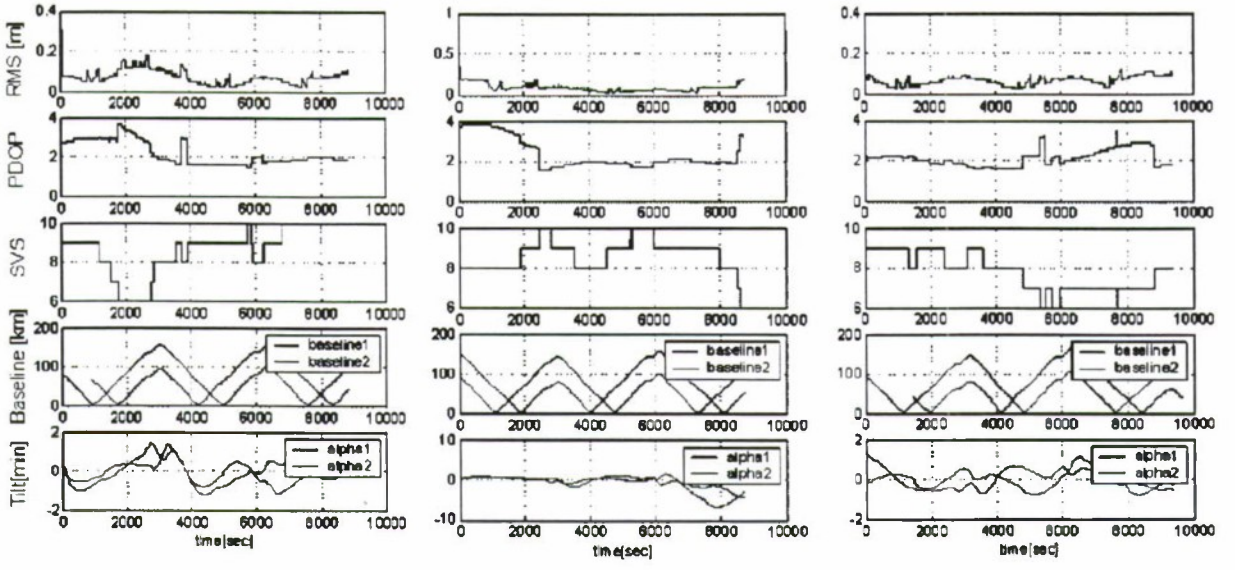

Fig.13

This information presents a view of the satellite navigation conditions during the flights and the accuracy of the vertical orientation of the GSU. The adequate numbers of visible satellites (typically 8 or 9) combined with the acceptable range of the geometric factor (PDOP < 2.5) provided good navigation solutions from differential processing despite baseline lengths exceeding 100 kms at times. The RMS deviations of the phase measurement based positioning were typical for navigation solutions under similar satellite visibility conditions.

Typical values of platform misalignment obtained were approximately ±1′. The accuracy of misalignment estimates carried out off-line was several arc-seconds, acceptable for integrated proccssing of the gravimetric data.

5.3. *Anomaly estimation*

To estimate the gravity anomaly, a filter with a cut-off frequency of 0.01 Hz was used. The resolution of such a filter in space, defined as half wavelength at half amplitude, equals approximately 4.5 kms at an aircraft spced of 90 m/sec. This corresponds to a map of anomalies at a scale of 1:450 000. The gravity anomaly was calculated as the free air anomaly at the survey altitude.

Line	Pass ID	Direction	Line	Pass lD	Direction
1	F010905-010	east	2	F010905-020	south-east
1	F010905-040	west	2	F010905-030	north-west
1	F010905-050	east	2	F010905-060	south-east
1	F010906-010	east	2	F010906-020	south-east
1	F010906-040	west (rejected)	2	F010906-030	north-west
1	F010906-050	east	2	F010906-060	south-east
1	F010908-010	east (rejected)	2	F010908-020	south-east
1	F010908-040	wcst	2	F010908-030	north-west
1	F010908-050	east	2	F010908-060	south-east

The anomaly was evaluated along two repeated lines: Line 1 (direction E-W) and Line 2 (direction NW – SE). There were 9 passes along Line1 and 9 passes along Line 2, described in the table below.

Passes F010906-040 and F010908-010 were rejected because of the low quality of the GPS data. On pass F010906-060 the angular rate sensor (ARS) offset exceeded acceptable limits. As a consequence, the error of platform misalignment increased to 8′. The excess ARS error was readily detected by the IGS control system. Once the platform levelling errors were eliminated, off-line processing gave satisfactory results for this pass.

Line 1	RMS (mGal)	Line 2	RMS (mGal)
F010905-010	0.70	F010905-020	0.36
F010905-040	0.37	F010905-030	0.53
F010905-050	0.66	F010905-060	0.35
F010906-010	0.80	F010906-020	0.50
F010906-050	0.61	F010906-030	0.56
F010908-040	0.75	F010906-060	0.83
F010908-050	0.37	F010908-020	0.31
		F010908-030	0.40
		F010908-060	0.32

The accuracy of the gravity anomaly estimation was determined in the following way. First, the systematic error, which did not exceed 1 mGal, was removed for each pass individually. It should be noted that it is possible to reduce the systematic error by increasing the time of reference measurements before and after each flight up to 1.5 hours. Then the average anomaly for all passes was evaluated along the line and the error of anomaly estimation was evaluated for each pass as the RMS deviation of the anomaly from the average value. The average error is approximately 0.6 mGal (1 σ). The RMS errors for each pass are given in the table.

Figs. 14 and 15 show the gravity anomalies along Lines 1 and 2 for all accepted passes. The mean value of the anomaly is indicated by a heavy dotted line on each graph.

In the authors' opinion, the main contribution to the error of gravity anomaly estimation in these tests was the GPS measurement error. This conclusion was made on the bases of indirect evidence: by comparing the GPS solutions for different base stations, combinations of carriers L1 and L2, and baseline lengths.

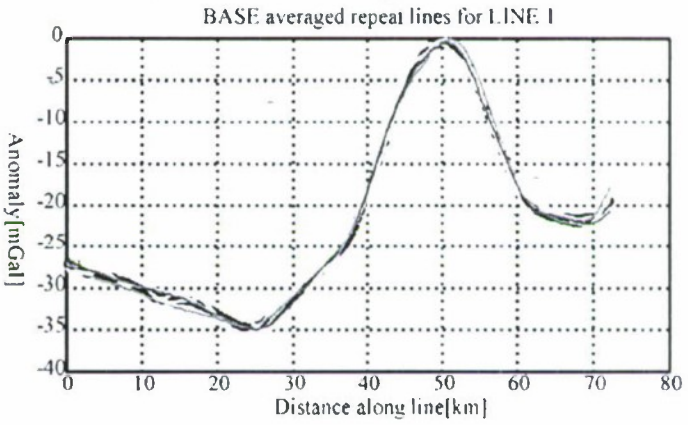

Fig.14

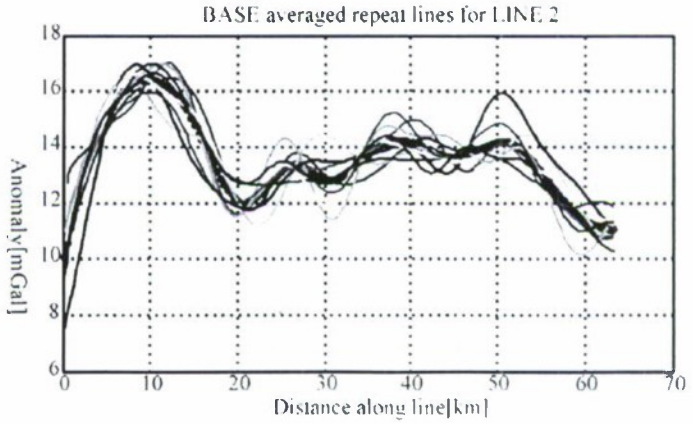

Fig.15

Conclusions

Versatile laboratory and flight tests of the GT-1A airborne inertial gravimetry system have demonstrated its efficiency, ease of installation and use, high performance, low noise levels and high spatial resolution. In the presence of vertical accelerations as high as 150 to 300 Gals, the error of gravity force estimation (1 σ) was 0.6 mGals with a bandwidth of 0.01 Hz and 1.0 mGals with a bandwidth of 0.0125 Hz. We expect that the accuracy of anomaly estimation can be enhanced one and a half to two times by using more precise GPS receivers and by decreasing baseline length by increasing the number of GPS base stations deployed.

Specifications of GT-1A Gravimeter

Range of gravitational acccleration measurement	9.76 to 9.84 m/sec^2
Dynamic range of disturbing acccelerations	
a) fine range	± 0.25 g
b) coarse range	± 0.5 g
Error in gravity anomaly estimation (1 σ) without altitude estimation errors:	
a) For autonomous operation of up to 2 months for marine version	0.3 to 0.5 mGals
b) For autonomous operation of up to 12 hours for ground and airborne versions	0.2 to 0.3 mGals
Error in gravity anomaly estimation (1 σ) including GPS-derived altitude estimation errors:	
a) With 0.01 Hz cut-off	0.5 mGals
b) With 0.0125 Hz cut-off	1.0 mGal
Spatial resolution at vehicle velocity V m/sec	
a) With 0.01 Hz cut-off	0.05 · V km
b) With 0.0125 Hz cut-off	0.04 · V km
Drift per 24 hours	0.2 ± 0.02 mGals
Accuracy of scale factor determination	10^{-4}
Attitude limits for both roll and pitch	± 45°
Operating temperature	-10 °C to +50 °C
Vibration tolerance between 5 and 35 Hz	0.2 g
Power consumption	150 W @ 27 Vdc
Weight including rotation table and shock mount	75 kg
Dimensions excluding rotation table and shock mount	600 × 600 × 750 mm
Service life	30,000 hours

References

1. **Berzhitzky V.N., Bolotin Y.V., Golovan A.A., Ilyin V.N., Parusnikov N.A., Smoller Y.L., Yurist S.S.** GT-1A Inertial Gravimeter System. Results of Flight Tests. Moscoiw State University, 2001.
2. **Berzhitzky V.N., Ilyin V.N., Smoller Y.L., Cherepanov V.A., Yurist S.S.** Triaxial gyro-stabilizer. Patent RF 2157966 dated 2000.01.17.
3. **Berzhitzky V.N., Ilyin V.N., Smoller Y.L., Yurist S.S.** Analogue to digital converter. Patent RF 2168269 dated 1999.12.23.
4. **Bogomolov O.D., Volnyansky V.N., Ermakov M.A., Ilyin V.N., Savelyev E.B., Smoller Y.L., Yurist S.S.** Gravimeter for measuring gravity force from moving carriers. Patent RF 2056642 dated 1993.07.09.
5. **Bolotin Y.V., Vavilova N.B., Golovan A.A., Kruchinin P.A., Parusnikov N.A., Tikhomirov V.V., Trubnikov S.A.** Airborne gravimetry: models, algorithms and software. Technical report. Faculty of Mechanics and Mathematics. Moscow State University, 2000.
6. **Bolotin Y.V., Golovan A.A., Kruchinin P.A., Parusnikov N.A., Tikhomirov V.V., Trubnikov S.A.** The airborne gravimetry problem. Some test results. Bulletin of Moscow State University. Math, Mech. Series. 1999, No.2 pp 36-41.
7. **Vavilova N.B., Golovan A.A., Parusnikov N.A., Trubnikov S.A.** GPS processing: models, algorithms and software. Technical report. Faculty of Mechanics and Mathematics, Moscow Statue University, 2001.
8. **Volnyansky V.N., Ilyin V.N., Nikitin B.P., Smoller Y.L., Yurist S.S.** Gyro-horizon. Patent RF 2062987 dated 1993.07.09.
9. **Volnyansky V.N., Ilyin V.N., Nikitin B.P., Smoller Y.L., Yurist S.S.** Gravimeter for measuring gravity force from moving carriers. Patent RF 2056643 dated 1993.07.09.
10. **Parusnikov N.A., Morosov V.M., Borzov V.I.** Correction problem in inertial navigation. M.: Moscow State University, 1982.
11. **Bolotin Yu.V., Golovan A.A., Parusnikov N.A.** Equations of airborne gravimetry. Algorithms and flight tests. Moscow State University, 2002.

BALLISTIC SUPPORT AND SUPERVISION OF RESEARCH AND TECHNOLOGICAL EXPERIMENTS OF FOTON SC*

G.P. Anshakov *), **Yu.G Antonov.** **), **A.I. Manturov** ***), **Yu.M. Ustalov** ****), **A.E. Kovaltsova** *****),
(State Rocket-Space Center "TsSKB-Progress", Samara, Russia)
Yu.N. Gorelov ******), **S.B. Danilov** *******)
(Samara State University, Samara, Russia)

Abstract

Results of updating methods, facilities and technologies of ballistic and navigation support (BNS), involved in "Foton" SC flight are presented. Methods and means of SC BNS provide for easy use of ballistic and navigation date in the interest of research and technological experiments.

A wide range of research and technological experiments within Russian and international space programs is made on "Foton" SC, success (efficiency) of experiments requiring the reception of various ballistic information. Increase in scientific hardware, installed on "Foton" SC, and complication of experiments and research, involving it, require continuous updating ballistic and navigation support (BNS) of SC flight.

SC ballistic and navigation support is a complex of software methods, algorithms, computing hardware with software and administrative measures, designed for receiving the desired ballistic and navigation information with the required accuracy and within the required time and its delivery to the user.

Diagram of Foton #12 ballistic data exchange is given in fig. 1. Orbit parameters estimation of SC flight is performed in Ballistic Center (BC) of Ground Control Complex (GCC) with the minimum use GCC measuring devices, which provides its economic efficiency. Checking, control and reception of data concerning results of experiments on FluidPac equipment is done with TeleScience equipment from ESRANGE receiving station (RS) in Kiruna, Sweden. Control implies transfer of SC Foton orbit parameters (OP), radio visibility zone (RVZ) and target designation (TD) to ESRANGE RS in order to set ESRANGE aerial system to bear on Foton with the required accuracy and time. Timely delivery of necessary data is done with the Center of General Designer (Center of GD) facilities, based in TsSKB. Information Telemetry Center of GD-Center takes part in operational SC ballistic and navigation support together with nominal Ballistic Center of GCC. Records of ballistic information exchange were developed during Foton #12 pre-launch processing jointly with European Space Agency (ESA); as well were developed procedures of processing and transmission of ballistic data from TsSKB to ESRANGE RS.

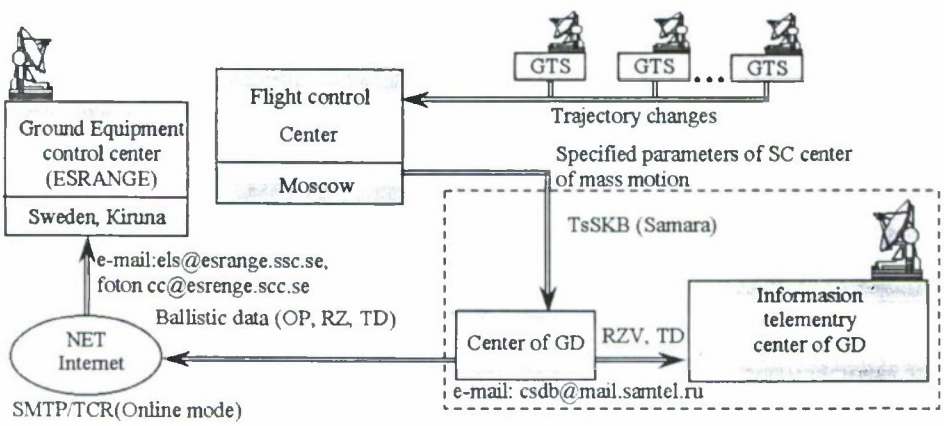

Fig. 1

*) The member-correspondent of Russian Academy of Sciences, First assistant of the general designer of centre;
**) The doctor of technical sciences, assistant of the general designer of centre;
***) The doctor of technical sciences, chief of a department;
****) The assistant of the chief of a department;
*****) The engineer;
******) The doctor of technical sciences, professor, pro-rector of university;
*******) The candidate of technical sciences, senior scientific employee.

The program complex is developed by TsSKB for modeling of "Foton" SC flight scheme and display in a quasi real time scale following navigation and ballistie information:

- eyelogram of pre-launeh operations at the launch site according to the reports;

- cyelogram of Foton SC injeetion to orbit by "Soyuz" launeh vehicle (LV); estimated trajeetory of LV aetive flight leg; LV current estimated coordinates and program pitch angle in the initial-launeh coordinate system;

- "Foton" SC flight seheme; estimated and actual (after SC motion parameters specified according to the trajectory measurement results are reeeived) "Foton" SC flight traek and RVZ of involved Control-Measuring Station (CMS) for the speeified time interval (up to 20 days); three-dimensional picture of the Earth with a "Foton" SC orbits; current "Foton" SC orbit parameters (fig. 2);

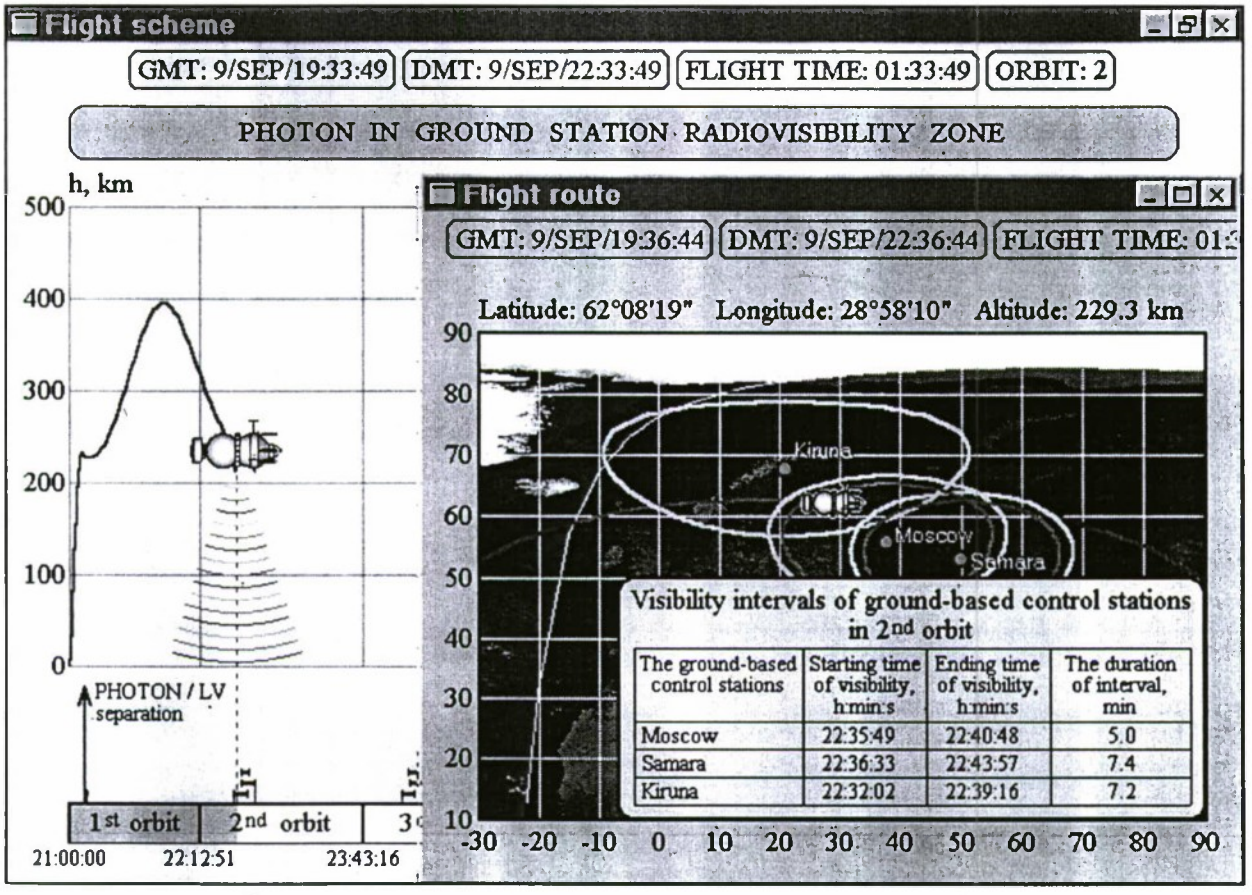

Fig. 2

- parameters of "Foton" SC braking mancuver, Descent Vehicle (DV) estimated deseent trajectory and eurrent eoordinates; the landing area; DV deseent traek, estimated landing point and ellipse of distortion; the scheme of search actions in DV landing site; DV actual landing point (fig. 3).

The first version of this program eomplex was suceessfully tested during flight of Foton SC # 12 in September 1999.

The additional software, allowing to estimate maximal levels of low-frequency on-board microaeeelerations within DV spaee or in its set points (in working zones of technological equipments), is included in structure of program eomplex during Foton-M pre-launeh proeessing. The estimations of on-board mieroaeeelerations are made by means of simulation of orbital and rotatory motions of SC in view of disturbing influence of the following external factors:

- the forees of acrodynamic braking;

- aerodynamic and gravitational torques, resulting to rotation of SC around the center of mass and, as a consequence, to advent of axipetal and rotational accelerations;

- inhomogeneity of the Earth gravitational field within DV space.

The modified version of program complex can be used not only for information supervision of "Foton" flight, but also for a choice of the rational "Foton" flight scheme, favouring to reduction of low-frequency microaccelerations on the board of "Foton" SC, at a stage of a design-ballistic substantiation.

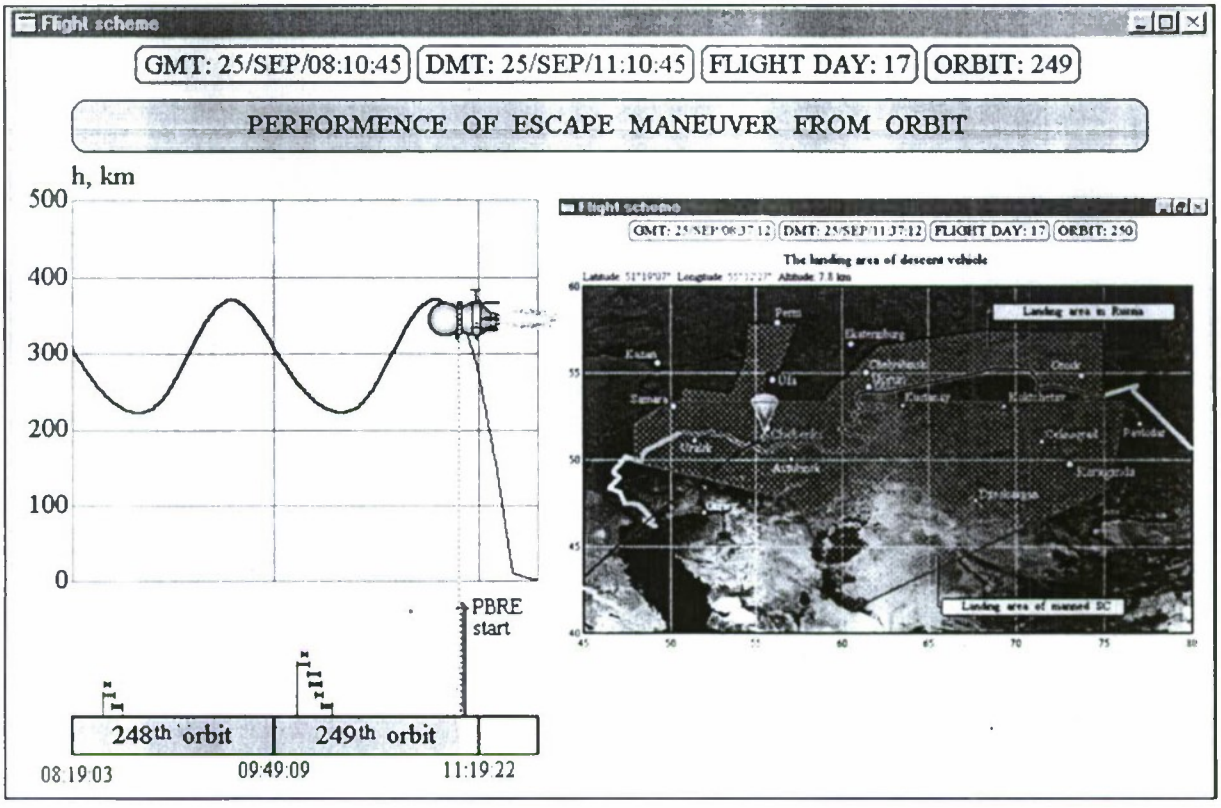

Fig. 3

Thus, BNS methods and devices developed by TsSKB and tested in nominal situations provide comfortable conditions for ballistic-navigation data usage to run scientific and technological experiments.

References

1. **Methods** of Ballistic Support and Supervision of Research and Technological Experiments of Foton SC / Anshakov G.P., Antonov Yu.G., Danilov S.B., Manturov A.I., Sapogina A.E., Ustalov Yu.M. // Proc. of the International Conference "Scientific and Technological Experiments on Russian Foton/Bion Recoverable Satellites: Results, Problems and Outlooks" (Russian Fedaration, Samara, 25-30 June 2000) – p. 301-312.

FAULT-TOLERANT ONBOARD COMPUTER FOR SATELTITE CONTROL LOOP*

Yu. G. Antonov*, Ya. A. Mostovoi*, V. N. Filatov, I. D. Yakushev****
*Russia, 443009, Samara, Pskovskaya st., TsSKB, tel: (846-2)-92-66-40,
fax: (846-2)-92-65-18, E-mail: csdb@mail.samtel.ru
**Russia, 103305, Moscow, Zelenograd, Building 107B, closed corporation NPO-ELAK, tel/fax: (095)-536-73-49,
E- mail: elak@telecom.sins.ru

Abstract

Key words: fault tolerance, fail-safe operation, software and efficiency.

The article deals with principles of Onboard Computer (central unit of Satellite Control Loop) fault tolerance and fail-safe operation from the integrated by criterion basis point of view.

C-5M Onboard Computer designed on the home-produced fully integrated elements is referred to. Its fault tolerance and fail-safe operation is assured with minimal delay from the moment of error occurrence and minimal losses in efficiency as concerns User's tasks.

While performing tasks from all Satellite onboard systems in multiprogramming mode, Onboard Computer and its software determinc ultimately efficiency of the Satellite's ability to solve special purpose tasks and its conceptual framework.

Ability of the Onboard Computer to continuously solve a required number of tasks within predetermined time in spite of probable faults and failures of its constituents is one of its essential properties. That is why, designers of Satellites and Onboard Computers are ready to promote high fault-tolerant performance by trebling and quadruple weighting / power characteristics, degradation of Onboard Computer efficiency and etc.

On-board Computer with stand-by elements does not insure fault-tolerance of the Onboard Computer, because probability of failure-free operation does not characterize to the full the property of fault-tolerance. For example, according to the operability analysis results obtained from the Ground Control System, an Onboard Computer with trebled elements and change over to the stand-by equipment through GCS, shows high probability of failure-free operation. However, it is apparent, that such an Onboard Computer cannot essentially be integrated into the Satellite Control Loop and be applied for Satellite attitude control or Satellite propulsion system control, because in case it is necessary to change the Onboard Computer to the stand-by equipment, the Satellite may be lost.

Thus, fault-tolerance and fail-safe operation of SCL-integrated Onboard Computers is provided when the following conditions are satisfied:

1. availability of stand-by equipment;
2. presence of built-in monitoring and control means with little lagging;
3. storage of non-corrupted "correct" data during fault of Onboard Computer elements.

Detection of errors in the Onboard Computer may be performed on the basis of their consequences detection by Satellite systemic facilities, because they appear in a certain period of time as deviations of control system phase coordinates within an allowable area. In this case, it is necessary to confirm, that the deviations appeared due to Onboard Computer errors.

As a result, an instruction for changing over the Onboard Computer to the stand-by equipment is obtained with a great delay – the system is non-stable, it is impossible to continue operation.

That is why, in various fault-tolerant Onboard Computers detection of errors is based on comparison of several homogeneous results, obtained parallel or in sequence in different stand-by channels by the same initial (basic) data. The comparison may be performed by hardware or software, and depending on it the error detection delay might differ.

Detection of errors may be performed by test self-checks as well. Such self-checks do not provide checking of all Onboard Computer units and thus become unreliable.

When it is necessary to restore correct data in the stand-by or failed units of the Onboard Computer, there may be used "backtrack" method, i.e. return to the preset breakpoint with correct data. Another way out is loading into the Onboard Computer units operating in parallel the deliberately correct data from operable units with skipping of incorrect data.

"Backtrack" is accompanied with single momentary disturbance of phase coordinates of the Satellite control system; the more the greater is the time period.

The described methods of fault-tolerance assurance lead to different delays and disturbances in control, and thereby, to alternatives in continuation of control system's operation after error elimination. Thus, sufficient resources of the Onboard Computer, which might have been used for solution of the user's tasks, are involved in fault-tolerance assurance.

The referred Onboard Computer C-5M, designed by the closed corporation NPO-ELAK has unique fault-tolerance characteristics – error detection and elemination, restoration of correct data is performed with minimal delay: several times during each computer operation.

It is achieved due to three channels operating in parallel, having several layers of software majority elements.

The unique fault-tolerance characteristics of the Onboard Computer assure high fault-tolerance of the entire Satellite, because monitoring of operability and changing over to the stand-by onboard equipment of the Satellite is performed by the Onboard Computer with minimal delay and high reliability.

Systems with software majorization lack convenience in use of popular types of microprocessors in synchronous operation and necessity to design special matrixes and custom-designed LSI.

As a result, Onboard Computer C-5M was designed without standard microprocessors on semi-customdesigned master matrix chips, thus, it does not have high absolute rate of operation.

However, the design with special-purpose LSI maser matrix chips allowed to introduce in Onboard Computer a special purpose menu, which provides maximal efficiency as concerns Satellite controlling.

A merit of no little significance of an Onboard Computer with such a design is that it is completely built on home-produced elements.

Software majorization also enables to reach high fault-tolerance with minimal loss in the processor efficiency as concerns user's mission: as compared to other methods of fault-tolerance assurance it is estimated to be 5-10 – fold.

Thus, the algorithmic efficiency of the Onboard Computer C-5M as concerns user's mission is not that bad, and in a number of cases out-performs efficiency of modern microprocessor-based Onboard Computers.

Onboard software for Onboard Computer C-5M is supported by the modern programming and debugging system, realized in PC-format. The user's tasks may be introduced through the assembler, designed for the C-5M, or in the high-level language as C for which there was designed an Onboard Computer C-5M compiler.

TsSKB designed high performance Onboard Real-time Operating System for the Onboard Computer C-5M.

This compact and high-rate Onboard Real-time Operating System allows to satisfy applications for task's solving on the basis of flexible non-synchronous priority discipline.

The Onboard Computer C-5M has a developed I/O device of modular design, which includes two multiplex command line modules designed in accordance with MIL STD 1553B.

Presence of two channels allows the Onboard Computer not only to control its "own" onboard equipment, but also to allocate a multiplex channel to form PC network.

This implicats ways for further perfection of Onboard Control Systems of promising Satellites.

The fact is that unique fault-tolerance of the Onboard Computer C-5M allows using it as a highly reliable control core, which alongside with solving of its own control tasks, can control stand-by simplier-organized high efficient micro-processor-based Onboard Computers, which solve subproblems of the Satellite Onboard Control System and which are interconnected with the Onboard Computer C-5M in a local net.

Non-net interfacing of fault-tolerant and fail-safe control core of the Onboard Computer C-5M with computational microprocessors as coprocessor in a non- majorization option is also possible.

OFF-LINE PROCESSING TASKS FOR INERTIAL GRAVIMETRY SYSTEM GT-1A*

Yu.V. Bolotin*, A.A. Golovan, N.A. Parusnikov*****
Laboratory of Control and Navigation, Faculty of Mathematics and Mechanics, Lomonosov Moscow State University, Leninskie Gory, 119992, Moscow, Russia, E-mail: navlab@moids.math.msu.su

Abstract

The main off-line processing tasks for inertial gravimetry system GT-1A are described.

Key words: airborne gravimetry, off-line processing.

During 2000 and 2001 the closed stock scientific and technological company ZAO NTP Gravimetric Technologies (GT) developed and FGUP Delphin manufactured the prototype version of a high precision, compact inertial gravimeter system (IGS) GT-1A. In September 2001 the first flight tests of GT-1A system were performed, the An-30 aircraft was used [1]. In presence of the vertical accelerations as high as 150 to 300 Gals, the error of gravity force estimation (RMS) was 0.53 mGal with a bandwidth of 0.01 Hz, and 1.0 mGal with a bandwidth of 0.0125 Hz.

The software for off-line data processing was developed by Lomonosov MSU Laboratory of Control and Navigation. Laboratory has a wide experience in software elaboration for airborne gravity surveys [2]. Cooperation between the MSU Laboratory and GT began in 2000. In 2000 and 2001 the MSU software was substantially modified to allow efficient operation with the GT-1A gravimeter. Here we describe, with brief remarks, the main off-line processing tasks have to be solved in the airborne gravity evaluation. Each of the task described bellow is the subject of independent discussion.

1. Fault detection, identification and compensation in data steams, synchronization errors fixing.
   Methods of analytic redundancy [3], [4], loose IGS-GPS Kalman integration algorithms are used.
2. IGS-GPS integration using Kalman-type smoothing algorithms. Purposes of this task are:
   - Check of the platform misalignment magnitude. By our opinion, the platform misalignment magnitude of 1.5-2 arc.min. during the flight is not critical for airborne surveys. Greater magnitude may cause difficulties in processing and decrease accuracy of gravity force estimation.
   - Estimation of alignment errors with accuracy approximately 5-10 arc.sec. These estimates are used in cross correlation technique in determination of the gravity force along the flight lines.
3. Processing differential GPS raw measurements. Navigation solutions:
   - Position determination using differential carrier phase observations.
   - Independent velocity determination using differential Doppler and carrier phase observations.
   - Independent acceleration determination using differential Doppler and carrier phase observations.
   - IGS-GPS tight integration.

   Peculiarities of these tasks:
   - Doppler solutions are used as initial approximations for corresponding carrier phase solutions.
   - Dual, single (L1 and L2) frequency and ionosphere-free carrier phases solutions are used for mutual cross checking.
   - Simultaneous processing of measurements from several Base stations and/or on-board GPS receivers if latter are used in survey.
4. Determination of the gravity force along the flight line. In this task the previous solutions are used:
   - Estimates of the platform misalignment.
   - GPS independent position, velocity and acceleration navigation solutions.
   - Eötvös corrections, estimation of relative GPS antenna position.
   - Estimation of shock mount deformation.

   Solution of the principal gravimetric equation [5] is performed using non-stationary adaptive Kalman filtering and smoothing. This approach allows more flexibility in reaction to possible data corruption,

*C. Sc,. Leading Research Scientist
**C. Sc,. Senior Research Scientist
*** D. Sc,. Professor

provides for non-stationary correlations of various kinds and minimizes the influence of boundary effects at the beginning and end of survey lines and during aircraft turns.

5. Grid leveling. Gravity accuracy estimation with line intersections.
6. Построение карт аномалий в свободном воздухе. An optimal algorithm is used, based on stochastic models of the gravity anomaly.

Described above off-line processing tasks are typical for any airborne gravimetry system. By our opinion, this systematization is useful for airborne gravimetry systems developing an testing.

References:

1. **V.N. Berzhitzky, Yu.V. Bolotin, A.A. Golovan, V.N. Iljin, N.A. Parusnikov, Yu.L. Smoller, S.Sh. Yurist.** GT-1A inertial gravimeter system. Results of flight tests. MSU Faculty of Mechanics and Mathematics, 2002.
2. **Yu.V. Bolotin, A.A. Golovan, N.A. Parusnikov** An Experienee in Design and Testing of Airborne Gravimetry Systems, in Proceedings of 8th International Conference on Integrated Navigation Systems. Saint Petersburg, Russia, CSRI Elektropribor, 2001.
3. **Мироновекий Л.А.** Функциональное диагностирование динамичееких енетем.Изд-во МГУ-ГРИФ, Москва-Санкт-Петербург, 1998.
4. **Голован А.А., Мироновекий Л.А., Парушников Н.А.** Алгоритмичеекий контроль навигационной информации е использованием аналитической избыточности. Оборонная техника, N 6-7, 1998
5. **Bolotin Yu.V., Golovan A.A., Kruchinin P.A., Parusnikov N.A., Tikhomirov V.V., Trubnikov S.A.** The airborne gravimetry problem. Some test results. Bulletin of Moscow State University. Math, Mech. series, 1999, No 2. pp 36-41.
6. **Н.Б. Вавилова, А.А. Голован, Н.А. Парусников, С.А. Трубников.** Математические модели и алгоритмы обработки измерений спутниковой навигационной системы GPS. Стандартный режим. М., Изательство Центра прикладных исследований при механико-математичееком факультете МГУ, 120 стр., 2001.

USING WIENER MODELS FOR DESCRIBING GYRO DRIFTS AND MEASUREMENT ERRORS IN INS STATE ESTIMATION*

V.A. Tupysev *
State Research Center of Russia - CSRI Elektropribor
St.Petersburg, Russia

Abstract

The comparative analysis of INS error behavior has been carried out for the case that Wiener and Markov models of gyro drifts and measurement errors are used to adjust Kalman filter.

Presented are the conditions for adjusting the filter that allow guaranteed estimation of the INS state under dynamic uncertainty in describing gyro drifts and measurement errors.

It is shown that Kalman filter adjustment to Wiener models is more preferable from the practical point of view, as it provides effective estimation of the INS state both in the cases that real processes have Markov properties and that their behavior is stepwise.

Key words: Kalman filtering, inertial system, guaranteed estimation.

At present methods of Kalman filtering are widely used with the aim to increase INS accuracy as they allow the INS state to be estimated by position and velocity measurements, including readings of a relative log, most effectively. The readings of the latter are treated as measurements of absolute velocity, while the current is treated as the measurement error.

This approach to the use of information from a relative log allows gyro drifts to be continuously subcalibrated simultaneously with INS damping.

The Kalman filtering method considered here is known to be optimal from the standpoint of INS state estimation accuracy if the Kalman filter adjustment complies with the real behavior of INS errors and measurement errors. The real behavior of these errors and measurement process in general form can be described by the following equations:

$$\dot{X} = \begin{vmatrix} \dot{X}_0 \\ \dot{X}_1 \end{vmatrix} = \begin{vmatrix} F_0 & F_2 \\ 0 & F_1 \end{vmatrix} \begin{vmatrix} X_0 \\ X_1 \end{vmatrix} + \begin{vmatrix} \xi_0 \\ \xi_1 \end{vmatrix} = FX + \xi \qquad \xi \in N\{0, Q\} \qquad Q = \begin{vmatrix} Q_0 & 0 \\ 0 & Q_1 \end{vmatrix}, \tag{1}$$

$$Z = HX + V \qquad V \in N\{0, R\},$$

where X_1 is the vector of disturbances and bias measurement errors, which also includes gyro drifts and parameters of the current.

It is generally accepted that gyro drifts can be described adequately by a sum of two components: constant drift described by the equations of the form

$$\dot{X}_i = 0, \tag{2}$$

and the drift described by the first-order Markov process of the form

$$\dot{X}_i = -\alpha_i X_i + \sigma_i \sqrt{2\alpha_i}\,\xi_i \quad . \tag{3}$$

The first-order Markov processes of the form (3) are also widely used to describe parameters of the current.

In view of the fact that in practice exact values of the parameters of these processes are unknown, the filter has to be adjusted under uncertainty of dynamics matrix F_1 that corresponds to the vector of disturbances and bias measurement errors X_1. In this case the real covariance D of the vector X can be determined from equation:

$$\left|\begin{array}{cc} \dot{D} & \dot{D}_2 \\ \dot{D}_2^T & \dot{D}_1 \end{array}\right| = \left|\begin{array}{cc|cc} \tilde{F} & -\Delta F & D & D_2 \\ 0 & F_1 & D_2^T & D_1 \end{array}\right| + \left|\begin{array}{cc|cc} D & D_2 & \tilde{F}^T & 0 \\ D_2^T & D_1 & -\Delta F^T & F_1^T \end{array}\right| + \left|\begin{array}{cc:c} Q_0 & 0 & 0 \\ 0 & Q_1 & Q_1 \\ \hdashline 0 & Q_1 & Q_1 \end{array}\right| + \left|\begin{array}{cc} KRK^T & 0 \\ 0 & 0 \end{array}\right|, \tag{4}$$

where $\Delta F = F_p - F$, F_p - design matrix.

$$\tilde{F} = F_p - KH,$$

K - the Kalman filter gain.

One of the possible approaches to the filter synthesis under these conditions is to use such adjustment of the filter that the matrix P calculated in the covariance channel of the Kalman filter is the upper bound for the real covariance D.

In the case of dynamic uncertainty of matrix F_1 considered here, it can be shown that guaranteed estimation of the state vector is provided when there exists $D_1^* \geq 0$ that obeys the system of equations

*Ph.D., Head of laboratory.

$$\begin{cases} Q_l - \Delta F_l D_l^* = 0 \\ F_l D_l^* + D_l^* F_l^T + Q_l \le 0 \end{cases} \quad (5)$$

where Q_l is the intensity matrix from (1), $\Delta F_l = F_{lp} - F_l$.

It is easy to check that for the case that matrices Q_l, F_l are diagonal, and condition

$$F_{lp} - F_l = \{f_{lp}\} - \{f_l\} \ge 0 \quad (6)$$

is satisfied, such matrix D_l^* does exist.

Assuming gyro drifts and parameters of the current are described by the first-order Markov processes of the form (3), where $\alpha_{min_i} \le \alpha_i \le \alpha_{max_i}$, condition (6) can be written as:

$$\alpha_i - \alpha_{p_i} \ge 0$$

As the exact value of α_i is unknown, it is evident that guaranteed estimates can be obtained when the Kalman filter is adjusted to the model

$$\dot{X}_i = -\alpha_{min_i} X_i + \sigma_i \sqrt{2\alpha_{max_i}}\,\xi_i . \quad (7)$$

Note that in the particular case that $\alpha_{min} = 0$, the process (7) will be described as Wiener

$$\dot{X}_i = \sigma_i \sqrt{2\alpha_{max_i}}\,\xi_i \quad (8)$$

and therefore if the filter is adjusted to the Wiener process (8), the estimation of the state vector X is also guaranteed.

To estimate the efficiency of the Kalman filter under parametric uncertainty conditions, the simulation of the filter adjusted to the Markov (3), (7) and Wiener (8) models of the current one was carried out with the following parameters $\alpha = 1/1\,\text{hour}$, $\alpha = 1/5\,\text{hour}$, $\alpha_p = 1/3\,\text{hour}$, $\alpha_{min} = 1/5\,\text{hour}$, $\alpha_{max} = 1/1\,\text{hour}$.

The simulation results allow the following conclusions:

1. If the filter is adjusted to the Markov model of the current when the real model is also Markov, it is impossible to establish an unambiguous relation between the calculated and the real root-mean-square errors (Figure 1). For example, if with $\alpha < \alpha_p$ for the Eastern component of the current the inequality $\sigma_{VE} < \sigma_{p_{VE}}$ is valid, then for the azimuth gyro drift ε_z the inverse inequality $\sigma_{\varepsilon z} > \sigma_{p_{\varepsilon z}}$ is fulfilled, and therefore it is impossible to provide guaranteed accuracy of all components of the state vector X.

2. Guaranteed accuracy for all the components of the vector X can be ensured when the filter is adjusted to models (7) and (8), which agrees with the results obtained theoretically (Figure 2).

3. Level of the losses in estimation accuracy, when both the calculated and the real models of the current are Markovian, is insignificant from the practical point of view as compared to the optimal adjustment of the filter (Figures 1, 2).

However the behavior of estimate errors changes considerably if one analyzes the efficiency of the filter adjusted to Markov models of disturbances and measurement errors under the condition that the behavior of real processes is of piecewise constant character (e.g. abrupt change in gyro drifts, change in the direction of the current).

The best illustration for the behavior of filter estimation errors in the case that real processes change this way is their behavior in the state vector estimation when the information from the relative log is processed under the condition that the current changes its direction abruptly.

The simulation results show that after the current changed stepwise, there observed a trend in the azimuth gyro drift estimate error, and, as a consequence, considerable increase of the latitude error (Figure 3).

The analysis of the Kalman filter procedures shows that the reason for this behavior of the azimuth gyro drift estimate error is bias in the discrepancy of measurements that comes to the filter input.

To eliminate this shortcoming, it is suggested that the Wiener model for the current be used instead of the Markov model to adjust the filter.

The expected positive effect of such adjustment is related to the fact that on the interval between stepwise changes of the real process this process is described by equation of the form (2).

Mismatch Δf_i between the design and the real dynamics matrices, if the filter is adjusted to the model (8), becomes equal to zero, and therefore the main reason for the losses in estimation accuracy, caused by the mismatch between the dynamics matrices, is eliminated.

The other reason for the losses in estimation accuracy is change of the real covariance of the estimate error at the moment of a stepwise change, however this change is in fact quickly compensated by the increase of the design covariance due to the presence of disturbance noises in the model that describes the Wiener process.

These conclusions are fully confirmed by the simulation results obtained under a stepwise change in the current when the Wiener process (8) is used as a design model of the current for adjusting the filter (Figure 4).

It should be stressed that the estimation procedure in continuous processing of measurements proves to be steady and effective in spite of the fact that dispersion of Wiener processes is an increasing function of time as opposed to real drifts and the current whose dispersion is limited.

It is noted that a similar effect of the filter behavior with the use of Markov processes in adjusting filters also shows itself when real gyro drifts change stepwise, as in this case bias in discrepancy of measurements also takes place.

It is stressed that Wiener models are also preferable from the computational point of view in adjusting the filter, as due to the properties of Wiener processes the description of two components: constant drift and the drift described by the Markov process can be replaced by the description of the total drift using one Wiener process and as a result the dimension of the filter will be made smaller.

The main conclusions of the discussion presented above can be formulated as follows:

1) Wiener models used to describe gyro drifts, bias measurement errors and the current provide effective estimation of the INS state both in the cases that real processes have Markov properties and that their behavior is stepwise, which is an advantage in practical implementation of INS state estimation procedures.

2) Adjustment of the filter to Wiener models provides guaranteed estimation of the whole INS state vector and in this sense the covariance matrix calculated in the filter covariance channel is a measure of accuracy of the state vector estimate.

3) Realization of Kalman filtering procedures with the use of Wiener models proves to be simpler than with the use of Markov models due to the fact that the filter state vector is of smaller dimension.

Figures 1-4 illustrate the root-mean-square errors in generation of the eastern component of the velocity V_E, coordinates φ, λ and the azimuth gyro drift ε_z with the filter adjusted in different ways and various descriptions of the current model. In Figure 1 the real behavior of the current is described by the Markov process with the parameters $\alpha = 1/1\,\text{hour}$, $\alpha = 1/5\,\text{hour}$ with the filter adjusted to the Markov process with $\alpha_p = 1/3\,\text{hour}$.

In Figure 2 the real behavior of the current is described by the same processes but the filter is adjusted to the Wiener process (8) with $\alpha_{max} = 1/1\,\text{hour}$.

In Figure 3 the current changes stepwise with $\sigma = 2$ knots with T = 10 hours when the filter is adjusted to the Markov process with $\alpha_p = 1/3\,\text{hour}$.

In Figure 4 the current changes stepwise with $\sigma = 2$ knots when the filter is adjusted to the Wiener process (8) with $\alpha_{max} = 1/1\,\text{hour}$.

To make the comparison of the results possible, disadjustment is assumed to take place at the instant T = 10 h.

As in practice the exact instant of a stepwise change is unknown, Figure 5 represents the simulation results for the case that the filter is adjusted to the Wiener process at T=0 and the current changes stepwise at T=10 h.

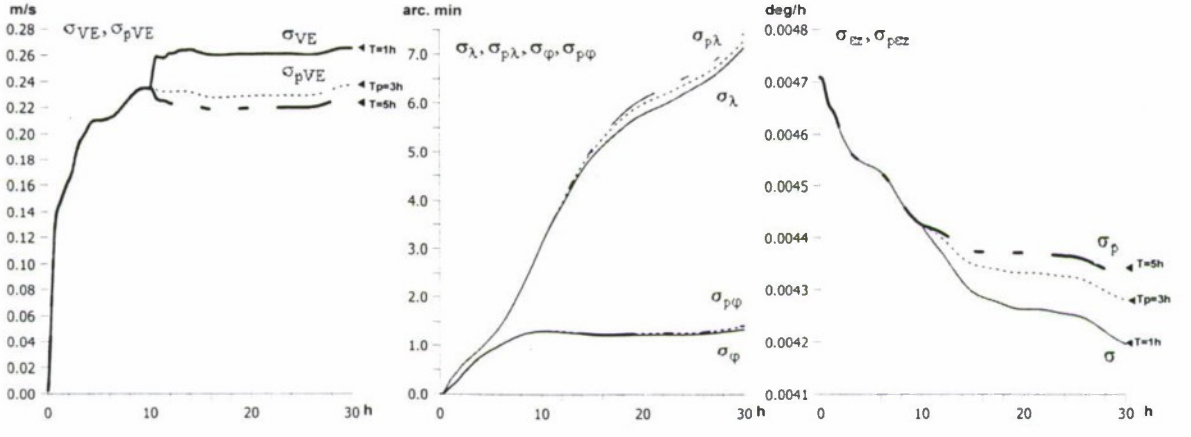

Fig. 1

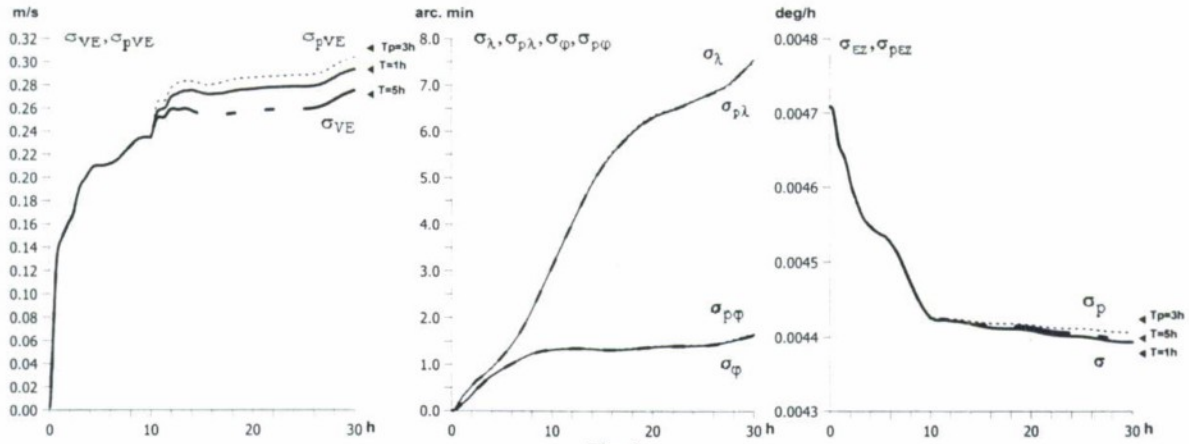

Fig. 2

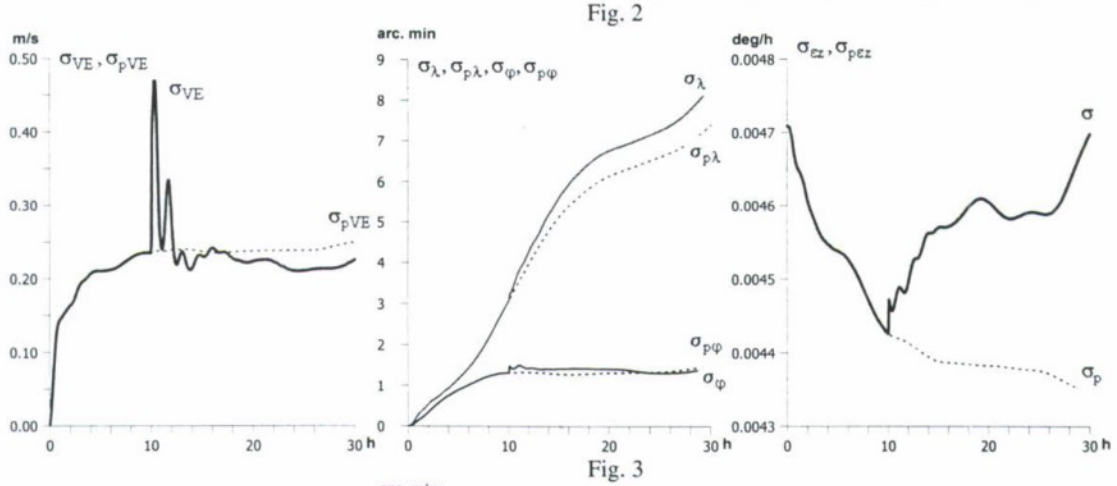

Fig. 3

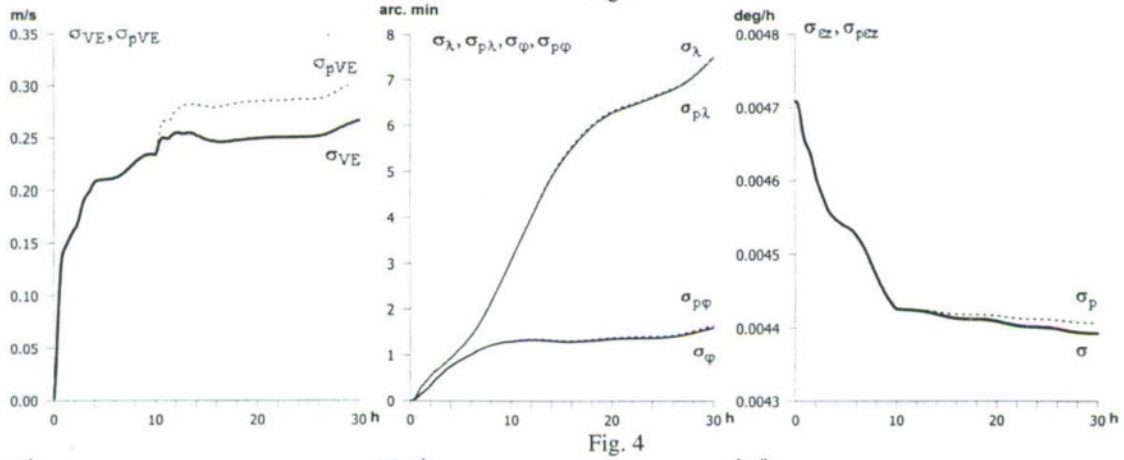

Fig. 4

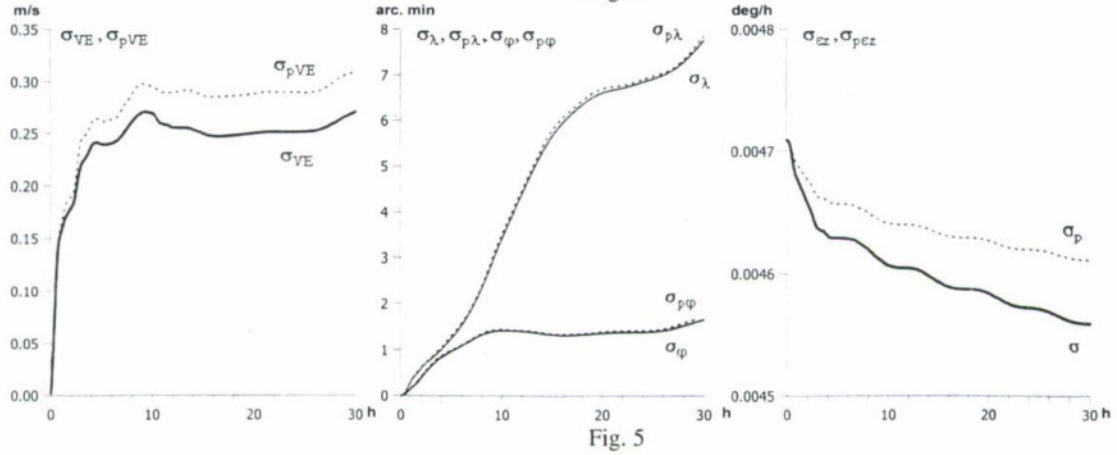

Fig. 5

THE USE OF AN AIRBORNE ELECTRONICALY AGILE RADAR * DURING AUTONOMOUS LANDING OF PLANES

G.V. Antsev*, V.A. Sarychev, V.A. Tupikov***, L.S. Tournetsky******
Joint-Stock Company «Radar mms»
37, Novosclkovskay St., 197349, St.Petersburg, Russia. E-mail:radar@radar-mms.com

Abstract

Key words: landing stage, IFR condition, aircraft, equipment, landing, airborne radar, ICAO, CNS/ATM concept

To guarantee a safe landing under IFR conditions, the should be supplemented with a requirement for aircraft to be equipped radar for control over performance landing

Introduction

Modern aviation landing without usc of ground equipment, i.e. with autonomous airborne systems, will significantly improve flight safety and regularity under conditions of operating semiimproved airfields, which is very important and timely for increasing the efficiency of aviation operation. It is well known that landing is the most complicated stage in the flight process and up to now the systems which ensure landing under Category III conditions of the ICAO metcorological minimum havc not bcen introduced into regular service yet.

On this report the main problems associated with the landing in IFR conditions are discussed, and a possibility of eliminating these problems with the use of airborne 8-mm-land radar is shown.

It is obvious from an analysis of complexities and drawbacks present at the terminal phase of a landing path under the IFR conditions that without their elimination it is impossible to reduce the probability of "missed approaches" and increase regularity of flights.

Thc main advantage of using the radar is the possibility of viewing a runway (its visualization) when this runway is not visually observable, and this per- mits eliminating the time shortage which causes psy-chological overstrain. For instance, in conditions corresponding to Category II of the meteorological minimum the available time may increasc several times from 6-10 s. Viewing the radar image of the runway and special pilotage-navigational marks, thc pilot can evaluate deviations from the landing path. The principal advantage is that on the base of information from the radar the decision hcight may be increased.

All the problems listed, among them the control over thc landing path terminal stage starting from a height of 60 m in IFR conditions to Categories II and III of the ICAO minimum, with the landing onto semiimproved airfields as well as taxiing, take-off run, landing run, detecting obstacles on runway and taxi tracks included, may bc solved using a "Vidimost" ("V-90") – type airborne radar of a 8-mm-wave band with a phased antenna array, which has been developed by our company. This radar exhibits the capabilities of high resolution fast (electronic) scanning of the antenna pattern and is an additional independent information source.

So, to guarantec a safe landing under IFR conditions, the CNS/ATM concept should be supplemented with a requirement for aircraft to be equipped with a "Vidimost" ("V-90") – type radar for control over landing, taxiing, take-off run, landing run, detecting obstacles on runway and taxi tracks. It should bc noted as well that such a radar not only supplements but also naturally fits into this concept, which confirms the timeliness of this radar development. Using the "Vidimost" – type radar is fully consistent with the CNS/ATM concept, as the landing technology implemented through the use of these equipment mates with existing and promising systems for communications, navigation and observation. This radar permits forming a four-dimensional navigation-parameter tunnel for most critical stages of flight and landing. The VID-95 has absorbed a broad range of advanced technologies accumulated and used in military avionics production – the virtually instantaneous beam throw-over by a millimeter-wave-land antenna using electronic scanning, presenting a color image of thc environment to the pilot, specifically on the windshield, efficient methods of data analysis and filtration, reliable monitoring and diagnostics, structural modularity and digital data exchange.

Such radar-tracking station givcs crew additional and independent from ground systems of landing thc channel of the information. Radar- tracking station should carry out mapping runway at call on landing and flight on a landing trajectory in conditions II and III categories meteominimum with maintenance of indication of the image runway in a rcal time scale, is similar to that it would bc possible visually to observe ahead at the rate of an aircraft.

Therefore, in summary it may be noted that the "Vidimost" ("V-90") – type radar makes up for a missing link in the ICAO new concept determining air transport traffic in the 21st century.

---

* D. Sc. Professor, General Director.
** D. Sc. Professor, Deputy of General Director.
*** D. Sc. Professor, Deputy of General Director.
**** D. Sc. Professor, Head of Department.

THE EFFICIENCY OF USING VELOCITY AND COORDINATE SATELLITE MEASUREMENTS IN DETERMINING GRAVITY ABOARD AN AIRCRAFT

O.A. Stepanov*, B.A.Blazhnov, D.A.Koshaev*****
State Research Center of Russia - CSRI Elektropribor, 30, Malaya Posadskaya, St. Petersburg, Russia,
E-mail: elprib@online.ru

Abstract

Key words: aerogravimetry, optimal filtering and smoothing, transfer functions, Butterworth filters, accuracy analysis, phase and Doppler satellite measurements

The paper considers the problem of gravity disturbance estimation solved by using the data from a gravimeter and phase and Doppler measurements from the satellite navigation system in the differential mode. The optimal solution of this problem is compared to the most commonly used solution in which the differences between the data from the gravimeter and derivatives from satellite measurements are processed with Butterworth filters in direct and in reverse time. The accuracy of gravity disturbance estimation is analysed for various gravity models and various (phase or Doppler) measurements. The effect of ambiguity of phase measurements on the accuracy of gravity disturbance estimation is investigated. Besides the analytical calculations, the paper presents and discusses the results obtained in the processing of the real air gravity survey data.

Introduction

When measuring gravity disturbance aboard a moving vehicle, the problem of compensation for vertical acceleration caused by aircraft dynamics is very importance. At present the accuracy of the state-of-the-art marine gravity survey is usually no less than 1 mGal [1-4]. This accuracy level is achieved without any external information about vertical motion of the vehicle. Until recently such accuracy was unattainable for aircrafts whose dynamics is much higher than for marine vehicles. The situation has changed drastically because of the new possibility to use high-accuracy information about vertical motion of the vehicle obtained from satellite navigation systems (GPS or GLONASS). The analysis for the state-of-the-art airgravimetry allows us to point out the following of its basic features [1-4, 9].

- Aerogravimetry often uses special modified marine gravimeters and gyrostabilized platforms.
- Compensation for vertical accelerations is only effective when phase and Doppler measurements are used in the differential mode - Differential GPS (DGPS).
- The achieved accuracy of gravity disturbance measurements is about 1-2 mGal with a spatial resolution of about 3-5 km. The main factors restricting the measurement accuracy are errors of the gravimeter itself and the platform used to level it.
- In the future the accuracy of measurements is expected to be raised to the level of 1 mGal with a spatial resolution of about 1-2 km. The accuracy of this level can be achieved owing to increase of gravimeter accuracy and improvement of processing algorithms, as well as due to gradiometers that are still being developed [12].

The paper investigates the algorithms for gravity disturbance estimation with the use of velocity and coordinate (altitude) satellite measurements.

In aerogravimetry gravity disturbance is commonly determined by using the so-called invariant (with respect to the vertical motion of the vehicle) algorithm. In so doing, the difference measurements are used. These measurements don't include true values of altitude, vertical velocity and acceleration. Usually the processing is carried out with stationary low-frequency Butterworth filters whose parameters (order and cutoff frequency) are selected empirically in order to make gravity disturbance estimation most effective [1-3]. At the same time the problem of gravity disturbance estimation can be formulated in the framework of the optimal approach.

The paper compares the procedures of processing using the Butterworth filters with the optimal solution.

The potential (achievable within the optimal solution) accuracy of gravity disturbance estimation is analyzed depending on the gravity properties and type of DGPS measurements. The paper also analyzes the effect of ambiguity of DGPS phase measurements conditioned by the uncertainty of integer number of periods on the accuracy of gravity disturbance estimation. This problem may seem insignificant, as the unknown integer number of periods is constant, while our interest in this problem is estimation of the second derivative of altitude. Nevertheless the solution of this problem is very important, as will be shown below. Besides the

---

* Leading researcher, D.Sc.
** Leading researcher, Ph.D.
*** Researcher, Ph.D.

analytical calculations, the paper presents and discusses the results obtained in the processing of the real air gravity survey data.

Statement of the problem

The measurements of the altitude and vertical velocity of the vehicle obtained from the DGPS and the data from the gravimeter can be represented as:

$$h^{\mathrm{DGPS}} = h + \delta h, \tag{1}$$

$$V_z^{\mathrm{DGPS}} = V_z + \delta V_z, \tag{2}$$

$$\tilde{g}^{\mathrm{gr}} = \dot{V}_z + \tilde{g} + \delta g, \tag{3}$$

where $h, V_Z, \dot{V}_Z$ - the altitude, vertical velocity and acceleration; $\delta h, \delta V_Z$ - the errors of measurements from DGPS; $\tilde{g}$ - gravity disturbance; δg - gravimeter errors.

In order to exclude unknown values $h, V_z, \dot{V}_z$, let us form the difference between the second integral of the gravimeter readings and the altitude from the DGPS, and the difference between the first integral of the gravimeter readings and the vertical velocity from the DGPS. Taking into consideration (1)-(3), these differences can be presented as follows:

$$z_h = \frac{\tilde{g}^{\mathrm{gr}}}{p^2} - h^{\mathrm{DGPS}} = \frac{\tilde{g} + \delta g}{p^2} - \delta h; \tag{4}$$

$$z_{V_z} = \frac{\tilde{g}^{\mathrm{gr}}}{p} - V_z^{\mathrm{DGPS}} = \frac{\tilde{g} + \delta g}{p^2} - \delta V_z. \tag{5}$$

in operator form.

The estimation problem consists in obtaining gravity disturbance using difference measurements (4)-(5). This problem can be considered both as a filtering problem, when only the measurements accumulated before the given point are used, and as a smoothing problem, when all the measurements obtained before and after the given point are used.

Specifying stochastic models for $\tilde{g}$, $\delta h, \delta V_Z$ and δg, one can solve this problem using the theory of optimal filtering or smoothing [10].

Often the difference between the gravimeter reading and the 2nd derivative of the altitude from the DGPS, and the difference between the gravimeter reading and the 1st derivative of the vertical velocity from the DGPS are used instead of (4), (5), i.e.

$$\tilde{z}_h = \tilde{g}^{\mathrm{gr}} - p^2 h^{\mathrm{DGPS}} = \tilde{g} + \delta g - p^2 \delta h; \tag{6}$$

$$\tilde{z}_{V_z} = \tilde{g}^{\mathrm{gr}} - p V_z^{\mathrm{DGPS}} = \tilde{g} + \delta g - p \delta V_z. \tag{7}$$

In practice the algorithms in which difference measurements (4), (5) or (6), (7) are processed with the use of low-frequency Butterworth filters: the forward filter - for the filtering problem and the forward and backward filters - for the smoothing problem, are widely used to estimate gravity disturbance.

Let us analyze the relationship between these algorithms and those based on the use of optimal stationary filters for the measurements (4), (5).

It should be noted that formally the following relations are valid between the differences (6), (7) and (4), (5):

$$p^2 z_h = \tilde{z}_h, \quad p z_{V_z} = \tilde{z}_{V_z}.$$

However due to rather low frequency of the data from the DGPS in (6), (7), there appears an additional error in numerical differentiation of altitude and vertical speed. As for the measurements (4), (5), owing to high frequency of gravimeter data output, integration errors are negligible.

The analysis of DGPS measurement errors

Statistic properties of DGPS measurement errors are very important in the study of the estimation problem under consideration. In order to determine these properties the phase and Doppler measurements, that had been obtained using dual-frequency geodetic *Novatel* receivers, were processed. This data was documented during flights aboard a small aircraft that was moving away from the reference receiver to the distance of up to 100 km. The measurements were received with a frequency of 1Hz. As the aircraft had no reference navigation system, the analysis of the error properties was based on linear combinations of measurements from which real signals (pseudoranges and pseudoradial velocities) were excluded. It was shown that errors in Doppler measurements are mainly of white-noise character with intensity $(0.01\mathrm{m/s})^2$ s. The errors in phase measurements also contain a

noise component whose intensity is evaluated to be at a level of $(0.005\text{m})^2$ s. Besides, they contain a slowly-varying component whose level and character depend on the relative position of the aircraft and the reference receiver. It was noted that for the L2 frequency the level of phase measurement error noise components is much higher than that for the L1 frequency. Thus the usage of phase measurements at the L2 frequency is only effective for ionospheric error compensation.

The comparison of optimal algorithms with the algorithms based on the usage of Butterworth filters

Let us compare the algorithms based on the usage of Butterworth filters that process the difference measurements (4), (5) or (6), (7) with the algorithms based on the usage of optimal stationary filters that process the differences (4), (5). In developing optimal algorithms the gravity disturbance model is assumed to be either the first ($\dot{\tilde{g}} = w$ - random walk) or the double $\ddot{\tilde{g}} = w$ integral of the white noise w. The application of such models will be substantiated a bit later.

The gravimeter errors are assumed to be null while the DGPS measurement errors, as is stated in the investigation, - white noise with the intensities as indicated above.

Using the differential equations for optimal filtering and smoothing estimates and the equations for the steady-state covariance matrices of the estimate errors [10], it can be shown that, under the assumptions made, the expressions given in Table 1 are valid for the transfer functions of optimal stationary algorithms.

Table 1. Expressions for transfer functions of gravity disturbance estimation algorithms

Problem	Data from DGPS	Gravity model	
		Random walk	Second integral of white noise
Filtering	V_z	$w_{B_2}(p)p$	$w_{B_3}(p)p(2p/\rho+1)$
	h	$w_{B_3}(p)p^2$	$w_{B_4}(p)p^2(\alpha p/\rho+1)$
Smoothing	V_z	$w_{B_2}(p)w_{B_2}(-p)p$	$w_{B_3}(p)w_{B_3}(-p)p$
	h	$w_{B_3}(p)w_{B_3}(-p)p^2$	$w_{B_4}(p)w_{B_4}(-p)p^2$

Here $w_{B_2}(p)=\dfrac{\rho^2}{p^2+\sqrt{2}p\rho+\rho^2}$, $w_{B_3}(p)=\dfrac{\rho^3}{p^3+2p^2\rho+2p\rho^2+\rho^3}$,

$w_{B_4}(p)=\dfrac{\rho^4}{p^4+\alpha p^3\rho+\dfrac{\alpha^2}{2}p^2\rho^2+\alpha p\rho^3+\rho^4}$ - transfer functions of the Butterworth 2nd, 3rd and 4th-order filters [7, 8]; $\alpha=\sqrt{2(2+\sqrt{2})}$; ρ - the cutoff frequency determined from the intensity $q_{\tilde{g}}$ or $q_{\ddot{\tilde{g}}}$ of the forcing noise w in the gravity model, and the intensity R_{V_z} or R_h of the noise in the measurements of the vertical velocity and altitude determined by using the expressions given in Table 2.

Table 2. Expressions for the cutoff frequency ρ of the Butterworth filter

Data from DGPS	Gravity model	
	Random walk	Second integral of white noise
V_z	$\left(q_{\tilde{g}}/R_{V_z}\right)^{1/4}$	$\left(q_{\ddot{\tilde{g}}}/R_{V_z}\right)^{1/6}$
h	$\left(q_{\tilde{g}}/R_h\right)^{1/6}$	$\left(q_{\ddot{\tilde{g}}}/R_h\right)^{1/8}$

Note that $w(-p)$ can be considered as a transfer function corresponding to the filtering procedure with the transfer function $w(p)$ in reverse time. This statement is based on the fact that derivatives in direct and reverse time are equal for the even order, but for the odd order they are equal in the absolute value and opposite in sign.

From the presented transfer functions it is clear that for the measurements (4), (5) the optimal stationary filtering and smoothing algorithms for the gravity models under consideration are reduced to differentiation of these measurements and usage of the Butterworth filters. The order and cutoff frequency of the filter are

determined depending on the accepted model of gravity disturbance, type of measurement under processing and intensity of measurement noise.

In the case that the measurements (6), (7) are used, the optimal filtering algorithm is reduced to the Butterworth filter for the random walk gravity model. At the same time for the gravity model described as the second integral of white noise the Butterworth filter does not provide any optimal solution for the filtering problem. To obtain this solution, it is necessary to use the derivative of these measurements.

However the optimal smoothing algorithms for both of the gravity models under consideration can be realized by processing the difference measurements (6), (7) in the forward and backward Butterworth filters.

The conclusions formulated here are valid for the models in the form of the first and second integrals of the white noise. Making use of the approximate procedure for developing optimal algorithms suggested in [7], it is, however, possible to show that these conclusions will hold true for more complicated models as well. According to this procedure the transfer function of the optimal algorithm is mainly determined by the crosspoint of spectral densities of the signal estimated and measurement errors and the inclination of these densities. Thus the gravity models considered here in the form of the first and second integrals of the white noise can be treated as an approximation of more complicated models for which the spectral densities $S_{\tilde{g}}(\omega)$ have an inclination of -40 or -80 dB per decade at the crosspoint with the lines $\omega^2 R_{V_z}$, $\omega^4 R_h$.

For example, the gravity model considered in [5, 6] can be approximated by the second integral of white noise. One of them is the so-called Jordan model [5]. The spectral density of this model along the straight section is as follows [5]:

$$S_{\tilde{g}}(\omega) = 2\alpha^3 \cdot \sigma_{\tilde{g}}^2 \cdot \frac{5 \cdot \omega^2 + \alpha^2}{(\omega^2 + \alpha^2)^3}. \tag{8}$$

Another model is considered in [6], its spectral density described as

$$S_{\tilde{g}}(\omega) = 4\alpha^3 \cdot \sigma_{\tilde{g}}^2 \cdot \frac{1}{(\omega^2 + \alpha^2)^2}. \tag{9}$$

Here $\sigma_{\tilde{g}}^2$ – the variance; $\alpha = V/\mu$; V – the the vehicle speed; μ - the correlation distance.

The analysis of the formula for the spectral density shows that with $\omega >> \alpha$ it can be approximated by the following expression:

$$S_{\tilde{g}}(\omega) \approx q_{\tilde{g}} / \omega^4, \tag{10}$$

corresponding to the description of gravity disturbance as the second integral of the white noise with the intensity which is the same as the intensity of the forcing noise for the corresponding model, i.e. $q_{\tilde{g}} = 10\alpha^3 \cdot \sigma_{\tilde{g}}^2$ or $q_{\tilde{g}} = 4\alpha^3 \cdot \sigma_{\tilde{g}}^2$.

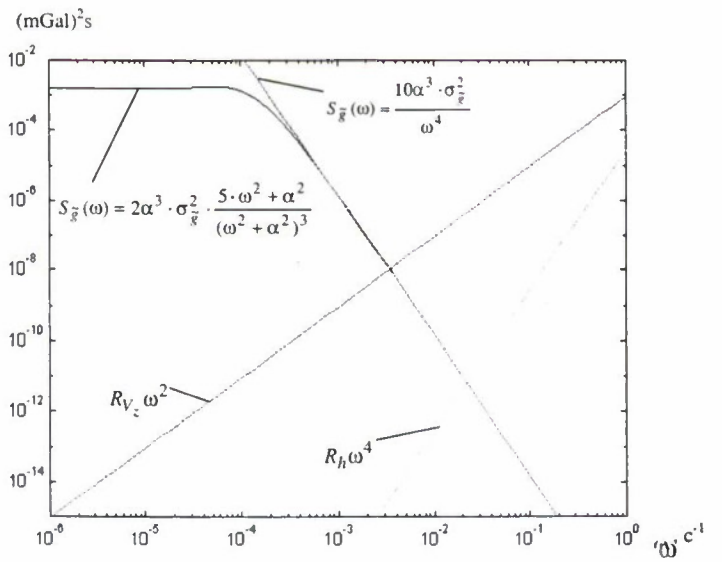

Fig. 1. The spectral density of the signal and measurement errors in the problem of gravity disturbance estimation

Fig. 1 shows the plots of spectral densities in the logarithmic scale, corresponding to the Jordan model and its approximation (10) for $\sigma_{\partial\tilde{g}/\partial l}$=1mGal/km, V=50m/s, as well as the spectral densities of the differentiated errors

in the vertical velocity $\omega^2 R_{V_z}$ and altitude measurements $\omega^4 R_h$ with R_{V_z} =(0.01m/s)^{2}s, R_h=(0.005m)^{2}s. It is clear to see that the Jordan model can be approximated with the acceptable accuracy by model (10) in the crosspoint area.

Thus, the conclusions regarding the model in the form of the second integral of the white noise can be extended with sufficient accuracy to the models that correspond to the spectral densities (8), (9).

Analysing potential accuracy of gravity disturbance estimation by using velocity and coordinate satellite measurements

The analysis of the potential accuracy of gravity disturbance estimation is carried out with the use of the expressions obtained from the solution of the matrix equations for steady-state covariance matrices for optimal filtering and smoothing errors (see Table 3).

Table 3. Expressions for gravity estimation error variances

Problem	Data from DGPS	Gravity model	
		Random walk	Second integral of white noise
Filtering	V_z	$1.41R_{V_z}^{1/4}q_{\tilde{g}}^{3/4}$	$3R_{V_z}^{1/2}q_{\ddot{g}}^{1/2}$
	h	$2R_h^{1/6}q_{\tilde{g}}^{5/6}$	$6.31R_h^{3/8}q_{\ddot{g}}^{5/8}$
Smoothing	V_z	$0.35R_{V_z}^{1/4}q_{\tilde{g}}^{3/4}$	$0.17R_{V_z}^{1/2}q_{\ddot{g}}^{1/2}$
	h	$0.33R_h^{1/6}q_{\tilde{g}}^{5/6}$	$0.14R_h\rho^5$

From these expressions it is clear that the accuracy of gravity estimation in the solution of the smoothing problem is 2–8 times higher than the accuracy achieved in the solution of the filtering problem depending on the type of the measurement and gravity model used. Note that this relationship is valid for any values of measurement and forcing noise intensities.

The expressions given above make it possible to obtain quantitative assessments of gravity estimation accuracy. The intensities of the forcing noises $q_{\tilde{g}}$, $q_{\ddot{g}}$ will be presented as $q_{\tilde{g}}=(\nabla g)^2 V/l$, $q_{\ddot{g}}=\nabla\tilde{g}^2 3V^3/l$, where V - the speed of the vehicle, ∇g - the RMS value of gravity increment at a distance of l, which is assumed equal to 1 km. Further, for simplicity, ∇g will be called a gravity gradient. Let the gradient ∇g values be 1, 3, 5, and 10 mGal/km and the speed V =50m/s, which is typical for an aerogravimetric survey. The RMS errors in gravity estimation for these conditions are given in Table 4.

Table 4. RMS errors for filtering and smoothing, mGal for V=50 m/s

Problem	Data from DGPS	Gravity model							
		Random walk				Second integral of white noise			
		∇g, mGal/km							
		1	3	5	10	1	3	5	10
Filtering	V_z	2.0	4.8	7.1	12.2	3.4	7.7	11.2	18.8
	h	1.1	2.4	3.6	6.1	0.8	1.8	2.7	4.5
Smoothing	V_z	1.1	2.9	4.4	7.8	0.8	2.2	3.5	6.7
	h	0.5	1.2	1.8	3.2	0.1	0.3	0.5	1.0

From the data in the Tables it may be conclude that

- The gravity estimation accuracy is much (2-8 times) lower in the case that the velocity measurement rather than the altitude measurement is used.
- It is only with the use of the altitude measurement the gravity estimation accuracy can be ensured at the level of 1 mGal.
- For the two models considered in the paper the accuracies of gravity disturbance estimation with the use of the altitude measurement in the solution of the smoothing problem are essentially different (by a factor of 3-

5). However when the filtering problem is solved with the use of velocity or altitude and the smoothing problem – with velocity, the accuracies differ no more than by a factor of 1.5.

Note that the steady-state variances for gravity disturbances were also calculated by solving the recurrent Riccati equation for the covariance matrix of the estimation error in the case that the gravimeter error δg is the white noise with the intensity $(5\text{mGal})^2\text{s}$. The differences between these results and those of the analytic calculations from Table 4 (where δg is assumed to be null) turned out to be negligible.

It was also established that the results obtained from the analysis of the potential accuracy for the Jordan model are close to the results that correspond to the gravity disturbance model as the second integral of the white noise with values a and $\sigma_{\tilde{g}}^2$ selected as $q_{\tilde{g}} = 10\alpha^3\sigma_{\tilde{g}}^2$. All this justifies the replacement of the Jordan model by a simpler description in the form of the second integral of the white noise in the development of the optimal algorithm or the accuracy analysis.

The effect of phase ambiguity on gravity disturbance accuracy

It is known that the processing of phase measurements generates the problem of integer ambiguity. This problem proves to be most urgent in filtering, as only measurements obtained before the given can be used.

Let us analyze a filtering error caused by phase measurement ambiguity. In so doing, assume that the measurements are processed by the optimal filter corresponding to the steady-state mode when the model of the gravity is the second integral of the white noise.

Assume that at a $t_{\nabla\Delta N}$ the integer number of periods $\nabla\Delta N$ is lost for one of phase measurements that is used to determine the altitude by the least-squares method. In this case the difference between the altitude measurement and the second integral of the gravimeter readings can be written as:

$$z_h = \Delta h + \delta h + K_h \lambda \nabla\Delta N \, 1(t - t_{\nabla\Delta N}), \tag{11}$$

where Δh - second integral of $\tilde{g} + \delta g$, λ - the wavelength of the DGPS signal; K_h - the corresponding element of the matrix gain used in the least-squares method, $1(\cdot)$ - a step function.

Taking account of the transfer functions of the optimal steady-state filter (see Table 1) and Eq. (11), it is possible to represent the component $\delta\tilde{g}_{\nabla\Delta N}$ caused by the $\nabla\Delta N$ as:

$$\delta\tilde{g}_{\nabla\Delta N}(p) = w_{\text{Б}_4}(p)\left(\alpha p/\rho + 1\right)p^2 K_h(p)\lambda\nabla\Delta N \exp(-pt_{\nabla\Delta N}). \tag{12}$$

First, estimate the level of $\delta\tilde{g}_{\nabla\Delta N}$ in the steady-state mode with the allowance made for changeability of K_h. Fig.2 shows a typical plot for the second derivative of the element $\lambda\ddot{K}_h$. Note the dominance of the oscillating component with amplitude of about 0.01mGal and frequency $\omega_{K_h} \approx 10^{-3}$ Hz (period of about 80 min). This component is caused by satellite motion relative to the Earth, and its frequency is much less than the Butterworth filter cutoff frequency. The peaks in $\lambda\ddot{K}_h$ are caused by the aircraft manoeuvring, when the survey is not realized. Therefore for the steady-state mode the following approximate equation is true for $\delta\tilde{g}_{\nabla\Delta N}$:

$$\delta\tilde{g}_{\nabla\Delta N}(t) \approx \lambda\nabla\Delta N \, \ddot{K}_h \, 1(t - t_{\nabla\Delta N}). \tag{13}$$

Taking into consideration the $\lambda\ddot{K}_h$ level (0.01mGal) and the possibility to determine $\nabla\Delta N$ by code measurements to the accuracy of a few unities of periods, it may be stated that for the steady-state mode the $\delta\tilde{g}_{\nabla\Delta N}$ error does not exceed 0.1mGal.

Let us analyze $\delta\tilde{g}_{\nabla\Delta N}$ at the transient mode, i.e. directly after $\nabla\Delta N$ appears in z_h. The transient time is determined by the time constant of the filter $T = 2\pi/\rho$. For this time the K_h may be considered a constant, i.e. $K_h(p) = K_h / p$. So, using the Laplace inversion [11], from (5), (6) it is possible to derive:

$$\delta\tilde{g}_{\nabla\Delta N}(t) = K_h\lambda\nabla\Delta N\rho^2\left\{\alpha b\exp\left(-a\rho(t - t_{\nabla\Delta N})\right)\cos\left(b\rho(t - t_{\nabla\Delta N})\right) + \exp\left(-b\rho(t - t_{\nabla\Delta N})\right)\times\right.$$
$$\left.\times\left[\frac{\alpha^2}{2}\sin\left(a\rho(t - t_{\nabla\Delta N})\right) - \alpha b\cos\left(a\rho(t - t_{\nabla\Delta N})\right)\right]\right\}, \tag{14}$$

where $a = \frac{1}{4}\left(\alpha - \sqrt{8 - \alpha^2}\right) \approx 0{,}38$, $b = \frac{1}{4}\left(\alpha + \sqrt{8 - \alpha^2}\right) \approx 0{,}92$.

Fig. 3 presents the plots of $\delta\tilde{g}_{\nabla\Delta N}$ against $K_h\nabla\Delta N$ as a function of the length of the path $L_{\nabla\Delta N} = V(t - t_{\nabla\Delta N})$ after the ambiguity had appeared. The values of the gradient ∇g are assumed to be the same as above. From these plots it is evident that $\delta\tilde{g}_{\nabla\Delta N}$ reaches inadmissible values of (70-230)mGal even

with ambiguity of one period ($\nabla\Delta N = 1$). It should be noted that, the higher is the gradient ∇g, the higher is the maximum value of the $\delta\tilde{g}_{\nabla\Delta N}$ but the faster it attenuates (see the lower plots in Fig. 3). This is due to the fact that the filter cutoff frequency ρ that defines the transient process for $\delta\tilde{g}_{\nabla\Delta N}$, is proportional to ∇g. Also note that the length of the path, along which $\delta\tilde{g}_{\nabla\Delta N}$ error decreases down to 1mGal, is (7-11) km.

Thus, when the filtering problem is solved with the phase measurement ambiguity even of one period, the accuracy substantially decreases on the path of several kilometres. Then the accuracy of gravity estimation reaches the same level as it had been before ambiguity appeared. From above it follows that it is necessary to solve the problem of phase measurements ambiguity.

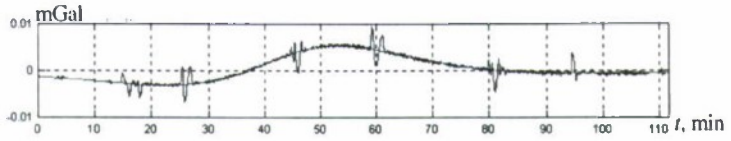

Fig. 2. The plot $\lambda\ddot{K}_h$ for the second difference of measurements

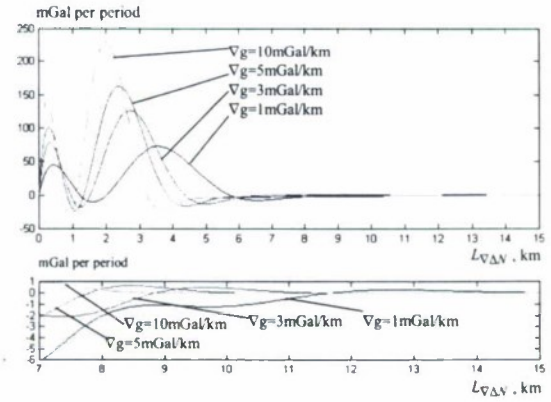

Fig. 3. Values $\delta\tilde{g}_{\nabla\Delta N}/(K_h\nabla\Delta N)$ for various gradients ∇g and speed 50 m/s

The results for the real data processing

The survey data used in the investigations was obtained with the use of the gravimeter Chekan-A developed in the CSRI "Elektropribor". The survey was performed during flights in Germany in the region with a gravity disturbance alteration of ~40 mGal. The average speed of the aircraft during the survey was 60m/s. The same profile was surveyed twice in opposite directions. In the processing corrections were entered for flight altitude, Eotvos correction, etc. The final estimation of real data processing accuracy was made by the comparison of gravity disturbance measurements for each profile in opposite flights. This method was found acceptable because the difference in coordinates in opposite flights did not exceed 200-400m, and the field gradients were about 1mGal/km. Gravity disturbance was estimated by two methods: by using the measurements (4), (5) that require integration of the gravimeter readings, and by using the measurements (6), (7) that require differentiation of altitude and vertical speed measurements. Since the gravimeter sensor corresponds to the transfer function $\frac{1}{T_{gr}p+1}$ with the time constant of about T_{gr}=40s, in order to restore a high-frequency component of gravity disturbance and vertical accelerations the output signal of the gravimeter was processed by using a circuit with the transfer function $T_{gr}p+1$. The gravity model was accepted as the second integral of the white noise. Remember that this model is close to the Jordan model. In accordance with the gravity model selected, the Butterworth filter of the 4th order with the cutoff frequency ρ=0.01Hz was used in the processing of altitude measurements, and the Butterworth filter of the 3rd order with cutoff frequency ρ=0.003Hz was used in the processing of vertical velocity measurements.

Two methods of measurement processing yielded close results. The difference between the gravity disturbance estimates at the same trajectory points (during the flight along the same straight section in opposite directions) in the solution of the smoothing problem was (1-2) mGal with the use of altitude measurements (see

Fig. 4), and (7-10) mGal - with vertical speed measurements. For filtering, these values increased by no less than 2-3 times.

The obtained level of errors exceeds the calculated (see Table 4) RMS errors of gravity estimation. To reveal the cause of the discrepancies, possible error sources were analyzed. The results of the investigations allow the following remarks.

- The contribution of vertical velocity measurement errors to the gravity disturbance estimation error is estimated at 10 mGal. This allows the conclusion that it is these errors that are the main cause that restricts the accuracy of gravity disturbance determination when velocity measurements are used.
- The contribution of altitude measurement errors to the total gravity error is estimated at the level of 0.7 mGal, which testifies to the presence of more substantial causes that determine the obtained accuracy level when altitude measurements are used.
- When the difference measurements (6), (7) are used, the level of the gravity disturbance determination error caused by the velocity differentiation error is 0.3 mGal, and the level of the error caused by the double altitude differentiation error is 0.5 mGal.
- The error in restoration of the gravimeter readings because of uncertainty of the time constant T_{gr} and the error caused by inaccurate time synchronization of the gravimeter readings and the DGPS measurements is much less than 1mGal.

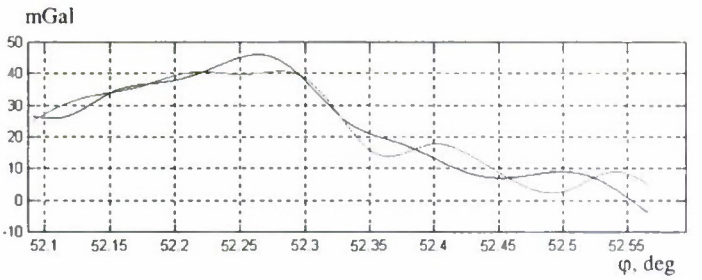

Fig. 4. The gravity estimates obtained in the solution of the smoothing problem for two opposite tracks along identical straight sections.

Conclusions

1. Optimal stationary filtering and smoothing algorithms have been analyzed, the results allowing the following implications:
   - The realization of optimal algorithms for gravity disturbance described as the random walk and the 2nd integral of the white noise is reduced to differentiation of differences between the integrals of the gravimeter readings and DGPS measurements with their subsequent processing by the Butterworth filters. The order and cutoff frequency of the filters that realize the optimal algorithm have been established depending on the gravity disturbance model, type of satellite measurement and measurement noise intensities.
   - Optimal algorithms designed for the gravity disturbance model as the 2nd integral of the white noise can be considered as algorithms close to optimal when gravity disturbance is described with the frequently used Jordan model.
   - When the differences between the gravimeter readings and derivatives of the DGPS data are used as measurements, the optimal filtering algorithm for the case that gravity disturbance is described by the random walk is reduced to the processing of these differences with the Butterworth filter. When gravity disturbance is described by the 2nd integral of the white noise, the processing of differences between the same measurements with Butterworth filters does not provide optimal solution to the filtering problem.
   - Optimal smoothing algorithms for the both models under consideration can be realized through the formation of differences between the gravimeter readings and derivatives of the DGPS data and by their processing with Butterworth filters of the appropriate orders in direct and reverse time.
2. The investigation of potential accuracy in gravity disturbance estimation has shown that:
   - In the smoothing problem the accuracy of gravity disturbance estimation is 2 to 7 times higher than the accuracy achieved in the filtering problem, depending on the type of the measurement and

gravity model. This relation does not depend on the intensity of forcing noises in the gravity disturbance model and measurement noise intensities.

- When the velocity measurement is used, the accuracy of gravity disturbance estimation is much (2 to 8 times) lower than in the case that the altitude measurement is used.
- Estimation is ensured to be at the level of 1mGal only in the case that the altitude measurement is used.
- For the two models considered in the paper the accuracies of gravity disturbance estimation with the use of the altitude measurement in the solution of the smoothing problem are essentially different (by a factor of 3-5). However when the filtering problem is solved with the use of velocity or altitude and the smoothing problem – with velocity, the accuracies differ no more than by a factor of 1.5.

3. It has been established that when the filtering problem for gravity disturbance is solved with the ambiguity of the phase measurements even of one period, the accuracy substantially decreases – down to 200 and more mGal, on the path of up to 10 km. In the steady-state regime the error in estimation of gravity disturbance caused by the ambiguity of the phase measurements can be as low as of 0.1 mGal.
4. In the processing of real gravimetric and satellite data the RMS value of differences between gravity disturbance estimates at the same point of the trajectory is (1-2) mGal for the smoothing problem with the use of altitude measurements and (7-10) mGal – with vertical velocity measurements.

References

1. **Hammada Y.** Optimal Versus Non-Optimal Lowpass Filtering in Airborne Gravimetry. Proceedings of the International Symposium on Kinematic Systems in Geodesy, Geomatics and Navigation. Banff, Canada, June 3-6, 1997. PP 633-640.
2. **Olesen A.V., Forsberg.R., Keller K., Gidskehaug A.G.** Airborne Gravity Survey of The Polar Sea North of Greenland. EAGE 61st Conference and Technical Exhibition – Helsinki, Finland, 7-11 June.1999.
3. **Bolotin Yu.A., Golovan A.A., Parusnikov N.A.** Dataware for aviation gravimetry problem. Proceedings of the Conference on oscillations and control theory. Moscow, 29 November, 2000.
4. **Abdelmoula F.** Ein Beitrag zur Bestimmung der Erdbeschleunigungsanomalien an Bord eines Flugzeuges. Aachen: Shaker, 2000 (Berichte aus der Luft-und Raumfahrttechnik) Zugl.: Braunschweig, Techn., Univ., Diss., 2000.
5. **Jordan S.K.** Self-consistent statistical models for gravity anomaly and undulation of the geoid. J. Geophys. Res. Vol. 77. N 20. 1972. PP 3660- 3670.
6. **Vassiliou A.A., Schwarz K.P., Wei M.** Study of the High Frequency Spectrum of the Anomalous Gravity Potential. Journal of Geophysical Research, 1987, vol. 92, No. B1, pp. 609-617.
7. **Chelpanov I.B. Nesenjuk L.P., Braginsky M.V.** Computation of navigational gyro devices characteristics. L. Sudostroyeniye 1978 (in Russian).
8. **Panteleev V.L.** Fundamental of marine gravimetry. M., Nedra, 1983 (in Russian).
9. **Blazhnov B.A., Nesenjuk L.P., Peshekhonov V.G., Sokolov A.V., Elinson L.S., Zhelesnyak L.K.** An integrated mobile gravimetric system. Development and test results. Proceedings of the 9th Saint-Peterburgs international conference on integrated navigation systems. 27-29 may 2002.
10. **Meditch J.S.** Stochastic optimal linear estimation and control. Mc. Graw Hill. New York, 1969.
11. **Korn G., Korn T.** Mathematical handbook for scientists and engineers. McGraw-Hill Book Company, 1968.
12. **Edwin H van Leeuwen**, Airborne Gravity Gradiometry. ATSE (The Australian Academy of Technological Sciences and Enginecring) Focus, No. 119, Nov/Dec 2001. http://www.atse.org.au/publications/focus/focus-vanleeuwen.htm.

LOW COST STRAPDOWN IMU/DGPS INTEGRATED NAVIGATOR WITH FUZZY LOGIC ADAPTIVE TUNING

B.W. Leach*, **R. Rahbari****, **J. Dillon*****
Flight Research Laboratory, Institute for Aerospace Research,
National Research Council of Canada, Ottawa, Canada K1A 0R6. E-mail:barrie.leach@nrc.ca

Abstract

Key words: strapdown navigation, DGPS, fuzzy logic, adaptive tuning

The Flight Research Laboratory (FRL) of Canada's National Research Council (NRC) uses low cost strapdown IMUs, medium accuracy INSs, state-of-the-art differential GPS (DGPS) and associated Kalman filter optimal integration algorithms for a variety of flight test applications. A prototype strapdown IMU/DGPS integrated navigator has been developed, based on a tactical grade IMU (the Litton LN-200 FOG IMU) and a NovAtel RT-20 DGPS receiver, for use on-board the FRL's research aircraft. A compact real-time hardware version of the integrated navigator is currently being flight tested and evaluated. These evaluations include assessing the performance improvements that are possible by using a fuzzy logic adaptive tuning algorithm to optimize the Kalman filter's measurement noise variances during flight.

Introduction

This paper describes the latest progress in an ongoing project (Refs. 1, 2) to develop a set of flightworthy hardware and software to optimally integrate strapdown IMU data (from a low cost Litton LN-200 IMU), along with NovAtel DGPS data, using the principles of Kalman filtering. The paper begins with a brief review of the instrumentation used for the recent flight testing on-board the Bell 206 research helicopter, including specifications of the inertial sensors in the LN-200 IMU (i.e., the gyros and accelerometers), the GPS/DGPS equipment being used, as well as the medium accuracy LTN-90-100 IRS used as a reference for evaluating integrated system performance. A real-time inertial alignment algorithm for initializing the attitude/heading is described, as is the error state feedback Kalman filter integrated navigation design. Then, some of the real-time hardware and software implementation details are given. Primary emphasis is placed on describing the important results and conclusions to be drawn from the flight testing of this real-time hardware/software configuration.

A conservative approach to the specification of the measurement noise variances in the real-time Kalman filter guarantees robust performance under virtually all flight conditions. However, it does mean that there are large portions of a typical flight where the maneuver dynamics are quite benign and the measurement noise tuning is far from optimal. To rectify this situation, a technique has been developed, using fuzzy logic concepts, for adaptively tuning the real-time Kalman filter to the predicted current conditions of the GPS/DGPS position and velocity measurement errors and associated noise variances. Using flight test data from the Bell 206 research helicopter, Kalman filter performance with the adaptive tuning algorithm is analyzed, and compared with that of non-adaptive tuning, over a wide variety of flight test dynamics. It is shown that the measurement residuals, and their predicted 1-sigma bounds, propagate in a more consistent, near optimal fashion with the adaptive tuning algorithm in place. As well, the estimates of accelerometer bias error, which are prone to artificial offsets with improper tuning, propagate within acceptable bounds when adaptive tuning is used; and, in general, all error state estimates are more accurate. The concluding section of the paper indicates future developments and specific applications of the low cost strapdown IMU/DGPS integrated navigator with fuzzy logic adaptive tuning.

1. Instrumentation details for Bell 206 flight testing of real-time strapdown navigator

A strapdown IMU/DGPS integrated navigator, employing an error state feedback Kalman filter, has been designed for use with flight test data from a Litton LN-200 IMU, integrated with NovAtel DGPS data, with a medium accuracy LTN-90-100 IRS being used as a reference for evaluating integrated system performance. Some of the details of these systems, as installed on-board the NRC Bell 206 research helicopter, are given below.

---

* Senior Research Officer
** Post Doctoral Fellow
*** Instrumentation Engineer

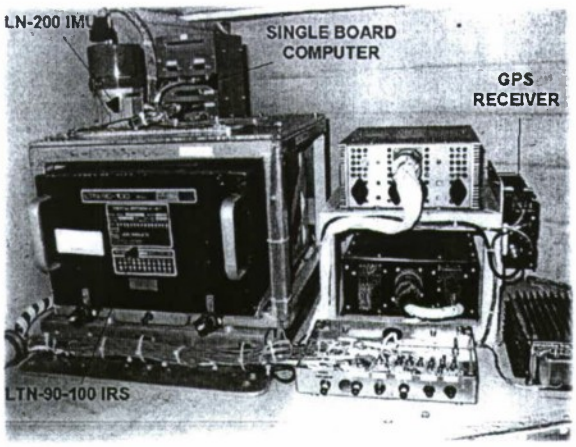

Fig. 1. Equipment installations in luggage compartment of Bell 206

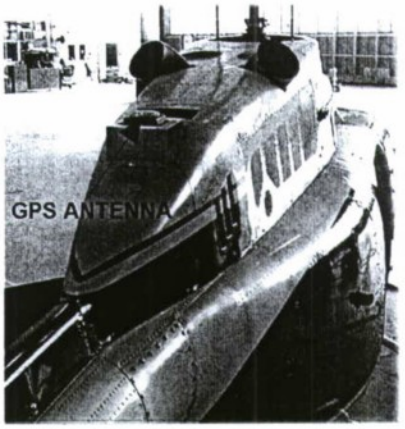

Fig. 2. GPS antenna installation on aft fuselage of Bell 206

Litton LN-200 IMU

The Litton LN-200 IMU (Fig. 1) is a low cost, small (i.e., a cylinder 9 cm high and 9 cm in diameter), lightweight tactical grade IMU that utilizes fibre optic gyros (FOGs) along with micromachined silicon accelerometers (SiAc's^{TM}) to measure 3-axis incremental changes in attitude and velocity. The unit purchased by the FRL is specified to have a gyro bias repeatability of less than 3 deg/hr, gyro scale factor accuracy of better than 300 ppm, a gyro random walk power spectral density (PSD) level of less than 0.15 deg/hr$^{1/2}$ and g-sensitive repeatability of 0.01 deg/hr/g. The accelerometer residual biases are less than 1,500 μg, scale factor stability is 1000 ppm, white noise PSD level is 50 μg/Hz$^{1/2}$ and axis misalignment is 300 μrad. Digital input/output is via an RS-485 serial data bus employing the IBM synchronous data link control (SDLC) protocol. Raw digitized delta angle ($\Delta\theta$) and delta velocity (Δv) IMU data are available from the bus at a 400 Hz rate. The resolution of the digital data output parameters, based on 16-bit words, is 1.90735 x 10^{-6} rad for $\Delta\theta$ and 6.10352 x 10^{-5} m/s for Δv.

NovAtel RT-20 GPS Receiver

A NovAtel PwrPak-II-RT20 GPS receiver served as the airborne GPS system, integrated with the LN-200 IMU, during the Bell 206 flight test program. This receiver has the capability of operating in a real-time DGPS mode, if required. A NovAtel Model 511 GPS antenna was installed on the aft section of the Bell 206 fuselage (Fig. 2). For real-time operation, the on-board receiver was polled for a GPS position/velocity solution at a 1 Hz rate. A GPS ground station was provided by a NovAtel GPS receiver card (Model 3151R OEM GPSCard), installed in a personal computer and connected to a stationary roof-top antenna (a Model 501 antenna with choke-ring). It was used as a reference station to provide differential GPS (DGPS) corrections, both for real-time and post-processing applications.

Litton LTN-90-100 IRS

A Litton LTN-90-100 Inertial Reference System (IRS), based on ring laser gyro technology, was installed on-board the Bell 206 for the flight tests, in the luggage compartment (Fig. 1). It provided supplemental inertial data (i.e., groundspeed, attitude/heading, linear accelerations, angular rates), recorded in the ARINC 429 digital data format, at 64 Hz. This accurate inertial reference information was used to evaluate the performance of the real-time Kalman filter-based strapdown navigator.

2. Software algorithms for alignment and navigation

Strapdown Inertial Coarse Leveling and Fine Alignment Processes

The integrated navigation software that has been developed includes an initialization sequence for coarse leveling and fine alignment. Coarse leveling (Ref. 3) is a method for rapidly initializing $\underline{\underline{C}}^{N}_{B}$, the direction cosine matrix (DCM) describing the aircraft attitude relative to a local level navigation (N) coordinate frame, to an approximate vertical attitude in the N frame. The method uses the average values (over several seconds) from the triad of strapdown accelerometers. Let $\underline{a}^{B} = [a_x\ a_y\ a_z]^T$ be the vector of averaged body axis accelerations and let $|\underline{a}^{B}|$ be the magnitude of $\underline{a}^{B}$. Then, define the unit vector, $\underline{u}^{B}_{ZL} = \underline{a}^{B} / |\underline{a}^{B}| = [u_1\ u_2\ u_3]$. The third row of the DCM is equivalent to the unit vector components, $C_{3,1} = u_1$, $C_{3,2} = u_2$, $C_{3,3} = u_3$. Initial values of pitch and roll angle (θ, ϕ) can then be computed from this third row, as follows:

$$\theta = \arctan \{ -C_{3,1} / (1 - C_{3,1}^2)^{1/2} \}; \quad \phi = \arctan \{ C_{3,2} / C_{3,3} \} . \tag{2.1}$$

Fine alignment is a method to precisely level the $\underline{C}^N_B$ matrix, in the presence of quasi-stationary disturbances, and estimate the horizontal earth rate components along the navigation (N) frame axes (Ref. 3). It is an iterative estimation / filtering process, based on calculating the double integral of transformed accelerometer-measured specific force, $\underline{a}^N_{SF}$, using the following simplified equations for the horizontal navigation components:

$$d \underline{C}^N_B / dt = \underline{C}^N_B (\underline{\omega}^B_{IB} \times) - (\underline{\omega}^N_{IN} \times) \underline{C}^N_B ; \quad \underline{\omega}^N_{IN} = \underline{\omega}^N_{IE} + \underline{\omega}^N_{Tilt},$$

$$\underline{\omega}^N_{Tilt} = K_2 \underline{u}^N_{ZN} \times \Delta \underline{R}^N_H ; \quad \underline{\omega}^N_{IE} = \underline{\omega}^N_{IEH} + \underline{u}^N_{ZN} \omega_e \sin lat,$$

$$d \underline{\omega}^N_{IEH} / dt = K_1 \underline{u}^N_{ZN} \times \Delta \underline{R}^N_H.$$

$$d \underline{v}^N_H / dt = \underline{a}^N_{SFH} - K_3 \Delta \underline{R}^N_H = \underline{C}^N_{BH} \underline{a}^B_{SF} - K_3 \Delta \underline{R}^N_H.$$

$$d \Delta \underline{R}^N_H / dt = \underline{v}^N_H - K_4 \Delta \underline{R}^N_H. \tag{2.2}$$

where $\underline{u}^N_{ZN}$ is a unit vector along the N frame vertical (Z) axis; $\underline{\omega}^B_{IB}$ is the body angular rate vector; $\underline{\omega}^N_{IN}$ is the angular rate of the N frame; $\underline{\omega}^N_{IE}$ is the earth rate vector; $\underline{\omega}^N_{Tilt}$ is an angular rate feedback term to correct tilt error in $\underline{C}^N_B$; $\Delta \underline{R}^N_H$ is position divergence; K_1, K_2, K_3, K_4 are feedback control gains for the fine alignment process (estimated using Kalman filtering); ω_e is earth rotation rate magnitude; and lat is geodetic latitude.

Equations 2.2 are integrated until $\Delta \underline{R}^N_H$ reaches an acceptable quasi-stationary equilibrium. At that point, $\underline{C}^N_B$ should be accurately leveled and $\underline{\omega}^N_{IEH}$ should be accurately estimated. The estimate of $\underline{\omega}^N_{IEH}$ is then used to initialize the $\underline{C}^N_B$ heading. This is done by defining $\underline{u}^N_{XE} = \{(\cos lat/\omega_{IEH}) \underline{\omega}^N_{IEH} + \underline{u}^N_{ZN} \sin lat\}$, where $\underline{u}^N_{XE}$ is a unit vector along the earth (E) frame X axis, as projected onto the N frame; $\underline{u}^N_{ZN}$ is a unit vector along the N frame vertical (Z) axis; $\underline{\omega}^N_{IEH}$ is the horizontal earth rate components at completion of fine alignment; and ω_{IEH} is the magnitude of the $\underline{\omega}^N_{IEH}$ two-element horizontal earth rate vector. The wander angle, α, of the wander azimuth navigation (N) frame can then be computed from the components of $\underline{u}^N_{XE}$ as:

$$\alpha = \arctan \{ -u_{XE2} / u_{XE1} \}, \tag{2.3}$$

Finally, the starting values for the Euler angles (i.e., θ, ϕ, ψ) used in the strapdown navigation process are

$$\theta_0 = \arctan \{C_{3,1} / (1 - C_{3,1}^2)^{1/2} \}; \qquad \phi_0 = \arctan \{ -C_{3,2} / -C_{3,3} \}; \qquad \psi_0 = - \alpha_0 , \tag{2.4}$$

where $C_{3,1}$, $C_{3,2}$ and $C_{3,3}$ are the elements of the third row of the $\underline{C}^N_B$ matrix, after fine alignment, and α_0 is the initial wander angle as determined from fine alignment and Eqn. 2.3.

Kalman Filter Design for Real-Time Integrated Navigator

Fig. 3 shows a block diagram representing the real-time error state feedback Kalman filter integration design being employed to optimally integrate IMU and DGPS data in the real-time error-corrected strapdown inertial navigator. Note that the INS/DGPS integration is of the so-called loosely-coupled form, in which GPS position and velocity components are used as primary measurements rather than the more fundamental GPS pseudoranges and pseudorange rates. Digitized delta velocity (Δv) and delta angle ($\Delta \theta$) IMU data and GPS height data are sent to a strapdown navigation algorithm that computes the standard inertial navigation outputs (i.e., position, velocity and Euler angles) at a 400 Hz rate. In the integration scheme, an error state feedback Kalman filter processes the differences between strapdown INS and DGPS position and velocity components as the primary Kalman filter measurements (at 1 Hz). The Kalman filter estimates the fundamental errors in the strapdown navigator and the DGPS components. These estimated errors are then fed back to correct the important navigation quantities 'on the fly' - primarily those of the strapdown navigator, but also those of the GPS receiver.

For development purposes, a fairly complete Kalman filter error state modeling has been employed (especially for the various gyro and accelerometer errors) in an offline version of the Kalman filter, consisting of a total of 42 error states. However, for the LN-200 IMU/DGPS real-time integration, it was found that a 22-element, reduced-order error state model was adequate. The 22 error states consist of: i) 3 INS position errors, ii) 3 INS velocity errors, iii) 3 INS tilt angle errors, iv) vertical loop acceleration correction error, v) 3 gyro offsets, vi) 3 accelerometer offsets, vii) 3 DGPS position offsets, and viii) 3 DGPS velocity offsets. All of the error states, other than the strapdown INS system error states (i.e., the first ten), are modeled as first-order Gauss-Markov processes (Ref. 4).

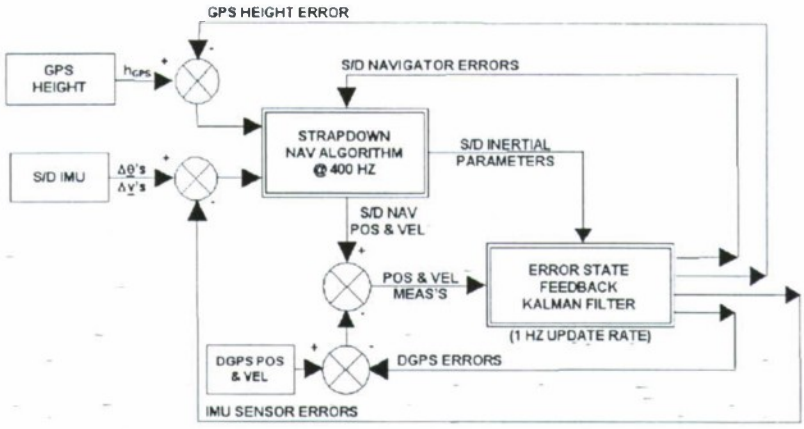

Fig. 3. Error state feedback Kalman filter design for real-time strapdown navigator

The Kalman filter measurements consist of six DGPS scalar components, namely: i) 3 strapdown INS - DGPS position differences and ii) 3 strapdown INS - DGPS velocity differences. The Kalman filter is implemented using Bierman's UDU^T mechanization algorithm (Ref. 5) for efficiency and robustness. The real-time version of the Kalman filter software has been hard coded to update at 1 Hz – one of the standard rates at which real-time GPS solutions are available from the RT-20 receiver.

3. Implementation details for real-time integrated navigator

Digital Interface Design for LN-200 IMU

The LN-200 IMU electrical interface (Fig. 4) consists of an RS-485 serial digital data bus and interface discrete lines. The protocol used is a simplified version of the IBM SDLC protocol, where the IMU is the bus station master operating in broadcast mode and the address data bytes are absent from the IMU messages. The protocol uses zero bit insertion to ensure a unique opening and closing flag of a zero, six ones, and a zero. The output data is sampled at 400 Hz and transmitted on the falling edge of an internally-generated 1.0152 MHz data clock. An optional 2-wire pair is also available for data synchronization purposes. A custom PC/104 interface board was designed at the Flight Research Laboratory to minimize the software overhead in processing IMU data. As the data bits are clocked into a shift register on the interface board, a comparison is made to remove artificially-inserted zero bits, before transferring bytes to a FIFO buffer. The data synchronization signal is used to trigger an interrupt on the interface computer. The interrupt handler simply reads from the FIFO, scales the raw data, and initiates the strapdown navigator.

Single Board Computer for Real-Time Navigation

A high performance PC/104 Single Board Computer is used to execute the strapdown navigation equations at 400 Hz and the error state feedback Kalman filter routine at 1 Hz. The computer is a TP400 from DSPDesign, using a National Semiconductor Geode GX1 CPU running at 300 MHz. The computer consumes approximately 3 W of power, which is dissipated using a passive heat sink. The computer and interface board are housed in a rugged aluminum box (see Fig. 1) with standard I/O connectors. The computer, interface board and LN-200 IMU are powered from aircraft 28 volts DC using two DATEL DC/DC converters that supply 5 Vdc and +/- 15 Vdc.

Interfacing and Timing Issues

In an off-line environment, it is possible to execute a fixed number of strapdown navigator iterations, then pause while the error state feedback corrections are computed using the Kalman filter. Due to the matrix calculations involved in updating the Kalman filter, it was not possible to complete the Kalman filter update within the strapdown navigator update period of 2.5 msec. Thus, the Kalman filter update calculations were distributed over the CPU idle time of several strapdown navigator iterations. Then, the feedback corrections were applied in the first strapdown navigator iteration following completion of the Kalman filter update. With the Geode GX1 300 MHz processor, a strapdown navigator iteration required 250 microseconds of CPU time, leaving 90% of the CPU time available for the Kalman filter update. At this CPU loading, the error state feedback corrections were calculated and applied within 12.5 msec of receiving a set of GPS measurements.

Software Implementation Details

The original off-line software program, written in Fortran, was converted to C for the real-time implementation. The Borland C compiler was used to create a DOS-based executable. In the near future, the

code will be ported to run on the QNX operating system. The strapdown navigator software is triggered by the interrupt service routine for the hardware interface board and, thus, runs at 400 Hz based on the LN-200 internal clock. The GPS data is processed by another interrupt service routine. Once a complete GPS measurement is available, the Kalman filter update is initiated as a lower priority task (i.e., it can be pre-empted by the strapdown navigator task). Since the IMU and GPS data have different clock sources, the issues of clock drift and jitter must be addressed. The software must be able to asynchronously iterate the strapdown navigator and Kalman filter update routines. This is achieved in the real-time implementation by calculating the terms of the Kalman filter state transition matrix as cumulative sums, within the strapdown navigator task, so that a complete state transition matrix is available when a set of GPS measurements arrives. The latency introduced by the RS-232 transmission time is accounted for by buffering the strapdown navigator outputs so that the INS/GPS differences are calculated at approximately the same instant in time, which is critical during highly dynamic maneuvering.

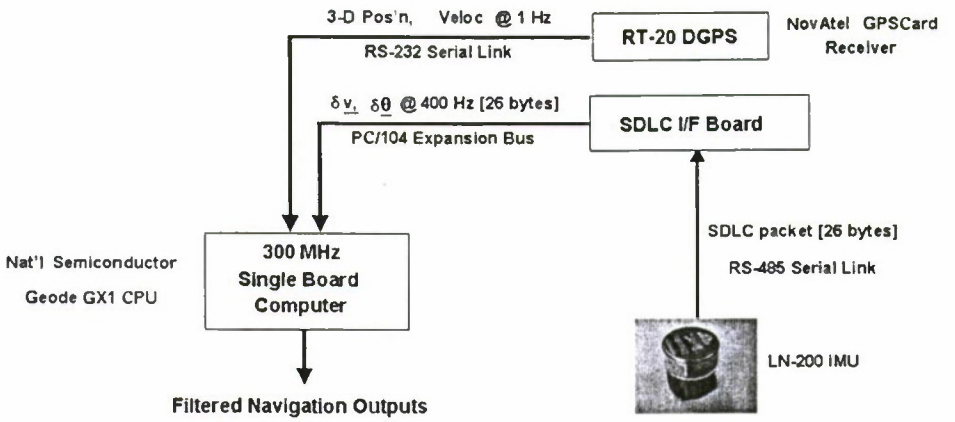

Fig. 4. Real-time strapdown navigator electrical interfaces

4. Real-time integrated navigation performance

Coarse Leveling / Fine Alignment Results

Coarse leveling / fine alignment software allows for a completely autonomous system that is not reliant on any external source of attitude / heading information for initialization. In order to optimize the performance of the coarse leveling / fine alignment software, data collected with the LN-200 IMU installed on-board the Bell 206 helicopter was used to adjust the alignment Kalman filter design parameters for robust performance. Estimating the four Kalman gains, with the alignment Kalman filter updating every second, resulted in foreground control reset equations (Eqns. 2.2) with a slightly under-damped response; thus, convergence was attained within a few minutes. As a result, staying on the ground for approximately 10 minutes prior to takeoff was found to be more than adequate to perform coarse leveling and fine alignment. In particular, it was found that the coarse leveling procedure only required 10 to 20 seconds of 400 Hz IMU data to attain a good solution for pitch / roll attitude.

Fig. 5 and 6 show a typical fine alignment response for a case in which the LN-200 IMU is being aligned using data collected on-board the Bell 206 with the engine running. Figure 5 shows the time series plots of the two measurement residuals, based on the horizontal measurement observations, $\Delta\underline{R}_{NX}$ and $\Delta\underline{R}_{NY}$, respectively. There is a typical mildly under-damped response, with an initial peak followed by a settling to steady state within approximately two minutes. Both measurement residuals stay well within the Kalman filter-predicted 1-sigma bounds (i.e., the dashed lines), implying a robust Kalman filter design. As well, all of the Kalman filter error states settle down to very small steady state values within about two minutes. Figure 6 shows the time propagation of the pitch, roll and heading angle estimates, as computed from N frame initialization Eqns. 2.2 to 2.4 throughout the fine alignment process. Pitch and roll angles do not change much, indicating that the coarse leveling results are reasonably accurate already. And comparisons with pitch / roll attitude from the LTN-90-100 IRS suggest that pitch / roll estimates from fine alignment are accurate to within 0.1 -> 0.2 degrees. Typically, heading angle alignment is not nearly as accurate as pitch / roll alignment. During fine alignment, the heading angle estimate starts at zero and very quickly reaches a steady state non-zero value within about two minutes. Using heading from the LTN-90-100 IRS for comparison, the error in the fine alignment heading was found to be about 8.5 degrees, which is consistent with residual gyro biases of approximately 1 deg/hr. Unfortunately, the quality of the gyros in the LN-200 IMU precludes a more accurate value of initial heading during fine alignment. However, we require only a nominal value for initial heading - in the navigation mode, the error state feedback process should quickly identify residual attitude / heading errors occurring in the strapdown navigator.

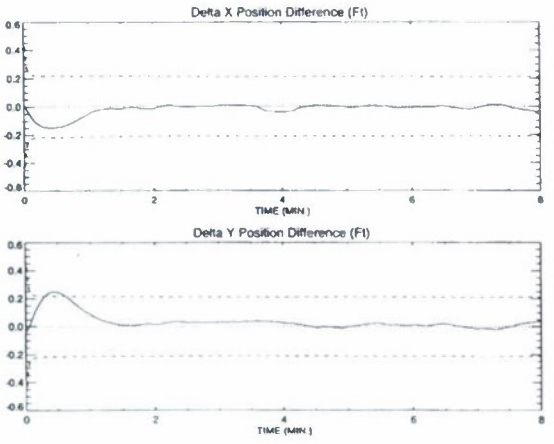

Fig. 5. Measurement residual time histories for alignment Kalman filter

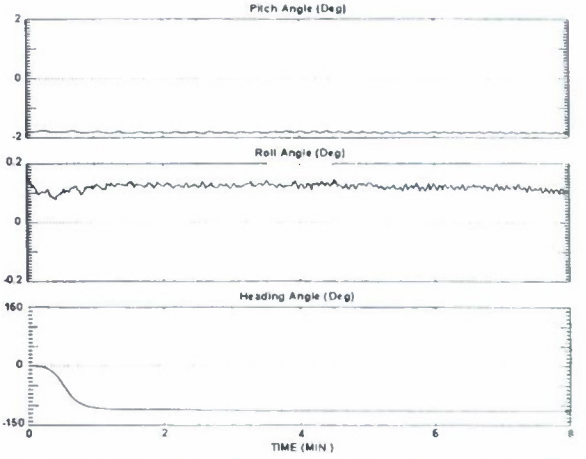

Fig. 6. Euler angle time histories during alignment process

Integrated Navigation Performance Results

Several dedicated flights were conducted with the Bell 206 to evaluate the performanee of the real-time navigator under typical helicopter flight dynamics conditions. The flight maneuvers performed included rather benign racetrack patterns all the way up to extremely aggressive ADS-33 military handling qualities maneuvers (Ref. 6). For one such flight, Fig. 7 shows the time histories of the three Euler angles (i.e., roll, pitch and heading angle). It is quite obvious that there is a great deal of dynamics occurring at several points during the flight, especially from the 40-minute mark on. The primary inertial reference system for assessing integrated navigation performance was a Litton LTN-90-100 IRS installed for the flight tests. IRS parameters being recorded, for comparison, included the Euler angles, track angle, groundspeed, linear acceleration components and angular rate components.

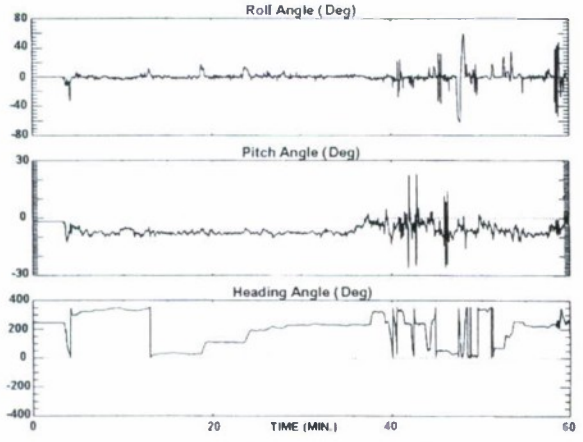

Fig. 7. Euler angle time histories

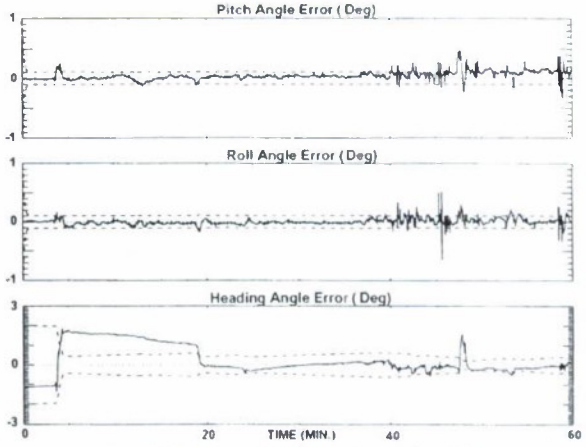

Fig. 8. Euler angle error time histories

For this flight, real-time strapdown navigator calculations of roll, pitch and heading angles were compared with those same quantities from the LTN-90-100 IRS. Absolute accuraey of LTN-90-100 roll and pitch angles is better than 0.05 degrees, and absolute heading angle accuracy is approximately 0.1 to 0.2 degrees. Figure 8 shows the differences between strapdown navigator outputs and the equivalent LTN-90-100 outputs, together with Kalman filter predicted uncertainty bounds (the dashed lines), for pitch, roll and heading during the flight. The pitch and roll angle differences easily lie within the +/- 0.1 degree uncertainty bounds during the henign segments of the flight (i.e., up to the 40-minute mark). And, even during the high dynamics maneuvers (i.e., the 40 –> 60 minute section), where piteh angle ean exceed 20 degrees in magnitude and roll angle is up to 60 degrees in magnitude, the pitch and roll angle differences only exceed the +/- 0.1 degree hounds occasionally. The heading angle difference is somewhat larger, as expected; but the differenee stays within the predieted uncertainty bounds (approximately +/- 0.5 degrees or less) for most of the flight (e.g., from the 20-minute mark onward). There is a large initial heading angle error of about 1.5 degrees at the beginning of the flight, attributed to a very aggressive helicopter maneuver at takeoff, whieh included an extremely large heading change prior to any signifieant forward veloeity. Eventually, the error state feedback Kalman filter identifies and corrects for this

heading angle error, after significant heading angle changes occur in the flight, so that the residual error can be observed and estimated accurately. As part of an overall heading alignment procedure, an operational consideration might be to always ensure that a sharp turn of 90 deg occurs, either during taxiing or just after take-off, to guarantee early observability of any initial heading angle error.

Figures 9 and 10 show the time histories of the Kalman filter's velocity error corrections and Euler angle error corrections that were being fed back, in real time, and applied to the strapdown navigator every second. These error corrections are quite small for most of the flight, and only become significant during the dynamic maneuvers, as expected. As with the Euler angle estimates (Fig. 8), these results have been duplicated off-line, using the off-line Kalman filter developmental software and the same set of initial conditions, thus confirming the accuracy of the real-time software. The results shown here have been based on a rather conservative tuning of the Kalman filter's measurement noise statistics, to handle the extreme cases of high dynamics and degraded GPS performance. The next section will discuss a real-time fuzzy logic adaptive tuning algorithm to optimize the Kalman filter under all dynamic conditions.

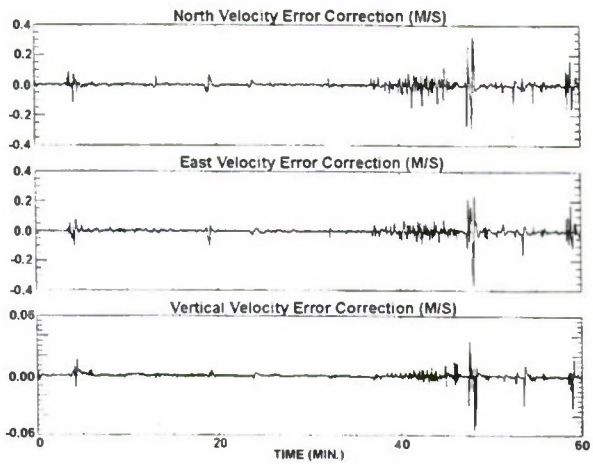

Fig. 9. Velocity error feedback corrections

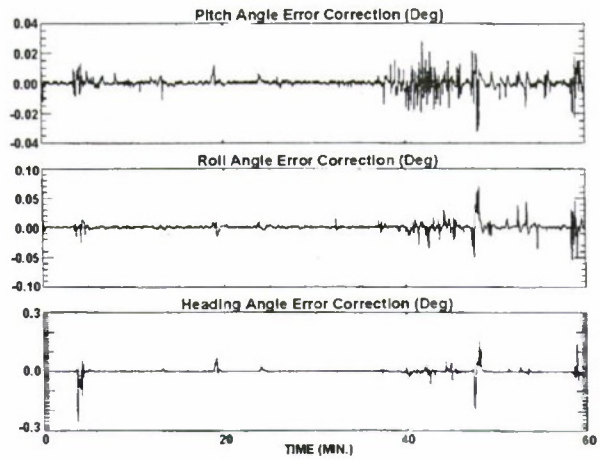

Fig. 10. Euler angle error feedback corrections

5. Fuzzy logic adaptive tuning

Adaptive Tuning for Optimal Performance

Preliminary tuning of the integrated navigator's Kalman filter measurement noise variances has been based on conservative, 'worst case' GPS measurement noise values derived from representative Bell 206 flight test data. The 1-sigma values of the DGPS noise processes have been specified to be relatively large (e.g., 1.5 m for position measurements and 1.0 m/s for velocity measurements), and larger yet for real-time, non-differential GPS (e.g., 5 m for position measurements and 1.5 m/s for velocity measurements). Also, the 1-sigma values of the Markov error states associated with the DGPS measurements have been specified, quite conservatively, as 5 m for position and 1 m/s for velocity. For the real-time non-differential GPS case, they have been specified as 20 m for position and 1.5 m/s for velocity. This conservative tuning guarantees that the Kalman filter will have robust, non-divergent performance under virtually all flight conditions. However, there are usually large portions of a typical flight for which the maneuver dynamics are quite benign. For those flight segments, the measurement noise tuning will be far from optimal and the error state estimates will not be as accurate as they could be.

It has been observed that GPS/DGPS measurement accuracy is usually closely linked to the level of helicopter maneuvering that is occurring. For helicopters, in particular, due to the location of the GPS antenna, there can be a sudden deterioration in GPS quality when the vehicle is in an unusual attitude, such as during a steep turning maneuver. Moreover, especially during periods of significant maneuvering, Kalman filter accelerometer bias estimates can exhibit artificial offsets if the GPS noise statistics are specified too tightly. These artificial offsets are usually associated with small, but significant, time skews in the GPS data relative to the inertial data. It is, thus, important to develop a technique that can detect significant maneuvering, in real time, and adjust the measurement noise parameters in the Kalman filter accordingly. An effective technique has been developed, using fuzzy logic concepts, for adaptively tuning the real-time Kalman filter to the predicted current conditions of the GPS/DGPS position and velocity measurement errors and equivalent noise variances.

Input / Output Variables for Fuzzy Logic Algorithm

To characterize the level of helicopter maneuvering, the following inertial parameters have been identified as useful: ϕ (roll angle), θ (pitch angle), p (body roll rate), q (body pitch rate), r (body yaw rate) and v_z (vertical

velocity). These parameters are the basis for fuzzy input variables used in a fuzzy logic algorithm that re-scales the GPS measurement noise parameters according to the level of helicopter maneuvering that is occurring at the time. Normally, this scaling parameter is the single fuzzy logic output parameter being used. In this manner, during benign straight-and-level flight, small values will be used for the GPS measurement noise variances. However, during any sort of significant helicopter maneuvering, the fuzzy logic algorithm will 'scale up' the GPS measurement noise parameters in a smooth, continuous fashion, consistent with the helicopter dynamics that are occurring, to better reflect the true GPS accuracy deterioration. In some cases, one scaling might be used for GPS position-based measurements and a different scaling for GPS velocity-based measurements.

Design of Membership Functions

Using Bell 206 flight data, dynamic ranges have been established for each inertial parameter, corresponding to maneuver levels identified as Low (L), Medium (M) or High (H) dynamics, consistent with the way that a knowledge expert would specify the heuristics of the problem in a meaningful manner. For a reduced set of three inertial input variables (i.e., $|\phi|$, $|v_z|$ and $|r|$), input membership functions have been designed as the overlapping triangular memberships, shown in Fig. 11, based on three-state (i.e., Low, Medium, High) dynamic ranges established for these inertial parameters. The memberships have overlaps in such a way that, for each crisp value, there exists at least one fuzzy value greater than zero (Ref. 7). The output membership functions (Fig. 11) have been designed in a symmetric fashion to represent three evenly distributed fuzzy output states (i.e., Low, Medium and High) spanning the range from 1 (no re-scaling) to 5 (maximum re-scaling). A maximum re-scaling of the GPS measurement noise standard deviation by a factor of 5 should be adequate (this will re-scale the measurement noise variance by a factor of 25). To evenly distribute the output membership functions, with peak points for the memberships at 1, 3 and 5 respectively, the universe of discourse has to start at –1 and end at 7. Since the 'center of area' is the defuzzification method being used, all the membership functions are shifted to the right by '1' so that, in particular, 'Low' starts from 0. Then, after defuzzification, the defuzzified value is shifted back to the left, corresponding to how each membership function was originally defined.

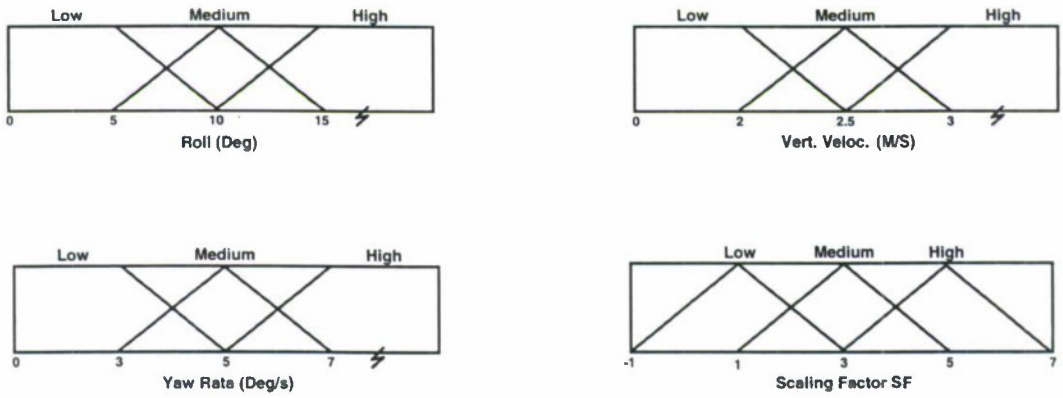

Fig. 11. Fuzzy logic input and output membership functions

Inference Rules and Technique

Inference rules for a reduced set of $|\phi|$, $|v_z|$ and $|r|$ as fuzzy input variables, and SF as the only fuzzy output variable, have been derived from the following set of heuristic logic statements:

IF $|\phi|$ = L THEN:
- IF {$|v_z|$ = H AND/OR $|r|$ = H} THEN SF = H
- IF {$|v_z|$ = M AND $|r| \leq$ M} THEN SF = M
- IF {$|v_z|$ = L AND $|r|$ = M} THEN SF = M
- IF {$|v_z|$ = L AND $|r|$ = L} THEN SF = L

IF $|\phi|$ = M THEN:
- IF {$|v_z|$ = H AND/OR $|r|$ = H} THEN SF = H
- IF {$|v_z| \leq$ M AND $|r| \leq$ M} THEN SF = M

IF $|\phi|$ = H THEN: SF = H

The above logic statements have been transformed into a complete fuzzy rule base so that the inference rules can be applied. The resulting knowledge base is a multivariable fuzzy system with 3 input fuzzy variables (x_1, x_2,

x_3) and one output variable (y), each having three fuzzy states (i.e., Low, Medium and High). Having three input fuzzy variables, each with three fuzzy states, means that a complete rule base will have 27 rules as the knowledge base. The rule base has been designed in a hierarchical fashion, based on the importance of each input variable in determining the output. The inference method implemented in this fuzzy rule base uses the fuzzy integral concept that has been developed in Ref. 8. The rule base has been designed in modules such that, for each fuzzy state of variable x_1, a different module of a two input / one output rule base applies (Ref. 9). However, since the crisp value of x_1 only hits two fuzzy states, only two modules (each module consisting of nine rules) will fire at a time. Each module consists of two inputs (x_2, x_3), and each input fires only two rules, so each module will fire four rules. Thus, since only two modules fire at a time, and each module fires four rules, there are a maximum of 8 rules out of 27 that need to be processed at each update time of the Kalman filter.

Adaptive Tuning Results

For a typical set of Bell 206 flight maneuvers, Fig. 12 shows time series of the three inertial input parameters that enter the fuzzy adaptive algorithm, as well as the output parameter, SF, that results. Roll angle magnitude and yaw rate magnitude reflect any significant turning maneuvers that occur, while vertical velocity magnitude shows any rapid helicopter ascents or descents. Based on the membership functions (Fig. 11) and inference rules that have been defined, the output variable, SF, is computed between the values of 1 and 5 (Fig. 12). It can be seen that SF varies with the level of maneuvering that is being measured by the three inertial parameters.

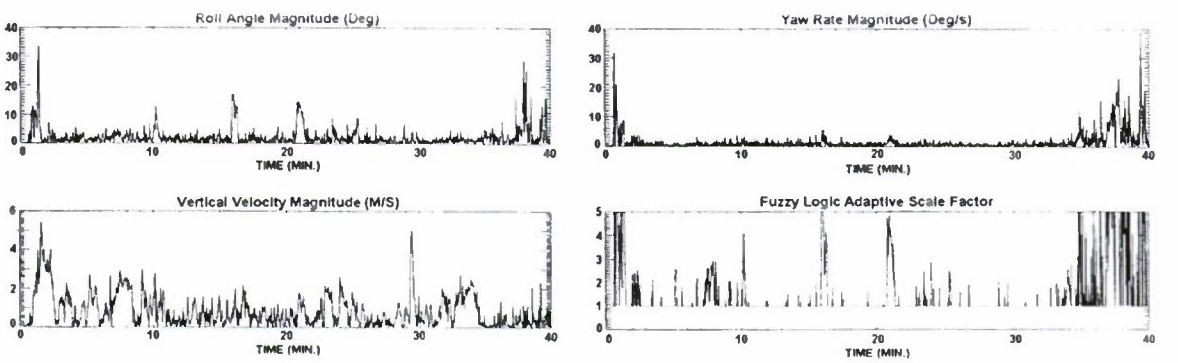

Fig. 12. Time histories of fuzzy input variables and output variable SF

By observing the measurement residual errors (innovations) that define the difference between actual measurements and measurement estimates predicted by the Kalman filter, the performance of the integrated navigation Kalman filter can be assessed. Theoretically, the residual errors should always lie within the filter-predicted standard deviation bounds. If GPS accuracy deterioration can be captured properly, using fuzzy logic adaptive tuning, then the Kalman filter error state estimates should remain 'near optimal', even during intervals of significant maneuvering. Adaptive tuning comparisons are shown for a flight in which a racetrack pattern is negotiated, followed by a series of dynamic flight test maneuvers. With no adaptive tuning being used, Figs. 13 and 14 show the residual errors and their Kalman filter-predicted standard deviations (dashed lines) for GPS horizontal position and horizontal velocity measurements. Note that the measurement noise statistics used for this comparison are not conservative, and reflect the situation during the benign, non-dynamic parts of the flight. As a result, the residual errors exceed the 1-sigma bounds whenever significant maneuvering occurs, especially towards the end of the flight. Figures 15 and 16 then show the same residual errors and associated standard deviations, but now with fuzzy logic adaptive tuning being used. With adaptive tuning, the 1-sigma bounds are computed at much higher levels during the dynamic maneuvers – a direct result of the 'scaling up' of the GPS measurement noise specifications. The residual errors now stay within the 1-sigma bounds, even during the most dynamic of the maneuvers, indicating a well-tuned Kalman filter. Also, with adaptive tuning, Kalman filter estimates of accelerometer offsets no longer develop artificial biases of several milli-g – another indication that the Kalman filter is working optimally. Being near optimal, adaptive tuning produces more accurate error state estimates, as indicated by the associated Kalman filter 1-sigma uncertainty bounds (not shown), especially during non-dynamic parts of a flight where the GPS measurement noise statistics have smaller values. And, as has been observed in some instances, this can be especially beneficial for improving heading angle accuracy. With the current hardware, the Kalman filter without adaptive tuning takes 12.5 milliseconds of compute time, and the adaptive tuning only takes an extra 300 microseconds. Thus, including the adaptive tuning algorithm will not add much overhead to the Kalman filter for a real-time implementation.

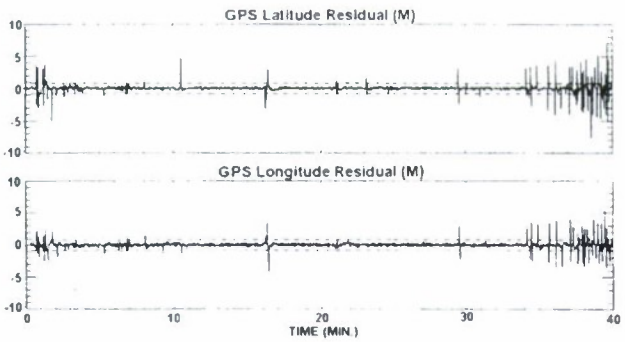

Fig. 13. GPS horizontal position residual time histories without adaptive tuning

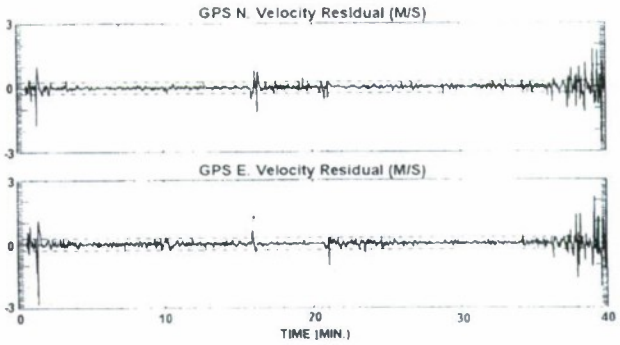

Fig. 14. GPS horizontal velocity residual time histories without adaptive tuning

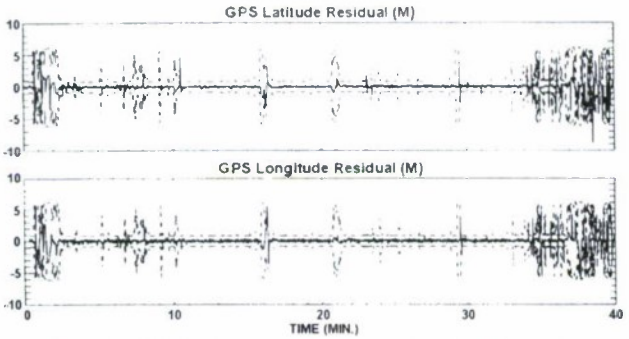

Fig. 15. GPS horizontal position residual time histories with adaptive tuning

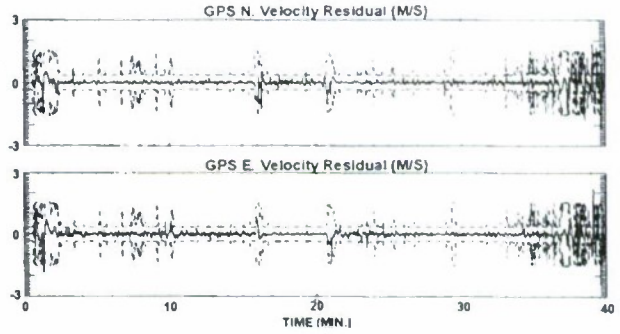

Fig. 16. GPS horizontal velocity residual time histories with adaptive tuning

Conclusions

1. A physically compact real-time strapdown navigator, based on a Litton LN-200 strapdown IMU integrated with a NovAtel RT-20 DGPS receiver, has been successfully flight tested on-board the NRC Bell 206 research helicopter.

2. The real-time performance of the strapdown navigator's alignment and navigation software compares well with results using off-line versions of the software.

3. A fuzzy logic adaptive tuning algorithm provides accurate real-time tuning of the GPS measurement noise variances to reflect maneuver-induced GPS accuracy deterioration, without adding much computational burden to the navigation Kalman filter.

4. Based on the performance seen to date, this integrated strapdown navigator is now being developed as the primary source of inertial navigation data on-board several NRC research aircraft, resulting in potential savings of $500,000.

5. Future work will concentrate on further enhancements to the fuzzy logic adaptive tuning algorithm to optimize its performance under all dynamic conditions. As well, consideration will be given to the potential cost / benefits of including a heading sensor (e.g., a directional gyro) as part of the integrated navigation package.

References

1. **Leach B.W.** Low Cost Strapdown Inertial/GPS Integrated Navigation for Flight Test Requirements // 6th Saint Petersburg International Conference on Integrated Navigation Systems – May 1999. RTO-MP-43 – P. 17-1 – 17-12. 2.
2. **Leach B.W., Hui K.** Flight Test Applications of Kalman Filter-Based Integrated Navigation Systems Using Differential GPS // Proceedings of 7th Saint Petersburg International Conference on Integrated Navigation Systems – May 2000. Saint Petersburg, Russia.
3. **Savage P.G.** Strapdown Analytics Part 1 and Part 2 // Strapdown Associates, Inc., Maple Plain, Minnesota, 2000.
4. **Maybeck P.S.** Stochastic Models, Estimation and Control Volume 1 // Academic Press, New York, 1979.
5. **Bierman G.J.** Factorization Methods for Discrete Sequential Estimation // Academic Press, New York, 1977.
6. Aeronautical Design Standard, Handling Qualities Requirements for Military Rotorcraft, ADS-33D // U.S. Army Aviation and Troop Command, St. Louis, MO, July 1994.
7. **Driankov D., Hellendoorn H., Reinfrank M.** An Introduction to Fuzzy Control // Springer-Verlag, Berlin, 1993.
8. **Tahani H., Keller J.M.** Information Fusion in Computer Vision Using the Fuzzy Integral // IEEE Trans. On Systems, Man and Cybernetics – 1990. Vol. 20 – No. 3 – P. 733-741.
9. **Rahbari R.** A New Inference Method for Multivariable Fuzzy Systems with Application in Industrial Control // Ph.D. Thesis, Department of Mechanical Engineering, The University of British Columbia, Vancouver, Canada, 2001.

INTEGRATED INERTIAL-SATELLITE SYSTEMS OF NAVIGATION, ATTITUDE CONTROL AND EXTERNAL TRAJECTORY MONITORING OF THE ORBITAL INJECTION VEHICLES. STRATEGY OF SYNTHESIS, CREATION EXPERIENCE AND ON-EARTH DEVELOPMENT RESULTS

V.D.Dishel *
N.A.Pylugin Automatics & Instruments Scientific Production Center (AISPC), Moscow, Russia
Vvedenscy st, 1, 117342, Moscow, Russia E-mail: nicolas@email.ru Fax 330-53-29

Abstract

Key words: filtering, navigation, algorithms, accuracy

The paper contains a united approach to synthesis of hybrid integrated system based on hardware and software combination of inertial and satellite navigation systems using GLONASS/GPS technologies systems and results of work aimed at the creation of them.

Schemes for hardware and software combination are designed, as well as block diagrams for the inertial control system with optimization of its elements' sensitivity axes orientation and the necessary redundancy level provision. The results attained using the advances in design and manufacturing of inertial instruments and satellite navigation equipment give us an opportunity to create control systems without traditional three-axis gyrostabilized platforms.

. It is shown that the main problem when using the hybrid integrated systems is to identify the inertial instrument coordinate system attitude errors and the gyro drifts. A generalized criterion is proposed taking into account the errors of the navigation problem solving as well as the inertial instrument coordinate system attitude errors. A unified approach to synthesis of Bayes-type algorithms being stable in the presence of disturbances and efficient from the computational point of view.

In the end of the report means and methods of on-earth development of systems with satellite navigation equipment included in the control loop are described based on the example of the integrated inertial-satellite control system for "Fregat" booster created in the AISPC. During flight test planned for the nearest future we hope to confirm the possibility of productive cooperation of inertial and satellite navigation systems

Introduction

A program of cardinal renovation of all the orbital injection vehicles is held now in Russia. Not only the existing vehicles are modernized, but also new launchers are developed, such as "Avrora", "Angara", "Fregat" and "Korvet" boosters and other.

Control systems for advanced cosmic missile complexes must resolve a much wider set of problems in order to fulfill the following tasks:

- ✓ implementation of new energetically profitable strategies of spacecraft orbital injection to different orbits using high-apogee schemes, including such orbits as geostationary(GSO) orbit with preliminary low-orbit phase control,
- ✓ launcher and booster control in case of launching from a vehicle including "air launch" using ANT-124 aircraft without loss of precision of the main problem solution,
- ✓ control of the descending parts in order to save them and use again many times ("Angara" launcher with rescued stage "Baikal"). Having the aforesaid in mind one can see that a search for new advantageous methods of navigation and attitude control systems which constitute the heart of control systems, solving the main part of the new problems, begins to play a great role.

Researches which were held in the state-owned enterprize AISPC during more than 20 years show that the main road for control systems development which provide the best solution of the enumerated problems with simultaneous achievement of radically new level of important parameters like precision, capability of self-contained functioning, multi-purposeness, weight and power consumption, comprises creation of hybrid integrated system based on hardware and software combination of inertial and satellite navigation systems using GLONASS/GPS technologies.

The efficiency of use of the GLONASS/GPS receivers in structure system of guidance and navigation of considered types of objects in many respects is defined by , as far as correct there was a way integration it with INS. It is caused by necessity of maintenance of close functioning INS and GLONASS/GPS receivers on considered active phase of flight.

The paper contains a united approach to synthesis of such systems and results of work aimed at the creation of them. In the framework of this approach it is shown that the requirement for reliable operation of hybrid integrated systems necessitates cooperative handling of the information from the inertial navigation system and

* Ph.D., Associate professor, Chief of Department of Complex Systems for Navigation, Guidance & Attitude Control

from the satellite navigation equipment beginning from the primary stage. The role and place of these systems are refined, and the specifications of the precision and operation parameters are justified for different launch conditions, different missions and so on. Schemes for hardware and software combination are designed, as well as block diagrams for the inertial control system with optimization of its elements' sensitivity axes orientation and the necessary redundancy level provision. The results attained using the advances in design and manufacturing of inertial instruments and satellite navigation equipment give us an opportunity to create control systems without traditional three-axis gyrostabilized platforms. We plan to use strapdown inertial systems instead. It is shown that the main problem when using the hybrid integrated systems is to identify the inertial instrument coordinate system attitude errors and the gyro drifts. A generalized criterion is proposed taking into account the errors of the navigation problem solving as well as the inertial instrument coordinate system attitude errors. A unified approach to synthesis of Bayes-type algorithms being stable in the presence of disturbances and efficient from the computational point of view. These algorithms provide periodic coordinate definition, velocities computation and identification of attitude errors as well as of the gyro drifts with the help of joint processing of signals from the aecelerometers, rotation velocity meters and from the satellite navigation equipment. An important advantage of the achieved results is the tolerance to coarse (1,0 ÷1,5 degrees) aimingf the command instruments complex before the start. Some special measures are designed in order to ensure stable operation of the satellite navigation equipment at different flight stages. Algorithms of inertial and satellite systems timing and fast algorithms of the movement equations integration are developed as well. Thanks to the aforementioned measures combined with special strategy of satellite navigation equipment sessions conduction navigation and attitude problem is solved with great precision. This leads to great precision of the orbital injection. Fro example, errors when putting a spacecraft to a geostationary orbit even from a movable start platform (air of sea) are 2÷4 times less than in case of control systems based on traditional stabilized-platform-type inertial navigation systems without correction.

A system of the described type is planned to use as well as a base for control systems of the separated rescued shuttle-type stages "Baikal". An analysis performed had shown that the flight conditions of this stage and precision requirements providing its soft landing in the destined area exclude practically design of a control system based on approaches different from those proposed in this paper. Specifically, the traditional inertial navigation systems with stabilized platform fail to success first of all as the result of limits caused by angles of gyrostabilized platform rotation.

In the end of the report means and methods of on-earth development of systems with satellite navigation equipment included in the control loop are described based on the example of the integrated inertial-satellite control system for "Fregat" booster created in the AISPC. During flight test planned for the nearest future we hope to confirm the possibility of productive cooperation of inertial and satellite navigation systems.

1. Statement of the task. Principles of an integration of inertial and satellite systems

Let's consider driving plant on the active legs with a large gang of an apparent velocity. This case envelops all types of tools of deduction of space-rocket engineering, including phases of launch of the launcher, accelerating and departure impulses booster [6], [7], flight of recoverable stages of the launcher after separating, descent vehicles and orbiters such as "«Buran", "«Shuttle" in atmosphere [5].

Let's consider(count), that the onboard control system has an inertial system (INS) or strapdown type (SINS), permitting with a desired frequency to measure parameters of an angular position of plant and vector of an apparent velocity.

The effectiveness of usage of instrumentation of satellite navigating (GLONASS/GPS receiver) in a structure system of guidance & navigation of considered types of plants in many respects is determined by , as far as valid there was a mode of an integration her(it) with INS. It is stipulated by necessity of security of tight operation INS and GLONASS/GPS receiver on the considered active legs of flight.

From performances INS by major is the high operational reliability, intrinsic to such systems, and guaranteed elimination of situations with miss of the information even during short time slices. It also predetermines that circumstance, that the integration should be produced in a condition of correction of the information INS with the help of the corrections which have been worked out GLONASS/GPS receiver. In such hybrid module GLONASS/GPS receiver fulfills, mainly, functions of instrumentation, ensuring reception of the measuring and digital information from selected navigation satellites and transmission them in on - board computer. The tasks of scheduling of time of realization of sessions, selection working navigation satellites , handling of the obtained measurements are decided in on - board computer. Such mode of an integration of the information allows maximum to take into account singularities of flight of considered types of plants, in particular possibility of their significant angular changes of aircraft attitude during sessions of navigational measurements, multiply to lower a stream of the information between on - board computer and GLONASS/GPS receiver, to reduce delays in usage of outcomes of sessions GLONASS/GPS receiver, that on the active legs is in essence important, to increase an exactitude of navigational definitions, to supply their reliability and reliability. The latter is reached

because during primary and secondary information processing it is possible to supply monitoring on reliability worked out in on – board computer of the navigational corrections by their comparison with practically faultless concerning reliability with output datas INS.

The significant g-loads and large gang of an apparent velocity on the active legs reduce in high rate of increase of errors of navigating because of errors of an inertial system, especially of errors of orientation of its coordinate instrumental base in an inertial system of coordinates.

Let's deliver the task of joint definition of an orthogonal matrix C, describing orientation of a stopway, and state vector $\mathbf{x}$, outgoing from a condition of minimization in some instant t_i magnitudes

$$J(C,\mathbf{x})=\frac{1}{2}\sum_{i=1}^{n}a_i\left(\mathbf{d}_i(\mathbf{x})-C_i\mathbf{d}_{p_i}(\mathbf{x})\right)^{\tau}\left(\mathbf{d}_i(\mathbf{x})-C_i\mathbf{d}_{p_i}(\mathbf{x})\right)+\frac{1}{2}(\mathbf{x}-\mathbf{x}^{-})^{\tau}W^{-}(\mathbf{x}-\mathbf{x}^{-}), \tag{1.1}$$

where J – criterion of an optimality,

C_i – some unknown orthogonal matrix, defining orientation frame of body concerning an initial inertial system of coordinates in an instant t_i,

$\mathbf{x}$ – m-component state vector which is not including parameters of orientation,

a_i – non-negative weighting coefficients everyone of vector $\mathbf{d}_i$,

τ – numeral of a transposition,

W^{-} – symmetrical positively semi-definite weight matrix,

The superscript "$^{-}$" for parameter concerns to his(its) a priori value.

Matrix C_i obeys to conditions of an orthogonality

$$C_i^{\tau}C_i=E, \qquad \det C_i=1 \tag{1.2}$$

Let's suppose, that two groups of parameters are accessible to measurement:

Three-dimensional unit vectors $\mathbf{d}=(d_1,d_2,d_3)^{\tau}$, assigned by projections (d_1,d_2,d_3) on an axis(axes) orientation frame of body . These measurements and calculated values, appropriate to them, $\mathbf{d}_{p_i}$ are connected by a relation

$$\mathbf{d}_i=C_i\mathbf{d}_{p_i}+\alpha_i, \qquad i=\overline{1,n}, \tag{1.3}$$

where $\alpha_i=(\alpha_{i_1},\alpha_{i_2},\alpha_{i_3})^{\tau}$ – vector of errors of measurements;

Vectors $\mathbf{h}$, connected with state vector $\mathbf{x}$ by a relation

$$\mathbf{h}_j=\mathbf{h}_j(\mathbf{x})+\mathbf{v}_j, \quad j=\overline{1,k}, \tag{1.4}$$

where $\mathbf{v}_j$ – error of measurements of vectors $\mathbf{h}_j$.

Let's consider(count), that a matrix C and the vectors of errors α_i, $\mathbf{v}_j$ belong to to known sets Ωc, $\Omega\alpha$ and Ωv accordingly.

According to criterion (1.1) matrixes C are in view of expressions (1.2) of a condition

$$\hat{C}(t)=argmin\,J(C), \tag{1.5}$$

where

$$\hat{C}(t)=\Phi(t,t_i,\mathbf{x})\hat{C}_i, \tag{1.6}$$

Φ – fundamental matrix of plant of control.

On the basis of properties of a matrix Φ we have

$$\hat{C}_i=\Phi(t_i,t,\mathbf{x})\hat{C}(t)=\Phi^{\tau}(t_i,t,\mathbf{x})\hat{C}(t) \tag{1.7}$$

Criterion (1.1) with registration (1.2) and properties of a track of a matrix can be submitted(shown) as

$$J=\sum_{i=1}^{n}a_i-\mathrm{tr}\left[C(t)P^{\tau}(t,\mathbf{x})\right]+\frac{1}{2}(\mathbf{x}-\mathbf{x}^{-})^{\tau}W^{-}(\mathbf{x}-\mathbf{x}^{-}), \tag{1.8}$$

where tr – label of a track of a matrix,

$P(t,\mathbf{x})$ – matrix of dimension (3x3), defined expression

$$P(t,\mathbf{x})=\sum_{i=1}^{n}a_i\Phi(t,t_i,\mathbf{x})\mathbf{d}_i(\mathbf{x})\mathbf{d}_{p_i}^{t}(\mathbf{x}) \tag{1.9}$$

In outcome we come to following statement of the task. On a population of measurements (1.3) and (1.4) to find in some instant t_i satisfying to conditions (1.2) matrix $\hat{C}$, estimation of a matrix C, and estimation of state vector $\mathbf{x}$, supplying a minimum to criterion (1.8)

2. Optimum parameter estimation of orientation

From expression (1.8) implies, that its first term does not depend neither from With, nor on vector $\mathbf{x}$. Therefore for reaching a minimum (1.8), and consequently and (1.1), it is enough to supply a maximization of a track of a matrix product tr [C (t) PT (t, x)] in view of a condition (1.2) with simultaneous deriving of the best estimation (by criterion of a minimum of conditional risk) state vector $\mathbf{x}$.

As is known [3], [4], any rectangular matrix can be shown as the singular expansion. Applying this confirmation to a matrix P, we shall receive

$$P = UД V^{\mathrm{T}} \tag{1.10}$$

Where U, V – appropriate (3x3) orthogonal matrixes,

Д – scalar matrix (3x3) with non-negative diagonal factors, and

$$\delta_{11} \geq \delta_{22} \geq \delta_{33} \geq 0 \tag{1.11}$$

Substituting expansion (1.10) in criterion (1.8) and leaving in it(him) only terms depending on a matrix of orientation, we shall have

$$J'(\hat{C}) = \mathrm{tr}(\hat{C}UД V^{\mathrm{T}}) = \mathrm{tr}(ДG), \tag{1.12}$$

where

$$G = U^{\mathrm{T}}\hat{C}V \tag{1.13}$$

According to the theorem of Euler [2] any orthogonal transformation(conversion) it is possible to present by flat rotation assigned unit vector γ and turn angle β. The matrix of orthogonal transformation(conversion), in this case G, expresses through component of vector of Euler as follows

$$G = e^{\beta} = E_{3x3} + \beta + \frac{1}{2}\beta^2 + \frac{1}{3!}\beta^3 + \frac{1}{4!}\beta^4 + \ldots = E_{3x3} + \beta\frac{1}{\beta}\sin\beta + \beta^2\frac{1}{\beta^2}(1-\cos\beta),$$

where β – skew-symmetric matrix composed from components $\beta_1, \beta_2, \beta_3$ of vector of Euler.

As a matrix G orthogonal, [2]

$$G = e^{\beta} = \begin{bmatrix} \cos\beta + \gamma_1^2(1-\cos\beta) & \gamma_3\sin\beta + \gamma_2\gamma_1(1-\cos\beta) & \gamma_2\sin\beta + \gamma_3\gamma_1(1-\cos\beta) \\ -\gamma_3\sin\beta + \gamma_2\gamma_1(1-\cos\beta) & \cos\beta + \gamma_2^2(1-\cos\beta) & \gamma_1\sin\beta + \gamma_3\gamma_2(1-\cos\beta) \\ \gamma_3\sin\beta + \gamma_3\gamma_2(1-\cos\beta) & -\gamma_1\sin\beta + \gamma_3\gamma_2(1-\cos\beta) & \cos\beta + \gamma_3^2(1-\cos\beta) \end{bmatrix} \tag{1.14}$$

The vector $\gamma = (\gamma_1, \gamma_2, \gamma_3)^{\mathrm{T}}$ is the eigenvector of an initial orthogonal matrix G, appropriate to its(her) eigenvalue, equal 1.

Substituting a matrix (1.14) in expression (1.12), we shall receive

$$J'(\hat{C}) = \delta_{11}[\cos\beta + \gamma_1^2(1-\cos\beta)] + \delta_{22}[\cos\beta + \gamma_2^2(1-\cos\beta)] + \delta_{33}[\cos\beta + \gamma_3^2(1-\cos\beta)] \tag{1.15}$$

Taking into consideration (1.11) and condition $0 \leq \gamma_1^2, \gamma_2^2, \gamma_3^2 \leq 1$ is obtained, that the maxima $J'(\hat{C})$ is reached at $\beta = 0$. Then the optimum estimation of a matrix $\hat{C}_{\mathrm{opt}}$ is given by expression

$$\hat{C}_{\mathrm{opt}} = UV^{\mathrm{T}} \tag{1.16}$$

With usage of expression (1.10) matrixes $\hat{C}_{\mathrm{opt}}$ are accepted by(with) an aspect

$$\hat{C}_{\mathrm{opt}} = PVД^{-1}V^{\mathrm{T}}, \tag{1.17}$$

where $Д^{-1} = \mathrm{diag}\left(\delta^{-1}{}_{11}, \delta^{-1}{}_{22}, \delta^{-1}{}_{33}\right)$.

We form a matrix of product $P^{\mathrm{T}}P$

$$P^{\mathrm{T}}P = V Д^2 V^{\mathrm{T}} \tag{1.18}$$

$$L^{-1} = VД^{-1}V^{\mathrm{T}}, \tag{1.19}$$

where

$$L = (P^{\mathrm{T}}P)^{1/2}, \tag{1.20}$$

And matrix L – symmetrical.

In outcome the optimum matrix $\hat{C}_{\mathrm{opt}}$ is from expression

$$\hat{C}_{\mathrm{opt}} = PL^{-1} \tag{1.21}$$

The grade of a matrix P is determined by a system of vectors $\mathbf{d}_i$ $(i = \overline{1,n})$. If among $\mathbf{d}_i$ There is even one triple of non-coplanar vectors, and the errors of measurements are rather insignificant, according to (1.21) definitions of optimum orientation is reduced to searching a squarc root from (3x3) of a matrix $\boldsymbol{P}$ and its eigenvalucs, i.e. diagonal units $\delta_{ii} > 0$, i =1,2,3.

The first task is decided with the help known [3], [4] procedures. Second – by searching the radicals of a characteristic polynomial of a matrix P

$$\det(\lambda \boldsymbol{E} - \boldsymbol{P}) = \lambda^3 - b_1\lambda^2 + b_2\lambda - b_3$$

With factors [4]

$$b_1 = tr\boldsymbol{P} = \sum_{i=1}^{3} \delta_{ii}, \quad b_2 = tr(\hat{\hat{\boldsymbol{P}}}), \quad b_3 = det\boldsymbol{P} = \prod_{i=1}^{3} \delta_{ii}, \tag{1.22}$$

Where $\hat{\hat{\boldsymbol{P}}}$ – affixed (3x3) a matrix for a matrix $\boldsymbol{P}$.

Let's discover connection of a factor b_1 and optimum estimation of a matrix. Let's consider product $\boldsymbol{P}^T\hat{\boldsymbol{C}}_{opt}$. With the registration (1.10) and (1.16) we have

$$\boldsymbol{P}^T\hat{\boldsymbol{C}}_{opt} = \boldsymbol{V}\ \boldsymbol{Д}\ \boldsymbol{V}^T \tag{1.23}$$

Then

$$tr\ (\boldsymbol{P}^T\hat{\boldsymbol{C}}_{opt}) = \sum_{i=1}^{3} \delta_{ii} = b_1 \tag{1.24}$$

If all vectors $\mathbf{d}_i$ $(i = \overline{1,n})$ lie in one plane, the matrix $\boldsymbol{P}$ – is dcgenerated. However, if among $\mathbf{d}_i$ There is even one pair linearly independent, i.e. not collinear vectors, the optimum matrix can be retrieved and in this case. For this purpose to evocative pair it is necessary to add vector component with it(her) non-coplanar triple, it is best – orthogonal initial plane. If it is more than not collinear vectors two, among them it is necessary to find a pair, most close to orthogonal and, as well as in the previous case to complete a system of initial coplanar vectors by a basis vector, orthogonal initial plane. Obviously, that at set values of errors of measurements and worst character of their distribution the maximum exactitude will be reached, if this triple consists of mutually orthogonal vectors.

Using properties of an affixed matrix from expression (1.10), we shall receive:

$$\hat{\hat{\boldsymbol{P}}}^T = (\boldsymbol{P}^T)^{-1}\det(\boldsymbol{P}^T) = (\boldsymbol{U}\boldsymbol{Д}^{-1}\boldsymbol{V}^T)\prod_{i=1}^{3}\delta_{ii} = \boldsymbol{U}\boldsymbol{Д}^*\boldsymbol{V}^T \tag{1.25}$$

where

$$\boldsymbol{Д}^* = \mathrm{diag}(\ \delta_{22}\delta_{33}, \delta_{11}\delta_{33}, \delta_{11}\delta_{22}\ ) \tag{1.26}$$

The expansion (1.25) allows to note

$$\hat{\hat{\boldsymbol{P}}}^{\frac{1}{2}} = \boldsymbol{U}\left(\boldsymbol{Д}^*\right)^{\frac{1}{2}}\boldsymbol{V}^T, \tag{1.27}$$

where

$$\hat{\hat{\boldsymbol{P}}} = \hat{\hat{\boldsymbol{P}}}^{\frac{1}{2}}\hat{\hat{\boldsymbol{P}}}^{\frac{1}{2}} \tag{1.28}$$

Let's consider now particular case of two observable vectors. From expressions (1.11), (1.22) follows

$$\delta_{33} = 0, \quad b_3 = 0, \quad \mathrm{rang}(\boldsymbol{P}) \le 2 \tag{1.29}$$

The secular equation accepts an aspect $\lambda^2 - b_1\lambda + b_2 = 0$,

And $\delta_{11} > 0; \quad \delta_{22} > 0; \quad \delta_{11} \ge \delta_{22}.$ (1.30)

Then

$$b_1 = \delta_{11} + \delta_{22}; \quad b_2 = tr\left(\hat{\hat{\boldsymbol{P}}}\right) = \delta_{11}\delta_{22} > 0 \tag{1.31}$$

as in this case $\hat{\hat{\boldsymbol{P}}}$ is symmetrical, for factors b_2, b_1 we shall have

$$b_2 = tr\left(\hat{\hat{\boldsymbol{P}}}\right) = \sum_{i=1}^{3}\left(\hat{\hat{\boldsymbol{P}}}_{ij}^{\frac{T}{2}}\right)^2$$

or

$$b_2 = a_1a_2\sqrt{(\boldsymbol{\Phi}_{t,t1,x}\boldsymbol{\Phi}_1 \times \boldsymbol{\Phi}_{t,t2,x}\boldsymbol{\Phi})^T(\boldsymbol{\Phi}_{t,t1,x}\boldsymbol{\Phi}_1 \times \boldsymbol{\Phi}_{t,t2,x}\boldsymbol{\Phi}_2)\cdot(\boldsymbol{\Phi}_{p1} \times \boldsymbol{\Phi}_{p2})^T(\boldsymbol{\Phi}_{p1} \times \boldsymbol{\Phi}_{p2})} \tag{1.32}$$

$$b_i = \sqrt{a_1^2 + a_2^2 + 2a_1 a_2 \cos(\xi - \xi_p)}, \qquad (1.33)$$

where about and about p – angles between vectors $\Phi_{t_j/1.x} d_1$ and $\Phi_{t_j/2.x} d_2$ and vectors $\mathbf{d}_{p_1}$ and $\mathbf{d}_{p_2}$ accordingly, and it is supposed, that 0 < about < p and 0 < about p < p.

3. Mathematical models used at measurement of apparent parameters with the help GLONASS/GPS receiver

Let's consider now application of the obtained outcomes for identification of errors of orientation of frame of body on the active legs of flight.

The equations of driving of a center of mass in an inertial system of coordinates(co-ordinates), as is known, look like

$$\frac{d\mathbf{V}}{dt} = \mathbf{g}(\mathbf{r}) + \dot{\mathbf{w}}; \qquad \frac{d\mathbf{r}}{dt} = \mathbf{V}, \qquad (2.1)$$

Where $\mathbf{V}$, $\mathbf{r}$ – velocity vector and position vector of plant generatrix state vector $\mathbf{x} = (\mathbf{V},\mathbf{r})^T$, $\mathbf{g(r)}$ – vector of gravitational acceleration, $\dot{\mathbf{W}}(\mathbf{t})$ – acceleration vector of forces of a not gravitational nature (apparent acceleration), mejeriment with the help of accelerometers of an inertial system.

For plants of spacc-rocket engineering connection between measured and actual values of vector of an apparent velocity is possible to set as

$$w_u(t) = C\, w(t) + \alpha_{w_i}, \qquad (2.2)$$

where

$$\mathbf{w(t)} = \int_{t_{j-1}}^{t} \dot{\mathbf{w}}(\mathbf{t})d\tau, \qquad (2.3)$$

C – unknown orthogonal matrix, which determines errors of orientation of a stopway in the CLAIM. Unknowns component of installation errors of accelerometers here concern also.

We shall recognize that all sessions of deriving and the handlings of the information from onboard receiver GLONASS/GPS are divided on two types: – standard and generalized. On first the definition (improvement) only of navigational parameters is made. On second – definition (improvement) both navigational parameters, and parameters of orientation. such separation is connected that the transients on components of state vector $\mathbf{x} = (\mathbf{V},\mathbf{r})^T$, describing a position of a center of mass, flow past faster, than on components describing orientation of frame of body . Therefore, using a principle of timing separation of processes of an estimation of fast and slow variables, an estimation of parameters C and $\mathbf{x} = (\mathbf{V},\mathbf{r})^T$ we shall conduct with a miscellaneous interval of a discretization.

We linearize a system (2.1) concerning a navigational search pattern. Then

$$\frac{d\Delta\dot{\mathbf{x}}}{dt} = F_x(\mathbf{x})\Delta\mathbf{x} + F_{\dot{w}}\,\Delta\dot{\mathbf{w}}(t), \qquad (2.4)$$

where Fx = $\frac{\partial F}{\partial \mathbf{x}}$, F? = $\frac{\partial F}{\partial \dot{\mathbf{w}}}$ – matrix of partial derivatives from vector of right members of a system (2.1) on state vector x and vector $\dot{\mathbf{w}}$ accordingly.

Solution of this linearized system shall present as [1]

$$\Delta\mathbf{x}(t) = \Phi(t)\Delta\mathbf{x}(t_{i-1}) + \Phi(t)\int_{t_{i-1}}^{t} \Phi^{-1}(\tau)F_{\dot{w}}\Delta\dot{\mathbf{w}}(\tau)d\tau, \qquad (2.5)$$

Where $\Delta\mathbf{x}(\mathbf{t}_{i-1}) = (\Delta\mathbf{v}(\mathbf{t}_{i-1}), \Delta\mathbf{r}(\mathbf{t}_{i-1}))^T$ vector of nautical faults in the moments (t_{i-1}, $i = 1,2,.....$) of realization of the generalized navigational sessions.

Is decomposable matrixes $\Phi(t)$, $\Phi^{-1}(t)$, $F_{\dot{w}}$ in a series(line) Tcylora on degrees $(t - t_{on})$, where t_{on} – refcrence value, $t_{i-1} \le t_{on} \le t$, and $\Phi(t_{on}) = E$. Here E – unit matrix of a size (6 ' 6). supposing it is as a matter of convenience $t_{on} = t_{i-1}$, to within the second terms of expansion we shall receive

$$\Phi(t) = E + F_x(x)(t - t_{on}) + \frac{1}{2}\left(\dot{F}_x + (F_x)^2\right)(t - t_{on})^2$$

$$\Phi^{-1}(t) = E - F_x(x)(t - t_{on}) - \frac{1}{2}\left(\dot{F}_x + (F_x)^2\right)(t - t_{on})^2 \qquad (2.6)$$

$$F_{\dot{w}}(t) = F_{\dot{w}}(t_{on}) + \dot{F}_{\dot{w}}(t - t_{on}) + \frac{1}{2}\ddot{F}_{\dot{w}}(t - t_{on})^2$$

Substituting the last relations in expression (2.5), after some transformations(convcrsions) we shall receive

$$\Delta x(t) = [E + (t - t_{on})C_{-1} + \frac{1}{2}(t - t_{on})^2 C_{tt}]\Delta x(t_{i-1}) + C_0 U_0(t) + (t - t_{on})C_t U_0(t) + C_\tau U_1(t) +$$

$$+ \frac{(t - t_{on})^2}{2} C_{tt} U_0(t) + (t - t_{on})C_{t\tau} U_1(t) + C_{\tau\tau} U_2(t), \qquad (2.7)$$

where following labels are entered as a matter of convenience

$$C_{-1} = F_x;\ C_0 = F_{\dot{w}};\ C_t = F_x F_{\dot{w}};\ C_\tau = \dot{F}_{\dot{w}} - F_x F_{\dot{w}};\ C_{tt} = \dot{F}_x + F_x^2; \qquad (2.8)$$

$$C_{t\tau} = F_x \dot{F}_{\dot{w}} - F_x^2 F_{\dot{w}};\quad C_{\tau\tau} = F_x^2 \dot{F}_{\dot{w}} - \dot{F}_x F_{\dot{w}} - 2F_x \dot{F}_{\dot{w}} + \frac{1}{2}\ddot{F}_{\dot{w}}$$

$$U_k(t) = \int_{t_{i-1}}^{t} \frac{(\tau - t_{on})^k}{k!} U(\tau)d\tau;\quad U(\tau) = \Delta\dot{W}(\tau) = \dot{W}(\tau) - \dot{W}_{\text{н}}(\tau) \qquad (2.9)$$

Returning to equations (2.1) and substituting cxpressions, appropriate to this equations, for matrixes of partial derivatives in (2.7), we shall receive

$$\Delta v(t) = \Delta v(t_{i-1}) + (t - t_{on})G\left[\Delta r(t_{i-1}) + 0{,}5(t - t_{on})\Delta v(t_{i-1})\right] + 0{,}5(t - t_{on})^2 \dot{G}\Delta r(t_{i-1}) +$$

$$+ \Delta w + G\int_{t_{i-1}}^{t} \Delta w(\tau)d\tau + \sum_{\upsilon=1}^{l} \delta v(t_\upsilon) + G\left[\sum_{\upsilon=1}^{l}\int_{t_\upsilon}^{t}\int \delta v_\upsilon(\tau)d\tau + \sum_{\upsilon=1}^{l}\int_{t_\upsilon}^{t} \delta r_\upsilon(\tau)d\tau\right] + \qquad (2.10)$$

$$+ \dot{G}\left[(t - t_{i-1})\sum_{\upsilon=1}^{l}\int_{t_\upsilon}^{t} \delta r_\upsilon(\tau)d\tau + \sum_{\upsilon=1}^{l}\int_{t_\upsilon}^{t}\int \delta r_\upsilon(\tau)d\tau\right],$$

where $\delta v_\upsilon(t) = v_{\text{н}}^{+}(t) - v_{\text{н}}^{-}(t)$; $\delta r_\upsilon(t) = r_{\text{н}}^{+}(t) - r_{\text{н}}^{-}(t)$; $\Delta w = U_0(t) = \int_{t_{i-1}}^{t} \Delta\dot{W}(\tau)d\tau$,

$v_{\text{н}}^{+}(t)$, $r_{\text{н}}^{+}(t)$ Navigational state vector in the moment t after an improvement in the moment t_ν ($t_\nu \le t$),

$v_{\text{н}}^{-}(t)$, $r_{\text{н}}^{-}(t)$ – value on the moment t of the same state vector in the supposition, that in the next moment t_ν the improvement was not produced,

$\delta v_\upsilon(t)$, $\delta r_\upsilon(t)$ – vector of discrepancies of navigational velocitics and coordinates(co-ordinates),

t_ν , $\nu = 1,2,3,...,\ l$ the momcnts, in which arc made improvements in standard navigational scssions. It is supposed, that on an interval $[t_{i-1}, t]$ is conducted l of such sessions,

$G = \frac{\partial g}{\partial r}$, $\dot{G}$ – matrix of a gravitational gradient and its(her) derivative(derivative) on time accordingly

$$G = \frac{\mu}{r^3}\left(3r^0 \cdot r^{0T} - E\right);\ \dot{G} = \frac{3\mu}{r^4}\left((v^T \cdot r^0)E - 5(v^T \cdot r^0)(r^0 \cdot r^{0T}) + (v \cdot r^{0T}) + (r^0 \cdot v^T)\right),$$

where r^0 – single position vector, μ – the gravity parameter is central of an attracting skew field.

The expressions for matrixes G and $\dot{G}$ are obtained for is central of an attracting skew field.

The formula (2.10) determines a deviation of vector of a navigational vclocity from an actual value to a flowing instant t in view of thc sessions, conducted on an interval, of navigational definitions.

Summarized deviation develops from:

- of navigational errors in the beginning of an interval t_{i-1} and thcir extrapolation by the currcnt moment t,
- of errors of vector of an apparcnt velocity incrtial system, stipulated by errors,
- of error of estimations updated with the help of standard navigational sessions, spent on a considered interval, of a search pattern.

The expression (2.10) allows on measurements receiver GLONASS/GPS to define(determinc) vcetor of errors of an apparent velocity. Really, we shall seleet the moment t conterminous with the moment of realization of the next generalized session, i.e. $t = t_i$. Let's suppose, that the exactitude receiver GLONASS/GPS is suffieient, that it was possible to eonsider(eount) error of estimation $\Delta v(t_{i-1}), \Delta r(t_{i-1})$ in the beginning of an interval and at the moment of an improvement $t = t_i$ $\Delta v(t_i) = v(t_i) - v_н^+(t_i)$ small as contrasted to as errors of an inertial system.

Integrating on an interval $[t_{i-1}, t]$ simultaneously in rate of flight of a set of equations

- Inertial navigation (analog of equations (2.1)) with accumulation on the basis(fundamentals) (2.3) observations of aeeelerometers and deriving $w_н(t_i)$,
- Updated driving (in view of spent on $[t_{i-1}, t]$ Standard navigational sessions),

In the moment $t = t_i$ we shall have veetor $v_н(t_i)$ (from the first system) and vector $v_н^+(t_i)$ – (from second). With their help, taking into consideration, that $\left| G \int_{t_{i-1}}^{t} \Delta w(\tau) d\tau \right| << |\Delta w(t)|$, from expression (2.10) we shall receive $\Delta w(t)$ and further estimation of veetor eolleeted on an interval $[t_{i-1}, t]$ of an apparent velocity $\hat{w}(t_i)(t_i) = w_н(t_i) + \Delta w(t_i)$.

proeessing logies, used in updated driving, of measurements of pseudo-distanee and the pseudo-velocities are built on the basis of minimization of eriterion (1.1) in the form(shape) of a special stable filter Kalman [5], [7]. Valued is the eight-measurement vector, first which six components consist of nautical faults of coordinates(eo-ordinates) (ΔL,Δr,ΔB) and velocities (ΔVL,ΔVr,ΔVb) plant in an orbital frame. Two represent others – fixed errors of distanee and radial velocity stipulated divergenees(separations) of phases and frequeneies of generators reeeiver GLONASS/GPS and navigation satellites.

4. Algorithm of an estimation of a matrix of orientation on the active legs of flight

Let's eonsider, that each active leg of flight is divided into a series of the above described intervals $[t_{i-1}, t]$. After their termination we obtain a population of veetors $w_н(t_i)$, $\hat{w}(t_i)$, (i =1,2,3 .....,) and their single analogs $w_н^0(t_i), \hat{w}^0(t_i)$. last it is possible to interprete as measurement such as (1.3). Let's limit by a case of conjugate measurements for two adjacent intervals $[t_{i-2}, t_{i-1}]$ and $[t_{i-1}, t_1]$ of the generalized sessions. Inside eaeh of them the standard sessions of navigational definitions will be earried out. Number of such sessions and their distribution it is enough, that the errors of orientation of above-stated unit vectors of an estimation were small as eontrasted to by turn angles, whieh is set by a required matrix C.

Let's construet of initial veetors the right orthogonal triples

$$\xi_+^0 = \frac{\hat{w}_{i-1}^0 + \hat{w}_i^0}{|\hat{w}_{i-1}^0 + \hat{w}_i^0|}; \quad \xi_-^0 = \frac{\hat{w}_{i-1}^0 - \hat{w}_i^0}{|\hat{w}_{i-1}^0 - \hat{w}_i^0|}; \quad \xi_\perp^0 = \xi_+^0 \times \xi_+^0;$$

$$\zeta_+^0 = \frac{w_{Hi-1}^0 + w_{Hi}^0}{|w_{Hi-1}^0 + w_{Hi}^0|}; \quad \zeta_-^0 = \frac{w_{Hi-1}^0 - w_{Hi}^0}{|w_{Hi-1}^0 - w_{Hi}^0|}; \quad \zeta_\perp^0 = \zeta_+^0 \times \zeta_-^0; \tag{2.11}$$

Then the optimum estimation of a matrix of orientation will be

$$\hat{C}_{opt} = 1/b_1 \cdot (\zeta_+^0 \xi_+^{0T} + \zeta_-^0 \xi_-^{0T}) \cos((\xi - \xi_p)/2) + (\zeta_+^0 \times \zeta_-^0)(\xi_+^0 \times \xi_-^0)^T \tag{2.12}$$

5. Structure of the integrated inertial – satellite system

In a control loop ereated in the last years in N.A.Pylugin Automatics & Instruments Scientifie Production Center (AISPC) of control systems of perspeetive tools of deduetion of the launeher "«Avrora", booster "«Corvette", "«Frigate", «Dm "- 03", launeher "«Flight" (project « Air start ») etc. is included 12-channel GPS/GLONASS reeeiver of spaee instrument making developed on a requirement speeifieation AISPC , and eompletely compatible on all aspeets of interfaees with other parts the inertial system of guidance & navigation. The strueture of GPS/GLONASS reeeiver is created outgoing from the requirement of seeurity of a high level of reliability during all operation life the inertial system of guidance & navigation. and consists of two independent eomplete sets. Now this integrated inertial – satellite system has passed all eyele of ground tests, both on

complex benches AISPC , and in a structure booster "«Frigate" in parent organization. During pilot-designer trials of plant, which should be held in a near future, will be, as it is expected, the possibility of effective joint activity of inertial and satellite systems of navigating is endorsed.

The successes, reached per the last years, in the field of creation of sensing probes of gyroscopic devices have allowed to begin projection of the strapdown inertial unit . On this base within the framework of a series, for example « the Gyroscope AI », forms the basis for universal high-precision strapdown integrated the inertial system of guidance & navigation by tools of deduction and space vehicle. Such system, being located on space vehicle, can supply control at all stages of flight of a space-rocket complex, since a pre-launch procedure, at stage of deduction and further during all time of maintenance of space vehicle on orbit.

6. Outcomes of mathematical modelling

For the analysis of quality of operation of offered algorithms and hardware structures the mathematical modelling of processes of navigating and definition of orientation on phases of launch of the launcher and accelerating impulses booster was conducted. Series of sessions of reception of the information with a special image selected navigation satellites GLONASS and GPS start at a stage of a pre-launch procedure for 15... 20 min up to a command of rise. The main purpose here consists in preliminary deriving of ephemerises those navigation satellites, which will be in a zone of the radioreview on phase of launch of the launcher. Further during flight everyone 40.. 50s. series of sessions of navigational definitions will be carried out. By results of coprocessing in onboard computer of the flowing observations INS and measurements from navigation satellites a method of a dynamic filtration the improvement of parameters of driving is carried out.

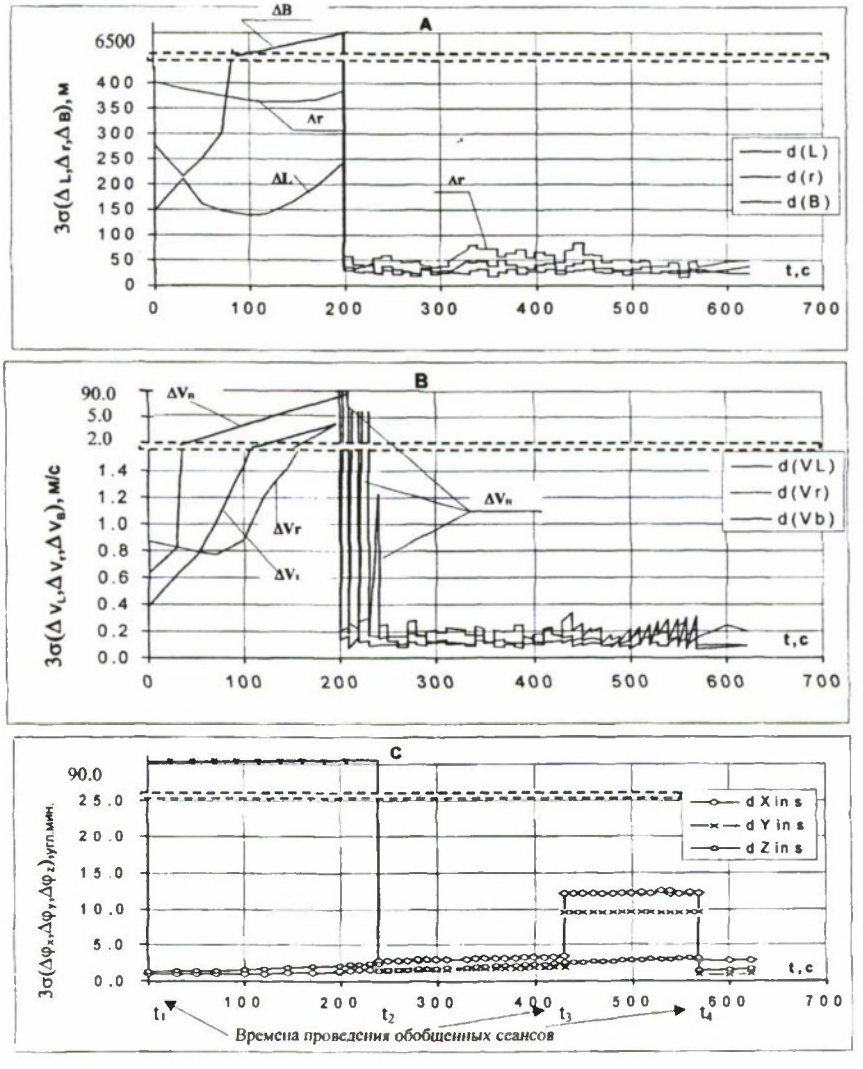

Limiting errors: coordinates(co-ordinates) (A), components of a velocity (B), parameters of orientation (C). Deductions of the launcher. $\Delta\varphi_Y(t_0) \le 90'$; $\Delta\varphi_X(t_0) = \Delta\varphi_Z(t_0) \le 1.0'$; $\Delta'\varphi_X = \Delta'\varphi_Y \le 0{,}3'$/min. $\Delta'\varphi_Z \le 0{,}4'$/min. Restricted visibility on start and in flight. Number navigation satellites < 5

On the initial stage of deduction the primal problem consists in possible earlier detection dominating among an other error of azimuth targeting strapdown intcgrated the inertial system of guidance & navigation . It is stipulated by rushing to reduce power losses, which are required on correction of a search pattern after an improvement of the indicated error. 3σ In model of errors GPS/GLONASS receiver and strapdown the inertial system all characteristic types of errors are included. Some outcomes of mathematical modelling are shown in a fig. (A,B,C). Definitions and calculations of navigational parameters on phase of launch of the launcher in an orbital frame – errors of coordinates as deviations in direction of radius of vector Δr, on a tangent in a search pattern ΔL and side direction and calculation of navigational parameters on phase of launch of the launcher in an orbital framc – errors of coordinates as deviations in direction of radius of vector Δr , on a tangent in a search pattern ΔL and side direction and calculation of navigational parameters on phase of launch of the of the launchcr in an orbital frame – knowledge, overstated as contrasted to by usual errors, of initial orientation of inertial tools $3\sigma(\Delta\varphi_y(t_0)) = 90'$ and restricted visibility navigation satellites. It is visible, what even in such complicated conditions the algorithms have shown steady operation on all phases of flight. To the extremity of deduction the rather high-prccision definition of all components of state vector is ensured. The similar picture is watched and during accelerating impulses fulfillcd on segments booster.

References

1. **R.Bellman.** Introduction to the Theory of Matrix, 1961.
2. **V.Branetz, I.Shmyglevsky.** Strapped-down Inertial Navigation Systems, M. 1992.
3. **F.Gantmather.** Theory of Matrix, 1967
4. **V.Voevodin, U.Kuznetsov.** Matrix and computation, 1984.
5. **V.D.Dishel, V.S.Lebedev.** Conceptual Basics of High Accuracy Navigation System for Space Shuttle Buran Lifting, Orbital Subarc, Descending and Landing on the Base of Information Composition from INS Satellite and Other Radiotechnique System. Proceeding of the First International Aerospace Conference, volume 6, pp 123-146, Moscow,28 September, 1992.
6. **V.D.Dishel, Y.V.Trunov, A.P Mezentsev, V.I.Reshetnikov.** Multi-Purpose Integrated Inertial-Satellite Attitude Control and Navigation System for Launchers, Boosters, and Spacecraft. The Institute of Navigation Proceedings of the 55th Annual Meeting, June 28-30,1999, Cambridge, MA, pp177-184.
7. **V.D.Dishel, V.L.Morgun.** Unified navigation system based on inertial navigation system and users navigation glonass and navstar systems. International aerospace congress, Theory, Applications, Technolog, Aug 15-19 1994, Moscow.

DEVELOPMENT AND PERFORMANCE ANALYSIS OF A TIGHTLY COUPLED GNSS/INS SYSTEM

B. Eissfeller*, Ch. Kreye, D. Sanroma**, Th. Lück****
Institute of Geodesy and Navigation (IfEN), University FAF Munich,
85577 Neubiberg (Germany), E-mail: Bernd.Eissfeller@unibw-muenchen.de

Abstract

Key words: GNSS performance, sensor integration, tight coupling

Apart from space and control segment the GNSS performance depends on several parameters, e.g. signal properties, multipath conditions, signal interruptions, signal-to-noise ratio, dynamics and receiver errors like thermal noise and oscillator instabilities.
The impact of these influences are based on the behaviour of the Phase Lock Loop (PLL) and the Delay Lock Loop (DLL) implemented in the GNSS receiver. To guarantee availability of a precise navigation solution the loop errors have to be significantly lower than the lock thresholds.
The first part of the paper presents investigations about the interaction of loop bandwidth, signal-to-noise ratio, accelerations, oscillator Allan variance and oscillator vibrations. In order to decrease the influence of receiver noise the tracking loop bandwidth has to be reduced. Consequently under high dynamic conditions or in a jamming environment the dynamics of the pseudoranges have to be removed from the loop signal to keep them in lock.
If the vehicle dynamics on the other hand is measured by a low cost INS, the range velocities, accelerations and higher derivatives can be computed by aid of inertial data.
In this context investigations about the different coupling principles between GNSS and INS are presented. With tight coupling the filtered INS-data is fed back directly into the GNSS receiver code and carrier tracking loops. A possible filter design for low cost INS-data and its transfer function are described.
In opposite to the unaided receiver the tightly coupled sensors are no longer depending on the accelerations but on the accelerometer bias and gyro drift behaviour of the INS. The Schuler frequency dominates the jitter value of the loops. The paper demonstrates that a gyro rate of approximately 1°/h is necessary to support the phase lock loop. Concerning the delay lock loop a gyro rate of 10°/h is sufficient.
In next part of the paper a simulation tool for a tightly coupled GPS/INS-Sensor is described. Used algorithms and sensor models are reviewed. The data flow beginning with original data and ending with the integrated navigation solution is presented. First simulation results are also shown. Advantages and problems of the coupled sensor system are mentioned.
The development of an experimental tight coupling system using the MITEL GPS Architect receiver and the LITTON LN-200 Inertial Measurement Unit is the key point of the final section of the paper. Besides hardware and software aspects methods of time synchronisation and data processing are addressed.

Introduction

The GNSS signal acquisition and tracking process is a two-dimensional signal replication process. In order to derive pseudoranges between satellite and receiver references of PRN code and the carrier frequency plus Doppler must be replicated and correlated with the incoming satellite signals. The signal generation is provided by a numerical controlled oscillator (NCO). The frequency alignment is controlled in a closed loop configuration. A basic structure of a delay (DLL) or phase lock loop (PLL) for a single SV is presented in figure 1.

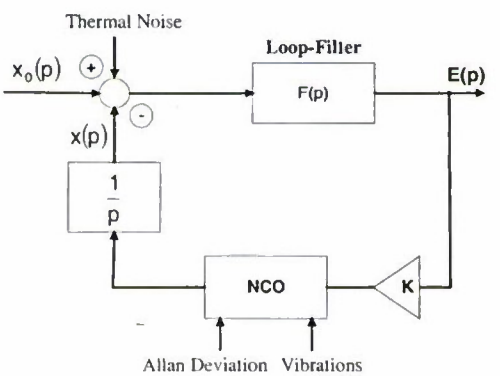

Figure 1. Rudimental delay or phase lock loop

* Univ.- Prof. Dr.- Ing., Vice-Director of the Institute of Geodesy and Navigation
** Dipl.- Ing. Research Associate

Only if this control loop is in lock pseudoranges and carrier phases can be obtained. When total GNSS measurement errors exceed the tracking threshold the receiver looses lock. These errors depend on carrier frequency f, signal to noise ratio C/N_0, preintegration time, loop bandwidth B_L, oscillator stability and receiver dynamics. As it can be seen in literature [e.g. WARD 1998] the rules-of-thumb concerning the tracking thresholds of PLL and DLL can be expressed by the following formulas:

$$\sigma_{PLL} = \sqrt{\sigma_T^2 + \sigma_A^2 + \sigma_V^2} + \frac{e(t)}{3} \leq 15^\circ \quad (1)$$

$$\sigma_{DLL} = \sqrt{\sigma_T^2 + \sigma_A^2 + \sigma_V^2} + \frac{e(t)}{3} \leq \frac{T_C}{6} \quad (2)$$

with

σ_{PLL}	PLL error	σ_{DLL}	DLL error
σ_T	Thermal noise (1-sigma)	σ_A	Allan variance oscillator jitter (1-sigma)
σ_V	Oscillator vibrations (1-sigma)	e(t)	Dynamic stress error
T_C	Chip length		

In relation to a GNSS like GPS using the L-band the tracking thresholds can be fixed to 8 mm for the phase lock loop and 5 m (Y) or 50 m (C/A) for the delay lock loop respectively.
As the first component of formula 1 and 2 the influence of the thermal noise should be investigated. Concerning the phase lock loop it can be obtained by the equation:

$$\sigma_T^2 = \frac{B_L}{C/N_0}\left(1 + \frac{1}{2 \cdot C/N_0}\right) \cdot \left(\frac{\lambda}{2\pi}\right)^2 \quad (3)$$

with λ carrier wave length
Depending on values for loop bandwidth and signal-to-noise ratio the resulting thermal noise can be presented in figure 2:

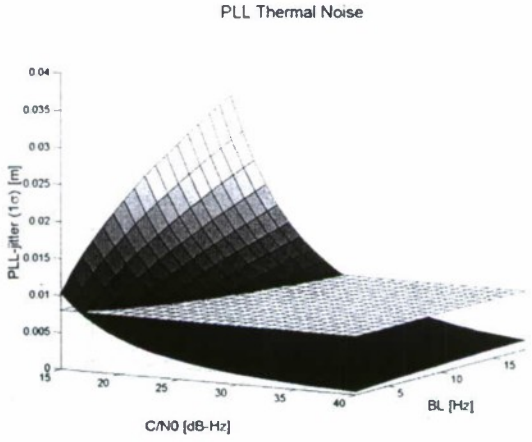

Figure 2. PLL thermal noise

In order to decrease the thermal noise a reduction of the filter bandwidth is necessary.
The errors caused by the oscillator are neglected in many accuracy investigations. The value for the Allan variance oscillator jitter conforms to its stability and can increase to 3 mm. The frequency variations caused by the receiver dynamics are called oscillator vibrations. Also this error can reach values up to 1.5 mm using a random vibration power curve of 4.8 g^2/Hz from 25 Hz to 250 Hz (0.1 mm vibration amplitude).
Especially in high dynamic environments the lock-in condition of the receiver loops cannot be kept. In this case the dynamic stress error e(t) violates the tracking threshold of the control loops.

$$e(t) = \frac{1}{\omega_L^2} \cdot \ddot{x}_0 \quad (4)$$

A reduction of the dynamic stress error without external aiding is only possible if the natural frequency of the loop filter ω_L can be increased. This however means a higher loop bandwidth at the same time. Higher thermal noise would be the result. The following graphs demonstrate the behavior of the total PLL-error in relation to different loop bandwidths:

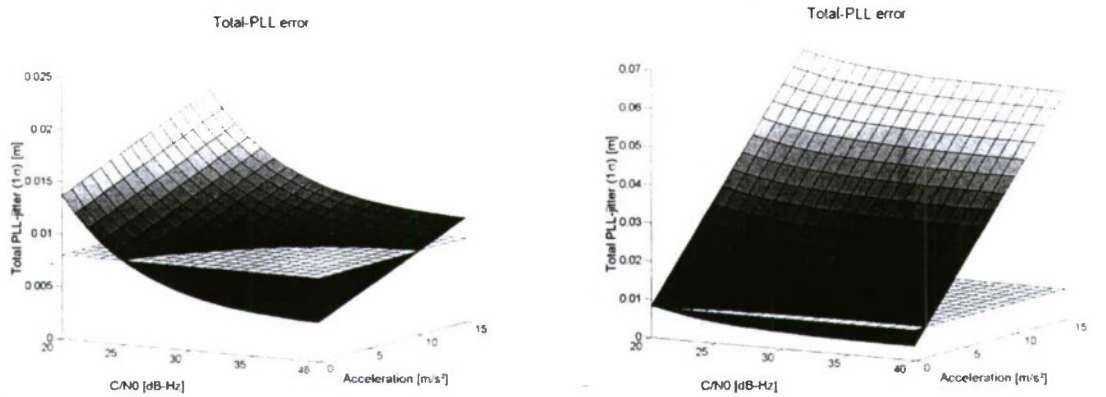

Figure 3. Total PLL-Error , loop bandwidth 15 Hz and 5 Hz

In opposite to the phase lock loop in the delay lock loop there are effectively only two performance characteristics: the code loop thermal noise error and the maximum line-of-sight dynamic threshold. The thermal noise error can be computed by:

$$\sigma_T = T_C \cdot \sqrt{\frac{B_L}{2 \cdot C/N_0} \cdot \left(1 + \frac{1}{T \cdot C/N_0}\right)} \tag{5}$$

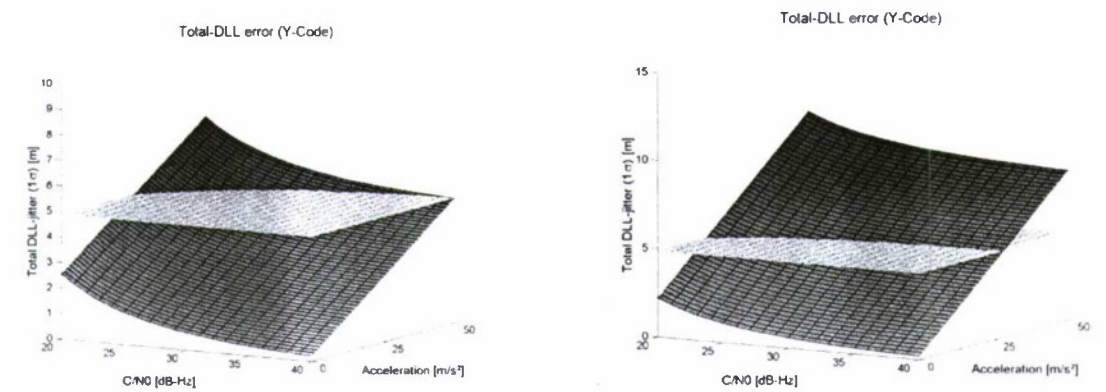

Figure 4. Total DLL-error, loop bandwidth 1.0 Hz and 0.75 Hz

As the thermal noise level of the code is much higher than the value of the carrier the loop bandwidth must be smaller. The lower robustness against dynamic stress can be compensated by carrier aiding of the code tracking loop. The variations of the total DLL error concerning the Y-Code is demonstrated in figure 4.

1. GNSS/INS Coupling Principles

Because of different error influences based on space segment, signal propagation or receiver noise the accuracy potential of a GNSS system is not sufficient for all applications. Additionally the availability and data frequency can be inadequate. Therefore many navigation or surveying systems use integrated GPS/INS systems to combine the only short-term stability of an INS sensor and the long-term stability but noise behavior of an GNSS sensor.
Different coupling principles of GPS/INS systems are possible. Most GPS/INS integrations are **loosely coupled,** giving up a great deal of performance in return for simplicity of integration. Using this principle the position and velocity estimates of a GNSS receiver are used as observations in an INS filter, thereby cascading two navigation filters (see figure 5; PVA: position, velocity, attitude). An estimation of INS errors, a reduction of GPS-noise and a bridging of GPS outages are possible. Yet single pseudoranges cannot be used to update the INS filter.
In a **close coupling** architecture only one navigation filter generates the integrated navigation solution with the information of GPS observations and INS navigation data (see figure 5). In this case the GPS measurements of pseudoranges and deltaranges are usable even when fewer than four satellites are tracked. Knowing the INS position lost ambiguity values can be restored more quickly.

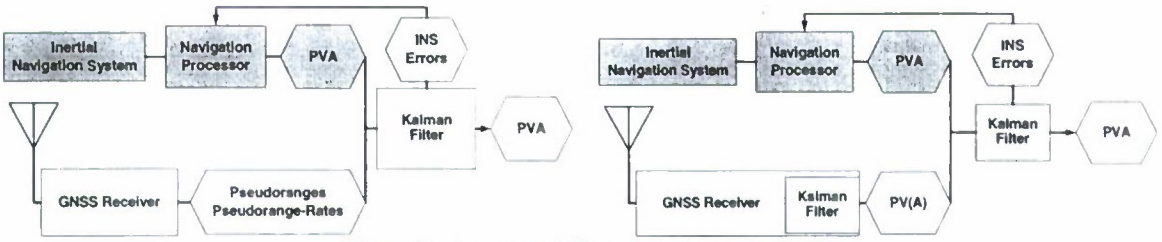

Figure 5. Loose and Close coupling principles

But in an observation environment with a low signal-to-noise ratio and high receiver dynamics no pseudoranges can be computed caused by transgression of the tracking thresholds of the PLL or DLL. In order to avoid this kind of GNSS outage additionally INS information (e.g. INS velocity) is added into the tracking loops of the receiver. Thereby the receiver dynamics can be subtracted from the rest of the signal. The dynamic stress error is minimized. Furthermore the loop bandwidth can be decreased to reduce the thermal noise error influence. This kind of GPS/INS integration is called **tight coupling** (see figure 6). Other advantages of this method are the fast reacquisition of lost satellite signals and the better anti-jamming performance. As the INS information influence the signal processing of the GNSS receiver the realization of this coupling principle requires special hardware equipment (see in the following sections of the paper).

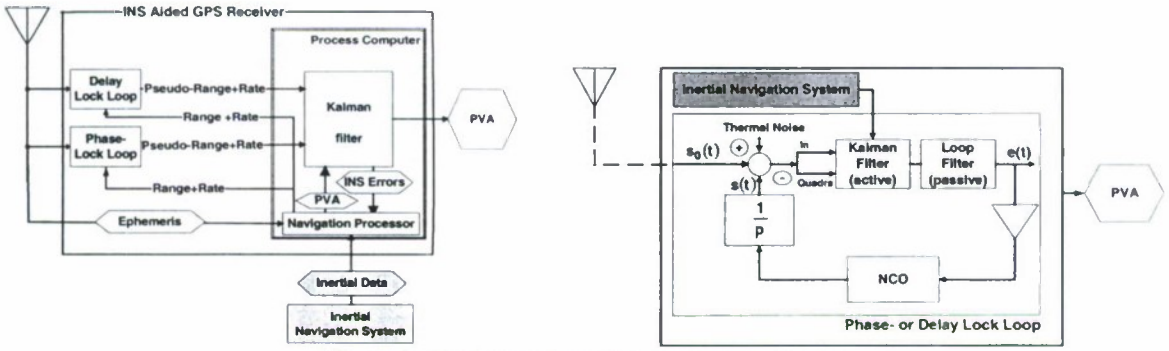

Figure 6. Tight and ultra-tight coupling principles

In **ultra-tight coupling** the Kalman filter is integrated on tracking loop level, i.e. each loop DLL and/or PLL is combining the early – late detector output with transformed and corrected range and rangerate data from the INS in an optimal filter. After this process the loop is closed by use of conventional control theory.

The basic principle may be described as follows for a 1st order digital DLL, where the state model may given as follows (process noise not considered)

$$\begin{bmatrix} \tau_{k+1} \\ T_{k+1} \\ \dot{T}_{k+1} \end{bmatrix} = \begin{bmatrix} (1-4B_L T) & 4B_L & 0 \\ 0 & 1 & T \\ 0 & 0 & 1 \end{bmatrix} \begin{bmatrix} \tau_k \\ T_k \\ \dot{T}_k \end{bmatrix} \tag{6}$$

with

τ_k	loop estimate of pseudorange	T_k	geometric range (satellite – receiver)
$\dot{T}_k$	geometric range-rate (satellite – receiver)	B_L	tracking loop bandwidth
T	pre-detection integration interval (20 msec for GPS)		

The following observations are used to up-date the loop filter :

i) Detector output (non-coherent E – L)

$$\begin{aligned} L_{DLL} &\equiv Q_E^2 - Q_L^2 + I_E^2 - I_L^2 + \varepsilon \\ &= 2\frac{a^2}{T_c}(2-d)(T_k - \tau_k) + \varepsilon \end{aligned} \tag{7}$$

with

a	amplitude of GPS signal	T_c	chip – length
d	correlator – spacing	Q, I	quadra-phase, in-phase signal
E, L	early, late	ε	detector noise

ii) INS derived range and range - rate

$$L_{INS} \equiv T_k + \hat{b}_{clock} + \hat{c}_{INS} + \varepsilon \tag{8}$$

$$\dot{L}_{INS} \equiv \dot{T}_k + \frac{d}{dt}\hat{b}_{clock} + \frac{d}{dt}\hat{c}_{INS} + \dot{\varepsilon} \tag{9}$$

with

b_{clock} clock – error estimate from central Kalman filter

c_{INS} inertial error estimate from central Kalman filter

This approach may be easily generalized for the carrier loop, carrier–aiding and higher order loops.

2. Theoretical Simulation

In order to study the improvements of GPS performance using the tightly coupling architecture a detailed investigation of the receiver loops behaviour have to be made concerning the additional INS information. In comparison to figure 1 the extension of e.g. the PLL configuration is presented in figure 7.

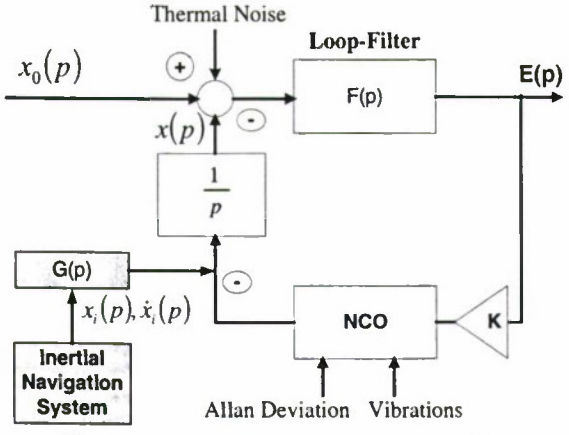

Figure 7. Tracking loop with inertial aiding

Using a theoretical simulation of the closed loop answers about the following questions should be available:

- What kind of filter function has to be used decreasing the error influence of the INS ?
- Is it possible to reduce the filter bandwidth and therewith the thermal noise ?
- What kind of INS is suitable to guarantee the tracking threshold conditions ?

Some fundamental knowledge about inertial navigation and signal processing are combined to develop a simplified but meaningful mathematical description of the discussed control loop.

The derivation of an observation equation is based on the fundamental equation of inertial navigation. The specific force a can be computed by:

$$\mathbf{a} = \ddot{\mathbf{x}} - \mathbf{g} \quad ; \quad \mathbf{g} = -\frac{GM}{R^3}\cdot\mathbf{x} = \frac{|\mathbf{g}|}{R}\cdot\mathbf{x} \tag{10}$$

with

a	specific force	x	position
g	gravitation	R	earth radius

Including a simple error model with an accelerometer bias B and a gyro drift D and restricted to the horizontal plane it can be written (t = time):

$$a + \delta a = \ddot{x} + \frac{g}{R}\cdot x \quad ; \quad \delta a = B + g\cdot D\cdot t \tag{11}$$

A transformation from time to frequency domain using the Laplace transformation and resorting yields to the following equation of inertial velocity:

$$\dot{x}_i = \frac{A(p)}{p} = \frac{\left(p^2 - \frac{g}{R}\right)}{p}\cdot x_0(p) - \frac{B}{p^2} - \frac{g\cdot D}{p^3} \tag{12}$$

In signal processing the closed loop configuration presented in figure 7 can be described as:

$$[p + K \cdot F(p)] \cdot X(p) = K \cdot F(p) \cdot x_0(p) + K \cdot F(p) \cdot G(p) \cdot \frac{\dot{x}_i}{p} \tag{13}$$

Thereby the added term contents the influence of inertial aiding.

Filter Design

Like it is shown in the equation 13 the effect of inertial data depends on the used filter function G(p). In relation to the tight coupling principle the dynamics of the pseudoranges should be subtracted from the total signal. According to this criterion G(p) have to be derived.

The dynamical tracking error E(p) is computed by:

$$E(p) = x_0(p) - x(p) \tag{14}$$

A combination of equation 12 and 13 yields to:

$$E(p) = \frac{\left[p - K \cdot F(p) \cdot G(p) \cdot \frac{p^2 + \frac{g}{R}}{p^2} \right]}{p + K \cdot F(p)} \cdot X_0(p) + \frac{K \cdot F(p) \cdot G(p)}{p + K \cdot F(p)} \cdot \frac{B}{p^3} + \frac{K \cdot F(p) \cdot G(p)}{p + K \cdot F(p)} \cdot \frac{g \cdot D}{p^4} \tag{15}$$

In order to guarantee the independeney of E(p) and X_0(p) the first term must be zero. This is possible if

$$\Gamma_0 \cdot p = K \cdot F(p) \cdot G(p) \cdot \frac{p^2 + \frac{g}{R}}{p^2} \tag{16}$$

Γ_0 designates in equation 16 the coupling coefficient between GNSS and INS. A value of one means the full integration capacity, zero signify the unaided GNSS receiver. Using equation 16 the filter function G(p) can be derived:

$$G(p) = \frac{\Gamma_0 \cdot p^3}{K \cdot F(p) \cdot \left(p^2 + \omega_s^{\,2}\right)} \tag{17}$$

with $\omega_S^{\,2} = \frac{g}{R}$ Schuler frequency

The amplitude response |G(ω)| of this filter function concerning a second order tracking loop can be determined by:

$$|G(\omega)| = \frac{\Gamma_0 \cdot \omega^4}{K \cdot \sqrt{\alpha^2 + \omega^2} \cdot \left(\omega^2 - \omega_S^{\,2}\right)} \tag{18}$$

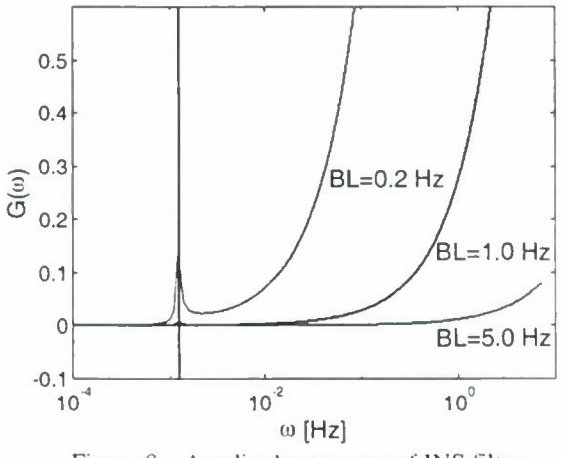

Figure 8. Amplitude response of INS filter

In order to evaluate the filter characteristics the result of equation 18 has been plotted in figure 8. An asymptotical trend can be seen at the Schuler frequency. Otherwise long term variations are suppressed. According to the chosen filter bandwidth high frequencies up to 1 Hz pass the filter nearly unchanged. As a basic approach this might be a reasonable solution based on the known short term stability of INS data. In a next step special filters have to be developed qualified for the characteristic error performance of the used inertial sensor.
If the presented filter function G(p) is inserted in equation 15 and after retransformation from frequency to time domain according to equation 4 the dynamical tracking error of the tightly coupled sensor can be derived (see equation 19). Assuming a coupling coefficient of one the dynamic tracking error is independent of the pseudorange acceleration. Instead of this INS errors like acceleration bias B and gyro drift D influence the tracking error.

$$e(t) = \frac{(1-\Gamma_0)}{\omega_L^{\,2}} \cdot \ddot{x}_0 + \frac{\Gamma_0 \cdot B}{\omega_L^{\,2}} \cdot \cos(\omega_S \cdot t) + \frac{\Gamma_0 \cdot D \cdot g}{\omega_L^{\,2}} \cdot \frac{\sin(\omega_S \cdot t)}{\omega_S} \qquad (19)$$

Simulation results

Using the dynamic tracking error presented in equation 19 the rules of thumb concerning the tracking thresholds of PLL and DLL (equation 1 and 2) can be evaluated for a tightly coupled configuration.
First a second order phase lock loop is investigated. The following graphs should demonstrate the influences of loop filter bandwidth B_L and INS error performance (accelerometer bias B, drift D) concerning the total loop error ($1-\sigma$). The current values are specified in the figure description. The coupling coefficient is fixed by 1.0.

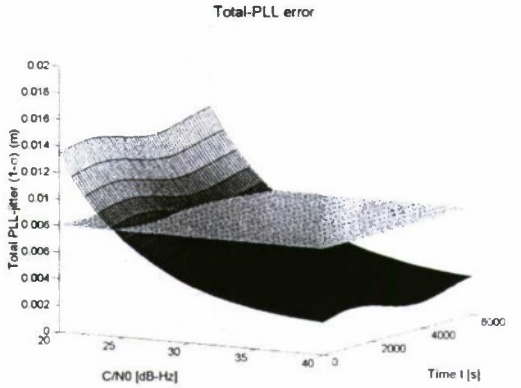

Figure 9. PLL; B_L: 15 Hz, D: 10.0°/h, B: 0.01 m/s^2

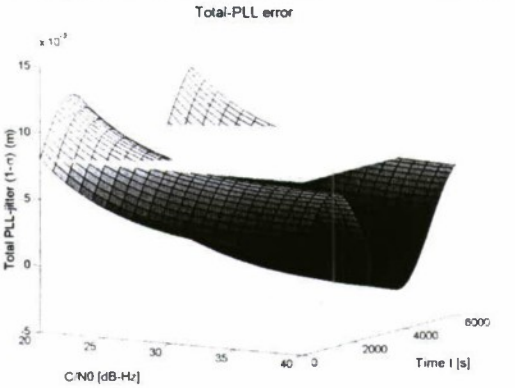

Figure 10.PLL; B_L: 5 Hz, D: 10.0°/h, B: 0.01 m/s^2

Because of the tight coupling architecture the PLL-error no longer depends on the pseudorange acceleration but on the time. The Schuler frequency dominates the error behavior of the tracking loop. If the loop bandwidth is decreasing an increase of tracking error can be recognized. At times of maximum amplitude the error transcends the tracking threshold already at higher signal-to-noise ratios C/N_0.

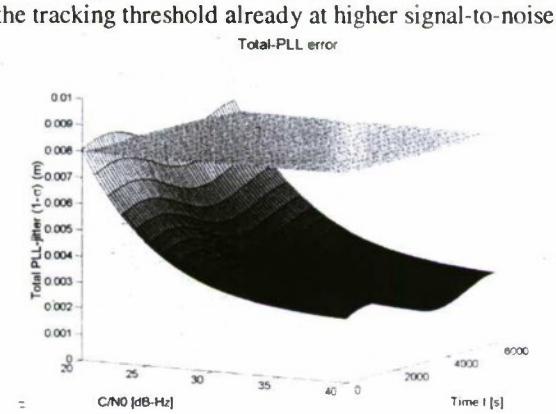

Figure11. PLL; B_L: 5 Hz, D: 1.0°/h, B: 0.01 m/s^2

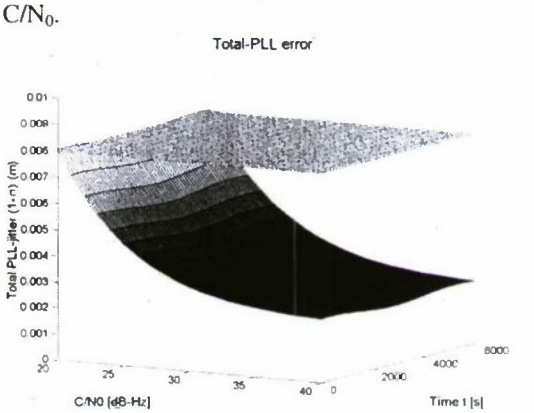

Figure 12. PLL; B_L: 5 Hz, D: 0.1°/h, B: 0.01 m/s^2

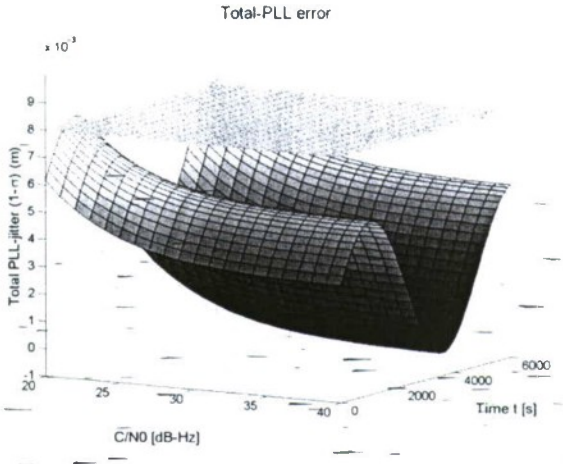

Figure 13. PLL; B_L: 2 Hz, D: 1.0°/h, B: 0.01 m/s^2

Like it is presented in figure 10, 11 and 12 using a more accurate inertial sensor reduce the amplitude of the Schuler frequency, so that the bandwidth can decreased again. But higher accuracy of the INS means increased costs. While a gyro rate of 10°/h can be provided by an INS with micro electrical mechanical technology (MEMS), 1°/h is only possible with a fiber optic gyro (FOG). Higher accuracy requirements are only provided by more expensive ring laser gyros (RLG) of high precision INS.

The following statements characterize the PLL investigations:

- Today MEMS-technology INS cannot meet the requirements to support the phase lock loop. Improvements of dynamical independence are disturbed by a high error level.
- A PLL support using high precision INS allow filter bandwidths down to 0.5 Hz. But expensive sensors limit the area of application.
- As a compromise INS with fiber optic gyros can be used. Like it is presented in figure 13 the PLL is kept in lock with an reduced bandwidth of 2 Hz.

The INS aiding of the code lock loop is less critical than of the PLL, but because of different chip length it must be distinguished between Y- and C/A-Code. An evaluation of equation 2 yields to the following results concerning the tight coupling configuration (figure 14 and 15):

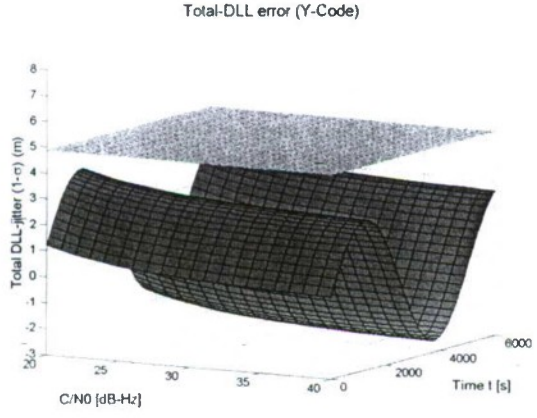

Figure 14. DLL (Y); B_L: 0.2 Hz, D: 10.0°/h, B: 0.01 m/s^2

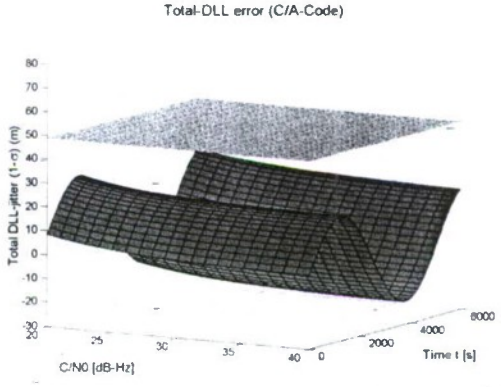

Figure 15. DLL(C/A); B_L: 0.5Hz, D: 20.0°/h, B: 0.01 m/s^2

An inertial sensor with a gyro drift of 10.0°/h is able to support an DLL with a loop bandwidth of 0.2 Hz tracking the Y-Code. The tracking threshold of nearly 5 m is not be violated down to an signal-to-noise ratio of 20 dB-Hz.

The loose-of-look condition concerning the C/A-Code rests with nearly 50 m. If a decrease of filter bandwidth down to 0.5 Hz is sufficient gyro rates of 20.0°/h keep the DLL in lock.

In opposite of the PLL to support a code tracking loop with INS data the today available MEMS technology INS meets the necessary requirements of tight coupling.

3. Numerical Simulation Tool

In order to verify the theoretical results and to prepare a planned practical test system a numerical **ti**ght **co**upling **sim**ulation tool (TICOSIM) is in development. For these purposes an existing implemented model of a generic GNSS receiver is extended and adapted with an INS simulation tool. Especially answers concerning the following questions are expected:

- What kind of INS filters are possible with different INS error models ?
- What happens in case of GNSS signal outages caused by the environment ? What means a GNSS outage concerning the system accuracy ?
- What kind of feedback effects have to be expected because of INS error estimation using observations of the combined system ?

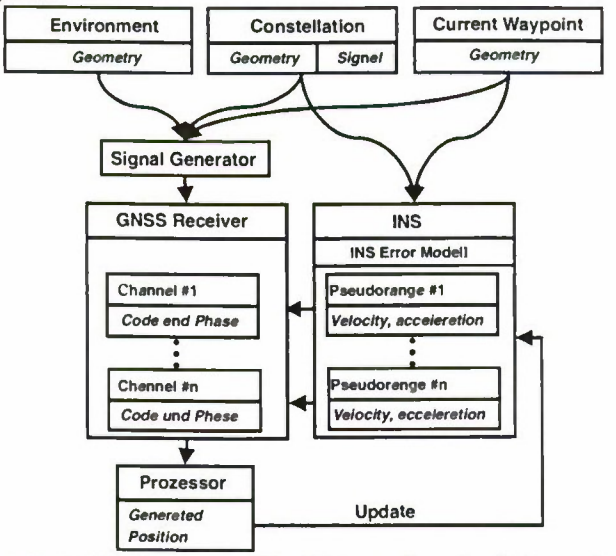

Figure 16. Diagram of the tight coupling simulation tool

Overview of the Control and Data Flow in TICOSIM

In figure 16 the control and data flow of the main processing modules is shown.

The **original data** consists of three parts: first the environment that allow to simulate GNSS signal outages caused by different objects like buildings or trees, second the constellation containing information about the satellite geometry and the GNSS signal structure and last the current waypoint data to describe the simulated position of the integrated GNSS/INS system over time.

Using this information the possible ranges between satellites and receiver are calculated and transformed in time and phase delays of the incoming GNSS signals. Furthermore in the **signal generator** the respective received signals s(t) are computed (see equation 20).

$$s(t) = a \cdot c(t-\tau) \cdot \sin(\omega t + \theta) \tag{20}$$

with:

c( )	code bit	τ	time delay
		θ	phase delay

At the same time in the **INS simulation element** the receiver waypoints are transformed into high frequency accelerations and gyro rates in a body fixed coordinate system. Using a specific INS error model systematic (accelerometer bias and gyro drift) and stochastic errors (noise) are added to the inertial data. Furthermore geocentric acceleration and velocity in an earth fixed coordinate system are obtained by a strapdown algorithm. In combination with the current satellite constellation the accelerations of the ranges can be calculated.

In order to derive the code and phase measurements from the incoming GNSS signals they have to be correlated with a replica signal generated by the **receiver model**. This is only possible if both carrier and code frequency and the phase delay is continuously tracked in the code and phase lock loops of each receiver channel. The mathematical model describing the loops consists of two coupled non-linear ordinary differential equations (21) and (22). Following the tight coupling principle the acceleration of the pseudoranges generated by the INS and transformed from meter to wavelength are added to the simulated phase lock loop (eq. 22). If carrier aiding is taken into account also the code tracking loop is supported by the INS information. The continuous solutions of these differential equations allow statements about the current stability conditions of the simulated control loops.

$$\Delta\tau = 2B_L T_c\left[i_e^2 - i_l^2 + q_e^2 - q_l^2\right] + \frac{\lambda}{2\pi c}\Delta\dot{\theta} + \frac{B_L T_c}{(2-d)\frac{S}{N_0}T}\delta S_\tau \tag{21}$$

$$\Delta\ddot{\theta} = \left(\xi\omega_L d_t + \tfrac{1}{2}\omega_L^2\right) i_p q_p + \ddot{\theta} + \frac{1}{2\frac{S}{N_0}T}\left(\frac{4\xi\omega_L}{T} + \omega_L^{-2}\right)\delta S_\theta - \ddot{\theta}_{INS} \tag{22}$$

In equation 21 and 22 i and q are the in- and quadra-phase components concerning the early e, late l and punctual p signal. The i and q components are the result of the correlation process in the receiver and can be approximated by:

$$i_r = \eta \cdot R(\Delta\tau - r)\cdot\sin(\Delta\theta)$$
$$q_r = \eta \cdot R(\Delta\tau - r)\cdot\cos(\Delta\theta) \tag{23}$$

The r takes on the values 0, +D/2 and –D/2 for the punctual, early and late channel respectively. The symbols in equation 21, 22, 23 mean:

B_L	noise bandwidth of the DLL	T_C	chip length of the code
λ	carrier wavelength	c	propagation velocity
$\Delta\tau$	code loop error	$\Delta\theta$	phase loop error
D	correlator spacing	S/N_0	signal-to-noise ratio
δS	detector noise (code and phase)	θ	line-of-sight (phase)
T	integration time of the correlator	ξ	damping factor
ω_L	characteristic frequency of the PLL	R( )	correlation function of the code

The **position processor** calculates a least square solution, using the ranges that the DLLs and PLLs in the receiver deliver.
The navigation solution of an unaided inertial sensor is drifting away over time. Especially the low-cost sensors that should be used in a practical system show only a short time stability. Therefore in fixed intervals the results of the position processor are used in a Kalman filter to improve the INS navigation solutions and to estimate the simulated error parameters of the inertial sensors. Concerning a practical system an evaluation of this feedback constellation is possible.

First results of the INS simulation element emphasize the influence of the receiver movement concerning the total pseudorange dynamics.
In this case slow land navigation is simulated along a testpath over 700 seconds presented in figure 17. The pseudorange acceleration to a satellite with 10 degree elevation without any receiver movement is a nearly constant value of –0.4 m/s².

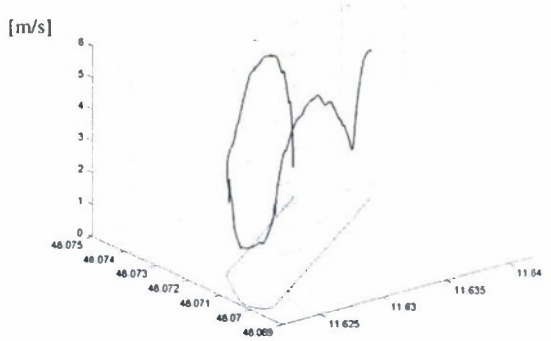

Figure 17. Course and velocity during the testpath

During the vehicle movement this acceleration change especially in turns for relatively large values (see fig. 18). Therefore also in land navigation the jerk stress should not be neglected especially if the bandwidth of the tracking loops is decreased.

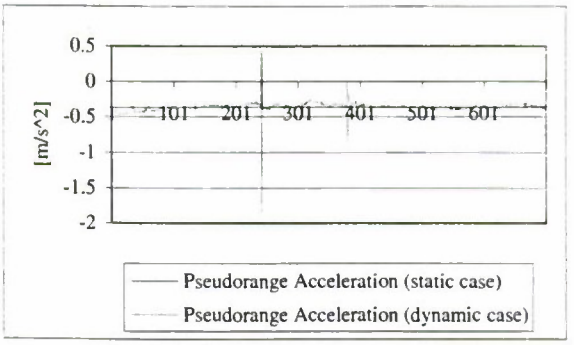

Figure 18. Influence of receiver dynamics

4. Prototyp System Development

The theoretical background of tight coupling and the results of the theoretical and numerical investigations define the configuration of the practical system. Both sensors GPS receiver and the inertial measurement unit have to meet special requirements.

First the internal code and phase tracking process of the receiver must be directly modified by the system developer. Therefore the implementation of the control loops have to be changeable. It must be possible to read out data from other sources and add them to the tracking loops. For this purposes we use the GPS Architect receiver card from MITEL. It is a development system intended for GPS receiver design operating in conjunction with a PC. The receiver software is written in C, can modified on a PC and then reloaded to the RISC processor of the receiver card. A block diagram of the GPS with all elementary components (RF front end, correlator, RISC processor, memory) and interfaces is shown in figure 19.

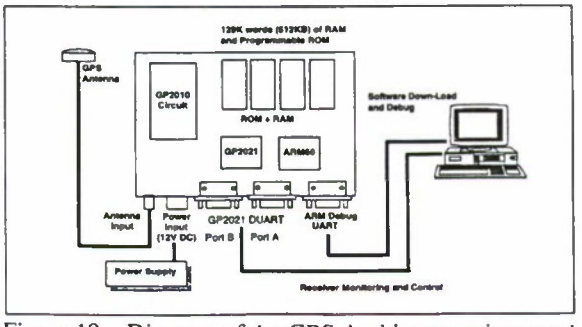

Figure 19. Diagram of the GPS Architect receiver card

As we investigated in the theoretical investigations a gyro drift of the INS nearly 1°/h is necessary to keep the phase tracking loops of the GNSS receiver in lock. This accuracy can be provided by a fiber optic gyro. Additionally the integration of GNSS and INS for dynamic applications requires an exact timing synchronization of the sensors. Therefore the possibility of external synchronization of the INS measurement frequency is an important property for this application. For this reasons we use the LN-200 Inertial Measurement Unit from LITTON. It provides the inertial data by a RS 485 data bus using the SDLC protocol with an output rate of 400 Hz.

In order to integrate the GPS and INS data they have to be synchronized to a common time table Therefore a time information must be added to every INS data set. Therefore a timing controller is used which is synchronized to GPS time by a PPS pulse. First of all a generated 100 Hz clock controls the INS data sampling process. Additionally a 1 Hertz pulse resets the internal time tag counter of the INS. These counter values are one element of every INS data set. Finally the internal latching of data is signalized by a digital pulse which can be temporally fixed by the timer card. Thereby the time synchronization can be controlled.

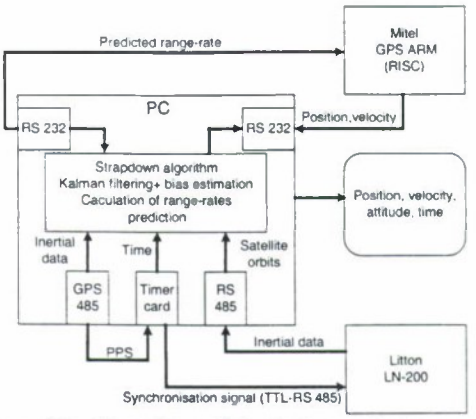

Figure 20. Data flow of the tight coupled system

In figure 20 an overview about the basic components and the data flow of the tightly coupled practical test system is presented like it is planned today. The central component of the test system is a software package running on a PC. The following tasks must be performed:

- Transformation of inertial data into navigation data using a strapdown algorithm
- Time synchronisation of GPS and INS data
- Estimation of INS errors using integrated position and velocity as observations
- Calculation of pseudorange, velocity and acceleration out of INS navigation data and satellite orbits
- Prediction of data at GPS tracking time

In order to decrease the complexity of the integrated system some simplifications are used. As the MITEL GPS Architect does not provide the PPS signal a second ordinary GPS card is used transferring the satellite orbit information at the same time. As a second simplification the estimation of the INS errors uses position and velocity as observations instead of pseudoranges. Therewith the principle of tightly coupling is not exactly be kept.

However concerning to the evaluation of improvement capabilities and difficulties correct results can be excepted using the presented system configuration

4. Outlook

On condition that the planned theoretical and practical investigations of the tightly coupled system show the unpredictable difficulties an increase of GNSS performance is possible. The basis for a development of a INS-aided GNSS receiver might be established. Including a price decrease of accurate INS sensors caused by further developments of the MEMS technology the use of tightly coupled GNSS sensors could become a standard for dynamical applications.

It might be expected that the integration of GNSS and INS systems become more closer in the future. But this only seems to be possible within the scope of a tight cooperation with a manufacturer of signal processing units of GNSS receivers.

5. Acknowledgement

The investigations and developments of a tightly coupled GNSS/INS sensor are founded by DLR (Deutsches Zentrum fuer Luft und Raumfahrt e. V.), FKZ 50 NA 9912.

6. References

Britting, Kenneth R. *(1971)* Inertial Navigation Systems Analysis, Wiley-Interscience

DiEsposti, Raymond et al. *(1998)* The Benefits of Integrating GPS, INS and PCS; Proceedings ION-GPS 1998

Eissfeller, Bernd *(1997)* Ein dynamisches Fehlermodell für GPS Autokorrelationsempfänger; Schriftenreihe Studiengang Vermessungswesen, Universität der Bundeswehr München, Heft 55

Eissfeller, Bernd *(1989)* Analyse einer geodätischen raumstabilisierten Inertialplatform und Integration mit GPS, Schriftenreihe Studiengang Vermessungswesen, Universität der Bundeswehr München, Heft 37

Kaplan, Elliott D. *(1996)* Understanding GPS-Principles and Applications, Mobile Communications Series; Artech House, Boston, London

Landry, Rene Jr. *(1999)* New Technique to Improve GPS Receiver Performance by Acquisition and Tracking Threshold Reduction; Research and Technology Organisation (RTO), Meeting Proceedings 43 (International Conference on Integrated Navigation Systems)

MITEL *(1997)* GPS Architect 12 Channel GPS Development System; version DS4605-2.5 March 1997, www.mitelsemi.com

Senott, Jim et. al. *(1997)* Robustness of Tightly Coupled Integrations for Real Time Centimeter GPS Positioning; Proceedings ION-GPS 1997

Titterton, D.H. and Weston, J.L. *(1997)* Strapdown Inertial Navigation Technology; IEE Radar, Sonar, Navigation and Avionics Series, The Lavenham Press

Ward, Ph. *(1998)* Performance Comparisons between FLL, PLL and a Novel FLL-Assisted PLL Carrier Tracking Loop under RF Interference Conditions; Proceedings ION-GPS 1998, p. 783-795.

Winkel, Jon O. et al *(1998)* SNSS Simulated Navigation Satellite System; Simulating a Generic GNSS Receiver in Virtual Environments; Proceedings of ION-GPS 1998

PHINS: THE FIRST HIGH PERFORMANCES INERTIAL NAVIGATION SYSTEM BASED ON FIBRE OPTIC GYROSCOPES

F. Napolitano*, T. Gaiffe, Y. Cottreau***, T. Loret****
Ixsea S.A.S. – 55, avenue Auguste Renoir – 78160 Marly le Roi – France
E-Mail : info@ixsea.com

Abstract

Key words: navigation system, fibre optic gyroscopes

Over the last twenty years the fiber-optic gyroscope (FOG) has evolved from a pioneering physics experiment to a practical device. Because their operational principle for sensing inertial rotation is not mechanical, but optical, FOGs are inherently quick to start, resistant to shock and vibration, light, compact and long lived. These characteristics make them particularly suitable for strapdown attitude and heading reference systems (AHRS) and they are now widely used in gyrocompass systems over the world. Progress in navigation grade FOG performance suggest that they should represent the next generation of rotation sensor for high performances inertial navigation systems (INS). In 2000, Ixsea built the first INS based on fiber-optic gyroscopes. Designed on the first place to meet the very high positioning requirements of marine and underwater applications (typically less than 5 m per hour drift with only velocity aiding) this INS, named PHINS, is now declined in four versions for marine, underwater, land and air applications. PHINS can be used either as an autonomous system or it can integrate external informations based on Kalman filtering to achieve the best performances. We will consider the structure of PHINS navigation algorithm with an emphasis on quality control and integration of specific acoustic sensors used in underwater applications. The performances of the system will be assessed based on several trials.

Introduction

Ixsea, formerly known as Photonetics, has been working on the Fibre Optic Gyroscope (FOG) technology since 1987. Based on 0.1 deg/h FOGs, we have developed in 1997 an attitude and true heading sensor known as Octans [16]. More than 200 are now used in projects all over the world, principally on survey vessels or underwater vehicles to provide better than 0.1 deg heading and 0.01 deg roll and pitch.

In 2000 Ixsea designed a complete inertial navigation system named PHINS using 0.01 deg/h FOGs and integrating a Kalman filter. PHINS Kalman filter is designed to optimally integrate informations from GPS, acoustic positioning systems, Doppler Velocity Log (DVL) and depth sensor. Depending on their availability they can be used simultaneously or separately, the PHINS being able to switch automatically between them. To achieve the bests performances models of each instrument specific errors are integrated in the filter. Moreover PHINS is able to detect failures in external sensors and to reject erroneous measurement.

Several trials have been done to validate PHINS performances, including trials on specially calibrated tracks and comparison with GPS RTK for survey and straight line trajectories. Over these trials PHINS performances were proved to be better than 0.02 deg accuracy for heading and 0.01 deg for roll and pitch, and less than 5 m per hour position drift with only velocity aiding.

1. System design

Much attention has been put on the mechanical design of PHINS (see figure 1). The actual system is a 16x16x16cm^3 box weighting only 3.8 kg. The power consumption is 12 watts. The box contains a high performance inertial measurement unit (IMU) and a digital signal processor (DSP) with the navigation software. Three connectors enable to plug external sensors.

The initial design of Phins was directed to marine and underwater applications. For underwater applications, PHINS is used as the positioning system of autonomous underwater vehicles (AUV) diving at 3000 m and doing pipeline or field survey for 24 hours without any human intervention. During these missions, PHINS can receive external informations from acoustic positioning systems and/or Doppler Velocity Log (DVL) . Acoustic positioning systems use acoustic transponder and compute position by triangulation. DVL are based on Doppler shift of acoustic waves reflecting on the seabed. Since acoustic positioning systems are costly and not easy to operate they are used mainly during the diving phase, so PHINS must be able to maintain its position with only velocity aiding for more than 20 hours with better than 5 m/h drift in straight line. In most missions mapping of the seabed is done using a multibeam echosounder requiring true heading and attitude from the PHINS.

---

* D. Sc. Mathematics and Computer Science
** CEO
*** Research Manager
**** Mechanical Engineer

Depending on the seabed or the depth, some part of the mission must be done without any external aiding (pure inertial mode). For marine applications PHINS is used to provide true heading and attitude to multibeam echosounder and as a positionning system available during GPS outages. It can also provide heave, surge and sway.

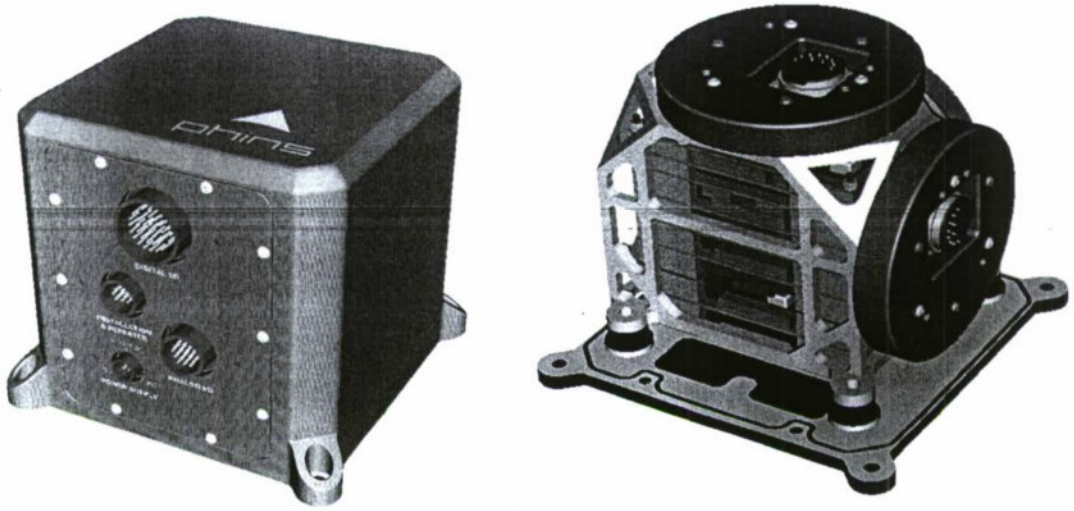

Fig. 1. PHINS mechanical design (16x16x16 cm^3, 3.8 kg)

Due to the type of mission described above, the following requirements were considered during the design of PHINS:

- it should be able to integrate informations from GPS, DVL, acoustic positionning systems and depth sensor
- the position error during long GPS outage (more than 100 seconds) should be within GPS accuracy
- the position drift using only DVL and no external position should be below 5 m/h (at 2 knots)
- the systems should provide quality informations on all data

2. Inertial measurement unit

The inertial measurement unit (IMU) is the core component of the system: it is formed by three FOGs and three accelerometers mounted on orthogonal axis.

2.1. Fibre optic gyroscopes

A fibre optic gyroscope (see [10] and the references therein for an account of FOG technology) is a ring interferometer made of a multiturn fibre coil enclosing an area A. Light entering the interferometer is divided into two counter propagating waves which return perfectly in phase after having travelled along the same path in opposite directions. When the FOG is rotating, a relativistic effect, known as Sagnac effect, induces a difference of transit time between the two waves which can be measured by interferometric means. The difference of transit time is proportional to the product of the rotation rate R and the area A enclosed by the coil (counted as many times as the fibre coil turn around A). In particular the sensitivity of the FOG can be increased by increasing the number of turn of the coil. Until a few years ago the use of FOGs in navigation systems was prevented by a parasite effect called Shupe effect. Shupe effect is a phase shift, resulting in increased bias, due to time varying temperatures experienced by different segments of the coil. Hopefully this effect can be almost completely eliminated by special winding of the fibre coil insuring that phase shifts effects are symmetrical and do not result in bias. Today high performances FOGs are equivalent in terms of performances to the best Ring Laser Gyroscopes (RLG). RLGs are based on the same relativistic effect as FOGs, however they are not based on fibre coil but on a ring configuration of mirrors. Due to the use of mirrors, the manufacturing process of RLG is much more delicate than the manufacturing process of FOG. Hence FOG are much cheaper to produce. Moreover RLG have very bad performances at low rotation speed and to eliminate this effect RLG are based on vibrating components which makes their life time shorter than FOG. These considerations imply that FOG should replace RLG for high performances navigation systems in the future.

FOGs manufactured by Ixsea cover the medium to very high performances range: from 0.1 deg per hour bias to 0.0003 deg per hour bias (used in space applications [15]). The characteristics of the FOGs used in PHINS are summarized in table 1.

Table 1: characteristics of FOG 120 used in PHINS

Bias stability over temperature range (-40 degC/ + 80 degC)	0.01 deg/h
In room bias stability	0.003 deg/h
Random walk	0.001 deg/sqrt(h)
Scale factor stability over temperature range (-40 degC/ +80 degC)	10 ppm
Scale factor linearity	3 ppm
Resolution	0.0012 arc sec

2.2. Accelerometers

The characteristics of accelerometers used in PHINS are summarized in table 2.

Table 2: characteristics of accelerometers used in PHINS

Bias stability	500 microG
Scale factor stability	500 ppm
White noise	100 microG/sqrt(s)

3. Navigation System of the PHINS

The navigation system of the PHINS is composed of three components: the IMU provide raw accelerations and rotations in body frame, the pure inertial navigation system resolves the inertial measurements in navigation frame and update the attitude, heading, velocity and position of the PHINS, the Kalman filter integrate measurement of the pure inertial system with measurement of external sensors to provide corrections to inertial system errors.

3.1. Pure inertial navigation system

3.1.1. Computation scheme

The scheme of PHINS pure inertial navigation system is given on figure 2. The computation involves two different process: first the gyros and acceleros measurement are integrated at high speed rate (300 Hz) in the body frame to provide elementary angles and speeds variations, then these elementary variations are integrated at a lower rate (100 Hz) to provide attitude, velocity and speed.

The integration of gyros and acceleros in the body frame corresponds to the integration of a non-linear differential equation. Due to the finite integration rate, the sums of angles and accelerations do not correspond exactly to the real movements of the body and they have to be corrected to account for the non-linearity which can lead to resonant errors. The non-linear corrections are called *coning* and *sculling* compensations.

The attitude update is based on a quaternion algorithm. The elementary angle variations obtained after coning compensations are integrated. Since the gyros output rotations with respect to an inertial frame, the earth rotation and craft rate must be subtracted before integration (the *craft rate* is the rotation of the body in the inertial frame due to the velocity of the body on the surface of the spherical earth).

Velocity and position are then updated taking into account the dependence of gravity on the position and the ellipsoidal shape of the earth. The earth model used is WGS-84.

An overview of inertial navigation systems equations can be found in any classical textbook (see [2] [13] and [14] for instance).

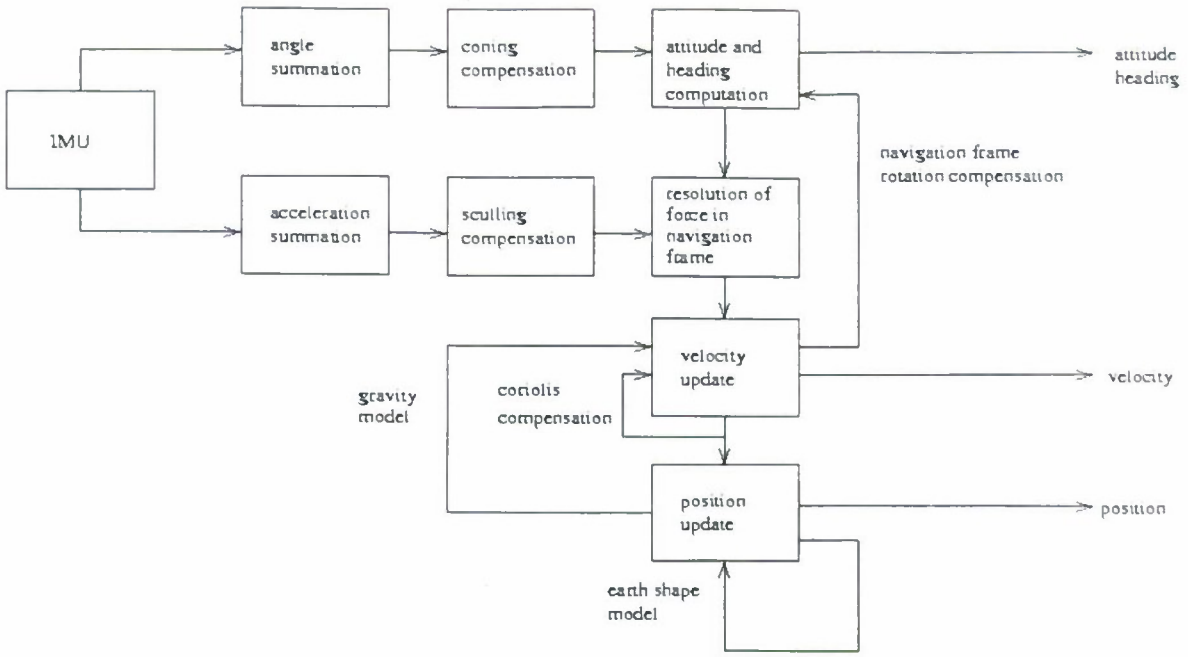

Fig. 2. scheme of pure inertial navigation system

3.1.2. Initial alignment

To initialise the navigation process it is necessary to dispose of initial attitude, heading, velocity and position. Initial position and speed should be provided by the user or by an external sensor. Initial attitude and heading are computed during a five minutes alignment stage occurring each time PHINS is switch on. During this stage PHINS doesn't need any external information.

The general principle of initial attitude and heading computation is the following: to know the attitude it suffices to know the vectors composing the navigation frame (east, north and up axes) ; the up axe is proportional to the gravity vector, the east axe is proportional to the derivative over time of the gravity vector in the inertial frame (due to the earth rotation around the north/south axe) and the north axe is the vector product of up and east axes. Since the accelerometers measure gravity and since the gyrometers can maintain the relation between the inertial frame and the body frame it seems that the initial attitude computation is very simple. However since the initialisation stage has to be done without external information, movements of the body have to be filtered and corresponding accelerations should be remove from accelerometers measurement. At the end of the initialisation stage the following performances are achieved: true heading error less than 0.1 degree, roll and pitch errors less than 0.02 degree.

3.1.3. Propagation of errors in pure inertial mode

As said before the pure inertial system is dependant both on the quality of data provided by accelerometers and gyrometers and on initial attitude, velocity and position errors obtained after the alignment. Since the gyros and acceleros data are integrated over time and since the velocity, position and attitude computations form a close loop, all these errors propagate with time and influence each other.

However it can be seen easily that the propagation of errors is bounded except for longitude error. The heading, roll, pitch, velocity and latitude errors of the pure inertial navigation system oscillate with time with three different periods: the Schuler period (84 mn), the earth rotation period (24 hours) and the Foucault period (24 hours secant latitude). For the PHINS the amplitude of the oscillation in heading, attitude and latitude is bounded roughly by the initial error in heading and the initial error in position. That is if the initial heading error is 0.1 deg the latitude error will oscillate with an amplitude of 0.1 deg and reciprocally if the initial latitude error is 0.1 deg the heading error will oscillate with an amplitude of 0.1 deg. Contrarily to attitude, velocity and latitude errors, longitude error is not bounded: it is the sum of three oscillating components with the period given above and a linear drift proportional to the bias of the gyros. Since the bias of the gyros used in PHINS is very small, the drift in longitude becomes apparent only after a very long time; over short period of time it is masked by oscillations due to initial errors.

3.2. Kalman filter

3.2.1. Computation scheme

The scheme of PHINS Kalman filter is given on figure 3 (see [5] [7] [8] [12] for general references about Kalman filter and [4] for Gauss original ideas about least square estimation). The goal of the Kalman filter is to use data provided by external sensors to improve the accuracy of the pure inertial system. Contrarily to classical approach used in civil marine applications like Dead Reckoning, were external sensor are used to replace inertial data, Kalman filter algorithm consist of an optimal integration of external and inertial data. Roughly speaking each time an external information is received by the PHINS (whether GPS, DVL, acoustic position, depth sensor,...) this information is compared to the information provided by the INS and errors of the INS and the external sensor are estimated. In particular the computation process of the Kalman filter is based on model of external and inertial sensors errors.

The error models of external sensor are specific for each type of sensor and some of them will be discussed in the next section. In general error of external sensors can be modelled as white noise or as first order Markov process.

The INS error equation of PHINS contains the following states: attitude and heading errors, velocity errors, position errors, FOG errors and accelerometers errors. All these errors propagates with time: for instance an error in the north speed propagates into an error in latitude which in turn propagates into an error in gravity model and so on. The equation of error propagation is obtained by partial derivative of the pure inertial navigation equations: for instance derivative with respect to heading provide the dependency of the INS errors with respect to heading error. Since the navigation equations are not linear, the linearisation of the error differential equation is only accurate to first order and classical Kalman filter cannot be used. Instead we use Extended Kalman filter [5]. The main algorithmic difference between classical and extended Kalman filter is the dependency, in the extended filter, of the error equation on the trajectory of the vehicle.

Apart from the error models, the key component of the Kalman filter is the *covariance matrix*. The covariance matrix is the covariance of the vector of all errors modelled in the filter (attitude, position, speed, ...). In particular it contains estimates of bounds of all errors and also correlations between different errors. The estimates of error bounds are crucial for quality monitoring. The correlations can be thought of as the "memory" of the filter. For instance suppose that the standard deviation of north speed given by the covariance matrix is 0.1 m/s, since the error in north speed propagates into an error in latitude, at the next step the standard deviation of latitude error will increase and the correlation between latitude error and north speed error will also increase meaning that at the next step a speed information can be used to correct the latitude error. In the same way since heading error propagates into speed and then position error, any speed or position information can be used to correct heading.

The computation process of the Kalman filter is as follows. On one side the pure INS is computing attitude, velocity and position based on inertial data (acceleros and gyros). These data are used to update the coefficients of the error equations and the error equation in turn is used to update the covariance matrix of the Kalman filter. If no external sensor is ever connected to the PHINS, this process continues forever. Then the only function of the Kalman filter is to provide error bound estimates. Once an external information is received (and after a prefiltering stage), this information is compared to the estimates of the INS. For instance if a position is received from a GPS receiver, the difference between GPS position and INS position is formed. This difference is the sum of the errors of the GPS receiver and the errors of the pure inertial system. These errors are discriminated in the Kalman filter observation unit based on the error covariance matrix. For instance and to simplify, if the difference between GPS and INS position is 10 meters while the standard deviation of INS is 1.0 m and the standard deviation of GPS is 20 meters it is likely that most of the error must be accounted to GPS. The possibility to discriminate between different types of errors is called *observability*. In general observability is not possible after the first measurement but it does increase with time since the differential equations of different errors are different. In particular, estimates of the Kalman filter tend to improve with time. Once the error have been discriminated the error of the inertial system are fed back into the INS and the errors of each instrument are fed back into its error model.

3.2.2. Robust observation and checking of external data

Some navigation Kalman filter integrate external sensors and inertial sensors errors in the same covariance matrix. In PHINS we have tried to separate the different model of errors when possible. The main advantage of the separation of error models are better observability, better numerical stability and reduced computation time. The better observability achieved is crucial to prevent the system to go into crazy estimations under special circumstances.

The observation scheme of PHINS Kalman filter is based on *M-estimates* [6] [9] [11] . In traditional Kalman filter, the correction to the INS after the reception of an external information depends linearly on the information received. This would be correct if external sensor errors could be modelled as white noise (or any process linearly driven by white noise). However in general external sensor data contains outliers with unbounded errors (for instance GPS jumps due to reflections or bad weather conditions). The direct integration of these outliers into the Kalman filter leads to unbounded errors in the estimated INS correction. The principle of M-estimates is to replace the linear dependency of the correction on the measured error by a bounded dependency and hence to reduce the effect of large deviation. This technique would be sub optimal from a theoretical point of view if we had to consider that the external sensors errors were perfectly modelled by white noise because it would slow the correction of inertial errors. However experience has shown that it is much better than traditional approach in real conditions, not only because of the robustness of the Kalman filter induced, but also because M-estimates enable to give much more confidence into external sensor (bad data will have few influence) and hence to compensate quickly inertial system errors. In PHINS Kalman filter, every external information is scaled before being put into the observation unit, and statistics of scaling over time are used to check for permanent errors of external sensors. Hence external data can not only be attenuated but also rejected. The rejection and bad quality flags provided for each sensor can then be used to monitor the integrity of the instruments and the quality of data provided by the system.

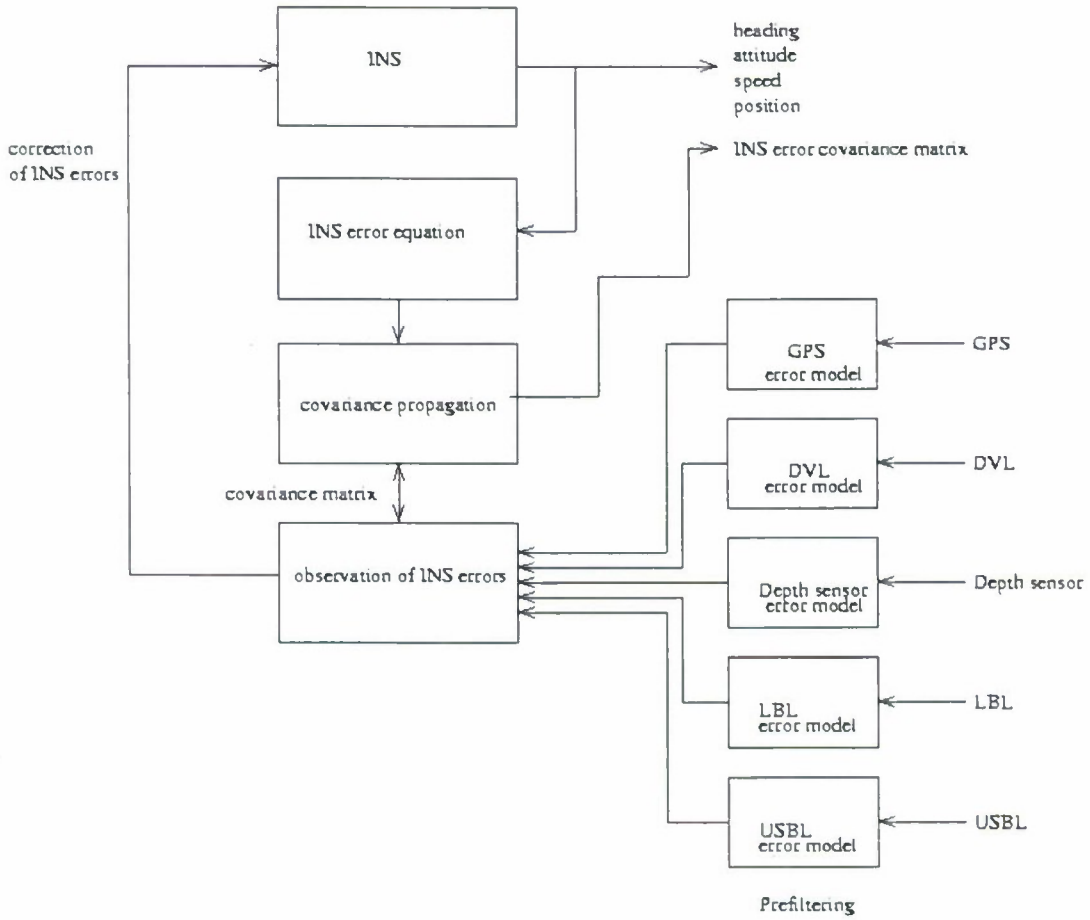

Fig. 3. scheme of PHINS Kalman filter

3.2.3. Models of acoustic sensors errors

Since GPS and depth sensor errors are well known we will concentrate on DVL, and acoustic positioning systems errors.

3.2.3.1. DVL errors

The following errors are taken into account into the DVL error model: white noise, scale factor and misalignment angle with respect to the PHINS. The scale factor and misalignment are modelled as random constant. Typical standard deviation for these errors after calibration of the instrument are 0.1deg for misalignment and 0.5% for scale factor (depending of course on the type of DVL connected to the PHINS). The white noise standard deviation is between 0.01 m/s and 0.03 m/s (for one second update rate). Since PHINS cannot estimates accurately very large DVL misalignment errors during normal operations a special procedure has to be done once for all to obtain a rough estimates which can be used for subsequent mission (as long as the PHINS and the DVL are not move with respect to each other). The principle of this calibration procedure is to compare PHINS position with GPS aiding with PHINS position with DVL aiding in Dead Reckoning mode (DR).

Today PHINS Kalman filter does not model DVL error due to current because the DVL is used only in bottom track mode and not in water track mode. In water track mode the DVL outputs velocity relative to the water layer and not relative to the seabed. We are now working on an extended model taking into account the effect of current so that PHINS would be able to use DVL even without bottom track. However it is likely that this error model will imply very poor observability for the Kalman filter. In this case special manoeuvres will have to be done to improve observability of current. For the moment when DVL without bottom track is the only external information available one can either navigate in DR mode or one can navigate in pure inertial mode. The position error could grow quickly in pure inertial mode however as soon as bottom track is available again PHINS will be able to correct most of the position error accumulated and hence continue to navigate with very high precision (see section 4).

3.2.3.2. USBL errors

The Ultra Short Base Line (USBL) system is an acoustic positioning system with two transponders. One transponder is on board a surface vessel and the other is placed in the underwater vehicle. USBL information consists of a range and an angle. The range is the distance between the surface vessel and the underwater vehicle, the angle is the angle in the navigation frame between them. Since the range computation is based on the knowledge of speed of sound velocity in water, it is subject to a scale factor error and a white noise error. The typical scale factor error is 0.5% of the range. The angle error is the sum of a white noise component, due to acoustic perturbation, and a slowly varying component directly related to the AHRS system on board the boat.

3.2.3.3. LBL errors

In general Long Base Line (LBL) systems consists of several acoustic transponder lying on the seabed and one transponder on board the underwater vehicle, each transponder being able to provide a range estimation to the underwater vehicle. Like for USBL, LBL range error can be modelled as scale factor error and white noise. Given four acoustic transponder on the seabed the position can be determined by triangulation. Moreover it is possible to use information coming from only one LBL transponder to estimate completely the INS position error because contrarily to GPS satellites the distance between PHINS and an LBL transponder is always quite short (less than a few kilometres). Hence the movement of the PHINS around the transponder allow complete observability of position errors (this assertion has been validated by simulation of LBL buoy based on GPS data).

3.2.3.4. Specific problems with acoustic systems

From what as been said it may seem that acoustic positioning systems are very easy to handle. However two different problems have to be considered.
First acoustic systems can interfere with each other and some of them have to be operated at a slow rate. This problem is completely solved by the use of Kalman filtering and a high class IMU: since the IMU is very accurate, the propagation of errors is very slow and the system only needs external information once in a while, because of Kalman filtering even with DVL aiding at a very low frequency the position error will grow very slowly since after every DVL information the filter will compensate for the accumulated position error and not only for the velocity error.
The second problem is more severe: since acoustic positioning systems are based on the propagation of sound through water (1500 m/s), position data given by LBL or USBL systems have a very important delay (they always arrive a few seconds after they are valid). To compensate these delays we have to consider the movements of the PHINS since the data were valid and the corrections applied to the INS during the latency time due to the use of other instruments.

4. System performances and tests results

4.1. Description of tests and summary of results

Four series of tests have been done to validate PHINS performanees and many trials using a ear equipped with a speedometer have been done during the development proeess. Among the four series of test, two were done in the south of Franee with eollaboration of Freneh marine researeh institute IFREMER, one was done in Japan for Tokyo University and one in the Orkneys Islands for Halliburton Subsea. This test were designed to validate the performances of PHINS with either GPS or DVL aiding. The tests with IFREMER and Halliburton were done in small boats and the tests in Japan were done on a calibrated track (using DVL aiding) and in a car (using GPS aiding and in pure inertial mode).
Using DVL aiding the following performanees have been obtained:

Position drift : - better than 3 m/h (at 2 knots) after ealibration of the DVL.
- better than 10 m/h (at 2 knots) without ealibration of the DVL

In pure inertial mode the following performanees have been obtained (after one hour GPS aiding):

Position drift : less than 3 m in 100 seeonds,
less than 0.8 miles per hour

When a DVL fix is available after pure inertial mode it reduees immediately most of the position error. For instanee after 100 seconds in pure inertial mode and one DVL fix the position error reduces to 0.2 m (instead of 3m). Moreover subsequent DVL fixes will eontinue to increase the position accuracy.

The performanees in heading and attitude with external aiding were validated in Ixsea faeility using speeially ealibrated tables and the results obtained have been eheeked by analysis of errors obtained during the tests at sea:

Heading error : less than 0.02 deg
Attitude error : less than 0.01 deg

4.2. Results of typical survey trajectory with DVL aiding only

Figure 4 shows a typical survey trajeetory realised during the tests with Halliburton. After the first five minutes alignment stage, the vessel is doing figures of eight during 25 minutes using GPS to improve its initial estimations, then for another 15 minutes the vessel goes in a straight line with both GPS and DVL to estimates DVL error, finally the vessel is doing a survey trajeetory with DVL aiding only during three hours. The survey trajectory consists of sixteen 1km lines spaced every 100 meters. The position error of the PHINS observed during this trial is shown on figure 5. The final position error is less than 5 m (the total distanee travelled is 22 km). Careful study of the error and position curves show that approximately half of the error is due to DVL scale faetor and half is due to the eombination of heading error and DVL misalignment error.

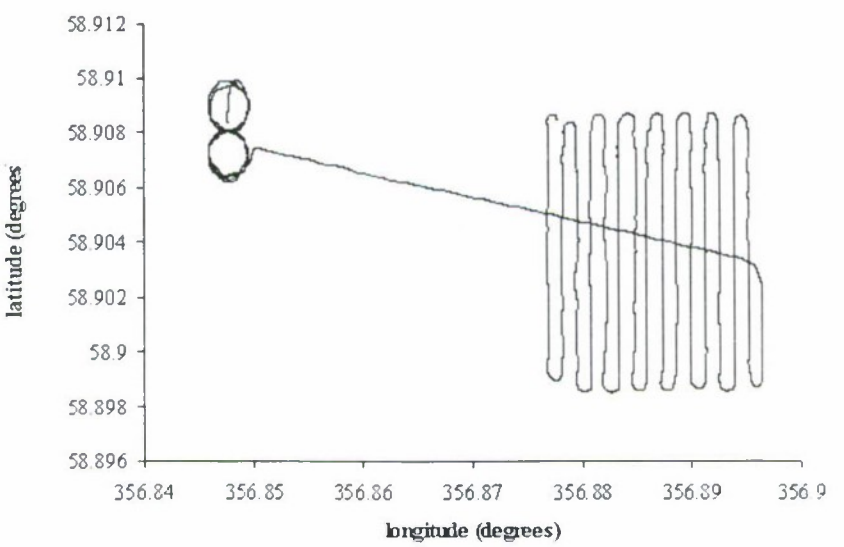

Fig. 4. survey trajeetory

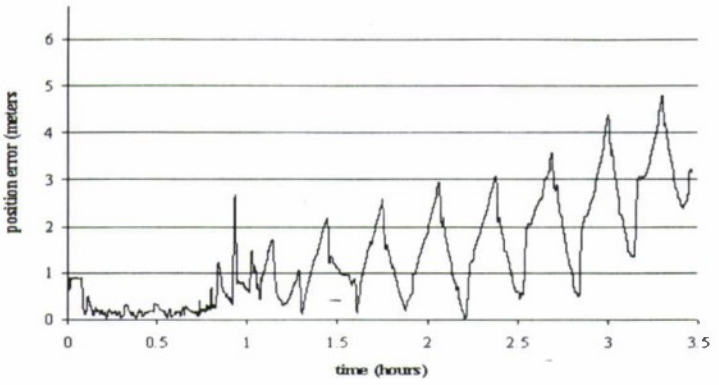

Fig. 5. position error versus time with DVL aiding only (after calibration stage with GPS)

Conclusions

PHINS is the first high performances inertial navigation system based on fibre optic gyroscopes. Several trials have proved that PHINS achieves very high performances. Its size, weight and power consumption makes it particularly suitable as the navigation system of small vehicles for which precise positioning is a critical issue. During its design a particular emphasis has been put on quality checking both for data coming from external sensors and for data provided by itself. This does not only improves the performances of the system but also provides the user the possibility to monitor in real time the quality of its navigation which can be crucial for certain applications or for post processing. Designed in the first place for marine and underwater applications, it can be connected not only to GPS and depth sensor but also to all types of acoustic sensors used in this field. PHINS is now declined in four versions for marine, underwater, land and air applications and its performances should allow him to become quickly a reference as a high-precision/low-cost navigation system in these area.

Acknowledgements

The first author thanks DR. Sam C. Bose for teaching him the principle of navigation systems during a Technalytics seminar and for fruitful discussions. IXSEA thanks the IFREMER for their technical support and for the opportunity to use their facilities during the first trials of PHINS.

References

1. **Bednarski, T., Muller, C.** Optimal bounded influence regression and scale M-estimators in the context of experimental design, preprint.
2. **Farrel, J.A., Barth, M.** The Global positioning System & Inertial Navigation, McGraw-Hill – 1999.
3. **Gaiffe, T.P., Morisse, J. Simonpietri, P. Martin, P., Lefèvre, H.C.** FOG multiplexing by time-shifted phase modulation, Fibre Optic Gyros 20th Anniversary Conference, H.C. Lefevre and K. Hotate ed., SPIE Proceedings, Vol. 2837 – 1996 – P. 132-140.
4. **Gauss, C.F.** Theoria combinationis observationum erroribus minimis obnoxiae - 1821, French translation by J. Bertrand, Mallet-Bachelier, Méthode de Moindres Carrés: Mémoires sur la combinaison des Observations par C.F. Gauss, Paris –1855. English translation by G.W. Stewart, Classics in Applied Mathematics no. 11, SIAM Press, Philadelphia – 1995.
5. **Grewal M.S., Andrews A.P.** Kalman Filtering Theory and Practice, Prentice Hall Information and System Sciences Series, Thomas Kailath ed.- 1993.
6. **Huber, P.J.** Robust Statistics, Wiley series in Probability and Mathematical Statistics, JohnWiley & Sons, New-York – 1981.
7. **Kalman, R.E.** A New Approach to Linear Filtering and Prediction Problems, *Transactions of the American Society of Mechanical Engineers (ASME), Journal of Basic Engineering*, 83 – 1960 – P. 35-45.
8. **Kalman, R.E., Bucy R.S.** New Results in Linear Filtering and Prediction Theory, *Transactions of the American Society of Mechanical Engineers (ASME), Journal of Basic Engineering*, 85 – 1961 – P. 95-105.
9. **Kremer, E.** *Robust credibility via robust Kalman filtering*, ASTIN BULLETIN, Vol. 24, No. 2 – 1994.
10. **Lefèvre, H.C.** *Fundamental of the interferometric fibre optic gyroscope*, Fibre Optic Gyros 20th Anniversary Conference, H.C. Lefevre and K. Hotate ed., SPIE Proceedings, Vol. 2837 – 1996 – P. 2-18.
11. **Neugebauer, S.P.** Robust Analysis of M-estimators of nonlinear models, Thesis, Virginia Polytechnic Institute and State University – 1996.
12. **Pollock, D.S.G.** A Handbook of Time-Series Analysis, Signal Processing and Dynamics, Signal Processing and its Applications, Academic Press – 1999.
13. **Titterton, D.H. Weston**, J.L. Strapdown inertial navigation technology, IEE Radar, Sonar, Navigation and avionics series 5, E.D.R. Shearman and P. Bradsell ed., Peter Peregrinus Ltd – 1997.
14. **Faurre, P.** Navigation inertielle optimale et filtrage statistique (in French), Méthodes mathématiques de l'informatique – 1, Dunod, Paris –1971.
15. **Wandner, K. Gaiffe, T., Cottreau, Y. Faussot, N. Simonpietri, P. Lefevre, H.** *Low noise Fiber Optic Gyroscopes for the Sofia Project*, Symposium Gyro Technology 1999 – Stuttgart.
16. **Gaiffe, T. Cottreau, Y. Faussot, N. Simonpietri, P. Lefevre, H. Ardilly, H.** *Marine Fiber Optic Gyrocompass with Integral Motion Sensor*, Symposium Gyro Technology 1999 – Stuttgart.

LOCAL NAVIGATION INTEGRATED SYSTEM ON THE BASE GNSS AND PSEUDOLITES NETWORK

V. Baburov, * N. Ivanszevich,**
E. Panov,* N. Vasilieva******
Branch Office FGUE "AUSRIRE" "AUSRIRE-Navigator"
Shkipersky protok, 19, 199106, Saint-Peterburg, Russia
E-mail" ausrire@navigat. ru

Abstract

Key words: Radio navigation system, pseudolite, navigation, landing, accuracy, non-equipped airdrome

The system, consisting of GNSS (GLONASS or GPS) and pseudolites system is considered as navigation integrated system. The opportunity of using such system on the non-equipped airdromes for deciding the navigation and landing tasks is estimated. The results of precision performances investigation are provided by integrated system, depending on the amount of pseudolites in network and its configuration are presented here. The using of such local system permits a landing performances on the level of Cat-I requirements of ICAO meteominimum to be provided without using the phase measurement methods.

Introduction

This investigation purpose is determined the capabilities of local integrated system, the navigation field to be comprised the fields of radio navigation satellite system GLONASS and/or GPS and pseudolites system to decade the tasks of the aircraft navigation and landing on the non-equipped airdromes.

The need for fields integration above mentioned systems are due to the following circumstances:

- radio navigation satellite systems don't provide the required navigation determinations of the reliability and accuracy, particularly for vertical component of the aircraft navigation in airdrome area and landing;
- ground radiators system don't provide the aircraft vertical determinations;
- the different navigation and landing facilities result in high cost of equipment both airborne and ground, which is needed to equip of the non equipped airdromes.

The numerous data that favor the reasonable use in sharing pseudolites with GNSS are in literature. However, they have the "point" character, where the point is characterized by space-time coordinates; the statistics are absent, describing the navigation integrated field behaviour for long interval, compared with period of repeatability of the GNSS navigation field configuration.

The recommendation of the optimum configuration of the pseudolite network, depending on the airport coordinates are absent, while, as known, GNSS field characteristics are varied on the space and time.

The authors of the report the main attention were given to study of mentioned factors in their investigations.

1. Investigation method

For determination of the positioning potential accuracy on operational constellation of the integrated system were taken up the digital simulation for geometrical factors (GF) computation with use of Monte-Carlo method in the following hypotheses:

- the real almanacs in UMA format are used for description of radio-navigation satellite system GPS,
- the minimal elevation angle of the Navigation Artificial Satellite of the Earth (NASE) over the horizon was 5 degree,
- the navigation task solution was carried out on the all Navigation Artificial Satellite of the Earth system,
- the pseudolites location coordinates conformed the "Pulkovo" airport coordinates.

Two type of computation were made:

- the points computation for time-moments with random access from equal one day interval,
- the computations for statistical characteristics which were proposed the accessed distributions configuration on equal one day interval. The geometrical configuration GPS-pseudolite- aircraft was modeling on 10 000 time moments.

---

* PhD, Sr Sc C, Branch Office Director
**PhD, Sr Sc C, Leading Research Scientist
*** Engineer
**** Chief Division

2. Geometrical characteristics of the operational constellation GPS and pseudolites.

The point computation results are presented in Figure 1. Four fragments (a, b, c, d) that are conformed the different pseudolites positions in respect of aircraft. In the first fragment pseudolite is located forward to North in respect of aircraft, in second – to South, ect.

As seen from computations of geometrical factors (GF) that improving of GF to issue unequal and strong depend on pseudolite azimuthal location in respect of aircraft. So a considerable improving of GF, to three times, can issue in some time moments. It is dependent on unequal distributed satellites GPS system on the sky and strong depends on day time for each particular selected point on the Earth's surface. Even one pseudolite location forward to such "lacuna" results in long-term (the navigation satellites constellation are varied quite slow) and cardinal improving of the constellation geometrical quality, used for navigation solution.

The ratio of GF on the altitude (or on plan coordinates) significantly depend on the number of N satellites, which are the aircraft radio visibility area: the smaller N, the more pseudolite contribution to the errors budget (i.e. the operational constellation quality of Navigation Artificial Satellite of the Earth (NASE) is worse). So, in N=7 (see points of second fragment Figure 1, conformed the pseudolites location to South), the error noise benefit from using pseudolites signals are near 300%, and in N=12 (points 2, 7, 9 the same fragment) the benefit are from 10% to 20%, thereby the small value conformes the more informative constellation of NASE (i.e. the GF of which is low). Such accuracy improvement would allow to use the satellite airborne equipment, operating on GNSS+APL for landing on the non equipped airdromes.

The "Pulkovo" airport the optimum of pseudolite location, as the computations are followed, is the South direction. It is noted, that in this case the considerable improvement of the noticeable reducing of GF in compliance with plan coordinates are issued.

For more objective estimation of this effect the additional computations, comprising histogram building the average magnitude (ξ) calculation, $\xi = \mathrm{VDOP}_{GPS} / \mathrm{VDOP}_{GPS+APL}$ and root-mean-square deviation $\sigma(\xi)$ were carried out. The results are given in Figure 2. Each of four fragments (a, b, c, d) are conformed the four directions to pseudolites: North, South, East, West. For each directions are given the differential distributions of magnitude ξ, the average and dispersion. The digital means of the interval are conformed the following diagram: first interval – [1.0 – 1.2]; second – [1.2 – 1.4);..., eleventh – [3.0 - ∞].

For "Pulkovo" airport the optimum of pseudolite location is to South direction, as it follows from given data. Thereby the benefit of using the additional navigational point (APL) to be in average 1.34. The optimum availability is explained by inequality of navigation field of GPS system.

3. Investigation of the latitude-longitudinal dependency of optimum azimuth from aircraft on APL.

Then the criticism of conclusions concerning the optimum azimuth on APL in respect to airport coordinates are tested. The modeling results are presented in Fugure 1, which is given average and root-mean-square the values of geometrical factors and their ratios ξ for marginal points of Russia territory, thereby the geometrical factors for GPS+APL system are given for different azimuthal directions on pseudolites (North, South, East, West).

The table representation manner is the same as in table 1.

The following conclusions can make on the computation results:

- There is the coordinate-azimuthal dependency of the maximum benefits of using APL, showing up more weak with approaching to USA territory, i.e. in the point with coordinates (45^0, 180^0)is observed practically the same value ξ in the all azimuth directions.
- The most effect of using one APL in GPS is observed in the point with coordinates (70^0, 30^0) the most removed (from considered) from continental part of USA.

4. Geometrical characteristics of the operational constellations GPS and some pseudolites.

HDOP and VDOP characteristics were studied in 0,1,2,3 and 4 pseudolites. The results of 10-th point computations on random time-moments are given in Figure 3 and 4 for HDOP and VDOP respectively. All directions from aircraft to APL conformed the following diagram: 1 APL – South; 2 APL – 1 APL is added to the East; 3 APL – previous configuration is added to 1 APL, located to the West, 4 APL – additional APL is located to the North.

The data provided follow:

First APL contribution is the most significant, 4 APL (for "Pulkovo") is the less informative.

a)

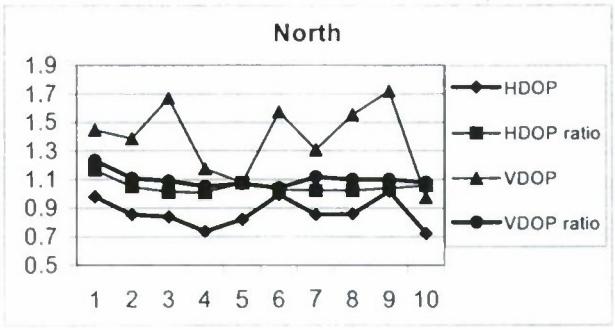

b)

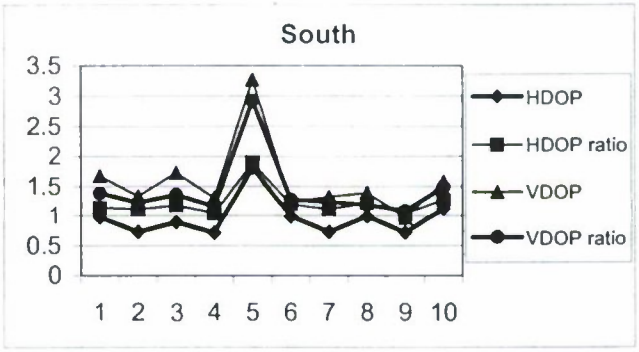

Fig. 1a,b. Geometrical factors and its ratios for different APLs locations in respect of aircraft

c)

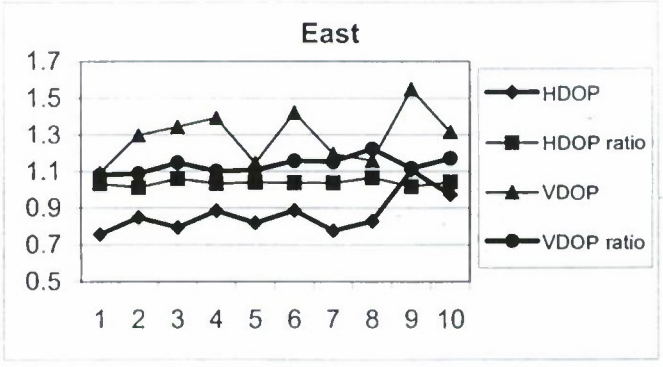

c)

d)

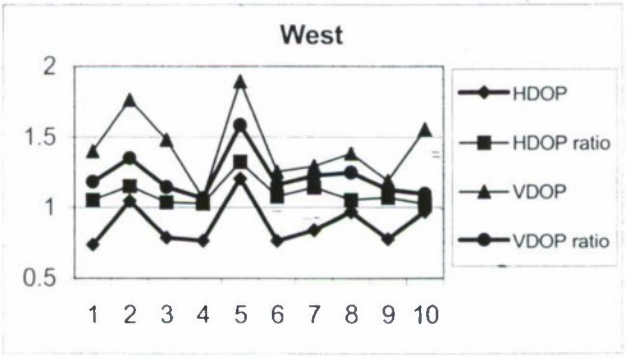

Fig. 1c,d. Geometrical factors and its ratios for different APLs locations in respect of aircraft

a)

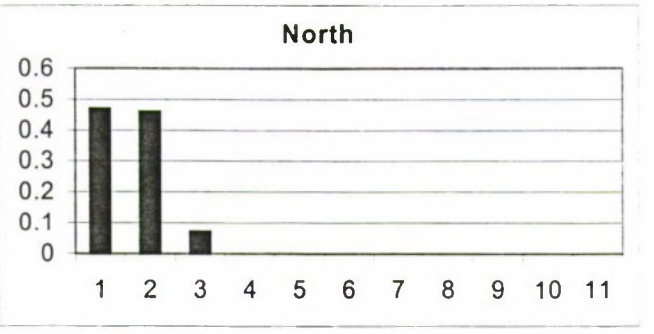

Mean 1.11, RMS 0.05

b)

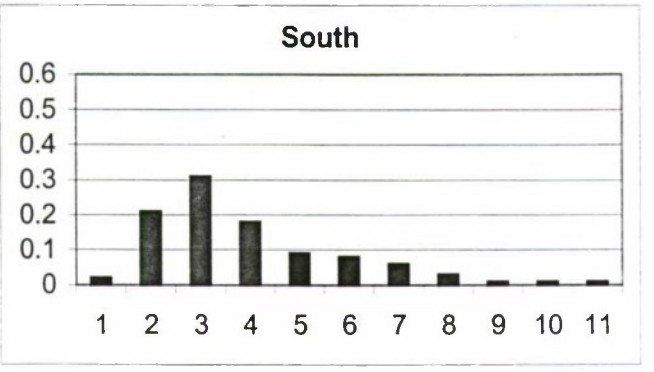

Mean 1.34, RMS 0.20

Fig. 2a,b. Distribution of ratios of altitude Geometrical factors for GPS system to altitude Geometrical factors for GPS system and APLs with APLs different locations of aircraft.

a)

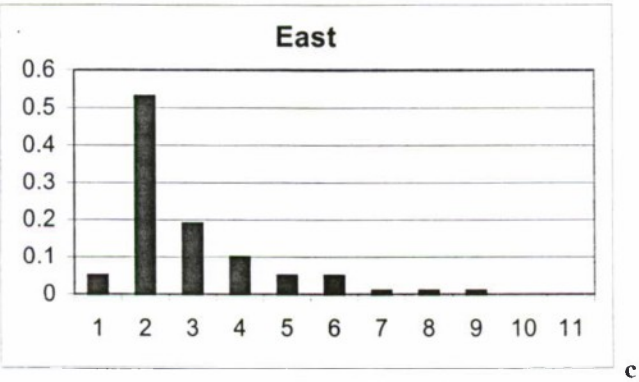

c

Mean 1.24, RMS 0.16

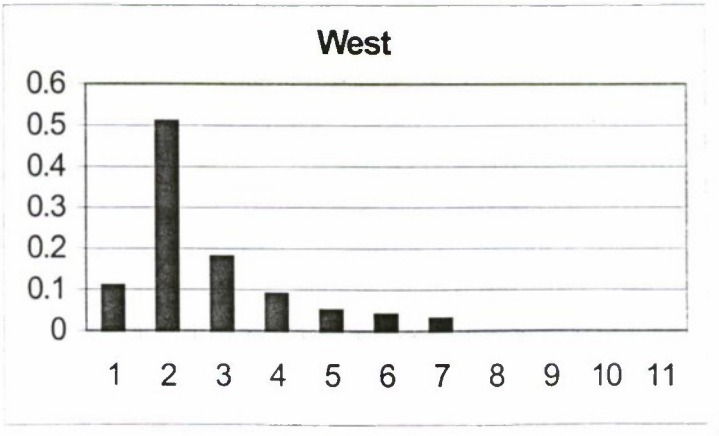

d)

Mean 1.22, RMS 0.14

Fig. 2c,d. Distribution of ratios of altitude Geometrical factors for GPS system to altitude Geometrical factors for GPS system and APLs with APLs different locations of aircraft.

The geometrieal faetor improvement depends on the assembly of visible GPS satellites eonstellation and varies in wide range from 1.30 (N = 14) to 1.93 (N = 8) on VDOP.

The modeling in aeeess volume n = 10 000 was earried out for estimations tested of average benefit and dispersion from using 4 APL.

Table 1: Accuracy positioning characteristics on GPS and GPS+APL depending on airport coordinates.

(φ,λ)	Performance	HDOP	North, ξ	South, ξ	East, ξ	West, ξ
70^0, 30^0	Average	0.818	1.042	1.092	1.093	1.034
	RMS	0.013	0.001	0.006	0.005	0.001
45^0,30^0	Average	0.988	1.144	1.074	1.041	1.092
	RMS	0.045	0.027	0.003	0.001	0.009
70^0,180^0	Average	0.830	1.26	1.149	1.072	1.067
	RMS	0.015	0.000	0.012	0.002	0.003
45^0,180^0	Average	0.937	1.091	1.096	1.046	1.073
	RMS	0.005	0.003	0.005	0.002	0.003

(φ,λ)	Performance	VDOP	North, ξ	South, ξ	East, ξ	West, ξ
70^0, 30^0	Average	1.482	1.171	1.309	1.305	1.178
	RMS	0.054	0.004	0.027	0.035	0.002
45^0,30^0	Average	0.461	1.310	1.214	1.246	1.338
	RMS	0.250	0.083	0.007	0.014	0.078
70^0,180^0	Average	1.542	1.150	1.381	1.272	1.266
	RMS	0.015	0.009	0.051	0.011	0.057
45^0,180^0	Average	1.328	1.209	1.217	1.202	1.246
	RMS	0.021	0.012	0.016	0.005	0.012

The results are presented in Figure 5 as two histograms, eonforming the aireraft different distance from APL: 27 400 m in altitude 400 m and 850 m in altitude 60 m. Each histogram sets the differential law of benefit distributions on vertieal geometrieal faetor as a result of using 4 APL's and its eharaeteristies – average and dispersion.

The digital means of interval are eonformed the following diagram: "1.2" – [1; 1.2]; "1.4" – (1.2; 1.4);... "3.0" –(2.8; 3]; ">3.0" – (3; ∞). The benefit average is unequal when two values of aireraft distanee to APL is seleeted and it is varied from 1.745 to 1.821.

Therefore, it is reasonable to set the optimum base values of APL's system for partieular airport in further development.

The aeeuraey improvement eharaeteristies as a result of using 4 APLs in different eoordinates of possible airports loeations on Russia territory and CNG eountries are provided in 2 - Table 2. The eonelusions are similar the previously obtained for 1 – APL: the far from the point with eoordinates (45^0, 180^0), the more the benefit.

5. Combined benefit estimation of using one and some APLs

The data provided previously eharaeterize the geometrieal properties of navigation field, eonfigured by GPS satellites system and pseudolites and one figure define the error positioning component due to by radio navigation parameter measuring (RNP). The following eomponent also enter in the eombined positioning error: time seales interaet timing errors of Navigation Artifieial satellite of the Earth (NASE), ephemerides errors, dissemination al errors (ionospherie and tropospherie), multiple refleetion errors and seleetive aeeess errors in GPS system.

If pseudolite operates in the loeal eontrol-eorreetive station mode, i.e. it radiates the additional information about differences between own eoordinates measured on GPS system and to runway referenee data, system errors and radio waves distribution errors are absent praetieally.

In literature the validated data on multiple refleetion errors for pseudolites are absent. Therefore this eomponent in eomputation is furter without eonsideration. Then the altitude measuring error will be speeified on known formula:

$$\sigma_V = \sqrt{2}\sigma G_{VDOP+ПС}$$

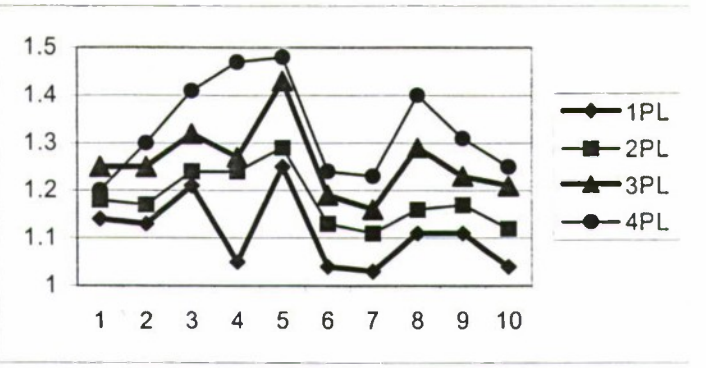

Fig. 3. Ratio of horizontal GF for GPS system to horizontal GF for GPS system and some APLs

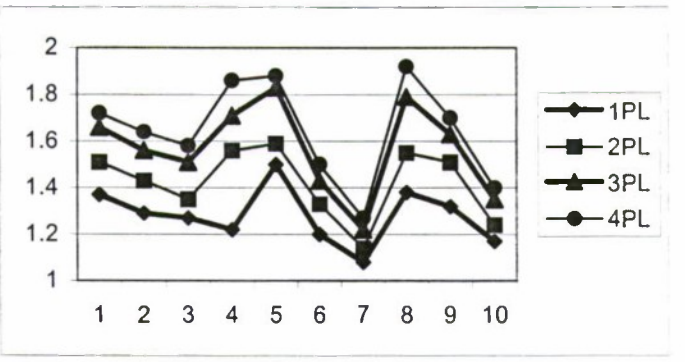

Fig. 4. Ratio of altitude GF for GPS system to altitude GF for GPS system and some APLs

a)

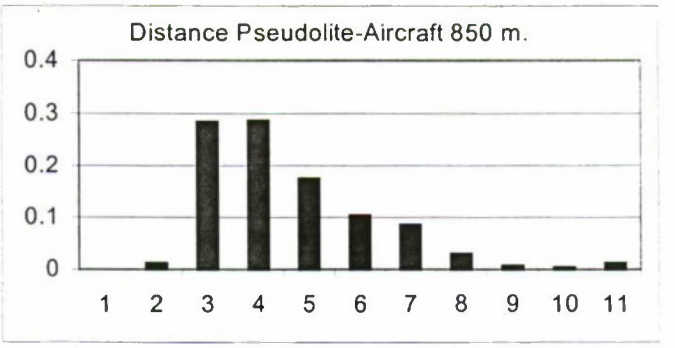

Mean 1.82, RMS 0.35

b)

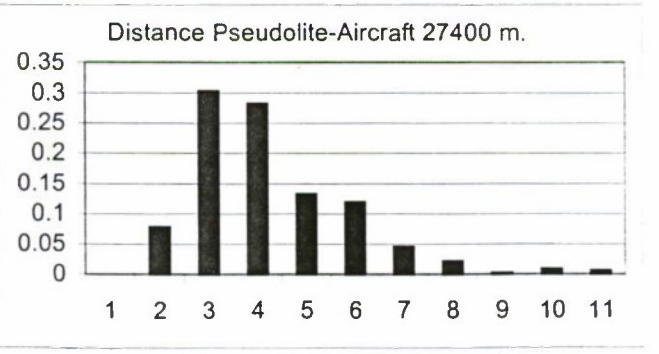

Mean 1.75, RMS 0.31

Fig. 5. Ratios distribution of altitude GF for GPS system to altitude GF for GPS system and 4 APLs with different APLs distances in respect of aircraft

The value $G_{VDOP APL}$ defines as $\overline{G}_{VDOP}/\overline{\xi}$. In $\sigma = 0.9$ m, conformed equipment type ACH-21, altitude measuring error is 1.43 m with 1APL and 0.76 m – with 4 APLs. In computations are accepted that $\overline{G}_{VDOP}$= 2.6, and $\overline{\xi}_4 = 1.821$. These data are obtained by modeling in volume access equal 10 000. The value $\overline{\xi}_1 = 1.34$ takes in Figure 2.

If pseudolite is not used for transmission of the corrective information, the additional systematic error (in SA is switch off) will be approximately 4 m without consideration of the multiple reflection errors on track APL-aircraft. In such a way the pseudolite using without mode of local control-corrective station (LCCS) (without another LCCS) is reasonable.

Conclusions

- As previous carried out computations shown, that using of pseudolites system by GPS system determinations will allow to provide in principle the aircraft landing on Cat-1, if one of APLs operates in mode of local control-corrective station.
- The improvement of geometrical properties of the operational constellations NASE GPS system depend on both the number of pseudolites and its location in respect of aircraft, which is in the point of accepted decision, in particular, from aircraft direction to APL and from "base" APL system, and from airport coordinates. For "Pulkovo" airport the vertical geometrical factor improvement and, consequently, the improvement of potential accuracy measuring is more 1.5 times.

IMPLEMENTATION AND TESTING OF GPS INTEGRITY MONITORING WITH SUPPLEMENTARY NAVIGATION SENSORS

Chang Sun Yoo*, Iee Ki Ahn**
Korea Aerospace Research Institute, Daejon, Korea, E-mail:csyoo@kari.re.kr, ikahn@kari.re.kr
Sang Jeong Lee***
Chungnam National University, Daejon, Korea, E-mail:eesjl@cslab.cnu.ac.kr

Abstract

Key words: GPS, inertial navigation, accuracy, integrity

GPS/INS integrated navigation system has distinct advantages that could compensate shortcoming of each ensor. GPS has been popular newly in a variety of application fields with its advantages of high precision without drift bias when it is compared to inertial navigation system. INS is able to keep navigation information abailable even though GPS has been interfered or jammed. In air navigation, GPS also will be used increasingly but be required solving its integrity in view of aircraft safety. GPS Integrity monitoring is the function to check a consistency of navigation solution from GPS observables and to inform user of warning if faulted signal is included in its observables. The error sources can be considered each in satellite, aircraft and ground sysem - hardware system failure, ephemeris error in satellite, data receiving or processing error, receiver malfunction in aircraft and data transmitting error, jamming, interference in ground system. Integrity monitoring is categorized into three types - Ground-based monitoring or GIC(GPS Integrity Channel), Redundant airborne sensors and RAIM(Reciver Autonomous Integrity Monitoring). Ground-based monitoring is method to obtain integrity information from DGPS reference system on the ground. Redundant airborne sensor or RAIM is method to be supplied its information from another supplementary onboard system or GPS receiver itself. Ground-based monitoring is realized through LAAS/WAAS but is expensive to implement. RAIM is attractive due to simple structure, low cost but have such shortcoming as the minimum number of satellite observables and the decreasing of availability. Integrated navigation through a combination of GPS and Inertial Navigation System can provide many advantage in solving continuity and integrity during GPS outages due to interference, jamming, etc. Its characteristic is to use all previous measurements through adaptive Kalman filter, while RAIM uses current snapshot information. Each additional information available can be used to check for slowly drifting types of faults that can not be detected without this redundancy. GPS/INS system could become alternative to increase GPS integrity performance. On this concept, navigation and error compensation algorithm has been developed on the basis of IMU(Inertial Measurement Unit) which consists of 3 FOG(Fiber Optic Gyroscopes) with 7.2°/h bias and 3 silicon micro-machined accelerometers and has been integrated into INS(Inertial Navigation System). GPS receiver with 12 channel, L1/L2 carrier signal has been added to result in loosely-coupled SDINS/GPS integrate navigation system. The data acquisition system consists of an industrial computer equipped with the 32-channel 16-bit AD converter as well as the IBM notebook computer. Industrial computer collects all raw data from FOGs and accelerometers and uses them for calculating all numerical algorithm by 40 Hz sampling frequency. GPS data is saved simultaneously during test by a notebook computer by 10Hz updating rate and provides both the external navigation information for correcting the navigation output of SDINS and the precise DGPS positioning output as the reference one to compare the results. Automobile tests were conducted in order to verify the developed system on the middle range, it took about 17 minutes to run the route near the Daeduk Science Town. In the procedure of automobile test, the initial alignment was conducted for 200 seconds before the car started to run. But one problem is that the resolution of FOG is not so accurate to measure the earth rotation rate. It means that it can not provide the initial yaw angle of the vehicle, so user needs either to input it artificially or input it from other information source such as magnetometer to supply it. At the starting point the car was aligned to the north direction (ψ =0°) and done the initial alignment procedure for 200 seconds. The trajectory of short range test for 7 minutes compared between GPS/INS and pure INS. The middle range test for 17 minutes show that the initial attitude after alignment was ϕ =1.183°and θ =-0.728° and the final attitude after the car stopped was ϕ =1.715°and θ =-0.674°. Position of integrated navigation system can be compared with DGPS reference position and the mean and standard deviation of position was summarized and shown. GPS integrity monitoring test using INS as supplementary navigation system has been done. On the basis of Kalman filter, the fault detection was implemented for INS/GPS integrated navigation system. First, navigation solution in INS is updated into new one through an addition of error states estimated from error model. Through estimated states and satellite ephemeris information, pseudorange between user and satellite can be calculated. The difference between the calculated value and the mesured one produce measurement and result in the residual. With the residual and the error covariance defined, Test statistic can be defined as SSR(Sum of Squared Residual). This method has characteristic that because SSR includes the previous all measurements, less number of satellite can be availlable than five satellites of RAIM. In Kalman filter, each residual also assumed uncorrelated each other. GPS integrity monitoring was done on the base of additional information from INS. The error characteristic of GPS is range bias drifts or jumps. It is not easy to distinguish a range bias drift of GPS with one of INS but more possible in case of jump error. The detection of fault is determined by comparing test static with the threshold estimated from false alarm. Through above analysis, integrated SDINS/GPS could not only be shown to provide higher accuracy than sole SDINS but also will be presented to give higher integrity than stand-alone GPS.

---

* M.Sc., Senior Researcher of Navigation and Control Group
** D.Sc., Head of Navigation and Control Group
*** D.Sc., Professor, Head of Electronic Laboratory

Introduction

GPS has been applied popularly in a variety of application fields with its advantages of high precision without drift bias when it is compared to inertial navigation system. In a case of the aviation navigation, GPS integrity as well as a precision became much more attractive subject in view of aircraft safety. Methods in implementation of GPS integrity monitoring may be categorized into two case - by GPS itself and by supplementary navigation sensor. The former is using RAIM(Receiver Autonomous Integrity Monitoring), which detects and identifies an faulted GPS with only raw measurements from GPS and provides conveniency and economic profit. The latter is using INS, altimeter, LAAS(Local Area Augmentation System which provide additional reference information to data processing unit interfaced with GPS receiver as primary means.

First in this thesis, navigation and error compensation algorithm has been developed on the basis of IMU(Inertial Measurement Unit) which consists of 3 FOG(Fiber Optic Gyroscopes) with 7.2°/h bias and 3 silicon micro-machined accelerometers and has been integrated into INS(Inertial Navigation System). GPS receiver with 12 channel, L1/L2 carrier signal has been added to result in loosely-coupled SDINS/GPS integrate navigation system. A developed SDINS/GPS system has been tested with ground vehicle and compared to Differential GPS with cm-level precision for evaluation of precision.

Next GPS integrity monitoring test using INS as supplementary navigation system has been done. In measurement data obtained from SDINS/GPS ground vehicle test, one faulted satellite of GPS constellation has been assumed and detected according to fault procedure using an residual information in Kalman filter, so that the capability of expansion to the case of multiple fault detection will be considered .

1. Structure of Navigation System

Strapdown INS Mechanism

The SDINS consists of two parts of calculation; rotational part (attitude determination) and translational part. Brief description of each part of navigation is defined as the following equations (1) and (2) ;

- rotational part : $\dot{\lambda}(t) = \frac{1}{2}\Phi(\lambda)\cdot\lambda(t)$, where $\Phi(\lambda) = \begin{bmatrix} \alpha & -\mathbf{q}^T \\ \mathbf{q} & \alpha\cdot\mathbf{I} - \mathbf{q}\times \end{bmatrix}$, (1)

- translational part : $\begin{bmatrix} \dot{\mathbf{r}}(t) \\ \dot{\mathbf{p}}(t) \end{bmatrix} = \begin{bmatrix} \mathbf{A}_\varphi(t) & t\cdot\mathbf{A}_\varphi(t) \\ \mathbf{0} & \mathbf{A}_\varphi(t) \end{bmatrix}\begin{bmatrix} \mathbf{r}_0 \\ \mathbf{p}_0 \end{bmatrix} + \begin{bmatrix} \mathbf{A}_\varphi(t)\cdot\mathbf{r}_\Delta(t) \\ \mathbf{A}_\varphi(t)\cdot\mathbf{v}_\Delta(t) \end{bmatrix}$, (2)

where $\mathbf{r}_\Delta(t) = \int_0^t (t-s)\cdot\mathbf{a}_g(s)\,ds \qquad \mathbf{p}_0 = \mathbf{v}_0 + \mathbf{u}_\varphi\times\mathbf{r}_0$

$\mathbf{v}_\Delta(t) = \int_0^t \mathbf{a}_g(s)\,ds \qquad \mathbf{a}_g(t) = \mathbf{A}^T(t)\cdot\mathbf{a}(t) + \mathbf{A}_\varphi^T(t)\cdot[\mathbf{g}(t) - \mathbf{w}_\varphi]$

$\lambda = [\alpha \quad \mathbf{q}]^T$ is the quaternion that describes the rotation of vehicle into the inertial frame. ω is the angular rate vector of the vehicle with respect to the inertial frame. $\mathbf{r}$ and $\mathbf{v}$ are the position and velocity vectors with respect to the navigation frame. $\mathbf{u}_\varphi = \Omega[\cos\varphi \quad 0 \quad -\sin\varphi]^T$ is a vector of the earth angular rate and ϕ is a latitude. Transformation matrices, $\mathbf{A}$ and $\mathbf{A}_\varphi$, represent ones from the inertial to the body frame and from the inertial to the navigation frame respectively.

Integrated SDINS/GPS Mechanism

Discrete error equation of SDINS is derived as equation (2) for implementing integrated SDINS/GPS navigation system. The vectors, $\delta\theta(t)$, $\delta\mathbf{r}(t)$ and $\delta\mathbf{p}(t)$, are error states – attitude, position and velocity, to be estimated and are determined by a method of Kalman filtering using a difference between the computed SDINS and the observed GPS values of the vehicle's navigation information : position and velocity

$$\begin{bmatrix} \delta\dot{\theta}(t) \\ \delta\dot{\mathbf{r}}(t) \\ \delta\dot{\mathbf{p}}(t) \end{bmatrix} = \begin{bmatrix} \mathbf{I} & \mathbf{0} & \mathbf{0} \\ \mathbf{A}_\varphi(t)\cdot\mathbf{V}_r(t) & \mathbf{A}_\varphi(t) & t\cdot\mathbf{A}_\varphi(t) \\ \mathbf{A}_\varphi(t)\cdot\mathbf{V}_v(t) & \mathbf{0} & \mathbf{A}_\varphi(t) \end{bmatrix}\begin{bmatrix} \delta\theta(t_0) \\ \delta\mathbf{r}(t_0) \\ \delta\mathbf{p}(t_0) \end{bmatrix} + \begin{bmatrix} t\cdot\hat{\mathbf{A}}_k^T\cdot\mathbf{u}_{\omega k} \\ t^2/2\cdot\mathbf{A}_\varphi(t)\cdot\hat{\mathbf{A}}_k^T\cdot\mathbf{u}_{ak} \\ t\cdot\mathbf{A}_\varphi(t)\cdot\hat{\mathbf{A}}_k^T\cdot\mathbf{u}_{ak} \end{bmatrix} + \begin{bmatrix} \tilde{\varepsilon}_{\theta\omega} \\ \tilde{\varepsilon}_{ra} \\ \tilde{\varepsilon}_{va} \end{bmatrix} \tag{3}$$

$$\mathbf{V}_r(t) = -\int_{t_0}^{t}(t-s)\cdot\hat{\mathbf{A}}^T(s)\cdot\mathbf{a}_0(s)\,ds\times \qquad \mathbf{V}_v(t) = -\int_{t_0}^{t}\hat{\mathbf{A}}^T(s)\cdot\mathbf{a}_0(s)\,ds\times$$

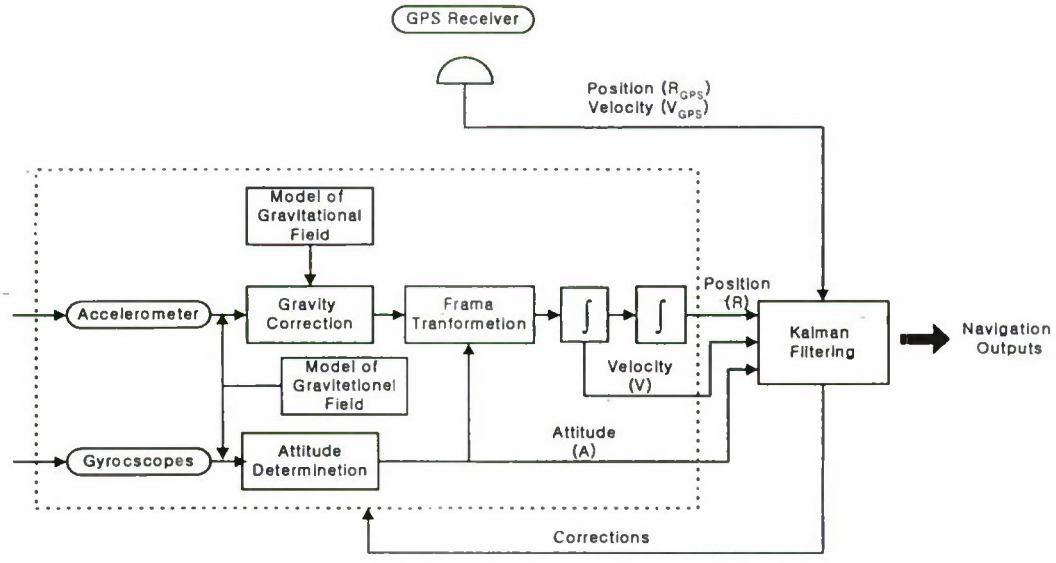

Fig.1. Structure of Integrated GPS/INS System

where the second term on the right hand side is the first approximation of corresponding integral and $\bar{\mathbf{A}}_k$, $\mathbf{u}_{\omega k}$ and $\mathbf{u}_{ak}$ are the mean value of the function $\mathbf{A}(t)$, $\mathbf{u}_{\omega}(t)$ and $\bar{\mathbf{u}}_{\mathbf{a}}(t)$ in the integration interval. The corrected vector for attitude, position and velocity can be found to be the solution of the Riccati equation of optimal control problem

$$\bar{\mathbf{u}}_{\omega,k} = -c_{\omega} \cdot \delta\bar{\theta}_k \quad , \quad \bar{\mathbf{u}}_{\mathbf{a},k} = -c_r \cdot \delta\hat{\mathbf{r}}_k - c_p \cdot \delta\hat{\mathbf{p}}_k \quad . \tag{4}$$

The coefficient of the corrected vector, c_{ω}, c_r and c_p, should be selected by trial and error and its value is set to be 5.0, 8.0, and 4.0 in this test.

2. Test of integrated INS/GPS

Hardware System Description

The developed integrated SDINS/GPS navigation system is composed of a three KVH's 1-axis interferometric type Fiber Optic Gyros(FOG) with a 7.2°/h gyro drift, one 3-axis Crossbow's silicon micro-machined type accelerometer with 30mg of bias and two NovAtel MiLLennium GSPCardTM GPS receivers for DGPS. IMU sets are installed on the one triad mounting frame which makes orthogonal axes and was shown on Fig. 2.

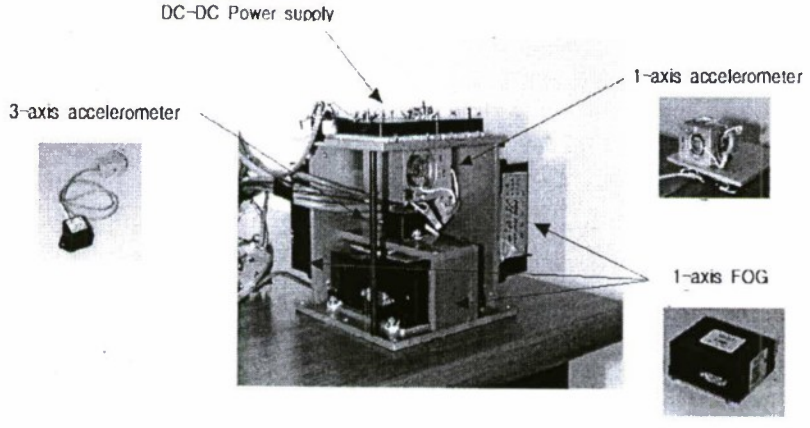

Fig. 2 Structure of Inertial Measurement Unit

Data Acquisition System

The data acquisition system(DAQ) consists of an industrial computer equipped with the 32-channel 16-bit AD converter as well as the IBM notebook computer. Industrial computer's CPU is a Pentium MMX 233 MHz with 64MB DRAM and it collects all raw data from FOGs and two accelerometers. Collected data from IMU is used for calculating all numerical algorithm defined in previous section inside the running time of 40 Hz sampling frequency. GPS data is saved simultaneously during the testing period by a notebook computer shown on Fig. 3. It provides both the external navigation information for correcting the navigation output of SDINS and precise DGPS positioning output as the reference one to compare the results. DGPS positioning result can be obtained from the post-processing software and its accuracy is so accurate as to be used as a reference value. GPS receiver's two communication ports support user-selectable bit rates of 300 - 115,200 bps. In real test, we chose 38,400 bps and the updating rate is 10 Hz.

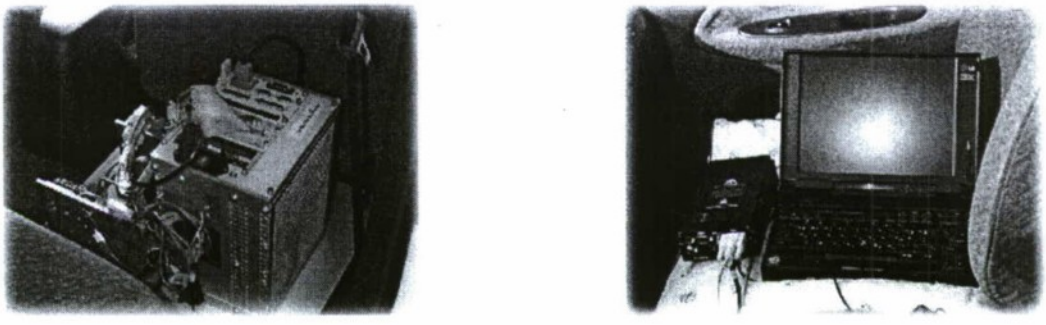

Fig. 3. Data acquisition system for IMU and GPS receiver

Test of integrated INS/GPS

All system described above were installed in automobile and automobile tests were conducted in order to verify the developed system on the middle range, it took about 17 minutes to run the route near the Daeduk Science Town.

In the procedure of automobile test, the initial alignment was conducted for 200 seconds before the car started to run. But one problem is that the resolution of FOG is not so accurate to measure the earth rotation rate. It means that it can not provide the initial yaw angle of the vehicle, so user needs either to input it artificially or input it from other information source such as magnetometer to supply it.

At the starting point the car was aligned to the north direction (ψ =0°) and done the initial alignment procedure for 200 seconds. Fig. 4.and Fig. 5 shows the trajectory of short range test for 7 minutes compared between GPS/INS and pure INS. Fig. 6 shows the trajectory of the middle range test for 17 minutes. The initial attitude after alignment was ϕ =1.183°and Θ =-0.728° and the final attitude after the car stopped was ϕ =1.715°and Θ =-0.674°. Position of integrated navigation system can be compared with DGPS reference position and the mean and standard deviation of position are summarized in Table 1.

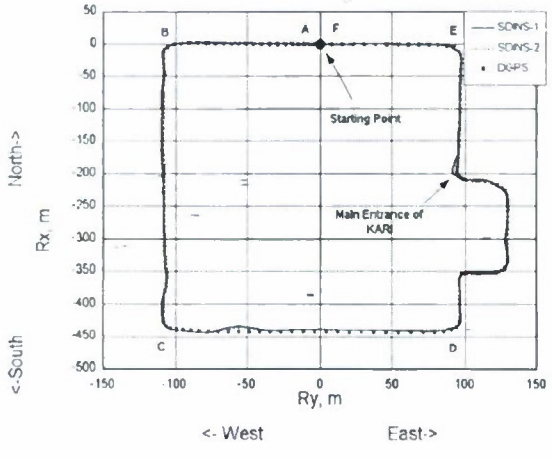

Fig .4. Trajectory of GPS/INS range test

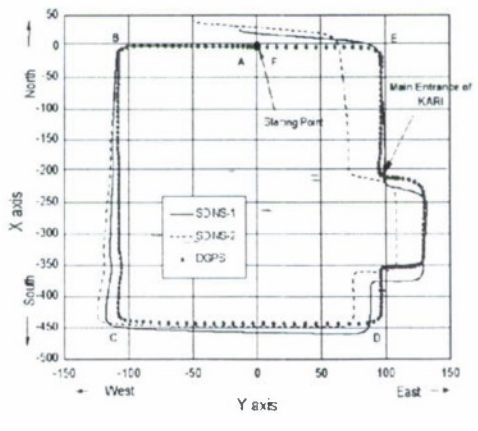

Fig. 5. Trajectory of pure INS range test

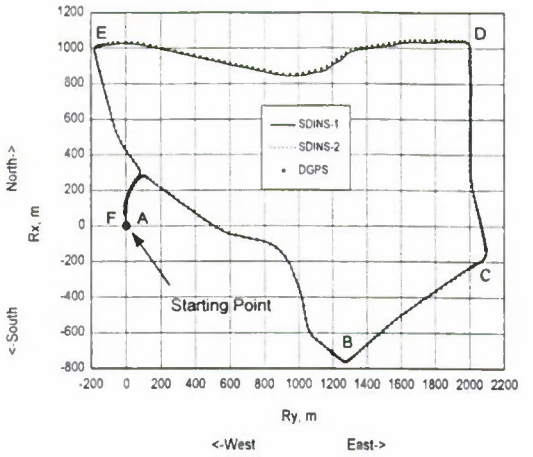

Fig. 6 Trajectory of middle range test

Period		Integrated SDINS/GPS		
		Δr_x (m)	Δr_y (m)	δr_z (m)
A-B	mean	0.1563	-2.0436	4.8414
	std (ó)	4.3548	4.3023	4.3378
B-C	mean	-4.1140	-4.6659	0.4898
	std (ó)	3.2862	3.4980	2.0238
C-D	mean	9.0662	-6.5153	-0.3832
	std (ó)	4.4695	2.0777	4.5908
D-E	mean	6.7169	-24.1905	5.3665
	std (ó)	4.9869	13.6930	6.6057
E-F	mean	-19.006	3.5515	-1.6698
	std (ó)	23.5526	13.4711	1.1439

Table 1. Statistics of position difference

3. GPS Integrity Monitoring in GPS/INS Integrated Navigation System

GPS Integrity monitoring has a function to check a consistency of navigation solution from GPS observables and to inform user of warning if faulted signal is included in its observables. GPS has become very popular but been required to provide fully 6×10^{-8} /Fhr integrity for aviation navigation in view of safety. Considering this integrity, redundancy in raw measurement or navigation solution is necessary. The error sources can be considered each in satellite, aircraft and ground system - hardware system failure, ephemeris error in satellite, data receiving or processing error, receiver malfunction in aircraft and data transmitting error, jamming, interference in ground system..

Integrity monitoring is categorized into three types - Ground-based monitoring or GIC(GPS Integrity Channel), Redundant airborne sensors and RAIM. Ground-based monitoring is method to obtain integrity information from DGPS reference system on the ground. Redundant airborne sensor or RAIM is method to be supplied its information from another supplementary onboard system or GPS receiver itself. Ground-based monitoring is realized through LAAS/WAAS but is expensive to implement. RAIM is attractive due to simple structure, low cost but have such shortcoming as the minimum number of satellite observable and the decreasing of availability .

Integrated navigation through a combination of GPS and Inertial Navigation System can provide many advantage in solving continuity and integrity during GPS outages due to interference, jamming, etc. Its characteristic is to use all previous measurements through adaptive Kalman filter, although RAIM to use current snapshot information. Each additional information available can be used to check for slowly drifting types of faults that can not be detected without this redundancy[9][10].

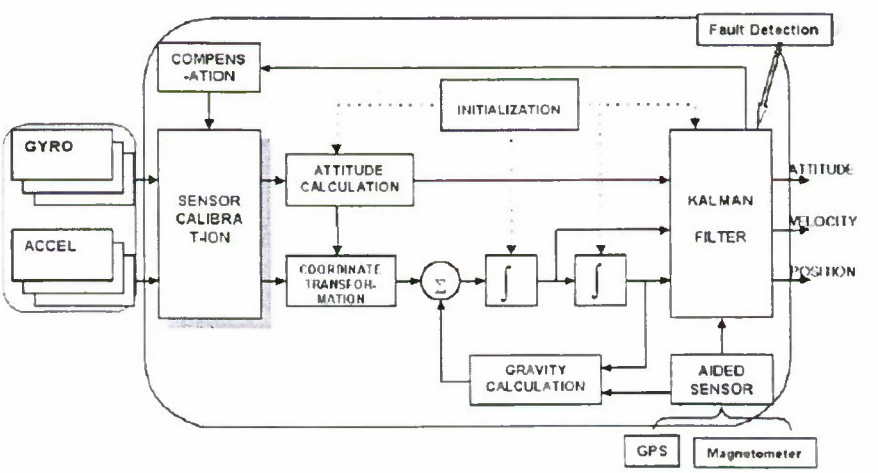

Fig. 7. Fault detection structure of GPS/INS integrated system

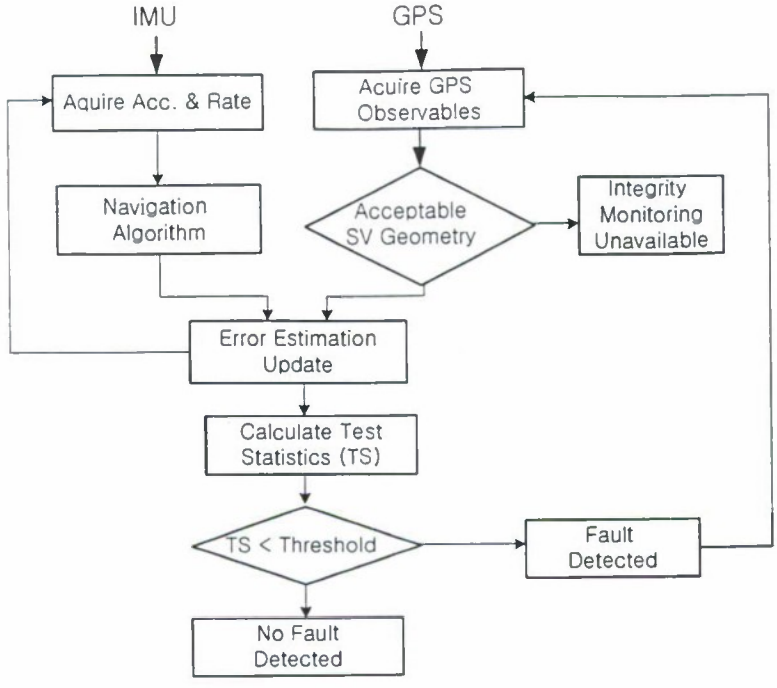

Fig. 8 Block diagram of fault detection in GPS/INS

Kalman filter

The central problem for the GPS receiver is the precise estimation of position, velocity, and time based on noisy observations of the satellite signals. This is an ideal setting for Kalman filtering. For the purpose of employing Kalman filter method in GPS solution it is necessary to introduce into consideration the dynamic model of the receiver. Three dynamic models of user are of interest for the analysis of GPS position accuracy: stationary, low dynamic and high dynamic[5,6].

Let us consider the low dynamics model of the user. In this case the position, velocity and clock bias and drift must be estimated leading to 8-element state representation. The corresponding dynamic model of errors is given by

$$\begin{bmatrix} \delta\dot{\mathbf{r}} \\ \delta\dot{\mathbf{v}} \\ \delta\dot{\mathbf{t}} \end{bmatrix} = \begin{bmatrix} \mathbf{0} & \mathbf{I} & \mathbf{0} \\ \mathbf{0} & \mathbf{0} & \mathbf{0} \\ \mathbf{0} & \mathbf{0} & \mathbf{F}_t \end{bmatrix} \begin{bmatrix} \delta\mathbf{r} \\ \delta\mathbf{v} \\ \delta\mathbf{t} \end{bmatrix} + \begin{bmatrix} \mathbf{0} \\ \eta_v \\ \eta_t \end{bmatrix}, \tag{5}$$

where $\delta\mathbf{t} = \begin{bmatrix} \delta b \\ \delta \mathrm{f} \end{bmatrix}$, $\mathbf{F}_t = \begin{bmatrix} 0 & 1 \\ 0 & 0 \end{bmatrix}$. η_v and η_t are a zero-mean uncorrelated Gaussian plant noise process with the covariance matrixes $\mathbf{Q}_v$ and $\mathbf{Q}_t$. Put $\delta\mathbf{x} = [\delta\mathbf{r} \quad \delta\mathbf{v} \quad \delta\mathbf{t}]'$. Then the corresponding model for a linear stochastic system (21) in discrete can be expressed in form

$$\delta\mathbf{x}_k = \Phi\delta\mathbf{x}_{k-1} + \xi_{k-1}, \tag{6}$$

where $\delta\mathbf{x}_k$ is the system state vector at time t_k, ξ_k is the zero-mean Gaussian vector sequences with the covariance matrix $\mathbf{Q}_k$, Φ is the state transition matrix with interval Δ:

$$\Phi = \begin{bmatrix} \mathbf{I} & \Delta\cdot\mathbf{I} & \mathbf{0} \\ \mathbf{0} & \mathbf{I} & \mathbf{0} \\ \mathbf{0} & \mathbf{0} & \Phi_t \end{bmatrix}, \qquad \Phi_t = \begin{bmatrix} 1 & \Delta \\ 0 & 1 \end{bmatrix} \tag{7}$$

The mathematical relationships between the covariance matrices of the continuous-time and discrete-time process noise of plant may be recalculation . The resulting value of the clock bias discrete time process noise matrix may be find.

The system output $\mathbf{z}_k = \left[\delta\vec{\rho}_k \quad \delta\dot{\vec{\rho}}_k\right]$ has the model equations

$$\mathbf{z}_k = \mathbf{H}_k \delta\mathbf{x} + \psi_k \,, \tag{8}$$

where ψ_k is the zero-mean measurement noise with the covariance matrix $\mathbf{R}_k$, $\mathbf{H}_k$ is the measurement sensitivity matrix:

$$\mathbf{H}_k = \begin{bmatrix} \mathbf{L}_k & 0 & 1_n & 0 \\ 0 & \mathbf{L}_k & 0 & 1_n \end{bmatrix}. \tag{9}$$

Let us establish an initial estimate of state $\delta\hat{\mathbf{x}}_0^+$ and the state covariance matrix $\mathbf{P}_0^+$. The state estimate and the error covariance of estimation is updated.

$$\begin{aligned} &\delta\hat{\mathbf{x}}_k^- = \Phi\delta\hat{\mathbf{x}}_{k-1}^+ \,, \\ &\mathbf{P}_k^- = \Phi\mathbf{P}_{k-1}^+\Phi^{\mathrm{T}} + \mathbf{Q}_{k-1} \,, \\ &\delta\hat{\mathbf{x}}_k^+ = \delta\hat{\mathbf{x}}_k^- + \mathbf{K}_k(\mathbf{z}_k - \mathbf{H}_k\delta\hat{\mathbf{x}}_k^-) \,, \\ &\mathbf{K}_k = \mathbf{P}_k^-\mathbf{H}_k^{\mathrm{T}}(\mathbf{H}_k\mathbf{P}_k^-\mathbf{H}_k^{\mathrm{T}} + \mathbf{R}_k)^{-1} \,, \\ &\mathbf{P}_k^+ = (\mathbf{I} - \mathbf{K}_k\mathbf{H}_k)\mathbf{P}_k^- \,. \end{aligned} \tag{10}$$

Taking into account a further construction of the GPS+SINS integrated system, the two approach for GPS solution is considered. First, it is interpolating the GPS data on the interval $[0,\Delta]$ with the time of discreteness d by using of the satellites position, the pseudorange and the delta range parabolic representations. This approach may be used only in post-flight analysis. Second, it is extrapolating on the same interval with the same discreteness. This approach may be used in real-time implementation

Fault detection

On the basis of above Kalman filter, the fault detection was implemented for INS/GPS integrated navigation system as follow. First, navigation solution $S_i^-(t)$ in INS is updated into $S_i^+(t)$ through an addition of error states estimated from error model.

$$x_i^+(t) = x_i^-(t) + \delta x(t) \,. \tag{11}$$

Through $x_i^+(t)$ and satellite ephemeris information, pseudorange $PR_{ic}^+(t)$ between user and satellite can be calculated. The difference between the calculated value $PR_{ic}^+(t)$ and the mesured one $PR_i^+(t)$ produce measurement $z_i^+(t)$

$$z_i^+(t) = PR_{ic}^+(t) - PR_i^+(t) \,. \tag{12}$$

For fault detection, the residual $\gamma(k)$ and the error covariance $V(k)$ is defined and Test statistic can be defined as SSR(Sum of Squared Residual) with the residual $\gamma(k)$ and the error covariance as follow

$$\begin{aligned} &\gamma(k) = z(k) - H(k) * x^-(k) \,, \\ &V(k) = H(k) * P^-(k) * H^T(k) + R \,, \\ &s^2(k) = \gamma^T(k) * V^{-1}(k) * \gamma(k) \,. \end{aligned} \tag{13}$$

This method has characteristic that because SSR includes the previous all measurements, less number of satellite is availlable than minimum five satellites is needed in RAIM. In Kalman filter, each residual also is uncorrelated each other. Because pseudorange residual is considered for each satellite, faulted satellite can be identified. In the above SDINS/GPS, GPS integrity monitoring was done on the base of additional information from INS. The error characteristic of GPS is range bias drifts or jumps. It is not easy to distinguish a range bias drift of GPS with one of INS but more possible in case of jump error.

When 'h' is the threshold estimated from false alarm, the detection of fault is determined as follow:

$$\begin{aligned} &\text{Faulted} \quad : S\ (k) > h \,, \\ &\text{Unfaulted} : S\ (k) < h \,. \end{aligned} \tag{14}$$

Through above analysis, integrated SDINS/GPS could not only be shown to provide higher accuracy than sole SDINS but also will be presented to give higher integrity than stand-alone GPS.

Conclusions

1. The integrated SDINS and GPS navigation system has been developed on the base of the chosen reference coordinates. This mechanization uses GPS as the external aids information system with Kalman filtering. This integrated SDINS and GPS navigation system was tested through the automobile test with the IMU and GPS receivers. GPS external information can improve the performance of pure navigation system : Strapdown INS. The ability of integrated navigation system to detect and correct the time dependent drift of SDINS was demonstrated and verified.

2. Based on field test data collected during the tests, the achievable position error is between 2.8 to 5.3m for time periods up to 7 minutes in short range test. Under middle range test conditions, integrated navigation system provides position accuracy of 9.1m in x axis, 6.6m in y axis and 5.4m in z axis.

3. In this paper investigation into improvement of SDINS/GPS for correcting GPS cycle slips was not proved and demonstrated. This typical feature is also important advantage of integrated SDINS./GPS navigation system. And also some deficiency of observable capability to correct the yaw angle of vehicle should be considered to be implemented especially on airborne applications.

4.Kalman filter for GPS integrity monitoring was derived. This will be served in detecting faulted satellite of GPS constellation according to fault procedure using an residual information in Kalman filter, so that the capability of expansion to the case of fault exclusion will be considered

References

1. KARI reserch report -*Technology Development of the Inertial Navigation and Global Navigation Satellite System*, UCEN99160, Aug. 2000
2. **S. J. Lee, C. S. Yoo, Y. H. Shim and J. C. Kim**, Performance Testing of Integrated Strapdwon INS and GPS //KSAS International Journal, Vol. 1, No. 1, 2000, pp.81-91.
3. **S. J. Lee, Naumenko, C. and Kim, J. C.**, Development of Correction Algorithm for Integrated Strapdown INS/GPS by using Kalman Filter //KSAS International Journal, 2001.
4. **C. S. Yoo and S. J. Lee**, A Case Study of RAIM using Parity Space Technique, KSAS Spring Conference, Korea, Apr. 1999
5. **C. S. Yoo and S. J. Lee** Study on Two-Failure GPS RAIM Problem, ICASE Autumn Conference,Korea, 2000
6. **R. G. Brown,** A Baseline GPS RAIM Scheme and a Note on the Equivalence of Three RAIM Methods. //NAVIGATION : Journal of the Institute of Navigation, 39(3):301-316, Fall 1992
7. **Mats Brenner,** Implementation of a RAIM Monitor in a GPS Receiver and an Integrated GPS/IRS, ION GPS-90, Sep19-21, 1990
8. **J. Diesel and S. Luu.** GPS/IRS AIME : Calculation of Thresholds and Protection Radius Using Chi-Squared Methods. In Proc. of ION GPS-95, vol. 2, pp 1959-1964, ION, 1995
9. **Farrel J., Barth M.**, *The Global Positioning System and Inertial Navigation*, McGraw-Hill, New York, 1999.
10. **M. Basseville and I. V. Nikiforov**, *Detection of Abrupt Changes : Theory and Application*. //Information and System Science Series. Prentice-Hall, Englewood Cliffs, N.J. USA, 1993

A COMPARISON OF TWO INTEGRATED AIRBORNE POSITIONING AND ORIENTATION SYSTEMS

O. Schiele, A. Kleusberg
Institute of Navigation, Stuttgart University, Geschwister-Scholl-Str. 24D, D-70174 Stuttgart, Germany
R. Horn
Institut für Hochfrequenztechnik und Radarsysteme, German Aerospace Center (DLR), Münchner Str. 20, D-82234 Weßling, Germany

Abstract

Key words: GPS, IMU, Integrated Positioning Systems, Airborne Sensor Positioning

Airborne remote sensing systems like Laser Scanners, Digital Line Cameras, Synthetic Aperture Radar (SAR) are systems of choice for fast acquisition of mass topographic data. For georeferencing purposes, these sensor systems rely on external positioning and orientation support of extremely demanding accuracy. Sensor position and orientation is typically provided by an integrated measurement and processing unit including a (differential) Global Positioning System (GPS) receiver and an Inertial Measurement Unit (IMU). Conventional analogue airborne photogrammetry and Digital Frame Cameras also benefit greatly from such external positioning/orientation provision.

Two such integrated sensor positioning and orientation systems are commercially available: the CCNS/AEROcontrol-IIb of IGI of Kreuztal/Germany and the POS/AV510 of Applanix of Richmond/Canada. These two systems were flown side-by-side in the DLR (German Aerospace Centre) fixed-wing aircraft during a SAR data acquisition mission. Post mission data processing of the GPS and IMU data yielded separate sensor trajectories (position, velocity, orientation) for the two systems at a data rate of 200 Hz for the POS/AV™510 and 50 Hz for the CCNS/AEROcontrol-IIb, for a total flight duration of about two hours and 40 min. The two trajectories are analysed and compared in order to identify any shortcomings in either system, and in order to cross-check if the two systems meet their advertised performance specifications.

Introduction

The positioning and orientation of airborne sensors with integrated GPS/IMU-systems is required for two reasons. First, the integrated system operated in real-time positioning mode provides guidance information to the pilot in order to maintain the planned flight schedule and to avoid data gaps between flight lines. Typical real-time accuracy requirement is of the order of several metres. Secondly, the integrated system must provide precise position and orientation for the sensor in order to georeference the sensor data. For this purpose the raw GPS data and raw IMU data are recorded during the flight and post-processed in the office.

For the most demanding applications, the pseudorange and carrier phase GPS data are recorded in the aircraft and simultaneously at a nearby GPS reference station at data rates of about 1 Hz. The IMU raw data consists of incremental angles (i.e. integrated angular velocity) and incremental velocity (i.e. integrated acceleration) at a much higher data rate. IMU data and GPS data are recorded using the same time scale, usually provided by the GPS receiver. The post-processing of the recorded data is done in either a centralised (or tightly coupled) approach, or in a decentralised (or loosely coupled) approach. In the centralised approach, the GPS raw data from both aircraft and reference station are directly combined with the IMU raw data to generate a time history (at the IMU data rate) of positions and orientation angles for the sensor platform. In the decentralised approach, the processing is done in two subsequent steps: first the GPS raw data from aircraft and reference station receiver are combined to generate the time history of the GPS antenna aboard the aircraft (at the GPS data rate). Then in a second step, the aircraft antenna positions are combined with the IMU raw data to generate a time history (at the IMU data rate) of positions and orientation angles for the sensor platform. For both approaches, the lever arms between IMU and GPS antenna, and between IMU and sensor platform must be taken into account.

Differential GPS positioning (i.e. GPS positioning involving a nearby GPS reference station) based on carrier phase measurements typically can achieve position accuracies better than 10 cm in three dimensions. This position accuracy level can hardly be improved with IMU data, especially since the IMU is rather insensitive to absolute position. Then the primary role of GPS and IMU data in such an integrated system is as follows, especially in the loosely coupled combination approach:

- The differential pseudorange and carrier phase measurements determine the GPS antenna trajectory aboard the aircraft (position and velocity) at the GPS data rate
- The GPS antenna trajectory data and IMU raw data serve to determine the IMU axes orientation and the IMU sensor calibration values
- The IMU data together with the lever arm data transfer the aircraft antenna trajectory into the trajectory of the remote sensing sensor

- The IMU data is used to interpolate the sensor position and the IMU axes orientation from the low GPS data rate to the higher IMU data rate
- The data from very accurate IMUs may be capable of smoothing out some of the random errors in the GPS determined trajectory.

The accuracy of the position and orientation determined with carrier phase based differential GPS and a precise IMU is rather difficult to assess, since other types of systems of comparable performance not exist. In the past several tests of such systems have been executed involving a comparison between positions and orientations of aero-photogrammetry cameras determined from aerotriangulation with the positions and orientations determined using integrated GPS/IMU systems, e.g. Cramer (2001), Heipke et al. (2001). A common problem of these comparisons is the requirement of precise knowledge of the interior orientation (in particular the focal length) of the camera, which is typically not known at the required accuracy level. Also, this kind of comparison can be done only for those rather few points of the camera trajectory, where a photogrammetric image was taken.

In the present article we will assess the accuracy potential of integrated GPS/IMU systems in a different way. We first observe, that there are four distinct parts contributing to the overall result for a decentralised integration approach:

- The GPS measurements obtained with the GPS receivers aboard the aircraft and at the GPS reference station
- The software used to determine the GPS antenna trajectory based on GPS carrier phase data
- The IMU measurements of incremental angles and incremental velocity
- The software used to combine the IMU raw data with the GPS determined discrete trajectory points.

Quite a number of articles have been written about the accuracy of differential kinematic GPS positioning, e.g. Raquet et al. (1998). It is typically an agreed opinion, that in benign environments close to the GPS reference station a position accuracy of better than 10 cm can be achieved. Therefore, in the present article we will concentrate on the accuracy limitations imposed by the remaining parts of the process, the IMU raw data generation and their combination with the GPS determined antenna trajectory in software. These parts of the process completely determine the orientation of the remote sensing sensor, and also determine the sensor's position between the low rate GPS points along the sensor trajectory.

We have flown a differential GPS system together with two IMUs of different makes simultaneously aboard the DLR research aircraft. The IMUs are manufactured by different companies and the IMU data are combined with the same GPS determined trajectory using independently developed software packages, possibly employing different error models and different adjustment algorithms. We then compare the result of these combinations and observe, that differences in the results are not to be attributed to the differential GPS but solely to the IMU measurements and the models employed in the combination software.

Before proceeding to this comparison we observe that such integrated systems do determine the position of the sensor, but cannot determine the orientation of the sensor. The IMU axes normally are not parallel to the axes of the remote sensing sensor system. It is always the IMU platform axes' orientation that is determined. Since sensor axes and IMU platform axes do not coincide in general, the (constant) angular offset between the two sets of axes must be determined by other means ("bore-sight alignment"). For the same reasons it is to be expected, that there is always an angular offset between the orientation parameters provided by processing data from different IMUs aboard the same aircraft. However, if both IMUs are rigidly attached to the aircraft structure, these offsets are expected to remain constant in time.

1. Description of the integrated systems

The two IMUs considered in this article are parts of the integrated GPS/IMU systems Applanix POS/AV510 owned by Stuttgart University and CCNS/AEROcontrol-IIb owned by DLR. The Applanix system consists of a dual frequency NovAtel MiLLenium GPS receiver, a Strap Down IMU named AIMU based on DMARS design of Inertial Science, Inc./USA, and a controller for system operation including real time positioning and raw data recording for GPS and IMU data. The AEROcontrol system consists of a dual frequency Ashtech Z-12 GPS receiver, a Strap Down LCR-88 IMU* of Litef/Germany, a controller for system operation including real time positioning and raw data recording, and software/hardware for flight guidance (CCNS).

Both IMUs consist internally of two two-degree-of-freedom dry dynamically tuned gyroscopes and three pendulous accelerometers delivering at the data interface three-dimensional time tagged measurements of

* The CCNS/AEROcontrol-IIb considered here is a predecessor of the CCNS/AEROcontrol-IId presently marketed by IGI of Kreuzial, Germany. The gyros of the IMU incorporated in the CCNS/AEROcontrol-IId are based on fibre optics technology.

velocity increments and of angular increments at data rates of 50 Hz and 200 Hz for the LCR-88 and the AIMU, respectively.

Both systems achieve their most accurate results in post-processing the recorded GPS pseudorange and carrier phase data from the aircraft GPS receiver and the GPS reference station, and thereafter integrating the IMU raw data with the GPS determined trajectory data. The determination of the GPS antenna trajectory is done with commercially available kinematic GPS software provided by the distributors of the respective systems as part of the overall software package. The integration of the GPS determined trajectory with IMU data and lever arm data is done with proprietary software tools of IGI and Applanix; either system uses the loosely coupled approach sketched above. The final result is the sensor position in terms of geodetic longitude and latitude and ellipsoidal height, the IMU axes orientation in terms of roll, pitch and azimuth angle (heading), and the respective accuracy estimates; the maximum data rate of the final result is the IMU data rate.

Based on the assumption that the aircraft GPS antenna trajectory can be determined through kinematic differential GPS carrier phase positioning with correctly resolved and fixed carrier phase ambiguities, the RMS accuracy specifications for the two systems are as follows (the range indicated for position accuracy accounts for the position accuracy dependence on distance from the GPS reference station). The figures given apply for 'typical flying conditions'.

Table 1: System performance specifications

	Position accuracy	Roll/pitch accuracy	Heading accuracy
Applanix POS/AV510	0.05 m to 0.30 m	0.005 deg	0.008 deg
IGI CCNS/AEROcontrol IIb	0.1 m + 1 ppm	0.01 deg	0.02 deg

2. Test flight set-up and data recording

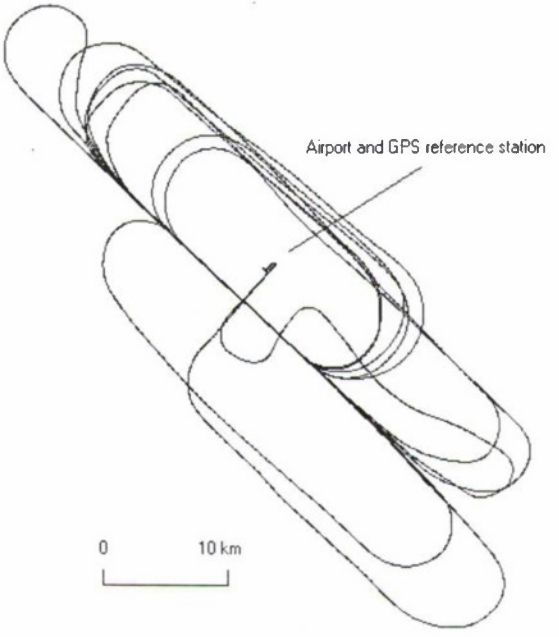

Fig.1. Test flight pattern

A test of the two integrated systems was scheduled during a regular test flight of the DLR Synthetic Aperture Radar system E-SAR close to the DLR facilities near Oberpfaffenhofen, Germany on March 16, 2001. The flight design called for 10 flights along a central line south-west of the DLR airport at an altitude of about 3700 m. The first four lines were flown in north-western direction, the remaining six lines were flown in south-eastern direction; flight duration for each line is about 2.5 min. The resulting flight pattern is shown in Fig. 1; direction North is upwards in Fig.1. During the flight the maximum distance to the GPS reference station located at the airport did not exceed 30 km; during the 10 central SAR lines, the distance did not exceed 10 km. The total flight duration was about 2 h 40 min.

For the purpose of this test, raw IMU data were recorded by both systems and GPS raw data were recorded by the NovAtel MiLLenium GPS receiver aboard the aircraft and an Ashtech Z-12 receiver at the GPS reference

station. The lever arms between the two IMUs and between the IMUs and the GPS antenna were measured conventionally with an estimated accuracy of one cm. These data together with the known geodetic co-ordinates of the GPS reference station form the basis for the data processing described below.

3. Data processing

As mentioned in the Introduction, this article concentrates on the performance of the IMU and the software used to integrate IMU data with the GPS determined trajectory. In order to keep this assessment free from influences of the different GPS receivers involved, only a single trajectory was computed using the NovAtel receivers both in the aircraft and at the GPS reference station. The 1 Hz DGPS data was processed with the PosGPS V3 software of Waypoint Consulting of Calgary, Canada. The GPS data were 'clean' and the data processing did not necessitate any operator intervention. The result of the carrier phase processing with fixed phase ambiguities was an uninterrupted 1 Hz sequence of WGS84 referenced longitude, latitude and ellipsoidal height of the GPS antenna covering the complete duration of the flight. These data together with the lever arm measurements between the two IMUs and the GPS antenna was input for the integration software.

The CCNS/AEROcontrol-IIb IMU data were integrated with the GPS determined trajectory using the software AEROoffice V4.0 of IGI. This processing was done at the IGI facilities by IGI staff. The result were longitude, latitude and ellipsoidal height for the AEROcontrol-IIb IMU centre and the AEROcontrol-IIb IMU orientation in terms of Roll, Pitch, and Heading angles, both at 50 Hz data rate. These 50 Hz trajectory data were made available to the authors. For the purpose of further evaluation and comparison, the positions were transformed to horizontal metric co-ordinates (Gauß-Krüger Easting and Northing with respect to the WGS ellipsoid) and heights above the WGS ellipsoid.

The Applanix AIMU data were integrated with the GPS determined trajectory using the software PosProc V2.1.4 of Applanix. This processing was done at the Institute of Navigation by the authors. The result were longitude, latitude and ellipsoidal height for the AEROcontrol-IIb IMU centre (lever arm between IMUs was taken into account) and the Applanix AIMU orientation in terms of Roll, Pitch, and Heading angles, both at 100 Hz data rate. For the purpose of further evaluation and comparison, the data were decimated to 50 Hz, and the positions were transformed to horizontal metric co-ordinates (Gauß-Krüger Easting and Northing with respect to the WGS ellipsoid) and heights above the WGS ellipsoid.

For the comparison of the positions and orientation angles, the data were separated into sequences covering 'typical flying conditions' (i.e. the 10 straight lines of SAR data acquisition) and 'non typical flying conditions' (i.e. everything else). Since the system performance specifications in Table 1 apply only for 'typical flying conditions', the following section 4 is restricted to the 10 straight lines of about 2.5 min duration each.

4. Results

For each of the ten straight lines, about 7500 3-d positions and orientation angles were now available for a direct comparison. We will perform this comparison in two steps. First we will look at differences in positions and orientation angles at the full second time marks coinciding with the time epochs of the GPS trajectory, and secondly we will look at subsets of position and orientation differences at the full data resolution of 50 Hz.

The 1 Hz data comparison is shown graphically in Figure 2 for the positions and in Figure 3 for the orientation angles. For each straight line segment about 150 data points are available. The differences are computed in the sense PosProc minus AEROoffice. A statistical summary for the differences is provided in Table 2.

Figure 2 and Table 2 clearly support the statement made in the Introduction, that the GPS determined trajectory is only minimally altered and/or improved by the integration software. Both integrated trajectories agree in the mean at the millimetre level. Standard deviations are 6 mm, 8 mm and 4 mm for Easting, Northing and Altitude, respectively. The maximum deviations from the mean do not exceed four times the standard deviation. No systematic behaviour is discernible in the position differences.

Table 2. Statistics for trajectory differences (1 Hz)

	Delta East	Delta North	Delta Alt.	Delta Roll	Delta Pitch	Delta Head.
Mean	-0.002 m	0.001 m	-0.002 m	0.292 deg	-0.043 deg	0.296 deg
Standard Deviation	0.006 m	0.008 m	0.004 m	0.010 deg	0.007 deg	0.026 deg
Max. Deviation	0.016 m	0.025 m	0.017 m	0.023 deg	0.022 deg	0.066 deg
Min. Deviation	-0.020 m	-0.028 m	-0.014 m	-0.031 deg	-0.026 deg	-0.051 deg

The plot of the differences of orientation angles in Figure 3 is dominated by the systematic and nearly constant offset from zero. This offset is to be expected, since we look at the differences between the orientation angles of two different IMUs. Such a constant offset is also present when the orientation of a remote sensing sensor is to

be determined, see section Introduction; the process of determining this offset is known by the name of bore-sight alignment. Under this aspect, of importance in the present context is the deviation of the angular differences from their mean values.

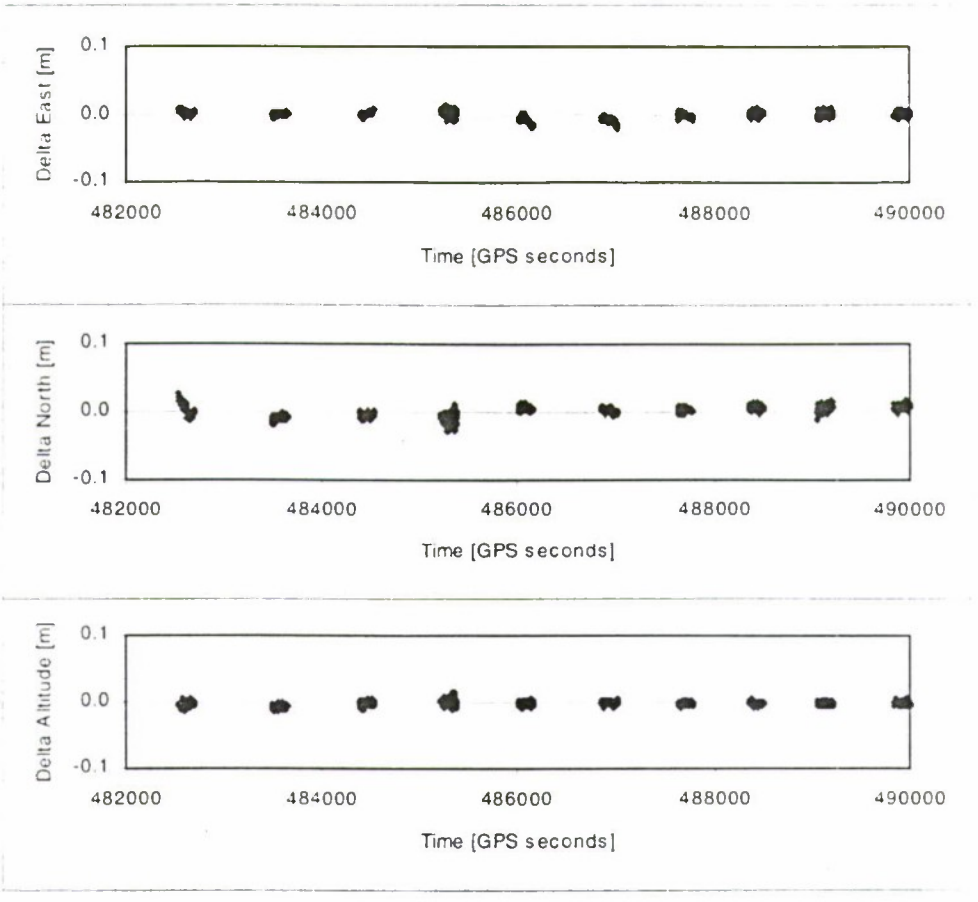

Fig. 2. 3-d position differences PosProc minus AEROoffice at 1 Hz

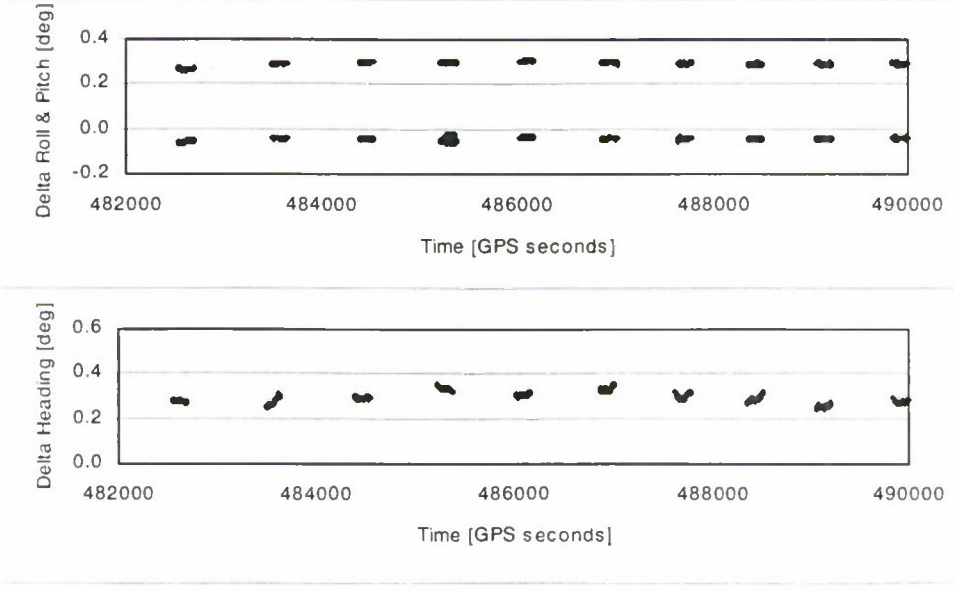

Fig. 3. 3-d orientation differences PosProc minus AEROoffice at 1 Hz

The statistics of these deviations from their mean value are listed in Table 2. The standard deviations for Roll, Pitch and Heading differences are 0.010 deg, 0.007 deg and 0.026 deg, respectively. The maximum deviations

do not exeeed four times the standard deviations. While no clear systematie behaviour is obvious from the plots of Roll and Pitch differences, sueh systematie trends are clearly diseernible in the Heading differences, e.g. in the second line. Overall the agreement is poorer in Heading than in Roll and Piteh; this is to be expeeted as Heading is less well determined in by an IMU than the other orientation angles.

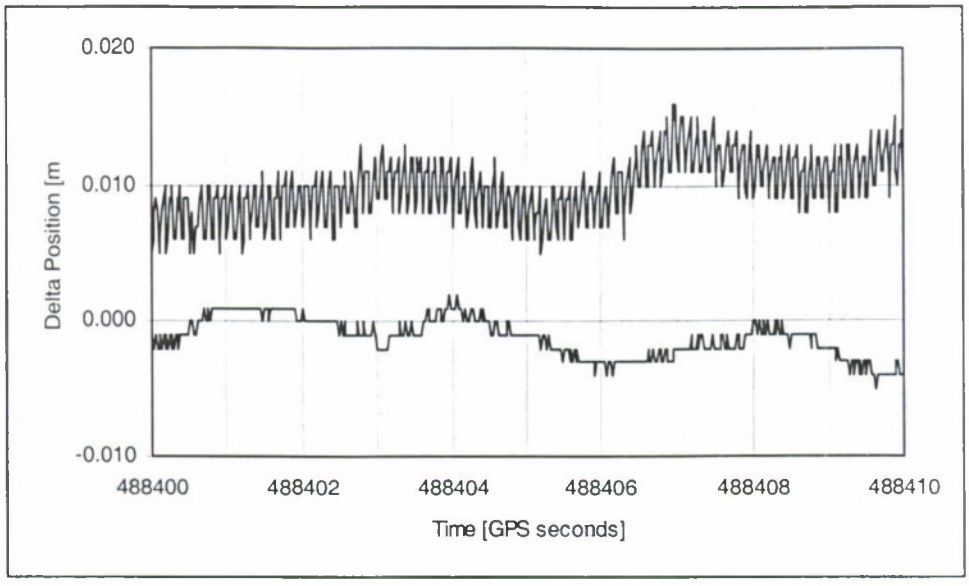

Fig. 4. Position differences PosProc minus AEROoffice at 50 Hz

As mentioned above a second type of comparison was done at the full data rate of 50 Hz. For this comparison a 10 second interval was arbitrarily seleeted showing data that is typieal for all ten straight lines. The ten second data span was taken from the eighth line. Figure 4 shows the differences in Northing (upper curve) and in Altitude (lower curve). The height differences basically show a linear behaviour between the full second epochs of GPS position updates, overlaid by data resolution noise (three deeimals are retained in the position data).

Quite different features are visible in the plot of Northing differences. Overlaid on the linearly interpolating eurve between full seeond epoehs is an oseillation with an amplitude of about 2 mm and a frequeney of exactly 10 Hz. The same amplitude and frequeney was found in the Easting differenees. Figure 5 shows for a one second interval the differences in Northing (upper eurve) and Easting (lower curve).

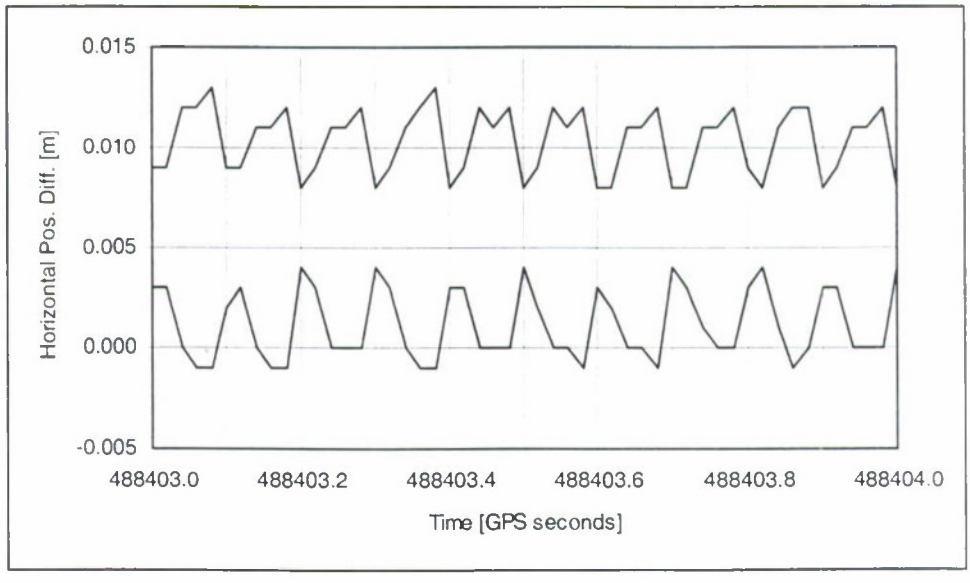

Fig. 5. Horizontal position differences PosProc minus AEROoffice at 50 Hz

Obviously the two curves are phase shifted by 180 deg. Recalling from Figure 1 that all lines were flown at Headings of approximately 135 deg or 315 deg, the two eurves of Figure 5 show a 10 Hz oscillation in flight

direction with an amplitude of about 3 mm. It is highly unlikely, that this translational oscillation between the IMUs really did happen during the flight. Whether this is an artefact of either of the two IMUs involved or an artefact of either of the two software packages used to integrate IMU data with GPS trajectory data is presently investigated.

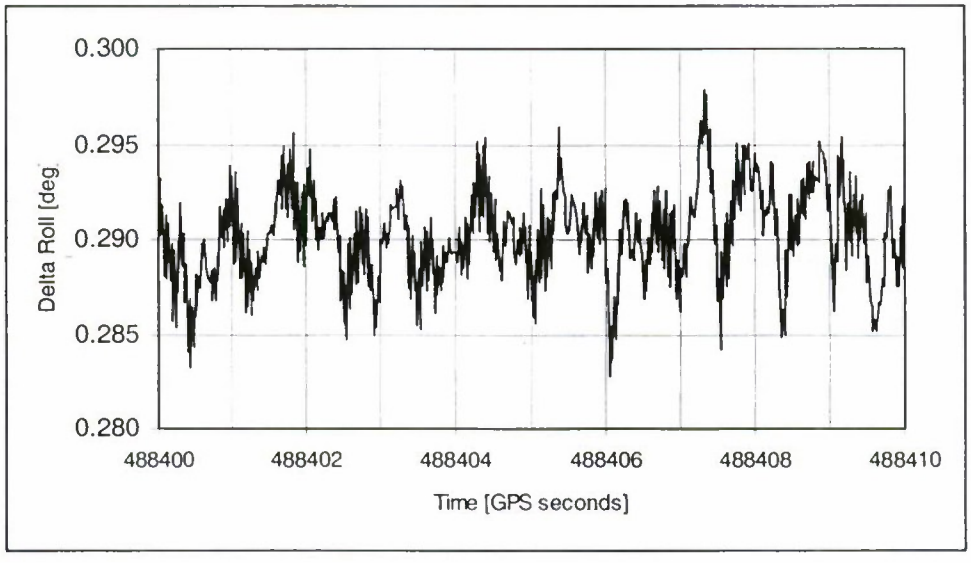

Fig.6. Roll angle differences PosProc minus AEROoffice at 50 Hz

No such 10 Hz oscillations were found in the 50 Hz orientation angle differences. As an example, Figure 6 shows the Roll angle difference for the same time interval depicted in Figure 4. The variation is typically within a band of about 0.01 deg and thus confirms the performance specifications listed in Table 1.

5. Conclusions

The comparison of the trajectories determined with two integrated GPS/IMU systems was restricted to those portions of the test flight with 'typical flying conditions' (straight lines). From the discussions of Section 4 we can draw the following conclusions:

The differences in 3-d position are at the millimetre to centimetre level. This is to be expected since the same GPS determined trajectory was combined with the data from the two IMUs. This also confirms that the GPS determined positions are modified only at an almost insignificant level by the IMU data integration.

The orientation angle differences between the two system consist of a constant offset and variations. The offsets result from differences between the IMU axes directions, which are unavoidable when mounting the IMU in the aircraft. Such offsets must be calibrated externally. The deviations of the orientation angle differences from their mean value are within the range resulting from the system performance specifications listed in Table 1.

The position difference data at 50 Hz update rate showed a 10 Hz oscillation horizontally in flight direction with an amplitude of about 3 mm. The possible causes for this oscillation are presently investigated. No similar oscillations were detected in the vertical co-ordinate and in the orientation angle differences.

Acknowledgements

The staff of Applanix Corporation and IGI mbH are acknowledged for their support in data processing and for continuing discussions related to system specifications and system performance issues.

References

1. **Raquet, J., Lachapelle, G. and T.E. Melgard (1998).** Test of a 400 km x 600 km Network of Reference Receivers for Precise Kinematic Carrier-Phase Positioning in Norway. Proc. ION-GPS'98, 407-416

2. **Cramer, M (2001).** Performance of GPS/Inertial Solutions in Photogrammetry. In: D. Fritsch and R. Spiller (Eds.) 'Photogrammetric Week '01', HerbertWichmann Verlag, Heidelberg, pp. 49-62.

3. **Heipke, C., Jacobsen, K., Wegmann, H. (2001).** The OEEPE test on integrated sensor orientation - results of Phase 1. In: D. Fritsch and R. Spiller (Eds.) 'Photogrammetric Week '01', Herbert Wichmann Verlag, Heidelberg, pp. 195-204.

A MINIATURE FOG WITH BUILT-IN DIAGNOSTICS AND INSTANT START-UP

V. Logozinski *, I. Safoutine **, V. Solomatin ***

Fizoptika Co.,
Mira avenue 100. 129626, Moscow, Russia. E-mail: solo@fizoptika.ru

Abstract

Key words: fiber optic gyro, start-up period, built-in diagnostics

In the report the most miniature fiber optic gyro (FOG) with the fastest start-up, extremely low power consumption (~0.5W) and with an ability of built-in diagnostics is presented. The principle of diagnostics, sensor's design and its performance, typical test results and an example of application are described.

1. Introduction

For some systems which operate in a waiting mode sometimes it is an advantage if the sensor has a short start-up period and built-in diagnostics. That allows to check serviceability of the sensor in a process of maintenance or during system activation.

In this report the miniature fiber optic gyro with a very short start-up period (~ 10 msec) and with an ability of practically instant (several milliseconds) built-in diagnostics is presented.

VG941-3AS sensor is a modification of VG941-3A which is being produced since 1998. VG941-3AS has smaller size, lower power consumption, very short start-up period and an ability of built-in diagnostics by external signal.

The fiber optic assembly is manufactured by technology developed in Fizoptika. All optical components are fabricated in series along one length of a fiber. At that the minimal optical losses are achieved. VG941-3AS demonstrates an excellent performance-to-size ratio.

2. VG941-3AS performance

Physical characteristics:
(see photo):

Weight - 30 gram
Size - ⌀ 24 mm x 50 mm
Power: - + 5 V (± 5%)
Operating temperature range - 30 °C ... + 70 °C

Fig. 1. VG941-3AS appearance

Main parameters

Parameter	Units	Value	Conditions, comments
Input range	deg / sec	± 600	Expandable on request
Bias variation (σ)	deg / sec	0.01	Steady state
Bias vs temperature	deg / sec	± 0.1	- 30 °C ... + 70 °C
Scale factor (SF)	mV / deg / sec	3.5	Nominal value
Scale factor variation (σ)	%	0.2	Steady state
Scale factor vs temperature (slope)	% / °C	-0.05 ... - 0.1	- 30 °C ... + 70 °C
Random walk (noise)	deg / hr √ Hz	0.004	Corresponds to output fluctuation at 1 sec averaging
Bandwidth	Hz	0 ... 1000	Analog output filter cut-off frequency
Start-up	Sec	0.01	
Power consumption	W	0.5	

* Dr., R&D Director
** B.Eng., Head of division
*** Dr., Executive Director

3. VG941-3AS design features

The overall drawing of sensor is presented in the picture. In process of VG941-3AS development a number of technical solutions was used in order to get a unique set of sensor's features.

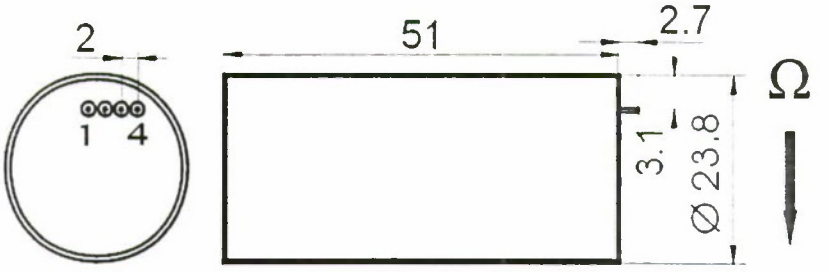

Fig.2. VG941-3AS overall drawing

Miniature size

The smallest dimensions for the fiber optic gyros were achieved due to:

- manufacturing of optical assembly of the sensor without splicing of the fiber ends between optical components;
- use of specialized optical fiber of a small diameter;
- mounting of the optical components (couplers and polarizer) on the quartz substrates of a smaller size;
- development of the new miniature electronic board.

The overall dimensions of processing electronic board were significantly reduced by use of the modern electronic components and due to essential redevelopment of the electronic modules, which are used in the sensors.

Low power consumption

Development and implementation of unipolar electronics OE-141AS with the modern components made possible a decrease of power consumption to 0.5 W (minimal value - 0.3 W).

Instant sturt-up

The minimal start-up period was one of the main purpose of the project. The typical value of start-up period for VG941-3AS sensors was realized as ~ 10 msec due to optimization of the transients processes in control circuit of PZT modulator. The minimal start-up period is estimated as 3 msec.

Built-in diagnostics of serviceability

In developed electronics the patented method of built-in diagnostics was realized. The operating principle and procedure are described in the next section.

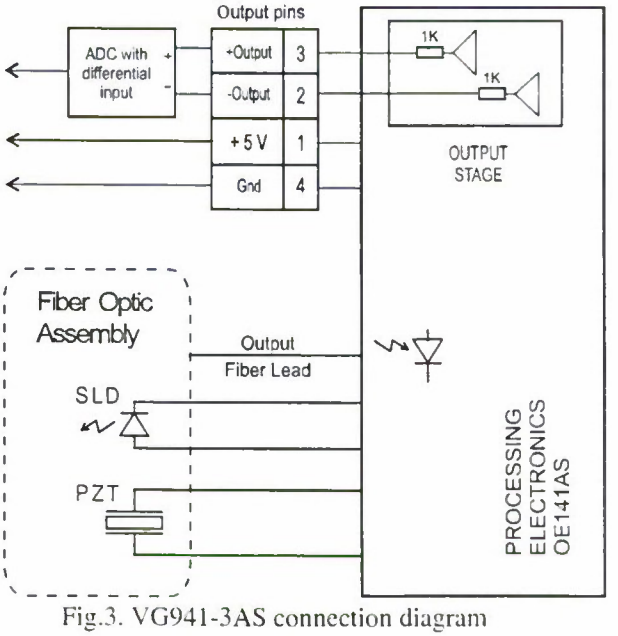

Fig.3. VG941-3AS connection diagram

The connection diagram of VG941-3AS is presented in the picture which includes also some details of the output stage of processing electronics and reflects an internal structure of the sensor.

The electronic board OE141-AS was developed to make its output signal compatible with the modern low-voltage ADC which are characterized by low noise level, high resolution and unipolar supply voltage. The balanced output has a bias of ~ 1 V.

4. The built-in diagnostics

The diagnostics of VG941-3AS is performed by measurement of its output when the test electrical signal is applied to the input of detecting module. The test signal is equivalent to the rotation signal at the output of photo-receiving module. As a test signal we have used the current through phase modulator. When the PZT modulator is excited at the frequency of fundamental radial resonance the value of excitation current is stable. Moreover, that signal coincides in frequency and phase with first harmony (rotation signal) at the output of photo-receiving module. If such signal is applied to the input of detecting module of electronics in the absence of rotation at FOG output the voltage of determined value and polarity appears. That is a criterion of FOG serviceability.

For implementation of described diagnostics into FOG electronics the several additional components were integrated (see picture): a meter of excitation current of phase modulator, amplifier and inverter with two control inputs. If control voltages (power supply) are applied to control inputs of inverter and amplifier the signal of excitation current is applied to the input of detecting modules of FOG electronics. In such a way FOG serviceability is checked by change of its output.

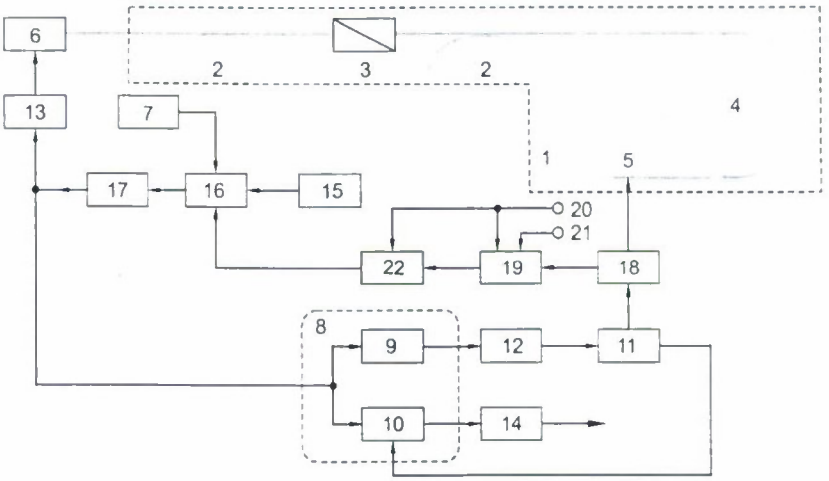

Fig.4. VG941-3AS block diagram:

1 – ring fiber interferometer
2 – fiber coupler
3 – polarizer
4 – fiber sensing coil
5 – phase modulator
6 – light source
7 – photo-receiving module
8 – demodulator
9 – AC detector
10- lock-in detector of 1-st harmony of modulation frequency
11 - controlled voltage generator
12, 13 – amplitude controller
14 - low-pass filter
15 - source of reference voltage
16 - summing unit
17 - regulator
18 - current meter
19 - controlled inverter
20, 21 – control inputs
22 - controlled amplifier

To stabilize the FOG scale factor the processing electronics stabilizes a light power entered into fiber and an amplitude of phase modulation.

At that the light power entered into fiber is stabilized by control of injection current of light source (6). The modulation amplitude of phase difference between counter propagating waves is stabilized by control of excitation voltage of phase modulator (5).

The inspection of FOG serviceability before beginning of measurements covers both optical module of FOG and its electronics.

When the control signals are not applied to the inputs (20, 21) FOG operates in ordinary mode of measurement of rotation rate (the signal at the output of preamplifier (22) is absent). At rest the FOG output should not exceed nominal bias value. If control voltage is applied to the input C1 (20) the signal of excitation

current of phase modulator comes to the input of summing unit (16). At that in the absence of FOG rotation a component at first harmony of modulation frequency appears in the signal at the input of demodulator (8). The amplitude of that component is proportional to the value of excitation current of phase modulator. After detecting by lock-in detector (10) it comes through the low-pass filter (14) to the FOG output. The required value of FOG output in this case confirms serviceability both of processing electronics and of FOG optical module, namely:

- DC component at the output of photo-receiving module (7) corresponds to required value, which is set by reference voltage source (15). In the opposite case the regulator (17) is in saturation and doesn't pass the signal of first harmony to the input of demodulator.
- a chain of phase modulator is in operational status. In the opposite case the value of excitation current significantly differs from required value.
- the detecting modules of processing electronics operate correctly.

In order to check the detecting modules of processing electronics under change of rotation direction the controlled inverter (19) is used. At applying of control signal to the input (21) the test signal is inverted. That is equivalent to change of rotation direction. At that the FOG output should change a sign by opposite one but save the same value. That is a confirmation of working order of detecting module under change of rotation direction.

Setup period of diagnostics signal (~ 200 mV) is of several milliseconds. A variation of diagnostics signal over temperature range (- 30 °C ... + 70 °C) doesn't excced ± 10%.

5. Test results

The typical dependencies which were obtained during testing of several VG941-3AS sensors are presented in this section.

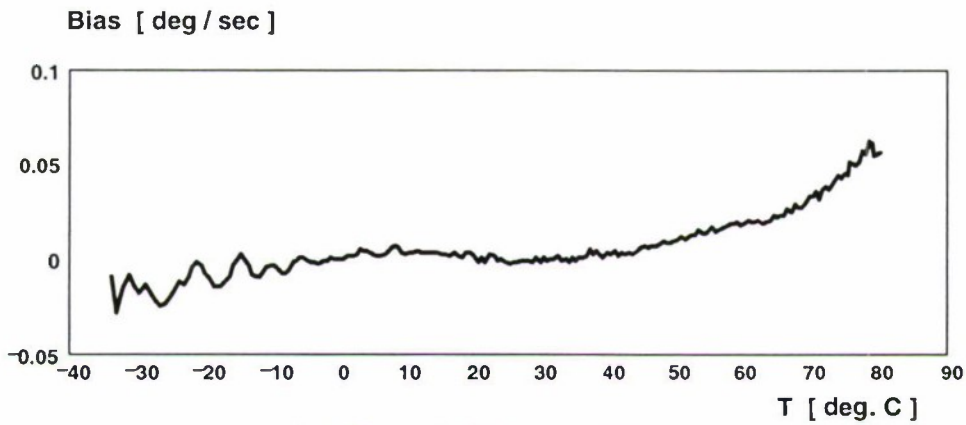

Fig.5. Bias variations over temperature range

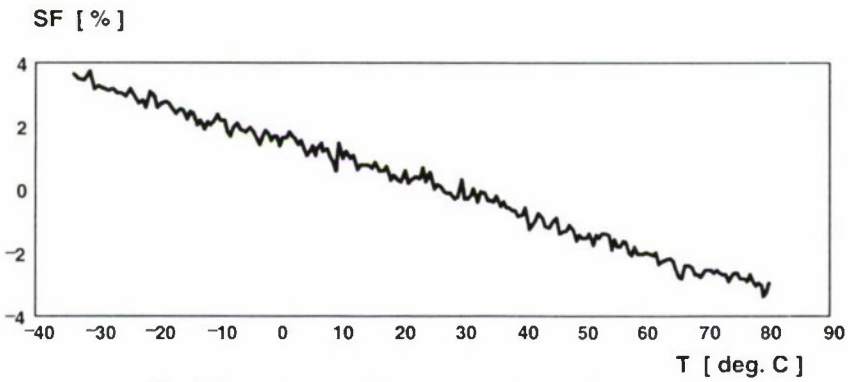

Fig.6. Scale factor variations over temperature range

The measurements were conducted in the following way:

- the sensor VG941-3AS was placed in a portable thermo-box and cooled to the temperature of ~ - 40 °C;
- the thermo-box was fixed on a rotation platform and supply voltage was applied to the sensor;
- the sensor was slowly heated and output data acquisition was performed during heating permanently.

1 - 2 hours were required to heat the sensor from - 40 °C to + 80 °C. For 20 seconds the sensor was rotated around its sensitivity axis for measurement of scale factor and for next 20 seconds the sensor was at rest for measurement of the bias.

The smooth (slow) components of the temperature dependencies are the repeatable functions of the temperature and can be compensated by polynomial correction on temperature.

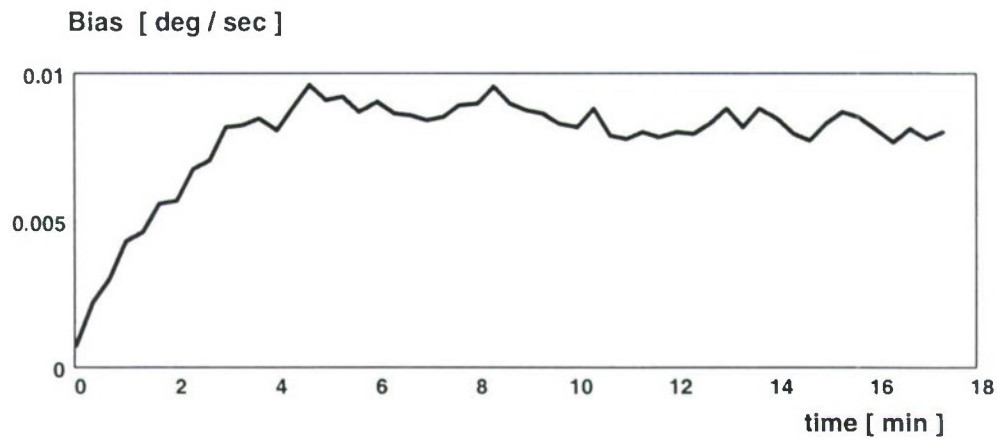

Fig.7. Bias variations during warm-up

The transient process of output signal (just after switch on) during self warm-up of the sensor is presented in the picture. Point averaging period for this measurement was of 20 seconds. The typical period of transient process is about 4 minutes.

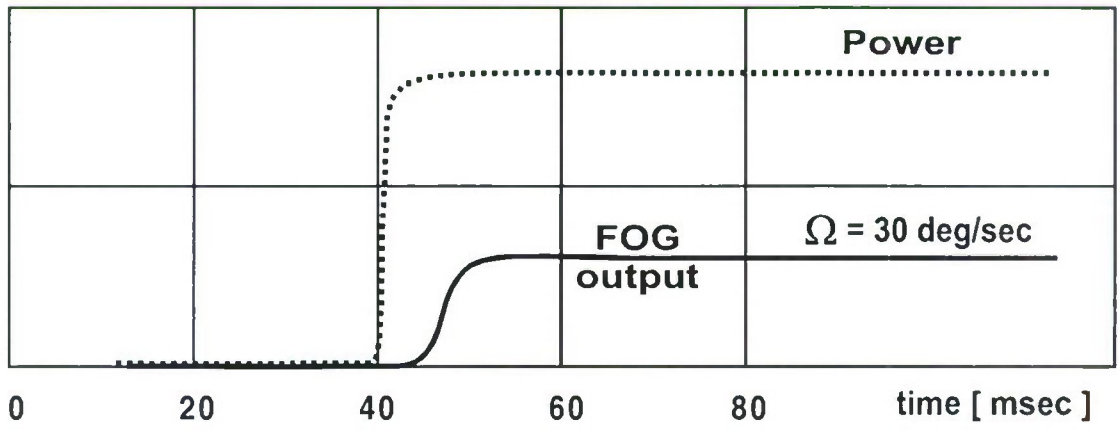

Fig.8. Transient start-up process

The transient start-up process of the sensor (see picture) was analyzed in the following way. The dormant sensor mounted on rotating platform was switched on during rotation. The value of rotation rate around sensitivity axis was of 30 deg/sec. Just after switching on the power consumption and output signal were recorded simultaneously. The start-up period was estimated as an interval between the moment of switching on and the moment when the output signal reached required level with 10% tolerance. For all tested sensors the start-up period was around 10 msec. The extreme start-up period for developed electronics can be estimated as 3 msec.

For one sensor the start-up period was measured at different temperatures from - 55 °C to + 75 °C. The transient process of output signal and start-up period were practically the same for all temperatures from that range.

6. Miniature 3-axis rate sensor. Example of application

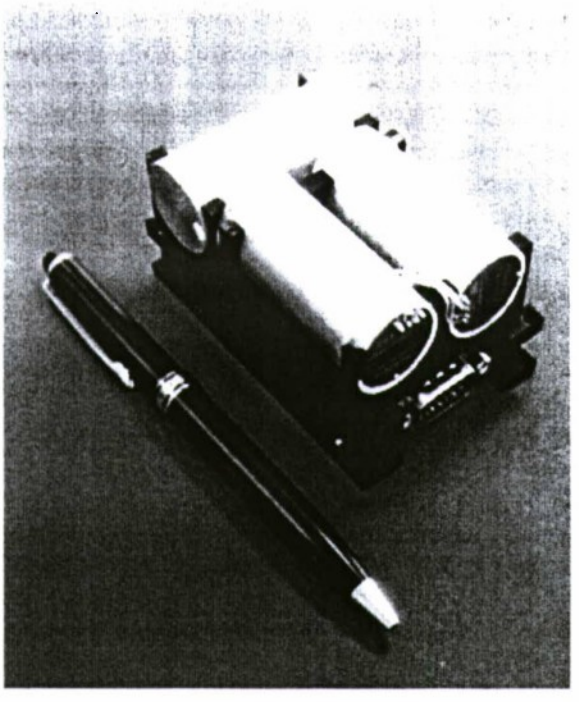

Fig.9. Miniature 3-axis rate sensor

Key features:

Weight	220 gram
Size	86 x 56 x 45 mm
Power	+5V
Output	digital RS485, 279 Hz repetition rate, 20-bit presentation of the angular rate veetor
Input range	± 600 deg/sec
Bias stability	30 deg/hr

In the picture you can see the miniature 3-axis rate sensor with digital output which was designed and assembled on basis of VG941-3AS sensors and digital board DC-7716. The key features of the system are presented above.

The digital board DC-7716 transforms the analog signals from VG941-3AS sensors to a serial digital eode. Output information (four three-byte words) comes via serial RS-485 interface. Data transmission rate via RS-485 interfaee is 38 Kbaud.

DC-7716 board contains:

- AD7716 sigma-delta ADC, 22 digits, four channels, maximum eonversion frequeney: 2232Hz, input range: ±2.5 V.
- ADSP2185 signal proeessor - 16 digits, fixed point, 32 MHz;
- Programmable flash memory (PROM) – 256 Kbytes;
- RS485 serial interfaee, transmission rate - 38 Kbaud (115 Kbaud - max.);

Main parameters of digital board:

1. ADC type: AD7716, Sigma-Delta, 22bits, 4 parallel ehannels, sampling rate - 1116 Hz, ±2.5V input.
2. Proeessor: ADSP2186, 16 bits, fixed point, 32 MHz.
3. Program flash memory - 256 KBytes.
4. Serial interfaee - RS485; maximal transmission rate - 115 KBauds.

The time dependencies of aeeumulated angle error for eaeh measuring axis are presented in the pieture below. The measurements were performed under steady-state conditions when the warm-up process for each sensor was eompleted. Before start of measurements the initial bias for each sensor was calibrated during 60 seeonds.

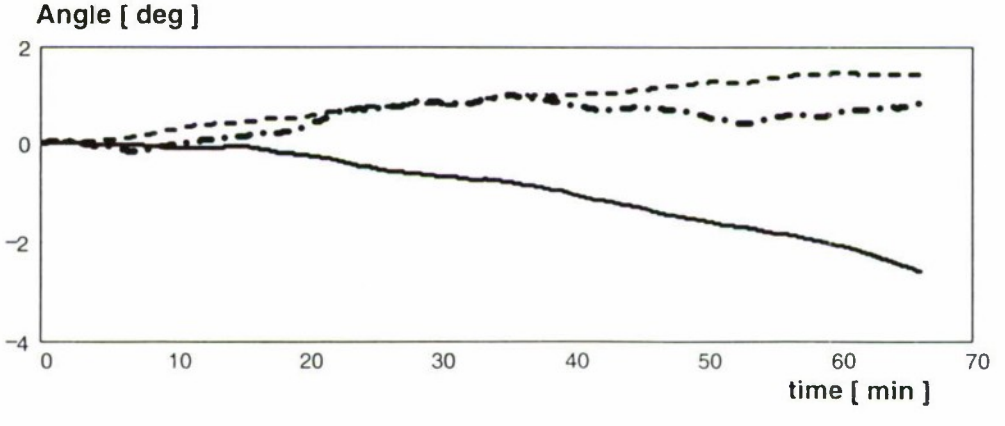

Fig.10. Accumulated angle error for each axis

PRECISION FIBER OPTICAL GYROSCOPE WITH LINEAR DIGITAL OUTPUT

V.E. Prilutskii*, Yu.K. Pylaev, A.G. Gubanov*****
"Antares", Russia, 410600, Saratov, Radishev St, 27,
tel/fax (8452) 73-37-90, E-mail: antar12@online.ru
Yu.N. Korkishko ****, V.A. Fedorov *******, E.M.Paderin ********
"Optolink", Russia, 103498, Moscow, Zelenograd, MIEE, Experimental Plant
"Proton", Tel/fax (095) 530-52-87, E-mail: korkishk@chem.mice.ru

Abstract

Key words: optical fiber, gyroscope, integrated optics, serrodine transformer, automatic control.

The design and industrial production problems of closed loop fiber-optic gyroscopes worked as a sensor of rotation rate are considered. This gyro is characterized by high accuracy and can be applied in the inertial systems of space navigation. General concept of configuration of optic path of gyroscopes with integrated-optic elements is presented. The features of the block diagrams and signal processing techniques are described.

Introduction

Per se the opportunity of commercial production of precision fiber–optic gyroscope (FOG) is directly determined by the level of technological base its main components and mainly polarization maintaining optical fibers and integrated optic circuits. So, working over the project on creation of high precision FOG gyroscope, the all our experience was used. All knowledge of principals and design features was applied. We used results, which were checked and experimentally confirmed. We had to create our own infrastructure to produce such components as multifunctional integrated optic element (MIOE), polarization maintaining fiber (PANDA), fiber splitter, fiber depolarizer (DP) and fiber coil (FC).

Some of the engineering solutions offered (related to fiber and integrated optical technologies and signal processing electronic devices) are protected by the patents and their efficiency is experimentally confirmed.

Developing the device of a high accuracy we don't exclude the creation of devices of middle and low grades of accuracy. Because of geometrical flexibility of FOG we get the lowest version without problem from high accuracy devices.

Compensation (zeroing) of Sagnac phase shift is carried out in the feedback closed loop FOG with the help of phase modulator (PM), which is placed on the ends of fiber loop, together with dynamic shift phase difference interfered light wave on the $\pi/2$ radian. In this case the control signal of the PM can be used to measure the rotation rate. It is well known that at such approach output characteristic of FOG is linear and scale factor (SF) is independent from parameters of most structural components of the device [1]. This is very important because if we process the information by means of a variable signal or a digital method, then along with the stability improvement of SF the number of the electronic factors which have an influence on the output signal error is essentially reduced.

Residual error measurement of rotation rate can be reduced with the help of algorithmic compensation of zero signal deviation or modification of SF (this is possible even for an open-loop FOG [2]). However it is clear, that in this case we must talk about compensation of only those error components, which depend on specified parameters (temperature, time etc.), i.e. predetermined. Random components can only be reduced (but not compensated!) with the help of effective design and engineer solutions and perfection of FOG component technology.

In this project we are trying to achieve the following error value (including random error) of main FOG features under environment conditions similar to exploitation on the space vehicles:

- bias repeatability, 3σ, °/h $\leq$ 0.1;
- random walk, $^{\circ}/\sqrt{h}$ ~ 0.005;
- scale factor repeatability, % $\leq$ 0.01.

---

* Branch Manager.
** Director General.
*** Ph. D. Degree, Deputy Director General.
**** Doctor of Phys.-Math. Science, Professor, Director General.
***** Doctor of Phys.-Math. Science, Professor, Technical Director.
****** Production Manager.

Main directions of technical release of the project are:

– use of single-mode fiber PANDA with strong birefringence and small loss for fiber coil symmetrical wound with length more then 1000 meters and diameter 140 millimeter;

– development and application of MIOE, produced by the proton exchange method, which performs the functions of Y – splitter, polarizer and PM;

– use of thermal stabilized semiconductor superluminescent diode (SLD) as a light source. The light power at the output of pigtailed single-mode waveguide is not less 2 mW;

– development of special data processing serrodine circuit with closed loop of feedback, which provides minimal errors in transformation and linear digital output both rotation rate and rotation angle cumulative value;

– development of a non-welding technology of assembling of the optical block.

1. Basic architecture and technologies

The general block diagram of the device, which will be the initial one, is shown on the Fig.1. This architecture type («minimum configuration»), as known [3], has a very important for the FOG practical application property of spatial and polarized reciprocity. This property provides high sensitivity to the rotation, and presence of a broadband phase modulator in the MIOE allows us to control phase shift of light wave on any to the beforehand given algorithm almost without distortion. Due to this fact there appears a new basic opportunity to achieve the accuracy limit of FOG, which is determined by optical components, (approaching the fundamental accuracy in the process of quality improvement).

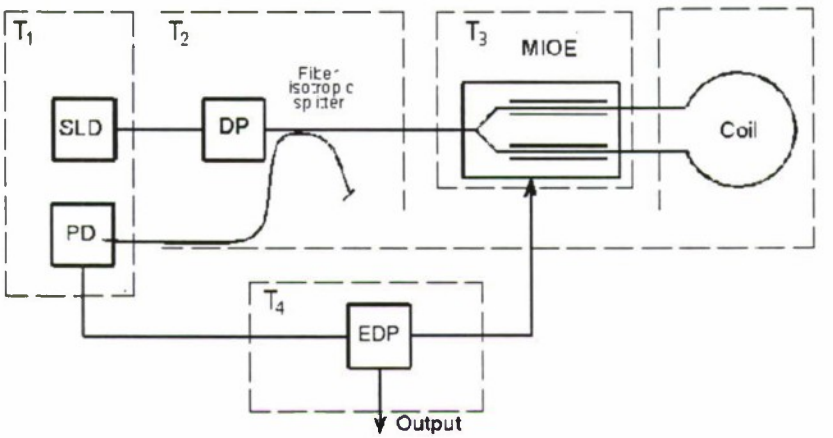

Fig.1. Fiber optic gyroscope minimum configuration. PD – photodiode

Four structure parts of FOG are marked by the dotted line on the scheme (Fig.1). These units have different functions, but the same production technology.

Such (base) technologies are as follows:

T_1 – semiconductor light emitter and receiver, T_2 – fiber components, T_3 – integrated optical element, T_4 – electronic (microelectronic) control.

Ownership of these technologies by a single enterprise allows us to develop and manufacture FOG in a full cycle (the raw and element base for them is accessible and relatively cheap).

2. FOG's block diagram

In the serrodine closed loop compensation of Sagnac phase difference $\Delta\varphi_c$ is realized by phase shift $\Delta\varphi_m$, brouht in the light wave sawtooth phase modulation on the line section (Fig. 2):

$$\Delta\varphi_m = \frac{\varphi_{rs} f \Delta\tau_g}{1 - \Delta t f},$$

where $\Delta\tau_g = \frac{Ln}{c}$ – time difference of light waves group delay, $f = \frac{1}{T}$ – frequency of sawtooth signal, φ_{rs} – sawtooth double amplitude, L – fiber coil length, n – fiber core refraction index, c – velocity of light in the vacuum, Δt – sawtooth reset time.

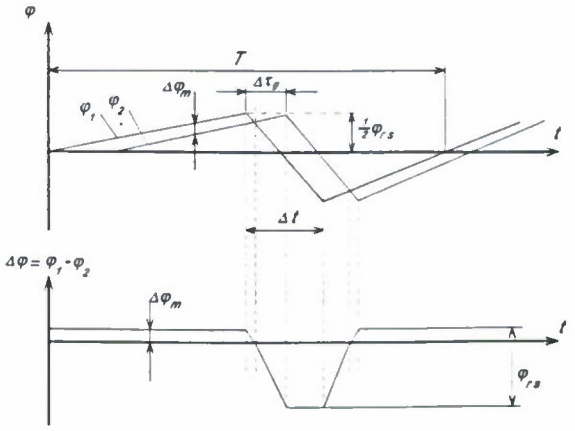

Fig. 2

Servomeehanism provides equality of these values with opposite signs, and expression of measured rotation rate Ω_{msr} (up to sign) is:

$$\Omega_{msr} = \frac{\lambda n}{2\pi D(1-\Delta t f)}(\varphi_{rs} \times f), \tag{1}$$

where λ – eentral wavelenght, D – fiber loop diameter (mean value).

Nonlinear dependenee of Ω_{msr} on the frequeney beeause of the presenee in (1) of a random variable Δt gives a main error of rotation rate measurement, whieh results in nonstability and nonlinearity. The use of a high-speed eleetronie eomponents allows to reduee Δt to the law, but nevertheless finite, value, thus providing an aeeeptable for most applieations SF error – with $\Delta t \to 0$ funetion (1) is linear rather f :

$$\Omega_{msr} = \frac{\lambda n}{2\pi D}(\varphi_{rs} \times f) \tag{2}$$

However, we ean solve this problem, if the value Δt is not redueed, but is speeially maintained equal to the half of a sawtooth signal period $\Delta t = T\ 2$ for any value of frequeney f . In this ease serrodine signal is transformed into the triangular waveform, and the Sagnae phase eontinuous eompensation problem is solved by periodie inversion of this signal on the input of PM with the same frequeney and expression (1) will be as follows:

$$\Omega_{msr} = \frac{\lambda n}{\pi D}(\varphi_{rs} \times f) \tag{3}$$

In the expression (3) as distinet from (2) frequeney f – is frequeney of the triangular waveform. Arising ehange for the worse (two times) of disereteness of transforming is eompensated by relative simplieity of reeeiving a symmetrie variable voltage of a triangular waveform with the given amplitude and with the frequeney, whieh is determined by error signal of main servomeehanism. And if we eount both positive, and negative peaks of this voltage, expression (3) beeomes equivalent to the (2).

Thus, having eonstants λ, n, D the measure of rotation rate is a multiplying $\varphi_{rs} \times f$. Obviously, it is impossible to measure phase amplitude φ_{rs} of sawtooth light wave modulation, as distinct from frequeney f . We can estimate the phase amplitude value with the help of voltage value, supplied on the PM, but in this ease we need exaet data of its transfer eharaeteristies, whieh is nonstabile itself. Generally, this method is very interesting and important, but unfortunately it is not investigated good enough by us. That is why we eoneentrate on the standard method of stabilization phase amplitude of sawtooth modulation with $\varphi_{rs} = 2\pi$ rad and additional servomechanism in the signal proeessing seheme. In this ease aeeording to expression (2) we have:

$$f = \frac{D}{\lambda n}\Omega, \tag{4}$$

where Ω – input rotation rate.

The fluetuation of values D and n have a thermodynamie eharaeter. For stabilization of these values a eoil is made by wounding fiber on the heat-insulated frame with symmetrie by raw paeking with stable tension.

The main disadvantage of semiconductor superluminescent diode is a strong dependence of its spectrum on the temperature – about 0,04 % per degree. It results in a temperature instability of SF in (4), equal, for example, to 1,6 % in a range of temperatures 0÷40 ^{O}C instead of required 0,01 %.To reduce this instability in the FOG there is a temperature controlling device, which maintains the temperature of a crystal oscillator on the given level with accuracy of 0,25 ^{O}C.

It is well known that the highest efficiency of classic dynamic phase difference shift of interference light wave in the fiber loop with simultaneous reduction of parasitic amplitude and polarization modulation is reached at the rectangular form of a so-called auxiliary (square-wave biasing) modulation with amplitude $\pi/2$ rad. and frequency $F = \dfrac{1}{2\Delta\tau_g}$, which corresponds to the eigen frequency of fiber loop.

Reliable realization of criterion $2F\Delta\tau_g = 1$ is provided when the voltage for auxiliary modulation is formed out of a reference variable signal, which frequency is stabilized by the quartz resonator. The frequency value of a given length of fiber loop, which guarantees the required accuracy of rotation rate measurement, is determined according to a condition (for silicon fibers) $F \cdot L \approx 10^8 (Hz \cdot m)$. For example, if $F = 96kHz$ then $L = 1070$ m.

It is not so easy to maintain the amplitude of auxiliary phase modulation at a level $\pi/2$ radian. The main problem is not in making a stable voltage of modulation. The problem is that even with a stable voltage, the phase amplitude is nonstable either as a light wavelength or as a transfer function of phase modulator etc. depending on chosen signal processing scheme and external factors. The cardinal solution of this problem is construction of servomechanism, which is automatically maintaining the value of interfered lightwave phase difference on the determined value. Gyro's response to the periodic excitation (a voltage pulse which is applied to the phase modulator) can serve as an error signal for such servomechanism.

In order to construct an automatic system of auxiliary phase modulation amplitude control the following algorithm of construction is offered:

– stable reference voltage forms amplitude voltage of auxiliary modulation U_{am}, which corresponds to the phase amplitude $\pi/2$ radian – the voltage is installed according to the maximum output signal of FOG at the given rotation rate with open-ended feedback of the main loop;

– precision resistance divider forms a similar voltage of modulation with amplitude equal $3U_{am}$;

– periodically at the given moments of time voltage 3 U_{am} is delivered on the modulator instead of a voltage U_{am} . the $3U_{am}$ frequency is considerably less then F, and the duration of the $3U_{am}$ delivery is sufficient for measurement of the response on disturbance by means of the device of sample and hold. It is clear, that at constant parameters of system there will be no reaction to such an excitation – error signal is equal to zero. But if, for example, the efficiency of phase modulator increases, phase amplitudes from both influences will also increase proportionally, but the photocurrent from main modulation U_{am} will decrease, and from revolting – will increase! This photocurrent difference will represent an error signal, by means of which the servomechanism reduces U_{am} until this difference turns to zero. With reduction of the phase modulator, the efficiency the process of regulation will proceed in opposite direction.

Fig. 3 shows a diagram, which explains the work of stabilization system

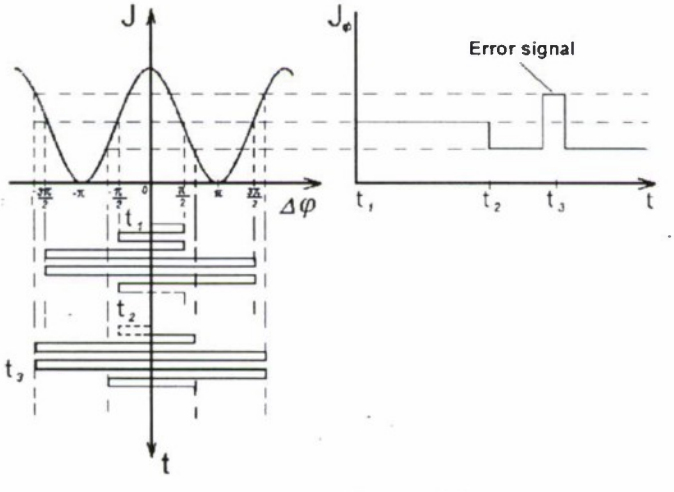

Fig.3 Auxiliary modulation.
On the diagram transition states aren't shown.

The value of phase amplitude of compensating modulation, equal to 2π rad, is easy to form from the reference voltage, which is used for forming calibration signal of auxiliary modulation – it is enough to transform it into the reference signal for sawtooth voltage with coefficient $4\ 3$. Thus stabilization system of phase amplitude of auxiliary modulation will automatically be the stabilizer of sawtooth phase amplitude. At the same time it is very important, that the disturbance caused by the sawtooth reset does not lead to the breakdown of the stabilization loop amplitude and vice versa, disturbance which is caused by calibration pulses does not lead to the breakdown in the Sagnac phase compensation loop.

The following fact makes the solution of this problem more complicated. The frequency of sawtooth voltage resets depends on the rotation rate, and consequently is a variable value. There are two operating modes: the mode of low and the mode of high rotation rates. In the first case the frequency of calibration pulses must not depend on the sawtooth frequency, because of frequency can be nearly zero, and may lead to an information loss. In the second case sampling time of phase amplitude has to depend on the sawtooth frequency, but we must avoid interaction of two stabilization loops. One of the variants of the algorithm of FOG work has been realized in this project.

To the mentioned above it is important to add the requirements of light source reliability (under the influence of environment factors), which is provided by SLD powering through the power light stabilizer (PLST), and the requirement of maximum possible attenuation of in-phase synchronous inducing on the input circuit of photodetector (PhD), that is provided by the galvanic isolation of this circuit from the rest of electronic components and by a differential amplification. As a result of this requirement, block diagram of FOG is (Fig4):

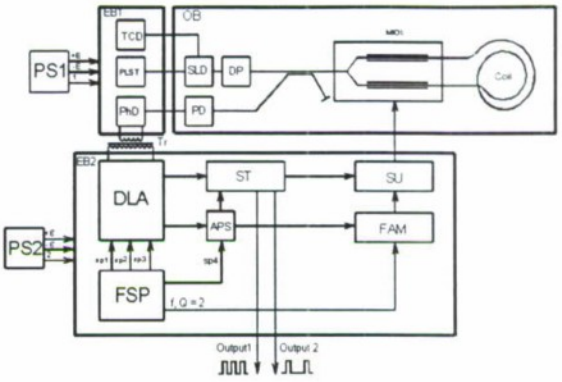

Fig. 4. Block Diagram of fiber optical gyroscope

PS1, PS2 – secondary power sources, EB1, EB2 – electronic blocks, OB – optical block; DLA -differential lock-in amplifier; FSP – former of synchronizing pulses; CT – serrodine transformer; APS – amplitude producing scheme; FAM – former of auxiliary modulation; SU – summation unit; SP1÷ SP4 – synchronizing pulses specifying algorithm of information processing; Tr – transformer

The functional content of the block diagram becomes clear by marking separate units and connections between them. We developed two versions of this scheme:

– with analog form of sawtooth modulation on the line section without fixation of the moment of "sawtooth " reset to the frequency of dynamic shift;

– with "staircase" form of sawtooth modulation on the line section with fixation the moment of "sawtooth " reset to the frequency of dynamic shift and full digital signal processing.

Advantages and disadvantages of both are well known.

3. Fiber coil and fiber components

FOG sensitivity to the rotation is mainly determined by the fiber coil design, its size, fiber type, and the wounding method. In this project it is efficient to use a single-mode polarization maintaining optical fiber PANDA with strong birefringence. Present technology level of fiber manufacturing on the "Optolink" LLC allows to produce fiber with following parameters:

– loss of optical light power, α	3÷4 dB/km;
– polarization beat length, L_p	≤ 2,5 mm;
– coefficient of intermode polarization coupling, h	$\leq 5 \cdot 10^{-5}$ 1/m;
– outer diameter, d	≤ 80 μm.

The expression for upper bound phase error of FOG, which appears as a result of the main destabilizing factor – polarized nonreciprocity [4] – leads to the dependence of minimal measured rotation rate on the fiber coil parameters:

$$\Omega_{\min} \sim \frac{\sqrt{hL_p}}{DL}.$$

This dependence is as follows: the transition from fiber coil on an elliptic fiber with parameters $L_p \approx 8$ mm, $h \approx 10^{-3}$ 1/m, $D \approx 80$ mm, $L \approx 200$ m (for example, ВГ910 device) to the fiber coil on the fiber PANDA with parameters $L_{p\approx} \approx 2{,}5$ mm, $h \approx 10^{-5}$1/m, $D \approx 140$ mm, $L \approx 1000$ m with other equal conditions value $\Omega_{\min}$ decreases more than 150 times.

Directed splitters, produced by the method of curling – fusion extraction from isotropic single-mode fiber, have the following typical parameters (λ = const) under the values of temperature, spectral, and polarization sensitivity division coefficient within the set limits:

– power division coefficient, % 50±1;
– extra power loss, dB 0,1.

Lyot fiber depolarizer was taken as a basis of depolarizer design construction well known like. The technology of manufacturing of this element provides achievement of the following parameters:

– optical power loss, dB < 0,5;
– residual light polarization at the width of a spectral line 15 nm, % < 0,1.

4. Multifunctional integrated optical element

One of the main fiber optical gyroscope's components is MIOE, which consists of integrated electro-optical phase modulator on the basis of Y – splitter formed at X-cut lithium niobate crystal. Integrated optical Y-splitter is manufactured by planar technology of high temperature proton exchange. The processes are held in the specially developed containers. The specially developed metals and dielectric films used as masks to provide locality proton exchange diffusion. Then by vacuum deposition of electrodes, the integrated electro-optical phase modulators are formed. This method was developed by "Optolink" LLC [5].

A very important advantage of proton exchange waveguides is following. In such waveguides the extraordinary refraction index is increasing, while refraction index of ordinary ray is decreasing. As a result, proton exchanged waveguides support propagation only extraordinary polarization modes (TE in our case). Therefore, it is no necessity to use in the fiber optical gyroscope a polarizer, which brings additional loss.

It is well known, that standard technology of proton exchange waveguide (APE-technology) applies a two-level process, which consists of a proton exchange, (melting benzoic acid as a rule) and subsequent annealing. It was recently obtained, that different defects are formed in the surface area of waveguide due to different phase transitions. These defects are sources of additional scattering of light. High-temperature proton exchange, in contrast to APE, does not allow any phase transitions, and, therefore, allows one to achieve the smaller optical losses and higher electro-optical coefficients.

The modeling Y – splitter with the help of the software "BPM-cad" produced by Optimave Corp. allowed us to choose an optimum function of Y-splitting.

After fabrication of Y – splitter and electrode deposition, first plates are cut (the angle is 10 degree to the Y axis). Then the end surfaces are polished, and finally they are coupled with input isotropic and two output anisotropic PANDA fibers. Then the packaging (installation into the case) follows and phase modulator electrodes are joined with outputs by means of welding.

Multifunctional integral optical element is a monoblock hermetic product, which can be connected to the optical block of fiber optical gyroscope by means of fiber waveguide welding and soldering phase modulator electrical outputs to the electronic blocks.

Main parameters of multifunctional integral optical component with operating wavelength 0,83±0,03 μm are following:

– optical power loss (at depolarized light), dB < 8;
– polarizer extinction ratio, dB > 40;
– division coefficient 0,5± 0,05;
– phase sensitivity of each of modulator, rad/V > 1.

5. Source and receiver of the light

As a light source is used emitter ILPN-330-4, which is produced by the enterprise "Ingect", Saratov. The emitter contains the following components:

1. Stripline SLD on the basis of double heterostructure system GaAs/GaAlAs with isolation by opposed *p-n* junction, which have an absorbe layer in the active area. Such design of SLD provides practically smooth

spectrum with halfwidth 15÷18 nm and with light power up to 1,5÷2 mW on an output built – in single-mode fiber waveguide.

2. Microcooler on the base of Peletie elements for maintaining SLD crystal temperature in the given range at joint operation with the thermal control device.

3. Thermoresistor for error signal formation in the thermal control device.

4. The photodiode on the basis of silicon p-i-n structure for formation of a steering command in the PLST.

All components in the ILPN -330-4 are placed in the standard hermetic case, with electric and optic pressure seals.

As a light detector the photodiode is used (on the basis of silicon p-i-n of structure such as FP1-850 K, produced by the same enterprise). The photodiode has electric current sensitivity to the wavelength $\lambda = 0{,}835$ μm not less than 0,3 A/W with delay time of a pulse signal front no more than 2 ns.

The photodiode is placed in the hermetic case with built-in multimode fiber waveguide

6. Electronic support of FOG

FOG electronic components are carrying out the following functions:

– the emitter to the power source connection with simultaneous stabilization of light power and SLD crystal temperature;

– signal transformation, amplification and synchronous demodulation from the optical block output;

– voltage forming for auxiliary phase modulation of light waves;

– voltage forming for compensative phase modulation of light wave;

– output signal forming.

Chief feature of all these schemes is that they are closed systems of automatic regulation with the first order of astatism. This allows improving dynamic properties of the device and decrease static errors all types.

On the Fig 5 the block diagram of the main regulation system, which supports the Sagnac phase difference close to zero, is shown.

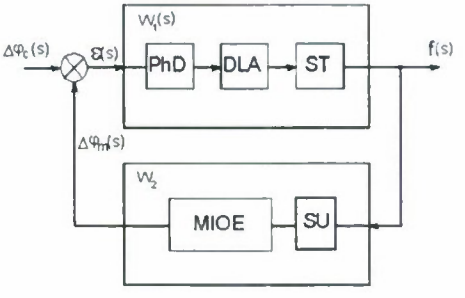

Fig. 5. The main regulation system block diagram: s – Laplace transformation symbol, $\mathcal{E}$ (s) – regulation error

Input (control) effect on this system is a Sagnac phase difference $\Delta\varphi_c(s)$, output signal is a pulses consequence, with frequency $f(s)$ which is proportional to the rotation rate (4), and the pulses number determines the rotation angle of the device with discreteness $\frac{\lambda n}{D}$. Transformation and regulation error is determined by the transfer function of the closed system by control effect and by error correspondingly. Electronic circuits, which include structural units of FOG, determine the transferring functions of the parts of the direct (straight) circuitry $W_1(S)$ and feedback W_2:

$$W_1(s) = \frac{\pi K}{2\varphi_{rs} V_\pi T_1 T_2 s}, \tag{5}$$

$$W_2 = 2\varphi_{rs}\Delta\tau_g, \tag{6}$$

where K – amplification coefficient of an open loop system; V_π – half-wave voltage of phase modulator; T_1, T_2 – time constant correspondingly integrator of the DLA and ST – block.

Dimensionality of Q-factor in our system K corresponds with the voltage (phase shift to the voltage transforming); and its value is determined by many optical and electrical factors: K value is proportional to the intensity of light, which is applied to the photodiode (this is a power of superluminescent diode and losses of optical

path); visibility of fringes (this level of light coherence and division factor of multifunetional integral optical component), photodiode efficiency, amplification factors of photodetector and differential synchronous amplifier, it has a maximum at optimum frequency and depth of auxiliary modulation.

Taking into account the relations (5), (6), we have transfer funetion on eontrol

$$F(s) = \frac{1}{2\varphi_{rs}\Delta\tau_g(1+Ts)} \tag{7}$$

and transfer function on error

$$E(s) = \frac{Ts}{1+Ts}, \tag{8}$$

where $T = \frac{V_\pi T_1 T_2}{\pi K \Delta\tau_g}$ – time constant, which determines dynamie features of FOG, its transmission band and dynamic regulation error.

Thus, according to (7) and (8), feedbaek elosed loop of main system of control effect is the inertia link of the first order, and the one of error – an inertia differentiator. By means of the well known methods of mathematical analysis (provided initial requirements to the preeision and dynamic characteristics of FOG are taken into account) we may estimate the potential range of the elements' parameters, which determine the T-value and their optimal values, which guarantee the stability and precision of the control system. But already these interrelationships may lead to the conclusion that in order to obtain good parameters of the FOG we should improve the Q-factor, (mainly its optieal eomponent), the effieieney of the phase-modulator (reduetion of V_π) and to inerease the length of fiber loop (an increase $\Delta\tau_g$), of course within the allowed limits. The qualitative advantage of this kind of FOG strueture is as follows: the eontrol error at the constant angular velocity is equal to zero and its eonstant nonaeeumalative value at the eonstant ehange of the latter.

To implement the circuit (loop) of the amplitude regulation of the compensative modulation the same structural units as for the main block are used. The only difference is that here the control effeet is carried out by means of the error signal (as a response to the mentioned calibration check). The algorithm of simultenious work of the feedbaek loops is arranged in such a way, so that they do not interact (as it may distort the operation), and to provide an independent reduetion of the controlled variables to the values $\Delta\varphi_c = 0$ and $\varphi_{rs} = 2\pi$. Under this condition in the set state (S=0) from (7) we automatieally get the expression (4) for SF.

One more feedbaek loop (in the stabilizer of power light) is intended to maintain the light power of SLD under the influence of the environment factors and in transition modes on the level corresponding to the nominal pumping eurrent at the given (normal) temperature. Here two important tasks are solved:

– the bandwidth of the FOG is stabilized, hence the noise level at its output;

– unauthorized (even minimum) exess of the allowed radiation power level that may cause SLD degradation is excluded.

Light power stabilizer bloek diagram is shown on Fig. 6.

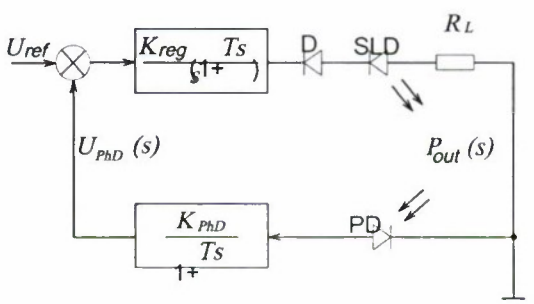

Fig. 6. U_{ref} – reference voltage, K_{reg} – regulator coefficient of amplification, D – protective diode, T – time constant of regulator circuits and photodetector, K_{PhD} – coefficient of amplification photodetector, R_L – load resistor, P_{out} – superluminescent diode light power, S – Laplace transform symbol, U_{PhD} – photodetector output voltage, PD – photodiode

Transfer charaeteristic of the light power stabilizer, its dependence P_{out} (S) on the seheme parameters and on time, is written with the help of Laplace transform symbols:

$$P_{out}(S) = \frac{K_{SLD}\left[K_{reg}(1+TS)U_{ref} - S(V_D + V_{SLD})\right]}{R_L S + K_{SLD}K_{reg}K_{PhD}}.$$

where: K_{SLD} – SLD efficiency, V_D and V_{SLD} – potential drop on the diode D and SLD respectively.

In the stable state mode $(S = 0)$ the light power, which is radiated by the SLD is:

$$P_{out} = \frac{U_{ref}}{K_{PhD}},$$

light power determined by the value of the reference voltage and photodetector coefficient. Thus the accuracy of P_{out} depends on the precision of the proportion – $\frac{U_{ref}}{K_{PhD}}$. The values U_{ref} and K_{PhD} are independent; that is why we must require the stability of U_{ref} and K_{PhD} for supporting P_{out} – stability of the whole system. Stability of U_{ref} is reached by application of precision stabilitron and resistors of forming circuit. The K_{PhD} stability is provided by the photodiode and amplifiers stability. Amplifier accuracy is reached by application of operational amplifiers with large coefficient in the circuit without feedback and precision resistors for feedback forming. Accuracy of power light stabilization system of SLD in the stationary state is determined by the accuracy of photodiode transfer characteristic.

The structure of feedback loop in the temperature control device is similar to the structure of loop in the light power stabilizer.

One of the factors that set a limit on the number of potential circuit engineering solutions for transformation of high-frequency opto-phase data on the angular velocity into the low-frequency electronic data is an extremely low sign level at the optic path output. For instance, at the rate of 0.1 °/h, power of the radiation source 2mW, total losses of optic path at the level of 20 dB, diameter and length of the fiber coil D=140 mm and L=1070 m, respectively, and the photodiode effectiveness at the level 0.3 A/W, the effective component of the photocurrent equals to the level 0.01nA. Under these conditions common-mode interference and inducing play an important part both at the electronic block input and at the power supply chain, as well as own noise and electronic stage shifts.

For supporting the relation sign/noise at the level, formed by the optic part of the FOG the following main solutions have been used during the design work:

– photodetector is produced on the basis of low noise wide-band amplifiers according to the scheme with a differential input and output (with a high level of geometric simmetrization of electric circuits, that connect the photodiode with the amplifiers);

– power supply chains of optical block, (as well photodetector) are decoupled galvanically from the power supply chains of the rest of the FOG;

– when the FOG is under regulation, a balance of the trimming arm in differential synchronous amplifier is provided to achieve maximal suppression of the phase coincidence inducing component, which is synchronous with the demodulation process.

Another special feature of electronic block is the following: to minimize the zero drifts of the FOG, which are caused by the bias in electric circuits, the data processing is carried out on the basis of the variable signal (or in a digital way) on all stages except one – the integrator of the main control system. This stage (cascade) is made on the precision IC, where the zero drifts within the whole temperature range may lead to the output drifts not more than 0,002 °/h.

The fiber optical gyroscope is powered from an external source with direct voltage 18÷36 V through three galvanic independent DC/DC transformers with output voltage ±15 V, ±12 V and ±5 V.

Power consumption does not exceed 6 watt in the set mode, and no more than 30 watt in a transitive mode during 0.1 second after switching-on.

At present time most units of the electronic block are produced on the basis of the solid-state technology. Improvement of this technology leads to better energy features. And, we hope, that at the same time precision factor will improve too.

7. Optical block assembly technology

A zero signal stability of a fiber optical gyro is provided not only by the quality of fiber components and multifunctional integral optical component, but also by the assembly technology of optical block. It is well known, that the welded connections of fibers are the reason of redundant losses of optical power and centers of cross connection between polarizing modes. As a result of this integration multifunctional integral optical component to the optical block is made by direct joining its waveguide with the ends of fiber loop and with one of the ends of input isotropic splitter (with length, sufficient for a spatial filtration of light). Depolarizer and photodetector are connected to the isotropic fiber by means of welding.

Conclusion

Calculation and experimental data, obtained at the "Antares", Saratov, and "Optolink" LLC Zelenograd, shows us that this fiber optical gyroscope configuration can be applied in the inertial navigation systems of space vehicles.

With transition to operation wavelength of 1,55 μm in the process of realization of algorithmic compensation, it is possible to improve parameters, given in the report, considerably.

References

1. **H.Lefevre** "The Fiber-Optic Gyroscope", Artech House, 1993.
2. **V. Logozinski, I. Safoutine, V. Solomatin** "Fiber Optic Gyro with Digitally Corrected Output", 8th Saint Petersburg International Conference on Integrated Navigation Systems, 2001, pp.49-56.
3. "**Optical** Gyros and their Application", RTO – AG -339, 1999.
4. **W.K. Burns** "Phase Error Bounds of Fiber Gyro with Polarisation – Holding Fiber", J.Lightwave Tech., V.4, №1, 1986.
5. **Yu.N. Korkishko, V.A. Fedorov, O.Y. Feoktistova** "$LiNbO_3$ Optical Waveguide Fabrication by High – Temperature Proton Exchange", J. Lightwave Technology, 2000,v.18, №4, pp. 562-568.

EXPERIENCE IN DEVELOPING AND CERTIFYING A STRAPDOWN INERTIAL NAVIGATION SYSTEM FOR CIVIL AVIATION (SINS-85) AND CREATING ON ITS BASIS MODIFIED SYSTEMS FOR CONTROLLING MARINE, GROUND-BASED, AND AEROSPACE OBJECTS AND SOLVING GEODETIC AND GRAVIMETRY PROBLEMS

S.P.Kryukov, G.I.Chesnokov, V.A.Troitskiy
(The Moscow Institute of Electromechanics and Automatics, Russia)

Abstract

Key words: strap down inertial system, laser gyro, certification

The paper presents results of developing and an experience of certifying the first Russian independent strap down inertial system (BINS-85) for civil trunk-route and medium-range trunk-route Il-96-300, Tu-204, Tu-334 aircraft and their modified versions. The BINS-85 system is fully compliable with Russian and international requirements to a similar type of equipment in terms of accuracy, availability time, reliability, output data, operation conditions, mass and size characteristics, and power consumption.

To create the BINS-85 system, the institute had to solve a number of scientific and technological problems, connected with the development and bringing its own production laser gyros and quarts accelerometers to the design figure, as well as with the system as a whole. Technological problems are, first of all, connected with the development and introduction of a set of aids for automated adjustment and alignment of the system with an equivalent accuracy of 3 ÷ 4 arc sec, and aids for implementation of an automated technique for an algorithmic reduction of gyro and accelerometer temperature errors, as well as compensation of relative position of sensitivity axes within the whole desired temperature range. BINS-85 full-scale production started in 2002.

On the basis of BINS-85 a number of modified versions of different applications were developed for sea vessels, aircraft, ground-based vehicles, both independent and integrated with SNS and other aids. These systems are at different development phases: from the pre-production phase to the technical proposal phase.

AOOT MIEA is a highly experienced company in creating inertial navigation systems (INS) and their sensors. Suffice it to mention gimbal INS: MIS-P, MIS-45, I-11, I-11-76, I-11-1, and I-21 still operated on Su-24, Tu-22M, Tu-95, Il-62M, Il-76, Il-86, Tu-154M, Tu-160, An-124, An-225 and other aircraft. The system of latest development - I-21 – in terms of its technical characteristics comply with the best world analogues, and out-performs them in operational conditions.

In their further development gimbal INSs have constraints. Therefore, in the 60-70-es active studies began worldwide on creating strap down inertial systems (BINS). To our opinion, the main advantage of BINS is cost and power consumption decrease, reliability and life increase (by 3-4 times) and, as a result, reduction of operation costs. This is achieved due to the absence of a gimbal suspension, incorporating precision angle transducers and gyro torquer, bearings, brush collectors, and so on. Another important BINS advantage is increase of informativity due to availability of information in the system on angular rates and linear accelerations body axes.

BINS advantages are revealed to the utmost when using laser gyros and "dry" accelerometers. They reduce availability time and power consumption by 3-4 times, as laser gyros and "dry" accelerometers have comparatively low and stable temperature coefficients of drift and scale factor, and therefore do not require an active temperature control system. Besides, of all known types of gyros, the laser gyro has the most stable scale factor (up to $1 \cdot 10^{-6}$) and does not require precise data converters, because it has a frequency output.

But creation of BINS for airborne application that would comply with ARINC-704 and ENLGS-3 requirements, required solving a number of complicated scientific and technical problems:

1. Developing precision laser gyros with the path length of no more than 28 cm and a "dry" gyro that has low and highly stable coefficients of drift and scale factor change within the whole operation temperature range.
2. Providing stability of relative position of the transducer sensitivity axes with an error of no more than 3 ÷ 4 arc sec.
3. Using high-performance computers that provide data acquisition from sensors and their processing, and building a "mathematical" platform.
4. Developing special-purpose software.
5. Developing automatic BINS calibration system, including laser gyro (LG) drift balancing, compensation of scale factor change, accelerometer zeroes, sensitivity axis misalignment and reduction of temperature error.

Comparison of accuracy characteristics of sensing elements for aviation INS and BINS of standard accuracy are given in Table 1.

Table 1. Sensing element accuracy requirements for INS and BINS of standard accuracy: $\Delta\varphi, \Delta\lambda \leq 3{,}7$ km for 1 hour flight at the 2σ

System	Gyros		Accelerometers		Adjustment accuracy
	Drift	Scale errors	Zero signal drift	Scale errors	
INS	0.02 degree/h	$6 \cdot 10^{-4}$	10^{-4} g during actuation $3.6 \cdot 10^{-4}$ during life	$14 \cdot 10^{-4}$	40 arc sec
BINS	0.015 degree/h	$5 \cdot 10^{-6}$	$5.3 \cdot 10^{-5}$ g in actuation $7.3 \cdot 10^{-5}$ during life	$7 \cdot 10^{-4}$	5 arc sec

The table shows that requirements to accuracy of BINS' sensing elements with respect to a number of parameters are substantially higher than those of gimbal INS' sensing elements of the same accuracy.

In accordance with the world tendencies, in the seventies AOOT MIEA started a research in the field of laser gyros and strap down INS (BINS). The research resulted in the development of the first home BINS in the period of 1984-1991 for Il-96-300 and Tu-204 airplanes – an I-42-IC system based on KM-11-1A laser gyros (LG), developed by NPO "POLUS", and AL-1 floating accelerometers developed by AOOT MIEA. In terms of accuracy and output parameters the I-42-IC system meets ARINC-704 requirements and for several years it was being lot-produced for first Il-96-300 and Tu-204 fixed wing aircraft. Main technical characteristics of the I-42-IC system are presented in Table 2.

Table 2

Main characteristics	1-42-1C	ARINC-704 requirements
Coordinate determination error, for 1 h of flight, km (2σ)	3.7	3.7
Ground speed determination error, km/h	21.6	21.6
Availability time, min	15	10
Pitch and roll output error, degree	0.1	0.1
True heading output error, degree	0.4	0.4
Mass, kg	38	20
Consumed power, VA	230	200
MTBF, h	2400	5000
Vibration resistance, g	1.5	0.5
Temperature range, °C	From –20 to +55	From –15 to +55

In terms of dimensions, power consumption and reliability the I-42-IC system was at a disadvantage (2÷3 times) in relation to western analogues, mainly because of non-compliance of the KM-11-1A device with western laser gyros: its volume was 3 times larger, power consumption – 6 times higher, and accuracy – 2 times lower than those of western gyros.

In this connection, AOOT MIEA made a decision to develop its own laser gyro LG-1 and small-size quarts accelerometer AK-6, in the production of which technological processes similar to those of LG-I are used. As far as the institute specialised in the development of electromechanical devices and gimbal INS, the technology of LG development was a new and complicated problem; to solve this problem there was created a specialised production line that included:

- an optical production with a high accuracy treatment of sytall and quarts;
- spraying on multi-layer interferential reflective coatings to mirrors – the technology of manufacturing mirrors with a multi-layer interferential coating (layer width is 0.15 mkm at an accuracy of 0.01 mkm) was developed;
- chemical treatment of quarts and sytall parts – chemical cleaning, chemical polishing, size etching;
- electro-vacuum production with thorough degassing quantum generator inner cavities and filling them with active gas mixture (He, Ne);
- work bays with special technological equipment for assembling and adjusting ring quantum generators;
- a test bay with automated benches to analyse LGs and included units.

On agreement terms a number of enterprises were attracted to develop metal alloys with a low temperature coefficient of linear expansion, high sensitivity piezoelectric plates, cold cathodes and other components.

The works were carried out in the following fields:

- obtaining a high accuracy at a small size (path length) of the device;
- improving reliability and extending life;
- probability of full-scale production.

LG-1 high accuracy and parameter stability were achieved by the development of a production process for mirrors with low losses and dissipation coefficients. In addition, a dither system with a special amplitude noising algorithm was developed. Temperature dependence of the device drift is algorithmically balanced.

To improve reliability and extend life time, all adhesive joints were expelled from the vacuum area of the quantum generator. All sytall joints with electrodes (eathode and anode) are made by indium soldering. This type of joints provides vacuum density and it does not emit foreign gas.

For electro-vacuum treatment of the quantum generator, special techniques of inner cavity degassing were developed that allow to retain active medium mixture. Reliable "ignition" of DC gas discharge in the quantum generator is provided by tripling excitation sources (voltage "-1500", voltage "+2800", ignition lamps).

Some techniques, processes and devices were granted with inventor's certificates.

Main technical characteristics of the LG-1 are presented in Table 3.

Table 3

Parameter description	Achieved level
Angular rate measurement range, degree/s	±90
Availability time, min	Not more than 2
Scale factor, arc s/pulse	0.9350 ± 0.0050
Scale factor instability	Not more than 10^{-5}
Systematic drift, degree/h	Not more than 1
Drift instability during actuation and from actuation to actuation, degree/h	Not more than 0.01
Drift noise component, degree/√h	Not more than 0.003
Operating temperature range, °C	-20 to +55
Volume, dm^3	Not more than 0.9
Mass, kg	Not more than 1.8
Dimensions (L x W x H), mm	145 x 130 x 47
Reliability (MTBF), h	More than 80 000 (design-basis)

A full set of technological and design documentation has been developed, prototypes have been manufactured, LG-1 design and preliminary tests have been carried out that allowed to send the device to the Serpukhov plant "Metallist" for its full-scale production. At present, all types of tests are completed at this plant, and the LG-1 laser gyro has been lot-produced since 1 January, 2002 with its acceptance by the customer representative.

LG-1 accuracy characteristics, dimensions, and life meet aviation BINS requirements. This device is the only laser gyro within its class lot-produced in the Russian Federation.

To measure linear accelerations, the BINS-85 system incorporates the AK-6 accelerometer.

The AK-6 features the use of quarts glass as structural material for a sensing element (pendulum) that has high stability characteristics in time under exposure to environment.

In the process of development and bringing a full-scale production to the design figure, the following structural and technological problems were solved:

- manufacturing a high-stability sensing element of quarts glass with coating that provides precision operation of the capacitive angle transducer;
- providing a high stability (within 10 arc s) zero signal and base in operation by using original structural solutions and high precision assembly technology (process).

Main AK-6 technical characteristics are given in Table 4.

Immediately after creating in MIEA a technological base for LG-1 and AK-6 production, and after obtaining the first device specimens, the institute started developing the BINS-85 system for standard digital flight and navigation integrated systems for Il-96-300, Tu-204 aircraft and their modified versions, and later for Tu-334 airplane.

Table 4

N	Technical characteristics	Values
1	Measurement range, g	±10
2	Zero signal drift during life, g	not more than $60 \cdot 10^{-6}$
3	Output signal slope error, %	not more than ±0.02
4	Stability of temperature coefficient slope of %/1°C in any temperature range of ±10°C	not more than 0.002
5	Stability of zero signal offset temperature coefficients, g/°C and base, arc s/°C, in any temperature range of ±10°C	not more than $6 \cdot 10^{-6}$ not more than 0.3
6	Operating temperature range, °C	-60 + +70
7	MTBF, h	not less than 100 000

Table 5 gives main technical characteristics of BINS-85 in accordance with Technical Specification requirements, actual characteristics, characteristics obtained by the present time, and ARINC-704 recommendations.

Table 5

Main parameters	Outlined in Specification 13266	Implemented	ARINC-704 Requirements
Error for determining			
- geographical coordinates	3.7 km for 1 hour	3.7 km for 1 hour	3.7 km for 1 hour
- ground speed components	14.4 km/h	14.4 km/h	21.6 km/h
- attitude (roll, pitch)	0.1 arc degree	0.1 arc degree	0.1 arc degree
- true heading	0.4 arc degree	0.4 arc degree	0.4 arc degree
Availability			
- autonomous alignment	10 min	10 min	10 min
- for desired heading	3 min	3 min	3 min
Number of output parameters	43	46	43
Consumed power	<200 W	95 W	<200 W
System mass	20 kg	20 kg	20 kg
MTBF	>5000 h	6350 h	>5000 h
Linear vibration resistance	1.5 g	1.5 g	0.5 g

In the process of BINS-85 development in addition to creating sensing elements, it was necessary to solve a number of complex problems, including:

development of a sensing element subunit that provides stability of accclerometer and gyro sensitivity axes relative position with an error of no more than 3÷4 arc s within the whole temperature range;

development of automatic BINS calibration system, including LG drift balancing, compensation of scale factor change, accelerometer zeros, transducer sensitivity axes misalignments, and algorithmic compensation of these errors change within the whole desired temperature range;

use of high-performance computers that provide sensor data acquisition, processing and building a "mathematical platform";

special-purpose software development.

In the period of 1994 ÷ 1996 the system underwent acceptance tests and interdepartmental tests, including flight accuracy and reliability characteristics verification tests. The system passed all kinds of ground tests to satisfaction. However, flight test results showed that errors for determining $\Delta\varphi$, $\Delta\lambda$ coordinates instead of 3.7 km for 1 hour of flight (2σ) in accordance with the Specification, were 5 km per 1 hour of flight, that corresponds to class II accuracy in accordance with ENLGS-3.

Analysis of acceptance, interdepartmental and flight test results allowed to find main reasons for increased navigation errors, the basic among them were sensing element temperature errors. In this connection, in 1999 the system was upgraded:

- technological margins of sensing element accuracy were increased;
- design of a number of subunits was changed, and a change-over to new LSI components was made;
- improved algorithms for alignment, orientation, and pre-flight calibration were implemented;
- system calibration techniques and algorithms as well as temperature error compensation were improved.

At the end of December, 2001 the Aviation Register of the Interstate Aviation Committee (AR MAC) issued an airworthiness certificate for the BINS-85 system to install it on an aircraft. This procedure completed a full cycle of BINS-85 developmental improvement and tests, including flight and qualification tests for compliance with class I accuracy requirements, as well as software certification for compliance with KT-178A.

The certification test program specified 14 flights with two BINS-85 systems on non-circuitous routes. Five-hour duration flights were made on IL-76MD airplane at 55.5° - 70° north and at 38° - 105° east. Autonomous initial alignment of BINS-85 was made at latitudes of up to 70° (Norilsk) under the ambient temperature of up to -20°C. In flight, the output information from BINS-85, SNS and SVS-85 was registered by a set of airborne trajectory measurement aids (CBTI), developed by LII (the Flight Test Institute) on the Notebook basis. The CBTI calculates and shows on the display BINS-85 main navigation parameter errors in real time. Post-flight evaluation of system and sensing elements errors was made on the basis of integrated inertial and satellite system data processing with the help of Kalman filter using software developed by LII. Test results show that statistical estimations of BINS-85 errors (at the level of $|m| + 2\sigma$) when determining coordinates do not exceed 3.7 km for each flight hour (allowance – 3.7 km per a flight hour), with respect to speed components do not exceed 3.7 m/s (allowance – 4 m/s), with respect to true heading do not exceed 16.2 arc min. (allowance – 24 arc min). Errors for determining other 38 parameters are also within the tolerance range. Fig.1 shows plots of

latitude and longitude errors in all implementations. The plots indicate that system accuracy margin is increased when the flight time is prolonged.

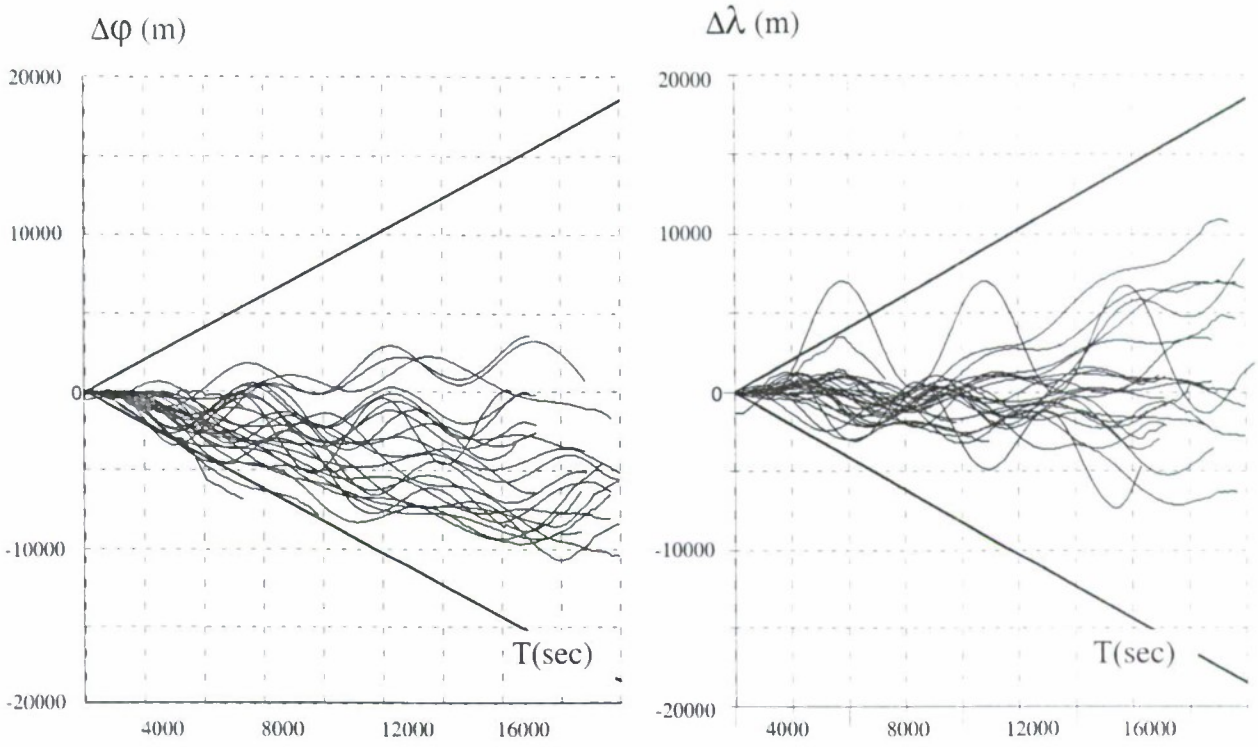

Fig.1. BINS-85 latitude and longitude errors in 28 implementations since 6.04.2001 to 2.08.2001

In the course of flight tests, in addition to determining main navigation parameter errors, errors of system's sensing elements were evaluated:

- systematic drift components of each LG during actuation;
- errors of accelerometer path scale factors.

Statistical assessments of these magnitudes are presented in Table 6.

Table 6

	LG drifts, degree/h			AK scale error, %		
	x	y	z	x	y	Z
|m| +2σ	0.021	0.032	0.026	0.09	0.11	0.12

Obtained assessments exceed approximately by 1.5 times these errors limit defined in the process of BINS-85 design with the help of calculations and mathematical simulation (in terms of LG drift - ≤0.015°/h, in terms of AK scale errors - ≤0.07%). In full-scale production sensing elements characteristics are supposed to be brought up to a desired level, and thus, technological accuracy margin will be provided during first two hours of system operation.

In addition to official tests on Il-76 MD, two BINS-85 systems were operated on Il-96-300. From August 2001 to February 2002 about 50 flights were made at 55.5° - 25° north and at 13° - 105° east. Flight time was from 5.5 to 9 hours. According to these flights results, hourly average errors for coordinate determination by BINS-85 system do not exceed 2.3 km in latitude, and 2.7 km in longitude.

One of the BINS-85 qualification problems was software (SW) certification. Due to home civil aviation integration into the world community, AR MAC introduced new "Requirements to airborne equipment and systems software when certifying aviation hardware" (KT-178A Qualification Requirements). The basis of KT-178A is RTCA/DO-178A document "Software considerations in airborne systems and equipment certification".

In accordance with ENLG-3, BINS-85 type systems directly influence flight safety and, therefore, apply to a "critical" category equipment for which a software level in accordance with KT-178A is defined as level I. Level I software certification required a large number of verification procedures with documents. It is worth mentioning that level I software certificate was obtained in Russia for the first time.

In parallel with the described works, full-scale production was being prepared, which begins from 2002 on the basis of cooperation of enterprises included into Aviapribor holding.

We should point out, that at present the BINS-85 system is the only home BINS that in accordance with domestic and international requirements can be used as a navigation and flight data sensor on aircraft of this class.

AOOT MIEA creates BINS-85-based modified versions of different application that are at different improvement phases now.

First of all, we should mention BINS-77 designed for An-70 transport aircraft. Its main difference from BINS-85 is availability of a multiplex communication link and extended operation conditions. At present flight qualification tests (FQT) are carried out within the aircraft (more than 400 flights have been made, mainly short flights and at the airport zone). FQTs are conducted with old, non-upgraded systems, therefore, navigation errors for the time being exceed the allowance. In 2002 we plan to replace them with systems upgraded using our BINS-85 experience, to conduct acceptance tests and complete flight qualification tests.

For civil aviation, BINS-120 system integrated with a satellite navigation system (SNS) has been developed. In accordance with the system Specification, under SNS receiver data transfer intervals, system error increment in geographical coordinates shall not exceed:

- 100m – during a 5-minute autonomous flight;
- 250 m – during a 10-minute autonomous flight.

By the present time SW has been debugged, prototype manufacturing is being finished, tests on the mobile laboratory have been completed. The results of the tests on the mobile laboratory, including tests in conditions when SNS outputs no data for a long time, verified that precision BINS integration with SNS allows to smooth out SNS noise, provide high accuracy navigation under rather long SNS data output intervals, and provides a basis for successful solving the tasks of ICAO Category III landing.

To solve geodetic and ground-based transport vehicle survey control tasks, a "Sitop" system was developed that in addition to BINS-85 incorporates SNS and an aerometric data unit. The system has two operation modes:

- correction from SNS and aerometric units;
- rate corrective action during periodic vehicle stops for no more than 30 seconds with a an interval of at least 5 minutes.

To improve accuracy, post-trip post-processing is provided. In the latter mode, an error of coordinate determining does not exceed 10 m, geodetic height – 8 m.

By the present time an experimental prototype has been manufactured, software has been debugged, the first phase of full-scale tests has been conducted, these tests show that the system accuracy is close to that of outlined in the Specification.

To study the scope for creating BINS that would comply with Navy's advanced requirements, in 1998 technical proposals were developed and one of the BINS-85 systems was full-scale tested on board hydrographical vessel GS-439. Prior to testing, software had been improved in the part of entering algorithms for autonomous initial alignment on the sea surface. Availability was increased up to 1 hour. Eight-hour mooring tests were carried out and twice the vessel put to sea for 4.5 hours. Plots for coordinate errors during sea tests are given in Fig.2.

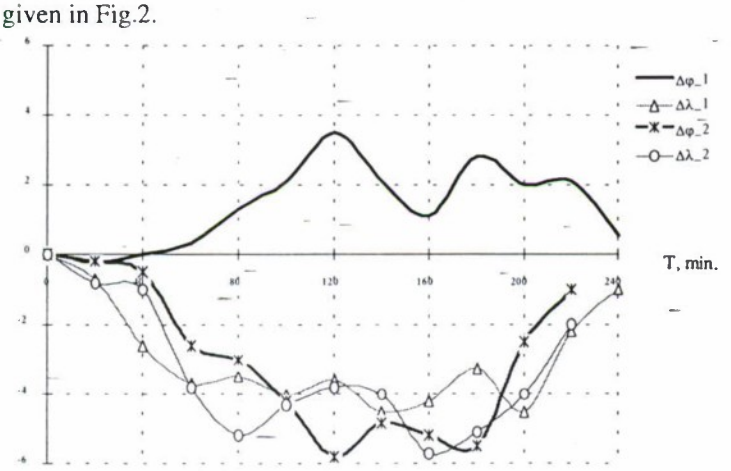

Fig.2

In the course of tests the principal feasibility of using aviation BINS on a sea vehicle was verified. These tests, theoretical solutions and statistical simulation showed the feasibility of creating a small-size, high accuracy BINS for Navy based on BINS-85 sensing elements and software, and using structural methods for accuracy improving.

AOOT MIEA is the leader in creating autonomous astroinertial systems and gravimetric integrated systems. Traditionally, to stabilise stellar monitors and gravimeters, special-purpose heavy, large-size gyroplatforms were built that caused problems when installing on board an aircraft. Therefore, when upgrading these integrated systems, it is supposed to use BINS-77 modified version with an increased number of angular data output, and to install the stellar monitor and gravimeter in the follower platform.BINS-85 modified versions can be used to control attitude of any airborne, seaborne and ground-based vehicle antennas.

PARTICULARITIES OF MULTI-COMPONENT ELECTROMAGNETIC SUSPENSIONS DESIGN*

G.A. Sapozhnikov*, S.V. Bogoslovsky, A.O. Kadkin*****
Saint-Petersbug University of Aerospace Instrumentation, Russia
190000, Saint-Petersburg,Bolshaya Morskaya st., 67, Russia E-mail: svb@aanet.ru

Abstraet

In the report the analysis of state on creation of measuring electromagnetic suspensions and supermodern devices on their basis is discussed. Mathematical models of magnetic suspensions on an alternating current for the first time are offered at simultaneous change of period and amplitude of a supply voltage. The method of synthesis of non-linear control is developed. The schemes of original measuring electromagnetic suspensions are adduced. As example of implementation is considered the six-component accelerometer with the electromagnetic suspension of a sensitive element. There are supports without mechanical contact of movable and fixed parts widely spread among devices and other equipment, which use rotation and movement of some units about others. Electrostatic and electromagnetic suspensions refer to those supports above all.

Key words: magnetic suspension, modeling

Electromagnetic suspensions of different types are of considerable interest as measuring instruments. But in this case it is natural to have a wish to reconceptualize their functions. Suspension is traditionally separated from transducer, and this does not lead to natural improvement of metrology characteristics. Only uniting of functions of suspension and transducer in one structure which generates an invariant characteristic connecting force and an informational parameter in one function, will solve the problem of creation of multi-axis singlemass appliances for measuring of the force and also the hole range of other physical parameters converted into force.

Electromagnetic suspensions not only decrease friction resistance, but also simultaneously give the exact information about displacement and forces defining movement of elements. So electromagnetic suspensions can be considered as multifunctional measuring suspensions.

Scheme and parameters of suspension depends on the requirements to a specific class of measuring devices. For example, displacement transducers should answer the requirements of high slope of an output signal, significant linear range, the symmetry of the characteristic to a zero signal, and absence of force influence on the part of the transducer.

Depending on a way of control of magnetic field value in the running clearance, electromagnetic suspensions are subdivided on passive and active ones. Suspension, which is used with auxiliary servo system, is called an active suspension. And suspension, where stability is caused by natural change of parameters of the basic system of a suspension, is called passive.

Advantages of active electromagnetic suspensions (AEMS) in comparison with passive ones are:

– higher stiffness and speed, because the obvious feedback makes easier the adjustment of a slope of change of current;

– opportunity to provide the lesser level of exciting moments;

– wider range of possible values of centering force.

When developing the measuring electromagnetic suspensions, it is preferable to choose the alternating-current suspensions with force characteristic as function of induction in the running clearance. The accuracy of induction measuring is much higher, when using the alternating-current transducers instead the direct-current ones. More over, alternating current has a demagnetizing effect on cores of electromagnetic converters, which essentially reduces the force measurement error because of residual magnetization of the core material. Researches indicate, that residual magnetization of the core material in the direct current measuring suspensions does not allow to make the force error less than 0.1-0.2%, even if core material is permalloy 79HM. One of the best material is ferrite 3000MT.

The frequency of supply voltage of AEMS electromagnetic converters depends on suspension rigidity, construction parameters, and dynamic properties of electromagnetic converters. It has great influence on selection of material for converter and on static characteristics of suspension.

The mathematical model of the differential alternating current electromagnetic force converter, when changing of amplitude and supply voltage period, has been constructed.

---

* D.Sc., Professor.
** D.Sc., Professor.
*** Aspirant.

Suppose, that at zero time ($t = 0$) voltage applied to eleetromagnet windings is as:

$$U(t) = U_m \sin\left(\frac{2\pi}{T} t + \gamma_0\right).$$

Set of equations, deseribing the differential eleetromagnetie foree eonverter:

$$\dot{X} = X_1;$$
$$\dot{X}_1 = -\frac{\lambda}{m} X_1 + \frac{a_1}{m} T_1 - \frac{b_1}{m} T_2 + \frac{a_2}{m} U_1 - \frac{b_2}{m} U_2 + \frac{a_3}{m} \psi_{21}^2 - \frac{b_3}{m} \psi_{22}^2 + \frac{F_{BH}}{m};$$
$$\dot{\psi}_{21} = -K\psi_{21} - \alpha_1 \dot{U}_1 - \beta_1 \dot{T}_1;$$
$$\dot{\psi}_{22} = -K\psi_{22} - \alpha_2 \dot{U}_2 - \beta_2 \dot{T}_2.$$

Differenee α_1 from α_2 and β_1 from β_2 is eaused by initial phase of eaeh of arms of the differential eireuit in the moment of applying of the eorresponding disturbance; F_{BH} - is impressed foree.

If eurrents are part of phase eoordinates, then the vector function F_m (eleetromagnetie force) in a set of equations of magnetic suspension mathematieal model ean be submitted as the bilinear form of phase eoordinates:

$$\mathbf{F}_m(\mathbf{X}) = \mathbf{X}^T \mathbf{D}_X \mathbf{X}.$$

Finding non-linear eontrol components

$$U(t) = U_A(t) + U_H(t).$$

$$\mathbf{U}_H(t) = \mathbf{N}\left\{\mathbf{F}_m[\mathbf{X}(t)] - \frac{\partial \mathbf{F}_m[\mathbf{X}(t_0)]}{\partial \mathbf{X}} \mathbf{X}(t)\right\},$$

when

$$\mathbf{U}(t_0) = -\mathbf{F}_2^{-1}(t_0)\mathbf{B}^T(t_0) \times$$
$$\times \{\mathbf{R}[\mathbf{X}(t_0), t_0]\mathbf{X}(t_0) + \varepsilon[\mathbf{X}(t_0)]\}'$$

$$\varepsilon[\mathbf{X}(t_0)] = \mathbf{Q}\left\{\mathbf{F}_m[\mathbf{X}(t_0)] - \frac{\partial \mathbf{F}_m[\mathbf{X}(t_0)]}{\partial \mathbf{X}(t_0)} \mathbf{X}(t_0)\right\},$$

$$\mathbf{Q} = -\left(\mathbf{A}^T - \mathbf{R}\mathbf{B}\mathbf{F}_2^{-1}\mathbf{B}^T\right)^{-1}\mathbf{R}; \mathbf{N} = -\mathbf{F}_2^{-1}\mathbf{B}^T\mathbf{Q}.$$

F_m in quite general case can be submitted as a bilinear veetor function of eurrents. If eurrents are part of phase coordinates, then the vector funetion F_m ean be submitted as the bilinear form of phase eoordinates:

$$\mathbf{F}_m(\mathbf{X}) = \mathbf{X}^T \mathbf{D}_X \mathbf{X}; \qquad \mathbf{U}_H(t) = \mathbf{N} \cdot \begin{bmatrix} \mathbf{X}^T(t)\mathbf{D}_X \mathbf{X}(t) - \\ -\mathbf{X}^T(t_0)\left(\mathbf{D}_X^T + \mathbf{D}_X\right)\mathbf{X}(t) \end{bmatrix}.$$

In aetive electromagnetic suspension with control of the running clearance by period of supply voltage the information value is time, and in pulse suspension with eontrol of the running clearance by control pulse repetition frequeney – is frequeney. It allows on the basis of such suspensions to develop the high-preeision souree information sensors, easily matching with a digital information-and-eomputation control eomplex.

The sensor of such type allows measuring three linear and three angular eomponents of aceeleration. It has the following technieal eharaeteristics:

Range of measurement, not less than	25 g
Instability of a zero drift from start to start, no more than	$2 \cdot 10^{-5}$ m / sec^2
Instability of steepness of an output characteristic of a linear acceleration, no more than	0.01 %
Threshold of a linear acceleration	$2 \cdot 10^{-6}$ m / sec^2
Threshold of angular acceleration	0.05 degrees / sec^2
Q-factor	10^6
Frequency band on high limit of measurements	from 0 up to 150 Hz.

The numerical values of angular component of acceleration are analytically determined outgoing from outcomes of measurement of linear component of acceleration and technical features of construction:

Overall dimensions of the complex ... . 60×60×60 mm.
Weight of the unit..... ..... 0.5 kg.

The second device created on the basis of the six-component accelerometer is the device for definition of small weights in zero-gravity conditions. The given device allows to determine with a high degree of accuracy the small weights, for example, received as a result of biological or chemical experiments in conditions of orbital flight.

Scheme of six-component accelerometer is discussed, also results of suspension body form optimization are obtained. Differences from well-known patent (Morrison cube) are discussed. The optimal form of suspension body is six component cross.

References

1. **G.A. Sapozhnikov, S.V. Bogoslovsky, A.T. Kizimov.** Theory and practice of electromagnetic suspension for measuring SPb, SUAI, 2001, P 384.

ACTIVE DAMPING OF THE ESG ROTOR NUTATION BY DRY FRICTION*

V.Z. Gusinsky*, O.I. Parfenov, S.V. Shipilov
State Research Center of Russia - Central Scientific & Research Institute Elektropribor,
St.Petersburg, Russia

Abstract.

Key words: electrostatic gyroscope, rotor nutation oscillation damping, controlled linear motion of the rotor, dry friction

A new technique for active damping of the ESG rotor nutation oscillations is considered. Intrinsic properties of the rotor suspension servo system and the vacuum chamber construction are used to produce a damping moment. The results of mathematical simulation and laboratory tests are given.

Introduction

At the present time and in the forcsecable future electrostatic gyroscopes (ESG) remain the most accurate among the other gyros [1]. The design principle that the ESG rotor should be noncontact in a high vacuum allows retarding and disturbing moments to be reduced to a minimum. However, this makes it difficult to fix the principal axis of inertia of the rotating rotor to a certain direction relative to the case or in space. Before the spin-up stator is energized, the position of the ESG rotor axis of symmetry is arbitrary. Then, in spinning-up, it causes nutation oscillations of the rotor, which prevent the information readout. The currently available aids and techniques for passive and active damping of nutation oscillations either take a lot of time to damp the rotor oscillations or call for complicated control systems [2 – 4].

One of the advantages of the suspension servo system in current use is the possibility to control linear motion of the rotor inside the vacuum chamber (VC). So, it becomes possible to provide periodic linear oscillations of the rotor until it touches (slides lightly) the inner surface of the vacuum chamber (for example, the limit stops that are used for the rotor fail-safe landing [5]). This sliding allows producing a dry friction moment oppositely directed to the instantaneous angular velocity of the rotor. As will be shown below, this moment damps the angular oscillations of the rotor.

1. The statement of the problem

Consider an ESG spherical rotor rotating about an arbitrary axis. At the same time the rotor performs some linear oscillation motions in the VC caused by a changing force generated by the suspension. When moving linearly, the rotor surface periodically comes into contact with the surfaces of the limit stops (supporting elements). The coordinate frame $OXYZ$ is fixed to the rotor, with the axes lying along the rotor principal axis of inertia. The coordinate frame $OX_IY_IZ_I$ is fixed to the stationary vacuum chamber. The rotor angular position relative to the case can be described by the Euler equations:

$$\begin{cases} \dot{\psi} = \dfrac{1}{\sin\vartheta}\left(\omega_x \sin\varphi + \omega_y \cos\varphi\right), \\ \dot{\vartheta} = \omega_x \cos\varphi - \omega_y \sin\varphi, \\ \dot{\varphi} = -ctg\vartheta\left(\omega_x \sin\varphi + \omega_y \cos\varphi\right) + \omega_z, \\ \dot{\omega}_x = \dfrac{1}{J_x}\left((J_x - J_z)\omega_z\omega_y + M_x\right), \\ \dot{\omega}_y = \dfrac{1}{J_x}\left((J_z - J_x)\omega_x\omega_z + M_y\right), \\ \dot{\omega}_z = \dfrac{M_z}{J_z}, \end{cases} \tag{1}$$

where J_z, J_x are the axial and equatorial principal moments of inertia of the rotor; ω_x, ω_y, ω_z, M_x, M_y, M_z are the projections of the angular velocity and external moments onto the corresponding axes; ψ, θ, φ are the Euler angles.

Below the term 'external moment' is used in reference to dry friction that arises every time the rotor surface comes into contact with the limit stops. (The moments due to residual gases, electric and magnetic fields are not taken into account, as they are negligibly small as compared to the dry friction moment). The dry friction

* D.Sc., Professor, Head of Department.

moment in the projections on the coordinate frame $OXYZ$ is as follows:

$$M = CM_1, \tag{2}$$

where C is the matrix of transition from $OX_1Y_1Z_1$ to $OXYZ$.

The matrix C is calculated as the product of rotation matrices that correspond to each of the Euler angles:

$$C = C_\varphi C_\vartheta C_\psi, \tag{3}$$

where

$$C_\psi = \begin{pmatrix} \cos\psi & \sin\psi & 0 \\ -\sin\psi & \cos\psi & 0 \\ 0 & 0 & 1 \end{pmatrix}, \quad C_\vartheta = \begin{pmatrix} 1 & 0 & 0 \\ 0 & \cos\vartheta & \sin\vartheta \\ 0 & -\sin\vartheta & \cos\vartheta \end{pmatrix}, \quad C_\varphi = \begin{pmatrix} \cos\varphi & \sin\varphi & 0 \\ -\sin\varphi & \cos\varphi & 0 \\ 0 & 0 & 1 \end{pmatrix}. \tag{4}$$

The moment M_1 is determined for each particular case of the limit stop arrangement as a sum of vector products of the contacting limit stop vector-radius by the friction force vector.

Denoting the distance from the center of the chamber to the limit stops by ρ, let us make the following assumptions:

- ρ is the same for all the limit stops;
- the ESG construction affords fail-free motion of the rotor when it comes into contact with the surface of the limit stops [5];
- the rotor suspension servo system (RSSS) is designed so that linear oscillations of the rotor only occur along the axis OX_1 and are described by the following equations:

$$X_1 = a \cdot \sin(\nu \cdot t); \quad |\sin(\nu \cdot t)| \le \frac{\rho}{a};$$

$$X_1 = \rho, \qquad |\sin(\nu \cdot t)| > \frac{\rho}{a},$$

where a and ν are the RSSS parameters, $a > \rho$;

- the friction force is constant.

The friction force vector is calculated by the formula:

$$F_i = F_o \frac{R_i \times \Omega_1}{|R_i \times \Omega_1|}, \quad i = 1,\ldots,n, \tag{5}$$

where F_i – the friction force vector;

i – the number of the limit stop;

F_o – the absolute value of the friction force;

R_i – the vector-radius of the i-th limit stop;

Ω_1 – the vector of the instantaneous angular velocity of the rotor in the coordinate frame $OX_1Y_1Z_1$;

n – the total number of the limit stops that come into contact with the rotor in the process of rotor damping.

$$\Omega_1 = C^T \Omega, \tag{6}$$

where Ω – the vector of the instantaneous angular velocity in the coordinate frame $OXYZ$.

Finally, the expression for the moment M_1 can be derived in the following form:

$$M_1 = \begin{cases} \sum_{i=1}^{k} R_i \times F_i, & if \quad X_1 \ge \rho, \\ [0\,0\,0]^T, & if \quad |X_1| < \rho, \\ \sum_{i=k+1}^{n} R_i \times F_i, & if \quad X_1 \le -\rho, \end{cases} \tag{7}$$

where k – the number of the limit stops that come into contact with the rotor as it displaces in the positive direction.

2. Computer simulation

The numerical integration of Equations (1) in view of the equations for M_x, M_y and M_z (2), (5) and (7) for some particular cases was carried out on a PC with the use of MatLab®.

The following parameters were varied:

- initial angular orientation of the rotor;
- initial rotation frequency of the rotor;

- friction coefficient;
- forced linear oscillation frequency of the rotor in the suspension.

The following parameters were fixed in the simulation:

- the rotor radius 0.025 m;
- the number of contacting limit stops n=4 (k=2);
- the arrangement of the limit stops in the VC: ψ_1=160°, θ_1=45°(limit stop 1), ψ_2=160°, θ_2=135°(2), ψ_3=-20°, θ_3=45°(3), ψ_4=-20°, θ_4=135°(4);
- the axial moment of inertia J_z=1.0*10^{-5} kgm^2;
- the equatorial moment of inertia J_x=0.9*10^{-5} kgm^2.

The computer simulation showed that during damping of nutation oscillations the gyro approaches the nearest limit stop regardless of the rotation frequency (20...40 Hz), forced oscillation frequency (10...40 Hz) and friction coefficient (0.1...0.4). Hence, from the initial positions ψ_o=160°, ϑ_o=40° and ψ_o=160°, ϑ_o=50° the rotor seeks the orientation ψ=160°, ϑ=45° (limit stop 1), while from the initial positions ψ_o=160°, ϑ_o=130° and ψ_o=160°, ϑ_o=140°- the orientation ψ=160°, ϑ=135° (limit stop 2). In so doing the higher is the initial rotation frequency of the rotor, the longer is the process of damping (in this calculation from 1...1.5 sec to 2...2.5 sec). The forced oscillation frequency f_k does not have a profound effect on the process of damping. At the same time the increase in the friction coefficient μ improves the damping efficiency, however it results in greater losses of the rotor angular rotation rate (in this calculation from Δf=5 Hz to Δf=10 Hz).

Fig. 1 shows one of the computational experiments.

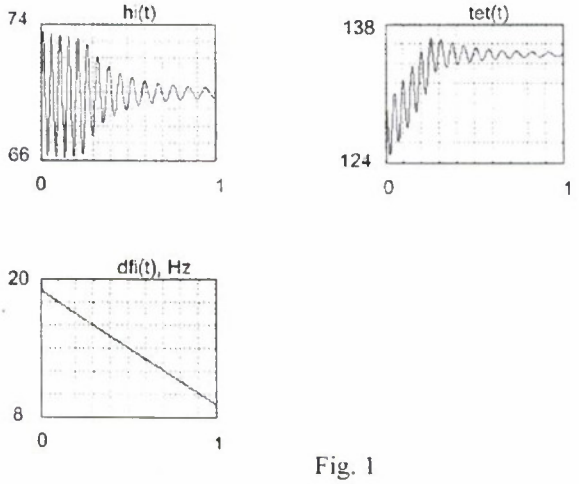

Fig. 1

Here

hi(t) – the plot of the angle χ against time. χ is related to the precession angle ψ as follows:

$$\chi = \psi - 90°; \tag{8}$$

tet(t) – the plot of the nutation angle ϑ against time;

dfi(t) – the plot of the rotor rotation frequency $\dot{\varphi}$.

Angles are given in degrees, t – in seconds, frequencies – in Hz.

Figures 2 and 3 show the plots of the damping time t_d against the rotor rotation frequency and friction coefficient.

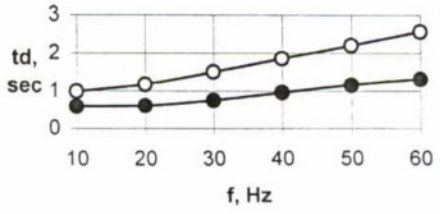

○ - the friction coefficient 0.1

• - the friction coefficient 0.2

Fig. 2

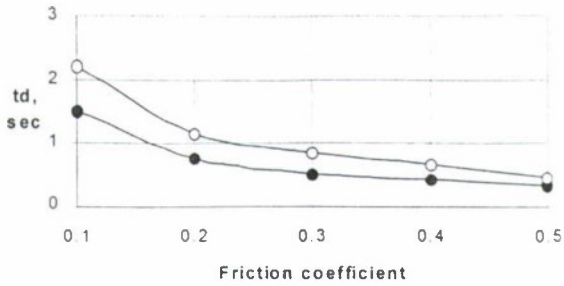

○ - the initial rotor rotation frequency 50 Hz
• - the initial rotor rotation frequency 30 Hz

Fig.3

3. Test results

The efficiency of the ESG rotor nutation oscillation damping by using the proposed technique was proved experimentally. The tests were carried out with the gyro case oriented vertically and horizontally for different angles of misalignment between the rotor and the case. In all tests after the damping procedure (that lasts no more than 30 sec) was completed, the rotor spin axis takes a fixed orientation, which is conditioned by the limit stops configuration regardless of the case orientation (horizon or vertical) and the initial orientation of the rotor relative to the case. The rotor oscillation amplitudes decrease from a few dozens of degrees of arc to some units of arc minutes.

Conclusion

The technique for damping nutation oscillations of the ESG rotor presented in this paper does not call for any sophisticated control systems, like those used for active damping methods. It does not disturb the thermal regime of the gyro because of the long Foucault currents effect as in the case of passive damping. The method proposed allows damping the rotor oscillations over a short period of time using the intrinsic properties of the rotor suspension servo system and the vacuum chamber design. The arrangement of the limit stops provides the required angular orientation of the rotor axis relative to the vacuum chamber.

References

1. **Peshkhonov V.G.** The key problems of the present-day autonomous navigation // Gyroscopy and navigation. № 1. 1996.– PP. 48 – 55. (In Russian).
2. **Lange B.** Active Damping of ESG Rotors with Mass-Unbalance Readout // Journal of Spacecraft and Rockets. – 1972. – Vol. 9, № 2. – PP. 667 – 675.
3. **Parkinson B.W., Lange B.** Active Damping of Free-Rotor Gyroscopes during Initial Spin-Up // Journal of Spacecraft and Rockets. – 1970. – Vol. 7, № 6. – PP. 667 – 675.
4. **Komarov V.N.** Active damping of the conducting gyro rotor nutation // Applied mechanics. Vol. 17, № 9, 1981. – PP. 99 – 105. (In Russian).
5. **Maksimov M.G., Paliy Yu.Ya., Shipilov S.V.** Selecting discrete support of the rotor for a strapdown electrostatic gyro // Gyroscopy and navigation. № 4, 1998.– PP. 98 – 99. (In Russian).

MATHEMATICAL MODELS OF THERMAL CONTROL SYSTEMS FOR MICROMECHANICAL GYROSCOPES*

M.A. Barulina*, V.E. Dzhashitov, V.M. Pankratov*****
Precision Mechanics and Control Institute, Russian Academy of Sciences,
24, Rabochaya St., 410028, Saratov, Russia.
tel. (845-2)-221693, (845-2)-222376, fax: (845-2)-222340,
E-mail: HrustovAV@forpost.ru or E-mail: iptmu@forpost.ru

Abstract

Key words: system of thermal control, nonlinear mathematical models, micromechanical gyroscope

In this paper set and investigated the problem of creation of active thermal control systems (TCS) of the microмechanical gyroscopes (MMG) providing at the minimal energy consumption, maintenance of the given temperature of the device in conditions of the determined and casual thermal influences. Nonlinear mathematical models reversive on semi-conductor Peltyer's thermocouples or on heating elements of thermal control systems of micromechanical gyroscopes are constructed. Analytical and computer research of the constructed models is carried out, qualitative and quantitative estimations of functioning of systems MMG - TCS are received at complex temperature influences.

Statement and the decision of the problem

Among the instrumental errors of micromechanical gyroscopic devices of inertial systems the temperature errors occupy the important place. As shown the cumulative experience of researches [1,2], application of thermal control systems of the absolute temperature of micromechanical gyroscopes (MMG) allows essentially (in some cases more than on the order) to increase their accuracy. Application of active thermal control systems (TCS) in micromechanical gyroscopes is especially important, that thermal influences on the device of an environment are in a wide range of temperatures (– 40 ÷ +85) °C.

At the same time there are questions investigated completely insufficiently such as the questions connected with a choice of the type of thermal control systems of micromechanical gyroscopes, maintenance of their given properties, definition of parameters of laws of regulation and heat-evolution, research of functioning systems MMG-TCS at the determined and casual temperature influences and some other.

The purpose of the present work is in the statement and the decision of the problem of working up of the theoretical and applied aspects of the analysis and synthesis of the active thermal control system for the micromechanical gyroscope, providing the minimal energy consumption, maintenance of the given temperature of the device in conditions of complex thermal influences and in reduction of thermal drift of a gyroscope.

Statement of the problem includes the following stages:

- Design of mathematical models of thermal control systems for micromechanical gyroscopes (reversive on semiconductor Peltyer's thermocouples or on heating elements with point-to-point control);
- Analytical and computer research of the constructed models, choice of parameters of the thermal control systems, type and characteristics of regulation laws, obtaining of qualitative and quantitative estimations of functioning of system MMG-TCS at the complex determined and casual temperature influences.

For achievement of the formulated problem nonlinear mathematical models of thermal processes in systems "MMG-reversive TCS on the basis of Peltyer's thermocouples" and "MMG-TCS on the basis of heating elements" are constructed and investigated. These models (fig. 1) contain systems of the perturbed ordinary differential equations of thermal balances and nonlinear laws of regulation of the temperature with the characteristics, analytical relation and program complexes for research of influence of a temperature field of micromechanical gyroscopes of periodic, step and casual temperature indignations:

$$c\dot{T}_1 + q(T_1 - T_2) + q_{M1}(T_1 - T_3) = Q_1,$$
$$c\dot{T}_2 + q(T_2 - T_1) + q_c(T_2 - T_c) = Q_2, \qquad (1)$$
$$c_M\dot{T}_3 + q_{M1}(T_3 - T_1) + q_{cM}(T_3 - T_c) = Q_3,$$

$$T_c = T_{cA}\sin\omega t + T_{co} + T_{cc} \qquad (2)$$

$$Q_1 = \left[-\varepsilon_T J(T_1 + 273) + \frac{J^2 R}{2}\right]nm, \qquad Q_2 = \left[\varepsilon_T J(T_2 + 273) + \frac{J^2 R}{2}\right]nm \qquad (3)$$

---

*The postgraduated student.
**Doctor of technical science, professor, the head of laboratory.
***Doctor of technical science, professor, the vice director in scientific problems.

TCS with Peltyer's thermoeouples

$$J = \begin{cases} J_{max}, & if \quad T_d - T_z \geq T_L \\ tg\alpha(T_d - T_z), & if \quad -T_L \leq T_d - T_z \leq T_L \\ -J_{max}, & if \quad T_d - T_z \leq -T_L \end{cases},$$

TCS with heating elements

$$J = \begin{cases} J_{max}, & if \quad T_z - T_d \geq T_L \\ tg\alpha(T_z - T_d), & if \quad 0 \leq T_z - T_d \leq T_L \\ 0, & if \quad T_z - T_d \leq 0 \end{cases}. \qquad (4)$$

$$T_d = \begin{cases} T_1, & if \quad the\ gauge \quad is\ located \quad on \quad working \quad side \\ T_3, & if \quad the\ gauge \quad is\ located \quad on \quad MMG \end{cases} \qquad (5)$$

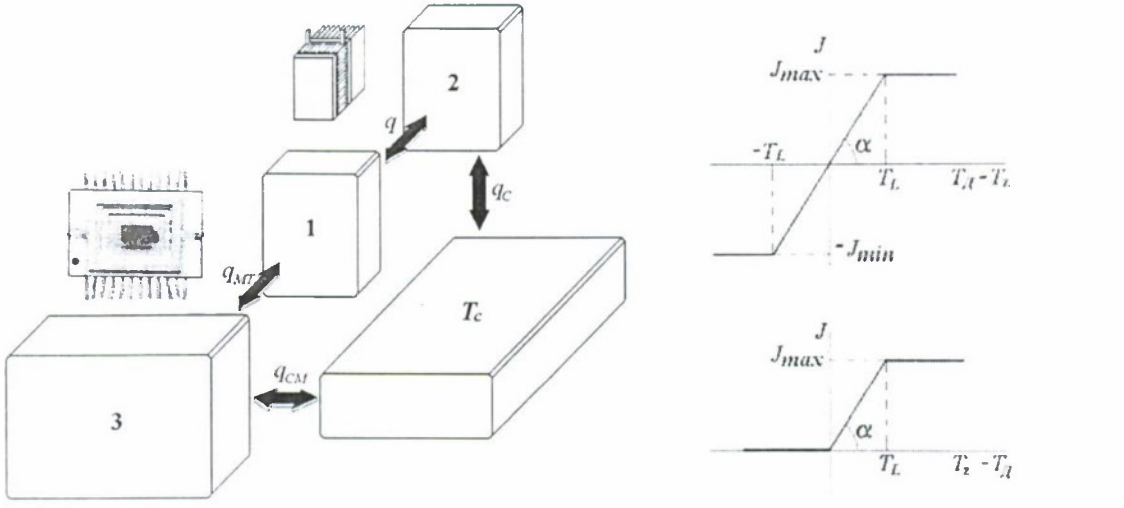

a) b)

Fig. 1. Thermal model of system "MMG-TCS" (a) and laws of regulation of temperature (b):
1,2 - accordingly working and external, contacting to an environment, side of thermocouples; 3 - chip with MMG

Inasmuch as laws of change heat-evolution of Peltyer's thermoeouples (3) and the law of regulation of temperature (4) have the nonlinear eharaeter, the eonstructed mathematieal model "MMG-TCS" is nonlinear. Therefore one of the basic methods of research of considered system (1) - (5) is mathematical modeling processes of functioning of system "MMG-TCS" by its numerieal integration and eomputer experimentation.

At the first stage the step changes of an ambient temperature in a range (-40÷85)°C were considered (fig.2a,b). As a result of these experiments there were determined a constant of time τ of transition process and rating values of eapacities TCS during at work in a lincar zone.

At the second stage the influence of harmonious change of an ambient temperature with the given amplitude T_{cA} and the period having the order of a constant of time τ transition proeess in MMG (fig. 2c). As a result of these experiments the choiee of parameters TCS describing thermal communieations MMG with Peltyer's thermoeouples and an environment were reeommended.

At the final stage the influence of casual temperature influenees on system "TCS – MMG" (fig. 3a) and an opportunity of occurrenee of a phenomenon of the determined chaos in system (fig. 3b, c) was investigated. Dependeneies of characteristics from time are shown on fig.3a and fig.3b, a phase portrait is shown on fig. 3c.

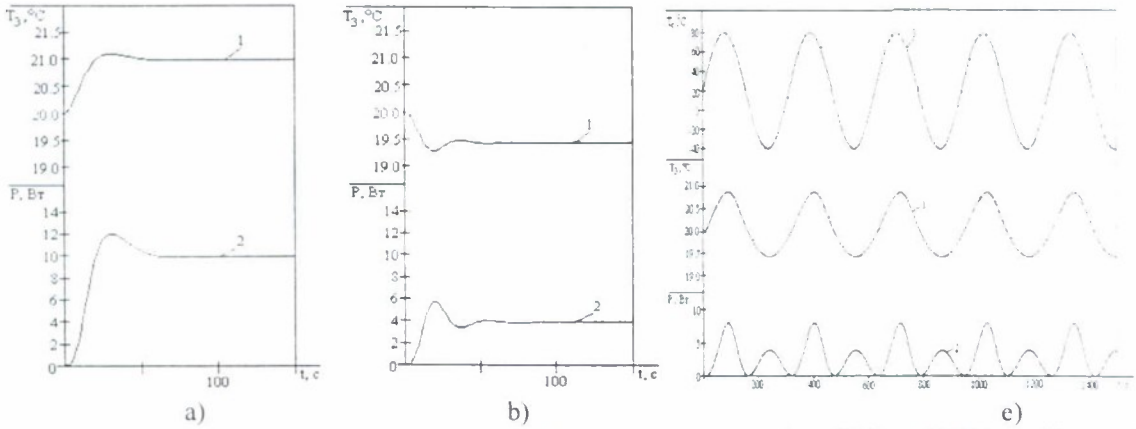

a) b) e)

Fig.2. Characteristics of system "MMG-TCS" at step from 20°C to 85°C (a), from 20°C to -40°C (b) and harmonic (c) changes of ambient temperatures:
1- temperature of MMG; 2 – power of energy consumption of TCS; 3- ambient temperature

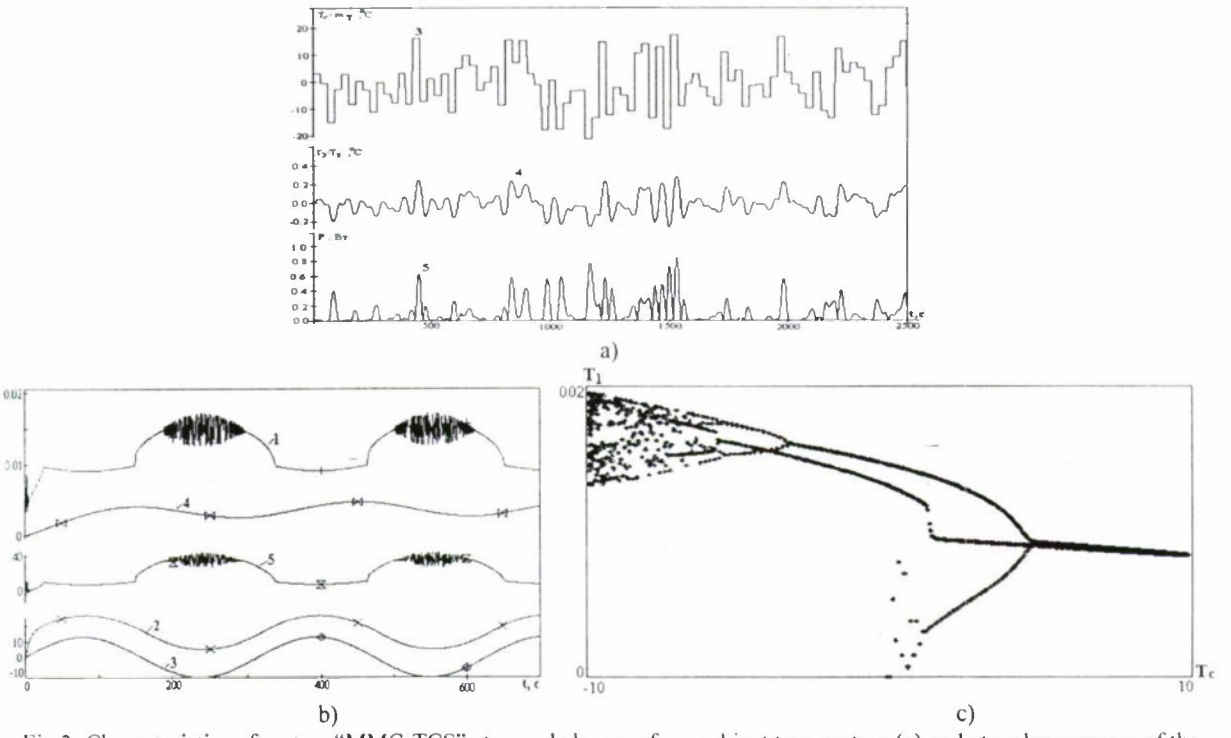

Fig.3. Characteristics of system "MMG-TCS" at casual change of an ambient temperature (a) and at a phenomenon of the determined chaos (b), (c): 1- temperature T_1 working side of thermocouples; 2 - temperature T_2 external side of thermocouples; 4 - temperature T_3 MMG; 3- ambient temperature T_c ; 5- power of energy consumption TCS

The analysis of results and conclusions

1. Results of research have shown, that with various constructive circuits of micromechanical gyroscopes it is expedient to apply reversive systems of a temperature control to stabilization of absolute temperature of chips with semi-conductor Peltyer's thermocouples. Feature of such systems of a temperature control is that they may work in reversive (cooling - heating) a mode at change of polarity of a proceeding current. It allows providing maintenance of given temperature MMG inside a range of change of an ambient temperature.

2. Unfortunately, disadvantage of such nonlinear systems of temperature's control is that at the certain combinations of parameters in them the phenomenon of the determined chaos may take place, that is the temperature on the working side of Peltyer's thermocouples gets chaotic character at a determined variable ambient temperature.

3. At realization of researches conditions of occurrence of the determined chaos are analytically revealed, the diagrams of stationary decisions containing regular, turning and singular points and areas of parameters of system at which this phenomenon is possible are constructed are determined. The carried out computer experiments have shown that arising at certain (relatives to relay) laws of regulation, a degree of heat-insulation of MMG and external side of thermocouples, an arrangement heat-sensing device, chaotic changes of temperature on the working side of thermocouples have insignificant influence on temperature of the chip with MMG (fig. 3b). This influence becomes more significant if the mass of the chip is less on some orders than the mass of thermocouples. However, occurrence of chaotic temperatures can be excluded by a choice of parameters of system.

4. In the certain cases application TCS on the basis of heating elements is possible for regulation of temperature in MMG. As have shown analytical researches the phenomenon of the determined chaos does not come in these systems of a temperature control, they are simpler and are reliable. The basic disadvantage of such TCS is that given temperature of MMG is necessary to choose at the top level of a range of an ambient temperature (for considered types MMG is +85 °C), what is not good for elements of the device and supporting electronics.

5. The constructed mathematical models, the developed program complexes and the carried out researches allow to give concrete recommendations for maintenance of the given thermal modes and for reduction of temperature errors of MMG with different overall-mass characteristics.

References

1. **Джашитов В.Э., Лестев А.М., Панкратов В.М., Попова И.В.** Влияние температурных и технологических факторов на точность микромеханических гироскопов // Гироскопия и навигация.-1999.- №3 (26). С. 3-17.

2. **Джашитов В.Э., Панкратов В.М.** Математические модели теплового дрейфа гироскопических датчиков инерциальных систем /Под общ. редакцией академика РАН В. Г. Пешехонова. - СПб.: ГНЦ РФ - ЦНИИ "Электроприбор", 2001.-150с.

HIGH-Q QUARTZ RESONATOR USING PIEZO-ELECTRIC EXCITATION AND CONTROL OF THE THIRD OSCILLATION MODE

Yu. A. Yatsenko*, V. V. Chikovani**

Ukrainian Center for Optical Instrument Technology
e-mail: chiko@public.ua.net

Abstract

Key words: resonator, sensitive element, gyroscope

Sensitive element investigation results made on the basis of quarts hemispherical resonator excited on the third vibration mode with the use voltage applied to ring-type piezoelectric member, the resonator is mounted on.

Introduction

Modern development tendencies in gyroscopy are characterized by motion to a miniaturization. To such sensors can be put Coriolis vibratory gyroscope (CVG), made both on the basis of hemispherical quarts, piezoelectric, metallic and other material resonators.

To day the certain results were achieved on miniaturization of CVG sensing elements. Hemispherical quartz resonator gyros of diameters 30 and 15 mm were developed by Litton (USA) [1], of diameter 20 mm by MIEA (Russia) [2]. Tineless hemispherical resonator and technology for its balancing was offered and developed by Medicon (Russia) [3]. Compound and stemless hemispherical quartz resonator were offered and developed by Ukrainian Center for Optical Instrument Technology (UCOpInTech) (Ukraine) [4, 5]. Besides, in UCOpInTech were developed and tested 17 mm and 25 mm cylindrical metallic resonator CVG, excited from the bottom of the cylinder.

The capability of a third mode standing wave vibration pattern control for stemless resonator designed by means of control voltages applied to a ring-type piezo-electric member (RPM) is investigated in the present study. The RPM is parted into 12 segments, each fourth of which is used as a positioning excitation electrode, and the remaining ones for control and pick off.

Design features

CVG design feature based on the hemispherical quartz resonator mounted on a RPM (see fig.1) is that the hemispherical resonator (it is not shown in a fig. 1) fastens on PRM with the help of a cement bonding, in region of its pole. Excitation the third vibration mode of the hemispherical resonator implements by means of voltages applied to RPM segments, arranged through angle 120 degrees. On the RPM undersurface 12 electrodes are formed through angle 30 degrees in view of segments. The upper face of the ring is completely metallized and is used as a common electrode. The frequency of the excitation signal is close to a natural frequency for the third vibration mode. The process of excitation of a hemispherical resonator with the help of RPM is that in the region of excitation electrodes there is a radial force, which affecting on a hemispherical resonator produces its deformation corresponding to the third vibration mode.

During measurements, pick up of the information was made both from RPM segments and from capacitive electrodes arranged by the edge of the resonator. The ring-type electrode 0 (see fig. 1) was basically used for initial excitation of the resonator. Signals from pairs of segments 4-7, 8-6, 12-3 move on the differential amplifiers 13, 14 and 15, relatively. The resonators, together with differential amplifiers, are in an evacuated chamber. The output signals were processed in the information-processing unit, which formed excitation signals as well. The hemispherical resonator oscillation registration, as researches have shown, is more effective when using capacity transducers, as the amplitude of radial oscillations by the edge of the resonator for the third mode is approximately two orders of magnitude more than near its pole region.

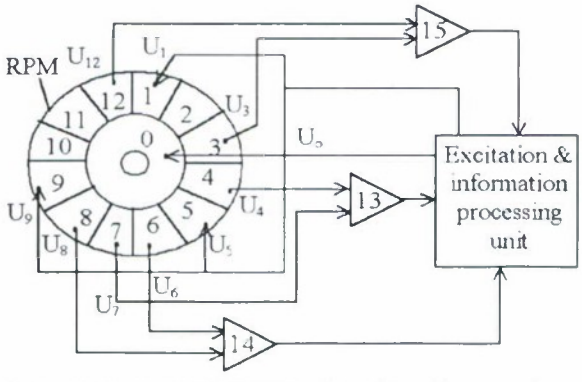

Fig.1. Measurement scheme (0 – piezo ring member , 1-12 - segments)

The third mode was used because of reduced sensitivities to resonator fixing and manufacturing imperfections, than that for the second mode. The latter was affirmed by experiments [5].

Experimental investigation results

The investigations were conducted for the resonator dia of 30 mms. The Q-factor of the resonator with RPM for the third vibration mode is about 10^6, the resonance frequency of oscillations is approximately equal to 13700 Hz, and steepness of the phase characteristic is about 1000 deg/Hz.

The comparative investigation of different pick-offs - capacitive one and RPM segments - have shown, that the capacitive transducer signals are registered at the excitation amplitude of 200 ... 300 mV. For RPM segments this value makes - 1.5 ... 2 V. It can be explained by that the output signal is formed by the difference voltage from the RPM segments, in which equal for all segment excitation signal components are present. Therefore, usage of combined method of measurement (excitation with RPM, and capacitive pick-offs is expedient).

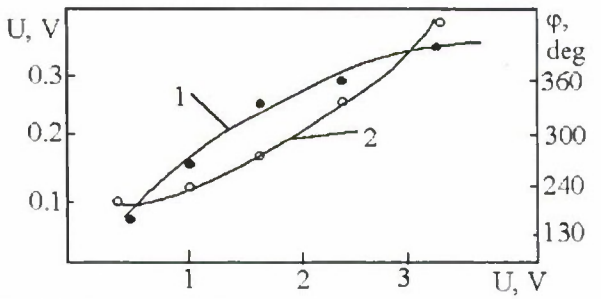

Fig. 2. Voltage applied to control segments vs. vibration wave amplitude

In a fig. 2 the dependency (curve 1) of capacitive electrode signal amplitude arranged by one of the nodes of oscillation for the third mode (above the 4-th segment) on voltage applied to the 4-th segment is shown. The increase of the voltage amplitude on the capacitive electrode with voltage growth applied to the nodal 4-th segment indicates the turn of the vibration pattern, when the current antinode comes nearer to the node. In the same figure the dependency (curve 2) of phase difference between the excitation signal and capacitive electrode signal is shown. It is visible, that the phase difference is also increased at the turn of the vibration pattern. This shows the capability of angular rate measurement based on phase measurements.

Conclusion

The capability of excitation of the third oscillation mode and its control in stemless resonator with the help of a ring-type piezo-electric member is shown in this investigation. This enables not to apply high-voltage initial excitation conventionally used in gyros of a considered type, and also to reduce the influence of manufacturing imperfections on a measuring error at the expense of using the third mode of oscillations. Besides the capability of angular rate measurement by the hemispherical resonator gyro, based on phase measurements is shown. This increases noise-proof features and considerably facilitates conversion of a signal to a digital form.

The obtained results allow to draw a conclusion, that the offered design of the resonator allows to realize a low-cost rate HRG with a sharp response to rotation, small overall dimensions and simpler circuits.

References

1. **W.W.Stripling, D.D. Lynch, J. R. Baskett.** Hemispherical Resonator Gyro: Principle, Design, and Performance./ Symposium Gyro Technology 1992, Stuttgart, Germany.
2. **E.A.Izmailov, M.M.Kolesnik, A.M. Osipov, A.V. Akimov.** Hemispherical Resonator Gyro Technology.Problems and Possible Ways of their Solutions./ 6-th S.-Petersburg International Conference on Integrated Navigation Systems. 1999.
3. **B.P.Bodunov, V.M.Lopatin, B.S.Lunin.** Development of tineless fused quarz hemispherical resonator./ 3-th S.-Petersburg International Conference on Integrated Navigation Systems. 1996.
4. **Yu.A. Yatsenko, S.F.Petrenko, V.V.Vovk, V.V.Chikovani.** Technological Aspects of Manufacturing of Compound Hemispherical Resonators for Small-sized Vibratory Gyroscopes./ 6-th S.-Petersburg International Conference on Integrated Navigation Systems. 1999.
5. **Yu.A. Yatsenko, V.V. Chikovani, L.V. Borisyuk.** Development of Stemless Quarts Hemispherical Resonator for Vibratory Gyroscope". Symposium Gyro Technology 2000, Stuttgart, Germany, September 19/20, 2000, Editor H. Sorg, pp.7.0-7.10.

ON THE MICROMECHANICAL VIBRATORY GYRO MOTIONS

S.A. Kharlamov[1]

Bauman Moscow State Technical University, Moscow, Russia
E-mail: sakharlam@mtu-net.ru

Abstract

Key words: micromechanical vibratory gyroscope, isotropic oscillator, anisotropic oscillator, microobservability

The models of micromechanical vibratory motions in the form of three-dimensional isotropic and two-dimensional anisotropic oscillators are considered. The problems of oscillator motion microobservability are discussed.

The micromechanical vibratory gyro is the object of many analytical considerations and practical efforts to develop miniature, low cost and reliable inertial sensors for a wide variety of applications. The gyro deserves the thorough analysis from the viewpoint of rational mechanics fundamentals. Three problems, related to the micromechanical gyro motion, are presented. Their solutions may be used as a sound foundation for a more deep understanding of gyro performance.

The first problem is to demonstrate that the three-dimensional isotropic linear oscillator may be used for the realization of inertial reference system which consists of the coordinate frame and time scale. By using the remarkable similarity of two body system motion in the celestial mechanics and the spatial isotropic oscillator motion [1] one can derive the fundamental properties of vibratory gyro which may be used as guidelines for the practical developments. To this end, the equation of motion of a point mass is written in the vector form

$$m\frac{d^2\mathbf{r}}{dt^2} + k_g\frac{\mathbf{r}}{r^3} = 0. \tag{1}$$

The equation represents a partial case of the Kepler two body problem where mass of one body is much larger than those of other. Similarly, the motion of mass joined to a large body (a spacecraft, for example) by a isotropic linear elastic suspension is defined by the following vector equation

$$m\frac{d^2\mathbf{r}}{dt^2} + k_e\mathbf{r} = 0. \tag{2}$$

To find the mass motions one should solve Eqs. (1) and (2) at the initial conditions

$$\mathbf{r}(0) = \mathbf{r}_0, \qquad \dot{\mathbf{r}}(0) = \mathbf{v}_0 = \mathbf{p}/m. \tag{3}$$

where $\mathbf{p}$ is and initial momentum of mass produced by an initial impulse.

Both equations have a common feature of motion, namely, the first integral in vector form

$$\mathbf{H} = \mathbf{p} \times \mathbf{r} = m\mathbf{v}_0 \times \mathbf{r}_0. \tag{4}$$

This integral means that the moment of momentum or angular momentum of mass relative to attractive center is a constant vector. Let introduce the angle α between the vectors of initial deviation and impulse according to the relation

$$\cos\alpha = \frac{\mathbf{p}\cdot\mathbf{r}_0}{pr_0} \tag{5}$$

and a unit vector $\mathbf{k}$ directed along $\mathbf{H}$,

$$\mathbf{k} = \frac{\mathbf{p}\times\mathbf{r}_0}{pr_0\sin\alpha}. \tag{6}$$

Depending on the angle α the motion of mass will be linear (to the center on out of the center at $\cos\alpha = 0$) or planar (at $\cos\alpha \neq 0$ mass moves in the plane perpendicular to the vector $\mathbf{k}$). In both gravitational and elastic problems, the most general motion is the well known motion along the elliptic trajectory. The major and minor axes of the ellipse can be selected as axes of the inertial coordinate frame. The fact that the constructed frame is really inertial has been proven both in celestial mechanics and in gyroscopy [2].

[1] Professor

As a unit of the time scale of the inertial reference system one can adopt the period of mass orbital motion which is equal

$$T_g = 2\pi\sqrt{\frac{ma^3}{k_g}}, \tag{7}$$

where a is the major axis of the trajectory called the Newton ellipse, and the period

$$T_e = 2\pi\sqrt{\frac{m}{k_e}} \tag{8}$$

of the orbiting of the isotropic oscillator mass along the trajectory called the Hooke ellipse.

In the special case where the initial displacement and velocity vectors are orthogonal, the trajectory is circular and the three-dimensional isotropic oscillator represents a model of rotor gyroscope. In another special case where both initial vectors are collinear, the trajectory is the straight line and the oscillator simulates a vibratory gyroscope. In the general case of elliptic trajectory, one has a model of hybrid rotor-vibratory gyroscope. The latter gyro can operate in the following manner. Let the spacecraft or body carries the oscillator the mass of which orbits along the Hooke ellipse and rotates. Then, the body rotation can be detected by detecting the Hooke ellipse rotation with respect to the body. In the body-fixed frame, the body rotations about the ellipse in-plane axes result to ellipse displacements proportional to the rotation angle. Thus, these rotations are well observable. In the case of body rotation about the axis perpendicular to the ellipse, then the ellipse relative displacements are detected by an observation of quadratic function of the rotation angle. Therefore, this body rotation is poorly observable.

The second problem is related with a treatment of two-dimensional anisotropic oscillator as a model of vibratory gyro in so-called whole angle measurement mode. The problem statement is stimulated by the well known fact that the perfect isotropy of any real engineering system is very difficult to attain. The equations of motion of the planar anisotropic oscillator written in the principal elasticity axes

$$\ddot{x} + (N-1)^2 x = 0, \quad \ddot{y} + (N+1)^2 y = 0 \tag{9}$$

can be transformed into the equations of motion in the so-called isofrequency axes

$$\ddot{X} + (N^2+1)X - 2NY = 0, \quad \ddot{Y} - 2NX + (N^2+1)Y = 0 \tag{10}$$

for two coupled identical single degree-of-freedom oscillators. At the specially selected initial conditions

$$X(0) = 0, \quad Y(0) = 1, \quad \dot{X}(0) = 0, \quad \dot{Y}(0) = 0 \tag{11}$$

these equations have the solutions

$$X(\tau) = \sin\tau \sin N\tau, \quad Y(\tau) = \cos\tau \cos N\tau \tag{12}$$

in the form of beatings for two mutually orthogonal axes. In the plane of oscillations, the trajectory of the oscillator mass fulfills a square over each period of these beatings.

If the isofrequency axes rotate about the axis perpendicular to the plane of oscillations then the equations of motion of the oscillator mass

$$\ddot{X} + 2\dot{Y}\dot{\theta} + (N^2 - \dot{\theta}^2 + 1)X - (2N + \ddot{\theta})Y = 0, \tag{13}$$

$$\ddot{Y} - 2\dot{X}\dot{\theta} - (2N + \ddot{\theta})X + (N^2 - \dot{\theta}^2 + 1)Y = 0 \tag{14}$$

have an exact solution

$$X(\tau) = \sin\tau \sin N\tau \cos\theta - \cos\tau \cos N\tau \sin\theta, \tag{15}$$

$$Y(\tau) = \sin\tau \sin N\tau \sin\theta + \cos\tau \cos N\tau \cos\theta \tag{16}$$

showing that the square rests fixed in the inertial coordinate frame and rotates relative to the isofrequency axes. Observing the trajectory of oscillator mass motion during the beating period allows one to the angular rate of square relative to the isofrequency axes. This angular rate is equal and opposed in direction to the measured angular rate if the anisotropic oscillator used as the vibratory gyroscope.

The third problem is connected with an attempt to find the boundary between the classical and quantum areas of consideration in the micromechanical inertial sensor study. The treatment is based on the concepts of microobservation and microcontrol formulated by A.A. Krasovsky [3] in 1976. The area of interest is the interaction of the micromechanical oscillator with classical and quantum versions of motion measurement system.

Naturally, the accuracy of the quantum motion measurement system is limited by the Heisenberg indeterminability principle

$$\sigma_p \sigma_q = h/2\pi \tag{17}$$

where σ_p is a standard uncertainty of momentum measurement, σ_q is a standard uncertainty of coordinate measurement, and h is the Planck constant. To find the similar limits for the classical measurement system A.A. Krasovsky [3] suggested the formula

$$\sigma_p \sigma_q = kT/\omega_0, \tag{18}$$

where k is the Boltzmann constant, T is an equivalent temperature which combine the oscillator temperature and so-called "noise" temperature of amplifiers, and ω_0 is the oscillator natural frequency. The comparison of accuracy limits of quantum and classical measurement systems for reasonable values of parameter in Eq. (18) shows that uncertainties of the classical system is nine orders of magnitude higher than those of the quantum system.

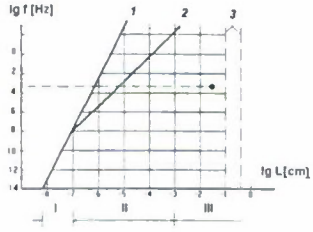

Figure 1

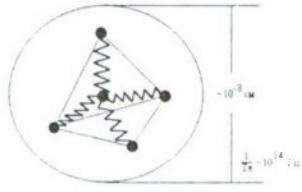

Figure 2

The possibilities of microminiaturizaton are shown in the plane "linear dimension—frequency" presented in Figure 1. The diagram borrowed in [3] contains the uncertainty barriers for the quantum (line *1*) and classical (line *2*) interactions of the measurement system and the control object, as well as the borders of the miniature component manufacturing technology (domain *3*). It is obvious that the microminituarization is naturally limited by the elementary vibratory gyroscope consisting of five silicon atoms and four covalent bonds as shown in Figure 2. This gyro has the overall size of order 10^{-8} cm and oscillation frequency of order 10^{14} Hz. It is located in the left bottom corner of the diagram.

The point in the diagram shows the location of a gyro which is developing long time by the Vector. It is clear that the possibilities to reduce gyro dimensions are not exhausted. One can hope that, in spite the micromechanical vibratory gyros are far from the "quantum borderline" today, they can approach it in the next future.

References

1. **Arnold V.I.** Huygens and Barrow, Newton and Hooke—the first steps of calculus and catastrophe theory from evolutes to quasicrystals [in Russian], Nauka. Fizmatlit. Moscow, 1989.

2. **Lynch D.** Vibrating gyro analysis by the method of averaging // 2nd Saint Petersburg International Conference on Gyroscopic Technology and Navigation, 1995.

3. **Krasovsky A.A.** Some problems of microcontrol // Zhurnal Tekhnicheskoi Fiziki, Vol. 46, No. 9, 1976, pp. 1804–1809 [in Russian].

THE PROBABILITY DISTRIBUTION OF THE INERTIAL DEAD RECKONING ERRORS

V.Sharov*, Y.Saraiskii**
Academy of Civil Aviation,
38, Pilotov str, 196210, Sankt-Petersburg, Russia. E-mail:aga@peterlink.ru

Abstract

Key words: dead reckoning errors , distribution,, RNP

Data of dead reckoning (DR) errors that have been collected during routine flights of Il-96-300 and post-flight procedures of the inertial reference system (IRS) checking are analyzed. A hypothesis of Laplace distribution of DR-errors is proposed. The results obtained may be used for the evaluation of IRS capability to meet the required navigation performance (RNP).

Introduction

The worldwide introduction of RNP concept increases the importance of permanent analysis of inertial dead reckoning errors because of IRS still remain the most important component of modern airborne navigation equipment. The reliable conclusion about the compliance of the equipment with the required navigation accuracy in each particular region may be made only on the base of experimental data. This article is devoted to the analysis of data that was collected by one of authors during flights of Il-96-300 and post-flight checks.

1. Technique of collection and processing of data

Aircraft Il-96-300 are equiped with three indepcndcnt IRS "Litton-90-100". For thc navigation mean coordinates are used however the crew can read original coordinates from each IRS . They were used as DR-coordinates. Coordinates obtained from GPS were considered as accurate. Coordinatcs were recorded every 30 min of flight on 6 aircraft. Totally 2193 measurements have been made for airborne time up to 11 hours.

The analysis presentcd is based on the errors that were calculated as differences bctween inertial coordinates (latitudes and longitudes) and GPS coordinates, taken for precisc. Coordinate errors $\Delta\varphi'$ and $\Delta\lambda'$ in minutes of arc were transformed to kilometers $\Delta\varphi=1.852\Delta\varphi'$; $\Delta\lambda=1.852\Delta\lambda'\cos\varphi$. Also radial error r have been calculatcd. For $\Delta\varphi$ and $\Delta\lambda$ values of means m_φ and m_λ,, variances σ^2_φ and σ^2_λ , correlation coefficicnts ρ for cach moment t were estimated. Standard errors σ_φ and σ_λ have been calculated as upper confidcnce limit (for the probability 0.999) because of samples had various sizes depend on t. Standard radial crrors σ_r were calculated as square root of mean value of r^2 .

2. Flight data analysis

Analysis have shown that non-stable stochastic processes $\Delta\varphi(t)$, $\Delta\lambda(t)$ have approximately zero expectations, correlation is insignificant, variances of latitude and longitude errors are alike and increasc since time of flight. It leads to the circular distribution with increasing σ_r that have been approximated as

$$\sigma_r = 0.69\,t + 0.92.$$

Under assumption of Gaussian distribution of $\Delta\varphi$ and $\Delta\lambda$ the radial error r has Rayleich distribution. In this case the radius of circle that includes present position of aircraft with P=0.95 can be calculated as

$$R_{Pe3}=\sigma_r(-\ln 0.05)^{1/2}=1.7308\,\sigma_r=1.17\,t+1.56.$$

This expression was intended to estimate the correspondence of IRS accuracy to RNP.

Nevertheless further thorough research based on Pearson and Kolmogorov criteria shown that the assumption about Gaussian distribution of $\Delta\varphi$ and $\Delta\lambda$ is inconsistent with data observed. It was found that the zero mean Laplace distribution with the probability density function

$$f(x)=(\nu/2)\exp(-\nu|x|) \qquad (2.1)$$

where ν-parameter depended on standard error of $\Delta\varphi$ and $\Delta\lambda$ ($\nu^2=2/\sigma^2$), is more suitable..

Fig.1 presents histogram of relative frequencies f^* of normalized errors for latitude St = $(\Delta\varphi-m_\varphi)/\sigma_\varphi$ and approximated probability density functions for t = 5 hours.

The Laplasian distribution of $\Delta\varphi$ and $\Delta\lambda$ leads to the bivariate distribution

$$f(\Delta\varphi,\Delta\lambda)=(\nu^2/4)\exp[-\nu(|\Delta\varphi|+|\Delta\lambda|)]. \qquad (2.2)$$

The following expression for the probability $P(R)=P(r<R)$ have been derived for this distribution

$$P(R)=1-e^{\nu R}-\nu\int_0^R e^{-\nu(\Delta\varphi+\sqrt{R^2-\Delta\varphi^2})}d\Delta\varphi.$$

---

* Post-graduate student, navigator of Il-96-300.

** D.Ph., Head of Airnavigation Chair.

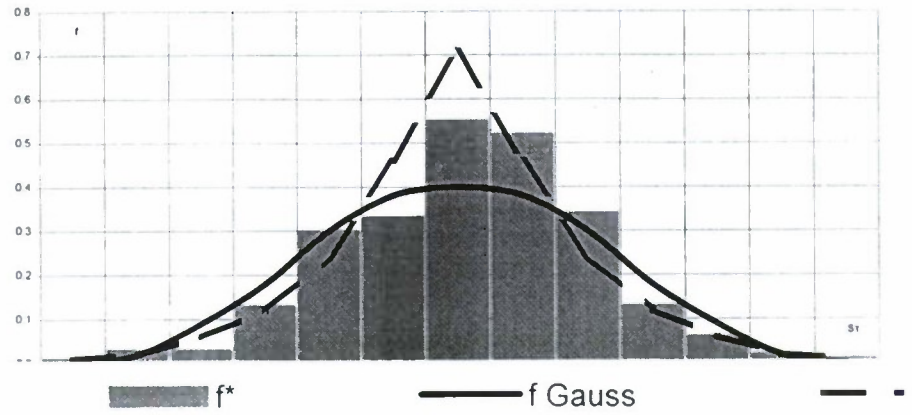

Fig.1 Distribution of Latitude Errors for t=5hrs. (n=164)

This probability can be calculated by numerical methods. The fact should be put into consideration that the hypothesis of Laplace distribution gives more pessimistic judgment of DR accuracy and ability to satisfy RNP. Nevertheless "Litton-90-100" provides relatively high accuracy. For example, it meets European B-RNAV requirements within 3.5 hrs of flight.

3. Analysis of post-flight checks data

IRS accuracy has also been estimated by comparison post-flight DR coordinates with published parking ramp coordinates. Differences between these coordinates have been divided by flight time to calculate "hour system errors" (HSR). The coordinates errors and radial differences for 478 flights have been collected and analyzed. The following performance data have been obtained (km per hour): m_φ=0.045, σ_φ=0.458, m_λ=.0.061, σ_λ=0.419, m_r =0.468, σ_r=0.523. Present data also have shown that the coordinate error distribution corresponds to Laplas distribution and therefore distribution of radial HSR is closer to bivariate Laplas distribution then Rayleich one (Fig.2).

Additional data which has been received from "Litton Aeroproducts" (Airbus-340, "Virgin Airline") contain 231 dates of HSR with following parameters (nautical miles per hour): m_r=0,555; σ_r=0.364. These data also have confirmed Laplace distribution.

There have been found no evidence of any dependence of IRS accuracy on region of flight, including the polar region. It was also found that HSR has a tendency for increase in the course of IRS exploitation time since 1998 to 2001 years.

In despite of high reliability of "Litton-90-100" failures and abnormal HSR (greater2 nm/hr) sometimes take place. From May 2000 to February 2001 there were 24 incidents in "Aeroflot", so permanent analysis of IRS performance is essential.

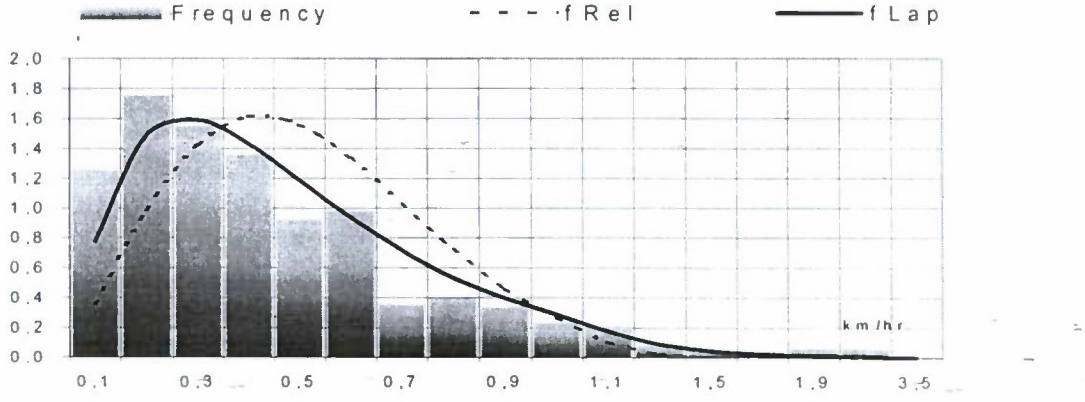

Fig2. Density of Radial HSR of "LTN-90-100" (n = 478)

Conclusion

1. DR-errors of latitudes and longitudes are non-correlated stochastic processes. They have increasing and approximately identical variances that corresponds to the circle distribution.

2. It is worth while to use the Laplace distribution of coordinate errors for the evaluation of probabilistic performance of IRS.

3. The monitoring of error data ensures opportune information about every IRS to detect its tendency to the deterioration

THE LINEAR ACCELERATION METERS UNIT WITH PRECISION QUARTZ ACCELEROMETERS AS SENSING DEVICES*

Kalihman L.Ya. *, Kalihman D.M. **, Kaldymov N.F.*, Nahov S.Ph.******
FSUE PC "Korpus", 1, Osipov St., 410019, Saratov, Russia, fax. 845.2.64.95.21

Abstract

Key words: the unit of linear acceleration meters, quartz pendulous accelerometer

In the report there is considered the construction principle of precision thermo-invariant unit of linear accelerations meters, which contains six nonorthogonally oriented quartz pendulous accelerometers, electronics designed to make output information, as well as thermo-invariance assurance system of the unit which is operating in control system of a descent space vehicle.

In modern control systems there are widely adopted linear accelerations accelerometers of different operation principles, for example, float accelerometers with electrical feedback, string accelerometers, and quartz pendulous accelerometers with electrical feedback.

There are widely spread the redundant systems containing more than three primary meters (accelerometers) where sensitivity axels are nonorthogonally orientated in regard to basic coordinate system connected with the device case.

Such systems ensure operation reliability in case of failure of several primary meters; allow making diagnostics of a failed device and switching it off.

Nevertheless, precise characteristics of the device are determined first by precision of primary meters - linear accelerations meters. Quartz pendulous accelerometers with feedback system can be referred as perspective linear acceleration meters. These accelerometers with small overall dimensions and mass, which is not exceeding 30 g, have high precise characteristics: scale factor error is 0,01-0,02 %, random component of zero signal from start to start is $1 \cdot 10^{-4}$g. The only difficulty restricting wide use of quartz pendulous accelerometers as primary meters is the temperature dependence of main characteristics because of nature properties of quartz, as well as temperature dependence of torque sensor of the accelerometer feedback system.

All together it results in non-linear character of dependence of quartz pendulous accelerometer scale factor and zero signal on the temperature.

Scale factor variation depending on temperature is characterized by the value of about $250 \cdot 10^{-6}$ g / °C, and zero signal variation – by the value of $45 \cdot 10^{-6}$ g/ °C. Taking into account that the range of operation temperatures for devices working in control systems of space vehicles is 0-40°C, it is easy to calculate that if the temperature changes by 40°C, the zero signal varies by $0.18 \cdot 10^{-2}$ g at the systematic component level is $5 \cdot 10^{-3}$g and the random component level is $0.5 \cdot 10^{-6}$g (for modern precision meters). Scale factor also varies similarly. It was found experimentally, that nonlinear dependence of the indicated parameters on temperature has a descending branch, an ascending branch and a point of inflection, which as a rule corresponds to the temperature, at which the quartz plate was mounted into the body of the accelerometer sensor. Therefore the units of linear accelerations meters with quartz pendulous accelerometers as primary meters in control systems of space vehicles are used nowadays only on conditions that temperature errors of quartz pendulous accelerometers are algorithmically compensated.

The algorithmic compensation is the entering of predetermined temperature dependences of accelerometers parameters into memory of the board computer or another special calculator operating together with accelerometers.

It is inconvenient when using the device, since board computers are usually overloaded with navigational and other problems to solve, and the special calculators complicate the system and raise its price.

The way to raise the precision for the unit of linear acceleration meters constructed upon quartz pendulous accelerometers by making the main characteristics invariant to modification of operation temperature without algorithmic compensation or thermostatic control is considered in the report.

The idea of the way is to use the heat power emitted by the electronics of the device to heat quartz pendulous accelerometers and at the same time to ensure temperature regulation (dumping of excessive heat power) by means of introduction of the passive heat controller into the device construction. Thus, the offered way allows to

---

* Candidate of engineering science, chief of department.
** Candidate of engineering science, chief of department.
*** Candidate of engineering science carrying on engineer - electromechanicses.
**** Chief designer.

provide the constant temperature (aecuracy ± 1°C) for sensors by passive means of regulating temperature field inside the device without using the additional power to heat them up and keep their temperature. **The temperature, lying by 5°C higher than the inflection point of temperature dependenees of basic eharaeteristies, is ehosen here as an operating point defining the temperature condition inside the device.** When such temperature stabilization is kept it bceomes possible to use the electronic analogue observer which works only on a linear branch of dependenee of aeeelerometer eharacteristies on temperature and ensures the control of high accuracy and the invariance of charaeteristics to temperature change.

The way is construetively realized in the deviee ULAM KX 69-042, designed at the enterprise "Korpus" aeeording to the requirements specifications of RCC "Energia" for the descent module of modernized spaceship "Soyuz-TM".

The device has passed all kinds of development tests, as well it has been tested as experimental equipment during flight tests of the spaceship "Progress".

The unit of linear acceleration meters (ULAM) (fig.1) contains six independent channels of measurement, eaeh of which has the quartz pendulous linear aceelerations meter (2) with built-in amplifier and temperature transmitter, seeondary power source (4) and information eonversion unit (3), which converts output voltage of the feed-baek amplifier into a unitary code.

The sensitivity axels of the accelerometers are oriented in 60° along the guiding lines of a eone with an half angle of 54,7356°; that is ensured by fastening of accelerometers at the panes of hexahedral pyramid with an angle of inclination of $35°15'52''$ (additional to an angle of 54,7356°) each pane to the supporting flat of device body (1), thus the axels of accelerometers are perpendieular to corresponding panes of the pyramid, and sensitivity axels of channels 1,3,5 and channels 2,4,6 form orthogonally related directions.

The passive (8) which structural layout is shown in fig. 2 is entered into the unit of linear aceeleration meters (fig. 1). The passive heat eontroller is loeated in the eavity of the truncated pyramid, on the panes of which six aceelerometers are fixed. Adjacency of the body of the passive heat controller to the surface of pyramid cavity is provided, and the passive heat eontroller eontains a pack of bimetallic plates (16), rod (14), slider (15), foundation (13), helieal (17) and flat (18) springs and heat-insulating hubs (19).

The pack of bimetallie plates (16) is installed between the end plane of the passive controller body (12) and the shoulder of the rod (14), the rod is located along an axel of the eontroller body with a possibility of axial movement in the case of thermal deformations of bimetallic plates. The slider (15) is fixed with a possibility of axial movement along the controller body. The foundation (13) is rigidly connected with the body (12) through heat-insulating hubs (19). The helieal spring (17) is located between a shoulder of the rod (14) and the components of the body (12), and the flat spring (18) is between the components of the rod and the slider, free space between the device body and hexahedral pyramid with aeeelerometers fixed on its basic grounds is filled with porous heat-insulator (10,11) (fig. 1).

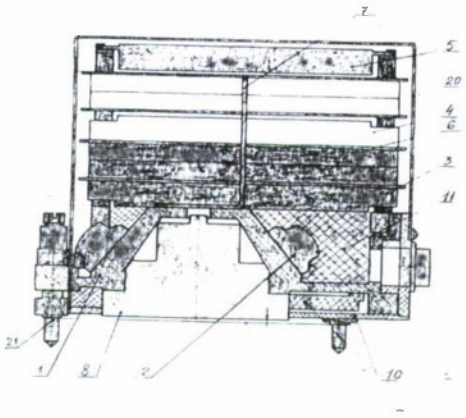

Fig.1

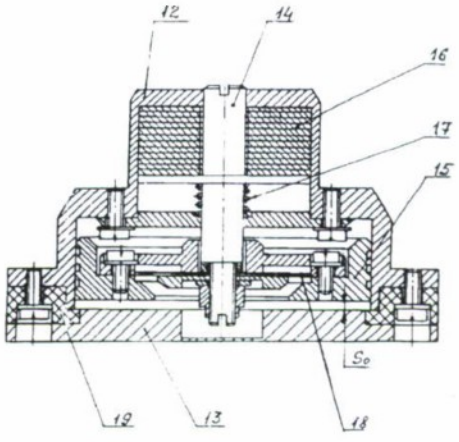

Fig.2

Electronics of the device (fig. 1) is six secondary power sources (4), six information conversion units (3) and the logic unit (5) (it is not considered as the unit performing a function, which is not connected with operation principle of the device) - are located as a paek above accelcrometers.

Between elcctronic units there are located heat-eonductors (6), connected to central heat conductor (7), the lower end of which is attached to the upper surface of the body of the passive heat controller (8). The joint operation of system of conductors (6, 7) and the passive heat controller (8) allows to guiding the heat power emitted by electronic units (3, 4, 5) to heat the device volume which is occupied by accelerometers (2); that

eliminates the overheating of electronic units and ensures accelerometers warming up. Thus in thermostatically controlled volume around of accelerometers there is ensured the temperature T =55±1°C which is on an ascending branch, above the inflection points of temperature dependence curves for parameters of device measurement channels. This creates conditions for the electronic observer (9), included into the structure of each information conversion unit (3), to perform its function – to ensure thermoinvariance for zero signal and scale factor of the measurement channel.

The electronic observer 9 (fig. 3) contains the bridge circuit (33), in diagonal of which the thermistor (34) (structurally located inside the accelerometer sensor), the measuring amplifier (35), analogue multiplier (36), precision reference voltage source (29) and adjusted resistors (32, 37, 38) are included. Analogue multiplier (36) has two inputs and one output, the output of the bridge circuit (33) is connected to the input of the measuring amplifier (35), the output of which is connected to the input of the integrator (23) through the adjusted resistor intended for equilibration of the circuit ensuring the thermoinvariance of the accelerometer zero signal. Simultaneously the output of the measuring amplifier (35) is connected to the first input of the analogue multiplier (36), and the second input of the analogue multiplier is connected to the output of the preliminary amplifier (22).

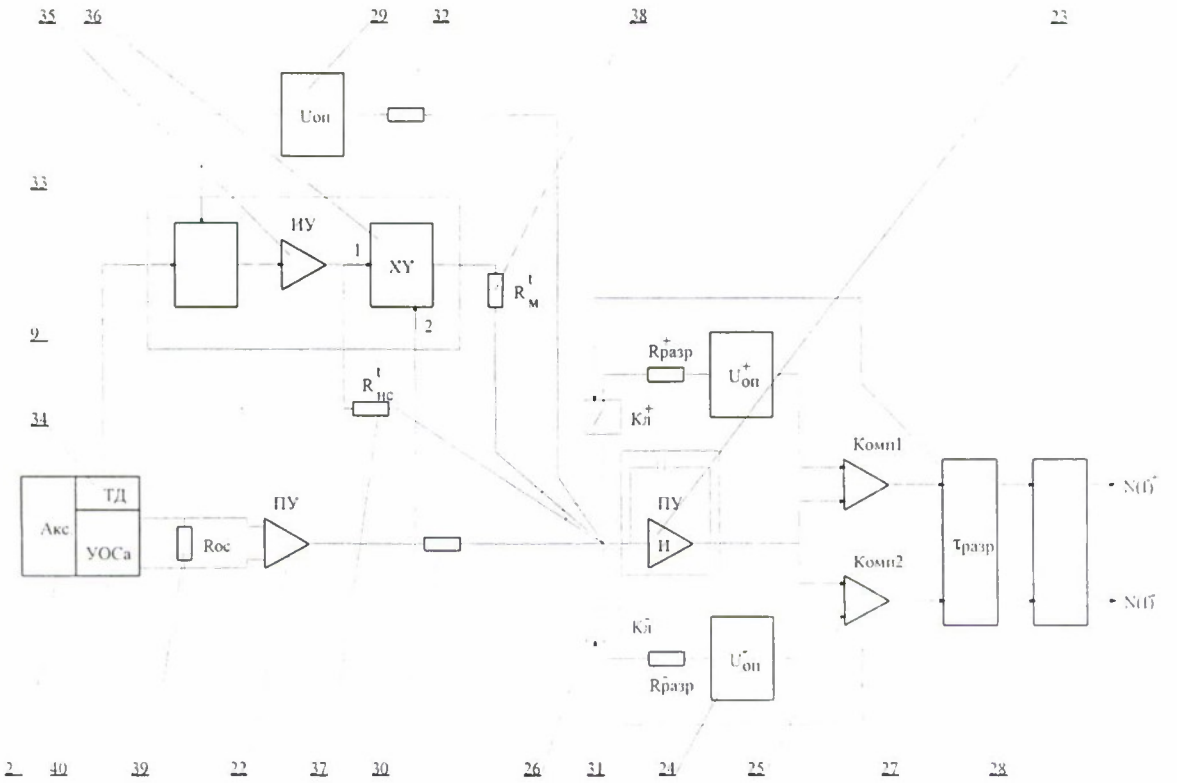

Fig. 3

The output of analogue multiplier is connected to the input of the integrator (23) through the adjusting resistor intended for equilibration of the circuit ensuring the thermoinvariance of the accelerometer scale factor. Simultaneously input of the integrator (23) through the adjusting resistor intended for compensation of systematic component of accelerometer zero signal, is connected to the output of the reference supply source (29), second output of which is connected to the bridge circuit (33).

The process of conversion of accelerometer feedback current into a unitary code made by the information conversion unit (3) is not considered (fig. 3) as widely known.

Let's only note, that: the integrator (23), two reference voltage sources (24), two comparators (25), electronic keys (26), scheme of time interval creation (27) (which contains binary counters, creator of interval duration...) and scheme of output information creation, i.e. impulses of a unitary code, (which contains the transistor key, pulse transformer ...) serve for the abovementioned conversion.

The electronic observer (9) which is entered into the information conversion unit (3) works as follows. The period of a tooth voltage at output of the integrator (23) is determined from the following ratio:

$$T = (I_{div} / I_{ch}) t_{dis} \qquad (1)$$

where I_{dis} - discharge current of the integrator (23), and I_{dis} = const, since the discharge current is created by the precision standard voltage source (24), included into a well-known converter scheme "voltage – frequency"; t_{dis} = const - time, during which the discharge of the integrator is carried out, the constancy of this value underlies the operation of a well-known converter scheme "voltage – frequency"; I_{ch} - charge current of the integrator (23). The charge of the integrator (23) is carried out by feedback current of the accelerometer, that's why temperature-dependent components are present in charge current.

$$I_{ch} = (1/R_{ch}) \cdot I_{fb} \cdot R_{fb} \cdot K_{pa}, \quad (2)$$

where $I_{fb} \cdot R_{fb} \cdot K_{pa}$ - current, output resistance of feedback circuit of the accelerometer and amplification factor of preliminary amplifier (22), accordingly; R_{ch} - resistance of the resistor (30) (fig. 3).

$$I_{fb} = I_{gfb} \pm \Delta I_{fb} \pm \Delta I_{gfbt} \pm \Delta I_{fbt}, \quad (3)$$

where I_{gfb} - feedback current, proportional to projections of linear acceleration vector on the sensitivity axle of the accelerometer at temperature of 30 ° C , $I_{gfb} = K^{30}_{s} g_{K}$,

ΔI_{fb} - zero signal of the accelerometer at temperature 30°C;

ΔI_{gfb} - modification of feedback current proportional to projection of linear acceleration vector caused by temperature instability of scale factor, $\Delta I_{gfb} = \Delta K_{s} \cdot g_{K}$,,

ΔI_{fbt} - temperature modification of accelerometer zero signal,

$K^{30}_{s} g_{K}$ - scale factor of the accelerometer at temperature of 30°C and projection of linear acceleration vector to a sensitivity axle of the accelerometer, accordingly,

ΔK_{u} - temperature coefficient of accelerometer scale factor.

For the accelerometer KX67-041, upon which the device ULAM KX 69-042 is implemented, temperature of 30°C corresponds as a rule to the inflection point of curves for temperature dependencies of the accelerometer characteristics, $\Delta K_{u} < \pm 250\ 10^{-6}$ 1/ ° C, for zero signal the similar factor is $\pm 45\ 10^{-6}$ g/ °C.

The observer (9) creates such compensation current of temperature dependence of a zero signal, that $\Delta I_{fbt} + \Delta I_{com} = 0$, and such compensation current of temperature dependence of a scale factor, that $\Delta K_{u}\, g + \Delta I''_{comp} = 0$.

This is performed as follows. An output signal from the diagonal of the bridge (33), the arm of which is the temperature sensor (34) multiplied by transmission factor of the measuring amplifier (35), supplied to the input of the analogue multiplier (36), on the second input of which the output there is supplied a signal from the output of the preliminary amplifier (22) proportional to measured acceleration, allows with the help of the balance resistor (38) to work out the amendment which compensates the change of feedback current due to temperature dependence of scale factor, i.e. it ensures $\Delta K_{u} g + \Delta I''_{comp} = 0$.

The compensation of temperature dependence of zero signal $\Delta I_{fbt} + \Delta I_{comp} = 0$ is carried out with the help of the resistor (30). Compensation is performed by using the precision reference supply source (29).

The device works within the range of environment temperature from 273 K up to 313 K (from 0°C up to 40°C) in different conditions of heat exchange, namely, at the presence of natural or reinforced convection according to measured accelerations, or at the absence of convection in conditions of imponderability, and of vacuum as well.

The high accuracy of main characteristics is ensured independently, without usage of algorithmic compensation, which requires much memory of the board calculator (BC) and creates difficulties in organization of BC software and in usage of the device.

The high accuracy of quartz pendulous accelerometers is achieved due to the invariance of its main characteristics, it is ensured without power expenditures but at the expense of usage of heat power emitted by electronics of the device.

Heat power removal from the electronic units in order to warm up the accelerometers at the same time eliminates the electronic units overheating, and that also raises precision characteristic of the device.

Characteristics of the device:
Measurement range is 10g.
Scale factor error is ±0.02 %
Random component of zero signal from start to start is 10^{-4} g in temperatures range of 0 - 40°C
Mass is 3 kg.

SIMULATION SOFTWARE AND HARDWARE IMPLEMENTATION FOR A LOW COST ELECTRONIC INERTIAL NAVIGATION SYSTEM TEST-BENCH

R. Giroux* , **R. Jr. Landry****
Dept. of electrical engineering – Ecole de technologie superieure,
1100 West Notre-Dame St., Montreal, Canada.
* e-mail: rgiroux@ele.etsmtl.ca ** e-mail: rlandry@ele.etsmtl.ca

R. Gourdeau***
Dept. of electrical engineering – Ecole Polytechnique de Montreal,
CP 6079, Succ.Centre-Ville., Montreal, Canada.
*** e-mail: richard.gourdeau@polymtl.ca

Abstract

Keywords: simulation, hardware, inertial navigation, algorithms, MEMS

This paper addresses the tools and materials used in order to setup a test-bench for the design of strapdown inertial navigation systems: a generic and flexible simulator that allows the simulation of different system's architecture scenarios, and an easy-to-use hardware implementation for real-time testing. In order to realize fast prototyping systems, to take advantage of modular design and to allow rapid real-time testing, a Simulink© Navigation System Simulator (SNSS) has been developed. The SNSS is designed in several modules allowing point-wise improvements or modifications, which do not affect the other modules. The SNSS will be a precious tool in the design of the innovative algorithm expected to be suitable for the use of MEMS inertial sensors in low cost navigation systems. The real-time testing is done with an off-the-shelf hardware architecture allowing direct use of Simulink© and Real-Time Workshop. At the end of its design phase, this software and hardware implementation will allow rapid prototyping and easy-to-use design for low cost GPS-aided electronic inertial navigation systems.

Introduction

For many years, low cost inertial navigation systems (INS) are subject of great interest. In the last decade, the development of Micro-Electro-Mechanical Systems (MEMS) has permitted mass production of devices, though reducing the cost of previously expensive sensors [1]. Applications for such systems are numerous and many researchers around the world are now spending efforts to integrate low cost and low precision sensors to INS (e.g. [2-8]). The 3D-ETSNAV research group, at the Ecole de technologie superieure, is part of the challenge and works toward the integration of MEMS inertial sensors in a fully operational GPS-aided navigation system.

Simulation of aided-INS systems is mandatory prior to real implementation in order to validate the design [9]. Furthermore, numerical analysis of algorithms behavior is necessary since the highly non-linear equations governing the system prohibit extensive analytical analysis. Simulation package tools available until now to achieve this goal are Matlab script files (www.gpsoftnav.com). However, modular and easy graphical design allowed by Simulink© urged us to conceive a simulator based on its blocksets, and new ones that has been created mainly for GPS and INS research and development. Also, it will allow us to do rapid real-time testing, which is a goal for the physical implementation. To our knowledge, only one simulator that uses Simulink© for INS budget error analysis has been already presented [10]. However, this simulator uses a flat earth hypothesis and neglects the earth rate and the transport rate in the computation of inertial measurements. Even if those rotation rates cannot be measured by the sensors (due to their low accuracy), it is believed that their effects on the true vehicle motion should be taken into account in the simulation. There is also a need to include a generic and flexible sensor model, with selectable characteristics, which permits the mimic of many MEMS sensors in an easier way.

The simulator presented herein is different in a few aspects. First, the measurement generation module takes into account all aspects that might influence its behavior. Also, this module includes a block function for the gravity model that allows the improvement of the gravity model accuracy independently of the other modules. On this aspect, in order to simulate the inertial measurement with high precision, the gravity model used must be more precise than the model used in the navigation algorithm.

---

* Ph.D. student.
** Ph.D., Professor.
*** Ph.D., Associate Professor.

Also, the simulator models the dynamic response of the sensors and simulates any specific characteristics of the sensor. Another interesting aspect of the SNSS resides in the simulation of geometrical configuration of sensors that permits redundancy analysis. Then, the sensor model can simulate different MEMS sensors response in any configuration. Finally, the modularity of the simulator and the use of an off-the-shelf hardware implementation allow the direct real-time testing of a previously simulated navigation algorithm. This will reduce significantly the time needed to design a low cost INS.

This paper will address the basis of the test-bench for MEMS-based INS, from a generic overview of the simulator to the hardware implementation. The first section will introduce the simulator, with basic mathematics about kinematic that constitute the core of measurements and trajectory generation. Then, the software architecture will be presented and the functionality of each module will be described. The next section will demonstrate the hardware used, from the sensors to the acquisition scheme. Finally, the expectations from this proof-of-concept demonstrator board will be addressed in the final section.

1. Software architecture and functionnality

As said previously, the software is designed in a modular perspective to allow easy reconfiguration of all sub-systems. After explaining the mathematical convention used in the theoretical development, the main modules of the simulator will be described in detail.

1.1 Mathematical background

The following mathematical conventions are introduced in order to evaluate sensors measurements: rate gyros and accelerometers; and to determine some kinematic variables from the desired trajectrory. The coordinate frames used are the follow:

- ✓ the earth-centered inertial (ECI) frame (i);
- ✓ the earth-centered earth-fixed (ECEF) frame (e);
- ✓ the local vertical (NED: North-East-Down) frame (v);
- ✓ the mobile frame (m).

Without loss of generality, the sensor frame is assumed to be coincident with the mobile frame.

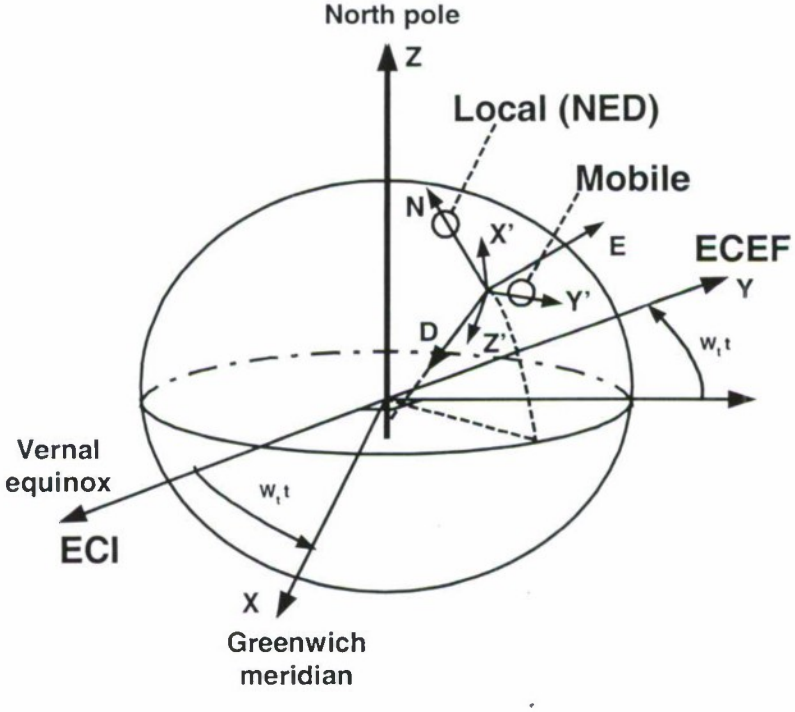

Figure 1.1: Representation of coordinate frames

To mitigate the complexity of mathematical expressions, the following conventions are used. The vector notation $[{}^{a}X_{b}]_{c}$ is read as follow: the vectored kinematic variable X of the frame b with respect to (w.r.t.) the frame a, measured w.r.t. the frame c. The rotation matrix from frame b to frame a is given by ${}^{a}R_{b}$. The Euler angle (roll, pitch and yaw) are respectively represented by (ϕ,θ,ψ) while the longitude/latitude pair is represented by (λ,φ). One dot over a variable means its first time derivative, while two dots correspond to its second time derivative. To simplify the expressions, the sine and the cosine of a variable X are written sX and cX, respectively. Also, the anti-symetric matrix of a vector $X = [x_1\ x_2\ x_3]^T$ is simply expressed by $S\{X\}$:

$$S\{X\}=\begin{pmatrix} 0 & -x_3 & x_2 \\ x_3 & 0 & -x_1 \\ -x_2 & x_1 & 0 \end{pmatrix} \tag{1.1}$$

The following subsections will introduce the different sub-systems of the SNSS, with respect to Figure 1.2, which shows their inter-relation.

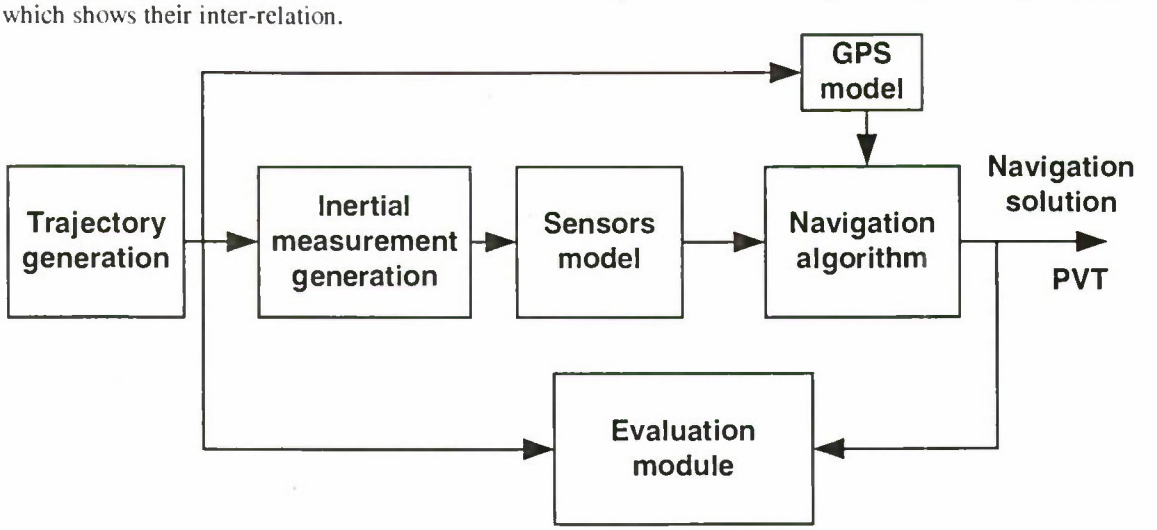

Figure 1.2: Top level modules of the SNSS

1.2 Generation of inertial variables

Rotation rate measurement

The rate gyro measures, in the sensor frame, the angular speed of the sensor frame w.r.t. to an inertial frame, which is the ECI frame in this specific case. This angular rate can be decomposed into several intermediate ones that are more common: the earth rate, the transport rate and the angular rate of the sensor frame w.r.t. the local frame, all of those measured in the sensor frame [11, 12]. These three components are respectively expressed in equation 1.2. Equations 1.3, 1.4 and 1.5 give the details of each component. All of the variables are known or can be obtained by the trajectory generation module.

$$\left[{}^{i}\Omega_{m}\right]_{m} = {}^{m}R_{e}\left[{}^{i}\Omega_{e}\right]_{e} + {}^{m}R_{e}\left[{}^{e}\Omega_{v}\right]_{e} + \left[{}^{v}\Omega_{m}\right]_{m} \tag{1.2}$$

$$\left[{}^{i}\Omega_{e}\right]_{e} = \begin{pmatrix} 0 & 0 & \omega_{T} \end{pmatrix}^{T} \tag{1.3}$$

$$\left[{}^{v}\Omega_{m}\right]_{m} = \begin{pmatrix} \dot{\phi} & 0 & 0 \end{pmatrix}^{T} + {}^{m}R_{v}\begin{pmatrix} 0 & \dot{\theta} & \dot{\psi} \end{pmatrix}^{T} \tag{1.4}$$

$$\left[{}^{e}\Omega_{v}\right]_{e} = \begin{pmatrix} 0 & 0 & \dot{\lambda} \end{pmatrix}^{T} + {}^{e}R_{v}\begin{pmatrix} 0 & -\dot{\varphi} & 0 \end{pmatrix}^{T} = \begin{pmatrix} \dot{\varphi}\, s\lambda & -\dot{\varphi}\, c\lambda & \dot{\lambda} \end{pmatrix}^{T} \tag{1.5}$$

Specific force measurement

The acceleration, or to be more precise the specific force, can be calculated by inverting the fundamental equation of navigation and isolating the needed variable [13]. Measured in the earth frame, the solution is given by equation 1.6, where ${}^{e}P_{m}$ is the position of the mobile w.r.t the ECEF frame and $g({}^{e}P_{m})$ is the gravity model.

$$\left[{}^{i}A_{m}\right]_{m} = {}^{m}R_{e}\left\langle {}^{e}\ddot{P}_{m} + 2S\left\{\left[{}^{i}\Omega_{e}\right]_{e}\right\}{}^{e}\dot{P}_{m} + S\left\{\left[{}^{i}\Omega_{e}\right]_{e}\right\}S\left\{\left[{}^{i}\Omega_{e}\right]_{e}\right\}{}^{e}P_{m} - g({}^{e}P_{m})\right\rangle \qquad (1.6)$$

Even if some variables can be obtained from the trajectory generator, the gravity acceleration vector has to be modeled. In order to conceive a simulator as close as possible to the reality, and in order to analyze the effect of different gravity models in navigation algorithms, the model of the gravity field for measurements generation has to be accurate. Hence, the use of non-spherical terms added to the spherical ones in the gravity model (or the use of a complex gravity representation) is mandatory.

It is worth nothing that the inertial measurement generation module is not the simulation of the raw data from the inertial sensors, but the computation of the ideal inertial variables (rotation rates and specific forces) that the mobile is subjected to when traveling along a specific trajectory. The raw data are coming from the sensor module, which takes the ideal inertial variable and corrupts them with errors, as will be explained in a next subsection.

1.3 Trajectory generation

The trajectory generation module was implemented with high precautions because it is the one that gives the kinematic variables information to the other blocks. The generation of the trajectory is based on the acceleration of the mobile w.r.t. the ECEF frame but measured in the local frame. With this information and its mathematical integration, and by use of the relation expressed by equation 1.7, one can obtain the acceleration of the mobile w.r.t. the ECEF frame, but now measured in the ECEF frame. Given this acceleration, the speed and the position w.r.t. the ECEF frame are easily obtained and the latitude/longitude (LATLONG) position can be computed.

$$\left[{}^{e}\dot{V}_{m}\right]_{e} = S\left\{\left[{}^{e}\Omega_{v}\right]_{e}\right\}{}^{e}R_{v}\left[{}^{e}V_{m}\right]_{v} + {}^{e}R_{v}\left[{}^{e}\dot{V}_{m}\right]_{v} \qquad (1.7)$$

Up to now, the trajectory generation is based on acceleration profile of the mobile w.r.t. the earth frame and measured in the local frame. A future add-on will consist in designing a graphical user interface allowing the user to "draw" a trajectory in a 3D map by means of via-points, as C. Eck did in is work [10] or input the software with real 3D trajectory scenarios.

Rotation matrices required by the previous equations are computed with variables obtained so far. The rotation matrix from the local frame to the earth frame (in equation 1.3) uses the LATLONG position. On the other hand, the rotation matrix from the earth frame to the mobile frame (equation 1.2) is calculated by matrix composition of the previous rotation matrix and another one obtained by use of Euler angles.

1.4 Sensor model

The output of this module is the simulated sensor measurements based on the ideal inertial variables given by the inertial measurement generation module. It will include many sensor characteristics and geometrical configurations. The sensor model is of great importance in the SNSS because a sensitivity analysis with respect to sensor characteristics and geometrical configurations will be performed on the navigation algorithm. Sensors will be modeled by using the following characteristic errors expressed in their stochastic form (but are not limited to):

- ✓ Bias errors;
- ✓ Scale factor errors, misalignments;
- ✓ Quantization;
- ✓ g sensitivity and g-squared sensitivity;
- ✓ Short-term errors;
- ✓ White noise;
- ✓ Etc...

These errors will be simulated whether by a constant, a constant with unknown prior value, random walk, drift, and any other kinds of mathematical formulation that will represent correctly of all kind of sensors (accelerometers and rate gyros). Figure 1.3 shows the scheme of implementation of the sensor model.

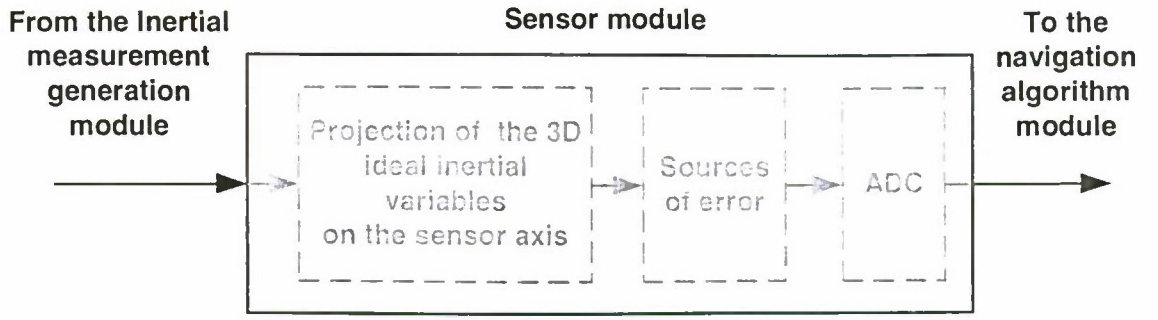

Figure 1.3: Single axis generic sensor model

1.5 Navigation algorithm

In this version of the simulator, the navigation algorithm that has been implemented is purely analytical and did not make use of any estimator to take into account the error model. It was simply designed for testing the measurement generation module and to analyze the propagation of round-off errors through the simulator modules in an ideal context. Equations 1.8 and 1.9 correspond to the analytical navigation equations in the ECEF frame. In the near future, the well-establish algorithm presented by Savage [14, 15] will be implemented.

$$ {}^{e}\dot{R}_m = -S\left\{\left[{}^{i}\Omega_e\right]_e\right\}{}^{e}R_m + {}^{e}R_m\, S\left\{\left[{}^{i}\Omega_m\right]_m\right\} \tag{1.8} $$

$$ {}^{e}\ddot{P}_m = -2S\left\{\left[{}^{i}\Omega_e\right]_e\right\}{}^{e}\dot{P}_m - S\left\{\left[{}^{i}\Omega_e\right]_e\right\}S\left\{\left[{}^{i}\Omega_e\right]_e\right\}{}^{e}P_m + g({}^{e}P_m) + {}^{m}R_e\left[{}^{i}A_m\right]_m \tag{1.9} $$

The simulator has already been validated for the error propagation with respect to finite computer calculation [16]. It appears that indeed, errors from that source is negligible over a long period of time (more than an hour without a refresh from GPS). Hence, their influence in further analyzes will not be taken into account.

2. Hardware implementation of a proof-of-concept real-time demonstrator

2.1 Sensors and raw data acquisition board

Aside the simulation, a prototype development board have been designed [17]. This board will be used to implement and test some of the theoretical solutions brought by the research. The raw data acquisition scheme is implemented in a Xilinx Virtex™ development board. Moreover, a sensor board has been designed and includes the following sensors:

- ✓ One three axis accelerometer assembly (ACH-04-08-05 of Measurement Specialties);
- ✓ Two dual axis accelerometers (ADXL202E of Analog devices);
- ✓ Two single horizontal axis rate gyros (ENC-03J of Murata);
- ✓ One single vertical axis rate gyro (ENC-05D of Murata);
- ✓ Two dual axis rate gyros (MicroGyro100 of Gyration) .

Those sensors are made with different kind of technologies and show specific characteristics. One of the goals of the theoretical studies is to assess the benefits of heterogeneous inertial information fusion. The actual platform will be of great interest at the time of experimental validation phase. The benefits sought are a more robust INS with regard to dynamic behaviours of the vehicle and a reliability improvement due to redundancy.

In the near future, the design will be enhanced with a three axis solid-state magnetometer (AP One Systems) and a low-cost GPS. Figure 2.1 shows a picture of the actual prototype board.

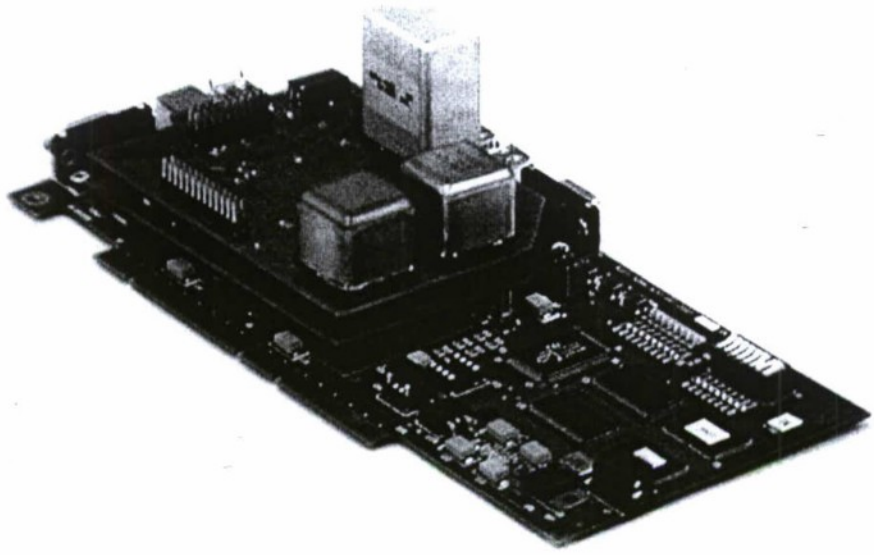

Figure 2.1: Development board for sensors acquisition scheme (accelerometers and rate gyros)

2.2 Real-time algorithm implementation

In order to easily test a simulated algorithm, a LYR Signal Processing Signal Master board SCB67x is used (figure 2.2). Two alternatives are possible: the navigation algorithm is tested in real-time with simulated data or the navigation algorithm is fully tested with real data.

No matter which alternative is chosen, the first step is to upload the desired Simulink block in the DSP on the LYR board, with Real-time Workshop and Code Composer Studio from Texas Instrument (TI). This upload is done with an Ethernet connection. If the inertial data are coming from the simulator, the board still communicate with Simulink by the Ethernet connection during the test. However, a very interesting feature of this hardware implementation resides in the possibility to test the algorithm with real inertial data. Figure 2.3 shows a schematic representation of a real-time execution of an INS algorithm, processing real data from the sensor board (figure 2.1) and a GPS receiver.

In this configuration, the sensor board acquires the raw data and performs a preliminary data processing. The data is then sent to the LYR Signal Processing Board, via many possible communication links:

- ✓ USB
- ✓ Firewire (IEEE 1394)
- ✓ PCI connector
- ✓ Serial proptocol

The real-time navigation algorithm processes the data from the inertial sensor board and the GPS in order to get the navigation solution, which is sent back to Simulink for graphical purposes and stored for further analyses. This implementation scheme is very user-friendly and permits rapid real-time testing of innovative algorithms with MEMS sensors.

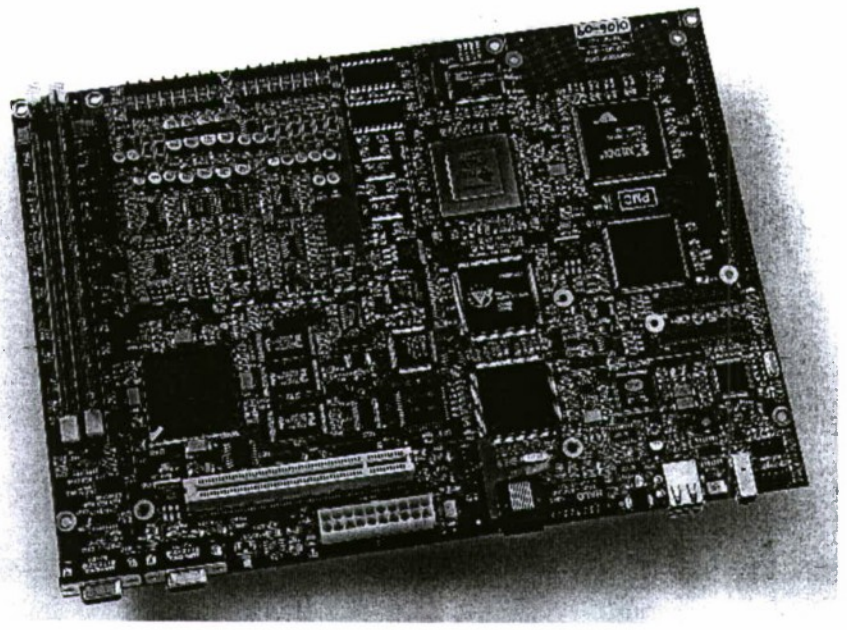

Figure 2.2: LYR Signal Processing Signal Master Board SCB67x

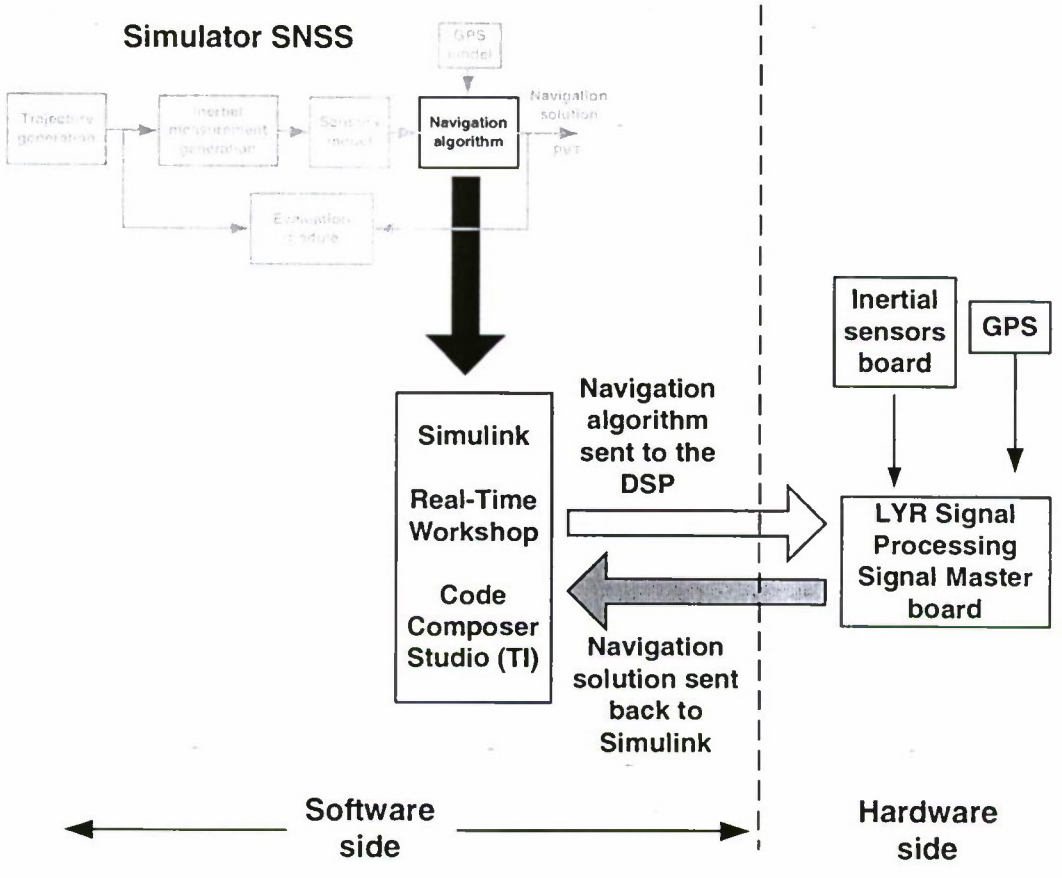

Figure 2.3: Rapid Real-time testing of simulated algorithms

Conclusions

This paper exposed the design of a Simulink© Navigation System Simulator (SNSS) associated with the hardware used to implement in real-time any kind of algorithms. The use of a simulator is mandatory in order to design a suitable algorithm that takes into account the specificity of low cost sensors like MEMS inertial sensors. The tools available since now have not been found adequate for our needs and urged the development of a modular and easy to reconfigure simulator. With the SNSS, many sensitivity analyses will be performed and among them: sensor noises and response bandwidth, geometrical configuration of the sensors, relevance of precise gravity model, refresh rate of external signals, etc. Another interesting feature of the simulator is the fast-prototyping capability due to its modular design and the use of the Real-Time Workshop of Simulink©, Code Composer Studio from TI and the LYR Signal Processing Signal Master board. A summary of features and advantages of the approach is shown at Table 1. Finally, the simulator will be refined during the project and new experiments will be done. At the end of the development phase, the SNSS and the associated hardware will constitute a powerful tool to make rapid designs and prototyping of Low-Cost GPS-aided INS.

Features	Advantages
Inertial measurement generation	✓ High precision gravity model ✓ Generation of ideal inertial variable w.r.t. any trajectories
Sensor model	✓ Generic sensor model ✓ Possibility of different geometrical configuration ✓ Selection of different kind of errors, allowing analyses of specific error contribution
Navigation algorithm	✓ Modularity allows modification of specific functionalities without disturbing the overall scheme: o navigation solution algorithm o error model o navigation filter o gravity model o GPS model ✓ Use of Simulink allows the direct transformation of navigation algorithms into a real-time executable platform
Hardware	✓ Sensor board allows the study of heterogeneous inertial information fusion ✓ Xilinx Virtex™ development board permits autonomous data acquisition (power source of 12 volts) ✓ LYR Signal Processing Signal Master board facilitates the validation of new navigation algorithms ✓ Communication links: o Ethernet o USB o Firewire (IEEE 1394) o PCI connector o Serial protocol

Table 1: Summary of features and advantages of the approach

Acknowledgements

The financial support for this work was partly provided by the Natural Sciences and Engineering Research Council of Canada (NSERC), the "Fonds québécois de la recherche sur la nature et les technologies" (NATEQ) and a research grant provided by Ecole de technologie superieure (ETS).

References

1. Lawrence, A., *Modern Inertial Technology: Navigation, Guidance and Control*, New York, Springer-Verlag, 1992.

2. Abershitz, A., K. Cohen, and R. Rubinets. *Performance Augmentation of Low Cost Sensors*, in *Joint 9th IFSA World Congress and 20th NAFIPS International Conference*, 2001.

3. Chen, G. and M. Harigae. *Advanced Carrier DGPS/MEMS-IMU Integrated Navigation with Hybrid System Models*, in *IEEE Position, Location and Navigation Symposium*, 2000.

4. Kourepenis, A., et al. *Performance of MEMS Inertial Sensors*, in *IEEE Position, Location and Navigation Symposium*, 1998.

5. Rios, J.A. and E. White. *Fusion Filter Algorithm Enhancements for a MEMS GPS/IMU*, in *Institute of Navigation National Technical Meeting*, 2002.

6. Luethi, P., T. Moser, and M. Uster, *Low Cost Inertial Navigation System*, Report, Swiss Federal Institute of Technology, Zurich, 2000.

7. Leach, B.W. and K. Hui, *Low Cost Strapdown Inertial/DGPS Integration for Flight Test Requirements*, Canadian Aeronautics and Space Journal, Vol. 45, No. 3, pp. 253 - 263, 1999.

8. Cannon, M.E., et al., *Low-Cost INS/GPS Integration: Concepts and Testing*, The Journal of Navigation, Vol. 54, No. 1, pp. 119 - 134, 2001.

9. Biezad, D.J., *Integrated Navigation and Guidance Systems*, AIAA Education Series, Virginia, USA, 1999.

10. Eck, C., J. Chapuis, and H.P. Geering. *Software-Supported Design and Evaluation of Low-Cost Navigation Units*, in *Proceedings of th 8th St-Peterburg International Conference on Integrated Navigation Systems*, 2001.

11. Santis, R.D., *Elements of Kinematics with Applications to Problems in Navigation and Robotics*, Ecole polytechnique, Montreal, 1999.

12. Marion, J.B. and S.T. Thornton, *Classical Dynamics of Particles and Systems*, 4th ed., Harcourt College, 1995.

13. Chatfield, A.B., *Fundamentals of High Accuray Inertial Navigation*. Progress in Astronautics and Aeronautics, Vol. 174, Virginia, 1997.

14. Savage, P.G., *Strapdown Inertial Navigation Integration Algorithm Design Part 1 : Attitude Algorithms*, Journal of Guidance, Control and Dynamics, Vol. 21, No. 1, pp. 19 - 28, 1998.

15. Savage, P.G., *Strapdown Inertial Navigation Integration Algorithm Design Part 2 : Velocity and Position Algorithms*, Journal of Guidance, Control and Dynamics, Vol. 21, No. 2, pp. 208 - 221, 1998.

16. Giroux, R., Landry, R. Jr. and Gourdeau, R. *Simulation Software for a Low Cost Electronic Inertial Navigation System*, in *International Conference on Guidance, Navigation and Control*, Harbin, China, 2001.

17. Giroux, R. *Low-Cost INS GPS*. in *52th International Astronautical Federation Conference, Poster session*, Toulouse, France, 2001.

A NEW RUSSIN STANDARD IN THE FIELD OF LOW-FREQUENCY MOTION QUANTITIES MEASUREMENTS

A.Ye.Sinelnikov*, V.N.Kudrjavtsev**
D.I.Mendeleyev Institute for Metrology, 19, Moskovsky pr. 198005, St. Petersburg, Russia
e-mail: niim2530@mail.convey.ru
P.A.Pavlov**
Saint-Petersburg State Electrotechnical University, 5, prof. Popov St., 197341, St. Petersburg, Russia
e-mail: PAPavlov@mail.eltech.ru

Abstract

Key words: standard, mechanical motion quantities, metrological characteristics.

The paper deals with the directions of work and the results obtained in establishing a new measurement standard in the field of mechanical motion quantities. The task to reproduce a group of constant and variable physical quantities with the help of a limited number of setups has been solved. The author outlines principals of creating three standard setups as well as results of their experimental investigations. A brief consideration is given for the approach accepted and used in Russia for the analysis of metrological characteristics of the standards intended for measuring mechanical motion quantities. Some perspective directions of further investigations are quoted.

Introduction

The Russian system of traceability in the important fields of measurements is basically the centralized one. The unit sizes are transferred from the primary standards, which are at the head of the State hierarchical chains, to working measuring instruments through the measurement standards of lower grades. In most cases the constant and variable physical quantities are reproduced therewith by different primary standards. For the most part, it was just in this way the low frequency motion quantities have been reproduced. For example, in Russia there has been used a standard for the constant linear acceleration unit, which includes two setups (turnable and rotational (centrifuges)), a standard of the variable aeeeleration unit (double eentrifuge), a standard for eonstant angular velocity, as well as highest precision setups for reproducing the variable linear acceleration (centrifuge with a controlled rotation axis), a setup for reproducing the variable angular acceleration and others.
However it should be noted, that in the standard for the field of scismometry, where the linear movement of a platform takes place and where it is sufficiently simple to relate the displacement, velocity and acccleration, all three indicated quantities are reproduccd. But it is clear, that in remaining cases of reproduction of low-frequency motion quantities the movable platforms of the standard can reproduce, in principal, several constant and variable quantities. Naturally, it is achieved by a signifieant eomplication of the standard. However, it is economically justified for the centralized system because it enables us to cut the attending personnel, to reduce the number of special thermostated boxes located on vibration-proof foundations, to automate completely the process of calibration, ete. The accuracy of determination of static and dynamic characteristics of measuring devices under study is improved, too. This approach, which has becn used in development of the present standard, can be also effective for instrument-building companies designing various measuring instruments.

Because of a great number of works, number of developments done and investigations completed, the present paper deals only with a brief review of the results obtained in establishing a new Russia standard based on the prineipals aeeording to whieh separate setups reproduce a certain number of physieal quantities.

Models And Calculatuion Methods

For the most of cases, when calculating and making investigations of the turnable and rotational setups use for reprodueing the motion quantities, a type of the setup is ehosen, models for reproduction uneertainty of each physical quantity are analyzed and then possible unccrtainty values are estimated. A similar approach has been used in the standard [1]. This approach is sufficiently simple and clear, but requires the researchers to understand the operation principles of the setup and its scparate parts in details and to provide carefully analysis of potential sources of uncertainties. This is most important for the development of complicated and high-precision setups, when there exist a potential risk to miss some sources of the uncertainty from consideration, particularly their

*D.Sc., Professor, Head of Laboratory.
**D.Sc., Lading Rescarch Scientist.

relationship. That is why for several decades in establishing the Russian standards they use the research and calculation methods based on direct differentiation of the vectors connecting an unmovable base with the center of masses of a device being investigated, located on moving platforms of the setups. In doing this, the unmovable base and turnable or moving at various velocities platforms are connected with the corresponding coordinate systems. As an example a simplified system of the coordinate axis of turntable and rotational platforms is taken from the review given in [2]. An appropriate parameters may provide to reduce the similar system to a system of axes of the turnable setups, centrifuge, centrifuge with the controlled direction of rotation axis, double centrifuge and some other setups.

To date, two main accelerometer types, the axial and pendulous ones (respectively, with the rectilinear and angular motion of a sensitive mass), have become most commonly used. Pendulous aeeelerometers are made with the horizontal or vertical axes of the sensitive mass suspension.

Let $O_0X_0Y_0Z_0$ be a rectangular coordinate system (Fig. 1), in which the O_0Z_0 axis is directed along a local vertical. The $O_0X_0Y_0Z_0$ system rotates at constant angular speed Ω, and vector $\bar{\Omega}$ is directed along the O_0Z_0 axis. The $O_1X_1Y_1Z_1$ coordinate system rotates with respect to the $O_0X_0Y_0Z_0$ system at constant angular speed ω and vector $\bar{\omega}$ is directed along the O_1Z_1 axis. At the initial moment, the O_1X_1 axis is parallel to the O_0X_0 axis, whereas, in the general case, the O_1Y_1 and O_1Z_1 axes make angle $\theta \neq 0$ with the corresponding axes of the $O_0X_0Y_0Z_0$ system. The transition from the $O_2X_1Y_1Z_1$ coordinate system, whose axes are parallel to those of the $O_1X_1Y_1Z_1$ system, to the $O_2X_2Y_2Z_2$ system is carried out by the following rotations: about the O_2X_1 axis through angle α, about the O_2Y_1 axis through angle β, about the O_2Z_1 axis through angle γ, and about the axis of the pendulum suspension through angle ψ. Here we assume two possible positions of the axis of the pendulum suspension: it coincides either with the O_2X_2 axis or with the O_2Z_2 axis. In Fig.1, the O_2X_2 axis is assumed to be the suspension axis, and the figure shows a rotation about this axis through angle ψ.

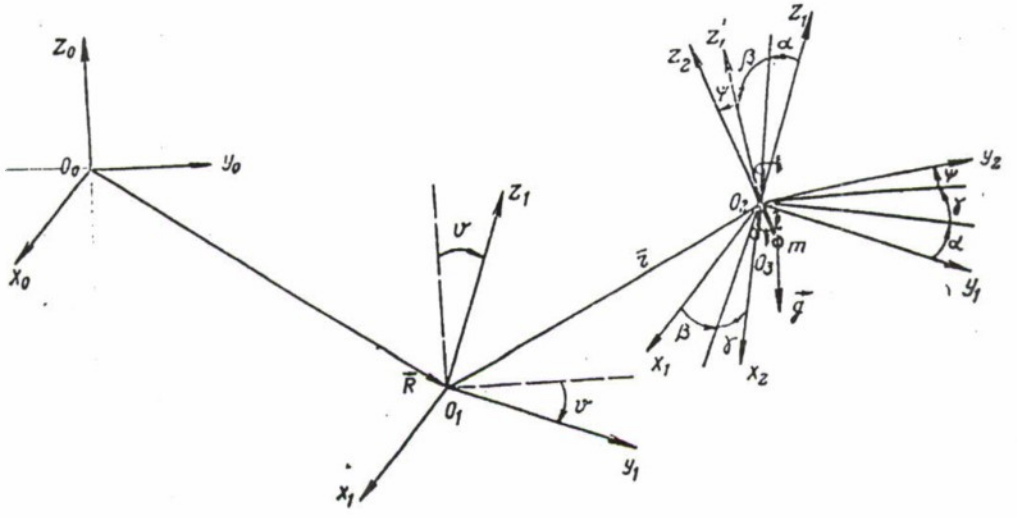

Fig. 1. Vector diagram

The relations between the projections of arbitrary vector $\bar{A}$ in the $O_2X_2Y_2Z_2$ and $O_2X_1Y_1Z_1$ coordinate systems are specified by one of the following orthogonal transformations:

$$A_{O_2X_2Y_2Z_2} = \Psi_i Q A_{O_2X_1Y_1Z_1}, \quad i = 1,2;$$

$$\Psi_1 = \begin{pmatrix} 1 & 0 & 0 \\ 0 & \cos\psi & \sin\psi \\ 0 & -\sin\psi & \cos\psi \end{pmatrix}; \quad Q = \begin{pmatrix} \cos\gamma\cos\beta + \sin\gamma\sin\beta & \sin\gamma\cos\alpha & -\cos\gamma\cos\beta + \sin\gamma\sin\alpha\cos\beta \\ -\sin\gamma\cos\beta + \cos\gamma\sin\beta\sin\alpha & \cos\gamma\cos\alpha & \sin\gamma\sin\beta + \cos\gamma\sin\alpha\cos\beta \\ \cos\alpha\sin\beta & -\sin\alpha & \cos\alpha\cos\beta \end{pmatrix} \quad (1)$$

$$\Psi_2 = \begin{pmatrix} \cos\psi & \sin\psi & 0 \\ -\sin\psi & \cos\psi & 0 \\ 0 & 0 & 1 \end{pmatrix};$$

Let us denote $\bar{R} = \overline{O_0O_1}$, $\bar{r} = \overline{O_1O_2}$, $\bar{l} = \overline{O_2O_3}$, where O_3 is the center of mass of the sensitive mass of an accelerometer. The positive direction of the measuring axis of an axial aeeelerometer is specified by one of the

unit vectors $\vec{e}_i = \vec{e}^{\,*}$ $(i = 1,2,3)$, then $\vec{l} = \overrightarrow{se^*}$. For a pendulous aeeelerometer, l is the length of the pendulum arm. In this case, the suspension axis coineides with one of the unit vectors $\vec{e}_i = \vec{e}^{\,0}$ $(i = 1,2,3)$. The acceleration at point O_3 reads

$$\vec{a} = \vec{L}, \tag{2}$$

where $\vec{L} = \vec{R} + \vec{r} + \vec{l}$.

Assuming $\vec{\Omega} = const$, $\vec{\omega} = const$, from Eq. (2) we find

$$\begin{aligned} \vec{a} = &-\vec{R}\left|\vec{\Omega}\right|^2 - \vec{r}\left|\vec{\Omega}+\vec{\omega}\right|^2 - \vec{l}\left|\vec{\Omega}+\vec{\omega}\right|^2 + \vec{\Omega}(\vec{R}\vec{\Omega}) + \\ &+(\vec{\Omega}+\vec{\omega})(\vec{r}(\vec{\Omega}+\vec{\omega})) + (\vec{\Omega}+\vec{\omega})(\vec{l}(\vec{\Omega}+\vec{\omega})) \end{aligned} \tag{3}$$

The equivalent force $\vec{F}$ of the inertial forces and weight $\vec{P}$, and the moment $\vec{M}$ of these forces, applied to the sensitive mass of an aceelerometer, respectively, equal

$$\begin{aligned} \vec{F} &= m[\vec{R}\left|\vec{\Omega}\right|^2 + \vec{r}\left|\vec{\Omega}+\vec{\omega}\right|^2 + \vec{l}\left|\vec{\Omega}+\vec{\omega}\right|^2 - \vec{\Omega}(\vec{R}\vec{\Omega}) - \\ &-(\vec{\Omega}+\vec{\omega})(\vec{r}(\vec{\Omega}+\vec{\omega})) - (\vec{\Omega}+\vec{\omega})(\vec{l}(\vec{\Omega}+\vec{\omega}))] + m\vec{g} \\ \vec{M} &= m\{(\vec{l}\times\vec{R})\left|\vec{\Omega}\right|^2 + \vec{r}\left|\vec{\Omega}+\vec{\omega}\right|^2 + (\vec{l}\times\vec{R})\left|\vec{\Omega}+\vec{\omega}\right|^2 \\ &-(\vec{l}\times\vec{\Omega})(\vec{R}\vec{\Omega}) - (\vec{l}\times[\vec{\Omega}+\vec{\omega}])(\vec{r}(\vec{\Omega}+\vec{\omega})) - (\vec{l}\times[\vec{\Omega}+\vec{\omega}])(\vec{l}(\vec{\Omega}+\vec{\omega}))\} + m(\vec{l}\times\vec{g}) \end{aligned} \tag{4}$$

It is convenient to represent veetors $\vec{R}$ and $\vec{r}$ as follows:

$$\vec{R} = \overrightarrow{R_H} + \overrightarrow{R_V}; \vec{r} = \overrightarrow{r_H} + \overrightarrow{r_V} \tag{5}$$

where $\overrightarrow{R_H}$, $\overrightarrow{r_H}$ are the "horizontal" components of veetors $\vec{R}$, $\vec{r}$ (aeeordingly, parallel to the $O_0X_0Y_0$ and $O_1X_1Y_1$ planes), and $\overrightarrow{R_V}$, $\overrightarrow{r_V}$ are the "vertieal" components of the same vectors. Allowing for Eq. (5), it follows from Eq. (4) that the projections of force $\vec{F}$ on the direetion of the measuring axis of an axial aeeelerometer and the projections of moment $\vec{M}$ on the suspension axis of a pendulous accelerometer, respectively, equal

$$\begin{aligned} F_{e^*} &= m\{\left|\vec{\Omega}\right|^2 (\overrightarrow{R_H}\times\vec{e}^{\,*}) + \left|\vec{\Omega}+\vec{\omega}\right|^2 ((\overrightarrow{r_H}+\overrightarrow{r_V})\vec{e}^{\,*}) - \\ &((\vec{\Omega}+\vec{\omega})\vec{e}^{\,*})(\overrightarrow{r_H}+\overrightarrow{r_V})(\vec{\Omega}+\vec{\omega}) + s\left|\vec{\Omega}+\vec{\omega}\right|^2 - s(\vec{e}^{\,*}(\vec{\Omega}+\vec{\omega}))^2\} + m(\vec{g}\vec{e}^{\,*}); \end{aligned} \tag{6}$$

$$\begin{aligned} M_{e^0} &= m\{\left|\vec{\Omega}\right|^2 (\vec{e}^{\,0}(\vec{l}\,\overrightarrow{R_H})) + \left|\vec{\Omega}+\vec{\omega}\right|^2 (\vec{e}^{\,0}(\vec{l}\times(\overrightarrow{r_H}+\overrightarrow{r_V}))) \\ &-((\overrightarrow{r_H}+\overrightarrow{r_V})(\vec{\Omega}+\vec{\omega})(\vec{e}^{\,0}(\vec{l}\times(\vec{\Omega}+\vec{\omega})))) - (\vec{l}(\vec{\Omega}+\vec{\omega})(\vec{e}^{\,0}(\vec{l}\times(\vec{\Omega}+\vec{\omega})))) + (\vec{e}^{\,*}(\vec{l}\times\vec{g}))\}. \end{aligned} \tag{7}$$

From the above general expressions it is possible to obtain the expressions needed to investigate one of the types of the devices with any of the setups. So, for the ease of investigations when the double centrifuge and the pendulum aeeelerometer with the vertieal axis of the sensitive mass suspension are used, the following values should be applied for the above expressions:

$$\begin{aligned} &\alpha \approx 0; \quad \beta \approx 0; \quad \gamma \approx 0; \quad \psi \approx 0; \quad \upsilon \equiv 0; \quad \vec{R} \neq 0; \quad \vec{r} \approx 0; \\ &\vec{\Omega} = const \neq 0; \quad \vec{\omega} = const \neq 0; \quad \vec{e}^{\,0} = \vec{e}_3. \end{aligned}$$

However, the expressions obtained in this way, have a general character and do not permit, in particular, to get a set of the uncertainties in reproducing the acceleration. In a general way, the quantities included in corresponding expression should be considered as the variable ones and not equal to zero. This makes it possible to estimate the real uncertainties of the setup. In this way an elongation of the eentrifuge arm and an angular motion of separate eentrifuge parts are taken into account and so on.

These expressions are not given here because they are too cumbersome. But you ean find those that are given for the ease of a double eentrifuge in [3].

A New Russian Standard

The new standard replaces two existing Russian standards intended for reproduction of constant and variable linear acceleration as well as provides the reproduction of variable angles with high accuracy. As it has been noted, a distinguished feature of the standard is its capability to reproduce preeisely with some separate setups certain number of physieal quantities or one of them both in the static or dynamic modes. Based on the equivalence principal, the intereonnceted inertial and gravitational methods are used in the standard [4], which has provided to inerease the accuracy and to extend the ranges of the quantities being reproduced.

The standard setups are loeated in thermal-stabilized boxes on a monolithic vibration-damping foundation with the mass of 3500 tons and are included into the system of standards in the field of graviinertial measurements (Fig. 2), whieh is situated in a forest zone, 40 km away from St. Petersburg.

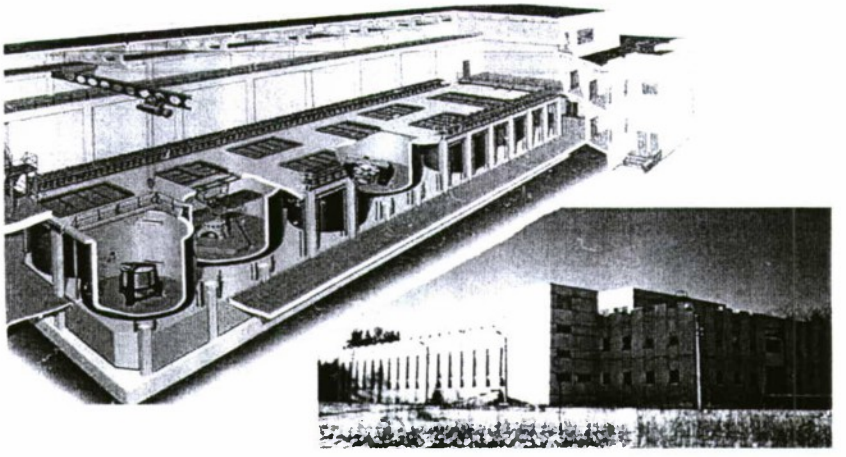

Fig. 2. Complex of standards in the field of graviinertial measurements

The standard comprises three setups. The constant linear accelerations are reproduced with standard setups ЭУП-3 and ДЦ-3, the variable (harmonie) aeeelerations – with the НЦ-3 and ДЦ-3 ones, the angels – with НЦ-3. Along with this, it is possible to reproduce the eonstant velocities as well as all listed physical quantities with various combinations of their values.

The standard turnable setup ЭУП-3 reproduces the constant linear acceleration within the range up to 1 g with the well known method of turn of the deviee being investigated in the Earth gravity field. When calibration and verifieation take plaee, a component of free fall aeeeleration $a=g\sin\varphi$ is directed along the measurement axis of the deviee being investigated, where φ is the deflection angle of the deviee measurement axis from the horizontal plane. In the setup (Fig.3) deviee is fixed to a special prism mounted on a shaft of the turnable table. For alignment of the prism surface into a horizontal position a liquid level and a sheer interferometer are used.

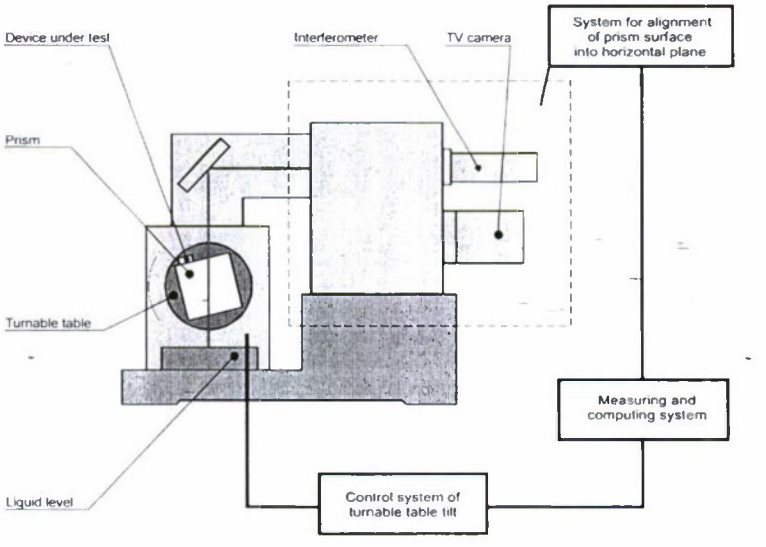

Fig. 3. Principal Scheme of Setup ЭУП-3

The appearance of the setup is given in Fig. 4.

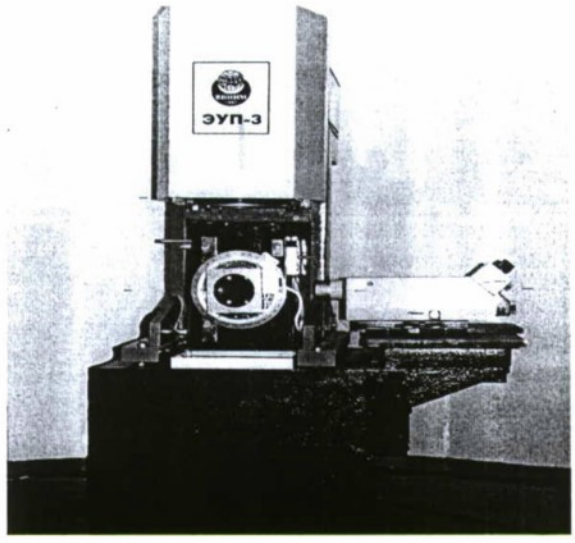

Fig.4. Standard Setup ЭУП-3. Electromechanical System.

Standard rotation platform with controlled direction of the rotation axis НЦ-3. The scheme of the setup is given in Fig. 5, photo of the electromechanical system is given in Fig.. 6.

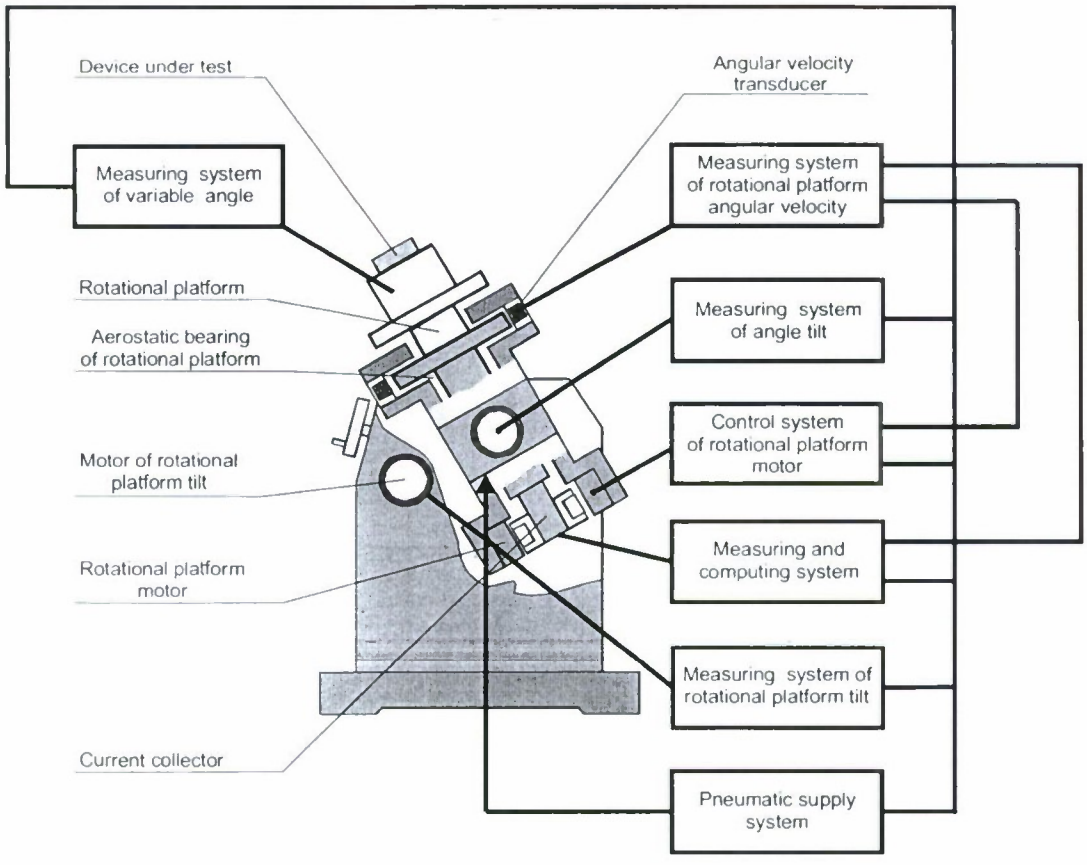

Fig.5. Principal Scheme of Setup НЦ-3

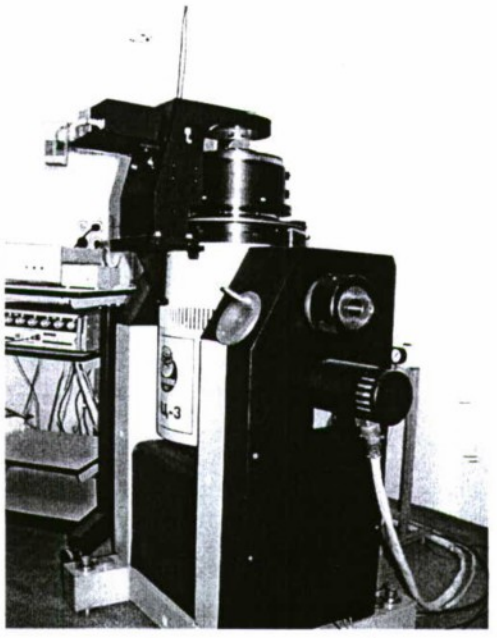

Fig. 6. Standard Setup НЦ-3. Electromechanical System.

The setup is intended to reproduce harmonic linear accelerations in the amplitude range up to 1 g within the frequency range 0,05-30 Hz, and variable angles in the range up to 360°. The harmonic acceleration being reproduced is $a=g\sin\varphi\cos\omega t$, where φ is the deflection angle between the platform rotation axis and the vertical, ω is angular velocity of rotational platform.

The device to be investigated is mounted on the rotor of the setup suspended on aerostatic bearings and rotated with a high precision system of an electric drive. Output signal of the device investigated as well as those of the transducers of platform inclination angles, an angular velocity of the rotor and other transducers not shown in figure, are transferred from the rotating platform to the corresponding measurement, control and calculating systems through a mercury current collector.

The acceleration amplitude determined by the turn angle of the platform in the Earth gravitational field, does not depend on the frequency determined by the angular velocity of the platform, which makes it possible to reproduce in the above frequency range the acceleration amplitudes equivalent to the acceleration amplitudes of the linearly-displaced platforms with the displacement amplitudes up to several hundreds meters. The setup accuracy is two order of magnitude higher therewith than that of the linearly-displaced platforms.

Fig. 7 shows possibilities of the setup developed as well as of setup ДЦ-3 as compared to the setup using the principal of a platform linearly moving within this frequency range.

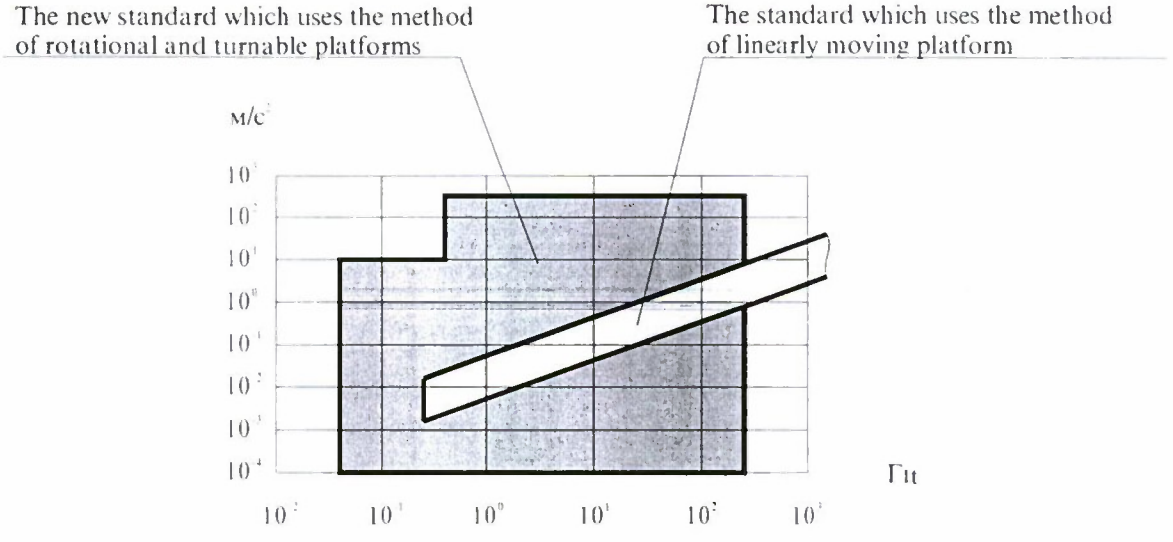

Fig. 7. Range of the reproduced acceleration amplitudes

The setup can be used too for reproducing constant linear acceleration. However in this case, its characteristics are limited with a relatively small length of the arm. If the mass center of a sensitive element of

the device being investigated is shifted with regard to the rotation axis of the platform, then a sum of harmonic and constant linear aceelerations is reproduced.

An important mode of operation for this setup is the mode of variable angle reproduction on the basis of goniometrie method. This problem has been solved in Russia on the State level, for the first time. As it is known, the standards reproducing plane angles unit, that exists in the world reproduce only a limited member of constant angles and are not able in many cases to be used for transferring the unit size to the device and transducers measuring variable angles.

For the first time the goniometrie method was suggested at the D.I.Mendeleyev Institute for metrology at the end of 60's. Since then it has been used in the process of establishing the aceeleration unit standards. On its basis the high preeision transducers of angle and angular velocity have been created too. In 70-80's two enterprises of our country developed a number of setups using this method as a basis, one of which was attributed as a state standard of Slovakia [6].

At present the leader in this field of work is the St. Petersburg State Electrotechnieal University [7]. The prineipal scheme of a corresponding part of the НЦ-3 setup is given in Fig-8.

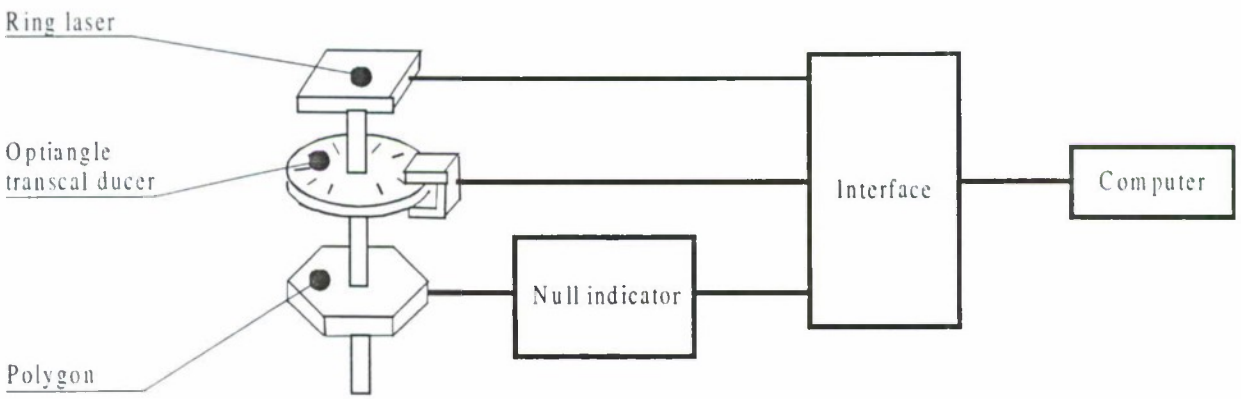

Fig.8. Principal scheme of the system providing reproduction of variable angles

The angle reproduction is realized with a rotating ring laser (RL) the output signal frequency of which is proportional to its angular velocity and the output signal phase is proportional to a rotation angle of the RL. The reproduced angle is:

$$\varphi = 2\pi \frac{N_\varphi}{N_{2\pi}},$$

where N_φ is the number of periods (pulses) of the RL output signal at the time of φ-angle reproduction,

$N_{2\pi}$ is the number of periods (pulses) of the RL output signal at the 2π radian angle.

Super-high seale faetor as well as scale linearity are very advantageous eharacteristies of the RL used as an angle transducer. However, some temporal instability of this coefficient causes the necessity to calibrate the RL on the angle 2π or some other already known angles. That is why when designing a standard for the plane angle unit, it is expedient to provide eomplexing in which along with the RL the transducers based on principally different physical effects are used. In the system developed, a holographic photoelectrie angle transducer was used, which has a less linear scale, but higher stability in time.

Such complexing along with the advantages indicated provides the possibility to realize the cross-calibration procedure [8], which makes it possible to determine systematic components of the uncertainty of both transducers.

In the scheme given in Fig. 8, polygon and a null indicator realize the secondary function and are intended for transferring the angle unit size to the standards of the next lower grade and to the working measuring devices. Application of the means indicated makes it possible, in principal, to obtain exeessive data as these means also can be engaged in the proeedure of cross-calibration.

The third standard setup ДЦ-3 is a system of rotated platforms with vertical axes of rotation and independent control system for platform rotation (double centrifuge).

Principal setup scheme is shown in Fig. 9

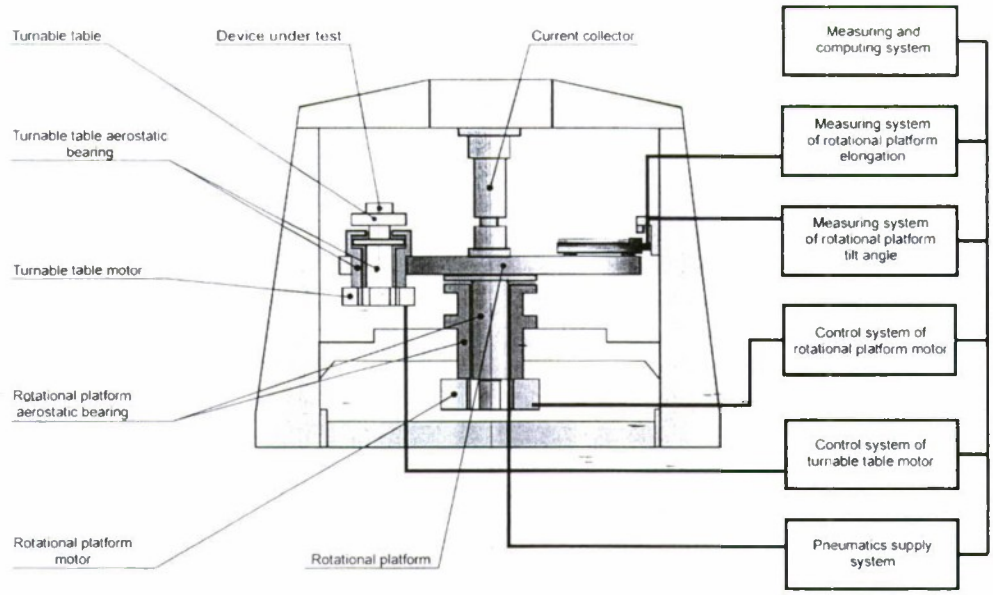

Fig. 9. Principal scheme of the Standard Setup ДЦ-3

On a central rotation platform of the setup the second platform, that is called a turnable table, is located. The distance between axes of rotation of the platform is R. The acceleration that is reproduced in a central point of a turnable table, $a=\Omega^2 R\cos\omega t$, where Ω and ω are the angular velocities of the rotor and turnable table. For each rotation platform, the drive, measurement, control and information processing systems are similar to the corresponding systems of setup НЦ-3. However, to increase the accuracy of constant linear acceleration reproduction, the systems providing measurement of deformational and thermal elongation of the rotor as well as measurement of a bending angle of the rotor in the process of its rotation.

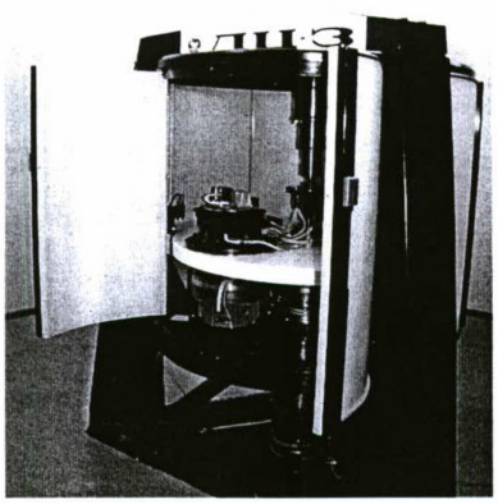

Fig. 10. Standard setup ДЦ-3. Electromechanical system

The setup operates in three modes. In the first mode the setup reproduces constant linear accelerations in the range up to 500 m/s^2, the central platform being rotated. In the second mode it reproduces harmonic linear accelerations in the amplitude range up to 250 m/s^2 and frequency range 0,5-30 Hz, both platforms being rotated in one direction. In this mode the setup has advantages similar to those of the НЦ-3 setup, but with a much wider amplitude range. A special aerostatic bearing of the peripheral rotation platform is designed for this setup. It can stand centrifugal forces up to 10000 N without any loss of accuracy. In the third mode, when the platforms are rotated in the opposite directions with the same angular velocity, the setup also reproduces harmonic accelerations, which amplitudes are the same as those of the linearly-displaced platform with the displacement amplitude equal to the distance between the platform axes. The absolute angular velocity of the peripheral platform is equal to zero, which makes it possible to investigate some gyroscopic devices.

The outside appearance of the electromechanical system of the setup is shown in Fig. 10.

The second and third setups can be used for simultaneous reproduction of constant and variable accelerations, as well as constant angular velocities in the range 0,3...180 rad/s with the uncertainties at the level $10^{-6}...10^{-7}$.

To achieve high metrological characteristics, the following things were done in the process of establishing the standard. The theory of "complex" standards was worked out; the method for reproduction of accelerations using the fixed point "1g" was studied; some systems comprising the setups, were designed or improved, including specialized aerostatic supports, means for measuring the elongation and bending angle of the rotation platforms in the process of their rotation on the basis of interferometric and capacitive transducers, multicircuit control systems using special motors, laser goniometric systems and interferometric systems for determination of

the horizontal plane position, mercury current collectors, etc. The principal scheme of a new setup was developed, which will enable us in future to replace the above setup and to provide the opportunity to reproduce variable angular accelerations as well.

Results Of The Standard Investigations

The standard has been investigated and certified according to the procedure intended for the derived unit standards. The works listed below have been done: 1) analysis of components of the uncertainty in reproducing the corresponding physical quantities, which have been obtained with the method described in section 2: 2) values of the indicated uncertainty components have been determined experimentally in relation to values, amplitudes and frequencies of the quantities being reproduced with the measurement systems, both consisting parts of the standard and the additional ones; 3) in accordance with the known metrological rules the uncertainties have been summed up.

Metrological characteristics of the standard are given in the table.

Unit reproduced	Setups	Range	Uncertainty valued according to type A	Uncertainty valued according to type B	Summed standard uncertainty
Constant acceleration	ЭУП-3, ДЦ-3	5×10^{-5}–500 m/s^2	1×10^{-5}–$2{,}5\times10^{-4}$ m/s^2	1×10^{-5}–6×10^{-4} m/s^2	1.4×10^{-5}–$6{,}5\times10^{-4}$ m/s^2
Variable acceleration in the frequency range 0.05 – 30 Hz	ДЦ-3, НЦ-3	10^{-4}–250 m/s^2	1.5×10^{-5}–$2{,}5\times10^{-3}$ m/s^2	3×10^{-5}–7×10^{-3} m/s^2	$3{,}2\times10^{-5}$–$7{,}5\times10^{-3}$ m/s^{22}
Plane angle in angular displacement	НЦ-3	0,2″–360°	0,04″	0,03″	0.05″

As irrespective of the standard being presented, there exist a state primary standard for the plane angle unit, which provides the reproduction of a limited member of constant angles, in particular, with the help of a 12-faced polygon included into this standard, a comparison has been made with a new standard reproducing the angles varying with time. Fig. 11 shows differences of the prism angle values, measured with the standard indicated.

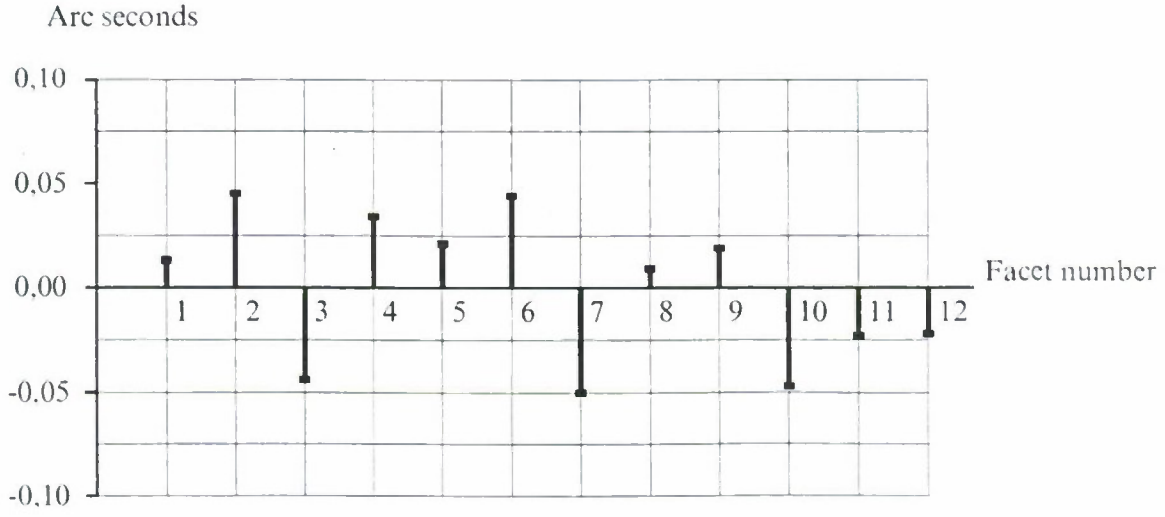

Fig. 11. Differences of the angle values of a 12-faced polygon, obtained as a result of comparison of the national plane angle standards.

An analysis of the curve presented makes it possible to conclude that the accuracy characteristics of the two standards are sufficiently close to each other. In connection with this it is suggested to apply the new standard for the key comparison (CCL-K3) being conducted by the BIPM.

Conclusion

The standard developed provides the metrological assurance within the field of the above motion quantities. The joint application of the standard and procedures of determining metrological characteristics of the accelerometers described, for example, in [1] and similar to them, makes it possible to determine these characteristics with a sufficiently high accuracy. Along with this, the results obtained during the development of the standard can be used in adjacent fields of measurements. In particular, as is generally known, the accuracy of determination of directions is often as important as the measurement of a vector modulus for solution of some problems, first of all, the navigational ones. Therefore the task of establishment of a radically new group of standards: standards of directions in space, is very urgent. This is quite a specific task for metrology because metrology only operates with the standards of physical quantities. In the process of development of the ЭУП-3 setup, the absolute method of determination of the horizontal plane on the Earth is investigated, which seems to be one of the steps in this direction.

Further investigations carried out with the aim to reproduce the physical quantities as well as the constant and variable angular accelerations with the help of one standard, seem to be the perspective ones.

Acknowledgements

In the above paper the authors have presented the results of the work carried out by a large group of scientists and engineers from the D. I. Mendeleyev Institute for Metrology, as well as from St. Petersburg State Electrotechnical University and the St. Petersburg Technical University and some other organizations. The authors express their gratitude to all of them.

The authors would like to express their special gratitude to Dr. A. Stolpner, director of Research and Production Enterprise "Metrological Systems" (the main manufacture of standard setups). It is hardly probable that without his participation, assistance and management of the works on creation of the major part of setups the described standard would come into being.

References

1. **IEEE** Recommended Practice for Precision Centrifuge Testing of Linear Accelerometers. Std 836-2001
2. **A.Ye.Sinelnikov, A.V.Gessan, E.P.Nilov.** Low Frequency Linear Accelerometers Test Uncertainties. Measurement, Control and Automation, 1979, №6. (In Russian)
3. **A.Ye.Sinelnikov.** About the Increase of Accuracy in Reproducing the Acceleration with the Help of Double Centrifuge. Metrology, 1978, №9. (In Russian)
4. **Ye.P.Krivtsov, V.N.Kudryavtsev, A.Ye.Sinelnikov.** Complex of standards in the field of gravitational measurements and the lines of its further development. 5th State Petersburg International Conference on Integrated Navigation Systems, May 25-27, 1998.
5. **B.E.Blanter, Ye.P.Krivtsov, D.P.Loukjanov, A.Ye.Sinelnikov, Ju.V.Filatov, Yu.N. Shestopalov.** State and perspectives of development of means for solid angle unit value transfer, angular velocity and acceleration on the basis of ring laser., Measurement technique , 1984, №7.
6. **Mokros J., Vu K.X.** Jemna mechanica a optika, 9 , 203, 1993.
7. **M.N.Burnashov., D.P.Loukjanov., P.A.Pavlov., Ju.V.Filatov.** The advancement of methods and means of laser dynamic goniometry Quantum electronics, т.30 , №2, с.141-146, 2000.
8. **M.N.Bournachev, Yu.V.Filatov, D.P.Loukjanov, P.A.Pavlov, A.Ye.Sinelnikov.** Reproduction of plane angle unit in dynamic mode by means of ring laser and holographic optical encoder, Proceedings of 2-nd EUSPEN international conference, Turin, May 2001.

DYNAMICS OF THE SENSITIVE ELEMENT OF THE MICROMECHANICAL ACCELEROMETERS

V.Yu. Raspopov*, Yu.V. Ivanov, S.A. Zotov*****.

Tula State University, 94, Lenin Avenue, Tula, Russia.

Abstract

Key words: accelerometer, sensitive element, silicon plate.

The dynamic of the accelerometers with monocrystallic pendulum for the parameters of indignations characterized by the angular movement of the base and linear displacement is researched.

The sensitive element of the micromeehanieal aeeelerometer is a silieon plate conneeted with the spring elements made together with the base body of the deviee. The sensitive element of the linear accelerometer fig.1 is in common the inertial mass m conneeted with the body by four spring erosspieees.

In common the eenter of the masses (point C) eoneerning the geometrieal eenter of thc masses (point O) is determined by the factors l_x and l_z. Thc output parameters of the sensitive element under thc action of aeeeleration "*u-g*" ("*u*"-acceleration of the displaeement of the base0 is linear y, and angular parameters of thc displacement of thc mass. The existence of the parameters l_x and l_z leads to thc appearance of the cross eonneetions between informative ehannels of the accelerometer, fig.2.

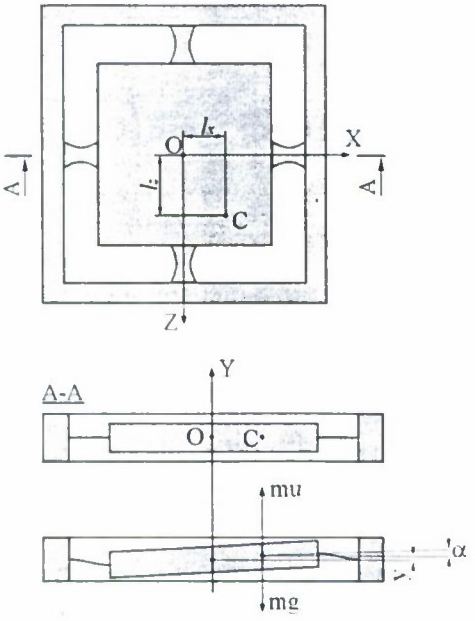

Fig. 1

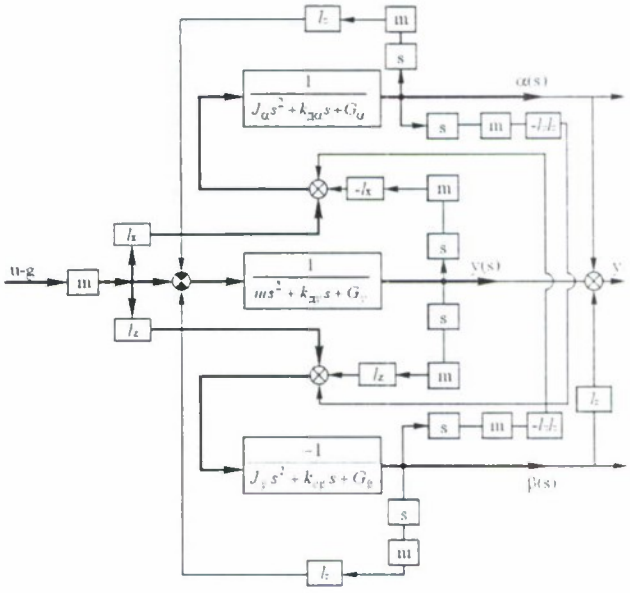

Fig. 2

Except the above mentioned parameters the dynamic of the aeeelerometer is found by the absolute factor of damper on channels: $k_{дy}$, $k_{дα}$, $k_{дβ}$, by rigidity of the suspender: G_y, $G_α$, $G_β$ and main inertia moments: $I_α$, $I_β$.

Mathematical model in aeeordanee with fig. 2 gives a possibility to eount thc frequency characteristics of the accelerometer.

The sensitive element of the angular accelerometer of the eompensatory transformation with the coils of the magnetoeleetrieal eonneetion is shown on the fig.3.

---

* Dr.Sc., Professor, Head of the Department of the Devices of Management of Tula State University.
** Dr. Sc., senior lecturer of the Department of the Devices of Management of Tula State University.
*** Postgraduate of the Department of the Devices of Management of Tula State University.

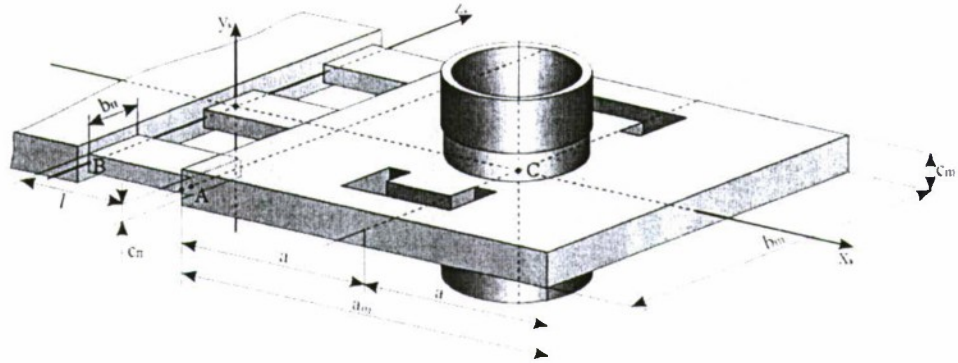

Fig. 3

The systems of the coordinates characterizing the position of the sensitive element of the accelerometer is shown on the fig.4.

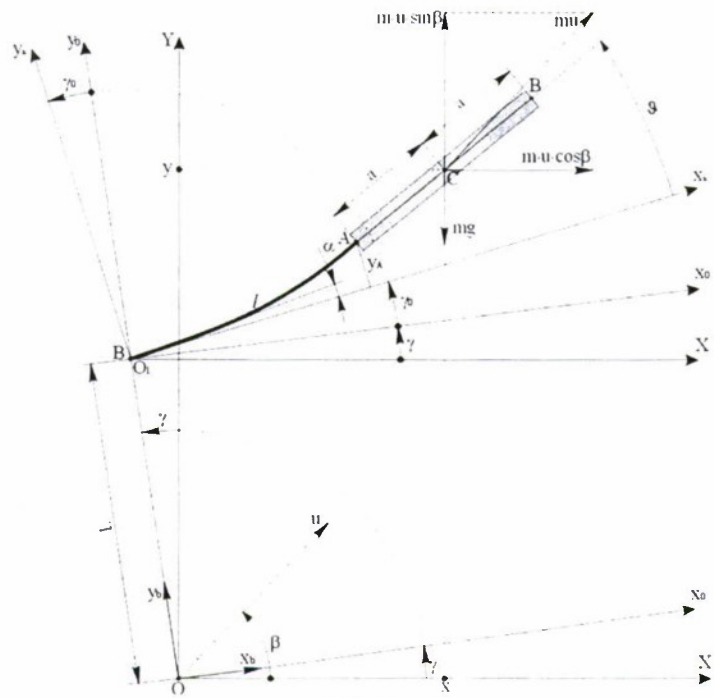

Fig. 4.

The equation of the movement of the sensitive element of the accelerometer are as following:

$$\left.\begin{aligned} &m\left(\ddot{y}_A + a\ddot{\vartheta} - (y_A + a\vartheta)\dot{\gamma}^2\right) + \left(k_{11} + K_{ЭМ}\right) y_A + \left(k_{12} + K_{ЭМ}a\right)\vartheta + k_д \dot{y}_A + \frac{k_{дy}}{a}\dot{\vartheta} = F + Q, \\ &J^*\ddot{\vartheta} + m\ddot{a}y_A - ma\left(y_A + a\vartheta\right)\dot{\gamma}^2 + \left(k_{21} + K_{ЭМ}a\right) y_A + \left(k_{22} + K_{ЭМ}a^2\right)\vartheta + k_д a\dot{y}_A + k_{дy}\dot{\vartheta} = Fa + Qa. \end{aligned}\right\} \quad (1)$$

Where: m - mass of the sensitive element, J^* - moment of the inertia according the axes crossing point A and perpendicular plane of drawing(see fig. 4), $k_д$, $k_{дy}$ - factors of damper under the linear and angular movement of the plate, k_{ij} - factors of the matrix of rigidity of the spring suspender, $K_{ЭМ}$ - factor of the back connection. F, Q - united forces having writing for angles γ_0 of the device on the base.

Analytical and numeral research of the system of equation (1) showed that the compelled movement of the sensitive element of the accelerometer may be seen as angular one according to the center of fluctuation. The distance from point A (see fig. 4) to the center of fluctuation for accelerometer of the direct and compensatory transformation will be determined under the following dependence:

$$c_ц = \frac{k_{12}a - k_{22} + J\omega^2}{k_{11}a - k_{12}}.$$

Where ω frequency of indignation, J- main moment of inertia.

INS INITIAL ALIGNMENT AND CALIBRATION ON MOVING BASE: ALIGNED AND REFERENCE SYSTEM INTERACTION*

L. Vodicheva*
Science and Production Association of Automatics
145, Mamina-Sibiryaka St., 620075, Ekaterinburg, Russia. E-mail: larisa@gduma.mplik.ru

Abstract

Key words: INS, initial alignment and calibration, moving base, Kalman Filter, decomposition

The problem of optimal interaction between aligned INS and reference Navigation System in the process of initial alignment, calibration and initial velocity determination on moving base is considered. The theoretical verification of the approach used in practice by Science and Production Association of Automatics (SPAA) is presented. The used approach requires the minimal number of parameters transmitted from a reference system to an aligned one. If Navigation System includes INS and INS error model can be described with sufficient certainty by finite number of parameters, proposed technique is shown to be optimal in accuracy.

The theory and applications of Initial Conditions Determination Systems (ICDS) are well developed. These function systems are destined for initial alignment, calibration and initial velocity determination. The significant success in this field was achieved by SPAA having developed for the first time in Russia the precision ICDS for Flying Vehicle (FV) being launched from moving carrier [1].

One of the problems of Flying Vehicle (FV) INS initial alignment on moving base with the help of more accurate carrier Navigation System (NS) is considered in the paper. This is optimization of interaction between two navigation systems. One of them is assumed to be a reference system. This is a carrier NS. Optimization criterion is ICDS accuracy. Restrictions are imposed by conditions of practical realization, in particular by number and list of parameters transmitted from a reference system to an aligned one. The results obtained in the process of SPAA developments are presented.

An aligned INS may use as a measurement unit both a gyro-stabilized platform with specific force sensors (SFS) mounted on it and a strapdown inertial measurement unit (IMU). To simplify arguments we shall consider linear measurement processing only. Angular measurement processing can be implemented similarly either separately or combined with linear measurement processing.

Outputs of a linear measurement channel are functions of motion and gravitation field parameters, and parameters of transformation of input values into output ones. The model of this transformation is known with some errors. We shall suppose any uncertainties of transformation to be transformation errors. These uncertainties are ICDS output parameters and include in addition to IMU errors uncertainty of simulated (either physically or mathematically) navigation frame initial orientation and uncertainty of initial velocity.

Optimal in accuracy algorithms of initial conditions determination may be obtained as integrated processing of all the measurements implemented on the carrier by Optimal Kalman Filter (OFK). In real systems as a rule both model of state vector changing and measurement model can be linearized and observed discrete dynamic system can be described as follows:

$$\begin{aligned} X(k+1) &= \Phi(k+1)\cdot X(k) + \Gamma(k+1)\cdot w(k) \\ Z(k+1) &= \mathrm{H}(k+1)\cdot X(k+1) + \vartheta(k+1), \qquad k = 1,2,...K, \end{aligned} \tag{1}$$

where $\Phi(k+1)$ is a state transition matrix; $\Gamma(k+1)$ is a state process noise transition matrix; $\mathrm{H}(k+1)$ is an observation matrix; $X(k+1)$ is n-element state vector; $w(k)$ is p-element state process noise vector; $Z(k+1), \vartheta(k+1)$ are m-element measurement and measurement noise vectors respectively.

For optimal approach measurement vector contains outputs of sensors included both in Flying Vehicle INS and carrier NS; state vector consists of parameters characterizing vehicle motion, gravitation field, measurement errors of aligned INS and reference NS. Estimates of state vector components on each update interval can be obtained by solving the equations (1) with the help of Kalman Filter recurrent procedure. However, practical realization peculiarities, in particular development of ICDS and carrier NS on different hardware by different groups of engineers, restrict the choice of ICDS algorithms. These algorithms are advisable to be constructed as two separate algorithmic units with minimal number of connections between them. A direct decomposition of equations (1) requires matrixes $\Phi(k+1)$ and $\mathrm{H}(k+1)$ to be presented as cellwise-diagonal ones. It is impossible since motion and gravitation field parameters are contained in state vector both of aligned INS and reference NS.

---

* Senior Research Scientist

Analyzing the technical solutions used in SPAA developments A. Zakharcev proposed another approach [2]. This approach is based on the Least Square Method (LSM) using total sampling of measurements. For this case the property of transitivity is strictly proved [3]. It is the transitivity property in connection with total sampling of measurements on observation interval that allows implementing decomposition of equations without losing optimality. This property consists in the following. The totality of measurements is divided into arbitrary sets in a way that measurement errors of different sets are not correlated. At first measurements of each set are processed separately, then obtained estimates are considered as new measurements and are processed jointly. The results of such a processing are the same as results of processing of all the measurements, i. e. they are optimal linear estimates.

The equations (1) can be represented by LSM fundamental equation:

$$Z = \mathrm{H} \cdot X + \vartheta, \tag{2}$$

where X is $(n+p \cdot K)$-element estimated vector; it includes n-element state vector at the beginning of observation interval $X(0)$ and p-element state process noise vector $w(k)$, $k = 0,...K-1$, at each update of Kalman Filter (1);

Z is $(m \cdot K+n+p)$-element measurement vector including three components; those are: $m \cdot K$ measurement errors $\vartheta(k), k = 1,...K$; n elements of a priori information about system initial conditions $X(0)$; p elements of a priori information about system noise $w(0)$;

H is measurement matrix represented in cellwise-diagonal form:

$$\begin{bmatrix} H_1 & 0 & 0 \\ 0 & H_2 & 0 \\ 0 & 0 & H_3 \end{bmatrix}, \text{where } H_1 = \begin{bmatrix} H(1)\cdot\Phi(1) & H(1)\cdot\Gamma(1) & \dots & 0 \\ H(2)\cdot\Phi(2)\cdot\Phi(1) & H(2)\cdot\Phi(2)\cdot\Gamma(1) & \dots & 0 \\ \dots & \dots & \dots & \dots \\ H(K)\cdot\prod_{r=1}^{K}\Phi(r) & H(K)\cdot\prod_{r=2}^{K}\Phi(r)\cdot\Gamma(1) & \dots & H(K)\cdot\Gamma(K-1) \end{bmatrix}, H_2, H_3$$

are identity n-dimension and p-dimension matrixes respectively.

ϑ is measurement error vector; the correlation matrix of measurement errors for equation (2) is cellwise-diagonal matrix as well composed of measurement errors correlation matrix, a priori estimation error correlation matrix and a priori system noise correlation matrix in OFK equations (1).

State vector $X(k)$ elements in equations (1) estimated by OFK are connected with vector X elements in equations (2) estimated by LSM as follows:

$$X(k) = \prod_{p=1}^{k}\Phi(p)\cdot X(0) + \sum_{p=1}^{k-1}\prod_{s=p}^{k}\Phi(s)\cdot\Gamma(p)\cdot w(p-1) + \Gamma(k)\cdot w(k-1) \tag{3}$$

State vector element estimates obtained by OFK and LSM equations are the same at the end of observation interval only. At the other updating moments the results may differ since state vector elements are estimated by LSM on the basis of all the samples over the observation interval $k = 0,...K$ and by OFK on the basis of the preceding samples $k < K$.

If all the measurements can be divided into sets in a way that measurement errors are non-correlated data processing can be decomposed into two stages. Two such decompositions correspond to main engineer approaches [4] to initial alignment on moving base. The first decomposition corresponds with reduction the problem to initial alignment on stationary base; the second one corresponds with special alignment technique on moving base. For the first decomposition measurements and a priori information relating to carrier NS are included into the first set and measurements and a priori information relating to aligned INS are included into the second set. In this case at the first stage data processing is implemented autonomously in aligned INS and carrier NS. At the second stage estimates obtained at the first stage are taken into account.

The mutual influence of estimates takes place if there are common parameters estimated in aligned INS and reference NS. For chosen decomposition these are parameters of motion and gravitation field. Using estimates of these parameters obtained by more accurate carrier NS it is possible to correct ICDS parameter estimates obtained by aligned INS. This approach conforms to compensation method when external measurement system is used for estimation of motion parameters and initial alignment on moving base is reduced to initial alignment on stationary base. The deficiency of this method reveals under return to recurrent form used in practical systems. This method is optimal for determined motion only. In general case it is suboptimal.

To construct the second decomposition we shall assume that carrier NS includes INS, i. e. the unit measuring the same vectors as aligned INS. Let us include all the NS measurements into the first set and the second set form as a difference between aligned INS and a chosen inertial unit of NS. In this case it is not motion and

gravitation field parameters, the number of which is proportional to the number of samples over the observation interval, to be the common estimated parameters. It is the errors of a chosen INS. If the error model of this INS can be described with sufficient certainty by finite number of parameters the method remains optimal even under returning to recurrent form. In this case optimal ICDS operation conforms to the scheme heuristically obtained and used in real systems developed in SPAA. This scheme can be briefly described as follows:

– the measurements of carrier NS are processed autonomously by recurrent optimal OFK procedure;

– simultaneously the difference signal between aligned INS and chosen inertial unit of NS is processed autonomously by recurrent optimal OFK procedure as well (this is vector matching [4]);

– at the end of autonomous processing the ICDS parameters obtained at the first stage are corrected by using the chosen inertial unit error estimates obtained at the first stage by processing all the measurements of NS; in addition the correction parameters transmitted from reference system to aligned INS are the functions of these errors constructed by analogy with parameters determined by ICDS.

–

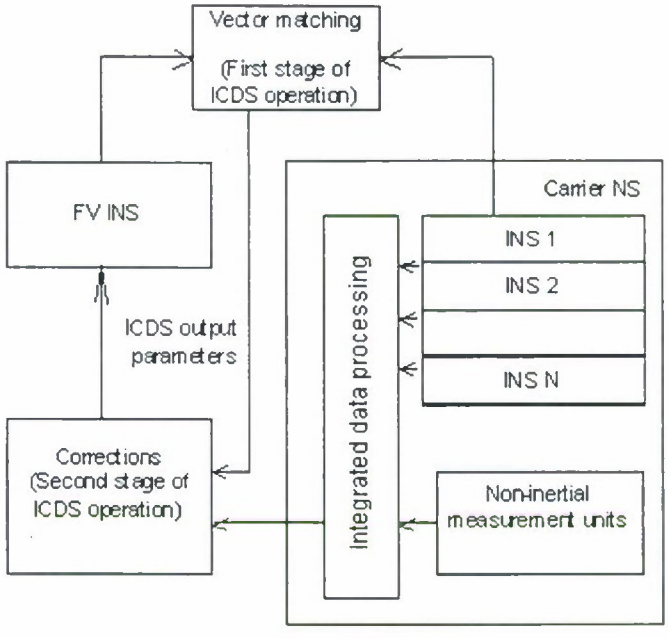

Matching scheme

The proposed scheme is the extension of well-known vector matching. The technique of vector matching is described in particularly in [4] for initial alignment that represents one of the ICDS problems under assuming that reference NS consists of one INS only and does not have errors. The proposed scheme has been named as the matching scheme. It is depicted on the figure. The implementation of ICDS algorithms based on the matching scheme requires minimal number of parameters transmitted from reference NS.

In conclusion let us note that the matching scheme is not managed to obtain directly from the equations (1). The transitivity property is strictly proved only for LSM using total sampling of measurements and the principal feature of the matching scheme is equivalence of two stages solution to the single stage solution using total sampling of measurements.

References

1. **Belsky L., Vodicheva L.** Stages of Development and Improvement of Precise INS Alignment and Calibration on Moving Base//5th Saint Petersburg Conference on Integrated Navigation Systems. – May 25-27, 1998. – pp. 66-74.
2. **Zakhareev A.** Improvement of the Use of Measurements Instruments on Moving Carrier for High Accurate Determination of INS Initial Conditions//PhD Dissertation (Technical Sciences), SPAA, Sverdlovsk, 1986. In Russian.
3. **Mudrov V., Kushko V.** Measurement Processing Technique: Quasiprobable Estimations. – Moscow.: Radio i Svyaz, 1983. – P. 304. In Russian.
4. **Lipton A.** Alignment of Inertial Systems on Moving Base. Electronics Research Center, Cambridge, Mass. national Aeronautics and Space Administration, Washington, D. C., 1967.

APPLICATION OF QUARTZ MICROMACHINING TO THE REALIZATION OF MICRO-GYRO*

Zhang Qiaoyun*, Lin Rile, Zhang Ting***,Li Maochen****, Lu Zhiqing*****
Sichuan Institute of Piezoelectric and Acoustooptic Technology, 400060,
Chongqing, China. E-mail: zhangqiaoyun69@sohu.com

Abstract

Key words: quartz, micromachined gyro, anisotropy etching

Micromachined gyro was made by using technologies directly derived from integrated circuit fabrication, it is easily to be mass- produced. It has following advantages: low costs, lightweight, resist high shock. In this paper, the basic structure and operation of quartz micromachined gyro are discussed. Mechanism and experiments of chemical anisotropy etching for quartz are described. The processing procedure of quartz tuning fork resonator is given. We have made quartz micro-gyros with the help of chemical etching technology. The sample's main specifications are as following: Driving frequency and pick-off frequency is about (10~12) kHz, quality factor (Q) is about 3000~5000, Scale factor is about 10mv/°/s, Bias stability is 3°/s.

1.Introduction [1][2]

There is a wide spectrum of emerging markets for micro-gyros with different performance requirements, including automotive purposes (airbags, collision avoidance systems, navigation, anti-skid and active suspension systems, etc.), consumer products (navigation, rehabilitation, toys, sport equipment, stabilization systems for video cameras, etc.), and industrial applications (stabilized platforms, angular measurements, robotics, etc.). Conventional gyros based on mechanical spinning rotors, laser technology or optical-fiber systems are too bulky, too expensive, or have a too modest reliability for these new mass-markets. Micromachined vibrating gyroscopes have a strong potential to meet the large market needs.

From the point of view of their mono-crystalline structure and their modulus of elasticity, quartz and silicon materials are good materials for micro-gyro. The quartz material has piezoelectric effect; the material's piezoelectric properties are particularly stable over temperature and time. Silicon is a semiconductor. Thus quartz has the advantage over silicon for devices in which leakage current should not exist between the various needed metallization . Clearly, as silicon is not piezoelectric, it requires more complex technologies to elaborate resonant devices. So, we select mono-crystalline quartz as the material for micro-machined gyro.

2. Basics of operation

Basic structure of quartz micro-gyro resonator is shown in fig. 1. An oscillator with closed loop constant gain circuit drives the driving tines at their resonant frequency of around 11KHZ. When the vibration tines are rotating at a rate about the input axis, a Coriolis torque will be produced, which cause the pick-off tines to vibrate in the plane perpendicular to the driven tines (see fig. 1). Electrical [1]charges are produced in the pick-off tines owing to piezoelectric effect, which are detected to obtain the output signal.

The angular motion around the output axis can be expressed by eq. (1) [3]

$$T=J\Theta''+b\Theta'+k\Theta \ . \tag{1}$$

Where J is the moment inertial of fork, K is the torsion stiffness of the support.

The general solution of Eq. (1) is

$$\Theta(t)=T\cos.(\omega t+\varphi) /J((\omega^2+\omega_0^2)+(\omega\omega_0/Q)^2) \ , \tag{2}$$

$$Y(t)=R\Theta(t)=2rwQ\cos(\omega t)/(A\omega) \ . \tag{3}$$

From eq. (3), we can conclude that the output signal voltage is in proportional to the input angular rate (w).

---

[1] * M. Sc., Senior engineer, Head of Laboratory.
** M.Sc., Engineer.
*** M.Sc., Engineer.
**** B.Sc., Senior engineer.
***** M. Sc., Professor, Leading Research Scientist

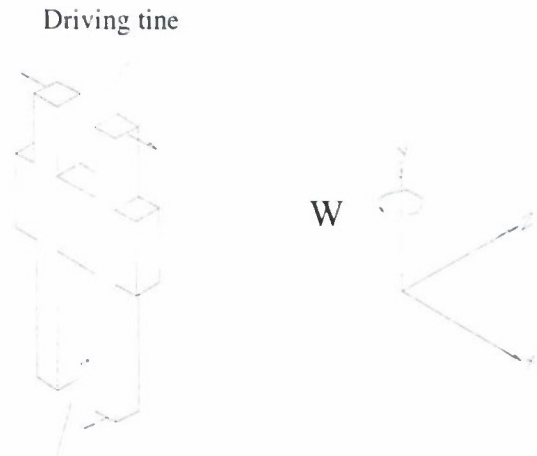

Fig.1 Basic structure of quartz micro- gyro resonator

3.Chemical etching technologies of quartz

The etching speed of a single crystal strongly depends upon the crystalline orientation of the surface being etched, the origin of this anisotropy is not clearly explained. The atomic density of the crystalline surface being etched seems to be a determining factor, the slowest etching speed generally corresponding to the densest plane [4][5] [6].

A very useful property of quartz is that it has a practically zero etching rate for all the planes parallel to its Z-axis. This property permits the realization of various shapes with steep flanks perpendicular to the Z-axis in any direction on "Z cut" substrates.

Quartz is etched in the warm mixture of hydrofluoric acid (HF) and ammonium fluoride (NH_4F) by the reaction [7]:

$$SiO_2+4HF \rightarrow SiF_4+2H2O.$$

SiF_4 is gas in the general conditions, but the complex compound is produced owing to SiF_4 react with HF in the HF solution.

$$SiF_4+2HF \rightarrow H_2SiF_6.$$
$$SiF_4+2NH_4F \rightarrow (NH_4)_2SiF_6.$$

The etching rate depends on the composition and temperature of etching bath. The property of the surface obtained depends strongly on the positive ions in the etching bath and its temperature. The surface roughness and etching rate is a function of the bath composition and its temperature [1].

Etching time controls the final thickness of etched quartz. This requires the bath temperature to be precisely monitored. The variation of bath temperature on 1□ will cause etching rate change about 0.1μm /min .

4. Processing [1] [2][3]

The chemical etching has advantage such as high etching rate, low cost and high anisotropy. The thickness and width of resonator being processed is a few hundreds of micrometers. So we manufactured the resonator with the help of chemical etching technology. Because the etching rate ratio (Vz/Vx, Vz/Vy) for mono-crystalline quartz is very large, we selected the Z-cut quartz as the materials to be micro-machined. Processes of quartz micro-gyro include RF sputtering thin film and e-beam resistance metallization, Substrate grinding and polishing, etching, photolithography and development. The process flow is shown in fig. 2.

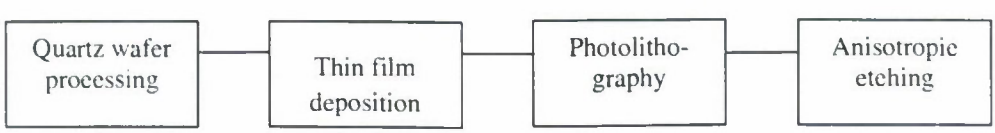

Fig. 2 Quartz resonator processing flow

4.1 Processing of quartz wafer

The processing of quartz wafer includes orientation, cutting, grinding and polishing, every step is all very important. If the surface of quartz wafer has much defects and scratches, they will become wider and deeper after etching. The flatness of wafer will be influeneed. In the worst ease the resonator will erisp. The elean room is neeessary for quartz wafers; the dust particle on the wafer surfaee will reduce the adhesion between the quartz and the thin film (Cr./Au). Bad adhesion of resist will seriously influence the etching processing.

4.2 Thin film deposition

Because the flatness and smoothness of resonator should be very high and the dimensions of resonator are very small, traditional chemical and mechanieal proteeting ways ean not be utilized to avoid the damage of the resonator surface. Two layers of metal films sueh as Cr./Au structure are used. The RF sputtering technology offers good adhesion for deposition of thin Kr/Au films on the quartz wafer.

4.3 Photolithography

The photolithography of quartz resonators includes the following steps

a. Designing the photolithography pattern and making the mask according to the dimensions of quartz wafer and the shape of resonator.

b. Coating and drying the photoresist on the quartz wafer.

e. Double side photolithography.

4.4 Chemical Etching

The principal requirements in processing the quartz resonator are the surface quality and the precision of dimensions. They are influenced by the faetors as follows: composition of etching bath, temperature, quality of the quartz material, quality of polishing and cleaning ete. We carried out a set of experiments utilizing etehing baths sueh as HF, NH_4F, NH_4HF_2, and KF with different concentrations and temperatures. The etehing rate depends strongly on the composition of etching bath and its temperature. The higher the temperature and the concentration, the greater the etching rate will be.

5. Experimental results

The configuration of our quartz miero-gyro is shown in Fig.3.The key feature is the assembly which contains the quartz resonator and suspension held in position by special adhesives. Fig.4 – 5 show the impedance-phase characteristies of driving axis and pick-off axis for our quartz micro-gyro tested in atmosphere respectively. The resonating frequeney of driving axis is 11.009KHZ and the resonating frequency of pick-off axis is 11.136KHZ. Quality factor of the resonator is about $(3\text{-}5)*10^3$. Fig.6 shows the test results of the rate-rotating table. It ean be seen from fig.6 that the seale factor is about 10mv/(°/s).

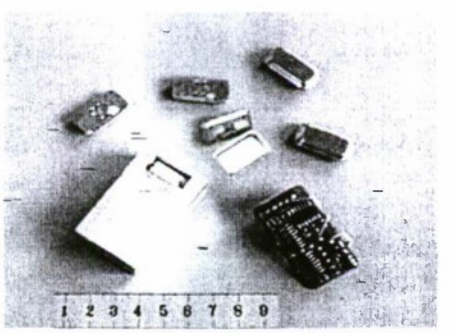

Fig.3 The configuration of quartz micro-gyro

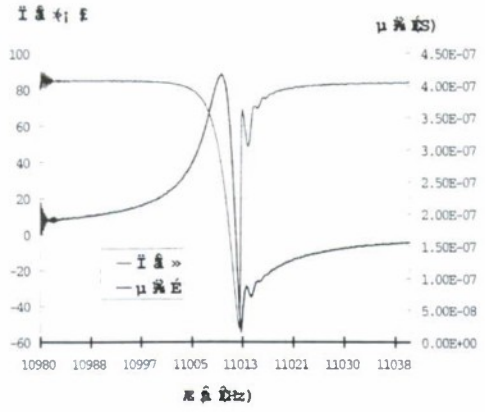

Fig.4 Impedance-phase characteristics of driving axis

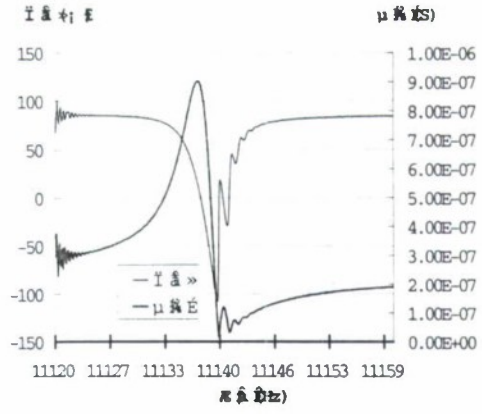

Fig.5 Impedance-phase characteristics of pick-off axis

6.Conclusion

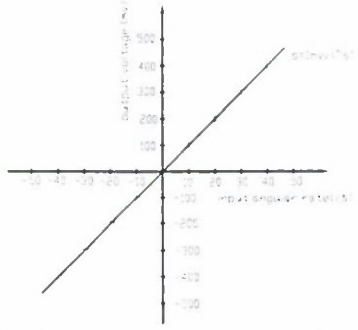

Fig.6 Output voltage versus input angular rate

Utilizing the chemical anisotropy etching, we have fabricated the quartz micro-gyro. The structure and experimental results of the quartz micromachined vibration gyro are presented. It is shown that the sensitivity is 10mv/(°/s), Bias stability is about 3°/s, Quality factor of the resonator is about $(3\text{-}5)*10^3$.

Our further work on the quartz micro- gyro includes: increasing the quality factor Q; Trimming the frequency mismatch between driving and pick-off mode; Making application-specific integrated circuit to improve the stabilized performance and reduce the volume of the instrument.

References

1. **Zhang Qiaoyun et.al,** Processing of the Quartz micromechanical gyroscope, second international symposium on inertial technology in BEIJING. 229-232.1998.10
2. **Danel JS.et.al,** Application of quartz micromachining to the realization of a pressure Sensor. IEEE International Frequency Control Symposium. 587-596.1993.
3. **G.N.Baker,** Quartz Rate Sensor from Innovation to Application, Symposium Gyro Technology, 11.1-11.20.1993.
4. **Vondeling J K.,** Fluoride-based etchants for quartz, Journal of Materials Science, 18, 304-314.1983.
5. **Monk David J.,** A review of the chemical reaction mechanism and kinetics for hydrofluoric acid etching of silicon dioxide for surface micromaching applications, Thin solid Films, 232.1-12.1993.
6. **Danel J S.,** micromachining of Quartz and its application to an acceleration Sensor, Sensor and Actuators, A21-23, 971-977.1990.
7. **Pellt Rangsten, et.al,** Etch rates of crystallographic planes in z-cut quartz-experiments and Simulation, J. Micromech. Microeng.18, 1-6.1998.

HIGH-PRECISION LAND-BASED GYROCOMPASS*

V.V. Kozlov*, A.A. Konovtchenko, A.P. Mezentsev***, L.A. Dudko****, A.I. Tereshkin*****
Kuznetsov RIAM, 55, Aviamotornaya st., Moscow, 111123, Russia
N.Yu. Mezhuev****
29 RI DM RF

Abstract

Key words: automatic gyrocompass, float gyro, plumb line sensor, functional diagram

High-precision land-based automatic gyrocompass (AGC), based on precise sensors – single degree of freedom floating gyroscope (FG), which work as angular velocity sensor, and 2-coordinates plumb line sensor (PLS) is given.

Analysis of AGC errors as well as an evaluation of contribution of all subsystems into the final error is developed. Operational characteristics of AGC for different working mode are presented.

Autimatic gyrocompass is intended for determination astronomical azimuth of dircctions optical axis autocollimator, axis is coincided with normal of mirror, fixed on gyro, in measuring range 0° to 360° and output azimuth magnitude in digital signals to outer devices and own indicator. AGC is classed as analytical gyrocompass, based on single degree of freedom floating gyroscope, measuring in angular velocity mode projection into sensetive axis (SA) horizontal component day Earth`s angular rate.

Gyrocompass arrangment diagram is presented in Fig. 1.

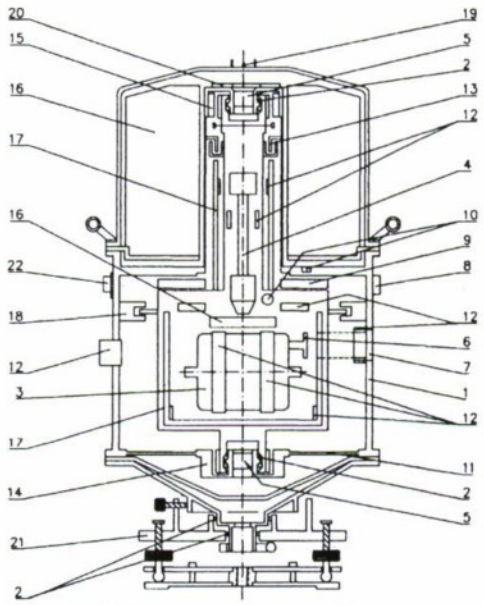

Fig.1 Girocompass arrangement diagram

1 - case, 2 - bearing, 3 - float giro, 4 - pendulum, 5 - slip-ring, 6 - mirror, 7 - illuminator, 8 - horizont indicator, 9 - heat modul, 10 - temperature sensor, 11 - membrane, 12 - heater, 13 - rate generator, 14 - angular-displacement sensor, 15 - motor, 16 - electronics unit, 17 - heat screen, 18 - angle sensor, 19 - goal arrangement, 20 - safety device, 21 - inclined whirl stand, 22 - connector

AGC disign features:

- main axis vertical orientaion, allows to minimazc exposure timc aftcr orientation alteration, and becomes possible for using FG with gas-bearing gyroscope axis and electromagnetic suspension for the sensetive element (SE), provides high stability g-depcndent moments.
- monitoring element (mirror), fixed on FG part, prescts basic direction (BD) and provides high stability of optical link SA FG with BD.
- electronic horizont indicator usage as light line provides high accuracy of axis rotation initial alignment sensetive clcmcnts unit (SEU) in vertical by according PLS signals.
- nonreduction transmission schedule of rotation and holding SEU, provides high operational life and fail-safety AGC characteristics.

Azimuth determination methods need to solve during AGC procesing such functional problems:

- projection SEU`s angular velocity measuring into SA FG;
- anglc α measuring – SA deflection from horizontal plane;
- velocity variation angle β measuring - deflection from horizontal planc axis of precession;
- turns of pivoted device part with SEU in azimuth planc, alignmcnt spccified angles relatively case and holding with required accuracy;
- measuring information assumption, storage under measuring cucle and data calclulation;
- input measured data and indicatin of output and service information;
- provision of heat regime SEU operation;
- components power provision.

Each problem solves by individual functional subsystem.

Device structure, all subsystem is given in Fig. 2.

---

*Head of Laboratory.
**Ph.D., Head of Laboratory .
***D.S., Professor, General director – Chief Designer.
**** Chief of Department.
***** Chief of Department.
******Senior Research Scientist.

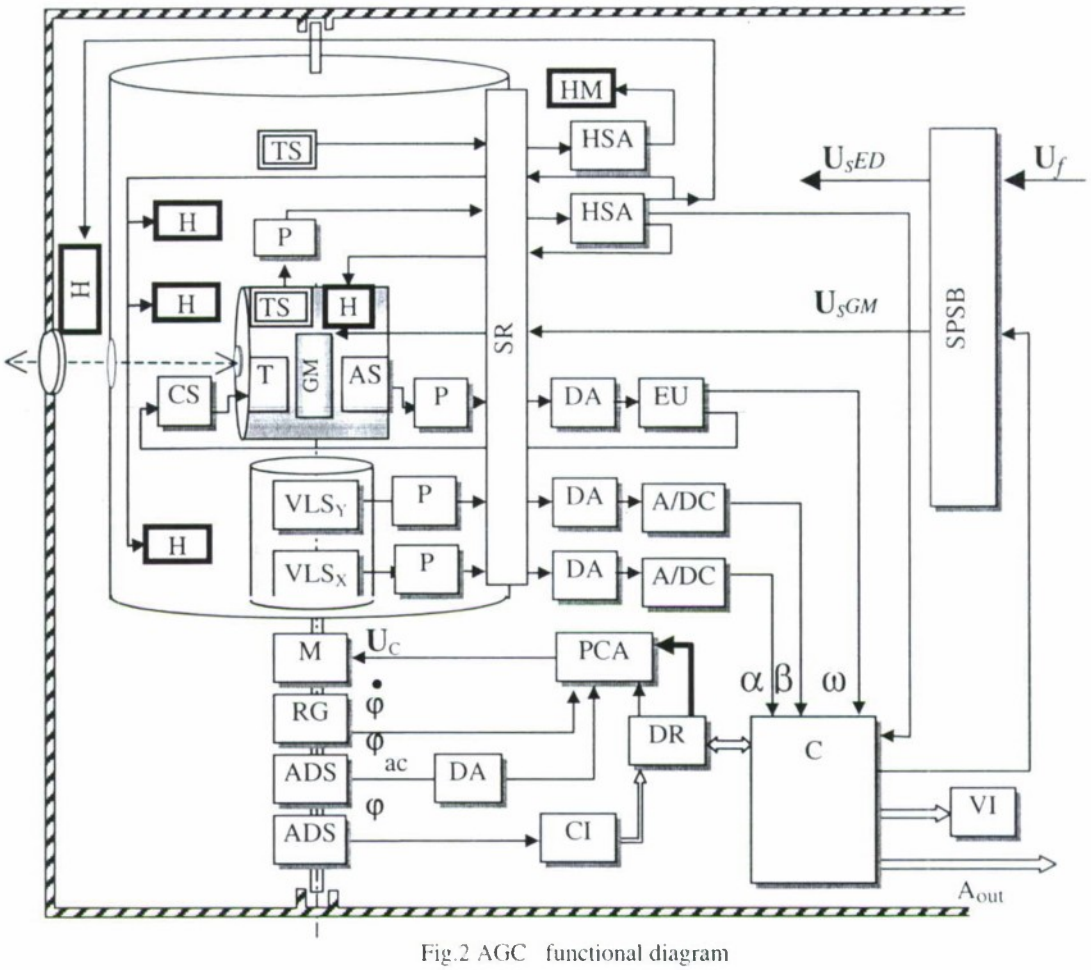

Fig.2 AGC functional diagram

Measuring angular velocity system includes preamplifier (P), discriminator amplifier (DA), electronics unit (EU) and current stabilizer (CS).

System measuring SEU`s turns from azimuth plane based on PLS, which consist 2 equal data convert channels. Each channel includes preamplifier, discriminator amplifier, A/D convertor (A/DC).

SEU`s alignment in specified angles of azimuth plane and holding SEU provides by consecutive operation from 2 systems.

Accurasy alignment system is analog control system with negative feedback and includes angular-displacement sensor (ADS), discriminator amplifier and precision capturing amplifier (PCA).

Transmission realizes on direct current motor (M).

SEU`s turn system intendes for quick turn in needed range of precision capturing system and realizes by digital control. Turn system ineludes code angular-displacement sensor with code invertor (ADS-CI), digital regulator (DR), direct current motor and analog control elements, which enters PCA.

Computer (C) intends to convert measuring data, azimuth computing and control all AGC systems.

Auxiliary subsystems intend power – SPSB and solve heatsetting problem. Heat setting system includes heat setting amplifiers (HSA), temperature sensors (TS), heaters (H) and heat module (HM).

Currently Kuznetsov RIAM have been developed eomplete design. AGC fabrication is keeping. Device exhibites such project characteristics:

Dimensions , mm	215 × 215 × 435
Weight, kg	14,5
Root-mean-square error, arc-sec	
- mode №1	4,4" at 10 min
- mode №2	5,6" at 7 min
- mode №3	10,6" at 4 min
- mode №4	20,2" at 2 min
Power consumption, W	
- measuring preperation	300 during 5 min
- azimuth measuring	25
Voltage – battery, V	22...29
Azimuth data, numerical	arc-deg, -min, -sec
Data trasmission interface	RS232C
Life time, years	20
Operational life, hours	30000

THE GENERAL METHODS FOR SYNTHESIS AND ANALYSIS OF HIGH-PRECISION ALGORITHMS FOR QUATERNIONS CALCULATION BY GYROS DATA*

A.P. Panov*,
National Technical University of Ukraine (KPI), Pobedy Prsp. 37, 03056, Kiev, Ukraine
Fax: 38 044 2417622 E-mail: nest@ntu-kpi.kiev.ua
M.V. Sinkov**,
Institute Problems Registration Information NAS of Ukraine, Shpaka Str. 2, 03113, Kiev, Ukraine
Fax: 38 044 4461491 E-mail: sinkov@ipri.kiev.ua
N.N. Aksenov***
Space Research Institute NAS and NSA of Ukraine, Glushkov Prsp. 40, 03187, Kiev, Ukraine
Fax: 38 044 2664124 E-mail: aks@space.is.kiev.ua

Abstract

Key words: strapdown inertial navigation systems, gyros, orientation quaternions, precession, coning algorithms, accuracy

The most general methods of the synthesis and analysis high-precision algorithms of rotation quaternions calculation on the base of gyros data are proposed. The specific feature of these methods is the construction and use of the generalized algorithms and generalized asymptotic estimates of theirs local errors (with arbitrary coefficients). In more detail coning algorithms of 6-th and 8-th order accuracy are considered. The comparative analysis of accuracy and performance of new and known algorithms is done. The efficiency of proposed method in comparison with other methods is demonstrated.

1. The synthesis and analysis problems of high-precision algorithms of rotation (orientation) quaternions calculations in onboard digital computers of Strapdown Inertial Navigation System (SINS) and Attitude and Heading Reference System are considered. These problems were actual at the initial stages of creation SINS and remain actual now. It can be illustrated by series of publications, in particular [1-10]. The solution of these problems should precede developments of programming tools for SINS CAD [3]. These problems are very important at implementation of SINS CAD in INTERNET environment using WWW technologies.
The high-precision algorithms of quaternions calculation are understood as algorithms of 6-th, 8-th and higher order accuracy [11]. In such algorithms high-precision transformations of integrating gyros readings (increments of angular quasicoordinates [11]) in components of quaternions of small rotations are performed. As computed components of quaternions are considered the Rodrig-Hamilton (Euler) parameters that are traditionally used in SINS. It is noted that offered methods of synthesis and analysis of algorithms may be effectively used and advanced also in the case of components calculations of the various nontraditional nonnormalized rotation quaternions and biquaternions (at apparent velocity calculation) [12]. In algorithms for calculation of Rodrig-Hamilton parameters are used as intermediate parameters the coordinates of orientation vector (Euler vectors) [1-11]. Through these parameters components of quaternions of small rotations are calculated.

2. The generality of methods of synthesis of algorithms consists of usage known ones [11] and construction of the new generalized algorithms of calculation of orientation vector coordinates. Such algorithms contain arbitrary factors (parameters), which enter also in the generalized estimations of local (on a step of calculations) algorithms errors [11]. The generalized estimations of local errors are found in the process of synthesis of the generalized algorithms [11]. The generalized algorithms and estimations of their local errors are synthesized for an arbitrary angular motion of the gyro package (rigid body or mobile object).

3. The generality of methods of the analysis of algorithms is based on construction and usage of the generalized asymptotic estimations of the rate constant of the algorithms global computational drift (drift rate) for particular cases of an angular motion of SINS gyro package. The analysis of algorithms assumes investigation of their some subset on accuracy and performance, and also optimization of algorithms on the base of preassigned criteria (on accuracy or performance) under the concrete calculations conditions [11]. The calculations conditions are determined by limitations on various parameters of an angular motion, on current step of calculations of quaternions in onboard digital computers, on characteristics of gyros (drift rate, etc.) and characteristics onboard digital computer (performance, the number of the digits, a ratio of execution time of various arithmetic operations). The generalized asymptotic estimations in the analytical form of computational loading for concrete onboard digital computers are calculated on the base of obtained estimations of the drift rates. These estimations are used for optimization with respect to performance of the subset of concrete high-precision algorithms [11].

4. The angular motion of rigid body in Euler classical case and its special cases (regular precession and coning motion) are considered [1-11]. In the Euler case the generalized asymptotic estimations of computational drift rate constant for any algorithm will contain the first integrals of angular rigid body motion [11].

---

* D.Sc., Professor.
** D.Sc., Professor, Head of Department.
*** Scientific Researcher.

In the case of the regular precession the generalized asymptotic precession [11] estimations of the drift rate contain as constant values the basic generalized algorithms characteristics, their local errors coefficients, and also precession parameters. As a main parameters of regular precession are used [11]: μ - precession angular rate, ν - angular rate of proper rotation, $\varepsilon = (\mu\ \nu)$ - dimensionless parameter, θ - nutation angle. The cases of direct (at $\vartheta < \pi/2$) and inverse (at $\vartheta > \pi/2$) regular precession are considered at the analysis of the algorithms.

The specific property of asymptotic preeession estimations of the rate drift constant and the estimations of the particular algorithms performance is their high accuracy. Relative errors of such estimations maybe about 0.0001 and less (at sufficiently small calculation step [11]). These estimations give (in opposite to others known [1-9] estimations) a full qualitative picture in a simple analytical form for any algorithm the relationships between rate drift or performance and algorithms characteristics, its local errors coefficients, calculation step and precession parameters. Coning single-frequency motion which most frequently used at the analysis of algorithm for quaternions calculation [1-11], turns out as special case from precession motion at $\varepsilon = -1$ under $\cos\theta > 0$ and $\varepsilon = 1$ under $\cos\theta < 0$.

5. It is shown, that the generalized asymptotic precession estimations of the algorithms performance may be used for the synthesis and analysis of the numerous adaptive precession [11] and coning [1-9, 11] algorithms (the calculations of the coordinates of orientation vector) on the base of appropriate "main" high-precision algorithms. The adaptive precession and coning algorithms have accuracy on two order above appropriate base algorithms at identieal eomputational complexity. The higher accuracy of the adaptive algorithms is reached using tuning of their eoefficients on precession or eoning motion of the gyro package (or mobile object).
The general methods of the synthesis and analysis of the adaptive eoning algorithms are eonsidered. Methods are based on usage: 1) the generalized algorithms (as base); 2) the generalized estimations of their local errors containing arbitrary factors; 3) the generalized estimations of a drift speed of base algorithms.

The examples of the synthesis of both known [7,9,11] and new adaptive coning three-step, four-step and five-step algorithms of 6-th and 8-th order accuracy on the base of appropriate 4-th order algorithms are given. All obtained adaptive algorithms are accompanied by the local errors estimations and the asymptotic estimations of the drift rate.

The efficiency of proposed general methods of the synthesis and analysis of the adaptive coning algorithms in comparison with ones based on Miller's approach [1,2,4,5,7,9] is shown.

With the help of the considered methods can be solved the problem of the synthesis of the local errors estimations for any selected algorithms and synthesis of the eonerete algorithms on the base of their local errors estimations. This problem is especially important for synthesis and analysis of precession and coning algorithms by using different methods (see [1-11]).

6. The considered general methods of the synthesis and analysis "traditional" algorithms may be effectively applied without essential changes at synthesis and the analysis of "nontraditional" algorithms for caleulation of quaternions using increments of multiple integrals of the coordinates of the angular rate vector [8]. Thus the numerous new adaptive algorithms with the appropriate asymptotic errors estimations for the cases of regular precession and coning motion may be synthesized.

References

1. **Ignagni M.B.** Efficient class of optimized coning compensation algorithms// Journal of Guidance, Control and Dynamics. Vol. 19, No.2, 1996, pp. 424- 429.
2. **Gusinsky V.Z., Lesyuchevsky V.M., Litmanovich Yu.A., Howard Musoff and George T. Schmidt**, A new procedure for strapdown attitude algorithms optimization as applied to stochastic motion input// Proceedings of the 3rd Saint-Petershurg International Conference on integrated navigation systems, 1996, pp. 3-12.
3. **Vodicheva L., Lookin N.**, Formalized AHRS algorithm representation as a SINS CAD unit// Proceedings of the 3rd Saint-Petershurg International Conference on integrated navigation systems, 1996, pp.32-43.
4. **Gusinsky V.Z., Lesyuchevsky V.M., Litmanovich Yu.A., Howard Musoff and George T. Schmidt,** A new procedure for deriving optimized strapdown attitude algorithms//Journal of Guidance, Control and Dynamics. Vol. 20, No.4, 1997, pp. 673- 680.
5. **Gusinsky V.Z., Lesyuchevsky V.M., Litmanovich Yu.A., Howard Musoff and Schmidt G.T.** Optimization of a strapdown attitude algorithm for a stochastic motion// Navigation: Journal of the Institute of Navigation, Vol.44, No.2, Summer 1997, pp. 163-170.
6. **Savage P.G.**, Strapdown Inertial Navigation Integration algorithms design. Part1: Attitude algorithms//Journal of Guidance, Control and Dynamics. Vol. 21, No.1, 1998, pp. 19- 28.
7. **Ignagni M.B.**, Duality of Optimal Strapdown sculling and coning compensation algorithms// Navigation: Journal of the Institute of Navigation, Vol.45, No.2, Summer 1998, pp. 85-95.
8. **Litmanovich Yu.A., Lesyuchevsky V.M., Gusinsky V.Z.**, Two new classes of strapdown navigation algorithms// Journal of Guidance, Control and Dynamics. Vol. 23, No.1, 2000, pp. 34- 44.
9. **Mark J.G. and Tazarles D.A.**, Coning algorithms taken into account nonideality frequency characteristics of gyro // Gyroscopes and navigation, No.1 (28), 2000, pp. 65-77.
10. **Pepelyaev S.E.**, New combined algorithm of determination of rigid body orientation// Izvestiya RAS, Rigid body mechanics, No.1, 2000, pp. 3-19.
11. **Panov A.P.** Mathematical foundations of inertial orientation theory. – Kiev: Naukova dumka, 1995. – 279 pp.
12. **Panov A.P.**, About new normalized and nonnormalized quaternions and hiquaternions for the orientation and navigation problem// III In Proc. Of Intern. Conference "Gyrotechnology, navigation, motion control and mobile object construction, April 19-20 2001. Kiev, pp. 211-214.

MULTIVARIATE ANALYSIS OF DIFFERENT INERTIAL NAVIGATION SYSTEMS – THE WAY TO THEIR VERSATILITY*

A.G. Andreev*, V.S. Ermakov, S.M. Yakoushin*****

Perm Scientific-Industrial Instrument Making Company,

106, 25th October Str, GSP-590, 614600, Perm, Russia. E-mail: root@ppk.perm.su. Fax(3422)45-12-19

Abstract.

Key words: navigation, simulation, designing, algorithms, accuracy

This paper deals with the application of the existed INS Flight Tests Simulation System (FTSS) for the optimization of INS design based on the multivariate analysis. For the first time this paper presents the comparative characteristics of INS main errors evaluations based on the traditional technique and that made with the help of the INS Flight Tests Simulation System. Application of the new technique allowed to define more precisely actual errors of inertial sensors – accelerometers and gyroscopes – that are the parts of the standard INS. Various applications of INS on different objects are reviewed. The multivariate analysis of influence of different sensor parameters (random error, non-linearity and instability of static characteristics scale factor, sensitive axes misalignment, pulls, cross-axis effects, etc.), dynamic operating conditions and data processing on INS outputs was carried out for all the above objects. Based on the study of the requirements imposed for the accuracy of the advanced multi-applicable INS, their size and operating conditions as well as on the results of the multivariate analysis of INS applications, the conclusion is made on the possibility of the development of two basic types of the universal INS (gimbaled and strapdown) with wide operating range.

Inertial Navigation Systems (INS) are aimed at the determination of moving objects angular position and coordinates. The main factor of the INS quality evaluation is the accuracy of its self-contained operation. At that, accuracy requirements are always in contradiction with two other important features – low cost and complicated operational environment (mostly unfavorable). Selection of INS that will totally meet the customer's requirements is a separate, rather difficult task because a lot of conflicting factors shall be considered.

It is not always possible to estimate the influence of one or another factor on INS parameters with the existed techniques of INS errors determination. The reason of it lies in the fact that INS algorithms are described by non-linear differential equations that can't be solved analytically while means of linearization are inadequate. Besides, the character of object movement in space also effects INS dynamic errors, especially those of the strapdown INS.

To overcome these difficulties the software – INS Flight Tests Simulation System – was developed, as well as methods of its application to different types of navigation systems.

For the first time this paper presents comparative characteristics of INS main errors evaluations based on the traditional technique and that made with the help of INS Flight Tests Simulation System (see Fig. 1, 2).

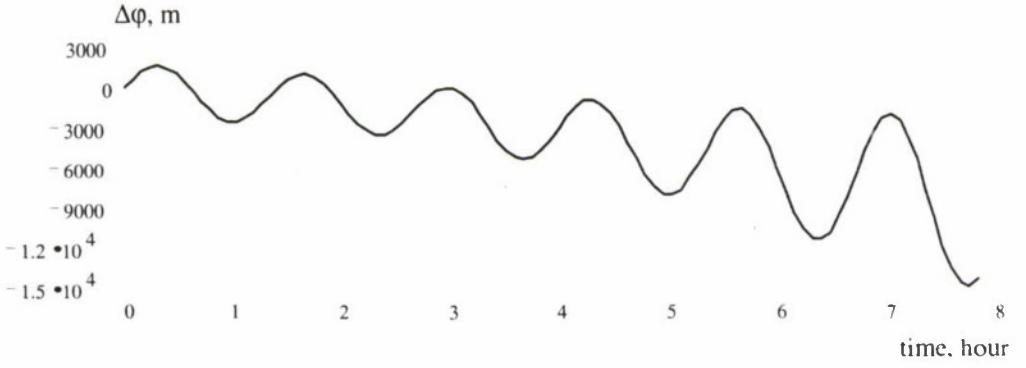

Fig.1. Difference in the positioning error evaluation on the basis of the traditional technique and that received with FTSS (influence of the INS initial alignment error with pitch angle $\Delta\vartheta = 3'$ was investigated)

* General Director.
** Executive Director.
*** D.Sc., Research Scientist.

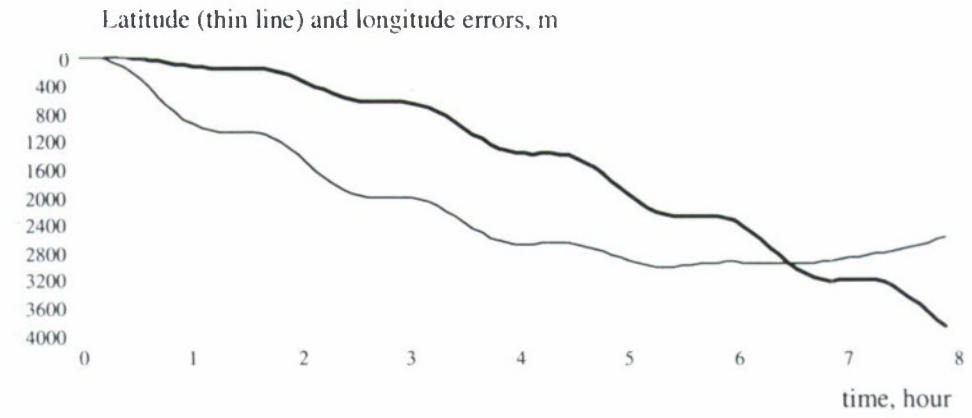

Fig.2. Gimbaled INS latitude and longitude errors due to initial alignment error $\Delta\psi = 3'$.

Application of the new technique allowed to define more precisely actual errors of inertial sensors – accelerometers and gyroscopes – that are the parts of the standard INS.

Two types of gimbaled INS – semi-analytical (with traditional dynamically-tuned gyroscopes) and analytical (with modulated dynamically-tuned gyros without torquers) – and a strapdown INS (with miniature dynamically-tuned rate sensors or fiber-optic gyroscopes) were investigated.

In this investigation project the sphere of possible applications of such systems was significantly extended compared to their present usage. It became possible thanks to high technical achievements of our Company in the development and production of very accurate inertial sensors and navigation systems.

On the whole, the following applications were studied including piloted and unmanned vehicles and robotics:

- aircrafts
- land systems
- in-tube defectoscopy
- drilling
- marine vessels.
-

The multivariate analysis of the influence of different sensor parameters (random error, non-linearity and instability of static characteristics scale factor, sensitive axes misalignment, pulls, cross-axis effects, etc.), dynamic operating conditions and data processing on INS outputs was carried out for all the above objects.

Error analysis of different INS types in the operating environment of the specified objects (angular and linear movement) was made.

Attention was also paid to INS errors due to improper initial alignment. With due account of allowed sensor errors as per specification (accelerometers, gyroscopes, rate sensors) their direct influence on the accuracy of the independent initial system alignment and their effect that arise during the coordinate reckoning of the moving object is shown. With allowance for possible integration of these inertial systems with odometer and/or satellite-aided measurements and short-time loss of information from them we present their accuracy parameters for the short periods of autonomous operation.

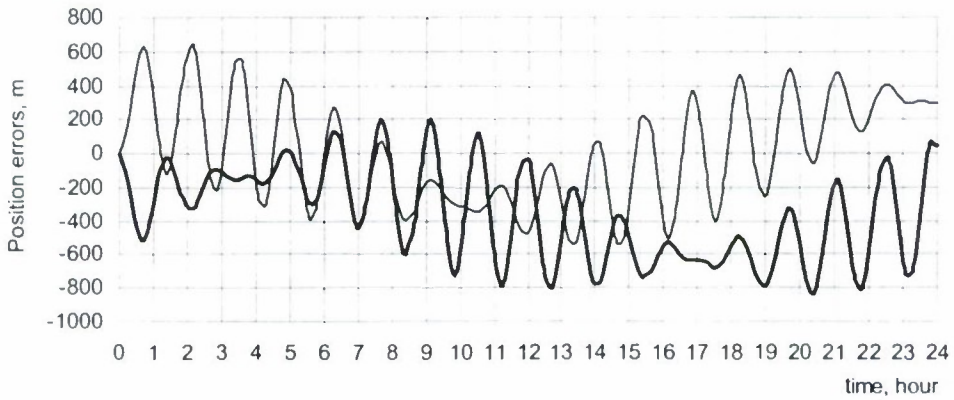

Fig.3. Gimbaled INS errors: random gyroscope drift 0.001 deg/h, accelerometer error 0.0005 m/s/s, initial alignment error (yaw - 20, pitch – 10, roll – 10 arc seconds).

Based on the study of the requirements imposed for the accuracy of the advanced multi-applicable INS, their size and operating conditions as well as on the results of the multivariate analysis of INS application, the conclusion is made on the possibility of development of two basic types of the universal INS (gimbaled and strapdown) with wide operating range. Figures 3 and 4 show the predicted accuracy parameters of the two types of the advanced universal INS in the autonomous operation mode.

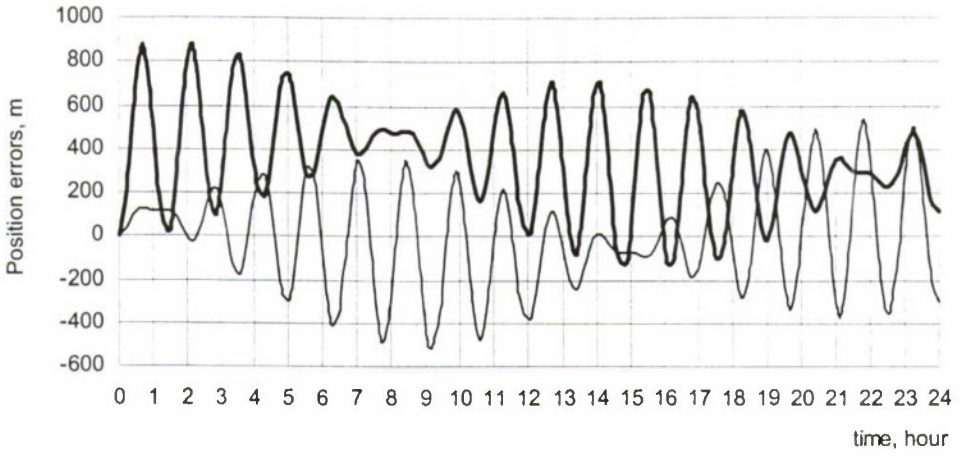

Fig. 4. Strapdown INS errors: the same conditions as for the gimbaled INS (see Fig.3)

Orientation on such an approach in the Company's prospective planning of the universal INS development will help to concentrate the efforts on the design of the units that may be adapted to different applications mainly by changes in their algorithms and interfaces.

ON APPLICATION OF THE MODULATING GYROSCOPE IN MARINE GYROCOMPASS *

V.S. Ermakov*, A.G. Maksimov, V.F.Kroupnov***, I.A.Dedok******
Perm Scientific-Industrial Instrument Making Company

Abstract

Sensitive elements of gyrocompasses shall meet the increased requirements of long and reliable service life without recalibration. Long and profound research has turned Company engineers attention to the gyroscope with the modulating principle of operation.

The main problem of the ship gyrocompasses based on DTG is the maintenance of the required service life. The weakest point here is the gyroscope ball bearing support. To provide the accuracy it is necessary to keep vacuum inside the DTG operating area, but vacuum badly influences the ball bearing lubrication, reduces its life time. In the modulating gyroscope the sensitive element is placed into the sealed ampoule where high vacuum is preserved. Modulating gyro bearings are located outside of the sealed ampoule and thus there operation conditions are more favourable than in DTG. When operating in standard pressure and temperature conditions the life time of the ball bearing support is 10000 hours and that of the gas dynamic bearing - 100000 hours.

It's worth pointing out the superiority of the gas dynamic bearing over the ball bearing in the terms of service life. Besides, the gas dynamic bearing increases the gyroscope accuracy. In serial production the cost of the gas dynamic bearing is comparable with that of the ball bearing support. This make the gas dynamic support more preferable in the applications where high accuracy and long service life are required.

Production costs of the modulating gyro sensitive element suspension machining are lower compared with DTG. The design of the modulating gyroscope allows to avoid the sensitive element disassembly for the adjustments in order to provide the required parameters of the gyroscope. Thus, the prime cost of the gyrocompass on the modulating gyro in serial production will be low.

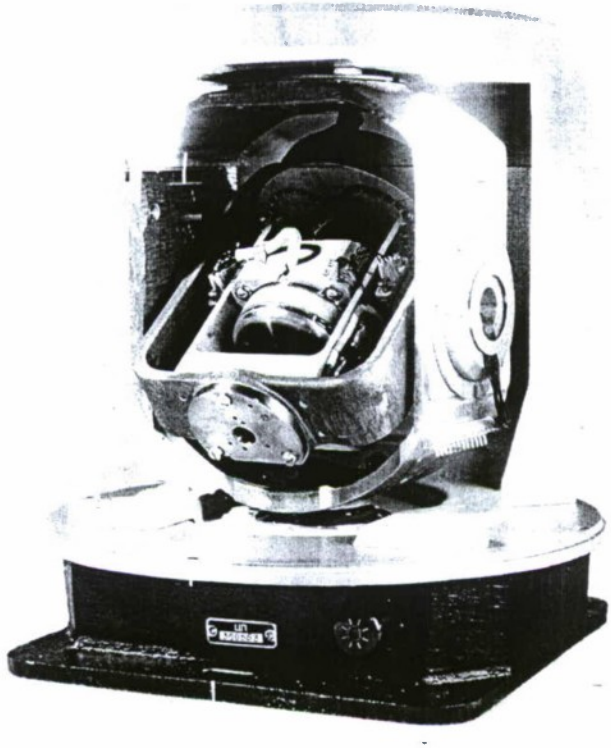

Fig.1. Cross Section of the Main Unit of the Gyrocompass "Geus"

* Honoured Doctor of Electrotechnical Sciences
** Research Engineers.
***Research Engineers.
****Research Engineers.

The investigation was carried out to determine the gyrocompass settling from the course displaced from the meridian to ± 90° and the gyroeompass behaviour near the meridian (stability and aeeuracy):

1. Determination of the gyrocompass settling aecuracy with deliberately low alignment and damping coeffieients.
2. Determination of the gyrocompass settling time with high alignment and damping eoeffieients.

Here we give the results of our investigation.

1. The this transition process the following value of coeffieients were seleeted:
2.

Ralignment = 80 kOhm
Rdamping = 220 kOhm

The settling time with the required aeeuraey from both displaeements (±90° from the meridian) was 3 hours 30 minutes.When settling was performed from the eourse +90°, the heading during the last hour made a eonstant value 338,8° (338,8° - eompass meridian).When settling was performed from the eourse -90°, the heading during the last hour made a constant value 337,9° (337,9° - eompass meridian). Differenee in the settled eourses is explained by the residual zone of insensitivity of diodes in the torquer eireuit and hysteresis of the generator with external excitation.

3. To reduce the settling time the eoefficients were ehanged:

Ralignment = 42 kOhm
Rdamping = 110 kOhm

The settling time with the required aeeuraey from both displaeements (±90° from the meridian) was 2 hours 30 minutes. When settling was performed from the course +90°, the heading during the last hour made a eonstant value 337,0° (337,0° - eompass meridian). When settling from the course -90°, the heading during the last hour made a constant value 337,8 (337,8°-compass meridian).

Conclusions

1. There is a zone of insensitivity, partieularly in the area of negative signals of the torquer. In this zone the course irregularly changes its sign and value.
2. There is an uncompensated azimuth drift that determines the settling course and in our ease it makes the pendulum rise to the definite height and escape the insensitivity zone of the torquer. 3. Settling time was not considered as an important factor at this stage investigation.
4. Non-linearity of the torquer voltage transfer charaeteristies was not taken into account. It is neeessary to take measurements for further eorrections of ω_{drift} in horizon and azimuth.

Problems that arise during gyroeompass adjustment, namely, hysteresis of the generator with external excitation that is used for control signal transmission to the gyroseope rotor as well as the insensitive zone of the eontrol eireuit mieroassembly ean be solved by the introduetion of the additional demagnetizing winding to the generator with external excitation and enhancement of the eontrol eireuit mieroassembly. Sueh modifieations may help to eliminate all the above problems and to achieve accuracy of 0,1° x see φ, that is higher than the present level of aeeuraey for the gyroeompasses of this grade.

FUNCTION-ORIENTED PROCESSORS AS THE BASIS FOR DIGITAL ELECTRONICS OF THE INTELLIGENT SENSORS FOR NAVIGATION SYSTEMS*

Niek A. Lookin*

Science & Production Association of Automatics, 145, Mamina-Sibiryaka St., 620075, Ekaterinburg, Russia
Institute of Engineering Science Urals Bransh of Russian Academy of Science, 34, Komsomolskaya St., 620219, Ekaterinburg, Russia
E-mail: lookin@imach.uran.ru

Abstract

Key words: sensor, functional-oriented processor, spline-approximation, function

Development of optimal functional-oriented processors (FOP) for fast function computation in navigation system sensor digital hardware is considered. The main expression for function computation by means of table-polynomial FOP realizing spline – approximation as a base numerical method is given as an example. Existence of minimum FOP hardware complexity for arbitrary analytical function has been justified. Formula of minimal possible polynomial power for given computation error is presented. Common scheme for FOP synthesis algorithm is considered.

Introduetion

Improvement of sensor electronics for achievement of high accuracy, stability and reliability is one of the main directions of navigation system development. Today electronic devices may occupy up to sixty percent (for example in fiber-optic gyro). These devices are mainly analog this restricts sensor accuracy, stability and sensitivity. Changing hard transformations in analog electronics by adaptive data and signal processing in digital hardware is one of the most perspective ways of sensor improving. Standard mathematical transformations such as elementary functions (for example y = Sin x) are often required. Standard microcontrollers (μC) and digital signal processors (DSP) used in sensor electronics have two main peculiarities:

• Most of the modern μC and DSP architectures are universal but their command sets are oriented to effective implementation of control procedures (μC) or signal algorithms (DSP). In some cases this may results in expensive hardware or time complexity especially if just small number of certain functions (such us Sin x) have to be computed in sensors.

• Standard μC and DSP can perform most of the required computational procedures for modern and perspective sensors with the help of software only (standard subroutines), it requires processing with high frequency (order of ten MHz). This results in high level of noise for sensitive circuits measuring very small parameters (for example, nanoamper current for hemispherical resonator gyro).

In the case when standard mathematical function (for example algebraic or trigonometric) computation with guaranteed accuracy is needed hardware computing with the help of functional-oriented processors (FOP) may be more efficient than μC and DSP. The paper is devoted to some problem of optimal FOP development

Functional-oriented processors and some problems of their architectures synthesis

FOP's application is useful and effective when high performance of computations is necessary. For example, mathematical coprocessors are most effective in achieving maximum performance for supercomputers [2]. It is interesting that additional hardware expenditures in that case are not very high [1]. Today FOP entirely may be produced as one chip of VLSI. This makes advisable their active usage them for mathematical functions computations in sensors electronics.

There are a number of methods providing either maximal computation speed for fixed hardware complexity or minimal complexity for fixed performance in development of optimal FOP. These methods have important significance for navigation systems sensors because of two main reasons:

• **Minimum** hardware complexity of electronics is required for most sensors. For example, all possible electronics and sensitive element for each axis of micromechanical gyro must be placed on single semiconductor chip. This is extreme but real case for actual sensors.

• **Maximum** data processing rate for control and stabilization feedback circuits is needed because high quality control and stabilization are required.

Thus simple and typical decisions on FOP realization that are used by designers may not be acceptable for perspective sensors requirements. Theory of optimal FOP development is still absent.

---

* PhD, Head of Department

Results of researches obtained by numerous scientists and engineers [2], [3], [4] show that table-algorithmic approach based upon polynomial spline approximation is one of the most perspective approaches to hardware realization of function computation. Method of the functions computation on FOP is based on the following expression:

$$F(X) = F(X1 + X2) = \sum_{i=0}^{m} (A_{(X1)})_i (X2)^i + \rho_{m+1}, \quad (1)$$

where $(A_{(X1)})_i$ are polynomial coefficients that represents some computable functions of argument X1; ρ_{m+1} is remainder expansion term. Binary digital code X may be represented always as $X = \chi 1 \cdot 2^{n_2} + X2$, where χ is "high order" part of argument X, n2 is a number of digits of the "low order" part named by X2. So if $X1 = \chi 1 \cdot 2^{n_2}$, then $X = X1+X2 = X1 \vee X2 = X1 \oplus X2$, i.e. we have simple disjunctive decomposition X: $\{X\} = \{X1\} \cup \{X2\}$ and $\{X1\} \cap \{X2\} = \varnothing$.

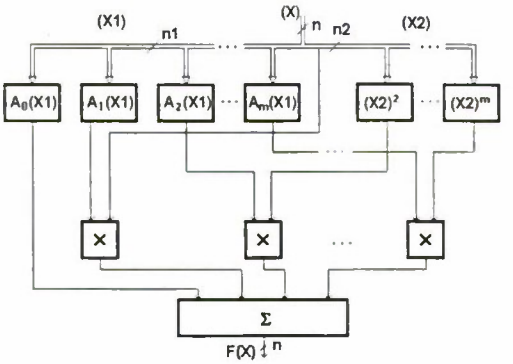

Basic FOP architecture

Following scheme of computation F(X) corresponds to proposed representation of argument X:

- code of argument X is divided on two independent components those are "high order" X1 and "low order" X2 in functions $(A_{(X1)})_i$ are computed independently;
- they are multiplied with corresponding terms $(X2)^i$, i = 0,1,...,m with final adding. FOP base architecture is represented on the figure.

FOP architecture consists of memory coefficient blocks (MC), multipliers (MULT), degree computation block (DB) and adder (S). Blocks MULT and DB implement parallel algorithm of concurrent multiplying all digits of co-factors (matrix type structure of multiplier). This hardware has homogenous structure. Besides MC blocks are memories so has homogenous structure as well. Thus nearly 80 percent of all the architecture are uniform that is preferable for FPGA implementation.

Using upper bound of computation complexity for schemes consisting of functional elements may allow establish the following. Hardware complexity for computation $(A_{(X1)})_i$ is evaluated as $L_{A(X1)} = O(2^{n1})$ and complexity for computation "low order" part of code, i.e. X2 is evaluated as $L_{(X2)^i} = O(n - n1)^2$). In generally it implies that L_{FOP} has one minimum for $n1_{opt}$ and $0 < n1_{opt} < n$. This implies the "slowest" FOP (with sequential function computation) not to be very low-cost. Though known point of view for computer science is loss of the performance because of decreasing hardware complexity. For example for optimal FOP computing Sin (x) with $\delta_f \le 2^{-31}$ n1 = 5 but not n1 = 0.

The minimal possible power m of polynomial for given computational error δ_f is the most important parameter for FOP development. Dependence between m and n1 is essential. For arbitrary analytical functions with any absolute magnitude not exceeding 1 correct formula is as follows:

$$m > \left| \left\lfloor \sqrt{(n1 + l - 1)^2 + n \cdot 2^{l(l-1)}} - (n1 + l - 1) \right\rfloor \cdot 2^l \right|, \quad (2)$$

where for n < 32 parameter l equal 1,2 or 3 depends on proportion $\frac{n1}{n}$.

On the ground of computation error for given mathematical function the upper bounds hardware and time complexity (L_A and L_T) for polynomial coefficient $(A_{(X1)})_i$ (L^{MC}), multiplication (L^{MULT}), exponentiation (L^{DB}) and final addition (L^S) may be obtained. Overall L_A and L_T estimates for FOP may be obtained as well.

Thus for FOP computing F(X) with δ_f = const optimal architecture synthesis algorithm consists of three main steps:

1^0. Determination $n1_{opt}$.

2^0. Determination $m = f(n1)$.

3^0. Evaluation of L_A and L_T for all FOP blocks and its architecture construction.

There are three basic types of FOP architecture, those are parallel (P-FOP), sequential (S-FOP) and mixed intermediate (PS-FOP and SP – FOP). P-FOP is preferable for function computation errors $\delta_f \le 2^{-16}$ and S-FOP for $\delta_f \le 2^{-32}$.

If FOP realization is based on FPGA, then MC, MULT, DB and S blocks may be implemented as a standard library VLSI element. In addition MC blocks may be implemented sometimes on the base of RAM. This allows computing different function at the expense of changing data in RAM.

Conclusion

1. Functional-oriented processors are effective means for digital data processing in electronics of navigation system sensors. In addition hardware and time computational complexity may be smaller then for standard microcontrollers or DSP.

2. For table-polynomial FOP computing functions by means of spline-approximation algorithms main architectural parameters depend on proportion between "low order" and "high order" parts of argument code. Formula for minimal possible power of polynomial representing analytic functions with arbitrary absolute magnitude not exceeding 1 is presented. It is proved that upper bound of hardware complexity has minimum for only one possible representation argument as combination "low order" and "high order" parts. This allows constructing optimal FOP architecture synthesis procedures. General form one of those procedures is presented as well.3. FOP application provides further improvement of navigation system sensors and makes the base for development of embedded intelligent for new generation sensors. Modes of measuring, monitoring, ensuring reliability and "vitality" will be provided in these sensors.

References

1. **Oransky A.M.** Hardware methods in computer science. – Minsk: BGU Edition, 1977. In Russian.
2. **Ercegovac M.D., Lang T., Muller J.-M., Tisserand A.** Reciprocation, Square Root, Inverse Square Root, and Some Elementary Functions using Small Multipliers. Research Report № 97-47, Ecole Normale Superériere de Lyon, Laboratoire de l'Informatique du Parallélisme, November 1997.
3. **Functional** oriented processors / Vodyaho A.I., Smolov V.B., Plyusnin V.U., Puzankov D.B.; Ed. by Smolov V.B. – Leningrad: Mashinostroenie, Leningrad branch, 1988. In Russian.
4. **Lookin N.A.** Problems of digital functional transformers architecture design // Architecture design automation for special-purpose processors. Coll. of papers. Ekaterinburg, Urals Bransh of RAS, pp 47 – 60. In Russian.

SYSTEM OF DIAGNOSTICS OF A CONSTRUCTION STRUCTURE STATE

A.A. Elizarov, B.S. Konovalov, S.F. Konovalov,
D.T. Mayorov, A.V. Polynkov, A.A. Trunov
Bauman Moscow State Technical University (BMSTU)
2nd Baumanskaya Str., 5, 107005 Moscow, Russia, E-mail: serguei.konovalov@mtu-net.ru
V.V. Yurasov
Scientific & Production Center "Automatics and Instrument Making" (SPC AIM), Moscow, Russia
Kwan Sup Lee
KRRI, Seoul, Korea

Abstract

Key words: accelerometer, inclinometer, spectrum, operation of bridges

The system of diagnostics of construction structures that capable (depending on variant of its set) of ensuring either periodic or continuous monitoring of a structure state under operation conditions is described in the paper. The system includes one accelerometer of compensation type with a vertical measuring axis and two compensation type inclinometers. The sensors are connected either to a computer or a microcontroller that provides three-component measurement of spectra of translational vibration and 2D measurement of inclinations. The information from the system is transmitted to the central computer by means of the radiomodem. Due to high resolution of the accelerometers, used in the system, and inclinometers of navigational class, it provides the sure measurement of oscillations of construction structures caused by traffic load, wind load, operation of lift equipment etc. The results of measurements of vibration spectra and inclination rate of different Moscow metal and ferroconcrete bridges, Moscow TV tower, the main building of Bauman State Technical University are presented in the paper. The fact that operation loading of tested structures in the case of enough long survey (about 30 minutes and more) in frequency range of 0.5 ... 30 Hz are equivalent to effect such as "white noise" is shown in the paper. The requirements to sensors of the system are defined in the paper.

Introduction

For prevention of emergency in service of such construction structures as bridges, TV towers, buildings it is necessary to carry out periodic inspection of their state. The part of construction elements can be inaccessible for direct inspection, and for this reason it is difficult to reveal that destruction of these elements, which can be dangerous for further service of a structure. At the same time some observable destruction of structure surface can be uncritical, as they have no effect on strength features of structure.

The objective information of destruction of elements of similar structures can be obtained from information of changing natural frequencies of vibration of structures and from occurrence of permanent speed of structure inclination.

The system of diagnostics of construction structures is capable (depending on its modification) to provide either periodic or continuous control of structures state during their operation.

♦

The high metrology characteristics of modern navigation devices and their decreasing prices allow to find for them new and sometimes unexpected application. The inclinometer of floated pendulous compensation type shown in Fig. 1 (which was designed approximately 20 years ago in joint research of SPC AIM named after academician N.A. Pilyugin and BMSTU) can be grouped with such devices. These devices provide the resolution at the level of 0.001 arc. sec and long-time stability of zero signal at the level of 0.03 arc. sec within the range of measured inclination up to 6°. To confirm so high resolution and stability of the inclinometer zero signal (or bias), it is necessary to provide rather careful checking both appropriate methodical and metrology furnishing. During this check three inclinometers were installed in a common case so that their measuring axes were parallel and the signal was concurrently registered from three devices. Doing so we assumed that the consistent changes of signals are indicative of change in the basis inclination, and inconsistent changes - of inherent drifts of devices. Most difficult problem is the determination of long-time stability of zero signal of devices. These experiments were performed in Institute of Physics of the Earth (city of Obninsk). The case with three devices under test was installed on the base located on basalt rock in the measuring mine at depth of 80 m. The constant temperature was kept by natural way; the measurements were conducted without man's participation. The total duration of the measuring was 2 months. Bias of all inclinometers relative to each other did not exceed 0.03 arc. sec. It is interesting to note that during all period of the measurements the matched harmonic changes of signals of three inclinometers (Fig. 2) were being registered. The period of the changes was 24 hour, and amplitude ~ 0.02 arc. sec. It has been established that the reason of these oscillations of the base are the tidal deformations of the crust caused by lunar and solar attraction (theoretically a greatest deflection of the vertical due to influence of the Moon is 0.035 ", and the Sun is 0.016 " appropriately).

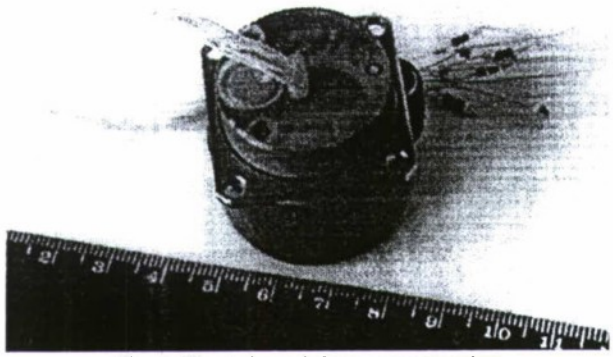

Fig. 1. Floated pendulous compensation inclinometer

The first our attempt of inclinometer application in area of studies of building structures was the use for the purpose of certification of measuring substructures in workshops and laboratories employed for testing navigation devices. The picture of motions of precision isolation substructure, installed in laboratory of navigational measurements of Harbin Polytechnical Institute (China), is shown in Fig. 3. Here, in addition to slow trend of the base through angle in value approximately equal to 0.03 arc. sec. during a day, the periodic motion with 24 hours cycle was revealed, and the speed of the substructure inclination was varied appreciably within a day. Moreover, the oscillation amplitude in direction NS (Fig. 3) was considerably greater the amplitude in direction EW (Fig. 4). It has been established that this periodic motion had been caused by sunlight heating of ground surface before the building. The second day of the tests was sunnier as compared with the first day, resulting in appropriate increase in the substructure inclination amplitude registered during the second day.

In process of preparing the measuring systems for testing the substructures, preliminary long term measurements were performed at laboratories of the department "Gyros and Navigation Complexes" placed on 10th floor of BMSTU Main building. In the case of long records the angular oscillations of the building were registered (mounting bracket of the device was fastened to the building fundamental wall). As it was found out, these oscillations have high-frequency components in frequency band 0.5 Hz ... 5 Hz (mainly these oscillations are translational motions) and low-frequency angular motions with period 24 hrs from the building inclinations caused by solar radiation. The plot of apex motion of the building (in sunny day on 19 April) corresponds to shape shown in Fig. 5. The fragment of the building motion due to solar radiation is presented in the right part of the Figure. The horizontal sections of the plots are well-recognized in the Figure and they are consistent with period of shading the surface by a cloud. It is interesting to note that the moment of stopping the building motion coincides with the moment of closing the sun by a cloud with an accuracy of 1...2 sec, and the motion restarts after leaving a cloud as fast as it stops. In studies of the building motion we have determined the following:

1. Random high-frequency translational oscillations of the building have the characteristic resonant frequencies in the spectrum, which are kept constant in observations over many years. These frequencies remain constant in conditions of various intensity of the building oscillations, observed at day and night time and, it is

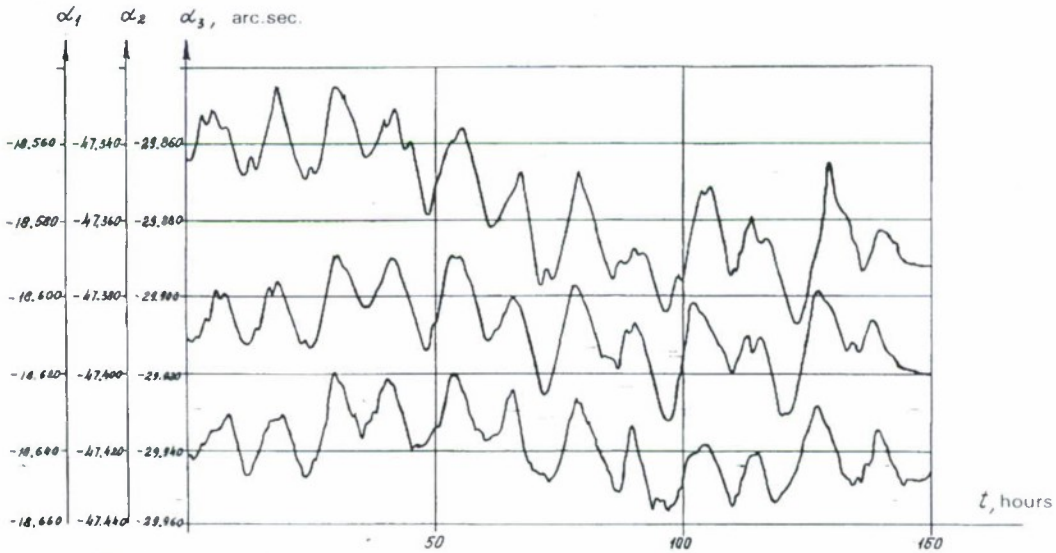

Fig. 2. Tidal oscillations of Earth's crust registered by 3 inclinometers

more probable they correspond to frequencies of main vibration mode shapes of the building.

2. Low-frequency oscillations of the building (with 24 hrs period) can change the amplitude depending on the season and the weather, but they are placed around the center which does not change its position relative to a vertieal.

These results have forced us to think of relation between registered parameters of the building motion and its teehnical state. However, we received the main impulse to development of similar system of early diagnosties of building structures when the tragedy had happened several years ago in Seoul, where the bridge span has fallen into Han river in rush hours. It is important to note that periodic inspection of the bridge, carried out in close time interval before the tragedy, have not shown any features whieh could be as indicatives of unsatisfaetory state of the bridge. The tragedy was accompanied with numerous victims, it had a large public resonance and, as a result, the governmental program on creation of system of early diagnostics of state of bridges has appeared.

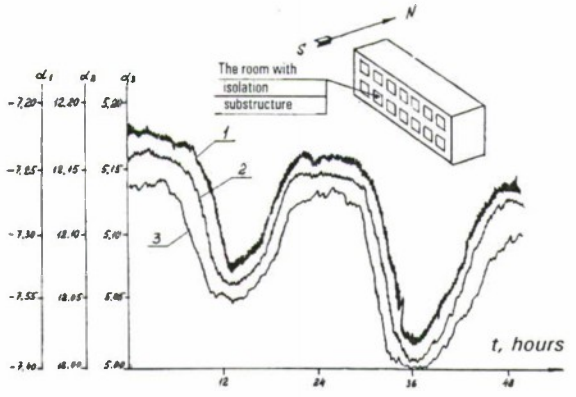

Fig. 3. Oscillations of isolation substructure in plane of meridian (Harbin)

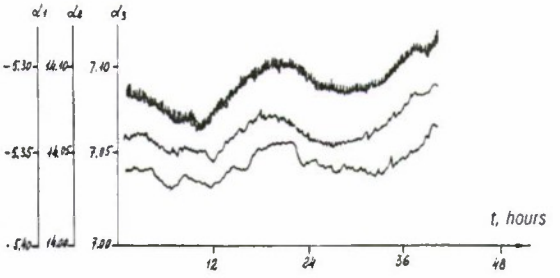

Fig. 4. Oscillations of isolation substructure in plane East-West (Harbin)

Department of "Gyros and Navigation Complexes" at Bauman Moseow State Technieal University has close relations with many firms in Republic of Korea and carries out joint development of accelerometers and inclinometers for last 10 years. Basing on experienee of using accelerometers and inclinometers in analysis of motion of building structures as well as on the information eontained in publieation [**Ahmed M. Abdel-Ghaffar, Robert H. Scanlan** Ambient vibration studies of Golden Gate Bridge: I. Suspended structure // Journal of Eng. Mech., Vol. III, No 4, April 1985.], we have offered one of Korean firms to execute joint developing the system of early diagnostics of a state of building structures bon the base of measuring speetra of their oscillations and slow angular motions. The results of this joint development are represented in the paper.

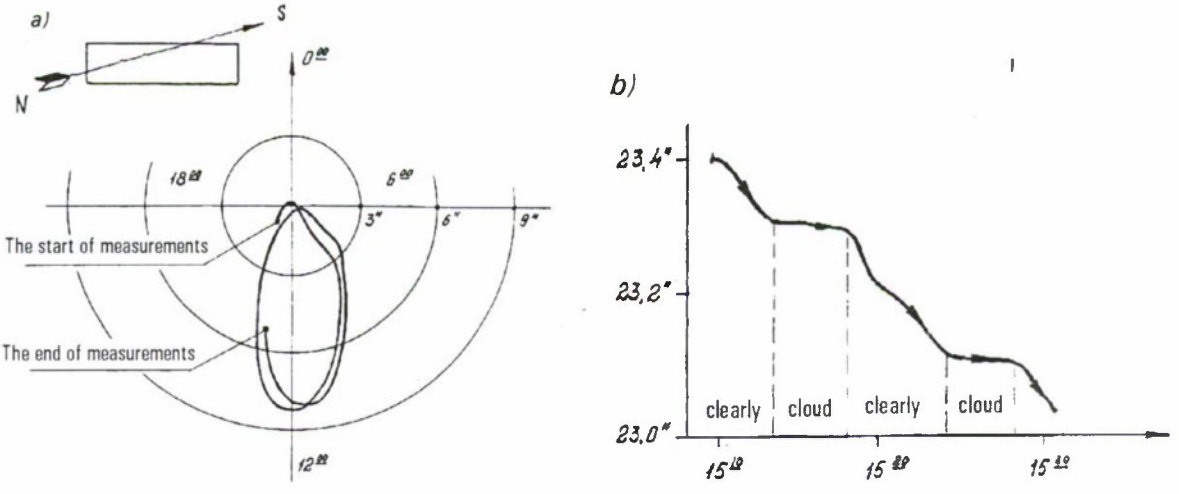

Fig. 5. a - daily motion of apex of the main building of BMSTU
b - the apex motion change with change of solar radiation

The first obvious indieation of the beginning of bridge disruption is the inelination of bridge deck being increased with time. For the bridge in a normal eondition the ehanges in the deck inelination are conneeted with ehanges with time of a statie load exposed to the bridge. Namely, it is eonnected with change in average intensity of traffie, and also with thermal deformation of elements of the bridge under ehanges of the ambient temperature, the solar radiation and availability of eontinuous wind load. For the bridge under destruetion, to these small

motions of reversible character which can be well observed by means of inclinometers, the irreversible angular motions can be added of the deck connected with such problems as sags of bridge support elements, occurrence of residual strains due to effect of great loads and disruption of construction elements of the bridge. Naturally, in the case of significant irreversible motions of the bridge deck the alarm signal should be produced with following stopping the bridge operation to carry out an additional thorough investigation of the bridge.

The second indication of the beginning of bridge disruption is a sharp change of the dynamic characteristics in bridge service. The sharp change of dynamic characteristics can testify of occurred destruction of separate supporting elements of the bridge, which provide its design rigidity. In case of detection of dynamic characteristic changes, also it is necessary to suspend operation of the bridge and to make thorough investigation of state of all bridge elements.

Dynamic characteristics of construction structures can be analyzed from frequencies of the main shapes (modes) of their oscillations. In common practice the special experiment is carried out to determine these frequencies. The springboard is installed on the bridge under test, from which the heavy automobile falls on a surface of the bridge with following exciting large oscillations of the bridge. These oscillations are easily registered with the help of rough accelerometers. The implementation of such experiment requires temporary removing the bridge from service and it is enough expensive and labour-consuming procedure. If we use highly sensitive accelerometers to measure parameters of the bridge motion, it makes possible to determine natural frequencies of oscillation shapes by more simple method without removing the bridge from service.

Dynamic effects of such environmental excitations as vehicular traffic, gusts of wind, water flow and waves acting to the bridge piers, produce small angular and translational vibration within frequency range from fractions of 1 Hz up to 30 Hz. These random effects applied to the bridge have non-stationary character, and the parameters of these effects are unknown. Proceeding from this, at first sight, it is impossible to receive authentic information of frequencies of the main shapes of the vibration by means of investigation of the bridge motion caused by these excitations. Nevertheless, with the help of installation shown in Fig. 6, we have conducted the investigations of bridge motions caused by service loads.

Fig. 6. The system of diagnostics of a construction structure state

The equipment includes two inclinometers with horizontal measuring axes (these devices make simultaneous registration of slow inclinations of the bridge and high-frequency translational acceleration in the frequency range up to 100 Hz) and one accelerometer with measurement range **2 g** and vertical measuring axis. The signals through the interface card enter the personal computer, where three arrays are formed, which correspond to three components of the bridge acceleration a_x, a_y, a_z . Number of elements of sampling the analog signal is N at step h by time. Thus, total time of the sampling is $T_1 = N \cdot h$. Spectral densities S_{ax}, S_{ay}, S_{az} are calculated in a computer for each sampling, and here the method of building spectrum is not essential as there is no restriction for using computer time. Then averaged spectrums are defined as follows:

$$\overline{S}_{ax} = \frac{1}{M}\sum_{n=1}^{M} S_{ax_n}; \quad \overline{S}_{ay} = \frac{1}{M}\sum_{n=1}^{M} S_{ay_n}; \quad \overline{S}_{az} = \frac{1}{M}\sum_{n=1}^{M} S_{az_n};$$

for number M of samplings, i.e. total observation time $T_2 = M\ N\ h$ Taking into account that higher frequency in the measured spectrum is 30 Hz, we have chosen h = 0.003 s for the measuring system. As the disturbance applied to the bridge has non-stationary character, and its parameters and dynamic characteristics of the bridge are unknown, it is impossible to estimate beforehand period T1 and T2 required for qualitative measuring spectrums of our interest. These periods were varied during experiments and their optimum values were determined for the following reasons:

1. It is desirable to have minimum time T_1 so that to execute the express control of measuring process.

2. While observing spectrums S_{ax}, S_{ay}, S_{az} with sampling duration T_1 within the range from 2 s to 100 s, considerable changing spectrums were registered from sampling to sampling. If the averaging time T_2 is within the range from 5...10 min, there are the same problems also for spectrums $\overline{S}_{ax}$, $\overline{S}_{ay}$, $\overline{S}_{az}$. With increasing time T_2 up to 20 minutes and more, the registering spectrums $\overline{S}_{ax}$, $\overline{S}_{ay}$, $\overline{S}_{az}$ keep constant view. It gives us the basis to consider that disturbing action on the bridge can be considered as stationary process when observation time is more than 20 minutes

3. If sampling time T_1 is within the range from 2 s to 10 s, then satisfied resolution in frequency is not provided due to the fact that close frequencies of vibration shapes are masked in averaged spectrums $\overline{S}_{ax}$, $\overline{S}_{ay}$, $\overline{S}_{az}$ ($T_2 = 30$ min). And with increasing T_1 from 2 s to 10 s the width of spikes in the spectrums becomes appreciably decreased and the new frequencies are revealed.

With changing T_1 within limits from 30 s to 200 s the registering spectrums $\overline{S}_{ax}$, $\overline{S}_{ay}$, $\overline{S}_{az}$ ($T_2 = 30$ min) keep unchangeable form. It gives us the basis to assume that satisfied resolution in frequency is provided at $T_1 \geq 30$ s.

Optimum values $T_1 = 30$ s и $T_2 = 30$ min have been determined for a number of bridges in Moscow, Seoul and Harbin as well as for the Ostankinskaya TV-tower in Moscow. Thus, they can be used in analysis of urban building structures without additional investigations. If needed to analyze some unique structures (for example, bridges with very long spans), the additional experiments may be required to define specific intervals T_1 и T_2. And procedure of choosing parameters T_1 и T_2 is held the same.

Results of measuring spectrums of a number of bridges located in Moscow (Fig. 7 ... 10) are given below.

The spectrums of oscillations of Ostankinskaya TV-tower are given in Fig. 11. On the basis of results of given measurements it is possible to do a number of conclusions.

1. For large number of investigated objects the distribution of resonant frequencies essentially differs from object to object and it is kept constant for each object irrespective of such factors as intensity of vehicular traffic, quantity and velocity of moving vehicles, phase of a day, the season, the weather. Their amplitudes of the registered peaks vary only. Such picture is possible only in the case when the investigated objects keep constant their dynamic characteristics, and also the input operating action is either white noise or slightly colored white noise. In this case the registered frequencies correspond to the actual shapes of oscillations of the bridge, and it is possible to consider them as criterions of estimating a structure state.

2. On the basis of results of measuring vibration spectrums of buildings and TV-towers caused by operating loading, conclusions can be done similar those obtained from analysis of the spectrums of bridge oscillations. However here, in high-frequency area of the spectrums the spikes, caused by existence of harmonic components in disturbing action, can be added, for example as, vibration connected with operation of such equipment as fans, machine tools etc. These spikes occur and disappear at switching on or switching out appropriate equipment. The frequencies of spikes caused by harmonic vibration from working equipment are located in frequency band above 15 Hz, which considerably exceeds natural frequencies of building oscillations (usually 5 Hz max.), and so they can be easily separated. More complicated picture is observed in measuring spectrums of oscillations of Ostankinskaya TV-tower (Fig. 12). Here spikes in the frequency band 12 ... 25 Hz can correspond to frequencies of the first tone of oscillations of steel tension ropes of the TV-tower, i.e. they correspond to actual oscillation frequencies of the structure. This question requires additional investigations.

Thus, it has been found that when measuring motions of bridges and building structures caused by operation loading, the spectrums are registered which look like summarized polyharmonic process and random noise. The frequencies, registered in lower area of the spectrum, correspond to frequencies of the basic shapes of oscillations of a building structure and they can be considered as criterions of estimating safety of the structures.

There are two variants of using the method designed for monitoring bridges and building structures.

1st method. Mobile system designed for monitoring construction structures (Fig. 6).

In this case a platform of the system is installed on bridge surface free from moving transport (for example, on a sidewalk), after aligning the platform in horizontal plane, the procedure of measuring spectrums of bridge oscillations and inclinations are carried out over observation period. If the site of installing the equipment is inconvenient to arrange the operator and personal computer, the system is capable of transmitting the information from its sensors by means of radiomodem to personal computer located in a vehicle. The experience shows that it is enough to have observation period in one position no more than 30 minutes to obtain the comprehensive information about spectrums of oscillations. Using the appropriate equipment, the team makes sequential measuring of motion parameters of the bridges in which Customer is interested and form preliminary speeds statistical information about frequencies of the oscillations shapes of and inclination rates of bridge deck.

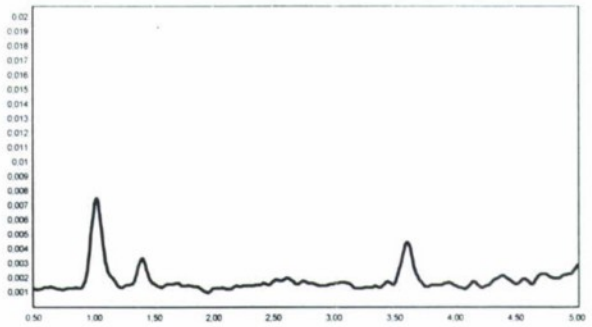

a) axis X

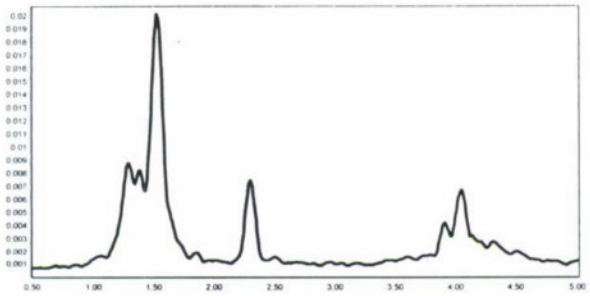

b) axis Y

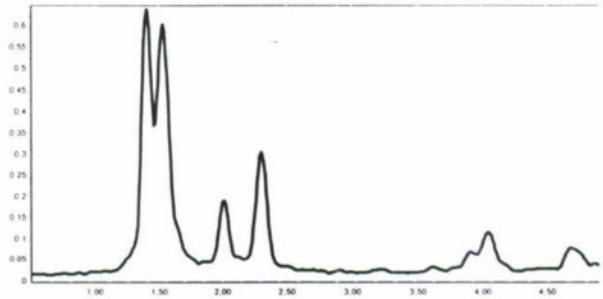

c) axis Z

Fig. 7. Sight and spectrums of Ust'insky Bridge oscillations

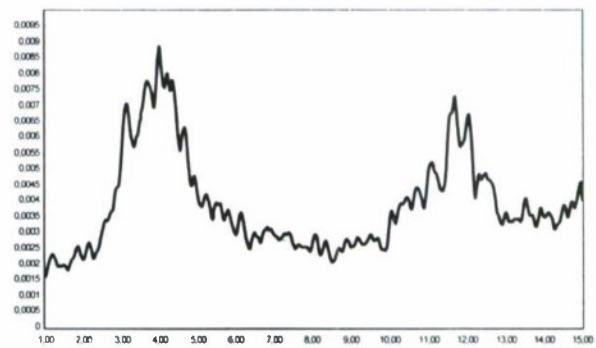

a) axis X

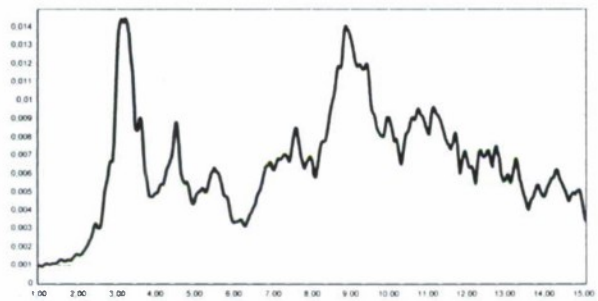

b) axis Y

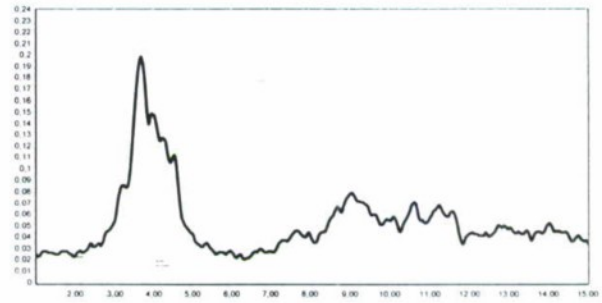

c) axis Z

Fig. 8. Sight and spectrums of Vysokoyauzsky Bridge oscillations (ferroconcrete bridge)

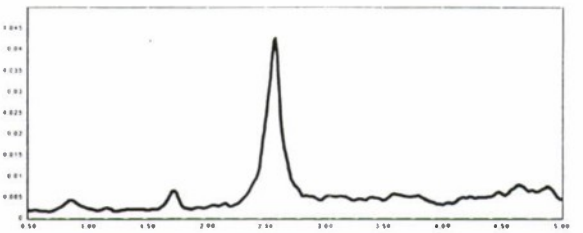

a) axis X

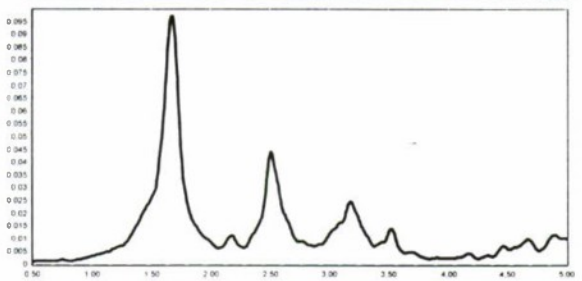

b) axis Y

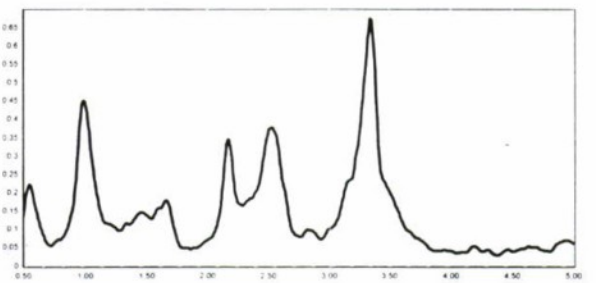

c) axis Z

Fig. 9. Sight and spectrums of Berezhkovsky Bridge oscillations

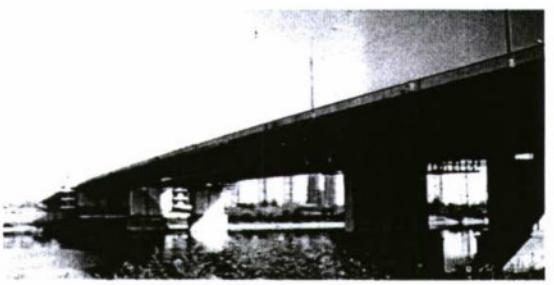

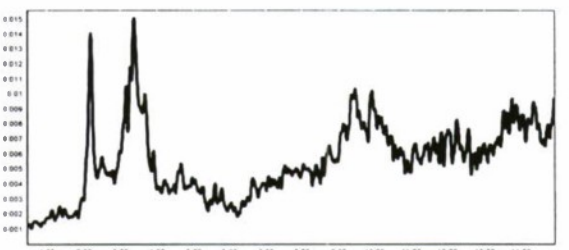

d) axis X

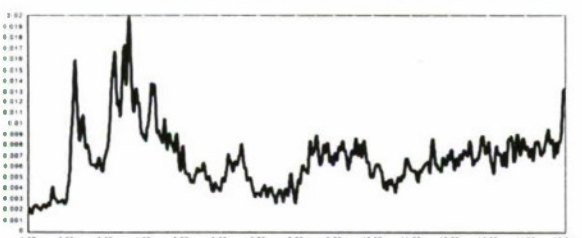

a) axis X

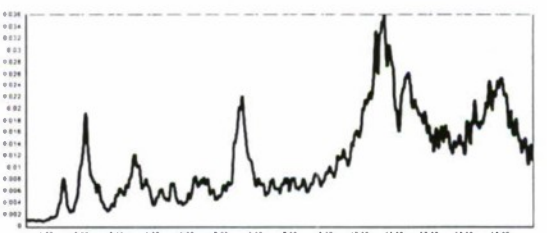

e) axis Y

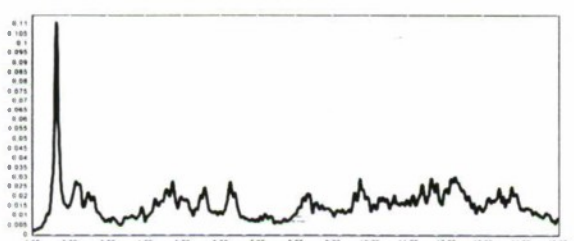

b) axis Y

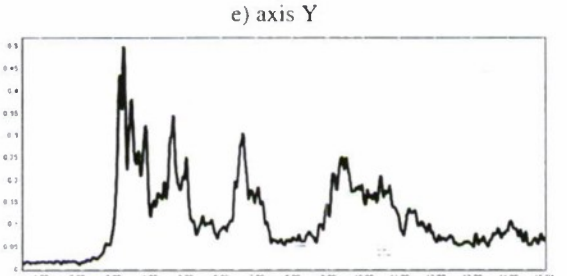

f) ось Z

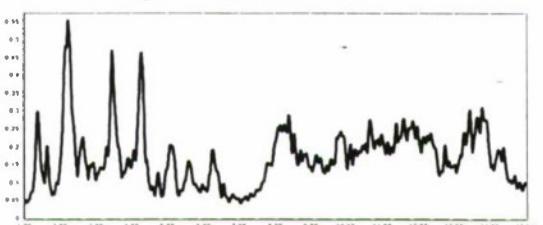

c) axis Z

Fig. 10. Sight and spectrums of Brateyevsky Bridge oscillations

spectrums a), b), c) - measured in the middle of the main metal bridge span.

spectrums d), e), f) - measured in the middle of side span made of reinforced concrete (approach trestle bridge)

The given instrumentation can be used for determining not only inclination rate, but absolute changes of angles of the bridge deck inclination as well, which vary from one regular test to another. However, the special mounting pads should be provided on a surface of the bridge to effect such measurements

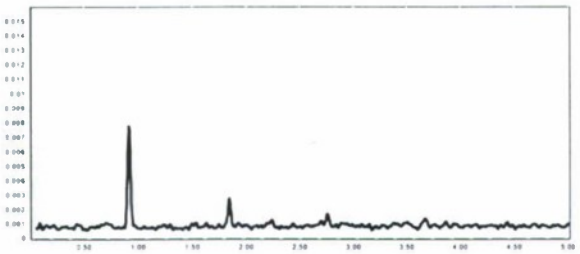

a) axis X

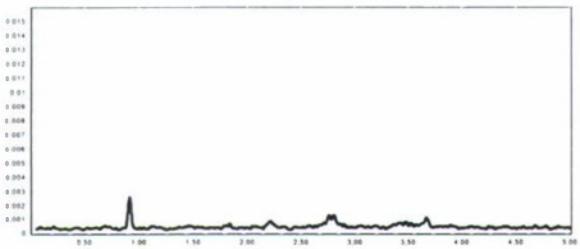

b) axis Y

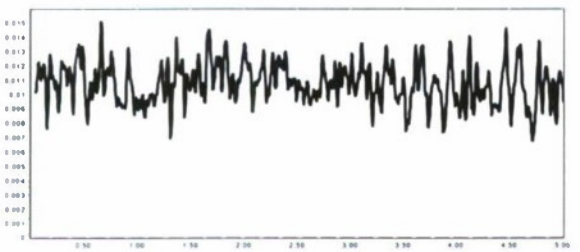

e) axis Z

Fig. 11. Low frequeney area of speetrums of oscillations of Ostankinskaya TV-tower at level of 47 m.

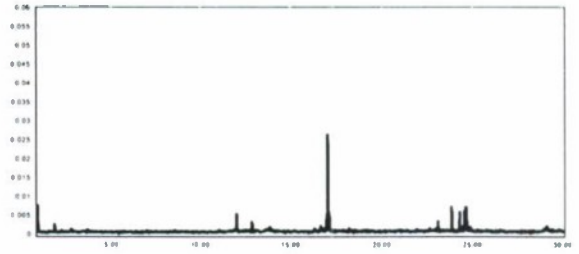

a) axis X

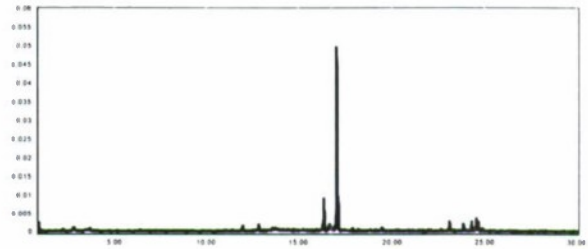

b) axis Y

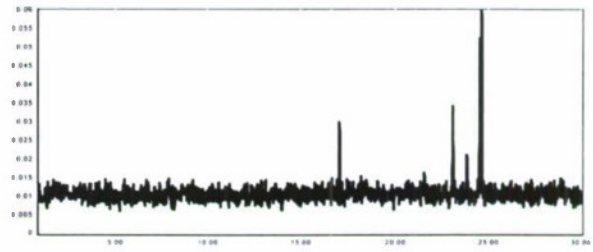

c) axis Z

Fig. 12. Full spectrums of oseillations of oseillations of Ostankinskaya TV-tower at level of 47 m..

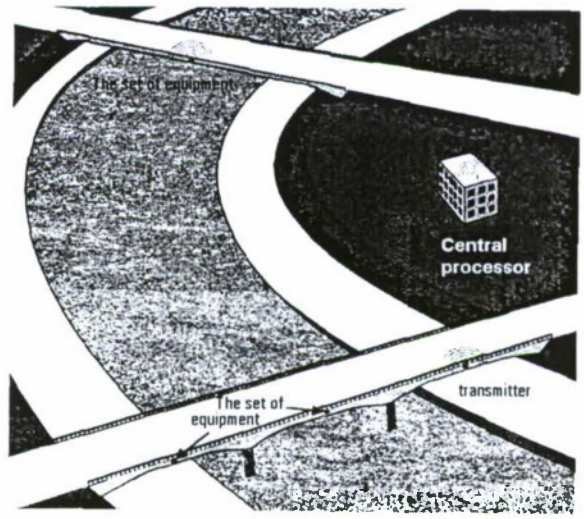

Fig. 13. Seheme of the stationary system

2nd method. The stationary system (Fig. 13).

This system is more expensive and eomplieated. sinee a triad of aeeelerometers with independent power supplies, mieroeontroller and radiomodem designed for linking eaeh sensor to the eentral processing unit is to be installed on eaeh span of the bridge. The eentral processing unit executes a continuous control of dynamie parameters and inelinations of a number of building struetures (for example, all bridges loeated in the city). Sueh system is more reliable. However, for realizing stationary system it is neeessary to develop eheap preeision inclinometers and accelerometers. In our view this task is quite realistic.

Conclusion

The present instrumentation makes possible to measure ehanges of inclinations and frequeneies of main vibration modes of bridges and other building struetures during their operation. The methods of deteetion of starting disruption of bridges and building struetures on the base of incremental inclinations of structures and frequeneies ehanging the main modes of their oseillations are developed. The disadvantage of both mentioned methods is the absenee of elear answer to question: what ehanges of strueture dynamie characteristics and ehanges of the inelination angles (or value of inelination rate) ean be eonsidered as eritieal indieations, whieh are signaling of neeessity to suspend serviee. It is obvious that these tasks should be solved separately for each object, however, for now there are no solutions of such tasks. The situation of uneertainty ean be solved with regard to the following cireumstance.

In designing bridges and other building struetures large safety factors are chosen, therefore only essential and eomplex destruetion of strueture construetion elements ean lead to an emergeney. In this ease a significant ehange of eonstruetion rigidity inevitably occurs whieh should result in eonsiderable ehanging the frequeneies of main vibration modes of the strueture. The small ehanges (about fraetions of pereent) of frequeneies values of main vibration modes should not be considered as an indication to alarming. Nevertheless, the absenee of precise eriteria for definition of dangerous states of struetures does not make possible to eliminate eompletely probability of appearanee of spurious alarm signals. However it is better than calm waiting for a erash.

CALIBRATION OF LASER INERTIAL MEASUREMENT UNITS ON THE BASIS OF GUARANTEEING ESTIMATION PROCEDURES

A.V. Chernodarov[*], S.A. Bystrov[**], V.V. Enyutin[***], and A.P. Patrikeev[****]
Air Force Engineering University, 3, Planetnaja St., 125190, Moscow, Russia, e-mail: chernod@mail.ru
Yu.D. Golyaev[*****] and M.S. Drozdov[******]
R&D Institute "Polyus", 3, Vvedensky St., 117342, Moscow, Russia

Abstract

Key words: laser gyro, random drift, calibration, filter, estimation, state observer, identification

This paper is devoted to the problem of improving the accuracy of inertial measurement units on the basis of Zeeman ring laser gyros (RLGs). The proposed solution of this problem relies on the inclusion in the technological cycle of RLG calibration, of guaranteeing procedures intended for estimation of random drifts and for parametric identification of their models. Such procedures imply the formation and integrated processing of observation that are redundant with respect to the standard calibration mode. A signal processing is considered which combines the potentialities of estimation filters and state observers. The results of experimental studies are given.

Introduction

The present state of strapdown inertial navigation systems (SINSs) is characterized by a wide application of ring laser gyros (RLGs). For laser SINSs (LSINSs), the problem of improving the operational characteristics of RLGs still remains topical. A conventional solution of this problem relies on the modernization of RLG hardware. Furthermore, the development of methods and means for integrated data processing (IDP) forms the necessary basis for the realization of both optimum estimation of RLG errors and algorithmic compensation for such errors brought about by causes that are constructional in nature. The application of the IDP makes it possible

- to perform RLG calibration from indirect measurements and also from correlations;
- to carry out identification of the mathematical models of RLG errors from experimental data and to employ them in order for the required qualities of LSINS accuracy to be maintained under changes in operating conditions;
- to make use of redundancy, both in information and in algorithms, in order to increase the accuracy and reliability of LSINSs.

Information redundancy of the initial alignment procedure for LSINSs creates conditions for unconventional approaches to the solution of the problem of sensor calibration. Such a solution is constructed, in this paper, with due regard for a priori known conditions for LSINS preparation for operational use, in particular, the condition for immovability of the LSINS base. The availability of information about exact values for at least one of the LSINS output parameters enables us to realize the procedures for guaranteeing estimation. Present-day approaches to the formation of the above-mentioned procedures rely on the optimization technique based on the H_∞ criterion [1]. Such optimization, as applied to integrated LSINSs, is aimed at restricting the effect of inadequacies inherent in the models of errors and disturbances on the reliability of state estimation of LSINSs and their sensors. With the LSINSs under actual operating conditions, the above inadequacies occur, for instance, due to the fact that statistical parameters of sensors deviate from their a priori assumed values as well as due to linearity and rounding errors.

The purpose of this paper is to show the possibilities of employing, first, guaranteeing estimation procedures for the improvement of RLG accuracy and for the reduction of RLG calibration time, and, second, the present-day computer-aided technologies for the automation of full-scale experiments that are performed with inertial measuring units.

---

[*] Cand.Sc., Head of Chair.
[**] Cand.Sc., Assistant Head of Chair.
[***] Cand.Sc., Instructor.
[****] Cand.Sc., Head of Laboratory.
[*****] Cand.Sc., Head of Department.
[******] Leading Engineer.

1. Analysis of Zeeman laser measurement units as calibration objects

The wide amount of laser gyros types goes from the different ways to overcome the lock-in phenomena. In Zeeman laser gyro [2] the difference between counterpropagating waves (dither) is created by applying a sign-changing magnetic field on active medium. This principal gives the possibilities to avoid applying the moving mechanical parts in gyro design. This is the reason for the high stability of Zeeman laser gyro to the mechanical shocks and vibrations.

The three-axis gyro ZLK-16-1 [3] is hermetic assembling of three ring lasers ZLK-16 and all necessary electronic parts. During the years of ZLK-16-1 applications, this device has proved itself as a good gyro for average accuracy navigation systems (less than 1°/h with preliminary calibration and 3...4 °/h without calibration).

Apparently, the outlook for future development of the devices of such a class is closely connected [3] with the widening of their capabilities on the basis of an increase in accuracy and also of improvement in the operation time. At present, the above-mentioned problem is solved with due regard for algorithmic compensation for the thermal drift $\Delta\omega_0(t)$ [3], i.e.,

$$\Delta\omega_0(t) = A_0(F)e^{-\frac{t}{\tau_1(F)}} + A_1(F)e^{-\frac{t}{\tau_2(F)}} + A_3(F), \tag{1.1}$$

where t is the time of device operation; F is the frequency of a dither, which is a function of the temperature; τ_1,τ_2 are time constants; $A_0, \ldots, A_3$ are the coefficients that are determined at the stage of certification of the device.

However, one can see that the value of the compensation signal (1.1) is dependent upon the stability of temperature conditions and it takes no account of other operational factors. Therefore, it becomes necessary to promptly estimate uncompensated residual RLG drift.

The problem of calibrating a laser inertial measurement unit (LIMU) in reference to residual RLG drifts can be successfully solved if we precisely know the geographical position and the orientation of measurement and moving trihedrals relative to one another. In practice, the above-mentioned conditions are generally not fulfilled. In the present paper, in order to overcome the difficulties mentioned, we propose to make use of the procedures that are redundant with respect to standard initial-alignment modes, specifically, the reckoning of the parameters of pseudoorientation of a LIMU having an immovable base. The output signals of the LIMU type ZLK-16-1, i.e.,

$$\overline{\Theta}_i = \int_{t_{i-1}}^{t_i} \overline{\omega}(\tau)d\tau \tag{1.2}$$

can be related to the Euler orientation parameters by the Bortz equation [4], whose approximate representation has the form

$$\dot{\overline{\Phi}} \cong \overline{\omega} + \frac{1}{2}\overline{\Phi}\times\overline{\omega} + \frac{1}{12}\left[\overline{\Phi}\times(\overline{\Phi}\times\overline{\omega})\right], \tag{1.3}$$

where $\overline{\Phi} = \{\Phi_x, \Phi_y, \Phi_z\}$ is the Euler vector; $\overline{\omega} = \{\omega_x, \omega_y, \omega_z\}$ is the vector of LIMU rotational rate, represented as projections on its own axes *Ox*, *Oy*, *Oz*.

We can make the Euler vector correspond to the direction cosine matrix (DCM) B, which characterizes the orientation of the aircraft-fixed coordinate frame *Oxyz* in relation to the inertial frame *OXYZ* [4], i.e.,

$$\mathrm{B}^T = \Phi^{-2}\overline{\Phi}\overline{\Phi}^T(1-\cos\Phi) + E\cos\Phi + \Phi^{-1}\breve{\Phi}, \tag{1.4}$$

where $\breve{\Phi} = \begin{bmatrix} 0 & -\Phi_z & \Phi_y \\ \Phi_z & 0 & -\Phi_x \\ -\Phi_y & \Phi_x & 0 \end{bmatrix}$; $\Phi = \sqrt{\overline{\Phi}^T\overline{\Phi}}$; E is an identity matrix.

If we vary relation (1.3) according to the parameters that enter in it, we can also derive a differential equation for the vector of LIMU errors $x = \{\Delta\overline{\Phi}, \Delta\overline{\omega}\}$, where $\Delta\overline{\Phi} = \{\Delta\Phi_x, \Delta\Phi_y, \Delta\Phi_z\}$ is the vector of errors of orientation parameters; $\Delta\overline{\omega} = \{\Delta\omega_x, \Delta\omega_y, \Delta\omega_z\}$ is the vector of RLG residual instrumental drifts.

From the elements of the matrix B one can find the angles $\overline{\psi}, \overline{\vartheta}, \overline{\gamma}$ of orientation of the aircraft-fixed coordinate frame (CF) *Oxyz* with respect to the inertial frame O_iXYZ [5]. In this instance, we assume that the original directions of axes of the above trihedrals coincide, and rotations are made as follows [6]: the first rotation is done by an angle of $\overline{\psi}$ radn. about the third axis *OZ*, the second rotation is performed by an angle of $\overline{\vartheta}$ radn. about a new position of the first axis *OX'*; the third rotation is done through an angle of $\overline{\gamma}$ radn. about a new position of the second axis *OY'*. In practice, however, it is necessary to determine the angles ψ, ϑ, γ of orientation of the aircraft-fixed CF *Oxyz* in relation to the geographical moving trihedral *ONHE*. Moreover, in aviation

applications, the axes Ox, Oy and Oz are pointing [5], respeetively, along the longitudinal, vertical (upwards), and lateral (rightwards) axes of an aircraft (Acft), and the axes ON, OE, OH are directed at a tangent to the geographical meridian, parallel, and the geodetic vertical. It is assumed that the original directions of the axes Ox and ON, Oy and OH, and also Oz and OE coincide, and rotations are made as follows: first rotation is done by an angle of ψ radn. about the axis OH, the second rotation is performed by an angle of ϑ radn. about a new position of the axis OE', the third rotation is done through an angle of γ radn. about a new position of the axis ON'. Having defined the DCM $B(\overline{\psi}, \overline{\vartheta}, \overline{\gamma})$ as a base one, we can determine the interrelation between the eoordinate frames considered above, using the following table.

B	B_1	B_3	P_3
$\overline{\psi}$	λ	ψ	$\pi/2$
$\overline{\vartheta}$	0	ϑ	$\pi/2$
$\overline{\gamma}$	$-\varphi$	γ	0

φ, λ are the geographieal latitude and longitude.

The appropriate DCMs are formed by assigning eoncrete values from the table to the angles $\overline{\psi}, \overline{\vartheta}, \overline{\gamma}$. For example, in determining the DCM B_3 we have $\overline{\psi} = \psi$, $\overline{\vartheta} = \vartheta$, $\overline{\gamma} = \gamma$, where ψ, ϑ, γ are the angles of yaw, pitch, and roll of an Acft. Taking this into account, the interrelation of the desired B_3 and the DCMs B and B_1 assumes the form

$$B_3 = BB_1^T P_3^T . \tag{1.5}$$

To form the DCM B_1, we can use either date obtained from a satellite navigation system (SNS) or "a priori" known position of a point at which LIMU calibration is carried out.

Using the elements of the DCM B_3, we can find the angles ψ, ϑ, γ of LIMU orientation with respeet to the trihedral $ONHE$. In order for the calibration proeess to be initialized, it is essential to know reference value of the angles mentioned. We can get these value by means of iterative refinement of their approximate values ψ_0, ϑ_0, γ_0, which were obtained using available aids, for instance, with the help of a magnetic compass and a balance level. Then the iterative process can be organized according to the Newton-Rafson technique [7]

$$\delta_i = \delta_{i-1} - \left(\frac{\partial \overline{\omega}_н}{\partial \delta} \right)_{i-1}^{-1} z_{\omega(i-1)} , \tag{1.6}$$

where $z_{\omega(i)} = \overline{\omega}_{p(i)} - \overline{\omega}_{н(i)} = [\omega_x \omega_y \omega_z]_i^T - P_3 B_{3(i)} P_3 B_1 \overline{\Omega}$; (1.7)

$\delta_i = \{\psi_i, \vartheta_i, \gamma_i\}$; $B_{3(i)} = B_3(\psi_i, \vartheta_i, \gamma_i)$; $\Omega = [0\,0\,\Omega]^T$;

ω_x, ω_y, ω_z are the projection of the vector of LIMU rotational rate on its own axes, formed from the RLG signal; Ω is the value of the angular velocity of Earth rotation.

It should be noted that procedure (1.6) can also be executed through the use of the angles of apparent rotation (1.2). In this instanee, the components of the vector $\overline{\omega}_{i(i)}$ are integrated on a given time interval.

For geodetically equipped plaees, the value of reference orientation angles or a part of them, for example, the angles of roll γ and pitch ϑ are known exactly. Their values can be used for the organization of guaranteeing procedures of LIMU state estimation on the basis of direet and indireet (1.7) observations. For the Kalman realization of the LIMU ealibration mode, the following observations ean be used as base ones

$$z_{\Theta(i)} = \overline{\Theta}_i - P_3 \int_{t_{i-1}}^{t_i} B(\tau) \overline{\Omega} d\tau . \tag{1.8}$$

The peeuliarities of proeessing of signals of the form (1.8) were eonsidered, for instanee, in [19]. In what follows, a technology is justified for the joint employment of noisy and exact observations for LIMU ealibration.

2. Construetion of guaranteeing proeedures for the estimation on a basis of the H_∞-optimization technique

Present approaehes [18] to the initial alignment of SINSs and to the calibration of their sensors rely on the teehnique for optimal Kalman filtering of observations eorrupted by noise. Furthermore, with an immovable SINS base, a part of the observed parameters can be known exaetly. The problem of proeessing of exaetly known parameters using the elassieal Kalman filter is an ill-posed one, beeause their eorrelation matrix $R_i = 0$ is singular and, consequently, a similar matrix P_i for estimation errors is singular, too.

In the present paper, the problem of combining the potentialities of state observers [8] and estimation filters is solved. Mathematically, a basis for such a combination can be the integration of deterministic and stochastic procedures used to form the necessary estimates. In this case, deterministic procedures can be considered as guaranteeing ones when we have discovered a disharmony and we tune the parameters of stochastic systems. The disharmony is generally accompanied by the filter divergence, and hence by the reduction in the reliability of the estimates obtained. The divergence, in turn, manifests itself in the fact that the actual estimation errors $\delta_j = x_j - \hat{x}_j$ differ considerably from their predicted mean-square values $\sigma_j = \sqrt{P_{jj}}$, where x_j, $\hat{x}_j$ are the j-th component of the SINS state vector and its estimate, respectively; P_{jj} is the j-th diagonal element of the matrix of weighting coefficients which characterize the degree of uncertainty of estimates.

Hence, the role of the guaranteeing tuning can be reduced to the formation of procedures intended to put a bound on estimation errors using a given level. To accomplish this, we propose to make use of the technique for estimate optimization based on the H_∞ criterion [1].

Assume that a SINS described generally by the differential equation

$$\dot{y}_p(t) = F(y_p, t) + G(t)\xi(t) \tag{2.1}$$

possesses discrete channels for making external measurements, i.e.,

$$z_i = h(y_i, i) + \vartheta_i; \tag{2.2}$$

$$\mu_i = l(y_i, i), \tag{2.3}$$

where $y(t)$ is an n-dimensional state vector of an undisturbed (ideal) SINS; $y_p(t)$ is an n-dimensional state vector of a disturbed (actual) SINS; $F(y,t)$, $h(y_i,i)$, $l(y_i,i)$ – n-, k-, and r-dimensional vector functions; $\xi(t)$ is a q-dimensional vector of SINS disturbaneies; $G(t)$ is the matrix of coefficients of relation; ϑ_i – k-dimensional vee-tor of disturbancies for external measuring tools. Relation (2.3) describes the parameters that are measured exactly.

The following equations for SINS errors can be made correspond to relation (2.1)-(2.3):

$$\dot{x}(t) = A(t)x(t) + G(t)\xi(t); \tag{2.4}$$

$$x_i = \Phi_i x_{i-1} + \Gamma_i \xi_{i-1}, \tag{2.5}$$

$$\Delta z_i = \hat{z}_i - z_i = H_i x_i + \vartheta_i; \tag{2.6}$$

$$\Delta\mu_i = \hat{\mu}_i - \mu_i = L_i x_i, \tag{2.7}$$

where $\hat{z}_i = h[y_{p(i)}]$; $\hat{\mu}_i = l[y_{p(i)}]$; $x_i = y_{p(i)} - y_i$; $\Phi_i = \Phi(t_i, t_{i-1})$, $\Gamma_i = \Gamma(t_i, t_{i-1})$ are transition matrices;

$H_i = \left.\frac{\partial h(y)}{\partial y}\right|_{y=y_{p(i)}}$; $L_i = \left.\frac{\partial l(y)}{\partial y}\right|_{y=y_{p(i)}}$; $A(t) = \left.\frac{\partial F(y,t)}{\partial y}\right|_{y=y_{p(i)}}$ are the matrices of partial derivatives.

In the general case [1], the solution of the estimation problem using the criterion H_∞ must provide the satisfaction of the inequality

$$\sup_{0\neq\xi,\nu\in l_2[0,\infty[} \frac{\|\eta\|_2^2}{\|\xi\|_2^2 + \|\nu\|_2^2} \le \gamma^2, \tag{2.8}$$

where $\gamma^2 \ge 0$ is a constant; $\nu_i = \Delta z_i - H_i\Phi_i\hat{x}_{i-1}$; $\eta_i = \Delta\mu_i - L_i\Phi_i\hat{x}_{i-1}$; $\|\xi\|_2^2 = \sum_{i=i_0}^{\infty} \xi_i^T \xi_i$.

In practical application [9], the interval for H_∞-optimization is bounded by the operation time of a dynamical system $i_0 \le i \le i_f$, and it is assumed that $\|\eta\|_2^2 < \infty$; $\|\xi\|_2^2 < \infty$; $\|\nu\|_2^2 < \infty$. Moreover, in order for condition (2.8) to be realized, we propose to make use of exact measurements (2.3). With such measurements, a part of the components of the vector δ_i in relation (2.8) is accessible for the error-free observation. This is corroborated by the model of the residual η_i between the actual observation $\Delta\mu$ and its predicted value $\Delta\hat{\mu}$, i.e.,

$$\eta_i = \Delta\mu_i - \Delta\hat{\mu}_i = L_i x_i - L_i \hat{x}_i = L_i\delta_i. \tag{2.9}$$

In addition, for residuals ν_i, we introduce the matrix R_i of weighting coefficients. Taking this into account, relation (2.8) can be represented as the following inequality:

$$J = 0{,}5 \sum_{i=i_0+1}^{i_f} \left\{ \|\nu_i\|^2_{R_i^{-1}} + \|\xi_i\|^2 - \gamma^{-2}\|\eta_i\|^2 \right\} \ge 0. \tag{2.10}$$

When using, as a cost function, the quadratic form of type (2.10), the solution of the problem of estimate op-

timization can be divided into two stages [10], namely: minimization of the cost function (2.10) by the appropriate choice of the estimates $\hat{x}_i$; provision of positive definiteness for a minimum of the quadratic form (2.10).

To solve the first part of the problem, we can employ the mathematical apparatus of the method of weighted least squares. In this case, to take into account the rate of change in the vector x_i, the cost function (2.10) can be represented in the Euler-Lagrange form [11]. Such a representation of the cost function enables us to carry out optimization using the Bellman-Shridhar technique [12], which is based on the formation of the Hamiltonian

$$\mathcal{H} = 0{,}5\left\{\|\nu_i\|^2_{R_i^{-1}} + \|\xi_i\|^2 - \gamma^{-2}\|\eta_i\|^2\right\} + \lambda_i^T\left\{\Phi_i \hat{x}_{i-1} + \Gamma_i \hat{\xi}_{i-1}\right\} \tag{2.11}$$

and on the solution of the canonical equations

$$\frac{\partial \mathcal{H}}{\partial \hat{x}_{i-1}} = \lambda_{i-1}^T; \quad (2.12) \qquad \frac{\partial \mathcal{H}}{\partial \lambda_i^T} = \hat{x}_i; \quad (2.13) \qquad \frac{\partial \mathcal{H}}{\partial \hat{\xi}_{i-1}} = 0 \quad (2.14)$$

given the boundary conditions $\hat{x}_{i_0}; \lambda_{i_f} = 0$, (2.15)

where λ_i is the vector of Lagrange multipliers.

Upon computing partial derivatives and upon solving the two-point boundary-value problem for the parameters $\hat{x}_{i/i}$ and λ_i by the method of invariant imbedding [12], we can obtain the following guaranteeing-estimation algorithm:

Prediction: $\hat{x}_{i/i-1} = \Phi_i \hat{x}_{i-1/i-1}$; (2.16)

$$P_{i/i-1} = \Phi_i P_{i-1/i-1}\Phi_i^T + \Gamma_i\Gamma_i^T; \tag{2.17}$$

Update: $\overline{P}_{i/i} = (P_{i/i-1}^{-1} + H_i^T R_i^{-1} H_i)^{-1} = P_{i/i-1} - P_{i/i-1}H_i^T (H_i P_{i/i-1} H_i^T + R_i)^{-1} H_i P_{i/i-1}$; (2.18)

$$P_{i/i} = (\overline{P}_{i/i}^{-1} - L_i^T \gamma^{-2} L_i)^{-1} = \overline{P}_{i/i} + \overline{P}_{i/i} L_i^T (\gamma^2 E - L_i \overline{P}_{i/i} L_i^T)^{-1} L_i \overline{P}_{i/i}; \tag{2.19}$$

$$\hat{\tilde{x}}_{i/i} = \hat{x}_{i/i-1} + P_{i/i} H_i^T R_i^{-1} \nu_i; \tag{2.20}$$

$$\hat{x}_{i/i} = \hat{\tilde{x}}_{i/i} - P_{i/i} L_i^T \gamma^{-2} \eta_i. \tag{2.21}$$

We can point out the following features and guaranteeing possibilities of algorithm (2.16)-(2.21):

- unlike the extended Kalman filter (EKF) [12], this algorithm permits one to process exact measurements for which $R_i = 0$, without the loss of positive definiteness of the matrix $P_{i/i}$;
- nonsingularity of the matrix $P_{i/i}$ is guaranteed by the appropriate choice of the parameter γ^2.

However, with the classical statement of the problem of guaranteeing estimation (2.8), the realization of its solution (2.16)-(2.21) involves the following difficulties: procedures of choosing the parameter γ^2 and of obtaining positive definiteness of the quadratic form (2.10) were not formalized. That is why, in practical applications [9] this parameter is generally selected in an empirical manner.

In order for the above-mentioned difficulties to be overcome, we propose an algorithm for guaranteeing estimation with adaptive tuning of the parameter γ^2, which also ensures positive definiteness of the quadratic form (2.10).

In constructing guaranteeing-estimation procedures, no assumptions concerning the character of the disturbancies ξ_i and ϑ_i were made. Furthermore, if weighting coefficients are given [9, 10] proportional to the covariancies of errors of estimates and observations, i.e., if $P_i = \mathrm{cov}\{\delta_i\}$, $R_i = \mathrm{cov}\{\vartheta_i\}$, then the kernel (2.16)-(2.18), (2.20) of algorithm (2.16)-(2.21) well be equivalent to the EKF. Formally, this permits one to make use of EKF properties in order to monitor and maintain the required characteristics of an estimating filter (2.16)-(2.21).

However, to discover the divergence, one needs information about real estimation errors δ_j. Such information is available only in mathematical simulation when we know an ideal phase path. In practical applications, the solution of this problem rely on the properties of the residual ν_i, which is related to the vectors of errors δ_i and ϑ_i by the following model:

$$\nu_i = \Delta z_i - \Delta \hat{z}_i = H_i x_i + \vartheta_i - H_i \hat{x}_i = H_i \delta_i + \vartheta_i. \tag{2.22}$$

Inasmuch as the errors δ_i and ϑ_i appear in relation (2.22) in an additive fashion, the Gaussion character of the residual ν_i can be considered only as a necessary, but not a sufficient condition for the no-divergence state of an estimation filter. If exact observations are made, the residual η_i, having the model (2.9), uniquely characterizes estimation errors. However, testing of the residuals for their Gaussian character in real time is a rather complex

problem. It is possible to simplify the process of divergence detection if we make use of the properties of a normalized residual and if we analyze the quadratic form

$$\hat{\beta}_i = \eta_i^T e_i^{-1} \eta_i , \qquad (2.23) \qquad \text{where } e_i = L_i P_i L_i^T .$$

Indeed, if the residual η_i is Gaussian in character, i.e. if $\eta_i \in N(0,e_i)$, the quadratic form (2.23) has the χ^2 distribution [13], namely, $\hat{\beta}_i \in \chi^2(r,2r)$, where r is the dimensionality of the vector η_i.

Using the properties of the χ^2 distribution and the rule of 3σ [13], we can form the tolerance β_r

$$\hat{\beta}_i \le \beta_r = r + 3\sqrt{2r} . \qquad (2.24)$$

The divergence of estimates is detected when the parameter $\hat{\beta}_i$ is out of tolerance. Here the retuning of a filter should be carried out so that condition (2.24) becomes identical.

It is advisable to perform the retuning basing on the procedures for sequential processing of components of the vector of residuals [14]. In practice [12, 15], the divergence of estimates and, as a consequence, the violation of condition (2.24), result from a decrease in the filter gain due to nonsingularity of the matrix $P_{i/i}$. Because of this, it is apparently expedient to increase the number of elements of the above matrix by the value ΔQ, such that condition (2.24) becomes identical, namely:

$$\frac{\eta_j^2}{L_j P_{i/j} L_j^T} = \frac{\eta_j^2}{L_j (\bar{P}_{i/j} + \Delta Q_j) L_j^T} = \beta_1 , \qquad (2.25)$$

where $P_{i/j}$ is the value of the matrix $P_{i/i}$ in relation (2.19) after processing the j-th component of the vector of the residuals η_i; $L_i = [L_1^T ... L_j^T ... L_r^T]^T$; $\beta_1 = 1 + 3\sqrt{2} \approx 5{,}2$.

In [16], it was shown that the following matrix satisfies condition (2.25):

$$\Delta Q_j = \bar{P}_{i/j} L_j^T q_j L_j \bar{P}_{i/j} , \qquad (2.26)$$

where $q_j = (\gamma_j^2 - e_j)^{-1}$; $\gamma_j^2 = [e_j^2 \beta_1 + (\eta_j^2 - \beta_1 e_j) e_j] / (\eta_j^2 - \beta_1 e_j)$.

Algorithm (2.16)-(2.21) for guaranteeing estimation can be represented, in view of expression (2.26), as its adaptive modification shown in Fig. 1.

In the execution of the adaptive algorithm, it is apparently possible to tune, from the exact observations $\Delta\mu_i$, the "a posteriori" matrix $P_{i/i}$ of weighting coefficients so that the generalized parameter $\hat{\beta}_i$ does not go over the specified tolerance β_1. Here, unlike conventional approaches [1, 9, 10] to the construction of estimation filters on the basis of the H_∞-optimization technique, the procedure used for the formation of the parameter γ^2 was represented in a formalized way.

3. Parametric identification of the models of RLG errors

The integration of LSINSs with the sensors of external data relies on a priori known models of their errors. However, while integrated navigation systems are in operation, RLG characteristics undergo certain changes. This has necessitated taking into account such changes in the models of RLG errors. Thus, the problem of identifying the parameters of the models of RLG errors arises. The above problem can be solved on the basis of correlative processing of the estimates of RLG instrumental drifts.

At present, it is deemed that it is possible to have an approximate [17] description of RLG random drifts as the Markov Gaussian first-order process

$$\Delta\dot{\omega} = -\alpha\Delta\omega + \xi\sigma\sqrt{2\alpha} \qquad (3.1)$$

with the exponential correlation function

$$R(\tau) = \sigma^2 e^{-\alpha|\tau|} , \qquad (3.2)$$

where $\alpha = \text{const} > 0$; $\xi \in N(0, 1)$; $R(0) = \sigma^2$ is the variance of RLG drift.

One can see that the construction of Eq. (3.1) corresponds to the model of LSINS errors (2.4).

In relation (3.1), (3.2), the quantity α is the parameter that is to be identified. In this case, the problem can be reduced to the finding of the value of α, which minimizes the quadratic function

$$F(\alpha) = \sum_{j=1}^{N} (\hat{R}_j - \sigma^2 e^{-\alpha\tau_j})^2 . \qquad (3.3)$$

$$\hat{R}_k = \frac{1}{N}\sum_{i=k+1}^{N+k} \overset{\circ}{x}_i \overset{\circ}{x}_{i-k}, \quad \overset{\circ}{x}_i = \hat{x}_i - m_x; \quad m_x = \frac{1}{N}\sum_{i=1}^{N} \hat{x}_i; \quad k = \overline{0, N}, \tag{3.4}$$

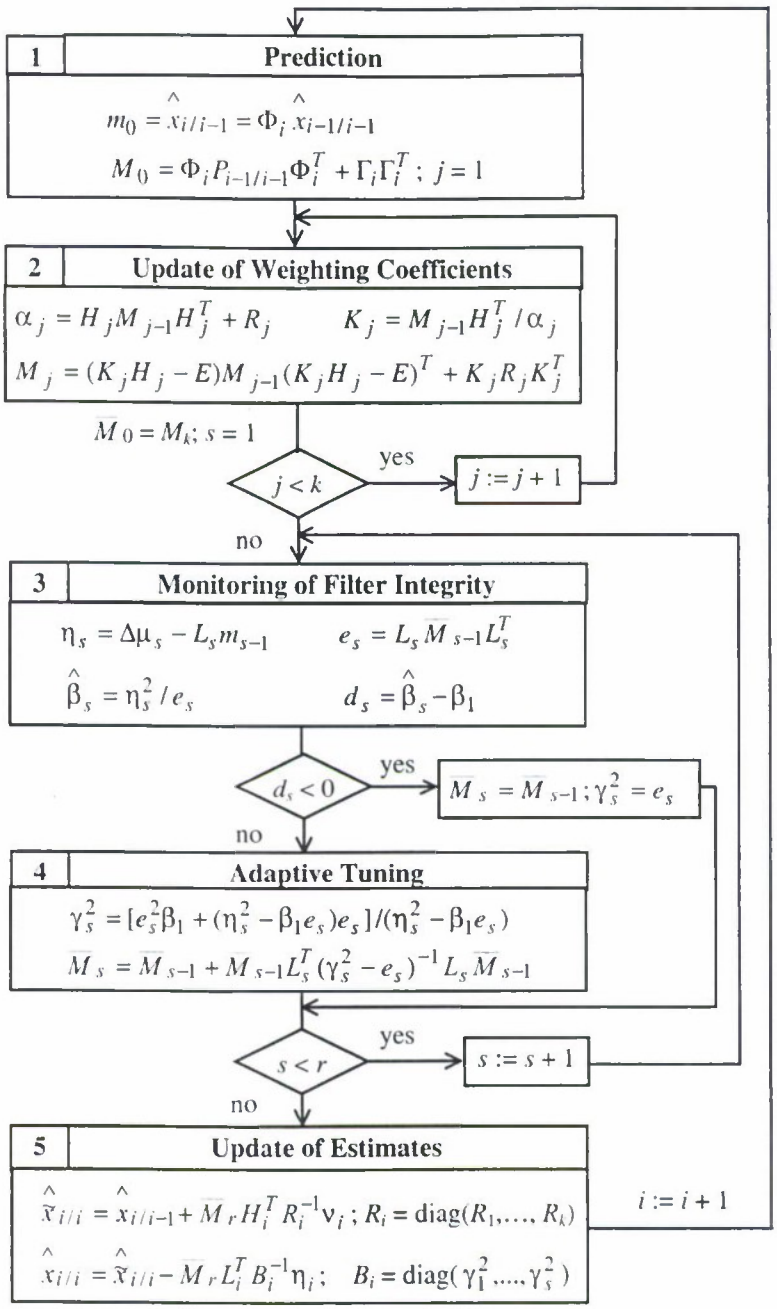

Fig. 1. Block-diagram of the algorithm of the guaranteeing estimation with adaptive tuning

$\hat{x}_i = \hat{x}(t_i)$ is the drift estimate for the appropriate RLG; N is the sample size; $\tau_j = k\Delta t$; $\Delta t = t_i - t_{i-1}$.

Differentiating function (3.3) with respect to α and putting the derivative equal to zero, we obtain

$$\frac{\partial F(\alpha)}{\partial \alpha} = -2\left(\sum_{j=1}^{N} \hat{R}_j - \sum_{j=1}^{N} \sigma^2 \tau_j e^{-\alpha\tau_j}\right)\sum_{j=1}^{N} \sigma^2 \tau_j e^{-\alpha\tau_j} = 0. \tag{3.5}$$

Considering that, for RLGs $0 < \alpha < 1$ and that the second multiplier in Eq. (3.5) has no influence on the solution, we can write

$$\sum_{j=1}^{N} \hat{R}_j = \sum_{j=1}^{N} \sigma^2 \tau_j e^{-\alpha\tau_j} . \qquad (3.6)$$

When the function $e^{-\alpha\tau_j}$ is expanded into the Maclaurin series $e^{-\alpha\tau_j} = 1 - \alpha\tau_j + \frac{1}{2}\alpha^2\tau_j^2 - \frac{1}{6}\alpha^3\tau_j^3 \ldots$

the form of Eq. (3.6) will depend upon the number of terms of this expansion, which are taken into account:

$$c\alpha + d = 0; \qquad b\alpha^2 + c\alpha + d = 0; \qquad a\alpha^3 + b\alpha^2 + c\alpha + d = 0; \ldots ,$$

where $a = \sum_{j=1}^{N} \frac{t_j^3}{6}$; $b = -\sum_{j=1}^{N} \frac{t_j^2}{2}$; $c = \sum_{j=1}^{N} t_j$; $d = \sum_{j=1}^{N} r_j - N = 0$;

$r_j = \hat{R}_j / \sigma^2$ is a normalized correlation function.

By solving these equations, we can estimate the parameter α with a certain degree of accuracy. Moreover, during the parametric identification on the basis of correlative processing of date (3.4) we can also estimate the variance of drift of the corresponding RLG, namely: $\sigma^2 = \hat{R}_0$.

The tuning procedure discussed above can be included in the technological cycle intended for LSINS preparation for operational use, taking into account a change in RLG characteristics during its operation. To improve the accuracy of calibration, prior to identification of the parameters of the models of RLG errors, the smoothing [20] of estimates of the LSINS state vector can be performed.

4. Analysis of the results of studies

A study of the possibilities of employing the procedures for guaranteeing estimation during the process of LIMU calibration has been carried out using a bench set of the ZLK-16-1 device, having an interface with a personal computer (PC). The interface was done on the basis of an industrially-made adapter intender for input/output of date through the PCI bus. This has made it possible to combine into an integrated structure general-purpose and special-purpose software-and-mathematical support (SMS) of the experimental work, which was developed in the C++, Builder, and Windows 98 environment; to make use of the modern graphical tools in order for an experiment to be performed; to impart the property of versatility to an automation-equipped working place (AEWP).

The block diagram of the AEWP is shown in Fig. 2. The LIMU was mounted on a geodetically tied-in and levelled rotary table. In the performance of the experiment, actual conditions for the preparation of the ZLK-16-1 device for operational use were formed. It was assumed that orientation of the device according to roll and pitch angles is known exactly, and azimuth orientation is known in error that is proportional to the deviation of the magnetic compass, approximately about 2°.

The positioning of a LIMU calibration point was performed from SNS averaged measurements. The processing of observations (1.8) and the angles ϑ, γ was carried out at a frequency of 5 Hz, and integration was performed at a frequency of 1 kHz. Some of the experimental results are shown in Figs. 3 and 4, namely: in Fig. 3a, control actions for ZLK-16-1 output signals are depicted; in Figs. 3b and 3c, output signals of an RLG are shown; in Figs. 4a and 4b, output signals of the adapter are shown; in Fig. 4c, an estimate of the residual drift of the RLG is shown.

The obtained accuracy of RLG residual-drift estimates is commensurable with similar results gained in the certification of the ZLK-16-1 device when its orientation is completely known.

The effectiveness of an algorithm for identification of the parameters of the RLG drift model was corroborated by mathematical simulation. In Fig. 5 are shown the normalized correlation functions r_r, r_a, and r_e: for the real drift, for "a priori" assumed drift, and for estimated drift, respectively. The following correlation intervals correspond to these correlation functions: τ_r =1000 sec, τ_a = 300 sec, $\tau_e \approx$ 967 sec, where $\tau = \alpha^{-1}$. One can see that $\tau_e \equiv \tau_r$.

Conclusions

Conditions for LIMU preparation for operational use permit one to combine the potentialities of stochastic and deterministic approaches to the estimation of the parameters of RLG state. Such a combination extends the prospects for improving the procedures of parametric identification and algorithmic compensation for RLG residual drifts under actual operating conditions. The calibration technology considered makes it possible to estimate generalized device drifts caused by errors that are both instrumental and computational in character.

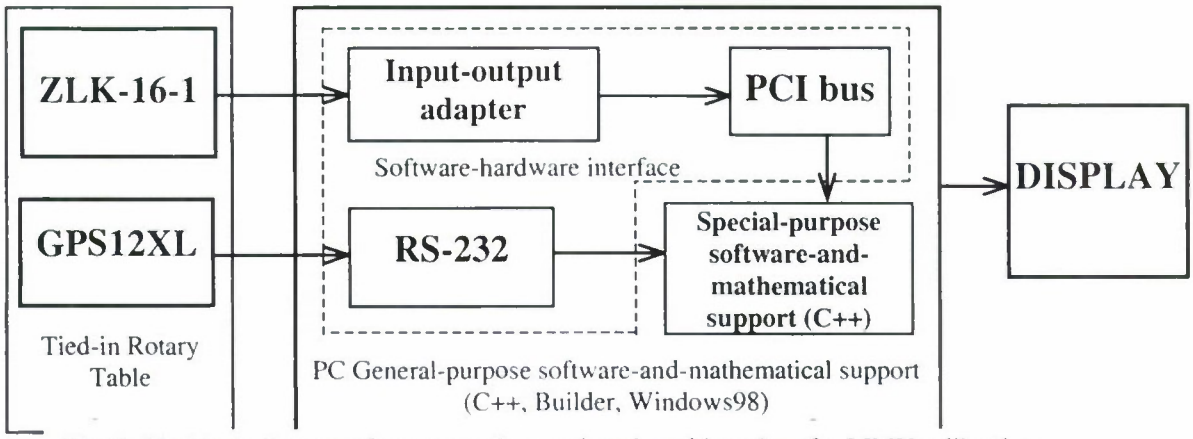

Fig. 2. The block diagram of an automation-equipped working place for LIMU calibration

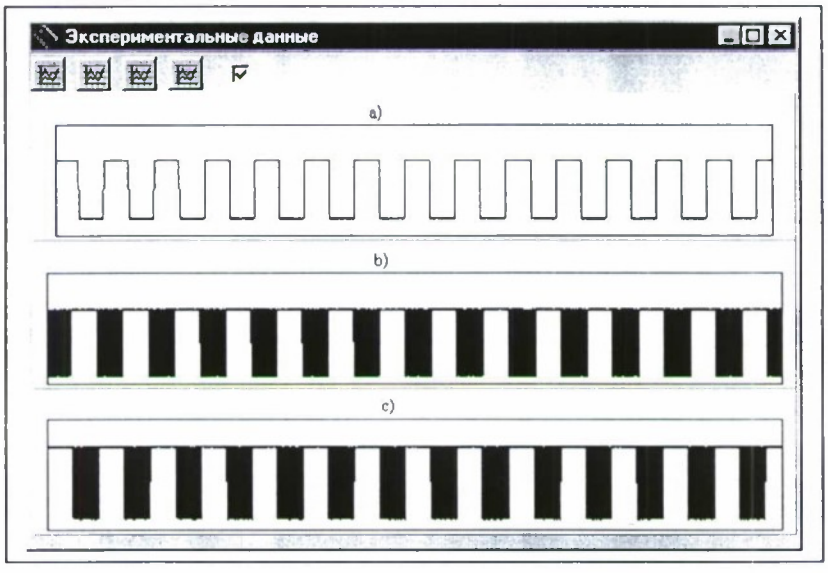

Fig. 3

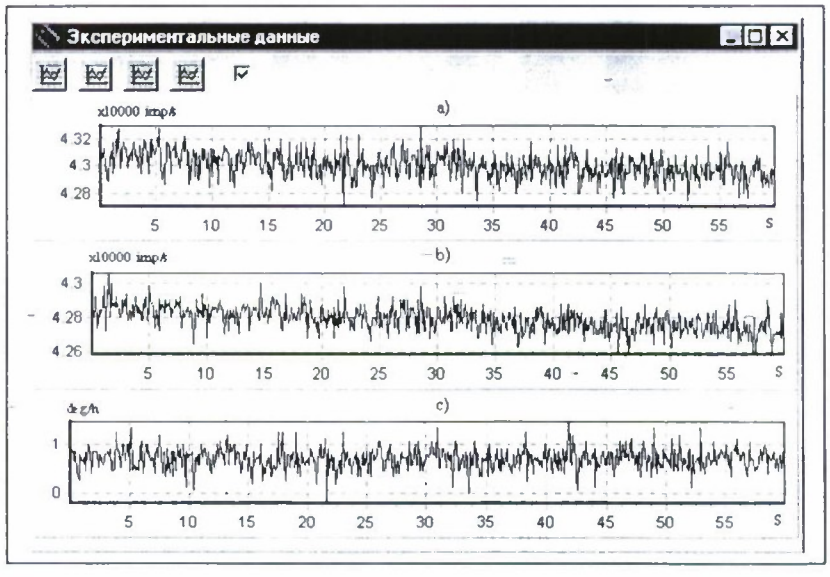

Fig. 4

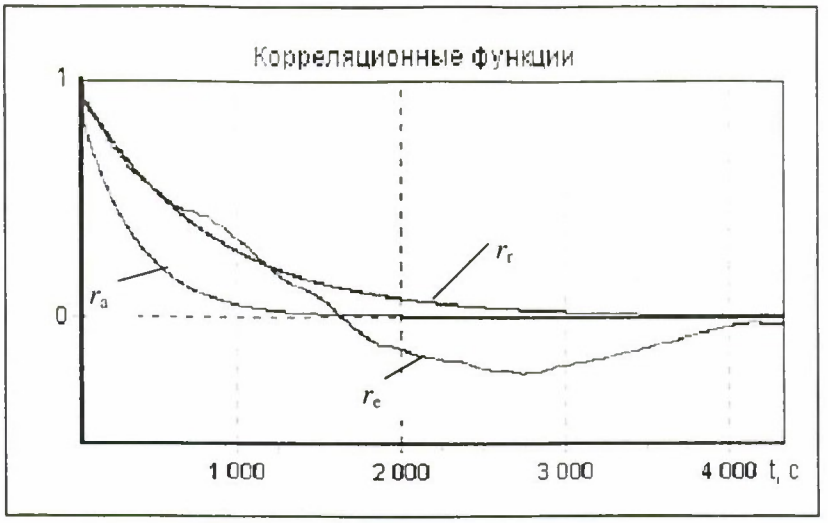

Fig. 5

References

1. **Souza C.E., Xie L.** Robust H_∞ filtering. In: Control and dynamic systems. – N.Y.: Academic Press, 1994. – Vol.65. – P. 323-377.
2. **Azarova V.V., Golyaev Yu.D., Dmitriev V.G., et. al.** Zeeman laser gyros. In: Optical Gyros and their Application. RTO-AG-339, Neuilly-sur-Seine Cedex, France, 1999, P. 5/1-29.
3. **Golyaev Yu.D., Drozdov M.S., Korjavy A.P., et. al.** Extension of the application field of Zeeman Laser gyro ZLK-16-1 // 5th St.-Petersburg International Conference on Integrated Navigation Systems. – SPb.: CSRI "Elektropribor", 1998. – P. 189-193.
4. **Bortz J.E.** A New Mathematical Formulation for Strapdown Inertial Navigation // IEEE Trans. on AES, 1971. – No 7. – P. 61-66.
5. **GOST 20058-80.** Aircraft dynamics in atmosphere. Terms, definitions and symbols. – M: Izdatelstvo gosstandartov, 1981. – 52 p.
6. **Bromberg P.V.** Inertial navigation systems theory. – M.: Nauka, GRFML, 1979. – 296 p.
7. **Forsythe G., Malcolm M., Moler C.** Computer methods for mathematical computation. – NJ.: Prentice-hall, Englewood Cliffs, 1977.
8. **Sage A.P., White C.C.** Optimum systems control. – N.J.: Englewood Cliffs, Prentice-Hall, 1982.
9. **Sugimoto S., Kubo Y., Ito A.** Static carrier phase differential positioning by applying the H_∞ filter // Proc. of the ION GPS'99 meeting, Nashville, TN, 1999. – P. 1241-1250.
10. **Hassibi B., Sayed A.H., Kailath T.** Linear estimation in Krein spaces. Part II: Applications // IEEE Trans. on Automatic Control. – 1996. – Vol. 41, No 1. – P. 34-49.
11. **Speedy C.B., Brown R.F., Goodwin G.C.** Control Theory. – Edinburgh: Oliver and Boyd, 1970.
12. **Sage A.P., Melse J.L.** Estimation theory with application to communication and control. – N.Y.: Mc Graw-Hill, 1972.
13. **Korolyuk V.S., Portenko N.I., Skorokhod A.V. and Turbin A.F.** A handbook of probability theory and mathematical statistics [in Russian]. – M.: Nauka, GRFML, 1985. – 640 p.
14. **Bierman G.J.** Factorization methods for discrete sequential estimation. – N.Y.: Academic Press, 1977. – 320 p.
15. **Fitzgerald R.J.** Divergence of the Kalman filter // IEEE Trans. on Automatic Control. – 1971. – Vol.16. – № 6.– P. 736-747.
16. **Chernodarov A.V., Enyutin V.V., Patrikeev A.P.** Initial alignment of complex inertial navigation systems on a basis of guaranteeing estimation procedures. [In Russian] // Гироскопия и навигация, submitted for publication.
17. **Loukianov D.P., Mochalov A.V., Recheel M.** Application of a laser gyro in track measuring systems. In: Optical Gyros and their Application. RTO-AG-339, Neuilly-sur-Seine Cedex, France, 1999, P. 14/1-14.
18. **Grewal M.S., Henderson V.D., Miyasako R.S.** Application of Kalman filtering to the calibration and alignment of inertial navigation systems // IEEE Trans. on AC. – 1991. – Vol. 36, No 1. – P. 4-13.
19. **Chernodarov A.V., Bystrov S.A., Enyutin V.V.** Alignment of inertial navigation systems on a basis of the joint procedures of forward and backward filtering of the increments of sensor signals // 8th St.-Petershurg International Conference on Integrated Navigation Systems. – SPh.: CSRI "Elektropribor", 2001. – P. 82-84.
20. **Chernodarov A.V., Enyutin V.V., Patrikeev A.P.** Diagnosis of integrated navigation systems on a basis of the joint U-D procedures of filtering and smoothing. [In Russian] // Гироскопия и навигация. – 2000. – №3(30). – Pp. 34-48.

A POWER GYROSCOPIC ATTITUDE CONTROL SYSTEM OF A SPACE VEHICLE RESOURCE-DK

A.V. Sorokin[1], **N.I. Bashkeev, V.V. Yaremenko**
FSUE "Command devices research institute", St-Petersburg , Russia. E-mail: info@niikp.spb.ru

U.G. Antonov[2], **N.A. Kuroedov, B.K. Suchkov**
FSUE "GNPRKTS "TSSKB - Progress", Samara, Russia. E-mail: csdb@mail.samtel.ru

E.I. Somov[3]
SCS «RI of problems of mechanical systems reliability», Samara, Russia. E-mail:pnms@sstu.samara.ru

Abstract

Key words: a space vehicle, an attitude control system, a power gyroscopic complex, a gyrodine, a gyroscope.

Is considered the power gyroscopic attitude control and stabilization system of a space vehicle «Resource – DK» for remote sensing of an Earth surface. Are elucidated the problems of selection of the design and kinematic schemes of power gyroscopic devices, is justified the expediency of usage of two-degree power gyroscopic devices (gyrodines). With the purpose of minimization of mass and power consumption the system from four identical gyrodines with two by two - parallel gimbal axes of gyroscopes is accepted. Are reduced the structural scheme of gyrodine and its main performances. Are described the design solutions and functional singularities of construction of the control moment gyroscopes, controlling drive, angle transmitter, electronic units, which base on wide experience of manufacturing and maintenance of similar devices. Are reduced the principles of construction of a system of reset of an accumulated angular momentum of power gyroscopic system.

The space vehicle «Resource – DK» (Fig. 1) is intended for multizonal detail exploration of an Earth surface from space. Its problem is the deriving of images of plants above ground in visible and infra-red radiation bands, ensuring of operating delivery of this information on a radio channel on the Earth and introducing this information to a broad audience of consumers. High-resolution on terrain, broad band of the review, the singularities of construction of instrumentation of observation cause the necessity of composite angular programmatic driving of space vehicle on orbit with major angular rates. This fact in combination with durable also determine singularities of an actuators construction of an attitude control system of space vehicle «Resource – DK».

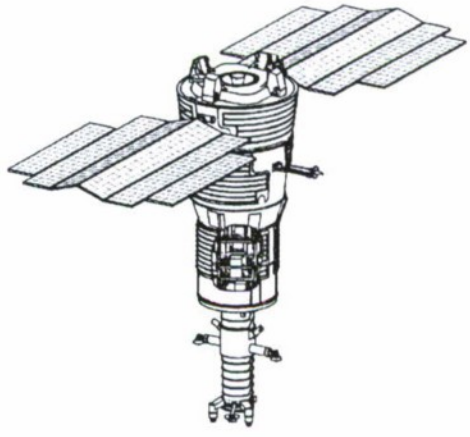

Fig.1

The actuators of an attitude control system of space vehicle «Resource – DK» are built on the basis of a power gyroscopic complex (PGC). This selection is explained by following circumstances:

- PGC allows to realize a programmatic attitude and stabilization of an angular position of space vehicle with minimum power losses and without expenditures of a propulsive mass; with its help, as displays experience, it is possible to create practically "non-flow" attitude control system even for such rather dynamical and durable space vehicle, what «Resource – DK» is;
- the wide-band control by a moment realizable by PGC, promotes reaching of split-hair accuracies of attitude required for space vehicle of such class;

[1] C. ph-m. s.
[2] D. t. s.
[3] C.t.s.

- usage of PGC allows to create around of space vehicle "clear air", favourable for operation of its optical units.

The high performance of application of PGC is reconfirmed by long-term practice of their maintenance on space vehicle of observation of the previous generations.

For precision attitude control systems of high-dynamic space vehicles is most expedient the application of PGC, built on the basis of power gyroscopic devices possessing property " to magnify a moment ", such as: pairs of three-degree gyroscopes or two-degree control gyroscopes, so-called gyrodines.

The PGC, built on the basis of pairs of three-degree gyroscopes, allow to have the very simple control laws by attitude. It is connected that such pairs, kinematic configuration is shown to which one in a fig. 2, allows to change separately an angular momentum on two axes, bound with a body of space vehicle, not changing it on third.

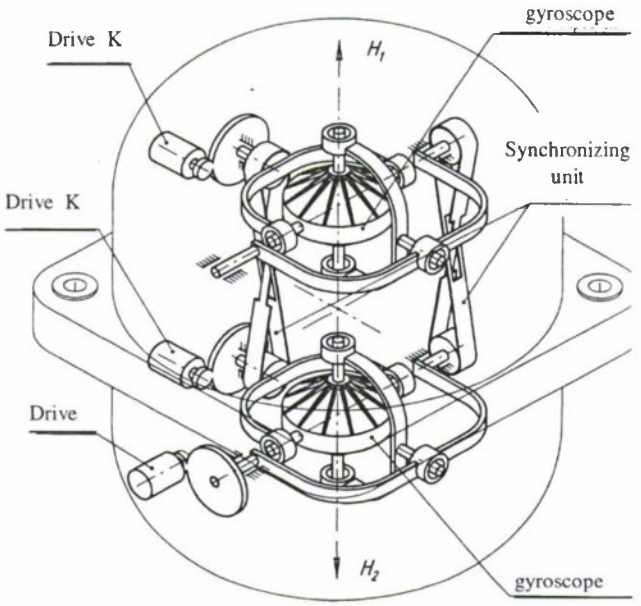

Fig.2

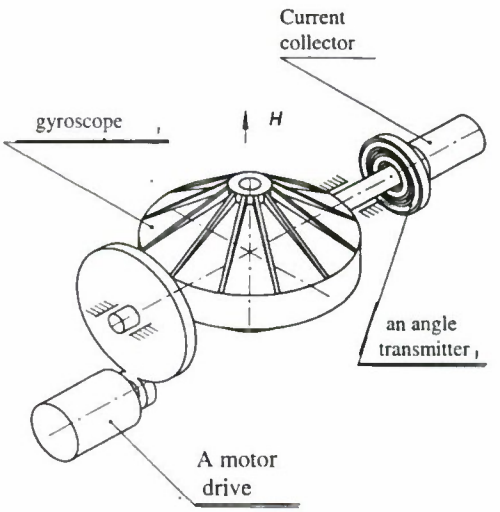

Fig.3

The structure of such PGC, as a rule, consists of two pairs of three-degree gyroscopes, one of which operates, for example, relatively to axes of a roll and pitch, and another – relatively to axes of a roll and yaw. Such scheme is specially convenient in cases, when the main, fastest programmatic turns are effected relatively to axis of roll, however this type of PGC differs by complication of construction, gimbal of each gyroscope has five rotation axes, that induces the difficulties in its manufacture and reduces in the high cost of articles.

Improving of performances of an airborne computers, accumulation of in-service experience of PGC, have made to possible the usage of more simple power gyroscopic devices – gyrodines. PGC, built on the basis of gyrodines, differ not only high manufacturability, but also good dynamic and operating performances, small overall dimensions and mass, broad possibilities for unification, but they require the realization of considerably more composite control algorithms. The kinematic configuration of gyrodine is shown in a fig. 3.

Structurally everyone gyrodine of the PGC of space vehicle «Resource – DK» consists of two devices: electromechanical and electronic. A structure of an electromechanical device consist of a control moment gyro (CMG), controlling drive and angle transmitter of turn of a gyroscope relatively to an axis of gimbal. The skeleton diagram of gyrodine is shown in a fig. 4.

The control moment gyro has a steel rotor rotated with a speed 10000 r.p.m. in ball bearings. Possessed experience displays, that at the indicated speeds of rotor rotation ball bearings can ensure the safe life till 10-15 years. As contrasted to by other alternate versions of supports: gas- or hydrodynamic, and also electromagnetic, ball bearings allow to decide a problem of making of CMG more costeffectively in mass and power consumption. For gyrorotor rotation is used the three-phase induction motor with consumed power 7-14 W depending on operational mode. The shank bore of the control moment gyro is hermetic and is

completed by helium-hydrogenous mixture at low pressure. For a diminution of a mass in a construction of CMG are used the aluminium alloys such as AMG.

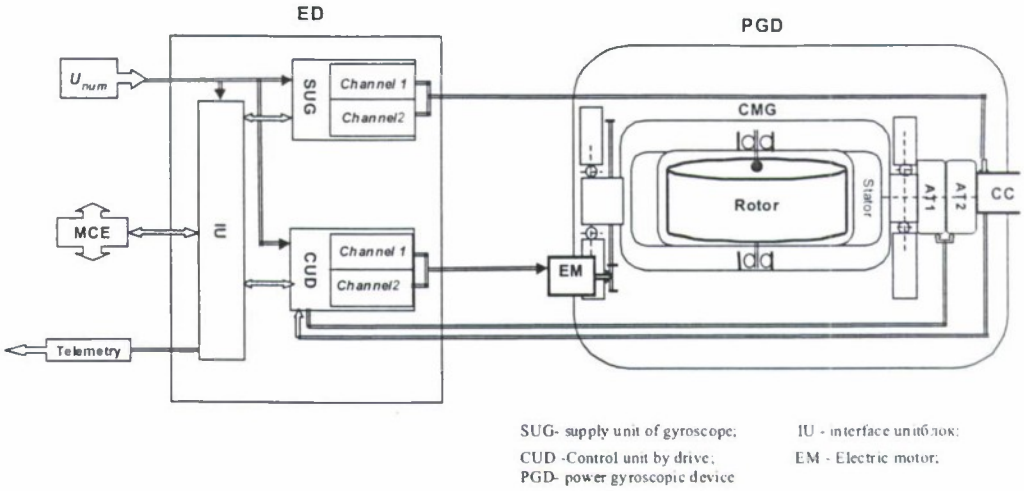

Fig.4

The controlling drive is built on the basis of brushless moment electric motor, the load-carrying part which one is maid as a three-phase motor of a direct current with excitation from permanent magnets manufactured from a material KS 37. The peak torque of a drive at a current of control 1,2 A equal to 1,2 Nm. The output axis of a motor is connected to a gimbal axis of the control moment gyro with the help of a gear supplied by device which take up backlash. The information on an angular position of a gyroscope relatively to a body is received with the help of an angle transmitter representing the two-reading sine-cosine multipolar rotated transformer, working in a phase condition. The accuracy of this transmitter, which one also used in a feedback circuit of a controlling drive (see fig. 4), does not exceed 2 angular min.

The electronic device contains units, which one provide all devices with a secondary current supply, a reception and conversion of the control signals and control instructions, a formation and issue of a code of a turn angle of the control moment gyroscope and the telemetry signals. The information exchange between the gyrodines and the control system implements on the multiplex channel of exchange according to GOST 26765.52-87.

For maintenance of required reliability, all main devices of gyrodine such as a gyromotor, a control drive, a sensor of an angular position of the gyroscope and the electronic units are doubled. Thus the back-up devices are in a «cold» reserve.

All elements of a gyrodine and have passed comprehensive improvement and practical approbation. The main characteristics of gyrodine are reduced in table 1.

Table 1

1	Maximum control moment, Nm	14.8
2	Angular momentum of rotor, Nms	94±2.4
3	Range of speed of turn of a gyroscope gimbal, grad/s	±8.6
4	Discreteness of speed of turn of a gyroscope gimbal, grad/s	0.0337
5	Accuracy of improvement of a gyroscope mean speed of turn, grad/s	0.02±0.02 x β
6	Range of angular measurement of turn of a gyroscope gimbal, grad	0 – 360
7	Accuracy of output of the information about an angular position of a gyroscope gimbal, no more, angular minute	15
8	Power consumption in the mode of stabilization, no more, W	45
9	Mass, no more, kg	48
10	Overall dimensions • CMG , mm • ED , mm	 445×300×280 150×480×310
11	Service life, years	8.5

Dynamic properties of gyrodine. For a research of dynamic properties of gyrodine were designed full nonlinear continuously - discrete model and series of the simplified nonlinear and linear mathematical models.

The full mathematical model of gyrodine allows the fundamental factors exhibited in a fig. 5, namely:

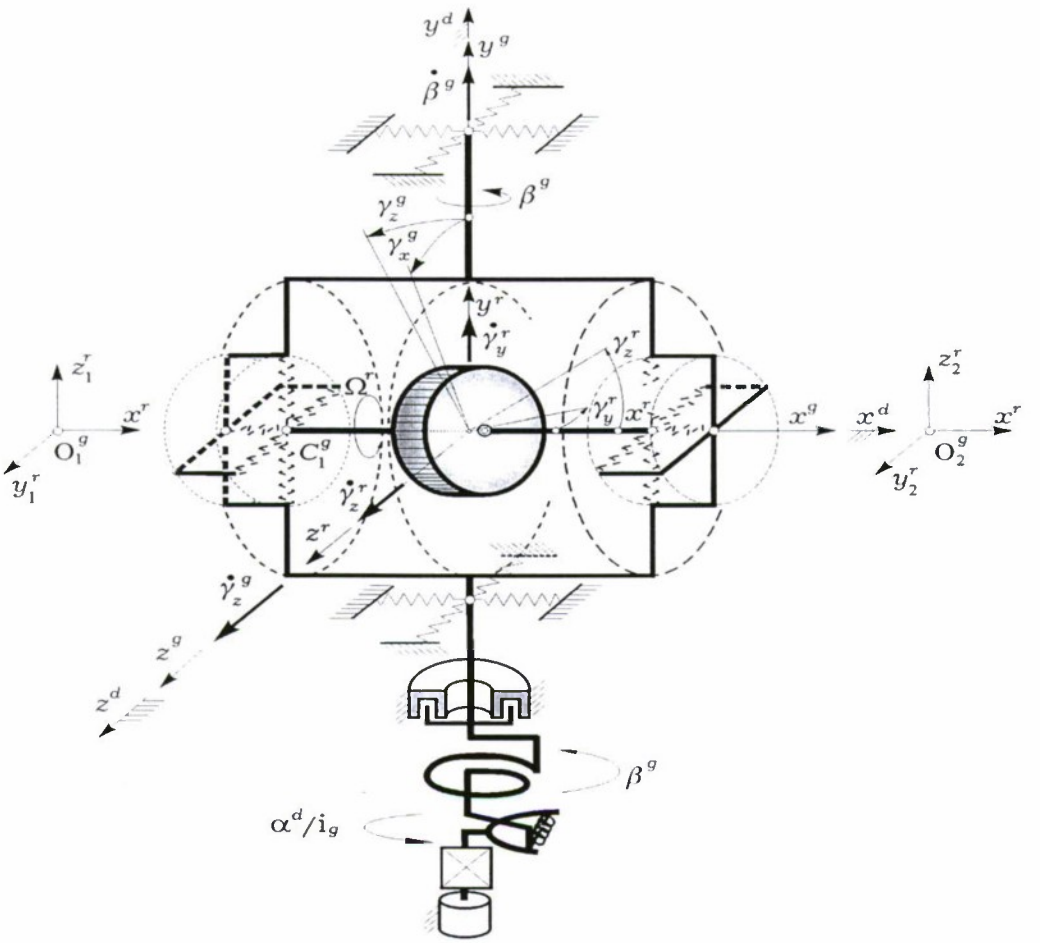

Fig. 5.

- Radial linear and angular displacements of a unbalanced rotor relatively to gyro-housing, stipulated by elasticity and damping of ball bearing;
- Dynamic of rotor rotation, radial linear and angular displacements of a unbalanced rotor relatively to gyro-housing;
- Radial and angular displacements of an gimbal axis of a gyro-housing, stipulated by elasticity and damping of ball bearings on this axis;
- Angular displacement of gyro-housing $\beta(t)$ relatively to an axis of it gimbal under an operation of a control moment of a drive and moment of friction forces in ball bearings;
- Moment of friction forces, kinematic inaccuracies and elasticity of teeth of an output cone of the reduction gearbox with the device which take up backlash;
- Own dynamic of a moment drive on a gimbal axis of a gyro-housing;
- Output signals of an angle transmitter $\beta(t)$ subject to its inaccuracies;
- Angular elasticity of mechanical fixing of a gyrodine body on space vehicle.

The simplified linear and nonlinear models of gyrodine, obtained from its full model as partieular eases, used for an installment research of dynamie influence of the separate factors and justifieation of values of gyrodine parameters. In particular was in detail investigated the influence of ball bearings elasticity on axes of a rotor and gyro-housing, elastieity of an output shaft of the reduction gearbox, and also elasticity of mechanical strengthening of a gyrodine body to a body of spaee vehiele. It has allowed to calculate values of stiffness and damping arguments of a gyrodine construetion, at whieh one the aeceptable value of its lowest resonance frequency is warranted. In a fig. 6 the dynamie of linearly inereasing pilot signal, whieh ensured by a controlling drive of gyrodine, with a maximum level of 8,6 grad/sec is exhibited by a numerical solution of a full mathematieal model of gyrodine under condition of a fixed foundation.

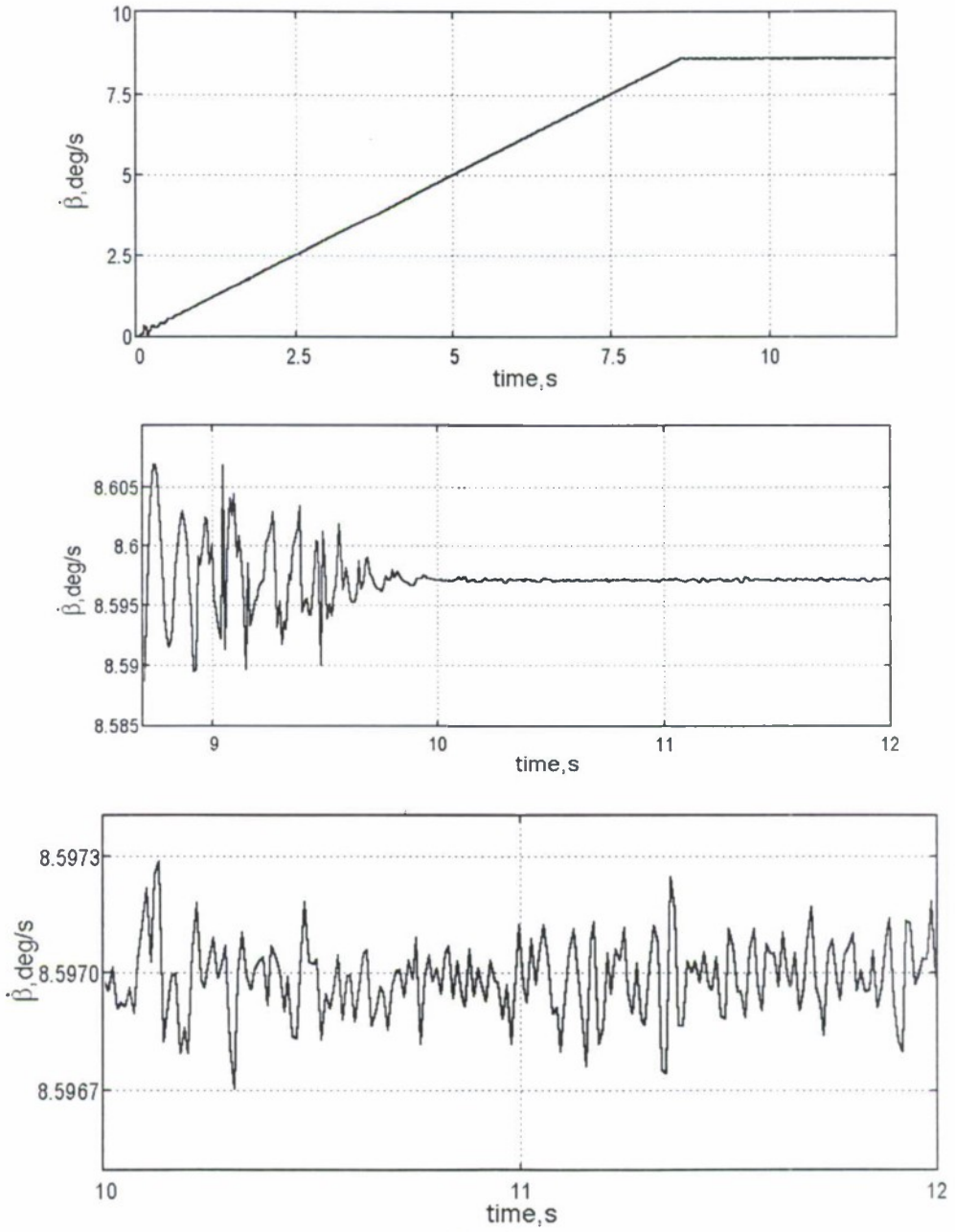

Fig. 6

The gyrodine safe life is reconfirmed by a major volume of experimental operations. A defining assembly in this respect is a rotor ball bearings. In this connection, the basic attention was given to service life tests of a gyroscope. In total on trials 13 gyroscopes were. From them 3 gyroscopes run more than 68000 hours, 3 gyroscopes - more than 90000 hours, 5 gyroscopes - more than 140000 hours and 2 gyroscopes - more than 150000 hours. Thus all their main parameters: starting and steady-state currents and the power consumption, readiness time, common vibration level, rotor rotation rate, dynamic disbalance laid within the limits of established tolerances. In particular, in a fig. 7 is shown the graph of a modification in accordance with operating time of one of defining arguments - steadied power consumption having tolerance in the documentation 7-14 W (for three gyroscopes).

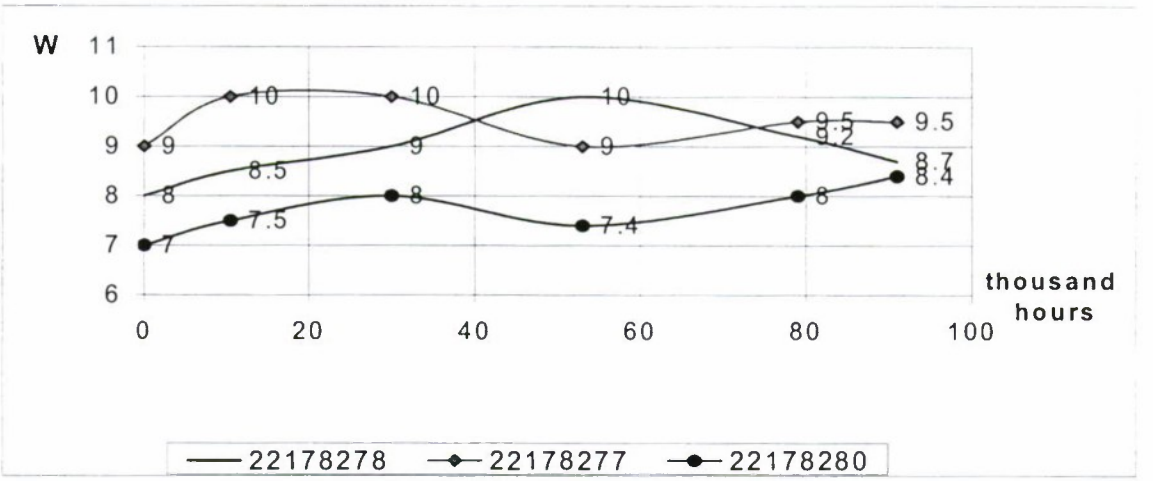

Fig. 7

According to requirements of reliability and dynamic responses of space vehicle «Resource – DK» the minimum amount of gyrodines, indispensable for control by its driving, is equal to four. In accordance with stringent restrictions on a mass and overall dimensions of an attitude control system of space vehicle «Resource – DK» and plants, unified with it, further increasing of this amount it are not exhibited possible.

At definition of the scheme of a gyrodines disposition in a coordinate system OXYZ, which bound with a body of space vehicle, allows requirements which demand to the attitude control system for ensuring of a given attitude of space vehicle. As the power gyroscopic devices are stopless, the functional capabilities of a power gyroscopic system on making control moment are determined by selected value of an angular momentum and disposition in a coordinate system OXYZ of gimbal axes of control moment gyroscopes in a body of gyrodine. Singularities of an aerodynamic configuration of space vehicle «Resource – DK», spectrum of its working orbits, and also the demanded operation conditions of scientific instrumentation are determine the restricted character of an angular rotation of space vehicle relatively to yaw axis OY and axis of a pitch OZ. For example, is not required alteration (changing) of a vector of an angular momentum of space vehicle from center of area of a variation up to its boundary on rays, collinear to axes OY, OZ. It, in turn, determines miscellaneous sizes of required area of a variation of an angular momentum of PGC on axes of a coordinate system OXYZ. As is known, at any installation diagram of gyrodines the evaluation of required rotation rate of gyroscopes conjugates with difficulties stipulated by "special" (singular) states of a vector of angles of rotation. The solution of this problem is simplified for the gyrosystem from 4 gyrodines with two by two parallel steering axes of gyroscopes, as a set of singular states of the gyrosystem in this case is minimized, and it is possible to use simple analytical relations for exposition of these states. In the even greater extent, the solution of a problem is simplified in the event case when for selection of a disposition of collinear groups to take into account the stipulated above configuration of required area of a variation of an angular momentum. These circumstances are taken into account for selection of the scheme of a gyrodines disposition for space vehicle «Resource – DK», introduced in a fig. 8. According to this scheme an axis of gyroscopes rotation and the plane OXY are parallel. An angle between rotation axes and plane OYZ (axis OY - axis of a minimum moment of inertia of space vehicle), $\alpha = 25$ deg, ensure optimal relations between sizes of area of a variation of an angular momentum on axes OX, OY, OZ.

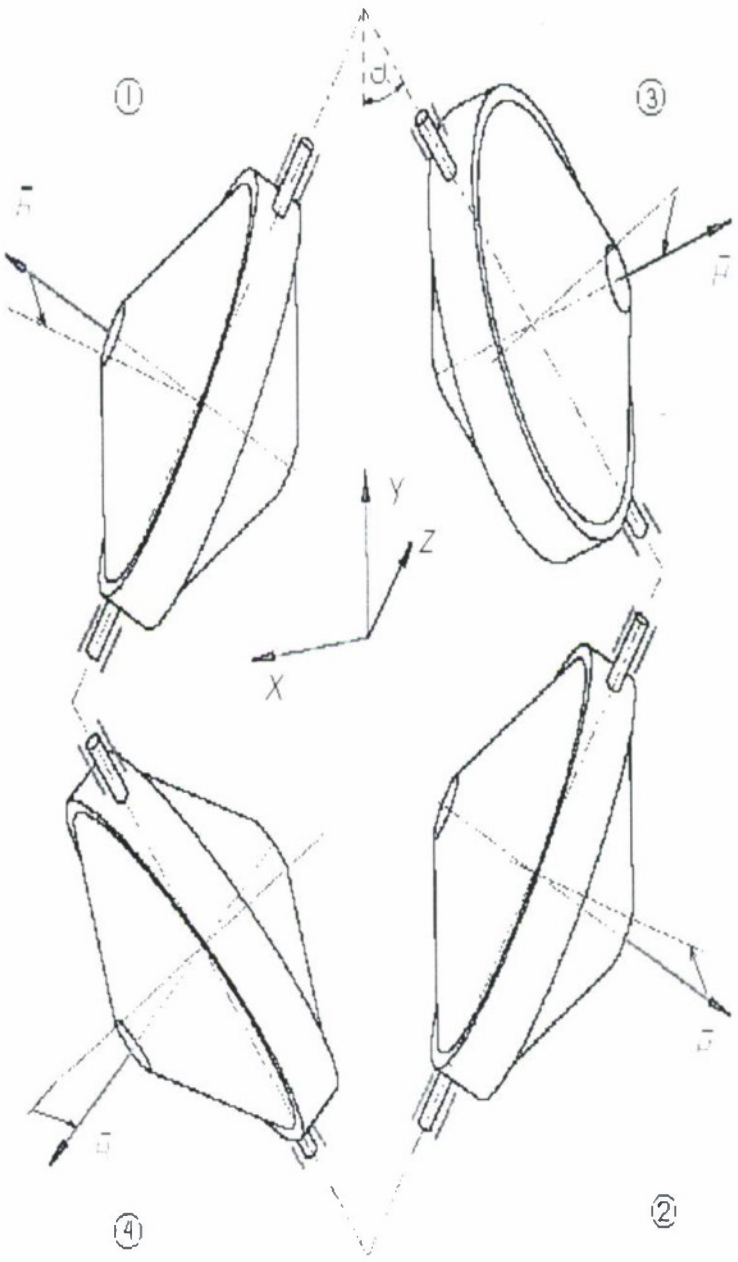

Fig.8

The maximum rotation rate of the control moment gyroscope ensured by controlling drive equal to 8,6 ^{0}/s. The positive inference about correspondence of this magnitude to requirements to an attitude control system of space vehicle is obtained by results of an estimation of two indexes, such as: an acceleration time of space vehicle up to a maximum rate at reorientation and maximum run error of programmatic motion of space vehicle in version of control with transiting of a vector of an angular momentum of the gyrosystem in an environ of singular states.

The application of PGC conjugates with necessity of a solution of a problem of its "unloading" in accordance with accumulation of an angular momentum under an operation of exterior moments. Thus the problem of a unloading is desirable for deciding so that the attitude control system was "non-flow", i.e. did not require a fuel rate available onboard space vehicle. The researches for space vehicle such as «Resource – DK» have shown, that for orbits with a perigee height is higher then 300 kms this problem is optimally decided with the help of a magnet system of reset of an angular momentum of a system "space vehicle + PGC", the mass of a magnet system is no more than 60 kgs, and mean power consumption is 55 W at magnitude of a dropped angular momentum up to 70 Nms. Besides, this mode of a unloading of PGC, as against a gravitation mode, does not require a special modification of attitude of space vehicle and by that does not restrict a possibility of operation of space vehicle on a

particular mission. The solution of problems of joint operation of PGC and a magnet system is connected with magnetic certification of installation sites of magnetometers and ensuring of magnetic compatibility of these systems of space vehicle.

For orbits with a perigee height less than 300 kms the efficiency of a magnet system is reduced in a result of increasing of the action of aerodynamic forces on space vehicle «Resource – DK». In this case the accumulation of an angular momentum is determined by component of an aerodynamic moment on an axis OZ.

The design-layout scheme of space vehicle allows with the help of a positional control of solar arrays and control by aerodynamic moment (on magnitude and sign) to retain an angular momentum in tolerance limits. The estimation of an aerodynamic moment, indispensable at indicated control, is effected under the information on an angular position of gyroscopes of gyrodines relatively to gimbal axes.

Usage of PGC in a structure of actuators of an attitude control system of space vehicle «Resource – DK», which built on the basis of gyrodines, together with magnetic and aerodynamic systems of its unloading allows to create costeffective, high-dynamic system with optimal weights and overall dimensions in all range of operation arguments.

AUTHORS INDEX

9th SAINT PETERSBURG INTERNATIONAL CONFERENCE ON INTEGRATED NAVIGATION SYSTEMS, 2002

Editor *A.K.Krytova*

Подписано в печать 21.05.02. Формат 70×108/16. Бумага офсетная. Гарнитура Таймс и Гельветика. Печать офсетная.
Усл.-печ. л. 38,4. Уч.-изд. л. 31,5. Тираж 300 экз. Заказ 313 от 21.05.02

Рег. № 020683 от 23.12.97
Государственный комитет РФ по печати

Государственный научный центр Российской Федерации – ЦНИИ «Электроприбор»
197046, С.-Петербург, ул. Малая Посадская, 30